Third Edition

Future Spacecraft Propulsion Systems and Integration

Enabling Technologies for Space Exploration

Paul A. Czysz
Claudio Bruno
Bernd Chudoba

Springer

PRAXIS

Springer Praxis Books

Astronautical Engineering

More information about this series at http://www.springer.com/series/5495

Paul A. Czysz · Claudio Bruno
Bernd Chudoba

Future Spacecraft Propulsion Systems and Integration

Enabling Technologies for Space Exploration

Third Edition

Springer

Published in association with
Praxis Publishing
Chichester, UK

PRAXIS

Paul A. Czysz
Parks College of Engineering, Aviation and Technology
Saint Louis University
St. Louis, MS
USA

Claudio Bruno
Department of Mechanical Engineering
The University of Connecticut
Storrs, CT
USA

Bernd Chudoba
Mechanical and Aerospace Engineering (MAE), AVD (Aerospace Vehicle Design) Laboratory
The University of Texas at Arlington
Arlington, TX
USA

Springer Praxis Books
ISSN 2365-9599 ISSN 2365-9602 (electronic)
Astronautical Engineering
ISBN 978-3-662-54742-7 ISBN 978-3-662-54744-1 (eBook)
DOI 10.1007/978-3-662-54744-1

Library of Congress Control Number: 2017937924

This Springer imprint is published by Springer Nature
The registered company is Springer-Verlag GmbH Germany
The registered company address is: Heidelberger Platz 3, 14197 Berlin, Germany

Foreword I

We are pleased to introduce the 3rd updated edition of *Future Spacecraft Propulsion Systems and Integration—Enabling Technologies for Space Exploration* by Czysz, Bruno and Chudoba.

The authors, a team of internationally renowned specialists in the fields of hypersonics, propulsion, and reusable vehicle conceptual design, are skillfully introducing the broad spectrum of past-to-present and present-to-future space missions. Starting with the historic-momentous flight of Sputnik 1 on October 4, 1957, this book step-by-step builds the case for future fully reusable and economically viable multi-flight space transportation systems for payloads and/or humans to Earth orbits and beyond. Adopting the mind-set *design-to-mission*, the authors are systematically introducing the potential and limitations of the full range of traditional to exotic propulsion cycles and flight vehicle design integration schemes.

In order to comprehend the variety of space missions, from Earth-orbit commerce to galactic space exploration, the authors begin with a highly interesting scenario of astronomical definitions, basics, and considerations of various interplanetary missions to still visionary journeys beyond our Solar System, e.g., to Alpha Centauri. This third edition of the book adds significant material emphasizing the comprehensive multi-disciplinary toolbox required for space mission and space technology forecasting. The overarching theme throughout this book is reusable systems, a necessary prerequisite toward a first-generation space infrastructure. In order to facilitate technology forecasting, the authors derive a system-level sizing methodology which is catalyst to correctly quantify what is needed to *design to mission*, a mandatory capability for futurists, decision-makers, CTOs, and engineers alike.

When reading this book, we are directly reminded of our own former professional career developing the reusable two-stage-to-orbit (TSTO) MBB SÄNGER II concept in Germany in the 1980s. This effort demanded us continuously screening international competitive concepts and technology preparatory activities including the development of dedicated technology demonstrators often requiring comprehensive international collaboration. During this highly stimulating era, the analogous conceptual and technological goals of the US single-stage-to-orbit (SSTO) National Aero-Space Plane (NASP) project created a tremendous hype which provided the impetus for the foundation of the *AIAA International Hypersonics Conference*, an international forum significantly promoted by Richard "Dick" Culpepper of Robert Barthelemey's NASP team. The first conference took place in 1992 in Orlando, Florida. Thanks to our increasing SÄNGER activities, the 1993 conference was hosted in Munich, Germany. Since then, the conference was renamed into *AIAA International Space Planes and Hypersonic Systems and Technologies Conference*. During the following decade, this conference was held each second year at various locations.

Two of the authors (Czysz and Bruno) were continuously attending and have been highly appreciated speakers and session chairmen. Their unique expertise delivered valuable inputs to upcoming reusable space transportation system concepts encompassing a variety of air-breathing propulsion systems and novel vehicle integration reasoning. It has been this rich and vibrant era of international reusable aerospace vehicle development which is uniquely

reflected in this 3rd edition of *Future Spacecraft Propulsion Systems and Integration—Enabling Technologies for Space Exploration*.

Unfortunately, our friend and conference promoter "Dick" Culpepper passed away in 2003. Our colleague and appreciated adviser and author Paul Czysz passed in 2013 after having been a mainstay in hypersonics and reusable space access for several decades. The whole hypersonics community is grateful for their valuable and enduring contributions. We are especially pleased to see an effective knowledge continuation with author Czysz working with author Chudoba since 2004. The 3rd edition of this book is testimony that this crucial body of propulsion and vehicle integration knowledge will be retained and continued.

Working with this book the reader will experience the immense amount of knowledge which can be made applicable for his specific objective by applying these experts' findings and recommendations. This book is a *must-read* for dedicated development work and studies in the field of spacecraft propulsion, flight vehicle integration, and its enabling technologies, as of today as well as for future missions and systems.

Heribert Kuczera & Peter W. Sacher
Members of the MBB-SÄNGER-Team (1988–1995), AIAA Associate Fellows
and authors of *Reusable Space Transportation Systems* (Springer, 2011)

Foreword II

It is indeed my pleasure to introduce the 3rd edition of *Future Spacecraft Propulsion Systems and Integration* by Czysz, Bruno, and Chudoba. This book starts by describing *the* seminal event in space exploration—the Russian launch of the Sputnik satellite—which occurred in 1957 and was the singular impetus for the creation of my agency, the Defense Advanced Research Projects Agency or DARPA one year later. DARPA is a bold agency that starts bold programs to explore unproven solutions to the most difficult problems for the Department of Defense. Like DARPA, this is a bold book that makes bold assumptions and hypotheses about how we should go about exploring the heavens. Many of these assumptions and hypotheses cannot be necessarily proven with what we know currently about the way the world works. However, I think the authors intentionally stretch our imaginations as they propose a vision for the exploration of our Solar System and beyond.

As I read this book, I found myself trying to imagine the heavens and the immensity of our universe. It humbles one to think about how large our world really is and Czysz, Bruno, and Chudoba do an excellent job of describing this world in a way that makes you want to suit up, jump in the next rocket, and go explore it.

But the rocket is the issue, isn't it? We don't have vehicles or propulsion systems that will let us explore the outer reaches of our world today. Czysz, Bruno, and Chudoba help the reader envision the propulsion concepts and flight vehicle systems that will be required to explore more of our universe. Using well-known equations and formulas, they offer vehicle and propulsion solutions that have the potential to help us break the bonds of Earth more efficiently than we can today. Will all of these concepts work? Do they all have merit? I would venture to say the answer is no but that should not stop us from applying the scientific method and some good, solid engineering rigor to these problem sets and from determining how we can build systems that take us to Mars and beyond.

Like DARPA's penchant for taking on high-risk, high-payoff projects, Czysz, Bruno, and Chudoba take on the high-risk but very high-payoff challenge of how to fully explore our solar system and beyond. So jump in, buckle up, and get ready for a wild ride.

Steven H. Walker Ph.D.
Acting Director, Defense Advanced Research Projects Agency (DARPA)
AIAA Fellow

Preface to Third Edition

The third edition of this book was born not only to update the state of the art of propulsion technology, but, more significantly, also to honor the memory of Paul A. Czysz, who was instrumental in proposing and leading the previous two editions. Paul Anthony Czysz died on August 16, 2013. He is credited with the development of a pragmatic system-level propulsion and aerospace design methodology. This was born from his design and testing experience in the USAF and at McDonnell Douglas, with the purpose of supporting the decision-maker by mathematically and visually identifying the available hardware solution space as a function of the mission. In addition to this book, Paul's work has been published in four books and in numerous technical articles. His original style in guiding and quantifying "design to mission" will remain a model for generations of engineers to come. A second difference with the two previous editions is the much greater emphasis placed on the integration of propulsion systems for hypersonic cruise aircraft and hypersonic accelerators facilitating space launch. This is the work of Professor Bernd Chudoba, the new co-author and specialist in this field.

The prime motivation for this book is the fact that humankind has been dreaming of traveling to space for a long time. In the early 1960s, there was a dedicated push to develop vehicle configurations that would permit us to travel to space and back through the atmosphere as readily and conveniently as flying on an airliner. That idea was unavoidably coupled with propulsion concepts that relied on capturing the oxygen within our atmosphere, instead of carrying it onboard from the ground up as expendable satellite launchers still do now. Given the slow technology progress since 1957, space access and space flight still suffer from limited performance due to high cost, mass consumption, and energy requirements, with consequent limited acceleration and relatively slow speed. During the 1960s, the concept of space travel extended beyond our planet, to our Solar System and the galaxy beyond (see Chap. 1), using power sources other than chemical, such as fission and fusion. It was then and still is recognized that any operational space flight transportation system is defined and limited by three key elements: (a) propulsion, (b) gravity, and (c) inertia. Future space flight requires advancing the understanding of all three areas. The first area (a) is primarily an engineering domain and is hardware driven, while the remaining two (b and c) are the domain of physics.

Accordingly, any significant advance in operational space capability will be a direct effect of revolutionary breakthroughs in high-thrust/high-efficiency propulsion and of gravity and inertia modulation. As the present outlook for breakthroughs in gravity and/or inertia is very uncertain, this book does focus on propulsion and the effect of its integration on the mission, the hardware and key technologies. The development of new manned space vehicles and launchers involves thousands of man-years. From the initial concept and through its gestation phase to the final product, how can the design team develop confidence in its performance and understanding of risks while committing very costly resources (see Chap. 2)? In this context, the trend toward space commercialization suggests the same approach seen with more conventional markets, where the mission objective is guided by continuous and sound evaluation of the product design and of its engineering or economics margins. This is in fact the integrated approach developed in Chap. 3.

Traveling to space in the near future is a multi-step process. The *first* is to realize a two-way transport to and from low Earth orbit (LEO); see Chaps. 4 and 5. This is a critical first step as it is the key to moving away from our Earth environment while being very expensive. In any future space scenario or market, economics dictates that travel to and from LEO must be frequent and affordable. From a vision of spacecraft parked in LEO, there are then several options. The geosynchronous orbit or geostationary orbit (GSO) is at an altitude of 35,853 km (22,278 statute miles) and has an equatorial orbital period of 24 hours, so it is stationary over any fixed point on Earth. These orbits are home to commercial telecommunication satellites.

The *second* critical step is an elliptical transfer orbit to the Moon. The orbital speed to reach the Moon is less than the speed to escape Earth's gravity, so the transfer orbit is elliptical (a closed curve) which does require less energy (but more logistics) than reaching GSO. Depending on the specific speed/orbit selected, the time to reach the Moon ranges from 56 to 100 hours. The Apollo program selected a 72-hour travel orbit from LEO (see Chap. 6). In terms of time, the Moon is truly close to us.

A *third* and far more eventful critical step is to achieve escape speed. This is a factor square root of two (about 1.41) faster than orbital speed. At escape speed and faster, the spacecraft trajectory is an open parabola or hyperbola. There is no longer a closed path for returning the spacecraft to Earth. So now we can move away from the gravitational control of Earth (not from gravity!) to explore our Solar System (see Chap. 7) and beyond.

There is a challenge of time, distance, and propulsion as we proceed farther and farther to explore our Solar System, then nearby Galactic space, and finally our galaxy. Exploring beyond our galaxy is technically far beyond our current or projected capabilities. Our understanding of propulsion, mass, inertia, and time will have to be different (see Chaps. 8 and 9). Understanding mass and inertia may be the most challenging. Inertia is a resistance to change of speed or direction. As we approach light speed, inertia/mass approaches infinity. As the mass approaches infinity, the thrust required to maintain constant acceleration approaches also infinity. Thus, at present, we do not know how to exceed the speed of light. If that remains the case, we are trapped within the environs of our Solar System.

An inertia-linked issue is human tolerance of continuous acceleration for long periods. Nominally that is assumed about three times the Earth's gravitational acceleration at sea level. At that acceleration, the time to reach a distant destination is numerically on the same order as the distance in light years. So, if a crewed spacecraft is to return to Earth within the lifetime of its occupants, we are again limited to about 20 light-years. That is within the distances to the seven or eight closest stars to our Sun.

As much as the authors would like to show how to travel in Galactic space, that will require breakthroughs in physics, not just propulsion. Until that time, we have much to explore and discover within the environs of our Solar System.

Coming down from Galactic space to life on Earth, these authors would like to acknowledge our spouses, Elena Prestini and Andrea Chudoba for their patience and support, and Christian Dujarric (formerly at ESA), Georg Poschmann (formerly at Airbus Industrie), Paul March at NASA, and Friedwardt Winterberg at The University of Nevada, for providing figures, articles, and comments. Special thanks go to our Editor at Springer, Ms. Janet Starrett-Brunner for her constant attention to our requests; without her, writing this book would have taken much longer.

East Hartford, Storrs, USA — Claudio Bruno
Arlington, Texas, USA — Bernd Chudoba
June 2017

Preface to First and Second Edition

Humankind has been dreaming of traveling to space for a long time. Jules Verne thought we could reach the moon with a giant cannon in the 1800s. In the early 1960s, there was a dedicated push to develop the vehicle configurations that would permit us to travel to space, and back through the atmosphere, as readily and conveniently as flying on an airliner to another continent and back. That idea, or intuition, was necessarily coupled with advanced propulsion system concepts, that relied on capturing the oxygen within our atmosphere instead of carrying it onboard from the ground up, as rockets developed in Germany in the 1940s did, and as satellite launchers still do. During the 1960s, the concept of space travel extended beyond our planet, to our Solar System and the galaxy beyond (see Chap. 1), using power sources other than chemical, such as fission and fusion. Not much is left nowadays of those dreams, except our present capability to build those advanced propulsion systems.

Traveling to space in the foreseeable future is a multi-step process. The first step is to achieve a two-way transport to and from orbit around our Earth, that is, a low Earth orbit (LEO); see Chaps. 2, 4, and 5. This is a critical first step as it is the key to moving away from our Earth environment. For any future development in space, travel that transits to and from LEO must be frequent and affordable. From a vision of spacecraft parked in LEOs, there are then several options. One is a geosynchronous orbit or geostationary orbit (GSO) that is at an altitude of 35,853 km (22,278 statute miles) and has an equatorial orbital period of 24 hours, so it is stationary over any fixed point on Earth. Another option for the next step is an elliptical transfer orbit to the Moon. The orbital speed to reach the Moon is less than the speed to escape Earth's orbit, so the transfer orbit is elliptical, and requires less energy to accomplish (but more logistics) than reaching GSO. Depending on the specific speed selected, the time to reach the Moon is between 100 and 56 hours. In fact, the Apollo program selected a speed corresponding to a 72-hour travel time from LEO to the vicinity of the Moon (see Chap. 6): in terms of the time needed to reach it, the Moon is truly close to us. All circular and elliptical orbits are, mathematically speaking, closed conics.

Another and far more eventful option is to achieve escape speed, that is a factor square root of two faster than orbital speed. At escape speed and faster the spacecraft trajectory is an open conic (i.e., a parabola or hyperbola), and there is no longer a closed path returning the spacecraft to Earth. So now we can move away from the gravitational control of Earth (not from gravity!) and proceed to explore our Solar System and beyond. However, after taking such a step, there is a challenge of time, distance, and propulsion as we proceed farther and farther to explore our Solar System, then nearby Galactic space, and finally our galaxy. Exploring beyond our galaxy is technically beyond our current or projected capabilities. In order to achieve travel beyond our galaxy, our current understanding of thrust, mass, inertia, and time will have to be different (see Chaps. 8 and 9). Mass/inertia may be the most challenging. An article by Gordon Kane in the July 2005 Scientific American entitled "The Mysteries of Mass" explains our current understanding of what we call mass. From another paper presented by Theodore Davis at the 40th Joint Propulsion Conference [Davis, 2004], we have the following statement:

> E = mc2 is the expression of mass-energy equivalence and applies to all forms of energy. That includes the energy of motion or kinetic energy. The faster an object is going relative to another object, the greater the kinetic energy. According to Einstein mass and energy are equivalent, therefore the extra energy associated with the object's inertia manifests itself in the same way mass manifests itself ... As a result, the kinetic energy adds to the object's inertial component and adds resistance to any change in the objects motion. In other words, both energy and mass have inertia.

Inertia is a resistance to change in speed or direction. As we approach light speed, the inertia/mass approaches infinity. As the mass approaches infinity the thrust required to maintain constant acceleration also approaches infinity. Thus, at this point we do not know how to exceed the speed of light. If that remains the case, we are trapped within the environs of our Solar System.

There is a second major issue. Human tolerance to a continuous acceleration for long periods has yet to be quantified. Nominally that is considered about three times the surface acceleration of gravity. At that rate of acceleration the time to reach a distant destination is numerically on the same order as the distance in light years. So if a crewed spacecraft is to return to Earth within the lifetime of its occupants, we are again limited to 20 light years of so. That is within the distance to the seven or eight closest stars to our star, the Sun.

As much as the authors would hope to travel in Galactic space, it will require a breakthrough in our understanding of mass, acceleration and propulsion. Until that time we have much to explore and discover within the environs of our Solar System.

Coming down from Galactic space to intelligent life on Earth, the authors would like to acknowledge the contributions of Elena and David Bruno, Catherine Czysz, Dr Babusci at the INFN (Italian Nuclear Physics Institute), Dr Romanelli at the ENEA Fusion Laboratories, Mr Simone, GS, H. David Froning, Gordon Hamilton, Dr Christopher P. Rahaim and Dr John Mason, Praxis Subject Advisory Editor. Special thanks go to Clive Horwood of Praxis, for his patience, constant encouragement, and prodding, without which writing this book would have taken much longer.

St. Louis, USA — Paul A. Czysz
East Hartford, Storrs, USA — Claudio Bruno

Contents

Notation

Abbreviations

AB	Airbreather (engine cycle), All-Body
AC	Alternating Current
ACES	Air Collection and Enrichment System (engine cycle)
AEC	Atomic Energy Commission
AEDC	Arnold Engineering Development Complex
AERE	Atomic Energy Research Establishment
AeroMech	conceptual design stability & control (software)
AFB	Air Force Base
AFFDL	Air Force Flight Dynamics Laboratory
AFRL	Air Force Rocket Laboratory
AGARD	Advisory Group for Aerospace Research and Development
AIAA	American Institute of Aeronautics and Astronautics
AI	Aerospace Institute
AIP	American Institute of Physics
ALES	Air Liquefaction and Enrichment System
ALHL	Air Launch Horizontal Landing
ALSS	Apollo Logistics Support Systems
AMTEC	Alkali Metal Thermal-to-Electric Conversion
ANSER	Analytic Services Inc
AoA	Angle-of-Attack
APL	Applied Physics Laboratory
ARC	Aerodynamics Research Center (at UTA), All Regeneratively Cooled (rocket)
ARCC	Air-breathing Rocket Combined Cycle
ARM	Asteroid Redirect Mission
ASEE	American Society for Engineering Education
ASI	Agenzia Spaziale Italiana (Italian Space Agency)
ASME	American Society of Mechanical Engineers
ASP	Aerospace Plane
ASPL	Advanced Space Propulsion Laboratory (NASA)
ASSET	Aerothermodynamic Elastic Structural Systems Environmental Tests (USA)
ATREX	Air Turbo Ramjet Engine with eXpander cycle
ATV	Automated Transfer Vehicle
AU	Astronomical Unit
AVD	Aerospace Vehicle Design (AVD Laboratory at UTA MAE, AVD Services LLC)
AVDS	Aerospace Vehicle Design Synthesis (software)
AW&ST	Aviation Week and Space Technology
BB	Blended Body

BEPR	Breakthrough Energy Physics Research
BG	Boost-Glide
BGRV	Ballistic Glide Reentry Vehicle
BNTEP	Bimodal Nuclear-Thermal Electric Propulsion
BOL	Beginning-Of-Life
BOR	Bespilotniye Orbitalniye Raketoplan (USSR unpiloted orbital rocketplane)
C/C	Carbon/Carbon (composites)
CBFR	Colliding Beam Fusion Reactor
C	Compressor, Chemical
CECE	Common Extensible Cryogenic Engine
CEM	Crew Exploration Module
CEO	Chief Executive Officer
CERMET	CERamics-METal
CERN	Conseil Européen pour la Recherche Nucléaire (European Organization for Nuclear Research)
CEV	Crew Exploration Vehicle
CFD	Computational Fluid Dynamics
CFR	Compact Fusion Reactor
CG	Center of Gravity
CGS	Centimeter-Gram-Second system of units (= cgs)
CIAM	Central Institute of Aviation Motors
CLV	Crew Launcher Vehicle
CO_2	Carbon dioxide
COIL	Chemical Oxygen-Iodine Laser
CONEU	Contiguous Continental Europe
CONUS	Continental United States
COPS	Comparative Operational Propulsion Systems
CRV	Crew Return Vehicle
CSP	Cryo-Solid Propulsion
CSS	Coaxial Slow Source
CT	Computerized Tomography
CTR	Controlled Thermonuclear Reactions
CTX	Compact Torus Experiment
CW	Continuous Wave
CXO	Corporate eXecutive Officer
DARPA	Defense Advanced Research Projects Agency
DB	Data-Base
DC	Deeply Cooled, Direct Current
D	Deuterium
DFP	Diluted Fusion Products (rocket)
DGLR	Deutsche Gesellschaft für Luft- und Raumfahrt
DNA	DeoxyriboNucleic Acid
DoD	Department of Defence
DOE	Department of Energy
DPF	Dense Plasma Focus
DRA	Design Reference Architecture
DR	Down Range
DRM	Design Reference Mission
DS	Decision-Support
DSN	Deep Space Network (NASA)
EAR	Excess Absolute Risk
ECH	Electron Cyclotron Heating

ECR	Electron Cyclotron Resonance
EM	Electromagnetic
ENEA	Agenzia nazionale per le nuove tecnologie, l'energia e lo sviluppo economico sostenibile (Italian National Agency for New Technologies, Energy and Sustainable Economic Development)
EP	Electric Propulsion
ERR	Excess Relative Risk
ERV	Earth Return Vehicle
ESA	European Space Agency
ESH	Expendable Spacecraft Hardware
ESI	Electrostatic Ion Thruster
ET	External Tank, Electric Thruster, Electrothermal
ETW	Engine Thrust-to-Weight ratio
EU	European Union
EVA	Extravehicular Activity (as in EVA suit)
EX	Exchanger
FDL	Flight Dynamics Laboratory (USAF)
FEL	Free Electron Laser
FF	Fission Fragments
FFRE	Fission Fragment Rocket Engine (NASA)
F	Fuel
FI	Fast Ignition
FIREX	FIeld-Reversed ion ring EXperiment
FMPT	First Materials Processing Test (program, Japan)
FOCAL	Fast Outgoing Cyclopean Astronomical Lens
FRC	Field-Reversed Configuration
FRM	Field-Reversed Mirror
FRX	Field-Reversed configuration plasma injector for magnetized target Experiment
FTL	Faster Than Light
GALCIT	Guggenheim Aeronautical Laboratory at the California Institute of Technology
GALEX	galaxy Evolution Explorer (NASA/JPL)
GCR	Galactic Cosmic Radiation, Galactic Cosmic Rays, Gas Core Reactor
GDL	Gas Dynamics Laboratory
GDM	GasDynamic Mirror
GEO	Geostationary Earth Orbit
GIE	Gridded Ion Engine
GMT	Greenwich Mean Time
GNIPGS	State Hypersonic Systems Research Institute (Russia)
GRASP	Gravity Research for Advanced Space Propulsion
GRC	Glenn Research Center (NASA)
GSFC	Goddard Space Flight Center (NASA)
GSO	Geosynchronous Orbit
GTO	Geostationary Transfer Orbit
GW	Gross Weight, Giga-Watt
H_2	Chemical formula for hydrogen gas
HALE	High-Altitude Long-Endurance
HC	Hypersonic Convergence
HED	High-Energy Density
HEO	Highly Elliptical Orbit
HL	Horizontal Landing
HMX	High Melting eXplosive (octogen)
HOTOL	Horizontal Take-Off and Landing

HRLV	Highly Reusable Launch Vehicle
HSCT	High-Speed Civil Transport
HTHL	Horizontal-Takeoff-Horizontal Landing (= HTOL)
HTOL	Horizontal-Takeoff-Horizontal Landing
HTPB	Hydroxyl-Terminated PolyButadiene
HTSC	High-Temperature SuperConducting
HyFAC	Hypersonic Research Facilities Study (NASA-sponsored study)
IAC	International Astronautical Federation Congress, International Astronautical Conference
IAEA	International Atomic Energy Agency
IAF	International Astronautics Federation
IAU	International Astronomical Union
ICAS	International Council of the Aeronautical Sciences
ICBM	Intercontinental Ballistic Missile
ICES	International Conference on Environmental Systems
ICF	Inertial Confinement Fusion
ICR	Inertial Confinement fusion Reactors
ICRP	International Commission on Radiological Protection
ICRU	International Commission on Radiation Unit
IEC	Electrostatic-Inertial Confinement
IEEEAC	Institute of Electrical and Electronics Engineers Aerospace Conference
IEEE	Institute of Electrical and Electronics Engineers
IGY	International Geophysical Year
IMLEO	Initial Mass in LEO
INEL	Idaho National Engineering Laboratories
INL	Idaho National Laboratories
IOC	Initial Operational Capability, In-Space Operations Corporation
IQ	Intelligence Quotient
IRBM	Intermediate-Range Ballistic Missile
IR	Infrared Radiation
ISABE	International Symposium on Air-breathing Engines
ISAS	Institute of Space and Astronautical Science (Japan)
ISECG	International Space Exploration Coordination Group
ISS	International Space Station
ISTC	International Science and Technology Center
ISTS	International Symposium on Space Technology and Science
ITAR	International Traffic in Arms Regulations
ITER	International Thermonuclear Experimental Reactor
JANNAF	Joint Army Navy NASA Air Force
JAXA	Japan Aerospace Exploration Agency
JBIS	Journal of the British Interplanetary Society
JHU	Johns Hopkins University
JIMO	Jupiter's Icy Moons Orbiter
JP	Jet Propellant
JPL	Jet Propulsion Laboratory
JSC	Johnson Space Center (NASA)
JUICE	JUpiter ICy moons Explorer
JWST	James Webb Space Telescope
K shell	Electron shell labeling (principal energy level)
KB	Knowledge-Base
KBO	Kuiper Belt Objects

KLIN	Meaning wedge in Russian, thermally integrated deeply cooled turbojet and rocket engine
KREEP	K = potassium, REE = rare earth elements, and P = phosphorus
KSC	NASA Kennedy Space Center
L shell	Electron shell labeling (principal energy level)
LACE	Liquid Air Cycle Engine
LANL	Los Alamos National Laboratory
LANTR	LOX-Augmented NTR
LASL	Los Alamos Science Laboratories
LDEF	Long Duration Exposure Facility
LDX	Levitated Dipole eXperiment
LEA	Liquid-Enriched Air
LEO	Low Earth Orbit
LESA	Lunar Exploration System for Apollo
LH_2	Liquid Hydrogen
LHC	Large Hadron Collider
LIGO	Laser Interferometer Gravitational-Wave Observatory
LLNL	Lawrence Livermore National Laboratories
LLO	Low Lunar Orbit
LND	Landing
LOCA	Loss Of Coolant Accident
LOX	Liquid Oxygen
LRE	Liquid Rocket Engine
LR	Lateral Range
LSS	Life Span Study
LTSC	Low-Temperature SuperConductors
LUNOX	Lunar-derived LOX
ly	Light-years
M shell	Electron shell labeling (principal energy level)
MagLev	Magnetic Levitation linear induction accelerator
MagLift	Magnetic Lifter
MAI	Moscow Aircraft Institute
MAKS	Multi-purpose Aerospace System
MAR	Mass Annihilation Rocket
MAV	Mars Ascent Vehicle
MBB	Messerschmitt-Bölkow-Blohm
McAIR	McDonnell Aircraft Company
MCF	Magnetic Confinement Fusion
MC	Magnetic Confinement
MCR	Magnetic Confinement Reactors, Magnetic Confinement Rocket
MDA	Multi-Disciplinary Analysis
MDC	McDonnell Douglas Corporation
MD	Module
MEO	Medium Earth Orbit
MFE	Magnetic Fusion Energy
MFPS	Mirror Fusion Propulsion System
MFTF	Mirror Fusion Test Facility
MGS	Manned Geosynchronous Earth Orbit (GEO) Servicing
MHD	Magneto-Hydro-Dynamic
MICF	Magnetic-Inertial Confinement Fusion
MIC	Magnetic-Inertial Confinement
MIF	Magnetic-Inertial Fusion

MIR	Lit. *peace* (space station run by the Soviet Union and later by Russia)
MITEE	Miniature Reactor Engine
MMC	Metal Matrix Composites
MMH/NTO	Monomethylhydrazine + Nitrogen Tetroxide (hypergolic propellants)
MMO	Mini-MagOrion (Miniature Magnetic Orion)
MMSEV	Multi-Mission Space Exploration Vehicle
MOL	Manned Orbiting Laboratory
MP^2	Multi-Purpose Plasma
MPD	Magneto-Plasma-Dynamic (= MHD thruster)
MR	Mass Ratio
MRX	Magnetic Reconnection Experiment
MSL	Mars Science Laboratory
MST	Madison Symmetric Torus
MSTO	Multi-Stage-To-Orbit
MTBM	Mean Time Between Maintenance
MTF	Magnetized Target Fusion
MTV	Mars Transfer Vehicle
NACA	National Advisory Committee for Aeronautics
NAL	National Aerospace Laboratory (Japan)
NASA	National Aeronautics and Space Administration
NASDA	National Space Development Agency (Japan)
NASP	National Aero-Space Plane
NATO	North Atlantic Treaty Organization
NBI	Neutral Beam Injection
NEA	Near-Earth Asteroid
NEO	Near-Earth Objects
NEP	Nuclear-Electric Propulsion
NERVA	Nuclear Engine for Rocket Vehicle Application
NEXIS	Nuclear-Electric Xenon Ion System
NextSTEP	Next Space Technology Exploration Partnership
NFL	National Football League
NFRC	Nuclear Fuels Reprocessing Coalition
NH	New Horizons
NIA	National Institute of Aerospace
NIAC	NASA Innovative Advanced Concepts (program)
NIF	National Ignition Facility
NIST	National Institute of Standards and Technology
n	Neutron
NP	Nuclear Propulsion
NPR	Nuclear Propulsion Research
NRC	National Research Council
NRL	Naval Research Laboratory
NRX	Nuclear Rocket Experimental
NSI	Nuclear Systems Initiative
NTER	Nuclear-Thermal Electric Rocket
NTO	Nitrogen Tetroxide
NTP	Nuclear-Thermal Propulsion
NTR	Nuclear-Thermal Rocket
NTREES	Nuclear-Thermal Rocket Element Environmental Simulator
NuSTAR	Nuclear Spectroscopic Telescope Array
N_2O_4	Dinitrogen Tetroxide
O_2	Oxygen

OCO	Orbiting Carbon Observatory, Oort Cloud Object
OD	Outer Diameter
ODWE	Oblique Detonation Wave Engine
OECD	Organization for Economic Cooperation and Development
OKB	Opytnoye Konstruktorskoye Buro (Russian, Experimental Design Bureau)
OMC	Open Magnetic Confinement
OMF	Open Magnetic Field
OMV	Orbital Maneuvering Vehicle
ONERA	Office National d'Etudes et Recherches Aérospatiales
OOPC	Other OPerational Costs
O	Oxidizer
OPA	Oxygen-Poor Air
Ops	Operations
OSTP	Office of Science and Technology Policy (White House)
OTV	Orbital Transfer Vehicle
OWE	Operating Weight Empty
OWEv	Operating Weight Empty (volume budget)
OWEw	Operating Weight Empty (weight budget)
PAMELA	Payload for Antimatter Matter Exploration and Light-nuclei Astrophysics
PBR	Particle Bed Reactor
PDE	Pulse Detonation Engine
PDRE	Pulse Detonation Rocket Engine
PDR	Pulse Detonation Rocket
PEMT	Purely Electro-Magnetic Thruster
PF	Poloidal Field
PP	Parametric Process
p	Proton
PY	Per Year
QED	Quiet Energy Discharge
QI	Quasi-Interstellar (= QIS)
QSH	Quasi-Single-Helicity
R&D	Research and Development
RAD	Radiation Assessment Detector
RAE	Royal Aircraft Establishment
RAM	Ramjet
RASC	Revolutionary Aerospace Systems Concepts
RAS	Russian Academy of Sciences
RBCC	Rocket-Based Combined-Cycle
RC	Right Circular (RC cone)
RDE	Rotating Detonation Engine
RDT&E	Research, Development, Technology, and Engineering
RFC	Reverse Field Configuration
RFI	Request For Information
RF	Radio Frequency
RFP	Reversed Field Pinch
RIAME	Research Institute of Applied Mechanics and Electrodynamics
RIT	Radio Frequency Ion Technology
Rkt	Rocket
RLV	Reusable Launch Vehicle
RMF	Rotating Magnetic Field
RSH	Reentry Spacecraft Hardware
RS	Rocket System (propulsion cycle, as in Ejector RS)

RSR	Roll Speed Ratio, Rapid Solidification Rate
RSS	Reentry Spacecraft Spares
RTG	Radioisotope Thermoelectric Generator
SABRE	Synergetic Air-Breathing Rocket Engine
SAE	Society of Automotive Engineers
SAFE	Subsurface Active Filtering of Exhaust
SAFFIRE	Self-sustained, Advanced-Fueled FIeld REversed mirror reactor
SAIC	Science Applications International Corporation
SBW	Switch-Blade Wing (= SWB)
SCORE	Stoichiometric COmbustion Rocket Engine
SCRAM	Scramjet
SCRJ	Supersonic Combustion Ramjet (also scramjet)
SCR	Solid Core Reactor
SC	Superconductor
SDIO	Strategic Defense Initiative Organization
SDI	Strategic Defense Initiative
SEI	Space Exploration Initiative
SEP	Solar-Energy Propulsion
SERJ	Supercharged Ejector Ram Jet
SL	Sea Level
SLS	Space Launch System, Sea-Level Static
SNAP	System for Nuclear Auxiliary Power
SNC	Sierra Nevada Corporation
SNRE	Small Nuclear Reactor Engine
SNTP	Space Nuclear-Thermal Propulsion
SOAR	Space Orbiting Advanced fusion power Reactor
SOX	Solid-Oxygen
SOZ	Solid-Ozone
SPACE	Space Propulsion Annular Compact Engine
SPHEX	SPHeromak EXperiment
SRM	Solid Rocket Motor (booster)
SR	Solar Radiation
SSME	Space Shuttle Main Engine
SSO	Sun-Synchronous Orbit
SSPX	Sustained Spheromak Physics Experiment
SS	Steady State
SSTC	Single-Stage To Cruise
SSTO	Single-Stage To Orbit
SST	Supersonic Transport
SSX	Swarthmore Spheromak Experiment
STAIF	Space Technology and Applications International Forum
STAR	Spaceplane Technology and Research
STP	Standard Temperature and Pressure
STS	Space Transportation System (Space Shuttle)
T III C	Martin Titan III C
TAD	Technology Availability Dates
TARC	Transmutation by Adiabatic Resonance Crossing
TAV	Trans-Atmospheric Vehicle
TCS	Training Course Series
TD	Thoria-Dispersed
TEPCO	Tokyo Electric Power Company, Inc
TESS	Transiting Exoplanet Survey Satellite

TF	Toroidal Field
TLC	Telecommunications
TMI	Three Mile Island
TM	Tandem Mirror
TMX	Tandem Mirror Experiment
TNO	Trans-Neptunian Objects
TOGW	Takeoff Gross Weight
Tokamak	To (roidal) ka (chamber) mak (machine)
TO	Takeoff
TPS	Thermal Protection System
TRISO	Tristructural Isotropic (fuel)
TRITON	TRImodal, Thrust Optimized, Nuclear Propulsion and Power System for Advanced Space Missions
TRL	Technology Readiness Level
TsAGI	Russian Central Aerodynamics Institute
TsIAM	Central Institute of Aviation Motor Development or CIAM
TsNIIMash	Central Research Institute of Machine Building
TSTO	Two-Stage-To-Orbit
T	Turbine, Tritium
TUG	Tugboat
TWA	Trans World Airlines
TWTO	Thrust-to-Weight ratio at Take Off
UAV	Unmanned Aerial Vehicle
UDMH	Unsymmetrical Diethyl-Hydrazine
UFO	Unidentified Flying Object
UHTC	Ultra-High-Temperature Ceramics
ULA	United Launch Alliance
UNSCEAR	United Nations Scientific Committee on the Effects of Atomic Radiation
UPS	United Parcel Service
USAF	United States Air Force
USA	United States of America
USN	United States Navy
USSR	Union of Soviet Socialist Republics (Soviet Union)
US	United States (America)
UTA	University of Texas at Arlington
UW	The University of Washington
VASIMR	VAriable Specific Impulse Magneto-plasma-dynamic Rocket
VATES	Virtual Autonomous Test and Evaluation Simulator (software)
VCCW	Vortex Combustion Cold-Wall (thrust chamber)
VCTR	Variable Cycle Turbo Ramjet
VDK	Jean Vandenkerckhove
VHRE	Vortex Hybrid Rocket Engine
VIRTIS	Visible and Infrared Thermal Imaging Spectrometer
VISTA	Vehicle for Interplanetary Space Transport Applications
VKI	Von Kármán Institute
VPK	Military-Industrial Commission of the Russian Federation
VTHL	Vertical-Takeoff-Horizontal Landing (= VTOHL)
VTOHL	Vertical-Takeoff-Horizontal Landing
VTOL	Vertical Takeoff and Landing
VT	Total volume, vertical takeoff
VTVL	Vertical-Takeoff-Vertical Landing
WB	Wing-Body

WHO	World Health Organization
WR	Weight Ratio
Wt	Weight
WU	Whittle Unit
W	Work
X	Experimental
ZFW	Zero-Fuel Weight
ZPE	Zero-Point Energy

Symbols

a	Cross-sectional semi-axis, semi-major axis of the transfer ellipse (Kepler's *elliptical* orbit), constant acceleration, plasma radius in the solenoid
a_0	Constant acceleration
a_{normal}	Acceleration perpendicular to flight path necessary to maintain a curved path
a_{sc}	Spacecraft acceleration
a_{x}	Axial acceleration
A	Propellant molecule, inlet area, atomic mass number, cross section of the reactor
$\vec{A}$	Vector potential
A, B	Constants for slender aircraft (state-of-the-art)
A_α	Mass number (nucleus emits an alpha particle)
A^+	Ion
$A^*, A_{\text{sonicthroat}}$	Rocket nozzle throat area
A_0	Airbreathing engine cowl stream tube area (inlet)
A_1	Airbreathing engine module cowl area (inlet)
A_2	Airbreathing engine module minimum area (inlet)
A_C	Airbreathing engine geometric air capture area (inlet)
A_{base}	Base cross-sectional surface area
A_c	Airbreather cowl area
A_C	Inlet air capture area
A_{cowl}	Airbreather cowl area
$A_{\max}$	Maximum cross-sectional surface area
A_z	Launch azimuth from true north
b	Cross-sectional semi-axis
$\vec{b}$	Local unit vector along $\vec{B}$
b/a	Vehicle normal cross-sectional geometry description (height and width)
B	Buildup factor, $B \equiv \left\vert\vec{B}\right\vert \equiv \sqrt{\vec{B} \cdot \vec{B}}$, $\vec{B} = B(x) \cdot \vec{b}$, poloidal magnetic field in the (r-z) plane
$\vec{B}$	Magnetic induction or magnetic field, magnetic field strength
$\vec{B}_{\min}, \vec{B}_{\max}$	Minimum value in the middle and a maximum value at the coil location
B_0	Mean magnetic field within the bottle
$\vec{B}_0$	Magnetic field necessary to stop pellet debris at a safe distance from the wall, magnetic field value in the solenoid
B_{ab}	Magnetic field value in the absorber
B_e	Magnetic field outside the separatrix (determined by the poloidal coil current)

$\vec{B}_{ext}$	External imposed magnetic induction or magnetic field, magnetic field strength
B_m	Magnetic-field intensity at the midplane
$B_{\max}$	Peak magnetic field within the bottle, magnetic field value in the mirror
$\vec{B}_p$	Tokamak magnetic field
$\vec{B}_{0p}$	Vacuum magnetic field
B_θ	Toroidal magnetic field along θ
c	Speed of light
c^*	Characteristic velocity
c_s	Plasma sound speed
C	Curve fit coefficient
C^*	Effective exhaust velocity
C_0	Collimation or coupling factor < 1 empirically accounting for the fraction of the impulse transmitted to the thrust plate by the debris
C_3	Characteristic energy (measure of the excess specific energy over that required to just barely escape from a massive body)
C_D	Drag coefficient (aircraft)
C_{D_0}	Drag coefficient (aircraft) for zero angle-of-attack (zero-lift drag coefficient)
C_L	Lift coefficient (aircraft)
$C_{L_{L/D\,max}}$	Lift coefficient (aircraft) at maximum aerodynamic efficiency
C_p	Heat capacity at constant pressure
C_{sys}	Constant system weight
C_T	Coupling coefficient
C_v	Heat capacity at constant volume
C/K	Kinetic energy losses chemical combustion can overcome
CO/F	Onboard (carried) oxygen-to-fuel ratio
CR	Inlet geometry contraction ratio ($A_{capture}/A_{throat}$)
d	Diameter of the receiving mirror on the spacecraft, distance
d_{acc}	Distance travelled at constant acceleration
dC	Number of neutrons captured by a nucleus
D	Aerodynamic drag (flight vehicle), cylinder diameter, diameter of the beaming mirror, absorbed dose, radiation dose
D_{Brems}	Bremsstrahlung radiation
D_{recom}	Radiation heat transfer due to recombination of electrons and ions
DR	Down range
e	Eccentricity, factor
e^-	Electron
E	Energy, energy to reach escape speed, internal energy, effective dose
$\vec{E}$	Electric field, radial electrostatic field
ΔE	Energy loss
E_B	Pellet energy release
E_f	Fusion heat release
E_{fus}	Energy released in a fusion reaction
$E_{fus,ij}$	Energy released in the reaction
E_i	Extraction potential, ion energy
E_{in}	Injection energy
E_k	Kinetic energy, kinetic energy of the fission fragments
$E_{\max}$	Maximum energy
E_p	Potential energy
E_{TW}	Engine thrust-to-weight ratio, sea-level static (SLS)
E/m	Energy density
f	Factor

$\vec{f}$	Lorentz force
f_b	Measure of the fuel burn fraction
f_{crw}	Crew member specific weight
f_D	Fraction for direct conversion
f_{ij}	Fraction of the fusion energy transferred to the plasma
f_n	Fraction of fusion energy associated with neutrons
f_s	Stoichiometric condition (stoichiometric fuel/air ratio)
f_{sys}	Variable system weight coefficient
f_T	Fraction used directly for thrust
ff	Fuel fraction (W_{fuel} / W_{TOGW})
$fuel/air$	Fuel-to-air ratio
F	D. Taylor correlation parameter, thrust, efficiency
$\vec{F}$	Lorentz force
$\vec{F}_g$	Gravitational force
g	Acceleration due to gravity
g_0	Gravitational acceleration at the surface of Earth
G	Universal gravitational constant
GW/S_p	Gross weight planform loading
h	Potential energy, altitude, altitude above surface, Planck constant
h_a, h_p	Geometry parameters for the example elliptical transfer orbit
h_0	Static enthalpy, freestream static enthalpy
h_S	Specific energy (energy/mass)
h_t	Total energy (stagnation energy)
H	Magnetic field intensity, equivalent dose
i	Orbital inclination, ionic current
i/F	Current absorbed per unit thrust (electric thruster)
I	Plasma current, radiation intensity, neutron flux
$\vec{I}$	Plasma current
I_{dsp}	Density specific impulse
I_p	Propulsion index, propulsion-propellant index
I_{pp}	Propulsion-propellant index
I_{ref}	Reference index
I_{sp}	Specific impulse, propulsion efficiency
I_{spe}	Effective specific impulse
I_{spf}	Fuel specific impulse
I_{str}	Structural index
$I_{sp} \cdot \rho_{ppl}$	Density impulse
I_{sp}/V_c	"Normalized" specific impulse
ICI	Industry capability index (= I_{TC})
$\vec{j}$	Current flux or current density (Lorentz force)
J	Potential energy per unit mass, fission heat release per unit propellant mass, energy density, potential energy per unit mass, microscopic kinetic energy per unit mass of the medium where potential energy has been released, heat of combustion, energy yield
$\vec{J}$	Current density vector
J_{II}	Current density component parallel to the equilibrium field
k	Boltzmann constant, boundary values
k_0	Constant of order unity that depends on the details of the trajectory
k_B	Boltzmann constant
k_{crw}	Crew member volume
k_{eff}	Effective neutron multiplication factor

k_m	Magnet constant
k_{mix}	Fuel-air mixing losses in combustor, as a fraction of the freestream kinetic energy
k_{ve}	Engine volume coefficient
k_{vs}	System volume coefficient
k_{vv}	Void volume coefficient
K	Constraint of constant helicity
K_{str}	Scaled structural fraction, correlation term
K_v	Scaled propellant volume fraction, maximum propellant volume available, correlation term, correlation parameter
K_{v_0}	Initial scaled maximum propellant volume fraction
K_w	Area ratio correlation parameter, wetted area to planform area ratio, correlation term
$K_{w_{78^\circ}}$	Area ratio correlation parameter for 78° wing/body leading edge angle
K/C	Kinetic energy/available chemical energy
KE	Kinetic energy, initial kinetic energy of the fusing pellet
L	Aerodynamic lift (flight vehicle), multiplier for body length, length of track, length of "bottle," trajectory distance (length), length of the solenoid
L_1, L_4, L_5	Lagrangian points
L_{ex}	Length of the expander
L_m	Length of the mirror
La	Launch site latitude
L/D	Lift-Drag ratio, aerodynamic efficiency
$(L/D)_{\max_{hypersonic}}$	Maximum hypersonic aerodynamic glide ratio
$(L/S)_{plan}$	Lift loading
LR	Lateral range
m	Mass, propellants combustion forms molecules of average mass, relativistic mass, mass of charged particle, propellant mass consumed
$\dot{m}$	Propellant consumption, mass flowrate of propellants, instantaneous propellant mass, mass flowrate
m_0	Rest mass (body at rest), fuel mass at rest, mass at rest
m_1, m_2	Mass of two bodies
m_e	Mass of electron
m_i	Mass of the plasma ion
m_{ppl}	Mass of propellant
$m_{spacecraft}$	Mass defect
Δm	Mass, propellants combustion forms molecules of average mass, relativistic mass
M	Mach number, mass of the central body, mass, generic "third body", spacecraft mass, mass (energy) of the parent nucleus
M_0	Initial Mach number, spacecraft mass
M_{aux}	Mass of the auxiliary system
M_{AB}	Maximum airbreathing Mach number
M_{cryo}	Cryoplant mass
M_f	Final mass of the ship at destination
$M_m = M_{mag}$	Magnet mass
$M_{powerplant}$	Powerplant mass
$M_{ppl} = M_p$	Mass of propellant, inert mass, inert propellant
M_{ppl_0}	Propellant mass at rest
M_R	Mass ratio ($M_R = W_R$)
M_{rad}	Radiator mass
M_{ref}	Refrigerator mass

M_s	Shield mass, blanket mass
M_{sc}	In-orbit spacecraft mass
M_{sun}	Mass of the Sun
M_{tot}	Total mass
MW	Average molecular weight
n	Number, plasma particle density, neutron
n_1, n_2	Particle number densities of the two reactants
n_e	Electron density
n_i	Equilibrium fuel ion density
n_j	Reacting ion species density
$n \cdot \tau$	Confinement parameter, Lawson parameter
N	Multiplier for nose cone length, number, volumetric density of nuclei
N_{crv}	Number of piloting crew
N_i	Number of ions per unit volume
N_x	Thrust required to provide the selected axial acceleration, axial thrust
N_z	Normal load factor
O/F	Oxidizer-to-fuel ratio
p	Pressure, proton
p^-	Antiproton
$\vec{p}$	4-vector in special relativity
P	Thrust power, power, jet power
P_{aux}	Auxiliary power needed to heat plasma
P_b	Loss due to bremsstrahlung
P_B	Bremsstrahlung radiation power
P_c	Combustor pressure
P_{cryo}	Cryoplant power
P_{el}	Electrical power
P_f, P_{fus}, P_{fusion}	Fusion power output
P_F	Thrust power
P_{inj}	Power injection
P_{jet}	Power of LANTR engine
$P_{\max}$	Maximum power reached at end of MagLev track
P_n	Neutron power per unit surface, target specific fluence
P_{rad}	Waste power to be radiated in space
P_s	Synchrotron radiation power
P_{spec}	Fusion power density in the reaction chamber, fusion power per unit volume that can be produced in the form of neutrons and charged particles
P_S	Loss due to synchrotron radiation
P_{thrust}	Power available for thrust
$P_{\gamma+\beta}$	Residual power of the combined gamma and beta particles
Py	Payload weight (= W_{pay})
P/F	Power absorbed per unit thrust (electric thruster)
q	Aircraft dynamic pressure, Coulomb charge, electric charge, factor
q_0	Aircraft dynamic pressure at stagnation point
q_c	Cumbustor dynamic pressure
$q_{radiated}$	Waste heat flux
$q \cdot \vec{E}$	Coulomb force
Q	Brayton cycle heat addition, energy added to the air by fuel combustion, energy gain (ratio between energy output and energy used to ignite), gain factor, fusion gain
Q_c	Heat of combustion
Q_{net}	Maximum air combustion energy

$Q_{rejected}$	Rejected heat
r	Distance between the center of mass of the two bodies, radius from the spacecraft center of mass to the center of mass of the central body, distance of the parallel rays from the Sun center, smaller of the two torus radii, spherical wire mesh of radius
r_1	Distance Earth to sphere of influence (Moon)
r_2	Radius of sphere of influence
r^*	Radius of an equivalent sonic throat that would give the nozzle mass flow, static pressure and temperature at the combustor exit
r^*_{ref}	Reference radius of an equivalent sonic throat
r_a, r_p	Geometry parameters for the example elliptical transfer orbit from LEO to GSO
$r_{antenna}$	Spacecraft antenna dish radius
$r_{base} = r_b$	Circular base radius
r_c	Flux conserver radius
r_m	Cylindrical solenoid of radius
$r_{nose} = r_n$	Body nose radius
$r_{O/F}$	Oxidizer-to-fuel ratio ($W_{oxidizer}$ / W_{fuel})
r_p	Plasma radius
r_{pay}	Payload-to-empty weight ratio (W_{pay} / W_{OEW})
r_s	Lunar sphere of influence, radius of magnetic separatrix
r_{str}	Structural fraction, structure-to-empty weight ratio (W_{str} / W_{OEW})
r_{use}	Useful load (W_{pay} + W_{crew})-to-operating empty weight (W_{OEW}) ratio
r_w	Tokamak geometry (wall radius), spherical or cylindrical chamber of radius
R	Geometry parameter (ellipse), gas constant, radius, laser range, pellet radius, mirror ratio, range, mirror ratio
R_0	Planet radius (e.g., average radius of Earth)
R_C	Tokamak geometry, radius of the reactor channel
R_D	Tokamak geometry
R_e	Reflectivity
R_{LE}	Radius at leading edge
R_N	Radius at vehicle "nose" or stagnation point
S	Radiating surface area, radiator area, wing surface area, US correlating parameter (Küchemann slenderness parameter), volumetric efficiency factor, entropy of the airflow, MHD interaction parameter, average distance, total journey distance, number of ion gyro-radii between the field null and the separatix
$S_{1/2}$	Midway distance, midpoint distance
$S_{plan}, S_{\mathrm{pln}}, S_p$	Planform area (area of the body projection on a planar surface)
S_{rad}	Radiator surface
S_{tr}	Strehl ratio
S_{wet}	Wetted surface area
SG	Bulk specific gravity
S/R	Non-dimensional entropy
t	Time to reach V
t_0	Length of time a reactor has been in operation
$t_{1/2}$	Half-life
$t_a = t_{acc}$	Acceleration time
t_b	Time for fuel burning (fusing), kinetic time
t_d	Destruction time, residence or transport time
t_e	Spacecraft journey duration in an Earth-bound observer frame of reference
t_{ES}	Round-trip time

t_m	Mission duration
$t_{mission}$	Ideal mission time
t_{sc}	Spacecraft journey duration in its own moving reference
t_t	Transit time
T	Thrust, temperature, US correlating parameter (Küchemann slenderness parameter), shape efficiency factor, multiplier to entropy S, gas static temperature, period of the ellipse, combustion temperature
$T_{1/2}$	Half-life
$T_{airbreather}$	Airbreather engine thrust
T_c	Combustor temperature
T_e	Electron temperature
T_H	Temperature in the blanket/exhaust system
T_i	Equilibrium fuel ion temperature
T_{ideal}	Ideal ignition temperature below which fusion power output is lower than power lost by Bremsstrahlung
T_j	Temperature of the jth species
T_{opt}	Optimal temperature
T_{rocket}	Rocket engine thrust
T_R	Radiator temperature
T_{sp}	Thrust per unit air flow
T/D	Thrust-to-drag ratio
T/W	Thrust-to-weight ratio
$T-D$	Thrust minus Drag, excess thrust
u	Gas velocity along MHD device
$\vec{u}$	Gas velocity along MHD device
u_τ	Velocity acquired at time τ under constant thrust
U	Magnetic energy
v	Light frequency
$v_\perp$	Velocity component normal to $\vec{B}$
v_{II}	Velocity component parallel to $\vec{B}$
$\vec{v}$	Velocity of electric charge; bulk velocity
v^*	Collisionality parameter defined as the ratio between the typical scale length along the magnetic field and the mean free path of Coulomb-driven collision
v_c	Characteristic velocity
v_{crv}	Crew member specific volume
v_{ex}	Exhaust velocity of the propellant being ejected
v_f	Final velocity
v_{ti}	Ion thermal velocity
V	Flight velocity, volume, internal volume
V_{flight}	Flight velocity
$\vec{V}$	Flow velocity
V_0	Flight velocity
$V_{1/2}$	Midcourse speed
V_{200}	Orbital speed for a 200 km orbit and escape
ΔV	Change in flight velocity (or flight velocity increment); incremental velocity, launch velocity increment (energy increment) to reach Earth orbit
$\Delta V_1, \Delta V_2$	Velocity increments to change orbital altitude
ΔV_{ab}	Airbreathing speed increment
$\Delta V_{airbreathing}$	Change in flight velocity (or flight velocity increment); incremental velocity
ΔV_{dp}	Difference of potential between two gids
ΔV_{pc}	Incremental velocity for an impulse turn (nonrotating Earth)

V_a	Velocity at the apoapsis (Kepler's elliptical orbit)
V_{av}	Average velocity
V_c	Combustor gas velocity, characteristic velocity associated with the mission (design speed)
$V_{circular}$	Orbital velocity (Keplerian circular orbit)
V_e	Specific impulse measured in m/s, speed of the mass ejected, bulk velocity, exhaust velocity, exhaust velocity acquired by the ion, material jet exhaust velocity, velocity of the mass ejected from the rocket, ideal specific impulse, debris velocity following the nuclear explosion
V_{esc}	Escape velocity
V_{fuel}	Injection fuel velocity
V_i	Injection speed
V_p	Velocity at the periapsis (Kepler's elliptical orbit), plasma volume
V_{ppl}	Propellant volume fraction
V_{sc}	Spacecraft speed in its own moving reference
$V_{tot} = V_{total}$	Total volume (= VT = V_T)
$\dot{w}$	Unit mass flow
w_r	Weighting factor for different types of radiation
w_T	Weighting factor for tissues/organs
$\dot{w}_{airbreather}$	Airbreather engine unit mass flow rate of propellant
$\dot{w}_{ppl}$	Unit mass flow rate of propellant
$\dot{w}_{rocket}$	Rocket engine unit mass flow rate of propellant
W	Weight, mass
W_{cprv}	Crew provisions weight
W_{crew}	Crew weight
W_{dry}	Dry weight
W_{empty}	Empty weight
W_{fuel}	Fuel weight
$W_{generator}$	Generator weight
W_{GW}	Gross weight (= gross mass)
W_n	Neutron wall loading
$W_{radiator}$	Radiator weight
$W_{reactor}$	Reactor weight
W_s	Surface heat flux
W_{TOGW}	Takeoff gross weight (= GW, gross weight)
W/S	Wing loading (classic aircraft)
W_{TOGW}/S	Wing loading
$W_{OEW} = W_{EO}$	Operating empty weight ($W_{OWE} - W_{pay} - W_{crew}$), ($W_{OEW} \approx W_{ZFW}$)
$W_{OWE} = W_{OE}$	Operating weight empty ($W_{OEW} + W_{pay} + W_{crew}$)
$W_{oxidizer}$	Oxidizer weight
W_{pay}	Payload weight
W_{ppl}	Propellant weight
W_R	Weight ratio (WR) = mass ratio
W_{str}	Structure weight
W_{use}	Useful load ($W_{pay} + W_{crew}$)
W_{tank}	Tank weight
W_{ZFW}	Zero-fuel weight, dry weight
x	Cross-sectional geometry parameter (top width/bottom width)
x, y, z	Cartesian coordinates
z_0	Axial coordinate corresponding to the midplane
Z	Atomic number
Z_0	Design altitude (airbreathing engine), geometric altitude

Z_α	Atomic number (nucleus emits an alpha particle)
ΔZ	Nucleus with charge difference change in atomic number
Z_{eff}	Effective charge
z	Axial direction of the reactor, cartesian coordinate
Z_j	Reacting ion species charge

Greek Letters

α	Ionization fraction, degree of ionization, percentage of initial mass, mass fraction of captured H atoms actually fused, matter-to-energy conversion fraction, ratio between engine power and mass, specific power, alpha decay (radioactive decay), specific power (thrust power per unit mass), ratio rotation frequency/ion diamagnetic rotation frequency
α^*	Power available per unit mass of the reactor
α_{cryo}	Specific power cryoplant
α_{mag}	Specific power magnet
α_{rad}	Specific power radiator
α_s	Specific power blanket
β	Prandtl-Glauert factor ($\beta = \sqrt{M^2 - 1}$), ratio between thermodynamic and magnetic pressure, beta decay (radioactive decay), parameter, thermal pressure/magnetic pressure, ratio between plasma pressure and magnetic pressure
β^-	Emission of an electron
β^+	Emission of a positron
β_{ext}	External imposed ratio between thermodynamic and magnetic pressure
$\beta_{\max}$	Maximum ratio between thermodynamic and magnetic pressure
γ	Flight path angle, specific heat ratio (heat capacity ratio), γ-ray wavelength (gamma radiation)
δ_{ppl}	Weight ratio
ε	Emissivity, deflection of the electromagnetic wave, bending angle, binding energy per nucleon, radiator emissivity
η	Efficiency, ideal Carnot efficiency
η_{aux}	Auxiliary efficiency
η_{carnot}	Carnot cycle efficiency
η_D	Direct conversion efficiency
η_{th}	Thermal conversion efficiency
η_T	Thrust conversion efficiency
θ	Nozzle half-angle, energy conversion efficiency of Builder, propulsion efficiency, azimuthal (circumferential) coordinate
κ	Thermal conductivity
$\vec{\kappa}$	Magnetic field curvature
λ	Approach angle to the Moon, arrival angle, laser wavelength, energy state, distance, global constant
λ_n	Neutron mean free path in the blanket
$\bigwedge$	Leading edge wing or body sweep angle
μ	Structure index, structure factor (= I_{str}), gravitational constant (= $M \times G$), standard gravitational parameter, payload ratio (payload mass/initial spacecraft mass), line absorption coefficient, magnetic moment
μ_a	Margin on inert weight
ρ	Density, charge density, gyration (spiral) radius, plasma density, volumetric density
ρ^+	Gas density with positive ion charges distributed, charge density

ρ^*	Ratio between the ion Larmor radius and the typical scale length transversal to the magnetic field
ρ_{fuel}	Fuel density
ρ_H	Average mass density of interstellar hydrogen
ρ_{ie}	Ion or electron gyration radius ("gyroradius") in the outer magnetic field
ρ_{mag}	Magnet density
$\rho_{oxidizer}$	Oxidizer density
ρ_{ppl}	Propellant density, mean propellant density
ρ_{rad}	Mass per unit surface of the radiator
ρ_s	Blanket density
$\rho \cdot u$	Mass flow per unit area
σ	Stephan–Boltzmann constant, fluid electrical conductivity, electric conductivity, neutron cross section, effective rate of capture per unit flux and unit nuclei surface density
σ_{stress}	Stress (= force/area)
$(\sigma \cdot v)_{ij}$	Reactivity
τ	Non-dimensional volume index, volume parameter, Küchemann parameter, slenderness parameter, duration (time to destination), confinement time, dimensionless quantity devoid of any units involving distance or time
τ_{78°	Küchemann parameter for 78° wing/body leading edge sweep angle
τ_E	Energy confinement time (ratio between the energy content of the plasma and the heating power)
τ_i	Fuel ion confinement time
τ_{ii}	Ion–ion collision timescale, timescale for the scattering of a trapped ion into the loss-cone
τ_N	Particle confinement time
τ_{SD}	Electron drag timescale
ϕ	Equivalence ratio, angle describing flight path geometry of the representative lunar trajectory, potential, ambipolar potential, barrier, plasma potential, flux of the axial magnetic field between the null point and the separatrix, magnetic flux
Ψ	Static compression enthalpy ratio
Ω	Gyration or cyclotron frequency, rotation frequency
Ω_{Di}	Ion diamagnetic rotation frequency

List of Figures

List of Tables

Introduction

We begin with the fundamental element, or you may say, the first step of traveling to space: orbiting around Earth or another celestial body. Consider an object orbiting the Earth; unless there are factors such interaction with the upper atmosphere, solar wind, and kinetic energy losses, the object will orbit indefinitely. The reason is that all objects in orbit are essentially falling around the body they are orbiting. This is relatively simple to illustrate. The acceleration of gravity at the surface of the Earth is 32.1741 ft/s^2 (9.8067 m/s^2) and that means, from Newton's Laws, in one second an object will fall 16.087 feet or 4.9033 meters from rest.

The radius of the Earth at the equator is 3,963.19 statute miles (6,378.14 km). If the Earth were a smooth sphere with the radius of the Earth's equator, then the distance traversed along the surface from a point A to a point B is 25,947 feet (7,908.7 meters), while this point B has "dropped" 16.087 feet lower than point A. Then, if an object were one foot above the surface of this perfect sphere, and traveling at a speed of 25,947 ft/s (7,908.7 m/s) parallel to the surface, then it would fall the same distance as the surface of the Earth curves and drops away from the starting point. That is, it would continuously fall "around the sphere" at an altitude of one foot, without ever striking the surface. In fact, it would be *in orbit* around the sphere. We can conclude that an object, when being in orbit around a body, is falling around that body at sufficient speed such that it does not move closer to the surface. Occupants in that orbiting body are not experiencing *zero gravity*; they do instead experience *zero net force*.

In order to show that, consider the acceleration of a body moving along a curved path that is at constant speed V, but with a constantly varying flight path angle. The acceleration perpendicular to the flight path that is necessary to maintain the curved path is given with

$$a_{normal} = \frac{V^2}{\text{radius}}$$

Using the equatorial radius of the Earth, with the magnitude of the speed V = 25,947 ft/s (7,908.7 m/s), the normal (perpendicular) acceleration is equal to the acceleration of gravity in magnitude, but acting in the opposite direction. Then, an object in orbit around a body is free-falling around that object without any net forces acting on that object. That is often described mistakenly but colorfully by the popular press as a condition of "zero gravity"; instead, it is the difference between two essentially equal and opposite forces. Microgravity would instead be a more appropriate term, for there is always a minute residual difference between gravity and normal acceleration. The balance tends to be so delicate that an occupant on an orbital station that sneezes can ruin a microgravity experiment. Technically, such disturbances go by the name of *microgravity jitters*.

Then, in order to go to space, we first need a transportation system from the surface of Earth to Earth orbit and return. In order to go to the Moon and beyond, for instance to Mars, we need a propulsion system that can leave Earth's orbit, and then establish an orbit around its destination object. We are able to do this to the Moon relatively easily with the currently operational propulsion systems. That is, because to reach the Moon, an elliptical orbit containing the Earth and Moon at its foci is sufficient. For reaching Mars, we must attain and exceed escape velocity. Mars requires a round trip of two years with current propulsion systems. Consequently, for the Mars journey, the required propulsion system that ensures minimum radiation damage to human travelers is still in the laboratory. In order to go Pluto and beyond, we need propulsion systems not yet built, but envisioned by people that seek to

travel beyond our Solar System. However, to travel much farther beyond Pluto remains, for the time being, only an expectation.

If you were to ask the question, *What is Space Propulsion?*, probably the most common answer would be: ... *Rockets* .... Beginning in 1957 with *Sputnik*, chemical rockets have propelled payloads and satellites into Earth orbit, to Mercury, Venus, Mars, and Titan (one of Saturn's satellites), and have propelled two *Pioneer* spacecraft (*Pioneer 10* and *Pioneer 11*) to the boundary between our Solar System and interstellar space. *Pioneer 10*'s last telemetry transmission to the NASA Deep Space Network (DSN) was April 22, 2002, having been launched on March 2, 1972. On January 22, 2003, the DSN recorded *Pioneer 10*'s last weak radio signal at a distance of 7.6 billion miles ($7.6 \bullet 10^9$ miles) from Earth. That signal took 11 hours and 20 minutes to reach DSN (Wolverton 2004). *Pioneer 11*'s last telemetry transmission was in 1995. Its journey has taken nearly 31 years, and it is now beginning to cross the boundary between our Solar System and interstellar space (the so-called Heliopause).

This is the problem we face with chemical rocket propulsion—the extremely long times to cover large distances, because the speed possible with chemical rockets is severely limited by how long the rocket motors can function. Had an operational *Pioneer* spacecraft reached a distance from Earth that is 100 times the distance the Earth is from the Sun (i.e., of the order of the Heliopause), it would take light around 14 hours to traverse the one-way distance. Then, a two-way communication requires 28 hours, four hours longer than one day! That is to say that, at light speed, *Pioneer 10* would have reached the Heliopause some 32 years ago! *Pioneer 10* is on its way to the red star Aldebaran, but it will not arrive there for more than another 2 million years (Wolverton 2004). The *Pioneer* spacecraft team that was present when the Pioneer spacecraft passed by Jupiter, Saturn, Neptune, or Uranus is no longer the group listening for the sporadic-distant signals being received from the *Pioneer* spacecraft. In reality, the *Pioneer* spacecraft moves so slowly, and that following its progress is beyond the practical ground-based tracking team's functional duration. Moving faster requires higher accelerations, but those are limited by the rocket propulsion systems available, human physiological constraints, and finally spacecraft hardware tolerance to acceleration (*g*-tolerance). To approach light speed or faster than light (FTL) speed, what is needed is not antigravity but antimass/anti-inertia. One primary question remains: *Is FTL possible?* One conclusion by (Goff and Siegel 2004) is:

> *... Current warp drive investigations* (*Goldin and Svetlichny* 1995) *apply general relativity to try to produce spacetime curvature that propagates at superlight speeds. Special relativity is preserved inside the warp field, but the contents are perceived to move at FTL speeds from the external frames. Such a classical warp drive cannot avoid the temporal paradox (i.e., time travel). If quantum systems are the only system that permits backward-in-time causality without temporal paradox, then any rational warp drive will need to be based on quantum principles. This means that until we have a workable theory of quantum gravity, research into warp drives based on General Relativity is probably doomed to failure. ...*

A second example of our chemical rocket speed limitations is a Pluto mission. The planet Pluto has a distance from the Sun varying from 2.78×10^9 to 4.57×10^9 statute miles, for an average of 3.67×10^9 statute miles. Depending on its distance, a one-way radio signal takes between 4 hours 10 minutes and 6 hours 48 minutes, to reach Pluto from Earth. Then, the two-way transmission from Earth and return takes from about 8 hours to 13 hours. That is a considerable time to consider communicating with and controlling a spacecraft. If a correction to its flight path, or a correction to its software programming, or remedying a problem is necessary, it will be between 16 and 26 hours before a return signal can confirm whether or not the action was successful. In that period of time, a great deal can happen to harm, injure, or destroy the spacecraft. Clearly, these spacecraft that are operating at the fringe of practical control because of the propulsion system's performance must essentially be robots, capable of diagnosing and correcting problems without human intervention.

The question is, *What propulsion performance is necessary to significantly change this chemical rocket paradigm?* The performance of a rocket is measured by its ability to change the magnitude of its speed in a given direction (velocity) by the ejection of mass at a

characteristic velocity. That change in the magnitude of the speed, ΔV, can be expressed in the simplest way as in Eq. (2):

$$\Delta V = g \cdot I_{sp} \cdot \ln(W_R)$$

$$\Delta V = c^* \cdot \ln(W_R)$$

where the characteristic velocity is given by

$$c^* = g \cdot I_{sp}$$

The weight ratio is defined as

$$W_R = \exp \frac{\Delta V}{g \cdot I_{sp}}$$

$$W_R = \frac{\Delta V}{c^*} = \frac{\text{Initial mass}}{\text{Final mass}}$$

with

$$(W_R - 1) = \frac{\text{Propellant mass}}{\text{Final mass}}$$

The specific impulse defined as the thrust produced per unit mass (weight) flow rate of propellant is given by

$$I_{sp} = \frac{T}{\dot{w}_{ppl}}$$

With these definitions, we do have just two *key parameters*: (1) the weight ratio, or mass ratio, which is just a measure of how much propellant is carried; (2) the characteristic velocity, or specific impulse, I_{sp}, which defines the performance of the propulsion system. The best cryogenic chemical rockets today have an I_{sp} of 460 s (4,462 m/s). That means that a (mass) flow of one kilogram per second generates 460 kg (4,462 N) of thrust. If our benchmark change of speed ΔV is the speed of light (299,790,000 m/s), then the specific impulse required for a mass ratio of 6 is 17,062,060 s. That is, one kilogram per second of propellant flow generates 17,062,060 kg of thrust. Or more pointedly, one microgram per second of propellant produces 17.06 kg of thrust! That is approaching a so-called *mass-less* thrust-producing system and is well beyond our current concept of generating thrust. Even if at some future time an I_{sp} of 100,000 s is achieved, the speed of light (299,790,000 m/s) is 170 times faster than the incremental velocity provided by a mass ratio of 6.

If our benchmark distance is one light-year, or 5,880 billion ($5{,}880 \times 10^9$) statute miles, or 1,602 times more distant than Pluto, to reach that distance in a 15-year one-way time, the specific impulse of the propulsion system would have to be 1,602 times greater than that of current rockets. If that was so, we could travel 1,602 times farther in the same 15-year time period. That is, the propulsion system I_{sp} must be 1,602 times 300 s (the best I_{sp} feasible with storable propellants), or 480,600 s, or a characteristic velocity of 4,713,000 m/s, about 1.6% of the light speed. The most advanced off the shelf electric propulsion we have today is capable of about 4,000 s, just 13.3 times greater than current storable propellant rocket specific impulse, so that we can travel 13.3 times farther in the same 15-year time period, or 48.8 billion statute miles. This enables us to reach the so-called *Oort Cloud*, the origin of long-period comets, and a region of space very distant from any major astronomical object outside of our Solar System. Clearly, we are confined to our Solar System if our travel time is going to be the duration of a human project team and our current propulsion systems. At the distance of one light-year and with current storable propellants, the travel time to one light-year distance from Earth is about 24,032 years. That is about the length of human recorded history. With our best Nuclear-Electric propulsion, the time to one light-year distance is 1,807 years.

Within our galaxy, *α-Centauri* (or Alpha Centauri) is one of the seven stars within 10 light-years of Earth, or *α-Centauri* is 6,580 times more distant than Pluto from Earth. Alpha

Centauri is the closest star system to the Solar System at 4.37 light-years (ly). In order to reach α-Centauri in a 15 year-long one-way travel, the specific impulse would have to be over 1.970×10^7 s, or the characteristic velocity 64% of light speed. If we could develop a propulsion system with an exhaust velocity equal to the speed of light, the specific impulse would be 30,569,962 s. Our galaxy is a spiral galaxy about 100,000 light-years in diameter with a central "bulge" about 20,000 light-years deep. Our Solar System is about 33,000 light-years from the galactic center. To reach past our galaxy to our nearest galaxy, *Andromeda*, that is 3,158,000 times more distant than Pluto, the I_{sp} would have to be on the order of 950×10^9 s, and the characteristic velocity would have to be an impossible 6.47×10^{12} or 21,600 times the speed of light. That velocity is not conceivable within our current understanding of physics.

Figure 1 shows the spiral galaxy Andromeda in ultraviolet wavelength by the GALEX Satellite and in visible light (see the GALEX/JPL Web site). The Andromeda galaxy is the most massive of the local group of galaxies, which includes our Milky Way, and is the nearest large galaxy similar to our own. The GALEX ultraviolet image shows regions of young hot, high-mass stars tracing out the spiral arms where star formation is occurring. The central white "bulge" is populated by old and cooler stars formed long ago, where a central supermassive black hole is very likely located. The GALEX image is compared to a visible light image. The stars in the foreground are stars in our galaxy, the Milky Way.

The ESA/NASA impression presents our Milky Way from an oblique angle (see Fig. 2):

> *...The black-hole system GRO J1655-40 is streaking through space at a rate of 400 000 kilometres per hour—4 times faster than the average velocity of the stars in the galactic neighborhood. The yellow star is our Sun. The black hole was formed in the disk at a distance greater than 3 kpc [kiloparsec] from the Galactic centre and must have been shot to such an eccentric orbit by the supernova explosion of the progenitor star. The runaway linear momentum and kinetic energy of this black hole binary are comparable to those of solitary neutron stars and millisecond pulsars. GRO J1655-40 is the first black hole for which there is evidence for a runaway motion imparted by a natal kick in a supernova explosion.* [Anon., 2012]

Related to this aspect of travel is the chance of discovering life, perhaps intelligent life (Asimov 1979). Such motivation has been the underlying purpose of all human exploration since *Homo erectus* started wandering and eventually moved out of Africa. Life, *as we know it at least*, may exist only under a narrow band of planetary conditions. For instance, a life-hosting planet must orbit a star or stars not too hot or too cold, it must be of the right density, and so on (Gonzalez et al. 2001). Figure 3, from Scientific American, shows the

Fig. 1 Andromeda Galaxy in ultraviolet wavelength and visible light (Courtesy JPL, 2005)

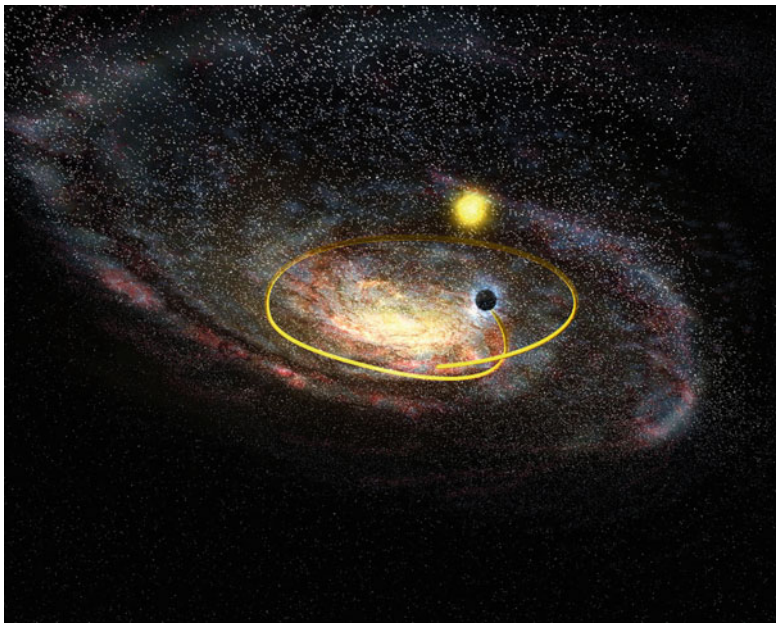

Fig. 2 Oblique view of our Milky Way galaxy and black-hole system GRO J1655-40 streaking through space (Courtesy ESA/NASA, 2012)

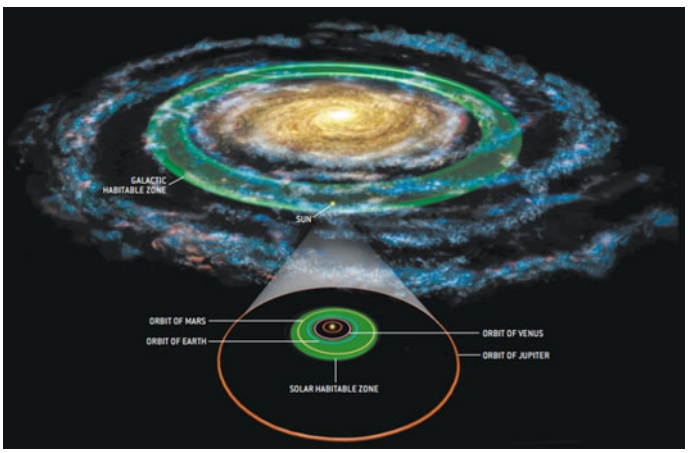

Fig. 3 Habitable zones of life and Earth-like Solar Systems (Gonzalez et al., 2001)

Galactic habitable zone and the Solar habitable zone. Toward the center of our galaxy, radiation would not permit biological life to exist. Outside the Galactic habitable zone, the planets forming around the stars tend to be gas giants, as their insufficient heavy-molecular weight materials inhibit the forming of rocky planets. The same is true for the solar habitable zone. Venus is too hot, and beyond Mars are only gas planets. Mars might have been habitable if it would have been larger and able to retain an atmosphere.

At this point in time, reaching other galaxies or even stars within our galaxy seems impossible, as physics tells us. Clearly, we must reach other galaxies by means other than conventional ejected mass propulsion. Distances and times involved are currently beyond comprehension, unless travel in Einstein's space–time coordinate can be accomplished. This is discussed in a speculative way in Chap. 9, as it is the only way we can leave the shackles of our own Solar System.

All travel within our own Solar System (and perhaps, sometime in the future, to distant places in our galaxy) depends on establishing first a regular, routine, and cost-effective schedule to reach Earth orbit. In other words, establishing a transportation system to Earth orbit is analogous to establishing the transcontinental railroad from Council Bluffs, Iowa, to Sacramento, California, in the late 1800s (Mazlish 1985; Ambrose 2000). That includes the space equivalent to the rail switching yard and marshaling yards that store and organize the materials to be shipped and that are returned. The key identifying characteristic of a transportation system is that the flow of goods and materials is a *two-way transport*.

One last observation. In the space organizations today, the buzzword is "technology" with the implication that without technology progress cannot be made, or that the next-generation launcher or satellite cannot be created without "new technology." Now, technology has played an important role in electronics, sensors, and communication systems. Technology has played a role in improving the materials available for launchers by making them lighter and with better characteristics. However, in the latter case, the new materials are not an *enabling technology* but only an *improvement technology*. New classes of orbital vehicles, space launchers, and their associated propulsion systems have been envisioned and have been capable of being constructed for well over 55 years. Clearly, the newly developed "industrial capability" makes it less difficult to fabricate these launcher configurations and propulsion systems today.

Figure 4 shows hypersonic airbreathing configurations that originated in 2015 and the 1960s, respectively. Both basic configuration concepts maintain a remarkable similarity despite different operational objectives. What has not changed is the composition of the air, the behavior of the air, and the physical characteristics of the air flowing over a body at high speed or low speed. Clearly, our ability to analyze the detail of the flow field and others has increased enormously. Still, our ability to perform multi-disciplinary analyses to create an efficient overall configuration, such understanding is based on vehicle synthesis knowledge which has been established decades ago. When comparing legacy configurations with today's configurations, it is obvious that the hypersonic and space flight requirements do indeed result in remarkably similar arrangements (*form-follows-function*), even when considering different design teams over a span of more than 50 years.

Remember that the *Saturn I* launcher was assembled from essentially scrap launcher tanks and engines, in order to demonstrate the feasibility of the *Saturn V*. Wernher von Braun excelled at the mastery of forecasting (predictive design), by being able to conceptualize products as pragmatic as possible during the initial sizing phase. That classic of space travel, *The Mars Project* (von Braun 1991), is an excellent example of a pragmatic forecasting study emphasizing the holistic or multi-disciplinary perspective.

If we have lost anything, it is the ability to make correct early decisions by utilizing quality forecasting (*sizing*) during the initial product gestation phase. The lack of defining the correct vehicle or system starting point ultimately clouds all follow-up decision-making that turns ideas and analyses into hardware. That is fraught with risk and uncertainty under the best of circumstances. To the authors, the difference between now and the past is the absence of retaining past design knowledge, the absence of extensive testing, and of the ability, or

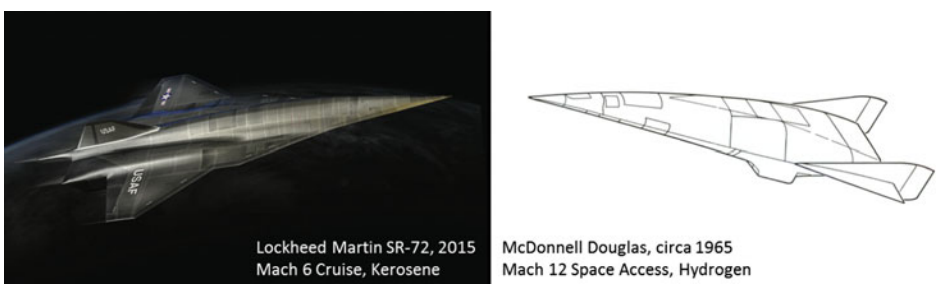

Fig. 4 Propulsion-integrated hypersonic (a) Mach 6 kerosene cruiser, and (b) Mach 12 hydrogen SSTO (Dillow 2015)

willingness, to alter designs when test results indicate there is a better path. All the scientific and technological progress and improved understanding we have acquired during the past 50 years has produced a paradoxical result: the ability to make decisions that turn studies and ideas into further high-fidelity paper studies and numerical analyses, with the ultimate goal of eliminating all risk and unanswered questions. This circular thinking shies away from multi-disciplinary holistic reasoning and from materially testing ideas and analyses; it prefers waiting for further proofs and further analyses. Test hardware failures, by identifying analytical limitations and the need to correct the hardware, are not failures, but milestones along the path to success. As Saint Paul said: ... *Test everything; retain only what is good* ... Clearly, a truly real failure is a test that fails and is therefore canceled, without learning the cause and its remedy. A path that is void of material hardware is a path of undefined limits and undefined requirements. The path to successful hardware is ... *success framed by your failures* ..., a viable early simulation and testing approach that enables you to know where the limits are, and why.

This book strives to describe vehicle-integrated advanced propulsion embodying this philosophy. It starts by looking at what was accomplished in vehicle design and propulsion after the Sputnik days of the 1950s, in order to improve the performance of the impressive but inefficient rocket launchers of that time. It then draws from the experience and attempts of the past to picture and suggest the future of the propulsion-integrated flight vehicle configuration concept. The logical framework for any true progress in hypersonic flight (which has to be considered as a stepping stone toward cost-effective space launch) and in-space launch and space transportation capability is that of the missions that such progress can enable. Thus, what follows will be marked by major yardsticks, from the first indispensable step, reaching Earth orbit more economically and routinely, to the building of a space infrastructure that is both technologically and economically viable, and, ultimately, in a far future, to human beings boldly exploring what lies in and beyond our Solar System.

References

Ambrose, S.E. (2000) *Nothing Like it in the World—The Men Who Built the Transcontinental Railroad 1863–1869*, Simon & Schuster, 2000.

Anon. (2012) "Image of the Day: Runaway Black Hole at Plane of the Milky Way", The Daily galaxy via http://chandra.harvard.edu/photo/2006/j1655/more.html, 06 July 2012

Asimov, I. (1979) *Extraterrestrial Civilizations*, Crown Publisher, 1979.

Dillow, C. (2015) "Inside America's Next Spyplane", *Popular Science*, June 2015.

Goff, A., and Siegel, J. (2004) "Can Conventional Warp Drive Avoid Temporal Paradox", AIAA paper 2004-3699, presented at the 40th *AIAA/ASME/SAE/ASEE Joint Propulsion Conference*, Fort Lauderdale, Florida, 11–14 July 2004.

Goldin, G.A. and Svetlichny, G. (1995) "Nonlinear Schroedinger Equation and Separation Property", *Journal of Nonlinear Mathematical Physics*, Vol. 2, No. 2, pp. 120–132.

Gonzalez, G., Brownlee, D. and Ward, P. D. (2001) "Refuges for Life in a Hostile Universe", *Scientific American*, Vol. 284, No. 10, October 2001, pp. 60–67.

Mazlish, B. (1985) "The Idea of Space Exploration", Article in *A Spacefaring People: Perspectives on Early Spaceflight* by A. Roland, NASA SP-4405, The NASA History Series, NASA, 1985, pp. 137–143.

von Braun, W. (1991) *The Mars Project*, 3rd printing. University of Illinois Press, 1991.

Wolverton, M. (2004) *The Depths of Space*, Joseph Henry Press, June 2004.

Overview

1

1.1 The Challenge

Space travel represents a daunting challenge for human beings. Space is seemingly devoid of any life-support elements for *Earth*-born humans. Remember that one of those life-support elements is gravity. As a consequence, human space travelers must carry all of their life-support systems along with them and find a way to create a sustained artificial gravity vector of yet-to-be-determined minimum or maximum value. For short *Earth* orbit missions, carried consumables and repair parts can be resupplied from *Earth* to provide a near-term, acceptable solution. For future long missions, the supply of consumables (oxygen, water, food, and power) must be self-sustainable onboard the spacecraft. Spare parts must be in sufficient supply to assure operation of critical hardware.

However, as humans attempt to explore further and further from *Earth*, the system that enables increasingly distance travels is still propulsion. In fact, food and other life-sustaining matter increase linearly with travel time and crew size, while Tsiolkovsky's law shows that accelerating a spacecraft by expelling mass (i.e., using Newton's third principle) needs a propellant mass that increases exponentially with increasing speed and initial mass. Thus, long travel times are a balance between the mass controlled by propulsion performance and the mass contributed by human support systems. No matter what support systems are available for humans, without appropriate propulsion, the necessary time and distance cannot be traversed. Clearly, whether human travelers or an automatic robotic system occupies the spacecraft, the propulsion system is the single key element. Remember, when imparting a velocity on a body in space, that velocity remains essentially unchanged. However, in order to orbit a distant object, the spacecraft must slow down to the initial speed of launch. This requires an equal propellant mass ratio that must be expended to decelerate the vehicle in comparison with the propellant mass ratio that was initially spent accelerating the vehicle. As we shall see, this propellant mass is not trivial.

1.2 Historical Developments

The former USSR orbited the first artificial satellite, *Sputnik*, in 1957 (Dickson 2001). Eleven years later, six Apollo missions to the moon enabled 12 astronauts to stand on the moon, explore its surface, and return samples (Stafford 1970). There was one short-lived attempt at building an orbital station, using an empty Saturn V upper-stage tank. The empty Saturn V, S-IV upper-stage tank, was outfitted to be inhabitable as the Skylab (McCurdy 1990; Anon 2012). After Skylab was permitted to enter the atmosphere and be destroyed, all US human exploration ended.

Not until the next century would the USA, using also Russian hardware, place a habitable orbital station into orbit. In that almost 30-year gap, the nations of the former Soviet Union (USSR) launched a series of Salyut orbital stations (Ivanovich 2008), culminating with MIR (Baker 2007), the seventh Russian orbital station. MIR had served successfully for 15 years, which was about three times its design life. Then in 2001, after suffering the ravages of solar radiation and the space environment, it was deorbited into the Pacific Ocean. This ended a long Russian history of humans living in space on an orbital station. In 2000, the International Space Station (ISS) (Harland and Catchpole 2002) was established in the Russian orbital plane of 55° and was constructed with a large fraction of Russian hardware (McCurdy 1990). Its resupply has been primarily a responsibility of Russia with its Progress/Soyuz launch system (Lardier and Barensky 2013; Hall and Shayler 2007), and many of the more massive components had been lifted with the Russian Proton launcher when the Space Shuttle (the US Space Transportation System or STS) was not available for the mission.

As with MIR, the key to successful utilization of an orbital station is the frequent and reliable transportation system that can regularly maintain supplies and rotate crewmembers. In effect, what is required is a "train" to and from space that operates with the scheduled frequency and reliability of a real train. The principal difference between a

P.A. Czysz et al., *Future Spacecraft Propulsion Systems and Integration*,
Springer Praxis Books, DOI 10.1007/978-3-662-54744-1_1

rocket-to-space and a train-to-space is that trains resemble a two-way transportation system for people and goods. When one of the authors (P.A. Czysz) visited Baikonur in 1990, the Soyuz launch complex had launched 92 Soyuz rockets in the previous 12 months, which is a very good record. However, other than allowing the return of astronauts, Soyuz still is a one-way transportation system.

The Russian experience assembles a primary database about humans and long-term exposure to near-*Earth* space and the microgravity and micromagnetic environment. In fact, the authors have had discussions with Russian researchers that indicate that the human physiology might become irreversibly adapted to microgravity after periods in orbit that exceed one year (Hansson 1987, 1991, 1993). Experiments that compared animal physiology response in low *Earth* orbit (LEO) to geostationary *Earth* orbit (GEO) using Rhesus monkeys (Hansson 1987, 1991, 1993) pointed out differences in adrenal cortex manufactured hormone effectiveness that were initially attributed to the absence of the *Earth's* magnetic field in configuring hormone receptor sites.

This experience shows how much remains to be learned about the adaptability of the human physiology and chemistry to space. In fact, one conclusion that might be drawn from the Russian data is that the human physiology is adaptable too. That is, the human physiology attempts to convert a gravity physiology into a microgravity physiology. There is a debate as to whether the gravity of the Moon is sufficient to induce a gravity physiology. Former astronaut Thomas Stafford commented that it might be, but only time spent on the Moon will tell (Stafford 1990). If the available data on the essential presence of a low-level magnetic field is confirmed, then that will be an additional environmental requirement for long-term human space travel. Since the ISS has been continuously occupied for more than 15 years, the USA is continuously gathering data on long-term orbital exposure on the Russian orbital plane of 55°.

As distances of missions from *Earth* will increase, the propulsion challenge increases because mission time increases. From a rational point of view, missions should be made within the possible lifetime of the project team, which is approximately 20 *Earth* years. *Earth* years are of significance and specified here, because as the fraction of light speed increases, the time dilatation for the crew increases. Taking time dilatation into account, a 20 *Earth*-year mission for the *Earth*-bound project team will not have the same time duration compared to the 20 years experienced for the space-based crew.

In principle, there are two classes of missions possible: (a) The first mission class is a one-way mission that explores a distant object and electronically communicates the information to *Earth*. Remember, if that is to a celestial object one light-year away, then communication will take a 2 *Earth*-year round-trip! (b) The second mission class is a two-way mission in which an article is returned to *Earth* after exploring a distant object. This can deliver a greater trove of information than the one-way mission. However, a return mission is the far more challenging mission architecture. If the returning spacecraft would travel at the speed of light, then the returning spacecraft will appear at *Earth* at the same time the light traveling from their destination shows them leaving!

1.3 Challenge of Flying to Space

A predisposition to use rockets derived from military ballistic missiles, forced by the military competition between the USA and the former USSR, curtailed efforts to develop alternatives to chemical rockets together with practical commercial developments. With the orbiting of Sputnik, the aircraft path to space, represented in the USA by the series of X-planes (Miller 2001) and in particular with the X-15 (Jenkins and Landis 2003; Gorn 2001; Evans 2013; Jenkins 2007), came to an end. With the X-15 demise, all efforts *to fly* to space ended and was replaced by the more familiar (but less practical) strategy based on blasting to space with expendable rockets derived from not-so-well-tried ballistic missile hardware, as early and as well current failures document. Like their ballistic missile progenitors, current expendable rockets are launched for the first, last, and only time. One recent development toward the reusable ballistic hardware lineage is the historic satellite-delivering flight of the *Falcon 9* on December 21, 2015, by SpaceX and the landing recovery of the first stage (Taylor 2015).

In this context, a reusable launcher is simply an expendable launcher with some parts reused a few times. Thus, neither the USA nor the former USSR have ever realized a truly commercial approach to space travel, although the former USSR was close to achieving a first step with the Energia/Buran system (Lozino-Lozinskiy 1989). Energia flew on its first flight with a cargo pod installed; Energia/Buran flew only once after that (Hendrickx and Vis 2007). The several Energia launchers and the two Buran hypersonic gliders were eventually scrapped or sent to museums. The roof of the assembly building at Baikonur collapsed in the late 1990s due to lack of maintenance, and perhaps the most ambitious and fully recoverable launcher and space-return glider system to have been ever built was no more. Both the USA and the former USSR have generated a large number of concepts that could fly directly to space and return on a sustained, frequent, and scheduled basis (Jenkins 2001; Hannigan 1994).

1.3.1 Vehicle-Integrated Rocket Propulsion

The subject of this book is space propulsion and vehicle integration. In exiting the *Earth's* atmosphere, the propulsion system and the flight vehicle configuration are inexorably linked. An aircraft that is a hypersonic glider exits the atmosphere on either rocket boosters or a first stage of a two-stage-to-orbit aircraft. As such it exits the atmosphere quickly, and the key exit design considerations are the high aerodynamic and mechanical loads encountered in the exit trajectory. Whether a new launcher such as the *Falcon 9* (SpaceX) or the now retired *Space Shuttle* (at the time NASA-operated), the physical phenomena are the same: The peak mechanical loads are occurring during ascent in the transonic region around Mach 1. In this case, aerodynamics is important but not vital. In contrast, the critical aerodynamic and thermodynamic (aerothermodynamic) loads are experienced during the entry glide, where thermal loads peak and must be controlled. As a consequence, the vehicle must always be controlled in flight such that its attitude and direction are within tight limits set by aerothermodynamics. The hypersonic glide angle-of-attack limits for high-performance hypersonic gliders lies between 11° and 15°, not the 40° of the US Space Shuttle Orbiter during the entry phase. Per design and operational strategy, the Russian Buran had a lower entry and hypersonic glide angle-of-attack when compared to the Space Shuttle. Russian Central Aerodynamics Institute (TsAGI) reports show that the Buran glide angle ranges between 30° and 35° (Neyland 1988a, b).

Like Buran, the high-performance hypersonic glider is best controlled by an automatic integrated flight control system that monitors the thermodynamic state of the vehicle as well as the aerodynamic and trajectory states. The sensor array provides real-time information to the control system that can maintain the correct attitude in a manner a human controller would not be able to accomplish. Clearly, it is the entry phase of the flight that "designs" the non-airbreathing class of vehicles. Since staging, that is, separation from its first-stage launcher, occurs in the Mach 8–12 range, the ascent propulsion system is usually a hydrogen/oxygen rocket. That means the configuration is designed for the entry glide phase; thus, propulsion does not determine the overall flight vehicle configuration concept.

1.3.2 Vehicle-Integrated Airbreathing Propulsion

An aircraft that uses airbreathing propulsion (airbreather) to exit the atmosphere has overall the same entry issues as the hypersonic glider. However, the capture of atmospheric air to create thrust by chemical combustion during the ascent phase is an additional and different issue, as it must configure the vehicle underside (aerodynamic compression side) as an integrated propulsion system that produces more thrust than drag, in addition to also producing lift. For the airbreathing propulsion system to function efficiently, the dynamic pressure and air mass flow per unit area must be higher than in a rocket exit (ascent) trajectory, as it is the airflow that enables the propulsion system to produce thrust in excess of drag for the vehicle to accelerate. Then, in this case, we have a propulsion-configured vehicle.

For a propulsion-configured vehicle, neither the shape of the vehicle nor the trajectory it flies is arbitrary. The airbreather does not exit the atmosphere quickly as the rocket does. The airbreathing accelerator stays in the atmosphere to the point where the transition to rocket propulsion occurs (usually Mach 8–12). The airbreathing propulsion system's mechanical, aerodynamic, and thermal loads act longer and are of greater magnitude compared to the rocket-powered vehicle. In fact, the dynamic pressure, that is, the pressure of the air impacting the vehicle, is about ten times greater than the entry dynamic pressure of the hypersonic glider. In this case, the principal thermal load is encountered during exit from the atmosphere. The vehicle must be configured such to generate sufficient excess thrust to exceed the atmospheric drag, overall providing a strong acceleration.

Clearly, the airbreather configuration is significantly different from the hypersonic glider, in that the hypersonic glider has not been configured to fly extensively in the atmosphere during ascent while producing thrust from a captured airflow. However, like the rocket-powered hypersonic glider, the airbreathing propulsion-integrated vehicle requires the same engine-off glide performance during the hypersonic entry flight path. However, with the thermal protection system (TPS) designed by the high exit loads, the entry loads and consequently vehicle configuration design are critical in maintaining stability and control while achieving an acceptable lift-to-drag ratio while gliding.

There is one exception as we will see in later chapters, where an airbreathing/rocket-powered hypersonic glider operates at a lower Mach number (compared to orbital Mach number of 25 plus). This vehicle can accommodate a retractable inlet working up to about Mach 5.

1.3.3 Choice of Propulsion System: A Multi-disciplinary Challenge

The question is always, why bother with airbreathing at all if it is that much of a technical and operational challenge. The answer is twofold.

(1) Oxidizer necessarily carried by rockets is heavy and requires more engine thrust to lift it into space.

A hydrogen/oxygen rocket, a vertical-launch vehicle with a 7000 kg payload has a gross weight in the 450,000–500,000 kg range and has a 50,000 kg operational empty weight (with the payload loaded). The engine thrust for a vertical takeoff is about 5950–6620 kN. In contrast, a modest performance combined-cycle airbreather vehicle that transitions to rocket at about Mach 12 has the same empty weight with payload installed, but a gross weight in the 200,000–225,000 kg range. The engine thrust for a vertical takeoff is about 2650–2980 kN. Most of the gross weight reduction is from the lesser amount of oxidizer carried and the lighter propulsion system weight. As a consequence, the installed thrust is about one-half, and the volume is less. A more advanced airbreathing system has the potential to reduce the gross weight to the 125,000–150,000 kg level (the attributes of different propulsion systems and their impact on size and weight are discussed in Chaps. 3 and 4).

(2) An operational system is sought that is capable of a large number of flights per year. This not only reduces recurring costs, but lessens resources required for launch and means that the system can operate at greater ease and has the potential to operate from more bases. Glebe Lozino-Lozinskiy had a concept for a spacecraft with a seven metric ton payload carried atop an Antonov An-225 (Interim HOTOL), with a second aircraft carrying the liquid hydrogen, launch facilities and staff (Parkinson 1991; Plokhikh 1989). It could literally launch a satellite from any facility that could accommodate a Boeing B747 or Airbus A380.

1.4 Operational Requirements

The USA was not the only nation to think beyond rockets. Figure 1.1 shows a spectrum of different launcher concepts investigated for a multitude of different mission objectives from the 1956 to 1981 time period (Miller 1993). Also, the Soviet Union studied rocket planes and hypersonic powered and unpowered vehicles (Encyclopedia Astronautica 2016). Some representative configurations are numbered in Table 1.1.

Examining the images of the launchers and spacecraft, we find an excellent cross section of the past 60 years. There are three configurations that have variable geometry features employing retractable straight wings for improved landing and takeoff, see #2, #10, and #11. All of the transatmospheric vehicles employ delta planforms, except for Harry Stine's low wing-sweep horizontal takeoff and landing (HTHL) concept (#3). Configurations #5, #7, #9, and #13 are two-stage-to-orbit (TSTO) concepts that employ either a subsonic, supersonic, or hypersonic carrier aircraft. The German *Sänger* configuration (#7) by MBB employs a hypersonic glider that carries onboard the propellant necessary to achieve orbit, maneuver, and return. Gleb Lozino-Lozinskiy's *Spiral* (#5) and Dassault's *Star-H* (#9) both have a different philosophy compared to MBB's *Sänger* with respect to the propellant to reach orbit. In their studies, it was more economical to carry the ascent propellant to preseparation altitude via a separate aircraft.

In fact, the question of propellant has many answers; the selection of a configuration concept and the propellant choice depends primarily on the mission and envisioned flight rate. Clear rules guiding the matching of mission-to-hardware have yet to be determined today. If the flight rate postulated in 1965 were real (74 flights per year), the answer would probably favor the TSTO MBB *Sänger* (hypersonic carrier aircraft) or *Interim HOTOL* (transonic carrier aircraft) type approach. All three of the designs shown in Fig. 1.1 share the idea to use the first stage (which staged the second stage at Mach number from 6 to 7) for a Mach 4.5–5 hypersonic cruise aircraft. If subcooled liquid methane were substituted for the hydrogen, with the same total energy content, the methane would occupy only 36% of the hydrogen tank volume. The 64% of the hydrogen tank would now make a perfectly well-insulated cabin for either carrying cargo or passengers. The useful range of such an aircraft would easily be in the 6500 nmi (12,040 km) category.

Of the vertical launch rockets in Table 1.1, the *Vostock* launcher from the former USSR (#14) is expendable. The *Vostock* launcher is designated SL-3. The growth version of this launcher is the SL-4, the *Soyuz* launcher. It is, in fact, from the former USSR, as the companies that supply the hardware and launch facilities for today's *Soyuz* are now in separate nations. The *Vostock* launcher is shown because *Soyuz* has achieved the launch rate required to support the 1965 USAF *Manned Orbiting Laboratory* (MOL) space station (Anon 2015a). It is noteworthy that in 1991, there were 92 launches from the three *Soyuz* pads at the Baikonur Cosmodrome. The other two the McDonnell Douglas (MDC) *Delta Clipper* (#15) and the General Dynamics *Millenium Express* (#16) are intended to be single-stage-to-orbit (SSTO) sustained use vehicles, although not at the rate required to support the 1965 MOL space station. Reusable vertical launch vehicles are important because they can lift heavy payloads to orbit when required by the mission, such as orbital assembly of space stations, or of the deep space and Mars vehicles represented by the Mars mission configuration concept #17. The horizontal takeoff mode unaided by thrust vectoring exacts a high price in terms of landing gear mass.

One recent development toward the reusable vertical-takeoff-vertical-landing (VTVL) launch vehicle is

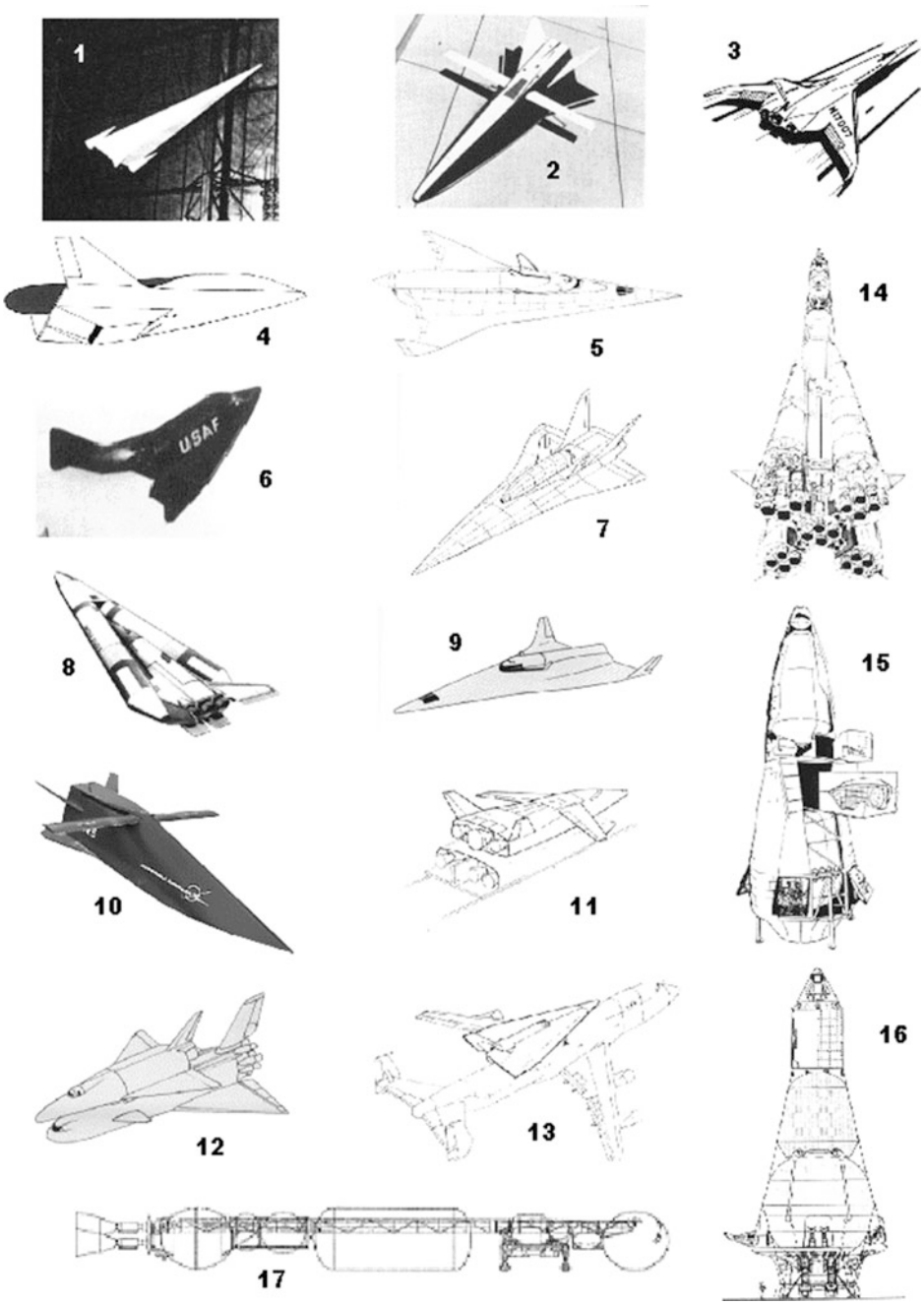

Fig. 1.1 Spectrum of launchers and spacecraft from 1956 to 1981

Table 1.1 Identification of configurations in Fig. 1.1

#	System	#	System
1	*HYARDS*, USAF, 1956	10	*FDL-7MC/MRS*, McDonnell Douglas, 1968
2	*Hyper III*, NASA, 1964	11	*TAV*, USAF, General Dynamics, 1981
3	*HTHL SSTO*, G. Harry Stine, 1957	12	*Spacemaster*, Martin Marietta, 1971
4	*Spaceplane*, USAF, 1960	13	*TAV*, General Dynamics, 1981
5	*Spiral*, NPO Molniya, 1962	14	*Vostok A-1*, OKB-1, 1961
6	*Dyna-Soar X-20*, USAF/Boeing, 1959	15	*Delta Clipper*, McDonnell Douglas, 1990
7	*Sänger II*, MBB, 1984	16	*Millennium Express*, General Dynamics, 1991
8	*Star Clipper*, Lockheed, 1964	17	Reference Mars Mission, Boeing, 1991
9	*Star-H*, Dassault, 1984		

the historic satellite-delivering flight of the *Falcon 9* on December 21, 2015, by SpaceX (Taylor 2015) and the following flights in 2016–2017 by SpaceX and Blue Origin. After the successful landing of the first stage of the SpaceX *Falcon 9*, Europe's Arianespace launch consortium issued a statement in early January 2016 that it does not see a need to change its overall expendable launch strategy. Arianespace Chairman and CEO Stephane Israel issued the following statement: "… *It's very complicated to see how this is going to evolve and to assess the economics of launch vehicle reusability*. … *It would be a mistake for us to put our heads down and chase somebody else's strategy*. …" (Svitak 2016). Such obvious discrepancy in overall launch strategy and outlook, as confirmed by Fig. 1.1, justifies the need for a competent generic vehicle sizing methodology to correctly advice decision-makers. The fundamental concept behind the generic, thus configuration-independent and therefore consistent, sizing methodology is introduced in Chaps. 3 and 4.

We have now established that, with the variety of launchers and propulsion required and available, to reach *Earth's* orbit is neither beyond the current capability, nor was it beyond the 1965 capability, nor should it be limiting the establishment of a routine and cost-effective space transportation system critical toward the establishment of a first-generation space infrastructure. In the words of one of these authors (P.A. Czysz): "… *So now it is to the future to achieve the dreams of the past generation* …".

Still, in the context of reusable versus "throwaway" or expendable launchers, it is a fact that the expediency of launching another expendable rocket, historically, has always won over the will to develop a commercial, sustained-use, multiple-launch spacecraft. As a consequence, the current "progressive" path is still the expendable rocket, albeit with some reusable parts. A lot has changed since Russell Hannigan wrote *Spaceflight in the Era of Aero-Space Planes* (Hannigan 1994). Today's space operational requirements revolve primarily around the following themes: (a) *space tourism* (primarily reusable sounding ascent space flight systems under development; note that most of these vehicles do not reach orbital velocity) (Seedhouse 2014); (b) *commercial satellite space launch* (established and dominated by expendable space launchers) (Isakowitz et al. 2004); (c) *ISS operation* (manned and unmanned flights utilizing expendable space launch systems since the retirement of the Space Shuttle) (Kitmacher 2010); and (d) *Solar System exploration* (unmanned probes utilizing expendable space launchers and NASA's heavy-lift Space Launch System (SLS) for unmanned and prospective human exploration missions) (Anon 2015b).

In October 1999 at the International Astronautics Federation (IAF) Congress in Amsterdam, an IAF paper reported that a US–Russian cooperation resulted in a hydrogen/oxygen rocket engine (the RD-0120, in the Russian classification) for the Energia launcher that had been fired on a test stand for 80 simulated launches and returns, with a throttle-up during ascent to 135% rated thrust (the US Shuttle engine, the SSME, throttles up to about 109% rated thrust). A manager from one of the US rocket launcher companies exclaimed: "… *This is terrible*; *we would have lost 79 launcher sales*! …" (Davis 1999). That mind-set explains why sustained operational use spacecraft historically never developed. The rocket launcher organizations never proceeded a path analogous to that taken by the Douglas Aircraft Company with the DC-3, DC-4, DC-6, DC-7, and DC-8 commercial transport family, to cite one example (Ingells 1979). From 1934 to 1974, this series of commercial transports went from reciprocating engines with propellers, with 150-mph speed and around 1000 miles range, to gas turbine powered jet aircraft, flying for 7000 miles at 550 mph. In the 60 years, from the first artificial satellite (Sputnik), the space launcher is still the liquid-rocket-powered ballistic missile of the late 1950s. The aerospace establishment has forgotten the heritage of its pioneers and dreamers. It has forgotten to dream, preferring to rely on a comfortable status quo (and certainly perceived safety by the shareholders). These historical motivations and current perceptions will have to be reassessed if a man is to travel in space for longer distances than those typical of the near-*Earth* environment.

A synthetic description of distances and time in our Solar System and our galaxy will illustrate this point.

1.5 Operational Space Distances, Speed, and Times

Envisioning the time and space of our Solar System, our Milky Way galaxy, and intergalactic space is a challenge for anyone. In terms of our current best space propulsion systems, it takes over one year to travel to our planetary neighbor, Mars. At the average distance, it can take up to 12 min for a microwave signal to reach Mars from *Earth*. Consider a rover on Mars that is approaching an obstacle or canyon. When the picture of that situational event is received on *Earth*, it is already 12 min behind actuality. By the time a stop signal reaches the rover, between 24 and 30 min have elapsed, depending on the promptness of the project team. It is another 12 min, or a 36- to 42-min elapsed time, before the project team knows whether the rover was saved, stalled, damaged, or destroyed. Consequently, with the control center on *Earth*, the time interval is too long to assure the rover remains operational, so an independent intelligent robot is a necessity.

Traveling to our remotest planetary neighbor, Pluto, requires a daunting 19 years. In terms of light speed, it is a mere 5 h 13 min, at Pluto's average distance from *Earth*. And this is just the outer edge of our planets, not of our Solar

System. To the edge of our Solar System, the boundary between our Solar System and the oncoming galactic space medium, the Heliopause, the light time is 13.46 h. Clearly, envisioning the size of our Solar System is a challenge. For example, our Sun is 109 times the diameter of the *Earth* and 1.79 times the diameter of the Moon's orbit around *Earth*, as depicted in Fig. 1.2. The Sun represents the single most massive object in our Solar System.

From the Sun, we can proceed outward to the outer edge of our Solar System and our nearest star, Proxima Centauri. Proxima Centauri is a very dim star; its slightly more distant neighbor, Alpha Centauri, is instead very bright, but they are near the Southern Cross and only visible from the Southern Hemisphere. A cross section of our local galactic space is shown in Fig. 1.3. Remember that an astronomical unit (AU) is the distance to an object divided by the *Earth's* distance from the Sun, so Jupiter is 5.20 AU from the Sun means that Jupiter is 5.2 times further from the Sun than *Earth* is.

Figure 1.3 spans the space from the Sun to our nearest stars, Proxima and Alpha Centauri. The space is divided into three zones. (1) The first zone contains the terrestrial planets; those are planets that are rocky, *Earth*-like in composition. These are Mercury, Venus, *Earth*, Mars, and a band of rocky debris called the asteroid belt. (2) The second zone contains the Jovian planets; those are planets that are essentially gas planets without a rocky core, but could have cores of liquefied or frozen gases. Within this band are the gas giants of Jupiter (11.1 times the diameter of *Earth*) and Saturn (9.5 times the diameter of *Earth*). Uranus and Neptune are 4 and 3.9 times the diameter of *Earth*, respectively. Jupiter is so massive that it is almost in the weight class of a sun. The radiation

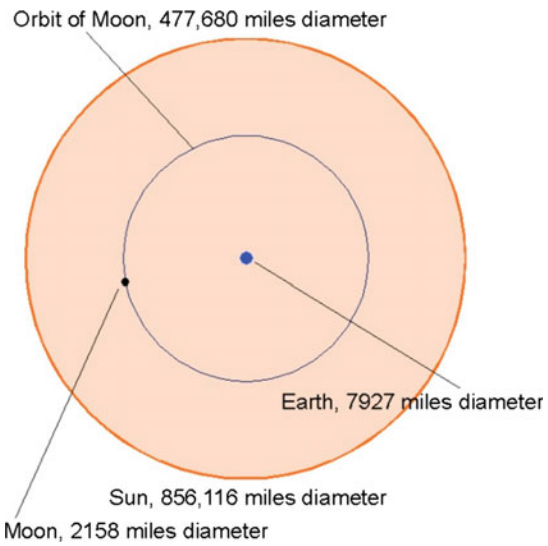

Fig. 1.2 Diameter of the Sun compared with the Moon's orbital diameter

associated with Jupiter is very intense and without significant shielding would be lethal to any human or electronics in the vicinity. The second zone extends to the boundary of our Solar System and the galactic medium, the Heliopause. (3) The third zone spans the distance from the Heliopause to the vicinity of Alpha Centauri. In this zone, you can see the Jovian planets and the terrestrial planets compressed into two narrow bands. That is, the size of our Solar System (100 AU) compared to the distance to our nearest star (149,318 AU) is very small indeed. The near galactic space contains a spherical shell about 140,000 AU thick that contains icy and rocky objects of differing sizes. Because the objects appear dark, they are very difficult to resolve in visible light. It is from this shell of objects that most long-term comets (such as Halley's Comet) appear to originate.

The volume of space encompassed by our Solar System traveling through the galactic medium is called the Heliosphere. Note that between the Heliopause boundary that defines the volume of space encompassed by our Solar System traveling through the galactic medium, and the nearest star, space is essentially devoid of any substantial objects. Even the Oort Cloud begins at a distance some 100 times greater than the Heliopause. If we look at distances measured in light travel time, these dimensions are reaffirmed. The outermost planet Pluto is 38.9 AU distant from the Sun. Even with these figures in mind, it is still difficult to visualize the size of our local space. That is important because it is the size of space that determines the character of the propulsion system needed.

The Sun is a logical reference point for visualizing size and distance. One approach to permit visualization of our Solar System is to scale down the system to comprehensible object sizes and distances. In order to do that, visualize the Sun not as a sphere 856,116 statute miles (1,377,800 km) in diameter, but as a 400 mm diameter (14.75 in) soccer ball. Doing so means the diameter of the *Earth* (7927 miles or 12,757 km) is about the diameter of a pea some 43 m from the soccer ball. Table 1.2 gives the diameter (mm) and distances (m or km) of the objects listed, from our Sun to our nearest galaxy.

In this analogy, Pluto is about one-half the diameter of the *Earth* and, on this scale, is at 1.7 km from the soccer ball. To illustrate now the snail's pace of our current travels, traveling to Pluto directly, e.g., without gravity assists from the massive planets, with our current chemical and future nuclear-electric or nuclear-thermal propulsion systems, would take 19 years, at the blinding speed of 220 mm per day on this scale. We truly move at a snail's pace in the dimensions of our Solar System! If we are to move faster, it is propulsion that will enable that greater speed. Over 19 years the true average speed to Pluto, using conventional propulsion as mentioned, is 32,326 ft/s (9.853 km/s). Of course that is an average, i.e., as if the spacecraft flew along

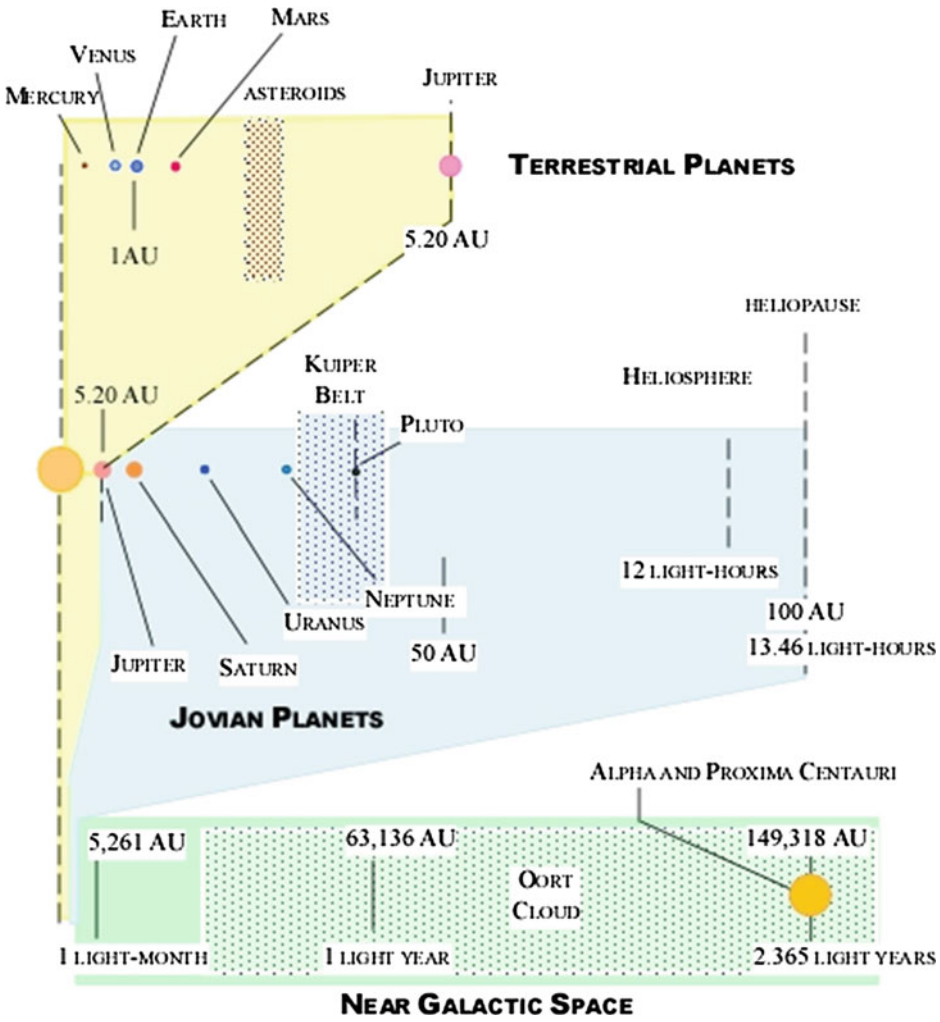

Fig. 1.3 Sun to near-galactic space in three segments

a radial path from *Earth* through the Sun and on to Pluto assuming they are all aligned. Since that is not the case, and since the actual trajectory is actually a curve longer than a radius, the actual speed should be faster. If we wanted the spacecraft to reach Pluto in one year, its average speed would have to be 19 times faster or 614,100 ft/s (187.2 km/s). In order to obtain such incremental speed, the specific impulse of the propulsion system would have to be not the 300 s of current chemical boosters, or the 3000 s (2942 m/s) of electric thrusters, but 5509 s (54,025 m/s). This number is well beyond our current capability.

In one popular space travel television show, it is merely required to specify the warp speed and pronouncing "engage" that (within several minutes or hours) enables to transport the crew of the *USS Enterprise* to their destination. In reality, nothing could be further from our understanding of established physics, as we know it today. The Heliopause (representing the boundary between our Solar System and the oncoming galactic space medium, within which our Solar System travels through space in the Milky Way) is 4.3 km on the soccer ball scale. One light-year is some 630 times farther, at some 2717 km from the soccer ball. That is the distance between St. Louis and Washington DC. Still, on this scale, the nearest star in our Milky Way Galaxy would be 11,433 km distant or 2660 times more distant than Pluto. If Proxima Centauri were in Tokyo, the soccer ball (Sun) would be in London! At our snail's pace of 220 mm per day, that is over 1400 centuries away! In order to reach Proxima Centauri within one year, we would have to travel at about 2.5 times the speed of light.

The galactic center is 13,500 times more distant than the nearest star (Harwit 1973; Kaufmann and Comins 2011). Then, if we could reach Proxima Centauri in one year at 2.5 times light speed, then it would still take 13,500 years to reach the galactic center (rotational center of the Milky Way)! If we were to reach the galactic center within one year, we would have to fly at 33,000 times the speed of light —or, in Mr. Spock's language, "… warp 5.5 …" (this assumes the speed of light is warp 1.0). The nearest galaxy-like structures are the small and large Magellanic Clouds. They are almost 85,000 times farther away than the nearest star. For us reaching the Magellanic Clouds in one year, we would have to fly a fantastic 212,500 times faster

Table 1.2 Scale of diameters and distances to objects in space

	Diameter (mm)	Distance	Distance units
Sun	400	0.00	m
Mercury	1.395	16.79	m
Venus	3.486	30.99	m
Earth	3.670	43.04	m
Mars	1.945	65.42	m
Asteroids		116.2	m
Jupiter	41.10	223.8	m
Saturn	34.50	410.6	m
Uranus	15.41	825.5	m
Neptune	14.68	1293	m
Kuiper Belt		1291	m
Pluto	1.834	1696	m
Heliopause		**4.304**	**km**
Oort Cloud		4.304	km
Oort Cloud		43.04	km
One light-year		**2717**	**km**
Proxima Centauri		11,443	km
Magellanic Cloud		$5.437 \cdot 10^8$	km
(M-31) Andromeda		$5.981 \cdot 10^9$	km

than the speed of light, at "warp 6.3." The nearest spiral galaxy M-31, Andromeda, is 930,000 times farther than our nearest star, and to reach Andromeda in one year, we would have to fly a mind-bending 2,325,000 times faster than the speed of light, at "warp speed" 7.4. If the desire is to travel the distance in one month, a quantity of 1.07 would have to be added to the warp speed. For a one-week travel time, 1.7 would have to be added, and for a one-day travel time, 2.6 would have to be added. Clearly, even at the speed of light, we are trapped within the area bounded by the nearest stars (see also Chap. 8). As we shall see, Einstein's concept of space–time, as a four-dimensional space, becomes an essential factor to comprehend and perhaps overcome this limitation.

Unless we are able to harness some other form of energy (perhaps, vacuum energy) and accelerate at unheard of accelerations, we will be forever confined to the region of our Solar System. In order to accelerate at these unheard of accelerations, we must discover not anti-gravity but anti-inertia. Otherwise, our resistance to changes in speed or direction will result in us being flattened to nothingness. Nick Cook described in Jane's Defense Weekly project GRASP (Gravity Research for Advanced Space Propulsion) with a similar goal, carried on by the partnership between The Boeing Company's *Phantom Works* and Eugene Podkletnov of Russia for a propellant-less propulsion system (Cook 2001).

1.6 Implied Propulsion Performance

In determining the limits imposed by a conventional thermal (chemical or even nuclear) propulsion systems, we will consider two options.

(1) The *first* is a two-way mission where the spacecraft accelerates to escape speed, or greater, departing low *Earth* orbit (LEO) along a trajectory that will intercept its destination object. When the spacecraft reaches the maximum speed allowed by the mass ratio and the propulsion system performance, it then coasts until the spacecraft must decelerate to match its destination velocity requirements. After deceleration, the spacecraft then does a propellant burn to place it in orbit around the destination object. The spacecraft releases a probe to gather data about the target object. After a predetermined period of exploration, the spacecraft accelerates to escape velocity from its destination object, then to its maximum speed determined again by the mass ratio and the propulsion system. It coasts at that speed until it must decelerate to be finally captured in *Earth* orbit. Figure 1.4 illustrates this notional round-trip.

(2) The *second* is to just do a one-way mission and launch a probe or lander to the target object, letting the orbiting spacecraft relay data back to *Earth*. As we shall see, in Einstein's space–time domain this may not be a viable

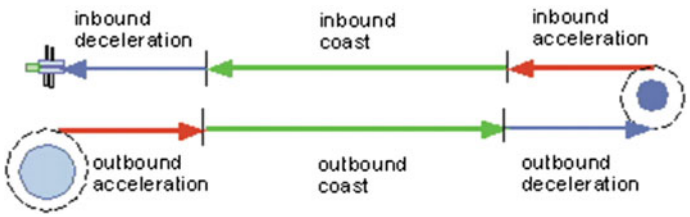

Fig. 1.4 Notional round-trip to a space destination from *Earth*, involving four plus and minus accelerations used to establish mission mass ratios

option for the *Earth*-bound mission managers. The critical element is the mass ratio for each acceleration and equal deceleration. Table 1.3 gives the total mass ratio from LEO for a one-way and a two-way mission. Included are the mass ratios for orbital transitions in the vicinity of *Earth* or the target object. It is assumed that, after each major acceleration, the empty propellant tanks are discarded to minimize future propellant expenditures. The propellant tanks weigh approximately 1.5% of the consumed propellant. The probe has a reference mass of 0.25 units and is launched from a spacecraft with a dry mass of 1.0 unit. That one mass unit does not include the expendable propellant tanks or the probe. In the two-way mission, the one mass unit spacecraft is returned to the *Earth*'*s* surface. The spacecraft 1.0 unit dry mass may be in the 5–50 t range for a practical deep-space spacecraft. The mass ratio (M_R) shown is from LEO to the end of the mission, either back to *Earth* or orbiting forever the destination object, as given in Table 1.3. The mass ratio for the two-way mission includes departing from the destination target and entering an *Earth* orbit on arrival in the vicinity of *Earth*. Clearly, the multiplying factor is somewhat larger than the mass ratio per acceleration squared.

The mass ratio required to lift the spacecraft from the *Earth*'*s* surface to LEO must multiply the mass ratios in Table 1.3. What determines the mass ratio is as follows: *one*, a practical limit; *two*, the propulsion system specific impulse. If a 10 t spacecraft was to be sent to space on a one-way mission, then spacecraft and propellant system mass in LEO would be 206 t (454,230 lb) for a mass ratio of 4 per each acceleration phase. An Energia configuration with 6 strap-on boosters could lift 230 t to LEO in an all-cargo configuration and could lift the 206 t spacecraft in one lift, as could Saturn V. But since the USA is, for now, without these superb heavy-lift machines, the lift must be done in multiple launches, see Table 1.4, followed by assembly in orbit using astronauts and cosmonauts doing space walks, waiting for NASA's Space Launch System (SLS) and the Chinese Long March 9 and SpaceX' *Falcon Heavy*.

From the data in Table 1.4, the number of lifts for a 206 t spacecraft to LEO could be a few as 6 and as great as 30, considering the heavier payload launchers. For a future combined-cycle propulsion system, the ratio of launcher mass to spacecraft mass (the launcher payload) can be reduced to about 21. That would reduce the launcher mass, but would not reduce the number of lifts to LEO unless the payload was increased. For deep-space mission and assembly of structures in orbit, nothing can replace an economical, fully reusable heavy-lift launcher, such as the Russian Energia was intended to be.

The challenge is greatest for a two-way mission and includes preservation of the propellant after a long stay in the space environment. The mass ratio for a two-way mission is daunting, as it multiplies the one-way mass ratio by 18.5, from 20.6 to 382. For the same 10 t spacecraft returned to Earth, the LEO mass that must be delivered into orbit is now 3820 t (8,423,100 lbs). Even with the 6-booster configuration for Energia, that would require 17 lifts to orbit. Without a reusable heavy-lift booster, such as Energia was intended to be, the viability of such missions is in serious doubt, as even the best, the Russian Proton, would require 191 trips to orbit!

We have said nothing yet as to the performance of the propulsion system (in terms of its I_{sp}), only estimated a reasonable value for the mass ratio required to move the spacecraft out of LEO and to its distant space destination. Any change in magnitude of the speed or a change in the direction of its velocity vector, either can represent incremental velocity (ΔV). For example, to change a LEO orbital plane by 13.5° requires a ΔV of 6000 ft/s (1829 m/s), see Chap. 5. A 90° orbital plane change corresponds to a 90° turn in space and requires 35,666 ft/s (10,871 m/s), that is 1.39 times the velocity increment as achieving LEO from an Earth! An aircraft can accomplish a modest load factor 90°

Table 1.3 Mass ratios for space exploration mission

M_R per acceleration (−)	2.0	3.0	4.0	5.0	6.0
One-way	4.86	11.3	20.6	33.1	49.1
Two-way	21.2	114	382	986	2163

Table 1.4 Current expendable and partially reusable rocket launchers

Launcher	Nation	Payload (t)	W_{GW}/W_{Pay} (−)	Number of lifts (−)
Shuttle	USA	20.4	100	10
Titan IV	USA	17.7	48.9	12
Ariane V	France	17.9	39.6	6
Proton	Russia	20.0	35.1	11
Zenit	Russia	13.7	33.4	15
LM-3B	China	13.6	31.8	15
Falcon 9	USA	13.2	38.3	16
Antares	USA	7.0	42.3	30

turn with only 20% more fuel consumed than flying level. In comparison, going to geosynchronous orbit from LEO can require as much propellant as achieving Earth orbit in the first place. Thus, moving about in space requires a very large amount of propellant indeed.

We have already spoken of specific impulse, I_{sp}, as an index of the propulsion performance in the *Introduction* chapter. I_{sp} is the thrust the propulsion system generates per unit of propellant mass flow consumed. When measured in seconds, the traditional engineering units, it is also the time a unit weight of propellant can sustain itself against *Earth* gravity. An I_{sp} of 455 s (4462 m/s) means that if the engine produces 1 N of thrust for 455 s, it will burn 1 kg of fuel. It as well means that 1 kg per 1 s of propellant flow generates 455 kg of thrust or 4462 N. That is, if *weight* (in newtons) is used as the unit of propellant, then specific impulse has the units of time (seconds):

$$I_{sp} = \frac{T}{\dot{w}} \quad \left[\frac{\text{N}}{\text{kg/s}} = \text{s (SI units)}\right] \tag{1.1a}$$

$$I_{sp} = \frac{V_e}{g_0} \tag{1.1b}$$

If *mass* (kg) is used more correctly as the unit of propellant, then specific impulse has the units of velocity (m/s):

$$I_{sp} \cdot g_0 = V_e = C^* \quad \left[\frac{\text{m}}{\text{s}} \text{ (SI units)}\right] \tag{1.2}$$

where $V_e = C^*$ is the specific impulse measured in m/s, which is the same as the effective exhaust velocity.

There are just two principal elements that determine the incremental velocity, ΔV: (1) specific impulse, I_{sp} (propulsion), and (2) mass ratio, M_R (propellant, hardware). For the one-way mission, there are two accelerations, the first a positive acceleration to maximum speed and a second, and equal, opposite acceleration (deceleration) from maximum speed to the spacecraft's initial speed. For the two-way mission, there are four accelerations, two on the outbound leg and two on the inbound leg.

Whether changing the magnitude of speed or changing direction, the only source of motive force is propulsion. Since there is no lift, the propulsion system must provide all of force required. Because there is no atmosphere, the spacecraft must carry not only fuel but also the oxidizer required to burn the fuel. The total propellant load, i.e., fuel *and* oxidizer, is many times greater than the fuel for an aircraft flying in Earth's atmosphere. We define propellant weight, $W_{ppl,}$ as follows:

$$W_{ppl} = W_{fuel} + W_{oxidizer} \tag{1.3}$$

Because rockets must carry the oxidizer onboard, the propellant weight just to achieve LEO from Earth is from 7 to 15 times the unfueled weight of the spacecraft. It is for this reason that for spacecraft, the measure of the total propellant carried is the "mass ratio," M_R, or the total vehicle mass divided by the unfueled mass of the spacecraft.

$$M_R = \frac{W_{TOGW}}{W_{OWE}} \tag{1.4}$$

Table 1.5 gives for a number of current propellants their I_{sp}, density I_{sp}, which is the propellants specific gravity times I_{sp}, oxidizer-to-fuel ratio (O/F), and mass ratio (M_R) required to accelerate from LEO orbital speed (25,656 ft/s or 7.820 km/s) to *Earth* escape speed (36,283 ft/s or 11.059 km/s), i.e., a velocity increment of 10,633 ft/s or 3.241 km/s.

The density specific impulse is the product of specific impulse and the average specific gravity of the propellants; we have

$$I_{dsp} = I_{sp} \cdot \delta_{ppl} \tag{1.5}$$

Overall, a high value of density I_{sp} is important for compact motor designs (when volume is at a premium).

Nuclear-powered electric propulsion should be used in low Earth orbit, resulting in an improved mass ratio for a given incremental velocity. As shown in Table 1.5, propellants in **bold** are hypergolic, that is they ignite (or even detonate) on contact. Hypergolics have the advantage that they are storable in space and have the highest density specific impulse. Propellants in *italics* are monopropellants that use the heat of a catalyst bed to decompose the liquid to

Table 1.5 Current chemical and nuclear rocket propellants characteristics

Fuel	Oxidizer	I_{sp} (s)	$SG\ I_{sp}$ (−)	O/F (−)	M_R (−)
UDMH	**N_2O_4**	**319**	**390**	**1.23**	**2.82**
Hydrazine	**H_2O_2**	**304**	**375**	**2.04**	**2.97**
Hydrazine	**N_2O_4**	**312**	**365**	**2.25**	**2.88**
JP-4	LOX	329	330	2.40	2.73
Nitromethane	–	*273*	*308*	*Monoprop*	*3.36*
Methyl Alcohol	LOX	297	282	1.15	3.05
Methane	LOX	329	247	2.33	2.73
Hydrazine	–	*218*	*219*	*Monoprop*	*4.56*
Hydrogen	N2O4	349	207	11.5	2.56
Hydrogen	LOX	455	170	6.00	2.07
Hydrogen	–	2000	149	Nuclear	1.15
Hydrogen	–	1200	90.0	Nuclear	1.32

a high-temperature gas; they have the lowest specific impulse. Hydrogen propellant used in nuclear rocket systems results in a low value for the density specific impulse. The propellants are ranked in order of specific gravity times I_{sp} ($SG \times I_{sp}$), where the bulk density of the propellant is expressed as bulk specific gravity. Generally, the higher this value, the less propellant volume required.

Figure 1.5 shows the specific impulse, I_{sp}, required to achieve a given velocity for a mass ratio of 4. The velocity is given in terms of statute miles per second with benchmarks in terms of the ratio to the speed of light. This chart has no relativistic effects included in the calculations. At 10% of the speed of light, the relativistic effect is 5.4%. The lowest value on the graph is Earth escape velocity, 36,283 ft/s or 11.059 km/s; the greatest speed is 4.85% of the speed of light for the 2050 ellipse. The current hypergolic and cryogenic rockets, representing US and European advanced systems, are indicated. From a talk given by Dr. Oleg A. Gorshkov of the Keldysh Research Center, the four capabilities that the center is working toward are indicated in Fig. 1.5 with the approximate year of availability.

The specific impulse required to reach 1% of light speed is at least two orders of magnitude greater than our expected advanced systems. Another two orders of magnitude are required if we are to attain light speed, i.e., four orders of magnitude greater than our expected advanced systems. That means achieving specific impulses of the order of 1–10 million seconds. This translates into the requirement that each kilogram per second of propellant flow produces 1–10 million kilograms of thrust (9.8–98 meganewton, MN). We have yet to speak of superluminal speeds, that is, traveling faster than light speed, but superluminal speed cannot be achieved until at least light speed is achieved. Assuming we can achieve the speed enabled by the specific impulse, I_{sp}, in Fig. 1.5, the question is: "… *how long is the travel time*? …"

Figure 1.6 shows the *Earth* time to travel one-way to within our Solar System, beginning with Mercury and ending with the Oort Cloud (shaded oval) and beyond. The

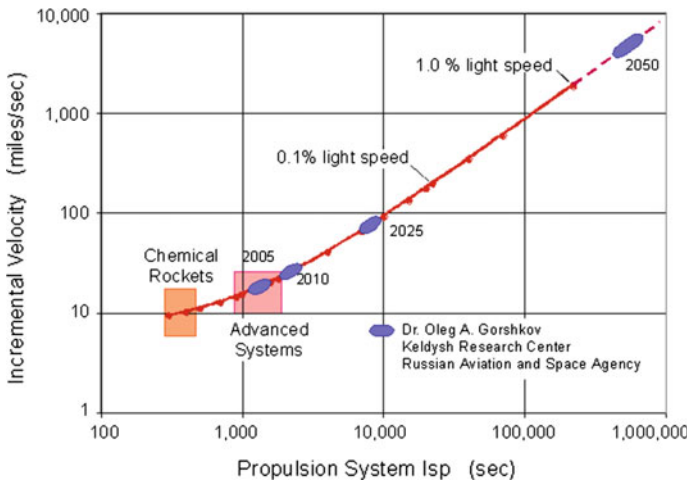

Fig. 1.5 Required specific impulse as a function of spacecraft speed for $M_R = 4$, with some projections

assumption is that we can achieve 0.1% light speed. To achieve 0.1% of light speed (983,580 ft/s) with a mass ratio of 4, an I_{sp} of 14,700 s is required. Figure 1.6 illustrates the staggering challenge of traversing space to objects in nearby Galactic space. With a propulsion system at least 10 times better than our projected advanced propulsion systems, the outer planets are readily accessible. Our nearest star, Proxima Centauri, is 4.2 light-years distant. Then, it will take an automatic spacecraft over 2500 years to reach Proxima Centauri. With the possible propulsion systems of Dr. Gorshkov, the nearest star falls at the 250 year travel time. The 7 nearest stars to our Solar System are within 10 light-years. That is another order of magnitude larger travel time. In terms of reaching the nearest galaxy, Andromeda, the time is 22 million *Earth* years.

Clearly, for the present time we cannot even reach our nearby stars' neighborhoods, much less the nearest galaxy. We are confined to our Solar System with an outlook that we may be able to only reach our nearest neighbor star in the future. Unless travel at greater that the speed of light is possible, we are as isolated as a culture in a petri dish. Note, however, that these times are for *Earth*-based observers, not for the crew of the spacecraft. Relativistic speeds create a sharp difference between these two times, see Chap. 9.

1.7 Propulsion Concepts Available for Solar System Exploration

In the previous section, it was shown how I_{sp} and mass control space travel and missions. If human exploration of our Solar System is the goal, then there are some time constraints to consider given the current knowledge of shielding from high-energy particles and radiation in space. There is a limit to the mass of shielding that can be incorporated into a spacecraft and yet retain a practical mass to accelerate from LEO. In addition, the ability to warn the space travelers to radiation that may encounter *Earth* is limited. Then, from other space sources and directions, the spacecraft will have to have a basic protection level plus a short-term safe house for more intense radiation. Since the first warning may be the arrival of the radiation, the danger is that the first encounter may be a lethal one, requiring the entire crew space to be placed in a safe house environment. Overall, the best insurance against this occurring is to minimize travel time!

From the point of view of radiation dose, statistically a trip of less than 1 year is relatively safe compared to a trip of over 2 years which is considered not safe, therefore requiring extra shielding, see also Appendix A. Exploring the Solar System via manned missions ideally means that the total travel time is on the order of 1 year to minimize the exposure of a human crew to hard space radiation, even with a shielded spacecraft. Russian experience with seven orbital stations, however, shows that even a 2-year mission in microgravity may generate irrecoverable physical damage. One solution is to provide a minimum level of acceleration, perhaps 1/5 of *Earth*'*s* gravity (approximately 2.0 m/s^2), and a weak magnetic field (at least 0.3 Gauss) analogous to *Earth*'*s* magnetic field. The real limitation, however, is that with current systems, a one-way travel time to the Heliopause (100 AU) appears feasible in 9.5 years. Such travel duration is too long for a human-carrying spacecraft, since we do not know how to construct spacecraft and supply resources for humans for a total transit period of 19 years. As a consequence, such missions will require a "robotic crew" instead.

The requirements for the propulsion system can be determined for a specific travel distance as a function of spacecraft weight with values selected for just two parameters, the total one-way travel time and the average acceleration of the spacecraft. The equations for the speed

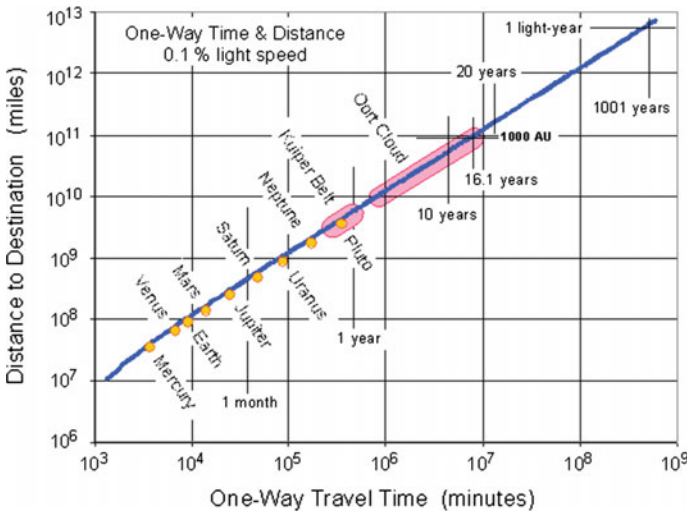

Fig. 1.6 One-way distance and travel time in *Earth* time

increment, ΔV, required over and above the orbital speed for the spacecraft to achieve its destination in the selected time, the spacecraft mass ratio, $M_{\text{R one-way}} = 4$, in *Earth* LEO for a one-way or two-way mission, the average specific impulse required to achieve the required ΔV, the acceleration time, t_a, from orbital speed to orbital speed plus ΔV, and the thrust N_x required to provide the selected axial acceleration (in g) are as follows:

$$\Delta V = \frac{\text{path length}}{\text{mission duration}} \approx \frac{\pi \cdot \text{radial distance}}{t_m} \left[\frac{\text{m}}{\text{s}}\right] \quad (1.6)$$

$$I_{sp} = \frac{\left(\frac{\Delta V}{g_0}\right)}{\ln M_R} = 0.7213 \cdot \frac{\Delta V}{g_0} \quad (1.7)$$

$$t_a = m_{\text{spacecraft}} \cdot \frac{\Delta V}{N_x} \text{ [s]} \quad (1.8)$$

$$N_x = m_{\text{spacecraft}} \cdot a_x \text{ [N]} \quad (1.9)$$

where g_0 is the surface acceleration on Earth, the specific impulse, I_{sp} (in seconds), the axial thrust, N_x, and the resultant axial acceleration, a_x.

Newton's Third Law-based propulsion will enable Solar System exploration within the previously discussed travel times only, if there is sufficient specific impulse and thrust. For the range of distances from 5 to 100 AU, the mass ratio, M_R, assumed for a one-way mission is 4, and for a two-way mission, the mass ratio assumed is 16. This determines the I_{sp} for the spacecraft, thus the performance of the propulsion system departing from LEO. The performance per unit distance traveled (in AU) can be determined from Table 1.6. In order to escape the gravity of *Earth*, the ΔV must be at least 3.238 km/s to provide an escape speed of 11.056 km/s.

For the mass ratio assumed in LEO, the propulsion system thrust required (in N) is about numerically equal to the I_{sp} for a 1000 kg spacecraft and an 82 AU mission. The thrust and specific impulse values required increase inversely with travel time. The 1.5-year mission-required I_{sp} is 6.3 times the 9.5-year mission, and the 0.5-year mission-required I_{sp} is 20.6 times the 9.5 year mission. That would put the propulsion capability in the *future system* capability, as shown in Fig. 1.5. The shortest mission time would be in the *possible systems* realm that researchers are expecting to be available much later this century. The challenge will be the thrust versus operating time required, as the mission time decreases. Probably the Russian chemical rocket engines hold the record for the longest continuous engine operation as achieved with the Kuznetsov NK-31 engine, the primary engine for the 1990s proposed Kistler Aerospace K-1 low-cost rocket (Kemp 2007).

In order to illustrate the magnitude of the propulsion performance required to achieve a rapid transit to a particular distant destination, a one-way mission to Pluto (39.4 AU average distance from the Sun) will serve as an example. The propulsion system performance required is given in Table 1.7. For the one-way trip, the $M_R = 4$ and the spacecraft mass is $m_{\text{spacecraft}} = 1000$ kg. For the shortest mission to Pluto, the propulsion system must generate 15 times the thrust and operate twice the duration compared to the longest mission time considered in Table 1.7. Given today's industrial capability in non-chemical space propulsion, the high thrust levels and long operation times required pose a serious challenge. Today's non-chemical (i.e., electric) space propulsion engine thrust is measured between 10 N to perhaps 100 N. Chemical rockets have operated realistically for perhaps an hour on the test stand. However, continuous operation for 17–20 h, with a restart 1 year later, is a daunting challenge. As a consequence, the spacecraft today are based on our current launch motor capability of high thrust over a relatively short operating time. What is needed is the development of a new deep-space propulsion system that has both higher thrust and longer operating times while being capable of ready storage and start-up after a long deep-space mission.

The thrust can be reduced, but there is a corresponding increase in the acceleration time; that is, the duration the propulsion system must operate. Depending on the engine providing the thrust, as outlined before there are limits to the duration a particular engine can provide thrust. The engine must operate to accelerate the vehicle as well as decelerate the vehicle at the end of the trip. Then, for the 9.5-year one-way mission, the engine must be in storage for 9 years before it is needed again to decelerate the vehicle. For the

Table 1.6 Propulsion performance for missions to the Heliopause and nearer

One-way mission time (years)	Acceleration in g (m/s^2)	Acc. time (h)	ΔV[a] (km/s)	I_{sp} (s)	T (One-way) (N)	T (Two-way) (N)
9.5	0.10	0.4069 AU	1.4366 AU	32.209 AU	3.923 M_{sc}	15.69 M_{sc}
1.5	0.50	0.5542 AU	9.7829 AU	219.33 AU	19.61 M_{sc}	78.45 M_{sc}
0.5	1.00	0.8390 AU	29.620 AU	664.08 AU	58.84 M_{sc}	235.4 M_{sc}

[a]From low Earth orbit
AU = Astronomical units
M_{sc} is the in-orbit spacecraft mass (kg)

Table 1.7 Propulsion performance for missions to Pluto for a 1000 kg spacecraft

One-way mission time (years)	Acceleration g (m/s^2)	Acceleration time (h)	ΔV[a] (km/s)	I_{sp} (s)	T (One-way) (N)
9.5	0.10	16.03	56.60	1270	3923
1.5	0.50	21.84	385.4	8640	19.610
0.5	1.00	33.06	1167	26,170	58,850

[a]From low Earth orbit

two-way mission, there are two 9-year storage periods in sequence. For the two-way mission, the acceleration, acceleration times, and thrust values are given in Table 1.8.

One of the rules-of-thumb in space operations within the Solar System is that 1000 s specific impulse and 1000 N are within the correct range for a properly sized propulsion system. You can see this is the case for the lower acceleration of 0.032 g (0.314 m/s^2) and a travel distance less than the distance to Pluto, for about the distance to Neptune. This 1000/1000 criterion applied to the Pluto distance means that the travel time would be 12.1 years, not 9.5 years. These criteria pose a challenge to existing propulsion technology represented primarily by chemical propulsion; in contrast, electric propulsion is playing a relatively minor role in satellite propulsion. At the same time, in-orbit assembly of spacecraft and propulsion systems may ease the single lift-to-orbit requirement, but assembly in space adds to the complexity and uncertainty of the mission. Structures of future spacecraft printed and assembled in space may be much lighter, without the need to withstand the initial space launch loads of the completely assembled structure.

One of the realities of the space environment is that there is no atmosphere; this makes it impossible to *convect* (via molecules) rejected heat to a surrounding gaseous medium. Operating chemical/thermal propulsion and support systems in space without convection means that waste heat associated with thermal propulsion, human beings, and equipment must be radiated away (via electromagnetic waves in the IR range) from necessarily large structures called radiators. The Space Shuttle Orbiter operated with its payload doors open because these contained integral radiators that rejected the waste heat (Miller 2001). Some of the waste heat can be used as an energy source to generate electrical and fluid power, but there remains a significant quantity to dispose of. Clearly, the spacecraft or orbital station is essentially an isolated thermal capacitor. Like an electrical capacitor, the greater the electrical charge, the higher the voltage. For the thermal capacitor, the greater the thermal energy stored, the higher the temperature.

An important parameter is the size of the radiator needed to reject the thermal energy to space by radiation. The Stefan law for radiated thermal energy is a function of the surface emissivity (i.e., the efficiency of the radiating surface, an emissivity of $\varepsilon = 0.9$ means that the surface is radiating 90% of the maximum possible energy), and the surface temperature raised to the 4th power. This is a very powerful function; if the absolute temperature is raised just by 10%, the total radiated energy is increased by 46%. One approach is to operate the radiators at the maximum possible temperature, based on the radiator material and the heat transfer fluid used to pump the thermal energy to the radiators. For a fixed maximum temperature (dictated by the melting point of the materials available), large waste heat fluxes, q_{radiated}, need an adequate radiating surface area, as indicated by the Stefan–Boltzmann Law for the rejected heat:

$$Q_{\text{rejected}} = q_{\text{radiated}} \cdot S\,[\text{W}] \tag{1.10a}$$

$$Q_{\text{rejected}} = \varepsilon \cdot \sigma \cdot S \cdot T^4\ [\text{W}] \tag{1.10b}$$

We obtain the heat flux:

$$q_{\text{radiated}} = q_{\text{R}} = \varepsilon \cdot \sigma \cdot T^4\ [\text{W/m}^2] \tag{1.11}$$

with the radiator area, S, given by

$$S = \frac{Q_{\text{rejected}}}{\varepsilon \cdot \sigma \cdot T^4} \tag{1.12}$$

Propulsion system options meeting the 1000/1000 criterion and using Newton's Third Law are (a) nuclear, and (b) electric, or (c) their combination. Conventional (thermal) nuclear propulsion (NP) has been tested through the 1970s (NERVA Project) (Dyson 2002; Dewar and Bussard 2009; Dewar 2004), resulting in an $I_{sp} \approx 900$ s and thrust $\approx 9 \times 10^5$ N, more than sufficient for a booster or launcher, but not quite adequate for long interplanetary travel. This type of nuclear propulsion (as shown in Chaps. 3 and 7) is perfectly suited for powering upper stages of a RLV (reusable launch vehicle), lifting heavy payloads from LEO to geostationary

Table 1.8 Engine thrust as a function of acceleration for two-way mission to Pluto (1000 kg spacecraft)

Acceleration g (m/s^2)	Acceleration time (h)	T (N)	I_{sp} (s)
0.100	16.03	3923	1270
0.070	22.90	2746	1270
0.032	50.09	1260	1270
0.010	160.30	392.3	1270

Earth orbit (GEO), and for powering a *space tug*. Direct heating of a propellant gas by the fission fragments (FF) has been proposed by Carlo Rubbia (Nobel Prize in Physics 1984). In principle at least, the material problem of the melting point has been bypassed. This should indeed produce a combination of specific impulse and thrust in the range desired for Solar System travel. A somewhat similar concept uses nuclear power to heat inductively a propellant, as done in wind tunnels using a Plasmatron, for instance in the Von Kármán Institute (VKI) facility.

Electric propulsion (EP) comes in many varieties. Common to all, however, is a typical low thrust per unit mass, and, for some, even a low thrust per unit cross section of the device, while the specific impulse may be more than adequate: Commercial ion thrusters are capable of 4000 s. To achieve the specific impulse and thrust combination already mentioned, magnetoplasmadynamic (MPD) thrusters are now considered the best candidates. They accelerate a plasma by the Lorentz force:

$$\vec{F} = \vec{j} \times \vec{B} \tag{1.13}$$

where the vector $\vec{j}$ is the current flux or current density, and $\vec{B}$ is the magnetic induction or magnetic field. MPD propulsion still needs large power to achieve a thrust of approximately 1000 N. Proposed solar power arrays would need acres of photovoltaic cells for energy harvesting to feed to a MPD thruster for, let us say, a manned Mars mission. In contrast, the combination nuclear power and MPD looks very appealing. Belonging to this same family is the so-called VAriable Specific Impulse Magnetoplasmadynamic Rocket, or VASIMR, in which the concept is further refined. Here, for a set amount of power, the product $F \times I_{sp}$ is constant, thus affording either low F and high I_{sp}, or vice versa. This feature may enable an interplanetary trajectory initiated from LEO. Carrol writes: "… *VASIMR is not a nuclear propulsion engine, but the electricity to make it work may come more readily from a high-yield nuclear powerplant, whose output is measured in megawatts, thousands of times that of solar power. And for humans, the kind of power generated by a nuclear source might be preferable on those long flights beyond the asteroids* …" (Carroll 2014).

Thus, either direct nuclear propulsion perhaps of the Rubbia type, or a combination of nuclear power plus electric propulsion is the current candidate propulsion system for Solar System exploration (see Chap. 7). The Rubbia concept could also function as a nuclear generator and could be alternative to VASIMR. In any case, due to thermal to electric conversion efficiency, at best about half of the nuclear power of any nuclear-powered system would be either lost in the exhaust or radiated into space (but some of the energy might be recycled). A recycling application would convert a portion of the waste power into electric power for a downstream electric propulsion thruster, or to boost the performance of the main electric propulsion thruster.

Although sketchy, these considerations show the importance of detailed energy and power budgets in planning efficient propulsion systems from fundamental physics. A relative newcomer technology that will help MPD propulsion is superconductor (SC) technology. Large $\vec{B}$ fields imply large and heavy copper coils. Ohmic heating of the coils limits the magnetic induction field, $\vec{B}$, in ground applications to about 1 T (tesla). On a space vehicle, lack of convective cooling would pose even more severe limitations. If, however, coils are made of materials kept superconductive either by active cryo-cooling or by using a cryogenic propellant such as LH_2, the magnetic field could be raised to as much as 10 T with a drastic reduction in mass and volume. Superconductivity will likely play a significant role in future propulsion fed by nuclear power.

Two alternatives to the nuclear and electric propulsion systems should be mentioned, despite them being not capable, at the moment, to satisfy the travel time requirement to even a few years at most. They are the *solar sail* and the *magnetic sail*. Both alternatives look appealing, largely because they seemingly do not need complex hardware or high power generation.

Solar sails exploit the *radiation pressure* of photons (light) emitted from the Sun to push a large surface (the "sail"). When properly oriented in space, solar sails operate much in the same way as the wind pushes a sailboat on *Earth*. Whether modeled as due to the Poynting vector, or due to photon recoil, the thrust level available is exceedingly small, decreasing with the square of the distance from the Sun. This limits the usefulness of the solar sail to the inner planets, like for a Mars mission (Percy et al. 2004). Contrary to what is intuitively assumed, the radial direction of the thrust can still be used to sail "against the wind" and be used for interplanetary missions to the inner planets. However, structural mass and low thrust rule out this propulsion concept for manned missions. (Seboldt and Dachwald 2008).

Magnetic sails work similarly, but the effect exploited is the solar wind (mostly electrons, protons and alpha particles) also radiated away by the Sun (Andrews and Zubrin 1990). However, instead of using their weak pressure on a physical sail, the spacecraft would generate a "frozen" magnetic $\vec{B}$ field inside a plasma cloud emitted from the spacecraft. The interaction between solar wind (i.e., the solar current) and the magnetic $\vec{B}$ field creates a Lorentz force. This is the force used for propulsion. Widely publicized, this propulsion concept is definitely capable of Solar System missions, but even in the foreseeable future the weak thrust, as in the case of the solar sail, is incapable of meeting the human travel-time criterion.

Unfortunately, none of the systems just discussed are capable of anything approaching light speed. As stated, these

propulsion systems confine us to our Solar System and long-duration missions (10 years or longer to Pluto, for instance). Chapter 9 will discuss some of those possibilities that might let us travel beyond our Solar System by reaching the speed of light quickly and traveling in "hyperspace" to our distant destinations.

Bibliography

Andrews, D.G. and Zubrin, R.M. (1990) "Magnetic Sails and Interstellar Travel", *Journal of The British Interplanetary Society*, Vol. 43, 1990.

Anon. (2012) "Skylab News Reference", Periscope Film LLC, April 2012.

Anon. (2015) "Declassified Manned Orbiting Laboratory (MOL) Records", National Reconnaissance Office, October 2015.

Anon. (2015) "Space Launch System at a Glance", Report NP-2015-09-83-MSFC, Marshall Space Flight Center, NASA, September 2015.

Baker, P. (2007) *The Story of Manned Space Stations – An Introduction*, Springer-Praxis Publishing Ltd., 2007.

Carroll, M. (2014) *Living Among Giants: Exploring and Settling the Outer Solar System*, Springer, October 2014.

Cook, N. (2001) *The Hunt for Zero Point*, Broadway Books, August 2003.

Davis, R. (1999) Private communication with P.A. Czysz at the 50th IAF Congress, Amsterdam, The Netherlands, 4–8 October 1999.

Dewar, J.A. (2004) *To the End of the Solar System – The Story of the Nuclear Rocket*, The University Press of Kentucky, July 2004.

Dewar, J.A. and Bussard, R. (2009) *The Nuclear Rocket – Making Our Planet Green, Peaceful and Prosperous*, 1st Edition, Apogee Books Publication, July 2009.

Dickson, P. (2001) *Sputnik – The Shock of the Century*, 1st Edition, Walker & Company, New York, 2001.

Dyson, G. (2002) *Project Orion – The True Story of the Atomic Spaceship*, Henry Holt and Company, April 2002.

Evans, M. (2013) *The X-15 Rocket Plane – Flying the First Wings into Space*, University of Nebraska Press, 2013.

Gorn, M.H. (2001) *Expanding the Envelope – Flight Research at NACA and NASA*, The University Press of Kentucky, 2001.

Hall, R.D. and Shayler, D.J. (2007) *Soyuz – A Universal Spacecraft*, Springer-Praxis Publisher, 2007.

Hannigan, R.J. (1994) *Spaceflight in the Era of Aero-Space Planes*, Krieger Publishing Company, 1994.

Hansson, A. (1987, 1991, 1993) Private communications with P.A. Czysz concerning the Soviet biomedical program, 1987–1993.

Harland, D.M. and Catchpole, J.E. (2002) *Creating the International Space Station*, Springer-Praxis Publisher, 2002.

Harwit, M. (1973) *Astrophysical Concepts*, 4th Edition, Astronomy and Astrophysics Library, Springer, September 2006.

Hendrickx, B. and Vis, B. (2007) *Energiya-Buran – The Soviet Space Shuttle*, Springer-Praxis Publisher, 2007.

Ingells, D.J. (1979) *The McDonnell Douglas Story*, Aero Publishers Inc., 1979.

Isakowitz, S.J., Hopkins, J.B. and Hopkins, J.P. (2004) *International Reference Guide to Space Launch Systems*, 4th Edition, American Institute of Aeronautics and Astronautics (AIAA), September 2004.

Ivanovich, G.S. (2008) *Salyut – The First Space Station – Triumph and Tragedy*, Springer and Praxis Publishing Ltd., 2008.

Jenkins, D.R. (2001) *Space Shuttle – The History of the National Space Transportation System – The First 100 Missions*, 3rd Edition, Midland Publishing, 2001.

Jenkins, D.R. (2007) "X-15: Extending the Frontiers of Flight", NASA SP-2007-562, NASA, 2007.

Jenkins, D.R. and Landis, T.R (2003) *Hypersonic – The Story of the North American X-15*, Specialty Press, North Branch, MN, 2003.

Kaufmann, W.J. and Comins, N.F. (2011) *Discovering the Universe*, 9th Edition, W.H. Freeman, New York, April 2011.

Kemp, K. (2007) *Destination Space – How Space Tourism is Making Science Fiction a Reality*, Virgin Books, May 2007.

Kitmacher, G.H. (2010) *Reference Guide to the International Space Station: Assembly Complete Edition*, CreateSpace Independent Publishing Platform, November 2010.

Lardier, C. and Barensky, S. (2013) *The Soyuz Launch Vehicle – The Two Lives of an Engineering Triumph*, Springer-Praxis Publisher, 2013.

Lozino-Lozinskiy, G.E. (1989) "BURAN: Its Creation and Prospects of Its Usage", paper presented at the *40th Congress of the International Astronautical Federation*, Malaga, Spain, 7–12 October 1989.

McCurdy, H.E. (1990) *The Space Station Decision – Incremental Politics and Technological Choice*, The John Hopkins University Press, New Series in NASA History, 1990.

Miller, R. (1993) *The Dream Machines: An Illustrated History of the Spaceship in Art, Science and Literature*, Krieger Publishing Company, July 1993.

Miller, J. (2001) *The X-Planes - X-1 to X-45*, 3rd Edition, Midland Publishing, Hinkley, UK, 2001.

Neyland, V.Y. (1988a) Private communication with P.A. Czysz, TsAGI, Moscow, 1988.

Neyland, V.Y. (1988b) "Engineering Problems and Methods of Preflight Development of Orbiters", unpublished TsAGI Report, Moscow [in Russian], 1988.

Parkinson, R.C. (1991) "The An-225/Interim HOTOL Launch Vehicle", AIAA Paper AIAA-91-5006, presented at the *3rd AIAA International Aerospace Planes Conference*, Orlando, Florida, December 1991.

Percy, T.K., Taylor, T. and Powell, T.C. (2004) "A Study of Possible Solar Sail Applications for Mars Missions", AIAA Paper AIAA-2004-3996, presented at the *40th AIAA/ASME/SAE/ASEE Joint Propulsion Conference and Exhibit*, Fort Lauderdale, Florida, 11–14 July 2004.

Plokhikh, V.P. (1989) "Sensitivity Analysis of SSTO Reusable Vehicle Parameters", IAF Paper IAF-89-223, presented at the *40th IAF Congress*, Malaga, 5–11 October 1989.

Seboldt, W. and Dachwald, B. (2008) "Solar Sails - Propellantless Propulsion for Near- and Medium-Term Deep-Space Missions", in *Advanced Propulsion Systems and Technologies, Today to 2020*, edited by C. Bruno and A. Accettura, AIAA, Reston VA., AIAA, March 2008.

Seedhouse, E. (2014) *Suborbital – Industry at the Edge of Space*, Springer-Praxis Publisher, 2014.

Stafford, T. (1970) Personal communication with P.A. Czysz at McDonnell Aircraft, St. Louis, 1970.

Stafford, T. (1990) Personal communication with P.A. Czysz at Paris Air Show, Le Bourget, 1990.

Svitak, A. (2016). "Arianespace: Next-Gen Ariane 6 Still The Answer to SpaceX Falcon 9", Aviation Week & Space Technology, 06 Jan 2016.

Taylor, J. (2015) "ORBCOMM-2 Mission", Final Press Kit, ORBCOMM, SpaceX, December 2015.

Thompson, M.O. (1992) *At the Edge of Space – The X-15 Flight Program*, Smithsonian Institution Press, 1992.

Wade, M. (2016) *Encyclopedia Astronautica*, see Index and 'Russian Rocketplanes', June 2016.

Our Progress Appears to Be Impeded

2

2.1 Meeting the Challenge

Prior to the 1930s, flying in aircraft was costly and potentially dangerous. There were fewer passengers and less cargo than required for profitability without government subsidy. The Douglas Aircraft Company design team took the train to New York City to meet with TWA officials rather than flying the airliners of the day, as there just had been a series of accidents including the one that Knute Rockne, the Notre Dame football coach, had perished on. Gene Raymond, the Chief Engineer for Douglas integrated the following three novel elements: (1) He used the newly dedicated GALCIT wind tunnel at the California Institute of Technology (Caltech) to experimentally verify the advanced aerodynamics of the new aircraft. (2) Raymond used the latest aluminum-stressed skin structure developed by Jack Northrop for Lockheed's aircraft fuselages. (3) The engines were the new Wright Cyclones radial air-cooled engines that developed 900 horsepower. Hence, Gene Raymond integrated the three principal elements for a successful aircraft from the newly demonstrated "industrial capability" (Loftin 1985). In 1932, the Douglas Aircraft Company introduced the DC-2 followed by the DC-3 in 1934 (Ingells 1979). The result was a commercial airliner that offered speed, range, and safety to the passenger while being profitable to the airlines without subsidy. The aircraft was a sustained-use vehicle that flew hundreds of times per year and therefore at an affordable price. By 1939, the DC-3 was flying tens of thousands of passengers for the airlines worldwide (Davies 1964).

Like the DC-3, there were other aircraft built from the available state of the art. One such aircraft was the operational Mach 3-plus SR-71 developed by Clarence (Kelly) Johnson's *Skunk Works* team at the Lockheed Burbank plant (Rich and Janos 1993; Miller 1995). The other aircraft was the North American X-15 research aircraft developed to investigate speeds up to Mach 6 (Jenkins and Landis 2003; Gorn 2001; Jenkins 2007; Evans 2013). Extensive wind tunnel testing established the aerodynamic characteristics of both, the SR-71 and X-15. The structure was high-temperature nickel-chrome alloys for the X-15 and β-titanium for the SR-71 in a structure analogous to a "hot" DC-3. The rocket engine for the X-15 was advanced from earlier rockets and has been developed to a level not yet installed on any aircraft. The turbo-ramjet propulsion for the SR-71 has yet to be duplicated 50 years later. For the X-15, one challenging goal was the flight-control system that had to transition from aerodynamic controls to reaction jet controls at the edge of space. For the SR-71, the challenge was to design an integrated control system for both the engine inlets and the aircraft for an operational range from high supersonic speeds to low landing speeds. This had not been done before, and it was accomplished before the era of integrated circuits and digital control. The goal for the X-15 was an approach to fly to space (by exceeding 100 km which is about 62 miles) as frequently as could be expected of an aircraft-launched experimental vehicle. By 1958, the X-15 was approaching 300 successful flights. The X-15 was achieving flight speeds of Mach 6.72 (7274 km/h or 4520 mph) and could briefly zoom to the edges of near-Earth space. Rockets of the day were single use and costly, with numerous launch failures. These aircraft were developed by engineers that did not ask "*What is the technology availability date?*" but rather, "*Where can we find a solution from what we already know or can discover?*" For both vehicles, the X-15 and the SR-71, solutions that were not previously known were discovered and used to solve the problems in a timely manner. From 1961 onward, that spirit enabled the Apollo team to fabricate a Saturn V rocket of a size that was previously inconceivable and succeed (Bilstein 1980).

2.2 Early Progress in Space

Also in 1957, during the International Geophysical Year (IGY), the USSR lofted the first artificial Earth satellite, *Sputnik I*, into low Earth orbit (Dickson 2001). Suddenly in the USA, the focus was on catching up, and space flight centered on vertical launch with expendable rockets, while

P.A. Czysz et al., *Future Spacecraft Propulsion Systems and Integration*,
Springer Praxis Books, DOI 10.1007/978-3-662-54744-1_2

the experimental aircraft experience and capability were discarded. With Sergei Korolev as the designer (Harford 1997), the USSR adapted a military intercontinental ballistic missile, the R-7A (NATO name SS-6 Sapwood), to be the first launcher (Clark 1988; Stine 1991). That launcher had the growth potential to become the current, routinely launched Soyuz launcher (Lardier and Barensky 2013; Hall and Shayler 2007). The first Sputnik weighed 150 kg, while the payload capability of the launcher was about 1500 kg indicating an impressive launch margin!

At the time, the President of the USA rejected the suggestions coming from many sides to adapt military ballistic missiles and insisted on developing a launcher sized specifically for the 1957 IGY (International Geophysical Year) satellite. That launcher, Vanguard, had almost no margin or growth potential (Launius and Jenkins 2002). There was about a 4 kg margin for the payload weight. After a series of failures, the first United States Army military IRBM (intermediate-range ballistic missile), the Jupiter missile, was modified into a satellite launcher, and *Explorer I*, the first satellite of the USA, was successfully launched. Since then, the former USSR, Russia, the USA and all the other space launcher-capable nations have focused on expendable launchers with the same strategy in ballistic missile utilization: they are launched for the first, last and only time.

As discussed in Chap. 1, during the 1960s there was an enthusiasm to reach space together with a very intense effort to obtain the necessary hardware. Technical developments were ambitious yet technically sound whilst being based on available industrial capability customized to pragmatically address the problem at hand. However, the complication was that the most capable vehicle configuration development, system designs, boosters, and spacecraft were associated with a military establishment, primarily the US Air Force. One goal was to have an on-demand global surveillance system with either a hypersonic glider (X-20 Dyna-Soar) with an Earth circumference boost-glide range capability (Godwin 2003; Houchin 2006), or a hypersonic boost-glide vehicle (Project Isinglass and Project Rheinberry) with a half-Earth circumference range capability (Rose 2008). Another goal was to establish a manned orbital laboratory (MOL) to assure a human presence in space and enable space-based research and Earth/space observations (Anon 2015; Baker 1996). The spacecraft launchers proposed had the capability for frequent scheduled flights to support an orbital station with a 21–27 crew complement, crew members being on six months rotating assignments. With the US government's decision that space is not a military but civilian responsibility, the civilian space organization (NASA) was tasked to develop their own hardware systems without the possibility to rely on military hardware. Consequently, most of the very successful system design efforts by the military organizations were unfortunately discarded by the civilian organizations, with the result that their system(s) never achieved the superior performance capability offered by the military systems.

After the Saturn V Apollo Moon missions starting in 1961, the short-lived Skylab experiment (1970) and the Apollo-Soyuz rendezvous (1975), the USA did have a dream to establish a space infrastructure and operational space systems. However, with the demise of the Apollo program and the elimination of the Saturn V heavy-lift capability in view of a future, yet to be realized NASA Space Launch System (SLS) vehicle (Anon 2015), there followed a 12-year period in which no crewed space missions were conducted, as all waited for the Space Transportation System (STS, or Space Shuttle) to enter into operation (Jenkins 2001). The dreamers, engineers, scientists, and managers alike, with visions of future possibilities, were put indefinitely on hold; the subsequent developments became myopic and focused on day-to-day activities requiring decades in development, and larger and longer funding profiles for minimal performance improvements. Armies of paper-tracking bureaucrats replaced small, dedicated, and proficient teams.

The USA is not the only nation that considered the establishment of an operational space infrastructure. Figure 2.1 shows a diagram one of the authors (P.A. Czysz) drew during discussions with V. Legostayev and V. Gubanov during the 1985 IAF Congress in Stockholm, Sweden, illustrating the USSR vision of a space infrastructure (Legostayev and Gubanov 1985). The sketch remains as drawn, with only the handwritten call-outs replaced by typed captions. This sketch shows a total space exploration concept, with certain capabilities unique to the Russian concept. One capability is a ground-based power generator and transmitter with the capability to wireless power satellites, lunar and Mars bases, and space exploration vehicles directly and also, via relay satellites, capable of powering other surface sites. In the 1930s, Nikolai Tesla stated that, with his wave-based transmission system, a Mars base or spacecraft traveling to Mars could be powered from Earth with less than 10% energy losses (Tesla 2014). With many years spent translating Tesla's notes and reports in the Tesla Museum in Belgrade, the Russians conducted numerous experiments using the cathode tubes that Tesla developed (Cook 2001). One of the authors (P.A. Czysz) saw such a tube when visiting the Tesla Museum in Smiljan, Croatia, in 1980, but most Western scientists are skeptical as to feasibility of such power transmitter.

The remaining elements of the Russian vision in 1985 are in common with other space plans. Their concept is built around an orbital station and free-flying manufacturing factories since manned space stations suffer from too many gravitational disturbances ("jitter") in the microgravity environment to be considered true "zero gravity." The space facilities are in low *Earth* orbit (LEO) and in geostationary

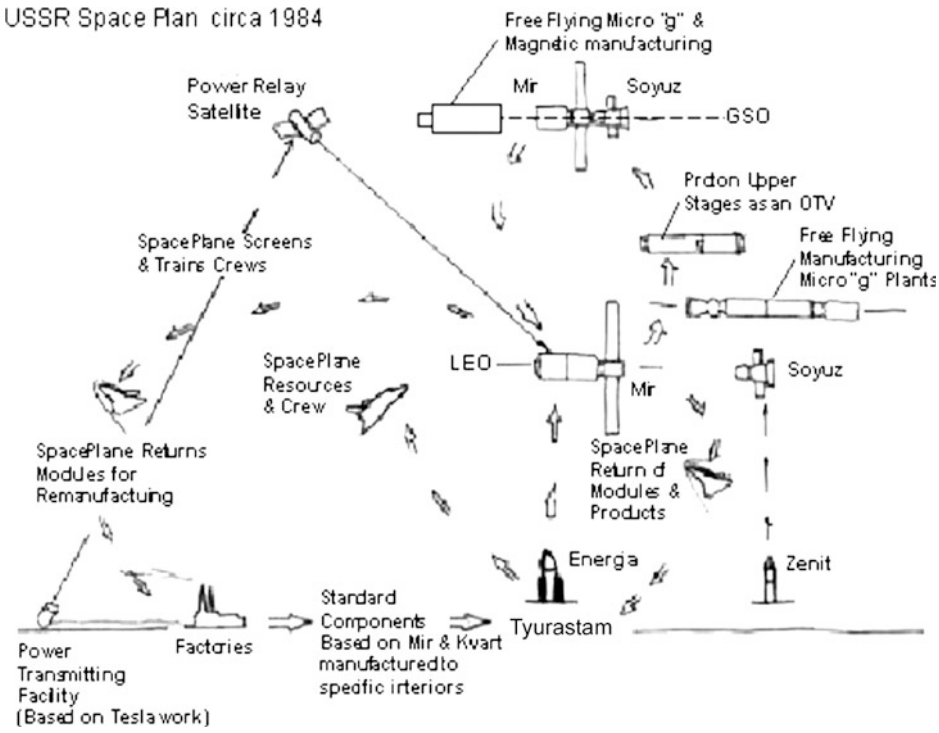

Fig. 2.1 A look at the future space infrastructure envisioned by Boris Gubanov and Viktor Legostayev of the former USSR based on having Energia operational. Circa 1984

orbit (GSO). An integral part of the Russian space plan is an orbital transfer vehicle (OTV) to provide movement of satellites and resources to and from LEO. Deep space exploration and establishing a permanent Moon base (Eckart 1999) were also part of the total space plan (see Chap. 6). The important part of the Russian concept is that it was based on hardware capability that they already had in use or was in development. The key difference from other space plans is that their now retired NPO Energia launcher (Hendrickx and Vis 2007) was a heavy-lift system that could launch either cargo payload vehicles (up to 280 t) or a manned glider (Buran) (Lozino-Lozinskiy 1989), see Figs. 2.7 and 2.11. NPO Energia was to provide a fully reusable heavy-lift system (Energia) and an aerospace plane (Buran) with the goal to support the orbital station and other human crewed systems.

There was a space transportation vehicle in the works at TsAGI (Plokhikh 1983, 1989) that could be considered analogous to the US National Aerospace Plane (NASP X-30) (Schweikart 1998). In 1986 per government decrees of January 27 and July 19, 1986, it was decided to develop the Russian equivalent of NASP, which is a Soviet horizontal-takeoff-horizontal landing (HTHL) single-stage-to-orbit (SSTO) aerospace plane. A technical specification had been issued on September 1, 1986, for a single-stage reusable aerospace plane system. Little is known about the design bureaus who submitted designs proposals, among them Tupolev (Tu-2000), Yakovlev (MVKS), and Energia. This would be an orbital station resource supply vehicle, with NPO Energia the workhorse of heavy-lift capability. N. Tolyarenko, who worked at TsIAM on the strategic reconnaissance ramjet-powered La-350 *Burya* and RSS-40 *Buran* missiles, told one of these authors (C. Bruno) that, were these to have been further developed into a first stage vehicle, we "*... would be on Mars by now ...*".

Another goal for the Russian and Ukrainian space groups was to greatly reduce the source of space debris, that is, inoperative satellites and spent third stages that remain in orbit (Legostayev and Gubanov 1985). Their approach would be to use the Buran glider and the aerospace plane(s) to return nonoperative satellites to Earth from LEO for remanufacture. The OTV would return nonfunctional satellites from GSO to LEO. As mentioned before, the unique difference has been the addition of beamed power from *Earth* via orbital relay to satellites and orbital stations from a ground power station. The power generation and transmission was based, as said, on concepts developed by the late Nikola Tesla with a reported progression of transmitted power up to 10 MW and efficiency over 75% from ground station to space station. This historical database is archived in both the Tesla Museums in Belgrade (Serbia) and in Smiljan (Croatia).

Just as the USA and the former Soviet Union had plans to develop space, so did Japan. Figure 2.2 shows a representation of an analogous plan presented by Japan's space organizations (at the time ISAS, NASDA, and NAL, now unified as JAXA) as they considered the future. As with the Russian concept, the Japan space organizations' concept is

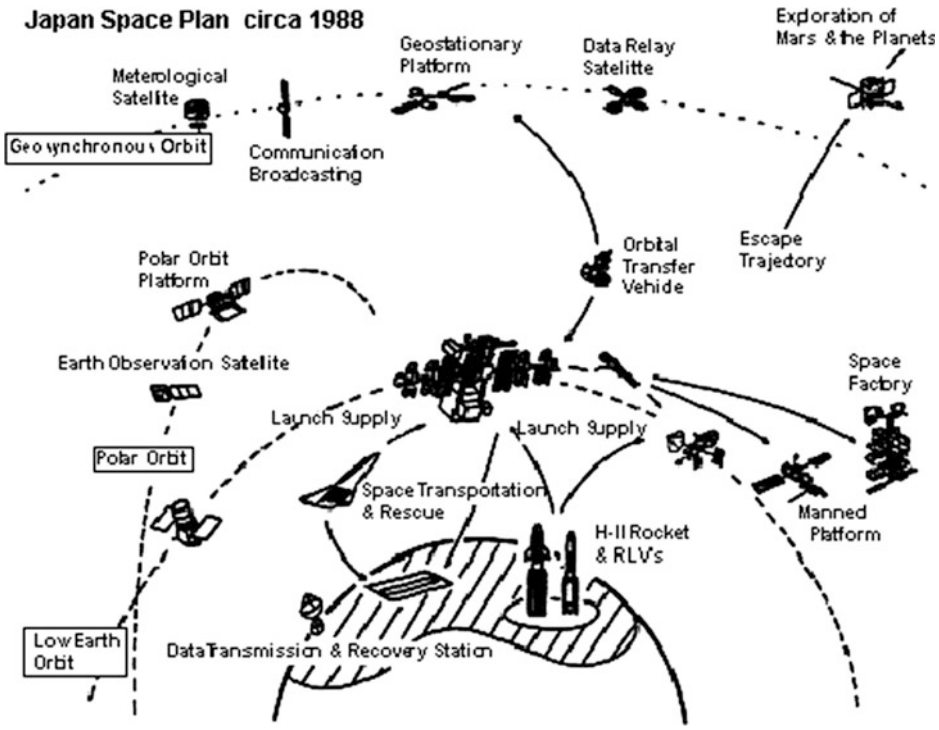

Fig. 2.2 A Japanese look to the future space infrastructure based on their development of an aerospace plane and significant orbital manufacturing assets, circa 1988

built around an orbital station and free-flying manufacturing factories, again independent from the station because of microgravity jitter. Their plan was very comprehensive and indicated a desire to establish commercial space operations. There are large space facilities in LEO, *Earth* observation platforms in polar Sun-synchronous orbit, and a variety of platforms in GSO. Integral to their space plan was an OTV to move satellites and resources to and from LEO. Deep space exploration and the establishment of a permanent Moon base was also part of the total space plan. There was an aerospace plane transportation vehicle in work at NAL (now JAXA) (Maita et al. 1991) that could be considered analogous to the US NASP. During the NASP project team visit to Japan in 1988, the Japanese concept was given significant print coverage and presented to the NASP team in considerable detail. Figure 2.3 shows an artist's rendition of the NAL aerospace plane. The configuration is a slender wing body with sharp leading edges and nose, required to minimize the hypersonic drag characteristics and to improve the reentry glide lift-to-drag ratio for *Earth* return. The plane is powered by a rocket-based combined-cycle (RBCC) propulsion system. The details are technically correct and indicate a competent design team working actual problems.

When the NASP team visited Japan, they received the vision of the Space Advisory Council of the international space activities shown in Fig. 2.4. Note that this Japanese perspective incorporated directly the world space plans as they existed in 1988. In fact, the Japanese plan indicates that in 1988 there was a multinational perspective toward establishing a functional space infrastructure that benefited each nation. This future was to be built around orbital stations and free-flying manufacturing factories in LEO and in GSO (Transferring industrial manufacturing to space for environmental reasons is also in the vision of Jeff Bezos, the Chairman of Amazon and owner of the Blue Origin space company.). Deep space exploration spacecraft were planned to the Moon and planets. However, problems with the engines for their H-IIB expendable launch system and the downturn in the national economy placed much of the Japanese vision on hold (or stretched out their vision much farther in time).

Clearly, many concepts have envisioned the future indeed, but the pioneers that expanded the scope of aviation are no longer there to make the dream reality. All that remains, it seems, are the skeptics, who say it is too expensive, or too dangerous, or impractical, or irrelevant.

2.3 Historical Analog

Experience with expendable vehicles is not limited to rockets, as illustrated by Fig. 2.5. In the 1800s, St. Louis, Missouri, was the *Gateway to the West*, and hundreds of thousands of pioneers passed through on their way to the West over a 70-year period. There is no record of how many Conestoga wagons, that departed St. Louis in the early and mid-1800s, ever returned. The settlers were, per their destination, on a one-way trip. One exception was the three

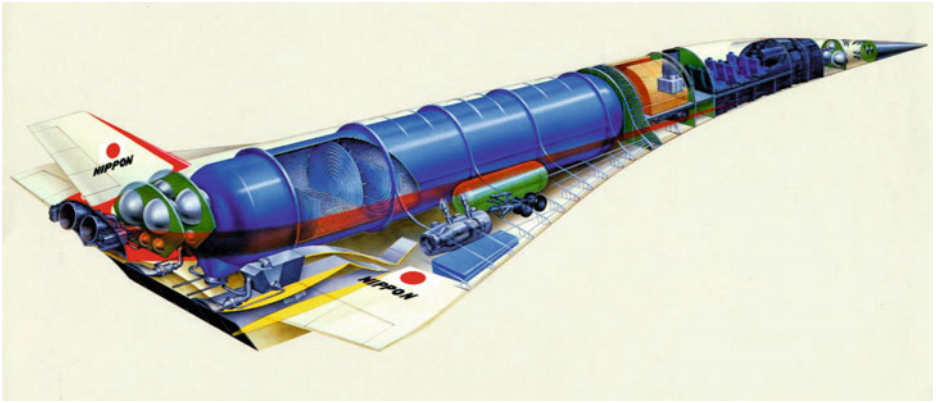

Fig. 2.3 Aerospace plane concept from Japan's National Aerospace Laboratories (*Courtesy* NAL)

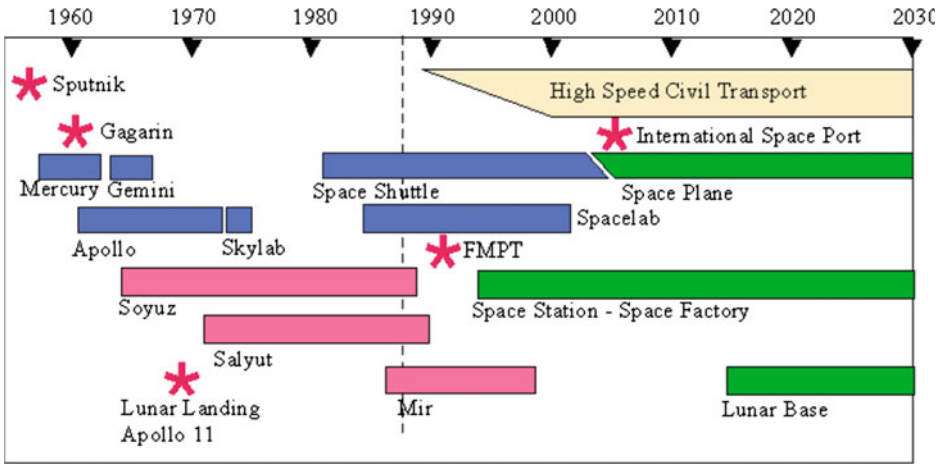

Fig. 2.4 International space plans as presented to the Space Advisory Council for the Prime Minister of Japan in 1988

Fig. 2.5 Expendable vehicles are for pioneers to open up new frontiers and establish a one-way movement of people and resources (expendable Conestoga wagon, circa 1860)

super-sized wagons that were sent to Santa Fe to return Spanish gold to St. Louis; they returned empty. Unlike the Space Shuttle external tank, the wagons were reused as construction materials at their final destinations.

A significant space infrastructure could have been constructed from empty central tanks during the period when the Space Shuttle (STS) was operational (Hunt 1998). At best there are some expendable launcher parts that can be refurbished, as in reusable launch vehicle (RLV) and highly reusable launch vehicle (HRLV) concepts, but this is a far cry from the sustained-use, long-life aircraft analog represented by the DC-3. The fact that each expendable launcher is launched for the first, last, and only time punctuates our failures. The expendable launcher market is limited, and so is the potential to justify further developments. All satellite-launching nations followed the same path, in a sort of "follow the leader" or "maintain the status quo" mind-set. The dream of a space transportation system was never permitted to become reality, unlike that of an airline transportation system.

The difficulty is that few transportation systems initially begun with an already existing, or ready-made, customer base. This is true for the first coal transport to the coast from York, England, in the early 1800s, or the US transcontinental railroad (Ambrose 2000). In the 1870s, the initial rail customer base established itself only after the transportation system was readily available and it was operated such to enable true two-way commerce. As depicted in Fig. 2.6, the railroad enabled the two-way transit necessary for the development of an economic frontier. According to the historical records, between 75 and 80% of the businesses founded in the westward expansion did not exist at the time

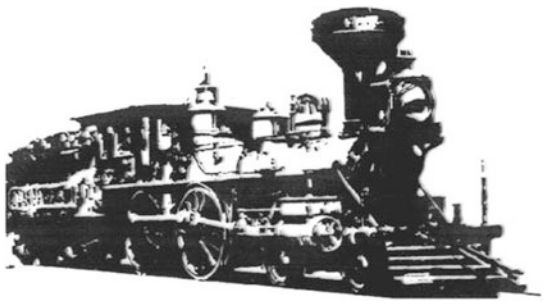

Fig. 2.6 Sustained-use vehicles industries used to open up new economic frontiers and establish scheduled, regular, sustained two-way flows of people, and resources

the railroad began. In the 6 years (1863–1869) that it took to build the transcontinental railroad, an enormous quantity of men and materials were consumed. Stephan Ambrose's book, *Nothing Like It in the World*, documents the dedication of the dreamers, surveyors, tracklayers, graders, engineers, and laborers that made the transcontinental railroad possible.

Compared to the task of designing, surveying and building the US transcontinental railroad, developing and launching the first sustained-use aerospace plane appears to be, at a first glance, less labor-intensive and less of a challenge. With the current approach of analyzing a future market, based on current mental notions and concepts of operation, such tactics does indeed demonstrate that no market initially does exist. An early result is the conclusion, as currently observed, that today's status quo (utilization of expendable launchers) may be sufficient, possibly even pointing to a perceived overcapacity. Clearly, planning a future space launch and in-space transportation system to such mental perception, that of a nonexistent market, will not yield a satisfactory argument for decision-makers today, nor in the future, nor would it have been convincing in the 1850s for trains nor in the 1930s for aircraft.

2.4 Evolution of Space Launchers from Ballistic Missiles

When the USSR lofted the first artificial *Earth* satellite (Sputnik I) into low Earth orbit by adapting a military ICBM, the R-7A (NATO's name: SS-6 Sapwood) became their first space launcher, see Fig. 2.7 (Clark 1988). That can be defined as a typical Russian design procedure. The USA has developed its expendable and partially reusable launchers in a similar manner. The US Army Redstone IRBM was the vehicle to launch the first US astronaut (Alan Shepherd) into space on a ballistic trajectory. The USAF Titan ICBM became the mainstay of the McDonnell Douglas Gemini manned spacecraft program.

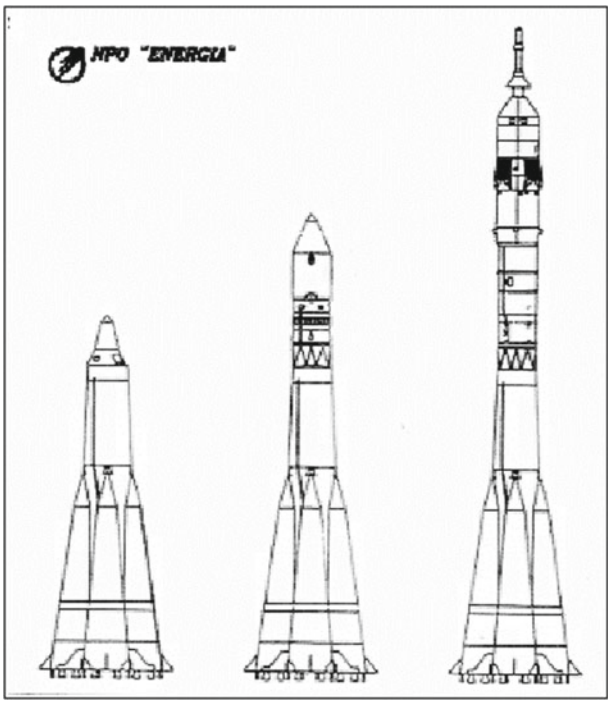

System	*Sputnik*	*Vostok*	*Soyuz*
Launch Weight (t)	267	287	316
Payload Weight (t)	1.55	6.7	8.8

Fig. 2.7 The conventional path for launcher development is the adaptation of a military ballistic missile (SS-6 "Sapwood") to a space launcher. "Sputnik" is an almost unmodified SS-6. "Soyuz" is a very capable, very reliable space launcher with hundreds of launches (over 90 per year)

The McDonnell Douglas Delta launcher began its career as the US Air Force Thor IRBM. The Thor core continues to serve even now, as the Boeing Delta II and Delta III launchers. The Convair Atlas launcher began as the USAF Atlas ICBM and was the launcher that puts the US astronaut John Glenn into the first Earth orbit in the Mercury capsule. The Atlas system keeps on living today, powered by the Russian-derived RD-170 rocket engines, as the Atlas V. Even in Europe, the ESA launchers have an industrial rocket hardware baseline approach to build on military-derived (e.g., the Vega) launching systems.

In fact, in order to begin, this was about the only alternative in existence. What it did, though, was to instill the operational concept of the expendable system as the most cost-effective approach, and with its low launch rate, to assure a continuing manufacturing base. Consider, for instance, the consequences if the first launchers were capable of just 10 launches before overhaul. In the early years, that might have meant only one or two launchers being fabricated, instead of 20. In comparison, the aircraft scenario was different because there were customers for all of the DC-3s that could be built, and literally hundreds of thousands of

potential and actual passengers. For space activities to change toward a dynamic infrastructure, a similar customer base has to develop requiring hundreds of flights per year, rather than 8–12.

In this context, the former USSR came closest. When one of the authors (P.A. Czysz) visited Baikonur in 1990, the civilian Soyuz launch complex had launched 90 Soyuz in the previous one-year period. The launch and countdown was based on a military counterstrike philosophy. There were about seven Soyuz and Soyuz payload combinations in active storage. These could be launched in about 12 h. On the day the author witnessed a Soyuz launch, the Soyuz arrived, transported horizontally on a train, at about 05:30 h. By 07:00 h, the Progress spacecraft (Progress is a Soyuz manned capsule reconfigured as a propellant and materials resupply vehicle) was horizontally integrated into the Soyuz launcher. It was then taken by rail to the launch site and erected. After 10:00 h, the propellant loading and countdown of the Soyuz launcher was executed by a neural network system of computers. The computer system "remembered" the Soyuz launch history over its several hundred launches. If any feature in the countdown matched a previous problem or potential problem, a service crew was sent to the launch pad to check the launcher. During this checking time, the countdown continued with only the item in question on hold. When the item status was confirmed as *ok*, that item was reinserted into the count. According to the Soviet launching officer on site, only 1 in 14 launches have had holds past the scheduled launch time for more than 15 min. During the visit, the Soyuz and Progress capsule was launched at 17:05 h that afternoon, see Fig. 2.8. In spite of the accomplishments of the Soyuz program, it remains until today an expendable launcher (Karashtin et al. 1990).

The heaviest lift launcher available in the former USSR was the Proton. The Proton was the result of an uncompleted intercontinental ballistic missile program. The Proton is powered by a hypergolic propellant rocket engine, the RD-253, in a unique arrangement. That is, a central larger diameter oxidizer tank is surrounded by six smaller fuel tanks, each with an RD-253 engine installed, as shown in Fig. 2.9. The hypergolic propellant-driven turbopumps start up so abruptly, that the sound is almost like an explosion! The launcher is one of the more reliable launchers available for heavier payloads, but like Soyuz, it is completely expendable. The Proton continues to be produced today, being offered as a reliable heavy-lift launcher by a consortium that includes Lockheed Martin. It was an important element in the construction of the International Space Station (ISS).

The Russian space organization wanted a launcher that was recoverable, that was reusable, and that was capable of heavy lift to orbit for a spectrum of missions, going from the support of facilities in LEO to deep-space missions (Gubanov 1984, 1988). With the USA initiation of the "Star Wars" space defense program (SDIO) and the Space Shuttle (STS), the Soviet military was convinced and they needed to counter a new military threat. They perceived (correctly) "Star Wars" as a system to destroy their warheads and warhead delivery systems. But they also perceived the Space Shuttle program as a disguise to create a direct-attack fractional orbit "space bomber." This perception would merge into what was to eventually produce the fully reusable heavy-lift vehicle Energia and the fully automatic military space plane Buran. By whatever method of calculation, the Soviets concluded that the Space Shuttle initiative was sufficiently important to build seven vehicles (Legostayev 1984). After NASA fielded the three operational shuttles, the Soviets were convinced that "the missing four" were hidden someplace, ready to launch at the Soviet Union in a manner similar to the ICBMs in missile silos (Lozino-Lozinskiy 1989). In fact, strange as it may seem, it was reported that

Fig. 2.8 Soyuz launch with Progress resupply capsule at 17:05 h in April 1991 from Baikonur Space Center, Tyuratam, Kazakhstan (photographed by the author P.A. Czysz)

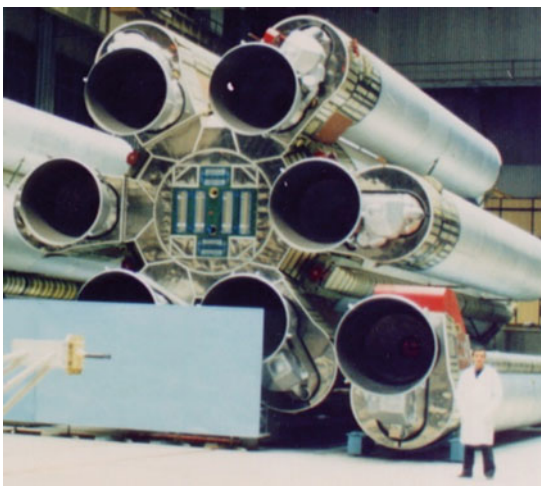

Fig. 2.9 Proton first stage in Moscow plant

just seven Buran airframes were fabricated, in a tit-for-tat response to the US shuttle program (Lozino-Lozinskiy 1990). The Buran glider was derived from Lozino-Lozinskiy's work on the BOR series of hypersonic gliders that began in the 1960s, analogous to the USAF Flight Dynamics Laboratory (FDL) efforts (Draper et al. 1971). According to Lozino-Lozinskiy, he had launched at least 24 test vehicles of the BOR family using scrapped ballistic missile stages (Lukashevich and Afanasiev 2009). The USAF Flight Dynamics Laboratory had launched several ASSET hypersonic glider test vehicles in the 1960s, but that has been the limit of the US flight experience (Draper and Sieron 1991; Hallion 2005).

The result of these Russian efforts was Energia, a heavy launcher capable of launching either cargo or a spacecraft (Buran) to space that was fully recoverable in its operational form. In its principal operational version, Energia was equipped with a side-mounted cylindrical cargo carrier that could be configured as a heavy-lift package to LEO, or a satellite package to GSO, a payload to be delivered to the Moon or Mars, and a deep space probe. Unlike the US Space Shuttle, the primary propulsion engines were all mounted on the center main tank, not on the Buran space plane itself. Because of the emphasis on astronauts, the US Space Shuttle evolved into a design that could never be flown without astronauts: the Space Shuttle had no heavy-lift canister or heavy-lift capability.

One of these authors (P.A. Czysz) drew the Energia concept of operation scenarios, see Fig. 2.10, during a lengthy discussion with Boris Gubanov at the IAC conference in 1984 (Gubanov 1984). There were few disposable parts. The side canister could be configured with just sufficient propulsion to reach LEO, or with sufficient propulsion (and less payload) for a Moon, Mars, or deep-space mission. The Zenit-based strap-on boosters were equipped with lifting parasail parachutes at the front and rear of the booster. The intent was to glide in the vicinity of the launch site for recovery. Since the boosters were liquid boosters equipped with NPO Energomash RD-180 rocket engines, there was little refurbishment required unlike the US solid propellant strap-on boosters on the Shuttle. These cost as much to refurbish as to build new. The Buran center tank has a very low ballistic coefficient, and using a Lockheed concept to reduce the heating with the thermal and antistatic coating applied to the booster, the entry into the atmosphere could be relatively easy. The center tank did a fractional orbit and was recovered in the vicinity of the launch site. Although never implemented in the first two test flights, the eventual operational capability planned was to recover all major components.

Said otherwise, Energia was to be the USSR's fully recoverable Saturn V equivalent. The booster configurations on the right side of Fig. 2.10 show the payload to LEO for the different strap-on booster configurations. For the four-pair configuration, the payload was carried in tandem with the center tank in a special powered stage. For the two-pair configuration, two payloads are shown, the canister and the Buran. The Energia M was a two strap-on booster arrangement for a lesser payload. The author (P.A. Czysz) saw Energia M in the Energia assembly building in 1990 (there is no reported flight of this version). Note the intended fly rate from three launch complexes: 1800 flights in 20 years, for an annual fly rate of 90, about the same as from the Soyuz launch sites. If the cost is the same as for the US

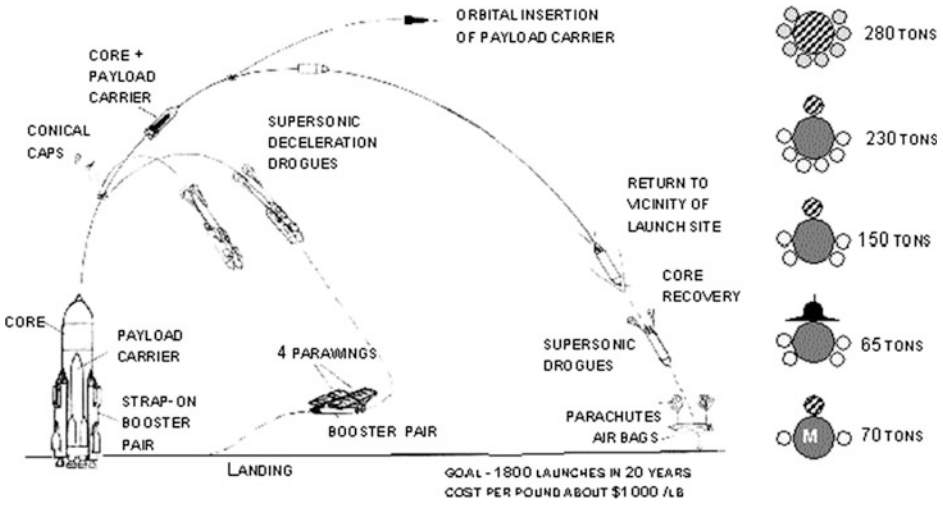

Fig. 2.10 Energia was an approach to achieve a fully reusable (all major components recoverable), extended-life launcher (at least 50 launches without overhaul) with an equivalent Saturn V heavy-lift capability that the USA discarded. The *right side* shows the strap-on booster configurations and payload to LEO. Energia M was developed as the smallest design configuration as a Proton rocket replacement, but lost the 1993 competition to the Angara rocket

Space Shuttle, US$1.32 billion for five flights and US$100 million for each additional flight, then with a mix of Buran and canister payloads, the payload cost to LEO ranges between US$450 and 650 per payload pound. Clearly, frequent flights of cargo-configured vehicles lower costs: the Energia would have been a wise investment. The Russians thought very highly of the Saturn V, but they were dismayed that the USA would summarily discard the Saturn V heavy-lift vehicle capable of lower cost to orbit (about $US5700 per pound payload in the 1980s) compared with the Space Shuttle.

The Energia had several launch configurations to optimize different size payloads for different orbits. The Zenit-derived (SS-16 missile) strap-on boosters were assembled together in pairs. The standard configuration was two coupled pairs, for a total of four individual strap-on boosters. In this configuration, the Energia could deliver 150 t to LEO in the cargo canister configuration and 60–70 t when carrying Buran. With three Zenit pairs, Energia could place 230 t in LEO with the side-mounted cargo canister. If an in-line cargo section was added to the center tank in lieu of the side-mounted canister, overall increasing the payload to 280 t that could be delivered to LEO, such payload capability would be an astonishing figure nowadays (the US Space Shuttle could only deliver less than 4% of this payload to LEO, and NASA's under construction SLS Block I capability is 70 t). It was this latter configuration that was the counter-*Star Wars* configuration.

Figure 2.11 shows a model of Energia (left) from an AIAA technical meeting display, with the side cargo canister mounted. Clearly visible is the forward and aft parachute packs on each strap-on booster. Utilizing the Zenit launcher as the strap-on booster meant that this part of the system was already a reliable component of the operational launch system. On the right is a night picture of Energia with Buran mounted and being prepared for launch (Gubanov 1998). The gray horizontal cylindrical tube is the crew access to Buran. The angled tube is an escape path to an underground bunker, in the event of a launch mishap. The two horizontal tubes in the lower part of the figure represent ducting that leads to the rocket exhaust chute under the vehicle. These are attached to eight vacuum cylinders on each side, equipped with compressors and a vent stack. When the hydrogen flow is initiated to the rocket engines, this system is opened and any vented hydrogen is drawn off, compressed, and burned in a vent stack.

The original plan was to construct three launch sites in close proximity, so that nine Energia/Buran and Energia/canister configured vehicles could be launched within three days in case of a Space Shuttle Star Wars attack. None of this was ever accomplished. The Russian space organization wanted also to replace Proton with a reusable vehicle. When one of the authors (P.A. Czysz) visited Baikonur in 1989, there was an Energia M being assembled consisting of only two Zenit strap-on boosters instead of four. It was their intent to make this the medium-lift launcher Proton replacement. With the side payload placement, Energia M could accommodate a payload canister or a smaller hypersonic glider, such as a crew rescue vehicle based on the BOR vehicles.

Figure 2.12 shows a modification to the Zenit strap-on booster, incorporating a skewed-axis wing (instead of four sets of lifting parachutes) and a turbojet with a nose inlet in

Fig. 2.11 A model of the Energia showing the strap-on booster parachute packs and cylindrical payload container (*left*) and the Buran space plane on the Baikonur launch complex (*right*). The RD-0120 engines are on the center tank, which is recoverable

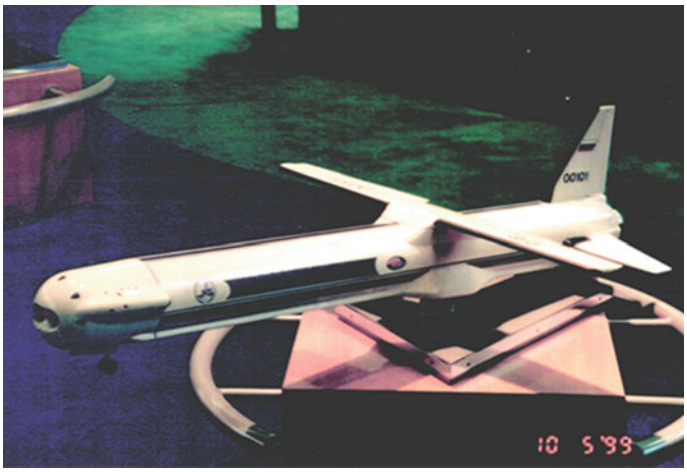

Fig. 2.12 Fly-back version of the Zenit strap-on booster as an alternative to lifting parafoils

the front of the booster for a powered return. This arrangement was shown at an American Institute of Aeronautics and Astronautics technical meeting in 1992 and has been retained in the reusable Baikal flyback booster for the Russian Angara family of modular launchers. Baikal has foldable wings and is powered by a turbojet with a nose air inlet that is faired during ascent and part of the reentry.

For readers who may wonder, the Buran arrangement is not a US Space Shuttle, or a copy of it. The Buran's intent was very different. P.A. Czysz visited the Buran assembly building at Baikonur in 1989. The glide angle-of-attack for maximum lift-to-drag ratio is 10°–15° less compared to the US Space Shuttle glide angle-of-attack. Buran is a fully automatic vehicle with a neural network-based control system. It landed for the first, last, and only time at the specially constructed runway at Baikonur without any human intervention. This took place during a snowfall and with significant 90° crosswind; it touched down within a few meters of the planned touchdown site (Buran Site Director 1989). As with all Soviet spacecraft, it was never intended to be controlled by a human pilot, except in a dire emergency. Its thermal protection system was (and still remains) unique due to its ability to handle lost surface tiles without risking damage to the airframe structure (Neyland 1988).

The manoeuver Buran reportedly performed during landing was much discussed in a 2002 article in Air and Space, but it was not a poorly executed automatic landing; in fact, it was strictly the result of the neural network flight-control computer decision. The computer was developed by the USSR Academy of Sciences, Siberian Branch, in Krasnoyarsk in the 1980s (Bartsev and Okhonin 1989) and built by a company in the Ukraine. The flight-control system had determined that during the entry, the actual lift-to-drag ratio (*L/D*) had exceeded the estimates used in the preplanned flight trajectory. As a result, the aerodynamic heating encountered by Buran during reentry would have been larger than expected due to the trim control surfaces deflections required at this modified *L/D* trim point. In order to avoid this flight point, Buran entered the approach pattern much faster than anticipated. If Buran was to land successfully, the excess speed had to be bled off. The neural network controller executed, without any input from ground control, a 540° turn rather than the initially planned 180° turn, thereby bleeding off the excess speed (Lozino-Lozinskiy 1990). As a consequence, Buran touched down at the planned landing point with the correct speed (Hendrickx and Vis 2007).

Figure 2.13 is a photograph taken from the Buran display in the Memorial Museum of Cosmonautics in Moscow. It shows conclusively that Buran is more closely related to the USAF Flight Dynamics Laboratory (FDL) hypersonic glider designs than to the Space Shuttle. In order for the leading edge vortex (a main source of lift) not to burst, the angle-of-attack would have been limited to the 25°–30° angle-of-attack range, not the 40°–45° operated with the Space Shuttle during the early reentry phase, a design approach causing stability and control challenges for the US design. In many aspects this is a very revealing photograph, as it documents the similarity of Buran with the high-performance (low-entry angle-of-attack) military hypersonic gliders that Draper, Buck, Goetsch, Dahlem, Neumann, Melvin and Sieron developed at the Flight Dynamics Laboratory (FDL) in the 1960s (Kirckham et al. 1975).

The burn marks on the visible right-wing elevon, see Fig. 2.13, indicate that its deflections during the entry portion of the flight were larger than anticipated, resulting in more severe heating exposure. Additional pictures in the Memorial Museum of Cosmonautics in Moscow show the underside of Buran after the flight; there are white streaks emanating from the gaps in the tiles. This indicates that the tile/aluminum interface temperature would have exceeded 100 °C had not the tile adhesive/phase-change material been present and active. This Russian adhesive incorporated a phase-change material that, in the event a tile was damaged

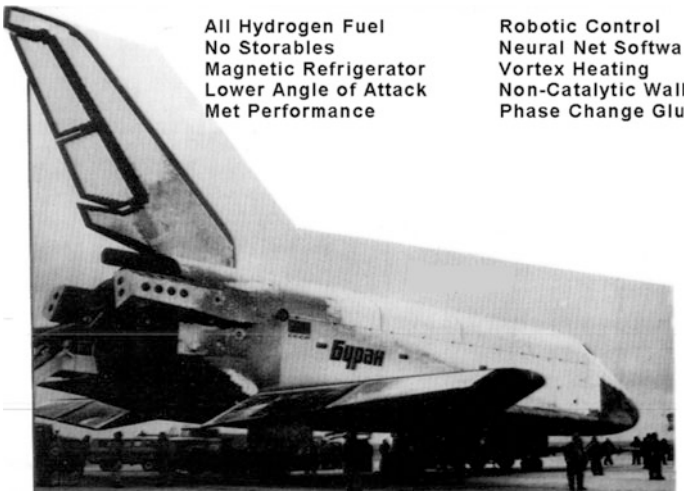

Fig. 2.13 Buran after landing on its first, last, and only flight. Note the trace of vortex heating emanating from the junction of wing and fuselage (apex). This matches the thermal mapping test at TsAGI and proves that the angle-of-attack was sufficiently low to prevent vortex bursting as it does on the Space Shuttle. The burned spot on the inboard elevon is the vortex core location

or lost, was capable of maintaining the interface with the aluminum structure at no more than 100 °C for several minutes at peak heating conditions, thereby preventing thermal damage. The intentional gaps with plastic spacers in the tiles permitted the vapor from the phase-change material to escape (they, as well, were mounted with a unique adhesive that acted as a thermal safety layer). V.Y. Neyland, one-time Deputy Director of the oldest Russian gasdynamic center TsAGI (founded in 1918) tested this strategy in one of the TsAGI wind tunnels, and one of these authors (B. Chudoba) has a copy of the data report (Neyland 1988). The thermal protection employed by the Buran was structurally robust in contrast to the brittle Space Shuttle tiles. During a 1989 visit to Russian research institutes, at the Komposit OKB, the author (P.A. Czysz) saw a Buran tile heated to white heat with an oxyhydrogen torch and then dropped into water, with no structurally visible damage to the tile.

Then, at the beginning of 1990, Russia had the hardware in test for a family of fully recoverable and reusable rocket-powered vehicles for medium and heavy lift. Despite such knowledge and capability accumulation, by the beginning of the twenty-first century, neither the USA nor Russia has an operational heavy-lift launcher on the order of the Saturn V (140 t payload to LEO). The Space Shuttle was limited to about 27.5 t payload to LEO with the Proton offering in excess of 100 t payload to LEO until its retirement in 1988. Thus, with both the US Saturn V discarded in lieu of the 2011 retired Space Shuttle and the demise of the Energia, there is no affordable heavy-lift launcher available to either the USA or Russia since the last 25 years. In the USA, the SLS, under development with engines derived from Saturn and the Space Shuttle, is promising a payload to LEO range of 70–130 t (for Block II). Its first flight is envisioned no sooner than November 2018 (Anon 2015).

2.5 Conflicts Between Expendable Rockets and Reusable Airbreathers

The fundamental question always posed is: "*Why airbreathers?*" One observation is that in-orbit specific energy (energy/mass) is a function of speed squared.

$$h_S = \frac{m \cdot g \cdot h + \frac{1}{2} \cdot m \cdot V^2}{W} \tag{2.1a}$$

$$h_S = \underbrace{h}_{\text{Potential energy}} + \underbrace{\frac{V^2}{2 \cdot g}}_{\text{Kinetic energy}} \tag{2.1b}$$

In Eq. (2.1a), W stands for mass. Then, if an airbreather reaches 12,000 ft/s rather than orbital speed of 25,573 ft/s, it achieves only 22% of the orbital energy. Using *specific energy,* this is correct. However, the launcher is much heavier at launch compared when entering orbit. Consequently, the *total energy* spent (Btu or MJ) is a very different value. Figure 2.14 shows the total energy for launch vehicles with four different propulsion systems and I_{sp}. The value of total energy at 12,000 ft/s (3658 m/s) is 70% of the orbital value, a much more significant value. Note also that all of the different propulsion system curves plateau to a single total energy value above 15,000 ft/s (4572 m/s) for an energy level of 10^9 Btu (1.055×10^9 kJ). The energy does not continuously increase with the square of the velocity, because the rocket engines are consuming the mass almost as fast as the specific energy is increasing.

However, as consistent as the energy levels are, the weight (mass) levels are not. Figure 2.15 shows the weight (mass) along the trajectory is a unique characteristic of each propulsion system. The weight-time history during the

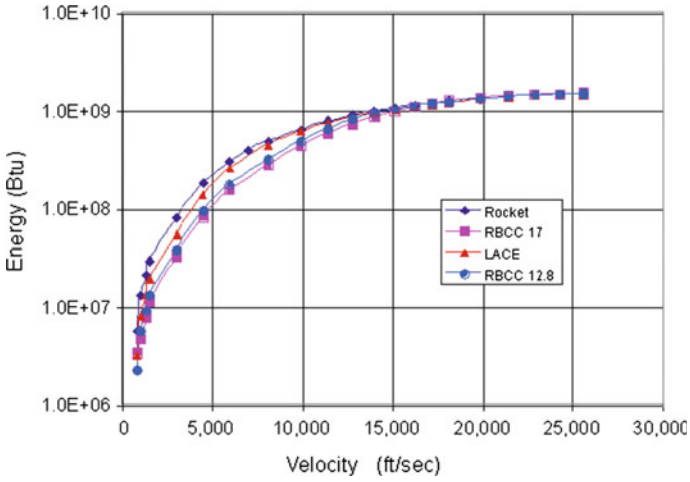

Fig. 2.14 As velocity increases, total vehicle energy approaches a plateau. Mass is being spent as fast as kinetic energy is increasing for all propulsion systems

ascent to orbit is given for four different propulsion systems as a linear function of the logarithm of the flight path energy. All have essentially the same on-orbit weight; note that a correctly selected propulsion system has little impact on the vehicle empty weight. For the three airbreathing concepts, once the "all-rocket" propulsion-stage is reached, the weight histories are essentially identical. Even simple airbreathing rockets like the LACE (Liquid Air Cycle Engine) or deeply cooled rocket that operates only to Mach 5 or 6 result in a substantial reduction in liftoff weight. In fact, increasing the airbreathing speed to Mach 17 from Mach 12 has much less impact compared to moving from Mach 6 to Mach 12. As shown, the propulsion system directly affects the oxidizer-to-fuel ratio at the beginning of the flight, when the thrust required is the greatest. Clearly, a reduction in the oxidizer-to-fuel ratio has the greatest effect, as the liftoff weights on the left-hand ordinate show in Fig. 2.15.

As developed in this chapter, system studies with what appear to be rational assumptions, such as turbojet low-speed propulsion or a combination of engines, doom the airbreathing launcher from its inception. In contrast, a combined-cycle propulsion system in which a single propulsion system can transition from one mode to another is the key to the success of the airbreathing launcher. As implied by Fig. 1.1 in Chap. 1, a multitude of design, build and test efforts have been chronicled from the past to the present, aimed at building an aircraft-like hypersonic vehicle that could fly to space and return. (Anon 1967; Hannigan 1994). However, as many valid programs that were initiated, there were as many programs seeking to discredit the airbreathing vehicle efforts.

Figures 2.16 and 2.17 show one such example of the conflict as presented in a briefing in the 1970s. The three aircraft shown in Fig. 2.16 are, from top to bottom: (a) an

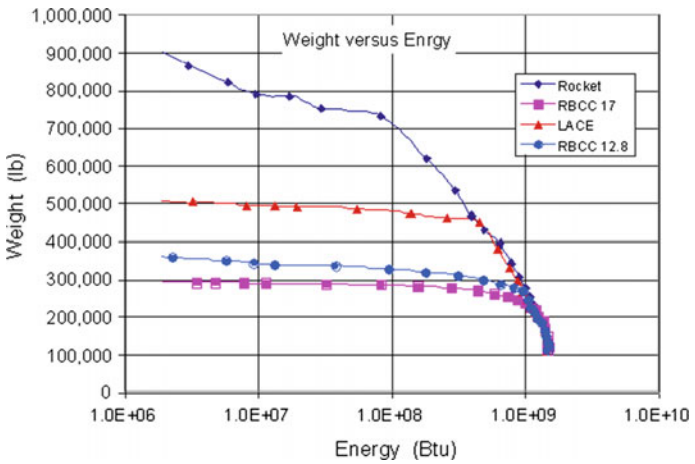

Fig. 2.15 The mass or weight history shows the differentiation of the propulsion systems in terms of initial (liftoff) weight and the convergence to a single on-orbit value

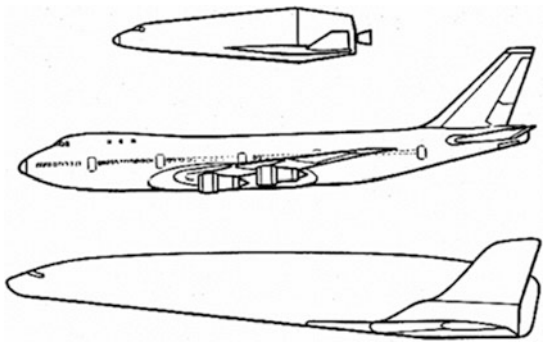

Fig. 2.16 Rocket advocate's vision of launchers that fly regularly to space. The all-rocket SSTO launcher (*top*) is smaller but heavier than the B747 (*center*). The airbreather launcher powered by a combination of 35 engines of four different types (*bottom*) is larger and heavier than the B747, discouraging the airbreather concept

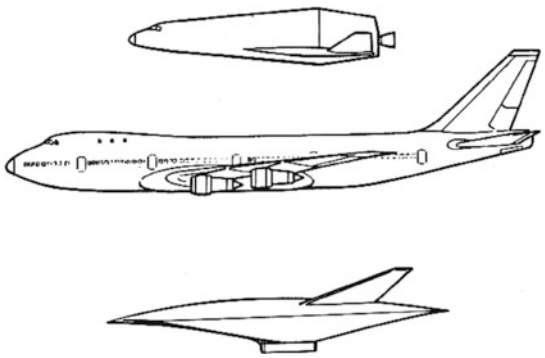

Fig. 2.17 A balanced vision of launchers that fly regularly to space. The all-rocket SSTO launcher (*top*) is smaller than the B747 (*center*). The airbreather launcher powered by a combined-cycle ejector ramjet/scramjet (*bottom*) is smaller and lighter than both, but is never been pursued as a launcher or hypersonic cruiser

all-rocket single-stage-to-orbit (SSTO) launcher, (b) a Boeing B747-100, and (c) an airbreather/rocket SSTO powered by a combination of 35 turbojet, ramjet, scramjet, and rocket engines. Such accumulation of nonintegrated individual propulsion systems does result in a clear weight penalty, since 3/4 of the installed propulsion systems are being carried as dead weight. As correctly depicted in Fig. 2.16, a very large airbreathing/rocket SSTO is the outcome because of the inert weight carried as nonoperating engines. Note that the turbojet is a very poor acceleration propulsion system that can consume more fuel compared to a rocket in some flight regimes. For many in the aerospace design community, this was a legitimate comparison considering the low launch rate of rocket launchers, the nonexistence of a viable civil need to increase the launch rate, and, for the rocket advocate, the absence of a good reason to replace the rocket.

However, the advocates of an integrated combined-cycle airbreathing/rocket SSTO have been proposing a very different system based on the integration of several different engines into a weight and volume optimized single combined propulsion system. The combined-cycle propulsion system can recover rejected heat and convert most of the recovered heat into thrust or system work. The three aircraft depicted in Fig. 2.17 are from top to bottom: (a) the all-rocket single-stage-to-orbit (SSTO) launcher, (b) the Boeing B747-100, and (c) an integrated combined-cycle airbreather/rocket SSTO vehicle. This not only saves energy, but also reduces entropy formation and drag.

The integrated combined-cycle airbreather/rocket SSTO aircraft depicted is from McDonnell Douglas Corporation, McDonnell Aircraft Company, St. Louis, Missouri, as presented by the USAF Flight Dynamics Laboratory (AFFDL). The combined-cycle propulsion system is integrated, thermally and physically, into one synergistic system. Then, the rocket, ramjet, and scramjet represent one and only one integrated propulsion system. The result is a vehicle with slightly less volume and empty weight than the all-rocket vehicle but about one-third its gross weight. The airframe and propulsion system had been designed for at least 100 flights before overhaul. At the flight rate anticipated in 1968, such operational requirement was sufficient for 8- to 10-year operation with commercial aircraft-type inspection and maintenance.

At the time, the perception has been that the simpler and increasingly reliable rocket was the least costly for the low launch rate required. A "catch-22" situation emerged since the launch rate could not be increased because of the selection of the rocket launcher as the primary space launcher system. With such presumption, the payloads that required a high launch rate never appeared, therefore self-justifying the rocket launcher selection. As a consequence, the expendable rocket launchers prevailed, and none of the integrated hypersonic airbreathing engine-airframe systems of the late 1950s and early 1960s were ever realized. Historically, much of the work done on these vehicles was for highly classified military programs with very limited access to information. It is a sad reality that most of this documentation is now shredded, lost, and forgotten. References (such as Stephens 1965; Anon 1966a, b; Brewer 1966) are the program references that document a small portion of what was accomplished.

The other great debate was single-stage-to-orbit (SSTO) versus two-stage-to-orbit (TSTO). Both have advantages and disadvantages depending on operational concept and geographical location. It is the operational requirement (mission, in military terms) that makes the decision. For the support of an orbital station, as discussed in Chap. 3, with a very specific payload requirement and specific launch sites to a given orbital inclination and altitude, a SSTO makes a good minimum operational equipment choice. If the operational mission is to deliver both crew and crew supplies in addition

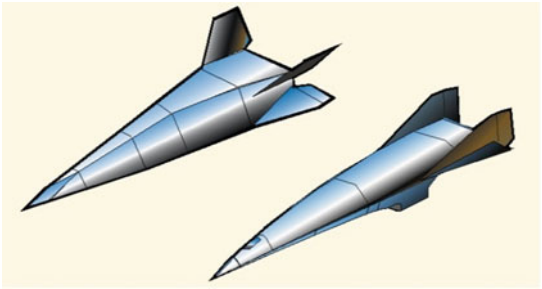

Fig. 2.18 Airbreather/rocket-derived hypersonic glider single-stage-to-orbit (SSTO) configuration (*left*), and airframe-integrated rocket ramjet/scramjet combined-cycle single-stage-to-orbit (SSTO) configuration (*right*)

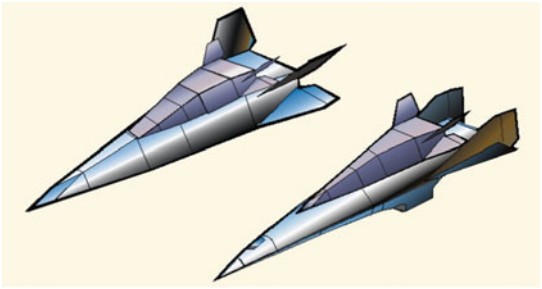

Fig. 2.19 Airbreather/rocket-derived hypersonic glider two-stage-to-orbit (TSTO) configuration with all-rocket second stage (*left*), and airframe integrated rocket ramjet/scramjet combined-cycle two-stage-to-orbit (TSTO) configuration with all-rocket second stage (*right*)

to large orbital payloads from different launch sites for different orbital inclinations and altitudes, then the TSTO offers a wider range of options and versatility. Figure 2.18 shows two SSTO configurations. The left configuration is an airbreathing-rocket propulsion system integrated into a hypersonic glider. The right configuration represents an airframe-integrated rocket ramjet/scramjet combined-cycle airbreathing propulsion system. Nominally, these are in the 7–10 metric ton internal payload class. Chapter 3 provides a discussion of the rocket propulsion hypersonic glider that was proposed in 1964 to support the Manned Orbiting Laboratory (MOL) with a 7 t crew or supplies payload. Except for the vehicle configuration, the overall concept was analogous to the Russian Soyuz-Progress capsule. Although many concepts were analyzed and designed, these concepts were not able to dislodge the expendable rocket as the dominating configuration concept for *any* mission role (due to the "catch-22" phenomenon discussed before).

For operational missions that deliver both crew and crew supplies, in addition to large orbital payloads from different launch sites for different orbital inclinations and altitudes, the TSTO offers a wide range of versatility. As shown in Fig. 2.19, there are two TSTO concepts and these have rocket-powered hypersonic gliders for second stages. Just as is shown for Energia in Fig. 2.10, a faired payload canister can be substituted for the hypersonic glider. If the nominal payload of the second stage returnable hypersonic glider is 7 metric tons, then the payload for the expendable canister second stage could be as large as 23 metric tons or a space station component approaching 28 metric tons. Then, the payload capability to orbit spans a 4:1 range.

With the flying capability of an airbreathing propulsion first stage, considerable offset is available to reach a latitude different from that of the launch site or to expand the launch window by flying either east or west to intercept the orbital launch plane. With this versatility to provide launch capability to different sites worldwide, the TSTO makes an excellent choice for a commercial space launcher. Note that the upper stage can have either a pointed nose or the spatular two-dimensional nose. The latter reduces the nose shock wave drag by as much as 40% (Pike 1977) and enables increasing vehicle volume without altering substantially aerodynamic characteristics. Pike began his work on minimum drag bodies in the mid-1960s. The spatular nose can be used on almost any hypersonic configuration, whether the SSTO or TSTO, whether a first stage or second stage.

Even though some excellent designs have originated in Germany, France, Russia, and the USA based on available hardware and existing industry capability with sufficient performance to LEO, none were ever able to dislodge the expendable rocket status quo. The launchers remained as they began, as ballistic missiles.

The hypersonic first stage can require more runway than what is available at airports worldwide. V. Plokhikh and the late Lozino-Lozinskiy proposed a TSTO based on the transonic Antonov An-225, an An-125 large cargo aircraft modified to carry a space launcher atop the fuselage (Plokhikh 1983). The NPO Molniya began to realize the MAKS (multipurpose aerospace system) project in the 1980s. The second stage can weigh up to 300 t. In this case, the fuselage of the An-225 can carry a portion of the launch crew and equipment. A second An-225 has sufficient volume to carry the liquid hydrogen required for the space launcher. In this case, the An-225 is more of a mobile launch platform than a first stage. With the range of the An-225, and the low-noise operation of the six turbofans that power it, the An-225 can make almost any commercial international airport a launch site.

Figure 2.20 shows the An-225 with a combined-cycle ramjet/scramjet-powered waverider mounted on top. The payload capability of the second-stage launcher is 7 t. This particular approach has the An-225 operating on hydrogen fuel and is equipped with an air collection and enrichment system in the cargo hold. That is, the hydrogen that is used to power the engines liquefies air and then separates the oxygen and nitrogen. The oxygen is liquefied and pumped into the launcher oxidizer tank (the launcher has no liquid

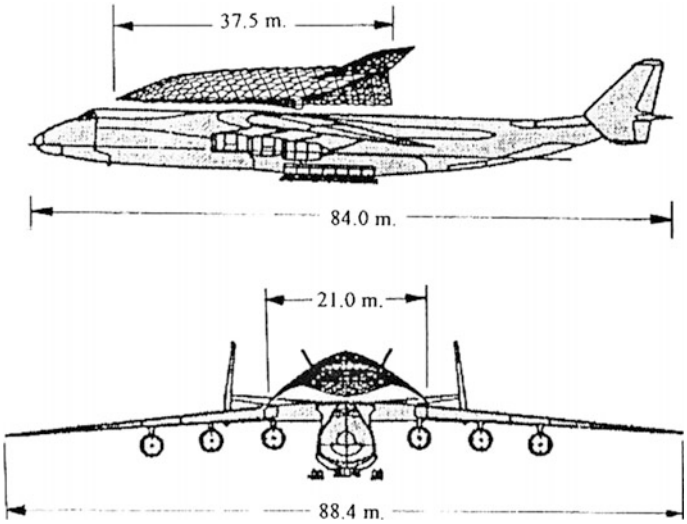

Fig. 2.20 Large transonic transport-based TSTO configuration with a combined-cycle powered waverider second stage

oxygen in its oxidizer tank at takeoff, only the liquid hydrogen tank is filled). This means that the two aircraft are heaviest not on takeoff but near the launcher separation point (Czysz and Little 1993). A LACE, deeply cooled air-breathing rocket, or the original HOTOL airbreathing rocket engine (RB545) would have provided a successful solution, see Chap. 4.

The use of the An-225 as a mobile launch platform is indeed a very practical commercialization concept for both space tourism (Mach 4 and 100 km altitude) and for a commercial point-to-point cargo delivery system (12,000 nmi in 90 min) as it eliminates noisy rocket launchers, provides an independent heading and altitude launch, and makes any commercial airport a potential launch point. This "Flying Circus" concept brings the launcher to the customer for a worldwide launch service for any country wishing to put a payload into orbit, send cargo to another point on Earth, or launch citizens on a tourist flight from their own country, not from the geographic location of possibly a foreign dedicated launch site. In the USA, Paul Allen's Scaled Composites Model 351 Stratolaunch or "Roc" is a similar concept currently under construction, see Fig. 2.21. Contrary to the An-225 carrier aircraft for HOTOL, the carrier airplane is being built from scratch. Powered by six turbofan engines, the carrier lifts the rocket second stage slung under the central wing section to a still unspecified "high altitude", where it is released and reaches orbit. According to press releases, the maximum take-off weight will be 1.3 million pounds, probably requiring a specially built runway. The Stratolaunch has been rolled out of its hanger for the first time on June 01, 2017. First flight is scheduled in late 2017, and first second-stage launch is planned for 2018 with commercial flights to be expected in the 2019 timeframe.

Steve Wurst of Space Access LLC, a RLV start-up, recovered some of the historic hardware from the "bone-yard" of The Marquardt Company, as its property was being sold in bankruptcy. Steve transformed hardware elements into a modern combined-cycle access to space launcher concept on private financing. As discussed before, reusable access to space launcher concepts did not fit the preconceived concepts of the government at the time and, short of

Fig. 2.21 Artist's rendition of Scaled Composites Model 351 for Stratolaunch Systems (*Courtesy* NASA). The design wingspan is 385 ft

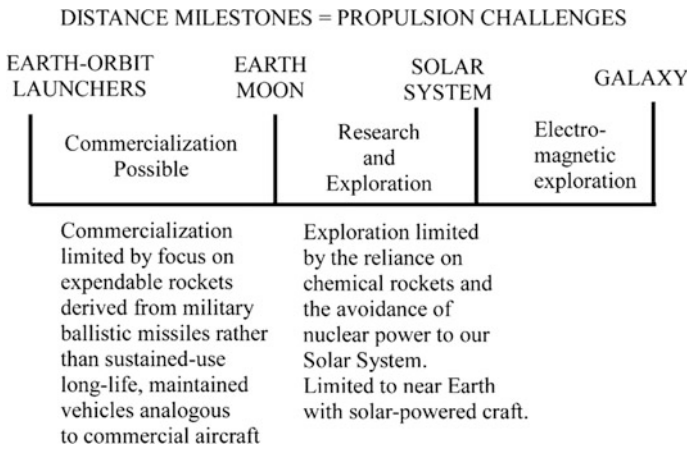

Fig. 2.22 Result is that the possibilities were never developed and impediments were sufficient to prevent any further hardware development of a truly sustained-use space launcher

turning the project into a government-sponsored program with government control, the project remained in the shadows. However, the overabundance of naysayers and skeptics, and the lack of dreamers continues to prevent the realization of a transportation system to space. Although reusing the first stage is being experimented with and operationally implemented by SpaceX (Falcon 9) and Blue Origin (New Shepard), the financial advantage of vertical-landing (VL) recovery by using pure rocket propulsion still must be demonstrated. For instance, the Falcon 9 flight that recovered the first stage lifted 22.3 t to LEO at the cost of $62M, thus still in the many tens of K$/kg. For the time being, we are still left with *Space Conestoga Wagons* and have yet to see the "railroad to space" evolve.

As indicated in Fig. 2.22, progress toward the future for both, Earth-based launchers and space exploration, appears to be impeded by the acceptance of the status quo. The key to breaking this stalemate is a propulsion system integrated into a sustained-use vehicle that can provide routine, frequent flights, and advance our space capabilities. The US X-planes proved that even high-speed research aircraft could be operated frequently and safely (Miller 2001), despite the need to air launch these aircraft from a modified B-50 in the early flight operations, and later from a modified B-52 (Lockett 2009).

Similarly, in space, nuclear propulsion is a vital necessity if we are ever to travel significant distances in practical times. Here, the mind-set is shaped by the fear of nuclear explosions in the atmosphere in case of accidents. Nuclear submarine reactors are reported to outlive the hull and are historically without nuclear accident. Accepting the disposable rocket, as today's standard space access system, and despite some inroads made by electric thrusters, this situation prevents scientific and safe crewed missions to deep-space destinations, see Chap. 7.

The missing elements are the dreams, determination, and resources analogous to those that were committed to the building of the transcontinental railroad (Ambrose 2000). In many respects, the challenges are less daunting although the environment is a great deal harsher nowadays. Note that we are not short of dreamers today, but we are lacking informed decision-makers due to outdated *future projects environment* tools, mind-sets, and overall poor design knowledge retention of past aerospace projects. Most hypersonic projects of the past were classified, thus the documentation necessary to dissipate skepticism tends to be unavailable. A modern generic design methodology, representing the foundation of a modern *Future Projects Office* capable of correctly advising the decision-maker, is introduced in Chap. 3.

2.6 Commercialization and Exploration Road Map

Incorporation of airbreathing offers many propulsion options. However, vehicle design choices are not arbitrary, since requirements and propulsion performance define the practical (technologically and commercially feasible) solution space. A priori assumptions and decisions can doom a complex project that without them would instead be successful.

2.6.1 Commercial Near-Earth Launchers Enable the First Step

One of the difficulties is the identification of the transportation need, and this at a time when there is an overabundance of expendable launchers that do not have the capability of high fly rates with the accompanying reduction of payload cost, per definition, see Fig. 3.1. This issue brings back the Conestoga wagon versus railroad comparison. Commerce with the western USA was never possible with the Conestoga wagons, as none ever returned since they were becoming building materials for the settlers instead. All of projections of future space business based on expendable

or limited reuse launchers are as valid as the business projections for the future railroad business based on Conestoga wagons in the early 1860s.

The late Dr. William Gaubatz, formerly of McDonnell Douglas Astronautics and manager of the Delta Clipper program, addressed this issue in his briefings on space development. Figure 2.23 represents our current status. Remember, however, that since Dr Gaubatz made his presentation, MIR has deorbited and crashed into the Pacific Ocean and the ISS has replaced it in 55° inclination orbit, followed by the retirement of the Space Shuttle after completion of ISS assembly in 2011. Expendable launchers can of course readily meet the military and commercial need, that is, suited to expendable launcher. Until a sustained-use launch system is operational, the payloads that warrant a high launch rate system will remain the subject of design studies only. In other words, without the railroad there will be no railroad-sized payloads for Conestoga wagons! The USA missed the opportunity to slightly modify the Space Shuttle main propellant tank to permit its use as a space structure, like the Saturn S-IVB. This could have been the starting point for building a space infrastructure (Taylor 2000). Note that the Space Shuttle main tank was intentionally not permitted to remain in Earth orbit and was deliberately crashed into the ocean.

For a true space transportation system to exist, a transportation system network has to be built, just as it was for the USA transcontinental railroad. Dr Gaubatz attempted to anticipate what the future might hold *if* an enabling space transportation system actually did exist. As shown in Fig. 2.24, the future space world envisioned becomes a crowded and busy place. Clearly, the availability of cost-effective near-Earth space launchers will enable this first step. One of the key enabling space structures is the "fuel station spaceport" network. Without these fuel stations, movement between orbital planes and altitudes is limited to specific satellites, such a GSO communication satellites with integral GEO-transfer propulsion. Note the "construction module storage" that can supply components for orbital, lunar and deep-space vehicle assembly in space. The "operations center" and "space station" provide a system to launch and control missions to the Moon, planets, and deep space. The "power station warehouse" provides hardware for the "power satellites" in GEO-Earth orbit. That, coupled with an "orbital servicing vehicle," can maintain this and other space resources. As seen earlier with the USSR space plan, there are "lunar spaceports" and "lunar orbiting satellites." There are also "space deployment and retrieval vehicles" as well as a "waste storage and processing facility" in high orbit. Hence, Fig. 2.24 provides a very comprehensive projection of future space if a suitable *scheduled*, *frequent*, *sustained* transportation, and heavy-lift capability is available. That is what is needed to plan for the future, not the current status quo.

There is a first step that can be made in propulsion to anticipate the future much as Steve Wurst did with his proposal. The key first step is off-loading some of the carried oxidizer by utilizing even partially airbreathing rockets, and designing for sustained operations over a long operational life with normal maintenance, not continuous overhaul and rebuilding. The design space available with current industrial capabilities and materials is readily identifiable, see Chap. 3. A cross section of propulsion options that are based on available and demonstrated hardware and materials is

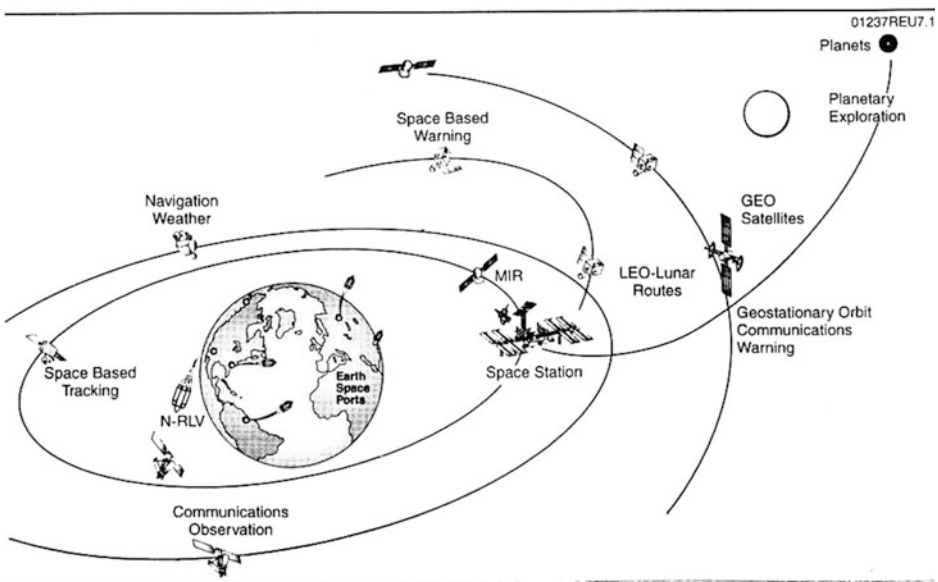

Fig. 2.23 Our current space infrastructure with MIR replaced by the ISS is limited to specific LEO and GSO without significant intra-orbit operations. Hubble is in the space-based warning orbit and is not shown

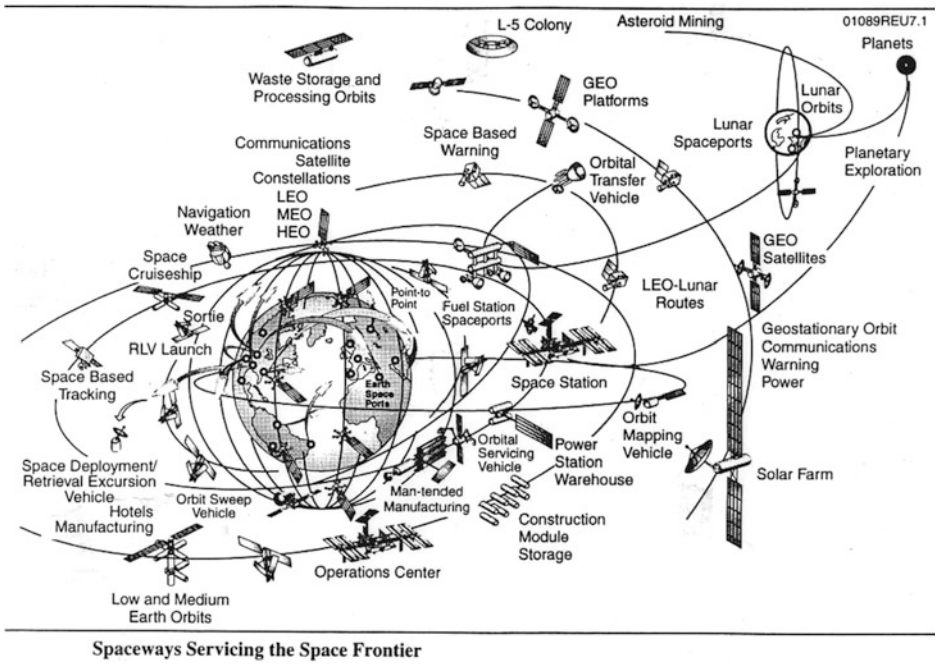

Fig. 2.24 One US look to the future space infrastructure that fully utilizes the space potential if a suitable *scheduled*, *frequent*, *sustained* transportation and heavy-lift capability is available

presented, and its pros and cons are discussed also in Chap. 3. The propulsion systems that are necessary to reach LEO are evaluated in Chap. 4 in terms of takeoff size and weight required for a specified payload.

For many decades the focus of the discussion has been, and rightly is, on the enabling space transportation system. As with the railroad analogy, emphasis has to be placed on an efficient two-way transportation system to and from LEO. The vehicle configurations discussed in what follows all have high hypersonic lift-to-drag (*L/D*) ratios. The reason for that is the corollary to the argument that if waiting times and launch delays are economically penalizing to commercial launch vehicles, the waiting times and return delays are also economically penalizing. However, the way the continents and national boundaries are distributed on the surface of *Earth* means that a returning vehicle may have to wait until its landing site comes within the lateral range (cross-range) capability, that is, with *L/D*. Figure 2.25 shows the waiting time in terms of orbits, as functions of the spacecraft lateral range capability and orbital inclination.

This chart was salvaged from the original 1964 work done for the MOL support vehicle, the McDonnell Douglas Astronautics *Military Model 176*. For Cape Kennedy orbital inclination, the waiting times for an Apollo type ballistic capsule (with very limited lateral range capability) can be 14 orbits or about 21 h. For nominal lifting bodies like Sierra

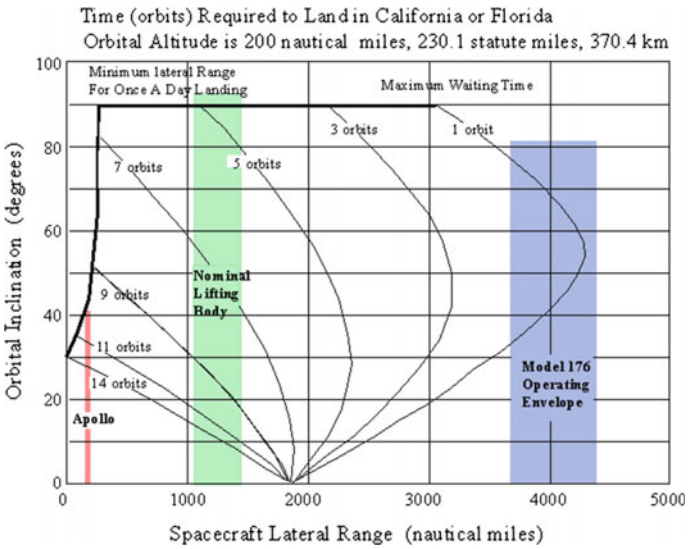

Fig. 2.25 Waiting time is costly for commercial space operations. Greater lateral (cross) range reduces orbital waiting time

Table 2.1 Return from orbit performance is configuration dependent

L/D (–)	0.5	1.3	1.7	2.2	2.7	3.2
LR (nautical miles)	200	1080	1700	2600	3540	4470
DR (nautical miles)	5800	9900	12,900	17,100	21,600	25,900
Waiting time at 28.7° (orbits)	14	11	8	4	1	<1

Nevada Corporation's *Dream Chaser* which is based on the Russian BOR and NASA's HL-20 mid-performance lifting body (Hoey 1994; Thompson and Peebles 1999; Reed and Lister 1997), the wait times vary from 11 orbits or about 16.5 h to 8 orbits and about 12 h delay. The class of vehicles discussed in Chap. 3, in contrast, would have no wait times. They can return at any time, any location in the orbit they are in, and land in CONUS (Continental United States). The longest return would be if the spacecraft were directly overhead the landing site: the spacecraft would have to circumnavigate the *Earth* in space, that is, in one orbital period of about 1.5 h. The spacecraft hypersonic aerodynamic performance and its resultant glide performance are shown in Table 2.1 in terms of lateral range (LR) and down range (DR) together with the maximum waiting time.

The implication of commercial operational requirements is the need to be able to return to the landing site from any orbital location on the current orbit. That requires a high hypersonic lift-to-drag (*L/D*) ratio glider. The Space Shuttle orbiter had a hypersonic *L/D* of between 1.1 and 1.3, sufficient to land at its intended site after one missed orbit, or a 1500 nmi lateral range. The hypersonic *L/D* performance of the class of high-performing lifting bodies such as X-24B, FDL-7, and Model 176 has, as discussed in Chap. 3, hypersonic *L/D* values from 2.7 to 3.2, meaning they can land in CONUS from any position on a low Earth orbit (400 nautical miles or less). Reed shows on page 156 of (Reed and Lister 1997) the cross-range distances plotted against hypersonic *L/D* for several vehicles returning from orbit. He does notice that the flat-bottom "race-horse" vehicles, such as the X-24B and Hyper III, have the greatest cross-range capability. An updated figure is presented in Fig. 2.26, showing the superiority of the FDL delta concepts and their derivatives (Model 176) in achieving the goal of no waiting in orbit. With the lateral range determined by the hypersonic *L/D* ratio, that is, the ability to turn (generate lift) with a minimum drag penalty, the significance of a sufficiently high hypersonic *L/D* is obvious for the return-from-orbit requirement. With the lateral range (cross-range) be determined, the down range performance can now be established, that is, the glide range in a straight-ahead glide.

Hence, this class of spacecraft can have a scheduled launch and return capability that minimizes waiting time and, more importantly for commercial passengers and crew, that can return in an emergency without waiting time. The correlation of lateral range, LR (in nmi), hypersonic *L/D*, and the resulting down range, DR (in nmi) is given by Eqs. (2.2) and (2.3) below.

$$\mathrm{LR} = 1.667 + 68.016 \cdot \left(\frac{L}{D}\right) + 706.67 \cdot \left(\frac{L}{D}\right)^2 - 91.111 \cdot \left(\frac{L}{D}\right)^3 \tag{2.2}$$

$$\mathrm{DR} = 4866.6 + 4.70417 \cdot \mathrm{LR} \tag{2.3}$$

For continental Russia, the longitudinal span is twice that of the USA, hence the *L/D* requirement for any time return is less, at approximately $L/D \approx 1.7$. Lozino-Lozinskiy was a

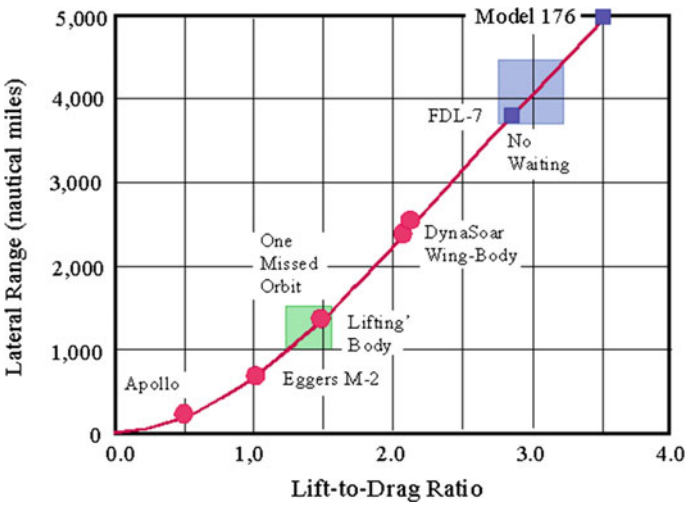

Fig. 2.26 Hypersonic lift-to-drag enables lateral (cross) range performance

strong advocate of the "no waiting emergency return," and his round-bottom BOR vehicles were capable of meeting the Russian *L/D* requirement (Lukashevich and Afanasiev 2009). Lozino-Lozinskiy had a forceful way of making his emergency return requirement much as Mr. McDonnell (Old Mac) had for the MOL support vehicle in 1964 (McDonnell 1999).

2.6.2 On-Orbit Operations in Near-Earth Orbit Enable the Second Step

The concept of the train yard as a center of operations for switching, long-haul train assembly, transfer of goods, refueling, and repair is applicable to a space marshaling facility. The remoteness of space parallels remote bases on Earth's surface, where the environment forces significant logistics operations to include propellant, cargo, repair parts, pilot accommodation, structures, and support items. The late Frederick (Bud) Redding formed a company, In-Space Operations Corporation (IOC), to exploit his orbital servicing and crew rescue vehicle *Space Cruiser* (Redding 2003). As originally conceived in 1980, the Space Cruiser was a low-angle conical hypersonic glider based on the McDonnell Douglas Model 122 (BGRV) experimental vehicle that was flown in 1966 (Hallion 2005). As initially conceived, the Space Cruiser had a length of 26 ft and could be folded to a length of 13.5 ft, see Fig. 2.27.

Redding adapted the design to incorporate an aft plug cluster engine configuration and storable propellants to create 13.3 kN (3000 lb) of thrust. The 4453 kg (10,000 lb) vehicle could perform a variety of missions using the 8 ft^3 forward payload bay and the 4 ft^3 aft payload bay. The Space Cruiser is capable of atmospheric entry and uses a small drogue parachute at Mach 1 followed by a multi-reefed parafoil to land safely on any flat surface. The Space Cruiser was intended to be operated by a pilot in an EVA suit (Griswold et al. 1982; Redding et al. 1983; Redding 1984). In 1983, Redding modified the configuration to an elliptical cross section which expanded the propellant quantity, as shown in a McDonnell Douglas Corporation trans-atmospheric vehicle (TAV) artist illustration from 1983, see Fig. 2.27. This particular configuration is based on a hypersonic glider research vehicle proposed to the US Air Force in 1964. It has sufficient volume and cross-range to act as a three-person rescue vehicle.

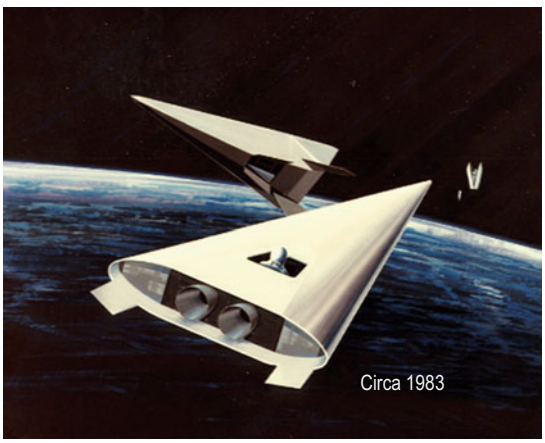

Fig. 2.27 "Bud" Redding's Space Cruiser launched from a transatmospheric vehicle to accomplish a satellite repair. The Space Cruiser is also able to serve as a three-person rescue vehicle

The Space Cruiser is a LEO service vehicle that can utilize the refueling station shown in Fig. 2.24. With its hypergolic propellant and small mass ratio, refueling was always a critical issue for the original Space Cruiser size. There were four basic tasks for the Space Cruiser as envisioned by Redding: (1) providing a one- or two-seat resource mover between spacecraft or orbital stations in close proximity; (2) providing a "Lifecraft" or emergency rescue vehicle; (3) providing a movable orbital workshop for repairing or maintaining nearby satellites; and (4) in the folded configuration, providing a camera mounted in the folded nose to act as a vehicle/satellite scanning system or an ad hoc reconnaissance vehicle free of the space station or shuttle.

For orbital transfer from low Earth orbits (LEO) to GSO and return, for collecting nonfunctional satellites in LEO for repair or disposal, for GSO refueling of sustained-use satellites, orbital busses, and tugs, there is a real need for a nuclear-powered tug. This nuclear-electric-powered tug can sustain in-orbit operations and maintain a functional orbital infrastructure, including space habitats, free-flying facilities, and power stations. In Chap. 5, several levels of space tug development are depicted using prior work of Dr. William Gaubatz, Tom Taylor, and "Bud" Redding. The most important determination is the quantity of propellant required (a) in LEO to implement the space infrastructure concepts represented in Figs. 2.23 and 2.24, and (b) to lift and accelerate the LEO propellant to low Earth orbit, unless both airbreathing launchers and nuclear-electric space propulsion are operationally available.

2.6.3 Earth-Moon System Enables the Third Step

The Earth-Moon system provides clear advantages which enable the next step to establish a solar system presence (Eckart 1999; Mendell 1985). Unlike artificial LEO orbital stations (MIR and ISS), the Moon as our natural space station is not devoid of indigenous resources, including water and gravity. Using Tom Stafford's report to Congress (Stafford 1991) as a data source on why we should return to

the Moon, the report summarizes the advantages of the Moon station compared to an Earth orbital station. It also shows the advantages of testing and evaluating human operations on a foreign, inhospitable planet before venturing far from Earth (possibly Mars), without the capability of easy and fast return. It also identifies the resources that can be obtained from the lunar surface and interior. With the discovery of water in the polar regions of the Moon in 2009, a clear incentive is provided to utilize the Moon as a resource depot for drinking water, fuel, and oxygen. A unit mass of liquid oxygen sent to LEO from the Moon may actually cost less than the same mass sent up from the Earth's surface. Mining of Helium-3 on the Moon could provide an energy source to power deep space exploration. Again, as in Earth orbit, the commercialization of sustained operations on the Moon is needed. Chapter 6 discusses Stafford's Congressional report and the need to return to the Moon.

2.6.4 Nuclear or High-Energy Space Propulsion Enables the Fourth Step

Nuclear or high-energy space propulsion is needed as a next step to explore the solar system. As discussed in Chap. 1, achieving much higher velocities in space compared to those velocities generated by practical rockets, requires high-energy and high-specific-impulse propulsion systems. Chapter 7 presents some specific systems that were under development or in conceptual formulation. Researchers at the high-energy particle research facilities speak of space-available energy in a different way than chemical propulsion engineers. If developments continue in our understanding of energy, we may actually be able to traverse the solar system nearly as quickly as the Earth–Moon system.

If someone had told Donald Douglas Sr. that just 35 years after the first DC-3 flew (first flight in 1935) a prototype supersonic transport would cross the Atlantic at Mach 2.0 (Concorde's first Atlantic crossing took place in 1971), he would have laughed in disbelief. In fact, he delayed the development of the DC-8 because he believed turboprops would hold the commercial market for over a decade before turbojets were commercially and economically practical. Nikola Tesla, before 1930, stated that with his electromagnetic energy transmitter he could power a base on Mars from Earth (the Russians have done it on an orbiting satellite). Leik Myrabo has done experiments on the laser powered vehicle LightCraft at Holloman Air Force Base, see Chap. 6. All these avenues are explored in the attempt to fulfill the need for a high-specific-impulse propulsion system. In planetary exploration, the *Holy Grail* is a propulsion system enabling a manned round trip to Mars in about 1 year; longer than that, cosmic radiation, solar flares, and re-adaptation to both Mars's and Earth's gravity may be lethal or crippling to the human crew. We need also to get to Pluto and the gas planets in a reasonable time. All of these systems can operate within the acceleration tolerances of the human being and spacecraft structures. For humans to be in a sustained acceleration much larger than $1g$ is probably untenable. Automatic, robotic spacecraft could accommodate instantaneous accelerations between 8 and $10g$ and sustained accelerations on the order of perhaps $3g$. This and other issues are explored and discussed in Chap. 7.

2.6.5 Very High-Energy Space Propulsion Enables the Fifth Step

Very high-energy space propulsion is essential for expanding our knowledge to nearby interstellar space, with fusion research eventually supplying the means. This would be simplified if we had an operational base on the Moon to mine helium-3, since in principle it would enable releasing thermonuclear energy with a minimum of neutronic radiation. Mastering of fusion, either steady or impulsive, to explore Galactic space would be an extremely ambitious next step, as distances are in the tens and hundreds of light-years. Even the closest stars are farther than a human lifetime away at current chemical rocket speeds, and even at fractional light speeds. This next step depends on the previous four and will probably not be realizable until they are accomplished. Nevertheless, it is possible to identify propulsion systems that can work and why and how they work. The difficulty in achieving even near light speed is the acceleration required, that is, by providing sufficiently large thrust. This is discussed in Chap. 8.

2.6.6 Light Speed-Plus Propulsion Enables the Sixth Step

This step requires an understanding of the physics of mass and inertia, both essential to reach speeds comparable to light speed or even above. If these are to be realized, then means to reduce or eliminate mass and inertia effects are likely required, unless the spaceship and its contents be flattened to a disk by the acceleration.

Light speed–plus propulsion is essential for expanding our knowledge to our Galaxy. Researchers can now theorize approaches for traveling at fractional light speed and even at greater than light speed based on General Relativity results. Our Galaxy is about 100,000 light-years in diameter and about 20,000 light-years thick at the center. It might contain up to 100 billion stars. The Earth is about 32,000 light-years from the center. Without the ability to travel in some sort of "hyperspace," as described in Chap. 1, the Galaxy is isolated

from our ability to explore it in any other way than by remote sensing. Except for our nearby galactic neighbors, our Galaxy is off-limits. The distances are almost not comprehensible. At 1000 times the speed of light, it would take 32 years for us to reach the galactic center.

Yet to consider super light speed is no more daunting than for the prior century researchers considering supersonic travel. There are concepts that are based on solid physics and some will be discussed in Chap. 9 in terms of what might be possible.

Bibliography

Ambrose, S. (2000) *Nothing Like It in the World*, Simon & Schuster, New York, November 2001.

Anon. (2015) "Declassified Manned Orbiting Laboratory (MOL) Records", National Reconnaissance Office, October 2015.

Anon. (2015) "Space Launch System at a Glance", NP-2015-09-83-MSFC, Marshall Space Flight Center, NASA, September 2015.

Anon. (1967) "A Study of Advanced Airbreathing Launch Vehicles with Cruise Capability", Lockheed Report IR 21042, Lockheed Aircraft Corporation, 1967.

Anon. (1966a) "Mission Requirements of Lifting Systems - Summary of Significant Results & Figures", McDonnell Aircraft Report B947, McAIR, prepared under NASA NAS 9-3562 (declassified 1970).

Anon. (1966b) "MA188-XAB Baseline Dual Mode Scramjet for the McDonnell Douglas Reusable Launch Vehicle Application", McAIR, Marquardt Letter to McAIR, 1966 (Confidential).

Baker, D. (1996) *Spaceflight and Rocketry—A Chronology*, Facts on File Publisher, January 1996.

Bartsev, S.I. and Okhonin, V.A. (1989) "The Algorithm of Dual Functioning (Back Propagation): General Approach, Versions and Applications", No. I07B, Preprint of Inst. of Biophysics SB AS, USSR Academy of Sciences, Siberian Branch, Krasnoyarsk, 1989.

Bilstein, R.E. (1980) "Stages to Saturn—A Technological History of the Apollo/Saturn Launch Vehicles", NASA SP-4206, NASA History Series, NASA, Washington DC, 1980.

Brewer, G.D. (1966) "Manned Hypersonic Vehicle", *Lockheed Horizons Magazine*, Issue 4, First Quarter, 1966.

Buran Site Director (1989) Discussion with P.A. Czysz during visit to Baikonur, April 1990.

Clark, P. (1988) *The Soviet Manned Space Program*, Salamander Books, London, November 1988.

Cook, N. (2001) *The Hunt for Zero Point*, Broadway Books, August 2003.

Czysz, P.A. and Little, J. (1993) "Rocket-Based Combined-Cycle Engine (RBCC)—A Propulsion Systems for the 21st Century", Paper AIAA-93-5096, presented at the *5th Aerospace Planes and Hypersonic Technologies* Conference and Exposition, Munich, Germany, 1993.

Davies, R.E.G. (1964) *A History of the World's Airlines*, Oxford University Press, December 1964.

Dickson, P. (2001) *Sputnik—The Shock of the Century*, Walker & Company, New York, 2001.

Draper, A.C., Buck, M.L. and Goesch, W.H. (1971) "A Delta Shuttle Orbiter", *Astronautics & Aeronautics*, Vol. 9, No. 1, January 1971, pp. 26–35.

Draper, A.C. and Sieron, T.R. (1991) "Evolution and Development of Hypersonic Configurations 1958–1990", Report WL-TR-91-3067, Flight Dynamics Directorate, Wright-Patterson Air Force Base, Ohio, September 1991.

Eckart, P. (Editor) (1999) *The Lunar Base Handbook—An Introduction to Lunar Base Design, Development, and Operations*, Space Technology Series, McGraw-Hill Publisher, 1999.

Evans, M. (2013) *The X-15 Rocket Plane—Flying the First Wings into Space*, University of Nebraska Press, 2013.

Godwin, R. (2003) Dyna-Soar: Hypersonic Strategic Weapons System, Apogee Books Space Series, Collector's Guide Publishing, July 2003.

Gorn, M.H. (2001) *Expanding the Envelope—Flight Research at NACA and NASA*, The University Press of Kentucky, 2001.

Griswold HR, Stein DS, Redding FW (1982) Integration of a Crewman into a high performance spaceplane. Paper SAE-820850, society of automation engineers, presented at the *12th intersociety conference on environmental systems*. San Diego, CA, Febr 1982.

Gubanov, V. (1984) Private communication with P.A. Czysz, 35th International Astronautical Federation Congress (IAC), Lausanne, Switzerland, 08–13 October 1984.

Gubanov, V. (1988) Private communication with P.A. Czysz, 39th International Astronautical Federation Congress (IAC), Bangalore, India, 08–15 October 1988.

Gubanov, V. (1998) Photographs from Gubanov in Figure 2.11, Private communication with P.A. Czysz, 49th International Astronautical Federation Congress (IAC), Melbourne, Australia, 28 September–02 October 1998.

Hall, R.D. and Shayler, D.J. (2007) *Soyuz—A Universal Spacecraft*, Springer-Praxis Publisher, 2007.

Hallion, R.P. (2005) "The History of Hypersonics: Or, 'Back to the Future—Again and Again'", AIAA Paper AIAA-2005-0329, presented at the *43rd AIAA Aerospace Sciences Meeting*, Reno, NV, 10–13 January 2005.

Hannigan, R.J. (1994) *Spaceflight in the Era of Aero-Space Planes*, Krieger Publishing Company, 1994.

Harford, J. *Korolev: How One Man Masterminded the Soviet Drive to Beat America to the Moon*, J. Wiley Publisher, March 1997.

Hendrickx, B. and Vis, B. (2007) *Energiya-Buran—The Soviet Space Shuttle*, Springer-Praxis Publisher, 2007.

Hoey, R.G. (1994) "Testing Lifting Bodies at Edwards", PAT Projects, Inc., in: Air Force/NASA Lifting Body Legacy History Project, see as well Air Force Report AFFTC-TR-85-11 (June 1985) Lancaster, CA, 1994.

Houchin, R.F. (2006) US *Hypersonic Research and Development — The Rise and Fall of Dyna-Soar*, 1944–1963, Space Power and Politics Series, Routledge Publisher, September 2006.

Hunt, D.R. (1998) "Reusing Space Shuttle External Tanks", Master of Aeronautical Science Thesis, Embry-Riddle Aeronautical University, September 1998.

Ingells, D.J. (1979) *The McDonnell Douglas Story*, Aero Publishers Inc., 1979.

Jenkins, D.R. (2001) *Space Shuttle—The History of the National Space Transportation System – The First 100 Missions*, 3rd Edition, Midland Publishing, 2001.

Jenkins, D.R. (2007) "X-15: Extending the Frontiers of Flight", NASA SP-2007-562, NASA, 2007.

Jenkins, D.R. and Landis, T.R (2003) *Hypersonic—The Story of the North American X-15*, Specialty Press, North Branch, MN, 2003.

Karashtin, V.M., Zemtsov, I.V. and Shulman, L.B. (1990) "Technology of Rocket and Space Pre-Launch Operations Control Systems Development", paper IAF-90-186, presented at the 41st *International Astronautical Federation Congress*, Dresden, Germany, 06–12 October 1990.

Kirkham, F.S., Jones, R.A., Buck, M.L. and Zima, W.P. (1975), "Joint USAF/NASA Hypersonic Research Aircraft Study", AIAA Paper AIAA-75-1039, presented at the *25th AIAA Aircraft Systems and Technology Meeting (ASM)*, Los Angeles, California, August 1975.

Lardier, C. and Barensky, S. (2013) *The Soyuz Launch Vehicle—The Two Lives of an Engineering Triumph*, Springer-Praxis Publisher, 2013.

Launius, R.D. and Jenkins, D.R. (Editors) (2002) *To Reach the High Frontier—A History of U.S. Launch Vehicles*, The University Press of Kentucky, November 2002.

Legostayev, V. (1984) Private communication with P.A. Czysz, *35th International Astronautical Federation Congress* (IAC), Lausanne, Switzerland, 08–13 October 1984.

LLegostayev, V. and Gubanov, V. (1985) Private communication with P.A. Czysz, 36th Congress of the International Astronautical Federation, European Space Conference, Stockholm, Sweden, 07–12 October 1985.

Lockett, B. (2009) *Balls Eight—History of the Boeing NB-52B Stratofortress Mothership*, LockettBooks, July 2009.

Loftin, L.K. (1985) "Quest for Performance—The Evolution of Modern Aircraft", NASA SP-468, NASA History Office, NASA, January 1985.

Lozino-Lozinskiy, G.E. (1989) "BURAN: Its Creation and Prospects of Its Usage", paper presented at the *40th Congress of the International Astronautical Federation*, Malaga, Spain, 7–12 October 1989.

Lozino-Lozinskiy, G.E. (1990) Private communication with P.A. Czysz and brief concerning BOR and Buran vehicles, 41st International Astronautical Federation Congress (IAC), Dresden, Germany, 06–12 October 1990.

Lukashevich, V. and Afanasiev, I. (2009) Space Wings, 2009 (in Russian).

Maita, M., Mori, T. and Ohkami, Y. (1991) "System Studies on STTO Space Plane", AIAA Paper AIAA-91-5012, presented at the *3rd International Aerospace Planes Conference*, Orlando, Florida, 03-05 December 1991.

McDonnell, S.N. (1999) "This is Old Mac Calling All the Team", Sanford N. McDonnell and McDonnell Douglas Corporation, 1999.

Mendell, W.W., editor (1985) Lunar Bases and Space Activities of the 21st Century, Lunar and Planetary Institute.

Miller, J. (2001) *The X-Planes—X-1 to X-45*, 3rd Edition, Midland Publishing, Hinkley, UK, 2001.

Miller, J.K. (1995) *Lockheed Martin's Skunk Works: The Official History*, Revised Edition, Midland Counties Publications, December 1995.

Neyland, V.Y. (1988) "Engineering Problems and Methods of Preflight Development of Orbiters", unpublished TsAGI report, Moscow [in Russian], 1988.

Pike, J. (1977) "Minimum Drag Bodies of Given Length and Base Using Newtonian Theory'', *AIAA Journal*, Vol. 15, No. 6, June 1977, pp. 769–770.

PlPlokhikh, V.P. (1983) Private communication with P.A. Czysz, 34th IAF-1983, International Astronautical Congress, 10–15 October 1983.

Plokhikh, V.P. (1989) "Sensitivity Analysis of Single-Stage-to-Orbit Reusable Vehicle Parameters", paper IAF-89-223, presented at the 4*0th IAF-1989, International Astronautical Congress*, Malaga, Spain, 07–13 October 1989.

Reed, R.D. and Lister, D. (1997) *Wingless Flight—The Lifting Body Story*, NASA-SP-4220, NASA, Washington DC, 1997.

Redding, F.W. (2003) "Hypersonic and Orbital Vehicles System", US 6530543 B2, U.S. Patent, March 2003.

Redding, F.W. (1984) "Spaceplane Technology and Research (STAR!)", Final Report DCS-11540, DARPA Order 4913, DCS Corporation, August 1984.

Redding, F.W. et al. (1983) "Spaceplane Examination", SRI International, Final Report, Contract FO4701-8IK-0001, Managed by the Air Force Space Division, Sponsored by DARPA Strategic Technology Office, 1983.

Rich, B.R. and Janos, L. (1993) *Skunk Works: A Personal Memoir of My Years at Lockheed*, Little Brown & Co, October 1993.

Rose, B. (2008) *Secret Projects: Military Space Technology*, Midland Publisher, September 2008.

Schweikart, L. (1998) *The Hypersonic Revolution: Case Studies in the History of Hypersonic Technology; Volume III: The Quest for the Orbital Jet: The National Aero-Space Program (1983–1995)*, 2nd Printing, Volume III, Air Force History and Museum Program, 1998.

Stafford, T. (1991) Editor "America on the Threshold—America's Space Exploration Initiative", Synthesis Group, Space Exploration Initiative, Chairman's Report to Congress, United States Government Printing, Washington DC, June 1991.

Stephens, R.R. (1965) "Mission Requirements of Lifting Systems—Engineering Aspects", Vol. I: Condensed Summary, and Vol. II: Mission Analysis - Spacecraft Selection—Performance Analysis", McDonnell Aircraft Company Report B831 for NASA Manned Spacecraft Center, contract NAS-9-3562, 1965.

Stine, G.H. (1991) *ICBM—The Making of the Weapon that Changed the World*, Orion Books, New York, 1991.

Taylor, T.C. (2000) "Commercial Space Habitation, 2000", Global Outpost, Inc., Lunar Development Conference: Return to the Moon II, Las Vegas, NV, 20–21 July 2000.

Tesla, N. (2014) *My Inventions: The Autobiography of Nikola Tesla*, Snowball Publishing, 2014.

Thompson, M.O. and Peebles, C. (1999) *Flying Without Wings—NASA Lifting Bodies and the Birth of the Space Shuttle*, Smithsonian Institution Press, April 1999.

Commercial Near-Earth Space Launcher: Understanding System Integration

3

Before there can be any space exploration, there must first be an ability to reach low Earth orbit (LEO) from Earth's surface. The required speed for LEO is given in Table 3.1. For all practical purposes, 100 nautical mile and 200-km orbital altitudes are equivalent.

Whether it is an expendable launcher or a sustained-use, long-life launcher, the launcher must reach the same orbital speed to achieve LEO. From here, the spacecraft can move to a higher orbit, change orbital planes, or do both. Reaching LEO is *the* crucial step because, as indicated in Fig. 2.5, the current system of launchers is representative of the Conestoga wagons that moved pioneers in the USA in just one direction: *west*. There is no record of any wagon returning to the *east*. The cost of traveling west was not reduced until the railroad transportation system was established that could (1) operate with a payload in both directions and (2) operate frequently on a scheduled basis. Both directions are key to establishing commercial businesses that ship merchandise west to be purchased by western residents, and raw materials and products east to be purchased by eastern residents. The one-way Conestoga wagons could never have established a commercial flow of goods.

Scheduled frequency is the key to making the shipping costs affordable so the cargo/passenger volume matches or even exceeds capacity. The same is true of course for commercial aircraft and as well for commercial space. In this context, it is worthwhile mentioning that the November 18, 2002, issue of *Space News International* presented an interview with the former NASA Administrator Sean O'Keefe that stated the projected cost for the five Space Shuttle launches per year had been US$3.2 billion before their retirement. That reduces to about US$29,000 per pound of payload delivered to LEO; for some missions, that cost could rise to US$36,000 per pound. The article stated that an additional flight manifest will cost between 80 and 100 million US$ per flight. If the Shuttle fleet would have sustained 10 flights per year, the payload cost would reduce to US$16,820 per pound. If the flight rate would have been two a month, the cost would be US$9690 per pound. *It is really the flight rate* that determines payload costs.

Figure 3.1 shows that the historical estimates of payload cost per pound delivered to orbit were correctly estimated and known to be a strong function of fleet flight rate for over 40 years. In the same figure, there are five estimates shown covering the time period from 1970 to Sean O'Keefe's data in 2002. In the 1971 AIAA *Aeronautics & Astronautics* article (Draper et al. 1971), the projected total costs for a 15-year operating period were given as a function of the number of vehicles. The payload costs were determined with the information provided in the article. This is shown as the solid red line marked Draper et al. One of the students in the author's aerospace engineering design class obtained the cost of crew, maintenance, and storage for 1 year of operation of a Boeing 747 from a major airline. The student used that data to establish for a Boeing 747 operations cost in maintenance, fuel, and personnel for 1-year operation of three aircraft with one in 1-year maintenance. The annual costs are fixed, as they would be for a government operation; then, assuming that same Boeing 747 operating with Shuttle payload weights and flight frequency yields a result shown in Fig. 3.1 as the line of green squares marked B 747. *These results show an infrequently used Boeing 747 fleet is as costly as it was operating the now retired Space Shuttle*.

This result shows that the airframe or system "technology" is not the issue. The real issue is the launch rate. This is an important finding, as most of the current new launch vehicle proposals are said to reduce payload costs through "new and advanced technology"—overall a statement that may not be correct. For the McDonnell Douglas TAV effort in 1983, H. David Froning and Skye Lawrence compared the cost per pound of payload delivered to LEO for an all-rocket hypersonic glider/launcher and a combined-cycle launcher (rocket-airbreather) operated as an airbreather up to Mach 12. Their analysis showed that the total life cycle costs for both systems were nearly identical, the vast difference in technology notwithstanding, and it was the fleet fly rate that made

P.A. Czysz et al., *Future Spacecraft Propulsion Systems and Integration*,
Springer Praxis Books, DOI 10.1007/978-3-662-54744-1_3

Table 3.1 Low earth orbital altitudes and speeds

Altitude (km)	185.2	200.0	370.4
Speed (m/s)	7794.7	7785.8	7687.1
Altitude (nautical miles)	100	108	200
Speed (ft/s)	25,573	25,544	25,220

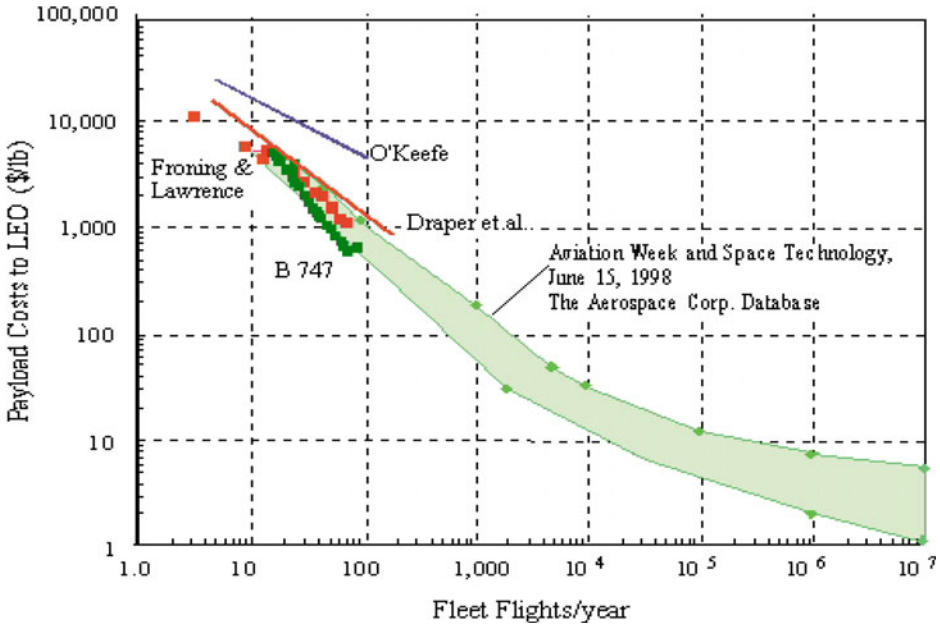

Fig. 3.1 Comparison of payload costs to orbit, from 1971 to 2003

the payload cost difference. The Froning and Lawrence data is the line of red squares. Jay Penn and Dr. Charles Lindley prepared in 1988 an estimate for a two-stage-to-orbit (TSTO) launcher that was initially an all-hydrogen vehicle, which then evolved into a kerosene-fueled first stage and a hydrogen-fueled second stage. Liquid oxygen was the oxidizer in all cases. They examined a wide spectrum of cost drivers such as insurance, maintenance, and vehicle costs; the study was published in *Aviation Week and Space Technology* in June 1998. This is shown in Fig. 3.1 as the light green area curve. Their analysis merges into the three previously discussed analyses. At the fly rate of a commercial airline fleet, the kerosene-fueled TSTO payload costs are in the 1–10 US$ per pound of payload. NASA Administrator O'Keefe's Space Shuttle data, published in *Space News International*, is shown as a solid blue line. The Space Shuttle data represents the highest payload cost data set, as shown in Fig. 3.1. As a point of interest, Dr. Charley Lindley, then a young California Institute of Technology Ph.D. graduate, worked for The Marquardt Company on scramjet propulsion for the first Aerospace Plane. The bottom line is, as stated by Penn and Lindley, "*... It is not the technology; it is the fly rate that determines payload costs. ...*".

Thus, one way to improve the launch cost issue would have been to schedule the Shuttle to operate more frequently or purchase surplus Energia launchers at the time. Given the stated NASA goals of US$1000 to US$l00 per pound of payload delivered to LEO by 2020, the solution is launch rate, not specifically or exclusively advanced technology. It is not specifically a technology issue because operational life and number of flights are design specifications. Clearly, operational life and number of flights do indeed govern durability, not necessarily technology. Translating the Penn and Lindley data into a single-stage-to-orbit (SSTO) all-hydrogen fuel launcher, the distribution results are shown in Fig. 3.2. Six categories of cost were adjusted for a SSTO launcher from the Penn and Lindley data, namely *propellant*, *infrastructure*, *insurance*, *maintenance*, *production,* and *RDT&E* (research, development, technology, and engineering). The costs of hydrogen fuel and oxygen oxidizer are essentially constant with flight rate, as they are new (recurring) for each flight. The one cost that changes the most is the amortized infrastructure cost. However, this cost and the other four costs (insurance, maintenance, production, and RDT&E) do not diminish until high commercial aircraft fleet fly rates are achieved. The corollary is that propellant (in this case hydrogen, not kerosene) does not become the primary cost until fleet flight rates in excess of 10,000 flights per year are achieved. This and larger fleet flight rates are achieved by commercial airlines, but are probably impractical in the foreseeable future for space operations.

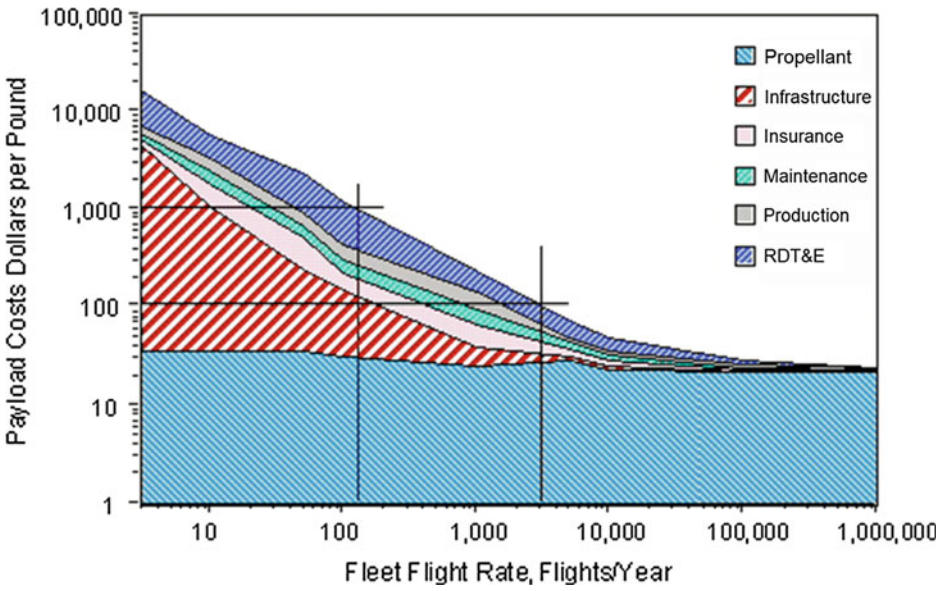

Fig. 3.2 Payload costs per pound based on fleet flight rate, after Penn and Lindley

From the Manned Orbiting Laboratory (MOL) (Anon 2015) requirements given in Chap. 1, near-future fleet flight rates will be in the hundreds per year, not hundreds of thousands. The NASA goal of US$1000 per pound can be met if the fleet launch rate is about 130 per year or 2.5 launchers per week. For a fleet of seven operational aircraft, that amounts to about 21 launches per year per launcher, assuming an availability rate of 88%, that is, about one flight every two weeks for an individual aircraft. At this point, the five non-propellant costs are about 30 times greater than the propellant costs. The NASA goal of US$l00 per pound to LEO requires about a 3000 fleet flight per year rate and a larger fleet. Given 52 weeks and a fleet of 33 launchers with an 88% availability rate, the weekly flight rate is 58 launches per week, yielding a fleet flight rate of 3016 flights per year. Such a fly rate demands an average of 8.3 flights per day! For this scenario, the five non-propellant costs are about three times greater than the propellant costs, that is, in the realm of the projected space infrastructure as shown in Fig. 2.23. Commercial aircraft exceed 1 million flights per year for the aircraft fleet. Consequently, the cost for commercial transports is primarily determined by fuel cost, not by individual aircraft cost. Then, whatever the future launcher system, for the space infrastructure envisioned by Dr. William Gaubatz in Fig. 2.23 to ever exist, the payload cost to LEO must be low enough due to a high enough launch rate to permit that infrastructure to pay its way to be built.

3.1 Missions and Geographical Considerations

The two main missions of interest, including civil and military considerations, are as follows: (1) hypersonic transportation in which cruise is a dominant mode and (2) orbital launch vehicles. The high-speed vehicle obviously has to takeoff from Earth, and either the vehicle or some part of it should land on Earth. Thus, the missions include the entire speed range from takeoff to cruise and to landing, or from launch to cruise and to orbit as desired in different vehicles. Then, an important question in the case of an accelerator vehicle for orbital launch is whether it should be the SSTO, the TSTO, or the multi-stage-to-orbit (MSTO) system. This question has to be examined in terms of two factors: (1) energy availability utilization and the technological needs, and (2) mission and geographical constraints. The first factor is addressed in Chap. 4. The second factor is briefly considered below.

It is well known that a typical velocity for an orbital launch vehicle to reach is about 7–8 km/s, and the geostationary transfer orbit (GTO) plane is about 7° off of the equator. In determining whether the required velocity is to be reached with one or more stages, the relation between a desired launch site and the GTO plane must be taken into account. In addition, several other considerations may be significant: (1) whether a horizontal or a vertical launch is

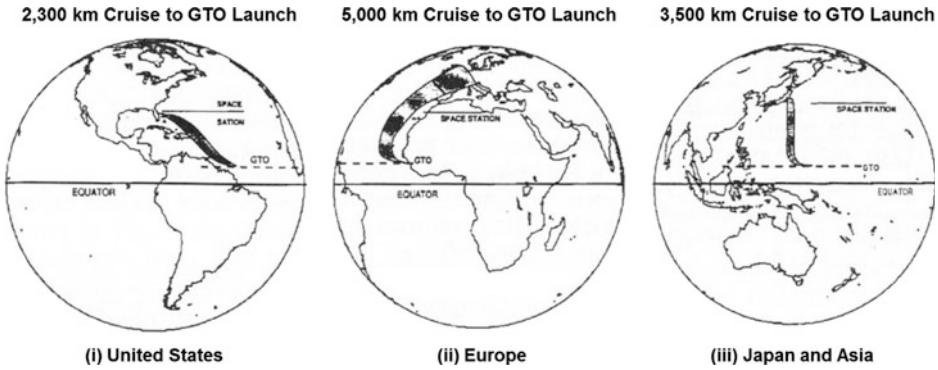

Fig. 3.3 Space launch trajectory

desired; (2) what type of landing is desired; for example, conventional aircraft-type landing; (3) whether the vehicle is required to place a spacecraft, for example, at an altitude that is suitable for rendezvous with an already available orbiter and to provide a significant increment in velocity or altitude; and (4) other uses to which the first stage of a multistage vehicle can be adapted, for example, a cruise-type hypersonic vehicle in a lower Mach number range.

One can examine the implications of those considerations for four typical geographical units on Earth: (1) a western European country, (2) Russia, (3) Japan, and (4) the USA. It may be pointed out that the extent of land in the Soviet Union is the largest among those. Also, China, India, and Indonesia are located favorably with respect to the GTO plane, with the latter two countries actually including land at 7° North latitude, see Fig. 3.3 (China is actually building a launching facility on the island of Hainan, on the Tonkin gulf). Heuristic reasoning then yields the following conclusions, based on allowing a flight of about 3000-km range between the launch site and the location of the GTO plane:

(1) A TSTO configuration may prove advantageous to European nations desiring horizontal launch and conventional landing capability.
(2) In the case of the USA and the cited Asian nations, either a SSTO or a TSTO system is practicable.
(3) A MSTO system provides no additional advantages compared to a TSTO system based on geographical considerations.

3.2 Energy, Propellants, and Propulsion Requirements

In today's space initiatives, there appears to be only one propulsion system of choice, the liquid or solid rocket. In fact, since the early 1950s a wide variety of space launcher propulsion systems concepts have been built and tested. These systems had one goal that of reducing the carried oxidizer weight, so a greater fraction of the gross weight could be payload. Another need was for frequent, scheduled launches to reduce the costs required to reach LEO from the surface of Earth. Without that frequency, launches would remain a one-of-a-kind event instead of a transportation infrastructure. Figures 3.4 and 3.5 give two representations for the SSTO mass ratio (weight ratio) to reach a 100 nautical mile orbit (185 km) with hydrogen for fuel.

In Fig. 3.4, the mass ratio is a function of the maximum airbreathing Mach number. Six classes of propulsion systems are indicated: (1) rocket-derived, (2) airbreathing rocket, (3) KLIN cycle, (4) ejector ramjet/scramjet, (5) scram-LACE, and (6) air collection and enrichment system (ACES). These and others are discussed in Chap. 4 in detail. The trend clearly shows that to achieve a mass ratio significantly less than rocket propulsion (about 8.1), an airbreathing Mach number of 5 or greater is required. This can be calculated by the equations that follow. For the gross takeoff weight, we obtain:

$$W_{\mathrm{TOGW}} = W_{\mathrm{R}} \cdot W_{\mathrm{OWE}} \tag{3.1a}$$

$$W_{\mathrm{TOGW}} = W_{\mathrm{OWE}} + W_{\mathrm{ppl}} \tag{3.1b}$$

$$W_{\mathrm{TOGW}} = W_{\mathrm{OWE}} + W_{\mathrm{fuel}} \cdot \left(1 + \frac{O}{F}\right) \tag{3.1c}$$

The weight ratio is obtained with

$$W_{\mathrm{R}} = \frac{W_{\mathrm{TOGW}}}{W_{\mathrm{OWE}}} \tag{3.2a}$$

$$W_{\mathrm{R}} = 1 + \frac{W_{\mathrm{ppl}}}{W_{\mathrm{OWE}}} \tag{3.2b}$$

$$W_{\mathrm{R}} = 1 + \frac{W_{\mathrm{fuel}}}{W_{\mathrm{OWE}}} \cdot \left(1 + \frac{O}{F}\right) \tag{3.2c}$$

For $(W_{\mathrm{R}} \neq 1)$, we obtain the following expressions:

$$(W_{\mathrm{R}} - 1) = \frac{W_{\mathrm{ppl}}}{W_{\mathrm{OWE}}} \tag{3.3a}$$

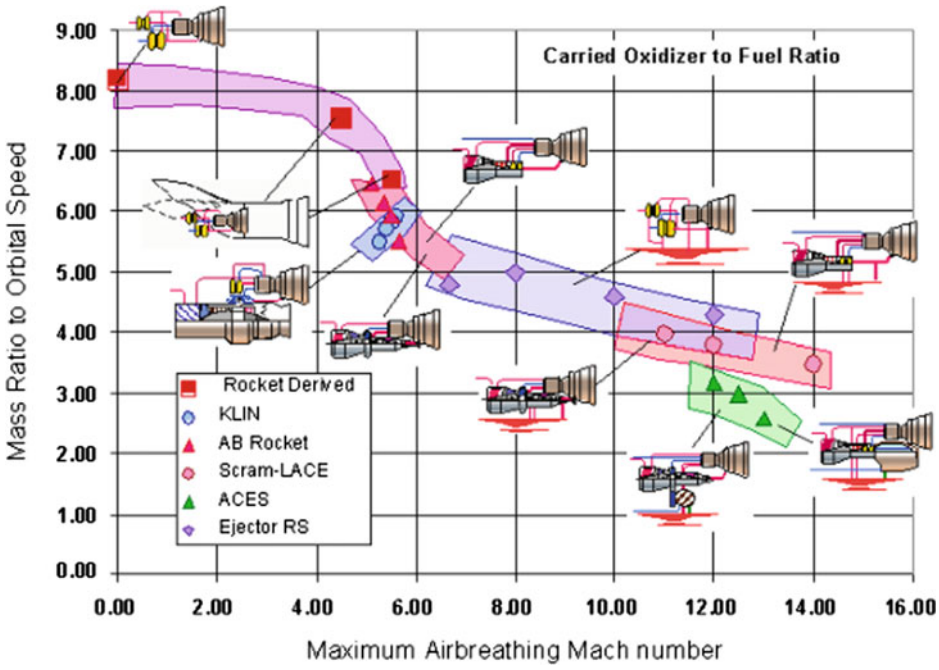

Fig. 3.4 The weight ratio to achieve a 100 nautical mile orbit decreases as maximum airbreathing Mach number increases

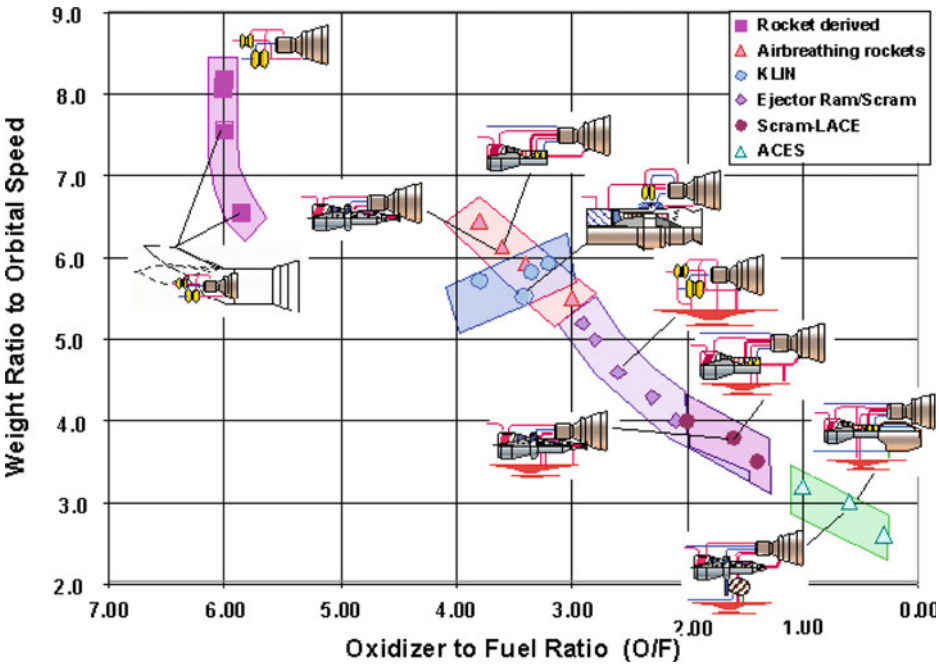

Fig. 3.5 The less oxidizer carried, the lower the mass ratio

$$(W_R - 1) = \frac{W_{fuel}}{W_{OWE}} \cdot \left(1 + \frac{O}{F}\right) \qquad (3.3b)$$

with

$$\frac{W_{fuel}}{W_{OWE}} = \frac{(W_R - 1)}{\left(1 + \frac{O}{F}\right)} \qquad (3.4)$$

where

W_{TOGW} = takeoff gross weight

$W_{OWE} = W_{fuel} + W_{empty}$ = operating weight empty

$\frac{O}{F}$ = oxidizer-to-fuel ratio

$$W_R = \frac{W_{TOGW}}{W_{OWE}} = \text{weight ratio} = \text{mass ratio}$$

Consequently, the weight ratio, hence the takeoff gross weight, is a direct result of the propellant weight with respect to the operational weight empty (W_{OWE}). The propellant weight is a direct function of the oxidizer-to-fuel ratio (O/F). In Fig. 3.5, the mass ratio is a function of the carried oxidizer-to-fuel ratio. Note that in Fig. 3.4, the mass ratio curve is essentially continuous, with an abrupt decrease at about Mach 5. In Fig. 3.5, the oxidizer-to-fuel ratio is essentially constant for the rocket-derived propulsion (about 6). There is a discontinuity in the oxidizer-to-fuel ratio curve between rocket-derived propulsion (value = 6) and where airbreathing rockets begin, at a value of 4. Based on the definition of fuel weight to W_{OWE} given by Eq. (3.4), the values from Fig. 3.4 result in a fuel weight-to-W_{OWE} ratio of approximately 1. That is, for all of these hydrogen-fueled propulsion systems, the fuel weight is approximately equal to the overall launcher weight when empty (W_{OWE}). The mass ratio is decreasing because the oxidizer weight is decreasing as a direct result of the oxidizer-to-fuel ratio. Consequently, an all-rocket engine using hydrogen fuel can reach orbital speed and altitude with a weight ratio of 8.1. An airbreathing rocket (AB rocket) or KLIN cycle can do the same with a weight ratio about 5.5. A combined-cycle rocket/scramjet with a weight ratio of 4.5 to 4.0, and an ACES needs 3.0 or less. Clearly, an airbreathing launcher has the potential to reduce the mass ratio to orbit by one-half (50%). That fact results in a significantly smaller launcher, both in weight and in size.

What that means is that, for a 100 t vehicle with its 14 t payload loaded, an all-rocket requires a gross weight of 810 t (710 t of propellant) and a 1093 t (10.72 MN) thrust propulsion system. With the oxidizer-to-fuel ratio reduced to 3.5, the gross weight is now 600 t (500 t of propellant) requiring a smaller 810 t (7.94 MN) thrust propulsion system. If the oxidizer-to-fuel ratio can be reduced to 2, then the gross weight becomes 200 t (100 t of propellant) resulting in a much smaller 270 t (27 kN) thrust propulsion system. For the same 810 t gross weight launcher with an oxidizer-to-fuel ratio propulsion system of 2, the vehicle weight becomes 405 t with a 67 t payload.

SSTO is shown because it requires the least launcher resources to reach LEO. Hydrogen is the reference fuel because of the velocity required for orbital speed: Any other fuel will require a greater mass ratio to reach orbit. A TSTO launcher will require two launcher vehicles, and it can have a different mass ratio to orbit (depending on fuel and staging Mach number), but the effect of increasing top airbreathing speed is similar. Since the ascent to orbit with a two-stage vehicle is in two segments, the lower-speed, lower-altitude segment might use a hydrocarbon fuel rather than hydrogen. The question of SSTO versus TSTO is much like the National Aerospace Plane (NASP) versus the Interim HOTOL arguments. The former is very good at delivering valuable, fragile cargo and crew to space complexes, while the TSTO with the option of either a hypersonic glider or a cargo canister can have a wide range of payload types and weights delivered to orbit. It is important to understand that they are not mutually exclusive. In fact, in all of the plans from other countries and in those postulated by Dr. William Gaubatz, both SSTO and TSTO strategies were specifically shown to have unique roles.

3.3 Energy Requirements to Change Orbital Altitude

Having achieved LEO, the next question is the energy requirements to change orbital altitude. The orbital altitude of the International Space Station (ISS) is higher than the nominal LEO altitude by some 500 km, so additional propellant is required to reach ISS altitude. The ISS is also at a different inclination than the normal US orbits (51.5° instead of 28.5°), and the inevitable increment in propellant requirement will be discussed in Chap. 5 when describing maneuvering in orbital space. As orbital altitude is increased, the orbital velocity required decreases, with the result that the orbital period is increased. However, because the spacecraft must first do a propellant burn to accelerate to the elliptical transfer orbit speed, and then it must do a burn to match the orbital speed required at the higher altitude, it takes significant energy expenditure to increase orbital altitude. Figure 3.6 shows the circular orbital speed required for different orbital altitudes up to the 24-h period GSO at 19,359 nautical miles and 10,080 ft/s (35,852 km and 3072 m/s). Figure 3.7 shows the circular orbital period as a function of orbital altitude, and at GSO, the period is indeed 24 h. Translating this velocity increment requirement into a mass ratio requirement calls for specifying a propellant combination. The two propellant combinations most widely used in space are the hypergolic nitrogen tetroxide/unsymmetrical dimethyl-hydrazine and hydrogen/oxygen (see Table 1.5 in Chap. 1).

The hypergolic propellants are room-temperature liquids and are considered storable in space without any special provisions. Hydrogen and oxygen are both cryogenic and require well-insulated tanks from which there is always a small discharge of vaporized propellants. Both the USA and Russia have experimented with magnetic refrigerators to condense the vaporized propellants back to liquids and return them to the storage tanks. The author (P.A. Czysz) saw the magnetic refrigerator to be used on Buran for all hydrogen/oxygen propellant maneuvering and station-keeping systems, had Buran continued development.

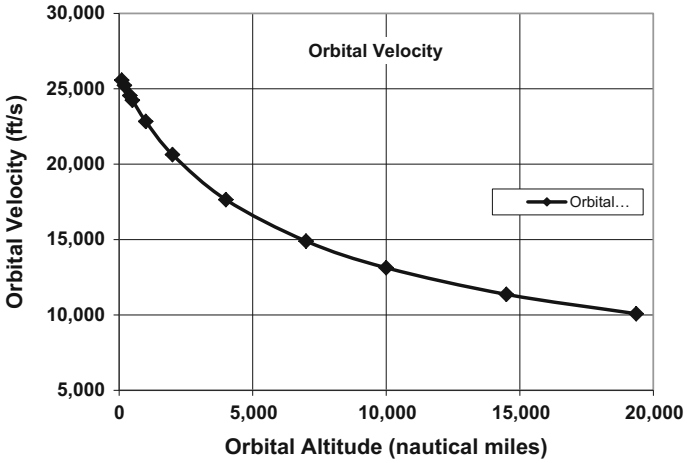

Fig. 3.6 Orbital velocity decreases as altitude increases

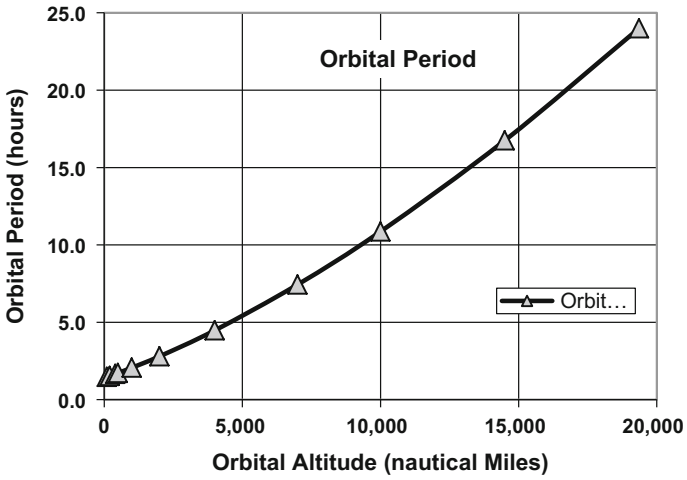

Fig. 3.7 Slower orbital speed means longer periods of rotation

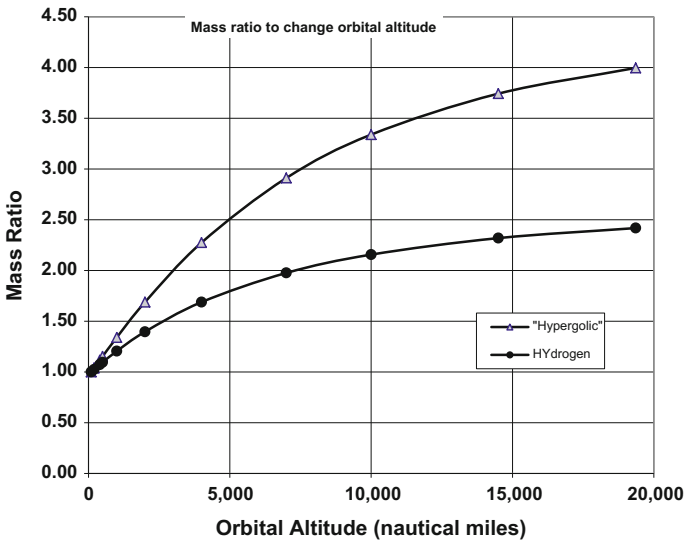

Fig. 3.8 To achieve higher orbit requires additional propellant

The resulting mass ratios for the two hypergolic propellants are shown in Fig. 3.8. The propellant for this orbital altitude change must be carried to orbit from Earth, as there are no orbital fueling stations now in orbit (see Fig. 2.23 for future possibilities). Consequently, if the weight of the object to be delivered to higher orbit is one unit, then the mass of the

system in LEO times the orbital altitude mass ratio is the total mass of the system required to change altitude.

To achieve GSO from LEO with hypergolic propellants, the mass ratio is 4, and for hydrogen/oxygen, it is 2.45. As an example, a 4.0 t satellite to GSO requires orbiting into LEO a *16.0 t spacecraft as an Earth launcher payload*. If that payload represents a 14% fraction of the launcher empty weight, then the launcher empty weight is 114.3 t. With the typical mass ratio to reach LEO of 8.1 for an all rocket system, the total mass at liftoff then becomes 925.7 t. Hence, it takes about 57.8 t of an all rocket launch vehicle to put 1 t in LEO, and 231 t of the same all rocket vehicle to put 1 t in GSO.

To achieve GSO from LEO with hydrogen/oxygen propellants, the mass ratio is 2.45. Consequently, a 4.0 t satellite to GSO requires orbiting into LEO a *9.8 t spacecraft as an Earth launcher payload*. If that payload represents a 14% fraction of the launcher empty weight, then the launcher empty weight is 70.0 t. For an ejector ram/scramjet-powered launcher (an airbreather) that flies to Mach 12, the mass ratio to reach LEO is 4.0 and the total mass at liftoff is 280.0 t. Hence, it takes about 28.6 t of launch vehicle to put 1 t in LEO for an ejector ram/scramjet-powered launcher that flies to Mach 12 as an airbreather, and about 70 t of the same ejector ram/scramjet-powered vehicle to place 1 t in GSO.

The advantage of airbreathing propulsion is that it requires a launcher that has an empty weight 39% less than the rocket launcher, and a gross takeoff weight that is 70% less for the same payload. This primary reason is rather obvious, since the airbreathing launcher carries some 210 t of propellant rather than the 811 t of propellant the all-rocket carries to achieve LEO speed and altitude; it does not use the large mass of oxidizer needed by an all-rocket system, replacing most of it with external air. The advantage of airbreathing propulsion is that less propellant and vehicle resources are required.

3.4 Operational Concepts Anticipated for Future Missions

For current concepts of expendable systems, the choice of the cylindrical configuration is practical: the solid boosters of the US Space Shuttle (STS) were indeed recovered off the Florida shore after separating at low Mach number. However, for reusable, long-life, and sustained-use vehicles, the requirements for glide range become important enough to differently shape the configuration of the launcher and launcher components.

As discussed in Chap. 2, the first example is that of a more conventional launcher designed from the start for 100% recoverable elements, and 80 flights between overhaul and refurbishment. Information about this launcher comes from a briefing on Energia that V. Legostayev and V. Gubanov supplied to one of the authors (P.A. Czysz) concerning the Energia operational concept (designed but never achieved, as Energia was launched twice from 1987 to 1988). Energia was a Soviet rocket designed by NPO Energia to serve as a heavy-lift expendable launch system as well as the booster for the Soviet/Russian Buran spacecraft program. The second example is that of a hypersonic glider and launcher system that was intended to operate over 200 launches before scheduled maintenance. This is from work from one of the authors' (P.A. Czysz) experience at McDonnell Douglas Corporation, which includes the hypersonic cruise vehicle work done for the NASA-sponsored *Hypersonic Research Facilities Study* (HyFAC) in the 1965–1970 time period (at McDonnell Aircraft Company), and the hypersonic space reentry glider work based on the USAF Flight Dynamic Laboratory FDL-7 glider series, the McDonnell Douglas *Model 176* MOL crew and resource resupply and rescue vehicle (at McDonnell Douglas Astronautics Company).

Recapitulating the observations from Chap. 2, Fig. 2.10 shows the goals of the Energia operational concept with all its components recoverable for reuse. The sketch was a result of discussion the author P.A. Czysz had with Viktor Legostayev and Vladimir Gubanov at several opportunities. The orbital glider, Buran, was a fully automatic system that was intended to be recovered at a designated recovery runway at the Baikonur space launch facility at Leninsk, Kazakhstan. (In order to confuse Western intelligence, the Baikonur site was always called Tyuratam, or coal mine, which is the first facility encountered when directed to Baikonur.) Buran had a very different operational envelope than the US Space Shuttle. In a briefing from Vladimir Yakovlich Neyland, when he was Deputy Director of TsAGI, the specific operational design parameters were presented. Among features of interest, Buran's entry glide angle-of-attack was said to be between 10° and 15° less compared to the Space Shuttle, resulting in an overall improved reentry lift-to-drag ratio. This is because Buran's glide range for one missed orbit was intended to be larger than that of the US Space Shuttle (STS). The center tank used an old Lockheed concept of a hydrogen gas spike (to reduce tank wave drag) and had overall very low weight-to-drag characteristics to execute a partial orbit for a parachute recovery at Baikonur. The strap-on boosters were recovered down-range using parasail parachutes or returned to Baikonur by a gas-turbine-powered flyback booster with a switchblade wing. It is important to point out that the basic design approach for Energia required to have all components recoverable at the launch site, in this case Baikonur.

In a November 1964 brief, Roland Quest of McDonnell Douglas Astronautics, St. Louis, presented a fully reusable

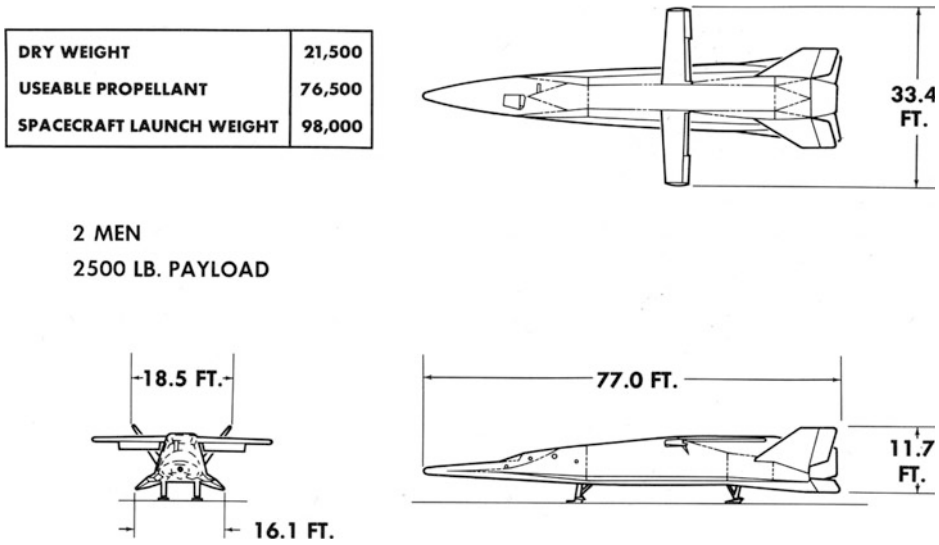

Fig. 3.9 Military Model 176 next generation spacecraft, November 1964 (McDonnell Douglas Astronautics Company)

hypersonic glider, the *Model 176*, intended to be the crew delivery, crew return, crew rescue, and resupply vehicle for the MOL crew (see Fig. 3.9).

One vehicle was to be docked with the MOL at all times as an escape and rescue vehicle. It could accommodate up to 13 persons, and as with the Energia-Buran system, all components were recoverable. Given the space infrastructure of the twenty-first century, it is important to recall that rescue and supply of manned space facilities require the ability to land in a major ground-based facility at any time from any orbit and orbital location. The cross- and down-range needed to return to a base of choice also requires high aerodynamic performance. Unlike airbreathing propulsion concepts limited to Mach 6 or less, an excellent inward-turning, retractable inlet can be integrated into the vehicle configuration derived from the FDL series of hypersonic gliders developed by the USAF Flight Dynamics Laboratory (Kirkham et al. 1975) and the work of the McDonnell Douglas Astronautics Company. The hypersonic work between both the McDonnell Douglas Astronautics Company and the McDonnell Aircraft Company residing under the McDonnell Douglas Corporation umbrella, and the USAF Flight Dynamic Laboratory (AFFDL) and McDonnell Douglas Astronautics Company provided a basis to converge the space and atmospheric vehicle developments to a common set of characteristics. Various aircraft and spacecraft configurations are shown in Fig. 3.10 (Draper et al. 1971; Draper and Sieron 1991).

The correlating parameter is the total volume, V, raised to the 2/3 power divided by the wetted area, S. The converged center value is 0.11 ± 0.03. The importance of this convergence is that the space configurations were moving away from the blunt-body (capsule) geometry and the atmospheric configurations away from the pointed wing-cylinders geometry, toward blended lifting bodies without any clearly defined wing (although there are large control surfaces, these primarily provided stability and control). This convergence of technical paths remained unrecognized by most, with only the USAF FDL and two or three aerospace companies (McDonnell Douglas being one) recognizing its importance to future space launchers and hypersonic cruise aircraft. These and other configurations were analyzed by the *Hypersonic Research Facilities Study (HyFAC)*. HyFAC confirmed the convergence of those two geometry lineages and subsequent families of vehicles. This observation has not yet been translated into application—the two branches remain separate until today. Consequently, we are still launching single expendable or pseudo-expendable launchers one at a time, for the first, last and only time.

3.5 Configuration Concepts

At McDonnell Aircraft Company, the author (P.A. Czysz) was introduced to a unique approach to determining the geometric characteristics required by hypersonic configurations with different missions and propellants. Figure 3.11 shows the principle of this approach. Normally, to increase its volume, a vehicle is made larger using linear (photographic) scaling. That is, all dimensions are multiplied by a constant factor. This means that the configuration characteristics remain unchanged except that the vehicle is larger. However, the wetted area is increased by the square of the multiplier, and the volume is increased by the cube of the multiplier. This can have a very deleterious impact on the size and weight of the design when a solution is converged. The McDonnell Aircraft Company approach, and as probably practiced by Lockheed and Convair in the 1960s, used the cross-sectional geometry of highly swept bodies to increase the propellant volume without a significant increase in wetted area.

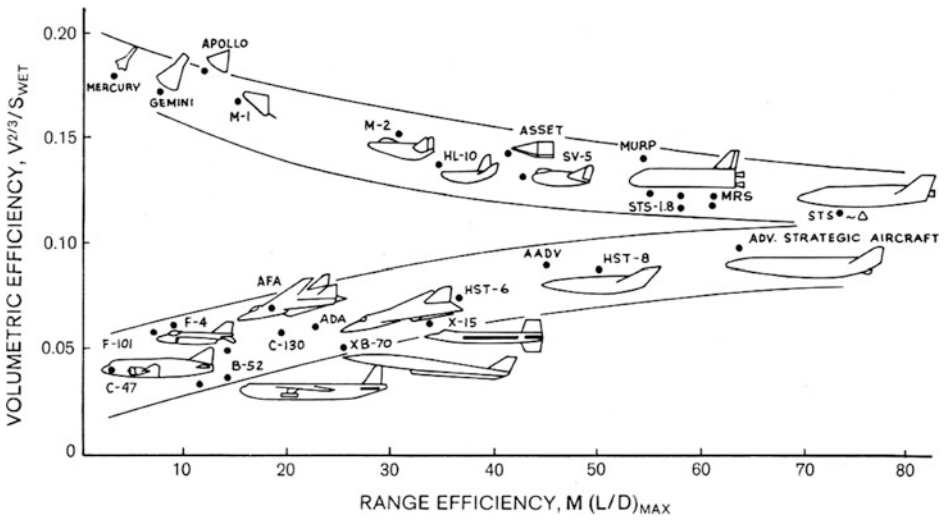

Fig. 3.10 Space and atmospheric vehicle development converge, so the technology of high-performance launchers converges with the technology of airbreathing aircraft (Draper et al. 1971; Draper and Sieron 1991)

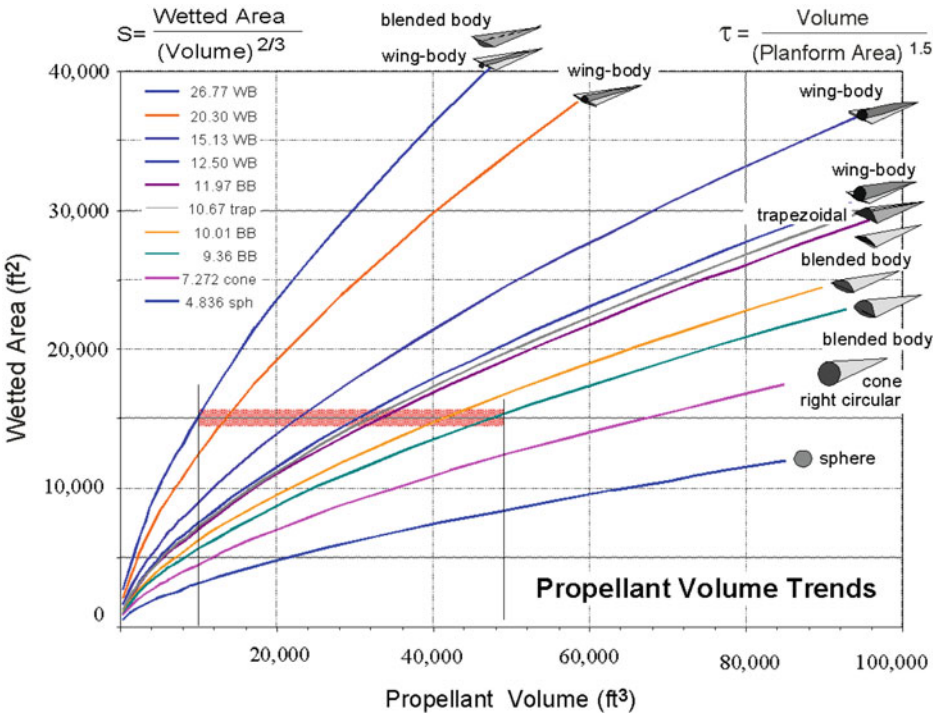

Fig. 3.11 A key relationship between volume and wetted area. Controlling drag, that is, skin friction resulting from wetted area, is the key to higher lift-to-drag ratios

As shown in Fig. 3.11, the propellant volume is plotted for a number of geometrically related hypersonic shapes as a function of their wetted area. The correlating parameter, S, is wetted area, S_{wet}, divided by the total volume, V_{total}, raised to the 2/3 power; this term is the reciprocal of the USAF FDL parameter in Fig. 3.10. The corresponding range of this parameter is 10.5 ± 2.0. As this parameter reduces in value, the wetted area for a given volume reduces. The most slender configuration is characteristic of an aircraft like Concorde. If a 78° sweep slender wing-cylinder configuration (S = 26.77) were expanded to the stout blended-body type (S = 9.36), the propellant volume could be increased by a factor of 5 without an increase in wetted area. If the original configuration were grown in size to the same propellant volume, the wetted area would be 3 times greater. Consequently, the friction drag of the S = 9.36 configuration is approximately the same, while the friction drag of the photographically enlarged vehicle is at least three times greater. Moving to a cone, the propellant volume is 6.8 times greater for the same wetted area. That is why the McDonnell Douglas Astronautics Company, Huntington Beach, *Delta Clipper Experimental* DC-X vehicle was a cone. It could accommodate the hydrogen–oxygen propellants within a wetted area characteristic of a kerosene supersonic aircraft.

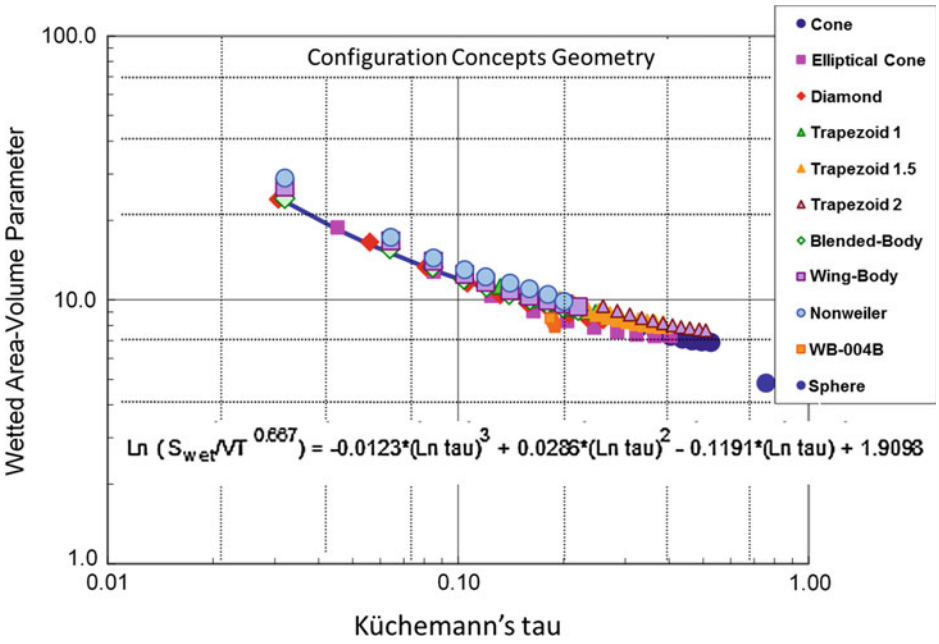

Fig. 3.12 Wetted area parameter from Fig. 3.11 correlates with Küchemann's tau yielding a geometric relationship to describe the delta planform configurations of different cross-sectional shapes. Note that $VT = V_{total}$

The correlating parameters with the area in the numerator and a volume raised to the 2/3 power in the denominator are characteristically used in the USA. The European correlating parameters associated with Dietrich Küchemann have volume in the numerator and area raised to the 1.5 power in the denominator (Küchemann 1960). The two approaches can be related as in the following equation sets. The US correlating parameters are given as follows:

$$S = \frac{S_{wet}}{(V_{total})^{0.667}} = \frac{K_w \cdot S_{plan}}{(V_{total})^{0.667}} \tag{3.5a}$$

$$T = \frac{S_{plan}}{(V_{total})^{0.667}} \tag{3.5b}$$

The European correlating parameters are:

$$\sigma = \frac{V_{total}}{(S_{wet})^{1.5}} = \frac{V_{total}}{(K_w \cdot S_{plan})^{1.5}} \tag{3.6a}$$

$$\tau = \frac{V_{total}}{(S_{plan})^{1.5}} \tag{3.6b}$$

with

$$K_w = \frac{S_{wet}}{S_{plan}} \tag{3.7}$$

$$S = \frac{K_w}{\tau^{0.667}} \tag{3.8}$$

The Roman (Latin) letters indicate US parameters in which the area is in the numerator. These parameters have values greater than one. The European parameters are indicated with Greek characters. These parameters have values less than one. Note that S_{plan} is the planform area (i.e., the area of the body projection on a planar surface), not the wetted area.

Figure 3.11 shows the value of S for a broad spectrum of hypersonic configurations. The values of S corresponding approximately to those in Fig. 3.10 are 12.5 through 8.3. This shows that the preferred configurations are all pyramidal planform shapes with different cross-sectional shapes that include a stout wing-body, trapezoidal cross sections, and blended body cross sections. Figure 3.12 shows that the value of S can be uniquely determined from Küchemann's tau for an equally wide variety of hypersonic configurations, including winged cylinders. Then, whether for hypersonic cruise configurations, airbreathing launchers, rocket-powered hypersonic gliders, or conventional winged cylinders, Küchemann's tau can be a correlating parameter for the geometric characteristics of a wide range of configurations. This means that specific differences in configurations are second order to the primary area and volume characteristics.

Supersonic cruise configurations using kerosene (such as Concorde) are in the 0.03–0.04 range of tau. Supersonic cruise configurations using methane are in the 0.055–0.065 range of tau. Hypersonic cruise configurations are in the 0.10 tau vicinity. Airbreathing space launchers are in the range of 018–020 tau. Rocket-powered hypersonic gliders are in the range of 0.22–0.26 tau. A correlating equation provides a means of translating Küchemann tau into the S parameter, $S_{wet}/V_{total}^{0.667}$. As implied in Fig. 3.12, as tau, τ, increases, the value of S decreases, meaning that the volume is increasing faster than the wetted area. This fact is crucial for a hypersonic aircraft since skin friction is a significant contributor to total drag. (In a well-designed hypersonic vehicle, friction

and wave drag have approximately the same value.) Later in the chapter, this parameter will be related to the size and weight of a converged design as a function of the industrial capability to manufacture the spacecraft. There are a wide variety of configurations possible. *But* if the requirements for a transportation system to space and return are to be met, the configurations spectrum is significantly narrowed (Thompson and Peebles 1999). Two basic configuration types are selected.

The *first* basic configuration type considers all-rocket and airbreathing rocket cycle propulsion systems that can operate as airbreathing systems to about Mach 6. For the rocket propulsion and airbreathing rocket propulsion concepts that are limited to Mach 6 or less, a versatile variable capture inward-turning inlet (DuPont 1999) can be integrated into the vehicle configuration derived from the FDL series of hypersonic gliders (Kirkham et al. 1975) and the work of the McDonnell Douglas Astronautics Company (see Fig. 3.16). Because of the mass ratio to orbit, these are generally vertical takeoff and horizontal landing (VTHL) vehicles. This is the upper left vehicle in Fig. 3.13.

The *second* basic configuration type considers airbreathing propulsion systems that require a propulsion-configured vehicle, where the underside of the vehicle is the propulsion system. The thermally integrated air-breathing combined-cycle configuration concept is derived from the McDonnell Douglas Astronautics Company—St. Louis, *Advanced Design* organization. This is a family of rocket hypersonic airbreathing accelerators and cruise vehicles (Pirrello and Czysz 1970). Depending on the mass ratio of vehicle, these can take off horizontally (HTHL) or be launched vertically (VTHL) and always land horizontally. The initial 1960s vehicle concept was propulsion configuration accelerated by a main rocket in the aft end of the body. Today, it can retain this concept or use a rocket-based combined-cycle (RBCC) propulsion concept. In any case, individual rockets are usually mounted in the aft body for space propulsion. This is the lower right vehicle in Fig. 3.13.

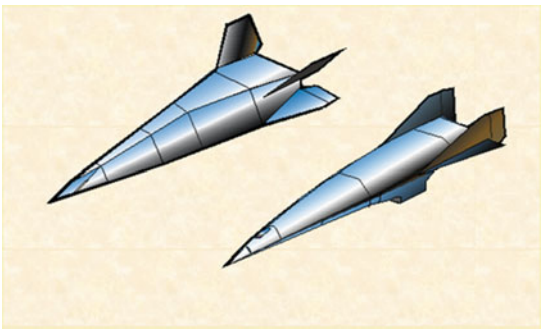

Fig. 3.13 Hypersonic rocket powered glider for airbreathing Mach < 6 and hypersonic combined-cycle powered aircraft for airbreathing Mach > 6

Both basic configurations are functions of tau; that is, for a given planform area, the cross-sectional distribution is determined by the required volume.

Both the hypersonic glider based on the FDL-7C and the hypersonic airbreathing aircraft in Fig. 3.13 have hypersonic lift-to-drag ratios in excess of 2.7. That means unpowered cross-ranges in excess of 4500 nautical miles and down-ranges on the order of the circumference of the Earth. These two craft can depart from any low-altitude orbit in any location and land in the Continental United States (CONUS) or in continental Europe (CONEU). Both are stable over the entire glide regime. The zero-lift drag can be reduced, for both, by adding a constant width section to create a spatula configuration. The maximum width of this section is generally the pointed body half-span. The pointed configurations are shown in Fig. 3.13. No hypersonic winged-cylindrical body configurations were considered, as these have poor total heat load characteristics and limited down-range capability. However, as a strap-on booster, the winged-cylindrical body configuration is acceptable.

The key to achieving the primary goal of reduced payload costs to orbit continues to be flight rate, and as in the case of the transcontinental railroad, scheduled services were supplied when as little at 300 statute miles of track (out of 2000 miles planned) had been laid (Ambrose 2000). Clearly, our flights to Earth orbit need to be as frequent as they can be scheduled.

The vertical-fin configuration arrangement has presented low-speed stability problems for many hypersonic glider configurations such as the X-24A, M2-F2, HL-10 and others. The high dihedral angle verticals for three of the four configurations in Fig. 3.14 are representative of the vertical fin orientation. The "X"-fin configuration was the result of an extensive wind tunnel investigation by McDonnell Douglas and the AFFDL that covered the speed regime from Mach 22 to Mach 0.3. A total of four tail configurations were investigated over the total Mach number range and evaluated in terms of stability and control; they are shown in Fig. 3.14. All of the configurations, except the first "X"-tail configuration, had serious subsonic roll-yaw instabilities at lower speeds. The "X"-tail configuration has movable trailing edge flaps on the lower anhedral fins, and the upper surfaces are all movable pivoting control surfaces at approximately 45° dihedral angle. This combination provided inherent stability over the entire Mach number range from Mach 22 to landing.

The FDL-7-derived hypersonic gliders (flat bottom) have a higher lift-to-drag ratio configuration than those similarly developed by Mikoyan and Lozino-Lozinskiy in Russia as the "BOR" family of configurations (curved bottom) because of differing operational requirements. Some of the first studies performed for NASA by McDonnell Aircraft Company and Lockheed (Anon 1970; Morris and William 1968)

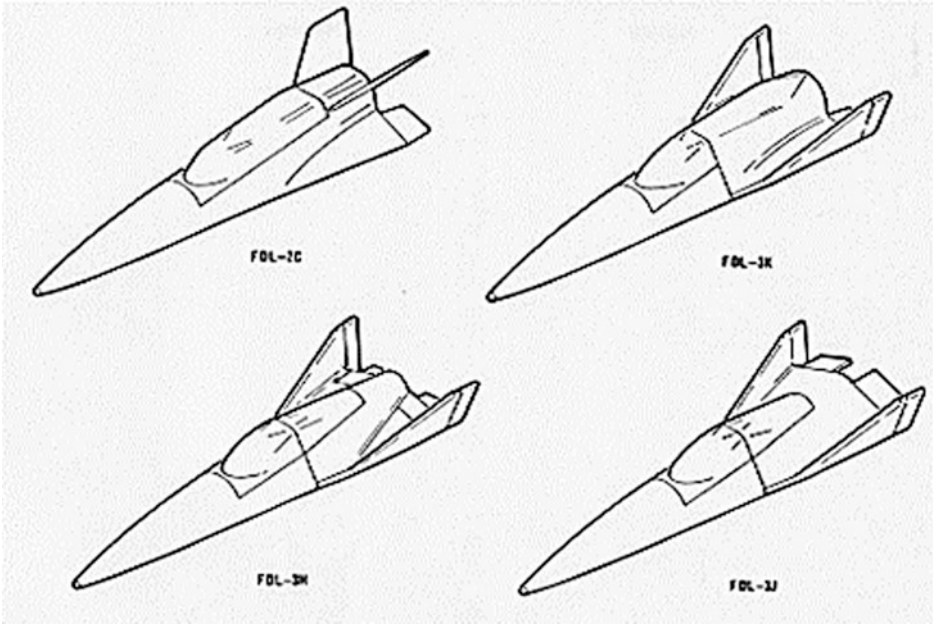

Fig. 3.14 Wind tunnel model configurations for tail effectiveness determination over hypersonic to subsonic speed regime (Mach 22 to 0.3)

identified as a need the ability to evacuate a disabled or damaged space station immediately, returning to Earth without waiting for the orbital plane to rotate into the proper longitude (see Chap. 2). Unfortunately, many of these studies were not published in the open technical literature and were subsequently destroyed. For a Shuttle or crew-return vehicle (CRV) configuration, the waiting period might last seven to eleven orbits, depending on inclination, or, in terms of time, from 10.5 to 16.5 h for another opportunity for entry. However, that might be too long in a major emergency.

In order to accomplish a "no waiting" descent with the longitudinal extent of the USA, that requirement demands a hypersonic lift-to-drag ratio of 2.7–2.9. The hypersonic vehicles based on the FDL-7 series of hypersonic gliders have demonstrated such capability. Given the longitudinal extent of the former USSR, that requirement translates into a more modest hypersonic lift-to-drag ratio of 1.7–1.9. Consequently, the Lozino-Lozinskiy BOR hypersonic gliders meet the requirement to land in continental Russia without waiting. This lower hypersonic lift-to-drag ratio meant that, if the deorbit rocket retrofiring was ground-controlled, Russian spacecraft could be precluded from reaching the USA. The BOR class of vehicles had been adopted by NASA as a potential ISS crew rescue vehicle (CRV). The X-24A, X-38, HL-10, HL-20, HL-40, and subsequently Sierra Nevada's *Dream Chaser* resemble, in fact, the primary concept of the BOR-4 vehicle. The BOR-4 vehicle is shown in Fig. 3.15 after recovery from a hypersonic flight beginning at about Mach 22 (Lozino-Lozinskiy 1989).

The BOR-4 picture was given to the author (P.A. Czysz) by Glebe Lozino-Lozinskiy at the 40th IAF Congress held in Malaga, Spain, in 1989 (Lozino-Lozinskiy 1989). Lozino-Lozinskiy was very familiar with the subsonic lateral–directional instability for this high dihedral angle fin configuration and, in the 1960s, constructed a turbojet-powered analog that investigated this problem. The solution was to make the aft fins capable of variable dihedral (as said, a power hinge was mounted in the root of each fin). At high Mach numbers, the fins were at about plus 45° as shown in Fig. 3.15. However, when slowing down to transonic and subsonic Mach numbers, the dihedral angle was decreased. At landing, the fins were at a minus 10° as shown by the dashed outline in Fig. 3.15. Thus, the BOR class of vehicles was a variable geometry configuration that could land in continental Russia; its stability could be maintained over the entire flight regime, from Mach 22 to landing.

The Model 176 began with the collaboration between Robert V. Masek of McDonnell Douglas Astronautics Company and Alfred C. Draper of USAF FDL in the late 1950s on hypersonic control issues. After a series of experimental and flight tests with different configurations, the "X"-tail configuration and the FDL-7C/D glider configurations emerged as the configuration that was inherently stable over the Mach range and had Earth circumference glide range (see Fig. 3.14). The result was the USAF FDL-7MC and then the McDonnell Douglas Astronautics Model 176. Figure 3.16 compares the two configurations. In the early 1960s, both configurations had windshields for pilot visibility (see Fig. 3.21). However, with today's automatic flight capability, visual requirements can be met with remote viewing systems. The modified FDL-7C/D configuration was reshaped to have flat panel surfaces, and the windshield provisions were removed, but it retained all of

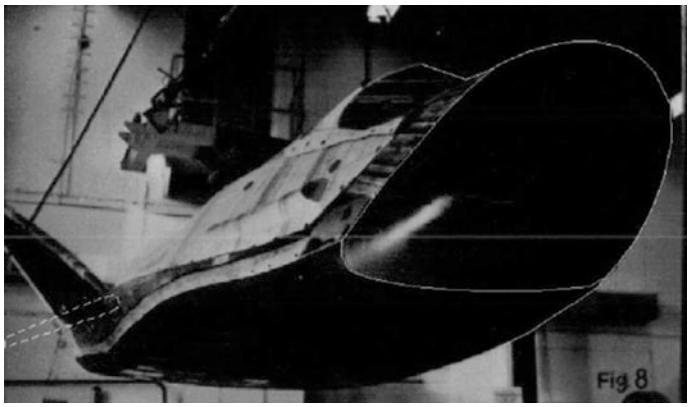

Fig. 3.15 BOR-4 after return from hypersonic test flight at Mach 22. The one-piece carbon-carbon nose section is outlined for clarity. The vertical tails are equipped with a root hinge, so at landing the tails are in the position shown by the *dashed line*. Thus, BOR-4 is stable in low-speed flight. If the variable dihedral were not present, BOR-4 would be laterally and directionally unstable at low speeds

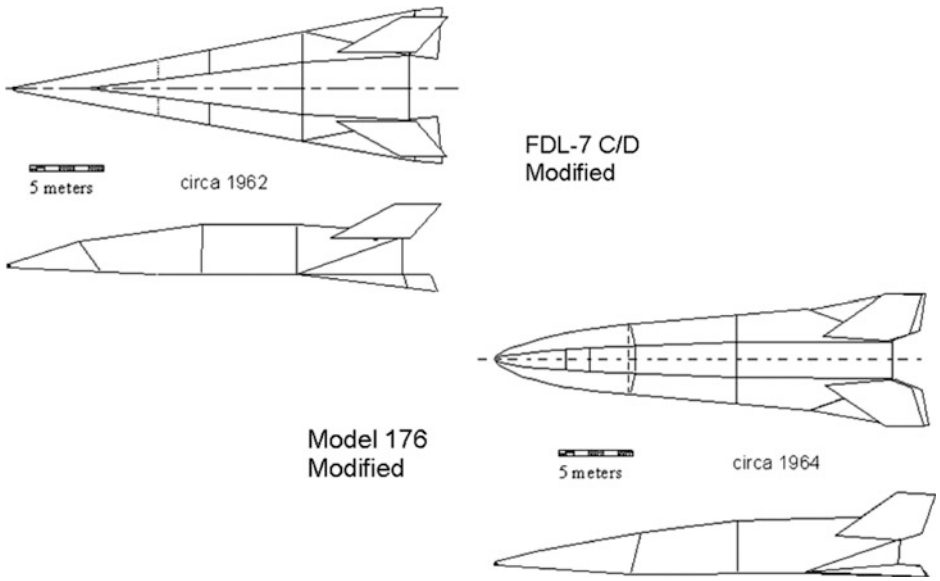

Fig. 3.16 FDL-7 C/D (*top*) compared with Model 176 (*bottom*)

the essential FDL-7 characteristics. In order to ensure the lift-to-drag ratio for the circumferential range glide, the Model 176 planform was reshaped incorporating a parabolic nose to increase lift while decreasing nose drag. A spatula nose would have also provided the necessary aerodynamic margin. However, the original configuration was retained with just the windshield provisions deleted (see Fig. 3.18).

The Model 176 was proposed for the MOL described in Chap. 2. It was a thoroughly designed and tested configuration with a complete all-metal thermal protection system that had the same weight of ceramic tile and carbon-carbon concepts used later for the US Space Shuttle, but was sturdier. A wind tunnel model of the McDonnell Douglas Astronautics Company Model 176 installed in the McDonnell Aircraft Company Hypervelocity Impulse Tunnel for a heat transfer mapping test is shown in Fig. 3.17. Note that conforming to the piloting concepts of the 1960s, it has a clearly distinct windshield that is absent from the configuration concept in Fig. 3.16. The wind tunnel model is coated with a thermographic phosphor surface temperature mapping system (Dixon and Czysz 1969). This system integrated semiconductor surface temperature heat transfer gauges (Dixon 1966) which permitted the mapping of the heat transfer to the model and full-scale vehicle. In addition, the model allowed accurate thermal mapping of the heat transfer distribution pertaining to the body and upper fins. From this data compendium, the surface temperatures of the full-scale vehicle with a radiation shingle thermal protection system could be determined, enabling the choice of the material and thermal protection system appropriate for each part of the vehicle.

The important conclusions that resulted from these heat transfer tests are that the geometry characteristics comprising of sharp leading-edges, flat-bottomed, and trapezoidal cross

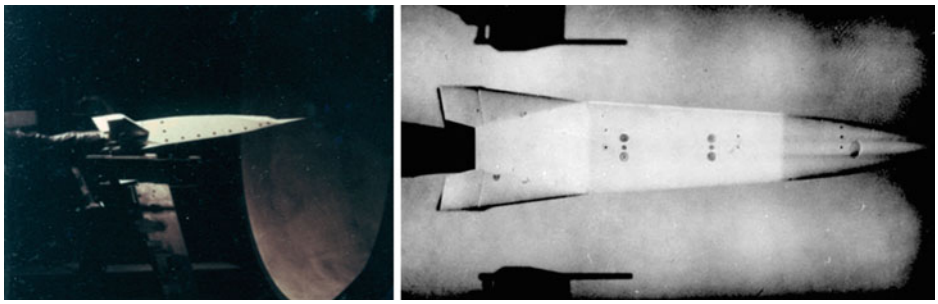

Fig. 3.17 Model 176 side and bottom view in the McDonnell Douglas Hypervelocity Impulse Tunnel (circa 1964)

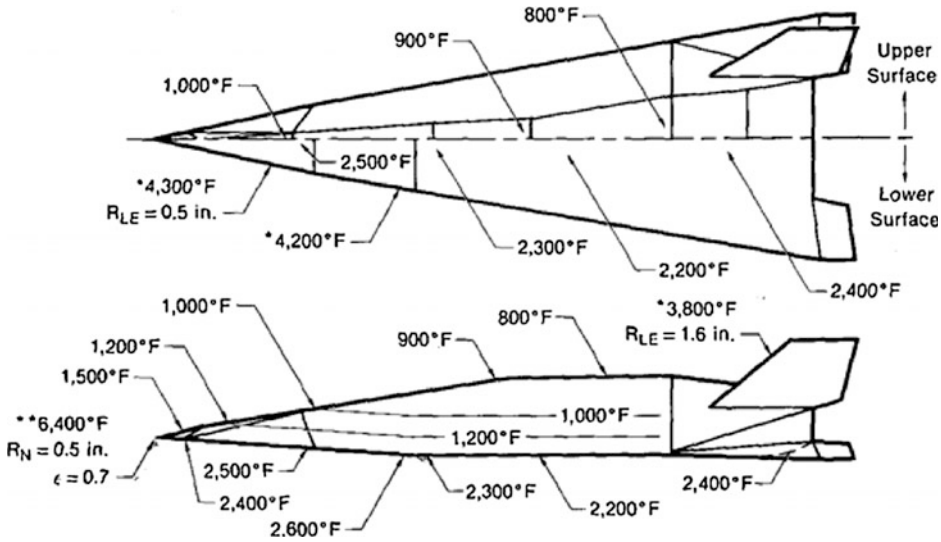

Fig. 3.18 FDL-7 C/D and Model 176 entry temperature distribution. Upper surface heating is minimized by cross-sectional geometry tailoring

section do reduce the heating to the sides and upper surfaces. The surface temperatures of the thermal protection shingles are shown in Fig. 3.18. In the range of angles-of-attack corresponding to maximum hypersonic lift-to-drag ratio, the sharp leading-edge corner separates and reduces the upper surface heating. Because of the separation, the isotherms are parallel to the upper surface and are 2100–2400 °F (1149–1316 °C) cooler than on the compression surface. The upper control fins are hot, but there are approaches and materials available for thermal management of control surfaces. The temperatures shown in Fig. 3.18 are radiative equilibrium temperatures. The temperatures with asterisks are the radiation equilibrium temperatures without employing thermal management. Thermally managed with nose water transpiration cooling (demonstrated in flight test in 1966) and heat pipe leading edges (demonstrated at NASA Langley in 1967–68), the temperatures of the nose and leading edges are 212 and 1300 °F (100 and 704 °C), respectively.

Except for the tail control surfaces, the vehicle is a cold aluminum/titanium structure protected by metal thermal protection shingles. Based on the local heat transfer and surface temperature, the material and design of the thermal protection system was determined, as shown in Fig. 3.19. It employs a porous nose tip with about a one-half inch (12.3 mm) radius, such as the Aerojet Corporation's diffusion-bonded platelet concept. Arc-tunnel tests conducted in the 1960s demonstrated that a one-half-inch radius sintered nickel nose tip maintained a 100 °C wall temperature in a 7200 R (4000 K) stagnation flow for over 4300s utilizing less than 1.0 kg of cooling water. The one-half-inch (12.3 mm) radius leading edges and the initial portion of the adjacent sidewall form a sodium-filled Hastelloy-X heat pipe system that maintains the structure at approximately constant temperature. Above the heat pipe, the sidewalls are insulated Inconel honeycomb shingles. Above those and over the top are diffusion-bonded multi-cell titanium. The compression side (underside) is coated columbium (niobium) insulated panels or shingles similar to those on the compression side of the Lockheed Martin X-33 that protects the primary structure as shown in Fig. 3.20. The upper all-flying surfaces and the lower trailing flap control surfaces provide a significant challenge. Instead of utilizing very high-temperature materials that can still have sufficient differential heating to significantly warp the surfaces, the approach was to adapt the heat pipe concept contained within the honeycomb cells perpendicular to the surface. This way the control surfaces heat loading was more isothermal, thereby reducing thermal bending tendencies and overall material temperature.

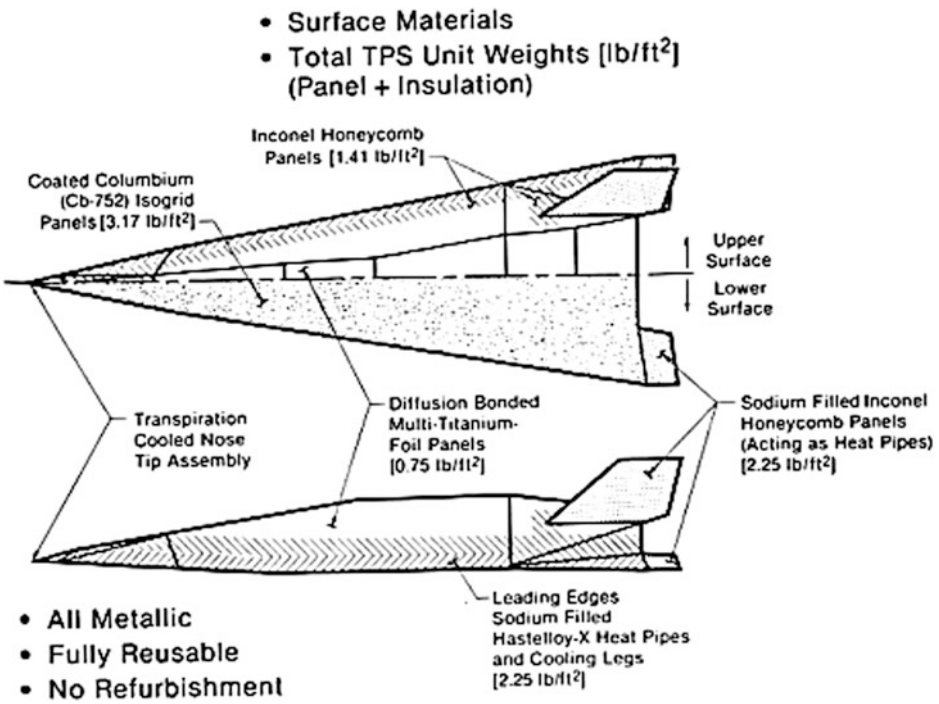

Fig. 3.19 FDL-7 C/D and Model 176 materials, thermal protection systems distribution based on temperature profile in Fig. 3.18

Fig. 3.20 McDonnell Aircraft Astronautics roll-bonded titanium structure (circa 1963), from *Advanced Engine Development at Pratt & Whitney* SAE Publisher (Mulready 2001). Today, this structure would be superplastically formed and diffusion-bonded from RSR (roll speed ratio) titanium sheets

The structure of Model 176 was based on diffusion bonding and superplastic forming of flat titanium sheets. Fifty years ago, the method was called "roll bonding," and it was executed with the titanium sealed within a stainless steel envelope and processed in a steel rolling plant. With a lot of effort and chemical leaching, the titanium part was freed from its steel enclosure. All of that has been completely replaced today by the current titanium diffusion bonding and superplastic forming industrial capability. The picture shown with Fig. 3.20 is from a Society of Automotive Engineers (SAE) publication entitled *Advanced Engine Development at Pratt & Whitney* by Dick Mulready. The subtitle is *The Inside Story of Eight Special Projects 1946–1971* (Mulready 2001). In Chap. 6, *Boost Glide and the XLR-129—Mach 20 at 200,000 Feet*, the McDonnell Aircraft boost-glide strategic vehicle is mentioned, together with the key personnel at the McDonnell Aircraft Company. Low thermal conductivity standoffs set the metal thermal protection insulated shingles off from this wall, resulting in an air gap between them. The X-33 applied the metal shingle concept but with significant improvement in the standoff design and thermal leakage, in the orientation of the shingles, and in the thickness and weight of the shingles. This is one aspect of the Lockheed Martin X-33 that can be applied to future spacecraft for a more reliable and repairable TPS compared to ceramic tiles. The titanium diffusion-bonded and superplastically formed wall was both the primary aircraft structure and the propellant tank wall. The cryogenic propellants were isolated from the metal wall by a metal foil barrier and via sealed insulation on the inside of the propellant tank.

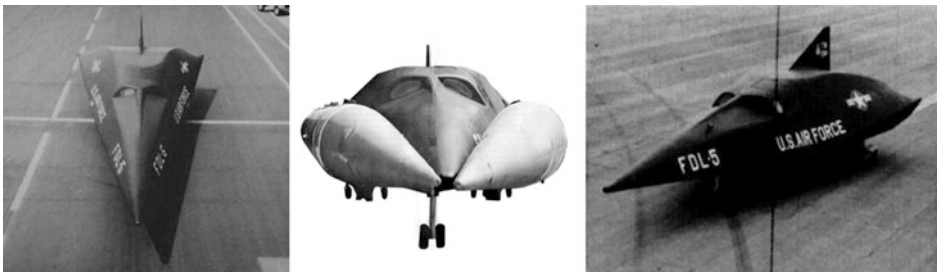

Fig. 3.21 Lockheed/USAF one-half scale FDL-5MA mock-up, representing a manned reusable spacecraft with conformal fuel tanks [reproduced from *Astronautics and Aeronautics* (Draper et al. 1971; Draper and Sieron 1991, USAF)]

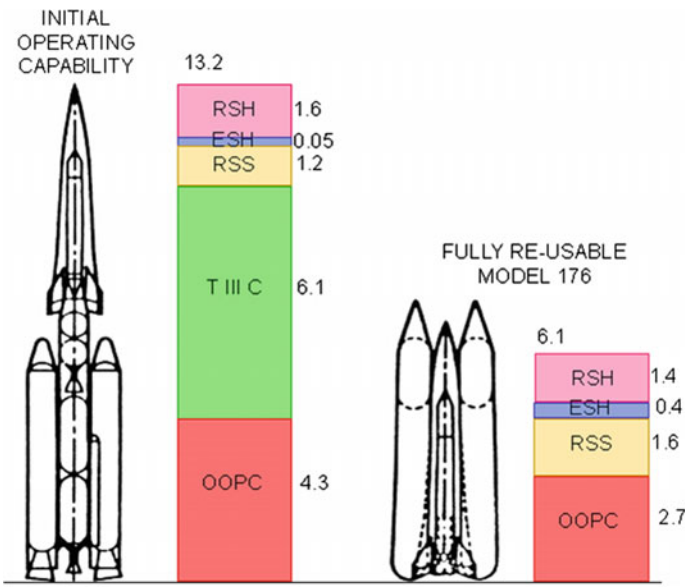

Fig. 3.22 Individual Model 176 launch costs for a 100-launch program, as projected in a McDonnell Douglas Astronautics Company 1964 brief (*RSH* reentry spacecraft hardware; *ESH* expendable spacecraft hardware; *RSS* reentry spacecraft spares; *OOPC* other operational costs; *T III C* Martin Titan III C cost)

The US Air Force Flight Dynamics Laboratory (USAF-FDL) fabricated a one-half scale mock-up of the FDL-5 configuration (Draper et al. 1971), see Fig. 3.21. The Lockheed/AFFDL effort generated with the FDL-5 an early FDL configuration which pioneered the compression sharing concept aimed at demonstrating acceptable yaw stability at speeds from Mach 2 to 19 and others. The strap-on tanks provided propellants to about Mach 6 or 7; then, the tanks separated; and the mission continued using internal propellants. Note the windshields installed in this 1960s mock-up. This was a vertical launch, horizontal landing configuration (VTHL). The intent was to provide the US Air Force with an on-demand hypersonic aircraft that could reach any part of the Earth in less than a half-hour and return to its launch base or any base within the CONUS. The early FDL-5 evolved at McDonnell Douglas Astronautics Company into Model 176, overall presenting a pinnacle in spacecraft development. However, in a very short period of time after this mock-up was fabricated, the path the USA took to space detoured, and most of this work was abandoned and discarded.

The ultimate intent was to begin operational evaluation flights with the Model 176 launched on a Martin Titan IIIC, as shown in Fig. 3.22. In 1964, the estimated cost was US $13.2 million per launch for a 100-launch program or about US$2700 per payload pound. As the system was further developed, two strap-on liquid hydrogen/liquid oxygen propellant tanks would be fitted to the Model 176 spaceplane for a fully recoverable system, as shown on the right side of Fig. 3.22. The estimated 1964 cost of this version was US $6.1 million per launch for a 100-launch program, or about US$1350 per payload pound. The launch rate for which the cost estimate was made has been lost in history, but to maintain the USAF MOL (Manned Orbital Laboratory) spacecraft, launch rates on the order of one per week were anticipated for both resupply and waste return flights. The latter flights could exceed the former in all of the studies the author is familiar with.

One of the most practical operational aspects of the FDL-5, FDL-7, and Model 176 class of hypersonic gliders was that the lifting body configuration forms an inherently

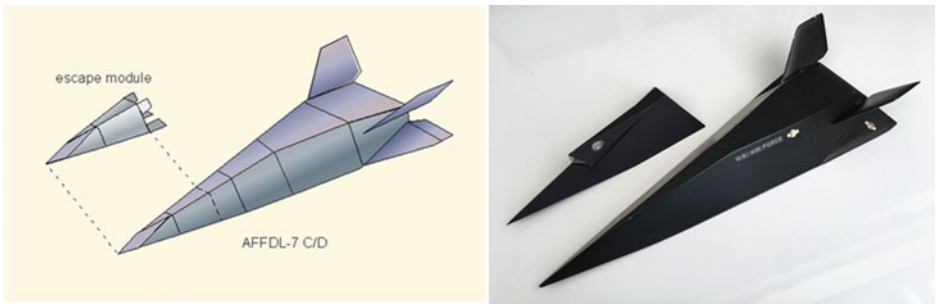

Fig. 3.23 USAF FDL-7C as configured by McDonnell Douglas Astronautics Company with an escape module capable of controlled hypersonic flight. Note that the demonstration model of the escape module on the right has a pop-up canopy to provide forward visibility for the pilot

stable (longitudinal and directional) hypersonic glider. Based on work by the McDonnell Douglas Astronautics on control of hypersonic gliders, the FDL-7 as configured by McDonnell Douglas Astronautics incorporated an integral escape module. As shown in Fig. 3.23, the nose section with foldout control surfaces was a fully controllable hypersonic glider capable of long glide ranges (though less than the basic vehicle, but greater than the Space Shuttle). Consequently, the crew always had an escape system that was workable over the entire speed range. As shown, the foldout control surfaces are representative of a number of different configurations possible.

3.6 Takeoff and Landing Mode

The switchblade wing version of the FDL-7C (i.e., the FDL-7MC) was the preferred version for the 1964 studies. The switchblade wing versions of the AFFDL FDL-7MC and the McDonnell Douglas Astronautics Model 176 configuration, without a windshield, are shown in Fig. 3.24. This was part of the McDonnell Douglas Astronautics TAV (transatmospheric vehicle) effort. The vehicle was powered by either an Aerojet air-turbo ramjet or an airbreathing rocket propulsion system. The inward-turning, variable capture area inlet (DuPont 1999) provides the correct engine airflow from landing speeds to Mach 5 plus. The propellant tanks were cylindrical segment, multi-lobe structures with bulkheads and stringers, able to support the flat metal radiative thermal protection shingles (similar to those initially planned for the canceled X-33). The nose was transpiration-cooled with a low-rate water-porous spherical nose. The sharp leading edges (the same leading edge radius was used for the nose tip) were cooled with liquid metal heat pipes. This approach was tested successfully during the 1964–1968 time frame and found to be equal in weight and far more durable than a comparable ceramic tile/carbon-carbon system. Whenever the landing weights were heavier than normal, the switchblade wing provided the necessary margin for these operations.

For a hypersonic cruiser aircraft, the takeoff mode is not an issue: It is a runway takeoff and runway landing. However, for a space launcher, the issue is not so clear-cut. With mass ratios for launchers much greater than for aircraft (4–8, compared to less than 2 for aircraft), runway speed may be impractical for some launchers with high mass ratios. Consequently, the principal space launcher option is vertical takeoff (VT) with horizontal landing (HL) remaining viable. However, for several launcher studies, the study directives mandated horizontal takeoff whatever the mass ratio. Many launcher studies have been thwarted by this a priori dictate of horizontal takeoff. In reality, horizontal or vertical takeoff,

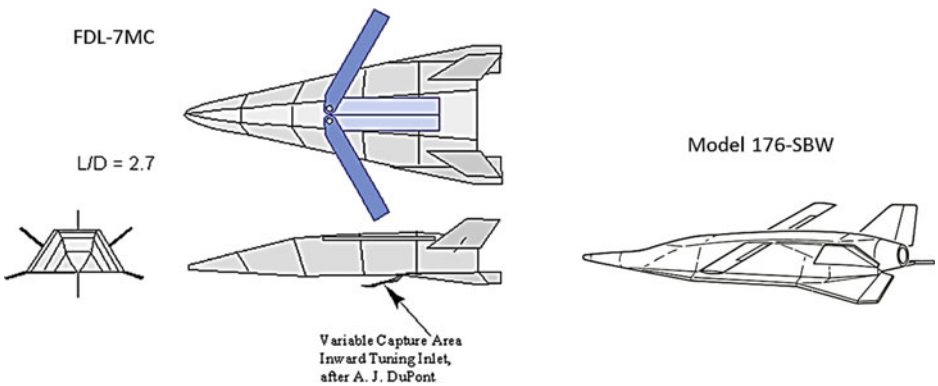

Fig. 3.24 USAF FDL-7MC and Model 176 equipped with a switchblade wing; FDL-7MC featuring the DuPont retractable inward-turning inlet for airbreathing rocket applications

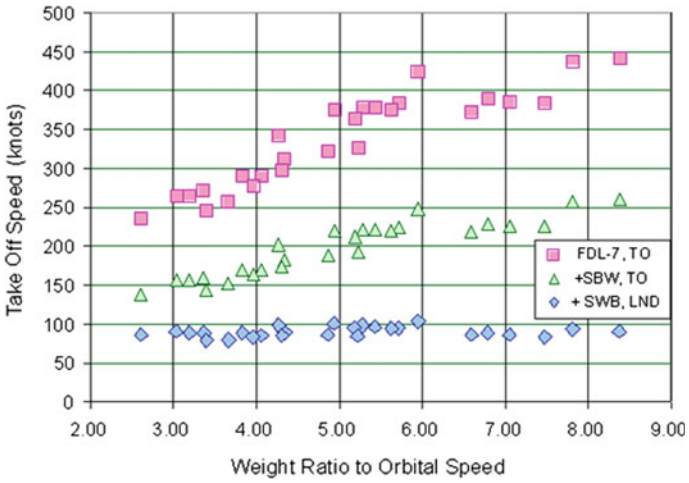

Fig. 3.25 Takeoff and landing speeds of minimum-sized launchers. *TO* takeoff; *LND* landing; *SWB* switchblade wings

like the configuration concept, is less a choice than a result of the propulsion concept selected. Horizontal takeoff requires that the wing loading be compatible with the TO lift coefficient the configuration can generate for the maximum takeoff speed limit. For high sweep delta planforms, such as that of the FDL-7MC and Model 176, the only high-lift device available is the switchblade wing and a retractable canard near the nose of the vehicle.

The basic FDL-7C and Model 176 lifting body configuration lineage was not designed for horizontal takeoffs. As shown in Fig. 3.25, the takeoff speed, as a function of the SSTO launcher mass ratio to orbital speed, is very high for the basic delta lifting body, even for low mass ratio propulsion systems (squares). With the lowest mass ratio, the takeoff speed is still 250 knots (129 m/s) and that is challenging for routine runway takeoffs. Landing and takeoff speeds are for minimum-sized vehicles, that is, values of tau in the range of 0.18–0.20 where the gross weight is a minimum. Adding the switchblade wing provides a reasonable takeoff speed for all mass ratios (triangles). The takeoff speed with the switchblade wing deployed is approximately also the landing speed with the wing stowed. All of the launcher vehicles have very similar empty plus payload weight (operational weight empty). The landing speeds are essentially constant for all configurations and propulsion systems, corresponding to the lower mass ratio values. With this approach, the landing and takeoff speeds are essentially equal, overall adding a degree of operational simplicity. Landing and takeoff speeds correspond to those of current military aircraft and civil transports, at least for the lower mass ratios (five or less). However, the landing speeds do increase with takeoff mass ratio, since the operational empty weight of the vehicle increases with mass ratio. An approach to make the landing speed approximately constant and to lower its value is to deploy the switchblade wing for landing (diamonds) (see Fig. 3.25). Then, the landing speed becomes very modest, even when compared with most civil transports and military aircraft.

Takeoff speeds for blended bodies in the 200–230 knot ranges were envisaged in the 1960s by using a very large gimbaled rocket motor to rotate upward causing the body to rotate, lifting off the nose wheel and eventually the entire vehicle with a thrust-supported takeoff. This concept was not implemented in an actual system. If the takeoff speed is too high for the propulsion system chosen (because of weight ratio), then the only way to decrease the takeoff speed is to increase the planform area for the system volume, overall requiring a reduction of the Küchemann tau. This unfortunately introduces a cascade of incremental mass increases that result in an exponential rise of the takeoff gross weight. This is illustrated in Fig. 3.26.

Figure 3.26 begins with a solution map of VT launchers, as represented by the shaded areas in the lower part of the figure. All of this data is for converged vehicle solutions, where the SSTO mission requirements are met and the mass and volume of each solution have converged. These solution areas represent a spectrum going from all rocket systems (far right) to advanced airbreathing systems (far left). These solution areas are for VTHL with thrust-to-weight ratio at takeoff (TWTO) of 1.35 and tau equal to 0.2. For comparison, the gross weight trends are shown for five different takeoff wing loadings. The horizontal takeoff and horizontal landing (HTHL) solutions for constant wing loading are shown for values of tau from 0.2 to 0.063. The point where VTHL and HTHL modes have the same gross weight represents the maximum weight ratio for which there is no penalty for horizontal takeoff. For example, at a takeoff wing loading of 973 kg/m^2 (200 lb/ft^2), the weight ratio is 5.5, representative of an airbreathing speed of Mach 6 $\pm$ 0.3. For a lighter takeoff wing loading of 610 kg/m^2 (125 lb/ft^2), the VTHL/HTHL boundary is now shifted to a weight ratio of 4.3, or an airbreathing Mach 10.5 $\pm$ 0.5. This wing loading

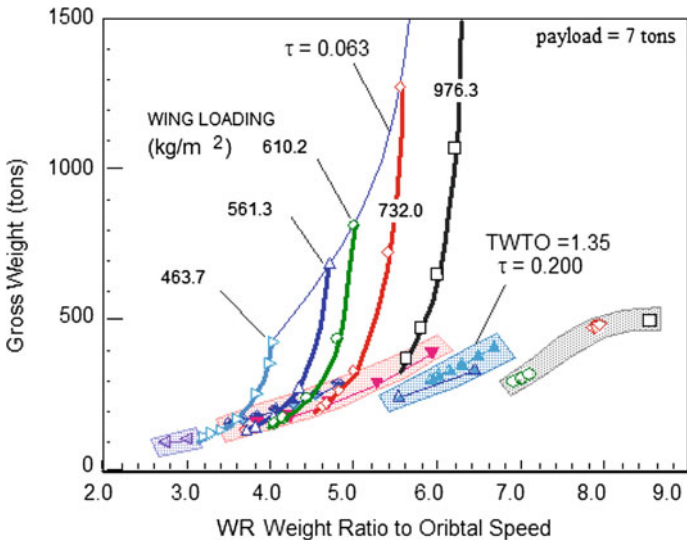

Fig. 3.26 Imposed horizontal takeoff requirement can radically increase takeoff gross weight unless the weight ratio is less than 4.5

is also correct to air launch in the Mach 0.72 at 35,000 ft region with horizontal landing (ALHL). For an even more reduced takeoff wing loading of 464 kg/m^2 (95 lb/ft^2), the VTHL/HTHL boundary is now set at a weight ratio of 3.4, or an airbreathing Mach 13 ± 1.0 for an ACES propulsion system. This latter wing loading is the wing loading that would represent the maximum airbreathing speed practicable and consistent with commercial transports.

For an airbreathing rocket, a mass ratio of 5.0 is achievable. That results in a gross weight of about 230 t. This is less than half the 480 t for an all-rocket case. However, if a horizontal takeoff requirement is imposed a priori, the lowest wing loading for which a practical solution exists is 610.2 kg/m^2. At that point, the gross weight for the horizontal takeoff solution is about 800 t, almost twice the all-rocket value. If the study team is not aware of the comparison to VT, the improper conclusion might be drawn that it was the propulsion system that caused the divergent solution. For lower wing loadings, the solution curve becomes vertical, and the solution will not converge.

The conclusion is, if the weight ratio is greater than 4.5, the best vehicle configuration is VT or an air-launched configuration (all of the vehicles have a horizontal landing mode). Again, it is important to let the characteristics of the converged solution themselves determine the takeoff and landing modes, if the lowest gross weight and smallest size vehicle are the project goals.

3.7 Transatmospheric Launcher Sizing

3.7.1 Vehicle Design Rationale

The major driver, in the development of launch vehicles for the twenty-first century, is reducing the cost of payload to orbit. This focuses vehicle characteristics toward a continuous use basis with the capability to recover fully operational the vehicle and payload if forced to abort the mission and if reduction of launch time and resources is required. Somewhat differently from commercial airliners, such requirements may become variously qualified and constrained in each country by its government and commercial policies, geography, and other considerations. There is a fundamental need to rethink the basic approach to conceptual design in terms of the technical requirements for meeting mission goals. This chapter provides an approach and a systematic method which is then applied to evolve various types of vehicles.

A. Theme

An approach to the conceptual design of transatmospheric vehicles is still a matter of debate. Although several design synthesis methods have been developed (Johnson 1991; Plokhikh 1989; Schindel 1989; Chudoba 2002; Coleman 2010), the difficulty is in rationalizing needs, capabilities, and opportunities. While it is fully recognized that airbreathing propulsion has a crucial role in meeting the goals of launch vehicles, and that the vehicle needs to be fully integrated in design, functions, and operation, the difficulty is estimating and matching available and required industrial capabilities to produce credible designs. There are invariably ambiguities and controversies associated with estimating available and required industrial capabilities, whether propulsion-propellant schemes, configurations and associated geometries, materials and structures, flight management, or controls, either considered individually or collectively. The approach taken in this section is directed toward clarifying and overcoming some of the ambiguities through the use of simple and direct basic principles and estimates. The outcome is what we do refer to as a *sizing approach*, representing the

implementation and numeric convergence of a vehicle system to sets of dependent and independent design parameters that enable in concert a specified mission.

B. **Objectives**

The authors' objectives in the development and use of the sizing methodology are as follows:

(1) Provide a quantitative sizing model based on simple principles and estimates to assess the feasibility of SSTO while accounting for system weight and volume as well as explicit margins. (SSTO configuration arrangement selected due to presenting the most challenging scenarios.)
(2) Provide simplified input requirements for screening parametric studies for parametrically screening trade spaces based on engineering experience that represents current and future manufacturing capabilities. Specifically, the authors identify a *current* set of volume and weight assumptions considered within today's industrial manufacturing and materials capabilities, and a *future* set which results from application of ongoing R&D worldwide. These two sets bound the possible *design space*.
(3) Apply the model to assess SSTO performance sensitivity to changes in assumptions and interaction between these assumptions.
(4) Extend the sizing model to TSTO and perform sensitivity analysis as for SSTO.
(5) Compare SSTO and TSTO performance.
(6) Assess the potential of air and LO_2 collection for both, SSTO and TSTO.

3.7.2 Vehicle Sizing Approach

In the development of subsonic atmospheric flight vehicles, it is accepted practice to adopt variants of a methodology developed more than half a century ago for conceptual design. The method is illustrated in Frederick et al. (1976) and Fig. 1 of Czysz and Murthy (1995). This method is based on historical data on design, test results, and operational experience and is responsible, for instance, for the wing & tube aircraft configuration traditionally found among commercial transports.

In the case of hypersonic vehicles, the total operational experience is small. Despite the lack of operational experience, the accumulated volume of historical design and test data has been extensive. However, when referring to historical design and test data that is not necessarily so. One author's (P.A. Czysz) career in hypersonic vehicles is based on the approach pioneered in the Mercury and Gemini reentry vehicles. That is, a conventional, cold, load carrying structure protected by relatively smooth radiation shingles (Altis 1967; Taylor 1965; Anon 1965a, b). When applying this approach to hypersonic cruisers, accelerators and gliders, coupled with wind tunnel testing over two decades did yield statistically weighted correlations for evolving optimal concepts that weighed less and had higher lift-to-drag than comparable conventional vehicles (Stephens 1965). Propulsion systems integrated into the vehicles during that time period spanned a broad spectrum of engines, ranging from turboramjets (Anon 1965a, b, 1969a, b) to scramjets (Anon 1966a, b; Altis 1967; Morris and William 1968). This led to the NASA-sponsored *Hypersonic Research Facilities Study* (HyFAC) (Pirrello and Czysz 1970) (see Fig. 3.27).

In this landmark study (Pirrello and Czysz 1970), the authors describe 102 hypersonic research objectives required

Fig. 3.27 Research program balance requires the evaluation of research potential and total costs of new candidate research facilities, both ground and flight (Pirrello and Czysz 1970)

to achieve Mach 12 flight. This compendium is matched with hypersonic research facility performance and cost requirements to achieve a significant fraction of those research objectives. In order to put the study into perspective, the *ground research facilities* represented about one-eighth of that effort, while the *flight research facilities* represented covered about seven-eighths of the effort. Clearly, the study was primarily a research aircraft effort with some consideration of required ground facilities. The objective of this chapter is to document a constant performance, volume, and mass convergence flight vehicle sizing procedure.

A. Approach

When the authors (P.A. Czysz and C. Bruno) began their careers in aerospace in the late 1950s (P.A. Czysz) and mid 1970s (C. Bruno), the standard practice was to begin design of aerospace vehicles by drawing constant wing area or constant weight concept aircraft. Each system component was independently sized, designed, and assembled. Common practice was to redraw and iterate each concept to approximately the same mission range. However, performance could differ significantly between concepts. This approach proved unsatisfactory for high-performance aircraft and particularly for high-speed vehicles.

Sizing aircraft concepts to *both* mission distance and maneuvering performance produced a change in how concepts were evaluated (Tjonneland 1988; Herbst and Ross 1969; Czysz et al. 1973; Plokhikh 1995). Decisions could now be made on equal performance aircraft of differing size and weight. This aircraft-sizing approach matched an aircraft configuration to mission performance requirements, then iterated the system weight and volume until assumed and computed were equal (Czysz et al. 1973). This is the approach taken in this chapter. The significant difference between a subsonic conventional aircraft and a hypersonic aircraft/space launcher is the propellant weight and its volume. For conventional commercial aircraft, the significant volume is that for the passengers.

Commercial transports have a *passenger volume* that approaches 80% of the total vehicle volume, while space launchers can have a *propellant volume* that approaches 80% of the total vehicle volume (Billig 1989). Although updated in subsequent references, this observation was also reported in earlier studies (Anon 1970). The reason is the much larger chemical energy required to reach altitude and speed of space launchers compared to those of airliners. Volume limitations were recognized early on as forcing a balance between aerodynamic performance (drag, mostly) and usable mission volume. As in the design of aircraft, credible space launcher sizing programs must size for constant performance, then consider both volume and mass in their convergence criteria. The mass ratio for the mission was determined independently by trajectory analysis. The volume of the vehicle was iterated until volume available equaled volume required and the mass ratio equaled the mass ratio required (Pirrello and Czysz 1970; Krieger 1990). The sizing procedure then does converge on system volume and weight. The interdependence of aerodynamics, propulsion, and structure required this approach to consider the flight vehicle as a single system, not an assembly of separate systems. The authors have always used this approach for hypersonic aircraft; that is, considering a constant performance vehicle system sized to mission weight ratio and volume requirements.

A significant number of critical conditions have to be met at high speeds. As with all high-performance vehicles, there are overriding demands with respect to industrial capabilities in propulsion, materials, and structures. For whatever reasons, launch vehicle design has continued in its present form with all-rocket schemes that include limited recovery and limited reuse capability after refurbishment. This is the reason payload-to-orbit cost has not been significantly reduced. Consequently, the approach to the conceptual design of hypersonic and space launch vehicles has to focus on payload-to-orbit cost and sustained use (Koelle 1995; Lindley and Penn 1997), see Chap. 2. The successful design of a high-speed vehicle rests on (a) what data and projections can be established, including results available from preliminary studies (Czysz and Murthy 1996; Vandenkerckhove and Barrére 1997) and (b) recognition of the fact that the most significant gains may only be realized from propulsion/propellant capabilities. These represent the principal challenge.

These engineering considerations go hand in hand with the fact that a hypersonic vehicle in atmospheric flight is characterized by vast exchange of matter and energy with the atmosphere while producing useful work. It should therefore be analyzed just as any thermal machine, with efficiency depending on minimizing the entropy rise of each exchange, see also Camberos and Moorhouse (2011). This approach has direct implications, among others, for reusability. Based on this reasoning, determining launch vehicle size should emphasize management of all forms of energy and propulsion as the principal elements, given the available industrial capability and freedom in selecting vehicle geometry configurations and concepts.

The objective of this chapter is to provide a set of parameters representing the industrial technologies (industry capability) available today to fabricate a launcher system vehicle. These are based on physical observations of the authors and private communication and exposure with industry representatives responsible for the industrial capability. Based on earlier work, a methodology is developed for the rational synthesis of reusable vehicles based on the

utilization of available data, projections, and characteristics of different configuration concepts. The methodology is then applied to the representative SSTO and TSTO launch system architectures, followed by addressing various limits for air-breathing propulsion as applied to SSTO and TSTO implementations incorporating air collection and air collection with separation. Note that the methodology applies to both aircraft and launch vehicles.

In this context, one recent development toward reusability is the historic satellite-delivering flight of the *Falcon 9* on December 21, 2015, by SpaceX (Taylor 2015) and the first flight of Blue Origin's reusable rocket *New Shepard* on April 29, 2015, to 58 miles altitude (Harwood 2015).

B. Sizing methodology

The approach described was applied to three vehicle classes: (A) the Douglas Aircraft Company *Phase I* systems studies of NASA-sponsored High-Speed Civil Transport (HSCT) resembling a supersonic commercial transport, which determined the *Phase II* configurations, sizes, and weights (Page 1986, 1987); over 30 airframe/propulsion system/fuel combinations were analyzed in Phase I, and three were selected for further study in Phase II. (B) The government funded recoverable SSTO vertical launch vehicle (Czysz 1991) by McDonnell Douglas Astronautics Company (later named the *Delta Clipper*); and (C) the sizing of demonstrator aircraft and reusable launch vehicles for the McDonnell Douglas Aeronautics and Astronautics Companies (Czysz and Murthy 1996; Czysz et al. 1997; Czysz and Froning 1997).

This approach was implemented in the early 1980s by J. Vandenkerckhove (VDK) as three separate computer programs, namely *SIZING*, *ABSSTO,* and *ABTSTO* (Czysz and Vandenkerckhove 2000). These sizing methodologies and software implementation generated some of the data utilized in this chapter. Development of the sizing programs began with the methodology described in *Hypersonic Convergence* (Czysz 1986), where we begin with the fundamental equation that defines the weight ratio to orbit.

$$W_{\mathrm{R}} = \frac{W_{\mathrm{TOGW}}}{W_{\mathrm{OWE}}} = \frac{W_{\mathrm{OWE}} + W_{\mathrm{ppl}}}{W_{\mathrm{OWE}}} = 1 + \frac{W_{\mathrm{ppl}}}{W_{\mathrm{OWE}}}$$

$$W_{\mathrm{R}} = 1 + \frac{W_{\mathrm{fuel}} + W_{\mathrm{oxidizer}}}{W_{\mathrm{OWE}}}$$

$$W_{\mathrm{R}} = 1 + \left(1 + \frac{W_{\mathrm{oxidizer}}}{W_{\mathrm{fuel}}}\right) \cdot \frac{W_{\mathrm{fuel}}}{W_{\mathrm{OWE}}} = 1 + \left(1 + \frac{O}{F}\right) \cdot \frac{W_{\mathrm{fuel}}}{W_{\mathrm{OWE}}} \tag{3.9}$$

The oxidizer-to-fuel ratio, *O/F* or $r_{O/F}$, is averaged over the trajectory and is equal to ($W_{\mathrm{oxidizer}}/W_{\mathrm{fuel}}$). For a given fuel and dry weight fuel fraction, the weight ratio is driven by the oxidizer-to-fuel ratio. Whatever the fuel choice, the weight ratio can be minimized if the oxidizer-to-fuel ratio can be minimized. The weight ratio may also be expressed in terms of the effective specific impulse, I_{spe}, with the following:

$$W_{\mathrm{R}} = \exp\left(\frac{\Delta V}{g \cdot I_{\mathrm{spe}}}\right) \tag{3.10}$$

The weight ratio, W_{R}, and effective specific impulse, I_{spe}, are functions of the oxidizer-to-fuel ratio for a given fuel. Rearranging the above equations, we arrive at two fundamental equations on which this sizing approach is built.

$$W_{\mathrm{OWE}} = \frac{V_{\mathrm{ppl}}}{S_{\mathrm{plan}}} \cdot \frac{\rho_{\mathrm{ppl}}}{W_{\mathrm{R}} - 1} \cdot S_{\mathrm{plan}}$$

$$W_{\mathrm{OWE}} = \frac{V_{\mathrm{ppl}}}{V_{\mathrm{tot}}} \cdot \frac{V_{\mathrm{tot}}}{S_{\mathrm{plan}}^{1.5}} \cdot I_{\mathrm{p}} \cdot S_{\mathrm{plan}}^{1.5} \tag{3.11}$$

The operational weight empty (W_{OWE}) is a product of three terms [see Eqs. (3.11a, b)]. In Eq. (3.11a), the first term $V_{\mathrm{ppl}}/S_{\mathrm{plan}}$ is determined by geometry, the second term $\rho_{\mathrm{ppl}}/(W_{\mathrm{R}} - 1)$ by the aero-thermo-propulsion system, and the third term S_{plan} by vehicle size.

With the appropriate substitutions as derived before, the propulsion index, I_{p}, is given as follows:

$$I_{\mathrm{p}} = \frac{\rho_{\mathrm{ppl}}}{W_{\mathrm{R}} - 1} \tag{3.12a}$$

$$I_{\mathrm{p}} = \left[\frac{\rho_{\mathrm{fuel}} \cdot \left(1 + r_{O/F}\right)}{1 + r_{O/F} \cdot \frac{\rho_{\mathrm{fuel}}}{\rho_{\mathrm{oxidizer}}}}\right] \cdot \left\{\exp\left[\frac{\Delta V \cdot \frac{T}{D}}{g \cdot I_{\mathrm{sp}} \cdot \left(\frac{T}{D} - 1 - \frac{\sin\gamma}{\frac{T}{D}}\right)}\right] - 1\right\}^{-1} \tag{3.12b}$$

The propulsion index, I_{p}, is the product of two terms. The *first term* is a function of the density of the propellants and their oxidizer-to-fuel ratio. The *second term* is more complex. It is a function of the propellant and engine selection; engine size, excess thrust over drag, and climb angle, γ, for a given increment of velocity. The propulsion index, I_{p}, can be evaluated along a trajectory or used as an index of a given propulsion/propellant system over an entire trajectory. Its magnitude is a function of maximum sustained speed of the vehicle and not a significant function of the specific propulsion type. In the authors' analyses for SSTO space launchers, based on SSME class turbopumps and operating pressures, the propulsion index spans the spectrum from an all rocket SSTO to an all airbreather SSTO, which is $\Delta I_{\mathrm{p}} = 4.0 \pm 0.5$. For any given vehicle speed, the larger the propulsion index, the smaller and lighter the vehicle. The

mean value of the propulsion index, as a function of the maximum sustained Mach number of the vehicle, is:

$$I_p = 107.6 \times 10^{-0.081 \cdot M} \tag{3.13}$$

The scatter around the mean is about ±10% from a subsonic cruise fighter with supersonic dash capability to a SSTO vehicle.

C. Fundamental sizing relationships

The non-dimensional volume index τ, introduced by D. Küchemann (Küchemann 1978) and credited to J. Collingbourne (Küchemann 1960; Collingbourne and Peckham 1967), relates volume to planform area. The W_{OWE} can now be related to vehicle design parameters. Although Küchemann calls τ a volume parameter, it can indeed be considered a slenderness parameter. This is clearly illustrated in Fig. 3.28 for a long-range, hypersonic aircraft sized with three different fuels: JP/kerosene (752 kg/m^3, 47 lb/ft^3), subcooled liquid methane (464 kg/m^3, 29 lb/ft^3), and subcooled liquid hydrogen (74.6 kg/m^3, 4.66 lb/ft^3). This is an order of magnitude range in fuel density. For a kerosene-fueled, low-volume per-unit-planform-area slender aircraft like a SST, τ = 0.03. As fuel density decreases, the value of τ increases to 0.039–0.147. For a high-volume per-unit-planform-area vehicle like a hydrogen–oxygen combined-cycle powered space launcher, τ can be in the 0.18–0.20 range.

Introducing τ, Eqs. 3.11a, b becomes:

$$W_{OWE} = \frac{\rho_{ppl}}{W_R - 1} \cdot \left(\frac{V_{ppl}}{V_{tot}}\right) \cdot \tau \cdot S_{plan}^{1.5}$$

$$W_{OWE} = I_p \cdot \left(\frac{V_{ppl}}{V_{tot}}\right) \cdot \tau \cdot S_{plan}^{1.5} \tag{3.14}$$

where

$$\tau = \frac{V_{tot}}{S_{plan}^{1.5}} \tag{3.15}$$

Recalling that

$$W_{OEW} = W_{OWE} - W_{pay} - W_{crew} \approx W_{dry} \tag{3.16}$$

it follows that

$$W_{OEW} = \left(\frac{\rho_{ppl}}{W_R - 1}\right) \cdot \left(\frac{V_{ppl}}{V_{tot}}\right) \cdot \tau \cdot S_{plan}^{1.5} - W_{pay} - W_{crew}$$

$$W_{OEW} = \left(\frac{\rho_{ppl}}{W_R - 1}\right) \cdot \left(\frac{V_{ppl}}{V_{tot}}\right) \cdot \frac{\tau \cdot S_{plan}^{1.5}}{(1 + r_{use})} \tag{3.17}$$

We now have the design variables related directly to the dry weight. However, a word of caution: the three weight terms in Eq. 3.16 and subsequently Eqs. 3.17a, b *are not* independent variables. They are related through the propellant and propulsion system. From Eq. 3.14a, b, it might seem that a low value of the propulsion index is desirable. In fact, for the combined volume and weight convergence point, the higher the propulsion index, the less the operational empty weight. This is because the other two parameter groups *are not* independent of the value of the propulsion index. As pointed out by Froning and Leingang (1990), r_{pay} (payload to empty weight ratio) is essentially a constant for most launch vehicles. Thus, Fig. 3.29 shows that the payload-to-gross weight ratio is only an artifact of the weight ratio to orbit. A much more meaningful ratio is the payload-to-empty weight ratio. This ratio is essentially constant with the air-breathing speed increment. The data for the comparison is for the payload only. The vehicles forming the data-base were manned, so adding a value for the crew weight to r_{pay} provides a value for the useful payload ratio r_{use}.

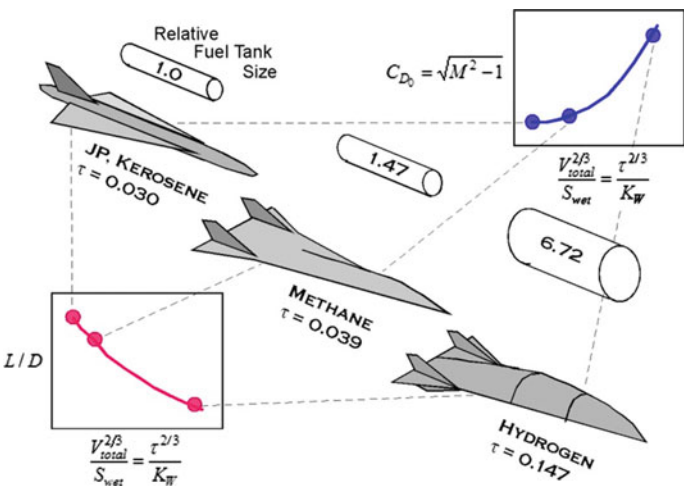

Fig. 3.28 Propellant density drives configuration concept and slenderness

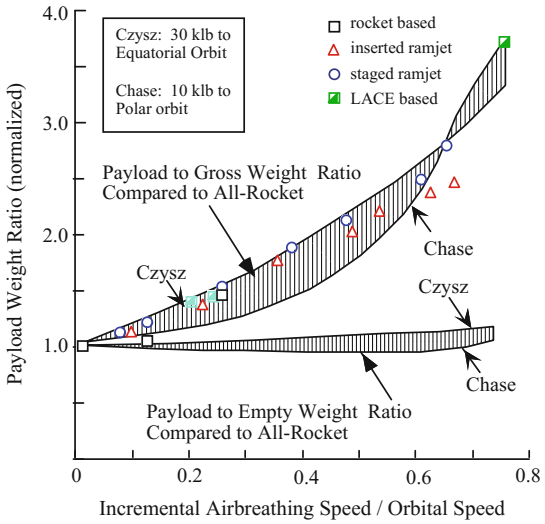

Fig. 3.29 Payload weight ratios show empty weight ratio as constant (essentially constant dry weight payload fraction)

Using one additional definition for structural fraction, r_{str}, the series of fundamental equations is complete with the following equation:

$$\frac{W_{str}}{S_{wet}} = \left(\frac{\rho_{ppl}}{W_R - 1}\right) \cdot \left(\frac{V_{ppl}}{V_{tot}}\right) \cdot \frac{r_{str}}{(1 + r_{use})} \cdot \frac{\tau \cdot S_{plan}^{1.5}}{K_w} \quad (3.18)$$

where

$$W_{str} = W_{OEW} \cdot r_{str} \quad (3.19)$$

$$K_w = \frac{S_{wet}}{S_{plan}} \quad (3.20)$$

Equation 3.18 now directly relates geometry-based parameters with the material/structure and propulsion-based parameters. Please note that the propulsion index, the propellant volume ratio, and the geometric terms directly affect the required structural weight per unit wetted (surface) area. The greater the propulsion-propellant system performance (i.e., the greater the value of I_p), the heavier the structural weight allowed for convergence, and therefore, the less technology is required. The corollary is that poor propulsion performance always demands structural and material fabrication breakthroughs.

D. Effect of τ on configuration concepts

In order to visualize the effect of Küchemann's τ, Fig. 3.30 shows blended-body configurations from very slender to very stout, with their associated value of τ, the ratio of wetted to planform surface, K_w, and the maximum lift-to-drag ratio at Mach 12. The minimum size configuration is the minimum volume vehicle consisting of only the propulsion-configured compression side of the vehicle and a flat upper surface. The stout vehicle is the stoutest still capable of overcoming transonic drag with a practical propulsion system and obtaining a high value of thrust minus drag.

E. Parametric sizing interactions

The relationship between τ and K_w (Czysz 1998) is dependent on the configuration concept. The premise for the sizing approach utilized in *Hypersonic Convergence* (Czysz 1986) is that families of geometries (geometry lineages) represent the characteristics of hypersonic vehicles rather than detailed and individual point designs. Given propulsion system characteristics and industrial capability, the result is a continuum of configuration concepts (solution topography) derived from the values of these geometric parameters that permit convergence within the technology limits set by the structural and propulsion indices. Thus, the converged configuration is a result of a multi-disciplinary parametric analysis and not an initial assumption.

Figure 3.31 shows the range of τ and K_w for a number of families of hypersonic configuration concepts appropriate for space launchers, all with 78° leading-edge sweep angle (see Sect. 3.9.1 for the full range of configuration concepts). Also shown, as a reference point, is the vertical launch rocket wing-body configuration with an aft wing, the NASA Langley WB004C configuration (Martinovic and Cerro 2002). The three propulsion integrated launchers (blended-body, wing-body, and Nonweiler waverider) are from converged design studies that supported the work by Escher (1993, 1995). The other configurations are from mathematical models for the surface area and volume (see Sect. 3.9.1 for detail). Combined-cycle engine launchers (which include hypersonic cruise aircraft) are powered by airbreathing propulsion over all or part of their flight path. The hypersonic glider configurations (with blunt bases) are ascent vehicles that return to earth unpowered and are based on the work at the USAF Flight Dynamics Laboratory (FDL) (Kirckham et al. 1975) in the 1960s. All of the vehicles include control surface areas in the total wetted area. The impact of geometry on the size and weight of a launch aircraft is clearly shown in Czysz and Murthy (1991).

In Fig. 3.28, the correlating parameter is not τ but $\tau^{2/3}/K_w = S^{-1}$. In one author's (P.A. Czysz) work experience in advanced design, the aerodynamic correlating parameter based on volume and area has been ratios of *areas,* not *volumes* (Anon 1965). In Vandenkerckhove and Barrére

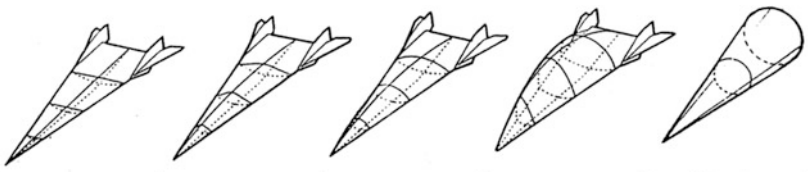

	Minimum	Slender	Nominal	Stout	Circular Cone
tau	0.032	0.063	0.104	0.229	0.393
K_W	2.44	2.51	2.64	3.39	3.61
$\beta \cdot C_{D0}$	0.0613	0.0639	0.0574	0.0809	0.0980
L/D M = 12	4.82	4.71	4.57	4.13	3.70

Fig. 3.30 The blended-body has a 7–1 volume range by upper body shaping

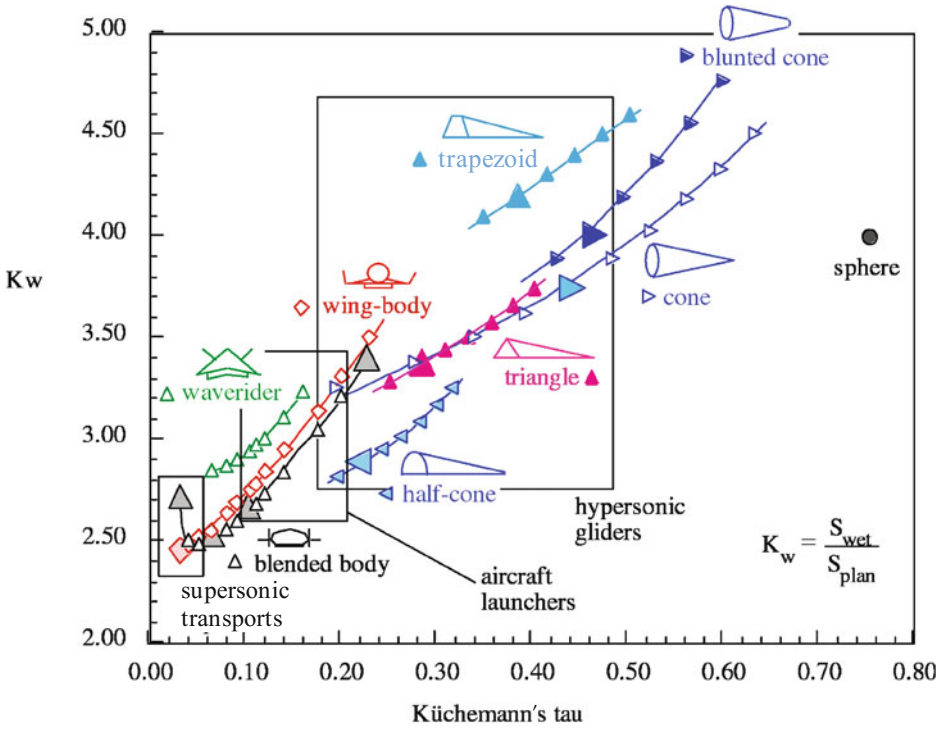

Fig. 3.31 The surface and volume continuum of hypersonic configuration concepts

(1997), both correlation parameters S and T are presented, where parameter S is called the *volumetric efficiency factor* and the parameter T is called the *shape efficiency factor*. Then, the same variables have been used, but in different combinations. The following transformations are helpful:

Küchemann's convention is:

$$\tau = \frac{V_{total}}{S_{plan}^{1.5}} = T^{-1.5} \tag{3.21}$$

US industry convention is:

$$T = \frac{S_{plan}}{V_{total}^{0.667}} = \tau^{-0.667} \tag{3.22}$$

$$\sigma = \frac{V_{total}}{S_{wet}^{1.5}} = \frac{V_{total}}{\left(K_w \cdot S_{plan}\right)^{1.5}} = S^{-1.5} \tag{3.23}$$

$$S = \frac{S_{wet}}{V_{total}^{2/3}} = \frac{K_w \cdot S_{plan}}{V_{total}^{2/3}} = \sigma^{-0.667}$$

$$S^{-1} = \frac{V_{total}^{2/3}}{S_{wet}} = \frac{S_{plan}}{T \cdot S_{wet}} = \frac{1}{T \cdot K_w} = \frac{\tau^{2/3}}{K_w}$$

$$\frac{V_{total}^{2/3}}{S_{wet}} = \frac{\tau^{2/3}}{K_w} \tag{3.24}$$

Equation (3.24c) is reflected in Fig. 3.28.

F. **Summary of parameter groups**

Parameter groups that dominate the sizing process are listed in the following discussion. The variables within these parameters are interrelated, so a change in one can result in a change in the magnitude of some of the other parameters. This means that the sizing process is very interdependent and interactive among propulsion, propellant, geometry-size, materials, and structural concept. Mathematically speaking, this interdependence is generally nonlinear: Thus, choosing which variable is known, and which must be solved for, does change the solution or even negates convergence. A second consequence of nonlinearity is that an analytical solution generally cannot be found in closed form but only by iterating an initial (and reasonable) guess. Later, sizing of high-speed aircraft will include discussions about propulsion, propellants, aerodynamics, and geometry clarifying these points, but one observation is that the weight ratio is a function of oxidizer-to-fuel ratio, see Eqs. 3.9a, b, c as are the resulting configuration characteristics. Consequently, the identification of the configuration concept is the result of parametric analysis and not the input.

$$\frac{\rho_{\text{ppl}}}{(W_{\text{R}}-1)} = I_{\text{p}} \propto \text{propulsion concept, propellant, aerodynamics, energy}$$

$$\frac{W_{\text{str}}}{S_{\text{wet}}} = I_{\text{str}} \propto \text{materials, structural concept, manufacturing capability}$$

$$\frac{V_{\text{ppl}}}{V_{\text{total}}} \propto \text{size, fineness ratio } (\tau), \text{ geometry}$$

$$\frac{W_{\text{str}}}{W_{\text{OEW}}} = r_{\text{str}} \propto \text{materials, size, fineness ratio } (\tau), \text{ geometry}$$

$$\frac{W_{\text{pay}}}{W_{\text{OEW}}} = r_{\text{pay}} \propto \text{approximately constant}$$

$$\frac{S_{\text{wet}}}{S_{\text{plan}}} = K_{\text{w}} \propto \text{size, fineness ratio } (\tau), \text{ geometry}$$

G. **External aerodynamics**

The sizing methodology includes a parametric solution technique that provides the vehicle size and weight as a function of τ. Vehicle drag and, therefore, thrust-to-drag ratio must be determined to correct the weight ratio for thrust-to-drag changes as a function of τ. As presented on pages 670 and 671 of Murthy and Czysz (1996), this is accomplished via empirical correlations extracted from wind tunnel and flight test data. These correlations had been prepared by Dwight Taylor while at McDonnell Douglas Corporation in the 1960s (private communication, Taylor 1983).

Briefly, Taylor's original correlation parameter was:

$$\sqrt{\left(\frac{V_{\text{total}}^{0.667}}{S_{\text{plan}}}\right)\cdot\left(\frac{S_{\text{wet}}}{S_{\text{plan}}}\right)^{1.5}} = \tau^{0.333}\cdot K_{\text{w}}^{0.75} = F \qquad (3.25)$$

In (Küchemann 1978), Küchemann provides a correlation for lift-to-drag ratio of the form:

$$\left(\frac{L}{D}\right)_{\text{max}} = \frac{A}{M}\cdot(M+B) \qquad (3.26)$$

where the constants A and B are as defined by Küchemann and the authors for slender aircraft (SoA = state-of-the-art):

1959 SoA	Future SoA	This chapter data-base
$A = 3$	$A = 4$	$A = 3.063$
$B = 3$	$B = 3$	$B = 3$

The aerodynamic correlations for drag and lift-to-drag ratio are then:

$$\left(\frac{L}{D}\right)_{\text{max}} = \frac{3.063}{M}\cdot(M+3) \qquad (3.27)$$

$$\beta\cdot C_{D_0} = 0.05772\cdot\exp(0.4076)$$

with

$$\beta = \sqrt{M^2-1} \qquad (3.28)$$

The zero-lift drag coefficient C_{D0} is a function of relative volume, relative wetted area, and Mach number. It is not necessary to add all drag terms (complete drag build-up) to determine total drag. The total drag can be estimated using the approach of Vinh (1993):

$$\beta\cdot C_D\cdot S_{\text{plan}} = \beta\cdot C_{D_0}\cdot(1+B)\cdot S_{\text{plan}} \qquad (3.29)$$

At the maximum L/D, B is equal to 2. That is, the classical case where the optimum induced drag for a symmetrical airfoil section is equal to the zero-lift drag. As developed by Vinh, the values for (1 + B) are:

Acceleration :	$C_L \approx 0.10(C_L)_{L/D\text{max}}$ and $(1+B) = 1.075$
Minimum fuel flow cruise :	$C_L \approx 0.82(C_L)_{L/D\text{max}}$ and $(1+B) = 1.75$
$(L/D)_{\text{max}}$ glide :	$C_L \approx 1.00(C_L)_{L/D\text{max}}$ and $(1+B) = 2.00$

Given a reference configuration and drag, the thrust to drag along the trajectory can be corrected for total volume. That is:

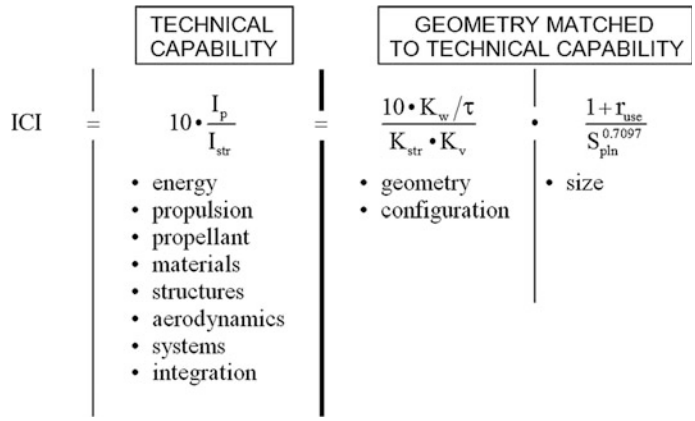

Fig. 3.32 The industrial capability index depends on technology and size of the configuration concept. Technology required equates to size and geometry of the configuration concept

$$\left(\frac{T}{D}\right)_{\tau} = \left(\frac{T}{D}\right)_{\tau_{\text{ref}}} \cdot \frac{(\beta \cdot C_{D_0})_{\tau_{\text{ref}}}}{(\beta - C_{D_0})_{\tau}} \tag{3.30}$$

$$(I_{\text{spe}})_{\tau} = (I_{\text{spe}})_{\tau_{\text{ref}}} \cdot \frac{(1 - T/D)_{\tau}}{(1 - T/D)_{\tau_{\text{ref}}}} \tag{3.31}$$

$$W_{\text{R}} = (W_{\text{R}})_{\tau_{\text{ref}}} \cdot \exp \frac{(I_{\text{spe}\,\tau})}{(I_{\text{spe}\tau_{\text{ref}}})} \tag{3.32}$$

Then, from the trajectory analysis, the drag corrected propulsion index (I_p) can be determined using Eq. 3.12a

$$I_{\text{p}} = \frac{\rho_{\text{ppl}}}{W_{\text{R}} - 1} (\text{in density units}) \tag{3.33}$$

The foregoing equations apply to an *accelerating space launcher vehicle*. In contrast, for *long-range cruise applications*, the correction must be introduced on the range equation, not the rocket acceleration equation (Czysz 1996).

H. Technology maturity determination

One result of the *Hypersonic Convergence* work (Czysz 1986) was the definition of a primary structure and propulsion interaction that controlled the size and weight of the aircraft, derived from Eq. 3.18. This evolved into the *Industrial Capability Index* (ICI) as a measure of the practicality of the vehicle under consideration, in terms of the industrial materials/fabrication/propulsion capability available. This index represents the relative measure of technological maturity. Maturity is the engineering capability to meet a specified goal. Overall, maturity involves capability in a number of areas: propulsion, aerodynamics, materials, manufacturing, and vehicle integration, as well as others. A definition of the ICI, is:

$$\text{ICI} = 10 \cdot \frac{I_{\text{p}}}{I_{\text{str}}}$$

$$\text{ICI} = 10 \cdot \left(\frac{\frac{\rho_{\text{ppl}}}{(W_{\text{R}} - 1)}}{\frac{W_{\text{str}}}{S_{\text{wet}}}} \right) \tag{3.34}$$

Figure 3.32 shows that the enabling capabilities are the propulsion system and the structural weight per unit surface area. Note that these are interdependent. If the structural index, I_{str}, is assumed larger (industrial technology less capable), and if the propulsion index, I_{p}, is not correspondingly increased (industrial technology more capable), the vehicle to be sized must become larger and stouter. The opposite is true if the propulsion index is improved, enabling a converged vehicle with higher structural weight per unit surface area. The technologies applicable to each side of the equation are indicated. The structural index is readily determined from current or projected industry achievements and manufactured hardware. The lower the *technology* of the materials and structural concept, the higher the value of the structural index (the heavier the structure per unit surface area).

The propulsion index is more indicative of the propulsion system hardware (turbopumps, heat exchangers, etc.) than of the thermodynamic cycle. If the propulsion index is determined from current hardware, then the ICI can be established. Taking the SSME engine hardware as a reference, the propulsion index from all-airbreather to all-rocket varies less than 15% when SSME hardware is applied to other propulsion cycles (Schindel 1989). For the SSME case, it will be found that the propulsion index is 57.0 ± 10 kg/m^3 (3.56 lb/ft^3 ± 0.5), and the structural index is 21 kg/m^2 (4.3 lb/ft^2) resulting in a value of 10 × ICI of 27.1 ± 5 m^{-1} (8.26 ± 1.5 ft^{-1}).

Equations 3.34a, b, as shown in Fig. 3.32, imply that for a given ICI there is a minimum-sized vehicle for each combination of geometric parameters. That is, the geometric solution can be less than the ICI in magnitude but not greater, and the greater the ICI, the more technology is required. If a small-sized vehicle is desired, then either the structural index must be reduced or the propulsion index must be increased. For instance, taking the demonstrated ATREX expander cycle of the Japanese ISAS (now: JAXA) (Tanatsugu and Suzuki 1986), it will be found that the propulsion index is 64.0 ± 10 kg/m^3 (4.02 lb/ft^3 ± 0.5), and the structural index is 19.5 kg/m^2 (4.0 lb/ft^2), resulting in a value of 10 × ICI of 32.1 ± 5 m^{-1} (10.0 ± 1.2 ft^{-1}). When the same ICI is desired, the structural index can increase to 23.7 kg/m^2 (4.86 lb/ft^2) without any change in vehicle size; alternatively, the vehicle planform area can be shrunk to 87% assuming the SSME industrial capability. A maximum index 10 × ICI = 37.7 ± 5 m^{-1} (11.5 ± 1.2 ft^{-1}) appears possible using the values from Tjonneland (1988).

Equations 3.34a, b can be mapped to show the available design space for a selected configuration (Czysz 1995), see Fig. 3.33 showing the design space map for the blended-body. It is important to recognize from Eqs. 3.34a, b that smaller vehicles are technologically more challenging compared to larger vehicles. Clearly, the most costly and technically challenging is the small demonstrator with zero payload, not the larger vehicle with payload capability. The technical capability indicated is what was judged to be available in the 1994 time frame. The small yellow circle symbols are the authors' evaluation of the 1994 ICI available in Europe. One author (J. Vandenkerckhove) focused on the maximum margin and minimum technology solutions that were the least slender (i.e., stouter). Another author (P.A. Czysz) focused on the solutions at the current industrial capability boundary.

The sizing process defined up to this point provides an indication of the possible design space, dependent on mission, configuration, propulsion, and propellant. The structural index, I_{str}, is straightforward. For non-space launchers (i.e., aircraft), the weight ratio is not the measure of propellant load, but of fuel fraction. For an aircraft application, the propulsion index, I_p, is given as follows:

$$I_p = \left(\frac{\rho_{ppl}}{W_R - 1}\right) = \frac{(1 - ff) \cdot \rho_{ppl}}{ff} \tag{3.35}$$

where

$$W_R - 1 = \frac{ff}{1 - ff} \tag{3.36}$$

$$ff = \frac{W_{fuel}}{W_{TOGW}} \tag{3.37}$$

As previously stated, the propulsion index, I_p, is a function of maximum sustained Mach number, so this sizing technique is not limited to space launchers. As applied to the high-speed commercial transport (HSCT), the propulsion index for kerosene fuel was 609 kg/m^3 (38.0 lb/ft^3) and 350 kg/m^3 (21.8 lb/ft^3) for liquid methane. That resulted in an ICI of 356.2 m^{-1} (108.6 ft^{-1}) for kerosene fuel. When the design space evaluation was executed for the HSCT, the result was not like that of Fig. 3.33. The minimum size and weight for a wing-body transport configuration with advanced variable bypass turbofan engines and hydrocarbon

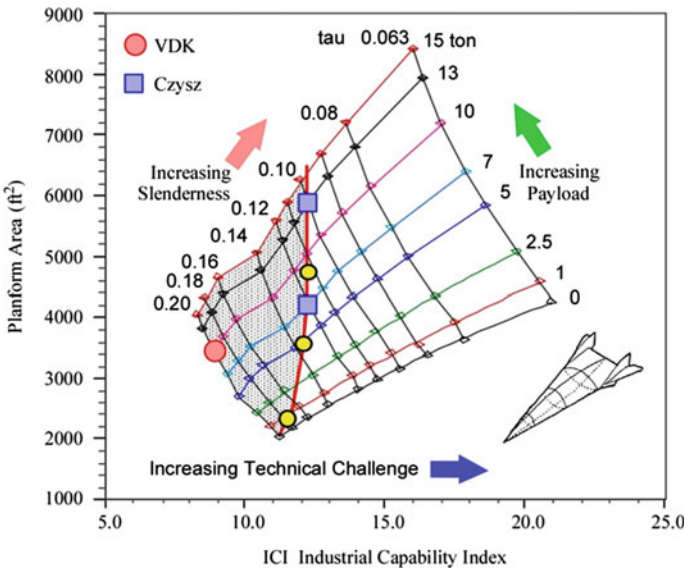

Fig. 3.33 Blended-body "design space" is bounded by realities of technology and geometry

fuel was obtained for $\tau \approx 0.035$, not $\tau \approx 0.20$ as in Fig. 3.33. Thus, this method provides a logical starting point for configuration development not based on conjecture or tradition but fundamental physical relationships. Consequently, much less time is needed to find a configuration that will converge.

3.7.3 Propulsion Systems

Airbreathing propulsion can be beneficial over a part of the flight trajectory. Historically, there are three broad categories of airbreathing propulsion:

(1) a combination of individual engines operating separately (sometimes in parallel, sometimes sequentially) that can include a rocket engine (Anon 1985);
(2) an individual engine (usually a rocket engine) operating in conjunction with one capable of more than one cycle mode (Tanatsugu et al. 1987; Nouse et al. 1988; Balepin et al. 1996), or a combined-cycle engine;
(3) a single, combined-cycle engine that operates in all of the cycle modes required, over the entire flight trajectory (Maita et al. 1990; Yugov et al. 1989).

For the single, combined-cycle concept, the engineering challenge is transitioning from one cycle to the next within a single engine. The transition from one engine cycle operation to another must be made *efficient* (on first law of thermodynamics basis, it means that the total energy losses must be minimized) and *effective* (on second law of thermodynamics basis, it means that when the energy is available for recovery as useful work, the energy conversion must be accomplished immediately or it becomes unrecoverable) (Curran 1993; Billig 1993). A category (3) engine is designed for minimum entropy rise across the cycle. The scope and limitations of these engines are discussed in detail in Froning et al. (1990), Czysz (1998), and several advantages to such a scheme have been identified (Escher 1995; Czysz and Little 1993; Czysz 1993).

A. Performance characteristics of airbreathing engines

The performance of an airbreathing engine is governed principally by the state properties of air and the vehicle characteristics that include: the captured mass flow, the inlet air kinetic energy, the energy released to the cycle by combustion with fuel, and the internal drag and energy losses through the engine flow path (Yugov et al. 1990). Evaluating these factors permits the establishment of performance boundaries based on first principles directly and addressing the highest-of-importance design drivers. The result is an altitude-speed (or equivalently, exhaust entropy-kinetic energy) envelope representation of performance potential and constraints for Brayton cycle airbreathing engines. The two boundaries are an altitude (equivalently, entropy state of exhaust gas) boundary and a velocity (equivalently, air kinetic energy to combustion energy ratio) boundary.

The first boundary is a function of the entropy of the gas exiting the propulsion system nozzle. Since the freestream entropy increases with altitude, for a fixed entropy rise engine cycle, the exhaust entropy also increases with altitude. The second boundary is a function of the kinetic energy of the freestream flow. At higher speeds, the air kinetic energy can significantly exceed the Brayton cycle combustion heat addition (to the airflow by combustion of a fuel). The ratio of maximum air combustion energy to kinetic energy is:

$$\frac{Q_{\text{net}}}{KE} = \frac{2 \cdot Q \cdot \eta_{\text{carnot}}}{V^2} \tag{3.38}$$

The Carnot cycle loss is the unrecoverable energy loss because the atmosphere (the cycle "cold end" receiver) is not at absolute zero temperature. A reasonable value for η_{carnot} is 0.79. The Brayton cycle heat addition, Q, for hydrogen is 1503 Btu/lb and for most hydrocarbons is 1280 ± 20 Btu/lb (Czysz 1986). From hydrocarbons to hydrogen, the Brayton cycle heat addition equals the air kinetic energy between 7100 and 7700 ft/s. As the vehicle speed increases, the combustion energy added to the airstream becomes a smaller fraction of the freestream kinetic energy. For hydrocarbons to hydrogen and for flight speeds between 14,200 and 15,400 ft/s, the Brayton cycle heat addition is 25% of the freestream kinetic energy. For hydrocarbons to hydrogen, and between 21,300 ft/s and 23,100 ft/s the Brayton cycle heat addition is 11% of the freestream kinetic energy. Energy input from combustion must overcome the losses that result from the external drag of the vehicle, energy losses associated with the internal engine flow, irreversible losses in the thermodynamic cycle, and supply as well the energy required for acceleration to orbital speed. Clearly, the energy available to overcome drag and provide acceleration is reduced by 4 every time the flight speed is doubled. The losses to overcome, however, are not a strong function of speed. The vehicle speed, when available energy just equals the drag energy, is the maximum airbreathing speed. For example, various losses may be expressed in the form of energy (energy losses) non-dimensionalized with respect to kinetic energy of the incoming air. Following this approach, we have:

Combustor drag losses:

$$\left(\frac{\Delta E}{KE}\right)_{\text{combustor}} = -\left(\frac{V_c}{V_0}\right)^2 \cdot \left(\frac{C_D \cdot S}{A_{\text{cowl}}}\right)_{\text{eng}} \tag{3.39a}$$

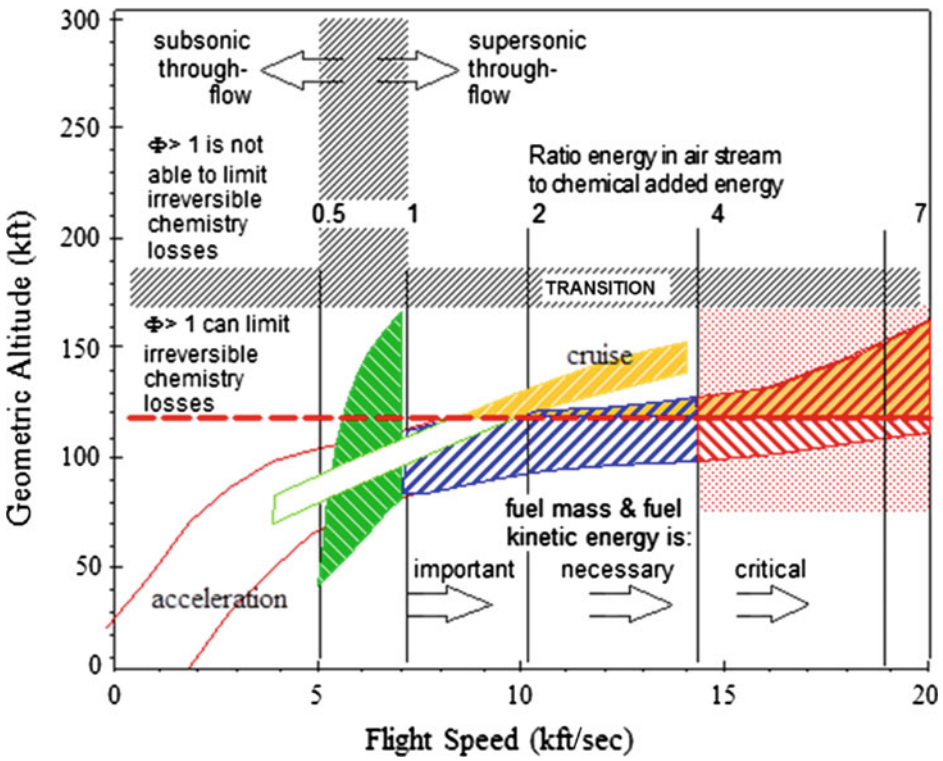

Fig. 3.34 As flight speed increases Brayton cycle operation is increasingly dependent on energy conservation, not fuel combustion

Fuel mixing losses:

$$\left(\frac{\Delta E}{KE}\right)_{\text{mix}} = -k_{\text{mix}} \cdot \left(\frac{V_c}{V_0}\right)^2 \tag{3.39b}$$

Vehicle drag losses:

$$\left(\frac{\Delta E}{KE}\right)_{\text{vehicle}} = -\left(\frac{C_D \cdot S}{A_c}\right)_{\text{vehicle}} \tag{3.39c}$$

Fuel injection losses:

$$\left(\frac{\Delta E}{KE}\right)_{\text{fuel}} = +\phi \cdot f_s \cdot \left(\frac{V_{\text{fuel}}}{V_0}\right)^2 \tag{3.39d}$$

Energy to accelerate:

$$\left(\frac{\Delta E}{KE}\right)_{\text{accel}} = -\left(\frac{T}{D}\right) \cdot \left(\frac{C_D \cdot S}{A_C}\right)_{\text{vehicle}} \tag{3.39e}$$

The only term that adds to the available energy of the air working fluid is the injected fuel energy. If the temperature of the fuel (in this case hydrogen) is scheduled so that the injected fuel velocity is equal to the flight speed, and the fuel injection angle is about 6°, then the injected fuel energy-to-kinetic energy ratio is $0.0292 \cdot \phi$. For an equivalence ratio of six, this provides an energy addition of 17.5%, or the equal of the maximum available combustion energy from fuel at 18,400 ft/s. Clearly, recovering normally discarded energy as thrust is just as critical as burning fuel in the engine. This is reflected in Fig. 3.34.

As the speed increases, the engine performance becomes more a question of energy conservation than of chemical combustion (Ahern 1992). The result is a spectrum of operation over the speed regime that was developed by Czysz and Murthy (1991) and is shown in Fig. 3.34. The figure illustrates the extent to which the kinetic energy of freestream air entering the vehicle inlet capture area and the fuel mass and internal energy become gradually more significant and critical as the flight speed increases. Thus, the operating limits of the airbreather can be clearly identified.

Examining Fig. 3.34, it should be clear that airbreathing propulsion is limited in both speed and altitude. The speed regime to the right of the energy ratio 4 line is questionable for an operational vehicle. It is possible for a research vehicle to investigate this area, but as we shall see, at the energy ratio 4 boundary the airbreathing vehicle has already achieved a significant fraction of the benefits from incorporating airbreathing. Consequently, from an energy viewpoint, a practical maximum airbreathing speed is 14,200 ft/s (4.33 km/s). To the right of this line, the payoff achieved compared to the resources required yields diminishing

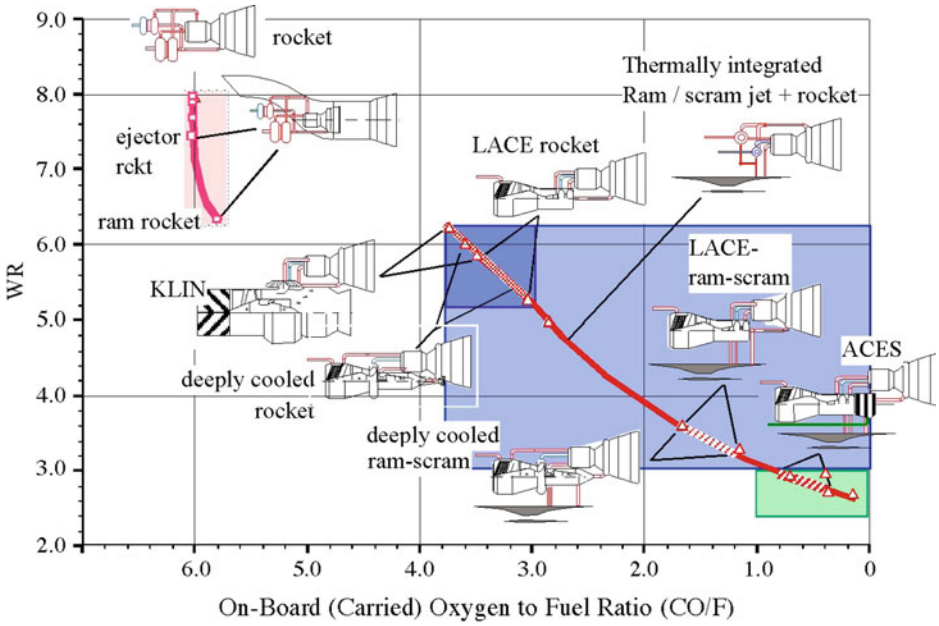

Fig. 3.35 Propulsion cycles determine carried oxidizer-to-fuel ratio (*CO/F*) and to-orbit weight ratio. To a 100 nmi orbit, weight ratio decreases with decreasing carried oxidizer

returns. The authors' contribution early on established a practical maximum for operational airbreathing launchers (Czysz 1992) at 3.9 km/s (12,700 ft/s) with the possibility to reach 14,000 ft/s (4.27 km/s), overall attainable via correct vehicle sizing, including compression side materials and minimum dry weight (Czysz 1995).

The altitude regime above 120,000 ft produces a degradation of thrust because increasing entropy limits the internal molecular energy that can be converted into bulk kinetic energy (exhaust gas velocity). Excess hydrogen is beneficial, providing abundant third bodies for the dissociated air molecules to recombine with up to a flight altitude of about 170,000 ft. Above that altitude, it is improbable a Brayton cycle engine can produce sufficient thrust. If excess fuel is used in Brayton cycle engines below 120,000 ft and less than 14,500 ft/s, it is to convert a fraction of the aerodynamic heating into net thrust via injection of the hydrogen at high velocity into the engine (such as the velocity corresponding to flight speed). Note that cruise engines operate at greater cycle entropy levels than acceleration engines.

Thus, up to this point, we have used first principles to establish that the vehicle will be stout, and not too small if it is to be built from available industrial capability (see Fig. 3.33). We have also established that it is not practical for an operational vehicle to exceed 14,200 ft/s in airbreathing mode. A flight velocity of 12,700 ft/s would be less challenging while retaining the benefits of airbreather operation.

B. Major sequence of propulsion cycles

There is a significant number of propulsion system options that have been studied. The authors have focused on those that are applicable to transatmospheric vehicles. The intent is to define the SSTO weight ratio and the onboard oxygen ratio carried by the vehicle. The smaller the weight ratio and the oxygen-to-fuel ratio, the smaller the size and gross weight of the vehicle. In terms of these parameters, the authors examined four principal propulsion categories with hydrogen as fuel, as shown in Fig. 3.35.

The *first* category is rocket-derived, air-augmented propulsion where the primary propulsion element is a rocket motor.

The *second* category is airbreathing rocket-derived propulsion where the propulsion elements are a rocket motor and an air/fuel heat exchanger.

The *third* category is the thermally integrated, combined-cycle engine propulsion where the principal element is a rocket ejector ramjet where the rocket ejector provides both thrust and compression (Nicholas et al. 1996; Der 1991).

The *fourth* category is the thermally integrated combined-cycle engine propulsion where the thermally processed air is separated into nearly pure liquefied oxygen and oxygen-poor nitrogen. The liquid enriched air is stored for later use in the rocket engine. Thermal integration means that the fuel passes through both rocket and the scramjet to scavenge rejected heat and convert it into useful work before entering the combustion chambers, increasing the specific impulse.

The combined-cycle concept dates back 55 years to the Marquardt Company (Escher 1995, 1996, 1999). Marquardt

had a propulsion concept that could go hypersonic with a single engine (Anon 1967). One of the Marquardt Company's concepts incorporated folding rotating machinery (Balepin et al. 1996) into their cycle. However, it is still a single engine that can go from takeoff to hypersonic speed.

1. *Rocket-derived propulsion*

Rocket-derived propulsion systems generally operate up to Mach 6 or less because of pressure and temperature limits of the air induction system. At Mach 6, inlet diffuser static pressures can typically equal 20 atmospheres and 3000 °R (1666 K). Although no rocket-derived propulsion systems are evaluated in this chapter, they are included for completeness in the comparisons. Overall, these propulsion systems can offer major advantages when applied to existing rocket launchers (Czysz and Richards 1998). As shown in Fig. 3.35, rocket-derived systems occupy the upper left-hand corner of the parameter space. The weight ratio to orbit is reduced proportionally to the thrust augmentation of the airbreathing system, but there is little change in the carried oxygen-to-fuel ratio. Examples of the rocket-derived air-augmented propulsion are as follows:

(1) Air-augmented rockets employ the rocket motor as a primary ejector (Nicholas et al. 1996; Mossman et al. 1960; Harper and Zimmerman 1942), so that some of the external airstream can be mixed with the rocket exhaust to increase mass flow and thrust at lower Mach numbers ($M < 6$), thus increasing the specific impulse. The rocket motor operates at its normal oxidizer-to-fuel ratio. The reduction of the mass-averaged exhaust velocity increases propulsion efficiency. This concept is not designed to burn the liquid oxygen in the entrained air. The weight ratio is reduced to 7.5 from 8.1, but the external air inlet system does add empty weight. However, with a mass ratio reduction of one-half, the system weighs less if the inlet system is less than 6.7% of the dry weight.
(2) The ram rocket is an air-augmented rocket cycle where the rocket is operated at a richer-than-normal oxidizer-to-fuel ratio enabling the oxygen in the entrained air to burn the excess fuel at the normal air-breathing air/fuel ratios for the fuel used (Scherrer 1988). The external airstream is mixed with the rocket exhaust to increase mass flow. Consequently, with the combustion of the excess fuel, thrust and specific impulse are increased at lower Mach numbers ($M < 6$). The weight ratio is reduced to 6.3, and the fuel-rich rocket operation reduces the oxygen-to-fuel ratio slightly. This is the best operational mode for the air-augmented rocket.

2. *Airbreathing rocket propulsion*

Airbreathing rocket-derived propulsion systems generally operate up to Mach 6 or less because of pressure and temperature limits of the air induction system. At Mach 6, inlet diffuser static pressures can typically equal 20 atmospheres and 3000 °R (1666 K). Airbreathing rocket propulsion concepts employ a method to reduce the temperature of air entering the inlet system so it can be compressed to rocket chamber operating pressures with reduced power requirements. There are two options: (a) The first option is to deeply cool the air just short of saturation and use a turbocompressor to pump the gaseous air into the rocket chamber; (b) the second option is to liquefy the air and use a turbopump to pump it into the rocket chamber (see Fig. 3.36). The rocket motor operates at nearly normal oxygen-to-fuel ratios, except that there is now a large mass of nitrogen also introduced into the combustion chamber. Again, the mass average exhaust velocity is reduced and the total mass flow increased, thus increasing thrust and propulsion efficiency. These propulsion systems are the darker shaded rectangle at the upper left-hand part of the shaded area in Fig. 3.35:

(1) The deeply cooled rocket is an expander cycle rocket developed by Rudakov and Balepin at CIAM (Rudakov and Balepin 1991) and Alan Bond for HOTOL. In Fig. 3.36, a more detailed view of the two airbreathing rocket cycles is shown. In the deeply cooled cycle, there is a hydrogen/air heat exchanger in the air inlet to capture the inlet air kinetic energy. This controls the air temperature entering the compressor and limits the work of compression and the compressor-corrected speed. The warmed hydrogen then enters the rocket combustion chamber to recover additional energy. The total thermal energy collected from the incoming air and hydrogen combustion chamber is then used to drive an expansion turbine which in turn drives a turbocompressor that compresses the cooled inlet air. That air can be cooled to nearly saturation by the hydrogen flow, then compressed to rocket operating pressures, and introduced into the combustion chamber. A rocket motor combustion chamber heat exchanger is necessary to provide sufficient energy to drive the turbomachinery. In effect, the rocket becomes an airbreathing rocket for Mach numbers less than 6. In this concept, there is no other air-breathing engine. This cycle reduces the mass ratio to the 5.2–6.0 range and the oxygen-to-fuel ratio to about 3.2. The main disadvantage is that flowrates, pressures,

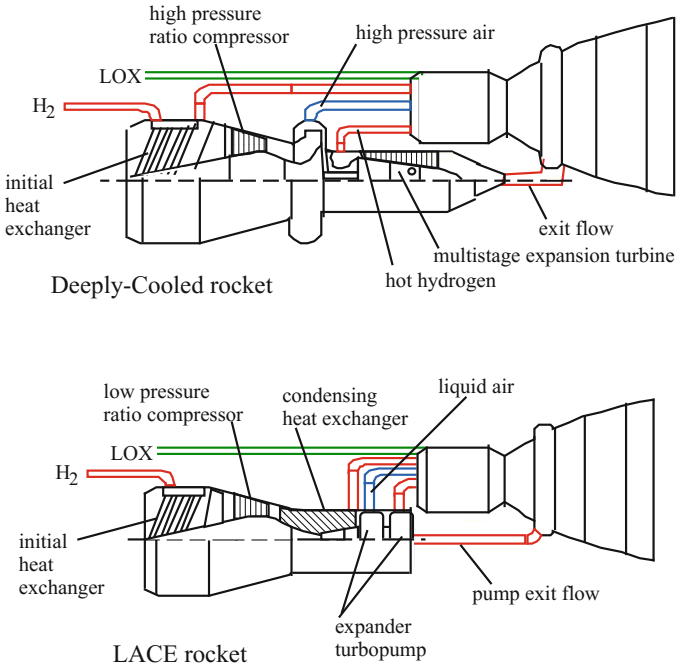

Fig. 3.36 Thermally integrated airbreathing rockets

and temperatures are interconnected by the heat exchangers and it is difficult to vary them operationally.

(2) The LACE rocket is the rocket part of the Aerospace Plane propulsion concept developed by the Marquardt Company in the mid-to-late 1950s (Escher 1966). LACE stands for **L**iquid **A**ir **C**ycle **E**ngine. It was examined in Russia (Rudakov et al. 1991; Balepin et al. 1993), Japan (Togawa et al. 1991; Miki et al. 1993; Ogawara and Nishiwaki 1989) and India (Anon 1988). As depicted in Fig. 3.36, this cycle, as with the deeply cooled, employs a hydrogen/air heat exchanger in the air inlet to capture the inlet air kinetic energy from the incoming air and it cools it to nearly saturation. The cooled air is then pressurized to a few atmospheres and flows into the pressurized liquefying heat exchanger. The total thermal energy collected from the incoming air and hydrogen combustion chamber is used to drive an expansion turbine which in turn drives a turbopump injecting liquefied air into the rocket motor. A heat exchanger in the rocket motor's combustion chamber is necessary to provide sufficient energy to drive the turbomachinery. In effect, the rocket becomes an airbreathing rocket for Mach numbers less than 6. In this concept, there are no other airbreathing engines. This cycle reduces the mass ratio to the 5.0–5.8 range and the oxygen-to-fuel ratio to about 3.

3. *Thermally integrated combined-cycle propulsion*

The fundamental element of the combined-cycle engine concept is a rocket ejector ram-rocket-ramjet thermally integrated into a rocket propulsion system (Lashin et al. 1993). In this section, the following two propulsion systems are the propulsion systems employed for the vehicle sizing studies: (a) LACE rocket ejector ram/scramjet, thermally integrated engine; (b) LACE-scramjet, thermally integrated engine. In the class of integrated ejector ram-scramjet propulsion, the integral rocket ejectors provide both thrust and compression at lower Mach numbers (Czysz and Richards 1998; Siebenhaar and Bulman 1995). The combination of ramjet and turbojet results in poor acceleration. However, the introduction of a deeply cooled turbojet that is thermally integrated with an expander rocket (KLIN cycle) (Balepin and Hendrick 1998) becomes analogous to the rocket ejector ram-rocket-ramjet, with the additional benefit of excellent low-speed performance. Examples of the thermally integrated engine's combined-cycle propulsion are as follows:

(1) Deeply cooled turbojet-rocket (KLIN cycle) is an adaptation of Rudakov and Balepin's deeply cooled rocket ramjet to a deeply cooled turbojet. The turbojet and rocket are thermally integrated. Unlike the ramjet, the precooler on the turbojet keeps the compressor air inlet temperature low to reduce compressor work and to increase mass flow and thrust. With the precooler, the turbojet does not see the inlet temperature associated with higher Mach number flight, so it appears to be at lower flight speed. The precooled turbojet provides a significant increase in transonic thrust. The precooled turbojet provides operation from takeoff to Mach 5.5 with rocket thrust augmentation when required, such as

in the transonic region. Above Mach 5.5, the turbomachinery is shut down and the rocket operates as a conventional cryogenic rocket. The KLIN cycle is equivalent to the ram rocket, ejector with combustion in secondary air cycle, in that the mass ratio is reduced to the 5.5–6.0 range and the oxygen-to-fuel ratio to about 3.4. However, it is not like this cycle in that it produces fuel-efficient, low-speed thrust.

(2) The deeply cooled rocket-ram-scramjet is the integration of the deeply cooled cycle developed by Rudakov and Balepin (1991) at CIAM and Alan Bond for HOTOL with a subsonic through-flow ramjet. In this cycle, the combustion energy of the incoming air and hydrogen in both rocket and ramjet is used to drive an expansion turbine, which in turn drives a turbocompressor. The incoming inlet air is cooled to nearly saturation in an air–hydrogen heat exchanger and then compressed to rocket operating pressures by the turbocompressor for introduction into the rocket combustion chambers. A heat exchanger in the rocket engine combustion chamber is necessary to provide sufficient energy to drive the turbomachinery. After leaving the expansion turbine, the hydrogen is introduced into the ramjet combustion chamber. At Mach 6 or less, the rocket is essentially an airbreathing rocket operating in parallel with a ramjet. Above Mach 6, the rocket is not used, and the ramjet operates as a supersonic through-flow ramjet (scramjet). After scramjet shutdown, the rocket operates as a conventional cryogenic rocket. In Fig. 3.35, the operational line is represented by the thick red line traversing the shaded area. For airbreather operation to the 12,000–14,000 ft/s range, this cycle can achieve weight ratios in the 3–4 range with oxygen-to-fuel ratios less than one.

(3) The LACE rocket-ram-scramjet is a **L**iquid **A**ir **C**ycle **E**ngine. It is like the Aerospace Plane propulsion concept developed by John Ahern at the Marquardt Company in the late 1950s. It was examined in the 1990s by Russia (Scherrer 1988; Rudakov and Balepin 1991), Japan (Rudakov et al. 1991; Balepin et al. 1993; Togawa et al. 1991) and India (Miki et al. 1993). In this cycle, the thermal energy from the incoming air and hydrogen combustion is used to drive an expansion turbine, which in turn drives a turbopump. The inlet air is cooled to nearly saturation by an air–hydrogen heat exchanger and then pressurized to a few atmospheres. It then flows into the pressurized liquefying heat exchanger. The turbopump pressurizes the liquid air to rocket operating pressures so it can be introduced into the rocket combustion chamber. A rocket motor combustion cham ber heat exchanger is necessary to provide sufficient energy to drive the turbomachinery. After exiting the turbomachinery, the hydrogen is introduced into the ramjet combustion chamber. At Mach 6 or less, the rocket is essentially an airbreathing rocket operating in parallel with a ramjet. The ramjet can convert to supersonic through-flow (scramjet) at Mach 6. Above Mach 6, the rocket is not used when the scramjet is operating. After scramjet shutdown, the rocket operates as a conventional cryogenic rocket. In Fig. 3.35, the operational line is represented by the heavy line traversing the shaded area. For airbreather operation in the 12,000–14,000 ft/s range, this cycle can achieve weight ratios in the 3–4 range with oxygen-to-fuel ratios less than one. The LACE cycles can achieve a specific impulse in the 4500 s and the Mach 6 to 3 range. Thermal integration provides about 1500 s of the 4500 s I_{sp}.

(4) The ejector ram-scramjet-rocket is an ejector ramjet thermally integrated with a rocket (Bulman and Siebenhaar 1995; Vandenkerckhove 1992a). The ejector may be a hot gas ejector and/or a rocket ejector. Remember, if the ramjet is a subsonic through-flow engine, then the scramjet is simply a supersonic through-flow engine. The maximum airbreathing speed can be selected from Mach 6 to at least Mach 14.5. At Mach = 6, the system is an ejector ramjet with the rocket ejectors distributed in the struts inside the ramjet engine module (Stroup and Pontez 1968). Above Mach 6, it is a conventional scramjet engine with variable configuration injectors to minimize internal drag (Czysz 1986). In Fig. 3.35, the operational line is represented by the thick line traversing the shaded area. This cycle can produce weight ratios from 6 to 3 depending on the maximum airbreathing speed. Despite its simplicity, it lacks the lower speed ($M < 6$) high-specific impulse of other cycles.

4. *Thermally integrated enriched air-combined-cycle propulsion*

These cycles are thermally integrated combined cycles except the thermally processed air is separated into nearly pure liquefied oxygen and oxygen-poor nitrogen. The liquid-enriched air is stored for use in the rocket engine during the ascent portion of the rocket's trajectory. The oxygen-poor nitrogen is introduced into the ramjet, creating the equivalent of a mixed-flow bypass turbofan. That is, the mass averaged exhaust velocity is reduced, but the specific impulse, engine mass flow, and thrust are increased. Thermal integration means that the fuel passes through both rocket

and scramjet to scavenge rejected heat and convert it into useful work before entering the combustion chambers, thus increasing the specific impulse. Examples of thermally integrated, enriched, air-combined-cycle propulsion are as follows:

(1) The ACES-LACE ejector ram-scramjet-rocket is an ACES (Hendrick 1996). ACES is an option added to the LACE system. The liquid air is not pumped to the rocket immediately, but passed through a fractionating system to separate the oxygen component as liquid-enriched air (LEA contains 80–90% oxygen) and nitrogen component as liquid oxygen-poor air (OPA contains from 2 to 5% oxygen) (Tagowa et al. 1991; Leingang et al. 1992). The oxygen component is then stored for use in the rocket's ascent portion of the flight. The oxygen-poor nitrogen component is injected into the ramjet to create a hypersonic bypass engine that increases engine mass flow and thrust and reduces the mass averaged exhaust velocity. At takeoff, this can significantly reduce the takeoff perceived noise. It is done for the same reasons a conventional mixed flow bypass gas turbine was invented. It was originally proposed for the space plane of the late 1950s and has been the subject of intense investigation in the 1960–1967 time period (Vandenkerckhove 1992a). For airbreather operation to the 12,000–14,000 ft/s range, this cycle can achieve weight ratios less than 3 with oxygen-to-fuel ratios approaching one-half.

(2) The ACES-deeply cooled ejector ram-scramjet-rocket is an ACES. ACES is an option added to the LACE system. The deeply cooled gaseous air is not pumped to the rocket immediately, but passed first through a vortex tube initial separator (at this stage, the LEA contains about 50% oxygen) and then into a cryogenic magnetic oxygen separator (unlike nitrogen, oxygen is diamagnetic). The oxygen component is then liquefied (LEA contains 80–90% oxygen and stored for use in the rocket's ascent portion of the flight. The gaseous component of oxygen-poor air (OPA) contains from 2 to 5% oxygen. The oxygen-poor nitrogen component is injected into the ramjet to create a hypersonic bypass engine that increases engine mass flow and thrust and reduces the mass averaged exhaust velocity. At takeoff, this can significantly reduce the takeoff perceived noise. It is done for the same reasons a conventional mixed-flow bypass gas turbine was invented. This system was tested in the laboratory (Vandenkerckhove 1992b), but has not as yet been developed as a propulsion hardware. For airbreather operation to the 12,000–14,000 ft/s range, this cycle can achieve weight ratios less than 3 with oxygen-to-fuel ratios approaching one-half.

C. Cycle comparison

When these propulsion systems are compared to the rocket, a number of observations are possible. The first of these regards the weight-ratio-to-orbit. Figure 3.37 shows the weight-ratio-to-orbit for the four categories as discussed in Fig. 3.35. The first two categories merge into a rocket-derived curve. The inserted ramjet and staged ramjet are integrated ejector ram-scramjet and rocket propulsion systems. The former have an airbreather inserted between two rocket operations (one from takeoff and the other from airbreather shutdown), while the latter have an airbreather function from takeoff followed by a rocket operation. Note that the weight ratio does not include propellant for orbital operations. If a nominal quantity were included, the weight ratio would be as indicated in the upper right-hand corner of the figure. The curve in the upper left indicates the region of applicability for rocket-derived propulsion systems. The other curve indicates the region of applicability for thermally integrated combined-cycle propulsion. The lower boundary of that area represents the maximum speed for airbreathing operation developed in Fig. 3.37. That achieves 88% of the maximum benefit possible with airbreathing in terms of weight ratio and velocity (about 22,000 fps, or 6.7 km/s). The technical, hardware, and economic challenges to achieve the last 12% of the weight ratio benefit by flying some 8000 ft/s faster probably exceed the benefits in the authors' opinion.

The sizing studies reported in this chapter focus on the shaded area, that is, airbreathing speeds between 6000 (1.83 km/s) and 12,000 ft/s (3.96 km/s). There is an area where the rocket-derived propulsion and combined-cycle propulsion are equivalent: This is the 5000–6000 ft/s (1.52–1.83 km/s) region, see Balepin et al. (1993) addressing this area. What Fig. 3.37 implies is that if an all-rocket gross weight is 7.5 times W_{OWE}, then a thermally integrated combined-cycle powered vehicle will be from 5.5 to 3.0 times W_{OWE}, depending on the maximum airbreathing speed. As shown in Fig. 3.30, the ratio of W_{pay} to W_{OWE} is essentially constant with airbreathing speed. Clearly, the combined-cycle propulsion reduces the gross weight by 2–4.5 times the W_{OWE}!

1. *Takeoff gross weight and takeoff mode*

In reality, horizontal or vertical takeoff, like the configuration concept, is less a choice than a result of the propulsion concepts selected. Figure 3.38 shows the impact of assuming vertical or horizontal takeoff for sized configurations with the

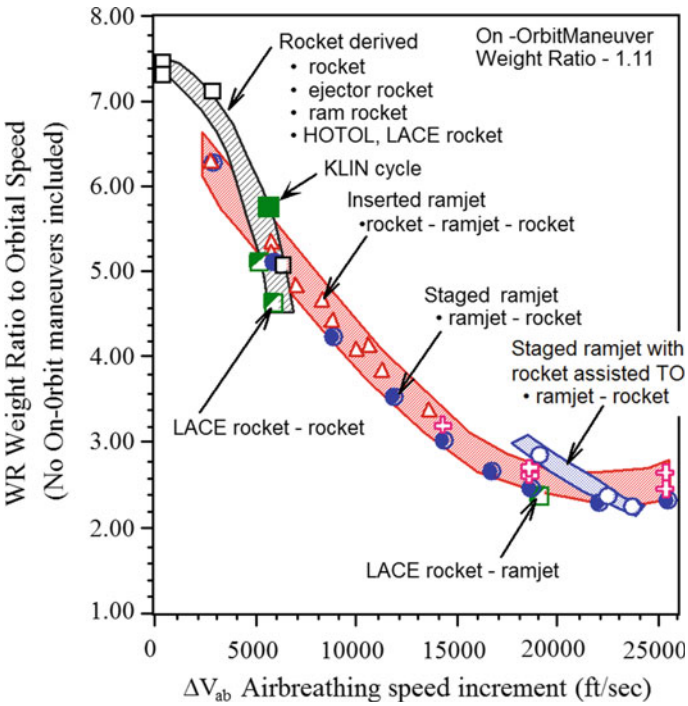

Fig. 3.37 Weight ratio reduction at 14,500 ft/s is 88% of maximum

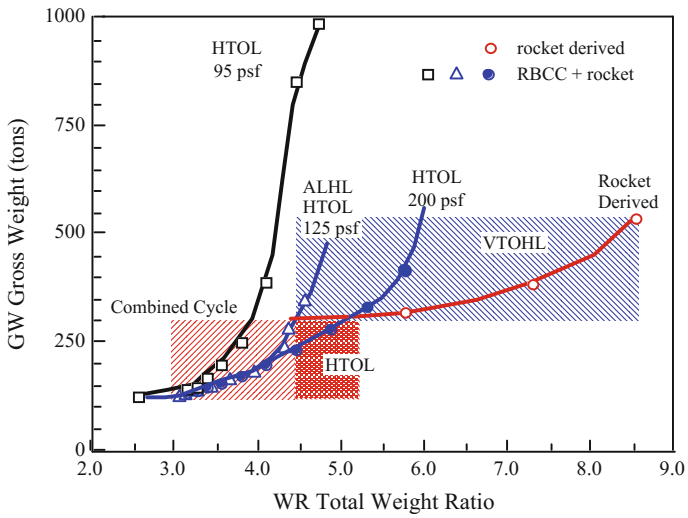

Fig. 3.38 Wing loading and weight ratio determine gross weight

same payload weight as a function of weight-ratio-to-orbit. Three different takeoff wing loadings were evaluated. VTHL takeoff thrust-to-weight ratio is 1.35. HTHL takeoff thrust-to-weight ratio is 0.75. Prior work suggested the nominal takeoff thrust-to-weight ratios, and no attempt was made to find an optimum takeoff thrust-to-weight ratio for each case. If the HTHL gross weight exceeds the VTHL gross weight, then the lighter vehicle is a VT mode. If thrust vectoring is available for nose wheel lift off, then the 200 lb/ft^2 (976 kg/m^2) is acceptable (Pirrello and Czysz 1970), although the takeoff speed is very high (about 344 knots).

The VTHL/HTHL boundary for 200 lb/ft^2 is a weight ratio of 5.2, or an airbreathing speed of about 7000 ± 1000 ft/s. For a takeoff wing loading of 125 lb/ft2 (610 kg/m^2), the takeoff speed is 291 knots, and the VTHL/HTHL boundary is now a weight ratio 4.3, or an airbreathing speed of 10,000 ± 1000 ft/s. This wing loading also applies to air launch horizontal landing (ALHL) in the Mach 0.72 at 35,000 ft region. For a takeoff wing loading of 95 lb/ft^2 (464 kg/m^2) and a takeoff speed of 254 knots, only the maximum airbreathing speed would permit horizontal takeoff. This wing loading is in fact too low to be practical for launchers as it drives the gross weight to unacceptable levels. The conclusion is that if the weight ratio is greater than 4.3, the best vehicle is a VT configuration or an

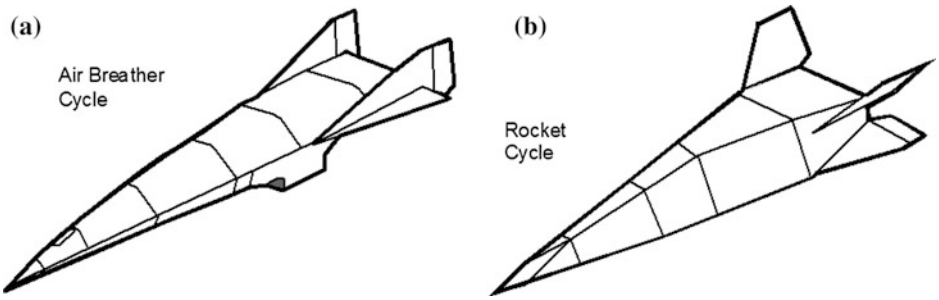

Fig. 3.39 Propulsion cycle determines configuration concept: **a** airbreather cycle (combined-cycle powered hypersonic aircraft); **b** rocket cycle (rocket-derived powered hypersonic glider)

air-launched configuration. For all vehicles considered in this report, the landing mode is horizontal.

Choosing the 125 lb/ft^2 (610 kg/m^2) takeoff wing loading means that only launchers with airbreathing speeds over 10,000 ft/s will be considered for horizontal takeoff. Thus, like the choice of the configuration concept, the choice of the takeoff mode is a result of engineering decisions—it is not an arbitrary selection! In terms of configuration concept selection, the choice is based on whether or not the airbreather is a rocket-derived or thermally integrated combined cycle. Landing wing loading is equivalent to a combat fighter, less than 45 lb/ft^2 (220 kg/m^2).

2. *Configuration concept*

Given the space infrastructure of the twenty-first century, it is important to recall that rescue and supply of manned space facilities requires the ability to land in a major ground-based facility at any time from any orbit and orbital location. [Similar considerations apply also to boost-glide weapon systems.] The cross and down-range needed to return to a base of choice also requires high aerodynamic performance. For the rocket-derived propulsion concepts that are limited to Mach 6 or less, an acceptable inlet can be integrated into the vehicle configuration derived, for example, from the FDL-7 series of hypersonic gliders developed by the Flight Dynamics Laboratory (Draper and Sieron 1991) and the work of the McDonnell Douglas Astronautics Company. The thermally integrated combined-cycle configuration concept is derived from the McDonnell Douglas Advanced Design organization in St. Louis. This is a family of rocket-accelerated hypersonic airbreathers (Czysz 1986). They can take off horizontally, vertically, or be air launched. In its initial 1960s propulsion configuration, the vehicle was accelerated by a main rocket in the aft end of the body. Today, it can retain this concept or use combined-cycle propulsion. In any case, rockets are usually mounted in the aft body for space propulsion.

Both the hypersonic aircraft and the hypersonic glider shown in Fig. 3.39 have hypersonic lift-to-drag ratios in excess of 2.7. That means unpowered cross-ranges in excess of 4500 nautical miles and down-ranges on the order of the circumference of the earth. Clearly, these two craft can depart from any low-altitude orbit in any location and land in the CONUS. Both are stable over the entire glide regime. The zero-lift drag can be reduced in both by adding a constant width section to create a spatula configuration. The maximum width of this section is generally the pointed body half-span. The pointed configurations are shown in Fig. 3.39. No wing-body (WB, winged-cylindrical body) configurations have been considered.

3. *Onboard (carried) oxidizer*

The question is, why all the trouble about airbreathers? Is not a rocket good enough? Perhaps for ballistic missiles, but not for vehicles that must achieve airline flight frequency, durability, and safety. The key to reducing size and weight, to enable the vehicle to abort at launch with vehicle and payload surviving in a failed operational state, is to reduce the onboard propellant and oxidizer. The rocket-derived propulsion reduces the weight-ratio-to-orbit but does not significantly affect the carried oxygen-to-fuel ratio. Both airbreathing rocket-derived propulsion and the thermally integrated engine combined-cycle engine reduce weight ratio and carried oxygen-to-fuel ratio. The ACES provides the greatest reduction in both weight ratio and oxygen-to-fuel ratio. Airbreathing rocket cycles (i.e., LACE or deeply cooled) can eliminate about 40% of the oxidizer from the launcher, so that for every 100,000 lb of hydrogen there is about 36,000 lb of liquid oxygen carried onboard instead of 600,000 lb for the pure rocket. For the thermally integrated combined-cycle propulsion, the liquid oxygen load can be only 200,000 lb. For the ACES propulsion, it might be possible to reduce the liquid oxygen load to 100,000 lb or less. The result is smaller, lighter vehicles that have better abort capability and have the potential of affordable sustained operations, with scheduled maintenance (Czysz and Froning 1995).

Ashford and Emanuel have compared ejector ramjet to the Oblique Detonation Wave Engine (ODWE). The ODWE can be one operating regime of a combined-cycle propulsion system (Townend and Vandenkerckhove 1994) when internal drag of the engine module becomes overly large as to significantly diminish the thrust-to-drag ratio at high hypersonic speeds (Vandenkerckhove and Barrére 1997).

3.7.4 Sizing Methodology and Software Implementation

Due to the demanding aerothermodynamics environment of hypersonic flight vehicles, the design of this class of aircraft requires a unique aerodynamic, propulsion, and structural integration logic, an integration level usually not found with traditional subsonic and supersonic aircraft. The design problem posed with hypersonic aircraft requires an advanced sizing logic since the hypersonic flight vehicle tends to have a fully blended geometry, where the "fully integrated body" must perform all functions (provide volume, lift, integrated propulsion, stability and control, payload housing, etc.).

A technical specialist's view of an aircraft can be that each technical discipline is independently responsible for that specialty's components and can independently optimize that component based on stated requirements for that component. In the past, for non-hypersonic aircraft, changes in each component were accounted for separately by each individual discipline. The interfaces were then checked and the elements were assembled. However, changing any one element evokes changes in many dependent elements. That is, a larger wing would require a larger engine, which would require more fuel, which would require more volume, and so on. For high-speed aircraft we have encountered in the past (Mach 3.5 or less), this approach was still acceptable. However, as speeds increase, this optimization of independent components does not lead to an integrated optimum. In fact, a very non-optimum result can be the outcome. This was strikingly clear in the 1960s for an aero-propulsion integration effort sponsored by the USAF and USN called Comparative Operational Propulsion Systems (COPS). An optimum airframe plus an optimum isolated nacelle resulted in a significant loss in performance when assembled into one unit. Clearly, a successful hypersonic system is not the assembly of a number of individually optimized subsystems.

As shown in Fig. 3.40, typical subsonic/supersonic sizing methodologies size the wing and propulsion system simultaneously, while the fuselage and empennage are sized independently. In contrast, the hypersonics convergence logic must consider the integrated aircraft, a clear departure from the traditional conceptual design methodologies (Chudoba 2002).

Integrating the volume (fuselage), aerodynamic surfaces (wing, empennage) and propulsion system simultaneously requires the explicit inclusion of volume in the convergence logic. In contrast, most subsonic design methodologies only check the wing fuel volume. This significantly advanced sizing logic is shown in Figs. 3.44 and 3.45.

Traditionally, the aircraft companies used constant gross weight analyses and photographic scaling as the primary approach for conducting design trades. Herbst (Herbst and Ross 1969, 1970) introduced to McDonnell Aircraft Company and one of the authors (P.A. Czysz) a scaling approach based on requirements, not fixed weight. In the requirements sizing approach, each component is sized iteratively until the entire system meets all of the requirements. Formerly, each configuration concept with the same weight had a different performance. Each sized configuration concept now has the same performance *with different size and mass*. Performed

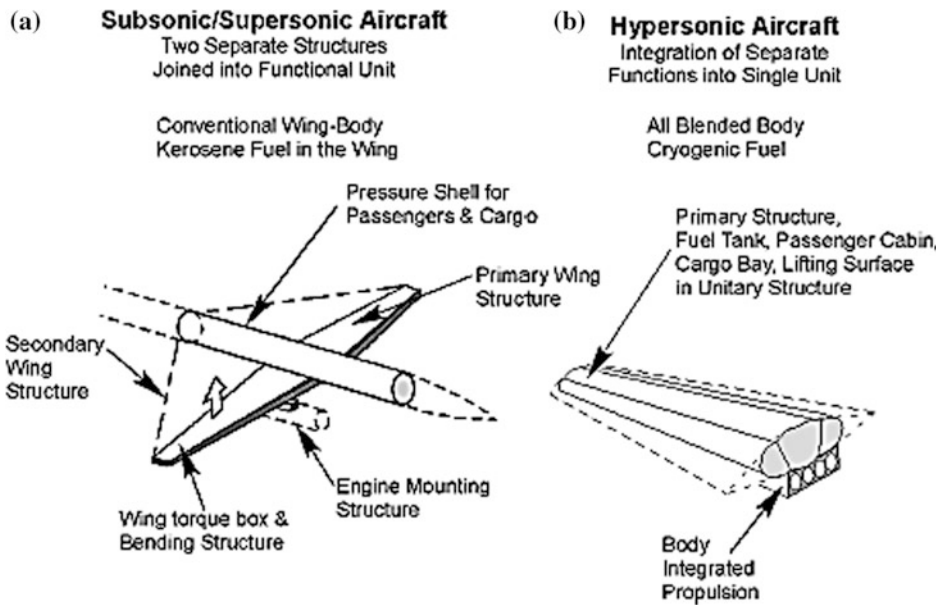

Fig. 3.40 A sizing perspective of geometric and functional **a** non-integrated subsonic/supersonic aircraft, and **b** highly integrated hypersonic aircraft

with a computer-aided design program, this approach was and still is revolutionary. Cycle time to evaluate a configuration concept was drastically reduced. With the sizing program, the system meets the specifications, but each component is not "the optimum within its own application" but what is optimally necessary for the entire system. In contrast, single component performance is insufficient to meet the integrated-system specifications.

The hypersonic sizing problem is both mass and volume challenged. Space launchers and passenger-carrying aircraft offer the additional volume problem of a bulk payload density approximately that of liquid hydrogen, that is, very low. The general sizing approach adopted is to specify the payload and propulsion system performance. An initial estimate is made for the planform area. The resultant iterations continue until volume available equals volume required.

In the following, three *sizing* implementation generations are presented that apply the relationships developed in Sect. 3.7.2: (A) *1st Generation:* P.A. Czysz; (B) *2nd Generation:* J. Vandenkerckhove; (C) *3rd Generation:* B. Chudoba.

A. *Hypersonic Convergence* sizing methodology (P.A. Czysz)

The first approach is based on Czysz's *Hypersonic Convergence* course (Czysz 1986). In designing an object, convergence, or closure, occurs when all the design variables are self-consistent and meet their goals. For instance, designing a football made of a new material will converge when, with the new material, the football will have its size and weight within the limits specified by the NFL rules, will bounce in the same way, can be grabbed without dropping, will be visible from a distance, and, when thrown, will reach at least the same distance of older footballs. This does not mean that the new football will be uniquely determined, but simply that its features will be within all specified constraints and will have margins within which it is still possible to make choices. In a similar manner, the objective of P.A. Czysz's methodology has been to provide a simple mass- and volume-based convergence logic to rapidly and correctly compare a wide variety of approaches to facilitate the conceptual design of space access vehicles and hypersonic cruise aircraft.

This approach correlates geometric data from references including (Pirrello and Czysz 1970; Tjonneland 1988; Billig 1989; Czysz and Murthy 1996; Czysz and Froning 1997). For a constant mission objective, this methodology selects a continuum of feasible configurations with basic vehicle volume and weight attributes, which are sized for a specific range of the Küchemann slenderness parameter τ. Specific τ values, which are capable to minimize or maximize the mission objective function, are selected to define prospective baseline vehicles. This approach is a general formulation of parametric sizing, correctly combining generic assumptions in a truly multi-disciplinary methodology. It is opposed to the more common practice of choosing a certain configuration or weight from the outset, and trying to optimize the vehicle via customizing a point design methodology. This approach benefits from simplifying, but not over-simplifying, the multi-disciplinary relations among classes of flight vehicles. These relationships are physically correct and consistent; thus, they are utilized to single out and assemble sets of parameters (parameter continuum) determining the so-called solution spaces. Having implemented a multi-disciplinary total-system convergence logic, this methodology enables to explore, physically understand, and visualize the relative merits of highly complex design trade studies. In the football analogy, a design space could be a set of curves on the weight-cost plane, with the thickness of the football skin demonstrating to be a primary football design-trade parameter. Within the limits of NFL weight rules, weight determines cost, this last being also a function of the skin thickness.

A.1. *Vehicle synthesis*

Vehicle synthesis is the task of synergistically combining chosen vehicle attributes and functional components aimed at obtaining a *converged* vehicle design that meets mission needs whilst considering specified requirements and constraints. For the initial vehicle definition, two key components are identified, namely the aerodynamic body of the vehicle (geometry configuration) and the propulsion-propellant system (propulsion concept). Concept components are described by a number of variables pertaining to their features, and the processes associated with them, that ultimately affect vehicle performance. The choices and constraints related to the concept components include, among others, their performance capability, the structural-material strength limitations or structural index, and the available industrial capability for manufacturing them. These may also be treated as variables during the conceptual design process (technology trades). Other choices and constraints pertaining to the mission may also be treated as variables during the conceptual design process. The task of synthesis then is to facilitate engineering consistency, correctness and convergence (closure or matching) among all vehicle variables across all disciplines such that the vehicle performs the desired mission.

Choosing dependent and independent variables implies also choosing their actual range of values. Such a choice must be rational, in many cases including projections based on available data and predictions. However, there are many instances in which the objective may be to set up performance or capability goals, and then, the choice of allowable variables and their ranges may need to be flexible.

When the mission needs or specifications change or become extensively defined and detailed, the problems of matching become complex, and the number of possibilities for matching or synthesizing reduces. In many cases, there may be a specific, major requirement for the vehicle. If that requirement is made the principal objective, one may have to establish special combinations of variables that ultimately meet that requirement. However, it is entirely possible that there is no convergence of the design within the ranges of variables given. A useful approach is to examine whether extending these ranges may possibly lead to a continuum of converged designs in the extended solution space topography.

In connection with vehicle synthesis, one often comes across the expression *vehicle optimization*. In the case of aircraft, missiles, launch vehicles, and spacecraft, which involve approximately the same number of variables as in hypersonic vehicle designs, there is a vast body of historical data and experience allowing optimization. However, even in this case, optimization cannot be carried out on strictly mathematical grounds. For instance, the shape of a hypersonic research aircraft to be dropped by the NASA B-52 at Edwards AFB can be optimized if one demanded maximum speed for a given thrust, subject to the requirement that length and weight of the vehicle be compatible with the B-52 wing-hardpoint load- and geometry limitations. This problem can be set up from first principles and solved based on well-established mathematical methods. However, if one would impose limits on wing loading and pilot seat dimensions, landing gear materials or propulsion installation, the overall lack of data, the inability to describe the parametric relations in analytical form, and other practical factors would render the mathematical problem untreatable. "... *It is very difficult to optimize mathematically a shoe ...*"

In particular, in the case of hypersonic and space launch vehicles, all these problems seem to arise mainly during the early conceptual design phase. It seems prudent, therefore, to *first* aim at multi-disciplinary and correct convergence of the highest-of-importance (reduced-order) design drivers of the vehicle, followed in a *second* step by highly accurate (high-fidelity) disciplinary optimization of the initially provided baseline design (via the first step) as the correct starting point. Even in the case of more conventional vehicles, the multi-disciplinary sciences and skills based on physics are at least as important as rational mathematical methods in producing successful designs.

Consequently, synthesizing a hypersonic or space launch vehicle consists of developing a physics-based methodology for obtaining a converged design. Whatever the methodology, it must allow options to improve it beyond the initial mission goals stated at the onset of a project.

The following section describes the multi-disciplinary relationships or parametrics required for developing the underlying hypersonic convergence relationships.

A.2. *Principal hypersonic convergence relationships*

For a fixed payload and crew weight, historical data-bases from the 1960s have been used to correlate the maximum propellant volume available for *hydrogen-fueled* aircraft to planform area (size):

$$K_{\mathrm{v}} = \frac{V_{\mathrm{ppl}}}{V_{\mathrm{total}}} \cdot S_{\mathrm{plan}}^{-0.07171} \tag{3.40}$$

$$\frac{V_{\mathrm{ppl}}}{V_{\mathrm{total}}} = K_{\mathrm{v}} \cdot S_{\mathrm{plan}}^{0.07171} \tag{3.41}$$

These correlations are for the four configuration concepts in Pirrello and Czysz (1970) (see Fig. 3.42). This correlation yields the maximum propellant volume ratio with high-density electronic payloads. Corrections for low-density payloads are also given in the same reference.

In order to determine the allowable structural weight per unit surface area, an estimate of the structural fraction is necessary. The initial correlation is based on one author's (P. A. Czysz) hypersonic aircraft experience. When this sizing approach was employed for the HSCT study, the Douglas Aircraft Company correlation results overlaid the hypersonic aircraft data (Page 1987; Czysz 1991). Other aircraft data indicate that, to first order, this approach produces results consistent with initial estimates. That correlation is:

$$K_{\mathrm{str}} = 0.228^{\pm 0.035} \cdot \tau^{0.20} \tag{3.42}$$

The approach does not integrate an engine design/performance program or trajectory analysis. These can be calculated on a separate Microsoft Excel spreadsheet. The adequacy of this approach is documented in Sect. 5 of Pirrello and Czysz (1970). Note that Eqs. 3.9a, b, c through 3.28a, b are dimensional, so all units must be dimensionally consistent. W_{OWE} is an American term that indicates the dry weight plus trapped fluids and crew consumables. It is slightly greater than the European W_{dry}, but with respect to parametric screening, the differences between W_{OWE} and W_{dry} are inconsequential.

The result, then, is two equations that give the operating weight empty, W_{OWE}, and the structural index, I_{str}, required for convergence.

$$W_{\mathrm{OWE}} = K_{\mathrm{v}} \cdot \tau \cdot \left(\frac{\rho_{\mathrm{ppl}}}{W_R - 1} \right) \cdot S_{\mathrm{plan}}^{1.5717} - W_{\mathrm{pay}} - W_{\mathrm{crew}} \tag{3.43}$$

$$\frac{W_{\mathrm{str}}}{S_{\mathrm{wet}}} = \frac{K_{\mathrm{str}} \cdot K_{\mathrm{v}} \cdot \tau}{K_{\mathrm{w}}} \cdot \left(\frac{\rho_{\mathrm{ppl}}}{W_{\mathrm{R}} - 1} \right) \cdot \frac{S_{\mathrm{plan}}^{1.5717}}{(1 + r_{\mathrm{use}})} = I_{\mathrm{str}} \tag{3.44}$$

$$I_{\mathrm{str}} = \frac{W_{\mathrm{str}}}{S_{\mathrm{wet}}} \tag{3.45}$$

Equation 3.44 clearly shows that for the same propulsion index and geometry, the smaller the planform area, the less the structural weight per unit surface area. In order to compensate and keep the structural index constant, the geometric parameter must increase accordingly, i.e., the vehicle must become stouter.

Integrating volume (fuselage), aerodynamic surfaces (wing, empennage), and propulsion system simultaneously requires to make volume appear in the convergence logic. At the heart of *Hypersonic Convergence* is the system of two equations, which solves for weight and volume simultaneously, see Eqs. 3.46 and 3.47.

The weight budget is given by:

$$W_{\mathrm{OEW}} = \frac{I_{\mathrm{str}} K_{\mathrm{w}} S_{\mathrm{plan}} + C_{\mathrm{sys}} + W_{\mathrm{cprv}} + \frac{T/W \cdot W_{\mathrm{R}}}{E_{\mathrm{TW}}} \left(W_{\mathrm{pay}} + W_{\mathrm{crew}}\right)}{\frac{1}{1+\mu_a} - f_{\mathrm{sys}} \cdot \frac{T/W \cdot W_{\mathrm{R}}}{E_{\mathrm{TW}}}} \tag{3.46}$$

The volume budget is given by:

$$W_{\mathrm{OWE}} = \frac{\tau \cdot S_{\mathrm{plan}}^{1.5}(1 - k_{vv} - k_{vs}) - (v_{\mathrm{crw}} - k_{\mathrm{crw}}) \cdot N_{\mathrm{crw}} - W_{\mathrm{pay}}/\rho_{\mathrm{pay}}}{\frac{W_{\mathrm{R}}-1}{\rho_{\mathrm{ppl}}} + k_{\mathrm{ve}} \cdot T/W \cdot W_{\mathrm{R}}} - W_{\mathrm{pay}} - f_{\mathrm{crw}} \cdot N_{\mathrm{crw}} \tag{3.47}$$

where

$$W_{\mathrm{OWE}} = W_{\mathrm{OEW}} + W_{\mathrm{pay}} + W_{\mathrm{crew}} \tag{3.48}$$

In these nonlinear expressions, all variables have been solved for in the trajectory analysis or are assumed constants except for W_{OEW} and S_{plan}, thus allowing for a unique solution. The weak nonlinearity of Eq. (3.47) suggests the solution is unique. Note that in this formulation, the wing loading (W_{TOGW}/S) will be known when W_{OEW} and S_{plan} are solved for. Therefore, a new sizing variable must be utilized, τ. The Küchemann slenderness parameter τ links planform area and volume. When held constant in the convergence logic, the resulting W_{OEW} and S_{plan} provide a unique solution with the required slenderness. With increasing τ, the vehicle will have more volume per unit planform area, thus will become stouter and *L/D* will decrease. Conversely, when τ is decreased, the vehicle will become more slender (see Fig. 3.41). In this integrated methodology, τ serves the same function as *W/S* does for the classical aircraft design approach. However, instead of linking wing area to weight, τ connects wing area to volume. This formulation allows for wing loading, weight, and volume to be solved simultaneously.

If the configurations shown in Figs. 3.31 and 3.42 are used within the assumptions of this approach, the geometry term in Eq. 3.44 (the "triple-K term") collapses into a single function, as given in Eq. 3.50.

$$\left(\frac{K_{\mathrm{w}}}{\tau}\right) \cdot \left(\frac{1}{K_{\mathrm{str}} \cdot K_{\mathrm{v}}}\right) = \left(\frac{K_{\mathrm{w}}}{\tau}\right) \cdot \frac{11.35^{\pm 2.29}}{\tau^{0.206}} \tag{3.49}$$

$$\frac{K_{\mathrm{w}}}{\tau} = \exp\left\{0.081 \cdot [\ln(\tau)]^2 - 0.461 \cdot \ln(\tau) + 1.738\right\} \tag{3.50}$$

In Fig. 3.43, the value of (K_{w}/τ) is presented for all configurations shown in Fig. 3.42. As indicated from the data in Fig. 3.31, the range of τ spans the complete spectrum of aircraft configurations from the SST *wing-body* (WB) configuration with $\tau = 0.03$ to a *sphere* with $\tau = 0.75$. Equation 3.50 is the curve through the data.

This means that given the propulsion and structural indices, to first order, the vehicle size can be readily estimated as a function of τ and a configuration concept. Thus, we obtain:

$$S_{\mathrm{plan}} = \left[\frac{\frac{\rho_{\mathrm{ppl}}}{(W_{\mathrm{R}}-1)}}{\frac{W_{\mathrm{str}}}{S_{\mathrm{wet}}}} \cdot \left(\frac{K_{\mathrm{w}}}{\tau}\right) \cdot \left(\frac{1}{K_{\mathrm{v}} \cdot K_{\mathrm{str}}}\right) \cdot \left(1 + \frac{W_{\mathrm{pay}}}{W_{\mathrm{OWE}}}\right)\right]^{1.409} \tag{3.51}$$

The *Hypersonic Convergence* logic provides an interesting simplification of the sizing process in that (1) the total aircraft volume and weight are converged simultaneously, and (2) the feasible design space for a given set of assumed constants is condensed into a single curve.

A.3. *Outline of methodology*

Aircraft synthesis methods have been available for many years; it may be useful to become familiar with them (Chudoba 2002; Coleman 2010).

The methodology for hypersonic and space launch vehicle convergence presented here is illustrated in Fig. 3.44 (Czysz and Murthy 1996). It is assumed that data sets on capabilities in propulsion, fuels, materials, and industrial manufacturing have been generated, based on past experience and extensions as well as on predictions from sizing

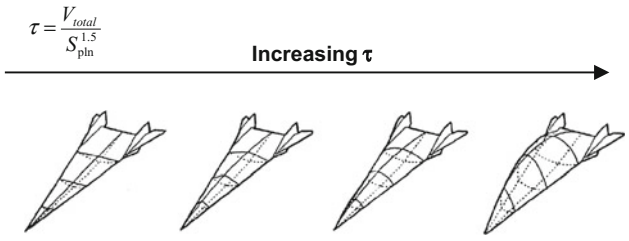

Fig. 3.41 Illustration of Küchemann slenderness parameter

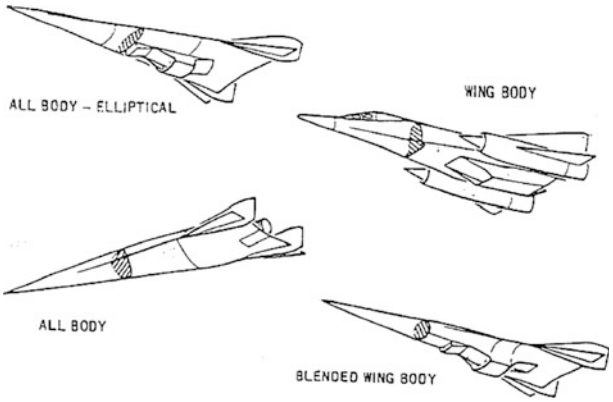

Fig. 3.42 Representative hypersonic configurations (Pirrello and Czysz 1970)

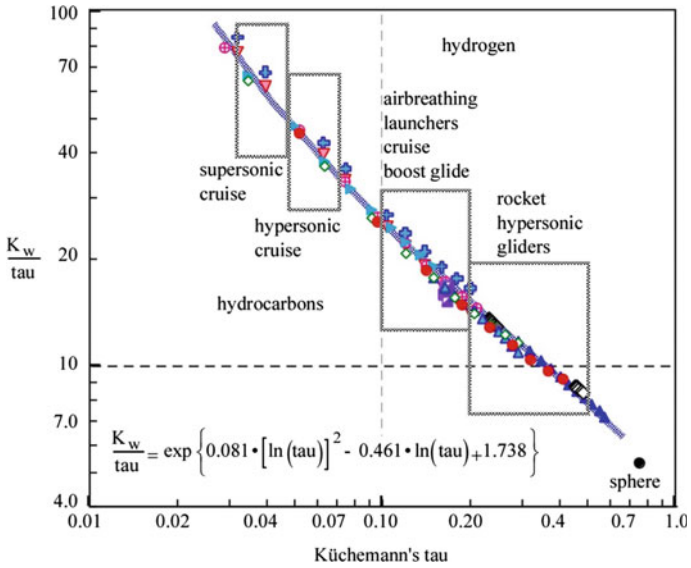

Fig. 3.43 Geometric parameters span the complete spectrum of aircraft configurations

programs. Given the mission, a reference vehicle is postulated and defined by adequately selecting key parameters. Then, a series of design spaces are constructed using these key parameters. Convergence to a vehicle design is sought based on the influence of these parameters on vehicle performance as calculated and plotted on the design spaces.

Figure 3.44 shows schematically how the reference vehicle can be varied based on characteristic parameters in the design space. Actual engineering choices require interpretation of the design spaces. Design spaces are generated from data on various aspects of vehicle design. Thus, the construction of design spaces is the most significant part of realizing vehicle convergence. Visibility, comprehensiveness, clarity, rationality, and thus consequently ease of interpretation are the main desired characteristics of design spaces.

Figure 3.45 shows how the same approach is implemented at the AVD Laboratory of one of the authors (B. Chudoba) (Coleman 2010).

A.4. *Design space concept and its utilization*

A design space is a parameter space of converged vehicles; it may involve two or more individual parameters or groups of parameters. In general, it is a multi-dimensional (multi-disciplinary) representation, but for practical reason is shown on a two-variable plane, and any other variable is used as a parameter. It visualizes and indicates what the available choices of the parameters being considered are.

A design space can be constructed in various ways, depending on the purpose for which it is to be utilized. One type of design space may show the performance attainable as a function of the parameters affecting performance. For example, for a hypersonic inlet of a cruiser working at a fixed Mach number, one may chart an enthalpy/freestream entropy space, where the contraction (area) ratio and the number of shocks are the parameters considered to examine the design space available at a particular flight Mach number (see Fig. 3.46). This space was obtained from the equations of mass and momentum conservation, the entropy gain equation, and shock-wave relationships. It illustrates the influence of the choice of contraction ratio and the number of shock waves on

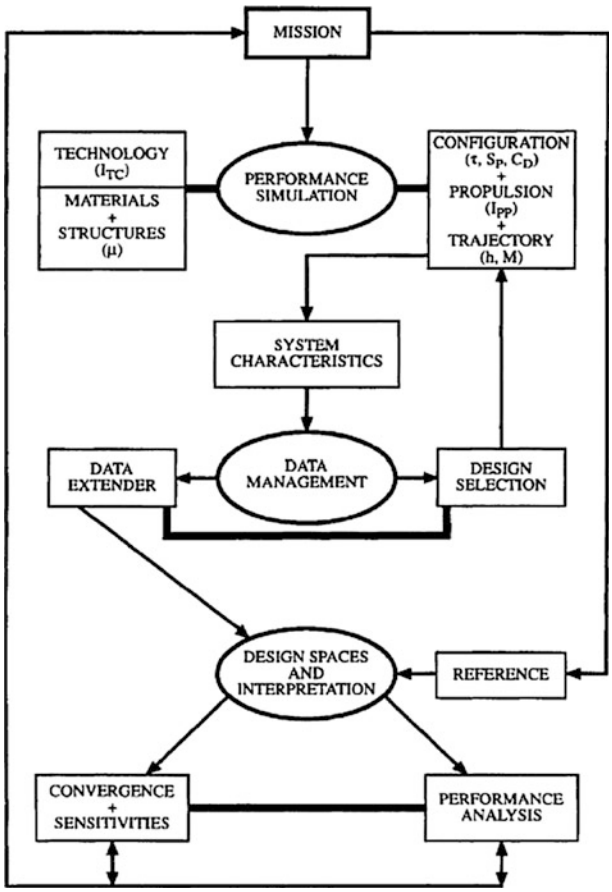

Fig. 3.44 Methodology for flight vehicle synthesis (Czysz and Murthy 1996)

losses, including the loss of energy available in the inlet during shock compression for a chosen mode of diffusion.

Similar charts can be constructed for flight at other Mach numbers, and one can examine the results with respect to an altitude-flight Mach number space showing a flight trajectory band. The results in Fig. 3.46 have been obtained under a number of assumptions, e.g., a calorically perfect, equilibrium gas, and constraints for the inlet configuration. The entire procedure adopted for the inlet also may be applied to other components of an engine, including a combined-cycle engine. Such a procedure is described in Billig and Van Wie (1987), Kutschenreuter et al. (1992). A set of design spaces have been established that show the attainable performance as a function of a series of parameters affecting performance; some may be utilized as variables and others retained as parameters in the construction of design spaces.

For transatmospheric launcher sizing, a design space is constructed in a slightly different fashion. This approach proves particularly useful in assessing the possibility of convergence of a vehicle that can meet the desired goals with reference to the indices, capability, configuration concept and its details, and various weight factors.

For example, a vehicle may be specified in terms of its orbital payload under various constraints, options, and limits. One can then choose a reference vehicle that, for available indices and capability, can perform the mission with a set of configuration and propulsion-propellant concepts. Said otherwise, varying the design space parameters will take the initial reference vehicle and (virtually) alter shape, weight, and materials within the allowed margins while still meeting mission goals (still converging). Interpreting the changes produced will show how to improve on the reference. Thus, constructing a series of design spaces in terms of the parameters affecting the vehicle design enables for each design space to show the effects of departing from the chosen reference conditions. In particular, it is of interest to establish the possible margins in the choice of various parameters with reference to the assumed, available indices, capability, concept and propulsion choices. Also, simultaneously, one can establish, from the design space, the need for improvements in the indices and capability before certain design changes can be realized.

As an example, one can construct a design space of converged vehicles with the structural index $I_{str} = W_{str}/S_{wet}$ and ICI $\equiv$ *Index* as variables, and using τ as a parameter. The reference vehicle is a blended-body concept powered by an RBCC propulsion system that transitions to rocket propulsion at 22,200 ft/s (Czysz 2004). The reference τ is assumed = 0.104.

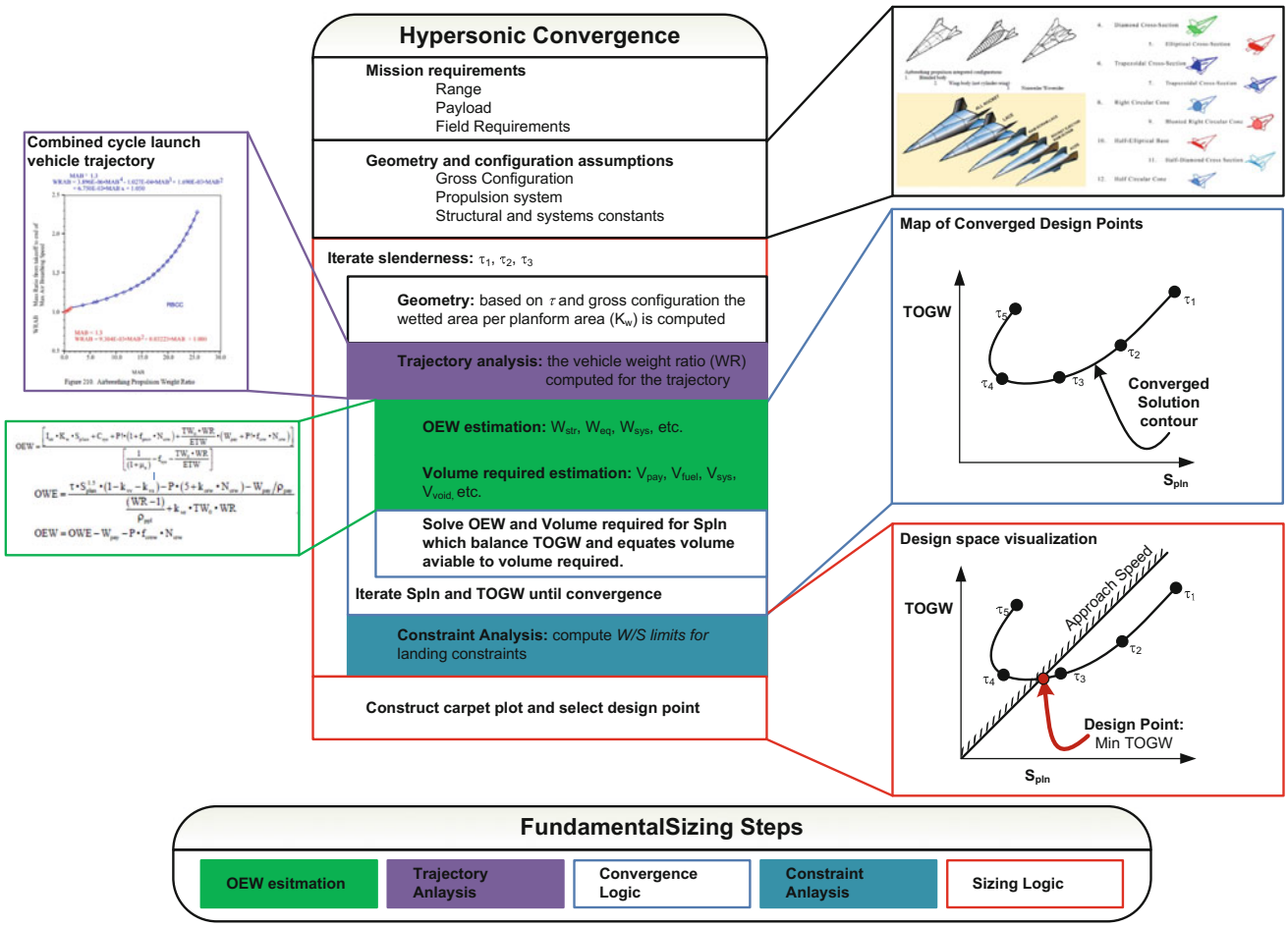

Fig. 3.45 Modern implementation of the *hypersonic convergence* sizing logic

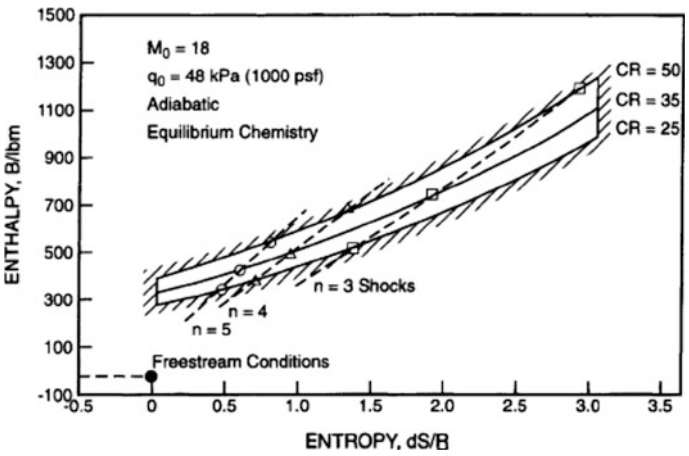

Fig. 3.46 Inlet design space possibilities (Czysz and Murthy 1996)

Figure 3.47 shows the 2-D design spaces. The chart on the left is a plot of I_{str} versus ICI obtained using their definitions. The curve intercepts the family of dashed lines τ = constant, also plotted, with τ varying from 0.032 to 0.229. The straight line I_{str} = 3.5 lbm/ft^2 is the state of the art in structural weight: All structures with $I_{str} > 3.5$ are realizable. Thus, as shown with the chart on the right, the space between this line and the curve (the shaded area) is the allowable design space defining the allowable design margins for an ICI index between 2 and 7. If we know what the *maximum* ICI is, the area shrinks to the left, and imposing a *specific* ICI it becomes a segment defining the actual design margin, that is the

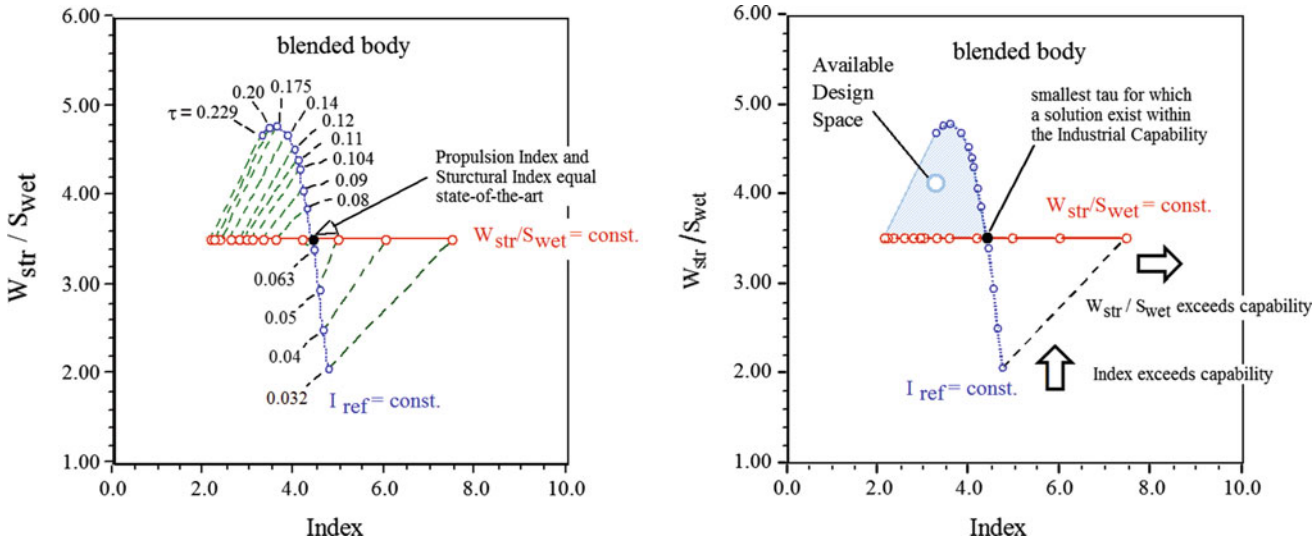

Fig. 3.47 Solution space and available design space definition for the blended-body configuration (RBCC propulsion system, airbreathing to 22,200 ft/s)

segment between the point (I_{str}, ICI) and the curve. In the instance, assuming ICI = 3.5 shows that with the materials at our disposal, it is impossible to converge on a blended-body shape more slender than $\tau \approx 0.063$.

In other words, Fig. 3.47 is a guide for locating the design convergence space. The area above the horizontal is where available capability in propulsion, material, and fabrication exceeds the minimum required. Both curves are a function of Küchemann's τ, and there are corresponding τ values on both curves, as indicated by the diagonal lines labeled 0.032, 0.104, and 0.229. The intersection of the two curves at the center represents the available ICI in materials and propulsion. To the right of the intersection, the required propulsion index is too large, or the required structural specific weight, I_{str}, is too light. The chart then maps the material, manufacturing, and structural capability, versus the propulsion/propellant capability. The shaded area represents solutions where there is convergence for a propulsion index that is less than the state of the art, and the required structural specific weight, I_{str}, is heavier than the state of the art. The distance between the arched curve and the horizontal curve is essentially the design margin.

The dashed lines are lines of constant τ between the two boundary solutions. The horizontal line is for I_{str} = 3.5 lbm/ft^2, with the Index ICI determined for each τ. The value of I_{str} is set by what is judged to be the current ICI for materials/structures at 1000 °C surface temperature. Since the initial reference τ was 0.104, the ICI was 4.09, thus higher than 3.5. The arched line is for the reference value of ICI = 4.09 with the maximum I_{str} for which convergence is possible. Given the reference value at τ = 0.104, the value of ICI is then corrected for the drag difference when changing τ (compared to the reference τ, which established the reference thrust to drag ratio).

The lower right portion of the chart represents an area where propulsion performance required is too great with respect to the ICI assumed feasible, while the specific structural weight I_{str} is too low. The upper left portion of the chart represents an area where propulsion performance required is less than the assumed ICI, and the specific structural weight I_{str} is greater than the minimum capable of being manufactured. Consequently, there is margin in both propulsion and structural weights in that portion of the design space, and the difference between the straight horizontal line assumed for I_{str} and the arched curve is the specific structural margin.

Note that each τ has a different industrial margin, that is, if the design will converge at I_{str} = 4.2 lbm/ft^2, then there is a 0.7 lbm/ft^2 margin over the assumed ICI of 3.5 lbm/ft^2. Thus, in design and manufacture, there is a built-in margin that will permit design convergence at the specified performance even at the heavier specific structural weight. For example, for τ = 0.11, and if the actual structural specific weight, as built, is 3.9 lbm/ft^2, there is no immediate drawback, providing that the design was converged for a structural specific weight greater than 3.9 lbm/ft^2 and less than 4.2 lbm/ft^2. The result is a larger vehicle, but one with greater margin for both payload and structural weight. Thus, the design space has margins defined by the maximum structural index that will permit convergence and the effective industrial capability. The former is primarily a function of the system thrust-to-drag ratio that determines the acceleration I_{sp} (I_{spe}), and the latter is determined by industrial state of the art or practice.

It is possible to generate allowable design spaces for every configuration and propulsion system concept. By interpreting the design space "maps," the topography can be immediately screened for feasible concepts while

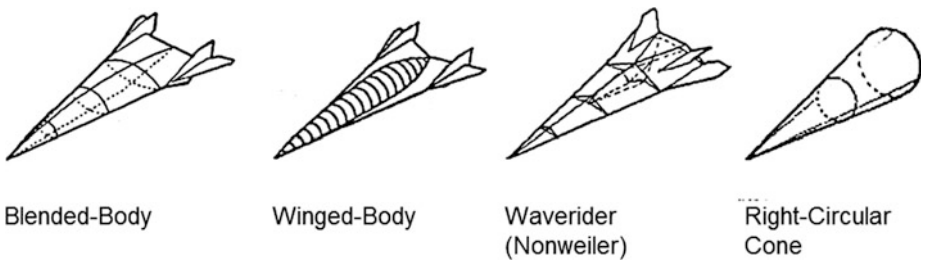

Fig. 3.48 Propulsion integrated configurations, 78° leading edge angle

deficiencies in state-of-the-art can be immediately identified as each concept has its own margins. In fact, the next section will show the design space for the four configuration concepts of interest in Fig. 3.48.

Each of the four configuration concepts has different solution spaces. Among non-conical vehicles, the blended-body has the greatest, and the waverider the least. The right-circular cone has the largest solution space of all four: It could be built as a SSTO vehicle with the SR-71/X-15 class of $I_{str} = (W_{str}/S_{wet})$ that is 55 years old. In that context, it offers no technology challenge unless the builders choose to create a technical challenge. This has been the configuration McDonnell Douglas chose for the SSTO Delta Clipper demonstrator, the DC-X, in the 1990s. It will prove an engineering challenge, but that is a much different issue. Remember that these are not expendable vertical launch cylindrical vehicles, but continuous use vehicles. Even the concept of a refurbishable-reusable vehicle is an incorrect concept with respect to these continuous use vehicles. The right-circular cone configuration will probably be confined to VTVL operations, as recently demonstrated by SpaceX (Taylor 2015).

Different choices of variables (or their combinations) establish a series of design spaces for the vehicle, so that in each case margins and limits become evident. Combining all of them determines whether or not the overall vehicle design will converge with respect to the entire set of parameters. However, before proceeding further, we summarize the elements of the vehicle synthesis procedure of the previous sections.

In Sect. 3.7.3, a spectrum of airbreathing engines in the altitude/speed trade-space has been evolved using the ratio of combustion-released energy to intake air kinetic energy and the air entropy level as parameters. The engines considered are restricted to the Brayton cycle variety. If other types of engines had been considered, the spectrum would have changed, at least in certain regimes of flight speed along with admissible variation in flight trajectory. In addition, other parameters would have become significant. Based on the concept of engine effectiveness, it has been shown that, compared to a rocket, an airbreathing engine provides the specific impulse that is about twice that of a rocket, and an effective specific impulse equal to that of the rocket, and the highest possible value of specific thrust based on air mass flow. In addition, the engine effectiveness is related to energy effectiveness based on energy availability considerations.

The next major consideration is that of materials and their available structural strength. In Sect. 3.7.2, an attempt has been made to examine the material–propulsion interface. Taking into consideration, the unavoidable limitations on structural strength as a function of temperature, and the need for thermal management for the vehicle as the flight speed increases, and for the propulsion system as the thermal equivalent of the kinetic energy of the inlet air increases, one could identify in the spectrum of engines and airframes the range of application of materials of different structural strength. Then, the structural material density and strength, as well as the thermal management system, add a number of new parameters for consideration.

In Sect. 3.7.2, the propulsion–vehicle configuration interface has been also considered, and several measures of performance are introduced, namely the structure index, I_{str}, the propulsion-propellant index, I_p, the mean propellant density, ρ_{ppl}, and the industrial technology capability index, ICI. In defining these in addition to the usual weight ratios, the size and geometry of the vehicles are identified with custom parameters and in the form of ratios, each of which has a distinct significance.

Regarding vehicles, four reference concept configurations and a number of propulsion concepts have been introduced; the latter include various possibilities for combining airbreathing engines and rocket motors combinations, noting that combined-cycle engines include airbreathing engines. For the vehicle configurations, aerodynamic data defines *L*/*D* and other parametrics. The engines are characterized by the parameters determining engine effectiveness. It is now intended to proceed to developing design spaces through a combination of which one may arrive at a convergence of the vehicle system to meet a given set of mission demands under a given set of constraints. The design spaces involve the vehicle and the propulsion-propellant parameters, generally in a multi-parameter space. Each design space developed helps to meet a particular design requirement by indicating the space in which to look for a possible solution relative to that requirement. The set of design spaces then should lead to overall vehicle system convergence.

What follows next are examples illustrating this hypersonic convergence method. A notable feature in the illustrations provided in the following section is that, while the methodology of vehicle synthesis is general enough, the type of vehicles considered is kept limited in that the number of concept configurations and propulsion-propellant configurations is restricted. This is not because of the inapplicability of the methodology to other cases, but because of the need to focus on those few basic configurations that could be examined minding the limitations in available data, possibly stemming from vehicle sizing routines and their projections.

A.5. *Applications of parametric design spaces*

In the current analysis, a hypersonic launch vehicle system has been considered so far only in terms of the flight vehicle and its propulsion-propellant characteristics. Even so, a large number of parameters enter into the description of the system and its performance characteristics. Up to this point, we have concentrated on obtaining a vehicle synthesis by evolving a methodology for combining a vehicle configuration with a propulsion-propellant configuration. The hypersonic convergence methodology by P.A. Czysz rests on the correlation of vehicle and propulsion-propellant parameters using available data and projections and estimates from sizing routines. The correlations can be applied to variations of a selected reference vehicle. The result is a set of options for a class of vehicles represented by the reference vehicle.

With the following, we discuss five design spaces that apply to a historic example of a reference mission and vehicle configuration concept.

A specific SSTO launcher is considered next as an historical example of application. That started in the USA as a project called NASP. The *National Aerospace Plane* (Augenstein and Harris 1993) started in July 1983 when the author (P.A. Czysz) found himself in the dining room of the Los Angeles Air Force Station being unexpectedly introduced as the manager of the McDonnell Douglas *Manned Aerospace Program* with Art Robinson of MDC Huntington Beach as his deputy manager. With Dwight Taylor of the McAIR aerodynamics department, Czysz set out to find a simple way to determine solution spaces for different mission–hardware–technology combinations: The outcome was the approach developed in Czysz (1986). In early 1984, the team was briefed about DARPA's *Copper Canyon* led by Robert Williams. The purpose was to develop a SSTO demonstrator based on Anthony (Tony) DuPont's engine and airframe concept, referred to as the *Government Baseline*.

Tony was the project manager for the Douglas-USAF Aerospace Plane project in the 1960s, and he brought forward some of the materials and structures from that effort. Tony's analysis indicated that his design could maintain a laminar boundary layer over the entire vehicle from Mach 0 to orbital speed, and his airbreathing engine concept would provide thrust in the atmosphere to orbital speed! His numbers were for a planform area of 2500 ft^2 with no disposable payload (payload was internal electronics and instruments). The empty weight was 25,000 lb, of which 2500 lb was instrumentation. The propellant load was 25,000 lb. That was a weight ratio of 2.0. With 50% slush hydrogen of density 5.13 lb/ft^3 (there was very little oxidizer on board), that yielded a propulsion index of about 5.5 and a resulting $\tau = 0.05$! Structural weight was about 55% of empty weight (about 12,000 lb), producing a structural index of 1.83 lb/ft^2, and that resulted in a ratio of propulsion index to structural index of 3.0 or, as later defined, an ICI of 30! That raised serious questions with the McAIR team. Consequently, the Czysz team took the four basic hypersonic configurations, see Fig. 3.48, and tried to determine what the requirements might be for each configuration lineage.

For the zero payload, minimum volume case, the four configuration concepts in Fig. 3.48 are examined. The propulsion index has been $I_p = 4.09$ lbm/ft^3. The right-circular cone again came to the rescue. That is, if the purpose of a demonstrator was to prove an RBCC propulsion system capable of reaching some fraction of orbital speed, and the configuration and the takeoff and landing modes were not critical, then the conical body would be satisfactory (again, that is why the McDonnell Douglas Delta Clipper/DC-XA became a cone). If, on the other hand, configuration and takeoff and landing modes were critical to the demonstration as the RBCC propulsion system, then there would have been an alternative design. In the end, there was no way to achieve even a fraction of orbital speed with the weights proposed, and this was the McDonnell Douglas Manned Aerospace team position. This caused serious problems with Mr. Williams and Mr. DuPont, who insisted that the McDonnell Douglas synthesis approach of "linking propulsion and structure" was fallacious, as those disciplines had always been considered independent before. That was an era when it was clearly believed that "research" could make any technology possible!

Figure 3.49 shows what the first McAIR estimates were for a series of airbreathing launchers to about Mach 14.5. The USAF Blue Ribbon Panel for Scramjets in 1968 led by Bernard Goethert came to the conclusion that from all of the data presented, a Mach 12 scramjet was well within the state of the art, and, given some additional experiments, possibly Mach 14.5 could represent a potential maximum airbreathing Mach number. This then became the McDonnell Douglas Manned Aerospace team position. The team with Aerojet-Sacramento and General Electric, Evendale, proposed in early December 1984 to build a *Copper Canyon* orbital demonstrator based on the McDonnell Aircraft blended-body. The aircraft would have a first flight in mid-1991, and after a 2-year flight test period, it would reach

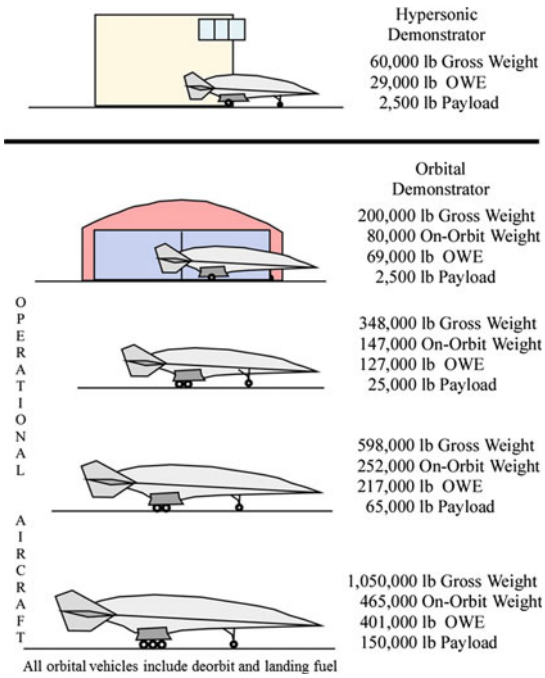

Fig. 3.49 An orderly progression of SSTO HTHL launchers beginning with a hypersonic demonstrator; circa 1983 (engine modules are a greater fraction of the vehicle length as size was reduced in 2004)

maximum airbreathing Mach number; thus, it would achieve orbital velocity and altitude in mid- to late 1993.

Aerojet-Sacramento had built a scramjet test facility based on an oxygen-rich hypergolic rocket engine and indeed tested a General Electric one-foot wide and a three-inch high combustion chamber designed by Pete Küchenreuter. In late 1994, *Copper Canyon* was terminated and NASP appeared under USAF sponsorship with Pratt and Whitney, Rocketdyne, Rockwell International, and General Dynamics now participants. Aerojet was dropped as a principal member to survive as a General Electric partner.

The vehicle was expected to carry a payload of 20,947 lbm with a weight ratio W_R equal to 2.70. The vehicle configuration concepts are the four reference shapes considered earlier, blended-body (BB), winged-body (WB), waverider or all-body (AB), and right-circular cone (see Fig. 3.48). The propulsion-propellant concepts consist of various types of RBCC engines, including the all-rocket and the all-airbreather engines, see Table C.1 in Czysz and Murthy (1996, page 624).

For the purpose of illustrating how design spaces work, a set of *reference conditions* is chosen for an RBCC propulsion system that transitions to rocket propulsion at 22,200 ft/s:

$V_{ppl} = 34,924\ \text{ft}^3$ $W_{pay} = 20,000\ \text{lb}$
$(T/D) = 3.2$ at $M = 12$ $I_p = 4.09\ \text{lb/ft}^3$
$\tau_{reference} = 0.10$ $W_R = 2.70$
ICI = 11.7 $I_{str} = 3.5\ \text{lb/ft}^2$
$I_{sp} = 1164$ s $I_{spe} = 800$ s

In the following, five design spaces are considered:

(1) The relation between the structure index, I_{str}, and the propulsion-propellant index, I_p, noting that I_{str} is included in ICI and I_p includes the vehicle drag associated with τ. Hence, the design space utilizes I_{str} and I_p as variables with τ as a parameter.
(2) The relation between the structure index, I_{str}, and vehicle planform area, based on the characteristics of four reference configuration geometries, for constant values of V_{pay}/V_{total} and V_{ppl}/V_{total} over a range of τ.
(3) The relation between W_{pay} and vehicle size, or τ, for various values of ICI.
(4) The relation between W_{pay} and the ΔV of airbreathing propulsion for various concept configuration geometries and with τ as a parameter.
(5) The relation between I_{str} and S_{plan} for various values of T/D and τ. This shows the influence of I_p and ICI on W_{pay} and V_{total}, as shown in items 1 and 3 above.

These five design spaces involve several performance indices, vehicle size parameters, and propulsion system energy effectiveness, in addition to prescribed mission requirements. The variables and the parameters are chosen to illustrate and to discuss various aspects of vehicle design. In most of what follows, the structural index I_{str} is treated as a variable to bring out the implications of the choice of materials. How to use the five design spaces is discussed below.

(1) AVAILABLE TECHNOLOGY DESIGN SPACE [available $I_{str} - I_p$ design space]

Referring to Fig. 3.50, considering the line I_{str} = const., the values of τ corresponding to I_p are determined on either side of the reference point assumed. With constant values of τ, the maximum possible values of I_{str} are determined corresponding to I_p values and joined by the arched line. The discussion of Fig. 3.47 in Sect. 3.7.4, A.4 above applies also to the current case.

Influence of configuration geometry: The effect of configuration geometry on available design space is illustrated in Fig. 3.50 assuming that the reference ICI is constant in all cases. Whereas the blended-body has the largest available design space among non-conical shapes, the conical body provides the largest design space. The highest value of τ for the maximum value of I_{str} permissible in the case of a conical body is about 0.393 compared with 0.175 for the blended-body, and the maximum value of I_{str} for the conical body is about 5.8 compared with 4.9 for the blended-body. Even in the case of a wing-body (WB), there is a margin in I_{str} of about 1.0.

The use of the conical body may be confined to VTVL missions due to very low S_{plan} when landing horizontally.

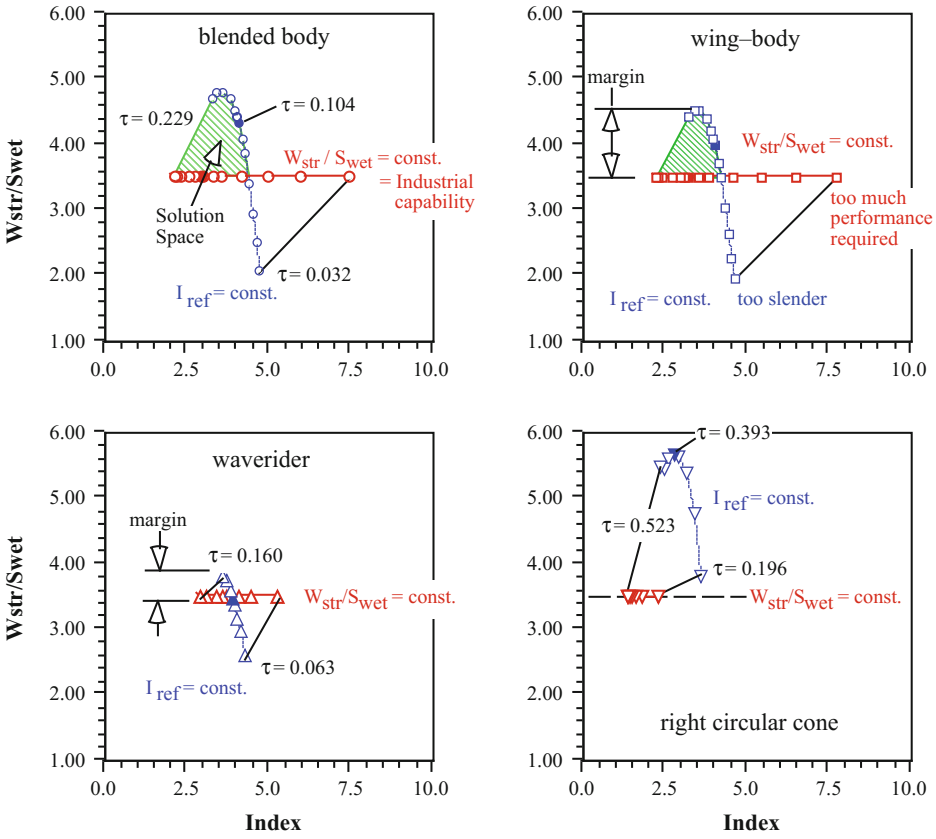

Fig. 3.50 Summary of the available design space for four different configuration concepts

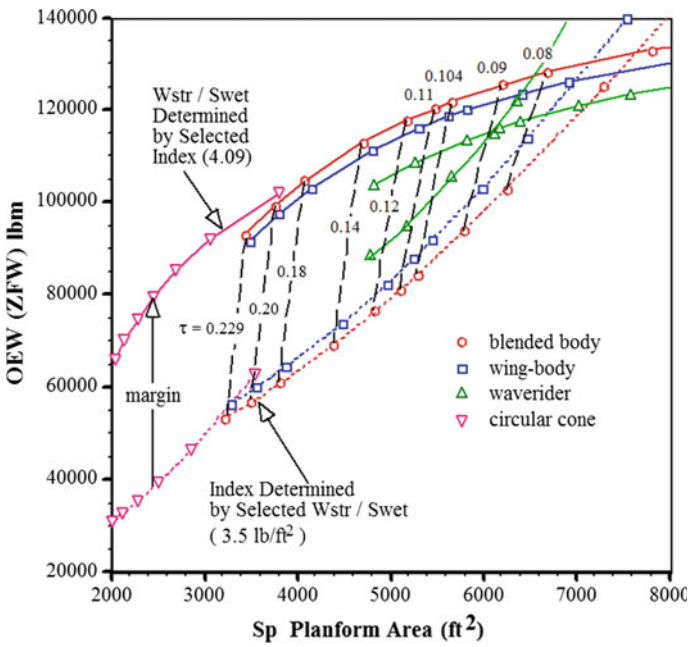

Fig. 3.51 Converged design space for four configurations, based on Fig. 3.50, with $W_{ZFW} \approx W_{OEW}$

However, the interesting feature is that the material and technology requirements are so small for this case that it becomes a natural candidate concept for a vehicle that must be reusable without refurbishing, a more stringent requirement than one with accepted refurbishment after each mission.

Margin in I_{str} and impact on size: An interesting question is whether the vehicle size, characterized by its planform area S_{plan}, changes appreciably if one tries to take advantage of the margin in I_{str} at a chosen value of τ. In examining this, one notices that I_{str} has an effect on W_{OWE}, the empty

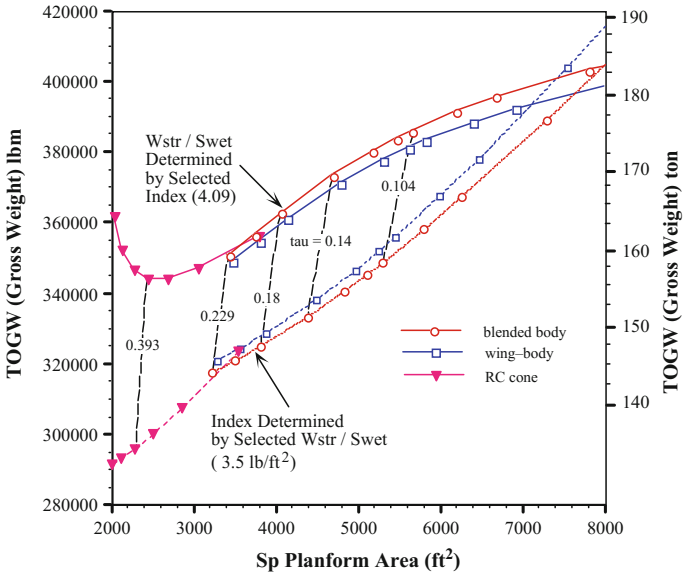

Fig. 3.52 Effects of varying S_p, τ, and I_{str} on takeoff gross weight

weight. Hence, a design space can be constructed for W_{OWE} and S_{plan} using τ as a parameter for the four reference configurations and two values of I_{str} (3.5 and 4.09 lb/ft^2). This is shown in Fig. 3.51. The I_p has been calculated at the same two values of I_{str}.

It is immediately apparent that while S_{plan} does not change much with I_{str}, W_{OWE} increases with I_{str} at constant τ: some design or technology compromise is necessary when utilizing the available margin in I_{str}. At the same time, whatever the margin, there is a gain in cost and manufacturing resulting from the feasibility of using less sophisticated materials and structures.

Margin in I_{str} and gross weight: Next, we assess the impact on W_{TOGW}, the gross takeoff weight, by utilizing the margin in I_{str} at constant τ and with the same two values of I_p. As in the case of W_{OWE}, one can obtain the change in W_{TOGW} resulting from increasing I_{str}, using τ as a parameter. The result is illustrated in Fig. 3.52. The I_p values required have been established at the two values of I_{str} as in Fig. 3.51. The extent of the increase in the case of three of the configuration concepts is shown in the figure.

There is a significant decrease in W_{OEW} and cost even for adopting part of the I_{str} margin available. As long as such cost savings can be realized, increases in W_{OWE} and W_{TOGW} may be acceptable. Note that in determining the I_{str} margin, both I_p and ICI have been taken into account.

ICI and size: With the correlation given by Eq. 3.52 (Czysz and Murthy 1996), the change in planform area with ICI has been presented before and is shown again for convenience in Fig. 3.53, using τ and W_{pay} as parameters in the case of a blended-body configuration.

$$I_p = 10 \cdot \frac{\rho_{ppl}}{(W_R - 1) \cdot I_{str}} \tag{3.52}$$

Based on the relations given in Eq. 3.52 and Fig. 3.52, one can establish, at first glance, that any vehicle concept will be a challenge when transitioning to rocket propulsion at less than 18,000 ft/s and with a planform area smaller than 2000 ft^2. It would require a gross weight of about 187,000 lbm, with an empty weight of 63,500 lbm for a payload weight of 10,000 lbm. Similarly, an airbreathing vehicle that is designed for minimum size would, for zero payload, require a 2100 ft^2 planform area with a gross weight of 140,000 lbm and an empty weight of 46,000 lbm.

Equation 3.52 can be remapped in the $S_{plan} - I_p$ space (recall the relation between I_p and ICI), as in Fig. 3.53, using τ and payload as parameters over the range of $0.20 \leq \tau$ 0.63, and $0 \leq$ payload ≤ 15 t. This figure provides a relation among planform area, τ, W_{pay}, and the propulsion-propellant index I_p and therefore ICI. In Czysz and Murthy (1996), an overlay of I_p for different propulsion systems is presented using the sizing routine presented in (Czysz and Vandenkerckhove 2000). Thus, one can obtain from a modified Fig. 3.53 the I_p required if a certain type of propulsion system is to be incorporated into a vehicle of given planform area and τ values. For more information, see Czysz and Murthy (1996).

Figure 3.53 can be extended to the other three configuration concepts, as shown in Fig. 3.54. Figure 3.54 also shows values for the size of vehicles with zero payload. It can be seen that, with the limitation posed by the maximum ICI index, the blended-body has the largest design space among the non-circular cross-sectional shapes, whereas the waverider has the smallest, mainly because the range of applicable τ values is quite small, although the L/D values are high. The right-circular cone derives its advantage from the high values of I_{str} that can be utilized. The variations of size are applicable

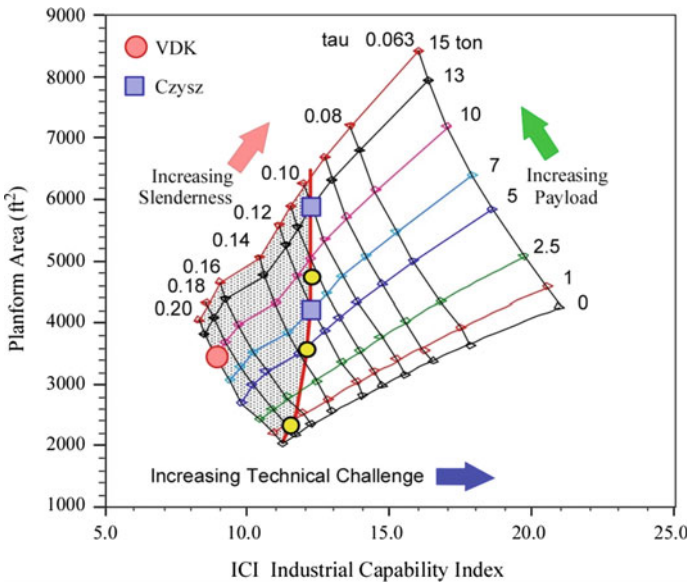

Fig. 3.53 Blended-body (BB) "design space" is bounded by realities of technology and geometry

for various propulsion options, from all-airbreather to all-rocket propulsion. One of the observations from the results presented is that aerodynamic efficiency (L/D) in terms of drag reduction does not seem to be a major driver in itself in hypersonic flight vehicles. If the thrust required for vehicle acceleration is available with high energy effectiveness of the propulsion-propellant system, compromises may be feasible with respect to both vehicle weight and shape.

(2) CONFIGURATION CONCEPT GEOMETRY [available $I_{str} - S_{plan}$ design space]

In discussing configuration concepts, the use is made of the Küchemann-derived S-variable, see Eqs. 3.24a, b, c:

$$S = \frac{S_{wet}}{V_{total}^{2/3}} = \frac{K_w}{\tau^{2/3}} \tag{3.53}$$

Both S, the vehicle slenderness, and K_w, the ratio S_{wet}/S_{plan}, increase as τ decreases, i.e., as the planform area increases for a given total volume of the vehicle. Attention is drawn to the aerodynamic, structural, and size characteristics presented for the four reference configuration geometries in Sects. 3.10 and 3.11 in Figs. 3.50 and 3.54. Those characteristics assumed airbreathing propulsion only up to 22,000 ft/s. Thus, an all-rocket engine is assumed to be used beyond that flight speed.

Based on the range of τ utilized for various configuration concepts in Fig. 3.54, one can then determine the variation of I_{str} as a function of S_{plan} using τ as a parameter, as shown in Fig. 3.55; I_{str} and τ are related via ICI (for I_p assumptions consistent with the McAIR 1963 scramjet work). The

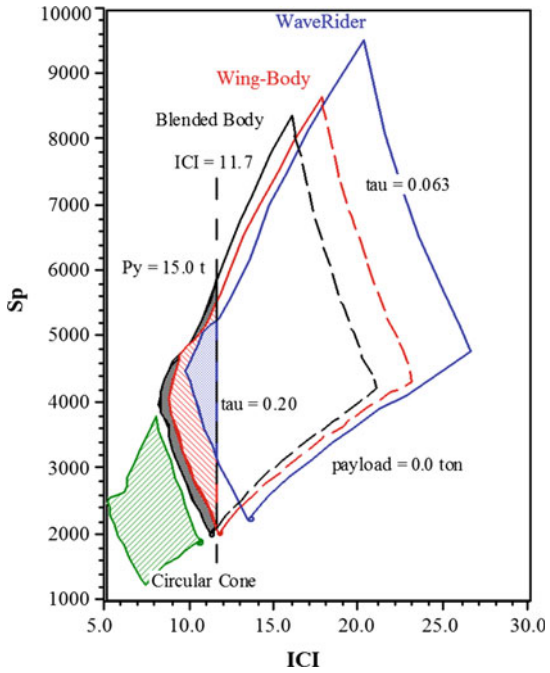

Fig. 3.54 ICI solution space map for four different configuration concepts

payload is assumed to be the same in all cases. Figure 3.54 also shows the reference value of I_{str}, and the points along the line of constant I_{str} indicate, by definition, a series of values of (τ, S_{plan}) for which the margin in I_{str} is zero.

One can observe from Fig. 3.55 that the highest permissible I_{str} and the lowest acceptable ICI occur at τ equal to about 0.175 for the blended-body (BB) and the wing-body (WB), at about 0.160 for the waverider, and at about 0.393

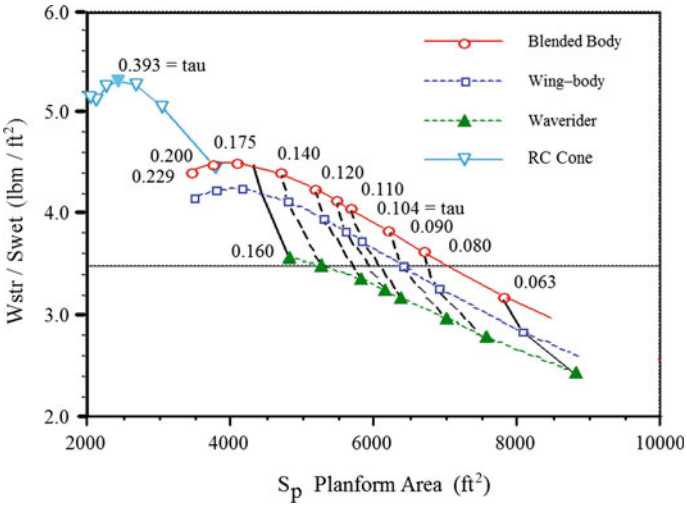

Fig. 3.55 Effect of configuration geometry on permissible structure index—using τ and S_{plan} as variables

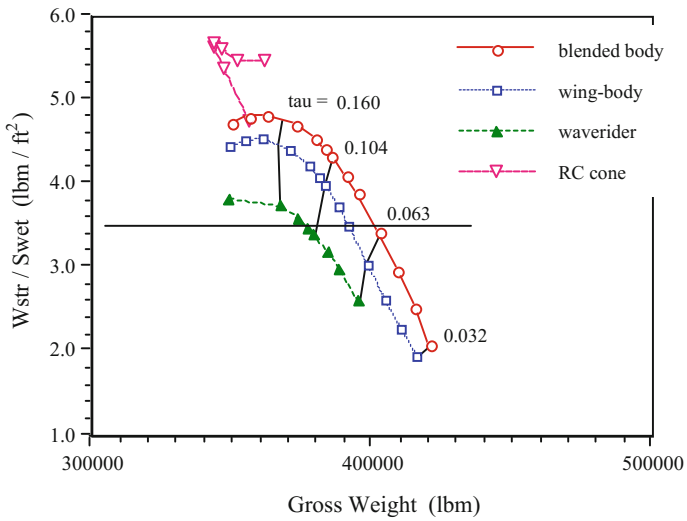

Fig. 3.56 Effect of configuration geometry on gross weight using τ as a parameter

for the right-circular cone. The larger τ values associated with less slender bodies seem to provide a larger margin in I_{str}. Thus, adopting a margin of 15% above the reference value of I_{str}, that is, using $I_{str} = 4.03$ lbm/ft^2, the waverider is entirely eliminated while the wing-body and the blended-body show a very limited margin. However, there is a clear advantage in the case of the right-circular cone because of its significantly broader ICI-range. The right-circular cone is, of course, restricted to VTVL missions.

It is also of interest to consider the variation of I_{str} with respect to W_{TOGW}, as in Fig. 3.56. A significant finding here is that the highest value of I_{str} occurs in the case of the non-symmetric body shapes. In addition, the highest values of I_{str} arise at about the same value of W_{TOGW}, whereas in the case of the right-circular cone, a considerably lower value of W_{TOGW} seems possible. The conclusion is that the choice of configuration geometry depends on the ICI available. In other words, given a value of ICI, the configuration geometry and the value of τ or slenderness determine the payload weight realizable with a chosen propulsion-propellant concept.

In these conceptual design exercises, note that (1) one must not start with a preconceived configuration before assessing the available margin in I_{str} and the associated value of τ in light of the available technology capability; and (2) when one obtains such numerical values as zero or negative payload, one must reexamine the configuration geometry, the slenderness (τ), I_{str} and ICI, and the I_p of the propulsion-propellant concept chosen. The zero-payload case does not need, in any rational approach, end in despair.

Based on the results given in Fig. 3.56, when a reference configuration is sought, the choice should be based on τ being no less than 0.393 for a right-circular cone, and no less than 0.175 for a blended-body (BB) and the wing-body (WB). Those

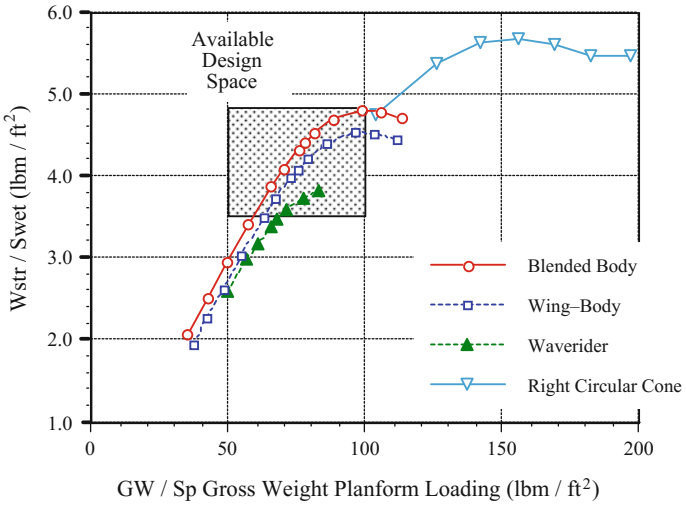

Fig. 3.57 Practical design space summary—effect of mission requirements such as horizontal takeoff and horizontal landing on configuration concepts

configurations will not be the lightest in terms of W_{TOGW}, but they correspond to the ICI available with the reference value I_{str} = 3.5 lbm/ft^2, and the I_p available with the propulsion-propellant concept under consideration. Every progress in ICI and I_p can be expected to lead to lower W_{TOGW} and to a higher payload ratio, provided one utilizes an appropriate configuration geometry. If the limits to improving ICI appear insurmountable, one can only investigate possible improvements in I_p and energy utilization effectiveness.

In order to examine the possibilities for other missions involving HTHL, one may cast Fig. 3.56 in a slightly different form as Fig. 3.57, where I_{str} is shown as a function of the gross weight planform loading or W_{TOGW}/S_{plan}. Utilizing a 15% margin in I_{str}, the available design space for the non-symmetric configuration concepts is, in fact, quite small when the takeoff wing loading is held in the range of 70 to 100 lbm/ft^2. (Some improvements may be possible with takeoff lift enhancing devices, while landing loads are generally small relative to the takeoff case.)

(3) PAYLOAD WEIGHT AND VEHICLE SIZE [available $W_{pay} - S_{plan}$ design space]

It may be pertinent to recall here the following observations from the earlier Sects. (1) and (2):

(a) The payload affects the ICI required, as shown in Fig. 3.54, noting the assumption that the propellant mass is proportional to payload mass.
(b) As the payload W_{pay} decreases, the empty weight W_{OWE} does not decrease in direct proportion.
(c) For a given value of Küchemann's parameter τ, a decrease in planform area demands an increase in available ICI, see Eq. 3.52.

In the following, all of the vehicles are assumed to be SSTO with a payload in the range 0–45,000 lbm. The propulsion-propellant concept is assumed to consist of air-breathing propulsion up to a flight speed of 22,200 ft/s. Initially, a blended-body configuration concept is considered, and, later, others are included.

The variation of I_{str} with respect to S_{plan} is mapped in Fig. 3.58, using τ and the payload as parameters. It can be observed that a 7 t payload is feasible with a value of I_{str} = 3.5 lb/ft^2 or an equivalent ICI. However, even allowing τ to increase to 0.2 from about 0.08 does not allow a margin of 15% in I_{str} at the peak value of I_{str}. With a margin of 15%, the smallest vehicle size allows a payload of 4 t, and a payload installed density (W_{pay}/V_{total}) of 6.0 lbm/ft^3, noting that τ becomes then about 0.22. If a smaller sized vehicle is attempted, then I_{str} must be reduced, and ICI and τ must be larger. A vehicle capable of 20 t payload can be attempted with the same margin in I_{str} but in a rather slender vehicle with practically no margin left to account for any uncertainties in ICI and I_p.

Considering the zero-payload case, some additional remarks are warranted in continuation of those made at the end of the previous section. Figure 3.58 shows the zero-payload case may be realized in two ways: (1) with higher I_{str} values, where W_{pay} = 0, but there is volume available in the vehicle for adding payload; and (2) with lower I_{str} corresponding to the case where no volume is provided for any payload, as in a demonstrator in which a bay is completely filled with high-density electronic instrumentation payload. It is clear that case (2) is not feasible with the reference value of I_{str} and the corresponding ICI assumed. In case (1), there is very little margin in I_{str}, and any attempt to make use of it tends to increase the value of τ. Thus, a zero-payload demonstrator may be as difficult to build as is a modest-payload vehicle, say with W_{pay} = 2.0 t, which may be equal to the mass of an instrument and data acquisition system.

In Fig. 3.59, the zero-payload case is shown with a minimum volume for all four reference configurations. The

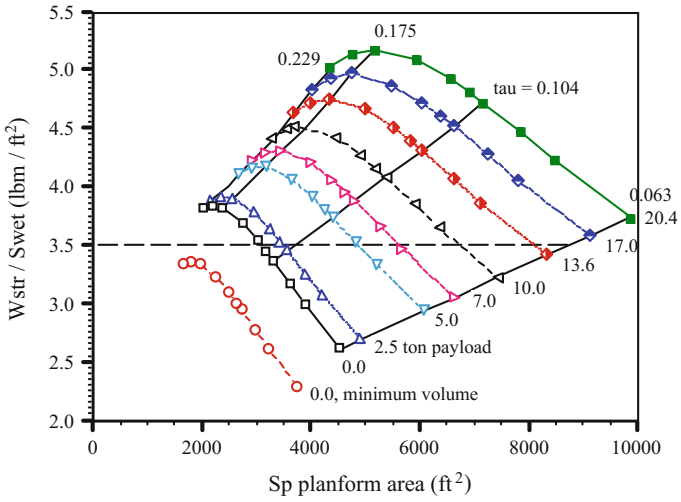

Fig. 3.58 Solution map for a RBCC SSTO showing the effect of choice of payload mass W_{pay} and Küchemann parameter τ on structure index I_{str} and planform area S_p spaces. Note the zero-payload values

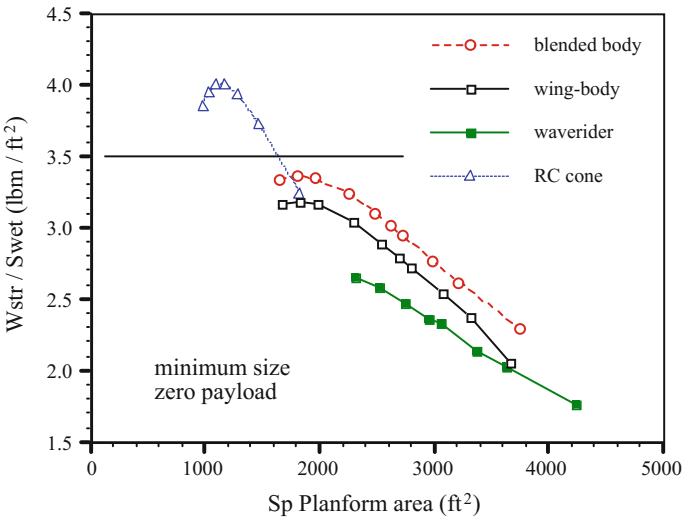

Fig. 3.59 Comparison of various configuration concepts for minimum-sized (zero-payload) demonstrator research vehicles, circa 1983

right-circular cone does provide a margin in I_{str}, whereas none of the other concept configurations are feasible at the reference I_{str} value and require a considerably higher ICI than the reference value. From the point of view of a demonstrator vehicle, if, for instance, the objective is to prove the performance of the propulsion system, then a conical body would be satisfactory within the available ICI since I_p has been included in obtaining the results. If the objective included assessment of aerodynamic performance or takeoff and landing, Fig. 3.59 suggests a vehicle with a payload of about 2–4 t.

The thermal load and the thermal management required are also significant issues in the development of a small vehicle. Thus, there may be a need to reconsider, even as reference, the available ICI and I_{str}.

(4) PROPULSION SYSTEM CONCEPT [available W_{pay} and ΔV design space]

There are solid reasons to believe that a propulsion concept based on a RBCC engine, which can be operated in different modes over various parts of a flight trajectory, may be superior to a combination of currently available separate engines (Czysz 1993). For example, estimates are available for the weights of SSTO and TSTO vehicles as a function of ΔV produced by airbreathing engines, as shown in Fig. 3.60. In this case, W_{OWE} is nearly constant, at about 6 times the payload, up to ΔV = 15,000 ft/s, and then increases to a value of 7–8 times the payload. Note that this applies to a blended-body configuration with τ = 0.104 and I_{str} = 3.5 lbm/ft^2, the reference values utilized throughout this section. The magnitude of W_{TOGW} changes with ΔV on account of the change in W_{pay}. It may be noted that, in these estimates, an arbitrary cross-range requirement was included.

It is now possible to map the change in I_{str} as a function of S_{plan}, utilizing ΔV for airbreathing propulsion and τ as parameters, as shown in Fig. 3.61. The lowest I_{str} margin occurs when the propulsion concept is entirely an

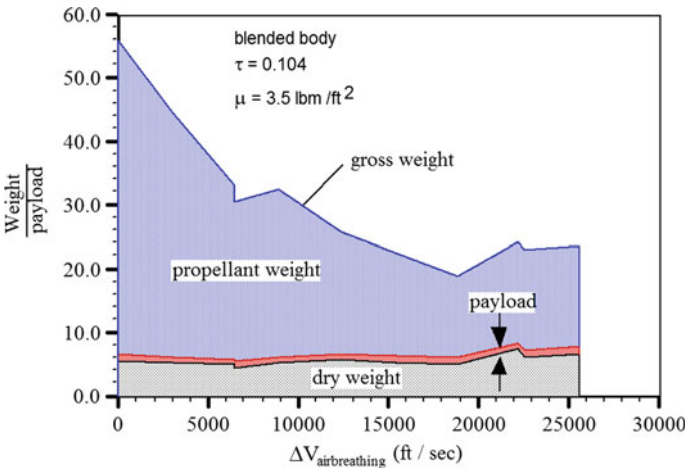

Fig. 3.60 Weight ratio as a function of airbreathing speed increment ΔV obtained for a specific vehicle (blended-body)

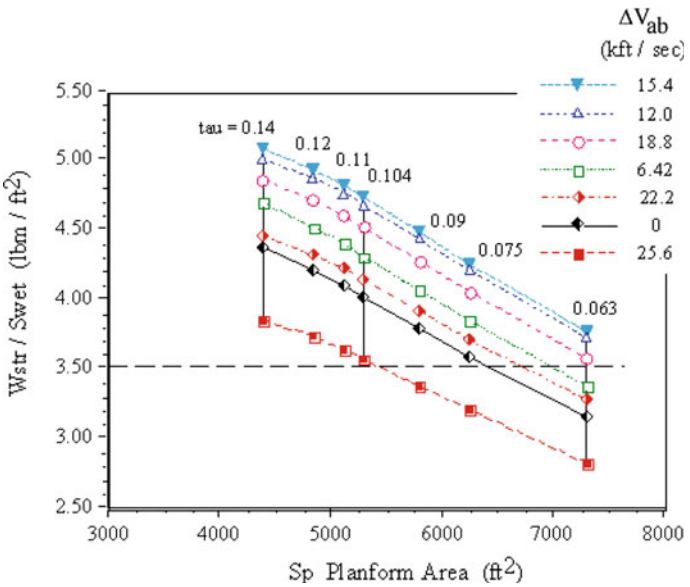

Fig. 3.61 Solution map for an RBCC SSTO propulsion concept that has different transition speed to rocket (ΔV airbreather) with margin in structure index, I_{str}

airbreather. The best margin seems to occur at ΔV = 15,400 ft/s, the value increasing with τ until the all-rocket propulsion system becomes superior compared to the all-airbreather.

For the reference payload, it is also interesting to see in Fig. 3.62 that W_{OWE} varies in a narrow band with respect to the slenderness parameter S, and thus, a tentative, average value estimated may prove adequate in initial analyses.

Next one may consider the variation of I_{str} with respect to the gross weight planform loading, utilizing ΔV for airbreathing propulsion and τ as parameters, as shown in Fig. 3.63. This figure provides a basis for examining launch and landing options. At low values of W_{TOGW}/S_{plan}, one can consider HTHL. At high values, VTHL may be the only choice, although an airborne launch (ALHL) may also be a solution along with other launch-assist schemes. At intermediate values of W_{TOGW}/S_{plan}, there may be an opportunity with vehicle rotation during launch assisted by thrust vectoring. Once unassisted HTHL operation is selected, the propulsion system concept is airbreathing over a significant portion of the speed regime.

The shaded area in Fig. 3.63 is the conventional takeoff and landing design area. In the partial thrust-supported area, one approach is to rotate the aircraft to a 15°–20° attitude at takeoff, and with the high T/D and E_{TW} of the RBCC propulsion system, the aircraft can climb just as a high E_{TW} ratio fighter in afterburner. Beyond the 140–150 psf range, a vertical launch or a launch from an airborne platform such as the An-225 or the Virgin Galactic Roc (Stratolaunch carrier aircraft) is more appropriate. Sled launches are as restrictive as vertical launches from fixed sites, and, therefore, a large measure of operational flexibility provided by the RBCC concept is lost. Not all agree with that assessment, but it is

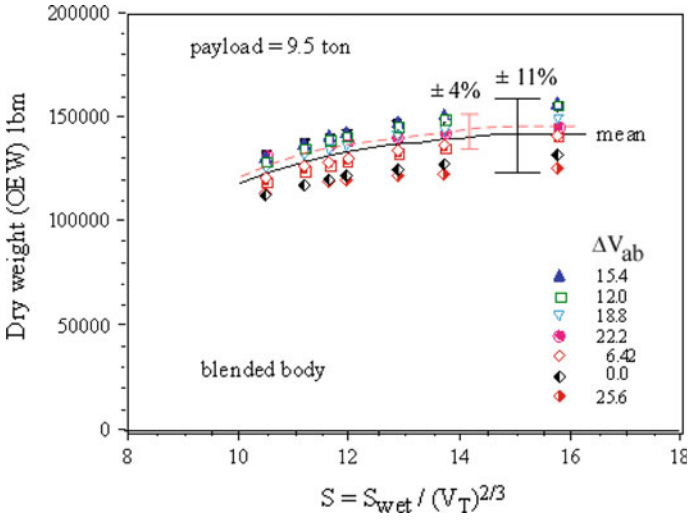

Fig. 3.62 Operational dry weight as a function of geometry (S) for a vehicle with a given payload for different ΔV obtained with airbreathing propulsion (payload = 9.5 t)

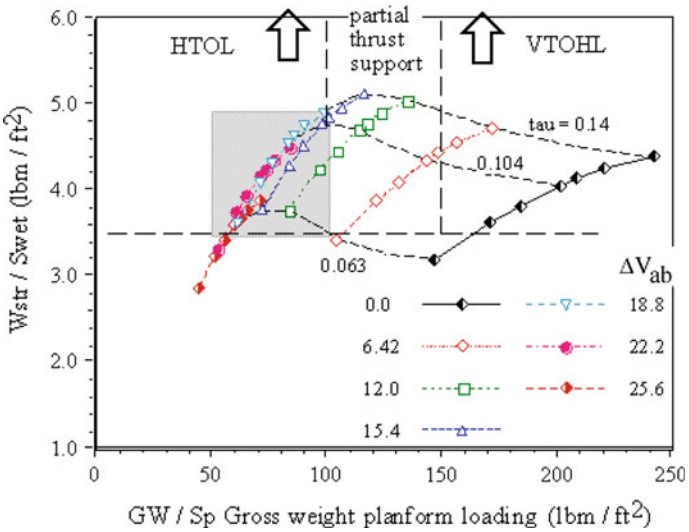

Fig. 3.63 Influence of launch and landing requirements on vehicle parameters for different ΔV obtained with airbreathing propulsion

the opinion of the authors (P.A. Czysz, B. Chudoba). In any case, there is a wide range of practical solutions available for RBCC propulsion concepts with airbreathing velocity increments between 12,000 and 22,200 ft/s.

(5) SYSTEM THRUST-to-DRAG RATIO [influence of I_p and ICI on W_{pay} and V_{total}]

This design space discussion is short as the message is also short and to the point. There is no substitute for thrust in an accelerating vehicle. It has been pointed out several times that the availability of large thrust is a major requirement in any launch vehicle, especially when airbreathing propulsion is included. In fact, there may be no substitute for thrust from many different considerations.

Considering for instance a blended-body, one can obtain the relation between I_{str} and S_{plan}, using parameters T/D averaged over the trajectory, and τ, see Fig. 3.64.

Three observations from this figure are as follows:

(1) The I_{str} margin available is a function of T/D. Vice versa, at a given I_{str}, larger vehicles need higher T/D.
(2) The slenderness of the vehicle, as represented by τ, is a major consideration in obtaining an increased margin with a given value of T/D.
(3) There is an imperative need to assess any propulsion-propellant concept simultaneously with available technology capability, the choice of vehicle size, and the flight trajectory.

Figure 3.64 shows that the quickest way to lose margin is to lower T/D ratio. Many of the all-airbreather concepts

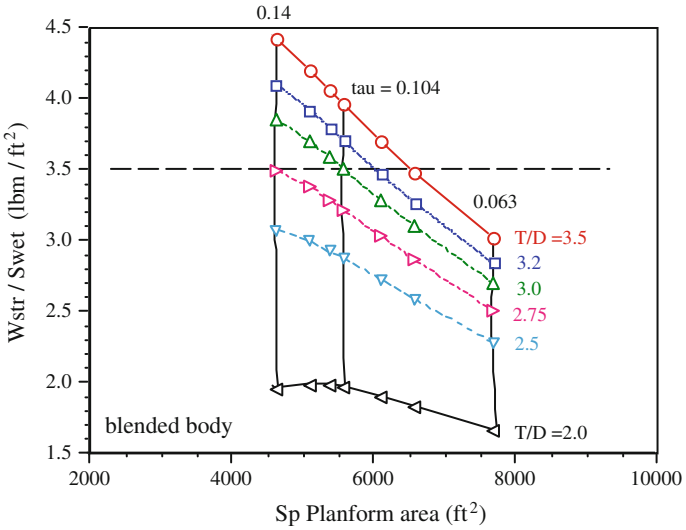

Fig. 3.64 Primary influence of thrust-to-drag ratio and τ on margin in structure index for a blended-body configuration

based on isolated turbojets and ramjets suffer from a low average *T/D* ratio. The net result of low *T/D* ratio is a specific structural weight that is well beyond the ICI. The single most important factor in obtaining results as reported herein is the RBCC propulsion system that can produce trajectory-averaged *T/D* ratios that are on the order of the all-rocket. It is also important to keep in mind the interrelationships among propulsion performance, slenderness, and material/structural requirement identified at the beginning of this chapter. It is far better to purchase increased thrust via a RBCC propulsion system for a stouter configuration than to seek the improbable low structural weight materials ('unobtainium'). Again, this is the authors' opinion. Much of the poor performance of airbreathers can be traced to the poor airbreathing *T/D* ratio. In the author's (P.A. Czysz, B. Chudoba) experience, for hypersonic aircraft, the most economical and lowest weight accelerator in the transonic region is a rocket. None of the converged hypersonic designs ($M \geq 8$) in the author's experience used turbojets for acceleration through the transonic region.

In order to summarize, in Sects. 3.7.4, an attempt has been made to show how key design options orchestrated by vehicle sizing can be examined using parametric design solution spaces (maps). These are built starting from a set of reference parameters after choosing configurations and propulsion-propellant concepts. There is no implication in doing so that a specific choice is better than others. The methodology developed by Czysz and others for seeking useful answers to questions in the evolution of the vehicle has been presented and illustrated with examples. These show the type of physical understanding and thus the rational guidance one can gain from design spaces. The illustrations provided clearly demonstrate the importance of realizing the best and most effective performance of the propulsion system and gaining the most margin with regard to materials and structures or the associated industrial capability, whether one is attempting a demonstrator for a specific purpose or a space launch vehicle. Conventional approaches to configuration concept evolution in aeronautics may not be appropriate for accelerating launch vehicles. In general, a reduction in the size of a vehicle for a given mission must not be motivated simply by cost reduction. There is no substitute for thrust, and that must be realized utilizing an appropriate propellant-propulsion system.

B. *ABSSTO* and *ABTSTO* sizing methodology (J.A. Vandenkerckhove)

The late Jean Vandenkerckhove thought this approach just described had merit and used it as a screening tool in his adaptation named "*SIZING.*" However, he did not think that the approximations, the separate Excel trajectory determination, separate ramjet/scramjet size, and performance determinations, were acceptable for his applications. Consequently, a more detailed approach was undertaken to solve and evaluate Eqs. 3.9a, b, c through 3.28a, b.

J. Vandenkerckhove began his adventure into airbreathing after an encounter with the co-author (P.A. Czysz) at a conference in London in 1983. J. Vandenkerckhove set out to show that only rockets had a future in launcher development. The approach used by Vandenkerckhove (1991a, b, 1992a, b) was to use an existing European-developed trajectory code, to which he added the vehicle characteristic information from Billig (1989) and data from a number of European references and from information gained in personal discussions with European aerospace engineers. For the propulsion performance, he constructed a one-dimensional ram-scramjet, nose-to-tail energy-based performance code (HYPERJET Mk #3) (Vandenkerckhove

1993), similar to those developed by Dr. Frederick Billig (1991) formerly of APL/JHU.

The final computer programs were identified as *ABSSTO* and *ABTSTO* for airbreathing SSTO and TSTO, respectively. The predicted results obtained were just the opposite of that anticipated, namely that incorporating airbreathing in the calculations produced a much better performance than with all-rocket propulsion.

In the mid-1980s, P.A. Czysz and J. Vandenkerckhove began a collaboration on airbreathing launchers. The objectives were:

1. Provide a quantitative sizing model based on simple and direct principles and estimates.
2. Provide simplified input based on engineering experience representing *past*, *current,* and *future* manufacturing capabilities for screening results of parametric studies.

The first step for J. Vandenkerckhove was to incorporate the sizing routines from Pirrello and Czysz (1970) into his codes; he also realized that imposing constant gross weight solutions should be avoided. The payload and crew weight were fixed. Rather than using a separate trajectory code to establish the required weight ratio, in J. Vandenkerckhove's sizing code implementation, engine design, performance, and trajectory were all integrated into a single program. The solution of the nonlinear set of equations was obtained iteratively, until the desired vehicle characteristics and performance assumed initially matched the output from the code within a small tolerance. The dry weight was determined by solving the weight and volume equations simultaneously.

J. Vandenkerckhove's implementations *ABSSTO* and *ABTSTO* represent a pragmatic software sizing approach for space launch and hypersonic cruise vehicles. Rather than selecting a configuration and scaling it, *ABSSTO* and *ABTSTO* develop a *design space* as a function of basic physical design variables from which the designer can select the combination which meets both the mission requirements and available technology.

Figure 3.65 shows the top-level process of the J. Vandenkerckhove convergence methodology as implemented in *ABSSTO* and *ABTSTO*. The basic processes follow the following steps:

Input

1. Define the mission, payload, configuration type, propulsion system, structural, and aerodynamic constants. These *independent design variables* can be iterated however the designer sees fit. For example, different design problems require exploring a variety of configuration types, while others may wish to explore mission sensitivities for a given configuration. In either case, the overall process leading to convergence does not change.
2. Define a range of Küchemann factors τ and make an initial guess for the planform area, S_{plan}. The planform area is iterated to converge the weight and volume budgets.

Analysis

For a given or assumed independent design variables, prepare the following for each Küchemann factor required:

1. Calculate the *L*/*D* and *T*/*D* (for launch vehicles) required for the trajectory analysis.
2. Calculate the weight ratio W_{R} from the trajectory analysis.
3. For the given W_{R} and the initial value of planform area, compute the operational weight empty (W_{OWE}); calculate from both the weight budget equation and volume budget equations.
4. Iterate the planform area until the W_{OWE} from the weight budget and the volume budget converge.
5. Complete the vehicle description (weight breakdown, volume breakdown, basic geometry, thrust requirements, etc.).
6. Calculate the ICI.

Repeat the process for each combination of τ and independent design variables desired.

Output

The output consists of the vehicle description and ICI for each combination of independent design variables and τ. The entire processes can be repeated for each individual stage in case a multi-staged vehicle is considered, beginning with the last stage and working backward to the first stage. For more information see Coleman (2008).

C. *Aerospace Vehicle Design Synthesis* (AVD-SIZING) sizing methodology (B. Chudoba)

In 1992, one author (B. Chudoba) was working as a future projects engineer with the European Airbus Industrie *Future Projects* department. During that time, he gained first-hand understanding of the very best industry had to offer, including the A380, A320 derivatives, the Concorde successor ESCT project, and others. This exposure uncovered the need to improve: (a) how future aircraft and launch vehicles are designed during the early conceptual design phase, (b) how to subsequently optimize the overall system, (c) how to efficiently orchestrate the early forecasting of enabling technologies and overall transportation architectures, and (d) how to implement an effective decision-making and team-integration process (Chudoba 2002). Ten years later, following the advice of Dr. Heribert Kuczera (European Space Agency FESTIP program director), he established the *Aerospace Vehicle Design*

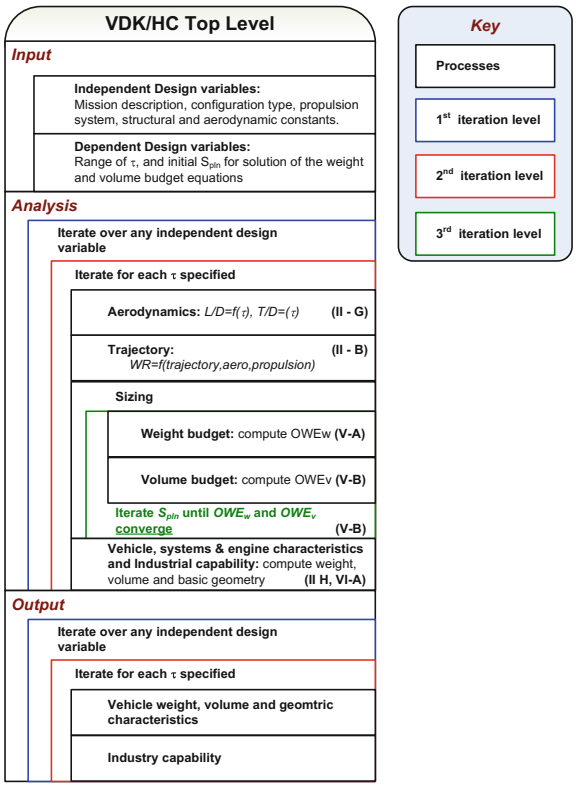

Fig. 3.65 Complete J. Vandenkerckhove convergence sizing methodology

(AVD) *Laboratory* at The University of Texas at Arlington and *Aerospace Vehicle Design* (AVD) *Services LLC* in collaboration with Professor Paul A. Czysz who led the hypersonic and reusable space launch research efforts for McDonnell Douglas. The AVD settings are synergistically continuing the research and professional technology forecasting services conducted by the late Professor Paul Czysz based on the complete *P.A. Czysz Technical Library*. Ever since, the goal has been to further refine the capability for aerospace systems conceptual design and strategic planning, overall challenging the stagnant aerospace product synthesis status quo observed (Chudoba and Heinze 2010).

The AVD-SIZING approach by this author (B. Chudoba) does advance the Czysz and Vandenkerckhove implementations introduced before. The AVD-SIZING methodology breaks down the boundaries between individual disciplines by attaching value to the importance of practical problem-solving with quality analyses while giving confidence through the originality of the insight gained and the practicality of the conclusions made. The best-practice AVD implementation is abridged in Fig. 3.66 (Chudoba et al. 2015). Note the integration of the *Customer Assets* organized via the data-domain (DB) and the knowledge-domain (KB), and the process-domain (PP) represented via the *AVD/Customer Interface* and *AVD Process*.

The development of new aerospace products necessitates thousands of man-years of effort. (For reference, the cost of R&D to develop the Airbus A380 airliner was between 1 and 2 billion euros.) Faced with committing resources from the early gestation of a new product, how can one develop assurance of its impact on the future market? Clearly, the success of vehicle, system, or architecture is primarily dependent on the quality of the underlying performance predictions and technology forecasts. The future projects team is responsible for correctly identifying the available product solution space and its risk topography—that means emphasis is on choosing the initial baseline design *correctly*. This requires a scenario-based, multi-disciplinary sizing methodology capable of uniquely trading the following real-world impact-domains: *marketplace*, *economical*, *societal*, *political*, *environmental*, and *technological*. The comprehensive representation of those impact-domains is largely missing in past and present hypersonics and space launch vehicle development methodologies. The AVD settings have been formed to challenge this early planning gap. *Consistency*, *predictability*, *realism*, *correctness,* and *transparency* are fundamental attributes of the AVD approach aimed at reducing the volatility of customer decision-making.

The AVD-SIZING methodology supports the early system definition and exploratory phase decision-making (Coleman 2010). After Paul A. Czysz's *Hypersonic Convergence* and Jean Vandenkerckhove's *ABSSTO* and *ABTSTO* software implementations, AVD-SIZING is the third-generation best-practice design and technology forecasting tool and methodology tasked to synergistically integrate both, the conceptual design team and corporate team (Chudoba et al. 2011). A unique data-base (DB) and knowledge-base (KB) system organize, utilize, and retain relevant data, information and knowledge from the rich past and present. The synthesis methodology introduced before then complements the systems-architect's task of identifying the *correct solution-space* in a multi-disciplinary context. AVD-SIZING reduces overall forecasting thus development risk by using industry endorsed solutions to increase overall decision-making efficiency (Chudoba et al. 2012). What follows is a brief description of the three principal elements of AVD-SIZING, which combined assemble a best-practice sizing methodology: (1) *data-base* (DB), (2) *knowledge-base* (KB), and (3) *parametric process* (PP).

1. DATA ENGINEERING: aerospace data-base (AVD-DB)

The first step in efficiently utilizing existing aerospace design understanding has been a systematic literature survey, which in itself has been an AVD ongoing effort throughout its existence. Sources of conventional and radical design data, information, and knowledge have been (a) public domain

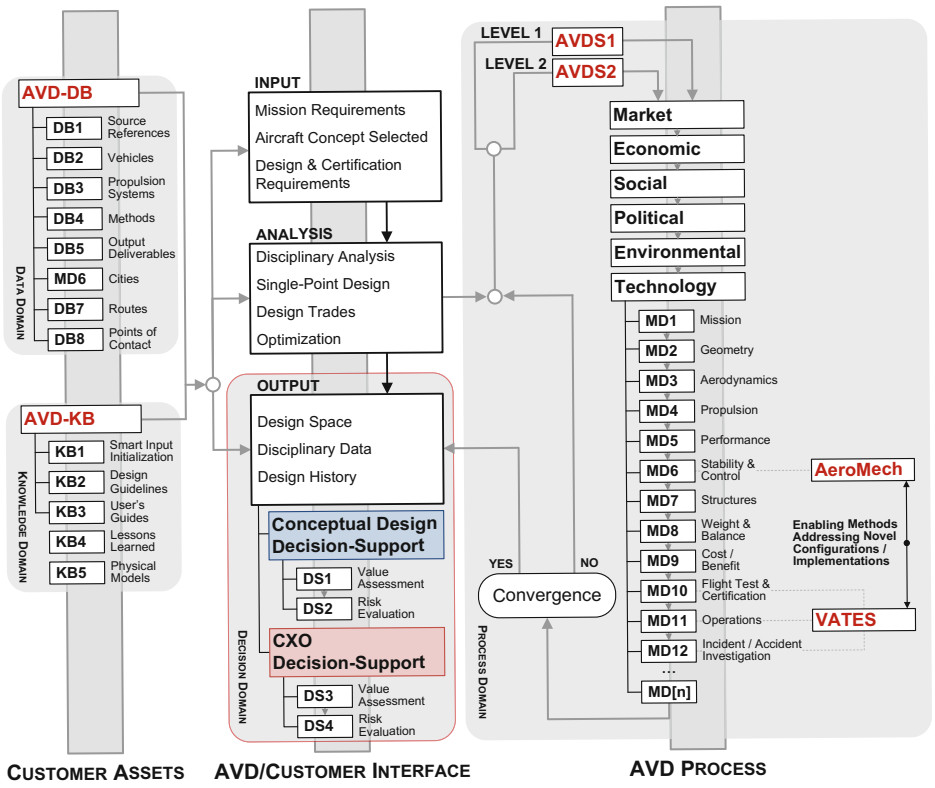

Fig. 3.66 Overview of *aerospace vehicle design synthesis* (AVDS = SIZING) methodology

literature, (b) institutions and industry internal sources, and (c) expert advice. For efficient handling of design-related data and information, a dedicated computer-based aircraft conceptual design data-base (AVD-DB) has been developed (Chudoba 2001; Chudoba et al. 2015a, b). This system stores and handles disciplinary and interdisciplinary literature relevant to the conceptual design (including methodologies, including disciplines like flight mechanics, aerodynamics, etc.), interview-protocols, flight vehicle case studies, (descriptive, historical, numerical information on conventional and unconventional flight vehicle configurations), results of simulation, flight test information, and others. AVD-DB can generate customer-tailored data sets, info-graphics, and data-driven market intelligence (Chudoba 2012; Chudoba and Gonzalez 2011).

The overall requirement in the creation of AVD-DB has been simplicity of maintenance and operation.

AVD-DB has matured to be the central instrument for managing aircraft design data and information toward a comprehensive and effective working tool (Haney et al. 2013; Haney 2016). Clearly, the quality of any data-base is only as good as the degree of completeness, actuality, and familiarity by the user. AVD-DB provides suitably selected, structured, and condensed flight vehicle conceptual design data and information, while accounting for as many design-related interactions as necessary, since the rationale for the evolution of aerospace systems is diverse, as a quick browsing of aerospace history reveals. Aerospace design disciplines and representative case studies showing design ingenuity have been selected to be included in AVD-DB; both need to be appreciated to efficiently serve the innovative designer to solve troublesome problems. AVD-DB embodies industry capability already attained and technologies explored in the context of the specific project.

In summary, AVD-DB represents an integrated data management solution, focusing on extraction, reuse, and capitalization of existing data assets.

2. KNOWLEDGE ENGINEERING: aerospace knowledge-base (AVD-KB)

The dedicated aircraft conceptual design knowledge-base (AVD-KB) collects, manages, and organizes knowledge. The primary objective in developing the AVD-KB system for more than twenty years has been to make legacy conventional and radical project design knowledge effortlessly available (Chudoba 2001). The particular strength of the system is that it enables the user to recall and then advance the understanding of high-speed aircraft and launch vehicle configurations by identifying their commonalties, peculiarities, lessons learned, and legacy design decisions, overall resulting in parametric design guidelines.

Particular emphasis has been placed on consistently grouping flight vehicle configuration-specific design

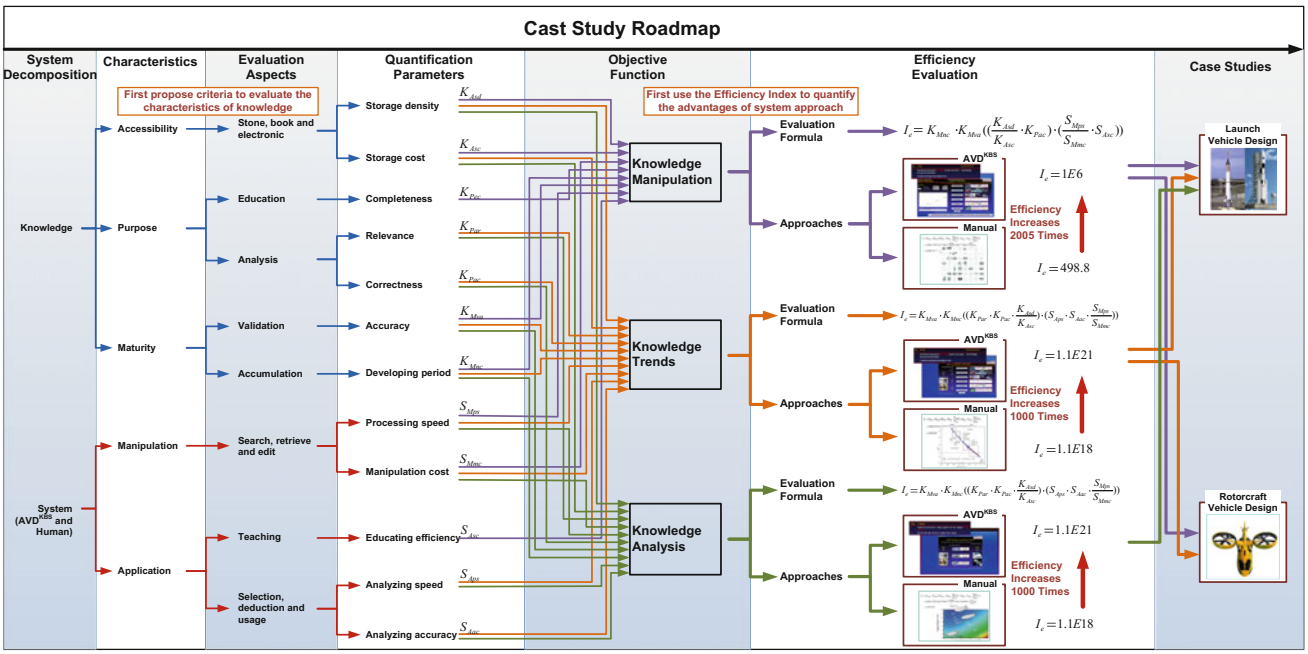

Fig. 3.67 Knowledge management case study roadmap (Peng 2015)

knowledge and experience. This enables the identification of generic flight vehicle parameters driving past case studies. The true novelty of AVD-KB is that the abstract nature of "knowledge' has been, for the first time, parameterized via the identification of logic knowledge categories, each represented via quantifying parameters with physical units. As an example, this approach enable us to quantify "team member knowledge-richness available versus knowledge-richness required" to address a specific project or problem (Peng 2015). Case studies enable the identification of key design drivers and variables with significant impact on the overall design, see the roadmap in Fig. 3.67. These design drivers form the basis to formulate relationships in the sizing methodology. In a successive step, knowledge-derived parametric design guidelines are developed. These show the continuum of the pertinent design characteristics in contrast to the narrow information supplied by typical single point-design solutions. In this way, AVD-KB also can show if legacy project assumptions and decision-making were flawed or still constitute a good foundation.

In summary, AVD-KB enables knowledge collection, retention, and utilization solutions with emphasis on standardizing and disseminating design-capability and smart design ("design-IQ"). Also, it enables smart input initialization, provides an accelerated learning environment, and formalizes parametric design guidelines where possible to facilitate continuous knowledge preservation.

3. PARAMETRIC PROCESS: aerospace sizing & solution-space screening (AVD-PP)

For each individual trade study, the total system design solution space is identified and visualized with the AVD parametric sizing program AVD-SIZING. AVD-SIZING is a best-practice constant mission sizing process capable of screening of a wide variety of conventional and unconventional vehicle configurations in the solution space. This approach has been developed through a thorough review of parametric sizing processes and methods from the 1960s to present for subsonic to hypersonic vehicles (Coleman 2010; Omoragbon 2016; Oza 2016; Gonzalez 2016). With this framework in place, the available solution space is identified including both technical and operational constraints.

Solution space screening implies visualizing multi-disciplinary design interactions and trends based on the Czysz and Vandenkerckhove foundation already described. The modular process implemented in AVD-SIZING relies upon an extensive library of robust methods for disciplinary analysis, and a unique multi-disciplinary analysis (MDA) sizing logic and software kernel enabling data storage, design iterations, and total system convergence.

The integration of the disciplinary methods library and the generic multi-disciplinary sizing logic enables consistent evaluation and comparison of radically different flight vehicles. The flight vehicle and architecture configuration-independent implementation of AVD-SIZING allows for rapid parametric exploration of the integrated flight vehicle system via a

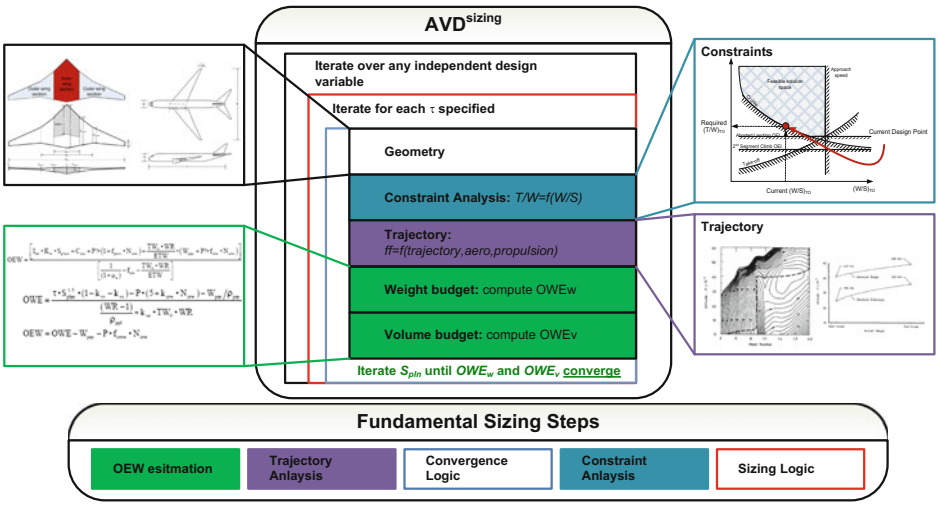

Fig. 3.68 Top-level AVD-SIZING methodology visualized via Nassi-Schneidermann structogram

convergence check of the mission-hardware-technology triple. Figure 3.68 visualizes the top-level sizing process schematic.

At the heart of AVD-SIZING are the weight and volume balance budgets. The results from the requirements in terms of geometry, performance constraints, and trajectory (weight ratio, *T*/*W* ratio, and vehicle geometry) are compared with the computed vehicle weight and volume available as required by the mission. For instance, once a slenderness τ is assumed, the planform area is iterated through the total design process until weight and volume available equal weight and volume required.

In summary, AVD-SIZING is a modular sizing methodology providing systems-level solution-space visualization based on the correct identification and utilization of highest-of-importance impact disciplines, descriptive variables, sound multi-disciplinary physics and future technologies. AVD-SIZING correctly integrates the disciplinary analysis environments and their method libraries into a total system convergence logic.

3.8 Available Solution Spaces: Examples

Having introduced the rationale of the *design solution-space topography* in Sect. 3.7, the following representative example applies this approach to a SSTO launcher. The output desired is (a) mass ratio required to reach LEO from the earth's surface, (b) the mass ratio to reach higher orbits, and (c) the impact of how often these systems operate on the cost of delivering payloads to orbit. This chapter is firstly establishing where a solution exists for the combination of propulsion system and geometry (hardware), mission and technology. Then, using a minimum of information representing the manufacturing capability of the aerospace industry, the minimum required description of the propulsion system and of basic hypersonic vehicle geometry trends, the solution space is identified. Note that in what follows the fuel is LH_2.

3.8.1 Single-Stage-to-Orbit (SSTO) Solution Space

The two principal parameters and relationships are as follows: (1) the operational weight empty (W_{OWE}) and (2) the ICI, as functions of the propulsion system, geometry, size, and material/structures manufacturing capability of industry, as given below. These two equations are solved simultaneously for planform area and ICI, given a specific payload and slenderness parameter.

As introduced earlier, the *weight budget* is given by:

$$W_{\mathrm{OWE}} = 10 \cdot \frac{I_{\mathrm{p}}}{I_{\mathrm{str}}} \cdot f(\mathrm{geometry}) \cdot \frac{1 + r_{\mathrm{use}}}{S_{\mathrm{p}}^{0.7097}} \tag{3.54a}$$

$$W_{\mathrm{OWE}} = W_{\mathrm{empty}} \cdot (1 + r_{\mathrm{use}}) \tag{3.54b}$$

$$W_{\mathrm{OWE}} = K_{\mathrm{v}} \cdot \tau \cdot I_{\mathrm{p}} \cdot S_{\mathrm{plan}}^{1.5717} \tag{3.54c}$$

The *volume budget* is related to the weight budget via:

$$W_{\mathrm{OWE}} = W_{\mathrm{OEW}} + W_{\mathrm{pay}} + W_{\mathrm{crew}} \tag{3.54d}$$

$$W_{\mathrm{OWE}} = \frac{V_{\mathrm{ppl}}}{S_{\mathrm{plan}}} \cdot \frac{\rho_{\mathrm{ppl}}}{W_{\mathrm{R}} - 1} \cdot S_{\mathrm{plan}} \tag{3.54e}$$

The factor $f(\mathrm{geometry}) \equiv f(\mathrm{geo})$ is defined as follows:

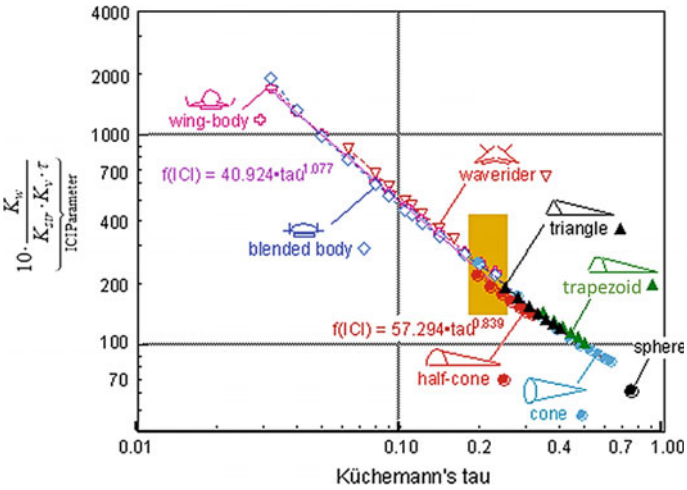

Fig. 3.69 Size-determining parameter group correlates with Küchemann's τ

$$f(\text{geo}) = \frac{K_w}{K_{\text{str}} \cdot K_{\text{v}} \cdot \tau} = f(\tau) \tag{3.55}$$

where

$$\text{ICI} = 10 \cdot \frac{I_{\text{p}}}{I_{\text{str}}}$$

$$\text{ICI} = \underbrace{10 \cdot \frac{K_w}{K_{\text{str}} \cdot K_{\text{v}} \cdot \tau}}_{\text{ICI Parameter}} \cdot \frac{1 + r_{\text{use}}}{S_{\text{plan}}^{0.7097}} \tag{3.56}$$

The ICI and W_{OWE} equations are solved simultaneously. The two principal terms in determining *size* are f(geo) and ICI. The ICI *parameter* is given in Fig. 3.69 as a function of τ.

As for previous geometric correlations, see Fig. 3.12, the different hypersonic configuration map does collapse into a single trend line as shown in Fig. 3.69. Note that the "ICI *parameter*" is not ICI. There are two correlating equations: one for values of τ less than 0.24 and one for values greater than 0.24. The orange shaded rectangle represents the typical SSTO solution space for both rocket and airbreathing propulsion systems. The reason the solution space is so narrow is that, whatever the propulsion system, for a given payload, the quantity of hydrogen fuel is approximately the same, and therefore, the volumes for the different propulsion systems are quite similar. With liquid oxygen 15.2 times denser than liquid hydrogen, the presence or absence of liquid oxygen has a significant weight impact, but a lesser volume impact. The K_v term is a function of τ and the configuration concept and details of this formulation can be found in Czysz and Vandenkerckhove (2000). Nominally K_{v} has a value of 0.4 for a wide range of τ and different configurations. The K_{v} term is a correlation term that defines the maximum volume available for the propellant as a function of vehicle size as defined by the planform area. The correlation is based on the author's (P.A. Czysz) experience in analyzing the results of hypersonic design studies spanning from 20 t to 500 t gross weight vehicles.

The ICI term consists of two elements, the propulsion index, I_{p}, and the structural index, I_{str}, (see Eq. 3.56a, b). For a broad spectrum of propulsion systems, I_{p} depends mainly on turbopumps: The I_{p} value for a given turbopump level of performance is almost constant. Assuming a Space Shuttle Main Engine (SSME) propulsion system, the propulsion index for a SSTO vehicle is 4.3. For a spectrum of propulsion systems from the SSME to an airbreather that can operate to Mach 14 for installation on SSTO vehicles, the propulsion index is 4.1 ± 0.2. The structural index is the total structural weight divided by the wetted area of the vehicle. This index is remarkably consistent over the passage of time. In 1968, the projected 1983 weight of an insulated aluminum structure, that is, both the structure and the propellant tank, was 3.5 lb/ft^2 (17.1 kg/m^2) (Pirrello and Czysz 1970). In 1993, NASA's estimated weight of the same insulated aluminum structure for a hypersonic waverider aircraft (both the structure and the propellant tank) was still 3.5 lb/ft^2 (17.1 kg/m^2) (Pegg et al. 1993). Using these values, the estimated range for the current value of ICI is 9–11. This then gives us a boundary to establish the practicality of SSTO vehicles with today's industrial capability. If the ICI is 9–11 or less, the concept is practical in terms of current industrial capability. If the ICI of a configuration/propulsion system is greater than the boundary value, then it is doubtful the concept is practical in terms of the current industrial capability. The distance of the concept under consideration from the ICI boundary is a measure of the margin, or lack of margin, with respect to the current state of the art. This is perhaps a more meaningful measure compared to less quantitative indices such as the popular TRL (Technology Readiness Level).

Based on these definitions, the solution space is presented graphically as a function of planform area S_{plan} (on the ordinate) and ICI (on the abscissa), with lines of constant payload

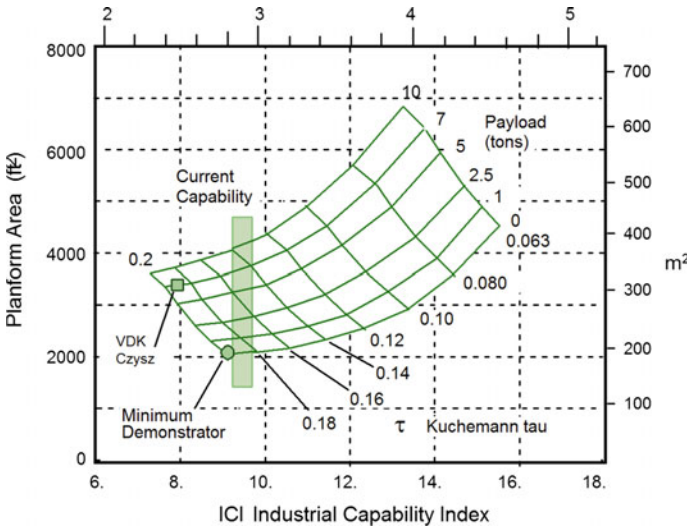

Fig. 3.70 SSTO hydrogen/oxygen rocket-cycle solution space

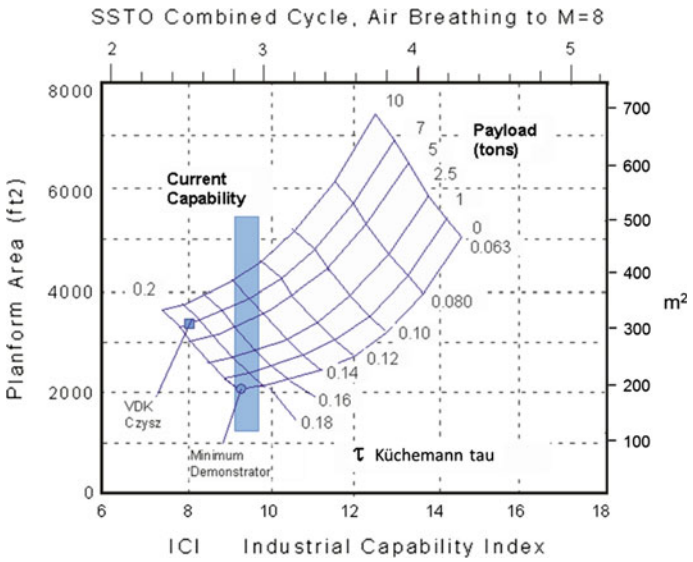

Fig. 3.71 SSTO ejector ramjet/scramjet cycle solution space (Mach 8 transition)

and τ forming the graphical results map. Three propulsion systems are presented for the SSTO to LEO mission (100 nm or 200-km orbital altitude), with payloads varying from zero to 10 t (metric tons). Küchemann's τ ranges from 0.063 to 0.20. The three propulsion systems evaluated are as follows:

(1) All-rocket topping cycle, similar to the P&W XLR-129 or the US SSME. For hydrogen/oxygen propellants, this system represents a hypersonic glider analogous to the FDL-7C/D, as in Fig. 3.70.
(2) Rocket plus ejector ramjet/scramjet operating as an airbreathing system to Mach 8, then transitioning to rocket to reach orbit. For hydrogen/oxygen propellants, the airbreather configuration is shown in Fig. 3.71.
(3) Rocket plus ejector ramjet/scramjet operating as an airbreathing system to Mach 12, then transitioning to rocket to orbit. For hydrogen/oxygen propellants, the airbreather configuration is shown in Fig. 3.72.

Figure 3.70 shows the solution map for the all-rocket configuration. The bottom scale is for ICI in English units (ft^{-1}) for I_p and I_{str}, and the top scale is for ICI in SI units (m^{-1}). The left scale is in English units, and the right scale is in SI units for the planform area. The vertical bar is the ICI boundary for the all-rocket topping cycle similar to the SSME (Jenkins 2001). Note that most of the design space is to the right of the ICI boundary at 9.0–9.5 ft^{-1}, that is, beyond the current state of the art. A kerosene-fueled supersonic cruise vehicle like Concorde has a low value of τ, about 0.035. A hydrocarbon-fueled hypersonic cruise vehicle would have a larger value of τ, about 0.063.

If the designer of a SSTO chose to pattern the design after a cruise vehicle, with a low value of τ, the design would not

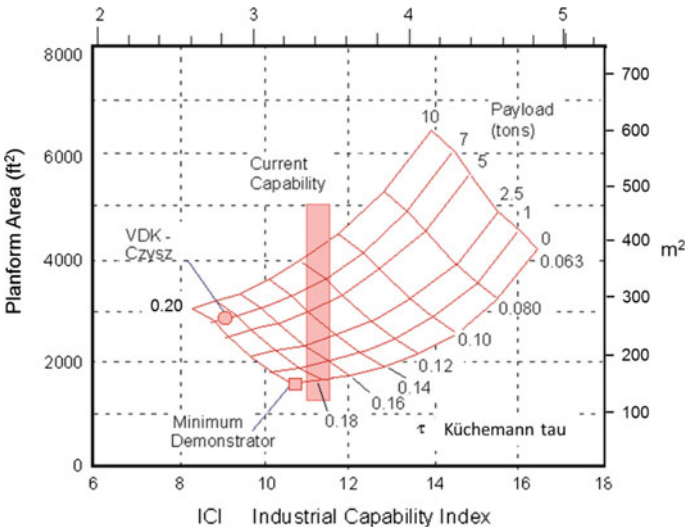

Fig. 3.72 SSTO ejector ramjet/scramjet cycle solution space (Mach 12 transition)

converge, no matter what resources were expended. Note that as the payload increases, the available design space increases. One of the dilemmas of hypersonic vehicle design is as well illustrated in this figure. Using reasoning based on subsonic aircraft, a smaller aircraft should be easier to fabricate and operate than a larger one. However, for a SSTO demonstrator, that is, a demonstrator that can actually achieve orbital speed and altitude, the opposite is the case. The minimum sized, zero-payload demonstrator is on the ICI boundary and at the maximum value of τ. An operational vehicle with a 7.0 t payload as analyzed by Czysz and Vandenkerckhove (2000) has a significant reduction of the ICI value needed. As the payload increases, the τ value at the ICI boundary decreases. Then, for a 10 t payload the minimum value of τ is 0.14. Note that it would be possible to build a hypersonic demonstrator that could achieve Mach 12 for, say, just 5-min flight time, but the mass ratio for that mission might be on the order of 1.8, far from the 8.1 ratio required to reach orbital speed and altitude.

Figure 3.71 shows the solution map for the rocket plus ejector ramjet/scramjet operating as an airbreathing system to Mach 8. The bottom scale is for ICI in English units for I_p and I_{str}, and the top scale is for ICI in SI units. The left scale is in English units and the right scale is in SI units for the planform area. The vertical bar is the ICI boundary for the rocket plus ejector ramjet/scramjet operating as an airbreathing system to Mach 8, and it is at the 9.0–9.5 ft^{-1} value, the same as for the all-rocket launcher. In terms of industrial capability required, this analysis points to an equality of requirements. As with the previous case, most of the design space is to the right of the ICI boundary, that is, beyond the current state of the art. Both the operational example and the demonstrator example have the same ICI value as the previous rocket case. Clearly, the Mach 8 airbreather is about equal, in terms of technical challenge, to the all-rocket vehicle.

Figure 3.72 shows the solution map for the rocket plus ejector ramjet/scramjet, this time operating as an airbreathing system to Mach 12. The bottom scale is for ICI in English units for I_p and I_{str}, and the top scale is for ICI in SI units. The left scale is in English units, and the right scale is in SI units for the planform area. The vertical bar is the ICI boundary for the rocket plus ejector ramjet/scramjet operating as an airbreathing system to Mach 12, and it is to the right of the previous two cases, at a value in the 11–11.5 ft^{-1} range. Clearly, a greater industrial capability fraction of the design space is available for converged designs, but those designs require a higher value of ICI. As with the two previous cases, most of the design space is to the right of the ICI boundary, that is, beyond the current state of the art. Both the operational example and the demonstrator example have a greater ICI value than the previous two cases.

In summary, as the value for the structural index can be assumed to be the same for all three cases presented, the Mach 8 airbreather is about equal, in terms of the technical challenge, to the all-rocket vehicle, but the Mach 12 airbreather represents a greater challenge particularly in propulsion.

It is important to note that the conventional aircraft design wisdom puts SSTO designs out of reach of current industrial capability. The SSTO challenges are similar for all-rocket and airbreather, but increasingly difficult as the Mach number, when airbreathing propulsion must transition to rocket propulsion, increases beyond Mach 8. Given the similarity of the industrial challenge, the question is: *What are the differences in weight for the airbreather compared to the all-rocket vehicle?* Figure 3.73 answers this key question. For approximately the same empty weight, the gross weight of the rocket vehicle is at least twice heavier compared to the

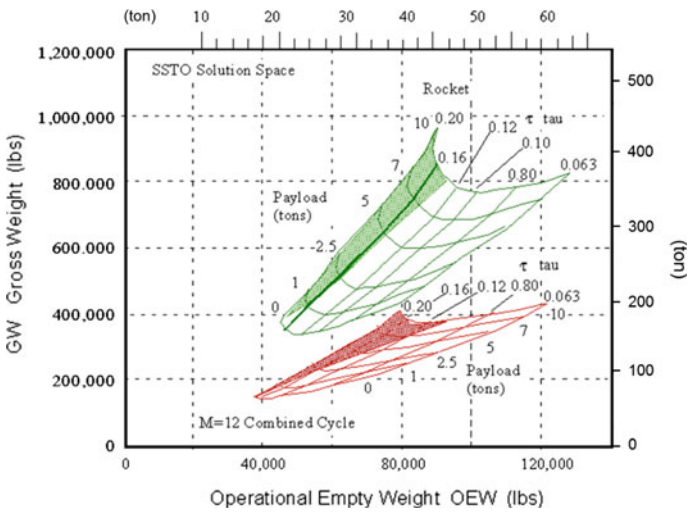

Fig. 3.73 SSTO Mach 12 (transition) combined-cycle propulsion has the advantage over the all-rocket design SSTO

combined-cycle vehicle. The shaded area indicates the area to the left of the ICI boundary in Figs. 3.70 and 3.72. Increasing the slenderness beyond $\tau \approx 0.12$ offers no benefit in reducing either the operational empty weight or the gross weight.

3.8.2 Transatmospheric Space Launcher: Lessons Learned

(1) In the authors' judgment, the real issue for space launcher organizations is not technology, but creating an operationally affordable vehicle that can be as reliable and frequent in delivering cargo to orbit as aircraft are efficient in delivering cargo to another city (Penn and Lindley 1998). The launcher that is at least partially airbreathing can meet the needs of frequent flights to orbit. This potential may still not be recognized by the space organizations, and typical of their positions is "... *the only propulsion system for the 21st century is rocket* ..." (Freeman et al. 1995). Less frequently flying heavy lift vehicles to LEO are a different matter, and vehicles designed for eventual full reuse, such as NPO Energia, are appropriate.

(2) Three vehicle sizing approaches of increasing generality and scope have been presented that integrate simultaneous volume and weight sizing solutions as function of configuration concept, propulsion, propulsion-aerodynamic-structural-energy efficiency, and trajectory. Methods of describing and visualizing the total parametric design space topography, and the design space where solutions are possible, have been described. The parameter interactions are such that a priori judgments often lead to non-converged results.

(3) A broad spectrum of potential airbreathing propulsion systems have been described, and their impact on weight ratio, takeoff mode, and size are presented to show the impact of airbreathing type of propulsion.

(4) The vehicle sizing approach described enables design to specific requirements. This provides greater physical insights into the multi-disciplinary hypersonic aircraft system interactions than do constant size exercises provide in comparison. With constant size, negative payloads can and do result. The physical interpretation of negative payload and the volume of that payload are obscure.

(5) The key to creating an affordable, flexible, and reliable launcher is a lightweight high-thrust propulsion system. A number of different engine cycles have been discussed in this chapter. Some employ turbo machinery as part of the cycle. The need for a high specific impulse and high thrust leads to the thermally integrated LACE ejector ramjet concept. The desire to reduce onboard carried oxidizer to a minimum leads to in-flight air collection and separation adaptation of the thermally integrated LACE ejector ramjet concept. As the NASA-sponsored *HyFAC* study clearly showed, as good as turbojets are for fighters, the poor launcher transonic acceleration makes non-integrated gas turbine engines an expensive price to pay for familiar conventionality.

(6) The TSTO or mobile-based SSTO with the Liquid Air Cycle Engine (LACE) incorporated into the subsonic carrier for collection purposes can already provide a flexible, fully reusable concept with only subsonic staging.

(7) For the SSTO without in-flight collection, the use of scramjets is mandatory. To represent the SSTO as an unachievable device in the near term is to discredit the pioneers of the late 1950s and 1960s who built and successfully tested these engines up to at least Mach 8

for the inlet diffuser, the exit, and their ability to duplicate conditions. With air collection, the use of scramjets is not essential, provided advanced light-weight high-internal pressure and temperature ramjets are available. With subsequent upgrades, scramjets with increased payloads have significant growth potential.

3.9 Hypersonic Configurations: Geometric Characteristics

This section collects the fundamental sizing relationships from *Hypersonic Convergence* (Czysz 1986) and then develops the geometrical relationships that are inherent in the approach.

3.9.1 Configuration Continuum

The fundamental premise of the approach is that the geometry of hypersonic vehicles relates to volume and area such that it can be approached parametrically rather than via single point designs. Ten families of hypersonic configurations have been developed in the *Hypersonic Convergence* data-base: All configuration geometries have delta planforms with the wing apex beginning at the nose. A NASA Langley cylinder-wing configuration (WB004C) was added as a reusable all-rocket reference point.

Overall, there are two scaling modes: (A) Hold the sweep angle constant and vary the volume by changing the maximum cross-sectional area; (B) hold the cross section constant and vary the wing sweep through 72° to 80°. The configurations and the pertinent equations are included in this chapter to enable the reader to develop the desired relationships. In this discussion, the authors used a fixed sweep angle of 78° for all configurations. All the curves shown are for pointed bodies.

To begin, *Hypersonic Convergence* is briefly reviewed to show the derivation of the three principal size-determining elements and where the geometric characteristic of a particular configuration does play a role. The three principal elements are as follows: (1) the ratio propellant volume to planform area, (2) the ratio propellant density to weight ratio minus one, and (3) the magnitude of planform area. The geometry of the configuration will be of first-order importance (highest-of-importance) in the first and third elements. The configuration will play a role in the second element, but only as a correction to the weight ratio term for thrust-to-drag ratio. Beginning with the definition of weight ratio, we have:

$$W_{\mathrm{R}} = \frac{W_{\mathrm{TOGW}}}{W_{\mathrm{OWE}}} \tag{3.57a}$$

$$W_{\mathrm{R}} = \frac{W_{\mathrm{OWE}} + W_{\mathrm{ppl}}}{W_{\mathrm{OWE}}} \tag{3.57b}$$

$$W_{\mathrm{R}} = 1 + \frac{W_{\mathrm{ppl}}}{W_{\mathrm{OWE}}} \tag{3.57c}$$

The fundamental definition of Operational Weight Empty (W_{OWE}) is given by:

$$W_{\mathrm{OWE}} = \frac{W_{\mathrm{ppl}}}{W_{\mathrm{R}} - 1} \tag{3.58a}$$

$$W_{\mathrm{OWE}} = \frac{V_{\mathrm{ppl}}}{S_{\mathrm{plan}}} \cdot \frac{\rho_{\mathrm{ppl}}}{W_{\mathrm{R}} - 1} \cdot S_{\mathrm{plan}} \tag{3.58b}$$

$$W_{\mathrm{OWE}} = W_{\mathrm{OEW}} + W_{\mathrm{pay}} + W_{\mathrm{crew}} \tag{3.58c}$$

Incorporating Küchemann's volume parameter

$$\tau = \frac{V_{\mathrm{total}}}{S_{\mathrm{plan}}^{1.5}} \tag{3.59}$$

we obtain

$$W_{\mathrm{OWE}} = \frac{\rho_{\mathrm{ppl}}}{W_{\mathrm{R}} - 1} \cdot \frac{V_{\mathrm{ppl}}}{V_{\mathrm{tot}}} \cdot \tau \cdot S_{\mathrm{plan}}^{1.5} \tag{3.60}$$

Introducing the geometric parameter K_{w}, the ratio of wetted (surface) area to planform area, and a correlation K_{str} for the structure weight fraction with respect to the W_{OEW}, we have:

$$K_{\mathrm{w}} = \frac{S_{\mathrm{wet}}}{S_{\mathrm{plan}}} \tag{3.61}$$

With

$$\frac{W_{\mathrm{str}}}{W_{\mathrm{OEW}}} = \frac{K_{\mathrm{str}}}{S_{\mathrm{plan}}^{0.138}} \tag{3.62}$$

and

$$K_{\mathrm{str}} = \frac{W_{\mathrm{str}}/W_{\mathrm{OEW}}}{S_{\mathrm{plan}}^{0.138}} \tag{3.63a}$$

$$K_{\mathrm{str}} = 0.228^{\pm 0.035} \times \tau^{0.206} \tag{3.63b}$$

We obtain a relationship for the technology of the airframe structure (including thermal protection) as related to the propulsion-propellant technology and geometry:

$$\frac{W_{str}}{S_{wet}} = \left(\frac{\rho_{ppl}}{W_R - 1}\right) \cdot \left(\frac{V_{ppl}}{V_{tot}}\right) \cdot \frac{\frac{W_{str}}{W_{OEW}}}{1 + \frac{W_{use}}{W_{OEW}}} \cdot \frac{\tau \cdot S_{plan}^{1.5}}{K_w} \quad (3.64)$$

With respect to the propellant volume fraction, V_{ppl}, the correlation from a series of detailed-design hypersonic cruise vehicles, from an F-15 weight class to an AN-225 weight class, provided the data-base. Because the correlation parameter K_v in Eq. (3.65a) is dimensional, two versions are given for both unit systems. The original correlations were for an all-electronic, high-density payload. Consequently, the initial value, K_{v0}, is scaled with respect the bulk density of the payload. This is the payload weight divided by the payload bay volume.

$$\frac{V_{ppl}}{V_{tot}} \approx K_v \cdot S_{plan}^{0.0717} \text{ (English)} \quad (3.65a)$$

$$\frac{V_{ppl}}{V_{tot}} \approx 1.1857 \cdot K_v \cdot S_{plan}^{0.0717} \text{ (Metric)} \quad (3.65b)$$

We obtain for the scaled propellant volume fraction:

$$K_v = K_{v0} - 6.867 \cdot 10^{-3} \cdot \tau^{-1} + 8.2777 \cdot 10^{-4} \cdot \tau^{-2} - 2.811 \cdot 10^{-5} \cdot \tau^{-3} \quad (3.66)$$

with

$$K_{v0} = 0.40 \cdot \left(\frac{\rho_{pay}}{5.0}\right)^{0.123} \quad (3.67a)$$

$$K_{v0} = 0.40 \cdot \left(\frac{\rho_{pay}}{176.5}\right)^{0.123} \quad (3.67b)$$

The payload fraction has been correlated for two classes of vehicles. Equation 3.68a is for the propulsion integrated configuration concepts with a body-integrated inlet ramp system and exhaust nozzle. Equation 3.68b is for the blunt-base rocket powered hypersonic glider configuration concepts. Note that the payload fraction is a function of both the geometrical slenderness and the absolute value of payload. The payload must be in metric ton for Eqs. 3.68a, b.

$$\frac{W_{pay}}{W_{OEW}} = \frac{e^{(2.10 \cdot \tau)}}{24.79} \cdot e^{[0.71 \cdot \ln(W_{pay})]}$$

$$\frac{W_{pay}}{W_{OEW}} = \frac{e^{(1.29 \cdot \tau)}}{25.4} \cdot e^{[0.71 \cdot \ln(W_{pay})]} \quad (3.68)$$

Equation 3.64 can then be written as:

$$\frac{W_{str}}{S_{wet}} = \frac{K_{str} \cdot K_v \cdot \tau}{K_w} \cdot \left(\frac{\rho_{ppl}}{W_R - 1}\right) \cdot \frac{S_{plan}^{0.7097}}{1 + \frac{W_{pay}}{W_{OEW}}} \quad (3.69)$$

This equation can be rearranged to yield a first-order or highest-of-importance estimate of the vehicle planform area based on the available industrial capability (technology), payload faction, and configuration geometry:

$$S_{plan} = \left[\left(\frac{K_w}{\tau}\right) \cdot K_{str} \cdot K_v \cdot \frac{\frac{\rho_{ppl}}{(W_R - 1)}}{\frac{W_{str}}{S_{wet}}} \cdot \left(1 + \frac{W_{pay}}{W_{OEW}}\right)\right]^{1.409} \quad (3.70)$$

The three primary terms are then:

$$\frac{\frac{\rho_{ppl}}{(W_R - 1)}}{\frac{W_{str}}{S_{wet}}} = \frac{I_p}{I_{str}} \quad (3.71a)$$

$$\left(1 + \frac{W_{pay}}{W_{OEW}}\right) = 1 + \frac{\exp(2.10 \cdot \tau)}{24.79} \cdot \exp[0.71 \cdot \ln(W_{pay})] \quad (3.71b)$$

$$\left(\frac{K_w}{\tau}\right) \cdot K_{str} \cdot K_v = \left(\frac{K_w}{\tau}\right) \cdot \frac{0.093 \pm 0.017}{\tau^{0.794}} \quad (3.71c)$$

A most likely value for K_v of 0.40 ±0.02 is assumed for the last term. For the (K_w/τ) term, ten families of hypersonic configurations from the *Hypersonic Convergence* data-base (Czysz 1986) are given. As introduced earlier, all configurations have delta planforms with the wing apex beginning at the nose. The NASA Langley cylinder-wing configuration (WB004C) has been added as a reusable all-rocket reference point. There are two different scaling modes. The first does fix the sweep angle and it varies the volume by changing the maximum cross-sectional area. The second does fix the cross section and it varies the wing sweep from 72° through 80°. For this report, the authors selected to fix the sweep angle at 78° for all configurations. The configurations and pertinent equations are provided here, enabling the reader to generate their own scaling models. All the curves shown in this reference are for pointed bodies. A spatula-body fixes the length and adds width and volume. Since the length determines the engine module height and length, a fixed length, but wider, vehicle can incorporate an increased number of the same engine modules into the configuration. This eases the concerns of the propulsion community with respect to engine module certification. The spatula-nosed waveriders from the University of Maryland have essentially the same characteristics as the blended-body (Mark Lewis, private communication, June 1997).

For the ten configuration families (geometry lineages) are constant 78° sweep-angle variable cross-sectional shapes. The rocket-derived propulsion includes LACE and deeply cooled rocket cycles. Airbreathing-derived propulsion-integrated hypersonic configurations are: (1) *blended-body*,

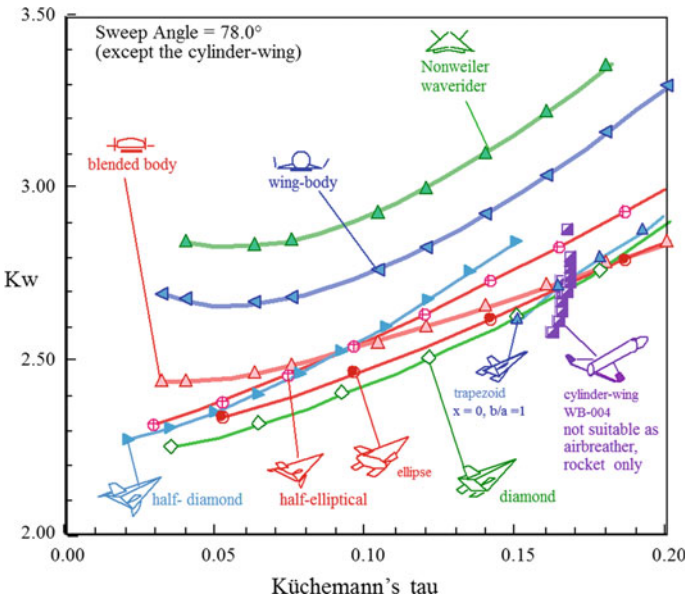

Fig. 3.74 Broad range geometric (surface and volume) design space for hypersonic configuration concepts spanning potential space launcher applications

(2) *wing-body* (not cylinder-wing), and (3) *Nonweiler waverider*. Rocket-derived hypersonic gliders are: (4) *diamond* cross section, base height to width 0.1–1.0; (5) *elliptical* cross section, base height to width from 0.1 to 1.0; (6) *trapezoidal* cross section, base top width to bottom width from 0 to 1.0; (7) *blunted* right-circular cone, nose-to-base diameter ratio from 0 to 0.3; (8) *half-diamond* cross section, base height to width from 0.05 to 0.5; (9) *half-elliptical* cross section, base height to width from 0.05 to 0.5; and (10) *half-blunted* right-circular cone, nose-to-base diameter ratio from 0 to 0.3. The eleventh configuration (11) is the NASA Langley cylinder-wing (WB004C) configuration (Martinovic and Cerro 2002), which is used as a vertical launch and recoverable rocket vehicle reference. The exposed wing area and diameter of the tank have been held constant. The volume changes by varying the length-to-diameter of the cylinder. This configuration has not been used in this book.

Figure 3.74 shows the wetted area to planform area ratio, $K_w = S_{wet}/S_{plan}$, versus τ for configurations that include aerodynamic control as surfaces as shown in Figs. 3.42 and 3.48. These are possible candidates for space launchers having values of τ less than 0.20 and lower values of wetted area to planform area ratio, S_{wet}/S_{plan}. The wing-body and Nonweiler waverider have larger values of wetted area to planform area ratio than integral wing-body configurations. The WB004C configuration has very different geometric properties compared to the highly swept integral wing-body configurations. It is essentially a constant τ configuration (0.162–0.167) over

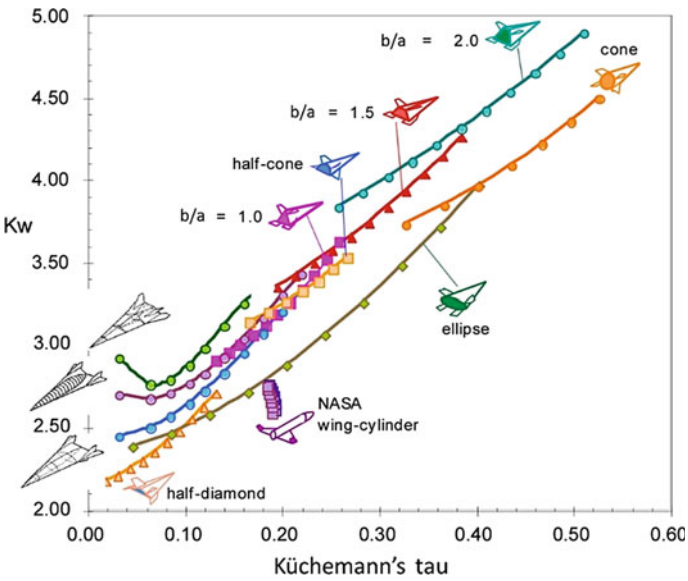

Fig. 3.75 Synopsis of the range of 11 geometric characteristics (surface and volume) of potential hypersonic vehicle configuration concepts

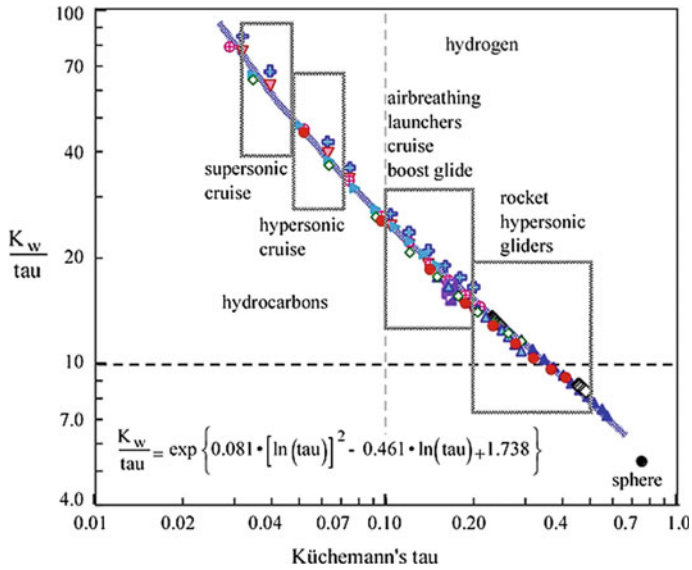

Fig. 3.76 Sizing geometry parameter, K_w/τ, is determined by τ

a 2 to 1 volume ratio, which means that volume changes require planform area changes. The full range of hypersonic shapes extend beyond $\tau = 0.20$. Figure 3.75 shows a broader range of configuration characteristics up to $\tau = 0.50$ that encompasses most hypersonic cruise aircraft, hypersonic accelerators or space launchers, and hypersonic gliders. That represents about the limit for a reasonable lift-to-drag ratio for an acceptable cross-range and down-range. Not shown is the *sphere* with a $\tau = 0.752$ and a $K_w = 4.00$.

The elliptical cone spans the widest range of τ and K_w as it progresses from an ellipse with a height 10% of its width to a circle. The diamond and trapezoidal shapes span similar ranges. There are two trapezoidal shapes. The first one with $(b/a) = 1$ has a height equal to the half width. The second one with $(b/a) = 2$ has a height equal to the width. The parameter in the sizing equation is the ratio of τ/K_w. That ratio is plotted in Fig. 3.76 for all of the configurations shown in Fig. 3.75. The result is the collapse of the geometric characteristics into nearly a single line, see Fig. 3.76. In this graph, the sphere is shown, and it has the lowest value of the (K_w/τ) term. Clearly, the sphere has the lowest W_{OEW} and the highest drag, making it a simple ballistic vehicle.

The different classes of vehicles and the propellants can be differentiated on Fig. 3.76. The denser the propellant, the smaller the propellant volume and the more slender the shape and the larger the planform area with respect to the propellant volume. The important conclusion is that as a first-order estimate, only τ needs be known. After the first order estimate, then the refinement of the estimate using different geometries can proceed. The primary determinant then is the propulsion index that results from a trajectory or cruise performance analysis. The remainder of this chapter gives the configuration concepts and the description of the geometric properties.

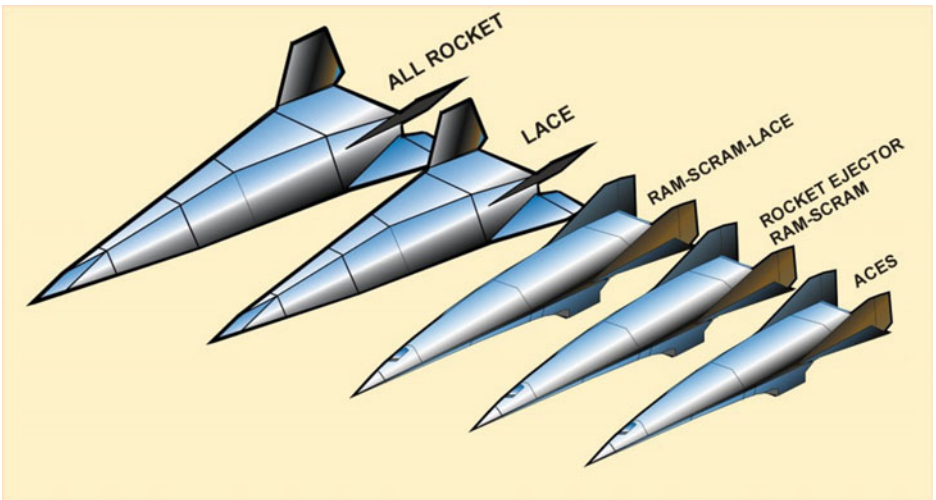

Fig. 3.77 A scaled family of rocket-based and ramjet/scramjet-powered hypersonic aircraft

Fig. 3.78 Airbreathing propulsion-integrated configuration concepts, 78° leading edge angle

3.9.2 Configuration Geometry Properties

There are a wide variety of configurations possible for reusable spacecraft. But if the requirements for a transportation system to space and back are to be met, the configuration spectrum is significantly narrowed. Two basic configuration types have been employed in the US.

One is for all-rocket and airbreathing rocket-cycle propulsion that can operate as airbreathing propulsion to about Mach 6, see upper left in Fig. 3.77. For the rocket propulsion and airbreathing rocket propulsion concepts, a versatile variable capture, inward turning inlet (DuPont 1999) can be integrated into the vehicle configuration derived from the FDL series of hypersonic gliders developed by the Flight Dynamics Laboratory and the work of the McDonnell Douglas Astronautics Company. Because of the mass ratio to orbit, these configurations are generally VTHL vehicles.

The other configuration lineage is for airbreathing propulsion systems that require a propulsion-configured vehicle, where the entire underside of the vehicle is an integrated propulsion system, see lower right in Fig. 3.77. The thermally integrated airbreathing combined-cycle configuration concept is derived from the McDonnell Douglas (St. Louis) *Advanced Design* organization. This is the family of hypersonic, rocket accelerated, and airbreathing cruise vehicles (Pirrello and Czysz 1970). Depending on mass ratio, these vehicles can takeoff horizontally (HTHL) or be launched vertically (VTHL) and always land horizontally. The vehicle concept initially conceived in the 1960s was an airbreathing, propulsion-configured vehicle accelerated by a main rocket in the aft end of the body. Today, such basic configuration can still retain this strategy or use a RBCC propulsion concept. Overall, both basic shapes are functions of τ, that is, for a given planform area, the cross-sectional distribution is determined by the volume required.

The following addresses configurations that are designed to be controlled in the entry glide and for airbreathers, and for the other class of vehicles to be controlled on the exit and entrance flight path. The first part deals with configurations specifically designed to integrate airbreathing systems and the second with hypersonic glider configurations.

Airbreathing Configuration Concepts. The section at the end of this chapter provides equations that give the geometric characteristics of airbreathing configurations. The airbreathing hypersonic vehicle is not just an aerodynamic shape with an engine attached, but indeed the compression side of the vehicle is the inlet, combustor and nozzle. At Mach 6, an isolated nacelle is almost as long as the airframe. A conventional freestream inlet, that is, one designed to operate at the freestream Mach number, is very difficult to control at hypersonic Mach numbers. Using the air vehicle as the propulsion system means that the engine inlet Mach number is considerably less than flight speed, and more amenable to stability and control. For the family of hypersonic vehicles shown in Fig. 3.78, the compression side is identical for all the blended-body configurations. In fact, to have the wing-body operate efficiently, it must have essentially the same underside as the blended-body. The Nonweiler waverider is a special case due to its conical flow field. There is the same number of ramps, but they are designed three-dimensionally to create a family of converging conical shocks.

General Hypersonic Glider Configuration Concepts. These vehicles have blunt bases and are appropriate for rocket-powered hypersonic gliders, such as the FDL-7 series. These configurations have been the basis of many hypersonic gliders by the US Air Force and others with an interest in significant cross-range and down-range over the past 50 years. These vehicles are very different from wing-body configuration concepts such as the Space Shuttle Orbiter, X-37 and XS-1 (first stage), or all-body (lifting body) configuration concepts like the X-24A, M2-F3, HL-10, Dream Chaser, and X-38, since they have substantially better performance with reduced entry heat load. It is possible to use some of the FDL-lineage configuration concepts, such as deeply cooled and LACE propulsion concepts that are limited to Mach numbers less than 6. The key to a successful airbreathing concept is the maintenance of sharp leading edges, in that they reduce drag and thus entropy production during flight. For more detail, see Czysz (1986).

The remaining figures in this section show the hypersonic glider and airbreathing cruiser/accelerator geometric

characteristics of configuration concepts and list related equations.

RIGHT-CIRCULAR POINTED CONE

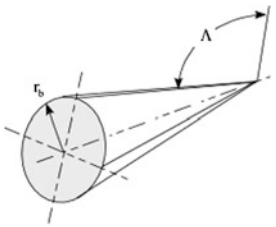

$$A_{\text{base}} = \pi \cdot r^2 \tag{3.72a}$$

$$S_{\text{plan}} = r^2 \cdot \tan \Lambda \tag{3.72b}$$

$$S_{\text{wet}} = \pi \cdot r^2 \cdot \left(1 + \frac{1}{\cos \Lambda}\right) \tag{3.72c}$$

$$V_{\text{tot}} = \frac{\pi \cdot r^3}{3} \cdot \tan \Lambda \tag{3.72d}$$

$$K_{\text{w}} = \pi \cdot \left(\frac{1}{\tan \Lambda} + \frac{1}{\sin \Lambda}\right) \tag{3.72e}$$

$$\tau = \frac{\pi}{3 \cdot \sqrt{\tan \Lambda}} \tag{3.72f}$$

$$\tan \Lambda = \frac{\pi}{3 \cdot \tau} \tag{3.72g}$$

$$\tau_{78^\circ} = 0.4826 \tag{3.72h}$$

$$(K_{\text{w}})_{78^\circ} = 4.160 \tag{3.72i}$$

$$0.54 \leq \tau \leq 0.39 \tag{3.72j}$$

BLUNTED CONE

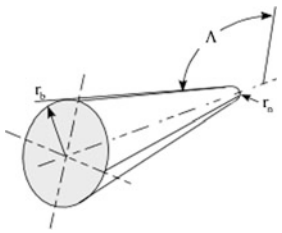

$$A_{\text{base}} = \frac{\tau \cdot r_{\text{b}}^2}{2} \tag{3.73a}$$

$$S_{\text{plan}} = r_{\text{b}}^2 \cdot \tan \Lambda \cdot \left[1 + \left(\frac{r_{\text{n}}}{r_{\text{b}}}\right)^2\right] + \frac{\pi \cdot r_{\text{b}}^2}{2} \cdot \left(\frac{r_{\text{n}}}{r_{\text{b}}}\right)^2 \tag{3.73b}$$

$$S_{\text{wet}} = \pi \cdot r_{\text{b}}^2 \cdot \left[1 + \frac{1 + \left(\frac{r_{\text{n}}}{r_{\text{b}}}\right)^2}{\cos \Lambda} + 2 \cdot \left(\frac{r_{\text{n}}}{r_{\text{b}}}\right)^2\right] \tag{3.73c}$$

$$V_{\text{tot}} = \frac{\pi \cdot r_{\text{b}}^3}{3} \cdot \left(1 - \frac{r_{\text{n}}}{r_{\text{b}}}\right) \cdot \left[1 + \frac{r_{\text{n}}}{r_{\text{b}}} + \left(\frac{r_{\text{n}}}{r_{\text{b}}}\right)^2\right] \cdot \tan \Lambda + \frac{\pi \cdot r_{\text{b}}^3}{2} \cdot \left(\frac{r_{\text{n}}}{r_{\text{b}}}\right)^3 \tag{3.73d}$$

$$(K_{\text{w}})_{78^\circ} = 4.600 \cdot \left(\frac{r_{\text{n}}}{r_{\text{b}}}\right)^2 - 2.350 \cdot \frac{r_{\text{n}}}{r_{\text{b}}} + 4.111 \tag{3.73e}$$

$$\tau_{78^\circ} = 0.3048 \cdot \left(\frac{r_{\text{n}}}{r_{\text{b}}}\right)^2 + 0.01875 \cdot \frac{r_{\text{n}}}{r_{\text{b}}} + 0.04826 \tag{3.73f}$$

$$0.00 \leq \frac{r_{\text{n}}}{r_{\text{b}}} \leq 0.30 \tag{3.73g}$$

$$0.4826 \leq \tau \leq 0.52 \tag{3.73h}$$

ELLIPSE

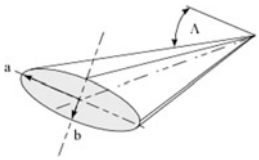

$$A_{\text{base}} = \pi \cdot a^2 \cdot e \tag{3.74a}$$

$$S_{\text{plan}} = a^2 \cdot \tan \Lambda \tag{3.74b}$$

$$S_{\text{wet}} = \pi \cdot a^2 \cdot \frac{(1+e)}{\cos \Lambda} \cdot \left(1 + \frac{R^2}{4} + \frac{R^4}{64} + \frac{R^6}{256}\right) + \pi \cdot a^2 \cdot e \tag{3.74c}$$

$$V_{\text{tot}} = \frac{\pi \cdot a^3 \cdot e}{3} \cdot \tan \Lambda \tag{3.74d}$$

$$(K_{\text{w}})_{78^\circ} = 2.404 \cdot \tau^2 + 2.920 \cdot \tau + 2.174 \tag{3.74e}$$

$$\tau_{78^\circ} = 0.4826 \cdot \frac{b}{a} \tag{3.74f}$$

$$0.01 \leq \frac{a}{b} \leq 1.0 \tag{3.74g}$$

$$0.0483 \leq \tau \leq 0.4826 \tag{3.74h}$$

$$e = \frac{b}{a} \tag{3.74i}$$

$$R = \frac{1 - e}{1 + e} \tag{3.74j}$$

DIAMOND

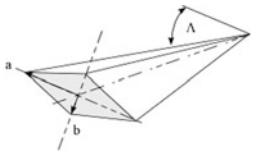

$$A_{\text{base}} = 2 \cdot a^2 \cdot e \tag{3.75a}$$

$$S_{\text{plan}} = a^2 \cdot \tan \Lambda \tag{3.75b}$$

$$S_{\text{wet}} = 2 \cdot a^2 \cdot \sqrt{1+e^2} \cdot \tan \Lambda + 2 \cdot a^2 \cdot e \tag{3.75c}$$

$$V_{\text{tot}} = \frac{2 \cdot a^3 \cdot e}{3} \cdot \tan \Lambda \tag{3.75d}$$

$$(K_{\text{w}})_{78^\circ} = 8.023 \cdot \tau^2 + 1.872 \cdot \tau + 2.173 \tag{3.75e}$$

$$\tau_{78^\circ} = 0.3074 \cdot \frac{b}{a} \tag{3.75f}$$

$$0.01 \le \frac{a}{b} \le 1.0 \tag{3.75g}$$

$$0.0307 \le \tau \le 0.307 \tag{3.75h}$$

$$e = \frac{b}{a} \tag{3.75i}$$

TRAPEZOID

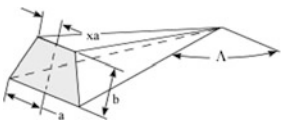

$$A_{\text{base}} = a^2 \cdot e \cdot (1+x) \tag{3.76a}$$

$$S_{\text{plan}} = a^2 \cdot \tan \Lambda \tag{3.76b}$$

$$S_{\text{wet}} = a^2 \cdot \left[(1+x) + \frac{\sqrt{e^2 + (1+x)^2}}{\cos \Lambda} \right] \tag{3.76c}$$

$$V_{\text{tot}} = \frac{a^3 \cdot (1+x) \cdot e}{3} \cdot \tan \Lambda \tag{3.76d}$$

$$(K_{\text{w}})_{78^\circ} = 2.906 - 2.022 \cdot \tau + 15.706 \cdot \tau^2 \tag{3.76e1}$$

$$\tau_{78^\circ} = 0.1535 \cdot x + 0.1538 \tag{3.76e2}$$

$$b/a = 1.0 \tag{3.76e3}$$

$$(K_{\text{w}})_{78^\circ} = 3.013 + 0.706 \cdot \tau + 5.438 \cdot \tau^2 \tag{3.76f1}$$

$$\tau_{78^\circ} = 0.2300 \cdot x + 0.2310 \tag{3.76f2}$$

$$b/a = 1.5 \tag{3.76f3}$$

$$(K_{\text{w}})_{78^\circ} = 3.093 + 1.064 \cdot \tau + 3.093 \cdot \tau^2 \tag{3.76g1}$$

$$\tau_{78^\circ} = 0.3075 \cdot x + 0.3075 \tag{3.76g2}$$

$$b/a = 2.0 \tag{3.76g3}$$

$$0.0 \le x \le 1.0 (\text{from triangle to square base}) \tag{3.76h}$$

$$0.154 \le \tau \le 0.615 \tag{3.76i}$$

$$e = b/a \tag{3.76j}$$

$$x = \text{top width/bottom width} \tag{3.76k}$$

POINTED HALF-CONE

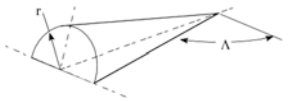

$$A_{\text{base}} = \frac{\pi \cdot r^2}{2} \tag{3.77a}$$

$$S_{\text{plan}} = r^2 \cdot \tan \Lambda \tag{3.77b}$$

$$S_{\text{wet}} = \frac{\pi \cdot r^2}{2} \cdot \left(1 + \frac{1}{\cos \Lambda} \right) + r^2 \cdot \tan \Lambda \tag{3.77c}$$

$$V_{\text{tot}} = \frac{\pi \cdot r^3}{6} \cdot \tan \Lambda \tag{3.77d}$$

$$K_{\text{w}} = \frac{\pi}{2} \cdot \left(\frac{1}{\tan \Lambda} + \frac{1}{\sin \Lambda} \right) + 1 \tag{3.77e}$$

$$\tau = \frac{\pi}{6 \cdot \sqrt{\tan \Lambda}} \tag{3.77f}$$

$$\tan \Lambda = \frac{\pi}{6 \cdot \tau} \tag{3.77g}$$

$$0.0307 \le \tau \le 0.307 \tag{3.77h}$$

$$(K_{\text{w}})_{78^\circ} = 3.220 \tag{3.77i}$$

$$\tau_{78^\circ} = 0.241 \tag{3.77j}$$

BLUNTED HALF-CONE

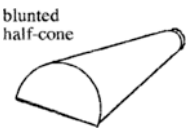

$$A_{\text{base}} = \frac{\pi \cdot r_{\text{b}}^2}{4} \tag{3.78a}$$

$$S_{\text{plan}} = r_{\text{b}}^2 \cdot \tan \Lambda \cdot \left[1 - \left(\frac{r_{\text{n}}}{r_{\text{b}}}\right)^2\right] + \frac{\pi \cdot r_{\text{b}}^2}{2} \cdot \left(\frac{r_{\text{n}}}{r_{\text{b}}}\right)^2 \tag{3.78b}$$

$$S_{\text{wet}} = \frac{\pi \cdot r_{\text{b}}^2}{2} \cdot \left[1 + \frac{1 + \left(\frac{r_{\text{n}}}{r_{\text{b}}}\right)^2}{\cos \Lambda} + 2 \cdot \left(\frac{r_{\text{n}}}{r_{\text{b}}}\right)^2\right] + S_{\text{plan}} \tag{3.78c}$$

$$V_{\text{tot}} = \frac{\pi \cdot r_{\text{b}}^3}{6} \cdot \left[\left(1 - \frac{r_{\text{n}}}{r_{\text{b}}}\right) \cdot \left[1 + \frac{r_{\text{n}}}{r_{\text{b}}} + \left(\frac{r_{\text{n}}}{r_{\text{b}}}\right)^2\right] \cdot \tan \Lambda + 2 \cdot \left(\frac{r_{\text{n}}}{r_{\text{b}}}\right)^3\right] \tag{3.78d}$$

$$(K_{\text{w}})_{78^\circ} = 58.592 \cdot \left(\frac{r_{\text{n}}}{r_{\text{b}}}\right)^2 - 25.755 \cdot \frac{r_{\text{n}}}{r_{\text{b}}} + 5.970 \tag{3.78e}$$

$$\tau_{78^\circ} = 0.1381 \cdot \left(\frac{r_{\text{n}}}{r_{\text{b}}}\right)^2 + 0.01643 \cdot \frac{r_{\text{n}}}{r_{\text{b}}} + 0.2409 \tag{3.78f}$$

$$0.2409 \leq \tau \leq 0.258 \tag{3.78g}$$

HALF-ELLIPSE

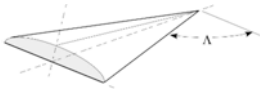

$$A_{\text{base}} = \pi \cdot a^2 \cdot \frac{e}{2} \tag{3.79a}$$

$$S_{\text{plan}} = a^2 \cdot \tan \Lambda \tag{3.79b}$$

$$S_{\text{wet}} = \frac{\pi \cdot a^2}{2} \cdot \left[\frac{(1+e)}{\cos \Lambda} \cdot \left(1 + \frac{R^2}{4} + \frac{R^4}{64} + \frac{R^6}{256}\right) + e\right] + S_{\text{plan}} \tag{3.79c}$$

$$V_{\text{tot}} = \frac{\pi \cdot a^3 \cdot e}{6} \cdot \tan \Lambda \tag{3.79d}$$

$$(K_{\text{w}})_{78^\circ} = 2.226 + 2.917 \cdot \frac{b}{a} + 4.689 \cdot \left(\frac{b}{a}\right)^2 \tag{3.79e}$$

$$\tau_{78^\circ} = 0.2413 \cdot \frac{b}{a} \tag{3.79f}$$

$$0.0241 \leq \tau \leq 0.241 \tag{3.79g}$$

$$e = \frac{b}{a} \tag{3.79h}$$

$$R = \frac{1 - e}{1 + e} \tag{3.79h}$$

HALF-DIAMOND

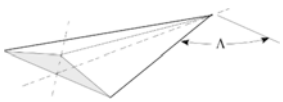

$$A_{\text{base}} = a^2 \cdot e \tag{3.80a}$$

$$S_{\text{plan}} = a^2 \cdot \tan \Lambda \tag{3.80b}$$

$$S_{\text{wet}} = a^2 \cdot [\sqrt{1 + e^2} \cdot \tan \Lambda + e] + S_{\text{plan}} \tag{3.80c}$$

$$V_{\text{tot}} = \frac{a^3 \cdot e}{6} \cdot \tan \Lambda \tag{3.80d}$$

$$(K_{\text{w}})_{78^\circ} = 2.228 + 1.865 \cdot \tau + 15.387 \cdot \tau^2 \tag{3.80e}$$

$$\tau_{78^\circ} = 0.154 \cdot \frac{b}{a} \tag{3.80f}$$

$$0.0154 \leq \tau \leq 0.154 \tag{3.80g}$$

$$e = \frac{b}{a} \tag{3.80h}$$

TRUNCATED DOUBLE CONE (circa 1965)

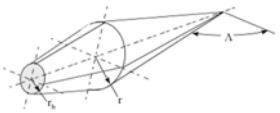

$$A_{\text{max}} = \pi \cdot r^2 \tag{3.81a}$$

$$S_{\text{plan}} = r^2 \cdot \tan \Lambda \cdot \left[1 + \left[1 - \left(\frac{r_{\text{b}}}{r}\right)^2\right] \cdot \frac{\tan \Lambda}{\tan(\Lambda - 3)}\right] \tag{3.81b}$$

$$S_{\text{wet}} = \pi \cdot r^2 \cdot \left[\frac{1}{\cos \Lambda} + \frac{1 - \left(\frac{r_{\text{b}}}{r}\right)^2}{\cos(\Lambda - 3)} + \left(\frac{r_{\text{b}}}{r}\right)^2\right] \tag{3.81c}$$

$$V_{\text{tot}} = \frac{\pi \cdot r^3}{3} \cdot \left[\tan \Lambda + \left[1 - \left(\frac{r_{\text{b}}}{r}\right)^3\right] \cdot \tan(\Lambda - 3)\right] \tag{3.81d}$$

$$(K_{\text{w}})_{78^\circ} = 3.622 \tag{3.81e}$$

$$\tau_{78^\circ} = 0.383 \tag{3.81f}$$

WING-CYLINDER (NASA Langley WB004C)

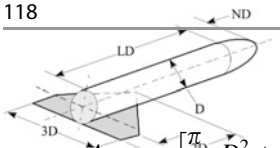

$$A_{\text{base}} = \left[\frac{\pi}{4}\cdot D^2 + 0.35\cdot D^2\right]\cdot 0.4444 \tag{3.82a}$$

$$S_{\text{plan}} = \left[3.375\cdot D^2 + \left(\frac{L}{D}\right)\cdot D^2 + \frac{\pi}{4}\cdot N\cdot D^2\right]\cdot 0.4444 \tag{3.82b}$$

$$S_{\text{wet}} = \left[\begin{array}{l} 7.12\cdot D^2 + \pi\cdot\left(\frac{L}{D}\right)\cdot D^2 + \frac{\pi\cdot D^2}{4} + \\ \frac{\pi\cdot N\cdot D^2}{4}\cdot\frac{ASIN(e)}{e} \end{array}\right]\cdot 0.4444 \tag{3.82c}$$

$$V_{\text{tot}} = 0.27\cdot D^3 + \frac{\pi\cdot D^3}{4}\cdot\left(\frac{L}{D}\right) + \frac{\pi\cdot N\cdot D^3}{6} \tag{3.82d}$$

$$\tau_1 = 0.1982 - 9.524E-5\cdot\left(\frac{L}{D}\right)_{\text{tank}} - 2.381E-4\cdot\left(\frac{L}{D}\right)^2_{\text{tank}} \tag{3.82e}$$

$$(K_{\text{w}})_1 = 2.193 + 0.128\cdot\left(\frac{L}{D}\right)_{\text{tank}} - 0.007524\cdot\left(\frac{L}{D}\right)^2_{\text{tank}} \tag{3.82f}$$

$$(K_{\text{v}})_1 = -0.2421 + 0.2109\cdot\left(\frac{L}{D}\right)_{\text{tank}} - 0.01438\cdot\left(\frac{L}{D}\right)^2_{\text{tank}} \tag{3.82g}$$

$$\tau_2 = 0.1899 + 4.286E-4\cdot\left(\frac{L}{D}\right)_{\text{tank}} - 2.381E-4\cdot\left(\frac{L}{D}\right)^2_{\text{tank}} \tag{3.82h}$$

$$(K_{\text{w}})_2 = 2.432 + 0.08833\cdot\left(\frac{L}{D}\right)_{\text{tank}} - 0.00438\cdot\left(\frac{L}{D}\right)^2_{\text{tank}} \tag{3.82i}$$

$$(K_{\text{v}})_2 = -0.07164 + 0.1625\cdot\left(\frac{L}{D}\right)_{\text{tank}} - 0.09571\cdot\left(\frac{L}{D}\right)^2_{\text{tank}} \tag{3.82j}$$

$$4 \le (L/D)_{\text{tank}} \le 8 \tag{3.82k}$$

$$0.186 \le \tau \le 0.193 \quad N = 1 \tag{3.82l}$$

$$0.184 \le \tau \le 0.189 \quad N = 2 \tag{3.82m}$$

$$e = \frac{\sqrt{2\cdot N - 1}}{N}\,\text{nose length} = N\cdot D \tag{3.82n}$$

BLENDED-BODY [BB] (McDonnell Douglas circa 1965)

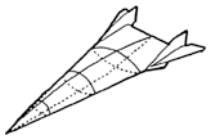

$$K_{\text{w}} = -62.217\cdot\tau^3 + 29.904\cdot\tau^2 - 1.581\cdot\tau + 2.469 \tag{3.83}$$

WING-BODY [WB]

$$K_{\text{w}} = -93.831\cdot\tau^3 + 58.920\cdot\tau^2 - 5.648\cdot\tau + 2.821 \tag{3.84}$$

NONWEILER WAVERIDER or ALL-BODY [AB] (circa 1960)

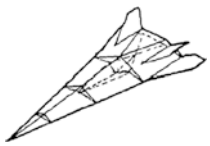

$$K_{\text{w}} = -533.451\cdot\tau^3 + 220.302\cdot\tau^2 - 22.167\cdot\tau + 3.425 \tag{3.85}$$

Bibliography

Ahern, J.E. (1992) "Thermal Management of Air-Breathing Propulsion Systems", AIAA Paper 92-0514, presented at the *30th Aerospace Sciences Meeting*, Reno, Nevada, January 1992.

Altis, H.D. (1967) "Hypersonic Scramjet Vehicle Study", Volume VII, Structures and Weights, MAC Report F666, McDonnell Aircraft Company, McDonnell Douglas Corporation, October 1967.

Ambrose, S. (2000) *Nothing Like It in the World*, 1st Edition, Simon & Schuster, New York, November 2001.

Anon. (1965a) "GE5/JZ6 Study, Wrap-Around Turboramjet, Turbo-Accelerator Propulsion System Study Data", Report SS-65-2, General Electric, December 1965 (confidential).

Anon. (1965b) "Structural Weight Estimation", Vol. 1, McAIR Report 747, circa 1965.

Anon. (1966a) "Hypersonic Ramjet Propulsion Program, Engine Performance", Marquardt Report 6112, The Marquardt Corporation, August 1966 (confidential).

Anon. (1966b) "MA188-XAB Baseline Dual Mode Scramjet for the McDonnell/Douglas Reusable Launch Vehicle Application", Marquardt Letter to McAIR, 1966 (confidential).

Anon. (1967) "A Study of Advanced Airbreathing Launch Vehicles with Cruise Capability", Lockheed Report IR 21042, The Lockheed Aircraft Corporation, 1967.

Anon. (1969a) "Comparative Propulsion Systems Concepts Study", U. S. Air Force Report AFRPS-TR-69-19, September 1969 (secret).

Anon. (1969b) "Variable Cycle Turboramjet GE14/JZ8", Preliminary Performance and Installation Manual, General Electric Report., U.S. Air Force Contract AF33615-69-1245, 1969 (confidential).

Anon. (1970) "Mission Requirements of Lifting Systems, Summary of Significant Results and Figures", McDonnell Aircraft Report B947 prepared under NASA NAS 9-3562, August 1965. (Declassified 1970.)

Anon. (1985) "Single-Stage-to-Orbit Concept Comparison', Aerospace Corporation Report 86-2602-301-ADA, October 1985.

Anon. (1988) "Hyperplane", 39th International Astronautical Federation Congress, Bangalore, India, October 1988.

Anon. (2015) "Declassified Manned Orbiting Laboratory (MOL) Records", National Reconnaissance Office, October 2015.

Augenstein, B.W. and Harris, E.D. (1993) "The National Aerospace Plane (NASP): Development Issues for the Follow-on Vehicle – Executive Summary", R-3878/1-AF, A Project Air Force Report, RAND, 1993, ISBN: 0-8330-1342-4.

Balepin, V.V. and Hendrick, P. (1998) "Application of the KLIN Cycle to Vertical Take-Off Lifting Body Launcher", AIAA Paper 98-1503, presented at the *8th AIAA International Space Planes and hypersonic Systems and Technologies Conference*, Norfolk, VA, 27-30 April 1998.

Balepin, V.V., Dulepov, N., Folomeev, E., Harchevnikova, G., et al. (1993) "Flight Liquid Oxygen Plants for Aerospace Plane: Thermodynamic and Integration Aspects", SAE Technical Paper 931452, Society of Automotive Engineers, April 1993.

Balepin, V.V., Maita, M., Tanatsugu, N., and Murthy, S.N.B. (1996) "Deep-Cooled Turbojet Augmentation with Oxygen (Cryojet) for a SSTO Launch Vehicle", AIAA Paper 96-3036, presented at the *32nd Joint AIAA, ASME, SAE and ASEE Propulsion Conference and Exhibit*, Lake Buena Vista, FL, 1–3 July 1996.

Billig, F.S. (1989) "Hypersonic Vehicles II", *Proceedings of the Short Course of Engine Airframe Integration,* School of Mechanical Engineering, Purdue University, July 1989.

Billig, F.S. (1991) "Propulsion Systems from Take-Off to High-Speed Flight", in: *High-Speed Flight Propulsion Systems,* edited by S.N.B. Murthy and E.T. Curran, Progress in Astronautics and Aeronautics, Vol. 137, AIAA, Reston VA, 1991, pp. 21–100.

Billig, F. S. (1993) "The Integration of the Rocket with a Ram-Scramjet as a Viable Transatmospheric Accelerator", AIAA Paper 93-7017. Also in Proceedings of the 11th ISABE, International Symposium on Air Breathing Engines, Vol. 1, Tokyo, Japan, 20–24 September 1993, pp. 173–187.

Billig, F.S. and Van Wie, D.M. (1987) "Efficiency Parameters for Inlets Operating at Hypersonic Speeds", Proceedings of the *8th International Symposium on Airbreathing Engines (ISABE)*, Cincinnati, OH, June 1987, pp. 118–130.

Camberos, J.A. and Moorhouse, D.J. (editors) (2011) *Exergy Analysis and Design Optimization for Aerospace Vehicles and Systems*, Progress in Astronautics and Aeronautics, Volume 238, Published by AIAA, Reston, Virginia, 2011.

Chudoba, B. (2001) "Aircraft Configuration Characterisation for Project Flight Mechanics", Issue 1, CoA Report NFP0106, College of Aeronautics, Cranfield University, April 2001.

Chudoba, B. (2002) *Stability and Control of Conventional and Unconventional Aircraft Configurations – A Generic Approach*, First Edition, Books on Demand GmbH, January 2002. (ISBN 3-8311-2982-7).

Chudoba, B. (2012) "A 21st Century Decision Aid; Aeronautics & Space Transportation Technology data-base", Final Contract Presentation, Hypersonics Research Directorate, National Institute of Aerospace (NIA), NASA LaRC, Hampton, VA, September 2012.

Chudoba, B. and Gonzalez, L. (2011) "A 21st Century Decision Aid; Aeronautics & Space Transportation Technology data-base; 2008 – Present International Hypersonic Projects", Final Contract Presentation, Hypersonics Research Directorate, National Institute of Aerospace (NIA), NASA LaRC, Hampton, VA, 12 October 2011.

Chudoba, B. and Heinze, W. (2010) "Evolution of Generic Flight Vehicle Design Synthesis", *The Aeronautical Journal*, Vol. 114, No. 1159, September 2010.

Chudoba, B. Coleman, G., Oza, A., Gonzalez, L., Haney, E., Ricketts, V. and Czysz, P. (2011) "Manned GEO Servicing (MGS) Crew Return Vehicle Sizing," Final Contract Report, National Institute of Aerospace (NIA), NASA LaRC and DARPA, Section in Final Report *"Manned Geosynchronous Earth Orbit (GEO) Servicing (MGS) Joint NASA/DARPA Study",* NASA SP-2012-598, MGS Study Team, NASA Headquarters and DARPA Tactical Technology Office, Washington, DC, 27 April 2011.

Chudoba, B., Coleman, G., Oza, A., Gonzalez, A. and Czysz, P. (2012) "Solution-Space Screening of a Hypersonic Endurance Demonstrator", NASA CR-2012-217774, August 2012.

Chudoba, B., Haney, E., Gonzalez, L., Omoragbon, A., and Oza, A. (2015a) "Strategic Forecasting in Uncertain Environments: Hypersonic Cruise Vehicle Research & Development Case Study", *The Aeronautical Journal*, Vol. 119, No. 1211, January 2015.

Chudoba, B., Oza, A., Gonzalez, L. and Omoragbon, A. (2015b) "Custom Decision-Support Solutions for Aerospace Systems Development", AVD Services LLC Dossier, November 2015.

Coleman, G.J. (2008) "Hypersonic Convergence Methodology and Example", AVD-Aero-001-2008, AVD Laboratory, Mechanical and Aerospace Department, The University of Texas at Arlington, April 2008.

Coleman, G.J. (2010) "Aircraft Conceptual Design – An Adaptable Parametric Sizing Methodology," Ph.D. Dissertation, The University of Texas at Arlington, Arlington, Texas, May 2010.

Collingbourne, J.R. and Peckham, D.H. (1967) "The Lift and Drag Characteristics of Caret Wings at Mach numbers between 5 and 10" C.P. No. 930, Aeronautical Research Council, February 1966.

Curran, E.T. (1993) "The Potential and Practicality of High Speed Combined Cycle Engines", *Hypersonic Combined Cycle Propulsion,* AGARD Conference Proceeding No. 479, AGARD, Neuilly-Sur-Seine, France, 1993, pp. Kl-9.

Czysz, P.A. (1986) "Hypersonic Convergence – High-Speed Aircraft Aero-Propulsion-Structure Systems Integration – Integrated Systems Approach to Identifying Solution Space", Volumes I-III, Course AE-P-452-50, 1992-93, Aerospace and Mechanical Engineering Department, Parks College, Saint Louis University, 1st Edition 1986.

Czysz, P.A. (1991) "Delta Clipper Sizing Program", unpublished work, McDonnell Douglas Astronautics Co., Huntington Beach, CA, May 1991.

Czysz, P.A. (1992) "Space Transportation Systems Requirements Derived from the Propulsion Performance", Paper IAF-92-0858, presented at the *43rd International Astronautical Federation Congress*, Washington, DC, September 1992.

Czysz, P.A. (1993) "Rocket Based Combined Cycle (RBCC) Propulsion Systems Offer Additional Options", *11th International Symposium on Airbreathing Engines (ISABE)*, Vol. 1, Tokyo, Japan, 20–24 September 1993, pp. 119–137.

Czysz, P.A. (1995) "Interaction of Propulsion Performance with the Available Design Space", *Proceedings of the XII International Symposium on Airbreathing Engines (ISABE),* Melbourne, Australia, September 1995.

Czysz, P.A. (1996) "Propulsion Concepts and Technology Approaches that Enable a Launcher for the XXI Century", *Proceeding of the 5th*

International Symposium, La Propulsion dans les Transports Spatiaux, 1996, p. 15.7.

Czysz, P.A. (1998) "Advanced Propulsion Concepts for the XXI Century", International Academy of Astronautics Workshop on Advanced Propulsion Concepts, The Aerospace Corporation, El Segundo, CA, January 1998.

Czysz, P.A. (2004) "Hypersonic Convergence", AFRL-VA-WP-TR-2004-3114, Volume 1 out of 3 Volumes, Wright-Patterson Air Force Base, December 2004.

Czysz, P.A. and Froning, H.D. (1995) "A Propulsion Technology Challenge - Abortable, Continuous Use Vehicles", Paper IAF-95-S.2.03, presented at the *46th International Astronautical Federation Congress,* Oslo, October 1995.

Czysz, P.A. and Froning, H.D. (1997) "A SSTO Launcher/Demonstrator Concept for International Development for a Flight Test Vehicle", in: *Proceedings of the International Workshop on Space Plane/RLV Technology Demonstrators,* Tokyo, Japan, March 1997.

Czysz, P.A. and Little M. (1993) "Rocket-Based Combined Cycle Engine (RBCC) - A Propulsion System for the 21st Century", AIAA Paper 93-5096, presented at the *5th International Aerospace Planes and Hypersonics Technologies Conference,* 03 December 1993.

Czysz, P.A. and Murthy, S.N.B. (1991) "Energy Analysis of High-Speed Flight Systems", in: *High-Speed Flight Propulsion Systems,* edited by S.N.B. Murthy and E.T. Curran, AIAA Progress in Astronautics and Aeronautics, Vol. 137, Reston VA, 1991, pp. 183–186.

Czysz, P.A. and Murthy, S.N.B. (1995) "Energy Management and Vehicle Synthesis", AIAA Paper 95-6101, April 1995.

Czysz, P.A. and Murthy, S.N.B. (1996a) "SSTO Launcher Demonstrator for Flight Test", AIAA Paper 96-4574, November 1996.

Czysz, P.A. and Murthy, S.N.B. (1996b) "Energy Management and Vehicle Synthesis", in: *Developments in High-Speed-Vehicle Propulsion Systems,* edited by S.N.B. Murthy and E.T. Curran, AIAA Progress in Astronautics and Aeronautics, Vol. 165, Reston VA, 1996, pp. 581–686.

Czysz, P.A. and Richards, M.J. (1998) "Benefits from Incorporation of Combined Cycle Propulsion", AIAA Paper 98-S.5.10, presented at the *48th International Astronautical Federation Congress*, Melbourne, Australia, October 1998.

Czysz, P.A. and Vandenkerckhove, J. (2000) "Transatmospheric Launcher Sizing", Chapter 16 in: *Scramjet Propulsion*, edited by E.T. Curran, and S.N.B. Murthy, AIAA Progress in Astronautics and Aeronautics, Vol. 189, Reston, VA, 2000.

Czysz, P.A., Dighton, R.D., and Murden, W.P. (1973a) "Designing for Air Superiority", AIAA Paper AIAA 73-38370, presented at the *AIAA 5th Aircraft Design, Flight Test and Operations Meeting,* St. Louis, MO, August 1973.

Czysz, P.A., Glaser, F.C, and LaFavor, S.A. (1973b) "Potential Payoffs of Variable Geometry Engines in Fighter Aircraft", *Journal of Aircraft,* Vol. 10. No. 6, 1973, pp. 342–349.

Czysz, P.A., Froning, H.D., and Longstaff, R. (1997) "A Concept for an International Project to Develop a Hypersonic Flight Test Vehicle", in: *Proceedings of the International Workshop on Spaceplanes/RLV Technology Demonstrators,* Tokyo, Japan, March 1997.

Der, J. (1991) "Improved Methods of Characterizing Ejector Pumping Performance", *Journal of Propulsion and Power,* Vol. 7, No. 3, 1991, pp. 412–419.

Dixon, W.P. (1966) "Precise Heat Transfer Measurement with Surface Thermocouples", Paper presented at the 8th Annual Rocky Mountain Spectroscopy Conference, Denver, CO., 1966.

Dixon, W.P., and Czysz, P.A. (1969) "Quantitative Heat Transfer Measurement Using Thermographic Phosphors", Optical Engineering, *Society of Photo-Optical Instrumentation Engineers Journal*, Vol. 7, No. 3, March 1969, p. 77.

Draper, A.C. and Sieron, T.R. (1991) "Evolution and Development of Hypersonic Configurations 1958–1990", Report WL-TR-91-3067, Flight Dynamics Directorate, Wright-Patterson Air Force Base, Ohio, September 1991.

Draper, A.C., Buck, M.L. and Goesch, W.H. (1971) "A Delta Shuttle Orbiter", *Astronautics & Aeronautics*, Vo. 9, No. 1, January 1971, pp. 26–35.

DuPont, A.A. (1999) "Further Studies of Optimized Inlets for Hypersonic Turbine Engines", Paper ISABE 99-7039, presented at the *14th International Symposium for Air Breathing Engines (ISABE)*, Florence, Italy, September 1999.

Escher, W.J.D. (1995a) "Rocket-Based Combined Cycle (RBCC) Powered Spaceliner Class Vehicles Can Advantageously Employ Vertical Takeoff and Landing (VTOL)", Paper AIAA 95-6145, presented at the *AIAA Aerospace Sciences Meeting,* Reno NV, January 1995.

Escher, W. (1995b) "Motive Power for Next Generation Space Transports: Combined Airbreathing + Rocket Propulsion," Paper AIAA 95-6076, presented at the AIAA *6th International Aerospace Planes and Hypersonics Technologies Conference,* Chattanooga, TN, April 1995.

Escher, W.J.D. (1966a) "A Study of Composite Propulsion Systems for Advanced Launch Vehicle Applications", Volume 1: Summary Report, Report 25, 194, Contract: NAS 7-377, Project: 5402, The Marquardt Corporation, 16 September 1966.

Escher, W.J.D. (1996b) "A Winning Combination for Tomorrow" Spaceliners", *Aerospace America,* Vol. 34, No. 2, February 1996, pp. 38–43.

Escher, W.J.D. (1999) "A U.S. History of Airbreathing/Rocket Combined-Cycle (RBCC) Propulsion for Powering Future Aerospace Transports – With a Look Ahead to the Year 2020", AIAA-IS-030, White Paper, Kaiser Marquardt, Van Nuys, CA, 01 June 1999.

Escher, W.J.D. and Czysz, P.A. (1993) "Rocket-Based Combined-Cycle Powered Spaceliner Concept", Paper IAF-93-S.4.478, presented at the International Astronautical Federation Congress, October 1993.

Frederick, J., Sutton, R., and Martens, R. (1976) "Turbine Engine Cycle Selection Procedure", in: *Proceedings of the 3rd International Symposium on Airbreathing Engines (ISABE),* DGLR-Fachbuch, No. 6, 1976.

Freeman, D.C., Talay, T.A. and Austin, R.E. (1995) "Single-Stage-to-Orbit - Meeting the Challenge", *Acta Astronautica*, Vol. 38, No. 4–8, February-April 1996, pp. 323–331.

Froning, H.D. and Leingang, J.L. (1990) "Impact of Aerospace Advancements on Capabilities of Earth-to-Orbit Ships", Paper IAF, presented at the *41st International Astronautical Congress,* Dresden, Federal Republic of Germany, 6–12 October 1990.

Gonzalez, L. "Complex Multidisciplinary System Composition for Aerospace Vehicle Conceptual Design," Ph.D. Dissertation, ASE Laboratory, Mechanical and Aerospace Engineering, The University of Texas at Arlington, Arlington, Texas, August 2016.

Haney, E. "Data Engineering in Aerospace Systems Design & Forecasting," Ph.D. Dissertation, ASE Laboratory, Mechanical and Aerospace Engineering, The University of Texas at Arlington, Arlington, Texas, April 2016.

Haney, E., Gonzalez, L., Omoragbon, A., Oza, A. and Chudoba, B. (2013) "Integrated Engineering data-base: A 21st Century Decision Aid," Proceedings of the 2013 ASEE Gulf-Southwest Annual Conference, The University of Texas at Arlington, Texas, March 21–23, 2013.

Harper, R.E. and Zimmerman, J.H. (1942) "An Investigation of Rocket Engine Thrust Augmentation with a Nozzle-Ejector System", Arnold Engineering Development Center Report TRD-62-42, March 1942.

Harwood, B. (2015) "Bezos' Blue Origin Completes First Test Flight of 'New Shepard' Spacecraft", Spaceflight Mow via CBS News, 30 April 2015.

Hendrick, P. (1996) "SSTO & TSTO LOX Collection System Performances: Influence of LOX Plant Architecture", Paper ICAS-96-3.8.3, presented at the *20th Congress of the International Council of the Aeronautical Sciences*, 8–13 September 1996.

Herbst, W.B. and Ross, H.G. (1969) "The Systems Approach to Systems Engineering", ASPR Inst., December 1969.

Herbst, W.B. and Ross, H.G. (1970) "Application of Computer Aided Design Programs for the Technical Management of Complex Fighter Developments Projects", AIAA Paper 70-364, presented at the *Fighter Aircraft Conference*, March 1970.

Jenkins, D.R. (2001) Space Shuttle: The History of the National Space Transportation System, The First 100 Missions, 3rd Edition, Midland Publishing, March 2001.

Johnson, D. (1991) "Beyond the X-30: Incorporating Mission Capability", AIAA Paper 91-5078, 1991.

Kirkham, F.S., Jones, R.A., Buck, M.L. and Zima, W.P. (1975) "Joint USAF/NASA Hypersonic Research Aircraft Study", Paper AIAA 75-1039, presented at the *AIAA 25th Aircraft Systems and Technology Meeting*, Los Angeles, California, August 1975.

Koelle, H.H. (1995) "Lunar Space Transportation - Cutting Costs of Logistics", Paper IAA-95-IAA.1.1.08, presented at the *46th International Astronautical Federation Congress*, Oslo, 03 October 1995.

Krieger, R.J. (1990) "A Summary of Features and Design Issues for Single-Stage-to-Orbit Vehicles", Paper AIAA 90-1932, presented at the 26th Joint AIAA/SAE/ASME/ASEE Propulsion Conference, Orlando, Florida, July 16–18, 1990.

Küchemann, D. (1960) "Aircraft Shapes and their Aerodynamics" (p. 227) in: *Advances in Aeronautical Sciences: Proceedings of the Second International Congress in the Aeronautical Sciences*, Vol. 3, edited by T. von Kármán, et al. Zürich, 12–16 September 1960.

Küchemann, D. (1978) *The Aerodynamic Design of Aircraft,* 1st Edition, Pergamon Press, New York, 1978, p. 214.

Kutschenreuter, P.H., Subramanian, S.V., Gaeta, R.J., Hickey, P.K., and Davis, J.A. (1992) "A Design Approach to High Mach Number Scramjet Performance," AIAA 92-4248, Aircraft Design Systems Meeting, Hilton Head Island, SC, 24–26 August 1992.

Lashin, A.I., Kovalevski, M.M., Romankov, O.N. and Tjurikov, E.V. (1993) "Combined Propulsion System for Advanced Multipurpose Aerospace Plane (ASP)", Paper IAF-93-S.4.479, presented at the *44th International Astronautical Federation Congress*, Graz, Austria, October 1993.

Leingang, J.L., Maurice, L.Q. and Carreiro, L.R. (1992) "Space Launch Systems Using Collection and Storage", Paper IAF 92-0664, presented at the *43rd International Astronautical Federation Congress*, Washington, DC, 28 August–05 September 1992.

Lindley, C. and Penn, J. (1997) "Requirements and Approach for a Space Tourism Launch System", *Acta Astronautica*, Vol. 52, No. 1, pp. 49–75, January 2003.

Lozino-Lozinskiy, G.E. (1989) "BURAN: Its Creation and Prospects of Its Usage", Paper IAF presented at the *40th International Astronautical Federation Congress*, Malaga, Spain, 7–12 October 1989.

Maita, M., Ohkami Y., Yamanaka, T. and Mori T. (1990) "Conceptual Study of Space Plane Powered by Hypersonic Airbreathing Propulsion System", Paper AIAA-90-5225, presented at the *2nd International Aerospace Planes and Hypersonics Technology Conference*, Orlando, FL, 29–31 October 1990.

Martinovic, Z.N. and Cerro, J.A. (2002) "A Procedure for Structural Weight Estimation of Single Stage to Orbit Launch Vehicles (Interim User's Manual)", NASA-TM-2002-211931, NASA Langley Research Center, September 2002.

Miki, Y., Taguchi, H. and Aoki, H. (1993) "Status and Future Planning of LACE Development", AIAA Paper 93-5124, presented at the *5th International Aerospace Planes and Hypersonics Technology Conference*, Munich, Germany, November–December 1993.

Morris, R.E. and William, N.B. (1968) "A Study of Advanced Air-Breathing Launch Vehicles With Cruise Capability", Volumes I–VI, NASA CR 73194-73199, Lockheed Report IR 21042, The Lockheed Aircraft Corporation, 1968.

Mossman, E.A., Rozycki, R.C. and Holle, G. F. (1960) "A Summary of Research on a Nozzle-Ejector-System", Martin Denver Research Report R-60-31, October 1960.

Mulready, D. (2001) Advanced Engine Development at Pratt & Whitney (The Inside Story of Eight Special Projects 1946-1971), SAE International, Warrendale, PA., 2001, ISBN: 0-7680-0664-3.

Czysz, P.A., and Murthy, S.N.B. (1996) "Energy Management and Vehicle Synthesis", in: *Developments in High-Speed-Vehicle Propulsion Systems,* edited by S.N.B. Murthy and E.T. Curran, *Progress in Astronautics, Vol. 165,* AIAA, Reston VA, 1996.

Nicholas, T.M.T., Narayanan, A.K. and Muthunayagam, A.E. (1996) "Mixing Pressure-Rise Parameter for Effect of Nozzle Geometry in Diffuser-Ejectors", *Journal of Propulsion and Power,* Vol. 12, No. 2, 1996, pp. 431–433.

Nouse, H., Minoda, M., et al. (1988) "Conceptual Study of Turbo-Engines for Horizontal Take-Off and Landing Space Plane", Paper IAF-88-253, presented at the 39th *International Astronautical Federation Congress,* Bangalore, India, 8–15 October 1988.

Ogawara, A. and Nishiwaki, T. (1989) "The Cycle Evaluation of the Advanced LACE Performance", IAF-Paper 89-313, presented at the *40th International Astronautical Federation Congress,* Malaga, Spain, October 1989.

Omoragbon, A. "Complex Multidisciplinary Decomposition for Aerospace Vehicle Conceptual Design and Technology Acquisition," Ph. D. Dissertation, ASE Laboratory, Mechanical and Aerospace Engineering, The University of Texas at Arlington, Arlington, Texas, September 2016.

Oza, A. "Integration of a Portfolio-Based Approach to Evaluate Aerospace R&D Problem Formulation into a Parametric Synthesis Tool," Ph.D. Dissertation, ASE Laboratory, Mechanical and Aerospace Engineering, The University of Texas at Arlington, Arlington, Texas, September 2016.

Page G. S. (1986) "Vehicle Synthesis Program (VSP)", Douglas Aircraft Memorandum C1-E82-ACAP-86-1381, McDonnell Douglas Corporation, December 1986.

Page, G.S. (1987) "HSCT Configurations for Phase II Analysis", Douglas Aircraft Memorandum AVI-ACAP-AAP-HAH5-108, McDonnell Douglas Corporation, August 1987.

Pegg, R.J., Hunt, J.L. et al. (1993) "Design of a Hypersonic Waverider-Derived Airplane", AIAA Paper 93-0401, presented at the *31st Aerospace Science Meeting and Exhibit*, Reno, NV, 11–14 January 1993.

Peng, X. (2015) "Formalization of the Engineering Science Discipline – Knowledge Engineering", Ph.D. Dissertation, AVD Laboratory, Mechanical and Aerospace Engineering, The University of Texas at Arlington, Arlington, Texas, May 2015.

Penn, J.P. and Lindley, C.A. (1998) "Spaceplane Design and Technology Considerations over a Broad Range of Mission Applications", IEEE Aerospace Conference, 21–28 March 1998.

Pirrello, C.J. and Czysz, P.A. (1970) "Hypersonic Research Facilities Study", Volumes I-VI, National Aeronautics and Space Administration Contract NAS2-5458 by McDonnell Aircraft Company (McAIR), NASA CR 114322–114331, October 1970.

Plokhikh, V. P. (1989) "Sensitivity Analysis of SSTO Reusable Vehicle Parameters", Paper IAF 89-223, presented at the *40th*

International Astronautical Federation Congress, 7–12 October, 1989.

Plokhikh, V.P. (1995) "Problems of Creating Reusable Aerospace Transporting Systems", Paper 95-V.4.05, presented at the *46th International Astronautical Federation Congress,* Oslo, 2–6 October, 1995.

Rudakov, A.S. and Balepin, V.V. (1991) "Propulsion Systems with Air Precooling for Aerospaceplane", SAE Technical Paper 911182, Society of Automotive Engineers, April 1991.

Rudakov, A.S., Gatin, R.Y., Dulepov, N.P., Koralnik, B.N., Harchevnikova, G.D. and Yugov, O.K. (1991) "Analysis of Efficiency of Systems with Oxidizer Liquefaction and Accumulation for Improvement of Spaceplane Performance", Paper IAF-91-270, presented at the *42nd International Astronautical Federation Congress,* Montreal, Canada, 5–11 October, 1991.

Scherrer, D. (1988) "Evaluation du Concept de Fusée-Statoréacteur Pour la Propulsion Hypersonique", ONERA Activities 1988, ONERA, Paris, April 1988.

Schindel, L. (1989) "Design of High Performance Ramjet or Scramjet Powered Vehicles", AIAA Paper 89-0379, presented at the *27th Aerospace Sciences Meeting*, Reno NV, January 1989.

Siebenhaar, A. and Bulman, M. (1995) "The Strutjet: The Overlooked Option for Space Launch", AIAA Paper 95-3124, presented at the *31st AIAA/ASME/SAE/ASEE Joint Propulsion Conference and Exhibit, July 1995.*

Stephens, R.R. (1965) "Mission Requirements of Lifting Systems - Engineering Aspects". Vol. I *Condensed Summary*, and Vol. II *Mission Analysis - Spacecraft Selection - Performance Analysis*, McDonnell Aircraft Company Report B831 for NASA Manned Spacecraft Center, Contract NAS-9-3562, 1965.

Stroup, K.E. and Pontez, R.W. (1968) "Advanced Ramjet Concepts – Volume 1: Ejector Ramjet Systems Demonstration", Final Report AFAPLTR-67-118, US AF Contract AF33 (615)-3734, The Marquardt Corporation, May 1968.

Tanatsugu, N. and Suzuki, K. (1986) "The Study of high Pressure Expander Cycle Engine With Advanced Concept Combustion Chamber", *Acta Astronautica*, Vol. 13, No. 1, January 1986, pp. 1–7.

Tanatsugu, N., Inatani, Y, Makino, T. and Hiroki, T. (1987) "Analytical Study of Space Plane Powered by Air-Turbo Ramjet with Intake Air Cooler", Paper IAF-87-264, presented at the *39th International Astronautical Federation Congress*, Brighton, UK, 8–15 October 1987.

Taylor, R. J. (1965) "High Temperature Airframe Weight Estimation", Paper SAE-0479, 24th Annual Conference, Denver, Colorado, 17–19 May 1965.

Taylor, D. (1983) "Aerodynamic Correlations", Private Communication with P.A. Czysz, McDonnell Douglas Corporation, 1983.

Taylor, J. (2015) "ORBCOMM-2 Mission", Final Press Kit, ORBCOMM, SpaceX, December 2015.

Thompson, M.O. and Peebles, C. (1999) *Flying without Wings: Before the Space Shuttle: Testing NASA's Wingless Aircraft*, 1st Edition, Crécy Publishing, Manchester, NH, 01 April 1999.

Tjonneland, E. (1988) "Survey of Integration Problems, Methods of Solutions, and Applications," Purdue University Short Course on *Engine-Airframe Integration*, West Lafayette, IN, July 1988.

Togawa, M., Aoki, T. et al. (1991) "A Concept of LACE for SSTO Space Plane", AIAA Paper 91-5011, presented at the 3rd International Aerospace Planes and Hypersonics Technology Conference, Orlando FL, December 1991.

Townend, L. and Vandenkerckhove, J.A. (1994) "External Afterburning and Shock-Confined Combustion in Supersonic Flow," APECS-VDK 001/94, European Space Agency (ESA) Contract 120285, May 1994.

Vandenkerckhove, J.A. (1991a) "A First Assessment of Scramjet-Propelled Single-Stage-to-Orbit (SSTO) Vehicles", WLC Phase 5, WP 260, Chapter 1, VDK System S.A., Brussels, Belgium, February 1991.

Vandenkerckhove, J.A. (1991b) "Further Assessment of Scramjet-Propelled Single-Stage-to-Orbit (SSTO) Vehicles", WLC Phase 5, WP 260, Chapter 1, Revision 1, VDK System S.A., Brussels, Belgium, October 1991.

Vandenkerckhove, J.A. (1992a) "A Peep Beyond SSTO Mass Marginality", Paper IAF 92-0656, presented at the *43rd International Astronautical Federation Congress*, Washington, DC, 28 August–05 September 1992.

Vandenkerckhove, J.A. (1992b) "SSTO Configuration Assessment", Chapter 2, Revision 1, VDK System S.A., WLC Phase 5, WP 260, Brussels, Belgium, August 1992.

Vandenkerckhove, J.A. (1993) "HYPERJET Mk-3, A Rocket-Derived Combined Engine", VDK System S.A. Report, April 1993.

Vandenkerckhove, J. and Barrére, M. (1997) "Energy Management", Chapter 16 in: *The Synerjet Engine – Airbreathing/Rocket Combined-Cycle Propulsion for Tomorrow's Space Transports*, SAE Progress in Technology Series, SAE PT-54, 1997.

Vinh, N.X. (1993) *Flight Mechanics of High-Performance Aircraft,* 1st Edition, Cambridge Aerospace Series 4, Cambridge University Press, 1993.

Yugov, O. K., *et al.* (1989) "Optimal Control Programs for Airbreathing Propulsion System or Single-Stage-to-Orbit Vehicles", paper IAF89-308, presented at the *40th International Astronautical Federation Congress*, Malaga, Spain, 7–13 October 1989.

Yugov, O.K., Dulepov, N.P. and Harchenvnikova, G.D. (1990) "The Analysis of Hypersonic and Combined Cycle Engines in the Propulsion System of the SSTO Vehicles", paper presented at the *41st International Astronautical Federation Congress,* Dresden, Germany, 6–12 October 1990.

Commercial Near-Earth Launcher: Propulsion Choices

4

As presented in Chap. 2, airbreathing propulsion advocates have been fighting a losing battle to change the space launcher paradigm from expendable rockets, that are launched for the first, last, and only time, to sustained-use launchers that are more like military airlift transports with long and frequent usage (Anon 1967). Chapter 3 has details of the debate that took place in the USA, where even a sustained-use rocket launcher proposed to support the military Manned Orbiting Laboratory (MOL) was discarded, as was MOL, as not having relevance in a purposely designated "civilian" space fleet. As a result, most if not all, of the military high-performance hypersonic glider design and performance data was forever lost, together with the benefits of these high-performance systems to the civilian space organization.

It must be admitted that airbreathing propulsion proposals, based on what were indeed rational assumptions when applied to rockets, resulted (and to many is still the case today) in large, ponderous, and too costly vehicles. Even though that was challenged, as shown in Figs. 2.16 and 2.17, lasting impressions were that airbreathers were too large and too expensive, and that they required too long a development period when compared to rocket-launching systems. This is factually contrary to the actual rocket record, an example being the total lack of a US man-rated space launch system during the 12-year period when the National Space Transportation System (STS or Space Shuttle) was being developed. Most interestingly, we again do experience this US manned launch vehicle void today. Despite a range of rocket-based space launch vehicles being under development for years, the US has no operational man-rated space launch system since the last flight of the Space Shuttle on July 21, 2011.

Chapter 3 also shows that, when propulsion systems are placed on a common vehicle platform like the lifting-body configurations, there are indeed differences in weights between rocket and airbreathing propulsion, but no significant size or industrial capability index differences. Then, the fact remains that, if we are to transition from the status quo today, as illustrated in Fig. 2.23, to the commercial space scenario in Fig. 2.24, something has to change to support the flight rate such a busy commercial infrastructure would require. However, it must be said that this particular status quo has been comfortable and profitable for the telecommunications and launcher industry so far.

In order to achieve a transportation system to space analogous to the transcontinental railroad, i.e., one that can support a commercial space infrastructure, this change must include an airbreathing launcher to meet the high flight rate requirements. The MOL was designed for 20–27 persons. The support spacecraft would carry 9–12 people or materials to resupply the station. For that goal, the payload planned was a 7 t payload (15,435 lb). An airbreathing launcher would be at least 1/2 the weight of the rocket vehicle in Fig. 2.16, requiring 1/2 the resources. The MOL study identified that each crewmember replacement would need to be accompanied by a 994 lb (450 kg) resource supply payload. For a 12-person crew replacement mission, that makes the crew replacement payload 15,228 lb, well within the 7 t payload capacity. The operating parameters of the MOL station were for a nominal 21-person crew. The same study determined that 47,000 lb (21,315 kg) of resources were required per crewmember per year. For one year, with a 21-person complement, that means 448 t (987,000 lb) of supplies needed to be lifted to the station for crew support, not counting propellants to maintain the station orbit. With 21 crewmembers, there are 4 flights per year required to meet the 6-month assignment requirement. To lift the crew supplies to the station would require 64 flights per year, not counting propellant and hardware replacement missions that may require another 5–6 flights per year. The number of flights to a large station is then at least 74 flights per year. From a military mission analysis, that would require a fleet

P.A. Czysz et al., *Future Spacecraft Propulsion Systems and Integration*,
Springer Praxis Books, DOI 10.1007/978-3-662-54744-1_4

of 10 aircraft (14, counting in operational spares) flying 7 times a year for 15 years, and a 100-flight operational life (Czysz 1999; Zagainov and Plokhikh 1991). When using instead the present rocket launchers, that becomes a total of 1050 launches by 1050 rockets. To the MOL designers of 1964, it was instead a fleet of 10–14 sustained-use vehicles operated over a 15-year period, plus repair and maintenance. That vast difference in outlook between the aircraft manufacturers and the ballistic missile manufacturers remains today. Sustained use remains a poor competitor to the expendable rocket rather than being adopted as a necessity for the future of commercial space.

Just as ground transportation has railroad trains, over-the-road tractor trailers, cargo trucks, busses, and automobiles, so space must have a variety of transportation vehicles with different payload capacities and fly rates. The USA is still lacking a heavy-lift capability as we once had with the Saturn V. The first flight of the dedicated US space exploration launch system (the SLS Block 1, capable of 70 t payload to LEO) is scheduled in 2018 (Anon 2015). We need the capability of sending heavy payload to the gas giants such as Jupiter and Saturn, moderate payloads to the outer planets, and modest payloads to the boundaries of our solar system (Anfimov 1997), all in comparable travel times. Airbreathing propulsion will not help us in space, but it can enable lighter, sustained-use launchers that increase the frequency to orbit and reduce the cost to a practical value that will enable more space infrastructure and space exploration.

4.1 Propulsion System Alternatives

Incorporation of airbreathing in launchers provides many propulsion options. However, vehicle design choices are not arbitrary as requirements and propulsion performance define practical solution spaces, as discussed in detail in Chap. 3. A priori decisions, such as horizontal takeoff versus vertical takeoff, can doom to failure an otherwise workable project. From the governing equations, the keys to succeed appear to be (a) offloading at least some of the carried oxidizer and (b) designing for sustained operations over a long operational life with maintenance, not continuous overhaul and rebuilding. As illustrated in Fig. 3.54, it is possible to readily identify the design space accessible with current industrial capability and materials.

New discoveries and industrial capabilities are always important, but, as was clearly demonstrated in the 1960s, neither discovery of new technologies nor the identification of technology availability dates (TADs and TRL as well) are necessary to fabricate an operational space flight system with more capability than the current hardware. Even a cursory review of the North American X-15 and the Lockheed SR-71 shows that the presence of bureaucratic roadblocks such as TAD and TRL would have meant neither aircraft would have ever been built or flown, but rather be replaced by paper studies. It was curiosity, resourcefulness, skill, and knowledge that enabled the North American and Lockheed teams to succeed. Governmental planning had little to do with their success. The teams adapted what was available and created what was not, and only if and when necessary. The latter is Theodore von Kármán's definition of an engineer (Vandenkerckhove 1986), as obtained as a personal note to Jean, one of von Kármán's last graduate students: "*Scientists discover what is, engineers create that which never was!*"

There is an excellent documented example of what is just written above in a book published by the Society of Automotive Engineers (SAE) entitled *Advanced Engine Development at Pratt & Whitney* by Dick Mulready. The subtitle is *The Inside Story of Eight Special Projects 1946–1971* (Mulready 2001). In Sect. 6, *Boost Glide and the XLR-129—Mach 20 at 200,000 Feet*, two McDonnell Aircraft Company persons are named, Robert (Bob) Belt and Harold Altus (sic) [The spelling should be Altis.]. The former was known to lead the "belt driven machine." Figure 4.1 comes from page 114 (Fig. 6.7) in that book. It compares the development testing of the XLR-129 turbopump to its design value of 6705 psia, with that of the NASA 350K turbopump that later became the main space shuttle main engine (SSME) component (Jenkins 2001). In the last paragraph of the section, the sentence reads: "*... The liquid oxygen turbopump was the next component in line. However, before it was funded, NASA had started the Space Shuttle campaign, and the Air Force gave the XLR-129 program to NASA, granting free use of the existing hardware to Pratt & Whitney. NASA promptly canceled the liquid oxygen turbopump because it would be unfair to our competitors to fund it. I bet there were times when NASA wished it had continued the program. ...*" And this is how a rocket engine disappeared with a run record of 42 simulated flights in the test chamber without any overhaul or repair.

With the following, we are applying the sustained-use viewpoint to the relevant cross section of propulsion system options based on available and demonstrated hardware and materials. A first introduction has been provided in Sect. 3.7.3 for developing the concept of the multi-disciplinary sizing methodology in Sect. 3.7.4. This chapter provides additional propulsion and airframe integration details as applied to commercial near-Earth launchers. Since airbreathing propulsion is most valuable over the atmospheric part of the ascent flight trajectory, the following three broad categories of airbreathing propulsion are further considered:

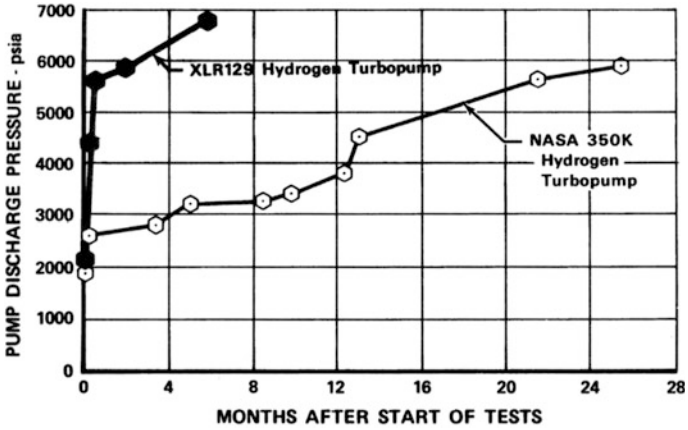

Fig. 4.1 Comparison of XLR-129 turbopump qualification history (circa 1965 for a 1960s program called ISINGLASS) with that of the space shuttle main engine (SSME) turbopump (NASA 350K), circa 1972 (Mulready 2001)

(a) Combination of individual engines operating separately (Anon 1985);
(b) Individual engine (usually a rocket engine) operating in conjunction with another engine capable of more than one cycle mode (Tanatsugu et al. 1987; Nouse et al. 1988; Balepin et al. 1996);
(c) Single combined-cycle engine capable of all cycle modes required over the entire flight trajectory (Maita et al. 1990; Yugov et al. 1989).

4.2 Propulsion System Characteristics

Assuming a combination of individual engines, the transition from one engine to another requires shutting down the first engine followed by transitioning to the second engine type which has already started, while maintaining or increasing flight speed. If the engine is airbreathing, then the flow path has also to be changed. In the past, switching the flow path from one engine to another has always been the system downfall. For a rocket engine operating in conjunction with another engine system, the operation is relatively straightforward. The key challenge is to control the fuel path to the engines. For the single combined-cycle concept, the engineering challenge is the smooth transition from one cycle to the next within a single engine. The transition from one engine cycle operation to another must be made *efficient* (on First Law basis that means the total energy losses must be minimized) and *effective* (on Second Law basis that means when energy is available for recovery as useful work, that conversion must be accomplished then or be lost).

An engine of category (c) is designed for the minimum entropy rise across the cycle. The scope and limitations of these engines are discussed in detail in references (Escher 1994; Czysz 1993a, b), and there are several advantages identified in such scheme. In the case of most airbreathing propulsion systems, the transition from one cycle to another is not a showstopper. In airbreathing propulsion, the two most important considerations to effectiveness and efficiency are as follows: (a) The airflow energy compared to the energy the fuel combustion can add to the flow, and (b) the internal airflow energy losses due to internal drag of strut injectors and cavities and to skin friction and fuel/air mixing.

4.3 Airflow Energy Entering the Engine

With a rocket propulsion system, all of the fuel and oxidizer are carried onboard the vehicle. As a consequence, other than atmospheric vehicle drag and the nozzle exit pressure compared to atmospheric pressure, the vehicle's speed relative to the atmosphere does not determine the propulsion system performance. The specific impulse, I_{sp}, is the thrust per unit propellant mass flowrate. Then, if more thrust is required more engine mass flow is required, i.e., a larger engine or increased chamber pressure to increase the mass flow.

With an airbreathing propulsion system, just the opposite is true. Because the air is entering the airbreathing engine via the vehicle inlet, see Fig. 4.2, the ability of the inlet to preserve energy, as the flow is slowed down in the inlet (for instance, by passing through a series of shock waves), is absolutely critical. The magnitude of the airflow kinetic energy recovered at the end of the inlet determines how much of the fuel–air combustion energy can be converted into thrust. Because the oxidizer is the oxygen in the air, there is a maximum energy that can be added per unit mass flow of air. Then, it is the capture area of the inlet and the airflow speed relative to the vehicle that rules how much *total* energy the burned fuel can add to the air stream. Ultimately, it is the difference between the energy lost in the inlet and the combustion energy that determines the thrust.

The energy of the air is a function of two quantities, (a) the energy of the air in the atmosphere (static enthalpy, in kJ/kg) and (b) the kinetic energy of the air stream (kinetic

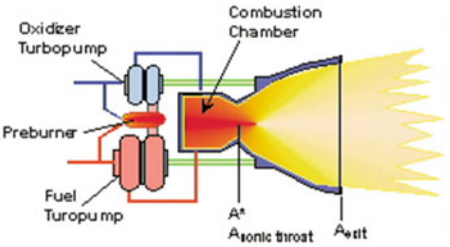

Liquid Propellant Topping Cycle Rocket Engine

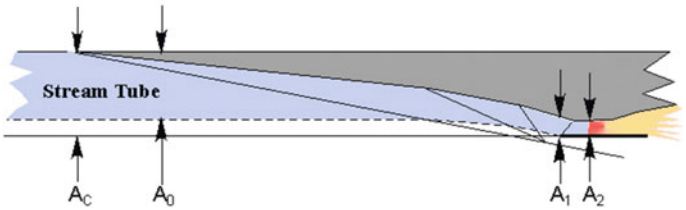

Air Breathing Engine Air Capture Inlet

Fig. 4.2 Liquid rocket engine carries its fuel and oxidizer onboard. By contrast, an airbreathing engine carries only fuel onboard, and the oxidizer is atmospheric air captured by the inlet. A_C = geometric capture area; A_0 = cowl stream tube area, which can be greater or less than A_C; A_1 = engine module cowl area; A_2 = engine module minimum area

energy, in kJ/kg), see also Eq. (2.1a). The *total* energy, or *stagnation* energy, is given as follows:

$$\underbrace{h_t}_{\text{Total energy}} = \underbrace{h_0}_{\text{Static enthalpy}} + \underbrace{\frac{V_0^2}{2}}_{\text{Kinetic energy}} \left(\frac{\text{J}}{\text{kg}};\ V_0 \text{ in m/s}\right) \tag{4.1a}$$

$$\underbrace{h_t}_{\text{Total energy}} = \underbrace{232.6}_{\text{Static enthalpy}} + \underbrace{\frac{V_0^2}{2000}}_{\text{Kinetic energy}} \left(\frac{\text{kJ}}{\text{kg}};\ V_0 \text{ in m/s}\right) \tag{4.1b}$$

The static enthalpy h_0 of air is assumed almost a constant over the altitude range over which the airbreathing propulsion system operates and is much smaller than the kinetic energy in flight: Total energy is essentially a function of the kinetic energy of the air stream. However, the energy Q added to the air by fuel combustion is approximately constant for each fuel. Thus,

$$Q = \left(\frac{\text{Fuel}}{\text{Air}}\right) \cdot Q_c \tag{4.2}$$

$$Q \quad \left(\frac{\text{kJ}}{\text{kg}}\right)_{\text{Air}} \quad \text{(Brayton cycle heat addition)}$$

$$Q_c \quad \left(\frac{\text{kJ}}{\text{kg}}\right)_{\text{Fuel}} \quad \text{(Heat of combustion)}$$

In an actual combustion, 100% of the fuel energy is not available to increase the energy of the air stream. (1) The first non-availability results because the atmospheric air is not at absolute zero. That loss of available energy is called the Carnot loss. Typically, the Carnot loss is about 21% of the input energy; then, around 79% is available. (2) The second non-availability in the combustor results from the temperature gradient in the combustor from the center of the combustor to the cooler wall. Typically, for metal walls in gas turbine engines and other airbreathing engines, that loss is about 4%. Then, 75% of the available combustor energy is available to produce thrust. (3) The third non-availability results from the energy required to mix the fuel and air at high combustor flow speeds (Swithenbank and Chigier 1969). This latter energy loss is a function of the kinetic energy of the fuel entering the combustor compared to the kinetic energy of the air stream.

These three non-availabilities are due to basic thermodynamics and gas dynamics. Nothing at this point has been included to account for friction and shock wave losses in the engine module. The ratio of the kinetic air stream energy to the hydrogen/air combustion heat addition is presented in Fig. 4.3 for the three energy non-availabilities.

These losses increase the entropy S of the airflow, and in fact the thermodynamic "free energy" available to do work is

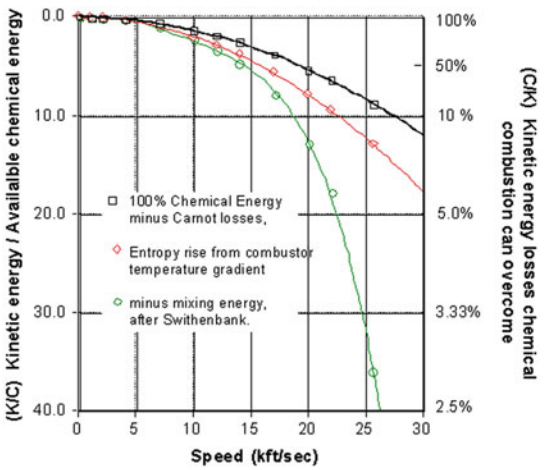

Fig. 4.3 Airflow energy compared to available chemical energy

the difference $E - T{\cdot}S$, not E (Fermi 1956). Anything producing entropy reduces free energy with a multiplier T. Remember 25,573 ft/s is the orbital speed at 100 nautical miles (Mach 23.52, 7.795 km/s, 25,573 mph). At orbital speed and with Carnot losses, the ratio of kinetic energy to energy added by burning hydrogen is about 9:1. That means, the kinetic energy of the air stream is 9 times the fuel combustion heat addition, an astonishing number. Therefore, if the air stream was to lose 11% of its energy (for instance, through friction), combustion of hydrogen fuel could not make up the deficit and there would be no net positive thrust. Adding losses caused by non-uniform combustion, that 9:1 ratio becomes about 12:1. At this point, the loss limit for the air kinetic energy is now more stringent, about 8%. Adding energy required to mix the fuel with the high-energy air, the ratio is about 38:1. The loss limit for the air kinetic energy is now 2.6%. That means that all of the internal inlet combustor-nozzle losses must be less than 2.6%, in order to just maintain thrust equal to drag, with no acceleration. That is very challenging.

The qualitative conclusion is that for a hypersonic airbreathing propulsion system the task is *not so much maximizing combustion efficiency*, but *minimizing air stream energy losses*. Clearly, hypersonic airbreathing propulsion becomes an energy conservation problem and that encompasses the entire vehicle. In fact, the entire vehicle must be conceived a thermal engine, with the energy and heat fluxes entering and exiting the vehicle "box" determining the work available, that is, $(Thrust - Drag) \times V_{flight}$. This is not necessary in a subsonic airplane, since those fluxes are very small compared to the fuel combustion power. For instance, the heat energy that enters the airframe is normally discarded, and that process is called cooling. If instead a portion of that heat energy could be recovered as useful work and converted to thrust, that could add heat corresponding roughly to 30% of the hydrogen fuel heat of combustion (Novichkov 1990a, b). Considering the loss limits discussed above, that is a very large energy addition.

Each fuel has a unique (a) heat of combustion (energy per unit mass of fuel) and a unique (b) fuel/air ratio that burns all of the oxygen in the air called the stoichiometric fuel/air ratio, f_s, see Table 4.1. When the heat of combustion and the fuel/air ratio are multiplied together, the result is the *Brayton cycle heat addition*, which is the energy added per unit mass of air. For the Brayton cycle heat addition, there are essentially two families of values of heat addition using conventional fuels: (1) hydrogen and acetylene, at 3498 kJ/kg and (2) hydrocarbons at 2954 ± 92 kJ/kg. There are indeed some exotic fuels at higher values, but these are very unstable or spontaneously ignite on contact with air. Since the total energy of the air (energy per unit mass of air) plus the square of the speed is a constant, there comes a speed when the energy of the air equals the energy added to the air by burning fuel. Clearly, the faster the aircraft flies, the smaller the fraction "fuel heat addition" becomes of the kinetic energy. Then, the ratio of the total enthalpy to the fuel heat addition ratio increases, as shown by Eqs. (4.3a)–(4.3c) for the fuel combustion energy (not including any losses):

$$\frac{h_t}{Q} = \frac{232.6}{Q} + \frac{500.0 \cdot V_0^2}{Q} \quad (V_0 \text{ in km/s}) \tag{4.3a}$$

$$\left(\frac{h_t}{Q}\right)_{\text{Hydrogen}} = 0.0665 + \frac{V_0^2}{6.995} \quad (V_0 \text{ in km/s}) \tag{4.3b}$$

$$\left(\frac{h_t}{Q}\right)_{\text{Hydrocarbon}} = 0.0787 + \frac{V_0^2}{5.907 \pm 0.18} \quad (V_0 \text{ in km/s}) \tag{4.3c}$$

From hydrocarbons to hydrogen, the Brayton cycle heat addition with Carnot losses equals the air kinetic energy between 2160 and 2351 m/s (7087–7713 ft/s). From hydrocarbons to hydrogen, the Brayton cycle heat addition with Carnot and non-uniform combustion losses equals the air kinetic energy between 2196 and 2019 m/s (6623–7208 ft/s). Then, for any speed above these speeds, the air kinetic energy is greater than the fuel combustion energy addition to the air stream. Second Law available energy losses make the problem a bigger problem because they limit the actual heat energy added to the air to less than the maximum values in Eqs. (4.3b) and (4.3c). For hydrocarbons, see Eq. (4.3c), there is a range in the heat of combustion (±0.18 range on the value in the denominator). With this, there is a practical limit to the combustion energy's ability to offset internal flow and frictional losses that can be determined from first principles. At that point, the airbreathing propulsion system can no longer accelerate the vehicle.

If we look at the other energy losses added to the Carnot loss, we see how much greater the air stream kinetic energy is compared to the fuel addition energy. This is what limits the application of airbreathing propulsion to space launchers. In terms of practical operational engines, the maximum flight speed is probably about 14,000 ft/s (Mach 12) and perhaps as much 18,000 ft/s (Mach 16.5) for research engines (that is, with no payload). The latter figure is 1/2 the specific kinetic energy (energy per unit mass) required to achieve orbit. Clearly, to achieve orbital speed with an airbreather propulsion system, a rocket is required for the final atmospheric acceleration in the trajectory (to obtain the ΔV required to reach orbit) and for all space operations due to lack of an atmosphere.

Table 4.1 Representative fuel properties

Fuel	Q_c (Btu/lb MJ/kg)	Q (Btu/lb MJ/kg)	Q carnot loss (Btu/lb MJ/kg)	Q carnot + non-uniform (Btu/lb MJ/kg)	Q_c·SG (Btu/lb MJ/kg)
Hydrogen	51,500	1504	1188	1038	3648
	119.95	3498	2763	2414	8485
Kerosene (JP-4)	18,400	1247	985.1	860.4	14,360
	42.798	2900	2291	2001	33,402
Methane	21,500	1256	992.2	866.6	8927
	50.009	2921	2308	2.015	20,765

4.4 Internal Flow Energy Losses

The performance of an airbreathing engine is primarily governed by the (a) state properties of air and by the vehicle characteristics that include (b) the captured inlet air mass flow, (c) the air kinetic energy entering the inlet, (d) the energy released to the cycle by combustion of the fuel, and (e) the internal drag and energy losses through the engine flowpath (Yugov et al. 1990). The energy losses in the air stream and the internal wave and friction drag of the engine module can dominate the energy budget. Evaluating these factors permits the establishment of performance boundaries based on first principles. The result is a representation of performance potential and constraints for Brayton cycle airbreathing engines defined by two parameters, altitude and velocity. As first introduced in Sect. 3.7.3, the vehicle performance is constrained by an *altitude boundary* (based on the entropy state of exhaust gas) and a *velocity boundary* (based on the air kinetic energy to combustion energy ratio), a visualization which is called the *flight envelope*, see Fig. 3.34. Both boundaries impact on lift available. In order to define these boundaries for the airbreathing hypersonic cruiser and accelerator, we need to first establish the magnitude of the engine internal flow losses.

Energy input into the combustion chamber must overcome all the losses that are a result of (1) the external drag of the vehicle, (2) the energy losses associated with the internal engine flow, (3) the irreversible losses in the thermodynamic cycle, and (4) it must as well supply the excess thrust minus drag ($T - D$) required for acceleration to orbital speed. As shown in Fig. 4.3, as the flight speed is increased, the kinetic energy becomes increasingly larger than the energy added by the fuel. As the flight speed is increased, the internal drag of the engine increases more rapidly than the airframe drag, so there is a point where the total drag is just equal to the thrust potential of the airbreathing propulsion system (decreasing with increasing speed because the fuel-added energy is becoming a smaller fraction of the air kinetic energy). That is then the maximum speed of the airbreathing flight vehicle. In Fig. 4.3, the losses are represented as a fraction of the flight kinetic energy. The drag losses are given as drag areas referenced to an area related to the propulsion system, see Fig. 4.2. Drag area is a universal way to represent drag energy losses. Multiplying the drag area by the local dynamic pressure, q, yields the first-order total drag which is defined as

$$D = C_D \cdot S \cdot q = C_D \cdot S \cdot \frac{\rho}{2} \cdot V^2 \tag{4.4}$$

The drag area is defined as

$$\frac{D}{q} = C_D \cdot S \quad (\mathrm{m}^2) \tag{4.5}$$

The first-order losses introduced above can be modeled as fractions of the flight kinetic energy. Those losses have been already introduced in Sect. 3.7.3 and are repeated here for convenience: (1) engine internal drag losses, (2) fuel/air mixing losses (after Swithenbank), (3) aircraft total drag, (4) kinetic energy added to the combustor flow by the hot gaseous fuel injection (not applicable for cold liquid-fuel droplet injection), and (5) energy required to accelerate the aircraft.

(1) Combustor drag losses:

$$\left(\frac{\Delta E}{\mathrm{KE}}\right)_{\text{combustor}} = -\left(\frac{V_c}{V_0}\right)^2 \cdot \left(\frac{C_D \cdot S}{A_1}\right)_{\text{eng}} \tag{4.6a}$$

(2) Fuel mixing losses:

$$\left(\frac{\Delta E}{\mathrm{KE}}\right)_{\text{mix}} = -k_{\text{mix}} \cdot \left(\frac{V_c}{V_0}\right)^2 \tag{4.6b}$$

(3) Vehicle drag losses:

$$\left(\frac{\Delta E}{\mathrm{KE}}\right)_{\text{vehicle}} = -\left(\frac{C_D \cdot S}{A_c}\right)_{\text{vehicle}} \tag{4.6c}$$

(4) Fuel injection losses:

$$\left(\frac{\Delta E}{\mathrm{KE}}\right)_{\text{fuel}} = +\phi \cdot f_s \cdot \left(\frac{V_{\text{fuel}}}{V_0}\right)^2 \tag{4.6d}$$

(5) Energy to accelerate:

$$\left(\frac{\Delta E}{\mathrm{KE}}\right)_{\text{accel}} = -\left(\frac{T}{D}\right) \cdot \left(\frac{C_{\mathrm{D}} \cdot S}{A_{\mathrm{C}}}\right)_{\text{vehicle}} \tag{4.6e}$$

In Eq. (4.6d), ϕ is the equivalence ratio.

The only positive term that adds to the available energy is the kinetic energy of the injected fuel. If the temperature of the fuel (in this case hydrogen) is scheduled so that the injected fuel velocity is equal to the flight speed, and the fuel injection angle is in the 6°–10° range, then the injected fuel energy to air stream kinetic energy ratio is 0.0292ϕ. For an equivalence ratio, ϕ, of 6, this provides an energy addition of 17.5% of the air stream kinetic energy. Consequently, recovering normally discarded energy as thrust is as critical as burning fuel in the engine in the first place. This will be discussed further on in this chapter, when identifying the operational zones available for Brayton cycle propulsion systems.

The principal culprit in the drag energy loss inside the combustion chamber, see Eq. (4.6a), is surface friction, and thus the wetted area of the engine (often referenced to the engine module cowl cross-sectional area), and the shock and wake losses from struts and injectors in the combustor flow. Note that friction scales directly with density and that must be minimized to maximize thrust. In order to keep the wetted area, and therefore skin friction loss, to a minimum, the combustor cross-sectional shape and length are critical. Cross-sectional shape is generally driven by integration considerations with the aircraft and has only limited variability, see Chap. 3. The combustor length used is based on both (a) experimental data (Swithenbank 1967; Swithenbank and Chigier 1969) and (b) Computational Fluid Dynamics (CFD) analyses where Second Law (available energy) losses must be considered (Riggins 1996). From both sources, the combustor length for maximum energy efficiency is about 0.40 m (15.7 in.). Swithenbank's measurements in a shock tube combustor test facility verified that for methane, atomized hydrocarbons, and hydrogen. With appropriate choice of injectors/mixers, the combustion time was 35 ± 5 μs (microseconds) over the combustor gas speed range of 6000–12,000 ft/s (1828–3658 m/s) (Swithenbank 1984).

With the wetted area minimized, the remaining task is to identify the shock wave and wake losses. This was done for four combustor configurations in Fig. 4.4 (Czysz and Murthy 1991). The total internal drag area for the four internal combustor geometries is shown in Fig. 4.5. In addition to the work by Czysz and Murthy, these were analyzed by students in the Parks College Hypersonic Propulsion and Integration class with the same results.

Case 2 is a set of five vertical struts with fuel or rocket injectors in the strut base, producing wake turbulence mixing that is characteristic of many ramjet/scramjet designs.

Case 1 is from Professor James Swithenbank of Sheffield University assembling a single horizontal strut with a line of trailing-edge triangles inclined a few degrees to the flow to form a lifting surface that create streamwise vortices for mixing. The fuel injection is from the strut base and at the base of each triangular "finger." The trailing-edge angle is sufficient to produce a subsonic trailing edge in the Mach 4 to 5 combustor flow. The trailing-edge vortex mixing is produced by a subsonic trailing edge on a lifting surface and was developed via experiments in the late 1960s.

Case 0 is an adaptation of the Swithenbank vortex mixing concept to a wall injector configured as a surface inclined to the wall with a subsonic trailing-edge angle, see picture on the right side in Fig. 4.4 (Swithenbank 1967; Swithenbank and Chigier 1969; Swithenbank 1984). The subsonic trailing edge produces the mixing vortex. The author (P.A. Czysz) was shown these injectors by Professor Swithenbank in 1988. The concept of a trailing-edge vortex on a lifting surface was also proposed by Townend (1986).

Case 3 is a shock-confined combustion zone formed between the body and the low-angle body shock wave when

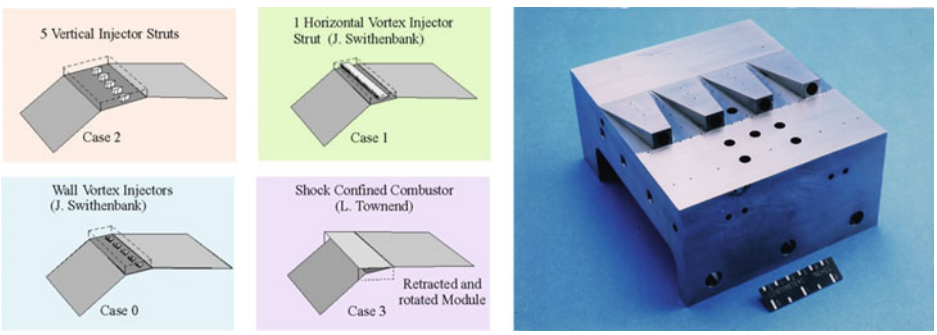

Fig. 4.4 Four representative ramjet/scramjet module configurations are presented schematically on the *left*. For clarity, the aircraft is compression side up, with the airflow from *right* to *left*. The picture on the *right* shows parallel fuel injectors. Their shape creates streamwise trailing vortices favoring mixing (*Courtesy* NASA)

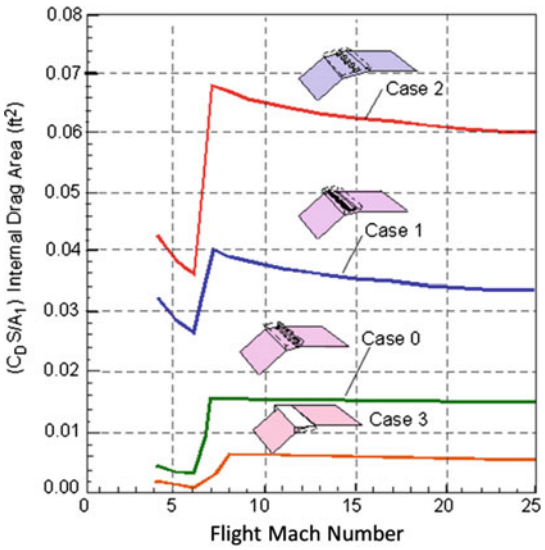

Fig. 4.5 Four very different internal drag areas divided by cowl area for the four combustor fuel injection configuration modules

the engine module is retracted. With Mach numbers on the order of Mach 10 or greater, the resistance of the shock system to normal flow is as great as a physical wall. This concept was successfully tested in an RAE facility by Leonard Townend in 1966 and offers the lowest losses of any configuration. It was also a configuration developed at McDonnell Aircraft under the leadership of H.D. Altis (Czysz 1999, Fig. 15).

For each of these cases, the internal drag area based on skin friction and shock wave drag ($C_D \cdot S$) was determined and referenced to the engine module cowl area as $(C_D \cdot S/A_1)_{engine}$ for each of the four engine module combustor configurations in Fig. 4.5 as a function of *flight* Mach number. Note that as the supersonic combustor through-flow begins (i.e., scramjet operation begins), there is a sharp increase in the internal drag. The stronger the shock waves and shock interference associated with the internal geometry, the sharper the drag rise.

With this information, it is possible to compare the magnitude of the internal engine drag to the external aircraft drag. The ratio of engine drag to aircraft drag can be determined casting the relationship as follows:

$$\frac{\text{Engine drag}}{\text{Aircraft drag}} = \frac{\left[\left(\frac{C_D \cdot S}{A_1}\right)_{eng} + k_{mix}\right] \cdot \left(\frac{q_c}{q_0}\right)}{\left(\frac{C_D \cdot S}{A_0}\right)_{air} \cdot \left(\frac{A_0}{A_1}\right)} \tag{4.7a}$$

$$\left(\frac{q_c}{q_0}\right) \leq \frac{A_0}{A_2} \cdot \frac{V_c}{V_0} \tag{4.7b}$$

$$\frac{A_0}{A_1} \approx \text{constant} \approx 7.0 \tag{4.7c}$$

The value for the aircraft drag area referenced to the geometric capture area $(C_D \cdot S/A_0)_{air}$ is essentially constant for the supersonic through-flow operation of the engine above Mach 6 and has a value of approximately 0.090. The engine airflow contraction ratio (A_0/A_2) depends on whether the engine is operating in supersonic or subsonic through-flow mode. Table 4.2 compares the combustor entrance conditions for the flight speed of 14,361 ft/s (4377 m/s). Once supersonic through-flow is established, the combustor static pressure and temperature remain essentially constant, as determined by Builder's thermodynamic analysis (Builder 1964). At 19,350 ft/s (5898 m/s), the contraction ratio for supersonic through-flow is 32:1, and for subsonic through-flow it is 128:1. Then, as the vehicle accelerates, the supersonic through-flow engine geometry and combustor are almost constant. For the subsonic through-flow engine, the combustor height becomes rapidly smaller and more intensely heated. The pressure and temperature are very high for the subsonic through-flow engine, to the point of being impractical-to-impossible to operate in a flight-weight combustor built from known materials.

Given the combustor conditions, it is now possible to determine the ratio of engine module drag to aircraft drag from Equation set (4.7a–4.7c).

The drag ratios for the four different combustor configurations of Fig. 4.4 are shown in Fig. 4.6. In steady flight, the mass flowrate entering the engine from the external free stream is constant while the density, velocity and flow area vary along the streamtube (flowpath) consistent with that constant mass flow. The result is that the dynamic pressure, q, of the flow, that is, the ability of the flow to generate force, is greatly increased, just as predicted by Eq. (4.5). That increase can be from 3 to 12 times the free stream value. That also means that the internal drag of the engine can exceed the external drag of the aircraft, which explains why internal drag losses are vital to the operation of the scramjet vehicle as shown in Fig. 4.6. This is a key result, because it quantifies how serious the engine drag can be as flight speed is increased, and why some historical engine programs struggled to exceed the Mach 10 to 12 regimes.

With a *retractable* vertical strut, it is possible to shift from the strut injector configuration to the wall injector configuration to maintain aircraft acceleration. If this configuration change is impossible, or is not made, accelerating much beyond Mach 10 is unlikely. It is therefore clear why engines with retractable strut concepts (Baranovsky et al. 1992a, b; Czysz and Vandenkerckhove 2000) are essential to high Mach number operation. The adaptation of the Swithenbank center strut to a wall-mounted vortex mixing injector was a significant improvement. Swithenbank developed the single horizontal strut with the trailing-edge delta fingers such, that although fixed, it had the potential to reach Mach 12. Townend's early pioneering in "shock-confined

Table 4.2 Combustor entrance geometry and conditions for 14,361 ft/s flight speed

Combustor conditions	A_0/A_2 (–)	V_c (ft/s; m/s)	P_c (atmosphere)[a]	T_c (K)	P_c (amagat)[b]
Supersonic through-flow	28.4	12,972 3954	1.10	1756	0.152
Subsonic through-flow	76.5	4495 1370	34.4	5611	1.325

V_0 = 14,361 ft/s, Z_0 = 124,000 ft, q_0 = 1122 lb/ft^2
V_0 = 4377 m/s, Z_0 = 37,795 m, q_0 = 57.72 kPa
[a]Referenced to sea-level pressure and density at 14.696 psia and 59 °F analogous to STP (standard temperature and pressure) conditions
[b]One amagat is local density divided by density at 14.686 psia and 0 °F, 0.002662 slugs/ft^3

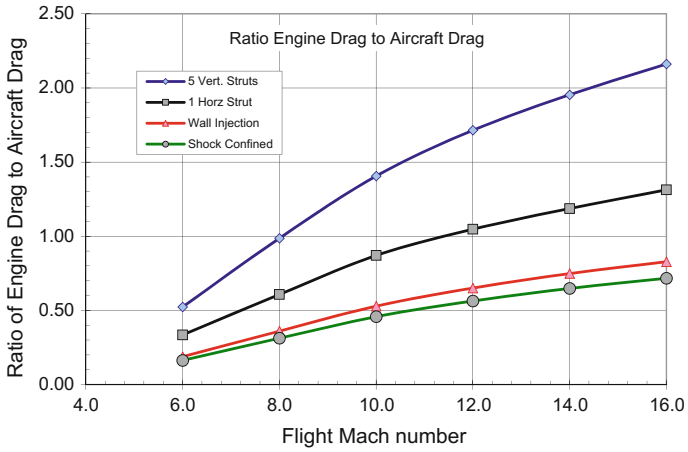

Fig. 4.6 Engine module configuration significantly affects performance

combustion" offered a significant reduction in propulsion system drag (Townend 1986). Ashford and Emanuel have compared the ejector ramjet to the Oblique Detonation Wave Engine (ODWE). The ODWE can represent one operating regime of a combined-cycle propulsion system (Townend and Vandenkerckhove 1994), when at high hypersonic speeds the internal drag of the engine module becomes as large as to significantly diminish thrust-to-drag ratio. The result is that the so-called propulsion acceleration specific impulse, or "effective specific impulse," based on thrust minus drag, is the important parameter for accelerating vehicles, not specific impulse alone as in cruisers. The effective specific impulse is given by

$$I_{spe} = \frac{T - D}{\dot{w}_{ppl}} \quad \left[\frac{\text{N}}{\text{kg/}s} = \text{m/s} \quad \text{(SI units)}\right] \tag{4.8}$$

We now have nearly everything necessary to determine what speed a scramjet-powered vehicle can reach based on available energy and thrust minus drag ($T - D$). There is one element missing, and that is altitude. Altitude is not limiting in the sense that combustion cannot be maintained; it can be limiting based on the value of the nozzle expansion entropy. Entropy is a thermodynamic quantity that relates to how much of the energy in the system is irreversible. That is, if energy (pressure) is expended to accelerate an airstream to supersonic speeds, then to slow it down sufficiently for mixing and combustion to take place, the air must be passed through a series ("train") of shock waves. The entropy-increase across the shock train determines how much of the initial pressure can be recovered. The greater the entropy rise, the larger the fraction of the initial pressure becoming unrecoverable (irreversible pressure loss). The same is true for any Brayton cycle engine (ramjet/scramjets and turbojets are Brayton cycles).

One characteristic of the atmosphere is that, as altitude increases, pressure decreases (at constant volume and temperature $\partial S/\partial p = -V/T$). As pressure decreases, entropy increases. The consequence for any propulsion cycle is that the higher the altitude, the higher the initial entropy in the atmosphere. Since most Brayton cycles have a constant increment of entropy across the cycle, this means that the higher the altitude, the larger the expansion-nozzle entropy. That entropy level determines how much of the chemical energy added to the air molecules through combustion can be recovered as exhaust velocity. The reason the combustion energy cannot be recovered as flow kinetic energy of the gas bulk motion (or flow velocity) is because the entropy limits the conversion of internal energy of the burnt gas (characterized by composition and temperature) to the molecules translation energy by collisions. To extract maximum momentum from high-temperature gas, this must be expanded down to the external pressure. Thermodynamically the driver of this process is the entropy gradient, and if atmospheric entropy is too high, expansion stops inside the

nozzle. The burnt expanding gas is said then to be "frozen." This "frozen" gas will be in a higher energy state compared to a gas in equilibrium with the atmosphere, which corresponds to the lowest internal energy and highest kinetic energy.

Equation (4.9) gives the critical entropy value based on the physical size of the nozzle and its expansion-nozzle half-angle determining expansion (Harney 1967). In the equation, (S/R) is the non-dimensional entropy, θ is nozzle half-angle, r^* is the radius of an equivalent sonic throat that would give the nozzle mass flow, static pressure, and temperature at the combustor exit, and r^*_{ref} is one inch (25.4 mm).

$$\left(\frac{S}{R}\right)_{\text{nozzle}} = \Sigma - 0.4 \cdot \ln\left(\frac{\tan\theta}{r^*/r^*_{\text{ref}}}\right) \tag{4.9}$$

with

$$\Sigma = 30.0 \quad \text{then there is no 'frozen' energy} \tag{4.10a}$$

$$\Sigma = 32.0 \quad \text{then about } 3\% \text{ of the dissociation energy is 'frozen'} \tag{4.10b}$$

$$\Sigma = 34.6 \quad \text{then about } 10\% \text{ of the dissociation energy is 'frozen'} \tag{4.10c}$$

If 10% of the chemical energy is "frozen" and cannot be recovered, there is a serious drop in exhaust gas velocity and a loss of thrust. Remember, in an airbreathing engine for thrust to be generated, the exhaust nozzle exit speed must be greater than the flight velocity. For the case presented in Table 4.2, the exhaust gas speed is just 9.7% greater than flight speed for the supersonic through-flow case and only 3.5% greater than flight speed for the subsonic through-flow case. Clearly, any loss of velocity producing energy is critical at this speed. For a particular engine, given the initial entropy of the atmosphere and the entropy increment of the engine, the onset of "frozen" flow can be identified (Glassman and Sawyer 1970). Then, the dissociation level becomes a function of altitude. We now have an altitude-sensitive or entropy-sensitive criterion for determining the physics of the flow and how it affects the magnitude of the net positive acceleration, see Fig. 4.7.

Above 175,000 ft, the static entropy increases to a level that makes continued control of the frozen dissociation by adding excess hydrogen improbable. There is a region where adding excess hydrogen can provide sufficient three-body collisions to reduce the degree of frozen oxygen and nitrogen dissociation. The excess hydrogen also is a better working fluid than air (its molecular weight is a factor 15 lower) and helps to contain the decrease in thrust from frozen chemistry effects. In the 170,000–180,000 ft altitude region, the atmospheric entropy is so large that even a large amount of excess hydrogen cannot control the irreversible effects. Above this altitude, it is probably not possible to achieve the desired airbreather performance.

With this understanding, we are finally able to determine the operating spectrum of a ramjet/scramjet propulsion system.

4.5 Spectrum of Airbreathing Operation

As introduced in Sect. 3.7.3, with increasing flight speed, the engine performance becomes characterized by energy conservation rather than by combustion; energy conservation becomes far more important than chemistry (Ahern 1992). Figure 4.8 presents a cross section of hypersonic glider trajectories and one maneuvering high *L/D* weapon (Boost Glide Reentry Vehicle, BGRV). Mercury, Gemini, and Apollo were ballistic capsules with very little lift. Shuttle and ASSET were hypersonic gliders with modest hypersonic *L/D* ratios (1.5–1.7). Model 122 was a precursor to BGRV to verify the trimmed rolling could be controlled by a nutating

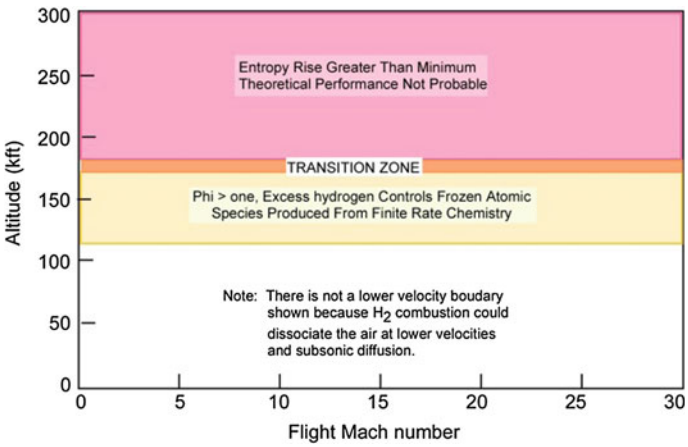

Fig. 4.7 Altitude boundaries determined by "frozen" chemistry

flare. Furthermore, rocket and airbreather exit trajectories are compared with the entry trajectories. The accelerating air breather launchers operate at the highest dynamic pressure (lowest altitude at a given speed). Then, entry heating for the airbreathing vehicle class is less than the exit heating. Cruise dynamic pressure is about equal to the capsule dynamic pressure. A cruise vehicle with a gliding return has less heating when gliding. In fact, one reason for boost-glide (BG) is that because of the pressure required to operate a scramjet, boost-glide always has less heating. Airbreathing exit operates at a greater dynamic pressure than even the BGRV maneuvering entry.

The result is a spectrum of operation over the speed regime developed by (Czysz and Murthy 1991) which is shown here again for convenience in Fig. 4.9. This figure illustrates the extent to which the kinetic energy of free stream air entering the vehicle inlet capture area and the fuel mass and kinetic internal energy become gradually more significant and critical as the flight speed increases. Thus, the operating limits of the airbreather can be clearly identified.

Figure 4.9 shows flight altitude versus flight speed, in kft/s. The corridor labeled "acceleration," which begins at zero speed and extends across the figure to nearly orbital speed (20 kft/s), is the flight corridor for airbreathing vehicles to reach orbital speed. This corridor is based on the dynamic pressure limits of accelerating airbreathing vehicles. The lower limit is based on structural weight and skin temperatures. The upper limit is based on having sufficient thrust to accelerate efficiently to orbital speed. The narrow corridor cutting across the acceleration corridor, labeled "cruise," is the corridor for hypersonic cruise vehicles to achieve maximum range. The vertical shaded area identifies the flight speeds at which a subsonic flow-through engine (ramjet) should transition to a supersonic flow-through engine (scramjet).

The shaded area between 5 and 7 kft/s is the transition region defined by Builder for hydrogen and hydrocarbon fuels as the region where kinetic compression to subsonic

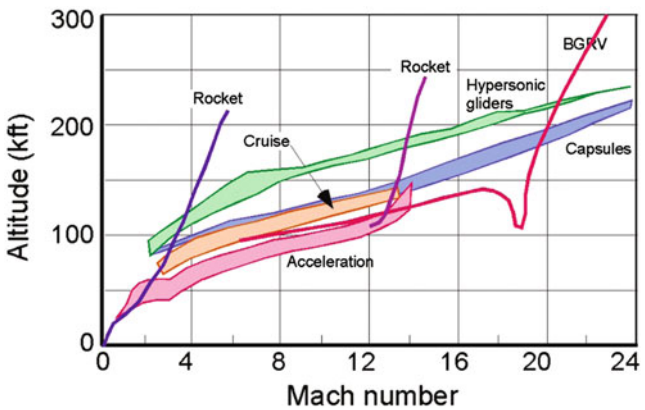

Fig. 4.8 Exit and entry trajectories overlaid

speeds ahead of the combustor alone yields optimum enthalpy compression ratio (Builder 1964). To the left of this area, mechanical compression is required to reach the optimum enthalpy compression ratio. In this area, engines are generally limited to the practical compression ratios achievable; they do not achieve the optimum enthalpy compression ratio. To the right of this area, the kinetic enthalpy compression ratio exceeds the value of the optimum enthalpy compression ratio. Then, diffusion of the air stream has to be limited in order to limit the enthalpy compression ratio (the engine through-flow speed is supersonic). This means that engine flow-through needs to remain supersonic, and flow-through speed increases as the flight speed increases.

The goal in limiting flow diffusion is to maintain a constant value for the optimum enthalpy compression ratio. Analysis of the Second Law of Thermodynamics by Builder does show that the engine design enthalpy compression ratio (rather than the design pressure ratio) and the fuel define the cycle efficiency. Hydrocarbon fuels are to the left side of the shaded area, and hydrogen is to the right side of the area. The vertical lines identified with the numbers 0.5, 1, 2, 4, and 7 represent the ratio of flight kinetic energy to the available fuel energy accounting for Carnot losses. As indicated by the arrows, to the left of the vertical shaded area engines are subsonic flow-through, and to the right of the vertical shaded area engines are supersonic flow-through. As pointed out in Eq. (4.6d), the kinetic energy of the injected, hot, gaseous fuel is a source of energy and momentum very useful to overcome the internal drag and mixing losses. As indicated by the arrows and text adjacent to the vertical lines, this energy addition becomes more critical to engine operation as the speed increases.

The speed regime to the right of the energy (airstream energy/chemical energy added) ratio = 4 line is questionable for an operational vehicle. It is certainly possible for a research vehicle to investigate this area but, as we shall see, at the energy ratio = 4 boundary, the airbreathing vehicle has achieved a significant fraction of the benefits from incorporating airbreathing in terms of the propellant required to achieve a given speed increment. As the energy ratio increases, the scramjet-powered vehicle thrust-to-drag ratio decreases. As the thrust-to-drag ratio decreases, the acceleration (effective) $I_{sp} \equiv I_{spe}$ decreases to the point where the high thrust-to-drag rocket uses less propellant for a given speed increment compared to the scramjet. At that point, the rocket engine is clearly a better accelerator than the airbreathing engine. From an energy viewpoint, a practical maximum airbreathing speed is about 14,200 ft/s (4.33 km/s).

Further to the right of this line, the payoff achieved compared to the resources required offers diminishing returns. That is, the velocity increment produced per unit propellant mass and volume flow is less for the airbreather. Beyond this point, a hydrogen/oxygen rocket requires less

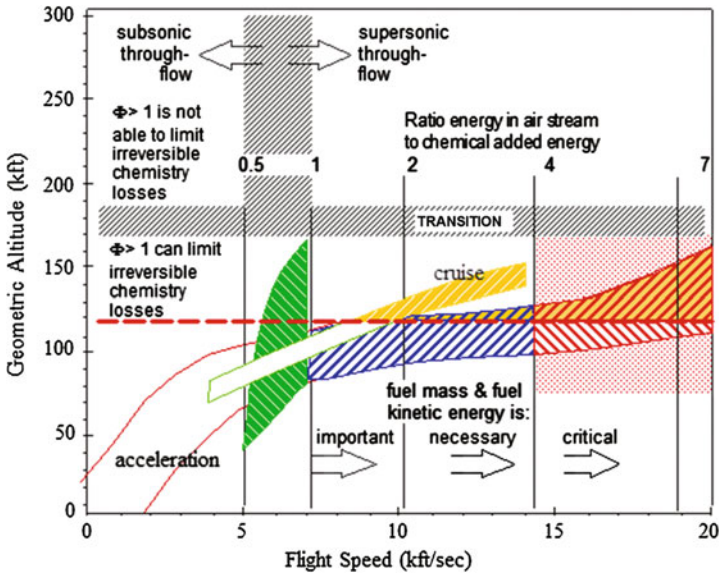

Fig. 4.9 Operating boundaries of Brayton cycle engines based on enthalpy and entropy analyses

propellant mass flow per velocity increment and less vehicle storage volume compared to the airbreathing engine. In terms of available energy and of the propellant required to produce a given velocity increment, the airbreather is outperformed by a hydrogen/oxygen rocket. This is a result of the fact that the thrust-to-drag ratio of the airbreather is diminishing as speed and altitude are increased, while the thrust-to-drag ratio for the rocket is increasing. For this operating regime, the acceleration (effective) I_{spe} of the airbreather falls below that of the rocket.

Returning to the consideration of entropy and applying the criteria from Eq. (4.9), the loss of exhaust velocity begins at about 120,000 ft (36,576 m), shown as a horizontal dashed line in Fig. 4.9. The altitude regime above 120,000 ft altitude produces a degradation of thrust because the increasing entropy levels limit the internal molecular energy that can be converted to kinetic energy and exhaust gas velocity. Dr. Frederick Billig of APL/JHU advocated the introduction of excess hydrogen in the flow to act as a molecular collision third body. In Eq. (4.6d), excess hydrogen means the equivalence ratio (ϕ) is greater than 1. For $\phi = 1$, nominally the fuel burns all of the oxygen available in the air. Excess hydrogen provides abundant third bodies for the dissociated product molecules to recombine to the minimum internal energy state (Billig 1989; Czysz and Murthy 1991). The hydrogen molecule dissociates into two hydrogen atoms. However, unlike other diatomic gases, atomic hydrogen in the exhaust has about 90% of the velocity potential as molecular hydrogen. Since it is a low molecular-weight gas, it is a better working fluid than air, producing pound-per-pound more thrust and higher specific impulse.

However, again due to entropy, adding excess hydrogen works up to a point. In terms of altitude, that point is about 170,000 ft (51,816 m). Between 120,000 ft and 170,000 ft, the excess hydrogen ameliorates the energy "frozen" in the non-equilibrium exhaust gas. Above that altitude, the entropy levels are such that, even with more third body collisions provided by hydrogen, the energy trapped in non-equilibrium products cannot be recovered and it is improbable that a Brayton cycle engine can produce sufficient thrust. Excess hydrogen fuel used in Brayton cycle engines below 150,000 ft and at less than 14,500 ft/s can convert a fraction of the aerodynamic heating into net thrust by soaking friction heating followed by injection and expansion of the heated hydrogen into the engine at a speed corresponding to flight speed. Note that cruise engines operate at greater cycle entropy levels compared to acceleration engines; they may therefore require a larger excess hydrogen flow compared to acceleration engines.

Up to this point, we have used first principles to determine that the vehicle will be stout, and not too small if it is to be built from available industrial capability, see Figs. 3.69–3.72. We have also established it is not practicable for an operational vehicle to exceed 14,200 ft/s in airbreathing mode, and apparently 12,700 ft/s would be less challenging while retaining the benefits of airbreather operation.

4.6 Design Space Available—Interaction of Propulsion and Materials/Structures

We have now established the most likely operational region for an airbreathing operational launcher from a first principles approach. The next question is: "*Are there materials available to operate in the Brayton cycle operating region?*" In this section, the role of coatings reducing heat transfer will not be discussed; while they can enhance structure survivability, most are proprietary and/or classified (for

instance, in the USA any related information is subject to ITAR). The approach taken here was first used in the 1965–1970 Hypersonic Research Facilities Study (HyFAC) for NASA (Pirello and Czysz 1970). The interest has been in identifying operational regions for different materials used on the compression side of hypersonic vehicles and near the nose, where radiation-cooled structures begin. Specifically, the heat transfer rate and surface temperature determined at a point 5 ft aft of the nose have been calculated for the vehicles in Fig. 3.13 as a function of Mach number, altitude, angle-of-attack and load factor and are shown in Figs. 4.10 and 4.11.

The load factor is the lift divided by the weight; in level flight, it is exactly 1. In a maneuver, such as a vertical or horizontal turn, or change in flight path angle, the normal load factor can be in the 2–3 range. The normal load factor, defined as the ratio of lift-to-weight, is usually expressed in units of g, the gravitational acceleration constant on the ground ($\approx$9.81 m/s^2). The angle-of-attack range has been selected from 1° to 20°, since this class of hypersonic aircraft develops their maximum lift-to-drag ratio at less than 20°. This range is much smaller compared to the reentry angle-of-attack range of the space shuttle (Jenkins 2001) or DynaSoar X-20 (Miller 2001) configurations that typically have glide angles in the 40°–45° range during the reentry phase. Correlating heating and lift results in an altitude versus Mach number chart for a particular material temperature, with load factor and angle-of-attack as parameters.

Figure 4.11 shows the assembled area plots for six representative radiation equilibrium temperatures (Pirello and Czysz 1970). Since 1970, the availability of materials has changed, so not all of the materials identified in the reference are available today. One notable example is Thoria-Dispersed Nickel (TD Nickel). Thoria is mildly radioactive and what was thought acceptable in 1967 is no longer acceptable 50 years later. Equivalent materials for 2100 °F (1147 °C) are carbon/carbon and silicon carbide/silicon carbide metal matrix composites manufactured in the USA and in the late 1980s by SEP at Bordeaux (later SNECMA, and currently Safran Snecma). TD Nickel was not considered for either Copper Canyon or the National Aerospace Plane (NASP or X-30). For a given material, the operational envelope and

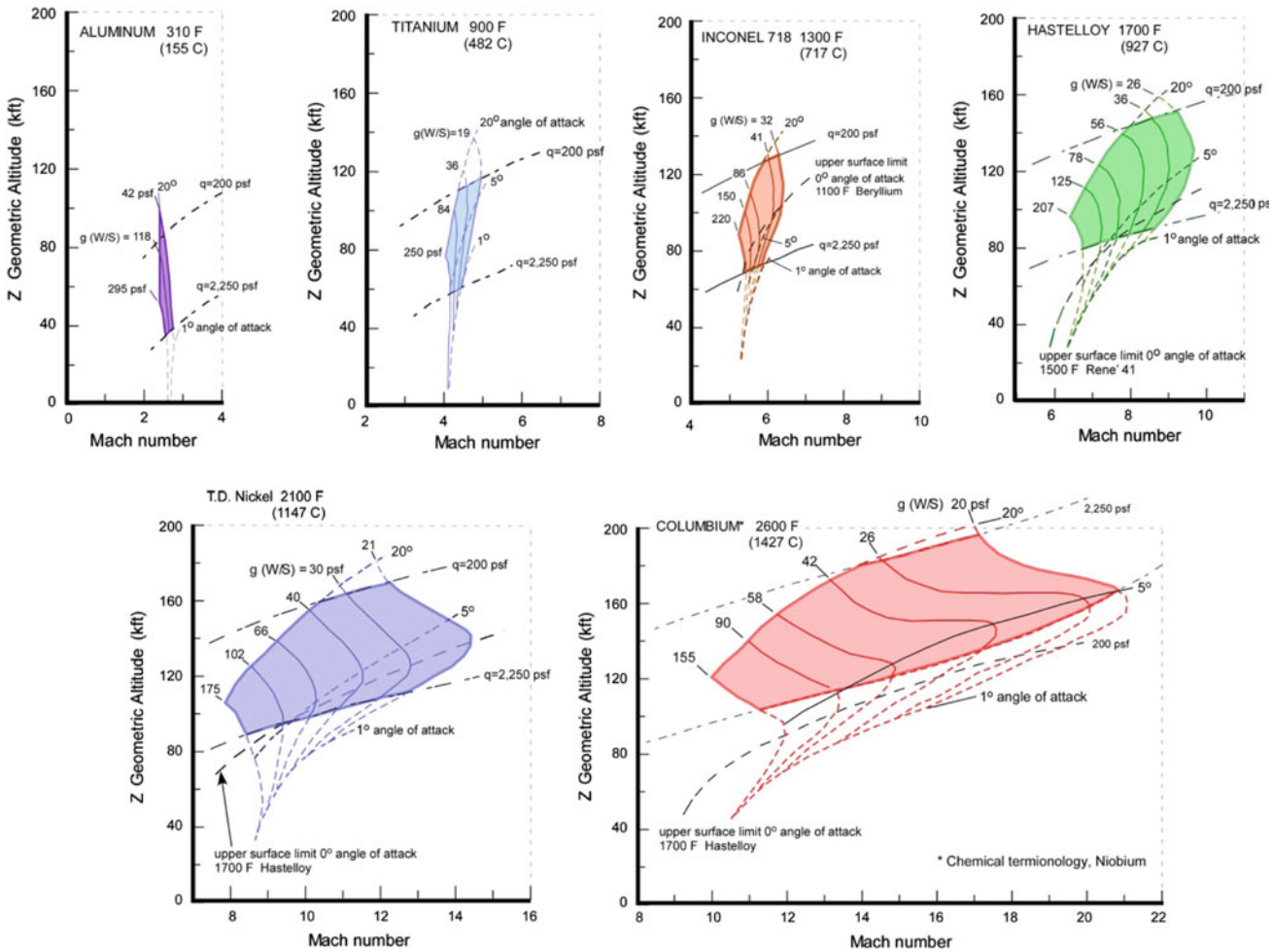

Fig. 4.10 Detailed performance envelopes for aluminum, titanium, inconel 718, hastelloy, thoria-dispersed nickel and columbium (niobium)

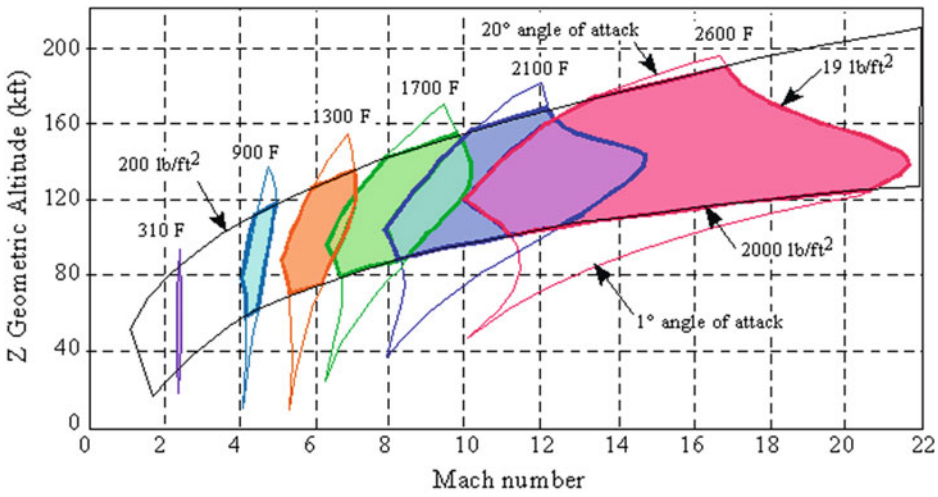

Fig. 4.11 Performance envelope of six materials. Temperature measured 5 ft (1.52 m) aft of the nose on a full-size operational vehicle

maximum speed for an aircraft has been determined as a function of angle-of-attack and load factor.

As shown in Fig. 4.10, each particular material has an operational region bounded by four limits. The left- and right-side limits are lift loading boundaries. Lift loading is defined as:

$$\frac{L}{S_{\text{plan}}} = N_z \cdot \frac{W}{S_{\text{plan}}} \quad (N_z \text{ is the normal load factor}) \quad (4.11)$$

with N_z representing the normal load factor and S_{plan} being the wing planform area. On the right side, this limit decreases as speed increases, because the aircraft becomes lighter as propellant is consumed and the aircraft accelerates toward orbital speed. The upper boundary of each area is determined by the 20° angle-of-attack, and the lower by 1° angle-of-attack. Note that the left boundary is not the same for each temperature area, because the aircraft becomes lighter as less propellant is consumed to reach cruise speed or orbital speed. The materials associated with each surface temperature and the magnitude of the maximum lift loading for each are given in Table 4.3.

Remember that the left and right boundaries are lift loads. If maneuvering at 3*g* is required (not impossible or unlikely for a hypersonic aircraft flying at high dynamic pressure), the wing loading corresponding to the minimum right-side lift loading becomes a maneuver lift loading three times the right-side minimum lift loading. In Fig. 4.10, that corresponds to 63 psf at Mach 10, instead of 21 psf at Mach 14 for the 2100 °F material at 0*g*, and to 78 psf at Mach 8, instead of 26 psf at Mach 10 for the 1700 °F material. Clearly, if a margin for an emergency maneuver is one of the operational requirements, then the maximum speed must correspond to the emergency lift load, not the 1*g* acceleration load.

The importance of lift loading in determining the maximum speed for a given surface temperature is not to be underestimated. If a vehicle is flying near its lift loading Mach limit, and for some reason the angle-of-attack, that is, the lift loading, must be changed, it may be mandatory to slow down before executing that maneuver. For an accelerating air-breather at 1500 lb/ft^2 (7.32 t/m^2) dynamic pressure, the 1*g* level-flight lift loading can be doubled by a 2° change in angle-of-attack, a very significant effect. Flight near a speed boundary could "over temperature," in pilot parlance, that is overheat, the windward compression surface (lower surface, or belly). Similarly, a reduction of the angle-of-attack to near 1° angle-of-attack could "over temperature" the expansion surface (upper surface). From this, for high-speed hypersonic flight it seems the straight and narrow flight path is the least demanding trajectory. With either the hypersonic glider or the airbreathing hypersonic cruiser and accelerator aircraft possessing a glide range approximately equal to the

Table 4.3 Material selections and maximum lift loading boundary for Fig. 4.11

Temperature (°F)	310	900	1300	1700	2100	2600
Temperature (°C)	154	482	704	927	1149	1427
Material	Aluminum	Titanium	RSR titanium[a] Inconel	RSR titanium[a] Hastelloy 1700	RSR MMC[a]	Coated niobium C–C C–Sic
Left boundary (lb/ft^2)	350	250	210	210	180	155
Limit (t)	1.71	1.22	1.03	1.03	878 kg/m^2	757 kg/m^2

[a]These materials are hot isostatically pressed, rapid solidification rate (RSR) titanium powders and metal matrix composites (MMC) made from RSR titanium powder with either silicon carbide fiber or Tyranno fiber reinforcement. Tyranno fiber and coating are patented materials of the UBE Corporation, Tokyo, Japan

circumference of the Earth, it may be better to continue around the Earth and land at the launch site, rather than attempting to turn back and overheat the structure.

An afterburning turbofan engine can increase its thrust by 42% by advancing the power lever to the afterburner position; additional fuel is then injected into the afterburner downstream of the turbine. This maneuver increases thrust by burning the oxygen left in the exhaust gas flow at the expense of increasing specific fuel consumption by 2.5 times (the I_{sp} is 40% of non-afterburning I_{sp}). In contrast, scramjets accelerate by increasing their angle-of-attack to increase the inlet mass capture and therefore thrust. The scramjet can easily double its thrust by an angle-of-attack increase of only a few degrees, at almost constant I_{sp}, by simply capturing more air flow. Then, while the afterburning turbofan in afterburner produces 1.42 times the thrust at 3.55 times the fuel flow, the scramjet produces 2.0 times the thrust at 2.1 times the fuel flow. Clearly, when a scramjet-powered vehicle chooses to accelerate, the pilot advances the throttle for the aircraft to increase its angle-of-attack in order to initiate and execute acceleration! This can produce very different reactions in human pilots who are not accustomed to see the angle-of-attack increase as the power lever is advanced. However, doing so can never give the automatic pilot any concern.

From Fig. 3.18 for the hypersonic glider, the maximum compression-side wall temperature is 2600 °F (1427 °C). This means that any vehicle achieving orbital speed with a vehicle in the FDL-7 class of performance must have materials capable of the same thermal performance on its compression side, whether rocket-powered or airbreather powered to orbital speed. In Fig. 4.11, the maximum temperature material is 4600 °F (2542 °C) for an airbreathing vehicle of either cruising or accelerating to orbit type. Clearly, an airbreathing vehicle capable of orbital speed must be built of the right materials to potentially achieve airbreathing operation in the Mach 12 to Mach 18 speed regime. Whether it is possible for the airbreather to operate in this range, considering what has already been said on Second Law energy losses, remains to be seen.

From a collaboration between P.A. Czysz and J. Vandenkerckhove in early 1984, practical maximum operational speeds for operational airbreathing launchers (Czysz 1992) have been established. These maximum operational speeds range between 3.9 km/s (12,700 ft/s, Mach 11.68) with the possibility to reach 4.27 km/s (14,000 ft/s, Mach 12.87) from a vehicle sizing, compression-side materials, and minimum dry weight approach (Czysz 1995). Many vehicles may not require operation above Mach 12. TSTO launchers concepts usually "stage" (i.e., release the second stage) in the Mach 6 to Mach 10 range, although some concepts stage at Mach 12. Hypersonic cruise vehicles are historically in the Mach 8 to Mach 12 range because of engine limitations, and also due to the very practical fact that flying faster does not improve block time, because of the longer climb and descent time and distances (Koelle 1989). For these cases, current titanium material systems match up well with the acceleration and cruise requirements.

Figure 4.12 shows two of these operational areas for two representative radiative equilibrium surface temperatures at 5 ft (1.52 m) aft of the nose, i.e., 1700 °F (927 °C) and 2100 °F (1149 °C). Radiative equilibrium occurs when the surface temperature is such that the total heat flux from the air above is radiatively rejected by the surface. These two temperatures are characteristic of hot isostatically pressed, rapid solidification rate (RSR) titanium powders, and of metal matrix composites (MMC) made from RSR titanium powder with silicon carbide fibers or Tyranno fiber/cloth reinforcement. These operational zones are from Fig. 4.11 with three values of lift loading shown. The lift loading lines have the same value in both operational areas. If the leading edges are thermally controlled by transpiration cooling or heat-pipe thermal pumping, then the materials shown are applicable for the primary metal thermal protection system based on shingles. The control surfaces will have to be fabricated with carbon–carbon or silicon carbide–carbon ceramic matrix materials because of their flow environment and also because of their structural thinness, as indicated in Fig. 3.18.

In Fig. 4.11, the cruise corridor corresponds to the highest flight Mach numbers for a given material. For instance, if an aircraft is flying at Mach 14 with a 1g wing loading of 19 lb/ft^2 (92.5 kg/m^2) and there is an operational problem that requires returning to base, unless the aircraft is slowed to about Mach 11 before attempting to climb, dive, or execute a 2g turn (lift loading now 38 lb/ft^2 (185 kg/m^2)), this maneuver will end in "over-temperaturing" the vehicle. This is one important reason to operate hypersonic vehicles with automatic controls, because actions consistent with instinctive subsonic or low supersonic aircraft piloting are fatal when flying hypersonic aircraft. Again, whether accelerating or cruising, any deviation from straight-line flight can be a source of "over-temperaturing" the thermal protection system (TPS).

4.7 Major Sequence of Propulsion Cycles

Section 3.7.3 introduced airbreathing propulsion systems in the context of parametric sizing and multi-disciplinary synthesis. The following expands the discussion to propulsion-integrated transatmospheric launchers.

There are a significant number of propulsion system options that have been studied and reported. In this chapter, 14 different classes of propulsion systems are discussed that are suitable for either hypersonic flight or transatmospheric

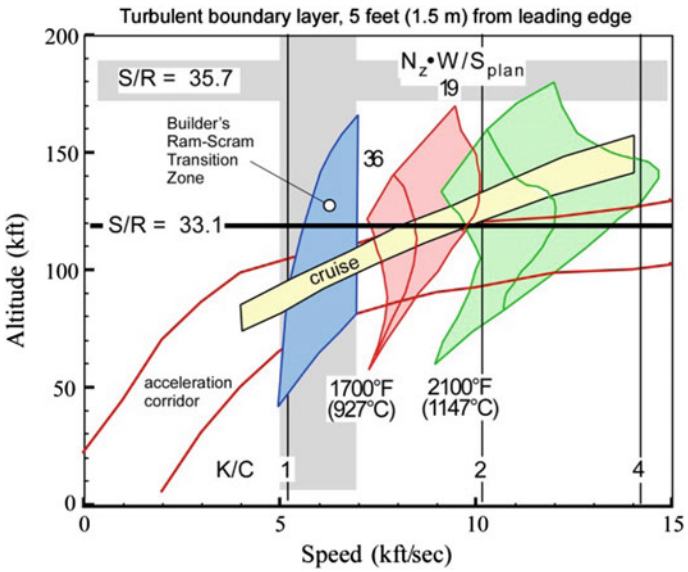

Fig. 4.12 Materials and engine operating regimes compared to the cruise and acceleration flight corridors. The ratio ($N_z \times W/S_{plan}$) is normal acceleration times wing loading in lb/ft^2

space launchers. The authors have focused on those that are applicable to SSTO and TSTO transatmospheric vehicles and hypersonic cruise vehicles. If the rocket ascent to orbit is deleted from the analysis, then a SSTO that uses airbreathing propulsion to Mach 10 is essentially the first stage of a TSTO vehicle. At the end of this chapter, SSTO and TSTO are compared following the work of the late Jean Vandenkerckhove in collaboration with the authors. The intent is to define the SSTO weight ratio and the onboard oxygen ratio carried by the vehicle.

As we have seen in Chap. 3, the smaller the weight ratio and the oxygen-to-fuel ratio, the smaller the size and gross weight of the resulting vehicle. In terms of mass ratio and oxidizer-to-fuel ratio to orbital speed, the authors examined 6 principal hydrogen-fueled propulsion categories, as shown in Figs. 3.4 and 3.5. The term "thermally integrated" is used in the description of these categories. "Thermally integrated" means that the hydrogen fuel has a role in all cycles integrating the combined-cycle engine; it collects thermal energy normally discarded as "cooling heat," finally turning that energy into useful work. This is accomplished by driving closed-loop power extraction units (Ahern 1983), or expansion turbines, or by converting heat into thrust via expansion. The combined-cycle concept dates back more than 50 years to The Marquardt Company (Escher 1998). Marquardt had a propulsion concept that would reach hypersonic speeds using a single engine (Escher et al. 1967; Escher 1995, 1996). One of The Marquardt Company's concepts incorporated folding rotating machinery (Escher and Czysz 1993) into their cycle; however, it was still a single engine that could go from takeoff to hypersonic speeds.

The following introduces seven principal airbreathing propulsion categories with hydrogen as fuel:

(1) The first category is the liquid-propellant, chemical rocket and rocket-derived air-augmented propulsion, where the primary propulsion element is a rocket motor. Solid rockets and hybrid rockets are not included as they are inherently expendable, limited-use engines not applicable to sustained-use vehicles.

(2) The second category is the airbreathing rocket, where the propulsion elements are a rocket motor and an air/fuel heat exchanger that supplies the rocket motor with atmospheric air as oxidizer over part of its trajectory. The British HOTOL, SKYLON, and further concepts developed by Alan Bond (Reaction Engines) represent such a propulsion system.

(3) The third category is the thermally integrated rocket–ramjet/scramjet engine, a combined-cycle propulsion system where the principal element is a rocket ejector ramjet/scramjet. The rocket ejector provides both thrust and low-speed compression. The rocket ejectors in the ramjet/scramjet are fuel ejectors when the thrust/compression augmentation is not required. Jean Vandenkerckhove's "Hyperjet" was in this class of engines.

(4) The fourth category is a combined-cycle based on a thermally integrated rocket and turbojet (often cited in the literature as "KLIN" cycle). In this case, thermal integration provides the turbojet pre-compressor air cooling for higher Mach number operation and greater thrust; the thermal energy recovered from the turbojet improves the rocket expander cycle operation. Invented by V.V. Balepin, formerly at the TsIAM Russian center, it is the only such known thermally integrated, turbine-based, combined-cycle propulsion system.

(5) The fifth category is a combined-cycle consisting of an airbreathing rocket thermally integrated with a rocket

ejector ram/scramjet. This system was first reported by Rudakov and Balepin (1991) at an SAE Aerospace America Conference in Dayton, Ohio.

(6) The sixth category is the thermally integrated engine combined-cycle propulsion analogous to the fifth category, except the thermally processed air is separated into nearly pure liquefied oxygen (so-called "enriched air") and oxygen-poor nitrogen, with the liquid oxygen-enriched air stored for later use in the rocket engine. The oxygen-poor nitrogen is introduced into the ramjet engine creating a bypass ramjet. With the greater mass flow and reduced exhaust velocity, the propulsion efficiency is increased.

(7) There is a seventh category spanning the above categories. In fact, the engines discussed in the above are all continuously running engines. In World War II, the V-1 flying bomb was powered by a pulsejet. This engine is an intermittently firing engine, consisting of an acoustically tuned pipe fed an explosive mixture that, when ignited, sends the combustion products wave traveling down the pipe. After the products exit the tube, the tube is effectively scavenged. New fuel is then injected and a new mixture forms, reloading the tube. The ignition process is then repeated, starting a new cycle. This periodic operation gives the pulsejet a characteristic cyclic rate and the characteristic sound that in the V-1's case gained it the nickname of the "buzz bomb," The modern development of the pulsejet is the pulse *detonation* engine, or PDE, where the volumetric explosion is replaced by a thin detonation wave, with a drastic increase of burning rate and power available, see for instance (Holley et al. 2012; Cocks et al. 2015). Three PDE versions of the continuous operation engines are included in the discussion at the end of this chapter. The first is a pulse detonation rocket (PDR) and the remaining two are the PDE-ramjet and the PDE-scramjet combined-cycles. More recently, rotating detonation engines (RDE) are being tested in the USA and France, where the detonation wave burns fuel and air while continuously rotating rather than by traveling axially (Cocks et al. 2016). Note that this subject is proprietary in France, being developed by MBDA for the military, and it is subject to ITAR (International Traffic in Arms Regulations) in the USA.

There is a discussion of each engine cycle in this chapter. However, before we can proceed, there are operational considerations giving additional insights into the application of the propulsion system to a launcher; these are presented in Table 4.4. There are three general performance groups: (1) one that has no airbreathing capability, (2) another that can reach Mach 5 to 6 airbreathing, and (3) the last group that can reach Mach 6 to 14, again in airbreathing operation. The nominal SSTO mass ratios to orbital speed and the normal airbreathing speeds at their transition to rocket propulsion are given in the top rows. As with all launchers, if the mass ratio is less than four, horizontal takeoff is not possible, and vertical takeoff with horizontal landing (VTHL) must be the takeoff and landing mode assumed.

In Table 4.4, the term "abortable on launch" is the capability of the launcher to safely abort the mission while being *on launch* and to *return* to the launch site. This does not just consist of an escape rocket firing and a payload capsule being recovered. It means, in aircraft terms, that the system aborts the launch and returns intact and functional to the launch or adjacent alternate site. The only vertical launch rocket that aborted its launch after an engine failure and landed vertically and safely on its launch pad was the McDonnell Douglas Astronautics experimental rocket, the Delta Clipper (Butrica 2003; Stine 1996; Hannigan 1994). The late astronaut Pete Conrad was flight director, and Dr. William Gaubatz was program manager. Other than current aircraft, no other space launcher has ever demonstrated that capability. One of the limitations to achieving abort on launch is indeed the mass of the oxidizer carried. The Delta Clipper had only a mass ratio of about 2.5. Had it been an operational orbital vehicle with a mass ratio of about nine, it may not have been abortable. If commercial space is to happen, in the authors' opinions it will be necessary to recover the launcher, functional and intact, and this capability is dramatically influenced by the oxidizer mass carried. It should be remembered that the oxidizer mass is always many times greater than the fuel mass; it is the oxidizer that affects the mass of the propellants the most.

Reuse and sustained operations imply that the returned vehicle is ready for another flight after an inspection. With today's rocket engines this is improbable, because they are designed for minimum weight and not for sustained use as aircraft engines are. Designing rocket engines for sustained use would require readopting the philosophy in place for the XLR-129. Flights before overhaul are indicative of an operational system that has sustained operational capability avoiding refurbishment after every launch. In 1964, the goals for the vehicle (McDonnell Douglas Model 176) to support the MOL and the XLR-129 were 100 flights before overhaul.

One of the serious impediments to commercial operations is that there is only one launch site available per launcher, with the exception of the Sea Launch platform, that can be towed to any oceanic location. This may be acceptable for the commercial communications satellite organizations, just as operations from one coal mine were acceptable for the first commercial railroad train in York, England. A commercial space transportation system will have to have the

Table 4.4 Comparison of continuous operation propulsion cycles

Characteristics	Continuous operation propulsion system concepts						
Propulsion concept	Rocket	Rocket-derived	Airbreather rocket	Turbojet-rocket combined cycle	Ejector rocket combined cycle	Airbreather rocket combined cycle	ACES
Candidate cycles	Topping, expander cycle	Air-augmented or ram rocket	LACE or deeply cooled	KLIN	Strutjet or ram/scram and rocket	LACE, or deeply cooled and ram/scram	LACE, deeply cooled and ram/scram
Category	First	First	Second	Fourth	Third	Fifth	Sixth
SSTO mass ratio (LEO) (–)	8.0–9.0	6.5–7.5	5.0–6.2	5.0–5.5	4.0–5.4	3.2–4.2	2.5–3.5
Airbreathing speed (Mach)	0	~5.0	5.0–6.0	~5.5	6.0–14	6.0–14	6.0–14
Abortable on launch	Improbable	Questionable	Possible	Possible	Likely	Yes	Yes
Reuse/sustained operation	No	Possible	Yes	Yes	Yes	Yes	Yes
Flights before overhaul (–)	100[a]	100	200	200	300	500	600
Onboard oxidizer (%)	Maximum	90	55	55	40	30	<10
Applicable to TSTO	Possible	Possible	Yes	Yes	Yes	Yes	Yes
Basing	Fixed	Fixed	Fixed	Multiple	Multiple[b]	Multiple	Multiple
Takeoff/landing	VTHL	VTHL	VTHL	VTHL	VTHL	HTHL option	HTHL
Configuration	External	External	Hypersonic	Hypersonic	Integrated	Integrated	Integrated
concepts	Tank + glider	Tank + glider	Glider	Glider	Airbreather	Airbreather	Airbreather

All can carry personnel or payload, but are automatic, autonomous vehicles
[a]80+ flight ground test without overhaul demonstrated by RD-0120
[b]Operates from numerous non-space launcher bases

characteristics of a UPS or Federal Express system to be truly commercial. Until the launchers are designed for a lower mass ratio, say, 4 or less, that will not be practicable. When a mass ratio of 4 or less is achieved, the entire concept of operations will change, because with the correct hypersonic configuration and propulsion system the time-consuming vertical assembly, fueling and month-long countdown will be eliminated. Runway operations will become the norm, opening more launch and return sites for distributed operations. Orbital plane changes and offset maneuvers will be far more economical when executed in ascent and not from orbit.

Another item in Table 4.4 is "applicable to TSTO." This is an important consideration. Most of the analysis discussed in this chapter is done for SSTO because this requires only one vehicle, it offers the best approach for sustained operations, and represents the most challenging. However, SSTO can create the impression of being a one-size-fits-all solution. The advantage of a TSTO solution is the payload to orbit flexibility. A SSTO with a 7 t (15,435 lb) payload to orbit is a hypersonic vehicle with an operational empty weight (OEW) of about 70 t (154,300 lb) and a gross weight (TOGW) of about 380 t (837,900 lb). That is a mass ratio to orbit of 4.9. The payload to Earth orbit is 10% of the vehicle empty weight that carries it. This means, whether people or support supplies, the payload is always 7 t. However, a hypersonic glider, that is the second stage of a TSTO, with a 7 t payload can be carried by a first stage that stages at Mach 11 and that has an OEW of about 35 t. Then, the payload to Earth orbit is 20% of the empty weight of the vehicle carrying it. The first-stage OEW is about 38 t, for a total empty weight of 73 t (161,000 lb). The total gross weight of the two stages is about 210 t (463,000 lb), with the second-stage gross weight at about 94.5 t (208,500 lb). That means a total mass ratio of 5.0. If the second stage is a cargo-only expendable cylinder, then for the same gross second-stage weight the payload would be about 17.5 t (38,600 lb). Then, the payload to Earth orbit is 50% of the vehicle empty weight that carries it. The gross weight is the same, so the mass ratio is the same. Thus, there is much more flexibility in the payload variety and weight that can be delivered to Earth orbit by the TSTO vehicle concept. In addition, the offset or orbital plane

maneuver would be carried by the first-stage flying as an aircraft in the atmosphere, not the stage reaching orbital speed and altitude (Czysz and Vandenkerckhove 2000). The propulsion conclusions apply to TSTO as well as SSTO.

4.8 Rocket-Derived Propulsion

Rocket-derived propulsion systems begin with the liquid-propellant rocket. Propellants are injected into a combustion chamber to burn at high pressure and temperature, and then their products exit via a sonic throat into an expansion nozzle that is designed to match the nozzle exit static pressure to the ambient atmospheric pressure, as shown in Fig. 4.2. For maximum performance, the nozzle exit pressure should be equal to the surrounding ambient pressure. However, atmospheric pressure ranges from 14.696 psi (101.3 kPa) at the surface to zero in space. Normally the nozzle size is specified by the area ratio, i.e., the exit area divided by the sonic throat area. The area ratio determines the ratio of the nozzle exit pressure to the chamber pressure. Once the chamber pressure is determined, then the exit pressure is determined. If the nozzle exit pressure is higher than the ambient pressure, the nozzle is termed "underexpanded" and the result is the nozzle flow suddenly expanding upon exiting the nozzle. When you see a picture of a rocket at high altitude or in space and see the exhaust blossoming into a large plume, this is an underexpanded nozzle. If the nozzle exit pressure is lower than the ambient pressure, the nozzle is termed "overexpanded" and the nozzle flow separates from the nozzle wall at a location that yields the approximate correct area ratio for the ambient pressure. If you see a picture of a rocket lifting off from a launching pad, you can see the flow exiting the nozzle is smaller in diameter than the actual nozzle diameter, a sign that this is an overexpanded nozzle.

Engines such as the Pratt & Whitney RL10-3 have a two-position nozzle. At lower altitudes, the nozzle area ratio is small (10–20). As the altitude is increased and the area ratio becomes too small, a nozzle extension slides over the nozzle increasing the area ratio (50–60). Thus, there are two altitude regions where the engine is correctly matched to the ambient pressure.

For most high-thrust rockets, the propellants are a fuel and an oxidizer. For some space maneuver and station-keeping rockets, the fuel is a monopropellant that is decomposed by a catalyst into gaseous products.

Rocket-derived propulsion involves installing the rocket as a primary nozzle in an air ejector system. The rocket induces airflow in the secondary air system, thereby increasing the total mass flow through the system. These systems are generally operated up to Mach 6 or less, because of pressure and temperature limits of the air induction system. At Mach 6, the inlet diffuser static pressures can typically equal 10–20 atmospheres and 3000 °R (1666 °K). These propulsion systems can offer major advantages when applied to existing rocket launchers (Czysz and Richards 1998) and are described below.

1. Chemical rocket. Figure 4.13 represents a typical turbopump-fed liquid-propellant rocket. A turbopump is generally a centrifugal compressor to pressurize the fuel, coupled to an expansion turbine driving the pump. The turbopump pressurizes the propellant feed system to the pressure required for engine operation. For the turbopump to function, some fuel and oxidizer are burned in a separate combustion chamber to generate the hot gases necessary to power the turbine, powering in turn the pump. Because this burned propellant does not contribute to the primary thrust of the rocket engine, the turbopump cycle rocket (such as the Rocketdyne J-2 for the Saturn V) has the lowest specific impulse, I_{sp}, for a given propellant combination.

A hydrogen/oxygen high-pressure engine has an I_{sp} of about 430 s. In the so-called "topping cycle" (such as in the Rocketdyne SSME), the turbopump exhaust, which is still rich in fuel, is introduced into the rocket motor, contributing to the engine total thrust. A hydrogen/oxygen high-pressure engine using this cycle has an I_{sp} of about 455 s. In an "expander cycle" (such as Pratt & Whitney RL-10), a liquid fuel, such as hydrogen, is vaporized and raised in temperature by passing through the engine cooling passages. The hot gases then drive an expansion turbine to drive the turbopump before being introduced into the combustion chamber. This engine has the highest I_{sp} for a specific propellant. A hydrogen/oxygen high-pressure engine has an I_{sp} of about 470 s. Some representative propellants are given in Table 4.5 with hypergolic propellants in bold. Hypergolic propellants are those that spontaneously ignite on contact with each other; monopropellants are in italics.

The chamber pressure assumed in Table 4.5 is 1000 psia (about 68 atmospheres), yielding the specific impulse values given in a nozzle with optimum area ratio. The I_{sp} is the thrust developed per unit mass flow and per second (lb/(lb/s)) or kg/(kg/s)). The I_{sp} is a function of the combustion temperature, chamber pressure, and the thermodynamics of the products of combustion. Since the thrust per unit mass flow is constant, the rocket engine thrust is a function of the total mass flow. Given the combustion temperature, the mass flow depends on chamber pressure and engine throat area. To obtain more thrust, either the pressure can be increased for the same size engine or the size of the engine can be increased. The rocket motor is necessary for space propulsion because it is independent of any atmosphere. Although a turbopump rocket engine is shown in Fig. 4.13, for some if not most, space applications, the propellant tanks are pressurized to feed propellant into the engine and there are no turbopumps.

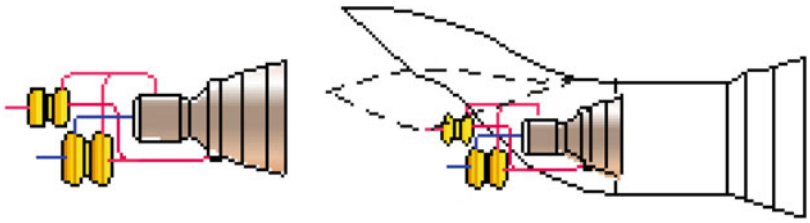

Fig. 4.13 Rocket-derived propulsion (*left* liquid-propellant rocket; *right* air-augmented rocket, ram rocket). *Blue* oxidizer. *Magenta* fuel. Pump and its turbine driver share a common shaft

Table 4.5 Representative propellants and their characteristics

Fuel	Oxidizer	I_{sp} (s)	SG·I_{sp} (–)[a]	*O*/*F* (–)
UDMH	**N_2O_4**	**319**	**390**	**1.23**
Hydrazine	**H_2O_2**	**304**	**375**	**2.04**
Hydrazine	**N_2O_4**	**312**	**365**	**2.25**
JP-4	LOX	329	330	2.40
Nitromethane	–	*273*	*308*	*Monoprop.*
Methyl alcohol	LOX	297	282	1.15
Methane	LOX	329	247	2.33
Hydrazine	–	*218*	*219*	*Monoprop.*
Hydrogen	N2O4	349	207	11.5
Hydrogen	LOX	455	170	6.00

[a]The product of specific impulse and the specific gravity (SG) of the propellant is termed density specific impulse and was used by the late V. Glushko of the GDL OKB to show the performance advantages of hypergolic propellants. All the I_{sp} are in vacuo

This is to clarify that the question of airbreather engines versus rocket applies only to flight in the Earth's atmosphere and concerns the large weight of oxidizer required by rockets, which increases the gross weight of the vehicle and increases the thrust of the rocket engines accordingly. Thinking along these lines, it appears intuitive that one way to increase the thrust of the rocket, for the same propellant flow, is to make it an "air-augmented" rocket.

2. Air-augmented rocket. Figure 4.13 employs the rocket motor as a primary ejector (Harper and Zimmerman 1942; Nicholas et al. 1996), so some of the external airstream can be mixed with the rocket exhaust to increase mass flow, thereby increasing thrust and specific impulse. These systems are generally operated up to Mach 6 or less, because of pressure and temperature limits of the air induction system. At Mach 6, the inlet diffuser static pressures can typically equal 10–20 atmospheres and 3000 °R (1666 °K). The rocket motor operates on its normal oxidizer-to-fuel ratio. The reduction of the mass-averaged exhaust velocity at low speed increases propulsion efficiency.

This simple concept is not designed to burn the oxygen in the entrained air. The weight ratio is reduced for an SSTO from 8.1 to 7.5. The sketch in Fig. 4.13 is notional, but the use of an inward-turning inlet with a variable capture area offers high mass capture tailored to the Mach number and provides high-pressure recovery. The retractable feature eliminates inlet drag at higher Mach numbers. True, the external air inlet system adds empty weight, but with a mass ratio reduction of 0.60, the air induction system weights less than the rocket, if the inlet system is less than 8% of the dry weight.

3. Ram rocket. Figure 4.13 is an air-augmented rocket cycle where the rocket is operated at a fuel-rich oxidizer-to-fuel ratio, so the oxygen in the entrained air can now burn the excess fuel at the normal airbreathing air/fuel ratios for the fuel used. Scherrer gives an excellent evaluation of the air-augmented rocket and the ram rocket based on ONERA research (Scherrer 1988). The external airstream is mixed with the rocket exhaust to increase mass flow. Combined with the combustion of the excess fuel, thrust and specific impulse increase at lower Mach numbers ($M < 6$). The weight ratio is reduced for an SSTO from 8.1 to 6.5. The sketch in Fig. 4.13 is notional, but the use of an inward-turning inlet with a variable capture inlet feature offers high mass capture tailored to the Mach number and provides high-pressure recovery.

The retractable feature eliminates inlet drag at higher Mach number. The external air inlet system adds empty weight. But with a mass ratio reduction of 1.6, the air

induction system weights less than the rocket if the inlet system is less than 24% of the dry weight. This is the better operational mode compared to the air-augmented rocket.

Neither of these latter two rocket configurations have found any significant applications yet, because of the opinion that the air-induction system might be too heavy for the benefit provided. That is very close to true for the air-augmented rocket, but it is not true for the ram rocket. A significant reduction in mass ratio can be realized for about a 5% increase in empty weight. Aircraft such as the SAAB-Scania Viggen, in fact, employ this method to increase the thrust of the gas turbine engine. The exhaust nozzle is an ejector nozzle, where the primary gas turbine exhaust induces ambient air into a secondary nozzle-mixer flow (Roed 1972).

4.9 Airbreathing Rocket Propulsion

Airbreathing rocket-derived propulsion systems are generally operated up to Mach 6 or less, because of pressure and temperature limits of the air-induction system (Miki et al. 1993). At Mach 6, the inlet diffuser static pressures can typically equal 20 atm and 3000 °R (1666 K). Airbreathing rocket propulsion concepts employ a method to reduce the temperature of air entering the inlet system; hence it can be compressed to rocket chamber operating pressures with reduced power requirements. There are two options: (1) One option is to deeply cool the air just short of saturation and use a turbo-compressor to compress the cold gaseous air to the rocket chamber pressure and inject it into the combustion chamber; (2) the second option is to liquefy the air and use a turbopump to pump the liquid air to rocket chamber pressure, then gasify it for injection into the rocket chamber, see Fig. 3.4. The rocket motor operates at nearly normal oxygen-to-fuel ratios, except that there is now a large mass of nitrogen also introduced into the combustion chamber. Again, the mass average exhaust velocity is reduced and the total mass flow increased, increasing thrust and propulsion efficiency.

4. Liquid air cycle engine, LACE rocket. Figure 4.14 is the rocket part of the Aerospace Plane propulsion concept developed by The Marquardt Corporation in the mid- to late-1950s, see Fig. 4.15.

The LACE (Liquid Air Cycle Engine) concept has been developed in Russia (Rudakov and Balepin 1991; Balepin and Tjurikov 1992; Balepin et al. 1993, 1995), Japan (Togawa et al. 1991; Miki et al. 1993; Ogawara and Nishiwaki 1989), and India (Gopalaswami et al. 1988). The thermodynamic principle of LACE is that a significant fraction of the energy required to liquefy the hydrogen is recoverable as available energy that can be converted to useful work. For a hydrogen-fueled aircraft, atmospheric air is an enormous source of energy, because of the 220–230 K temperature difference. Via a hydrogen/air heat exchanger, atmospheric air can be cooled as the liquid hydrogen is boiled, requiring no energy expenditure from the aircraft's systems. Ahern (1983, 1992) was associated with the development of the first LACE system in the USA when working with the scramjet team at The Marquardt Company in 1958. As part of that work, Ahern proposed a closed helium heat pump that avoided the problem of having two phase changes in the hydrogen/air heat exchanger (air being liquefied as hydrogen is gasified) and of having a hydrogen heat exchanger in the air inlet. To the author's knowledge, this concept has never been developed beyond the laboratory stage. Ahern also had a concept of recovering the aircraft aerodynamic heating with the hydrogen flow to the engine, and using that energy to create useful work (electrical, hydraulic, and air handling work) and engine thrust (thrust from supersonic hydrogen fuel jet injected into the scramjet combustor). This will be further discussed in the section on ramjets/scramjets.

As depicted in Fig. 4.14, this cycle employs a hydrogen/air heat exchanger in the air inlet to capture the inlet air kinetic energy from the incoming air and to cool it to nearly saturation. The cooled air is then pressurized to a few atmospheres and then flows into the pressurized liquefying heat exchanger. The total thermal energy collected from the incoming air and hydrogen combustion chamber is used to drive an expansion turbine, which in turn drives a turbopump that pumps liquefied air into the rocket motor. A rocket motor combustion chamber heat exchanger is necessary to provide sufficient energy to drive the turbomachinery (Tanatsugu et al. 1987). In effect the rocket becomes an airbreathing rocket for Mach numbers less than 6. In this concept, there is no need for another airbreathing engine. This cycle reduces the mass ratio to the 5.0–5.8 range and the oxygen-to-fuel ratio to about 3.5.

5. Deeply cooled rocket. As depicted in Fig. 4.14, this cycle employs a hydrogen/air heat exchanger in the air inlet to capture the inlet air kinetic energy from the incoming air and cool it to nearly saturation. Unlike the LACE cycle, the next step is to compress the cold air via a turbo-compressor. This controls the air temperature entering the compressor and limits the work of compression and the compressor corrected speed. The warmed hydrogen then enters the rocket combustion chamber to recover additional energy. The total thermal energy collected from the incoming air and hydrogen combustion chamber is then used to drive an expansion turbine, which in turn drives a turbo-compressor that compresses the cooled inlet air. That air can be cooled to nearly saturation by the hydrogen flow, then compressed to rocket operating pressures and introduced into the combustion chamber.

This cycle was independently developed at TsIAM (Rudakov and Balepin 1991) and by Alan Bond for

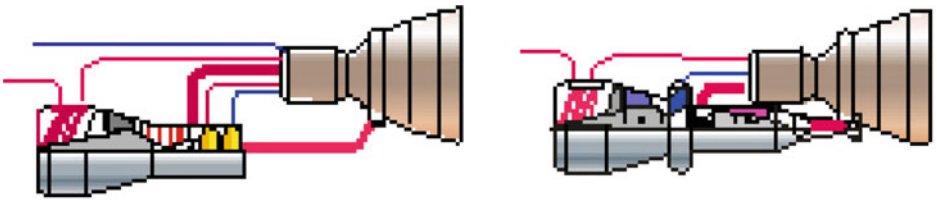

Fig. 4.14 Airbreathing rockets (*left* LACE rocket; *right* deeply cooled rocket). The cooling heat exchanger is the structure ahead of the compressor. See text for operation

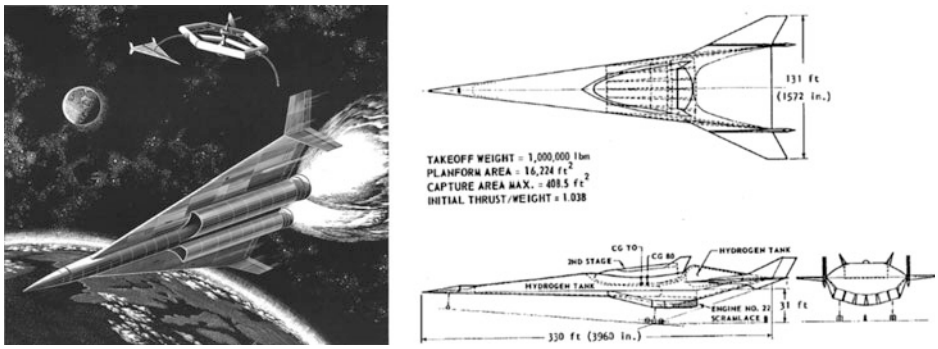

Fig. 4.15 Marquardt's first generation (1963) (Anon 1963) and second generation (1966) (Escher 1966) baseline Aerospace Plane (ASP) with scramjet engine

HOTOL. A rocket motor combustion chamber heat exchanger is necessary to provide sufficient energy to drive the turbomachinery in an expander cycle. Both Rudakov and Balepin of TsIAM and Tanatsugu of JAXA, Japan, employ heat exchangers in their rocket combustion chamber. Alan Bond did not for the HOTOL engine, as it could have adversely affected its performance at higher Mach numbers. In effect, the rocket becomes an airbreathing rocket for Mach numbers less than 6. In this concept, no other airbreathing engine is required. This cycle reduces the mass ratio to the 5.2–6 range and the oxygen-to-fuel ratio to about 3.4. There is a significant discussion of whether a liquefying system is equivalent in weight to a deeply cooled gaseous system. In most studies the authors are aware of, it is an even trade-off and other considerations should be used to make the selection.

With a suitable inlet system, airbreathing rockets can be integrated into flat-bottomed hypersonic glider configurations, see Fig. 3.9, as the forebody compression system required by a ramjet/scramjet, see Fig. 4.2, is not needed. Figure 4.16 shows such an inlet, an inward-turning, variable capture area inlet (DuPont 1999), that has been wind tunnel tested to Mach 5 plus. The mechanical details are not shown, but the mechanical actuation and integration is similar to the movable ramps on current supersonic military fighters. The movable lower inlet can be designed to retract flush with the lower surface when not in use. Since the outer surface of the lower cowl is the only surface that experiences entry heating, this system is much lighter than an outward-turning inlet. Note that in the low-speed position, the exit of the lower ramp flow is parallel to the lower vehicle moldline. Thus, all of the inlet structure is inside the fuselage moldline except the lower movable ramp. The inlet has the advantage of turning the flow inward, so there is no bulge in the moldline produced by an outward-turning inlet, such as the half-conical 2-D or pitot inlets on the Dassault Mirage aircraft. It also has the advantage of changing capture area to match the increasing corrected airflow requirement as speed is increased. The inlet meets or exceeds the military inlet recovery specification over the entire Mach range.

This class of propulsion systems can be airbreathers to Mach 5.5, and it is not necessary to have a fully developed airbreather configuration like the Mach 6 Lockheed Martin HTHL SSTC (single-stage to cruise) hypersonic cruiser SR-72, or the Mach 12 McDonnell Douglas HTHL SSTO accelerator, see Fig. 4 found in the *Introduction* chapter. Overall, a variable capture inward-turning inlet, integrated into a non-propulsion contoured flat-bottom hypersonic glider configuration, provides a satisfactory system (Balepin and Hendrick 1998). Figure 4.17 shows an inward-turning inlet incorporated into a hypersonic glider configuration with the engine system represented in Fig. 4.14, the LACE or deeply cooled rocket propulsion system. The rocket is installed much as it would be for an all-rocket configuration.

In 1983, McDonnell Douglas proposed the TAV (transatmospheric vehicle) concept incorporating the DuPont variable capture area, inward-turning inlet concept. The baseline airframe was the AFFDL developed FDL-7 flat-bottom hypersonic glider configuration. Figure 4.18 shows four artist sketches made for a USAF TAV competition in 1983. Note the retractable inlet for a powered

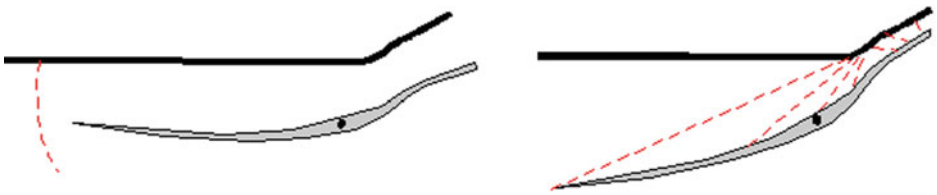

Fig. 4.16 Variable capture area, inward-turning inlet

landing with an airbreathing rocket. The USAF requested a horizontal takeoff machine (HTHL), and in doing so the gross weight increased by over a factor of 2. This is compared to the VTHL (vertical takeoff horizontal landing) configuration concept as implemented with the Boeing X-37 (Orbital Test Vehicle) (Weeden 2010) or the NASA selection of three private space companies including the Sierra Nevada Corporation Dream Chaser Spacecraft for commercial ISS resupply services as announced in early January 2016 (Morring 2016).

Note that the X-37 resembles a wing-body configuration, the Dream Chaser an all-body configuration (round-bottom lifting body), and the FDL-7 series an all-body configuration (flat-bottom lifting body). All three vehicle configuration concepts differ with respect to a multitude of attributes as introduced in Chap. 3. In summary, for a notional ISS return, all three vehicles would have significantly differing hypersonic glide and landing performances as expressed by down-range/cross-range capability, field performance, etc., overall dictating aspects like space operation (i.e., orbital waiting times), landing site selection and retrieval, and much more. The parametric sizing methodology introduced in Chap. 3 has been developed to correctly identify the *required* versus the *available* total vehicle solution space topography to directly support informed decision-making.

4.10 Thermally Integrated Combined-Cycle Propulsion

As the Mach number increases, the kinetic energy of the air increases with the square of the speed. As we have seen in Fig. 4.3, the kinetic energy of the air rapidly exceeds the thermal energy available to be transferred to the engine working fluid, air. The fraction of the combustion energy, rejected as unavailable for conversion to useful work, is also significant. In a modern turbojet engine, only about 23% of the fuel combustion energy is actually converted to thrust, and 44% is discarded out of the exhaust nozzle unused except to heat the atmosphere (Kroon 1952; Flack 2005). With commercial high bypass ratio engines, about 31% is converted to thrust. Then, it is critical to examine what part of the energy, which has been carried onboard the aircraft, has *not* converted to useful work or thrust. Any increase in the useful work conversion ratio reduces the propellant carried onboard, thus reduces the gross weight and the overall size of the vehicle. The result of this analysis and of many previous efforts has been the *thermally integrated* combined-cycle propulsion system.

The combined-cycle engine concept fundamental element began as a rocket ejector ramjet–scramjet (Stroup and Pontez 1968), thermally integrated into a rocket propulsion system, and that has a long history in hypersonics as early workers realized that the hypersonic vehicle in atmospheric flight must obey the rules of any thermodynamic cycle. An excellent discussion of the subject, by one who was already working in supersonic combustion engines in 1958, is by Curran (1993). Another early pioneer, Dr. Frederick Billig, added many insights into the advantages of thermal integration (Billig 1993). Other countries were also working on thermally integrated concepts, and one excellent source is from TsAGI (Lashin et al. 1993). In the class of integrated ejector ram–scramjet propulsion, the integral rocket ejectors provide both thrust and compression at lower Mach numbers (Buhlman and Siebenhaar 1995a, b). The combination of a separate ramjet and turbojet results in poor acceleration. However, the introduction of a deeply cooled turbojet thermally integrated with an expander rocket (KLIN cycle)

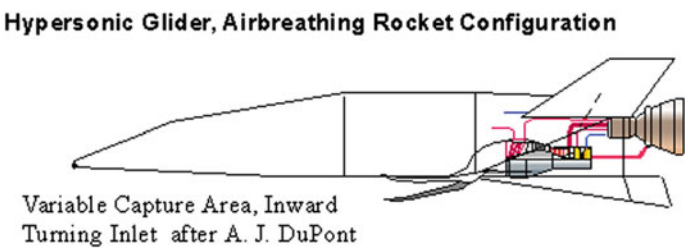

Fig. 4.17 Airbreathing rocket configuration concept

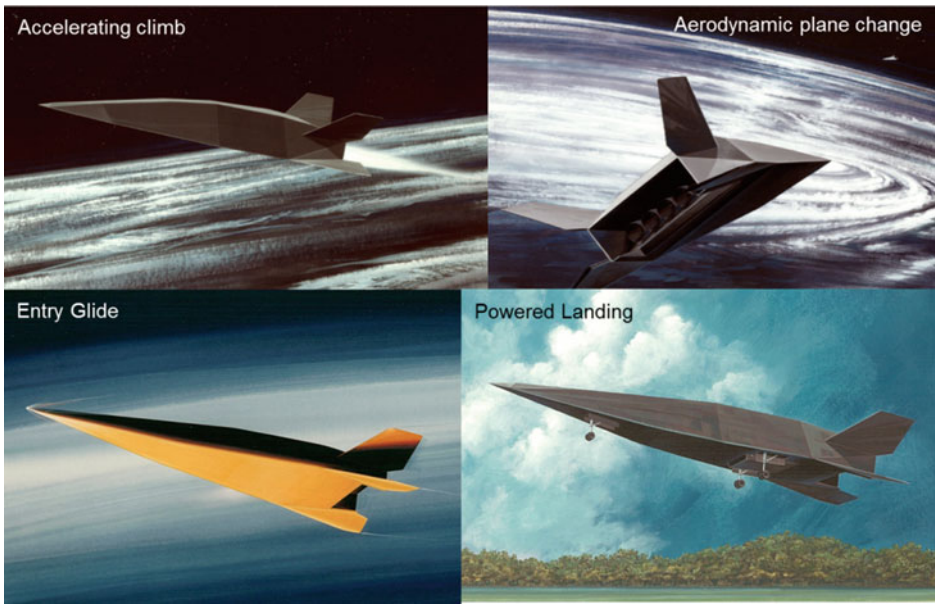

Fig. 4.18 McDonnell Douglas TAV concept from 1983

(Balepin and Hendrick 1998) is analogous to the rocket ejector ram-rocket–ramjet, with an additional benefit of excellent low-speed performance.

6. Deeply cooled turbojet-rocket (KLIN cycle). Figure 4.19 is an adaptation of Rudakov and Balepin's deeply cooled rocket ramjet into a deeply cooled turbojet-rocket. The turbojet and expander cycle rocket are thermally integrated (Balepin and Hendrick 1998). Unlike the ramjet, the pre-cooler on the turbojet keeps the compressor air inlet temperature low to reduce required compressor work and to increase mass flow and thrust. With the pre-cooler, the turbojet does not see the inlet temperature associated with higher Mach number flight, so it "appears" to be at lower flight speed. The pre-cooled turbojet provides a significant increase in transonic thrust. However, even with the increased transonic thrust, the turbojet remains a poor transonic accelerator. Clearly, the KLIN cycle operates with the rocket as a team. Whenever the turbojet thrust is not adequate to maintain a higher value of effective specific impulse, the rocket engine operates to add additional thrust and increases the effective specific impulse, as defined below. The specific impulse is given by

$$I_{\mathrm{sp}} = \frac{\text{Thrust}}{\text{Propellant flow}} = \frac{T_{\mathrm{rocket}} + T_{\mathrm{airbreather}}}{\dot{w}_{\mathrm{rocket}} + \dot{w}_{\mathrm{airbreather}}} \qquad (4.12)$$

We obtain the effective specific impulse

$$I_{\mathrm{spe}} = \frac{\text{Thrust-Drag}}{\text{Propellant flow}} = I_{\mathrm{sp}} \cdot \frac{\frac{T}{D} - 1}{\frac{T}{D}} \qquad (4.13)$$

Because of its lower thrust in the transonic region, a hydrogen-fueled turbojet is about equivalent in effective specific impulse to a hydrogen-oxygen rocket. In afterburner operation, the rocket outperforms the turbojet. Thermally integrated together, the combination is better that the sum of the individual engines, as demonstrated in Fig. 4.20. The thermal energy from both rocket and turbojet is used to power the expansion turbines that drive the propellant turbopumps. If there is remaining excess energy, it can be added to a heat exchanger upstream of the turbojet combustor. The pre-cooled turbojet provides operation from takeoff to Mach 5.5 with rocket thrust augmentation when required, such as in the transonic region. Above Mach 5.5, the turbomachinery is shut down, and the rocket operates as a conventional cryogenic rocket.

7. LACE rocket-ram–scramjet. Figure 4.21 is the engine family in Fig. 4.14 integrated with a ramjet. As in Fig. 4.20, the results with a LACE rocket will be similar to the deeply cooled rocket. The airbreathing rocket operates only to Mach 6 or less, so the companion engine is a subsonic through-flow ramjet. In this cycle, the thermal energy from the incoming air and hydrogen combustion is used to drive an expansion turbine that in turn drives a turbopump. A rocket motor combustion chamber heat exchanger is

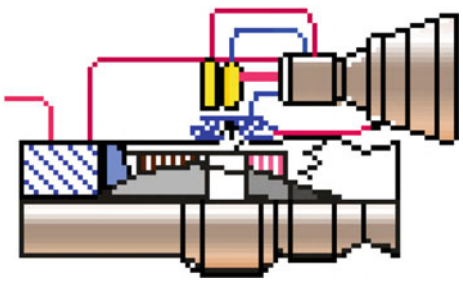

Fig. 4.19 Deeply cooled turbojet-rocket (KLIN cycle, thermally integrated turbojet-rocket)

necessary to provide sufficient energy to drive the turbomachinery. After leaving the expansion turbine, the hydrogen is introduced into the ramjet combustion chamber. The inlet air is cooled to nearly saturation by an air-hydrogen heat exchanger, and then pressurized to a few atmospheres. It then flows into the pressurized liquefying heat exchanger. The turbopump pressurizes the liquid air to rocket operating pressures, so it can be introduced into the rocket combustion chamber. After exiting the turbomachinery, the hydrogen is introduced into the ramjet combustion chamber.

At Mach 6 or less, the rocket is essentially an airbreathing rocket operating in parallel with a ramjet. The ramjet can convert to a supersonic through-flow engine (scramjet) at Mach numbers above Mach 6, but the rocket is now a conventional cryogenic rocket, not an airbreathing rocket. Above Mach 6, the rocket is normally not used when the scramjet is operating. After scramjet shutdown, the rocket operates as a conventional expander cycle cryogenic rocket.

8. Deeply cooled rocket-ram–scramjet. Figure 4.21 shows the integration of the deeply cooled cycle developed by Rudakov and Balepin at TsIAM and Alan Bond for HOTOL (Parkinson 1991) with a subsonic flow-through ramjet. In this cycle, the recovered thermal energy from the incoming air and hydrogen combustion in both, the rocket and the ramjet, is used to drive an expansion turbine, which in turn drives a turbo-compressor. The incoming inlet air is cooled to nearly saturation in an air-hydrogen heat exchanger, and then compressed to rocket operating pressure by the turbo-compressor so it can be introduced into the rocket combustion chamber. A rocket motor combustion chamber heat exchanger is necessary to provide sufficient energy to drive the turbomachinery. After leaving the expansion turbine, the hydrogen is introduced into the ramjet combustion chamber. At Mach 6 or less, the rocket is essentially an airbreathing rocket operating in parallel with a ramjet. Above Mach 6, the rocket is normally not used, and the ramjet operates as a supersonic through-flow ramjet (scramjet). After scramjet shutdown, the rocket operates as a conventional cryogenic rocket.

4.11 Engine Thermal Integration

When discussing propulsion, hypersonic flight or atmospheric entry, the question of cooling is always prominent; *cooling* implies discarding the rejected energy (Ahern 1983, 1992). *Thermal management* implies that a fraction of the rejected energy creates useful work or thrust (Barrère and Vandenkerckhove 1993). The concept of thermal management begins typically with two separate engines that are thermally integrated by having the fuel (in this case hydrogen) flowing through both engines before a portion of the collected thermal energy is extracted as useful work. This first example is limited to an airbreathing Mach number of 6, and the airframe is not a part of the thermal integration concept.

Figure 4.20 is from (Rudakov and Balepin 1991) and shows the performance of a Japanese LACE rocket with a pressurized liquefier, as part of a SCRJ-LACE system (Aoki and Ogawara 1988; Togawa et al. 1991; Yamanaka 2000, 2004), and of a Russian deeply cooled rocket, integrated with a ramjet (Rudakov and Balepin 1991). The solid line identifies the deeply cooled rocket by Rudakov. The central dashed line identifies a hydrogen ramjet by Rudakov. When simply *operated independently*, the combined thrust and fuel flow produces about a 500 s I_{sp} increase, as indicated by the lower dashed line identified as combination of rocket/ramjet. When *thermally integrated*, the fuel flows through both engines, collecting thermal energy from both rocket and ramjet, which is used to power the expansion turbines driving the turbo-compressor. The same two engines, when thermally integrated, provide a 1500 s increase in I_{sp} over the combination of rocket/ramjet, as indicated by the top dashed line.

Then, between Mach 2 and Mach 6, it is possible to have the thrust of a rocket and the specific impulse of a military subsonic turbofan, e.g., 4500–4000 s (specific fuel consumption from 0.8 to 0.9 kg/s per kg of thrust). This concept could be preceded by the development of the airbreathing rocket, which does produce a tangible benefit for operational

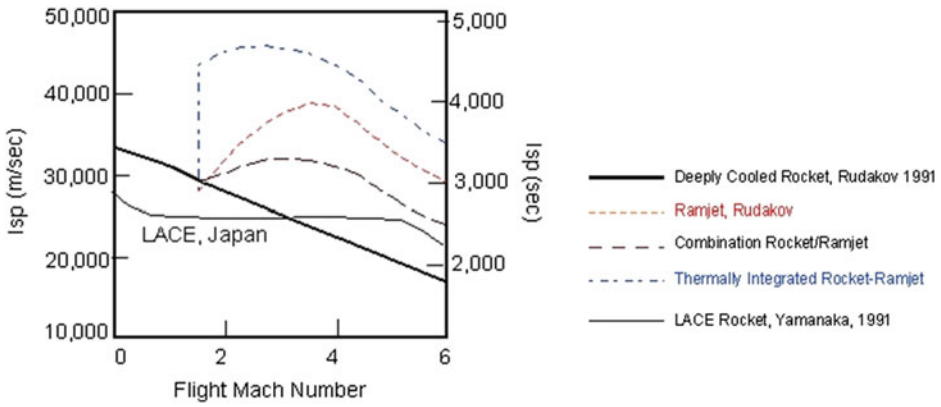

Fig. 4.20 Benefits of thermal integration from Rudakov and Balepin (1991)

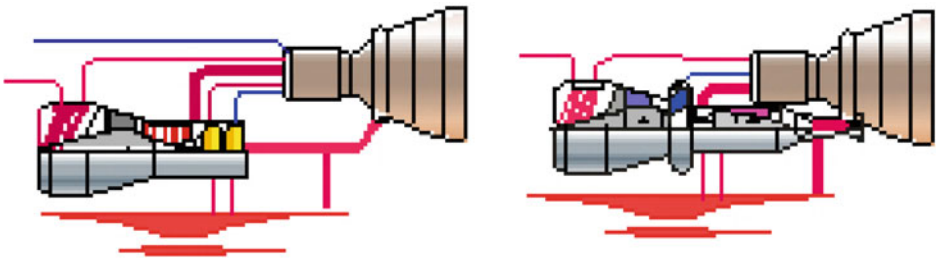

Fig. 4.21 Airbreathing rocket thermally integrated combined cycle. *Left* LACE-based combined-cycle. *Right* deeply cooled combined-cycle

launchers based on existing rocket engines and hardware technology. This initial step could deliver an interim operational capability in terms of a sustained-duration-use rocket launcher, in parallel with the development of the ramjet engine to be incorporated later into this propulsion system, eventually developing into a scramjet version of the ramjet. When these principles are applied to SSTO and TSTO launchers, size and weight (both dry and gross weights) are reduced.

These three propulsion systems could profoundly affect the size and weight of both SSTO and TSTO launchers if they were applied. Their advantage is that they are fabricated of tested and demonstrated hardware utilizing current industrial capability. Alan Bond and Alexander Rudakov were pioneers in the construction of actual hardware with operational potential; current work by Reaction Engines for the SABRE engine documents that it is possible to build integrated engines with technology already available (Davies et al. 2015). Unfortunately, today's status quo environment in aerospace propulsion steadfastly maintains rocket engines as the primary known standard, thus better than new concept solutions. Today, we observe a prevailing rocket advocacy to the exclusion of all or most else. A promising development in the UK has been the November 2015 announcement by BAE Systems plc and Reaction Engines Limited for BAE Systems of a strategic joint investment and collaboration to accelerate Reaction Engine's development of SABRE (Gallagher and Webster-Smith 2015). SABRE (Synergetic Air-Breathing Rocket Engine) resides in category (2) out of the 7 categories discussed here. It is an airbreathing rocket, where the propulsion elements are a rocket motor and an air/fuel heat exchanger that supplies the rocket motor with atmospheric air as oxidizer over part of its trajectory.

4.12 Total System Thermal Integration

When discussing propulsion in the context of hypersonic flight or transatmospheric vehicle ascent/entry, the question of cooling must be examined in the context of total energy management or integration. In the case of the SR-71, aerodynamic heating was mostly absorbed by the structure, having the surface operate at radiative equilibrium temperature. Then, the SR-71 is classified as a hot structure vehicle and therefore it required a material that maintained its strength at high temperature (i.e., in the 660 °C range and that was beta-titanium). During flight, the thermal energy had to be removed from the crew compartment and equipment bays. That thermal energy plus the thermal energy rejected by the engine both were transferred to the fuel. Discussions of the SR-71 design state that the fuel temperature entering the engine was over 600 °C (Merlin 2002; Goodall and Miller 2003). In this case, all of the thermal energy was discarded as hot fuel; note that hot fuel itself does not provide useful work or engine thrust. With a high-temperature coking hydrocarbon as fuel used as heat sink, this was a rational approach (utilizing the fuel as the heat sink for cooling purpose) as there was hardly any option to extract the recovered energy (heat) from the liquid hydrocarbon.

Let us now consider a system-level thermal integration approach. When synergistically utilizing fuel as a very capable heat transfer medium, the structural concept should be unlike the SR-71 *hot structure* and more like a *cold structure* protected by a combination of metal radiation shingles, radiating about 95% of the aerodynamic heating back to space. Structure cooling includes a *thermal management system* that converts about half of the thermal energy entering the airframe into useful work and thrust. Figure 4.22 illustrates a system-level thermal integration approach (Ahern 1992). The skin panels in the nose region, engine ramps and nozzle region, and the combustion module are one side of a heat exchanger system, which "pumps" aerodynamic heating into an energy extraction loop. The very cold hydrogen passes through skin panels that absorb the incoming aerodynamic heating. The energy extraction loop lowers the heat-absorbing hydrogen temperature and then passes it to another heat exchanger panel. Consequently, the liquid hydrogen goes through a series of energy additions and subtractions until it reaches the combustion chamber where it is injected as a high-speed hot gas producing thrust, see Figs. 4.4 and 4.23. This concept goes back to the original Aerospace Plane (ASP) effort for the US Air Force, to which The Marquardt Corporation was one of the

contractors, see Fig. 4.15. At that time, John Ahern worked with Charles Lindley, Carl Builder, and Artur Magar, who originated many of these concepts.

Figure 4.23 depicts a typical closed-loop heat pump loop identified in Fig. 4.22 as a rectangle with "EX" (exchanger) inside, and the fuel wall injection system. This particular loop is for one of the inlet ramps ahead of the engine module. The three heat exchangers form a closed-loop system, where thermal energy extracted from the skin panels is used to power an expansion turbine that drives the working fluid compressor. The *net work* extracted can be used to power electrical generators, hydraulic pumps, refrigeration units, or fuel boost pumps. With hydrogen as fuel, the vehicle is independent of ground power sources and can self-start as long as there is hydrogen in the fuel tanks. Eventually, the fuel reaches the engine module where it picks up the heat transferred to the combustor walls. When the hydrogen reaches its maximum temperature, it is injected into the combustion chamber via series of Mach 3 nozzles at a low angle to the wall. The size of the nozzles can be small and approach the equivalent of a porous wall. The result is that the hydrogen acts as film cooling for the wall, reducing the wall friction as well as the heat transfer rate. For a Mach 3 wall nozzle, the kinetic energy of the injected fuel also creates thrust.

The thrust per unit fuel flow, I_{spf}, is given in Eqs. (4.14a) and (4.14b) for hydrogen.

$$I_{spf} = 9.803 \cdot T^{0.5197}\ (\text{s})\ T \text{ in Rankine} \tag{4.14a}$$

$$I_{spf} = 13.305 \cdot T^{0.5197}\ (\text{s})\ T \text{ in Kelvin} \tag{4.14b}$$

At 2000 °R (1111 K), the hydrogen specific impulse is 509 s, or better than a hydrogen/oxygen rocket. For a scramjet engine with an equivalence ratio larger than one, this can produce 30% or more of the engines net thrust (Novichkov 1990a, b). Applying this approach and using Builder's Second Law, the impact of fuel temperature injected through Mach 3 nozzles in the combustor wall, see Fig. 4.24, can be assessed.

One measure of airbreathing engine performance is the energy conversion efficiency θ. The energy conversion efficiency is defined here as follows:

$$\theta = \frac{V \cdot T}{Q_c \cdot \dot{w}_{fuel}} \tag{4.15a}$$

$$\theta = \frac{V \cdot I_{sp}}{Q_c} \tag{4.15b}$$

$$\theta = \frac{V \cdot T}{Q \cdot \dot{w}_{air}} \tag{4.15c}$$

with

$$I_{sp} = \frac{\theta \cdot Q_c}{V} \tag{4.16}$$

and V the flight speed. At hypersonic speeds, the value of θ is almost constant, ranging between 0.55 and 0.60 from Second Law analysis (Builder 1964). That means that as speed is increased, the specific impulse must decrease. Figure 4.24 shows three I_{sp} values, decreasing from upper left to lower right. The top solid line is for an ideal engine with no internal losses. The middle solid line shows the I_{sp} from Builder's analysis including the losses from Swithenbank's injector system (Case 0, Fig. 4.5). This is the value of the I_{sp} if the vehicle was in cruise mode; that is, thrust equal to drag ($T = D$), with no acceleration. The bottom solid line shows the effective or acceleration I_{sp} based on engine net thrust minus aircraft drag, I_{spe}; this is the I_{sp} for an accelerating aircraft that must have thrust greater than drag. If there is no acceleration (that is, $T - D = 0$), then the value of effective I_{sp} is zero ($I_{spe} = 0$). The gray band is the sizing breakeven I_{sp} for a hydrogen/oxygen rocket and a hydrogen-fueled airbreather. Since the bulk volume of 100 kg of 6:1 liquid oxygen–hydrogen is 0.26 m^3, and that of 100 kg of subcooled liquid hydrogen is 1.34 m^3, the breakeven I_{sp} is a function of volume and I_{sp} together. As Mach 12 (13,050 ft/s) is approached, the propulsion system efficiencies become similar. That is, the propellant masses required to achieve a unit change in velocity are equal.

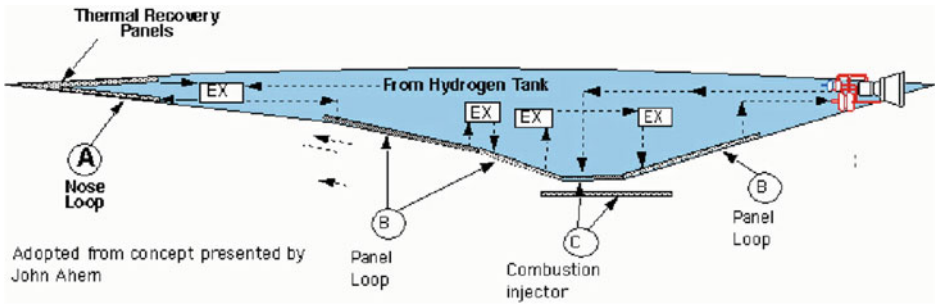

Fig. 4.22 System thermal integration

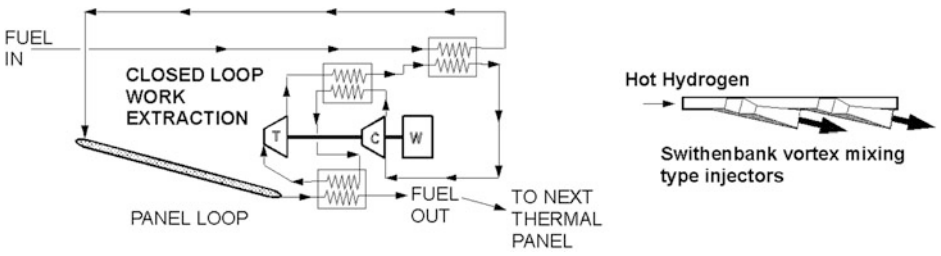

Fig. 4.23 Closed cycle heat pump (after Ahern) and combustor fuel injection. The external appearance of the Swithenbank injectors is shown in Fig. 4.4

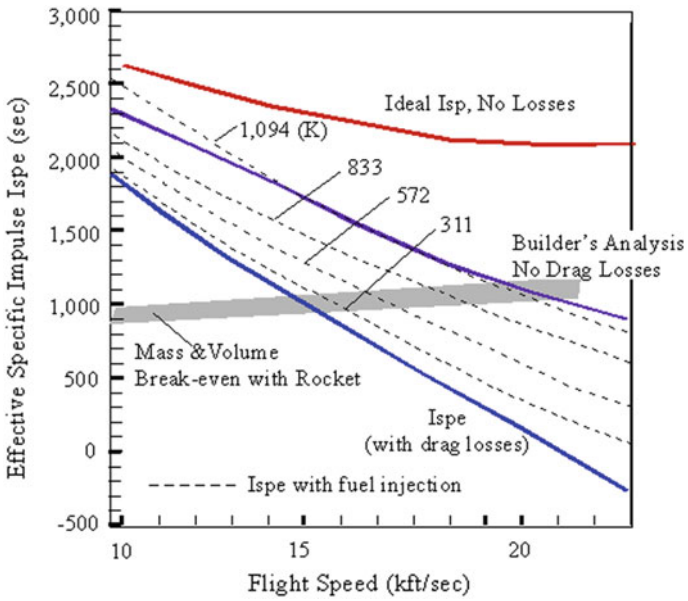

Fig. 4.24 System thermal integrated specific impulse

For some airbreathing systems, the rocket propellant mass required to achieve a unit change in velocity is less than for the airbreathing system, and so the volume requirements for the rocket propellant are about 1/5th that for the airbreather system. For the Swithenbank injectors, that breakeven speed is Mach 15.0 (16,312 ft/s). However, at the breakeven speed, the airbreather is just equal to the rocket, and even if no higher speed is sought, a higher I_{sp} is always welcome. That higher I_{sp} comes through system thermal management.

The impact of thermal management is illustrated in Fig. 4.24 by the four dashed lines for the specific impulse of the thermally integrated system. The temperature of the injected hydrogen is given in Kelvin. As the injected fuel temperature increases, the injected fuel energy offsets a greater fraction of the internal drag losses. If the injected hydrogen temperature can reach 1094 K (1969 °R), then all of the internal drag losses generated by the Swithenbank injector concept have been compensated for. The airbreathing engine energy and entropy limitations presented in Fig. 4.9 are still in effect. At Mach 15 flight speed, the effective I_{sp} can be increased by over 600 s. It requires a detailed engine analysis to quantify a specific value for a given system, but the general trend is correct. Recovered thermal energy can be converted into useful work and thrust to increase performance (Ahern 1992; Barrère and Vandenkerckhove 1993; Novichkov 1990a, b).

9. Ejector ram–scramjet-rocket. Figure 4.25 is an ejector ramjet thermally integrated with a rocket. The ejector may be a hot gas ejector and/or a rocket ejector. Remember, if the ramjet is a subsonic through-flow engine, then the scramjet is simply a supersonic through-flow engine. The maximum airbreathing speed can be selected from Mach 6 to at least Mach 14.5. At Mach less than 2, the system is an ejector ramjet analogous to a ram rocket system, except the rocket ejectors are distributed in the struts inside the ramjet engine module (Stroup and Pontez 1968). At Mach numbers greater than 2, the engine is a conventional ramjet with the rocket injectors now functioning as hot hydrogen injectors. Subsonic thrust is generated in the same manner as a ramjet, and the supersonic hydrogen injection acts as an aerodynamic isolator. Above Mach 6, it is a conventional scramjet engine with variable configuration injectors to minimize internal drag as discussed earlier in this chapter (Gounko et al. 2000).

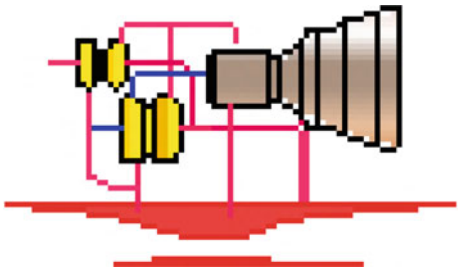

Fig. 4.25 Integrated ejector ram–scramjet-rocket

This propulsion concept was the backbone of the effort to create an airbreathing launcher and hypersonic cruiser discussed in conjunction with Fig. 3.13, and it represented the Marquardt effort from 1959 until 1963 to achieve the first aerospace plane (ASP) for the US Air Force shown in Fig. 4.15, and the effort of the Applied Physics Laboratory, Johns Hopkins University, to achieve a scramjet missile for the US Navy (Rife and Cantelon 2010; Werrell 1985). In all cases, the rocket community argumentations overpowered those supporting the advantages of airbreathing propulsion, and an all-rocket solution was adopted in every case.

There have always been, and still remain, arguments that scramjets will not work, and that the [notorious] analogy is with trying to light a match in a supersonic wind tunnel. However, Professor James Swithenbank of Sheffield University has the correct analogy, and that is lighting a match inside a Concorde traveling at Mach 2. Both, the surrounding air and the match are at the same relative velocity, as is the hot hydrogen which is injected into the engine via the injection devices, and assuming the supersonic flow-through airflow velocity and hydrogen injection velocity are matched to be the same. For the Mach 13 (14,137 ft/s) case shown in Table 4.2, the hydrogen injection velocity and the combustor through-flow speed would be the same at a gas temperature of 660 °C (933 K, 1220 °F). For a slower Mach 8 (8700 ft/s) case, the combustor through-flow speed is 7100 ft/s (Mach 6.53, 2164 m/s) and the hydrogen gas temperature required is a modest 293 °C (566 K, 585 °F). Then, in reality, the fuel and air are essentially at static conditions with very little differential speed and shear. Clearly, Swithenbank's analogy, that the scramjet is like lighting a match for a cigar while tasting *Champagne* on Concorde, is the correct one.

When one of the authors (P.A. Czysz) was a young engineer at Wright Patterson Air Force Base, he was assigned as Chief Engineer to the high temperature hypersonic tunnel at Hypervelocity Branch, Aircraft Laboratory at the Wright Air Development Division. The high-temperature hypersonic tunnel was a nominal Mach 4 wind tunnel heated with a zirconia pebble bed. Nominal air temperatures were in the range 2500–1500 K (4500–2700 °R). The pressure, temperature, and velocity in the test section were very close to those of a scramjet operating at a Mach 8 flight condition. The Aero-Propulsion Laboratory assigned Paul James Ortwerth and then Squadron Leader E. Thomas Curran to investigate the possibility of testing a scramjet combustor in the high-temperature hypersonic tunnel.

Squadron Leader Curran was familiar with the work Professor James Swithenbank was doing in a similar facility in Montreal, Canada. The result was an experiment that used the test section of the high-temperature hypersonic tunnel as a scramjet combustor. A 7.6-cm-wide flat plate model, 19 cm long with five hydrogen injection ports, located at 1/4th of the model length from the model nose, was placed in the 12.7 cm test section (Burnett and Czysz 1963). The model was installed on an injection system, so the duration of the time in the test section could be controlled. There were a series of pressure taps running down the model centerline. The gas plenum chamber in the model was equipped with thermocouples to measure the hydrogen temperature. Both color Schlieren and infrared ciné film (motion picture film format) recordings of the flow field were made. The infrared film was filtered to center on the high-temperature water emission radiation. Figure 4.26 shows two of only a few surviving photographs from the test; all of the original ciné film was burned to recover the silver.

In Fig. 4.26, the left picture is a color Schlieren with a horizontal knife-edge. The red above the model indicates a reduction in density, whereby the green/blue does indicate an increase in density. The shock waves from the model and gas injection are clearly visible. The red hydrogen injection is also clearly visible. The model plenum chamber thermocouple gave a hydrogen temperature of 300 ± 15 °C (573 ± 15 K), which is an indicator that the test section air and hydrogen speeds were very similar. From Table 4.2, the 7100 ft/s test section speed corresponds to a flight speed of 8000 ft/s as does the 2500 K stagnation temperature. The picture on the right is from the infrared film camera and clearly shows the water formation approaching the hydrogen injection holes, an indicator that combustion delay was minimal. Professor Swithenbank's data correlations for over 1000 test runs give a time to complete combustion of 35 ± 5 μs for gaseous fuels. At this airflow speed, the distance traveled is about 2.98 ± 0.4 in. (6.6–8.6 cm) and is very close to the data from the pictures. A later analysis showed a very close correlation between the schlieren and infrared pictures and thus confirmed the combustion distance from pressure measurement (Czysz 1993b). Then indeed, hydrogen will burn very well in a scramjet!

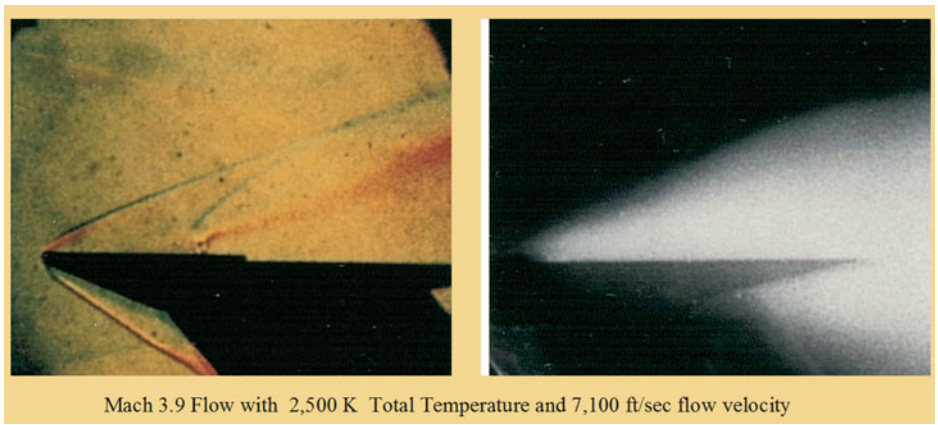

Fig. 4.26 300 °C hydrogen injected into supersonic air stream at flight conditions corresponding to a scramjet combustor for an aircraft flying at Mach 8 (tests circa 1962)

4.13 Thermally Integrated Enriched Air Combined-Cycle Propulsion

These cycles are thermally integrated combined-cycle propulsion systems analogous to the *LACE rocket-ram–scramjet* and the *deeply cooled rocket-ram–scramjet*, except the thermally processed air is separated into nearly pure liquefied oxygen (LEA: Liquid Enriched Air; LACE: Liquid Air Cycle Engine; and ACES: Air Collection Enrichment System) and gaseous nitrogen (OPA: Oxygen-Poor Air). This is possible because the boiling point of liquid oxygen is 90.03 K, and the boiling point for liquid nitrogen is 77.2 K. Just as in a fractionating tower for hydrocarbons, where hydrocarbons of different boiling points can be separated, the oxygen can be liquefied while the nitrogen remains gaseous.

This means that most of the oxidizer carried onboard the launcher is not loaded at takeoff but loaded during the flight to orbit. The result is that the carried oxidizer-to-fuel ratio at takeoff is less than for a non-ACES system. Thus, the takeoff gross weight and engine size are reduced. Whether also the volume (size) of the launcher is reduced depends on the volume of the ACES system (Bond and Yi 1993). The maximum weight of the launcher is then near the ascent climb to orbital speed and altitude, rather than at takeoff. The process is executed in steps, through temperature gradients where a fraction of the oxygen is liquefied at each step. As in all chemical processes, the difficulty increases as the oxygen purity increases, and for a flight-weight system there is a practical limit. The liquid-enriched air has purity in the 85–90% oxygen range and is stored for use in the rocket engine during the rocket ascent portion of the ascent trajectory. The oxygen-poor air contains 2–5% oxygen and is introduced into the ramjet, creating the equivalent of a mixed-flow bypass turbofan. That is, the mass-averaged exhaust velocity is reduced but the specific impulse rises, overall increasing engine mass flow and thrust.

Thermal integration means that the fuel passes through both rocket and scramjet to scavenge rejected heat and convert it into useful work before entering the combustion chambers. This increases the specific impulse while at the same time oxidizer is being stored for the ascent to space. Just as for the LACE and deeply cooled rocket, both rocket and ramjet must operate as an acceleration system until efficient scramjet operation is reached. The Mach number for air separation and collection is usually in the Mach 3 to Mach 5 region. The ACES cycle is a very good cycle for launchers that require a launch offset to reach an optimum launch latitude and time window, for instance, when the vehicle must cruise some distance until the ascent to orbit point is reached. This approach is applicable to SSTO vehicles. The ACES cycle has more significant payoffs for TSTO launchers that must fly an offset, because the air separation plant is in the first stage, not in the stage that continues its ascent to orbit.

A good example of this is reaching the ISS at 55° orbital inclination from Cape Canaveral, at 28.5° latitude. The Space Shuttle loses a significant fraction of its payload because of the propellant required to move the orbital plane during a rocket ascent. In order to rotate the orbital plane 26.5° requires a significant weight ratio increase to achieve low Earth orbit (this will be further discussed in Chap. 5). However, a "first stage" or carrier vehicle (with second-stage release at subsonic to hypersonic velocities utilizing an air-breathing engine) flying in the atmosphere can achieve the plane change with a much smaller fraction of the propellant required compared to the plane change using rocket thrust (Space Shuttle), because the first stage accomplishes the turn simply using aerodynamics. The rocket, during the acceleration-turning flight, has thrust at least twice its weight with an effective I_{sp} of around 400 s, while the aircraft has the thrust of 1/6th its weight with a specific impulse about 10 times larger, see Fig. 4.20. This expands the launch window because the launcher can fly to intercept the ascending node

of the desired orbit and not be confined to when the ascending node and launch site latitude coincide. The figure of merit for these systems is the weight of LEA collected per weight of hydrogen. A practical value is 6 kg of LEA per kg of hydrogen; for more details see (Czysz and Vandenkerckhove 2000). Examples of the thermally integrated enriched air combined-cycle propulsion are as follows:

10. ACES-LACE ejector ram–scramjet-rocket. Figure 4.27 shows an air collection and enrichment system (ACES) (Ogawara and Nishiwaki 1989) added to propulsion system #6. The liquid air is not pumped to the rocket immediately, but passed through a liquid fractionating system to separate the oxygen component as liquid-enriched air (LEA contains 80–90% oxygen) and nitrogen component as liquid oxygen-poor air (OPA contains from 2 to 5% oxygen) (Balepin 1996). The oxygen component is then stored for later use in the rocket ascent portion of the flight. The oxygen-poor nitrogen component is injected into the ramjet, to create a hypersonic bypass engine that increases engine mass flow, thrust and reduce the mass-averaged exhaust velocity. In the 1960s, hardware development was undertaken by the Linde Corporation under an Air Force contract. Sufficient hardware was fabricated to design the operational system and confirm performance. ACES most significant penalty is the volume required for the fractionating separator. For hydrogen-fueled hypersonic cruiser and transatmospheric space launchers, volume is a critical parameter, when increasing it becomes a significant size and weight penalty. However, this propulsion strategy can significantly reduce the takeoff perceived noise. ACES was invented for the same reasons a conventional mixed-flow bypass gas turbine was invented. ACES was originally proposed by the Air Force Aero-Propulsion Laboratory for the space plane of the late 1950s (Leingang et al. 1992; Maurice et al. 1992) and was the subject of intense investigation in the 1960–1967 time period (Leingang et al. 1992). Most of the original Air Force work was for a TSTO vehicle, although application to SSTO was investigated. For airbreather operation to the 12,000–14,000 ft/s range, its cycle can achieve weight ratios less than 3 with oxygen-to-fuel ratios approaching one-half.

11. ACES-deeply cooled ejector ram–scramjet-rocket. Figure 4.27 is an ACES option added to propulsion system #7. Even in the 1950s, the paramagnetic properties of liquid oxygen were noted by the LACE and ACES investigators (Leingang 1991). Patrick Hendrick was a graduate student under the late Jean Vandenkerckhove in 1988, when he observed that Siemens sold an exhaust gas analyzer measuring gaseous oxygen based on its diamagnetic properties. The magnetic susceptibility of oxygen at its boiling point (90.03 K) is 7699×10^{-6} in cgs units (centimeter-gram-second system of units), that is, as large as some chromium and nickel compounds.

During a visit to Jean Vandenkerckhove at his Brussels residence, Hendrick (1996) discussed his concept of gaseous air separation using the magnetic properties of oxygen. Collaboration with Vladimir V. Balepin resulted in the addition of a vortex tube pre-separator based on the small temperature difference in the liquid temperature of nitrogen and oxygen. The result was a new approach to the ACES concept with much lower total volume requirements than the liquid fractionating equipment. The deeply cooled gaseous air is not pumped to the rocket immediately, but passed first through a vortex tube initial separator (at this stage the LEA contains about 50% oxygen) (Lee et al. 2003a, b), and then into a cryogenic magnetic oxygen separator. The oxygen component is then liquefied as LEA (LEA contains 80–90% oxygen) and stored for use in the rocket ascent portion of the flight. The gaseous nitrogen component of oxygen-poor air (OPA) contains from 2 to 5% oxygen. The oxygen-poor nitrogen component is injected into the ramjet, to create a hypersonic bypass engine that increases engine mass flow, thrust and reduce the mass-averaged exhaust velocity.

At takeoff, this system can significantly reduce takeoff noise, for the same reasons a conventional mixed-flow bypass gas turbine was invented. This system is in the laboratory phase consisting of studies and testing, but has not as yet been developed as propulsion hardware. At this point in time, it has the potential to significantly reduce the volume and weight required for an ACES system, but is not yet proven. For airbreather operation to the 12,000–14,000 ft/s range, this cycle can achieve weight ratios less than 3 with oxygen-to-fuel ratios approaching one-half (1/2).

4.14 Comparison of Continuous Operation Cycles

To compare the continuous operation cycles, Fig. 3.5 is repeated as Fig. 4.28. In Fig. 4.28, weight ratio to LEO, that is the takeoff gross weight divided by the on-orbit weight, is represented for different engine cycles as a function of the net oxidizer-to-fuel ratio. These may be divided into two groups represented by (a) rocket-derived propulsion and (b) airbreathing rockets.

The rocket-derived propulsion class is represented by cycles: (1) rocket, (2) air-augmented rocket, and (3) ram rocket. For this class, the oxidizer-to-fuel ratio is essentially constant at a value of 6. As a ram rocket, the weight ratio to LEO decreases from 8.1 to 6.5. There is only a minimal payoff for the air-augmented rocket; without burning the oxygen in the air, there is insufficient thrust increase to make a significant difference in weight ratio.

There is a discontinuity in the oxidizer-to-fuel ratio curve between the rocket-derived propulsion value of 6 and where airbreathing propulsion begins, at a value of 4. The second

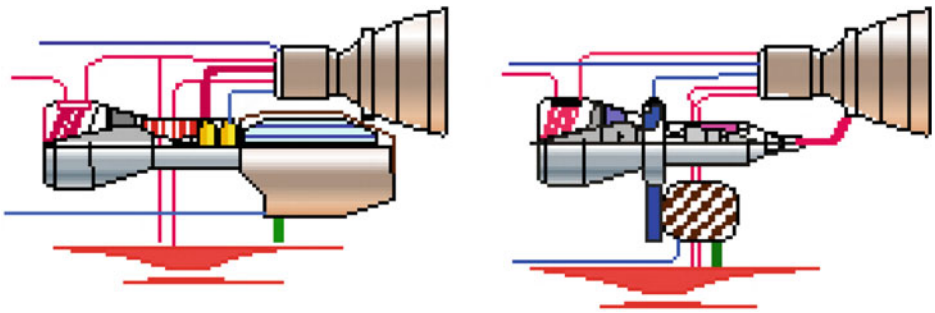

Fig. 4.27 Air collection and enrichment cycle (ACES). *Left* LACE-based combined-cycle. *Right* deeply cooled combined cycle

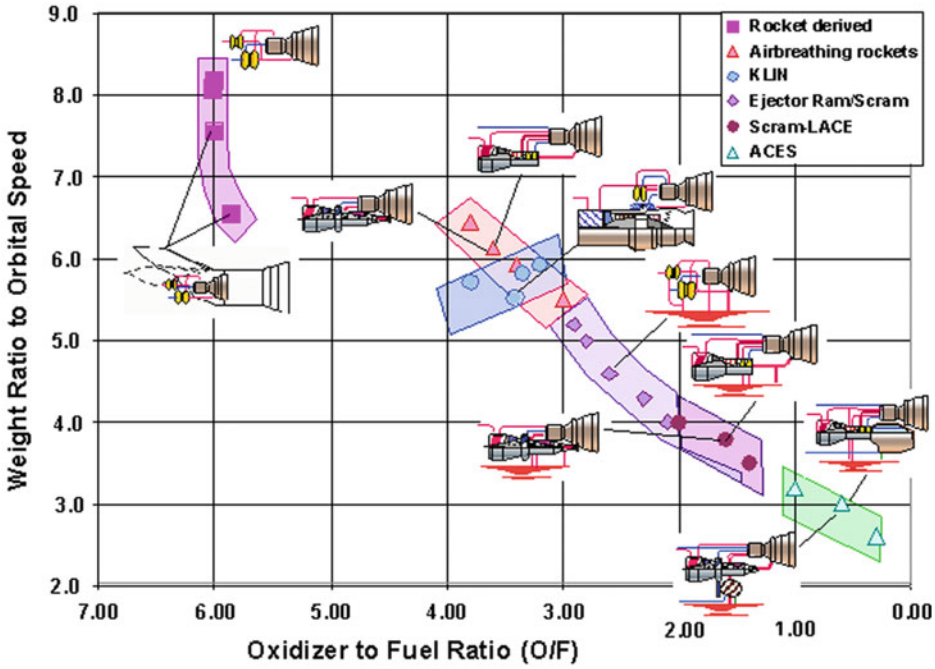

Fig. 4.28 The less oxidizer carried, the lower the mass ratio

class, represented via the airbreathing propulsion cycles, moves down to the right reducing in weight ratio and oxidizer-to-fuel ratio to values 2.5 and 0.5, respectively.

From Eq. (3.4), the relationships involving weight ratio are:

$$W_{\mathrm{R}} = 1 + \frac{W_{\mathrm{ppl}}}{W_{\mathrm{OWE}}} \tag{4.17a}$$

$$W_{\mathrm{R}} = 1 + \frac{W_{\mathrm{fuel}}}{W_{\mathrm{OWE}}} \cdot \left(1 + \frac{O}{F}\right) \tag{4.17b}$$

The TOGW is defined as

$$W_{\mathrm{TOGW}} = W_{\mathrm{R}} \cdot W_{\mathrm{OWE}} \tag{4.18a}$$

$$W_{\mathrm{TOGW}} = W_{\mathrm{OWE}} \cdot \left[1 + \frac{W_{\mathrm{fuel}}}{W_{\mathrm{OWE}}} \cdot \left(1 + \frac{O}{F}\right)\right] \tag{4.18b}$$

Equation (4.17b) directly links the weight ratio to orbit to a function of the oxidizer-to-fuel ratio and the weight of fuel divided by the operational weight empty (dry weight plus trapped fluids, crew, and payload). Then, the $W_{\mathrm{fuel}}/W_{\mathrm{OWE}}$ ratio is multiplied by 1 + (O/F) to produce the weight ratio (W_R). If the $W_{\mathrm{fuel}}/W_{\mathrm{OWE}}$ ratio is approximately constant, then there is a direct benefit in incorporating airbreathing propulsion. The gross weight is reduced and the total engine thrust is reduced, greatly reducing the size, complexity, and cost of the propulsion system. If the $W_{\mathrm{fuel}}/W_{\mathrm{OWE}}$ ratio is approximately constant, then increased engine and turbopump size and weight are a consequence of continuing with rocket propulsion systems.

When rearranging Eq. (4.17b), we obtain

$$\frac{W_{\mathrm{fuel}}}{W_{\mathrm{OWE}}} = \frac{W_{\mathrm{R}} - 1}{\left(1 + \frac{O}{F}\right)} \tag{4.19}$$

Remember, in this equation the oxidizer/fuel ratio is the oxidizer/fuel ratio carried on the launcher with its associated weight ratio, not the rocket engine oxidizer-to-fuel ratio. The importance of Eqs. (4.17b) and (4.18b) and of the chart is

that it shows the gross weight is a function of one airframe parameter, W_{OWE}, and of two propulsion parameters, and that it is directly proportional to the carried oxidizer-to-fuel ratio. When reducing the carried oxidizer, and the gross weight and resultant engine thrust decrease proportionately.

Beginning with the rocket point in Fig. 4.28 at a weight ratio of 8.1 and ending at the ACES weight ratio of 3.0, a straight line connects all hydrogen-fueled propulsion systems except the air-augmented rocket and ram rocket. The reason these two lie outside is because the engine oxidizer-to-fuel ratio stays essentially unchanged and the reduction in weight ratio comes from the air entrained, but not burned, in the ejector system.

Analyzing the data in Fig. 4.28, the result is a value for $W_{\text{fuel}}/W_{\text{OWE}}$ equal to 1.05 ± 0.06. Then, regardless of the propulsion system, the quantity of fuel carried by a hydrogen-fueled launcher that achieves LEO lies between 99 and 111% of the W_{OWE}. This only holds true for a hydrogen/oxygen propulsion system with a 6:1 oxygen/fuel ratio and a stoichiometric air/fuel ratio of 35.4:1. A hydrogen/oxygen rocket with a 7:1 oxidizer/fuel ratio will have a different value. This is an important result of the governing equations, as it fixes the fuel weight regardless of the propulsion system and focuses on the real problem, the weight of the oxidizer carried.

As shown by Eq. (4.17b), the launcher weight ratio is only a function of the carried oxidizer-to-fuel ratio, and the weight ratio is determined by the propellant combination. From the propellant combinations in Table 4.5, the value of $W_{\text{fuel}} = W_{\text{OWE}}$ for the different rocket propellant combinations has been calculated and given in Table 4.6. Note that hydrogen carries the least fuel per W_{OWE}. With an oxidizer-to-fuel ratio of 6, that means the propellant load is 7.3 times the W_{OWE}. The hydrocarbons are five times greater and with an oxidizer-to-fuel ratio about 2.35, the propellant load is 17 times the W_{OWE}. The propellant load of hypergolic propellants ranges from 19 to 20 times W_{OWE}. From Table 4.6, we can see why one of the famous Russian rocket engine designers, Valentin Petrovich Glushko, chose the room temperature liquid UDMH and N_2O_4 for Proton and the submarine-launched ballistic missiles (Chertok 2011).

The importance of this relationship is that with minimal information, a reasonable estimate of the fuel and propellant weight compared with W_{OWE} is available. Hydrogen provides the least weight ratio to orbit. Because the density of hydrogen is low, the volume required is the greatest.

The weight ratio is decreasing because the oxidizer weight is decreasing as a direct result of the oxidizer-to-fuel ratio. Then, from Fig. 4.28, when using hydrogen fuel, (A) an all-rocket engine can reach orbital speed and altitude with a weight ratio of 8.1. (B) An airbreathing rocket (AB rocket) or KLIN cycle can do the same with a weight ratio about 5.5. (C) A combined-cycle rocket/scramjet with a weight ratio of 4.5–4.0, and (D) an ACES has weight ratio of 3.0 or less. Clearly, an airbreathing launcher has the potential to reduce the mass ratio to orbit by 60%! It becomes obvious that a significantly smaller launcher is the result, both in weight and size, and presumably also less expensive. In order to achieve this operationally, the design goal must be to *reduce the carried oxidizer*.

It is more difficult if not impossible to achieve this continuous progression of propulsion systems with fuels other than hydrogen. Methane is a cryogenic fuel, but it does not have the thermal capacity to liquefy or deeply cool air, so the hydrocarbon equivalent of a LACE or deeply cooled cycle is not possible. Ramjet/scramjet engines are possible with most of the liquid fuels, although hydrocarbons decomposition into carbon-rich compounds (coking) will limit the temperature, which ultimately limits the maximum speed obtainable.

Examining the operational regions for each cycle, note that:

(1) *Chemical rocket, air-augmented rocket, and ram rocket* maintain essentially a constant oxidizer-to-fuel ratio, with the weight ratio to achieve orbit decreasing because of the increased thrust produced by the air ejector system. For a vehicle with a rocket W_{OWE} equal to 76 t and assuming the W_{OWE} of other propulsion systems at 76 t (plus any differential weight for the propulsion system), the W_{TOGW} for the three systems is:

Cycle	W_R (–)	O/F (–)	W_{TOGW} (–)	Savings[a] (t)	Payload (t)
Rocket	8.10	6.00	616 t	0	7.0
Air-augmented rocket	7.50	6.00	616 t	0	6.0
Ram rocket	6.50	5.80	543 t	73	15.4

[a]With respect to an all-rocket SSTO launcher

For the same liftoff weight of 616 t, the payload for the three systems is 7.0, 6.0, and 15.4 t, respectively. As is usually the case for the air-augmented rocket, the increased system weight is not offset by the increase in thrust, unless the oxygen in the secondary air is burned. For the ram rocket, the payload is more than doubled. The ram rocket is not any kind of technology challenge, as many afterburning turbojet engines have ejector nozzles (such as the mentioned Saab J-35 Viggen). The ram rocket is a simple way to increase payload to orbit using the same rocket engine, or to reduce the size and cost of the rocket engines for a fixed payload.

(2) *LACE rocket, deeply cooled rocket, and cooled turbojet-rocket (KLIN cycle)* are other propulsion system concepts that build onto the basic rocket engine for increased performance. This propulsion system creates

Table 4.6 Fuel weight to operational weight empty for propellant combinations from Table 4.5

Fuel	Hydrogen	Hydrogen	Kerosene	Methane	Hydrazine	UDMH
Oxidizer	O_2	N_2O_4	O_2	O_2	N_2O_4	N_2O_4
Relative fuel volume (–)	14.83	16.24	6.51	13.47	6.20	10.73
Relative oxidizer (–)	5.25	7.73	2.09	2.05	1.52	0.819
W_{fuel}/W_{OWE} (–)	1.05	1.15	5.02	5.12	6.20	8.42
W_{ppl}/W_{OWE} rocket (–)	7.35	14.4	17.0	17.1	20.2	18.7

UDMH = unsymmetrical dimethyl hydrazine

an airbreathing rocket operating to about Mach 5.5. All of the hardware required for the thermodynamic processing of the air has been built in one form or another over the last 55 years. No differentiation in weight is made for the liquid air cycle versus the deeply cooled. Historical data suggests that these two systems are essentially equal in total system weight.

One of authors (P.A. Czysz) saw a 1 m^3 liquid hydrogen/air heat exchanger operate for 1 min at Mitsubishi Heavy Industries in 1988 at outside air conditions of 38 °C and 90% relative humidity without any water condensation on the heat exchanger tubes. The runtime was short because the container capturing the liquid air was overflowing and running down the ramp. So again, this is not a technology issue, but (rather disappointingly) simply a decision-to-proceed issue. The KLIN cycle has the advantage of thrust for landing without the operation of a heat exchanger to provide the rocket with airbreathing capability. For a rocket vehicle with W_{OWE} equal to 76 t and assuming the same W_{OWE} for other propulsion systems plus any system-specific differential, the W_{TOGW} for the two systems is:

Cycle	W_R (–)	O/F (–)	W_{TOGW} (t)	Savings[a] (t)
LACE-deeply cooled rocket	6.40	3.85	476	140
LACE-deeply cooled rocket	6.00	3.60	443	173
LACE-deeply cooled rocket	5.50	3.10	404	212
KLIN cycle	5.70	3.40	432	184

[a]With respect to an all-rocket SSTO launcher

Even considering the weight of the heat exchangers, the conversion of the rocket to an airbreathing rocket to Mach 5.5 offers considerable savings in weight and engine thrust. This straightforward improvement to the rocket engine offers major cost reductions (Czysz and Richards 1998). For the same liftoff weight of 616.2 t, the payload for the airbreathing rocket systems and the KLIN cycle is between 24 and 38 t. Had the Delta Clipper program survived and, had an airbreathing rocket been considered, the payload could have been increased and the gross weight reduced. Instead, Delta Clipper employed four RL-10A-5 liquid-fueled rocket engines.

(3) *LACE rocket-ram–scramjet and deeply cooled (DC) rocket-ram–scramjet* have the advantage of providing a weight saving equal to the ejector ram–scramjet, but with an intermediate step. For the ejector ram–scramjet propulsion system, the benefits cannot be realized until an operational scramjet is developed and qualified for flight operations. The advantage of the airbreathing rocket is that it can be an effective first step based on existing hardware arranged in a different manner, and that can achieve approximately 60% of the eventual scramjet benefit without any new engine development. An operational system can be operating and realizing this benefit while the scramjet is being developed at its own pace, to be integrated later into the airbreathing rocket system (as envisioned by A.S. Rudakov), in order to realize the final 40% improvement. During that time, the airbreathing rocket system and the air vehicle have been proven in operation. No differentiation in weight is made for the liquid air cycle versus the deeply cooled. Historical data suggests that the systems are essentially equal in total system weight. For a vehicle with a rocket W_{OWE} equal to 76 t, and the W_{OWE} of other propulsion systems also fixed at 76 t plus any differential for the propulsion system, the W_{TOGW} for the two systems is:

Cycle	W_R (–)	O/F (–)	W_{TOGW} (t)	Savings[a] (t)
LACE rocket-ram–scramjet	4.00	2.00	283	334
LACE-DC rocket-ram–scramjet	3.50	1.40	245	372

[a]With respect to an all-rocket SSTO launcher

Integration of the ram–scramjet into the airbreathing rocket system realizes the gains Rudakov reported in Fig. 4.20, by reducing the gross weight by more than half. We are now approaching the weight of a vehicle that can safely abort on launch. With a weight ratio of 4 or less, the potential for horizontal takeoff becomes a real possibility, and a true, safe abort-on-launch capability, could be reality.

(4) *Ejector ram–scramjet-rocket* operational area overlaps the airbreathing rocket and airbreathing rocket-ram/scramjet operational areas. The complete spectrum for the ejector ram–scramjet-rocket is given below. At the higher weight ratios, the ejector ram–scramjet overlaps the airbreathing rockets. The advantage of the latter is that it can be developed from existing hardware and does not require the development of a new engine, the scramjet, for operational application.

There is a clear advantage for the application of airbreathing rockets to launcher before the application of scramjets. The lower weight ratios overlap those of the airbreathing rockets integrated with the ejector ram–scramjet engine. Again, the initial operating capability offered with the airbreathing rocket is built onto, rather than being replaced by, a new system. Building on the airbreathing rocket offers the advantages of expanding the capability of a proven operational system rather than introducing a new vehicle, an important advantage for this propulsion system. If the scramjet was a developed propulsion system at this point in time, beginning with the airbreathing rocket might not be the preferred choice. However, attempts to take this path began in the late 1950s and have yet to yield even a small-scale operational weight engine.

Recent developments are encouraging (Gallagher and Webster-Smith 2015; Davies et al. 2015; Norris 2015). But as of today, there is neither an operational size scramjet nor research and development size scramjet that has the necessary maturity for integration into an operational vehicle. One author (B. Chudoba) is involved to develop the logic successor to the X-51 scramjet demonstrator (Osborn 2015). Clearly, with the availability of rocket ejectors, the ejector ram–scramjet has low-speed thrust and does not require an additional propulsion system for takeoff and low-speed acceleration. If propellant remains after entry, the engine can provide landing and go-around thrust.

For a vehicle with a rocket W_{OWE} equal to 76 t and the W_{OWE} of other propulsion systems also at 76 t, plus any differential for the propulsion system, the W_{TOGW} for these systems is:

Cycle	W_R (–)	O/F (–)	W_{TOGW} (t)	Savings[a] (t)
Ejector ram/scramjet-rocket	5.50	3.40	396	220
Ejector ram/scramjet-rocket	5.20	3.00	372	244
Ejector ram/scramjet-rocket	5.00	2.80	365	260
Ejector ram/scramjet-rocket	4.50	2.50	317	299
Ejector ram/scramjet-rocket	4.23	2.00	296	320
Ejector ram/scramjet-rocket	4.00	1.75	278	338
Ejector ram/scramjet-rocket	3.50	1.40	241	375

[a]With respect to an all-rocket SSTO launcher

The ejector ram–scramjet, operating to airbreathing Mach numbers from 6 to 14, offers the ability to reduce the gross weight by more than 50%.

(5) *ACES-LACE ejector scramjet-rocket*, *ACES-deeply cooled ejector scramjet-rocket* is another concept that dates back to the late 1950s, and, like the scramjet, has not proceeded beyond the ground test phase. This concept did have much full-sized, flight-weight hardware built and tested successfully in the 1960s. The difficulty has always been the sensitivity of SSTO space launchers to volume demands. This propulsion system is very attractive for TSTO launchers with the air collection and separation system in the first stage (Rudakov et al. 1991). A number of these have been designed, but none have proceeded beyond the concepts stage. This will be discussed later in the chapter dealing with mission-sized launcher systems.

If indeed there is a problem with this propulsion system concept, it is the volume required for the liquid air separator. For volume-limited applications, the size and weight of the airframe increase. It remains to be designed and demonstrated that the volume reduction potential of the deeply cooled gaseous separation is real (Lee et al. 2003a, b). As a result, both systems are being treated as equal-size, equal-weight, and equal-performance systems.

For a vehicle with a rocket W_{OWE} equal to 76 t and the W_{OWE} of other propulsion systems also defined to 76 t, plus any differential for the propulsion system, the W_{TOGW} for this system is:

Cycle	W_R (–)	O/F (–)	W_{TOGW} (t)	Savings[a] (t)
ACES-scramjet	2.90	0.50	252	364

[a]With respect to an all-rocket SSTO launcher

Even though the weight ratio is less than for the ejector ram–scramjet-rocket, the gross weight is not due to the air separation system volume.

4.15 Conclusions with Respect to Continous Operation Cycles

Carl Builder was one of The Marquardt Company's team members that developed the Air Force scramjet program. Carl Builder, Lindley (1965), and John Ahern were responsible for developing the thermodynamic analysis for the scramjet. The standard approach for the ramjet and its extension to scramjets was based on an isentropic stagnation conditions analysis, where First Law inefficiencies were evaluated in terms of stagnation pressure losses, and of aerodynamic analysis of the engine flow path based on local Mach numbers and aerodynamic characteristics. For a subsonic flow-through engine (ramjet), where the heat addition is done at subsonic speeds, and where maximum pressure and temperatures do not exceed (typically) 20 atm and 1800 K, this type of approach is quite acceptable.

However, for supersonic through-flow engines (scramjet), the heat addition is at supersonic Mach numbers and the Fanno and Rayleigh solution characteristics change sign (Scott and Riggins 2000). The isentropic stagnation pressure and temperature can reach 1000 atm and 6000 K. For this case, a different approach was sought. It was based on static conditions, not stagnation, the cycle being analyzed using a Second Law approach based on un-recovered (lost) available energy and entropy increases (Builder 1964). The original work was done in the late 1950s. By 1960, the Air Force scramjet program associated with the aerospace plane began falling apart, and this group sought employment elsewhere. Builder joined the Rand Corporation in the strategic planning department, giving up on further scramjet work because his work had been so close to completing a successful program and yet it was to be scrapped arbitrarily in favor of rockets.

At the urging of The Marquardt Company scramjet manager, Artur Magar, Builder finally published in 1964 a partial description of the approach (Builder 1964). One of the authors (P.A. Czysz) and a colleague from Douglas Aircraft Company, Gordon Hamilton, visited Builder in 1984 to discuss the unfinished portion of his work. As a result, a paper was prepared that documented the complete approach (Czysz 1988a). Although the original paper is now over 50 years old, the conclusions reached by Builder are as applicable today as then. In fact, in reading this book, the reader should come to the same conclusions. The tragedy is that in the intervening 55 years, there has been no change in the space launchers propulsion systems, design, or fabrication. Forty years after the Wright Brothers' first flight, jet power aircraft were flying in both Great Britain and Germany and by 50 years the first British commercial jet transport was approaching operational status. As in the past, each rocket still flies for the first, last, and only time. The following paragraphs are Builder's conclusions from 1964, verbatim.

Before summarizing, it would be well to note that the analyses and figures presented are based upon an ideal gas analysis. It is well recognized that the behavior of air is not ideal at high temperatures, above about 3500 or 4000 °R. However, this analysis is restricted to the static conditions throughout the cycle, so the errors due to non-ideal behavior may not be as large as they would if stagnation conditions were being used. For example, the optimum compression enthalpy ratios determined in this analysis are generally under ten, which means that the temperatures at the end of the compressive device would be under 4000 °R, because of this, it is believed that the trends and characteristics which have been presented for the Brayton Cycle family are quite valid, even if the specific values or curves are subject to adjustment for non-ideal gas effects.

What conclusions can be drawn from this treatment of the Brayton Cycle family of airbreathing engines? First: we should note that a thermodynamic analysis on Mollier coordinates for the static gas conditions provide a consistent treatment of the complete spectrum of engines in this family.

Second: an optimum amount of compression can be defined which depends only upon the overall processing efficiency of the heat-energy input of the cycle. That optimum amount of compression is compared to that available from ram stagnation of the engine airflow, a clearer insight is gained into the factors, which are common to the natural evolution of the turbojet, the conventional ramjet, and the supersonic combustion ramjet.

Third: the energy conversion efficiency of the Brayton Cycle appears to continuously improve with speed, even approaching orbital velocities. It has been shown that the amount of compression is an important consideration in determining the energy conversion efficiency. Thus, we should not be overly preoccupied with the efficiency of compressive devices or the attainment of the maximum amount of compression possible. It is over-compression which causes the drop-off of conventional ramjet efficiencies above 10,000 fps.

Finally, what does this analysis tell us with respect to potentially new engines lurking in the spectrum of chemical airbreathing propulsion? The turbojet, conventional ramjet, and supersonic combustion ramjet are clearly the dominant occupants of the three distinct regions of desired compression: mechanical, stagnation, and partial diffusion. However, we seem to lack engines for the transition regions. The turbo-ramjet is a hybrid, which spans two of the three regions, but is probably not the best possible choice for the

region in-between. In the Mach 3 to 5 regime, an engine having very modest mechanical compression with high processing efficiencies might be very attractive. In a sense, a fan-ramjet might be a suitable name for such a cycle; the duct-burning turbofan and the air-turborocket could be considered close cousins to this hypothetical engine. At the higher speed end, around Mach 10, we can postulate a very efficient engine called the transonic combustion ramjet. There is still another important class of possibilities offered just outside the confines of the Brayton Cycle family: engines with non-adiabatic compression and expansion processes as a result of heat exchanges between the air and fuel. We might find a complete new spectrum of such engines awaiting our discovery.

At the time Builder wrote the AIAA-64-243 paper, a major effort was underway to develop, in a single engine, the characteristics of the combined turbojet and ramjet. The concept was called a turbo-ramjet (Doublier et al. 1988; Escher 1966).

4.16 Pulse Detonation Engines

4.16.1 Engine Description

Based on non-continuous through-flow, a pulse detonation engine (PDE) is a cyclical operation engine analogous to the World War II pulse jets (Neufeld 1995; Hellmold 1999). This engine fires cyclically, resulting in an intermittent engine thrust. The engine consists of an acoustically tuned pipe, fed by a detonable mixture inside that, when ignited, sends the combustion products wave traveling down the pipe ahead of a detonation wave. After the products exit the tube, the tube is effectively scavenged, new fuel is then injected, and a new mixture forms, sort of reloading the tube. The ignition process is then repeated, starting a new cycle. This periodic operation gives the PDE a characteristic cyclic rate and the characteristic sound that, in the V-1 case, gained it the nickname of "buzz bomb."

A comparison of the pulse detonation rocket engine (PDRE) or pulse detonation engine (PDE) with today's standard rocket and turbojet cycles can show the potential of this propulsion system. A PDRE is a cylindrical tube with a defined length. The PDRE is an intermittent internal combustion/detonation engine with three strokes, namely *injection*, *detonation*, and *exhaust*, as shown in Fig. 4.29. The PDRE is characterized by mechanical simplicity, and high compression ratio compared to continuous combustion engines. The PDE/PDREs have the potential to significantly reduce the cost and complexity of today's liquid-propellant rocket engines; they present novel alternatives to current gas turbine and/or rocket engines. The PDE/PDRE has the potential to provide dramatic improvements in both costs and performance for space propulsion applications. This is due primarily to the fact that detonations provide a more efficient mode of combustion over the conventional constant pressure approach of current engine technology. Large reductions in pumping, plumbing, and power requirements appear also possible with the PDE/PDRE. The self-compressing nature of the detonation combustion could dramatically reduce the need for massive oxidizer/fuel turbopumps. Pump pressure is 10 atm instead of 300 atm. Corresponding reductions in plumbing, structural requirements and pumping power are thought possible with the PDE/PDRE. Practical engineering issues and subsystem technologies still need to be addressed to ensure that this potential is realized.

The PDE/PDRE possesses a significantly higher power density compared to conventional rocket designs. Detonation combustion produces large pressure increases in the combustion chamber (over and above those produced by pre-combustion turbopumps), creating large thrust forces at the chamber thrust wall. The result is a very high thrust for an engine of equivalent dimensions compared to today's state-of-the-art propulsion systems, provided of course that the repetition rate is sufficiently high. Alternatively, an equivalent amount of thrust could be generated with a more compactly designed PDE/PDRE. Because additions in PDE/PDRE load-bearing structure do not increase proportionally with gained chamber thrust forces, the PDE/PDRE does also possess a much higher thrust-to-weight ratio than current chemical rocket engines.

As shown in Fig. 4.29, the basic cycle has one detonation wave traveling down the tube. One way to increase the thrust is by making a multiple-tube engine (Norris 2003) as was being developed by Pratt & Whitney. Note that in the referenced article, a single detonation wave tube is shown, which is satisfactory for sea-level testing. In all of the work done on PDEs for this chapter, they have been equipped with expansion nozzles just as in the case of a rocket engine, see Fig. 4.30. Another approach is to operate the detonation wave tube so there are multiple pulses traversing the tube (Norris 2003).

The flow characteristics in a pulse detonation engine have been modeled previously using a variety of methods including zero-dimensional, one-dimensional, and two-dimensional unsteady analyses. All three of these levels are useful, but provide different types of information. Zero-dimensional analyses provide fast, global parametric trends for the unsteady operation of a PDE. One-dimensional models provide a first indication of the dominant wave processes and the manner in which they couple with the

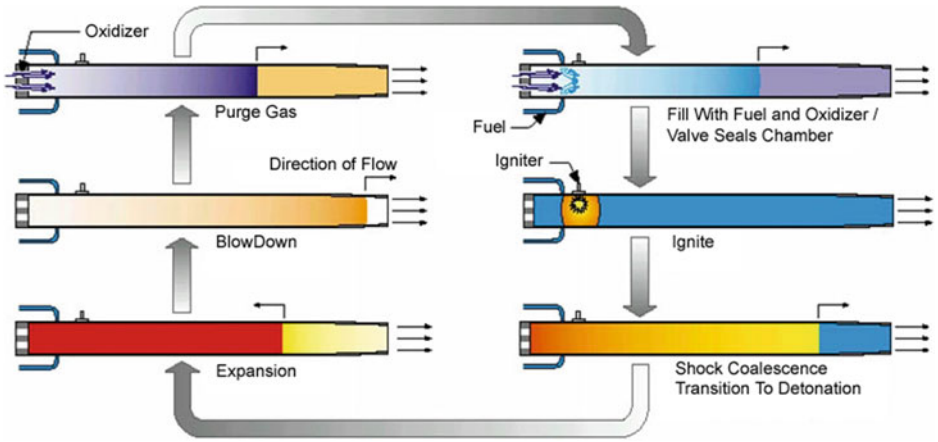

Fig. 4.29 The pulse detonation rocket engine (PDRE) operational cycle

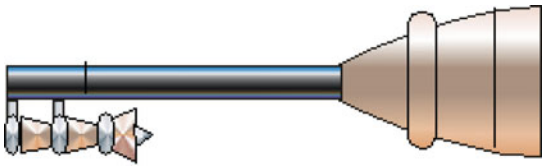

Fig. 4.30 Pulse detonation rocket engine (PDRE)

overall engine/vehicle system at a cost that is intermediate between zero- and two-dimensional models. Two-dimensional models have the capability of identifying the dominant multi-dimensional effects (e.g., fuel/air mixing) and their level of importance. However, multi-dimensional modeling requires a substantial investment in computational resources. Some specific areas of PDE/PDRE operation are inherently dominated by multi-dimensional phenomena, and the only way to address these phenomena is by modeling the entire multi-dimensional process.

4.16.2 Engine Performance

Analysis of engine flowpath physics, anchored to available experimental and CFD data, has shown performance to be dependent on the propellant combination, the feed system, and other design parameters. It is only through detailed component energy balancing, coupled with unsteady detonation analysis and modeling of losses, that accurate estimates of the PDE/PDRE performance may be obtained. Three key parameters that determine performance are *nozzle length* compared to the detonation tube length, *fill fraction* (i.e., whether there are multiple detonation waves present in the engine), and *detonation frequency*.

The first factor is *nozzle length*. Nozzle lengths can double the I_{sp} for a hydrocarbon-fueled PDRE (Kailasanath 2002). Data from (Daniau 2002) indicates that a divergent nozzle does not adversely affect the cycle time. Detonation frequencies in the 140 Hz range for hydrogen-oxygen and 110 Hz for hydrocarbon-oxygen mixtures are possible. The importance of the information is that for a fully airframe-integrated PDE with the aft-body forming the nozzle, a beta parameter in the 5–6 range enhances PDE performance. Beta is the ratio between nozzle length and combustion chamber length. The combustion chamber length is not the entire tube length, the forward part of the tube being where the fuel and oxidizer mix and combustion is initiated, as shown in Fig. 4.29.

The second factor that affects the performance of the PDE is the *fill fraction*. In an ideal detonation wave tube, see Fig. 4.29, the products of combustion exit the tube and the tube is purged before the next charge is introduced. An option is to introduce a new charge into the tube before the cycle is complete. In this case, the fill fraction is less than 100%. That is, only a certain fraction of the tube receives a new charge. A reduction in the fill factor directly affects the I_{sp} of the engine, no matter at what frequency. In this chapter, a 100% fill and a 60% fill fraction were used. The partial fill case provides 38% greater I_{sp} when compared with the full fill case. The former is referred to as "full fill," and the latter is referred to as "partial fill" in the propulsion characteristics and sizing results.

The third factor affecting performance is the *detonation frequency*. In a chart shown by Kailasanath (2002), the real difference in the performance of the PDE versus the ramjet is governed by the detonation frequency of the PDE. The chart depicts experimentally determined thrust versus the frequency for the PDE compared to a ramjet. For the PDE, as the frequency is increased, the thrust increases almost linearly. For a modest frequency PDE operating at one-half the maximum frequency of 35 Hz, the thrust is 2.25 times the ramjet thrust. Since the reason for rocket-driven ejectors in the ramjet engine is to obtain greater thrust at low-speed, the pulse detonation engine has significant potential to increase low-speed performance over that of a ramjet. For this chapter, a thrust of twice the subsonic through-flow ramjet engine has been used, see Fig. 4.31.

In the low-speed flight regime, there is insufficient kinetic energy to produce a static compression enthalpy ratio, Ψ, sufficient to sustain ramjet operation. The rocket ejector ramjet is a means of providing sufficient nozzle enthalpy and pressure ratio to have an efficient ramjet at speeds lower than Mach 2.5. The PDRE does not depend on ram pressure; with the PDE ejector, it has sufficient pressure ratio to operate at zero flight speed as either a pulse detonation rocket or as an airbreathing pulse detonation engine analogous to the rocket ejector ramjet. So, the question was to predict its potential performance using Builder's analysis.

The original Brayton cycle analysis by Builder (1964) was based on the static enthalpy rise within the engine. Builder called the term (Ψ) the static enthalpy compression ratio h/h_0, where h_0 is the freestream static enthalpy. If C_p = constant, then $\Psi = T/T_0$. The extension of Builder's original work by Czysz (1988a) has continued that nomenclature. Heiser and Pratt (2002) and Wu et al. (2003) use static temperature ratio for the value of Ψ, so there is about one-unit difference between the two definitions of Ψ in the 5000–6000 ft/s range, with the temperature ratio definition being the lower value. The comparison in performance is made using the energy conversion efficiency θ, that is, what fraction of the input fuel energy is converted into useful thrust work.

The energy conversion efficiency has been already defined before with Eqs. (4.15a)–(4.15c); we further have:

$$\theta = \frac{V \cdot T}{\frac{\text{Fuel}}{\text{Air}} \cdot Q_c \cdot \dot{w}_{\text{air}}} \tag{4.20a}$$

$$\theta = \frac{V \cdot T_{sp}}{Q} \tag{4.20b}$$

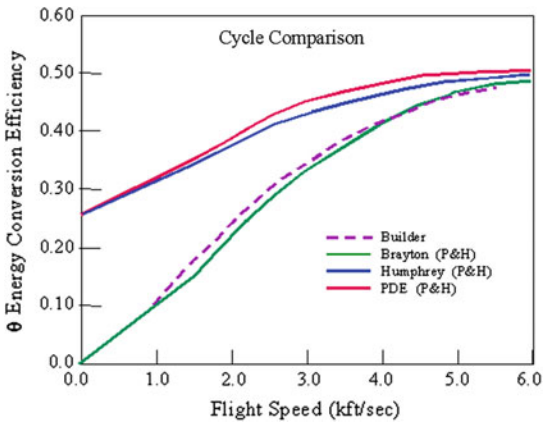

Fig. 4.31 The pulse detonation engine (PDE) cycle compared with the Brayton cycle. P&H indicates the (Heiser and Pratt 2002) paper

With specific impulse and specific thrust defined as

$$I_{sp} = \frac{\theta \cdot Q_c}{V} \tag{4.21}$$

$$T_{sp} = \frac{\theta \cdot Q}{V} \tag{4.22}$$

It is important to observe that as velocity is increased, both the specific impulse, I_{sp} (thrust per unit fuel flow) and specific thrust, T_{sp} (thrust per unit air flow) decrease inversely proportional to velocity, even though θ may increase with velocity to a plateau value. Making a direct comparison between the energy conversion efficiency of Builder (θ) using the enthalpy ratio Ψ and the temperature ratio definition of Ψ by Wu et al. (2003) and Heiser and Pratt (2002) did not produce a clear cut conclusion. The comparison for θ between (Builder 1964) and (Heiser and Pratt 2002) is rather good, considering that the values for Builder were independently done prior to 1964 using a Second Law approach that minimized the cycle entropy rise. Nevertheless, the clear advantage in the lower speed range for the PDE is shown in Fig. 4.31.

The Humphrey cycle is a cycle that has been used as a surrogate for the pulse detonation cycle to estimate performance. As shown in Fig. 4.31, it provides a good representation of the PDE energy conversion efficiency. The energy conversion efficiencies were converted into I_{sp} values, see Eq. (4.16), and the PDEs compared with conventional ram–scramjets. The more informative parameter, for an acceleration-dominated SSTO application, can be obtained from a comparison of effective specific impulse, that is, the acceleration specific impulse using the $T - D$ difference rather than thrust, T, alone. For I_{spe} estimations, the aircraft drag was determined from historical data for the two configurations of interest (Pirrello and Czysz 1970).

12. Pulse detonation rocket engine (PDRE). Figure 4.30 depicts a rocket PDE (or PDRE). The PDRE usually is charged with a near stoichiometric mixture of fuel and oxidizer, and they can be any detonable fuel and oxidizer combination. For estimating the performance of launchers, only hydrogen has been used here as fuel. The primary advantage of this system is reduced complexity and weight in the propellant fluid pressurization systems. The PDR is charged with fuel and oxidizer to generally less than 10 atm. The resulting pressure peak behind the detonation wave can exceed 1000 atm. The very uniform pressure behind the detonation wave yields a constant thrust pulse.

In one of the research institutes located outside Beijing, China, and at The University of Texas at Arlington's (UTA) Aerodynamics Research Center (ARC), there are

high-performance shock tube wind tunnels driven by a detonation wave tube, rather than the conventional hydrogen/oxygen combustion driver. The result is a very uniform drive-pressure profile and longer run times. The advantages are that the charge to the driver tube is a few atmospheres compared to the conventional tens to a hundred atmospheres. The detonation wave itself delivers compression and heating without a mechanical pump. Made flight weight, the PDR is a device which is operating at a cyclic rate rather than with a single firing. It can be installed in any rocket-powered aircraft or launcher, just as the rocket engine was installed, with the expansion nozzles located at the same place.

13. Pulse detonation rocket/ramjet engine. The evolution of a PDRE/PDE-based combined-cycle engine is reported as a Russian concept (Kailasanath 2002). This Russian concept can operate over a range of flight conditions going from takeoff to hypersonic flight. The PDE can be integrated into an airframe in the same manner as a rocket and ram–scramjet. For the low-speed flight regime, and until there is sufficient kinetic energy to produce a static temperature ratio, Ψ, sufficient to sustain PDE operation, a strut-integrated PDRE functions very much like a rocket ejector strut, except with less complexity and high-pressure fluid systems.

Figure 4.32 shows a Russian concept for a PDRE/ramjet PDE that is equivalent to a rocket–ramjet system, which can operate as an airbreathing system up to Mach 6 (Kailasanath 2002). (1) In the first operating region, to about Mach 2.3, the engine operates as a pulse detonation rocket ejector ramjet with the PDR replacing the rocket ejector. (2) Above Mach 2.5, the PDR acts as an ejector and is a hydrogen ejector, with a downstream-pulsed oxygen injection which stabilizes a periodic detonation wave in the engine ahead of the nozzle contraction. In this case, the ramjet nozzle is driven by a detonation wave process. The shock system around the PDR ejector and the ejected hydrogen pressure isolates the detonation process from the inlet, and prevents regurgitation of the shock system. (3) Above Mach 6, the PDR is the propulsion system, analogous to the airbreathing rocket or ejector ramjet–rocket. A representative installation is shown in a hypersonic glider (FDL-7 family) at the top of Fig. 4.32.

14. Pulse detonation rocket/ramjet–scramjet engine. Figure 4.33 shows a Russian concept for a PDE/ramjet/ODWE equivalent to a rocket-ram–scramjet system as described in Kailasanath (2002). The PDE module is shown integrated into a blended-body configuration airbreathing vehicle much as a rocket ejector ramjet–scramjet is integrated. Except for the pulsed nature of the ejector strut operation, the engine is essentially a rocket ejector ramjet. The engine spans the operational envelope from takeoff to perhaps a little above Mach 15.

(1) The PDRE operation is confined to the strut during the low-speed phase of the operation. (2) For the PDE engine above Mach 6 flight, the propulsion configuration is an airbreathing PDE that incorporates elements of the rocket PDE, with the kinetic compression of the rocket ejector ramjet producing a pulsed detonation wave within a steady flow device. This concept is equivalent to a LACE or deeply cooled airbreathing rocket. (3) For speeds greater than Mach 6, the propulsion converts to a steady-state operation as an oblique detonation wave engine (ODWE), as it is necessary to transition the detonation wave from an oscillating (back and forth) wave structure to a steady oblique detonation wave structure. In this operating mode, it is equivalent to a scramjet (Kailasanath 2002). In this latter mode, the engine works using a continuous detonation process and is now a steady-state engine. (4) Above the maximum airbreathing speed, the PDR provides the thrust to orbital velocity. At the top of Fig. 4.33, a representative installation in a propulsion-configured airbreathing configuration is shown. Externally there is little difference in the configuration compared to the conventional scramjet installation, except for perhaps a longer engine cowl.

The pulse detonation propulsion systems offer considerable promise to reduce weight and propellant pumping challenges. Note that PDREs are in a period of experimentation and development, and most of the engineering is still classified. The question remains: Can the eventual operational hardware developed capture the promise shown in the analytical studies? In the following section, we assume that operational hardware has captured the promised performance, so a valid measure of the propulsion system potential is presented.

4.17 Conclusions with Respect to Pulse Detonation Cycles

The three pulse detonation engine systems are compared in a single table in a similar manner to the continuous engine cycles. For a vehicle powered by a conventional continuous rocket engine, the W_{OWE} is 76 t (metric tons); the equivalent PDR W_{OWE} is 70 t because of the lesser total vehicle volume and the lesser propellant pumping hardware and weight. The assumption has been that the engine weight is the same as an equivalent thrust conventional rocket engine. This is yet to be demonstrated with operational engine weights, but it is a reasonable expectation considering the much less complicated hardware required. With these considerations, the W_{OWE} of 70 t is equivalent to the conventional all-rocket.

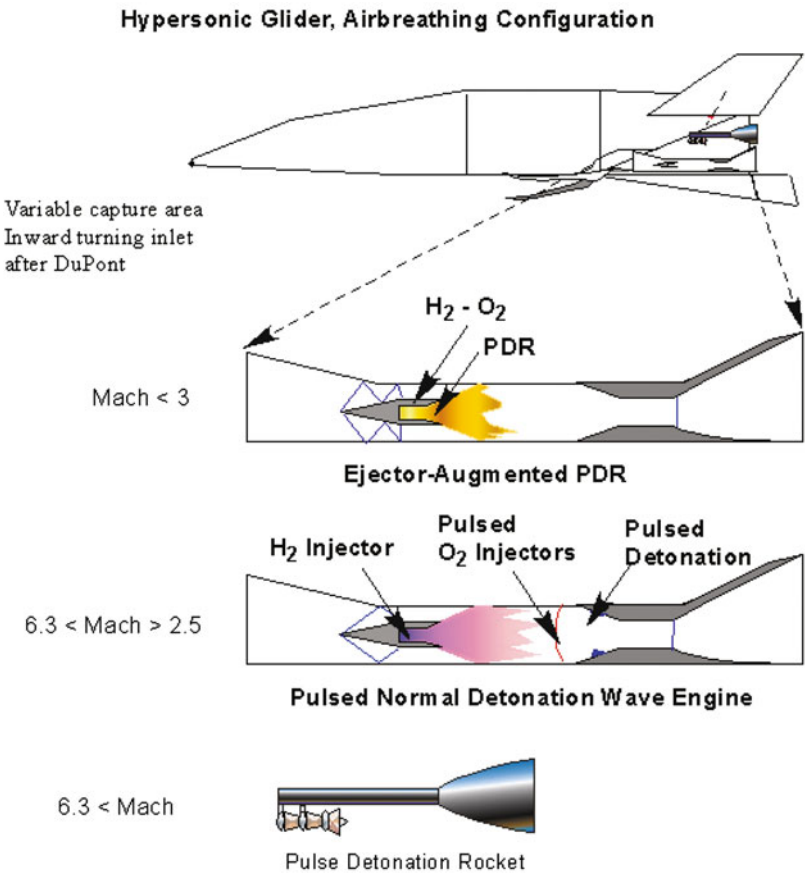

Fig. 4.32 Integrated PDRE ramjet combined cycle

For other propulsion systems, the W_{OWE} is 70 t plus any differential weight for the propulsion system. The W_{TOGW} for the three systems is:

Cycle	W_R (–)	O/F (–)	W_{TOGW} (t)	Savings[a] (t)
Pulse detonation rocket	8.10	6.00	567	49
Pulse detonation rocket/ramjet	5.10	4.60	357	259
Pulse detonation rocket/ram/scramjet	3.20	1.80	224	392

[a]With respect to an all-rocket SSTO launcher

Perhaps the PDEs are the beginning of the Builder conclusion more than 50 years ago, "*There is still another important class of possibilities offered just outside the confines of the Brayton Cycle family: engines with non-adiabatic compression and expansion processes as a result of heat exchanges between the air and fuel* and engines with non-steady *operation* (non-italics by the authors). *We might find a complete new spectrum of such engines awaiting our discovery.*" (Builder 1964)

4.18 Comparison of Continuous Operation and Pulsed Cycles

Adding the PDEs to the results in Fig. 4.28, the result is Fig. 4.34 that gives the SSTO mass ratio (weight ratio) to reach a 100 min (185 km) orbit with hydrogen fuel as a function of the maximum airbreathing Mach number for both continuous and cyclic operation engines. Seven classes of propulsion systems are indicated: (1) rocket-derived, (2) airbreathing (AB) rocket, (3) so-called KLIN cycle, (4) ejector ramjet, (5) scram-LACE, (6) air collection, and enrichment systems (ACES) and (7) pulse detonation derived engines (PDR/PDRE). As in Fig. 4.28, there is a discontinuity in the results. If the mass ratio to orbit is to be significantly reduced, the carried oxidizer-to-fuel ratio (oxygen and hydrogen) must be reduced to 5 or less. That means at least an airbreathing rocket or airbreathing PDR is required to achieve that threshold.

The weight ratio, hence the takeoff gross weight, is a direct result of the propellant weight with respect to the W_{OWE}. As introduced earlier (Sect. 4.14), the propellant weight is a direct function of the oxidizer-to-fuel ratio (O/F):

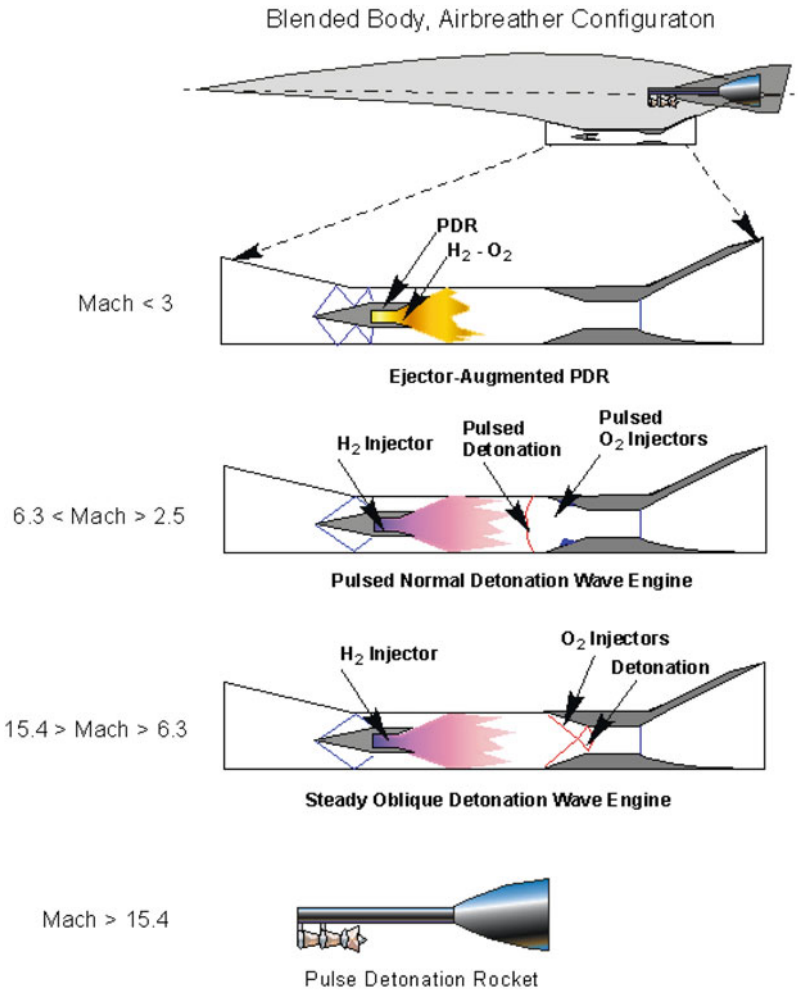

Fig. 4.33 Integrated PDRE ram–scramjet combined cycle

$$W_{\mathrm{R}} = 1 + \frac{W_{\mathrm{ppl}}}{W_{\mathrm{OWE}}} \tag{4.23a}$$

$$W_{\mathrm{R}} = 1 + \frac{W_{\mathrm{fuel}}}{W_{\mathrm{OWE}}} \cdot \left(1 + \frac{O}{F}\right) \tag{4.23b}$$

The TOGW = W_{TOGW} is defined as usual

$$W_{\mathrm{TOGW}} = W_{\mathrm{R}} \cdot W_{\mathrm{OWE}} \tag{4.24a}$$

$$W_{\mathrm{TOGW}} = W_{\mathrm{OWE}} \cdot \left[1 + \frac{W_{\mathrm{fuel}}}{W_{\mathrm{OWE}}} \cdot \left(1 + \frac{O}{F}\right)\right] \tag{4.24b}$$

$$\frac{W_{\mathrm{fuel}}}{W_{\mathrm{OWE}}} = \frac{W_{\mathrm{R}} - 1}{\left(1 + \frac{O}{F}\right)} \tag{4.24c}$$

Remember, in these equations, the oxidizer/fuel ratio is the oxidizer/fuel ratio carried on the launcher with its associated weight ratio, not the rocket engine oxidizer/fuel ratio. The importance of the equation set is that the gross weight is a function of one airframe parameter (W_{OWE}) and two propulsion parameters, and that the gross weight is directly proportional to the carried oxidizer-to-fuel ratio (O/F). Reduce the carried oxidizer, and the gross weight and resultant engine thrust decrease proportionately.

Beginning with the rocket point in Fig. 4.34 at a weight ratio of 8.1, and moving to the ACES with weight ratio of 3.0, a straight line between these points connects all of the continuous hydrogen-fueled propulsion systems. The exception are the PDRs, lying below the continuous propulsion curve: hence, their $W_{\mathrm{fuel}}/W_{\mathrm{OWE}}$ ratio is *less than one*.

The PDR is essentially equivalent to the rocket in terms of weight ratio to orbital velocity. The PDE/ramjet is equivalent to a rocket–ramjet system and lies in line with the thermally integrated KLIN cycle at a higher oxidizer-to-fuel ratio and lower weight ratio. Clearly, the PDE/ramjet has an oxidizer-to-fuel ratio about one unit greater than the KLIN cycle, and about one-half unit less in terms of weight ratio.

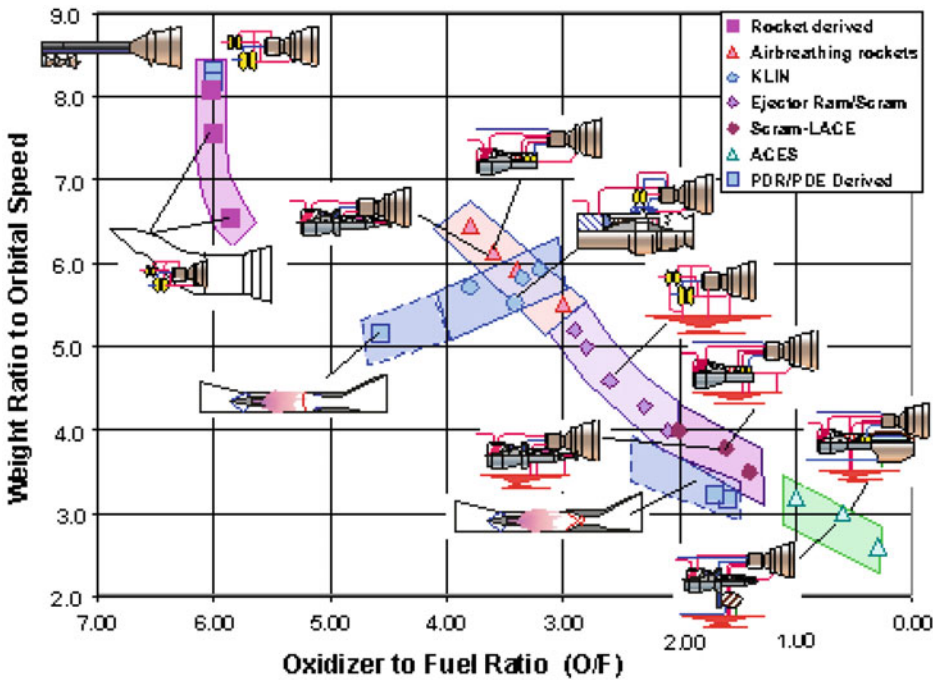

Fig. 4.34 The PDE improves the total weight ratio

In terms of characteristics, the PDE/ramjet appears to be more like a thermally integrated rocket/turbojet than the airbreathing rocket propulsion systems. In terms of the impact on operational systems, the next set of charts will size launchers to the same mission and payload to enable us to evaluate the propulsion system differences in terms of launcher system size and weight.

The PDE/ram–scramjet system is equivalent to the thermally integrated airbreathing rocket-ram–scramjet systems. It lies to the left (greater *O*/*F* ratio) of the thermally integrated ram–scramjet cycles at a slightly lesser weight ratio to orbital speed near the RBCC propulsion systems of Yamanaka (scram-LACE), Builder (ejector ram–scramjet), and Rudakov (deeply cooled-ram–scramjet). From the cycle analysis, the PDE appears to have performance advantages and disadvantages with respect to the continuous cycles (lesser weight ratio but greater oxidizer-to-fuel ratio), trades that must be evaluated in the context of launcher-sizing programs.

These three propulsion configurations have been further evaluated in detail. The overall process of exploring the thrust-to-weight ratio, cost of development, and overall payload capability for the variety of propulsion systems and matching flight vehicle integration has to examine the configurations without bias. Only such "generic" parametric modeling approach is able to correctly determine the relative merits of the "best" configuration implementation. At this point in our discussion, these ideas require further parametric investigation to finalize the comparison.

Clearly, while most conventional propulsion systems have fuel weights approximately equal to the W_{OWE}, the PDE propulsion systems have fuel weights that are less than W_{OWE}, hence the advantage of PDE systems. This weight advantage appears to represent a simple and fundamental correlation facilitating to judge hydrogen/oxygen propellant SSTO results. As shown in Table 4.6 for other fuels, the ratio will not be one.

In determining the launcher size for each propulsion system concept, an important parameter is the installed engine thrust-to-weight ratio. A non-gimbaled (that is fixed and not steerable by pivoting the engine) rocket engine for space operation could have an engine thrust-to-weight ratio as large as 90. For a large gimbaled engine, such as the space shuttle main engine (SSME), that value is about 55 for the installed engine. We use this value as the reference value for our comparisons. The liftoff thrust generally determines the maximum engine thrust for the vehicle. For a given vehicle thrust-to-weight ratio at liftoff or takeoff, $(T/W)_{\mathrm{TO}}$, the weight of the engines is a function of the required vehicle thrust-to-weight ratio at liftoff, the thrust margin, the weight ratio, and the W_{OWE}. Thus:

$$W_{\mathrm{engine}} = W_{\mathrm{R}} \cdot \left(\frac{T}{W}\right)_{\mathrm{TO}} \cdot \frac{W_{\mathrm{OWE}}}{\left(\frac{T}{W}\right)_{\mathrm{engine}}} \qquad (4.25)$$

The weight ratio is the total mission weight ratio including all maneuvering propellant. For vertical liftoff, the launcher thrust-to-weight ratio is at least 1.35. For horizontal takeoff, the launcher thrust-to-weight ratio is in the 0.75–0.90 range. Usually, if the horizontal takeoff thrust-to-weight ratio exceeds one, there is a significant weight penalty (Czysz and Vandenkerckhove 2000). The engine thrust-to-weight ratio, $(T/W)_{\text{engine}}$, has been a constant source of controversy and discussion for airbreathing engines. One approach to avoid such arguments before the actual sizing procedure begins, and that has stopped the sizing process from assessing the true potential in the past, is to find a suitable relationship for determining the engine thrust-to-weight ratio. For the authors' purpose, that procedure is to assume the total installed engine weight is a conservative constant equal to that of the all-rocket launcher. The resulting engine thrust-to-weight ratio, $(T/W)_{\text{engine}}$, for all other propulsion systems, can then be determined as:

$$\left(\frac{T}{W}\right)_{\text{engine}} = \frac{W_{\text{R}}}{W_{\text{R}_{\text{rocket}}}} \cdot \frac{(T/W)_{\text{TO}_{\text{vehicle}}}}{(T/W)_{\text{TO}_{\text{rocket}}}} \cdot \frac{W_{\text{OWE}}}{W_{\text{OWE}_{\text{rocket}}}} \cdot \left(\frac{T}{W}\right)_{\text{rocket}} \tag{4.26a}$$

$$\left(\frac{T}{W}\right)_{\text{engine}} = \frac{W_{\text{R}}}{8.1} \cdot \frac{(T/W)_{\text{TO}_{\text{vehicle}}}}{1.35} \cdot 1.55 \tag{4.26b}$$

$$\left(\frac{T}{W}\right)_{\text{engine}} = 5.03 \cdot W_{\text{R}} \cdot \left(\frac{T}{W}\right)_{\text{TO}_{\text{vehicle}}} \tag{4.26c}$$

Evaluating Eqs. (4.26a)–(4.26c) for the data in Fig. 4.34 results in Fig. 4.35, showing the engine thrust-to-weight ratio, $(T/W)_{\text{engine}}$, as a function of weight ratio to orbital speed, W_{R}, with minimum maneuver propellant. There is one calibration point in the open literature from 1966: William J. Escher completed the testing of the SERJ (supercharged ejector ramjet) to flight duplicated engine entrance conditions of Mach 8, the maximum airbreathing speed for SERJ (Escher et al. 2000, 2001). In those tests, the flight-weight engine would have had an installed thrust-to-weight ratio of 22, had it been installed in an aircraft. From Fig. 3.4, the mass ratio for an airbreathing speed of Mach 8 is 5. From Fig. 4.35, the range of values for a weight ratio of 5 is 25–27. Clearly, the SERJ engine would have had a weight just slightly larger than the assumed all-rocket engine weight.

The simple approach above estimates the operational weight of an arbitrary propulsion system. However, a word of caution: This approach estimates the installed engine thrust-to-weight ratio for an integrated propulsion system. It will not estimate the weight of the engine airbreather approach shown in Fig. 2.15, as that is an impracticable system by any standard. It is very easy to have estimates that destroy an airbreathing approach in that, to some, they appear perfectly reasonable when in fact they are based on misinformation. The relationship given with Eqs. (4.26a)–(4.26c) will give a realistic and obtainable value, given the industrial capability available today and based on the history of actual integrated airbreathing cycles.

Figure 4.35 shows that air-augmented rockets and ram rockets have lower engine thrust-to-weight ratios because of the secondary air duct weight. The ACES system has a lower engine thrust-to-weight ratio because of the weight of the air separation hardware. And, as postulated, PDEs have a higher *engine* thrust-to-weight ratio because the pumping hardware is lighter than the conventional rocket turbopumps, with a lower required launcher *takeoff* thrust-to-weight ratio. One of the advantages of wing-supported horizontal takeoff is an acceptable lower engine thrust-to-weight ratio. As discussed earlier in conjunction with Fig. 3.29, if the mass ratio permits horizontal takeoff without serious weight penalty, it has the operational advantage to open up more launch sites coupled with less strenuous engine thrust-to-weight requirements.

4.19 Integrated Launcher Sizing with Different Propulsion Systems

The real measure of a propulsion system performance, when installed in a vehicle and sized to a defined payload and mission, is when being compared to other propulsion systems. For the evaluation of the propulsion systems in this chapter, the reference mission is a SSTO mission, launching into 200 km (108 min) orbit with a 28.5° inclination and carrying a 7 t payload with a carried net density of 2.83 lb/ft^3 (45.33 kg/m^3). The sizing has been accomplished using the sizing program described in Chap. 3 (Czysz and Vandenkerckhove 2000) and using the configurations in Fig. 3.13. Hypergolic propellants are carried for in-orbit maneuvering, corresponding to a ΔV of 490 m/s. That results in a weight ratio for in-orbit maneuvering of 1.1148. The orbital maneuvering propellant includes propellant to circularize the orbit and a retro-burn to deorbit the vehicle.

All of the weight ratios presented in this chapter include the orbital maneuvering weight ratio of 1.1148, a value assumed constant for all propulsion systems. That is, the weight ratio of 8.1 for the all-rocket includes the 1.1148 weight ratio, so the actual weight ratio just to achieve orbital velocity is 7.2659. The primary sizing equations are repeated here for convenience. For details of the range of values, and

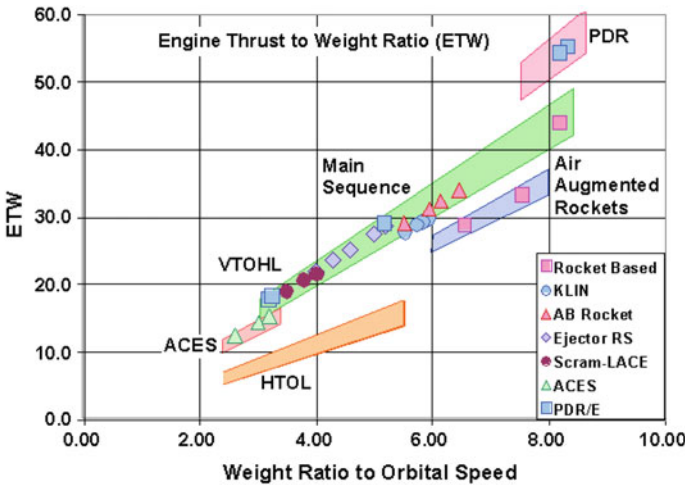

Fig. 4.35 Engine thrust-to-weight ratio decreases with weight ratio

the definition of the terms, see Chap. 3 and (Czysz and Vandenkerckhove 2000). The equations are solved simultaneously for the planform area and Küchemann's τ. Then, the other vehicle characteristics can be determined for that specific solution.

The weight budget is given by:

$$W_{\mathrm{OEW}} = \frac{I_{\mathrm{str}} K_{\mathrm{w}} S_{\mathrm{plan}} + C_{\mathrm{sys}} + W_{\mathrm{cprv}} + \frac{(T/W)_{\mathrm{TO}} \cdot W_{\mathrm{R}}}{(T/W)_{\mathrm{engine}}} \left(W_{\mathrm{pay}} + W_{\mathrm{crew}}\right)}{\frac{1}{1+\mu_{\mathrm{a}}} - f_{\mathrm{sys}} \cdot \frac{(T/W)_{\mathrm{TO}} \cdot W_{\mathrm{R}}}{(T/W)_{\mathrm{engine}}}} \tag{4.27}$$

The volume budget is given by:

$$W_{\mathrm{OWE}} = \frac{\tau \cdot S_{\mathrm{plan}}^{1.5}(1 - k_{\mathrm{vv}} - k_{\mathrm{vs}}) - (V_{\mathrm{crw}} - k_{\mathrm{crw}}) \cdot N_{\mathrm{crw}} - W_{\mathrm{pay}}/\rho_{\mathrm{pay}}}{\frac{W_{\mathrm{R}}-1}{\rho_{\mathrm{ppl}}} + k_{\mathrm{ve}} \cdot (T/W)_{\mathrm{TO}} \cdot W_{\mathrm{R}}} - W_{\mathrm{pay}} - f_{\mathrm{crw}} \cdot N_{\mathrm{crw}} \tag{4.28}$$

with

$$W_{\mathrm{OWE}} = W_{\mathrm{OEW}} + W_{\mathrm{pay}} + W_{\mathrm{crew}} \tag{4.29a}$$

$$W_{\mathrm{OEW}} = W_{\mathrm{OWE}} - (W_{\mathrm{pay}} + W_{\mathrm{crew}}) - W_{\mathrm{trapped\ fluids}} - W_{\mathrm{consumed\ fluids}} \tag{4.29b}$$

The above-summarized approach was originally developed for application to "Copper Canyon" and the National Aerospace Plane (NASP) programs (Schweikart 1998). It was used in the Phase 1 screening of 32 high-speed civil transport concepts (Douglas Model 2229) for the effort NASA sponsored with Douglas Aircraft Company (Bunin 1991; Graf and Welge 1991). The solution was adapted to MathCad by a Parks College graduate student, Ignacio Guerro, for use in the Senior Capstone Aerospace Design Course. Douglas Aircraft checked the solutions against a number of subsonic transports, and the author (P.A. Czysz) checked the solutions against the hypersonic aircraft concept of McDonnell Aircraft Advanced Engineering. Overall, the comparisons between this approach and specific converged design data are very close.

The three key determinants of the airframe empty weight are the (1) total volume, the (2) total surface area, and the (3) structural index. The first two are geometry-determined, and the latter is the total airframe structure (no equipment) divided by the total wetted area. Table 4.7 gives data related to 10 different structural approaches developed over the past 45 years and their impact on the empty weight of a launcher with a 7 t payload and a weight ratio of 6. They are listed in increasing weight per unit wetted area.

Except for structures 8 and 10, all are cold primary structure constituted by an internally insulated cryogenic integral propellant tank, protected by internally insulated metal thermal protection shingles that stand off from the structure/tank wall and provide an insulating air gap. The metal shingles are formed from two sheets of metal with a gap filled with a high-temperature insulation material. The edges are sealed so a multi-layer vacuum insulation can be employed, if needed. Structure 8 has the same thermal protection system, but the propellant tank and primary structure are separate, that is, representing a non-integral tank. Structure 10 is a non-integral tank concept with an external hot structure, separated from the propellant tank by insulation and air gap (like the fuselage of the X-15) (Jenkins 2007). The SR-71 and X-15 wings are hot structures that are not protected by insulation, and the structure and fuel soak up all the aerodynamic heating. In these cases, the determining structural parameter is the hot strength and stiffness of the material. In all other cases, the determining structural parameter is the cold strength and stiffness of the material. All the concepts protect the structure or tank with passive insulation, except concept 1 that uses propellant (fuel) to pump (convect) heat away from the structure and convert it into useful work, see Figs. 4.22 and 4.23.

Table 4.7 Specific weights of structures and associated structural indices

Source	I_{str} (metric) (kg/m^2)	I_{str} (imperial) (lb/ft^2)	W_{OWE} (t)
(1) NASA, active, 1993 (Pegg et al. 1993)	13.8	2.83	33.3
(2) NASA, passive, 1993 (Pegg et al. 1993)	16.6	3.40	43.4
(3) HyFAC, passive, 1970 projection to 1985	17.1	3.50	45.5
(4) VDK, passive, future	18.0	3.68	49.6
(5) VDK, passive, current	21.0	4.30	65.8
(6) HyFAC, passive, 1970 1970 industrial capability	22.0	4.50	72.1
(7) HyFAC, passive, 1970 1966 industrial capability	22.7	4.66	76.7
(8) HyFAC, passive, 1970 non-integral tank	25.4	5.20	96.5
(9) HyFAC, passive, 1970 1970 hypersonic demonstrator	29.3	6.00	130.6
(10) HyFAC, hot structure, 1970 non-integral tank	32.5	6.66	163.4

4.20 Structural Concept and Structural Index

Structures 1 and 2 in Table 4.7 are from reasonably recent reports (1993) concerning metal thermal protection systems (TPS) with current advanced titanium and metal matrix composite materials. Structures 3, 6, 7, 8, 9, and 10 are from the seminal Hypersonic Research Facilities Study (HyFAC) conducted for NASA by McDonnell Aircraft Company, Advanced Engineering Department, from 1968 to 1970 (Pirrello and Czysz 1970). One of the authors (P.A. Czysz) was the Deputy Study Manager for that program. Except for structure 3, which anticipated the development of advanced titanium, metal matrix composite materials, and high-temperature plastic matrix materials, the other concepts employ high-temperature chrome-nickel alloys and coated refractory metals for the thermal protection shingles that enclosed the vacuum multi-layer insulation. Structure 9 represents an effort to minimize the cost of a short flight time research vehicle (5 min) at the expense of increased weight by using more readily available high-temperature materials.

Structures 4 and 5 have been the work of the late Jean Vandenkerckhove (VDK) and the late author (P.A. Czysz) to characterize the high-temperature metal and ceramic materials available at the time in Europe. Carbon/carbon, silicon carbide/carbon, and silicon carbide/silicon carbide structural material from SEP, Bordeaux (now SAFRAN/SNECMA, Bordeaux), and metal matrix composites from British Petroleum, Sudbury, along with the conventional aircraft materials, have been characterized from information supplied by the major European aerospace manufacturers. At that time, no materials from the former Soviet Union were included. Notice that the structural concepts center on the HyFAC study structural data. These representative values have been used in most of the work completed by the authors.

The two structural indices used by J. Vandenkerckhove for a weight ratio 6 launcher result in a W_{OEW} of 49.6 t employing VDK *future,* and 65.8 t employing VDK *current*. The same vehicle using the 1970 McDonnell Douglas structural index results in 72.1 t *current* and 45.5 t *future* (projected to 15 years in the future, to 1985). Assuming the current availability of materials and manufacturing processes equivalent to 1970, then the vehicle empty weight ranges between 65.8 and 72.1 t. Assuming the current availability of materials and manufacturing processes equivalent to the 1985 projection (and from what the authors saw at SEP, Bordeaux, BP, Sudbury, and NPO Kompozit, Moscow), then the vehicle empty weight ranges between 45.5 and 49.6 t. Note that these values should span what is possible with readily available materials today, as much as the Saturn V was constructed from what was available in 1965. As we see from Table 4.7, the non-integral structural concepts are not competitive, resulting in a W_{OEW} of 96.5 t for a passively insulated tank, and 163.4 t for a hot structure concept. The 1993 results from (Pegg et al. 1993) show some weight reduction in the passive structural concept of the order of about 5%, not a critical item. The focus on future launcher must be durability over a long period of use, not one-time lightness. The design, build, and operations philosophy must be akin to that of the Boeing B-52, not of an ICBM.

The cold, insulated integral tank structural concept employed in these studies remains appropriate and valid. The concept has withstood the test of many challenges, but remains the lightest and lowest-cost approach to high-temperature, hypersonic aircraft structure that has been established by practice (Pirrello and Czysz 1970). The primary structure is principally aluminum with steel and titanium where strength is a requirement. The aerodynamic surface is made by interleaved smooth shingles with standoff

and insulation material that provide a high-temperature radiative surface to dissipate to space most of the incoming aerodynamic heating. Less than 3% of the incoming aerodynamic heating reaches the aluminum structure. The HyFAC data dates back to circa 1968 and is built on the materials and insulation available then. With advanced RSR materials and superplastic forming with diffusion bonding, together with silicon carbide and carbon fiber reinforcements to fabricate metal matrix composites (MMC), the values in Table 4.7 should be conservative.

The active TPS values are from a more recent source, as given by Pegg et al. (1993). Depending on the duration of the flight, that heat can be absorbed in the airframe thermal capacitance or removed by an active thermal management system (see Figs. 4.22 and 4.23). For some short duration (10 min or less) research flights and some orbital ascent flights, no active thermal management system is necessary. For a long-duration cruise flight, some means of moving the incoming thermal energy to a site where it can be disposed of or used to perform mechanical work is required. The original concept from the 1970s has been implemented, using high-temperature refractory metals such as columbium (niobium), tantalum, molybdenum, and Réne 41 and other refractory alloys, which have densities larger than steel (9000–17,000 kg/m^3).

Clearly, today's RSR titanium, RSR metal matrix composites (MMC), titanium aluminide, carbon/carbon, and silicon carbide/silicon carbide composites can achieve the same temperature performance at much less weight. The weight estimates based on scaling of the 1970 data are therefore very conservative. The configuration concept uses conventional aircraft construction techniques for most of the aircraft; the shingles are well within the current manufacturing capabilities considering the hot isostatic pressing, superplastic forming, and diffusion bonding available in the gas turbine industry. For longer-duration flights required for long-range cruise, the advantages of active thermal management are clear. With current materials, whether actively thermally managed for cruise, or passively thermally managed for exit and entry, it should be possible in the 2016-plus timeframe to build a structure for a hypersonic aircraft that is between 3.0 lb/ft^2 and 4.0 lb/ft^2 (14.6 and 19.5 kg/m^2) using materials and processes available today.

The W_{OWE} is a function of the structural index, I_{str}, and a weak function of the weight ratio to orbit W_R, see Fig. 4.36. There is a 15% margin on the W_{OEW} assigned by the sizing equations. The W_{OWE} that applies to the sizing results in this book is given by Eq. (4.30):

$$W_{OWE} = 65.8 \cdot [0.003226 \cdot (I_{str})^2 - 0.04366 \cdot (I_{str}) + 0.4943] \cdot (0.02369 \cdot W_R + 0.8579) \tag{4.30}$$

4.21 Sizing Results for Continuous and Pulse Detonation Engines

For the evaluation of the different propulsion systems, see Table 4.7, structural concept 5 (VDK *current* at 21.0 kg/m^2) has been used. The propulsion systems, see Fig. 4.34, have

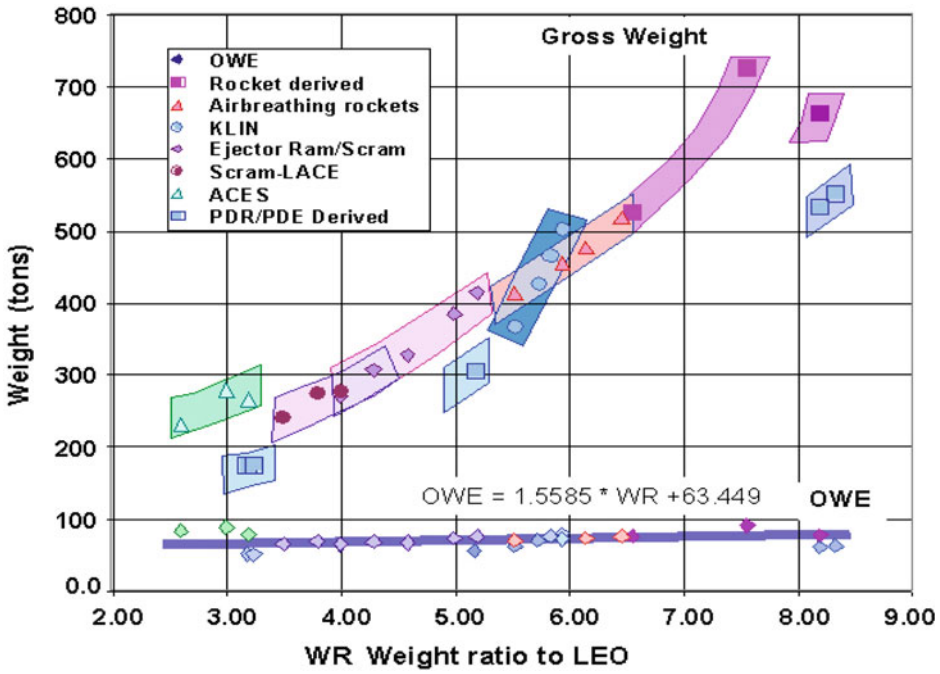

Fig. 4.36 Gross weight decreases significantly as weight ratio decreases. Operational weight empty is almost constant

been installed in the appropriate configuration concept and sized to mission. Figure 4.37 presents W_{TOGW} and W_{OWE} as a function of oxidizer-to-fuel ratio, and Fig. 4.36 presents W_{TOGW} and W_{OWE} as a function of weight ratio. Each of these presentations provides different perspectives of the sizing results and the characteristics of the propulsion systems.

Whenever presenting results as a function of oxidizer-to-fuel ratio, Fig. 4.37, there is always the discontinuity between the rockets and the airbreathing systems. For the rocket-derived systems, the all-rocket is not the top point, but the second from the top. The air-augmented rocket is heavier than the all-rocket, because the thrust increase and reduced oxidizer-to-fuel ratio do not offset the weight of the ejector system. This is clearly shown in Fig. 4.36, as the air-augmented rocket has a mass ratio of 7.5 and is heavier than the all-rocket. Below that point, the W_{OWE} value is on top of the correlation line indicating a heavier empty weight. The ram rocket, in which the oxygen in the ejector secondary air is burned, is a different case, and the weight and oxidizer-to-fuel are less than the all-rocket. The ram rocket has a gross weight similar to the PDE. The difference is that the ram rocket is at the end of its improvement capability while the PDE is just at the beginning of its potential improvement cycle. The pulse detonation rocket (PDR) has a gross weight similar to the ram rocket, with much less complexity. The important result is that either can reduce the gross weight by 200 t! This is comparable to the highest values of the airbreathing rockets and the KLIN cycle.

Clearly, the incorporation of some airbreathing in the rocket, whether an ejector burning fuel in the secondary air stream (ram rocket) or by direct airbreathing rocket (LACE, deeply cooled rocket or KLIN cycle), results in a significant advantage in gross liftoff weight and engine size and thrust reduction (in fact, a 28% reduction).

Direct airbreathing rockets (LACE, deeply cooled rocket, or KLIN cycle) form a group in the center of both charts (Figs. 4.36 and 4.37) and are in the 3–4 oxidizer-to-fuel ratio and in the 5.5–6.5 weight ratio area. These propulsion cycles form the first steps in airbreathing propulsion and are capable of reducing the gross weight from nearly 700 t (metric tons) to 400–500 t. Their maximum airbreathing Mach number is in the 5–6 range.

The important aspect is that this is a beginning capability that, with adaptation to further airbreathing (scram-LACE), can achieve gross weights in the 200–300 t range. As shown in Fig. 3.4, as the airbreathing speed is increased, both the oxidizer-to-fuel ratio and mass ratio decrease until Mach 12 airbreathing speed is reached, when further increase of airbreathing speed does not result in additional decrease in the mass ratio. This results from the fact that, as shown in Eqs. (4.12) and (4.13), both thrust and specific impulse for an airbreathing system decrease with the inverse of speed while drag could increase. When the effective specific impulse (based on thrust minus drag) falls below the effective specific impulse of a rocket, the rocket is a better accelerator. As a consequence, attempting to fly to orbital

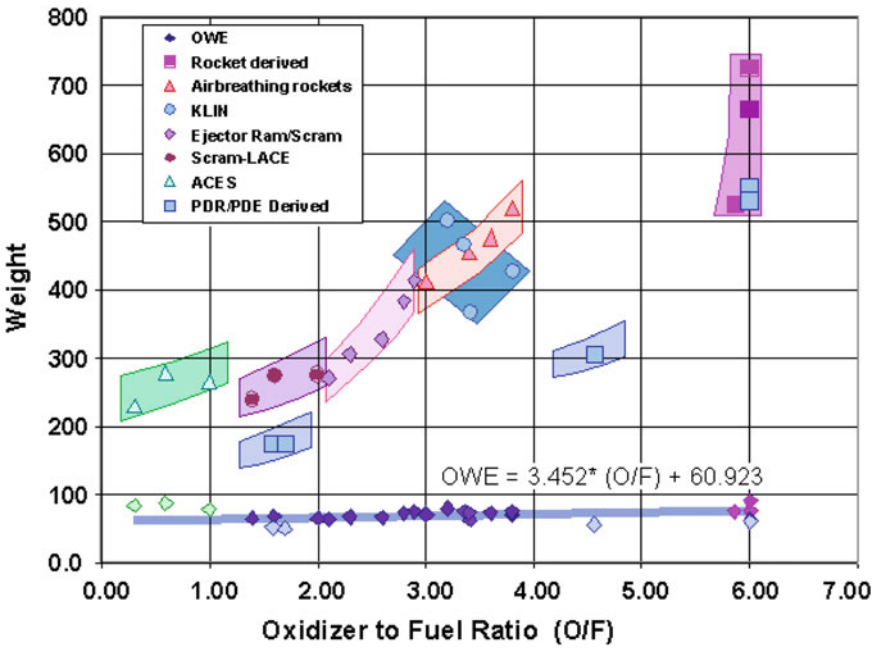

Fig. 4.37 Gross weight decreases significantly as oxidizer-to-fuel ratio decreases. Operational weight empty (empty weight plus payload) is nearly constant

speed with an airbreather will result in a larger vehicle that requires more propellant.

Air collection, enrichment, and separation (ACES) began as a recommended system beneficial for TSTO launchers. As discussed in Chap. 2 and later in this chapter, for the TSTO application the ACES system presents significant advantages. However, for the SSTO configuration implementation, the additional volume requirement in the orbital vehicle can carry penalties, depending on the system design chosen. Even though ACES has both a lower weight ratio and lower oxidizer-to-fuel ratio, its gross weight is about the same as the ejector ram–scramjet and the scram-LACE and scram–deeply cooled. In both plots (Figs. 4.36 and 4.37), the W_{OWE} is heavier than (above) the correlation line, as was the air-augmented rocket.

What does fall below the W_{OWE} correlation line are the PDE points. That is for two reasons: (1) less volume required and (2) lower weight of propellant pumping systems. In Fig. 4.35, it is almost possible to envision a new main sequence of PDEs parallel and lower than the continuous operation engines. As this class of engines is developed into operational systems, the potential exists for this class to reduce both, the rocket class and airbreather class, in gross weight and empty weight. What is not clear at this point is, whether the cyclic engine can have variants equivalent to the airbreathing rocket and its ACES derivative. These latter engine types may remain as continuous operation engine cycles only.

If we take the W_{OWE} results and subtract the 7 t payload to yield the W_{OEW}, then it is possible to see how volume affects the magnitude of the empty weight. Figure 4.38 shows the empty weight value as a function of the total vehicle volume. The correlation is rather good. First, notice that the triangles representing the ACES propulsion system have almost the largest volumes. The largest is the air-augmented rocket. This clearly explains the W_{OWE} values in the previous two graphs where the W_{OWE} values were greater than the correlation curve through the other cycles. It is also clear that the PDEs have some of the lowest volume values for the propulsion systems presented. Clearly, the variation in empty weight can primarily be explained by variation in total volume. The W_{OWE} is also a function of the structural index and the weight ratio to orbit, see Fig. 4.36. As given in Eq. (4.30), we now can determine the mean W_{OWE} for any other structural index than the VDK *current* at 21.0 kg/m^2 and any mass ratio.

When representing the data in Fig. 4.36 in terms of total volume rather than weight, this results in Fig. 4.39. Clearly, the ACES systems lie above the main sequence of propulsion systems (large shaded area) and the PDEs lie below the main sequence of propulsion systems. Whether the PDE-ramjet and PDE-scramjet areas can be connected remains to be seen, there should be no technical reason why future PDE systems would not span that area.

What we can conclude so far is:

(1) The structural concept for an insulated cold primary structure is an important decision that can have a significant impact on vehicle empty weight. For launchers, passive thermal protection is more than adequate. However, for a cruising vehicle, passive insulation permits too much of the aerodynamic heating to reach the cryogenic tanks, and an active heat removal scheme is required. Pegg et al. employed fuel as the heat transfer agent (Pegg et al. 1993). Others include water, water-saturated capillary blankets, and other phase-change materials between the backside of the shingle and the integral tank structure outside surface. All of these are appropriate for most of the structure for blended-body or all-body configurations. The leading edges are based on sodium heat pipes that move the thermal energy to a lower temperature area or a heat exchanger. Control surfaces are a case-by-case basis, and each is designed based on configuration and local flow conditions. In terms of the total vehicle and an advanced concept initial sizing, these have minimal impact on the final size and weight. But if the reader wishes to refine the estimate, the values in Table 4.7 can be improved by the following first-order correction. This correction assumes that the leading edges are 10% of the total surface area, and the control surfaces are 15% of the total surface area. Note that the corrections are based on values from (Pirrello and Czysz 1970) for an operational vehicle.

$$I_{str} = 5.87 + 0.75 \cdot (I_{str})_{\text{Table 4.7}} \tag{4.31}$$

Then, the VDK *current* structural index would become 21.6 kg/m^2.

(2) Given the thermal protection system and structural concept, the next most important determinant of the empty weight is the total volume of the vehicle, see Fig. 4.38. In some cases, the total volume is a response to the change in oxidizer-to-fuel ratio; in other cases, it is the inherent volume of the propulsion concept (ACES and PDE systems) as shown in Fig. 4.39.

(3) The gross weight is a direct result of the weight ratio to orbit (Fig. 4.36), which is determined by the propulsion system oxidizer-to-fuel ratio (Fig. 4.34).

(4) The threshold values for the oxidizer-to-fuel ratio and weight ratio, that clearly separate airbreathing systems from rocket-derived vehicles, are 3.9 and 6.5, respectively (Figs. 4.37 and 4.36). At these values, the W_{OWE} for a launcher with a 7 t payload is 71.48 t, the gross

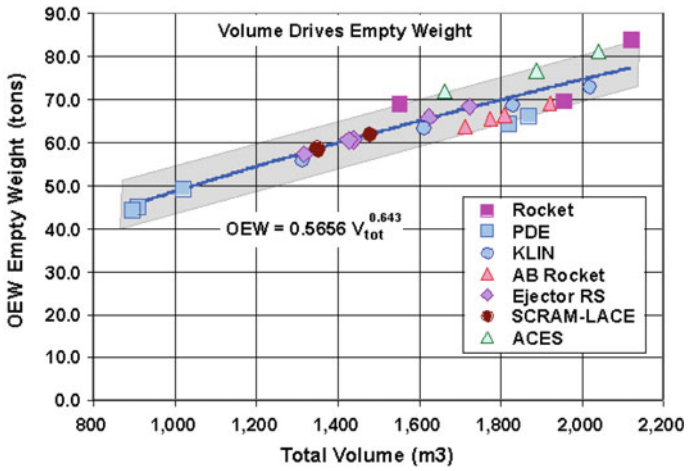

Fig. 4.38 Total volume decreases as the weight ratio decreases, except for ACES propulsion system

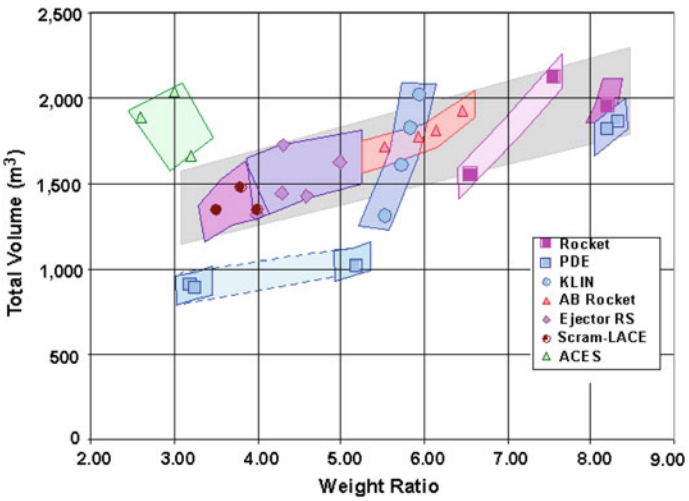

Fig. 4.39 Empty weight is less if total volume is less. ACES is heavier because volume is greater

weight is 510 t, overall less than the 690 t for the all-rocket case.

(5) The ACES system for a SSTO will have a greater volume than a corresponding ejector ram–scramjet propulsion system. Even though the weight ratio and oxidizer-to-fuel ratio are less, some of the weight ratio and oxidizer-to-fuel advantages may be offset (Figs. 4.37 and 4.39).

(6) Because of the reduced pumping system weights and the lesser installed volumes, the pulse detonation propulsion systems will have a smaller volume and less weight than a corresponding sustained operation propulsion system.

(7) Propulsion system weight has been assumed to be a constant, equal to that for the all-rocket with a gross weight of 690 t, liftoff thrust of 932 t, and a propulsion system weight of 16.9 t. The exceptions are the air-augmented rocket in which an ejector structure has been added to the airframe, the ACES system in which the air separation system has been added to the LACE or deeply cooled airbreathing rockets, and the PDEs where the conventional turbopumps have been replaced by lower-pressure-ratio turbocompressors (Fig. 4.35).

4.22 Operational Configuration Concepts: SSTO and TSTO

For the *rocket-derived vehicles*, the configuration is the hypersonic glider derived from the Air Force Flight Dynamics Laboratory FDL-7 C/D (Draper and Sieron 1991). This configuration is depicted accelerating to orbit in Fig. 4.40. As depicted, it is powered by either a LACE or a deeply cooled airbreathing rocket. Although sized as a SSTO vehicle, it could also represent the second stage of a TSTO accelerating to orbital speed. At the altitude shown, the Mach number is greater than 6, so the inward-turning inlet is retracted. As *Model 176*, see Fig. 3.9, the McDonnell Douglas version for MOL (Anon 2015), it was designed in 1964 for a fleet of 10 vehicles to fly between 75 and 90

flights per year with an individual aircraft flight rate between overhaul of 200 and an operational life of 25 years.

For the *airbreather-derived vehicles*, the configuration is derived from the McDonnell Blended Body, as shown in Fig. 4.41. The configuration is depicted in an accelerating climb with a combination of rocket and ramjet power as the vehicle accelerates through the transonic flight regime. It is depicted climbing from a C-5A Galaxy air launch, but it could just as easily have separated from an An-225 *Mriya*. If this were a TSTO vehicle, a smaller version of the vehicle in Fig. 4.40 would be on top, and separation would be in the Mach 8 to 14 range. As one of the reference operational vehicles for the 1970 HyFAC study (Pirrello and Czysz 1970), this airbreathing launcher was the first stage of the TSTO vehicle that staged at Mach 10 to 12. Later, as the CFD (Computational Fluid Dynamics) verification model for Copper Canyon and the subsequent NASP program (Schweikart 1998), it was a SSTO configuration which has been as well publicized as the *Orient Express* (Conway 2008; Davies 1998). Again, the design goals were for frequent flight, spanning a long operational life with significant flights between overhaul, as for the Model 176. Unfortunately, no actual goal numbers have survived.

In the authors' opinion, for a versatile and payload-flexible launcher, a TSTO vehicle offers the best options. And there have been some elegant and practical TSTO launchers designed, but unfortunately never built. Figure 4.42 shows two of those launchers, the MBB *Sänger* (upper) and the Dassault Aviation *Star-H* (lower). The MBB *Sänger* program also conceived the first stage being constructed as a hypersonic transport carrying over 200 passengers (Kuczera and Sacher 2011; Koelle et al. 2007). This highly refined blended wing-body was developed through extensive wind tunnel testing, including the detailed testing of the second-stage separation at Mach 7 in the Ludwig-Tube facility at the Göttingen DLR Institute in Germany (Jacob et al. 2005).

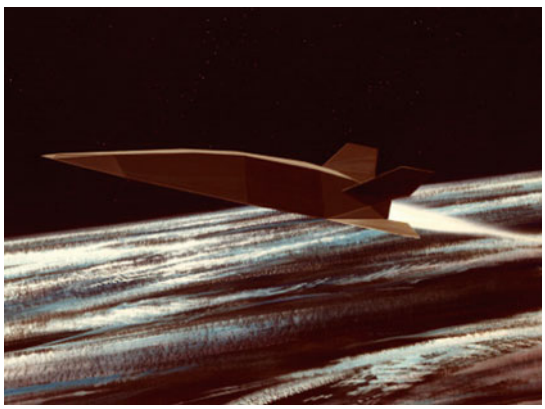

Fig. 4.40 LACE rocket-powered VTHL SSTO with a gross weight of 450 t, a weight ratio of 5.5 and an oxidizer/fuel ratio of 3.5

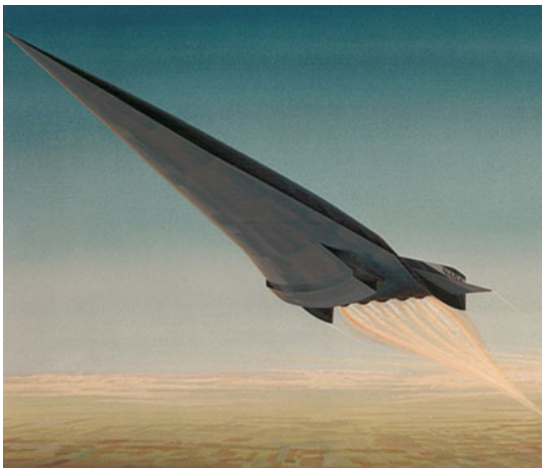

Fig. 4.41 Ejector ram–scramjet-powered HTHL SSTO with a gross weight of 300 t, a weight ratio of 4.3 and an oxidizer/fuel ratio of 2.2

The second stage of the MBB *Sänger* was a flat-bottom hypersonic glider that carried the ascent propellant and payload to orbit. It was designed as an automatically piloted vehicle. Considering that the net density of a passenger cabin is about 80 kg/m^3 and that of subcooled hydrogen is 76 kg/m^3, a hydrogen tank makes a perfect cabin for a weight of passengers equal to the weight of the hydrogen, with much less thermal insulation requirements. Switching the fuel to subcooled methane means that there is volume for both the passengers and methane, replacing the hydrogen and oxygen for the launcher.

Dassault Aviation *Star-H* used a different approach for the second stage (Kuczera and Sacher 2011; Kingsbury 1991). Since the thermally protected second-stage glider is the most costly, the Dassault Aviation *Star-H* approach has been to minimize its size and have it carry payload only; the propellant and thrust has been provided by a separate expendable rocket. This reduces the size of the hypersonic glider, in this case depicted as the Hermes (Hannigan 1994). This was also the philosophy of Gleb Lozino-Lozinskiy in the Mikoyan *Spiral 50-50* concept that dates back to 1968 (Harford 1997).

Both the MBB *Sänger* and the Dassault Aviation *Star-H* are elegant designs that could have been successful, in principle, had they been built. However, both suffered from a propulsion community mistaken assumption that the turbojet was the best accelerator for lower speed operation between Mach 2.5 to Mach 3.0. The resultant massive over-and-under turbojet/ramjet propulsion system of the MBB *Sänger* and the turboramjet propulsion system of the Dassault Aviation *Star-H* appear to have been their downfall. A rocket ejector ramjet or airbreathing rocket would have provided excellent acceleration capability instead.

In Chap. 3, we compare a TSTO powered by a rocket ejector ramjet with a TSTO powered by a turboramjet (Czysz

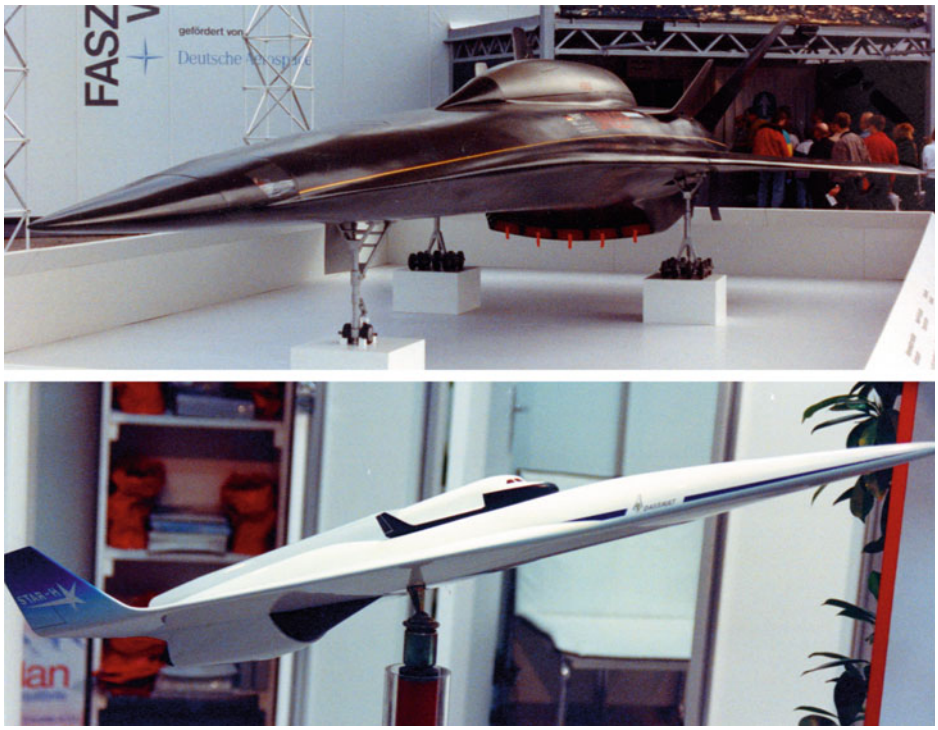

Fig. 4.42 Two elegant TSTO designs. The MBB Sänger (*top*) and Dassault Aviation Star-H (*bottom*)

and Vandenkerckhove 2000). Both TSTO launchers have been sized to deliver a 7 t payload to 463 km in a 28.5° inclination orbit. The staging Mach number selected is 7, which is the same as for the MBB *Sänger* system. In comparison, the turboramjet launcher consists of a second stage weighing 108.9 t, carried by a 282.7 t first stage for a total liftoff weight of 393.0 t. The rocket ejector ramjet launcher consists of a second stage weighing 118.4 t, carried by a 141.6 t first stage for a total liftoff weight of 261.0 t. We observe a significant weight difference; the ejector ramjet thrust is nearly constant from transonic to staging speeds, while the turboramjet at staging speed is only providing 25% of the transonic thrust. The turboramjet has significantly more thrust at takeoff, but that is not as important as maintaining a constant supersonic acceleration. The result is that the turboramjet launcher suffers a 50% gross weight penalty at takeoff when compared with the ejector ramjet launcher case.

If a commercial hypersonic transport version of the first stage was contemplated, then the propulsion system would have to be changed to a cruise-focused system, replacing the acceleration-focused system of the launcher. The *acceleration-focused system* must maximize thrust minus drag, $T - D$, and minimize zero-lift drag, C_{D0}. The *cruise-focused system* must maximize aerodynamic efficiency, L/D, and propulsion efficiency, θ. This change in focus almost precludes a single system from doing both missions. The exception might be Rudakov's combined cycle with the performance shown in Fig. 4.20. The attempt to get one gas turbine-based propulsion system to do both is the weakness of most of these legacy TSTO programs. Yet TSTO launchers are an excellent option, and with a suitably powered TSTO, a substantial saving in gross weight can be realized together with significant payload flexibility. Note that the more recent NASA-DARPA *Horizontal Launch Study* from 2011 (Bartolotta et al. 2011) does indeed employ gas turbine propulsion with the transonic carrier vehicle, as does the British Aerospace Interim HOTOL study from 1991 (Parkinson 1991), the NPO Molniya MAKS study from 1976 to 1981 (Lozino-Lozinskiy and Bratukhin 1997; Lozino-Lozinskiy et al. 1993), the recent 4-turbojet WhiteKnightTwo carrier aircraft being built by Virgin Galactic (Anon 2016), and Paul Allen's 6-turbojet carrier aircraft Stratolaunch (Anon 2014).

In the 1990s, Paul A. Czysz and the late Jean Vandenkerckhove extensively examined the SSTO compared to the TSTO based on rocket ejector ram–scramjet propulsion (Czysz and Vandenkerckhove 2000; Vandenkerckhove 1991, 1992a, b, 1993a, b). Figure 4.43 compares the takeoff gross weight (W_{TOGW}) results, and Fig. 4.44 compares the dry weight (W_{OEW}) results. Note that any crew for space operations, or crew rotation on an orbital station, are considered payload and not crew, that is, pilots. Nine comparisons are made as described below:

(1) SSTO with VDK *current* structural concept (reference: 21.0 kg/m^2) with 15% dry margin and crewed (piloted) by two crewmembers with provisions for orbital stay, powered by ejector ram–scramjet of VDK design, *Hyperjet* Mk 3 (Vandenkerckhove 1993a).

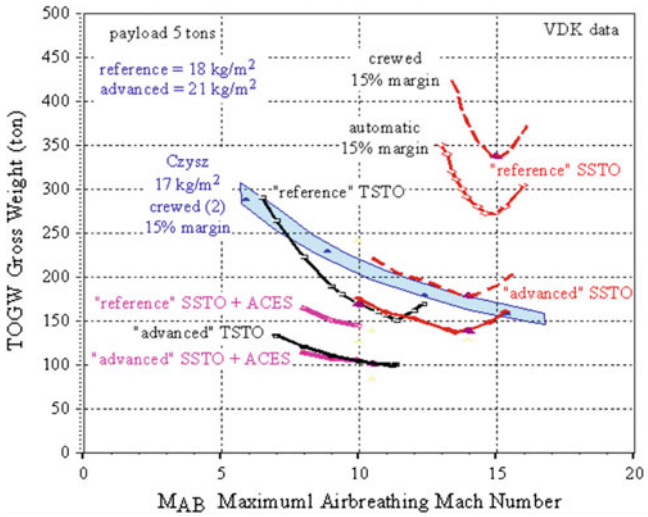

Fig. 4.43 Comparison of SSTO and TSTO results for W_{TOGW}

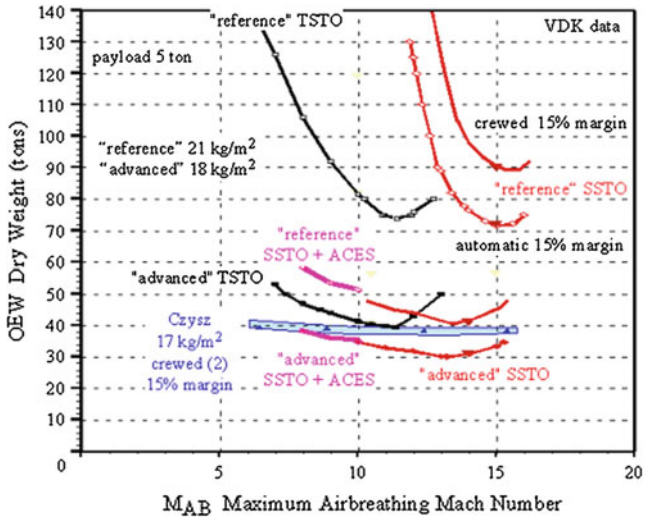

Fig. 4.44 Comparison of SSTO and TSTO results for W_{OEW}

(2) SSTO with VDK *current* structural concept (reference: 21.0 kg/m^2) with 15% dry margin and piloted by automatic flight control system, powered by ejector ram–scramjet of VDK design, *Hyperjet* Mk 3 (Vandenkerckhove 1993a).
(3) SSTO with VDK *future* structural concept (advanced: 18.0 kg/m^2) with 15% dry margin and crewed (piloted) by two crewmembers with provisions for orbital stay, powered by ejector ram–scramjet of VDK design, *Hyperjet* Mk 3 (Vandenkerckhove 1993a).
(4) SSTO with VDK *future* structural concept (advanced: 18.0 kg/m^2) with 15% dry margin and piloted by automatic flight control system, powered by ejector ram–scramjet of VDK design, *Hyperjet* Mk 3 (Vandenkerckhove 1993a).
(5) SSTO with Czysz structural concept from McDonnell HyFAC Study (17.0 kg/m^2) with 15% dry margin and piloted by automatic flight control system, powered by engines with maximum airbreathing Mach numbers from 6.0 to 12.0 from the engine sequence in Fig. 3.4 (Pirrello and Czysz 1970).
(6) TSTO with VDK *current* structural concept (reference: 21.0 kg/m^2) with 15% dry margin and piloted by automatic flight control system, powered by ejector ram–scramjet of VDK design, *Hyperjet* Mk 3 (Vandenkerckhove 1993a).
(7) TSTO with VDK *future* structural concept (advanced: 18.0 kg/m^2) with 15% dry margin and crewed (piloted) by two crewmembers with provisions for orbital stay, powered by ejector ram–scramjet of VDK design, *Hyperjet* Mk 3 (Vandenkerckhove 1993a).
(8) SSTO with VDK *current* structural concept (reference: 21.0 kg/m^2) with 15% dry margin and piloted by automatic flight control system, powered by ejector ram–scramjet of VDK design with ACES (air collection, enrichment, and collection).
(9) SSTO with VDK *future* structural concept (advanced: 18.0 kg/m^2) with 15% dry margin and piloted by automatic flight control system, powered by ejector ram–scramjet of VDK design with ACES (air collection, enrichment, and collection).

Because a specific engine design has been considered, the results have much sharper minima compared to the generic engine concepts. In Fig. 4.43, we can see the impact of piloted (crewed) systems for both "reference" SSTO and "advanced" SSTO launchers. For the reference case, the gross weight increment is almost 70 t. The minimum gross weight occurs at Mach 15 maximum airbreathing speed for the "reference" SSTO structural concept and Mach 14 for the "advanced" SSTO structural concept. The gross weight is driven by the difference in empty weight shown in Fig. 4.44. In this figure, the 20 t difference in W_{OEW} is clearly seen for the "reference" structural concept. The results from *Hypersonic Convergence* (Czysz 1987) are close to the results obtained by VDK's "advanced" solutions. The difference is that the family of combined-cycle propulsion systems yields a design point at each Mach number, whereas the VDK results are for a particular ejector ramjet engine configuration.

Examining the TSTO results, there are two interesting observations. (1) The first is that the minimum empty weight of both TSTO stages is about the same compared to the single SSTO system for both the "reference" and "advanced" structural concepts. This means that other than design and

engineering costs, the airframe cost based on weight should be quite comparable. Note that the design, engineering, and production costs are not the driving costs in launcher operations, see Fig. 3.2. (2) The second is that the gross weight for the "reference" TSTO is only slightly greater than the "advanced" SSTO, and that the "advanced" TSTO presents one of the lowest gross weights. This is due to the fact that much less mass (second stage only) must be delivered to orbit for the TSTO, compared to the entire (non-staging) SSTO vehicle. Clearly, the TSTO can have an acquisition and cost advantage over the SSTO implementation. If both vehicles are automatic, then crew costs are not a distinguishing factor.

The last comparison is the addition of ACES (air collection, enrichment, and separation) to the SSTO propulsion system. This permits the SSTO to have an offset capability analogous to the TSTO as it collects the enriched air oxidizer for ascent into orbit. Jean Vandenkerckhove and Patrick Hendrick wrote the complete ACES performance code themselves rather than depend on 1960s programs. The performance of the hardware came primarily from two sources, John Leingang in the USA (Leingang et al. 1992) and M. Maita and his colleagues with the National Aerospace Laboratories (now JAXA) in Japan (Maita et al. 1990). The results show that the addition of ACES to SSTO results in the SSTO vehicle weight now being equivalent to the TSTO vehicle. The results are different than those from Figs. 4.36 and 4.37; this is due to the fact that the Vandenkerckhove results are based on a detailed system analysis of individual hardware items, while the results presented with Figs. 4.36 and 4.37 are based on correlated results. However, the results are not that dissimilar in that both suggest that a SSTO with ACES is as light as an advanced TSTO.

Examining Figs. 4.36 and 4.37, there are a number of options that yield very similar results. Considering the "advanced" SSTO with automatic flight controls for a maximum airbreathing Mach number of 14, and the "reference" TSTO with automatic flight controls for a maximum airbreathing Mach number of 12, and the "reference" SSTO plus ACES with automatic flight controls for a maximum airbreathing Mach number of 10, we have three different systems, two of which use current materials and fabrication capability, with essentially the same gross weight and different empty weights. Considering the "advanced" TSTO with automatic flight controls for a maximum airbreathing Mach number of 12, and the "advanced" SSTO plus ACES with automatic flight controls for a maximum airbreathing Mach number of 10, we have two different systems with essentially the same gross weight and similar empty weights.

Clearly, there are two approaches to reach minimum weight launchers. One approach is to focus on TSTO with inherent payload size and weight flexibility, or alternatively focus on SSTO with ACES and a more focused payload capability, such as discussed for the Model 176 resupply and crew rescue vehicle for the MOL.

4.23 Emerging Propulsion System Concepts in Development

This section will discuss two propulsion systems that operate in a manner different from conventional airbreathing chemical combustion systems.

(1) The first propulsion system originated in the former Soviet Union, probably in the 1970s, as a total energy concept that coupled aerodynamic forces with electromagnetic forces, thereby requiring a local plasma flow to exist for the system to work. The name given by its inventor, the Russian V. Freishtadt, to the system is *Ayaks* (АЯКС), or Ajax, and is described as a magnetohydrodynamic (MHD) energy bypass system. If the flow inside (or even around) the aircraft is sufficiently ionized, i.e., in the plasma state, then the MHD system is equivalent to an induction generator that can remove energy (reduce velocity) from the flow in the form of an electrical current, with minimal aerodynamic diffusion (Tretyakov 1995). This reduces the energy lost through shock waves in conventional inlet aerodynamic deceleration, at the price of increasing drag. If that electrical power is transmitted to the equivalent of an induction motor (a Lorentz force accelerator), then electromagnetic interaction with the plasma can add energy (increase velocity) back to the flow.
The motivation for the MHD system is the realization that the electromagnetic energy transfer suffers less of an entropy rise (irreversible energy loss) than aerodynamic diffusion and expansion, therefore the net thrust is greater. If the flow field around the aircraft is a plasma, flow energy (Gorelov et al. 1995) can be removed at the nose by an MHD generator that alters the shock wave structure around the vehicle, overall reducing the total drag (Batenin et al. 1997). Again, because the flow is ionized, the flow in the propulsion inlet system can be turned by MHD Lorentz forces instead of physical inlet ramps, a form of morphing. That may dramatically reduce the weight and mechanical complexity of the inlet/nozzle system. In this chapter, the focus is on the energy bypass system, and it must be noted that a

rigorous evaluation of all concept elements has not been made, so that this concept is still controversial.

(2) The second propulsion system is creating heated air to produce thrust not by combustion, but by the interaction between matter (air) and intense electromagnetic radiation (either by a *laser* or by a *microwave beam*). The advantage is that only some working fluid (usually water) is needed to produce thrust; water is dense when stored liquid while producing a low molecular-weight gas when heated. Matter does not need to be combustible. Since the energy source is remote from the vehicle, a directed energy beam (from Earth, or the Moon, or a space station or wherever) must provide the power to the vehicle to produce thrust. This vehicle is named *Lightcraft* by its inventor, the late Professor Leik Myrabo, formerly at Rensselaer Polytechnic Institute.

4.23.1 MagnetoHydroDynamic (MHD) Energy Bypass System

The initial Ajax system information came from two sources (Novichkov 1990a, b). One was from a Russian document and the other an article in *Space Wings of Russia and the Ukraine* in the September 1990 magazine Echoes of the Planet/Aerospace. The article states that the project has originated in the State Hypersonic Systems Scientific Research Enterprise (GNIPGS) in St Petersburg, which was headed by Vladimir Freishtadt. The article elaborates on the cooperation of industrial enterprises, the Technical Institutes, the VPK (Military Industrial Commission), and the RAS (Russian Academy of Sciences). All the discussions with individuals about Ajax stress both the global range capability at hypersonic speeds and the directed energy device for peaceful purposes. Interestingly, the use as a space launcher is not mentioned.

Beginning in 1990, in Russian and Ukrainian literature articles started to appear about a new long-range hypersonic aircraft named Ajax, whose development had begun at least 10 years earlier. Its propulsion system employed a coupled magnetohydrodynamic (MHD) element that (reportedly) significantly increased the performance of and decreased the size of the hypersonic vehicle. With the available literature and after discussions by the authors with Russian and Ukrainian citizens, there was sufficient information to use first principles to analyze the system and determine whether the concept provided a real advantage.

In September 1996, as part of the Capstone Design Course, AE P 450-1, and the Hypersonic Aero-Propulsion Integration Course, AE P 452-50, at Parks College, Saint Louis University, a student design team took on the task of analyzing Ajax. The resulting performance increase reduced

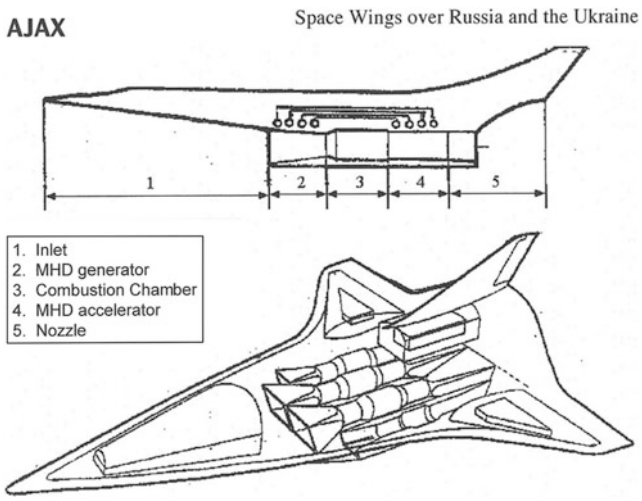

Fig. 4.45 Ajax from article by *Space wings over Russia and the Ukraine*

the size and weight of the performance-sized aircraft (Esteve et al. 1977). The student team members were Yago Sanchez, Maria Dolores Esteve, Alfonso Gonzalez, Ignacio Guerrero, Antonio Vicent, and Jose Luis Vadillo. Professor Mark A. Prelas, Department of Nuclear Engineering, University of Missouri-Columbia, was an advisor to the student team. After touring a number of Russian nuclear facilities, he provided first-hand knowledge of the ionization devices that are reported to be key components of the Ajax system.

From Novichkov (1990a) comes a sketch of the propulsion system with the coupled MHD generator-accelerator showing the energy bypass concept, see Fig. 4.45. The simple sketch gives a cross section similar to any airframe-integrated propulsion system, in which the bottom of the vehicle hosts the propulsion system, and the forebody is indeed the front part of the inlet. Also from Novichkov (1990b) are the features of the Ajax system and reasons the Ajax system was developed. They are as follows:

(1) *Energy bypass* via a coupled MHD generator-accelerator system (Gurianov and Harsha 1996; Carlson et al. 1996; Lin and Lineberry 1995): a portion of the free stream kinetic energy bypasses the combustion chamber, to reduce the entropy rise associated with aerodynamic diffusion and to augment the combustion process.

(2) *Reforming* of hydrocarbon fuel via a thermal decomposition process, followed by an electrical arc process into a high hydrogen fraction fuel, with about 20,200 Btu/lbm heat of combustion. It is assumed that the products are gaseous hydrogen, ethylene, and other combustible species, and possibly carbon monoxide. The quantity of water used or the disposal of the excess

carbon for this process is unclear (experimental data and analyses from various sources, including Russian, support qualitatively the relevance of this feature).

(3) *Ionization* of the airflow at the nose of the aircraft and of the airflow entering the engine, probably generated by the Russian-developed Plasmatron or, as reported by other Russian researchers, by streamers. One of these Plasmatron devices is operating in the plasma wind tunnel test facility at the von Kármán Institute (VKI) near Brussels. The former may alter the shock system surrounding the aircraft to reduce drag and to permit the MHD nose generator to extract enthalpy kinetic energy from the flow. The latter permits the MHD generator-accelerator to function with the magnetic field strengths possible with superconducting magnets and the flow velocities present within the engine module to produce a flow energy bypass system (Tretyakov 1995; Gorelov et al. 1996), (Russian information supported by analysis and available databases.)

(4) *Powering of the fuel-reforming process* by an MHD generator in the nose of the vehicle (Batenin et al. 1997), that with a particle beam generator in the nose, produces a plasma bubble at the vehicle nose and results in a reduction of the vehicle total drag (Gurijanov and Harsha 1996; Tretyakov 1995; Gorelov et al. 1996; Smereczniak 1996). Reportedly, a nose plasma bubble capable of absorbing radar waves is present in the Russian "Topol" ICBM (Russian information with experimental data obtained by one of the authors (C. Bruno) under an Italian research collaboration effort with the Russian Academy of Sciences (RAS-Novosibirsk)).

(5) *Increase in the combustion efficiency* within the engine by means related to injection of plasma or hydrogen ahead of the fuel injector struts (Tretyakov et al. 1995) (Russian information with experimental data obtained under Italian collaboration research effort with RAS-Novosibirsk.).

(6) *Diversion* of the bypassed energy to a directed energy device on an intermittent basis for peaceful purposes. Purposes listed are as follows: reduction of the ice crystal formation over Antarctica to reduce the size of the ozone hole, space debris burning (e.g., see Campbell and Taylor 1998), ionosphere and upper atmosphere research, ozone generation, communication with artificial satellites, water surface and atmosphere ecological conditions diagnostics, ore deposits prospecting, Earth vegetation research and monitoring, seismic conditions and tunnel monitoring, ice conditions and snow cover monitoring, and long-range communication and navigation.

In January 2001, Alexander Szames of *Air et Cosmos* interviewed Nikolai Novitchkov and Vladimir L. Freishtadt (Szames 2001). The article states that the project originated in the State Hypersonic Systems Research Institute (GNIPGS) in St Petersburg. Vladimir Freishtadt was the OKB Director, with members Viktor N. Isakov, Alexei V. Korabelnikov, Evgenii G. Sheikin, and Viktor V. Kuchinskii. It is clear from the literature that Ajax is primarily a global range hypersonic cruise vehicle. All the discussions with individuals about Ajax again stressed both the global range capability at hypersonic speeds and the directed energy device for peaceful purposes.

When the illustration shown in Fig. 4.46 was published in Paris in December 1999, it showed a vehicle concept that corresponded to correct hypersonic design criteria and a flow field significantly modified by MHD interaction. A paper presented in the 1997 IAF Congress held in Turin, Italy, provided details of an axisymmetric MHD nose generator; it describes in particular the nose MHD device that reportedly powers a fuel-reforming process of unknown description (Batenin et al. 1997). Its intent is to drive the device that creates plasma ahead of the nose. Researchers from Novosibirsk have stated such tests have been conducted in their hypersonic, high-temperature wind tunnels and presented very similar pictures. An AIAA paper by Dr. J. Shang of the Air Force Research Labs has similar data.

One of the difficulties with the MHD propulsion system analysis is that the only realistic analysis possible is for an

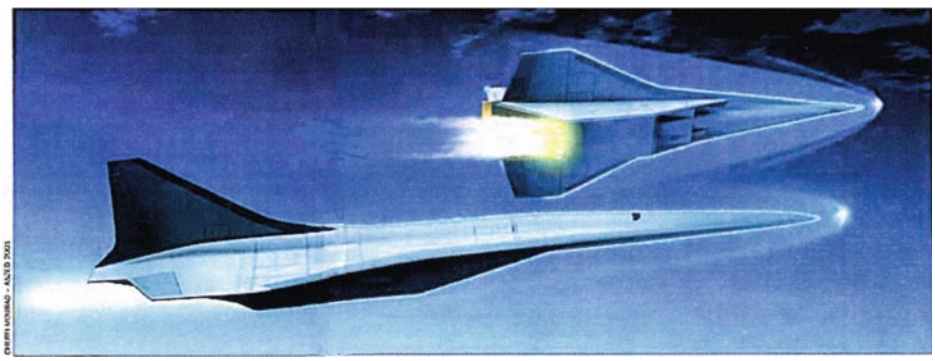

Fig. 4.46 Ayaks illustration in *Air et Cosmos* by Alexandre Szames from information obtained from Vladimir Freishtadt, the Program Director of AYAKS

aircraft in a free stream flow field without any ionization. The Szames illustration was also confirmed by Russian researchers who have stated that the propulsion system and aircraft operate as if they were in a modified Mach number gas flow field. In fact, the flow around the aircraft and entering the engine is a plasma flow. None of the aircraft or propulsion analyses these authors have done have actually considered this plasma flow field since the understanding of coupling and then solving the equations of electromagnetism (Maxwell) simultaneously with the Navier–Stokes equations of aerodynamics are still incomplete. Thus, the work by the authors investigated over the years the feasibility of single elements of only Ajax, see Bruno et al. (1997, 1998), Bruno and Czysz (1998), Czysz and Bruno (2001), Lee et al. (2002a, b, 2003a, b), Bottini et al. (2004) and concluded each element per se was feasible as claimed, but rigorous simulation of an integrated engine flowpath is still missing. Note that the plasma effect is not the same as a simple thermal modification of the gas properties. In contrast, since the atmosphere ahead of the flying aircraft has very low density, ionization followed by MHD interaction with the external upstream flow field appears definitely feasible and may be intense, covering to some extent the flowfield downstream.

The reported performance of an Ajax vehicle mission includes a 13,812 km (7458 nmi) range at Mach 8 and 33 km altitude for a mission duration of 129 min. Cruise speed is then 8005 ft/s. From historical aircraft performance correlations, the climb and descent time and distance are 46 min and 1250 nmi, respectively. With ground operation, the approach in Chap. 3 yields a cruise distance of 6208 nmi (11,497 km) and a mission time of 130 min. For a fuel fraction of 50%, we obtain a range factor predicting 16,590 km (8958 nmi). The sketch of Ajax, see Fig. 4.45, indicates a Küchemann τ of about 0.10. That yields a hypersonic, purely aerodynamic, lift-to-drag ratio $L/D_{\text{hypersonic}} = 4.1$. The integrated propulsion system and gravity relief result in a final $L/D_{\text{hypersonic}} = 4.7$. The reported heat of combustion for Russian reformed kerosene is about 30,000 Btu/lbm. With a 50% propulsion energy conversion efficiency, the $V{\cdot}I_{\text{sp}}$ is 1921 nmi (3557 km) and the I_{sp} is 1457 s. The resulting range factor is 9024 nmi (16,712 km). If low-level ionization were to be employed to reduce the cruise drag, then the mission range would be 25,309 km (13,666 nmi) in 204 min. Clearly, the reported Ajax performance is an Earth-circling range (more than antipodal) in three and one-half hours (Earth circumference is about 40,075 km or 21,639 nmi around) (Bruno et al. 1998).

For a cruise flight system, the total heat load can be an order of magnitude greater than for an atmosphere-exit trajectory. Then, some form of continuous energy management is required to prevent the airframe thermal capacitance from being saturated by excess energy (Pirrello and Czysz 1970). The heat capacity of some of the reformed hydrocarbon fuels can be greater than hydrogen. From the Szames article, the heat of formation is given as 62,900 kJ/kg or 59,620 Btu/lb for the case of reformed methane. In the case of Ajax, the thermal energy is not discarded but used to create thrust. As indicated in the Szames article, the Ajax system is an energy management system that minimizes the shock losses (entropy rise of the total aircraft system in hypersonic flight) and makes converted kinetic energy available for applications. The fraction of the thrust energy provided by the recovered aerodynamic heating reported in the Russian references, 30%, is in agreement with prior analyses (Czysz 1992; Ahern 1992).

MHD flows are governed by the interaction of aerodynamic and electromagnetic forces. As a result, the key MHD parameters have to contain elements of both. The seven most important considerations and parameters are (1) cyclotron frequency, (2) collision frequency, (3) the MHD interaction parameter, (4) the load parameter, (5) the Hall parameter, (6) the Hartmann number, and finally (7) the gas radiation losses. These parameters characterize and also constrain the performance of a MHD system. Parameters 1–2–3–7 are the four discussed in this chapter. One of the authors (C. Bruno) provided information related to the impact of each of these parameters. Four of them are critical to the operation of the MHD generator and accelerator in determining the existence and intensity of the Lorentz force (Bottini et al. 2003), that is the force that accelerates or decelerates the airflow via electromagnetic energy interaction with the ions in the plasma-containing flow. If the Lorentz force is not present, there is no electromagnetic acceleration or deceleration of the gas.

4.23.1.1 Cyclotron Frequency and Collision Frequency

Consider the motion of a single charged particle in a magnetic field $\vec{B}$. A single charged particle spirals around the $\vec{B}$ field lines with the electron cyclotron frequency. The charged particle of an ionized gas is thus guided ("confined," in plasma parlance) by the magnetic field (and thus can be separated by ions and create an $\vec{E}$ field and a voltage), but only on the condition that its mean free path (the distance a particle travels between collisions) is greater than the cyclotron radius. If this were not the case, after a collision with another particle, the particle would be scattered away from its spiral trajectory and "diffuse" across the field lines. This condition is the same as saying that the collision frequency must be less than the cyclotron frequency. The condition for guidance, accounting for collision frequency and cyclotron frequency, scales with B, pressure and temperature according to the following equation:

$$10^{-3} \cdot \left[\frac{B \cdot T^{1.5}}{p \cdot (1-\alpha)}\right] \gg 1 \tag{4.32}$$

where B = magnetic field strength (in tesla), T = gas static temperature (K), p = static pressure (atm), and α = ionization fraction. The left-hand side of Eq. (4.32) is the Hall parameter. Since the numerical factor in front of Eq. (4.32) is on the order of 10^{-3}, it is clear that this condition requires very high magnetic field strength, B, or very low pressure, p, or very high ionization fraction, α. Very high (non-equilibrium) electron temperature T_e can satisfy this last condition, provided B is on the order of 1 T or greater and pressure is on the order of 0.1 atm. This places a stringent condition on the operation of a MHD device. It is clear that this rules out equilibrium ionization for all practical purposes (the equilibrium temperature would have to be unrealistically high, of order of many thousand K), and that extraction can work efficiently after a certain amount of dynamic compression, but not inside the combustion chamber, where the pressure is of the order of 1 atm for a supersonic through-flow combustor and between 10 and 20 atm for the subsonic through-flow combustor. This condition favors hypersonic cruise vehicles, as their typical dynamic pressure (hence internal pressures) are at least 1/3 that of an accelerating launcher.

4.23.1.2 MHD Interaction Parameter (S)

The interaction parameter, S, defines the strength of the interaction, or coupling, between the magnetohydrodynamic energy and the airflow. S appears naturally by writing the fluid-dynamic Navier–Stokes equations and adding the electromagnetic Lorentz force to the momentum balance, therefore much simplifying the actual physics. The MHD interaction parameter is defined as

$$S = \frac{\sigma \cdot B^2 \cdot L}{\rho \cdot u} \tag{4.33}$$

with σ = fluid electrical conductivity (Ω m), ρ = gas density (kg/m^3), u = gas velocity along MHD device (m/s), and $\rho \cdot u$ = mass flow per unit area (kg/m^2/s). S is proportional to σ, so the plasma ion density must be sufficiently high for the field $\vec{B}$ to modify the airflow; a rule of thumb is at least 10^{14}–10^{16} charged particles/cm^3, but this depends also on $\vec{B}$ intensity.

The mass flow per unit area along a vehicle increases by 25 or more from the nose to the engine area as the flow is compressed. This means that the Russian installation of a nose MHD device and plasma generator, to drive the hydrocarbon fuel arc reforming process and alter the surrounding flow field to reduce drag, is using basic physics to advantage. Again, the nose mass flow per unit area is about an order of magnitude less for a hypersonic cruise vehicle compared to an accelerating space launcher, favoring the application of MHD to cruise vehicles. For the cruise vehicle, the pressure is less and the ionization potential to create a plasma much greater than for an accelerator, see Fig. 4.9. Note that the magnetic field strength, B, is squared, so a doubling of the $\vec{B}$ field increases the interaction by a factor of 4. The mass flow per unit area inside the combustor is too large to have a significant interaction at moderate magnetic field strengths. That is why the MHD generator and accelerator are placed where the local Mach number is higher and the mass flow per unit area and pressure are less. The $\vec{B}$ field for the MHD generator and accelerator is usually greater than that required for the nose device, because of the larger mass flow per unit area.

Work on application of $\vec{B}$ fields to propulsion, heat transfer, flow control, and drag reduction continues, although implementation in practical devices is not yet known. A recent survey of the status of the art in this field is in Poggie et al. (2016).

4.23.1.3 Radiative Losses

The plasma transport equations include energy transport. In terms of temperature, T, the radiative energy transport (loss) is the left side of Eq. (4.34):

$$\frac{\partial k \cdot T}{\partial t} + \frac{2}{3} \cdot k \cdot T \cdot \vec{V} \cdot v_i = \left(\frac{D_{recom}}{\sqrt{T}} + D_{Brems}\sqrt{T}\right) \cdot \alpha \cdot N_i \tag{4.34}$$

where the two terms on the right-hand side are the radiation heat transfer due to recombination of electrons and ions, D_{recom}, and the Bremsstrahlung radiation contribution, D_{Brems}. The number of ions per unit volume, N_i, and the degree of ionization, α, multiply the radiation heat transfer terms. Again, α needs to be a compromise, since it raises S but drives also radiation losses, and a similar compromise exists for the temperature T. Note that Eq. (4.34) is an approximation of the physical photonic distribution: depending on T, and for sufficiently large α, the photon mean free path may become so short that radiation can be confined inside the plasma and emerge as loss only at its boundary.

4.23.1.4 MHD Summary

The four MHD parameters briefly discussed: the (1) cyclotron frequency, (2) collision frequency, the (3) MHD interaction parameter, and the (4) gas radiation losses. Those four parameters do provide the minimum criteria for a MHD system to operate successfully. It is critical that any system seeking to operate as an MHD system must meet the criteria for the Lorentz force to exist in the first place. Although

appearing to be applicable to space launchers, the MHD energy bypass system is thus limited by the internal pressure in the propulsion system. The result is that an MHD system that has significant potential for a global range cruise aircraft actually will have only minimal potential for a space launcher (Bottini et al. 2003). In contrast to the propulsion case, the MHD interaction with the external flow, for reducing drag and permit electromagnetic deflection of the airflow (instead of a physical ramp system), is instead applicable to both, cruise aircraft and space launcher, because the external flow pressure is low in both cases.

4.23.2 Electromagnetic Radiation Propulsion

One of the limitations of the space launcher is the quantity of propellant that must be carried to achieve orbital speed. Even the most optimistic airbreathing system has a mass ratio of 4, the propellant is three times the operational weight empty. During the 1987 International Astronautical Congress held at Brighton, England, Viktor Pavlovitch Legostaev, General Designer of RSC Energia, approached the author to discuss space developments in the Soviet Union (Legostaev 1984). Part of the material presented was an experiment where a vertical launch rocket used water as a propellant and the energy to vaporize the water and produce thrust was provided by a focused microwave generator. An altitude of about a kilometer was achieved. Material was also presented from the Nikola Tesla museum in Belgrade, Serbia (Tasić 2006). In the translated Tesla manuscripts (Tesla 2007), there was a discussion of projected electromagnetic energy with minimum transmission losses. Tesla's claim was that a base on the Moon or Mars could be powered by a suitably located generator on Earth. Legostaev presented some data to the effect that experiments projecting energy from Siberia to an orbiting satellite and retransmitting the energy to Moscow achieved the transmission efficiencies Tesla had predicted. The picture of the power generating tube Legostaev showed was identical to the tube the author (P.A. Czysz) saw at the small museum at Tesla's birthplace in Smiljan, Croatia. In both cases, the evidence presented supported that a remote-powered vehicle was possible.

Note that direct propulsion by "pushing" a spacecraft to space by photon momenta had been proposed by Sänger (1956), and A. Kantrowitz extended the concept to laser-driven ablation propulsion (Kantrowitz 1978).

Professor Leik Myrabo, of Rensselaer Polytechnic Institute, Troy, New York, was developing a spacecraft based on focused electromagnetic energy (laser or microwave) for at least 20 years (Myrabo 1982, 1983, 2001; Myrabo et al. 1988, 1998). In this case, the vehicles are toroidal, the toroid forming a mirror to focus the received electromagnetic energy to vaporize and ionize water and air. Thus, the propulsion system becomes an MHD-driven space launcher. Myrabo demonstrated with USAF support a scale model propelled by a laser at Lawrence Livermore Laboratory (Myrabo and Lewis 2009). The importance of the Myrabo concept is that it is truly a combined-cycle concept. Through a series of propulsion configuration variants, the single spacecraft becomes four different MHD propulsion systems that can, in principle, reach low Earth orbital (LEO) speed and altitude, all powered by projected power, see Fig. 4.47. The power emitting system can be on Earth or in orbit. If there is an orbital power generator, spacecraft can be powered to the Moon (see Chap. 6), or a satellite can be powered to geosynchronous orbit with a minimum of Earthbound resources. If the power generator is placed on the Moon, then the system can provide propulsion to the nearby planets and moon systems. This concept is very interesting because it has the least onboard propellants of any system and hence provides the smallest weight.

The *Lightcraft* vehicle is an axisymmetric vehicle that begins its liftoff under beamed power, in this case from an orbiting laser, as shown in Fig. 4.48. Selective illumination of the laser windows provides lateral thrust, so sideways translation movement is possible in addition to vertical movement. In the liftoff phase, the propulsion system is configured for vertical takeoff or landing. Although forward acceleration to high subsonic speed is possible, the propulsion system soon transitions to the airbreathing rotary pulsejet mode. In this case, the rotating outer ring provides linear acceleration by ejecting an air plasma from an MHD engine segment. As speed increases, the entire vehicle acts as an MHD airbreathing fanjet to cover the supersonic and hypersonic speed regimes. In its final configuration, the pulsejet configuration now operates as a rocket, for instance with water as a working fluid (see Myrabo references for details and Chap. 5).

Since its inception, this concept has evolved, but the basic axisymmetric shape with toroidal mirrors to focus the

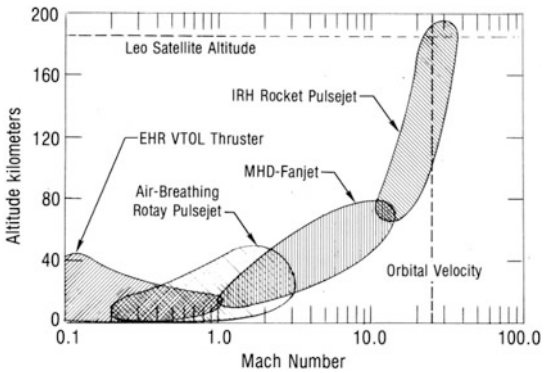

Fig. 4.47 Laser/microwave heated MHD spacecraft operating envelope enabled by a series of propulsion configuration adaptations

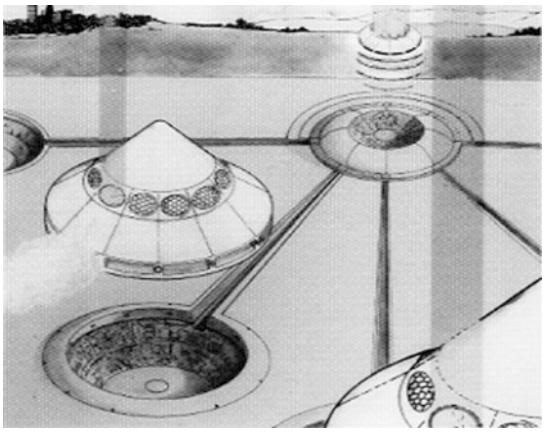

Fig. 4.48 Laser/microwave heated MHD spacecraft by Leik Myrabo of Rensselaer Polytechnic Institute, Troy, New York

radiated energy for producing a plasma remains. After Myrabo's death, R&D in this area was continued in Germany and the USA, where high power lasers are also investigated as weapons (a laser "gun" is currently being tested by the US Navy). Experimental data and the status of this technology can be found in Schall et al. (2007), Eckel and Schall (2008) and scaling laws in Yabe and Uchida (2007). For the theoretical foundations of the key interaction between laser and matter for propulsion applications, see (Phipps and Luke 2007).

4.23.3 Variable Cycle Turboramjet

Repeating part of the conclusion from Builder's 1964 report, there is an observation about a (then) hypothetical engine, the air turboramjet. To quote,

> … In a sense, a fan-ramjet might be a suitable name for such a cycle; the duct-burning turbofan and the air-turborocket could be considered close cousins to this hypothetical engine. At the higher speed end, around Mach 10, we can postulate a very efficient engine called the transonic combustion ramjet. There is still another important class of possibilities offered just outside the confines of the Brayton Cycle family: engines with non-adiabatic compression and expansion processes as a result of heat exchanges between the air and fuel. We might find a complete new spectrum of such engines awaiting our discovery. … (Builder 1964)

Such engines have been discovered, but have unfortunately never been pursued. In Fig. 4.49, there is a thumbnail insert of an original sketch of a variable cycle turboramjet based on the Rocketdyne SSME, sketched sometime in the early 1980s. Unfortunately, the identity of the sketch's source has long been lost. But it shows the ingenuity that was routinely discarded in favor of the rocket status quo. Although the details of the engine's operation are also lost, the originality in adapting an existing fixed cycle rocket engine with a fixed specific impulse to a variable cycle, airbreathing turboramjet/rocket is evident. As shown in the enlarged drawing based on the sketch, a rotating gas generator provides the power for the low-pressure ratio compressor. The engine operated as rocket-based turboramjet at lower Mach numbers and then transitions to the conventional rocket for the higher Mach numbers. With the flow-through LOX injector, if the airbreather thrust cannot provide sufficient low-speed acceleration, then the rocket could be ignited to provide an additional boost.

Who knows what the launchers of today would be like if innovations like this, based on current operational hardware, had been allowed to proceed. Dr. Nikolai Tolyarenko, formerly at TsIAM and more recently at the International Space University (Strasbourg), showed in 2010 to one author (C.

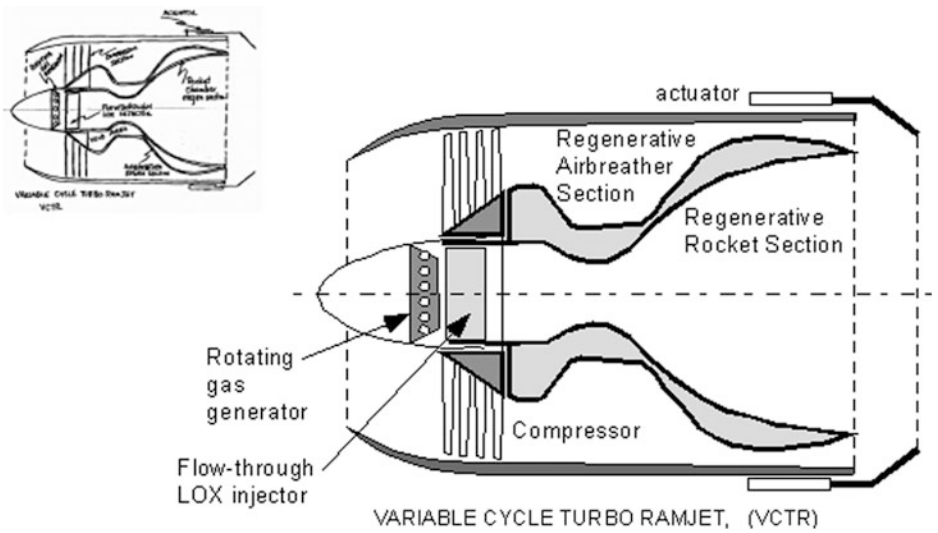

Fig. 4.49 Sketch of variable cycle ramjet based on Rocketdyne SSME, circa 1983

Bruno) a 1960s movie of the launch of the ramjet-powered *Buran* RSS-40 cruise missile he helped design, and said "... *were we let free to develop it, we would be on Mars now* ...."

It is not a lack of ideas or hardware concepts, or the lack of technology that confines us to low-performing rockets today, but a lack of imaginative designs based on correct decision-making, thus leadership to implement those ideas.

4.23.4 Aero-Spike Nozzle

The performance of the propulsion systems in this section is based on the conventional convergent-divergent nozzle, see Fig. 4.50 (Sutton and Biblarz 2010). At low altitudes, external atmospheric pressure causes the nozzle flow to separate from the nozzle wall (overexpanded in Fig. 4.50).

Because the nozzle exit area is now larger than the overexpanded flow, the transonic base drag can be very large. The 2-D and 3-D aero-spike nozzle, on the other hand, can accommodate higher external pressure while reducing base drag. The difference is that the convergent–divergent nozzle has one combustion chamber and throat, whereas the aero-spike nozzle has a number of smaller rocket chambers around the 2-D or 3-D periphery of the central 2-D or 3-D spike. To the author's knowledge, one of the first tests of an aero-spike nozzle was in the Cornell Aero Labs transonic wind tunnel in the late 1950s and early 1960s.

The Saint Louis Science Center sponsored the Russian Space Exhibition in 1992, when one of the authors (P.A. Czysz) was able to participate in some technical sessions with the Russian engineers. One engineer the author met was Konstantin Petrovich Feoktistov, who was the designer of Voskhod, Soyuz, Salyut, and Mir, and formerly a member of the Sergei Pavlovich Korolev team. Even though it is now over 50 years since the Russian Moon landing program (Johnson et al. 2014), the action of Glushko's OKB to block hardware from being delivered to Korolev is still resented. During the technical meetings, there would be angry exchanges in Russian between Valentin Glushko's OKB members and Feoktistov. When the author was able to visit Moscow and Saint Petersburg on an educational exchange in 1993, he was able to visit Feoktistov at his apartment. Feoktistov had a bookcase on one wall that was filled with his design studies. One was for a multi-launch space launcher designed around an aero-spike nozzle that he had tested full-scale.

The Lockheed Martin X-33 subscale VTHL SSTO employed the 2-D or linear aerospike engine (Stine 1996; Butrica 2003; Miller 2001). Among the numerous suggested applications of the 3-D aerospike engine is the TSTO *Orion-III* aerospaceplane in the epic science-fiction film *2001: A Space Odyssey* that employed a combined-cycle propulsion system with two aft fuselage-embedded 3-D aerospike nozzles (Bizony 2014; Frayling 2015), see Fig. 4.51.

4.23.5 ORBITEC Vortex Rocket Engine

In a conventional rocket engine, there is an ejector plate at the base of the combustion chamber that injects fuel and oxidizer into the combustion chamber at a specified fuel-to-oxidizer ratio. The key challenge is to control the combustion process such that heat transfer to the walls is minimized. The group that best controlled wall heating was probably the former Soviet Union rocket engine designers, see (Kalmykov et al. 2008), and in the 1990s one of the authors (C. Bruno) was offered information on a vortex combustion-powered rocket engine developed in the Soviet Union (Golovitchev 1990).

Eric Rice, President of ORBITEC until 30 September 2008, had a different approach with his founding team some years ago. This approach involved controlling combustion

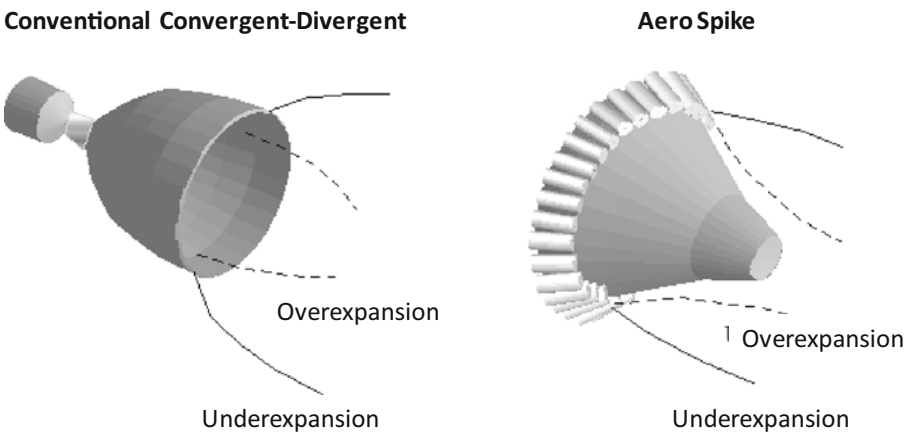

Fig. 4.50 Two 3-D expansion-nozzle configurations alternatives

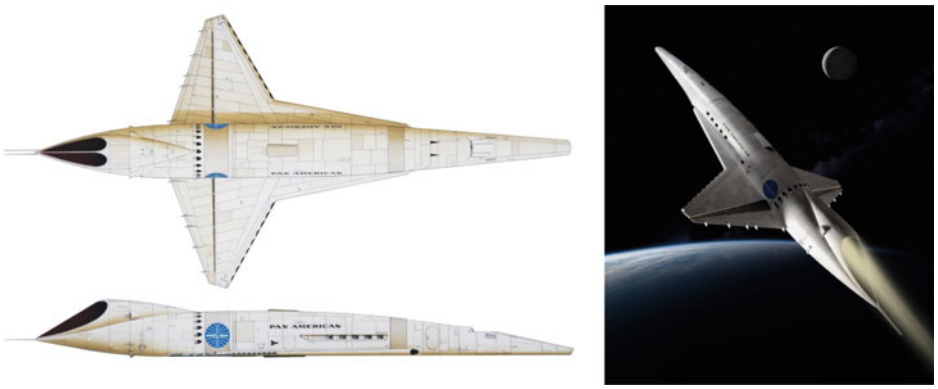

Fig. 4.51 Orion III 2-view artwork by Simon Atkinson (www.satkinsoncreativearts.com) and large display model by B. P. Taylor

and wall heating using the intense mixing and combustion driven by interaction between vortical flows.

ORBITEC's patented Vortex Combustion Cold-Wall (VCCW) thrust chamber employs a unique propellant swirl injection method that generates a pair of coaxial, co-swirling counter-flowing vortices in the combustion chamber. Combustion of the propellants is confined to the inner vortex. The outer vortex cools and protects the chamber wall from excessive heat loads that ordinarily result from the hot combustion products. Successful testing has demonstrated operation flexibility, burning various propellant combinations including gaseous oxygen/gaseous methane, gaseous oxygen/RP-1, liquid oxygen/RP-1, gaseous oxygen/gaseous hydrogen, liquid oxygen/gaseous hydrogen, gaseous oxygen/gaseous carbon monoxide, and liquid oxygen/liquid propane. "*... ORBITEC is also applying the coaxial vortex flow field to hybrid rocket engine systems that produce fuel regression rates significantly higher than conventional hybrid configurations. This increase in fuel regression rate enables the use of a simple circular grain port and leads to significant gains in performance, reliability, and durability of hybrid systems ...*" [ORBITEC].

A vortex cylindrical combustion chamber burning gaseous oxygen and gaseous hydrogen at a mixture ratio of 6 was equipped with an acrylic chamber (measured wall temperature ~60 °C) for optical visualization of the combustion zone (~3000 °C). The acrylic chamber clearly showed the central core combustion vortex away from the acrylic wall. Specific impulse efficiencies of about 98% have been obtained in non-optimized lab-scale chambers.

Current efforts apply VCCW thrust chamber assemblies at chamber pressures of 1000 psi and thrust levels of 7500–30,000 lbf (this thrust was reached in 2015) using liquid oxygen/gaseous propane, liquid oxygen/gaseous methane, liquid oxygen/liquid methane, and liquid oxygen/RP-1. RP-1 is a kerosene blend specially formulated for application as rocket propellant. These efforts were initially supported by lab-scale, large prototype and flight-weight engine testing, computational fluid dynamic simulations, and numerical analysis of the vortex flow field. Orbitec is now a subsidiary of Sierra Nevada Corporation (SNC), the commercial space company approved in 2016 for NASA funding of its proprietary *Dream Chaser* hypersonic glider competing with SpaceX and Orbital ATK for lifting cargo to the ISS. Although no decision has been made, the Orbitec engine may eventually power the SNC *Dream Chaser* shuttle.

The advantage of vortex combustion is that it opens up the opportunity of considering different propellant approaches. One such approach consists of novel versions of the hybrid rocket engine.

4.23.5.1 Vortex Hybrid Rocket Engine (VHRE)

With the goal of achieving practical and functional hybrid rocket propulsion systems, ORBITEC has patented a unique hybrid propulsion technology called the vortex hybrid rocket engine. Rather than injecting oxidizer parallel to the fuel port at the head-end, as in a classic hybrid, oxidizer is injected tangentially through a swirl ring at the aft-end of the fuel grain. This injection method generates a bidirectional, co-axial vortex flow field in the combustor. The swirling, high-velocity gas enhances heat transfer to the fuel surface which, in turn, drives high solid-fuel regression rates. Testing has already demonstrated regression rates up to 650% faster than a classical hybrid for a given mass flux. The rapid regression rate allows the use of a single cylindrical grain port which offers significant benefits including (1) increased volumetric grain loading, (2) simplified grain manufacture and grain mechanical strength, and (3) reduced grain sliver at engine burnout. Additionally, the unique flow field enhances mixing and increases combustion efficiency.

ORBITEC has applied vortex hybrid technology to paraffin and other fuel blends. With paraffin, extremely high regression rates, compared with classic hybrids with rubber-based fuels, have been obtained. Blending paraffin

and other fuels adds another degree of freedom for tailoring the regression rate to precise specifications and may provide fuel strength advantages over pure paraffin.

The vortex hybrid rocket engine features:

- Application flexibility,
- Very high regression rates,
- Simplified grain geometry,
- Reduced grain sliver at burnout,
- Increased volumetric fuel loading,
- Enhanced combustion performance,
- Excellent safety and low risk,
- Low cost and reusability,
- Significantly large design, experimental, and analytical database.

To appreciate these features, one must understand conventional hybrid engines. In the classical hybrid engine, the fuel and oxidizer are physically separate and stored in different phases. Classic hybrid rocket engines have several important operational and safety advantages over both liquid-propellant and solid-propellant rocket engines. Unlike solid-propellant grains, solid-fuel grains are inert, insensitive to cracks and imperfections, and safe to manufacture, transport, store, and handle. Like liquid-propellant engines, hybrid engines can be throttled, but require only half the feed system hardware. Due to their relatively simple design and inherent safety, classic hybrid engines should display lower manufacture and launch costs than current propulsion systems.

However, current classical hybrid engines suffer from low solid-fuel regression rates, low volumetric loading, and relatively low combustion efficiency. Common solid fuels, such as hydroxyl-terminated polybutadiene (HTPB), usually regress quite slowly compared with solid propellants. Complex cross-sectional geometries with large burning surface areas must be employed to obtain the necessary fuel flow rate consistent with the desired thrust level. Such grains require large cases and display poor volumetric loading and high manufacturing costs. The fuel may occupy as little as 50% of the total grain case volume. As the grain webs thin down near the end of burn, they are prone to release fuel chunks which results in sharp thrust pulses.

The combustion of fuel and oxidizer in a classic hybrid occurs in a boundary layer flame zone, distributed along the length of the combustion chamber above the fuel surface. Portions of the propellants may pass through the chamber without reacting. Secondary combustion chambers at the end of the fuel grain are often employed to complete propellant mixing and increase combustion efficiency. These chambers add length and mass to any conventional design and may serve as a potential source of combustion instability. These drawbacks are avoided in the vortex hybrid rocket engine (VHRE).

The vortex hybrid propulsion system has the potential to mature into a significant size range of propulsion systems. The systems would be suited for applications ranging from zero-stage strap-on boosters to pump-fed, large, reusable first-stage boosters and second-stage sustainer engines for highly reusable launch vehicles. The vortex hybrid is also efficient in smaller sizes and should find applications as propulsion for orbit transfer stages, orbital maneuvering systems for space vehicle propulsion, the *Orion* crew exploration vehicle escape capsule propulsion, and for orbit insertion kick stages. Additionally, the vortex hybrid has the potential to serve as an in-space refuel-able propulsion system. Such a system would be refueled in space by fuel grain cartridges and pre-packaged liquid-oxidizer tanks launched for the purpose and continue to serve for extended periods from a parking orbit in space. ORBITEC has been evaluating the use of vortex hybrid upper-stage propulsion for satellite and booster applications. Another family of applications concerns a vortex hybrid that would make use of in situ resources from a lunar or Martian base. In more advanced future systems, propellant supplies could be delivered from lunar resources at lower energy due to the weaker gravity well of the Moon. For example, it may be feasible to produce metallic fuel grains of aluminum to burn with oxygen extracted from oxides present in lunar regoliths.

4.23.5.2 Stoichiometric Combustion Rocket Engine (SCORE)

SCORE is a high-performing, low-thrust, gaseous hydrogen/oxygen rocket engine designed by ORBITEC to operate at a stoichiometric mixture ratio as part of the water rocket program being sponsored by DARPA for Earth orbit spacecraft.

SCORE is a small (20 lbf) on-orbit spacecraft rocket engine intended to serve as the primary thruster for the water rocket system. The water rocket calls for the use of liquid water as a propellant supply. The liquid water is electrolyzed on orbit into hydrogen and oxygen gas, which is then stored and used as needed for orbital maneuvers. Because the propellants are made from water, they are available in stoichiometric proportion, and the overall performance of the propulsion system is optimized by using all of the available propellant. This approach also eliminates complicated, heavy, and costly cryogenic storage systems while providing high performance.

Other applications include reboost/repositioning for orbiting facilities such as the ISS space platforms or spacecraft. The water rocket has several major advantages over conventional stored liquid propellants such as MMH/NTO.

It offers dramatically improved I_{sp}, it is environmentally friendly, and its lack of toxicity simplifies launch operations. In addition to these advantages related to the propulsion system, the water rocket also doubles as a battery; stored hydrogen and oxygen gas may be converted back to water to generate electricity in a fuel cell during periods of darkness.

The water rocket requires a long-life engine that can deliver high performance at relatively low thrust in the harsh conditions of high-temperature stoichiometric combustion. SCORE uses ORBITEC's patented cold-wall vortex flow field to accomplish just that. The vortex protects most of the chamber wall from combusting propellants whilst minimizing the heat load. Development work has progressed toward a flight-type engine which is regeneratively cooled and will exhaust to simulated altitude conditions.

4.23.5.3 Cryogenic Hybrid Rocket Engine Technology

This technology originated in both Europe, at the Aerospace Institute in Berlin, see (Lo et al. 2005), and in the USA, where ORBITEC has developed technology in cryogenic hybrid rocket engines. This patented family of engines uses a cryogenic solid as the fuel (or oxidizer) grain. The cryogenic hybrid offers the safety and relative simplicity of hybrid engines coupled with the performance of cryogenic bipropellant engines. The latest addition to this family, the ACHRE-I, uses a solid-oxygen (SOX) grain with liquid-hydrogen fuel. Fully loaded, the ACHRE holds a 5 kg SOX grain and produces 120 lbf thrust. Liquid hydrogen is used both as the fuel for firing and the coolant for the SOX grain formation process. The ACHRE is intended for use as a high-performance launch vehicle kick stage or orbital transfer vehicle. Future work with the ACHRE will explore the use of solid-ozone (SOZ) mixed in with the SOX grain. Addition of 50% SOZ will result in a significant performance gain: the specific impulse is increased by nearly 20 s.

Numerous successful hot-firing tests have been performed with various propellant combinations with ORBITEC's "workhorse" Mark II cryogenic hybrid rocket engine, exploring solid oxygen/gaseous hydrogen, solid hydrogen/gaseous oxygen, solid carbon monoxide/gaseous oxygen, solid methane/gaseous oxygen, and other solid hydrocarbon fuels.

Bibliography

Ahern, J.E. (1983) Briefing for Robert Williams on Second Law Thermodynamics, DARPA Copper Canyon manager, Washington, DC, 1983.

Ahern, J.E. (1992) "Thermal Management of Air-Breathing Propulsion Systems", AIAA Paper 92-0514, *30th Aerospace Sciences Meeting*, Reno, Nevada, January 1992.

Anfimov, N.A. (1997) "In Searching for an Optimal Concept of Future Russian Reusable Space Transportation System", in: Proceedings of the *International Workshop on Spaceplane/RLV Technology Demonstrators,* Tokyo, Japan, 10–12 March 1997, pp. 67–96.

Anon. (1963) "Marquardt Needs Advanced Propulsion Engineers", Full-Page Advertisement, Aviation Week & Space Technology, 20 May 1963.

Anon. (1967) "A Study of Advanced Airbreathing Launch Vehicles with Cruise Capability", Lockheed Report IR 21042, The Lockheed Aircraft Corporation, 1967.

Anon. (1985) "Single-Stage-to-Orbit Concept Comparison', Aerospace Corporation, 86-2602-301-ADA, October 1985.

Anon. (2014) "Stratolaunch Eagles', Stratolaunch Systems, Orbital ATK, 2014.

Anon. (2015a) "Space Launch System at a Glance", NP-2015-09-83-MSFC, Marshall Space Flight Center, NASA, September 2015.

Anon. (2015b) "Declassified Manned Orbiting Laboratory (MOL) Records", National Reconnaissance Office, October 2015.

Anon. (2016) Virgin Galactic – Human Spaceflight Vehicles Fact Sheet", Virgin Galactic, February 2016.

Aoki, T. and Ogawara, A. (1988) "Study of LACE Cycle for SSTO Space Plane", Paper IAF-88-252, presented at the *39th International Astronautical Federation Congress*, Bangalore, India, 08–15 October 1988.

Balepin, V.V. (1996) "Air Collection Systems", *Developments in High-Speed-Vehicle Propulsion Systems*, edited by S.N.B. Murthy and E.T. Curran, Progress in Astronautics and Aeronautics Series, Vol. 165, AIAA, Reston VA, 1996, pp. 385–419.

Balepin, V.V. and Tjurikov E.V. (1992) "Integrated Air Separation and Propulsion System for Aerospace Plane with Atmospheric Oxygen Collection", SAE Technical Paper SAE-92-0974, *Society of Automotive Engineers, Aerospace Atlantic Conference*, Dayton, OH, 07–10 April 1992.

Balepin, V.V. and Hendrick, P. (1998) "Application of the KLIN Cycle to Vertical Take-Off Lifting Body Launcher", AIAA Paper 98-1503, *8th AIAA International Space Planes and Hypersonic Systems and Technologies Conference,* Norfolk, VA, 27–30 April 1998.

Balepin, V.V., Dulepov, N., Folomeev, E., Harchevnikova, G., *et al.* (1993) "Flight Liquid Oxygen Plants for Aerospace Plane: Thermodynamic and Integration Aspects", SAE Technical Paper 931452, Society of Automotive Engineers, April 1993.

Balepin, V.V., Czysz, P.A., Maita, M. and Vandenkerckhove, J. (1995) "Assessment of SSTO Performance with In-Flight LOX Collection", AIAA Paper AIAA-95-6047, presented at the *AIAA 6th International Aerospace Planes Conference*, Chattanooga, TN, 1995.

Balepin, V.V., Maita, M., Tanatsugu, N., and Murthy, S.N.B. (1996) "Deep-Cooled Turbojet Augmentation with Oxygen (Cryojet) for a SSTO Launch Vehicle", AIAA Paper 96-3036, presented at the *32nd Joint AIAA, ASME, SAE and ASEE Propulsion Conference and Exhibit*, Lake Buena Vista, FL, 1–3 July 1996.

Baranovsky, S.I., Davidenko, D.M. and Levin, V.M. (1992a) "Combustion Chamber of Ramjet for Aerospace Plane", Vol. 3, presented at the *9th World Hydrogen Conference*, Paris, June 1992, pp. 1583–1591.

Baranovsky, S.I., Davidenko, D.M. and Konovalov, I.V. and Levin, V. M. (1992b) "Experimental Study of the Hydrogen Supersonic Combustor", Vol. 3, presented at the *9th World Hydrogen Conference,* Paris, June 1992, pp. 699–1708.

Barrère, M. and Vandenkerckhove, J. (1993) ''Energy Management'', Paper ISABE 93-7016, presented at the XI International Symposium on Air Breathing Engines, Tokyo, Japan, September 1993.

Bartolotta, P.A., Buchen, E., Engelund, W.C., Huebner, L.D., Moses, P.L., Schaffer, M., Voland, R.T., Voracek, D.F. and Wilhite, A.W.

(2011) "Horizontal Launch: A Versatile Concept for Assured Space Access," NASA SP 2011-215994, Report of the NASA-DARPA Horizontal Launch Study, December 2011.

Batenin, V.M., Bityurin, V.A., Ivanov, G.S., Inozemzev, N.N. and Gorozhankin, P.A. (1997) "Electromagnetic Complex Concept for the Horizontal Start and Landing of a Reusable Air-Space Aircraft", paper presented at the *48th International Astronautical Congress*, Turin, Italy, 06–10 October 1997.

Billig, F.S. (1989) "Hypersonic Vehicles II", *Proceedings of the Short Course of Engine Airframe Integration,* School of Mechanical Engineering, Purdue University, July 1989.

Billig, F. S. (1993) "The Integration of the Rocket with a Ram-Scramjet as a Viable Transatmospheric Accelerator", AIAA Paper 93-7017, Vol. 1, Proceedings of the 11th ISABE, International Symposium on Air Breathing Engines, Tokyo, Japan, 20–24 September 1993, pp. 173–187.

Bizony, P. (2014) "The Making of Stanley Kubrick's 2001: A Space Odyssey", 1st Edition, Taschen, August 2014.

Bond, W.H. and Y, A.C. (1993) "Prospects for Utilization of Air Liquefaction and Enrichment System (ALES) Propulsion in Fully Reusable Launch Vehicles", AIAA Paper AIAA-93-2025, presented at the *29th AIAA/SAE/ASME/ASEE Joint Propulsion Conference,* Monterey, 28–30 June 1993.

Bottini, H., Bruno, C. and Czysz, P.A. (2003) "Is The MHD Scramjet Really An Advantage?" AIAA 2003-5046, presented at the *39th AIAA/ASME/SAE/ASEE Joint Propulsion Conference and Exhibit*, Huntsville, Alabama, 20–23 July 2003.

Bottini, H., Bruno, C. and Czysz, P.A. (2004) "Analysis of Kerosene-Fueled MHD SCRJ Cruiser Performance", paper AIAA 2004-4127, presented at the *40th AIAA/ASME/SAE/ASEE Joint Propulsion Conference,* Fort Lauderdale FL, 12–14 July 2004.

Bruno,C. Czysz, P.A. and Murthy, S.N.B. (1997) "Electro-Magnetic Interactions in Hypersonic Propulsion Systems", paper AIAA 97-3389, presented at the *33rd AIAA/ASME/SAE/ASEE Joint Propulsion Conference*, Seattle WA, 6–9 July 1997.

Bruno, C. and Czysz, P.A. (1998) "*An Electro-Magnetic-Chemical Hypersonic Propulsion System*," AIAA Paper 98-1582, presented at the AIAA 8th International Spaceplanes and Hypersonic Systems and Technologies Conference, Norfolk, Virginia, 27–30 April 1998.

Bruno, C., Golovitchev, V.I. and Tretyakov, P.K. (1998) "New Trends in Improving Hypersonic Vehicles Aerodynamics and Propulsion Flow Control by External Energy Supply", Paper 98-0-1-08V, *21st International Symposium on Space and Technology (ISTS)*, Omiya, Japan, May 1998.

Buhlman, M. and Siebenhaar, A. (1995a) "The Strutjet: The Overlooked Option for Space Launch", Paper AIAA-95-3124, presented at the *31st AIAA/ASME/SAE/ASEE Joint Propulsion Conference,* San Diego, CA, 10–12 July 1995.

Buhlman, M. and Siebenhaar, A. (1995b) "The Strutjet Engine: Exploding the Myths Surrounding High Speed Airbreathing Propulsion", Paper AIAA-95-2475, presented at the 31st AIAA/ASME/SAE/ASEE Joint Propulsion Conference, San Diego, CA, 10–12 July 1995.

Builder, C.H. (1964) "On the Thermodynamic Spectrum of Airbreathing Propulsion", AIAA-64-243, *1st AIAA Annual Meeting*, Washington, DC, June–July 1964.

Bunin, B.L. (1991) "Update on Douglas' High-Speed Civil Transport Studies", N94-33450, NASA-CP-10087, 1st High-Speed Research Workshop, Williamsburg, Virginia, 14–16 May 1991.

Burnett, D.R. and Czysz, P.A. (1963) "Supersonic Hydrogen Combustion Studies", AEDC ASD-TDR-63-196, Project Nr. 3012, Task Nr. 301201, Aerodynamic Division, Directorate of Engineering Test, Air Force Systems Command, Wright-Patterson AFB, Ohio, April 1963.

Butrica, A.J. (2003) *Single Stage to Orbit – Politics, Space Technology, and the Quest for Reusable Rocketry*, The John Hopkins University Press, October 2003.

Campbell, J.W. and Taylor, C.R. (1998) "Ground-Based Laser Propulsion for Orbital Debris Removal", in: *Space Technology and Applications International Forum (STAIF)-1998*, ed. by M.S. El-Genk, American Institute of Physics CP420.

Carlson, C.P.P., Kessler, R. and Schmitt, E.W. (1996) "Magnetohydrodynamic Generator Design for a Combined-Cycle Demonstration Powerplant", *Journal of Propulsion and Power*, Vol.12. No. 2, March–April 1996.

Chertok, B. (2011) "Rockets and People: The Moon Race (Volume IV)", 1st Edition, NASA SP-2011-4110, NASA History Series, NASA History Program Office, 2011.

Cocks, P.A.T., Holley, A.T., Greene, C.B. and Haas, M. (2015) "Development of a High Fidelity Simulation Capability", AIAA paper 2015-1823, presented at the *53rd AIAA Aerospace Sciences Meeting,* Kissimmee, FL, Jan. 5–9, 2015.

Cocks, P.A.T., Holley, A.T. and Rankin, B. (2016) "High Fidelity Simulations of a Non-Premixed Rotating Detonation Engine", AIAA paper 2016-0125, presented at the *54th AIAA Aerospace Sciences Meeting*, San Diego CA, Jan. 4–8, 2016.

Conway, E.M. (2008) "High-Speed Dreams: NASA and the Technopolitics of Supersonic Transportation, 1945–1999", 1st Edition, New Series in NASA History, John Hopkins University Press, October 2008.

Curran, E.T. (1993) "The Potential and Practicality of High Speed Combined Cycle Engines", in: *Hypersonic Combined Cycle Propulsion,* AGARD Conference Proceeding No. 479, AGARD, Neuilly-Sur-Seine, France, 1993, pp. Kl-9.

Czysz, P.A. (1987) "*Hypersonic Convergence – Technology Interdependance Inhibits Technology Independence*," © McDonnell Douglas, April 1987, Purdue University Engine-Airframe Integration Short Course, July 1987.

Czysz, P.A. (1988) "Air Breather vs. Rocket: Is the Rocket the Only Reliable, Demonstrable Space Propulsion System?", presented at the *SAE Aerospace Atlantic Conference & Exposition*, Dayton, OH, April 1993.

Czysz, P.A. (1988a) "Thermodynamic Spectrum of Airbreathing Propulsion", SAE Technical Paper 881203, presented at the *Future Transportation Technology Conference and Exposition*, San Francisco, CA, 08–11 August 1988.

Czysz, P.A. (1992) "Space Transportation Systems Requirements Derived from the Propulsion Performance", Paper IAF-92-0858, presented at the 43rd IAF (International Astronautical Federation) Congress, Washington, DC, September 1992.

Czysz, P.A. (1993a) "Rocket Based Combined Cycle (RBCC) Propulsion Systems Offer Additional Options", in: *11th ISABE Proceedings*, Vol 1, Tokyo, Japan, 20–24 September 1993, pp. 119–137.

Czysz, P.A. (1993b) "Hydrogen Combustion Studies – Revisited", presented at the *1993 JANNAF Propulsion Meeting Conference,* Monterey, CA, 15–19 November 1993.

Czysz, P.A. (1995) "Interaction of Propulsion Performance with the Available Design Space", in: *Proceedings of the XII International Symposium on Airbreathing Engines* (ISABE), Melbourne, Australia, September 1995.

Czysz, P.A. (1999) "Combined-cycle Propulsion - is it the Key to Achieving Low Payload to Orbit Costs?", ISABE Paper 99-7183, presented at the XIV International Symposium on Air Breathing Engines (ISABE), Florence, Italy, 11 September 1999.

Czysz, P.A., and Bruno, C. (2001) "MagnetoHydroDynamic Coupled Ramjet Propulsion System: A Perspective", Paper ISABE 2001-1230, presented at the *XV ISABE Symposium*, Bangalore, India, September 2–7, 2001.

Czysz, P.A. and Murthy, S.N.B. (1991) "Energy Analysis of High-Speed Flight Systems", in: *High-Speed Flight Propulsion Systems*, edited by S.N.B. Murthy and E.T. Curran, Progress in Astronautics and Aeronautics Series, Vol. 137, AIAA, Reston VA, pp. 183–186.

Czysz, P.A. and Richards, M.J. (1998) "Benefits from Incorporation of Combined Cycle Propulsion", AIAA Paper 98-S.5.10, presented at the *48th International Astronautical Congress*, Melbourne, Australia, October 1998.

Czysz, P.A. and Vandenkerckhove, J. (2000) "Transatmospheric Launcher Sizing" in Curran, E.T. and Murthy, S.N.B. *Scramjet Propulsion*, Progress in Astronautics and Aeronautics Series, Vol. 189, Reston VA., Chapter 16, 2000.

Daniau, E. (2002) "Pulse Detonation Engine: Concept, Performance and Applications", ISU/AAAF Short Course, Versailles, France, May 2002.

Davies, R.E.G. (1998) "Supersonic (Airliner) Non-Sense: A Case Study in Applied Market Research", Paladwr Press/Airlife Publishing Ltd, 1998.

Davies, P., Hempsell, M. and Varvill, R (2015) "Progress on Skylon and SABRE", Paper IAF-15-D2.1.8, presented at the *66th International Astronautical Federation (IAF) Congress*, Jerusalem, Israel, 12–16 October 2015.

Doublier, M., Pouliquen, M. and Scherrer, D. (1988) "Combined Engines for Advanced European Launchers", Paper IAF-88-251, presented at the *39th International Astronautical Federation (IAF) Congress*, Bangalore, India, 08–15 October 1988.

Draper, A.C. and Sieron, T.R. (1991) "Evolution and Development of Hypersonic Configurations 1958–1990", WL-TR-91-3067, Flight Dynamics Directorate, Wright-Patterson Air Force Base, Ohio, September 1991.

DuPont, A.A. (1999) "Further Studies of Optimized Inlets for Hypersonic Turbine Engines", ISABE 99-7039, *presented at the XIV International Symposium of Air Breathing Engines (ISABE),* Florence, Italy, September 1999.

Eckel, H.A. and Schall, W. (2008) "Laser Propulsion Systems", in *Advanced Propulsion Systems and Technologies: Today to 2000*, edited by C. Bruno and A.G. Accettura, AIAA Progress in Astronautics and Aeronautics Series, Vol. 223, AIAA, Reston, VA., Chapter 14, March 2008.

Escher, W.J.D. (1966) "A Study of Composite Propulsion Systems for Advanced Launch Vehicle Applications – Volume 1: Summary Report", Report 25,194, Ref.: 5402/855/5580, NASA Contract NAS7-377, Marquardt Corporation, Rockedyne Lockheed California Company, Van Nuys, CA, September 1966.

Escher, W.J.D., Flornes, B.J. et al., (1967) "A Study of Composite Propulsion Systems for Advanced Launch Vehicle Applications", Marquardt Corporation Final Report, NASA Contract NAS7-377, Van Nuys CA, April 1967.

Escher, W.J.D. (1994) "Motive Power for Next Generation Space Transports: Combined Airbreathing + Rocket Propulsion", private communication with P.A. Czysz, 1994.

Escher, W.J.D. (1995) "Rocket-Based Combined Cycle (RBCC) Powered Spaceliner Class Vehicles Can Advantageously Employ Vertical Takeoff and Landing (VTOL)", AIAA Paper 95-6145, presented at the 1995 AIAA Aerospace Sciences Meeting, January 1995.

Escher, W.J.D. (1996) "A Winning Combination for Tomorrow's Spaceliners", *Aerospace America,* Vol. 34, No. 2, February 1996, pp. 38–43.

Escher, W.J.D. (1998) "A History of RBCC Propulsion in the U.S. - A Personal Recounting", White Paper, Kaiser Marquardt, Van Nuys, CA, 1998.

Escher, W.J.D. (2001) "The Seven Operating Modes of the Supercharged Ejector Scramjet (SESJ) Combined-Cycle Engine", Paper AIAA-2001-34041, presented at the *37th AIAA/ASME/SAE/ASEE Joint Propulsion Conference,* Salt Lake City, Utah, 08–11 July 2001.

Escher, W.J.D. and Czysz, P.A. (1993) "Rocket-Based Combined-Cycle Powered Spaceliner Concept", Paper IAF-93-S.4.478, presented at the *45th International Astronautical Federation Congress,* October 1993.

Escher, W.J.D., Roddy, J.E. and Hyde, E.H. (2000) "Marquardt's Mach 4.5 Supercharged Ejector Ramjet (SERJ) high-Performance Aircraft Engine Project: Unfulfilled Aspirations Ca. 1970", Paper AIAA-2000-3109, presented at the *36th AIAA/ASME/SAE/ASEE Joint Propulsion Conference and Exhibit, Huntsville*, Alabama, 16-19 July 2000.

Esteve, M.D. et al. (1977) "ODYSSEUS, Technology Integration for a Single Stage to Orbit Space Transport Using MHD Driven Propulsion", Senior Design Study, Parks College of Aerospace and Aviation, Saint Louis University, St. Louis, MO, 1977.

Fermi, E. (1956) *Thermodynamics,* 1st Edition, Chapter 5, Dover Publications, New York, June 1956.

Flack, R.D. (2005) *Fundamentals of Jet Propulsion with Applications*, 1st Edition, Cambridge University Press, January 2005.

Frayling, C. (2015) "The 2001 File: Harry Lange and the Design of the Landmark Science Fiction Film", 1st Edition, Reel Art Press, December 2015.

Gallagher, B. and Webster-Smith, R. (2015) "BAE Systems and Reaction Engines to Develop a Ground Breaking New Aerospace Engine", Press Release, Reaction Engines and BAE Systems, 02 November 2015.

Glassman, I. and Sawyer, R.F. (1970) The Performance of Chemical Propellants, NATO AGARDograph 129, Technivision Services, Slogh (UK). Chapter II.C, January 1970.

Golovitchev, V.I. (1990), personal communication.

Goodall, J. and Miller, J. (2003) *Lockheed's SR-71 'Blackbird' Family*, 1st Edition, AeroFax, Midland Publishing, March 2003.

Gopalaswami, R., Gollakota, S., Venugolapan, P., Nagarathinam, M. and Sivathanu, P.A. (1988) "Concept Definition and Design of a Single-Stage-To-Orbit Launch Vehicle HYPERPLANE", Paper IAF-88-194, presented at the *39th International Astronautical Federation (IAF) Congress,* Bangalore, India, 08–15 October 1988.

Gorelov, V.A., Gladyshev, M.K. et al. (1995) "Ionization Near Hypersonic Vehicles: The Experience of Numerical, Laboratory and Flight Investigations", paper AIAA 95-1940, presented at the *26th AIAA Plasmadynamics and Lasers Conference*, San Diego, CA, 19–22 June, 1995.

Gorelov, V.A., Gladyshev, M.K., Kireev, A.Y., Korolev, A.S., Yegorov, I.V. and Byzov, V.N. (1996) "Computational and Experimental Investigations of Ionization near Hypersonic Vehicles", *Journal of Spacecraft and Rockets*, Vol. 33, No. 6, November–December 1996.

Gounko, Y.P., Kharitonov, A.M., Latypov, A.F., Mazhul, I.I. and Yaroslavtsev, M.I. (2000) "Technique for Determination of Heat Fluxes and Force Characteristics of Ramjet/Scramjet Models in a Hot-Shot Wind-Tunnel", Institute for Theoretical and Applied Mechanics SB RAS, Novosibirsk, 2000.

Graf, D.A. and Welge, H.R. (1991) "1989 High-Speed Civil Transport Studies - Summary", NASA CR-187545, Contract NAS1-18378, HSCT Concept Development Group, Advanced Commercial Programs, McDonnell Douglas Corporation, September 1991.

Gurijanov, E.P. and Harsha, P.T. (1996) "AJAX - New Directions in Hypersonic Technology", AIAA Paper 96-4609, presented at the *7th Aerospace Planes and Hypersonic Technologies Conference,* Norfolk VA, April 1996.

Hannigan, R.J. (1994) *Spaceflight in the Era of Aero-Space Planes*, 1st Edition, Krieger Publishing Company, 1994.

Harford, J. (1997) *Korolev: How One Man Masterminded the Soviet Drive to Beat America to the Moon*, 1st Edition, John Wiley & Sons, April 1997.

Harney, D.J. (1967) "Similarity of Nonequilibrium Air Expansion in Hypersonic Nozzles", USAF FDL-TM-67-1 (AD664084), Air Force Flight Dynamics Laboratory, Wright-Patterson AFB, Ohio, May 1967.

Harper, R.E. and Zimmerman, J.H. (1942) "An Investigation of Rocket Engine Thrust Augmentation with a Nozzle-Ejector System", Arnold Engineering Development Center Report TRD-62-42, March 1942.

Heiser, W.H. and Pratt, D.T. (2002) "Thermodynamic Cycle Analysis of Pulse Detonation Engines", *AIAA Journal of Propulsion and Power*, Vol. 18, No. 1, pp. 68–76.

Hellmold, W. (1999) *Die V1 – Eine Dokumentation*, 1st Edition, Bechtermünz Verlag, 1999.

Hendrick, I.P. (1996) "SSTO and TSTO LOX Collection System Performances: Influence of LOX Plant Architecture", Paper ICAS-96-3.8.3, presented at the *1996 International Council of the Aeronautical Sciences,* Sorrento, Italy, 08–13 September 1996.

Holley, A.T., Wong, W.Y., Rowland, R.A., Meyers E.T., and Freese, R.A. (2012) "Combined Experimental and Modeling Pulsed Detonation Engine Combustor Performance Evaluation Technique", JANNAF paper presented at the CS/APS/EPSS/PSHS Joint Subcommittee Meeting, Monterey CA 3–7 December 2012.

Jacob, D., Sachs, G. and Wagner, S. (Editors) (2005) "Basic Research and Technologies for Two-Stage-to-Orbit Vehicles", Final Report of the Collaborative Research Centres 253, 255 and 259, Deutsche Forschungsgemeinschaft, Wiley-VCH Verlag, December 2005.

Jenkins, D.R. (2001) *Space Shuttle: The History of the National Space Transportation System, The First 100 Missions*, 3rd Edition, Midland Publishing, March 2001.

Jenkins, D.R. (2007) "X-15: Extending the Frontiers of Flight", NASA SP-2007-562, NASA, 2007.

Johnson, M., Stevens, N. et al. (2014) *For the Moon and Mars: N-1 – A Reference Guide to the Soviet Superbooster*, 1st Edition, ARA Press, March 2014.

Kailasanath, K. (2002) "Recent Developments in the Research on Pulse Detonation Engines" (Invited), Paper AIAA-2002-0470, presented at the *40th AIAA Aerospace Sciences Meeting & Exhibit*, Reno, NV, 14–17 January 2002.

Kalmykov, G.P. *et al.* (2008) "LOX-Hydrocarbon Engines in Russia", in *Advanced Propulsion Systems and Technologies: Today to 2000*, edited by C. Bruno and A.G. Accettura, AIAA Progress in Astronautics and Aeronautics Series, Vol. 223, AIAA, Reston, VA., Chapter 14, March 2008.

Kantrowitz, A. (1978) "Laser-Assisted Propulsion Research", in: *Radiation Energy Conversion in Space*, ed. by K.W. Billman, AIAA Progress in Aeronautics and Astronautics Series, Vol. 61, p. 271.

Kingsbury, N.R. (1991) "Aerospace Plane Technology: Research and Development Efforts in Europe", GAO/NSIAD-91-194, *Report to the Chairman, Committee on Science, Space, and Technology, House of Representatives*, United States General Accounting Office, July 1991.

Koelle, D.E. (1989) "On the Optimum Cruise Speed of a Hypersonic Aircraft", IEEE Aerospace and Electronic Systems Magazine, Vol. 4, No. 5, May 1989, pp. 13–16.

Koelle, D.E., Sacher, P.W., and Grallert, H. (2007) "Deutsche Raketenflugzeuge und Raumtransporter-Projekte", 1st Edition, Band 34, Die Deutsche Luftfahrt, Buchreihe über die Entwicklungsgeschichte der Deutschen Luftfahrttechnik, 2007.

Kroon, R.P. (1952) "Turbojet Performance Manual", Engineering Department, Dept. A-1200, Westinghouse Electric Corporation, Aviation Gas Turbine Division, 1952

Kuczera, H. and Sacher, P.W. (2011) *Reusable Space Transportation Systems*, 1st Edition, Springer/Praxis Publisher, London, January 2011.

Lashin, A.I., Kovalevski, M.M., Romankov, O.N. and Tjurikov, E.V. (1993) "Combined Propulsion System for Advanced Multipurpose Aerospace Plane (ASP)", Paper IAF-93-S.4.479, presented at the *44th International Astronautical Federation Congress*, Graz, Austria, October 1993.

Lee, Y.-M., Czysz, P.A. and Bruno, C. (2002a) "Magnetohydrodynamic Energy Bypass Performance Analysis for Hypersonic Vehicles", paper AIAA 2002-3571, presented at the *38th AIAA/ASME/SAE/ASEE Joint Propulsion Meeting*, Indianapolis, IN, 7–10 July 2002.

Lee, Y.-M., Czysz, P.A., Bruno, C. and Petley, D. (2002b) "Implementation of Magnetohydrodynamic Energy Bypass Process for Hypersonic Vehicle" Paper IECEC-20174, presented at the *37th AIAA/IEE/ASME/SAE/ANS/AIChE Intersociety Energy Conversion Engineering Conference*, Washington DC, 28 July–01 August 2002.

Lee, Y.M., Nikolic-Tirkas, B., Tarrant, G.S., Balepin, V., Petley, D. and Czysz, P.A. (2003) "Vortex Tube Air Separation Applications for Air Collection Cycle Hypersonic Vehicles", Paper AIAA-2003-374, presented at the *41st AIAA Aerospace Sciences Meeting and Exhibit,* Reno, NV, 06–09 January 2003.

Lee, Y.-M., Czysz, P.A., and Bruno, C. (2003) "Implementation of Magnetohydrodynamic Energy Bypass for Hypersonic Vehicles", Paper IAC-03-S.5.07, presented at the *54th International Astronautical Congress,* Bremen, 28 September–03 October 2003.

Legostaev, V.P. (1984) Private communication with P.A. Czysz, 38th International Astronautical Congress (IAF), Brighton, UK, 10–17 October 1984.

Leingang, J.L. (1991) Personal communication with P.A. Czysz, Dayton, OH, 1991.

Leingang, J.L., Maurice, L.Q. and Carreiro, L.R. (1992) "Space Launch Systems Using Collection and Storage", Paper IAF 92-0664, presented at the *43rd Congress of the International Astronautical Federation*, Washington, DC, 28 August–05 September 1992.

Lin, B.C. and Lineberry, J.T. (1995) "An Assessment of T-Layer MHD", Paper AIAA 95-1933, presented at the *26th AIAA Plasmadynamics and Lasers Conference*, San Diego, CA, 19–22 June 1995.

Lindley, C.A. (1965) "Performance of Air Breathing and Rocket Engines for Hypervelocity Aircraft", in: Proceedings of the *4th International Council of the Aeronautical Sciences (ICAS) Congress*, Paris, 1964, Spartan Books, Washington, DC, 1965, pp. 941–976.

Lo, R.E., Adirim, H., Pilz, N., Schildknecht, A. *et al.* (2005) "Acquisition and Evaluation of Cryo-Solid Propulsion (CSP); Final Report: Summary of Most Important Results", Technical Report TR Nr.36/03-2005, Aerospace Institute (AI), Berlin, Final Report to the European Space Agency ESA ESTEC, Contract 16830/02/NL/CP, Noordwijk, The Netherlands, March 2005.

Lozino-Lozinskiy, G.E. and Bratukhin, A.G. (Editors) (1997) *Aerospace Systems: Book of Technical Papers*, 1st Edition, Publishing House of Moscow Aviation Institute, Moscow, 1997.

Lozino-Lozinskiy, G.E., Skorodelov, V.A. and Plokhikh, V. P. (1993) "International Reusable Aerospace System MAKS - Present State of the Art and Perspectives", presented at the *5th AIAA/DGLR International Aerospace Planes and Hypersonics Technologies Conference*, Munich, Germany, 30 November–03 December 1993.

Maita, M., Ohkami Y., Yamanaka, T. and Mori T. (1990) "Conceptual Study of Space Plane Powered by Hypersonic Airbreathing

Propulsion System", Paper AIAA-90-5225, presented at the *2nd International Aerospace Planes Conference*, Orlando, FL, 29–31 October 1990.

Maurice, L.Q., Leingang, J.L. and Carreiro, L.R. (1992) "The Benefits of In-Flight LOX Collection for Air Breathing Space Boosters", AIAA paper, presented at the *4th International Aerospace Planes Conference*, Orlando, FL, 01–04 December 1992.

Merlin, P.W. (2002) "Mach 3+ NASA/USAF YF-12 Flight Research, 1969-1979", Monographs in Aerospace History #25, NASA SP-2001-4525, 2002.

Miki, Y., Taguchi, H. and Aoki, H. (1993) "Status and Future Planning of LACE Development", Paper AIAA-93-5124, presented at the 5th International Aerospace Planes & Hypersonics Technology Conference, Munich, Germany, 30 November–03 December 1993.

Miller, J. (2001) *The X-Planes - X-1 to X-45*, 3rd Edition, Midland Publishing, Hinkley, UK, 2001.

Morring, F. (2016) "Dream Chaser Wins Spot in 2nd Round ISS Cargo Contract", Aviation Week & Space Technology, 14 January 2016.

Mulready, D. (2001) *Advanced Engine Development at Pratt & Whitney (The Inside Story of Eight Special Projects 1946-1971)*, SAE International, Warrendale, PA., 2001, ISBN: 0-76800664-3.

Myrabo, L.N. (1982) "A Concept for Light-Powered Flight", Paper AIAA-78-698, presented at the *18th AIAA Joint Propulsion Conference*, Cleveland, OH, 21–23 June 1982.

Myrabo, L.N. (1983) "Advanced Beamed-Energy and Field Propulsion Concepts", NASA-CR-176108, BDM Corporation publication BDM/W-83-225-TR, Final Report for the California Institute of Technology and Jet Propulsion Laboratory under NASA contract NAS7-1000, Task Order RE-156, May 1983.

Myrabo, L.N. (2001) "World Record Flights of Beam-Riding Rocket Lightcraft: Demonstration of 'Disruptive' Propulsion Technology", Paper AIAA-2001-3798, presented at the 37th AIAA Joint Propulsion Conference and Exhibit, Salt Lake City, UT, 08–11 July 2001.

Myrabo, L.N. *et al.* (1988) "Apollo Lightcraft Project", NASA-CR-184749, Final Report, prepared for NASA/USRA Advanced Design Program, 4th Annual Summer Conference, Washington, DC, 13–17 June 1988.

Myrabo, L.N. and Lewis, J.S. (2009) *Lightcraft Flight Handbook: LTI-20*, 1st Edition, Apogee Books, May 2009.

Myrabo, L.N., Messit, D.G. and Mead, F.B. (1998) "Flight and Ground Tests of a Laser-Boosted Vehicle", Paper AIAA-98-3735, presented at the *34th AIAA/ASME/SAE/ASEE Joint Propulsion Conference and Exhibit,* Cleveland, OH, 13–15 July 1998.

Neufeld, M.J. (1995) *The Rocket and the Reich – Peenemünde and the Coming of the Ballistic Missile Era*, 1st Edition, The Free Press, 1995.

Nicholas, T.M.T., Narayanan, A.K. and Muthunayagam, A.E. (1996) "Mixing Pressure-Rise Parameter for Effect of Nozzle Geometry in Diffuser-Ejectors", *Journal of Propulsion and Power,* Vol. 12, No. 2, 1996, pp. 431–433.

Norris, G. (2003) "Pulse Power", Flight International, Vol. 163, No. 4887, 1–23 June 2003, pp. 50–52.

Norris, G. (2015) "Air-breathing Sabre Concept Gains Credibility", Aviation week & Space Technology, 30 July 2015.

Nouse, H., Minoda, M., *et al.* (1988) "Conceptual Study of Turbo-Engines for Horizontal Take-Off and Landing Space Plane", Paper IAF-88-253, presented at the *39th International Astronautical Federation Congress,* October 1988.

Novichkov, N. (1990a) "Space Wings of Russia and the Ukraine", Article in Magazine *Echoes of the Planet/Aerospace*, Moscow, September 1990.

Novichkov, N. (1990b) Private communication, 41st International Astronautical Federation Congress (IAF), Dresden, Germany, 06–12 October 1990.

Ogawara, A. and Nishiwaki, T. (1989) "The Cycle Evaluation of the Advanced LACE Performance", Paper IAF-89-313, presented at the *40th International Astronautical Federation Congress,* Malaga, Spain, October 1989.

Osborn, K. (2015) "AF Chief Scientist: Air Force Working on New Hypersonic Air Vehicle", Defense Tech, 01 June 2015.

Parkinson, R.C. (1991) "The An-225/Interim HOTOL Launch Vehicle", AIAA Paper AIAA-91-5006, presented at the *3rd AIAA International Aerospace Planes Conference*, Orlando, Florida, December 1991.

Pegg, J., Hunt, L. and Petley, D.H. (1993) "Design of a Hypersonic Waverider-Derived Airplane", Paper AIAA-93-0401, presented at the *31st AIAA Aerospace Sciences Meeting and Exhibit,* Reno, NV, 11–14 January 1993.

Phipps, C.R. and Luke, J.R. (2007) "Laser Space Propulsion", in: *Laser Ablation and Its Applications*, Springer, New York. Chapter 16, 2007.

Pirrello, C.J. and Czysz, P.A. (1970) "Hypersonic Research Facilities Study", Volumes I–VI, National Aeronautics and Space Administration Contract NAS2-5458 by McDonnell Aircraft Company (MCAIR), NASA CR 114322-114331, October 1970.

Poggie, J., McLaughlin, T. and Leonov, S. (2016) "Plasma Aerodynamics: Current Status and Future Directions", Journal Aerospace-Lab, AL 10-01, December 2015.

Rife, J.P. and Cantelon, P.L. (2010) "Speeds Up to Orbital': A History of the William H. Avery Advanced Technology Development Laboratory", John Hopkins APL Technical Digest, Vol. 28, Number 4, 2010, pp. 306–323.

Riggins, D.W. (1996) "Brayton Cycle Engine/Component Performance Assessment Using Energy and Thrust-based Methods", Paper AIAA-1996-2922, presented at the *32nd AIAA Joint Propulsion Conference and Exhibit,* Lake Buena Vista, FL, 01–03 July 1996.

Roed, A. (1972) "Development of the Saab-Scania Viggen", Canadian Aeronautics and Space Journal, Vol. 18, June 1972, pp. 167–175.

Rudakov, A.S. and Balepin, V.V. (1991a) "Propulsion Systems with Air Precooling for Aerospaceplane", SAE Technical Paper 911182, Society of Automotive Engineers, April 1991.

Rudakov, A.S., Gatin, R.Y., Dulepov, N.P., Koralnik, B.N., Harchevnikova, G.D. and Yugov, O.K. (1991b) "Analysis of Efficiency of Systems with Oxidizer Liquefaction and Accumulation for Improvement of Spaceplane Performance," Paper IAF-91-270, presented at the *42nd International Astronautical Federation Congress,* Montreal, Canada, October 1991.

Sänger, E. (1956) "Flight Mechanics of Photon Rockets", *Aero Digest*, 1956, p. 68–73.

Schall, W.O., Eckel, H.A., and Bohn, W.L. (2007) "Laser Propulsion Thrusters for Space Transportation", in: *Laser Ablation and Its Applications*, ed. by C.R. Phipps, Springer, New York, Chapter 17, 2007.

Scherrer, D. (1988) "Evaluation du Concept de Fusée-Statoréacteur Pour la Propulsion Hypersonique", ONERA Activities 1988, ONERA, Paris, April 1988.

Schweikart, L. (1998) "The Hypersonic Revolution: Case Studies in the History of Hypersonic Technology; Volume III: The Quest for the Orbital Jet: The National Aero-Space Program (1983–1995)", 2nd Printing, Volume III, Air Force History and Museum Program, 1998.

Scott, T. and Riggins, D.W. (2000) "Work Interaction in Quasi-One Dimensional Flows", Journal of Propulsion & Power, Vol. 16, No. 6, pp. 1053–1059.

Smereczniak, P. (1996) "Electromagnetic Drag Reduction (EMDR) Program", Contract F33657-96-D-2004-0002, Developed for Aeronautical Systems Center Planning Directorate (ASC/XR), 1996.

Stine, G.H. (1996) *Halfwhere to Anywhere – Achieving America's Destiny in Space*, 1st Edition, M. Evans and Company, Inc., October 1996.

Stroup, K.E. and Pontez, R.W. (1968) "Advanced Ramjet Concepts – Volume 1: Ejector Ramjet Systems Demonstration", Report AFAPLTR-67-118, US AF Contract AF33(615)-3734, The Marquardt Corporation Final Report, May 1968.

Sutton, G.P. and Biblarz, O. (2010) *Rocket Propulsion Elements*, 8th Edition, Wiley Publisher, New York, February 2010.

Swithenbank, J. (1967) "Hypersonic Airbreathing Propulsion", Progress in Aerospace Sciences, Vol. 8, Pergamon Press, New York, 1967, pp. 229–294.

Swithenbank, J. (1984) Oral presentation on scramjet research at Sheffield University, May 1984.

Swithenbank, J. and Chigier, N.A. (1969) "Vortex Mixing for Supersonic Combustion", XXI (International) Symposium on Combustion, The Combustion Institute, Pittsburgh, PA, 1969, pp. 1154–1162.

Szames, A. (2001) "Enquête sur une énigme: l'avion hypersonique Ajax", Air et Cosmos, No. 1777, January 2001, pp. 22–24.

Tanatsugu, N., Inatani, Y, Makino, T. and Hiroki, T. (1987) "Analytical Study of Space Plane Powered by Air-Turbo Ramjet with Intake Air Cooler", Paper IAF-87-264, presented at the *International Astronautical Federation (IAF) Congress*, Brighton, UK, October 1987.

Tasić, J. (2006) "The Name of Nikola Tesla in Belgrade: Following the Trail of Light", BelGuest, Summer 2006.

Tesla, N. (2007) *Nikola Tesla: Colorado Spring Notes, 1899–1900*, 1st Edition, BN Publishing, June 2006.

Togawa, M., Aoki, T. et al. (1991) "A Concept of LACE for SSTO Space Plane", AIAA Paper 91-5011, presented at the *3rd International Aerospace Planes and Hypersonics Technologies Conference*, December 1991.

Townend, L. (1986) Oral presentation to NASP technical team on scramjet test in 1966, Hampshire, UK, April 1986.

Townend, L. and Vandenkerckhove, J. (1994) "External Afterburning and Shock-Confined Combustion in Supersonic Flow", APECS-VDK 001/94, ESA contract 120285, European Space Agency, 1994.

Tretyakov, P. (1995) "Supersonic Flow Around Axisymmetric Bodies with External Supply of Mass and Energy", Institute of Theoretical and Applied Mechanics SB RAS, Novosibirsk, Russia, 1995.

Tretyakov, P.K., Golovitchev, V.I. and Bruno, C. (1995) "Experimental and Numerical Study of Counterflow Jet Flame Stabilization in a Supersonic Air Stream", paper presented at the *XII International Society of Air Breathing Engines (ISABE)*, Melbourne, Australia, 10–15 September 1995.

Vandenkerckhove, J.A. (1986) Personal communication with P.A. Czysz about Von Kármán at CalTech, March 1986.

Vandenkerckhove, J.A. (1991) "A First Assessment of Scramjet-Propelled Single-Stage-to-Orbit (SSTO) Vehicles", WLC Phase 5, WP 260, Chapter 1, VDK System S.A., Brussels, Belgium, February 1991.

Vandenkerckhove, J.A. (1992a) "A Peep Beyond SSTO Mass Marginality", Paper IAF-92-0656, presented at the *43rd International Astronautical Federation Congress*, 28 August–05 September 1992.

Vandenkerckhove, J.A. (1992b) "SSTO Configuration Assessment", Chapter 2, Revision 1, VDK System S.A., WLC Phase 5, WP 260, Brussels, Belgium, August 1992.

Vandenkerckhove, J.A. (1993a) "HYPERJET Mk #3, A Rocket-Derived Combined Engine", VDK System Report, April 1993.

Vandenkerckhove, J.A. (1993b) "Comparison Between Ejector-Ramjets & Turbo-Ramjets for T.S.T.O. Propulsion", Paper AIAA-93-5095, presented at the *5th International Aerospace Planes and Hypersonics Technologies Conference*, Munich, Germany, 30 November–03 December 1993.

Weeden, B. (2010) "X-37B Orbital Test Vehicle Fact Sheet", Secure World Foundation, 23 November 2010.

Werrell, K.P. (1985) *The Evolution of the Cruise Missile*, 1st Edition, Air University Press, September 1985.

Wu, Y., Ma, F. and Yang, V. (2003) "System Performance and Thermodynamic Cycle Analysis of Air-Breathing Pulse Detonation Engines", Journal of Propulsion and Power, Vol. 19, No. 4, July–August 2003.

Yabe, T. and Uchida, S. (2007) "Laser Propulsion", in: *Laser Ablation and Its Applications*, ed. by C.R. Phipps and Luke, J.R., Springer, New York, Chapter 18, 2007.

Yamanaka, T. (2000) "Innovative Breakthroughs to a Reusable STS", private communication with P.A. Czysz, 2000.

Yamanaka, T. (2004) "Fundamentals of Airbreathing Rocket Combined Cycle (ARCC) Engine and Design of an ARCC Engine Powered Single-Stage-To-Orbit (SSTO) Vehicle", Beyond the Atmosphere CDROM, July 2004.

Yugov, O. K., et al. (1989) "Optimal Control Programs for Airbreathing Propulsion System or Single-Stage-to-Orbit Vehicles", Paper IAF-89-308, presented at the *40th IAF Congress, International Astronautical Federation*, Malaga, Spain, October 1989.

Yugov, O.K., Dulepov, N.P. and Harchenvnikova, G.D. (1990) "The Analysis of Hypersonic and Combined Cycle Engines in the Propulsion System of the SSTO Vehicles", presented at the *41st IAF (International Astronautical Federation) Congress*, Dresden, Germany, October 1990.

Zagainov, G.I. and Plokhikh, V.P. (1991) "USSR Aerospace Plane Program", Paper AIAA-91-5103, presented at the *3rd International Aerospace Planes and Hypersonics Technologies Conference*, Orlando, FL, 03–05 December 1991.

Earth Orbit on-Orbit Operations in Near-Earth 5

Although not in the frontline technical or popular press, a critical element in reaching space beyond Earth is establishing the space infrastructure around the planet Earth. The concept of this infrastructure as a train marshaling and switching yard is appropriate, a difference being the difficulty of access. The rail control center serves as a center of operations for switching, long-haul train assembly, transfer of goods, refueling, and repair. Likewise, the orbital stations serve as centers for switching payloads between carrier and the required orbit, long-haul space exploration vehicle assembly, transfer of goods to human habitats and manufacturing facilities, return, refueling, and repair coordination. This is no trivial activity, and it will take a commitment as dedicated as the Apollo program to achieve. In this day and age, a correspondent return on investment must be shown. In a step-by-step discussion, we will document the resources necessary to supply what is needed by this space infrastructure as a function of the vehicle-integrated propulsion systems.

Chapter 4 presents those propulsion systems with which we can effectively build reduced oxidizer-to-fuel ratio launchers that are lighter and smaller than conventional expendable rockets. In fact, the remotely powered, directed electromagnetic energy system of the late Professor Leik Myrabo requires even less carried onboard propellants, a huge advantage in seemingly resource-absent space. Note that as long as the principal launchers are expendable launchers for military and commercial needs, the available payloads will be *only* those suitable for infrequent expendable rocket launches. As discussed in the context of Chap. 2, the payloads will then remain consistent with Conestoga wagons until there is an operational railroad equivalent. Until a sustained-use launch system is operational, the payloads that warrant a high launch rate system will remain the subject of design studies only! Until such sustained-use launch system is operational, the flight rate will remain insufficient to build the global space infrastructure needed to support space operations. If the Space Shuttle main propellant tank would have been slightly modified to permit its use as a space structure before the retirement of the STS in 2011 (Hale 2012), like the empty S-IVB third stage of the Saturn V and second stage on the Saturn IB (Bielstein 1980), this could have been the beginning of a space infrastructure as a first step (Taylor 1998, 2000). However, the Space Shuttle main tank was instead intentionally crashed into the ocean, wasting such valuable asset.

Assuming the capability existed for sustained space launches to establish an operational near-Earth orbit space infrastructure, there are serious performance and propellant refueling challenges that need to be immediately addressed. Because of the activity required by the elements of the near-Earth orbit infrastructure, the quantity of propellant required in space and, more importantly, the quantity of launcher propellant required to lift from the Earth surface that very propellant into low Earth orbit (LEO) are truly prodigious, unless a non-chemical rocket is used. For a true space transportation system to exist, a transportation system network has to be built just as it was for the US transcontinental railroad. The late Dr. William Gaubatz, formerly of McDonnell Douglas Astronautics and former director of the Delta Clipper DC-X program (Butrica 2003; Stine 1996; Hannigan 1994), attempted to anticipate what the future might hold if a space transportation system actually would exist, as shown in Fig. 5.1. Dr. Gaubatz shows the elements necessary to build the infrastructure, but unfortunately does not address the assets required to establish and sustain that infrastructure.

Figure 5.1 presents a functional orbital infrastructure, including space habitats, free-flying facilities, and power stations at several levels of development, using prior work of Dr. Gaubatz. Table 5.1 lists the orbital vehicles and platforms and their diverse functions facilitating a true space infrastructure. Future global space is a crowded and busy place although a snapshot would show only single elements (points) in space, not trajectories. The key enabling space structures are the fuel station spaceports and orbital servicing vehicles. Without these vehicles, movement between orbital

P.A. Czysz et al., *Future Spacecraft Propulsion Systems and Integration*,
Springer Praxis Books, DOI 10.1007/978-3-662-54744-1_5

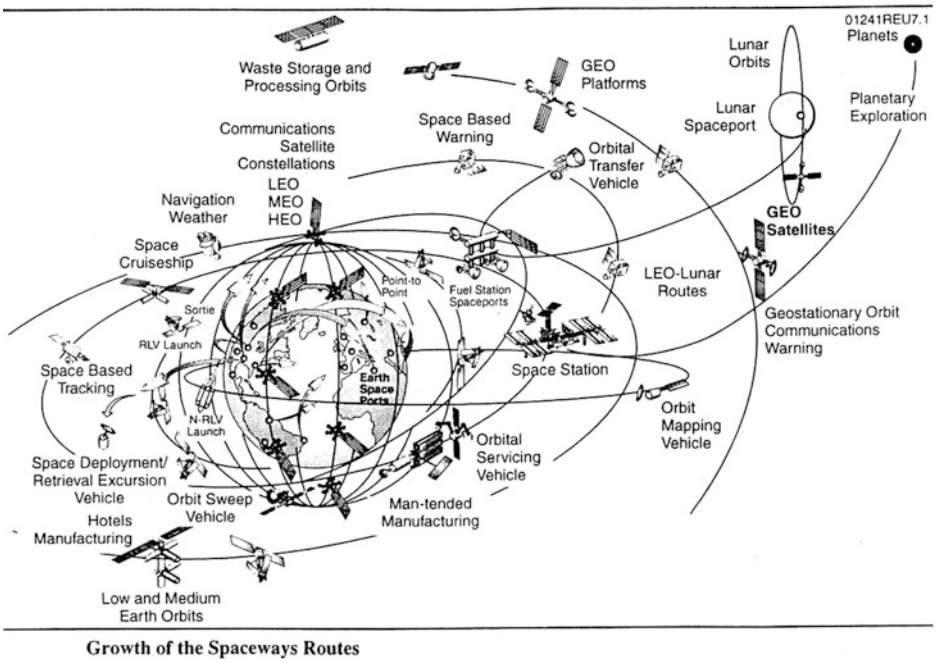

Fig. 5.1 Growth in spaceway routes. Future space infrastructure envisioned by Dr. William Gaubatz, if enabled by a space transportation system and in-space operations system to support the infrastructure

planes and altitudes is limited to specific satellites, such as GSO communication satellites with integral geotransfer propulsion. With servicing centers equipped with construction module storage, they can supply components for orbital, lunar, and deep-space vehicle assembly in space. The operations center/space station provides a system to launch and control missions to the Moon, the planets and deep space. Like the USSR plan introduced in Chap. 2, there are lunar spaceports and lunar orbiting satellites. There are space deployment and retrieval vehicles as well as a waste storage and processing facility in high orbit. Then, this outlook provides a comprehensive projection of future space if a suitable (a) scheduled, frequent, and sustained transportation and (b) heavy-lift capability are available as the key prerequisites. In short, these two "critical mass" enabling elements are needed to plan for the future, not the current status quo.

What is not shown in the visualization by Dr. Gaubatz, see Fig. 5.1, is a solar power station that beams power to the Earth's surface, space assets, or a power station warehouse that provides hardware for the power satellites in geostationary Earth orbit. It remains to be seen whether a solar power station has the energy conversion efficiency to provide affordable energy to Earth or space assets comparable to nuclear power stations. In this context, a source of excellent information on solar power stations is from reports by H.H. Koelle, formerly at the University of Berlin (Koelle 1961; 1995). In fact, the singular reliance on photovoltaic power generation may doom all power stations until a more efficient and more durable conversion system can be identified. As proven by the NASA LDEF (Long Duration Exposure Facility) materials evaluation satellite, space is a very hostile environment and we have yet to identify slowly deteriorating or non-deteriorating materials and construction concepts, including those for solar panels. Nikolai Anfimov, of the Russian TsNIIMash (Central Research Institute of Machine Building), in a private communication with author P.A. Czysz, had stated that the hub of the Russian MIR orbital station, exposed to the space environment for 15 years in orbit, was so riddled with cosmic-Galactic radiation particles (e.g., *Fe* ions) that it was beginning to leak, even though there were no visible holes. Clearly, the complexity and extensive nature of the space infrastructure implies that a significant commitment of human and monetary resources is necessary if we are to go beyond the two currently operating solitary orbital stations (ISS and Tiangong-1) with limited capability.

In fact, infrastructure demands access to space and maneuvering in space. Spacecraft must be lifted to orbit more economically than possible now and, once there, must be able to change their orbit to reach propellant depots, crewed maintenance and space stations, space hotels, TLC (Telecommunications) and scientific satellites, and rescue vehicles ("lifeboats"). All these in-space missions require more economical in-space propulsion for space tugs and orbital maneuvering vehicles (OMVs) not only to raise or lower orbit and to rendezvous, but also to change orbital plane. Operation must be more economical both in terms of energy and mass. Accordingly, this is the focus of this chapter.

Table 5.1 Space infrastructure vehicles and missions, from Fig. 5.1

	Orbital system	Function	Orbit
1	Sustained-use launcher	High frequency, modest payloads	LEO/MEO
2	Expendable launcher	Low frequency, heavy payloads	LEO
3	Point-to-point transfer	Points on Earth or orbit	
4	Operations center/space station	Operations coordination/research	LEO/MEO
5	Orbital servicing vehicle	Maintains in-orbit vehicles	All
6	Fuel station spaceport	Refuels orbital vehicles	LEO
7	Space-based manufacturing	Human based low *g* manufacturing	LEO
8	Man-tended manufacturing	Robot based micro*g* manufacturing	LEO/GEO
9	Orbital sweep vehicle	Orbital cleanup vehicle	All
10	Waste storage and processing vehicles	Processes and disposes human and manufacturing wastes	HEO
11	Navigation/weather	Supports travel network	LEO/MEO
12	Orbital mapping vehicle	Measures resources and geography	LEO/MEO
13	Space-based warning	Military and asteroid warning	HEO/GEO
14	Space-based hotel	Space tourism facilities	LEO/MEO
15	Space Cruiser vehicle	Human transport and rescue	LEO
16	Communication satellite constellations	Supports telecommunication systems	All
17	Orbital transfer vehicle	Orbital altitude/plane change	All
18	LEO-lunar vehicle	Transport to Moon and return	LEO
19	Space deployment retrieval vehicle	Recovers spent vehicles	All
		Replaces spent vehicles	
20	Space excursion vehicle	Placement of new systems	LEO
21	GEO platforms/satellites	Micro*g* and magnetic field space	GEO
22	GEO communications and warning vehicles	Fixed equatorial position	GEO
23	Lunar spaceport system	Lunar transportation/research hub	Lunar
24	Lunar orbital vehicles	Support lunar activities	Lunar
25	Planetary exploration vehicles	Near- and deep-space vehicles	LEO/Lunar

5.1 Energy Requirements

The concept of the train yard as a center of operations for switching, long-haul vehicle assembly, transfer of goods, refueling, and repair is not unrealistic for the first-generation space infrastructure. As we shall see, the energy requirements are greater for mobility in the vicinity of Earth than to reach LEO. There is a clear need for a nuclear-powered tug for orbital transfer from LEO to geostationary orbit (GSO) and return, see Chap. 7. There is also a need for collecting, repair, or disposal of non-functional satellites in LEO and GSO; for the refueling of sustained-use satellites; for orbital busses and tugs; and, generally speaking, for sustained in-orbit operations and maintenance. As we shall see, this implies a first step that must be taken as far as vehicle-integrated propulsion to anticipate the future.

5.1.1 Getting to Low Earth Orbit: Energy and Propellant Requirements

At nonrelativistic speed, all of the classical orbital mechanics from near-Earth to the edge of our solar system and beyond are based on Newton's fundamental law of gravitational attraction. The assumption is that the gravitational force, $\vec{F}_g$, acts throughout the universe in the same way. Newton's law of universal gravitational force between the mass of two bodies, m_1 and m_2, with the distance, r, between the center of mass of the two bodies is given by:

$$F_g = G \cdot \frac{m_1 \cdot m_2}{r^2} \tag{5.1}$$

The universal gravitational constant, G, is

$$G = 6.67408 \cdot 10^{-11} \frac{\mathrm{m}^3}{\mathrm{kg\,s}^2} \tag{5.2}$$

Gravity is probably one of the most mysterious forces in the universe. In fact, while our everyday experience of gravity is commonplace, our understanding is very limited. The law has been well tested on Earth and in the vicinity of the Earth. However, when astronomers attempt to use Newton's fundamental law of gravitational attraction to predict the motion of stars orbiting the center of the Galaxy, they sometimes must grapple with strange results. The most distant man-made objects are *Pioneer 10* launched in 1972 and *Pioneer 11* launched in 1973. *Pioneer 10* is now more than 8 billion miles from Earth. On January 23, 2003, the tracking stations picked up the last feeble transmission from the probe's radioactive isotope (plutonium)-powered transmitter (Folger 2003; Wolverton 2004). As *Pioneer 10*'s feeble signal faded from detection, the spacecraft seemed to be defying Newton's law of gravity because it was slowing down as if the gravitational attraction from the Sun was growing stronger the farther away it traveled. *Pioneer 11* also slowed down in a similar manner. The *Ulysses* space probe, which has been orbiting the Sun for 13 years, has also behaved in a manner characteristic of an unknown force slowing it down.

In the case of the *Pioneer 10* and *Pioneer 11* probes, the most distant man-made objects, this perceived irregularity led for some time to postulate that Newton's law changed with increasing distance. *Pioneer 10* launched in 1972 and *Pioneer 11* launched in 1973. *Pioneer 10* is more than 10 billion miles from Earth. On January 23, 2003, the tracking stations picked up the last feeble transmission from the probe's radioactive isotope (plutonium)-powered transmitter (Folger 2003). As *Pioneer 10*'s feeble signal faded from detection, the spacecraft seemed to be defying Newton's law of gravity because it was slowing down as if the gravitational attraction from the Sun was growing stronger the farther away it traveled. *Pioneer 11* also slowed down in a similar manner. The *Ulysses* spacecraft orbiting the Sun also behaved as if an unknown force slowed it down. This so-called *Pioneer Anomaly* was eventually explained as reported in Chap. 9 (Turyshev et al. 2004), but there is some scant evidence that perhaps gravity does not act in the same way on a galactic scale. Our Galaxy makes one rotation in about the time from when dinosaurs began to inhabit the Earth to now. Perhaps on that time and distance scale, gravity may act differently. Until more is understood, we will continue with the traditional assumption of gravity acting the same throughout the universe, but also need to acknowledge that the farther we travel and the longer we are in space, we may be departing from the expected.

The law of gravity rules the attraction between two masses. When in motion, then the law that governs the two-body problem (that is, a large central body and a moving smaller body) yields Kepler's three laws of motion. Although gravitational forces can be formulated for N number of bodies, the only analytic (closed-form) solutions found are for $N = 2$. Numerical solutions are possible, but these involve the use of the largest computers; they are used only when the simple two-body problem is suspect (such as predicting a Mercury orbiter trajectory) or high navigational accuracy is required (Logsdon 1997). The Keplerian *circular* orbit relationships between two bodies are given below (Koelle 1961):

$$V_{\text{circular}} = \sqrt{\frac{M \cdot G}{r}} \quad [\text{km/s}] \tag{5.3a}$$

$$V_{\text{circular}} = \sqrt{\frac{\mu}{r}} \quad [\text{km/s}] \tag{5.3b}$$

$$V_{\text{circular}} = \sqrt{\frac{\mu}{R_0 + h}} \quad [\text{km/s}] \tag{5.3c}$$

$$\text{Period} = 2 \cdot \pi \sqrt{\frac{r^3}{\mu}} \quad [\text{s}] \tag{5.4a}$$

$$\text{Period} = 2 \cdot \pi \sqrt{\frac{(R_0 + h)^3}{\mu}} \quad [\text{s}] \tag{5.4b}$$

where μ = gravitational constant = $M{\cdot}G$, M = mass of the central body, r = radius from the spacecraft center of mass to the center of mass of the central body, R_0 = planet radius, and h = altitude above surface.

The gravitational parameters and the orbital speeds for a 200-km orbit and escape are given in Table 5.2 for selected bodies.

From Eqs. (5.1), (5.3a, b, c) and (5.4a, b), the orbital velocity decreases and the orbital period increases as the spacecraft altitude is increased, see Figs. 3.6, 3.7 and 3.8. The two-body equations assume non-rotating masses. If the central body is rotating, then its rotation can add a velocity vector increment to the launcher vehicle, dependent on the latitude of the launch site and the launch azimuth. Figure 5.2 shows the required velocity increment from the Earth's surface to the orbital altitude (in nautical miles).

Both the non-rotating Earth and rotating Earth (launch site at the Equator) velocity increments required are shown in Fig. 5.2. These are not the velocities in orbit, but the velocity increment (energy increment) that determines the mass ratio to reach simultaneously the given orbital altitude and required orbital speed. The speed of the Earth's surface at the Equator is 463.6 m/s (1521 ft/s). That reduces the launch speed increment (ΔV) to 7331.05 m/s (24,052 ft/s) if the launcher is launched due east (90° latitude from true north) at the Equator. If the launcher is launched due west, then the launcher must cancel out the easterly motion, so the

Table 5.2 Gravitational characteristics of nearby planets and Earth's Moon

	Venus	Earth	Moon	Mars	Jupiter
μ (km^3/s^2)	324,858.8	398,600.4	4902.8	42,828.3	126,711,995.4
R_0 (km)	6061.8	6378.14	1737.4	3397.0	71,492
V_{200} (km/s)	7.203	7.784	1.680	3.551	42.10
V_{esc} (km/s)	10.187	11.008	2.376	5.022	59.538

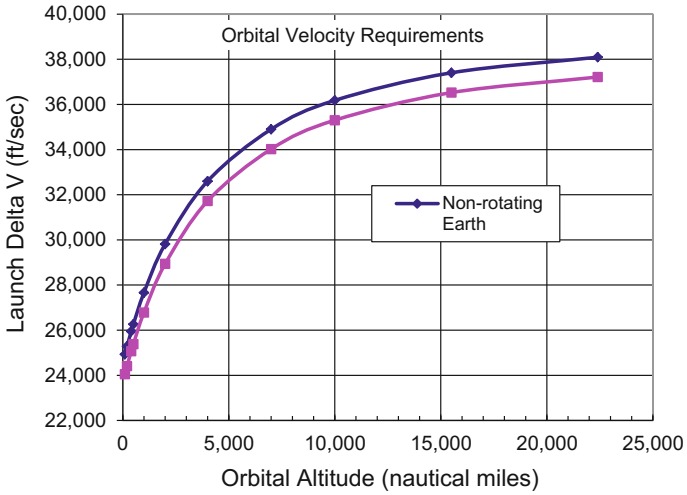

Fig. 5.2 Launch velocity increment to reach Earth orbit

launch speed increment (ΔV) is 8258.25 m/s (27,094 ft/s). For a true east launch, the launch velocity increment as a function of the launch site latitude La is:

$$V_0 = V_{\text{circular}} - 1521 \cdot \sin(La) \quad \text{[ft/s]} \tag{5.5}$$

For a due east launch, the inclination of the orbit is equal to the latitude of the launch site. Figure 5.3 shows the velocity increment for the launch ΔV as a function of the launch site azimuth for a due east launch with a number of launch sites indicated. In reality, the launch azimuth will not always be due east. The launch azimuth for a non-rotating Earth at a given orbital inclination and launch site latitude is:

$$\sin A_z = \frac{\cos i}{\cos(La)} \tag{5.6}$$

with A_z = launch azimuth from true north, and i = orbital inclination.

Equation (5.6) defines the minimum inclination for an orbit as the latitude of the launch site and a true east or west launch (90° or 270°). For the rotating Earth case, a correction to the launch azimuth and velocity must be made by the vector addition of the eastward velocity of the Earth and the launch velocity vector. But Eq. (5.6) will give the minimum azimuth and a good first-order value. For a Sun-synchronous orbit (SSO at 98°) from a launch site at 45° latitude, this value is −11.4° or an azimuth of 348.6°. For the International Space Station (ISS) orbit (55°) from Kennedy (28.5°), the azimuth angle is 40.7° or just north of northwest. Consequently, when the Space Shuttle launched from Kennedy, the spacecraft had to roll to position the wing plane perpendicular to 40.7° and then proceed along its launch trajectory.

Given the incremental velocity required to achieve a circular orbit, the next step in discussing the infrastructure logistics is to determine the quantity of launch propellant required to place a given quantity of propellant into LEO for interorbit maneuvering.

5.2 Launcher Propulsion System Characteristics

Section 3.1 provides the governing equations and methodology for determining launcher size to achieve a given velocity increment with a given payload mass. The sizing process is the same for determining the quantity of launch propellant required to place a given quantity of propellant (payload) into LEO. The difference is that for a fixed-volume payload bay, each propellant combination has a different bulk density and therefore a different tank volume occupied for a fixed propellant mass. Overall, the role of the propellant delivery vehicle is analogous to that of an Air Force tanker aircraft. Its role is to deliver fuel to in-flight operational

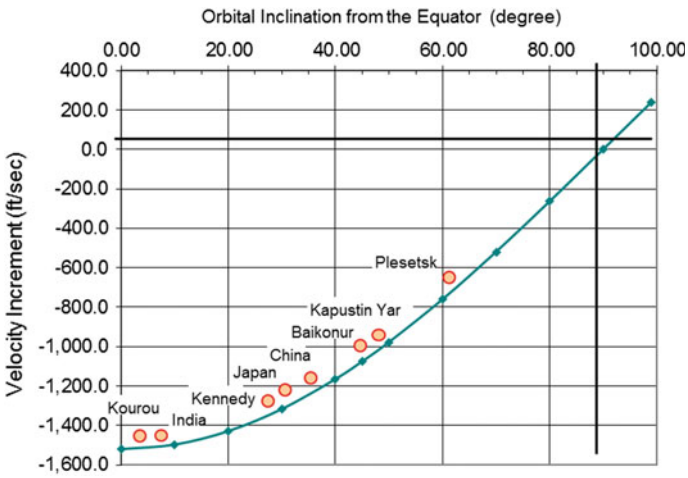

Fig. 5.3 Velocity increment to 200-nm orbit for orbital inclination. Some launch centers are indicated

vehicles on demand and on a sustained operational basis. In this case, the role of the LEO tanker is to routinely deliver propellant to an orbital refueling station in LEO. Being a dedicated tanker, the cargo container is a propellant tank, with provisions for transferring propellant in orbit. In microgravity, special design considerations are necessary (e.g., that the propellant is adjacent to the transfer pumps), but much of this has been accomplished for some time in space and is a known and established design practice.

In all cases, the LEO tanker is an automatic vehicle that has sustained, frequent use and routine exit and entry of the atmosphere attributes. In short, it is not an expendable or a reusable expendable vehicle. As a consequence, the best configuration choice for the LEO tanker is the hypersonic glider or air-breathing launcher, as shown in Figs. 2.18 and 2.19, and Figs. 4.39–4.41. With the following, four different launcher propulsion systems are evaluated for the tanker to LEO mission:

(1) Hydrogen/oxygen rocket, e.g., based on the Pratt & Whitney XLR-129 (Mulready 2001).
(2) Hydrogen/oxygen LACE rocket, based on the Pratt & Whitney XLR-129.
(3) Rocket ejector ram–scramjet airbreathing to Mach 10, transitioning to a hydrogen/oxygen rocket, based on the Pratt & Whitney XLR-129.
(4) Rocket ejector ram–scramjet airbreathing to Mach 12, transitioning to a hydrogen/oxygen rocket, based on the Pratt & Whitney XLR-129. (Note: All rocket technology was sold in 2013 from Pratt & Whitney to Aerojet-General, of Sacramento, CA.)

The design payload selected here is 19 t (41,895 lb) of propellant with a bulk density of 999.4 kg/m^3 (62.4 lb/ft^3). A launcher for the design payload was sized for each of the four propulsion systems. For different propellant densities, the size and weight of the launcher is different. These corrections are discussed later in this chapter and are given in Fig. 5.4.

5.2.1 Propellant Ratio to Deliver Propellant to LEO

The propellant ratio is defined here as the propellant mass burned by the launcher to achieve LEO, divided by the propellant load carried to LEO. Mass and density of the propellant affect the size of the launcher, and this sensitivity has been evaluated. The launchers are sized using the methodology described in Chap. 3. The vehicle assumptions are the same as outlined in Chap. 4, except that a permanent propellant tank replaced the accessible payload bay. For the design payload and payload density, the sizing results are given in Table 5.3.

The propulsion system selection determines the key parameter for an orbital tanker, which is the propellant burnt to lift the orbital maneuver propellant, divided by the propellant delivered. The LACE rocket is an adaptation of an existing operational rocket engine and requires good engineering design and testing, but it is not a technological challenge. The LACE rocket offers a greater than 50% reduction in the propellant required to deliver the design payload of 19 t of propellant to LEO, as shown in Table 5.3 and Fig. 5.5.

Because of the LACE rocket's greater thrust over drag ratio *T/D*, the propellant ratio is slightly better than a rocket ejector ramjet utilizing atmospheric air up to Mach 6. A piloted vehicle is at a disadvantage for an orbital tanker in that the provisions for the pilot increase the propellant required for delivering the orbital propellant to LEO. Clearly, transitioning to an airbreather vehicle configuration offers the potential to reduce the propellant required to deliver the orbital maneuver propellant by 38 and 52%, respectively. Proceeding beyond an airbreathing Mach number of 12 results in an increase in the propellant required to deliver the orbital maneuver propellant, see Fig. 5.5.

The important conclusion from this analysis is that as a first step, basing the propulsion system on an existing rocket motor

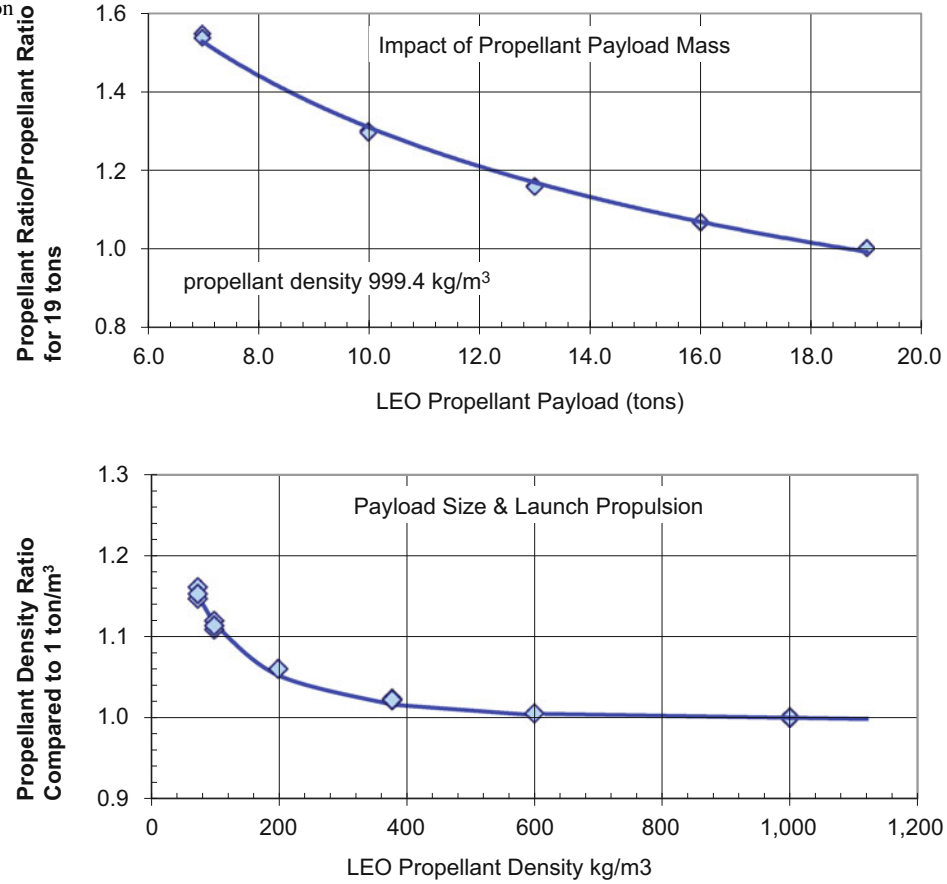

Fig. 5.4 Propellant required as a function of payload mass and density

Table 5.3 Launchers sized to deliver 19 t of propellant to LEO

	H_2/O_2 rocket FDL-7C/D	LACE rocket FDL-7C/D	RBCC Mach 10 airbreather	RBCC Mach 12 airbreather
Planform area (m^2)	600	370	301	268
W_{eng} (t)	27.95	11.85	11.13	8.92
W_{OEW} (t)	97.86	57.9	46.73	40.18
W_{OWE} (t)	116.9	76.9	65.73	59.18
W_{ppl} (t)	892.9	379.2	235.2	181.0
W_{TOGW} (t)	1,010	456.1	300.9	240.1
Propellant ratio (–)	47.0	20.0	12.4	9.53

Design payload is 19 t (41,895 lb) of propellant with a bulk density of 999.4 kg/m^3 (62.4 lb/ft^3)
LACE Liquid Air Cycle Engine; *RBCC* Rocket Based Combined Cycle

(LACE rocket), offers a 57% reduction in the propellant required to deliver the orbital maneuver propellant. It is important to note that this step does not require a technological breakthrough, but only an adaptation of an existing operational propulsion system. A key observation is, even with the best propulsion system for the launcher, it requires 10 lb of launcher propellant to deliver 1 lb of orbital maneuver propellant to LEO. It becomes clear that the orbital maneuver vehicle needs to be a very efficient user of orbital propellant.

In the above exercise, the design payload selected has been 19 t (metric tons). If that payload mass is increased, there is a gradual decrease in the percentage of the propellant required to deliver the orbital maneuver propellant, as shown in the top chart of Fig. 5.4. However, if the payload is instead decreased, the propellant required to deliver the orbital maneuver propellant increases quickly. As shown in the top chart of Fig. 5.4, at 7 t LEO propellant payload, the propellant required to deliver the orbital maneuver

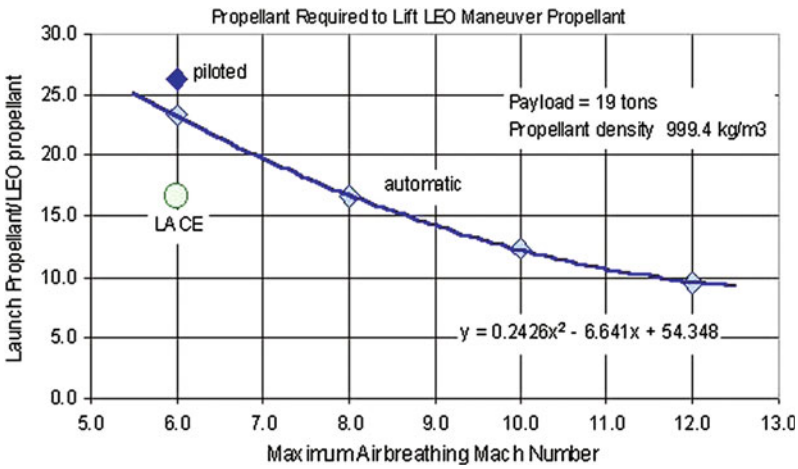

Fig. 5.5 Launch propellant required to lift orbital maneuver propellant to LEO with a rocket ejector ramjet. All-rocket ratio = 47

propellant is 50% greater compared to the 19 t LEO propellant payload case. The correlating curve fit is:

$$\frac{W_{\mathrm{ppl_{launcher}}}}{W_{\mathrm{ppl_{LEO}}}} = 3.5531 \cdot W_{\mathrm{pay}}^{-0.4339} \tag{5.7}$$

where W_{pay} is in t.

Orbital maneuvering vehicles (OMVs) are powered by a mix of propulsion systems and propellants. A parametric sizing effort has established the variability of the ratio of launcher propellant to propellant payload with payload propellant bulk density and payload mass. A representative set of orbital maneuver propulsion systems is given in Table 5.4. This is only meant to span a selected range of relevant systems and is by no means all-inclusive or comprehensive. The density I_{sp} (bulk specific gravity, SG, times I_{sp}) is a measure of the relative volume taken by the propellant system. In that respect, the hypergolic propellants take always less volume compared to a hydrogen-fueled system.

For propellant bulk densities greater than 700 kg/m^3 (43.7 lb/ft^3), there is no change in the propellant/payload ratio. That is, the propellant payload volume does not influence how much propellant is required to deliver the orbital maneuver propellant; in contrast, the payload mass has a major impact. For propellant bulk densities less than 700 kg/m^3 (43.7 lb/ft^3), there is an increase in the propellant required to deliver the orbital maneuver propellant. That is, now both, the propellant mass and the volume of the orbital maneuver propellant, determine the size and volume of the launcher. The result is an increase in propellant required to deliver the orbital maneuver propellant, as shown in the bottom chart of Fig. 5.4. The correlation curve fit for propellant bulk densities less than 700 kg/m^3 (43.7 lb/ft^3) is:

$$\frac{W_{\mathrm{ppl_{launcher}}}}{W_{\mathrm{ppl_{LEO}}}} = 3.189 - 0.3524 \cdot X + 0.0263 \cdot X^2 \tag{5.8}$$

where $X = \rho_{\mathrm{ppl(LEO)}}$, the propellant density in LEO.

The range of launcher propellant required to lift one mass unit of orbital maneuver propellant to LEO ranges from 47 to 9.5. Compare this to a Boeing 767-200 carrying 216 passengers over a 5800 km distance: The fuel consumed is 2.6 mass units per one mass unit of payload. The oxidizer-to-fuel ratio for the airbreather to Mach 12 is 3.14, and the resulting fuel-to-payload ratio is 3.02. That implies that the airbreathing launcher is only about 16% less efficient in its propulsion system flying to Mach 12 than a Mach 0.85

Table 5.4 Characteristics of space propulsion systems for orbital maneuvering vehicles

	Hypergolic rocket	Hydrogen/oxygen rocket	Solar electric	Nuclear electric
Fuel	Hydrazine	Hydrogen	Lithium	Lithium
Oxidizer	Nitrogen Tetroxide	Oxygen	none	none
Bulk density (kg/m^3)	1229	378.0	533.7	533.7
I_{sp} (s)	290	460	3200	9000-plus
Density I_{sp} (s)	357	174	1705	4797

transport. Concorde, flying 100 passengers at Mach 2.04 over a 6300 km distance, consumed about 8.3 mass units of fuel per one unit payload mass. Consequently, the air-breathing launcher is more efficient than Concorde in terms of fuel usage.

After finding the propellant required to lift the orbital maneuver propellant to LEO, the task remains to establish how much orbital maneuver propellant is required.

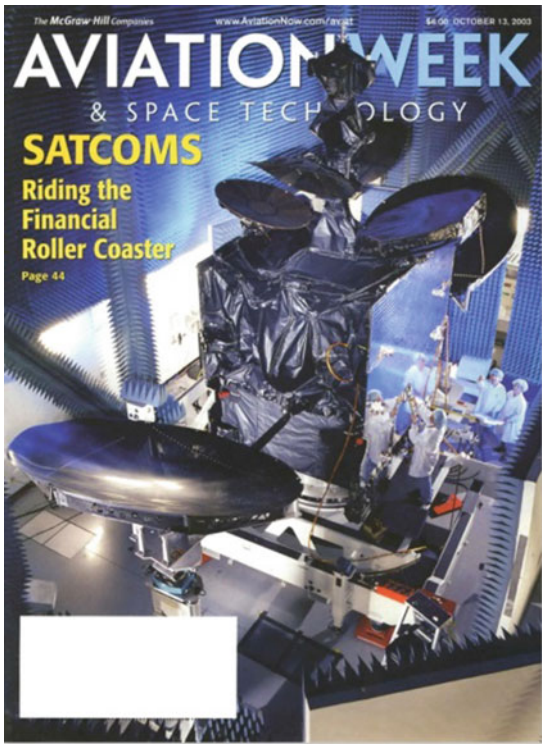

Fig. 5.6 Representative reference satellite (Covault 2003)

5.2.2 Geostationary Orbit Satellite Size and Mass

The first step is to examine a number of GSO satellites from the open literature and determine a representative reference value. The goal is to generate a "reference GSO satellite" that is heavy enough to represent future satellites and then provide a reasonable estimate of the orbital propellant required. Table 5.5 gives the dimensions of the satellite main body with all antennas folded. The mass ratio determined for the "beginning-of-life" mass and the "empty" mass is the propellant required for maintaining the GSO orbit and station-keeping due to orbital precession.

The cover of *Aviation Week & Space Technology* of October 13, 2003, has a picture of the Boeing Satellite Systems 601B for broadcast and broadband multimedia services, see Fig. 5.6 (Covault 2003). This is not unlike the reference satellite listed at the bottom of Table 5.5. Having identified a reference satellite, the next question is how much propellant will be required to change its altitude and orbital inclination?

5.3 Maneuver Between LEO and GEO, Change in Altitude at Same Orbital Inclination

The nominal LEO altitude assumed here is 100 nm (185.2 km) or around 200 km (108 nm). Reaching a higher-altitude orbit is usually a two-step process, as shown in Fig. 5.7 for the GSO example.

For a general elliptical orbit, the lowest altitude is the periapsis and the highest is the apoapsis specifically for selected bodies:

Table 5.5 Characteristics of a number of GSO satellites (Karol 1997)

System	Length (m)	Width (m)	Height (m)	Volume (m^3)	Beginning-of-life (BOL) mass (kg)	Empty mass (kg)
ASTRA-1F	4.51	3.41	2.80	43.2	1803	1279
EHF-7	3.35	3.35	3.35	37.7	1224	868
INTERSAT 707	4.69	2.41	2.19	27.2	3649	1760
APSTAR 1A	6.58	2.16[a]	2.16[a]	24.1	584	414
CHINSAT 7	6.58	2.16[a]	2.16[a]	24.1	557	395
N-STAR-B	3.05	2.40	2.20	27.3	1617	2057
INMARSAT III	2.10	1.80	1.71	16.7	1098	778
AMOS-1	1.22	1.68	1.92	10.5	579	410
Reference	3.40	2.80	2.80	26.7	2267	1608

[a]Diameter, cylindrical configuration

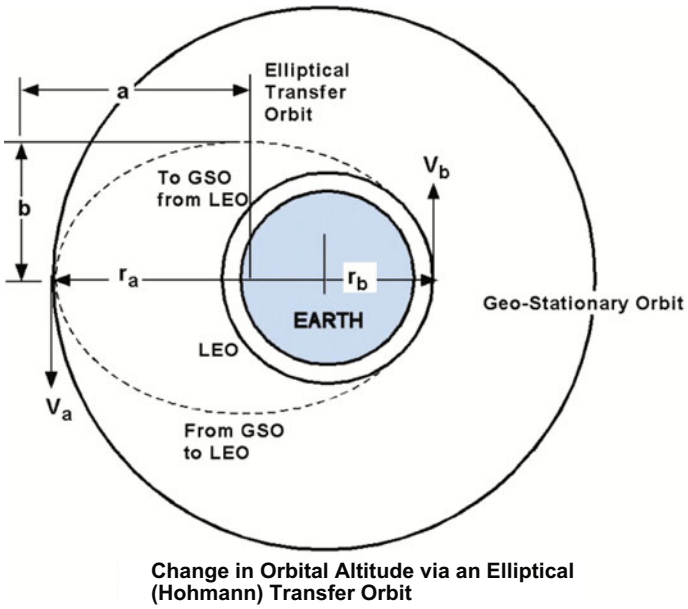

Fig. 5.7 Transfer ellipse to change orbital altitude

General	Sun	Earth	Moon
Periapsis	Perihelion	Perigee	Perilune
Apoapsis	Aphelion	Apogee	Apolune

The first step is an elliptical transfer orbit to the orbital altitude desired, which requires a propulsion burn to leave the low-altitude orbit. The second step is a propulsion burn to match the circular orbital velocity at the desired higher orbital altitude. The process to return to the lower orbital altitude requires a burn to match the elliptical orbital speed at the higher altitude, then a second propulsion burn to match the lower circular orbit speed. This is a minimum energy transfer orbit, or Hohmann Transfer (Logsdon 1997). Equations (5.3a)–(5.3c), Eq. (5.4a) and (5.4b) provide the magnitude of the circular orbital velocity at the desired altitude.

Figure 5.7 shows the geometry for the example elliptical transfer orbit from LEO to GSO. The information needed is the elliptical orbit velocities for the lowest orbital altitude (periapsis) and the highest orbital altitude (apoapsis). The following equations provide the orbital parameters for Kepler's *elliptical* orbits. We obtain for the velocity at the periapsis

$$V_p = \sqrt{\frac{2 \cdot \mu}{R_0 + h_p} + \frac{\mu}{a}} \tag{5.9}$$

The velocity at the apoapsis is

$$V_a = \sqrt{\frac{2 \cdot \mu}{R_0 + h_a} + \frac{\mu}{a}} \tag{5.10}$$

The semimajor axis of the transfer ellipse is given with

$$a = \frac{(R_0 + h_a) + (R_0 + h_p)}{2} \tag{5.11}$$

and the eccentricity, which defines the shape of the orbit, is defined as

$$e = \frac{(r_a - r_p)}{(r_a + r_p)} \tag{5.12}$$

The period of the ellipse is

$$T = 2 \cdot \pi \sqrt{\frac{a^3}{\mu}} \tag{5.13}$$

All Kepler orbits are conic sections. In this general sense, an orbit is a path through space defined by a conic section. There are two closed orbital solutions (circular and elliptical) and two open (not returning) orbital solutions (parabolic and hyperbolic). For a circular orbit, the eccentricity, e, has to be equal to zero. For an elliptical orbit, the eccentricity, e, has to be less than one. For a parabolic orbit, the eccentricity, e, has to be equal to one. For a hyperbolic orbit, the eccentricity, e, has to be larger than one.

To increase orbital altitude, the velocity increments are then

$$\Delta V_1 = V_p - V_{\text{circular,p}} \tag{5.14a}$$

$$\Delta V_2 = V_a - V_{\text{circular,a}} \tag{5.14b}$$

To decrease orbital altitude, we obtain

$$\Delta V_1 = V_{\text{circular,a}} - V_a \tag{5.15a}$$

$$\Delta V_2 = V_{\text{circular,p}} - V_p \tag{5.15b}$$

Then, to increase orbital altitude requires a propulsion burn at periapsis to accelerate to elliptical orbit speed, followed by a propulsion burn at apoapsis to increase the spacecraft speed to circular orbit speed at the higher altitude. To decrease orbital altitude, there is a propulsion burn at apoapsis to slow the spacecraft to elliptical orbit speed, followed by a propulsion burn at periapsis to decrease the spacecraft speed and circularize the orbit at the lower altitude. Specifically, transferring from a 100-nm (185.2-km) LEO to a 19,323-nm (35,786-km) GSO orbit (refer to Fig. 5.7 for the geometry of the transfer maneuver and the location of the velocities called out), the orbital velocity for a 100-nm (185.2-km) circular orbit is 25,573 ft/s (7795 m/s). For an elliptical transfer orbit, the orbital velocity at the 100-nm (185.2-km) perigee is 33,643 ft/s (10,254 m/s) and 5235 ft/s (1596 m/s) at the 19,323-nm (35,786-km) apogee. The orbital velocity for a 19,323-nm (35,786-km) circular orbit is 10,088 ft/s (3075 m/s).

5.3.1 Energy Requirements for Altitude Change

Referring to Fig. 5.7, to initiate the transfer maneuver, the spacecraft must be 180° away from the desired point in the GSO orbit. At that point, a rocket burn is required to increase the spacecraft velocity from 25,573 to 33,643 ft/s, an incremental velocity of 8070 ft/s (2460 m/s). The spacecraft is now in an elliptical trajectory toward the 19,323-nm (35,786-km) apogee. When the apogee is reached, the elliptical orbital velocity is 5235 ft/s (1596 m/s), that is slower than the 10,088 ft/s (3075 m/s) required for a GSO circular orbit. Then, at apogee, a rocket burn provides 4853 ft/s (1479 m/s) velocity increment necessary to circularize the orbit, otherwise the spacecraft will continue along its elliptical trajectory. The total velocity increment is 12,923 ft/s (3939 m/s).

In order to return to LEO, the opposite sequence of events is necessary. Again, at the orbital location opposite the location point in the LEO orbit, a retroburn of minus 4853 ft/s (1479 m/s) velocity is necessary to slow the spacecraft to the elliptical orbit apogee velocity of 5235 ft/s (1596 m/s). When approaching the 100-nm altitude, the elliptical orbit speed is approaching 33,643 ft/s (10,254 m/s). In order to achieve a 100-nm circular orbit, a retroburn of minus 8070 ft/s (2460 m/s) is necessary to reach the 100-nm circular orbit speed of 25,573 ft/s (7795 m/s).

For the round-trip described above, a total of four rocket firings are required for a total incremental velocity of 25,846 ft/s (7878 m/s), a velocity greater than the incremental velocity to reach LEO!

We conclude that to change orbital altitude requires the expenditure of energy. The energy amount required depends on the altitude change desired. The incremental velocity required to move from a nominal 100-nm or 200-km orbital altitude is given in Fig. 5.8. The incremental velocity curve is highly nonlinear. A 6000 ft/s (1829 m/s) incremental velocity will permit an altitude change of about 3000 nm (5556 km). However, a burn of twice the velocity increment, 12,000 ft/s (3658 m/s) will permit an altitude change of about 13,000 nm (24,076 km), which is 4.3 times larger compared to the first case.

5.3.2 Mass Ratio Required for Altitude Change

The previous section provides the methodology to determine the magnitude of the incremental velocity to achieve a given orbital altitude change, in a fixed orbital inclination. The propulsion systems described in Table 5.4 provide the specific impulse, I_{sp}, for each of the four systems considered. Since there is no atmospheric drag in space, the ideal weight ratio Eq. (5.16) applies:

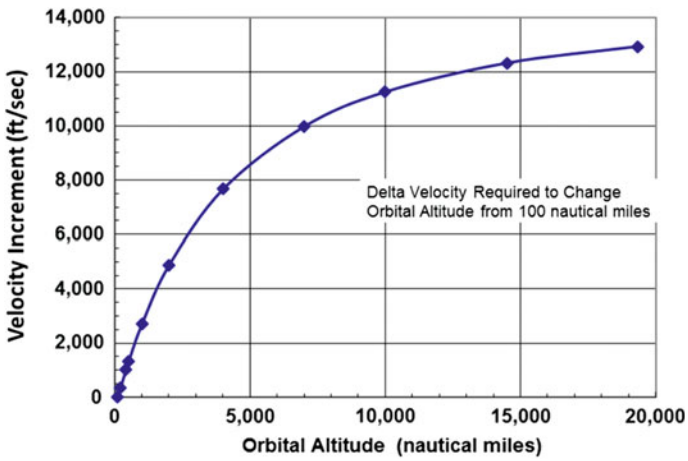

Fig. 5.8 Velocity requirement to change orbital altitude can approach one half of the orbit speed

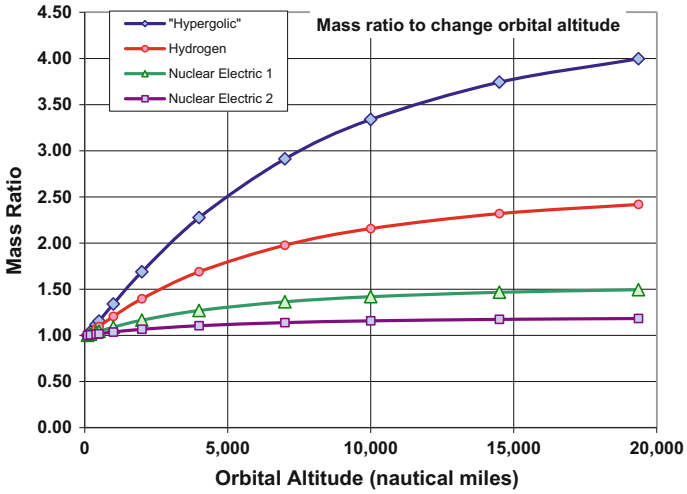

Fig. 5.9 Mass ratio required to change orbital altitude is very dependent on the propulsion system performance (I_{sp})

Table 5.6 Sized orbital maneuver vehicles (OMV) for a one-way mission from LEO to GSO

Propulsion	Gross mass (t)	Propellant (t)	W_{OWE} (t)	W_{OEW} (t)	$W_{R\ one\text{-}way}$ (–)	Thrust (kN)
Hypergolic	12.01	9.00	3.01	0.738	3.996	58.67
H_2/O_2	7.14	4.16	2.98	0.716	2.418	35.02
Solar electric	4.80	1.59	3.21	0.945	1.134	4.71
Nuclear electric	3.60	0.345	3.25	0.985	1.046	3.53

$$W_R = \frac{\Delta V}{g \cdot I_{sp}} \tag{5.16}$$

Translating the incremental velocity data and specific impulse data into weight ratio yields Fig. 5.9. The weight ratio for the four propulsion systems described in Table 5.4 is provided as a function of orbital altitude. The weight ratios for the LEO to GSO orbital altitude change are as follows: (1) 4.00 for the hypergolic propulsion system; (2) 2.39 for the oxygen/hydrogen propulsion system; (3) 1.55 for the solar electric propulsion system; and finally, (4) 1.11 for the nuclear electric propulsion system. The acceleration specified for the chemical rocket-powered OMV is 0.5 g. For the electric thruster-powered OMV, the acceleration is 0.1 g.

The gross weight of the one-way OMV is straightforward, and the sizing program balances the propellant required versus the capacity of the propellant tank that determines the operational empty weight (W_{OEW}). The sized OMV for each of the propulsion systems transporting a 5000 lb (2268 t) satellite is given in Table 5.6.

The gross weight for the one-way mission is:

$$W_{TOGW} = W_R \cdot (W_{OEW_{OMV}} + W_{satellite}) \tag{5.17}$$

$$W_{ppl} = (W_R - 1) \cdot (W_{OEW_{OMV}} + W_{satellite}) \tag{5.18}$$

Note that the operational empty weight (W_{OEW}) is essentially constant. It is larger for both electric propulsion configurations because of the solar panels for the solar electric and the radiators for the nuclear electric. As in the case for the launchers, the primary difference in the weights and thrust values is the result obtained for the carried propellant. The propellant mass for the hypergolic rocket is 34 times larger compared with the nuclear electric rocket. The propellant load required is reduced by (a) the increasing specific impulse, I_{sp}, of the propulsion system and (b) the reduction in mass and thus engine thrust and propellant flow rate.

Unlike the space launcher, where the payload is about 1/7 of the W_{OEW}, for the orbital maneuver vehicle (OMV) the payload is larger than the W_{OEW}. The W_{OEW} differs from "empty" or "dry" weight in that all of the fluid lines are filled and any trapped fluids or propellants are included in the W_{OEW}. The operational weight empty (W_{OWE}) is the W_{OEW} plus the payload. That is, the vehicle operationally is ready but without the propellants loaded. The satellite (payload) weight for the OTV is 2.268 t. The Russian *Progress* capsule can deliver 3.5 t to LEO, and the European Space Agency (ESA) Automated Transfer Vehicle (ATV) can deliver 7.67 t to the ISS orbital altitude of 249 nm (Catchpole 2008).

Table 5.7 Payload size versus OMV for a hypergolic propulsion system with a one-way mass ratio of 4

W_{Pay} (t)	W_{GW} (t)	W_{ppl} (t)	W_{OEW} (t)	W_{OWE} (t)	T (kN)
2.268	12.01	8.991	0.735	3.02	58.7
3.50	18.32	13.71	1.106	4.61	89.9
3.650	19.08	14.28	1.148	4.80	93.6
4.00	20.86	15.61	1.245	5.24	102
4.50	23.38	17.50	1.380	5.88	115
5.50	28.40	21.25	1.641	7.14	139
6.50	33.36	24.97	1.891	8.39	164
7.50	38.28	28.65	2.130	9.63	188

If the OMVs in Table 5.6 are extended to different payload masses for the hypergolic propulsion system, the size and mass trends can be established as given in Table 5.7.

For payloads larger than 4.9 t, the 19 t of propellant payload delivered to LEO by the tanker launcher is insufficient for a LEO to GSO mission. This is shown for hypergolic propulsion, because as advanced propulsion enters orbital operations, the propellant requirement will substantially reduce, even for the heavier payloads. The propellant load scales as the mass ratio minus one. Then, for the nuclear electric propulsion system, the propellant load for the 7.5 t payload OMV is only 1.07 t, and for the solar electric propulsion system, it is 4.71 t. However, as long as the principal orbital maneuver propellant of choice is hypergolic, the orbital propellant requirements will steadily increase. The ESA ATV meets a current need. With the Space Shuttle retired, a more substantial thrust OMV is required to reboost the International Space Station (ISS), while some mechanism is required to provide service capability to the Hubble Space Telescope if necessary. If the Hubble Space Telescope was to be placed at the same orbital inclination as the ISS, but at a higher altitude, the Hubble Space Telescope could be serviced from the ISS without the need for an equivalent Space Shuttle system.

The gross weight of the two-way OMV is more complex, because the OMV must carry the return-to-LEO propellant to GSO in the first place. The sizing program balances the total propellant required versus the capacity of the propellant tanks that determines W_{OEW}. The sized OMVs for each of the propulsion systems transporting a 5000 lb (2.268 t) satellite are given in Table 5.8.

The gross weight for the two-way mission is:

$$W_{GW} = [W_R \cdot (W_{OEW_{OMV}} + W_{satellite})] \cdot W_R \tag{5.19a}$$

$$W_{GW} = W_{OEW_{OMV}} \cdot W_R^2 + W_R \cdot W_{satellite} \tag{5.19b}$$

The propellant weight for the two-way mission is:

$$W_{ppl_{to\,LEO}} = (W_R - 1) \cdot W_{OEW_{OMV}} \tag{5.20}$$

$$W_{ppl_{to\,GSO}} = [W_R \cdot W_{OEW_{OMV}} + W_{satellite}] \cdot (W_R - 1) \tag{5.21}$$

As would be expected, the to-GSO and return OMV is significantly larger than the one-way vehicle, see Table 5.8. Other than being larger, the same comments apply to the two-way OMV as the one-way OMV. Launching to GSO with the current multistage rockets, the propellant in the upper stage (usually third stage) contains the propellant for the elliptical GEO stationary transfer orbit, and the GSO circularization propellant is carried in the GSO satellite. Sizing the one-way mission gives some indication of the upper stage propellant mass required to place the payload into GSO transfer orbit. Given the function of the OMV, the two-way mission is the logical sizing mission.

With a conventional rocket-powered OMV (for instance, the *Jupiter* tug proposed by Lockheed Martin), rocket engines of approximately the correct thrust are available. For example, a hypergolic restartable rocket in the 50–60 kN range is available from the Ukrainian Yuzhnoye Design Office and organization and is the YUZ-U-29 rocket propulsion system for the Tsyklon launcher. The specific impulse is 289 s for a total installed engine thrust-to-weight ratio 49.1 and a thrust of 56 kN. The hydrogen/oxygen

Table 5.8 Sized OMVs for the two-way mission from LEO to GSO to LEO

Propulsion	W_{GM} (t)	W_{ppl} (t)	W_{OWE} (t)	W_{OEW} (t)	$W_{R\ Two\text{-}Way}$ (–)	T (kN)
Hypergolic	27.07	23.70	3.37	1.10	16.00	119.5
H_2/O_2	10.98	7.79	3.19	0.925	5.71	53.83
Solar electric	5.99	2.59	3.39	1.12	2.22	5.87
Nuclear electric	3.79	0.494	3.30	1.03	1.23	3.72

rocket in the 35 kN range is available both from the USA and from the former USSR. The collaboration of NPO Energomash, Khimki, has produced a LOX/LH_2 in-development engine of the correct thrust level, the ENM-C-36. The specific impulse is 461 s. The Pratt & Whitney RL10 is also an upper stage candidate. As the RL10 is an expansion turbine cycle, its potential operational life is very long compared to a conventional rocket engine.

Electric-powered engines for the solar electrical and nuclear electrical propulsion systems are a challenge in that there are no engines or engine clusters available in the thrust class required. The largest electric thrusters are in the former Soviet Union and are about 1 N in gross thrust! At 1/10 *g* acceleration, the total velocity increment of 12,923 ft/s (3939 m/s) is achieved in 1.11 h. At 1/100 *g* acceleration, the time required is 11.16 h, and this choice of acceleration would reduce the thrust to the 5–6 kN range, at the expense of the maneuvering time that would increase correspondingly.

The only future electric thrusters that appear capable of such thrust levels are magnetoplasmadynamic (MPD) thrusters, e.g., the VASIMR (Variable Specific Impulse Magnetoplasma Rocket) engine, see Chap. 7 (Diaz 2000). It may not be possible to fabricate solar panels of the size necessary to drive an electric thruster in the 5–6 kN thrust level, given the low-energy conversion efficiency of solar panels. A 0.57 N thruster with a 50% energy conversion efficiency (still unavailable) would require an input from the solar panels of about 30–40 kW. A 5700 N thruster, by analogy, would require an input of some 300 MW to 400 MW, an unheard of power level for solar panels. The largest multimedia communication satellites carry solar panels of 5–6 kW total power. This would be 1000 times greater. At that power level, to reach an incremental velocity of 12,923 ft/s (3939 m/s), the acceleration time is 46.5 days, operationally practicable for some GSO operations but unacceptable to commercial TLC (Telecommunications) operators. An order of magnitude increase in thrust to 5.7 N would reduce the transit time to 4.6 days, a more acceptable level. Consequently, that may be the first objective in developing thrusters for the solar electric OMV.

We now have both the quantity of launcher propellant required to deliver the OMV propellant to LEO and the OMV propellant required, in each of the three orbital maneuver missions. We are now in the position to determine the total mass units of propellant (launcher and OMV) required per unit mass of the satellite for each of the four space propulsion systems.

5.3.3 Propellant Delivery Ratio for Altitude Change

In Fig. 5.10, the ratio of the total mass units of propellant (launcher and OMV) required per unit mass of the satellite is presented for the four in-space propulsion systems and the four launcher propulsion systems, namely those in Table 5.9.

Figure 5.10 shows the dramatic reduction in the total propellant mass (launcher and OMV) required per unit mass of the satellite, for the two electric OMV propulsion systems, by advancing the performance of the launcher propulsion system. By incorporating a LACE system into an existing hydrogen/oxygen rocket, the propellant required to deliver 1 mass unit of propellant to LEO is reduced by 56%. Proceeding to a Mach 12 ram/scramjet produces another 50% reduction in the required propellant to deliver 1 mass unit of propellant to LEO. Clearly, instead of the 190.5 mass units of propellant required, LACE reduces that number to 83.1, and a Mach 12 ram/scramjet further reduces that number to

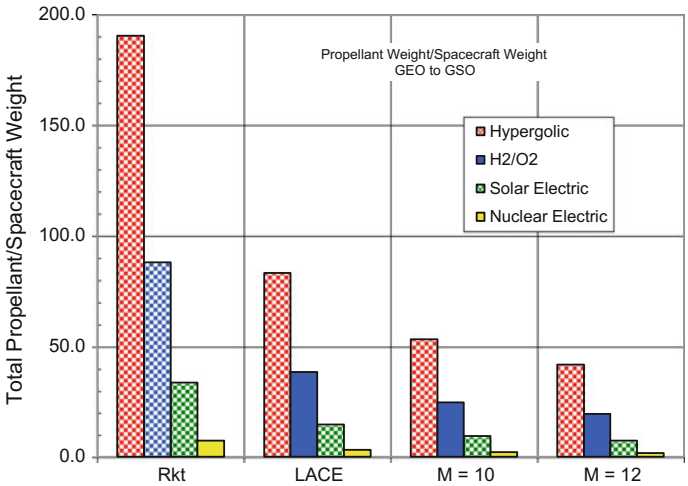

Fig. 5.10 Ratio of total propellant weight/satellite weight

41.8 propellant mass units required to deliver 1 mass unit of propellant to LEO. However, the real gains occur when propulsion of both launcher and OMV propulsion is improved.

Figure 5.11 focuses on the electric propulsion for the OMV and the more efficient launcher propulsion systems. The propellant required to deliver 1 mass unit of propellant to LEO is between 3.5 and 0.5. Then, it becomes practicable to deliver propellant to LEO, as the propellant cost is no more than the propellant to deliver a unit mass of payload in a commercial transport. Although it is nearly prohibitive in terms of hypergolic space rockets and conventional launch rockets to deliver significant quantities of orbital maneuver propellant to LEO (the actual figure is 190.5 kg of propellant per kilogram of LEO propellant delivered), the future holds a dramatic reduction in that quantity by a factor of about 20 just by using hydrogen/oxygen propulsion in space, and a combination of hydrogen/oxygen rocket and airbreathing propulsion for the launcher. With space electric propulsion and the hydrogen/oxygen rocket, plus airbreathing propulsion for the launcher, that ratio can be reduced to the range 1–3 kg of burnt propellant per kilogram delivered to orbit. At this point, the orbital tanker is now competitive with a KC-135 or KC-46 for refueling missions.

5.4 Changes in Orbital Inclination

An orbital plane change is a much more challenging propulsion space maneuver than an orbit change. A large expenditure of energy is required to achieve a small change in the orbital plane. A propulsive plane change is an impulse turn and is executed with the thrust line perpendicular to the orbital path and in the direction of the plane change. The incremental velocity for an impulse turn is given by Eq. (5.22) for a non-rotating Earth:

$$\Delta V_{\mathrm{pc}} = 2 \cdot \sqrt{\frac{\mu}{R_0 + h}} \cdot \sin\left(\frac{\alpha}{2}\right) \tag{5.22}$$

with the standard gravitational parameter for Earth defined as

$$\mu = 1.407645 \cdot 10^{16} \ \frac{\mathrm{ft}^3}{\mathrm{s}^2} \tag{5.23}$$

and with the average radius of Earth

$$R_0 = 3442.5 \,\mathrm{nmi} \tag{5.24}$$

As indicated in Eq. (5.22), the higher the orbital altitude, the smaller the incremental velocity for a given plane

Table 5.9 Launcher and OMV propulsion options

Launcher propulsion	OMV propulsion
Hydrogen/oxygen rocket based on the P&W XLR-129	Hypergolic, restartable, long-life rocket closed turbopump cycle rocket
LACE rocket based on the P&W XLR-129	Hydrogen/oxygen restartable, long-life expander or closed-cycle rocket
Rocket ejector ram/scramjet to M = 10 + hydrogen/oxygen rocket	Electric MHD thruster with lithium fuel powered by solar panels
Rocket ejector ram/scramjet to M = 12 + hydrogen/oxygen rocket	Electric MHD thruster with lithium fuel powered by nuclear reactor

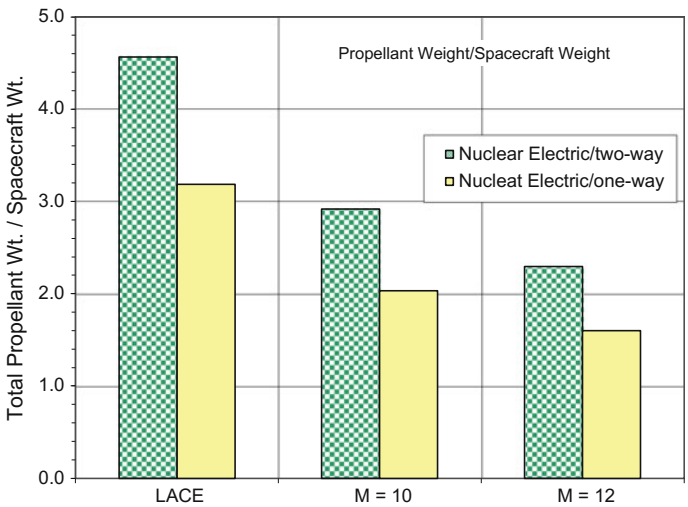

Fig. 5.11 Ratio of total propellant weight to satellite weight for two electric propulsion systems

change. Travelling to that higher orbital altitude requires propellant, as we have just seen in the previous section. Consequently, there is an opportunity for a trade-off, depending on whether or not the change in orbital altitude propellant plus that of the reduced plane change impulse turn is less than the propellant consumed by a dip to lower altitude followed by an aerodynamic turn plane change and pull-up. From Eq. (5.22), the incremental velocity per 1° change in orbital plane is about 446 ft/s (135.9 m/s) at an orbital altitude of 100 nm. Then, a modest 5° plane change requires an incremental velocity of 2230 ft/s (679.7 m/s).

The right sketch in Fig. 5.12 depicts an orbital plane change in LEO and in a higher-altitude elliptical orbit. In order to accomplish this, a rocket burn is required to put the spacecraft into the elliptical orbit, then at apoapsis a rocket burn to rotate the orbital plane and a final rocket burn to return the spacecraft to the lower-altitude circular orbital speed. As we shall see, there is an angle above which this procedure requires less incremental velocity than a lower orbital altitude plane change.

The left sketch in Fig. 5.12 depicts an orbital plane change in LEO performed by entering the Earth's upper atmosphere with a high lift-to-drag ratio hypersonic glider and executing a thrust-equals-drag aerodynamic turn at maximum hypersonic aerodynamic glide ratio, $(L/D)_{\text{max hypersonic}}$. This maneuver requires a hypersonic glider, but it enables a much larger orbital plane change for the same propellant consumed. With conventional rocket propulsion, this method of changing the orbital plane uses always less energy. This was first analyzed and presented by Dr. Wilbur Hankey in 1959 when at the Air Force Flight Dynamics Laboratory at Wright-Patterson Air Force Base, Ohio (Dr. Hankey has been later an Emeritus Professor with the Wright State University in Dayton, Ohio) (Hankey 1988).

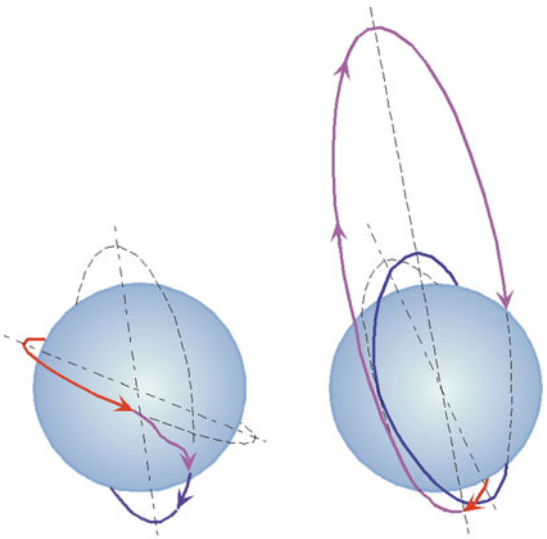

Fig. 5.12 Orbital plane change via an aerodynamic turn in the upper atmosphere (*left*) and an impulse turn executed during an elliptical transfer orbit to 22,400-nm orbit (*right*)

5.4.1 Energy Requirements for Orbital Inclination Change

Using Eq. (5.22), the variation in incremental velocity with altitude as a function of plane change angle is given in Fig. 5.13 for five orbital altitudes, from 100 nm (185.2 km) to 19,323 nm (35,786 km). For a 90° plane change at 100-nm orbital altitude, the incremental velocity is just over 35,000 ft/s (10,668 m/s). Compare that to the incremental velocity for the orbital altitude change from 100 to 19,323 nm of 12,900 ft/s (3992 m/s) in Fig. 5.8. As a consequence, the incremental velocity requirements for an orbital *plane* change are much more demanding than an orbital *altitude* change. For an incremental velocity of 12,900 ft/s, an orbital plane change of about 29° is possible. Overall, that is a smaller plane change than required to move from the latitude of NASA Kennedy Space Center (KSC) to the latitude of the International Space Station (ISS).

Shown in Fig. 5.14 is the ΔV for an impulse turn made from the GSO orbital altitude of 19,323 nm (35,786 km), which requires about 11.5 h to execute. This is one of the lower-energy solutions for the plane change. Increasing the altitude of the impulse turn to 36,200 nm (67,042 km) decreases the incremental velocity to about 1000 ft/s (304.8 m/s), but increases mission time to 24 h. As shown, the breakeven orbital plane change is about 50°. Then, if the orbital plane change is less than 50°, it is best executed from the spacecraft's orbital altitude without any orbital altitude change. However, there remains the interesting possibility of using aerodynamics to change the orbital plane (Chudoba et al. 2011; Cerro et al. 2012).

The aerodynamic plane change requires slowing the hypersonic glider to about 22,000 ft/s (6706 m/s) to enter the upper atmosphere between 240,000 and 260,000 ft (73,152–79,248 m) altitude. At that point, the rocket engines are ignited and a thrust-equals-drag ($T = D$) turn through the orbital plane change angle desired, and at the lift coefficient corresponding to maximum hypersonic (L/D), is initiated. The aircraft is then leveled at the correct orbital heading, and the engines are reignited to regain orbital velocity. For the class of hypersonic gliders evaluated, this maneuver requires a total velocity increment of about 1022 ft/s (311.5 m/s) to dip into the atmosphere, turn aerodynamically, and pull up to

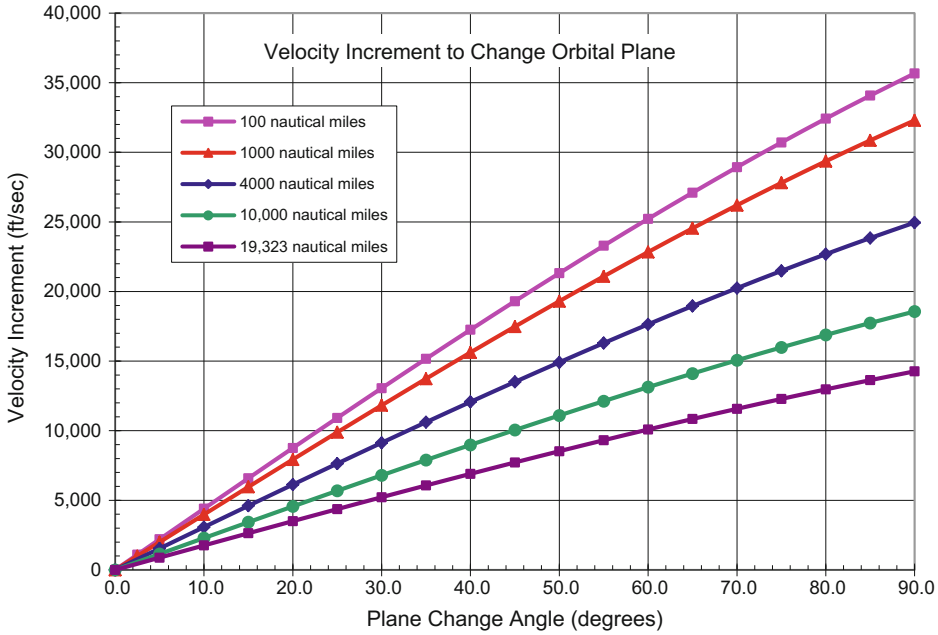

Fig. 5.13 Velocity increment to rotate orbital plane for different orbital altitudes. Higher altitude requires less energy

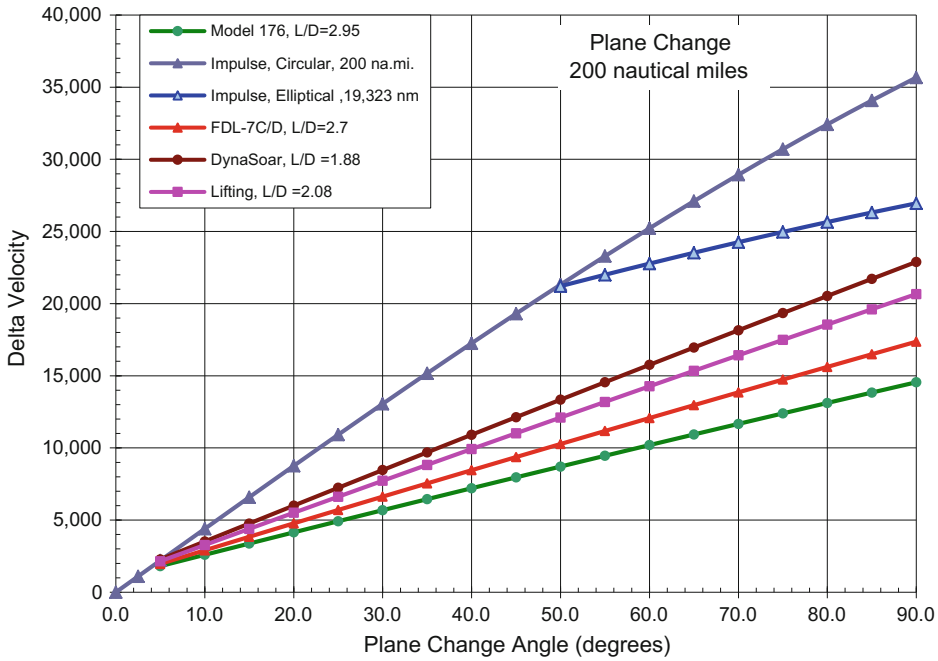

Fig. 5.14 Velocity increment as a function of turn method and plane angle change

the initial orbital altitude and speed. The incremental velocity required to execute the orbital turn is a function of the lift-to-drag ratio, as presented in Fig. 5.14 where it is compared to an orbital impulse turn.

The lift-to-drag ratio at Mach 22 varies from 1.88 to 2.95 for the four hypersonic gliders presented. This performance can be represented as a curve fit as follows:

$$\Delta V_{\text{turn}} = 1022 + C \cdot \left(\frac{L}{D}\right) - 0.0883 \cdot \left(\frac{L}{D}\right)^2 \text{ (ft/s)} \quad (5.25a)$$

with

$$C = 2317.2 - 2545.6 \cdot \left(\frac{L}{D}\right) + 1040.9 \cdot \left(\frac{L}{D}\right)^2 - 144.45 \cdot \left(\frac{L}{D}\right)^3 \quad (5.25b)$$

As shown in Fig. 5.14, the aerodynamic plane change requires significantly less energy compared to the impulse

turn. For the *Model 176* hypersonic glider configuration, see Chap. 3, the incremental velocity required is about 40% of the impulse turn requirement. Even a rather modest *X-20 Dyna-Soar* lift-to-drag ratio of 1.88 offers a plane change requirement of around 60% of the incremental velocity required by an impulse turn. The Space Shuttle Orbiter had a lift-to-drag ratio of about 1.5, and the Russian Buran had about 1.7. For the Space Shuttle and Buran orbiter configurations, blunt wing leading edges and nose reduced their hypersonic lift-to-drag ratio well below two.

Figure 5.15 depicts a USAF Flight Dynamics Laboratory FDL-7 C/D glider making a plane change to rendezvous with another orbital vehicle seen in the distance (top right corner of image). In actuality, the rocket engines would be firing, but the artist omitted the engine plume to clarify the orientation of the maneuver. The hypersonic glider is generally a second stage of a TSTO vehicle sized as an automatic OMV, specifically for plane change maneuvers. The design payload is the same as for the space OMV, a 2268 kg (5000 lb) payload. A traditional in-space OMV (a space tug) cannot enter the Earth's atmosphere; hence, it is limited to space operations only. In contrast, the hypersonic glider has the capability to enter the atmosphere when needed to operate as an optional rescue vehicle. The hypersonic glider has an Earth's circumference glide range and can return to Earth without any prior preparation or waiting in orbit. With a payload bay of 36.5 m^3 (1289 ft^3) capacity, it can accommodate nine to twelve persons in pressure suits in an emergency situation.

Table 5.3 provides the specific impulse, I_{sp}, for each of the four OMV propulsion systems. For operation in the space environment, since there is no atmospheric drag, the ideal weight ratio equation applies, see Eq. (5.16). In contrast, the hypersonic glider does experience about an 8% reduction in I_{sp} due to atmosphere drag during the aerodynamic turn maneuver. Combining the incremental velocity and specific impulse data into weight ratio yields Fig. 5.16.

5.4.2 Mass Ratio Required for Orbital Inclination Change

Figure 5.16 presents the mass ratio for the four propulsion systems described in Table 5.4 and the four hypersonic gliders indicated in the column headings. Note that (1) with the hypergolic propellant, the mass ratio quickly becomes impracticable. The curve was terminated at a mass ratio of 10 and a 50° plane change. (2) With the hydrogen/oxygen rocket, the same mass ratio permits an 85° plane change. Extending the time for the plane change by transitioning to an elliptical transfer orbit and executing the plane change at 19,323 nm (35,786 km) GSO orbital altitude reduces the mass ratio to 6 for a 90° plane change. (3) The solar electric propulsion system and the nuclear electric propulsion system, when vehicle-integrated to perform aerodynamic plane changes, provide the only practicable mass ratios for an operational infrastructure. The mass ratios for a 90° orbital turn are between 11 and 5. The mass ratios for the 32° impulse turn orbital plane change are 4.53 for the hypergolic engine, 2.62 for oxygen/hydrogen, 1.15 for solar electric, and 1.05 for nuclear electric, as shown in Table 5.10. The acceleration specified for the chemical rocket-powered OMV is 0.5 *g*. For the electric thruster-powered OMV, the acceleration is 0.1 *g*.

The gross weight of the plane change OMVs is straightforward, and the sizing program balances the propellant required versus the capacity of the propellant tank that determines W_{OEW}. The sized OMVs, for each of the propulsion systems transporting a 5000 lb (2.268 t) satellite,

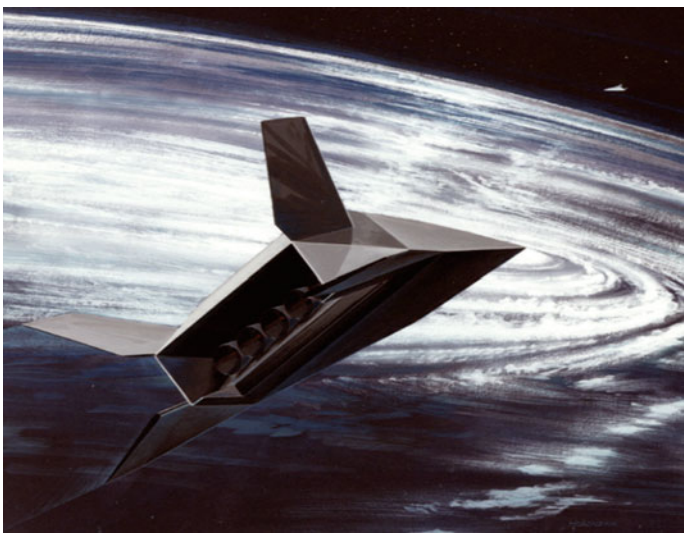

Fig. 5.15 A notional space glider based on the FDL-7 configuration performing an aerodynamic orbital plane change

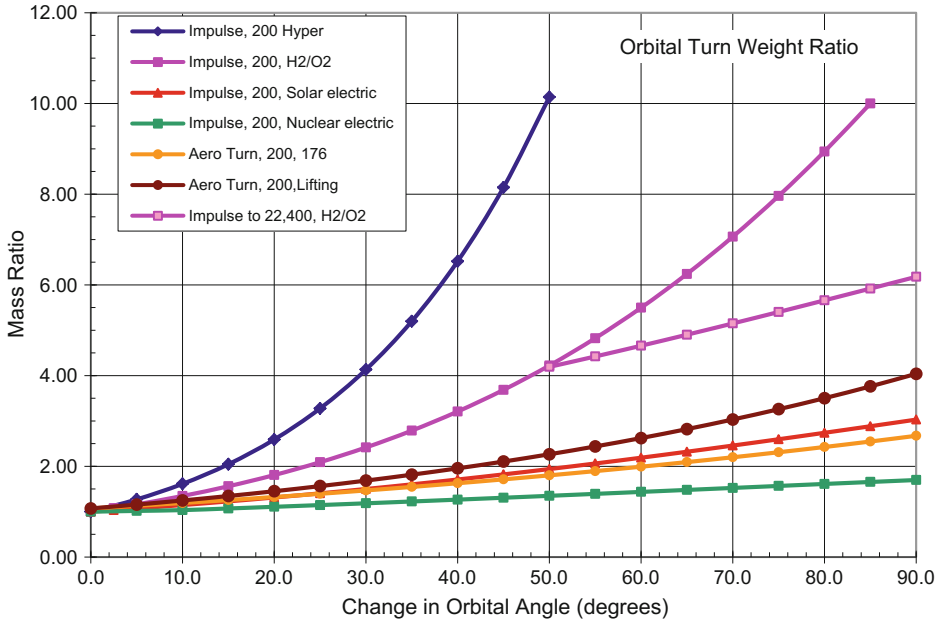

Fig. 5.16 Mass ratio requirements for orbital plane change

Table 5.10 Sized OMV for a 32° plane change at 200-km altitude for a 2,268 kg satellite

Propulsion	W_{GW} (t)	W_{ppl} (t)	W_{OWE} (t)	W_{OEW} (t)	W_R (–)	T (kN)
Hypergolic	13.83	10.78	3.05	0.786	4.529	67.8
H_2/O_2	7.82	4.80	3.02	0.716	2.619	38.3
Solar electric	5.38	1.91	3.47	1.20	1.147	10.6
Nuclear electric	3.82	0.397	3.42	1.15	1.050	7.49

are given in Table 5.10. The gross weight for a single mission is:

$$W_{GW} = W_R \cdot (W_{OEW_{OMV}} + W_{satellite}) \tag{5.26}$$

The propellant weight for the single mission is:

$$W_{ppl} = (W_R - 1) \cdot (W_{OEW_{OMV}} + W_{satellite}) \tag{5.27}$$

Note that the operational empty weight (W_{OEW}) of the OMV is essentially constant. It is larger for the electric propulsion configurations, because of the solar panels for the solar electric propulsion system and the radiators for the nuclear electric propulsion system, see Chap. 7. As in the case for the launchers, despite varying weight and thrust values, the primary differences are the weight and volume required for the carried propellant. The propellant mass for the hypergolic rocket is 27 times larger when compared with the nuclear electric rocket. Again, the propellant load is reduced with increasing I_{sp} of the propulsion system, and the resulting reduction in mass, subsequent engine thrust and propellant flow rate. Unlike the space launcher, where the payload is about 1/7 of the W_{OEW}, for the OMV the payload is larger than the W_{OEW}. The W_{OEW} differs from empty or dry weight in that all of the fluid lines are assumed filled, and any fluids or propellants trapped are included in the W_{OEW}. The operating weight empty, W_{OWE}, is the operating empty weight, W_{OEW}, plus the payload and crew, overall resembling the vehicle operationally ready but without the propellants loaded.

The ideal hypersonic glider for plane change maneuvers is usually a second stage of a TSTO vehicle sized as an automatic OMV specifically for plane change maneuvers. The design payload assumed here is 2.268 t (5000 lb). With a mass ratio of 1.603, the OMV is sized for a 32° plane change capability, the same as the impulse turn OMV. The size and mass characteristics are given in Table 5.11. At Mach 22, the glider has a hypersonic *L/D* of 2.70. At this speed, the glider is in orbit acting as a plane change OMV. An alternate design is shown with a design payload to accommodate the heaviest satellite in Table 5.5, which has a beginning-of-life (BOL) weight of 3650 kg. The vehicle scales as the square-cube law, as the ratio of masses, 1.609, is just slightly greater than the ratio of areas 1.354 raised to the 3/2 power, that is 1.576. As would be expected, the W_{OEW} ratio 1.362 scales with the area ratio.

Because the glider is a hypersonic glider and not just a space structure, it requires more resources to construct and operate. However, it is the only OMV with a true escape and rescue capability for an orbital facility crew. It might be better to design the glider to more demanding requirements,

Table 5.11 Hypersonic glider (FDL-7 C/D) for 32° plane change at 200-km altitude

$W_{pay\ satellite}$ (t)	W_{GW} (t)	W_{ppl} (t)	W_{OEW} (t)	W_{OWE} (t)	S_{plan} (m^2)	T (kN)
2.268	8.33	3.13	2.93	5.20	42.33	40.8
3.650	12.15	4.61	3.99	7.64	57.33	60.1

Table 5.12 Hypersonic glider (FDL-7 C/D) for variable-degree plane change at 200 km and 2.268 t satellite

Plane change	W_{MR} (–)	W_{ppl} (t)	W_{OEW} (t)	W_{OWE} (t)	W_{GW} (t)	S_{plan} (m^2)
90.0	3.228	14.69	4.33	6.60	21.29	59.59
62.0	2.313	7.57	3.49	5.76	13.13	49.29
32.0	1.603	3.13	2.93	5.20	8.33	42.33
32.0	1.603	3.47	3.49	5.76	9.23	49.29

so it can have a more versatile operational life. Table 5.12 gives the sizing of a hypersonic glider with a 2268 kg payload for three plane change capabilities. Increasing the plane change capability from 32° to 62° (+93.8%), the W_{OEW} increases just 19.1%. W_{OEW} and W_{dry} determine the cost of the spacecraft. W_{GW} determines the operational cost. In this case, the W_{GW} is 57% larger. Designing for a larger plane change capability like 62°, but operating at a 32° plane change, has only a minimal increase in the resources required over a spacecraft specifically designed for a 32° plane change, see the last two rows of Table 5.11. It would be practicable and highly desirable to design for greater operational capability. Since the hypersonic gliders are designed to operate with hydrogen/oxygen propellants, the availability of engines is not critical; a number of engines from either the USA or Russia are suitable.

We now have determined both, (a) the quantity of launcher propellant required to deliver the OMV propellant to LEO and (b) the OMV propellant required in each of three orbital maneuver missions. At this point, we can determine for each of the four space propulsion systems the total mass units of propellant (launcher and OMV) required per unit mass of the satellite.

5.4.3 Propellant Delivery Ratio for Orbital Inclination Change

For the OMV impulse turn, Fig. 5.17 shows the dramatic reduction in the total propellant mass (launcher and OMV) required per unit mass of the satellite by advancing the performance of the critical component, the launcher propulsion system. Incorporating a LACE system into an existing hydrogen/oxygen rocket, the propellant required to deliver one mass unit of propellant to LEO is reduced by 56%. Proceeding to a Mach 12 ram/scramjet produces another 50% reduction in the required propellant to deliver one mass unit of propellant to LEO. Clearly, instead of the 228.2 mass units of propellant required to deliver one mass unit of propellant to LEO, the LACE launcher propulsion system reduces that number to 99.6, and a Mach 12 ram/scramjet launcher propulsion system further reduces that to 50.0 propellant mass units. However, the real advances occur when *both*, the launcher *and* the OMV propulsion systems, are improved.

Similar to Fig. 5.11, Fig. 5.18 focuses on the electric propulsion system for the OMV and the more efficient launcher propulsion systems. In this case, the propellant/satellite weight ratio required to deliver one mass unit of propellant to LEO is between 4.5 and 2. Subsequently, delivering propellant to LEO is no longer impracticable as the cost of propellants burnt is comparable with that of delivering a unit mass of payload in a commercial transport aircraft.

In contrast, utilizing conventional hypergolic space rockets and conventional expendable launch rockets for delivering significant quantities of orbital maneuver propellant to LEO is still prohibitive (228.2 kg of propellant per kilogram of LEO propellant delivered). Clearly, substantial improvements are enabled when (a) using the hydrogen/oxygen propulsion system in space, (b) when using the hydrogen/oxygen rocket in combination with the airbreathing propulsion system for the launcher, and (c) with the application of electric propulsion in space and the hydrogen/oxygen rocket and airbreathing propulsion for the launcher, that ratio can be reduced to a figure of about 3 or maybe 2. In short, the orbital tanker is now competitive with a KC-135 or the more modern KC-46 for refueling missions.

Since the hypersonic glider is part of a VTHL TSTO launch system, the first stage is used only once to launch the glider. After reaching orbital altitude and inclination, the space propellant tankers are used to replenish its operational propellants. Table 5.13 gives the propellant to satellite weight ratio for a *FDL-7C/D* hypersonic glider and two satellite weights. The *Model 176* hypersonic glider would have an even smaller value of this ratio, while the *X-20 Dyna-Soar* and the lifting body would have a larger value of the ratio. This table corresponds to the values in Table 5.11.

The hypersonic glider is capable of larger and less expensive plane changes. As we have seen in Table 5.12, the increase in capability is possible for a reasonable investment in vehicle size. This table corresponds to the values in

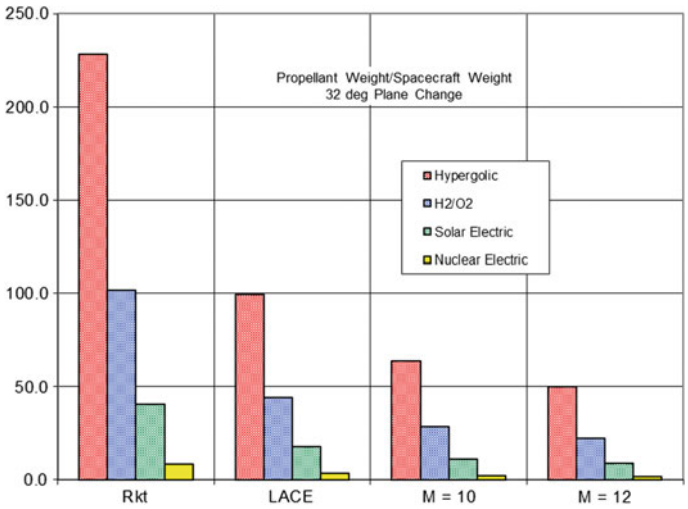

Fig. 5.17 Ratio of total propellant weight to satellite weight

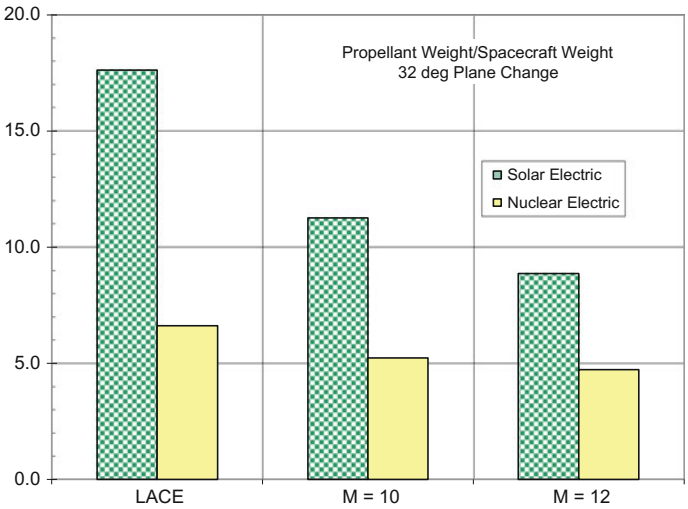

Fig. 5.18 Ratio of total propellant weight to satellite weight for solar and nuclear electric propulsion

Table 5.13 Ratio of total propellant weight to satellite weight for an FDL-7C/D hypersonic glider with a 32° plane change capability and two satellite weights

$W_{Satellite}$ (kg)	Launcher propulsion			
	Rocket (–)	LACE (–)	M = 10 (–)	M = 12 (–)
3650	60.6	26.5	16.9	13.3
2268	73.5	32.1	20.5	16.1

Table 5.11 for three levels of design for the plane change hypersonic glider. As shown in Table 5.12, the last row in Table 5.14 is for the 62° orbital plane change design spacecraft operating a 32° plane change.

Observations pertaining the OMV results are as follows:

- It is clear that the better propulsion system of the orbital tanker results in reduced resources required to transport the propellant to LEO.
- There is a clear advantage for an airbreathing launcher when considering sustained space operations.
- Compared to the impulse turn OMV, the hypersonic glider requires less total propellant to accomplish its mission, requiring only about 65% of the impulse turn OMV propellant, see Table 5.15.

In summary, for performing orbital plane changes, hypersonic gliders have clear advantages. Even for the

Table 5.14 Ratio of total propellant weight to satellite weight for FDL-7C/D hypersonic glider and three plane change angles for four launcher propulsion systems

Plane change (degree)	Launcher propulsion			
	Rocket (–)	LACE (–)	M = 10 (–)	M = 12 (–)
90	310.9	135.7	86.7	68.2
62	160.2	70.0	44.7	35.1
32	66.2	28.9	18.5	14.5
32[a]	73.5	32.1	20.5	16.1

[a]Sized for 62° plane change operated over a 32° plane change

Table 5.15 Ratio of total propellant weight to satellite weight for the FDL-7C/D hypersonic glider compared to the hydrogen/oxygen propellant OMV designed for a 32° plane change for four launch propulsion systems

Plane change	Launcher propulsion			
	Rocket (–)	LACE (–)	M = 10 (–)	M = 12 (–)
Hypersonic glider	66.2	28.9	18.5	14.5
H_2/O_2 OMV	101.7	44.4	28.3	22.2

hypersonic glider designed for a 62° plane change, while flying a 32° plane change (last row of Table 5.14) requires less propellant compared to an impulse OMV. The hypersonic gliders require less propellant to be lifted to orbit and offer an escape and rescue capability not available with impulse turn OMVs.

5.5 Representative Space Transfer Vehicles

Each OMV has approximately the same W_{OEW} as indicated in Tables 5.10, 5.11 and 5.12. However, each OMV has a different configuration that is determined by the characteristics of the individual propulsion system, as depicted in Fig. 5.19.

The two chemical rocket-powered OMVs are similar and conventional. Although having different gross weights, they are similarly sized. The satellite attaches to an equipment module mounted on the front end of the propellant tank, where the guidance and control systems and all subsystems are housed, see Fig. 5.20. There would be a stowed communications antenna and solar panels for power in the equipment module (not shown).

The solar electric propulsion system does require much larger solar panels than shown. Current communications satellites have solar panels in the 25–30 m (82–98 ft) total span for thrusters with less than 1/10th the thrust required for the solar electric OMV. Some of the limitations of this system are the current low thrust levels, the continuously degrading solar panel output (aging), and the unwieldy size of the solar panels for such a vehicle. Nuclear electric has the same problem as the solar electric, in that current thrusters have less than 1/10th the thrust required for the nuclear electric OMV. This system does have the advantage that the power output is sufficient and constant. The nuclear electric OMV requires large radiators to dissipate the rejected thermal energy from the reactor to space. Their exact size depends on the nuclear system chosen and the thermodynamic cycle to power the electric generators. The nuclear reactor will be a space-designed reactor and not based on Earth-based nuclear power stations. A most likely candidate is some type of gas-cooled reactor.

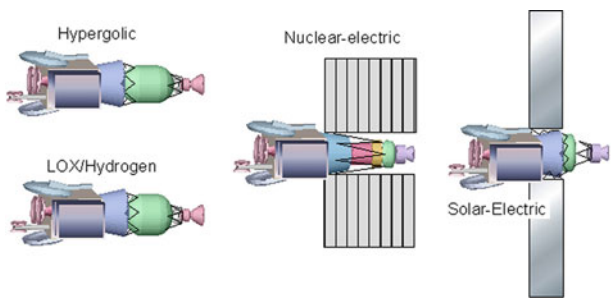

Fig. 5.19 Relative size and general configuration of OMVs

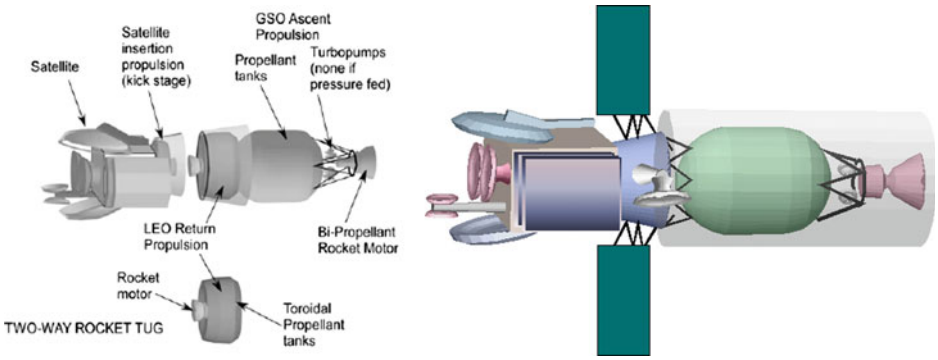

Fig. 5.20 LEO-GSO-LEO two-way OMV with shield

A round-trip operational OMV that travels from LEO to GSO and returns to LEO is shown in Fig. 5.20. The solar panels are just sufficient to power the system electronics and other electrical subsystems. A communication link to Earth and space-based ground stations is indicated. Because the intended life expectancy is multiple years, and recalling the damage one of these authors (P.A. Czysz) witnessed on the LDEF (Long Duration Exposure Facility) satellite, a shield over the tank structure and engine is necessary, as shown in phantom in Fig. 5.20. The equipment module can be made robust enough not to require a separate shield. As with the MIR orbital station, the solar panels on an operational OMV will probably have to be replaced within its lifetime.

The orbital plane change OMV can change the orbital plane by an (a) impulse turn in orbit or an (b) aerodynamic turn in the upper atmosphere. The impulse plane change OMV is very similar to the OMV as shown in Fig. 5.20 and is shown on the left side of Fig. 5.21. The aerodynamic plane change OMV is shown in the right side of Fig. 5.21. Both are sized for a 32° plane change with a 2268 kg (5000 lb) satellite. The impulse plane change OMV cannot enter the Earth's atmosphere, therefore limiting it to space operations. The hypersonic glider OMV has the capability to enter the atmosphere to operate as a rescue vehicle. The glider has a glide range equal to the Earth's circumference and can return to Earth without any prior preparation or waiting in orbit. With a payload bay of 36.5 m^3 (1289 ft^3) capacity, it can accommodate nine to twelve persons in pressure suits in an emergency situation.

5.6 Operational Considerations

Given the characteristics of the OMVs, the question is how to build an operational infrastructure in addition to the OMVs. The next five subsections will attempt to put the needs for an operational infrastructure into perspective. In fact, one of the most critical issues, if not the most critical, is the orbital propellant resources required to sustain an operational infrastructure. The availability of an infrastructure architecture and infrastructure hardware is important, but without propellant all grinds to a standstill. The infrastructure will probably be configured in some type of constellation, distributing resources over the infrastructure shell around the Earth. Since nowadays resources are scarce, the operators of the infrastructure must be a frugal group, not wasting any reusable resource or hardware. This consideration hints at private entrepreneurs rather than to the traditional space agencies as the main players. And, finally, having populated the infrastructure with human beings that

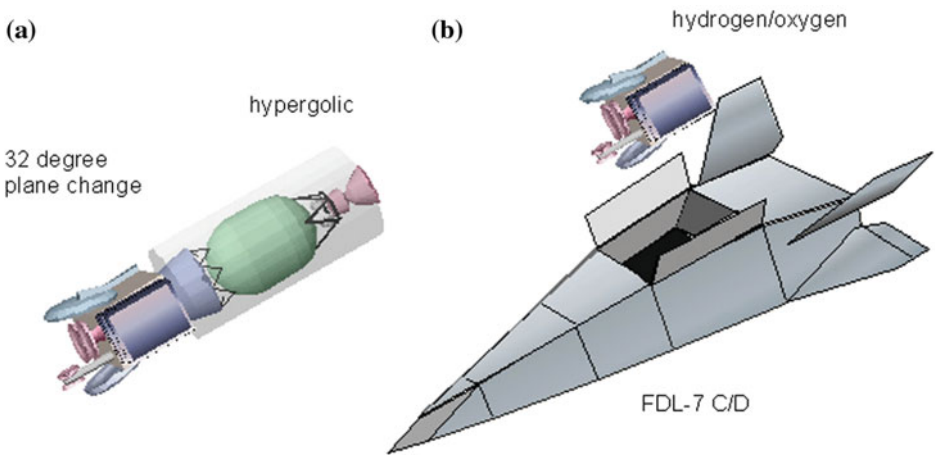

Fig. 5.21 OMV for **a** impulse turn and **b** hypersonic glider for aerodynamic turn

are not pilots, but workers with identified tasks, and tourists hoping to see and experience space, a viable and readily available rescue and return capability is a necessity.

5.6.1 Missions Per Propellant Delivery

It is worth repeating that the critical issue is the orbital propellant resources required to sustain an operational infrastructure. As the results given with the previous subchapters have shown, the existing expendable rocket launcher systems and hypergolic propellant space rockets force a level of launcher performance and activity that make any but limited space operations impractical, and this is witnessed by the current status quo. Figures 5.10 and 5.11 with Figs. 5.17 and 5.18 show that the expendable rocket launcher and hypergolic rocket OMV spend over 200 kg of propellant to deliver 1 kg of OMV propellant to LEO. The solution anticipated is to use airbreathing launchers and nuclear electric-powered OMVs. Then, the requirement reduces to a figure on the order of 2 or 3 to deliver propellant to LEO and on the order of 5 to deliver to LEO propellant required for orbital plane changes. It would appear that the operational infrastructure envisioned by the late Dr. Gaubatz in Fig. 5.1 must wait for the deployment of the correct propulsion systems for both, the synergistic "twins" consisting of the operational space launcher and the operational OMV.

The next critical issue is the following: Given the propellant is delivered to LEO in 19 t (41,895 lb) increments, how many missions can the OMVs complete from a single delivery? Figure 5.22 and Table 5.16 give the number of missions for the impulse OMVs executing two different missions, and the aerodynamic turn mission for the FDL-7 C/D hypersonic glider with a lift-to-drag ratio of 2.7.

Although heavier than the impulse OMV, the efficiency of the aerodynamic plane change maneuver permits the hypersonic glider OMV to have 45% greater mission capability from the same orbital tanker propellant load. Solar electric and nuclear electric are not appropriate propulsion systems for vehicles that fly in the upper atmosphere, because of the solar panels and radiators associated with those systems.

5.6.2 Orbital Structures

The concept of space ways depicted in Fig. 5.1 is dependent on the capability to manufacture space structures as standard items on a limited production line, comparable to the aircraft assembly line. Although the USA, Japan, and Europe have manufactured individual modules for the International Space Station (ISS) over its more than 10-year construction time (and a similar length characterize the Chinese *Tiangong-1*), these are one-of-a-kind items, hand-built at great expense. The only nation known to manufacture space structures with standardized components on a limited production line is the former Soviet Union.

Figure 5.23 shows one picture of one of a number of orbital station major components being manufactured in a factory in the Moscow area. In this picture, the orbital station module is being integrated with its *Proton* launcher, at the manufacturing plant for immediate detection of interface problems that can be addressed during the manufacturing process, not later on the launch stand. Each of the modules and components has different functions, but, such as automobiles and aircraft, each has been tailored to a specific mission based on installed equipment and a common structural core. The costs and time to manufacture the components have been minimized using this approach.

The organization of the manufacturing line, and the use of standardized components that can be gleaned from the plant pictures, is quite impressive. The pictures of this plant are now more than 35 years old. It is not known whether the

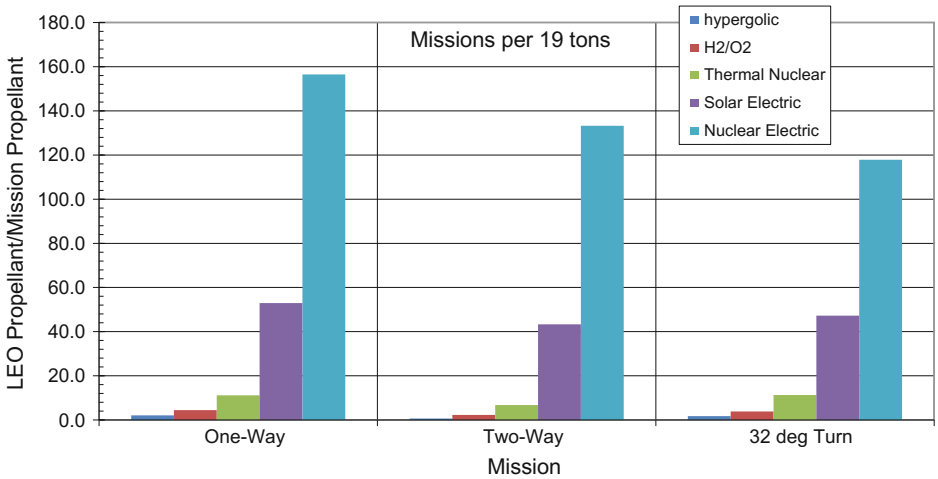

Fig. 5.22 Orbital maneuver missions per 19 t propellant payload for five different OMV propulsion systems

Table 5.16 Number of orbital missions per 19 t (metric ton) propellant payload for 2268 kg satellite payload for the OMV

Mission	Launcher propulsion				
	Hypergolic (–)	H_2/O_2 (–)	Solar electric (–)	Thermal nuclear (–)	Nuclear electric (–)
Impulse OMV LEO to GSO and return	0.71	2.3	4.3	6.8	133
Impulse OMV 32° plane change	1.7	3.8	4.7	11	118
Hypersonic glider 32° plane change		5.5			

Fig. 5.23 Large orbital station in final assembly and integration with its Proton booster. Moscow factory, circa 1989

plant or manufacturing capability remains in present Russia. This is the only plant of its kind known to the authors, and it should be the model for manufacturing components for an operational space infrastructure instead of relying on building single, one-of-a-kind custom components. One of the very important observations of the Russian approach to space payloads is that the payload and delivery stage are integrated as a part of the manufacturing process and not left to cause future delays on the launch pad. Note the Proton booster on the right-hand side of the photograph. In this context, a technology revolution is the advent of additive manufacturing, facilitated by low- or micro-gravity and vacuum. This last makes plasma torches easier and more convenient to use.

5.6.3 Orbital Constellations

One of the Senior Capstone Design course project teams at Saint Louis University, USA, looked at the near-Earth infrastructure postulated by the late Dr. William Gaubatz. The project topic was to analyze what would constitute the first step in the development of that infrastructure. The title of the project was *Space-Based Satellite Service Infrastructure* (Shekleton et al. 2002). Among other results found was that as the number of structures in space continually increases, the need for a space-based service infrastructure continues to grow.

The increasing human presence in space calls for creative support and rescue capabilities that will make space an "easier" and safer frontier. In addition, over 2200 functioning unmanned satellites are currently populating Earth's orbits. These include a variety of commercial, military, weather, and research satellites, many of which require servicing or ultimately removal from orbit as space debris at some point in time. As a first step, the student team determined that significant space facilities are necessary to achieve support of an initial "catalyst" infrastructure. As shown in Fig. 5.24, there is a requirement for distributed facilities (Shekleton et al. 2002).

The primary facility identified is a twin propellant tank arrangement with living quarters, repair shop, and a parts storage straddling the two propellant tanks. A much larger and modified version of the "elliptical" Space Cruiser is shown in Fig. 5.25; this vehicle has been identified as the

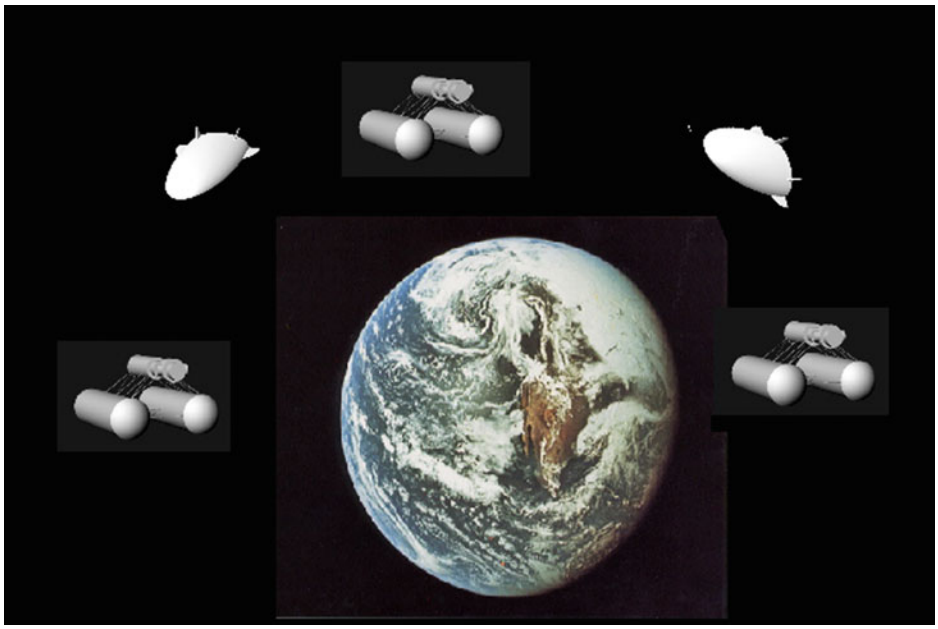

Fig. 5.24 Student design team results in terms of orbital systems hardware

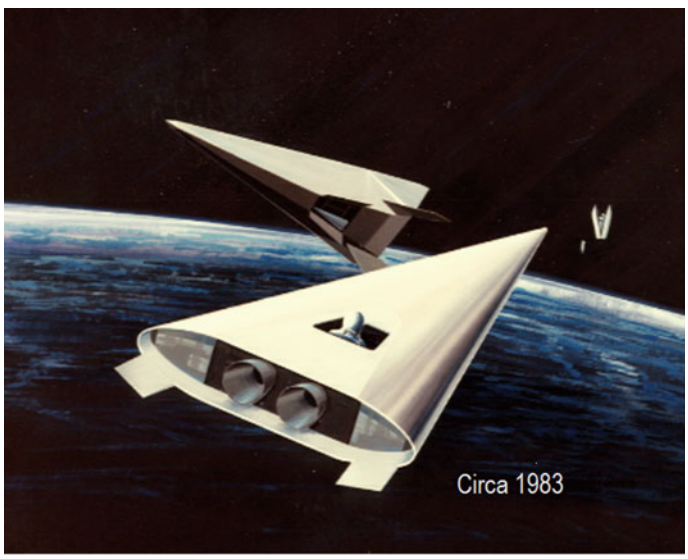

Fig. 5.25 "Bud" Redding "elliptical" Space Cruiser launched from a transatmospheric vehicle to accomplish a satellite repair

primary OMV. The elliptical cross-sectional hypersonic glider has been modified to a captured shock cross section (waverider) based on the work of Mark J. Lewis when at the University of Maryland (Lewis 1993), see Fig. 5.24. The initial concept of the "waverider," first implemented with North American's supersonic B-70 Valkyrie strategic bomber, can be attributed to the developments by (Eggers and Syvertson 1956).

The OMVs are deployed from the service facilities on an as-needed basis for non-routine maintenance and repair and on a scheduled basis for operational satellites and facilities. The gliders have limited facilities as habitats but have sufficient provisions for 3- to 5-day deployments away from the main service facility. The space station has not been chosen as a support base, because of the large quantity of propellant stored and the large inventory of spare parts and repair facilities required. One of the service facilities could be in orbital proximity to the space station if that is operationally required. The propellant storage could accommodate about 100 t of propellant or up to five propellant tanker payloads. The propellant tanks are segregated to accommodate hypergolic and hydrogen/oxygen propellants separately. Cryogenic propellants will need cryo-coolers and much energy to operate them (cooling needs about 20–100 times the amount of energy to be extracted). The hypersonic gliders are capable of escape and rescue missions for up to 15 persons. This constellation has been considered the foundation on which to build an operational space infrastructure.

5.6.4 Docking with Space Facilities and the ISS

Examining Fig. 5.1, we see a variety of space structures (facilities) that are unique to each facility's function, in time an aspect that is probably the norm for space facilities. In reality, we are just beginning because there is no existing space infrastructure with the exception of the ISS and, on a limited basis, the Chinese Tiangong-1 station. At best, there are specific missions to specific orbital assets (such as to Hubble, before the retirement of the US Space Shuttle). As published in the aerospace literature, the European (Columbus Laboratory) and Japanese (Japanese Experimental Module, Kimbo) laboratory modules for the International Space Station needed over 5 years to complete at large financial cost (Baker 2012). The high-maintenance and consequently high-cost Space Shuttle retired in July 2011, shortly after the completion of the ISS assembly.

Existing orbital facilities are expensive, and visiting vehicles must conform to standards and requirements based on vehicle and facility idiosyncrasies. For now, there is no consistent set of standards and requirements in sync with the commercial industries. Eventually, the transportation vehicles will have to provide the requirements for the orbital baseline infrastructure, including the definition of transportation cycles in analogy to how airports are defining air transportation. Commercial platform markets include transportation-related support services, habitation, and in-space service industry support.

The most economical space facility ever flown was the US Skylab (Anon 2012). It was a Saturn S-IVB stage modified for habitation and launched empty. Instead of being the prototype of future space structures for the initial phase of infrastructure building, it was summarily and unwittingly permitted to decay from orbit and burn up in the atmosphere. Skylab was placed into a 435-km (235 nm) orbit at an inclination of 50° (Furniss 2001). Skylab was in orbit from May 14, 1973, to July 11, 1979, (6 years, 5 months, and 25 days). It was launched empty and was sent crews via a Saturn rocket and an Apollo capsule. There were three missions to crew Skylab: Skylab 2 for 28 days, Skylab 3 for 59 days, and the final Skylab 4 for 84 days, for a total of 171 days occupied. The last crew departed Skylab on February 8, 1974, just 8 months and 26 days after being put into orbit. Clearly, Skylab remained unused for over 5 years. Unfortunately, there was no mechanism to maintain Skylab in orbit, and on July 11, 1979, it entered the atmosphere over Australia. Again, instead of being a prototype for an economical first step toward an orbital station, it was a one-of-a-kind experiment only. The next philosophical path taken was then to create an "optimum" space station, the "perfect" creation of NASA that took almost 26 years before another American astronaut crewed a US orbital station. In that time period, the former Soviet Union placed seven orbital stations into orbit, ending with the orbital station MIR. Note that since the retirement of the Space Shuttle in 2011, the USA is still devoid of a US man-rated space launch system to LEO.

There exists an analogous situation involving the STS (Space Transportation System, or Space Shuttle) which retired in 2011. The Space Shuttle external tank is a giant cylinder 154 ft (46.7 m) in length and 27.5 ft (8.4 m) in diameter containing 73,600 ft^3 (2083 m^3) of propellants. That is about 369,600 lb (167.63 t) at a 6:1 oxygen/hydrogen ratio by mass. The lithium–aluminum external tank weighs 58,250 lb dry. Each Space Shuttle mission discarded the external tank after it had achieved 99% of full orbital velocity. This means significant energy had been invested in the external tank, only about 260 ft/s (79 m/s) short of orbital velocity. With a very small investment, the external tank (ET) could have been placed into orbit and become the initial building block for orbital facilities other than the International Space Station, at a fraction of the cost.

At one time, the government was encouraging organizations to put this empty space asset to a useful application (Commerce Business Daily 1988). One of the individuals taking this seriously was Thomas Taylor, CEO of Global Outpost. He and his company championed the salvage of the external tank for over two decades (Taylor 1980, 1998;

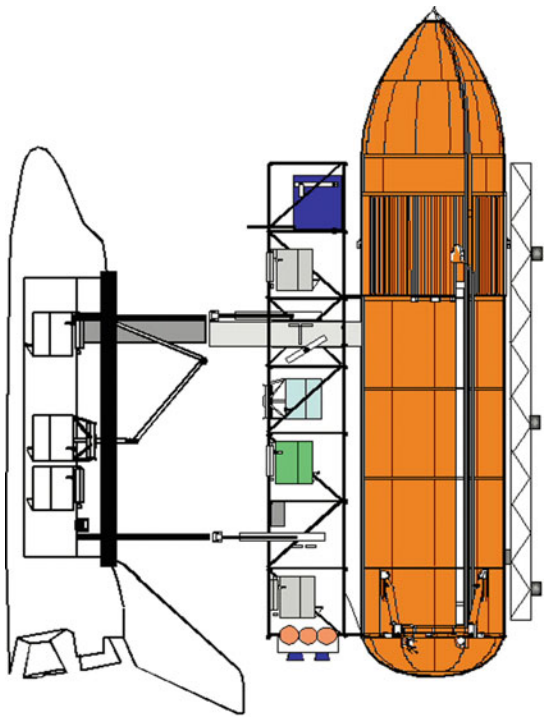

Fig. 5.26 An orbital infrastructure station fabricated from discarded Space Shuttle main propellant tanks with a Space Shuttle docked for resupply

Gimarc 1985). Global Outpost developed a salvage method using the Space Shuttle with NASA assistance. The organization had won the right to "five ET's in orbit at no cost" and had worked out a salvage procedure with NASA (Anon 1993). The concepts shown in Figs. 5.26, 5.27 and 5.28 are based on concepts developed by Thomas Taylor and Global Outpost Inc.

At the time, there were several possibilities for the empty external tank:

(1) The external tank could be used as it was intended to be used, as a hydrogen/oxygen propellant storage facility, using the orbital refueling launchers to supply propellants on a scheduled basis. The tank could accommodate 8.8 of the 19 t propellant deliveries by the orbital propellant tanker.
(2) The aft dome of the external tank could be cut to provide a 10.3 ft (3.14 m) diameter hole permitting the use of 55,000 ft^3 (1557 m^3) of the interior as a hangar for the OMVs.
(3) Just as with the Saturn S-IVB stage, the external tank could be launched, with some modifications so that at least one external tank could accommodate a human habitat. This modification is the basis for the sketches in Figs. 5.26, 5.27, and 5.28.
(4) An inflatable habitation structure is possible using the NASA TransHab or Bigelow Aerospace 8.0 m (26.25 ft) diameter and 8.2 m (26.90 ft) long inflatable structure (Kennedy et al. 2000). A fabricated volume would be transported uninflated in a sustained-use space launcher described in Chap. 3 and inflated on orbit for sustain use. The habitat is capable of resisting high-speed particle impact and providing environmental controlled life-support interior. A first prototype was launched to the ISS on April 16, 2016, was successfully connected and inflated, and is being evaluated throughout 2016 and into 2018, when a decision by NASA on its viability will be made.

Habitation requires cargo and passenger services. Each new industry will require cargo in both directions. The change from one type of transportation to another has always evolved into major commercial centers of industry, such as harbors and airports. Emerging commercial space ways have to expand the capabilities around the Earth and then to the Moon. Transportation is and will remain *the* major catalyst. The cost reduction stimulates the accelerated growth and expansion. Harbors start small, grow, and reach out to their customers with docks and wharfs; the space harbor will be no exception.

The external tank modified for crewed habitation and equipment and parts storage facility as conceived by Taylor (1980) is shown with the NASA Space Shuttle Orbiter docked with the crew transfer structure deployed between the orbiter air lock module and the external tank, see Fig. 5.26. This mission would have been for an equipment/parts resupply mission, for crew rotation, or as a mission adjunct. However, since the Shuttle had a limited useful operational life, its retirement opened the pathway toward a sustained flight rate spacecraft. The one actually designed for that purpose (for the USAF MOL in 1964) was the Air Force Flight Dynamics Laboratory *FDL-7C/D* and the McDonnell Douglas derivative, the *Model 176*. The modified external tank shown in Fig. 5.27 is shown docked with the crew transfer structure deployed between the *FDL-7C/D* or MDC *Model 176* air lock module and the external tank. As before, this could have been an equipment/parts resupply mission, crew rotation, or as a mission adjunct.

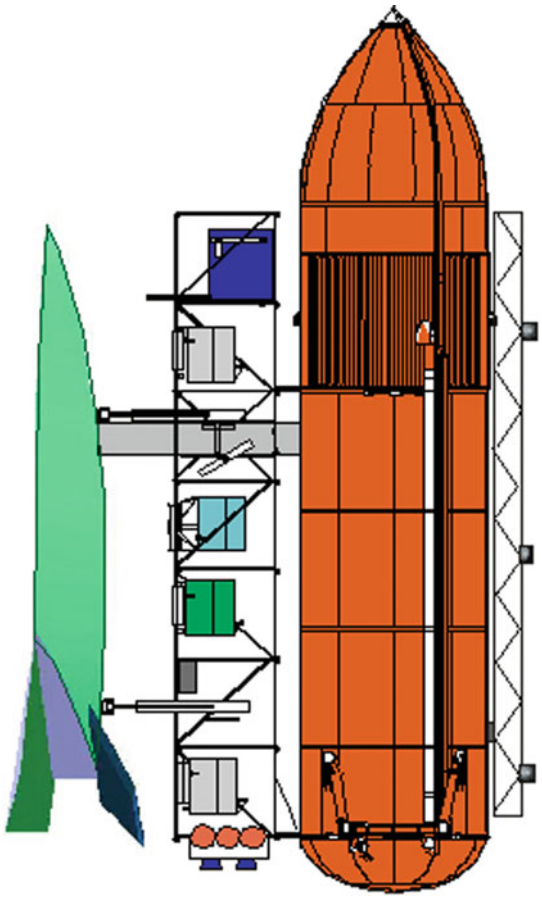

Fig. 5.27 An orbital infrastructure station fabricated from discarded Space Shuttle main propellant tanks with a hypersonic glider resupply spacecraft analogous to MDC *Model 176*

The concept of the Space Cruiser has been introduced in Chap. 2, see Fig. 2.26. This vehicle enables the external tank (ET) to take on the role of a maintenance, repair, and orbital transfer center, much as that developed by the Parks College design team (Shekleton et al. 2002). The Space Cruiser dates back over 40 years. The authors first were aware of the concept when one of the authors (P.A. Czysz) was manager of the McDonnell Douglas Aerospace Vehicle

Group in 1983. The late Mr. Redding visited the author and briefed him on the Space Cruiser concept. As originally conceived in 1980, the Space Cruiser is a low-angle conically shaped hypersonic glider similar to the McDonnell Douglas Model 122 (BGRV) experimental hypersonic vehicle that was flown in 1966 (Hallion 2005).

As initially conceived, the Space Cruiser length is 26 ft but can be folded to a 13.5 ft length, see Figs. 5.25 and 5.28. Redding adapted the design to incorporate an aft plug nozzle cluster configuration and storable propellants to create 13.3 kN (3000 lb) of thrust. The 4453 kg (10,000 lb) vehicle is to perform a variety of missions using the 8 ft^3 forward payload bay and the 4 ft^3 aft payload bay. The Space Cruiser is capable of atmospheric entry and uses a small drogue parachute at Mach 1 followed by a multi-reefed parafoil to land safely on any flat surface. The Space Cruiser has been intended to be operated by a pilot in a space suit (Griswold et al. 1982). In 1983, Redding modified the configuration to an elliptical cross section aimed at expanding the propellant quantity, as shown in a 1983 McDonnell Douglas Corporation transatmospheric vehicle (TAV) artist illustration, see Fig. 2.25 (Redding et al. 1983; Redding 1984). Mr. Redding formed an organization shortly before his death to preserve the work on the Space Cruiser and seek future development, the In-Space Operations Corporation (IOC).

In Fig. 5.28, the external tank modified for crewed habitation and an equipment and parts storage facility is shown with several space maneuvering vehicles docked to the support structure. From the top-right, there is a round-trip to GSO rocket transfer vehicle, see also Fig. 5.20; the center-right shows a solar electric orbital transfer vehicle, see also Fig. 5.19. At the bottom-right, there is a folded Space Cruiser with a satellite for transfer to another facility. At top-left, there is a hypersonic glider aerodynamic plane change vehicle, and at bottom-left, a full length Space Cruiser is shown docked. The Space Cruisers shown in Fig. 5.28 are 2.4 times larger than the original Space Cruiser (62 ft or 18.9 m in length). They have 13.5 times more volume and greater capability because the propellants are now cryogenic hydrogen and oxygen with magnetic refrigerators to all to eliminate propellant losses. These, like all the orbital maneuver vehicles, are automatic control vehicles that can carry crewmembers when necessary. In this figure, the salvaged external tank was thought to be an operations center for orbital maneuver vehicles necessary to move satellites and provide on-site repair and maintenance and non-functioning satellite removal.

With the Shuttle demise, all these potential developments ceased and the 2008 financial crisis reduced the forecasts of commercial use of space. As of this writing, conventional rockets are the only form of launchers, although emphasis is on cost reduction by automatic landing and reuse of first stages fueled by kerosene or liquid methane. Blue Origin and Space-X are two companies involved in these developments.

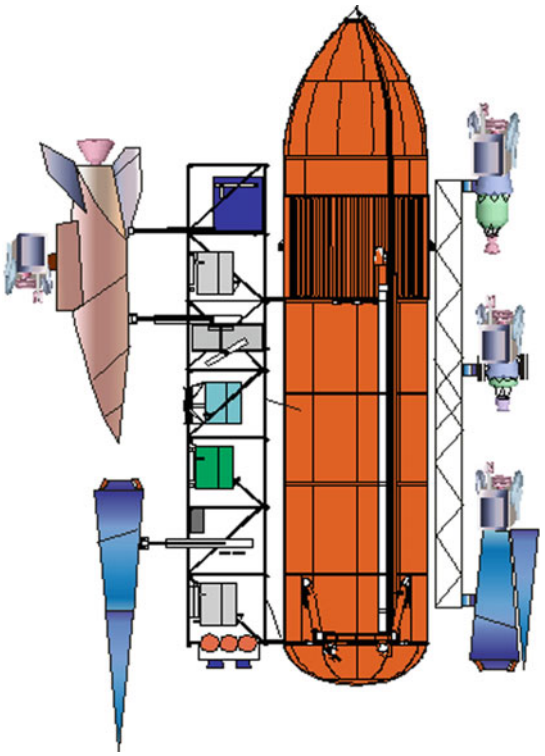

Fig. 5.28 An orbital infrastructure station fabricated from discarded Shuttle main propellant tanks with docked In-Space Operations Corporation (IOC) Space Cruiser, a hypersonic orbital plane change vehicle, and OMVs

5.6.5 Emergency Rescue Vehicle

Whether it is the orbital facility support vehicle, the hypersonic glider aerodynamic plane change vehicle, or the Space Cruiser, these vehicles can serve as an immediately available escape and rescue vehicle in case of an emergency. With these vehicles recovering in the Continental United States (CONUS), or Continental Europe (CONEU), they are capable to reenter to reach these locations without waiting in orbit for the correct orbital position due to their superior inherent extended crossrange and downrange hypersonic glide performance.

The orbital facility support vehicle has the capability to accommodate nine to thirteen crew, depending on the medical circumstance (litter patients or ambulatory). This means that with a fleet of these vehicles, the space facilities need not be only partially manned; the high-performance return vehicles provide safe return for the fully crewed facilities. These vehicles have been designed in the past to be able to generate 75–90 flights a year and to be launched in less than 24 h. This implementation scheme presented provides a true capability to build an operational infrastructure as envisioned by the late Dr. William Gaubatz in Fig. 5.1.

5.7 Observations and Recommendations

This chapter has demonstrated the very large resources required to support the delivery of propellant for an operational infrastructure if conventional rocket launchers are used with conventional hypergolic rockets for space operations. It is required that sustained-use airbreathing launchers and nuclear space propulsion be developed into an operational system *if* an operational space infrastructure is ever to exist.

The key to achieving an initial operating capability with an infrastructure is not to throw away valuable (reusable) assets in lieu of very costly and long delivery-time optimum solutions that have little tolerance or durability when encountering off-design conditions and unexpected events. Some of the missed opportunities include usage of the salvaged Space Shuttle main external tank (ET) that could have been put to use as identified by Thomas Taylor. The authors observe the following:

(1) The emerging partly reusable launch vehicles by Space-X and Blue Origin in the USA, and those being designed by Airbus in EU, will probably bring more cost-effective transportation and commercial ventures to LEO.
(2) Salvaged hardware in orbit will provide commercial opportunities and transportation markets in LEO.
(3) Human-operated commercial services in orbit will emerge as the lower-cost transportation options emerge.
(4) The transportation node in LEO is important to the commercial world, because the mode of transportation changes in LEO.
(5) The cost for countries interested in positioning on the trade routes of the future is lower than ever and will be commercial.
(6) A new method of cooperation between government and the private sector must be found.
(7) In the mid- to far-term, access to asteroids rich in ice ("dark comets") may provide water and oxygen for crew support and propellants for conventional and nuclear rockets, see Sect. 7.6.
(8) Space Tourism will serve as a stepping-stone or *primer* supporting (1) through (7).

Bibliography

Anon. (2012) Skylab News Reference, Periscope Film LLC, April 2012.

Anon. (1993) "Global Outpost Inc. and NASA Enabling Agreement", No. 1564-001-00A, Rev. 3, 20 April 1993 (included a cash deposit for five external tanks on orbit)

Baker, D. (2012) *International Space Station: 1998–2011 (all stages) (Owner's Workshop Manual)*, Haynes Publishing, November 2012.

Bilstein, R.E. (1980) "Stages to Saturn – A Technological History of the Apollo/Saturn Launch Vehicles", NASA SP-4206, NASA History Series, Washington, DC, 1980.

Butrica, A.J. (2003) *Single Stage to Orbit – Politics, Space Technology, and the Quest for Reusable Rocketry*, The John Hopkins University Press, October 2003.

Catchpole, J.E. (2008) *The International Space Station: Building for the Future*, Springer Praxis Publisher, July 2008.

Chudoba, B. Coleman, G., Oza, A., Gonzalez, L., Haney, E., Ricketts, V. and Czysz, P., (2011) "Manned GEO Servicing (MGS) Crew Return Vehicle Sizing", Final Contract Report, National Institute of Aerospace (NIA), NASA LaRC and DARPA, Section in Final Report "Manned Geosynchronous Earth Orbit (GEO) Servicing (MGS) Joint NASA/DARPA Study," NASA SP-2012-598, MGS Study Team, NASA Headquarters and DARPA Tactical Technology Office, Washington, DC, 27 April 2011.

Cerro, J.A. (Editor), Chudoba, B., Coleman, G. (Contributors AVD Laboratory), et al. (2012) "Crew Transfer Options for Servicing of Geostationary Satellites", *71st Annual Conference of the Society of Allied Weight Engineers*, Bad Goegging and Manching, Germany, 5-10 May, 2012.

Covault, C. (2003) "Use It or Lose It", *Aviation Week & Space Technology*, Vol. 159, No. 15, 13 October 2003, pp. 44–46.

Diaz, F.R.C. (2000) "The VASIMR Rocket", *Scientific American*, Vol. 283, No. 5, 01 November 2000.

Eggers, A.J. and Syvertson, C.A. (1956) "Aircraft Configurations Developing high Lift-Drag Ratios at high Supersonic Speeds", NACA RM A55L05, NACA, 05 March 1956.

Folger, T. (2003) "Nailing Down Gravity", *Discover Magazine*, Vol. 24, No. 10, October 2003, pp. 34-40.

Furniss, T. (2001) *The History of Space Vehicles*, Thunder Bay Press, January 2001.

Gimarc, J.A. (1985) "External Tank Applications in Space Manufacturing", *7th Princeton/AIAA Conference on Space Manufacturing*, AIAA, October 1985.

Griswold, H.R., Stein, D.S. and Redding, F.W. Jr. (1982) "Integration of a Crewman into a High Performance Spaceplane", SAE Paper TP-820850, *12th Intersociety Conference on Environmental Systems, Society of Automation Engineers*, San Diego, CA, 19-21 July 1982.

Hale, W. (2012) *Wings in Orbit: Scientific and Engineering Legacies of the Space Shuttle (1971–2010)*, NASA/SP-2010-3409, December 2010.

Hallion, R.P. (2005) "The History of Hypersonics: Or, Back to the Future - Again and Again", AIAA Paper 2005-0329, *43rd Aerospace Sciences Meeting*, Reno, NV, 10-13 January 2005.

Hankey, W.L. (1988) *Re-Entry Aerodynamics*, AIAA Education Series, Renton VA, January 1988.

Hannigan, R.J. (1994) *Spaceflight in the Era of Aero-Space Planes*, Krieger Publishing Company, 1994.

Karol, J.M. (1997) "1996 Space Launch Activities", ANSER Report SAD 97-1, Arlington, VA., 1997.

Kennedy, K.J. *et al.* (2000) "Inflatable Structures Technology Handbook", Chapter 21: Inflatable Habitats, NASA Johnson Space Center, Draft 05, July 2000.

Koelle, H.H. (1995) *Werden und Wirken eines Deutsch-Amerikanischen Raumfahrt-Professors*, 2nd Edition, Wissenschaft & Technik Verlag, Berlin, May 1995.

Koelle, H.H. (Editor) (1961) *Handbook of Astronautical Engineering*, McGraw-Hill Book Company, New York, 1961.

Lewis, M. (1993) "The Use of Hypersonic Waveriders for Aero-Assisted Maneuvering", *Journal of the British Interplanetary Society*, Vol. 46, 1993, pp. 11–20.

Logsdon, T. (1997) Orbital Mechanics: Theory and Applications, John Wiley & Sons, Inc., October 1997.

Mulready, D. (2001) *Advanced Engine Development at Pratt & Whitney (The Inside Story of Eight Special Projects 1946–1971)*, SAE International, Warrendale, PA., 2001, ISBN: 0-7680-0664-3.

Redding, F.W. (1984) "Spaceplane Technology and Research (STAR)", Final Report DCS-11540, DARPA Order 4913, DCS Corporation, August 1984.

Redding, F.W. et al. (1983) "Spaceplane Examination", SRI International, Final Report, Contract FO4701-8IK-0001 to DARPA Strategic Technology Office, Menlo Park CA, 1983.

Shekleton, M., Patel, M., Muravyeva, I. and Steele, K. (2002) "Space-Based Satellite Service Infrastructure", Senior Course Design Project Final Report, Parks College of Engineering and Aviation, Saint Louis University, St. Louis, MO, 2002.

Stine, G.H. (1996) *Halfwhere to Anywhere – Achieving America's Destiny in Space*, M. Evans and Company, Inc., October 1996.

Taylor, T.C. (2000) "Commercial Space Habitation, 2000", Global Outpost, Inc., Lunar Development Conference: Return to the Moon II, Las Vegas, NV, 20–21 July 2000.

Taylor, T.C. (1998) "Salvage Hardware Apparatus and Method for Orbiting Objects", US 5813632 Patent, Inventor: Taylor, Thomas C., September 1998.

Taylor, T.C. (1980) "Commercial Operations for the External Tank in Orbit", paper presented at the 80-89 American Astronautical Society (AAS), 18th Goddard Memorial Symposium, Washington, DC, 27-28 March 1980.

Turyshev, S.G., Anderson, J.D. and Nieto, M.M. (2004) "The Study of the Anomalous Acceleration of the Pioneer 10 and 11", *22nd Texas Symposium on Relativistic Astrophysics*, Stanford University, Stanford, 13–17 December 2004.

Wolverton, M. (2004) *The Depths of Space*, Joseph Henry Press, June 2004.

Earth–Moon System: Establishing a Solar System Presence

6

The Earth's Moon is a natural satellite that has been suggested was created by a Mars-sized body that crashed into the Earth very early in the history of the Earth, about 4.5 billion years ago. The latest sky surveys give an age of our Solar System of about 4.7 billion years. With the Soviet, American, Japanese, Chinese and Indian lunar mapping satellites, the Soviet automatic rovers, and the Apollo landings, a significant amount of information has been gained about the Moon (Spudis 2003). Even with this information, there is much more to be learned from exploring the Moon and understanding its geology and structure. During the 1960s there were plans to use the Apollo system for lunar exploration. ALSS (Apollo Logistics Support Systems) and LESA (Lunar Exploration System for Apollo) were efforts within NASA to define the equipment and operational requirements to explore the Moon. Unfortunately, none of these plans ever reached realization. Using the 1991 report to congress entitled *America on the Threshold,* Thomas P. Stafford, former Apollo astronaut and Lieutenant-General USAF (Ret.), as Chairman of the Synthesis Group, Space Exploration Initiative, assembled a number of documents reasoning that we should return to the Moon (Stafford 1991). Figure 6.1 shows the cover and inside page from that report.

Note that the Moon is shown in front of the planet Mars with the Solar System in the background. General Stafford provides the argument for the Moon as a stepping-stone to Mars and space. It is important to recognize that it is not just a stepping-stone, but an important operational near-Earth space base that does not require orbital re-boosting. However, recent interest in lunar exploration does not even conceive the Moon as a key orbital asset, but just as a location visited nearly 50 years ago. Again avoiding a commitment for establishing a permanent natural orbital station as an Earth asset, the emphasis is rather on a high-visibility mission, or missions, for example to a nearby asteroid (Covault 2008). The reason is we will become "Moonstruck" and ignore the deeper-space manned missions. Given the state of the global economy, there is indeed a chance that after visiting the Moon again, the cost, and its inevitable overruns, may deter decision makers from authorizing going any further.

Instead, the Moon is very important as a base of operations for space exploration. The Moon can be a launching point for vehicles to explore our Solar System and nearby space. A non-rocket launcher that has the difficulty of being justified on Earth can readily provide lunar escape speed. Equipment, rovers, and habitats can be developed on the Moon for use on Mars. With the resources of an operational base, equipment that needs modification can be maintained on the Moon to avoid a return to Earth. Systems can be modified until successful operation on the Moon provides high confidence of reliable operation on Mars. One of the critical features of this natural satellite is that there are no propulsion requirements to keep it in a stable orbit, unlike LEO orbital stations (Mir and ISS). Also unlike artificial orbital stations, the Moon is not devoid of indigenous resources, including gravity. It is possible to show the advantages of the Moon compared to an Earth orbital station.

6.1 Earth–Moon Characteristics

The Moon, at least on the side we can see, is characterized by bright, rugged, heavily cratered highlands and large sparsely cratered, level dark areas called by Galileo Galilei "maria" or "seas" in Latin, shown in Fig. 6.2. The Moon has a mass of 1/81.3 of the Earth mass. Analysis of the lunar rocks returned by the Apollo astronauts indicates an age of about 4.5 billion ($4.5 \cdot 10^9$) years. The orbit of the Moon around Earth is nearly circular, the eccentricity, e, being only slight ($e = 0.0549$); its inclination to the plane of the ecliptic is 5.145°. The plane of the ecliptic is the plane containing most of the planets orbiting the Sun (except the planet Pluto). The Earth to Moon distance ranges from 406,700 to 356,400 km from Earth, with a mean of 379,700 km

P.A. Czysz et al., *Future Spacecraft Propulsion Systems and Integration*,
Springer Praxis Books, DOI 10.1007/978-3-662-54744-1_6

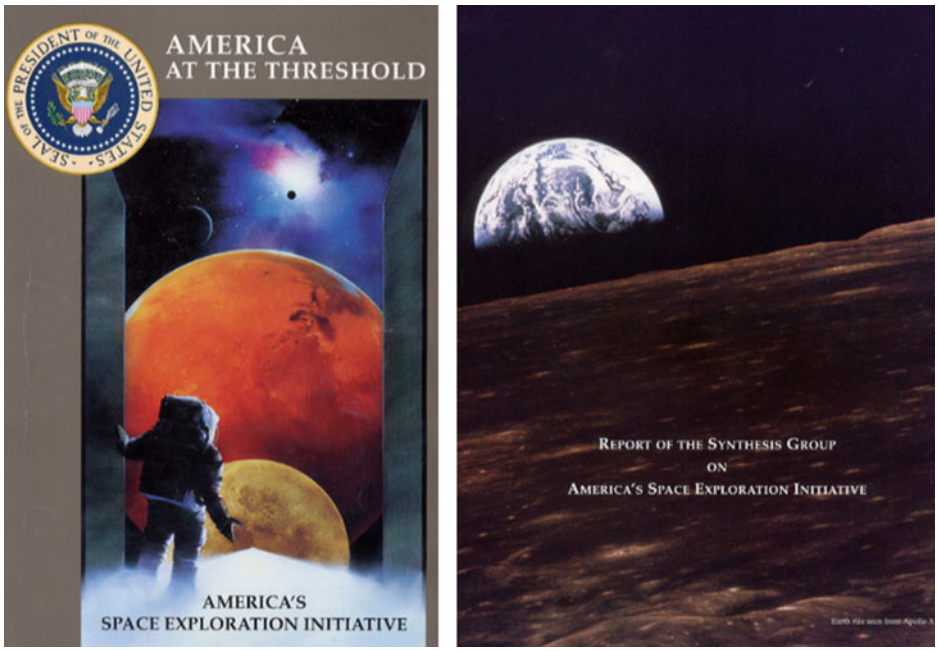

Fig. 6.1 A presidential study to continue the exploration in the future by General Thomas Stafford (retired), an Apollo and Apollo–Soyuz astronaut. The key to expanding human exploration of the solar system is the exploration of the moon and the establishment of a moon-base that is the prototype for mars and other human-compatible planets

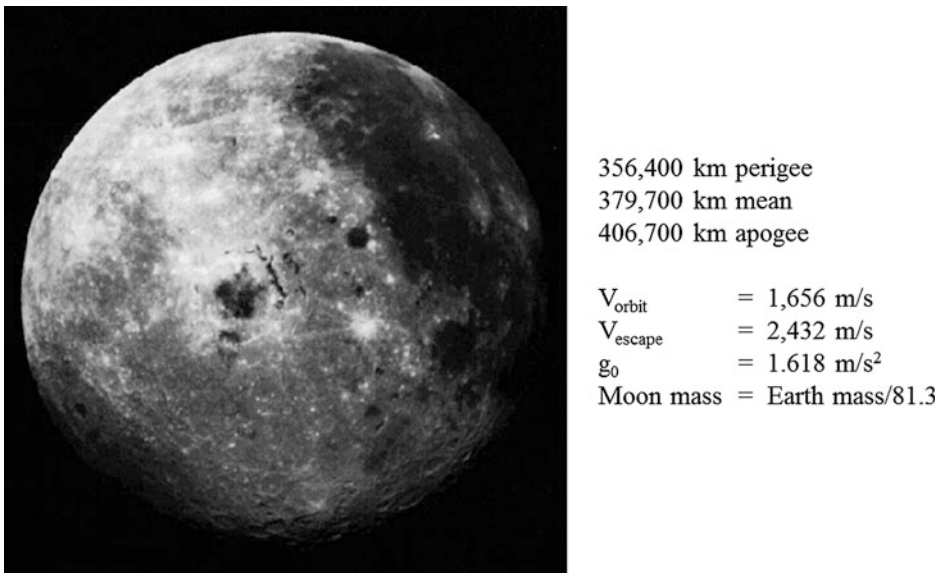

Fig. 6.2 Orbital parameters of the Moon and distances from Earth

(252,711 statute miles to 221,456 miles from Earth, with a mean of 235,934 miles). Nominal orbital speed is much lower than Earth, 1656 m/s (5433 ft/s), and nominal escape speed is 2342 m/s (7683 ft/s). The acceleration of gravity at the Moon surface is 1.618 m/s^2 (5.308 ft/s^2), about one-sixth that of the Earth.

In Fig. 6.3, when the Earth–Moon distance is 384,400 km (238,854 statute miles), the center of mass (and rotation) of the Earth–Moon system is offset from the Earth's center by 4671 km (2902 miles), that is, at 379,729 km (235,952 statute miles) from the Moon. That center of rotation is called the *barycenter*. The gravitational sphere of influence of the Moon, when it is at 384,400 km (238,854 statute miles) from Earth, is 66,183 km (41,124 statute miles). At that distance, the gravitational attraction of the Moon will be greater than that of the Earth and will therefore control the motion of approaching spacecraft. Consequently, in calculating the trajectory when the lunar sphere of influence is crossed, a conical patch is required to approximate the Moon approach trajectory. Since the conical patch is an approximation, the correct trajectory solution must be obtained by numerical integration.

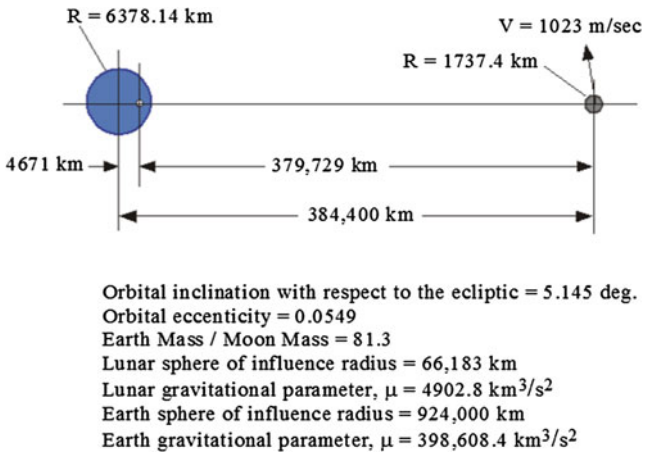

Fig. 6.3 The Earth–Moon system revolves about the barycenter some 4600 km from the center of the Earth. The Moon rotates about that center at an average speed of 1023 m/s, so any vehicle traveling from Earth must match that speed to orbit the Moon

The Moon travels around the Earth in a counterclockwise direction at 1023 m/s (3356 ft/s), and added to the Moon's orbital velocity, nominally 1655.9 m/s (5433 ft/s) at 50 km (31.07 miles) orbital altitude, this is the velocity that a spacecraft must possess to capture a stable lunar orbit. The Moon covers about 13.177° per day (0.54904° per hour) in its orbit, so the travel time to the Moon gives the lead angle at injection to the lunar transfer trajectory.

A typical lunar trajectory is shown in Fig. 6.4, and this is similar to the Apollo trajectories. The usual approach in planning an Earth–Moon trajectory is to specify the approach angle to the Moon (λ) and evaluate the resultant lunar trajectory inside the lunar sphere of influence. The approach angle is then varied until the desired lunar orbit is obtained. Remember, the lunar sphere of influence is a function of the distance from Earth to the Moon, as given by the Laplace method:

$$r_s = r_1 \cdot \left(\frac{M_{\text{Moon}}}{M_{\text{Earth}}}\right)^{2/5} \tag{6.1a}$$

with the mass ratio

$$\frac{M_{\text{Moon}}}{M_{\text{Earth}}} = \frac{1}{81.3} \tag{6.1b}$$

The distance r_2 = 66,183 km (41,124 statute miles) given in Fig. 6.3 is for the 384,400 km Earth–Moon distance. The Earth–Moon distance varies, as said, from 406,700 km to 356,400 km with a mean of 379,700 km, so the lunar sphere of influence ranges from 70,023 to 61,362 km, with a mean of 65,374 km (43,510 miles to 38,129 miles with a mean of 40,621 miles). The lead angle for launch, in this particular case 27.9°, is a function of the transfer trajectory time from injection to intersection of the Moon's sphere of influence. In all cases, the injection speed into an Earth–Moon transfer trajectory is less than the Earth's escape speed, 10,946 m/s (35,913 ft/s), so all of the lunar transfer trajectories are elliptical orbits. The minimum energy transfer ellipse is a *Hohmann transfer* ellipse to the Moon's orbit, followed then by a propulsion burn to match the Moon's orbital speed of 1023 m/s. This transfer orbit minimizes energy but requires the greatest time to reach the Moon's orbit, that is, 109.5 h. For safety, the Apollo trajectory was designed to reach the Moon in less than that, that is, 72 h. Remember the conical patch technique is very simple for planning interplanetary missions, but it is only an approximation for Earth–Moon missions, and precise numerical integration is required for any specific trajectory. However, the approximate approach does not influence the selection of propulsion systems for lunar missions and is satisfactory for the purposes of this book.

Launching a spacecraft to the Moon for a specific arrival time requires very accurate velocity control as shown in Fig. 6.5. The Moon travels in its orbit around Earth at

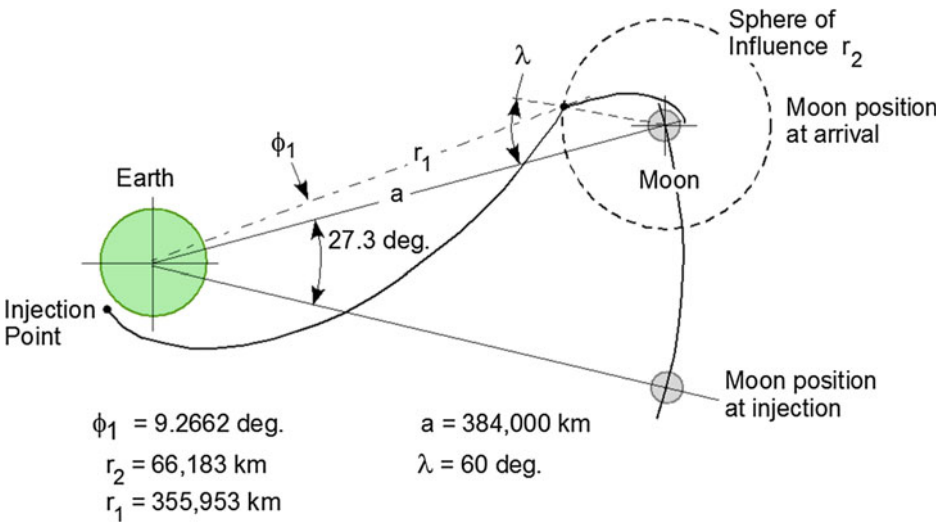

Fig. 6.4 Flight path geometry of the representative lunar trajectory

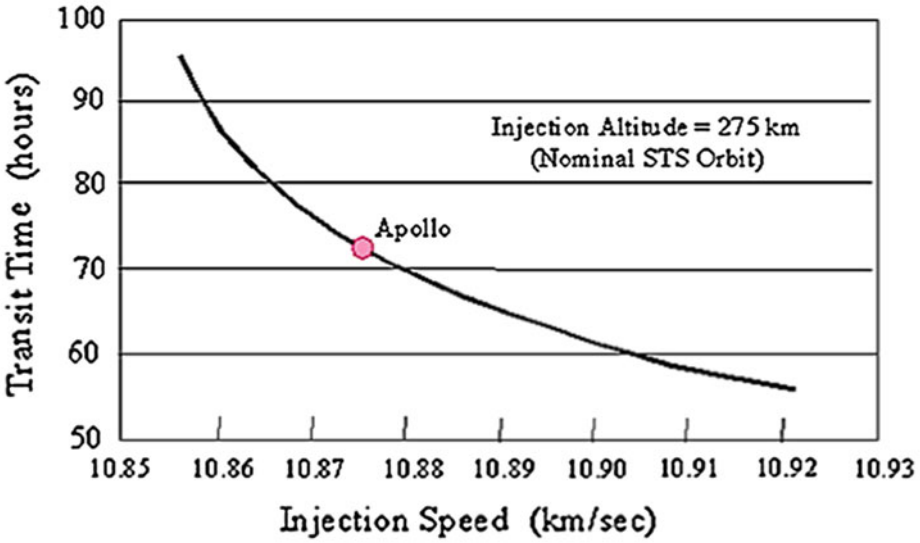

Fig. 6.5 Earth orbit injection speed is less than escape speed, so the trajectory to the Moon is a transfer ellipse analogous to LEO to GSO transfer ellipse (V_{esc} = 10.946 km/s) (Brown 1998)

1023 m/s (3356 ft/s) at an angular rate of 13.177° per day (0.54904° per hour). To achieve the Apollo mission 72-h transit time, the precision of the injection speed had to be at least less than 1 m/s (a difference of 0.01 km/s, or 10 m/s, can change the arrival time by 5 h). The important fact is that all of the trajectories are ellipses and all eventually return to the Earth periapsis after completing a longer or shorter portion of the ellipse.

Errors in the exact trajectory will not "lose" a spacecraft in space. However, the time to complete an elliptical trajectory matters, and therefore, the issue is acquiring the precise point of intersection between the transfer ellipse and the Moon's sphere of influence, as this point sets the rest of the trajectory to the Moon. A 1 s error puts this intersection over 1 km in error and can have serious impact on the resultant lunar trajectory, so timing is critical. This is not meant to make the lunar trajectory a technology challenge, but only to clarify the requirements. The late 1960s technology was adequate for at least eight Apollo missions to the vicinity and surface of the Moon.

6.2 Requirements to Travel to the Moon

As shown in Fig. 6.6, traveling to the Moon is a multi-step process. The first step is to achieve low Earth orbit (LEO), nominally set at 100 nm or 185.3 km. From that orbit, spacecraft can achieve higher orbits or be injected into a lunar or planetary transfer orbit. The International Space Station (ISS) is nominally in a 275 km (148.5 nm) orbit. All of the calculations performed in this section for lunar transfer orbits are for a 275 km circular Earth orbit. The first step is to determine the requirement to reach a circular Earth orbit. For that, a single-stage-to-orbit (SSTO) launcher was selected as this is the most demanding. A two-stage-to-orbit (TSTO) launcher will have lesser mass ratio requirements. Table 6.1 gives the launcher requirements for LEO with a hypothetical SSTO launcher.

Achieving even a modest airbreathing capability can reduce the lift-off mass of the launcher by a factor of 2, simultaneously reducing vehicle and propulsion system size. With a lesser oxidizer load and an operational design focus,

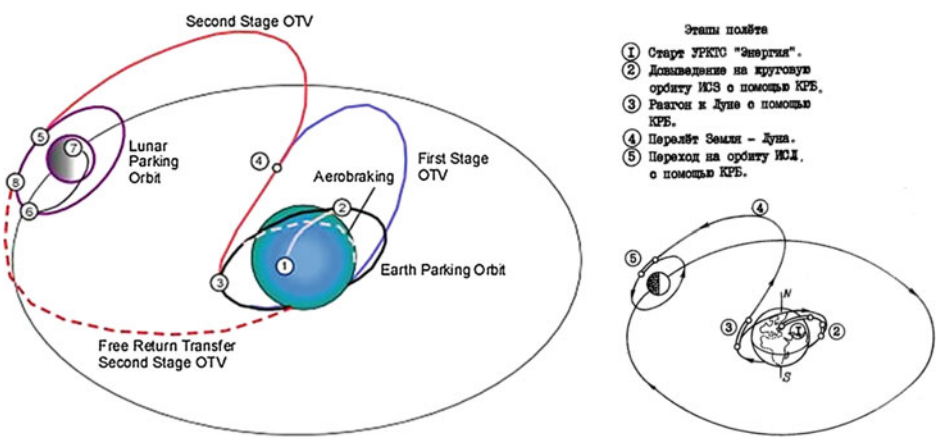

Fig. 6.6 Transfer trajectory from Earth orbit to lunar. From an original briefing chart from a presentation by V. Gubanov at the European Space Conference in Bonn, Germany, April 1984

Table 6.1 Launcher requirements to achieve circular low Earth orbit

h (km)	h (nm)	V_{orbit} (km/s)	V_{escape} (km/s)	$M_{R\ rocket}$ (−)	$M_{R\ combined\ cycle}$ (−)
185.2	100.0	7.7930	11.021	8.07	4.06
275.0	148.5	7.7403	10.946	8.28	4.16
370.4	200.0	7.6854	10.869	8.37	4.20

Table 6.2 Injection speed and transit time to Moon from 275 km circular orbit

$t_{t\ Lunar}$ (h)	V_i (km/s)	ΔV (km/s)	ΔV (ft/s)	$M_{R\ hypergolic\ rocket}$ (−)	$M_{R\ nuclear\ rocket}$ (−)
119.5	10.854	3.111	10,207	2.986	1.172
88.0	10.86	3.118	10,230	2.993	1.172
75.0	10.87	3.128	10,263	3.004	1.173
65.5	10.89	3.148	10,328	3.025	1.174
58.5	10.91	3.168	10,394	3.046	1.175
56.0	10.92	3.178	10,427	3.057	1.176
54.0	10.93	3.188	10,460	3.068	1.177

the possibility of more frequent and lower cost to orbit is a reality. In terms of Moon missions, the propulsion advances associated with the launcher have the greatest impact. With respect to in-space operations, the options available in the near term are about the same as for the Apollo missions.

Having achieved LEO, the next step is to inject the spacecraft into a trans-lunar elliptical transfer orbit. From the data in Fig. 6.5 (Brown 1998), the requirements for the transfer ellipse are determined for a range of travel times, see Table 6.2. The travel duration of 119.5 h is the lowest-energy Hohmann transfer ellipse. The shortest time corresponds to a speed approaching escape speed, 10.946 km/s, see Table 6.1.

If and when a *nuclear electric rocket* or a *nuclear thermal rocket* becomes available (see Chap. 7), the reduction of the propellant required for the trans-lunar trajectory will be significant. The propellant mass in terms of the operational weight empty (W_{OWE}) will reduce from about 2.0 times the W_{OWE} to about 0.17 times the W_{OWE}, a reduction of some 91.5% in propellant mass. As with the orbital manoeuvre vehicles (OMVs) described in Chap. 5, the major hurdles for the nuclear electric propulsion system are thrust and the magnitude of the rejected heat that determines the space radiator mass.

The difficulty with all elliptical transfer orbits is the time it takes to return to Earth if the trajectory is not precisely corrected at the intersection with the lunar sphere of influence. For the Hohmann transfer ellipse, 119.5-h trip time, the elliptical orbital period is approximately *10 days*, 5 h. For the 70-h lunar trip time, the injection speed is 10.88 km/s and the transfer ellipse orbital period is approximately *16 days*, 15 h. For the 58.5-h lunar trip time, the transfer ellipse orbital period is approximately *40 days*, 22 h. And finally, for the 54.0-h lunar trip time, the transfer ellipse orbital period is approximately *135 days*, 21 h. Thus, the faster you go, the larger the orbit eccentricity and length if the trajectory to the Moon is not precise.

All of these elliptical trip times are longer than the resources carried by the Apollo spacecraft could last, so either a redundant or very reliable rocket system, or a sufficient resource reserve is necessary. With the proper selection of the arrival angle (λ), the propellant requirement for the transfer trajectory to the lunar sphere of influence can be almost negligible, or at least sufficiently manageable not to significantly affect the sizing of the total propellant mass. Only a numerical analysis for each specific trajectory will yield that quantity correctly; such analysis does not affect the selection of the propulsion system and therefore does not need to be done for the purposes of this book. The last table (Table 6.3) deals with the propellant requirements to land on the Moon's surface and to take off from it.

Table 6.3 lists the minimum mass ratios to the lunar surface from the lunar parking orbit, and back from the lunar surface to the lunar parking orbit. As for the Apollo lunar ascent module, a hypergolic propellant is a reasonable choice until nuclear rockets or other non-chemical launching systems are operational. The hypergolic rocket requires no igniter and is the most reliable starting engine available, providing the propellant isolation valves *do not* leak. (If there is a leak, the lunar spacecraft will probably be totally destroyed by a violent explosion. With the demise of

Table 6.3 Arriving or departing the Moon with a hypergolic propellant rocket

h (km)	h (nm)	V_{orbit} (km/s)	V_{escape} (km/s)	$M_{R\ orbit}$ (−)	$M_{R\ escape}$ (−)
50.0	27.0	1.656	2.342	1.756	3.082
122.3	66.0	1.623	2.296	1.820	3.313

clean machine shops with dust and oils contamination controls that existed for the Mercury, Gemini, and Apollo programs, the potential for contaminated surfaces and leaking hypergolic isolation valves remains a concern today). The 112.3-km lunar orbit has a 2-h period and makes a good lunar holding orbit if a rendezvous there is required. The mass ratio to descend to the surface, with some margin, is about two. A mass ratio of 3.5 is sufficient for the escape manoeuvre. The spacecraft essentially falls toward Earth once it clears the lunar sphere of influence.

As the spacecraft approaches Earth, it can be traveling at a speed greater than the lunar injection speed and escape speed. Consequently, it is necessary to have braking rocket propulsion or aerodynamic breaking in the upper atmosphere to slow the spacecraft speed to be captured in an Earth orbit. In the case of a braking rocket, the returning spacecraft must have an available mass ratio similar to that in Table 6.2. In the case of a spacecraft braking aerodynamically in the upper atmosphere, the attitude is one for maximum drag. If the spacecraft resembles a lifting body configuration, it may roll upside-down and lift-down to increase the energy dissipated and decrease the heating intensity, as the heating pulse is spread out over a longer time in the upper atmosphere. The actual mission mass ratio will depend on trajectory and configuration specifics, but these tables give the reader an estimate of the propulsion and propellant requirements. Note that a round-trip to the Moon from LEO can require less mass ratio than an out and back mission to GSO.

6.2.1 Sustained Operation Lunar Trajectories

The Apollo trajectories and the Saturn V delivery system provided the necessary transport to the Moon and return in the late 1960s. With a near-Earth orbital space infrastructure established (see Chap. 5), it is not necessary to have a direct flight to the Moon with expendable hardware. Both Russia and the USA contemplated a Moon base and the systematic flights necessary for its support and staffing. Figure 6.6 is a composite of both approaches, based on briefings and reports from the early 1980s. The figure is from a brief given by V. Gubanov to the space organization of the former Soviet Union, and presented at the 1984 European Space Conference in Bonn, Germany. The original figure is in Cyrillic and has been translated. The presentation by V. Gubanov describes a multi-step approach that begins with an "artificial" Earth orbital station, and then moves to the Moon as the Earth's "natural" orbital station. After the Moon station is established and operational, the tested and proven Moon facilities are used to design a *Mars* facility, and the Moon is used as a launching platform for the human expedition to Mars. In the original Gubanov brief, there is a single transportation vehicle that moves from LEO to the lunar parking orbit and returns. In the Science Applications International Corporation (SAIC) study from 1984 for an initial operational Moon base, a two-stage transportation system using Orbital Manoeuvre Vehicles (OMVs) is proposed (Anon 1984a, b).

In the future with an operational Moon base, Earth-based launchers deliver the lunar base materials to LEO for integration to an OMV. The first OMV puts the system into an Earth elliptical orbit, and the second-stage OMV stages at the correct time for another Earth elliptical orbit that intersects the lunar sphere of influence, see Fig. 6.4. Both OMVs return to LEO for continued use. There is the option for the lunar payload to be transferred to a lunar surface delivery vehicle in lunar orbit, or to descend directly to the lunar surface, as the mission requirements dictate. Just as the Earth launchers can deliver to LEO, or return lunar payloads from LEO, there is a lunar launcher that delivers and returns payloads from low lunar orbit (LLO). Since the second-stage OMV must execute an aerobraking manoeuvre in the Earth's upper atmosphere, it must have at least a capsule configuration for braking with a finite lift-to-drag ratio (such as the Apollo heat shield or a Mars aerobraking design with an asymmetric cone configuration). Technologically, the choice in this case is between reusable heat shields or ablatives, the latter requiring refurbishment or replacement after each re-entry flight.

6.2.2 Launching from the Moon Surface

The lunar launcher that delivers and returns payloads from low lunar orbit (LLO) requires propellant to reach LLO and return to the surface. We have already said that nominal orbital speed is much lower than that for Earth, 1656 m/s (5433 ft/s), and requires a much smaller mass ratio to reach and return from LLO. The nominal escape speed is 2342 m/s (7683 ft/s), or about one-third of the Earth nominal LEO speed. From Table 6.3, we see that the mass ratio to reach LLO is 1.82, or about 3.5 for a round-trip back to the surface. This is a modest mass ratio, but all of the propellants must be delivered from Earth at a very high cost in expended propellant (see Chap. 5), unless propellants can be manufactured in situ. This provides an opportunity for a non-conventional launch capability, solving the difficult operational problem associated with using Earth to function as a launcher to LLO. The lunar surface acceleration of gravity is 1.618 m/s^2 (5.308 ft/s^2), then the weight of the equipment is one-sixth of what it is on Earth; the force required for *lifting* construction equipment is less as the required strength of their materials. Humans on the Moon will still be limited by having to work in pressure suits doubling also as radiation shields when outside, and in environmentally controlled habitats and facilities.

Launching payloads from the Moon surface is therefore attractive. With rockets, only a modest amount of propellants is needed. However, given the inherent thermodynamic inefficiency of rockets (overall instantaneous energy efficiency in a few tens percent), the low lunar gravity suggests also alternative means to achieve escape speed, among them magnetic accelerators and laser-driven propulsion. The first practical means of launching payloads and/or vehicles from the lunar surface to LLO, or to accelerate them to lunar escape speed for deep-space missions, are electrical railguns and their variants such as the "magnetic levitation linear induction accelerator," or MagLev driver (Batenin et al. 1997; Loftus 1999; Post 1998, 2000; Bruno 2008). Such a launcher must have a straight path to reduce structural stresses and cannot follow the curved surface of the Moon. Figure 6.7 shows the track of a railgun (or MagLev) launcher capable of both lunar orbital and lunar escape speed. The length is determined by the acceleration the payload can tolerate. These electrical devices have a substantial advantage on the Moon, as there is no atmospheric drag to overcome. The most significant motivation and challenge is to move materials efficiently, either for construction or for manufacture, from in situ lunar resources.

In Fig. 6.7, the 35 km long track is flat and supported off the lunar surface. These drivers are to reduce as much as possible the need for propellants ferried from Earth or even when manufactured in situ (in either case, an expensive solution, although water has been found to exist in at least one lunar south pole crater). Solar energy is available during the long Moon day; the solar constant there being about 1.35 kW/m^2, some 10% higher than on Earth due to the lack of an atmosphere. Thus, solar energy could be collected more easily and readily than on Earth to generate electricity. This overall strategy is potentially cheaper than manufacturing or ferrying propellants and could then provide the energy needed for orbiting payloads with lunar railguns (Bruno 2008). Railguns capable of accelerating large caliber projectiles and of replacing naval guns are being tested on US Navy ships.

A railgun variant is the MagLev or "magnetic lifter," or MagLift. The MagLift accelerates a payload in the same way as the railgun, that is, via the Lorentz force, but uses magnetic repulsion to prevent physical contact with the electrically conductive rail(s) and avoids friction. It is not designed to reach escape speed: it replaces only the first stage of a conventional rocket. For instance, installed on the Moon, it could accelerate a single-stage rocket up to half of the lunar escape speed. Magnetic lifter concepts can significantly affect lunar-based transportation. By levitating the launcher and providing the initial acceleration or boost, fuel weight is eliminated or reduced, enabling larger payloads and/or less costly launches. This strategy to accelerate payload can be self-standing or can complement rocket propulsion. Because it does not need consumables (other than electricity) and has no moving parts, MagLev/MagLift launch-assist technology is inherently geared to high launch rates, and provided power generation is available. Rates would be limited by the time to prepare the launcher and carrier (the 'sled') assemblies. The MagLev track and supporting facility are inherently capable of rapid turnaround.

A MagLift-assisted launch would be accomplished by mounting the payload-containing vehicle piggyback on a carrier structure (sled). The sled accelerates along a fixed track as power is fed to embedded magnetic coils by a dedicated power generation or energy storage system. The coils interact with magnets (permanent or not) on the bottom of the sled to provide both levitation and the propulsion Lorentz force necessary to accelerate the assembly. Part, or all, of the sled desired speed is obtained in this way. Once the required velocity is attained, for instance, if it is less than escape or orbital speed, the vehicle's own rocket is activated, until reaching final speed and/or orbit. MagLift/MagLev acceleration is limited by track length and vehicle/payload sturdiness. After the launch vehicle is released, the carrier sled is slowed to a stop, for instance electromagnetically, to recover part of the sled energy and store it, and then is returned to the starting end of the track for reuse.

This ideally simple scenario must account for the fact that Lunar railgun/MagLev systems are constrained by power available, track length and acceleration. In fact, neglecting for simplicity the lunar gravitational work, the thrust power P to accelerate a mass m to a final velocity V along a track of length L and with a constant acceleration a_o is given by

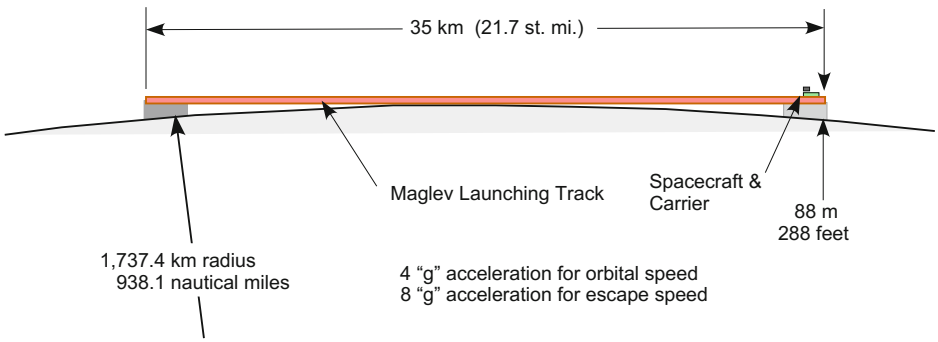

Fig. 6.7 Track for a notional superconducting MagLev launcher on the Moon. The launcher provides a non-chemical propulsion means to achieve lunar escape speed

$$P = m \cdot a_0 \cdot V \tag{6.2a}$$

$$L = \frac{a_0 \cdot t^2}{2} \tag{6.2b}$$

$$V = a_0 \cdot t \tag{6.2c}$$

where t is the time to reach V. From Eqs. (6.2a), (6.2b) we obtain for the track length

$$L = \frac{V^2}{2 \cdot a_0} \tag{6.3}$$

Equation (6.3) describes a hyperbola on the (a_0, L) plane. Then, per unit mass, escape velocity can be reached by using a combination of acceleration and track length, so that neither a too intense acceleration nor an excessively long track is necessary. The payload for exploration of the Jovian planets and Mars will require that the magnitude of the acceleration is limited to less than 3–5 times the Earth's gravitational acceleration. Considering a simple insertion trajectory into an escape orbit demonstrates the critical dependency on track length, L. For instance, a $3g$ acceleration (96.52 ft/s^2 or 29.73 m/s^2) and launch speed just exceeding escape, i.e., 8200 ft/s or 2.5 km/s, need a minimum track length L = 348,313 ft or 105.1 km and a $3g$ acceleration lasting about 85 s. Constructing such track on the Moon will exceed technical and financial capability for decades to come. For simply gaining a ΔV = 500 m/s with the same acceleration, the V^2 dependence predicts a much more manageable 4.2 km long track.

Energy-wise, the energy E to reach escape speed V is of course independent of a_o and L:

$$E = \frac{m \cdot V^2}{2} \tag{6.4}$$

For instance, a 1 t payload needs approximately 3 GJ (3 MJ/kg) to reach Moon escape speed. This is not a large figure per se (it is equivalent to the heat given off by burning completely 717 kg of gasoline with air), but power is. In fact, since velocity changes during acceleration, the *maximum* power is:

$$P_{\max} = m \cdot (a_0)^{1.5} \cdot (2 \cdot L)^{0.5} = m \cdot a_0 \cdot V \tag{6.5}$$

The power required is a stronger function of the acceleration than of L. In the case just made (V = 2.5 km/s, $a_0 = 3g$), the maximum power, reached at the end of the track, is 74.3 kW per kg of payload. This means 74.3 MW/t, the power of a medium-size terrestrial gas turbine. On the Moon there is no air, and the only in situ power source is the sun. At 1.35 kW/m^2 and 12% photovoltaic efficiency, the area needed is $458.6 \cdot 10^3$ m^2, or a square field with the dimensions ($677 \cdot 677$) m^2 filled with solar cells. A possible solution to the power problem is to store energy harvested by solar cells, and to release it when needed, or to use nuclear power, see Chap. 7. In the end, a MagLev solution for lunar transportation will depend on the nature of the payloads to be accelerated, i.e., how much acceleration they can tolerate without damage.

A second potential lunar launch system is the LightCraft concept of the late Professor Leik Myrabo (1982, 1983), Myrabo et al. (1987). This is described in Chap. 4 as an Earth launcher, but the LightCraft has also a deep-space configuration where thrust can be produced by interaction of the solar wind with the laser/microwave beam. As shown in Fig. 4.46, the installation of the laser/microwave projector takes much less space than for the MagLev device because it requires no track.

Laser beams are an attractive means of carrying concentrated power over distance. In vacuo, their power is not dissipated by interaction with gas molecules, and diffraction cannot take place. Thermal blooming is absent, and the beam (theoretically) stays coherent. These advantages suggest using a laser as a primary power source beamed to a spacecraft to supply power and accelerate it. Atmospheric effects (accounted for by the so-called Strehl ratio S_{tr} of order 10^{-1}) result in a laser range, R, given by the (approximated) Rayleigh equation

$$R = D \cdot d \cdot \sqrt{\frac{S_{tr}}{24.4 \cdot \lambda}} \tag{6.6}$$

where

D diameter of the beaming mirror,
d diameter of the receiving mirror on the spacecraft,
S_{tr} Strehl ratio $\approx$ 0.1, and
λ laser wavelength (Eckel and Schall 2008)

For instance, a CO_2 laser (λ = 10.6 mm) beamed by a 5 m diameter mirror could be received by a 1 m diameter mirror at about 140 km, assuming a Strehl factor 0.5.

In space, this range can be higher, since the Strehl ratio is close to 1. Chemical oxygen-iodine lasers (COIL) have been surpassed by electrically powered diode lasers already tested on vehicles and on ships, although their power is still limited to a few tens of kW. Free electron lasers (FEL) (Marshall 1985) may work in a range of wavelengths; continuous wave (CW) or pulsed mode operation is an important issue directly affecting thrust.

Once received, the power can be used in a variety of propulsion strategies. A semi-empirical quantity, the "coupling coefficient" C_T expresses how much of the incident power is converted into thrust. C_T depends on the particular strategy chosen to produce thrust from the power transmitted by the laser beam and permits analysis of Moon-launching without bothering with the specifics of propulsion. If sufficiently large, or lasting, or both, laser power becomes thrust capable of lifting a payload from the Moon and injecting it

into orbit. Notice that small lasers are still capable of acceleration (of course, thrust produced must be at least equal to the lunar weight), but the Rayleigh equation sets a crude distance and time limit on how long acceleration may last. In fact, if a_0 is the acceleration (assumed constant) imparted to the craft, T is the thrust, V the lunar escape speed, t the escape time, neglecting gravity work for simplicity, it must be

$$a_0 = \frac{T}{m} \tag{6.7a}$$

$$R > \frac{a_0 \cdot t^2}{2} \tag{6.7b}$$

$$V = a_0 \cdot t \tag{6.7c}$$

and eventually the minimum acceleration a_0 must satisfy the conditions:

$$\frac{T}{m} > \frac{V^2}{2 \cdot R} \tag{6.8a}$$

$$\frac{P}{m} > \frac{V^2}{2 \cdot C_T \cdot R} \tag{6.8b}$$

Thus, the issue is laser *fluence*. For instance, a 1000 kg payload accelerated by a CW CO_2 laser beamed by a D = 5 m mirror, received by a 1 m focusing mirror and assuming a Strehl coefficient = 0.5, needs about 21 m/s^2 (T = 21,000 N) to accelerate to lunar escape speed within 140 km of the laser range. The minimum power required, if the coupling coefficient is 1000 N/MW, turns out to be P = 21 MW, a striking figure and unfeasible at this time with a *single beam*, but that may become feasible in a few years from now. In any event, Eqs. (6.8a), (6.8b) points to the fact that "shipping" payload from the Moon requires significant installed power. As in the case of railguns, power may be a combination of solar and nuclear energy. Stored solar energy is probably insufficient at lower acceleration, since the spacecraft need to be illuminated for longer periods. Takeoffs and landings are vertical with minimum surface footprint. The basic concept has been demonstrated (Myrabo et al. 1998; Myrabo 2001). In terms of potential for deep-space acceleration and launching from the lunar surface, this concept has the most potential and the least acceleration load on the spacecraft.

As with all of these schemes, a significant amount of material must be either fabricated on the Moon or lifted from the surface of the Earth, which requires an even greater mass of propellant to reach LEO and the Moon. Clearly, the trade-off question is: *Does the propellant saved in lunar launches and the propellant required to deliver that propellant to the Moon (or to* in situ *manufacture on the Moon) justify the cost of the facility?* With current chemical propellants the answer is *no*. We have seen that the ratio between propellant mass required to deliver a payload to its destination and the payload mass is too large. However, as higher-thrust solar electric and nuclear electric propulsion systems become operational, the cost of these propellants will fall dramatically and non-rocket launch facilities on the Moon will in all probability become practical.

6.3 History

The history of our visits to the Moon are listed as a reminder that we have not returned to the Moon, since the last Apollo 17 astronauts departed the surface of the Moon on December 14, 1972, nearly half a century ago. In the decade beginning in the mid-1960s there were probes, landers, rovers, lunar satellites, and even 12 American astronauts that briefly visited the surface. Since then only *Clementine*, the *Lunar Prospector*, the *SMART-1* electric thruster-powered probe, *Chang'e-1*, *Chandrayaan-1,* and *Kaguya* with its two auxiliary satellites have orbited or visited the Moon. (The second Chinese *Chang'e-2* orbited the Lagrangian point L2.)

After the few brief visits to the Moon, subsequent Apollo missions and any sustained exploratory visit to the Moon were scrapped. The very efficient and capable heavy launch system, Saturn V, was discarded as having no future use. Today a heavy-lift system to LEO is still missing, and the NASA's Space Launch System (SLS) is being built at great cost. The closest for regaining that capability was the Russian *Energia* launcher that was scrapped after just two successful launches, following the disintegration of the Soviet Union. Most recently, on August 03, 2016, the private company *Moon Express* has received formal approval from the Federal Aviation Administration (FAA) to launch its MX-1 lunar lander to deliver a commercial package to the Moon in 2017 (Brown 2016).

Scientifically, the Moon still conceals many mysteries about its past history that remain to be discovered. There are unexplained anomalies in surface composition, there is the massive, violent bombardment of the Moon that occurred about four billion years ago, there is the question of water ice in the shadowed south polar region, and whether ^{3}He (or helium-3, a very interesting fusion "fuel", see Chap. 8), hydrogen, and oxygen can be recovered from the surface in a sustained operation. Briefly, past exploration has been by the former Soviet Union and the USA. More recently, the European Space Agency (ESA), Japan, India, and China and the USA plan to send more unmanned spacecraft to the Moon in an attempt to resolve some of its unanswered questions and in preparation for future crew landings.

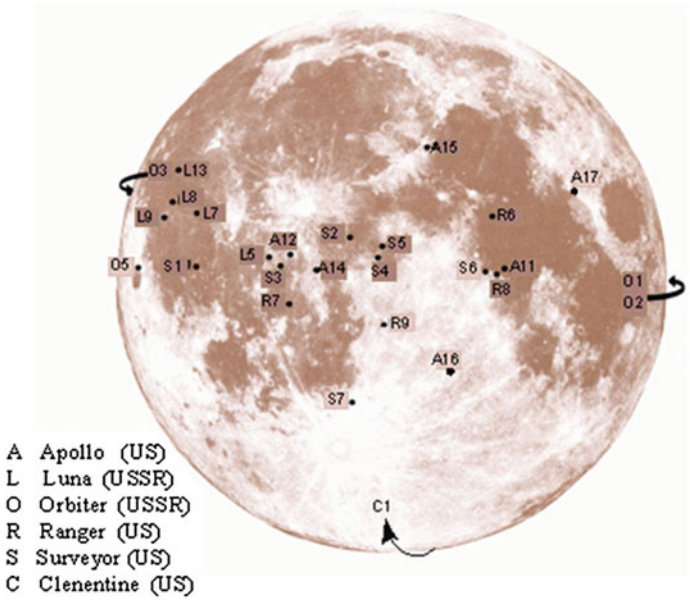

Fig. 6.8 We have been there before with probes, landers, orbiters, and human visitors. Apollo was a manned Moon mission beginning with the Apollo 10 lunar mapping mission, and ending with Apollo 17. Luna was a USSR robotic lander and rover series, Orbiter was a series of USSR flyby and orbital photographic mapping missions, Ranger crashed into the surface relaying pictures as it did, Surveyor was a lander mission series, and Clementine was an orbital mapping and resources survey mission

Figure 6.8 shows where the different systems have reached the Moon's surface and some of the lunar orbital systems.

6.3.1 USSR Exploration History

- *Luna 1, 2, 3* Luna 3 returned the first pictures of the near and far side of the Moon.
- *Luna 9, 13* First successful soft landings on the lunar surface.
- *Luna 16, 17* First automatic probe to return samples and have robot rovers to traverse the lunar surface and avoid craters.
- *Orbiters 1, 2, 3, 4, 5* All missions were successful and mapped the lunar surface in detail.

6.3.2 USA Exploration History

- *Ranger 7, 8, 9* Nine Rangers were launched; the last three sent back pictures of the lunar surface as the probe crashed into the surface.
- *Surveyors* All successfully landed on the lunar surface and took scientific measurements.
- *Apollo 11, 12, 14, 15, 16, 17* human landings on lunar surface, local exploration, and 15, 16, 17 mineral (ilmenite) sample collection.
- *Clementine* Lunar mapping and resource survey; first to find evidence of water in southern hemisphere craters.
- *Lunar Prospector* Lunar mapping and resource survey.
- *SMART-1* First ESA lunar probe sent from LEO to LLO with an ion electric thruster.

6.3.3 India Exploration History

- *Chandrayaan-1* Lunar mapping and mineral resource survey.

6.3.4 Japan Exploration History

- *Kaguya* (Selene) High-definition video mapping with two auxiliary satellites for precision mapping capability.
- *Lunar-A* Future lunar satellite to fire probes into the lunar surface.

6.3.5 China Exploration History

- *Chang'e-1* First Chinese probe mapping the lunar surface.

This brief listing of lunar exploration history and probes has been assembled in the hope that these would not be the last. All missions aided in our understanding of the Moon and have already radically changed our perception of the Moon and its origin. There is much more to the Moon than a nearby object to be explored for its history, natural resources, and structure. The most important aspect of the Moon is that it can be a natural orbital station, it can be a staging base for deeper exploration of space, and it can be an operational training base and systems development test site for hardware that will eventually permit us to confidently and safely have humans establish a base on Mars.

Technically, Apollo–Soyuz was not a lunar mission, but it was the precursor to the cooperation that led to the ISS being established in orbit. When one of these authors (P.A. Czysz) visited the Space Museum in Moscow, the centerpiece of the Museum (in 1990) was the Apollo–Soyuz spacecraft joined together and hanging in the rotunda. In the Leninsk Museum outside of Baikonur Space Center one finds a tribute to the spacecraft commanders, Tom Stafford and Alexei Leonov. Also within the tribute is some of the space artwork of Leonov, who was quite an accomplished artist. The last Saturn and Apollo moon launch departed Kennedy Space Center on July 15, 1973 at 19:50 GMT and brought to an end the US exploration of the Moon and an era of accomplishments that, just a few years previously, were thought impossible and a luxury that nobody should afford.

6.4 Natural Versus Artificial Orbital Station Environments

Tom Stafford provides a very clear view of what might be if we take advantage of the Moon's potential (Stafford 1991). Stafford's Synthesis Group, in defining the Space Exploration Initiative (SEI), placed significant emphasis on the utilization of the Moon as an orbital operational base. Stafford's report goes into significant detail on how this could be accomplished, beginning with a reconstituted and electronics-upgraded Saturn V/Apollo program. In discussing the finding with General Stafford at the 1991 Paris Air Show, he related the frustration in the inability of industry to manufacture the Saturn V hardware, especially the Pratt & Whitney J-2 hydrogen/oxygen rocket engine and the Rocketdyne one-million-pound thrust F-1 rocket engine. It became apparent that the human machining and tooling skills had disappeared with the aging and retiring of skilled craftsmen, since computer-controlled machining was not an adequate substitute.

Nearly 45 years after the Apollo missions, with all of the technology improvements since then, the 1960s hardware capability could not be reconstituted. What was thought impossible prior to the Apollo missions now is impossible because the only operational crewed vehicle we had, the Space Shuttle (STS), not only was incapable of anything approaching a lunar mission but was retired with the last flight of *Atlantis* on July 21, 2011, closing the 30-year Space Shuttle program. Since then, the USA has been without a domestic man-rated space access system.

If we are to take advantage of the Moon as an orbital station, it must be with the new SLS launcher hardware being built by NASA, that will be capable of lunar missions. Its funding is decided on a year by year basis, and plans exist to use it to sustain a space presence with frequent flights. In fact, President Obama's directive is to focus efforts on Mars exploration, and forbids using NASA funds for the Moon (Sutter 2010; Martin 2016).

6.4.1 Prior Orbital Stations

Not to belabor the point, but the most operational experience in an artificial orbital station is still possessed by the former Soviet Union and today's Russia. In discussing that experience with Vladimir Gubanov of the production company Energia, it is clear that the Russian engineers and researchers are aware of the limitations of a crewed artificial orbital station. Gubanov's presentations to the Russian government clearly emphasized an operational Moon-based orbital station as a precursor for venturing to Mars, and as a launching platform for automatic spacecraft space exploration. The artificial orbital stations that have been operational are listed below. Salyut 6 was re-activated after a serious hypergolic propellant leak forced evacuation of the station. An innovative adaptation of Earth-based tools to operate in space by a single cosmonaut permitted repair of the propellant system. Mir was in orbit some 15 years.

- *SkyLab* USA civil space station, 1972.
- *Salyut 2, 3, 4* USSR military orbital stations, 1973, 1974, and 1977.
- *Salyut 1, 4, 6, 7* USSR civil orbital stations, 1971, 1974, 1977, and 1982.
- *Mir* USSR civil orbital station, 1986.
- *ISS* USA with Russia, European, and Japanese participation, 1999.
- *Tiangong-1* Chinese precursor of *Tiangong-2*, a Chinese crewed space laboratory, 2011.

6.4.2 Artificial Orbital Stations

An artificial orbital station is an isolated man-made habitat for humans to exist in the inhospitable and hostile environment of space. Figure 6.9 shows Mir in orbit near the end of its 15 years in space and during the deorbit over the South Pacific. Figure 6.10 shows the International Space Station (ISS) in 2006 and finally assembled in 2016 in orbit. Mir was not as elaborate as ISS, but until its abandonment, it was the longest-lived functional orbital station.

The artificial orbital station's modular design allows different functional modules to be added as needed. Note that, in the absence of a US supply and rescue vehicle to date, the Soyuz capsule is still the only man-rated supply and rescue vehicle for the ISS. There is a Soyuz attached to the ISS (lower side of ISS in Fig. 6.10), but there is no Soyuz attached to Mir because the picture was taken by the last crew departing Mir before its entry into the atmosphere. Since both stations had their origins in the Russian station modules, there is a similarity of structure.

The characteristics of such a station require its sustained and continual support to sustain a human crew over the operational life of the station, as given below. The defining characteristics of an artificial Earth satellite/orbital station are the following:

1. The station is without any self-sustaining resources, and must be continuously resupplied.
2. The orbital station is the only inhabitable facility; survival outside the orbital station can be by space suit only and is limited by the life-support resources of the space suit.
3. The microgravity environment begins to induce significant physiological changes in the human crew for orbital stay times that exceed roughly 6 months.
4. Solar and space radiation are serious hazards over long orbital stays. The dose per astronaut is about 90 mSv/year, see Appendix A. A *safe house* is required for the crew to wait out hazardous solar events (e.g., unpredictable solar flares).
5. Solar wind and atmospheric drag require propulsion burns to sustain orbital altitude. Failure to re-boost operational orbital altitudes can result in atmospheric entry and destruction of the orbital station.
6. The orbital station must be attitude-controlled to maintain solar panel and antenna orientation.
7. Solar radiation is currently the sole, sustained, renewable power source via solar cells. Power varies between 75 and 90 kW. Solar-driven heat engines (Stirling or Rankine cycles driving generators) and nuclear power systems are yet to be considered or designed, much less tested or implemented.
8. With human inhabitants, there is a critical requirement for means of rapid evacuation to Earth. This was one of the overriding considerations of the support systems for the 1964 USAF Manned Orbiting Laboratory (MOL) (Anon 2015). Only Russia has implemented a rescue system, sized for the station crew, which is attached to the orbital station whenever the crew is on board the station. Had the former Soviet Union not collapsed, the Lozino-Lozinskiy BOR-4 hypersonic gliders would be that crew re-supply/escape system, rather than the Soyuz ballistic capsule.

If the orbital station is to be more than a crewed pressurized container, then a sustained support and transportation system must be an integral part of the orbital station system. In terms of the ISS that was and is not the case, even when the Space Shuttle was operational. As discussed in Chap. 5, a LEO infrastructure is a demanding operation because nothing associated with the infrastructure is self-sustaining. Everything must be supplied from the Earth's surface. Then, unless some type of gravitational acceleration (of magnitude required to overcome human physiological changes, yet to be determined) is generated,

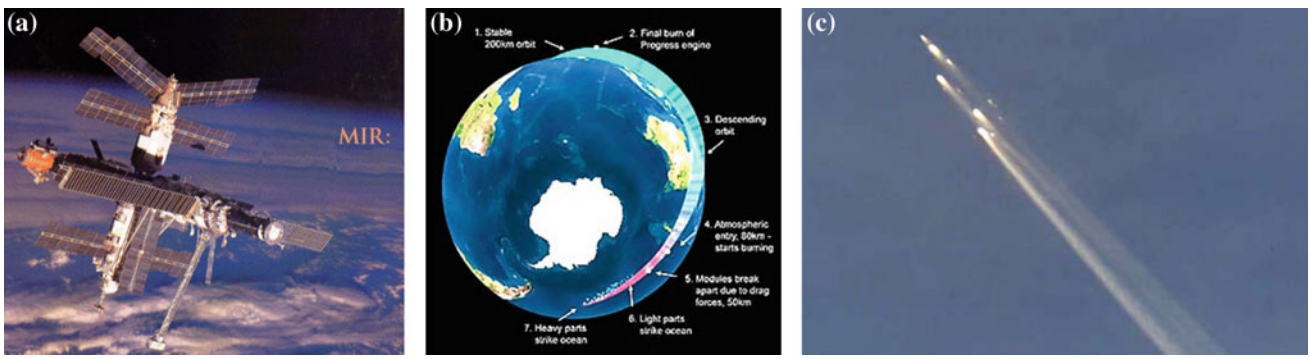

Fig. 6.9 From *left* to *right*: **a** orbital station Mir in its 15th and last year of operation before deorbit. **b** Mir final orbit and descent schematic (Bryce 2001). **c** Mir deorbit over South Pacific

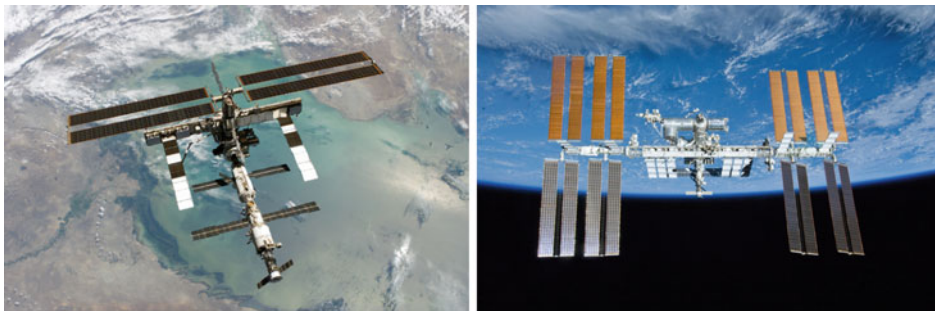

Fig. 6.10 International space station (ISS) in orbit in 2006 on *left*, and in 2016 on *right*

long-term human habitation will have serious health risks. Considering these challenges, General Stafford and his synthesis group determined that there is an approach that avoids most of these complications.

6.4.3 Natural Orbital Stations

A natural orbital station is a habitat for humans to exist located on a natural satellite of Earth. It is true that the Moon's environment is also an inhospitable and hostile environment. But in the presence of gravity and a soil surface, there are options that do not exist for the artificial orbital station. General Stafford's *Synthesis Group* is not the first to study the Moon as a suitable operational crewed orbital station. Science Applications International Corporation (SAIC) generated such concept in a 1984 report for the initial operational Moon base; see Hoffman and Niehoff (1985). The characteristic of such a station is that it does not require continual support to sustain a human crew over the operational life of the station, as given below.

The defining characteristics for the natural Earth satellite (Moon) station are:

1. The lunar station can be self-sustaining for food and water, given construction of pressurized transparent domes and soil-processing equipment. Automated operation can last from 10 to 20 years with nuclear power. This station can be a prototype robotic facility for eventual deployment on Mars (Bayón-Perez 2002).
2. Solar and space radiation hazards exist, but underground facilities negate risk, see Fig. 6.11. Habitats near the lunar north pole (near the *Peary* crater) might be ideal, as they may be permanently illuminated, but enjoy a thermally benign environment (Bussey et al. 2005).
3. Both external modules and below-surface facilities at least 1 m deep provide multiple habitable locations that undergo less temperature extremes and offer protection from damaging solar radiation, Fig. 6.12.
4. Natural gravity about one-sixth that of Earth provides some gravitational force. Whether it is sufficient to trigger gravity-based beneficial physiological reactions remains to be established. The orbital and escape speeds are lower than from Earth.
5. The beam-powered LightCraft and the magnetic levitation (MagLev) accelerator are both options and alternatives to pure rocket launch from the lunar surface.
6. Possibilities for in situ manufacturing of hydrogen and oxygen for rocket propellants from elements in the lunar soil deposited from the solar wind or comets exist. One of the chief components of the solar wind is atomic hydrogen (protons). Water was found in November 2009 to be present near the south pole.
7. Assembling of prefabricated equipment and structures from Earth is possible, Fig. 6.12.
8. No space walks required; surface assembly uses mostly standard construction equipment.
9. Solar radiation and ^{3}He mining are sources of renewable, aneutronic fusion power (see Chap. 8).
10. Lunar facilities inhabitants can evacuate to subsurface facilities or other surface modules in the case of solar flares or other occurrences, Fig. 6.11.
11. Return to Earth is free once lunar escape speed is reached and the spacecraft passes beyond the lunar sphere of influence.

Figures 6.11 and 6.12 show both the underground and surface concept structures being designed by ESA and the Japanese Space Agency. None of these requires a technical breakthrough to be built. Available industrial capability in the USA, Europe, or Asia can develop the first-generation facilities and assembly equipment necessary to establish an initial operational capability (IOC). As more is learned about the lunar environment and surface conditions, systematic improvements can be incorporated.

At the European Space Conference in Bonn, Germany, in 1984, where V. Gubanov presented the rationale basis for Fig. 6.6, the Japanese Space Agency NASDA (now JAXA) presented a comprehensive plan and an approach for returning to the Moon and establishing a permanent habitat. Unfortunately, it had been too long since Apollo, and the engineers that for the first time created "that which never

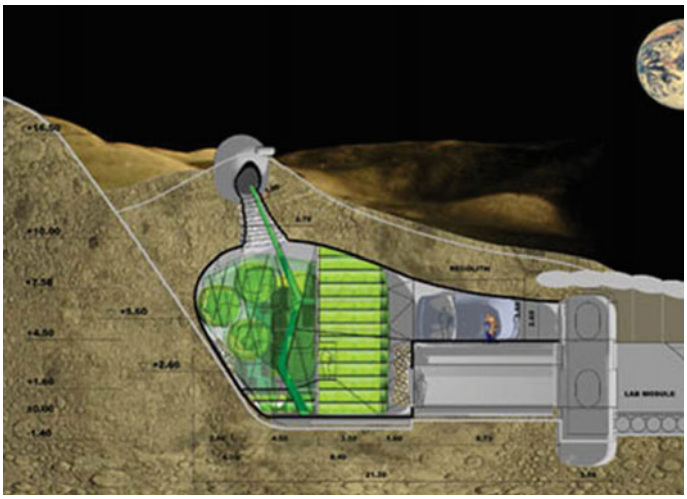

Fig. 6.11 ESA concept for underground lunar habitat

Fig. 6.12 ESA concept for long-term lunar structures to form a village on the moon

was" were not in attendance. The audience expressed severe skepticism about whether humans would ever return to the Moon. The approach and plan were well-thought-out and do-able, given significant engineering of practicable and operational Moon facilities. There seemed to be a misunderstanding between what is feasible at laboratory level, still requiring a substantial technology R&D budget, and what needs to be engineered based on operationally practicable industrial capability (already demonstrated by Apollo).

Using the Moon as an operational base makes propulsion choices less costly and easier to make for deep-space missions. Spacecraft speeds on the order of 13,500 m/s (44,291 ft/s) are possible with non-chemical rockets with low mass ratios (1.4 with a nuclear rocket, instead of 20 for a hydrogen/oxygen rocket and 98 for hypergolic rockets), a first advantage. There is a clear advantage for testing and evaluating human operations on a foreign, inhospitable planet that is just 70 h away, before venturing far from Earth without the capability of easy and fast return. General Stafford found that, on a per pound basis, the cost of liquid oxygen sent from the Moon to LEO may actually be less compared to lifting the same mass up from the Earth's surface.

High-energy material (^{3}He) recoverable from the lunar surface can power deep-space exploration and Earth-based fusion power plants when cryogenic, magnetic confinement reactors are available (see Chap. 8). For launches into our Solar System and for astronomical observatories on its dark side, the Moon is a natural choice. Using the Moon greatly reduces the magnitude of the resources required from Earth. Again, as in Earth orbit, the commercialization of sustained operations on the Moon is more practicable for high-frequency lunar missions.

6.5 Moon Base Functions

A permanent operational base on the Moon has many more options than an artificial orbital station. Perhaps one of the most important functions relates to the future exploration of Mars. We left the Moon in a hurry, not even completing the scheduled missions. There is much left un-discovered on the Moon. The lunar mapping satellites *Clementine*, the *Lunar Prospector,* and *Chandrayaan* have found mineral deposits that can be exploited for fabrication of Moon-launched

deep-space missions. As an astronomical observatory, it has advantages over Hubble in terms of size and accessibility. Some of the most intriguing features of establishing a permanent lunar foothold are listed and discussed below.

6.5.1 Martian Analog

Figure 6.13 is from General Stafford's report on America's Space Exploration Initiative (Stafford 1991). The figure shows sites on Mars and the Moon that have features in common and could be used to evaluate facilities and equipment destined for deployment on Mars. Before these are deployed on Mars, they can be put to good use for building a Moon operational base, their performance evaluated and modifications made while in relatively close proximity to Earth. Although the Moon has no atmosphere, while Mars has a tenuous atmosphere that can generate massive seasonal dust storms, the key similarities are those associated with the surface features.

The Moon has essentially no surface pressure; Mars has a surface pressure that is everywhere lower than 10 millibar (about 1/100 atm). On Earth, the pressure of 10 millibar corresponds to an altitude of 29,300 m (96,127 ft), so there is very little atmosphere on Mars. Humans require a full pressure suit over altitudes of 55,000 ft (16,764 m); in that respect, full pressure suits are required on both Mars and the Moon. The acceleration of gravity on Mars is 3.707 m/s^2 (12.162 ft/s^2), on the Moon about half of that, that is 1.62 m/s^2 (5.309 ft/s^2). On the Martian surface, the temperature is approximately 218 K (−67 °F) (it depends on the season) and on the Moon approximately 215 K (−73 °F).

With the surface conditions being rather similar, this makes the Moon an excellent Mars evaluation site. With lower gravity, it will be easier to move about on the Moon and assemble equipment and facilities, but the difference with Mars is not so large that operation of the hardware cannot be established fairly well. One of the uncertainties with Martian operations is that of the density variation of the atmosphere at the time of entry. As a result, the landing ellipses (the set of points of most probable landing location, or elliptical error probability) are quite large. If cargo material is being pre-positioned, even if the same landing coordinates are selected, the landing sites of crew and cargo missions could be 5 km (3.1 statute mile) apart. Then, part of the Mars equipment evaluation will be the ability of the astronauts to locate and move the equipment to the same location. For a human mission to Mars, that very aspect may be a truly critical element.

6.5.2 Lunar Exploration

Both Soviet Union and the USA left the Moon after a few brief encounters without really exploring it. We do know from the early Soviet *Luna programme* pictures that the far side of the Moon (the side that is always facing away from the Earth) is far different than the near side. Figure 6.14 is a composite of a near-side photograph with a far-side photograph, so the differences can be compared (Berman 2003). With the far side always invisible from Earth, it will make for a major challenge for human astronauts to explore the area. The *lunar maria* on the near side were formed at different times. From the lunar samples returned by the Apollo astronauts, the age of the samples varies from $4.5 \cdot 10^9$ to $2.6 \cdot 10^9$ years. There are no *lunar maria* on the far side—so whatever process produced the large flat areas on the near side was absent on the far side.

Clementine and the *Lunar Prospector* have identified the surface materials on both the near and far side of the Moon and recorded the elevations, as shown in Fig. 6.15 (Spudis 2003). Figure 6.15 shows the enormous extent of the South Pole-Aitken basin (in purple, on the bottom of the right image) that stretches across some 2500 km (1553 st. mi.).

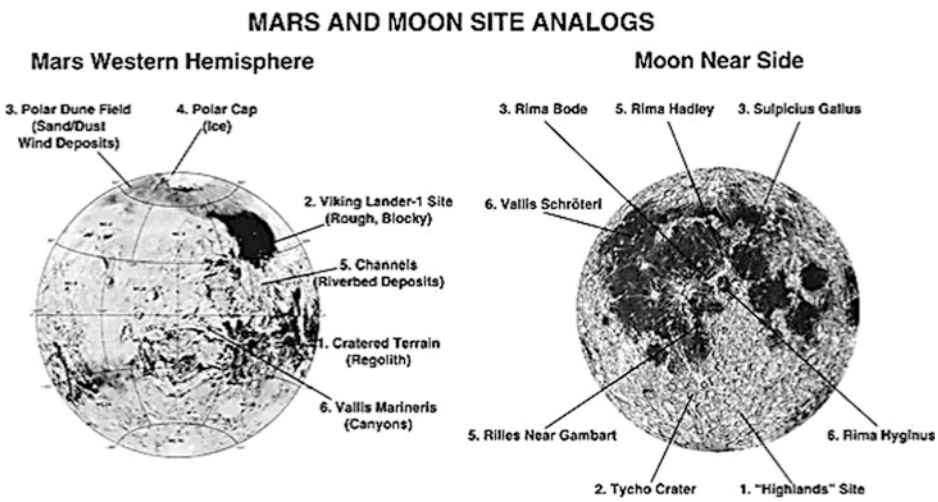

Fig. 6.13 From Thomas Stafford's report to US Congress: the comparison of representative lunar sites with representative Martian sites

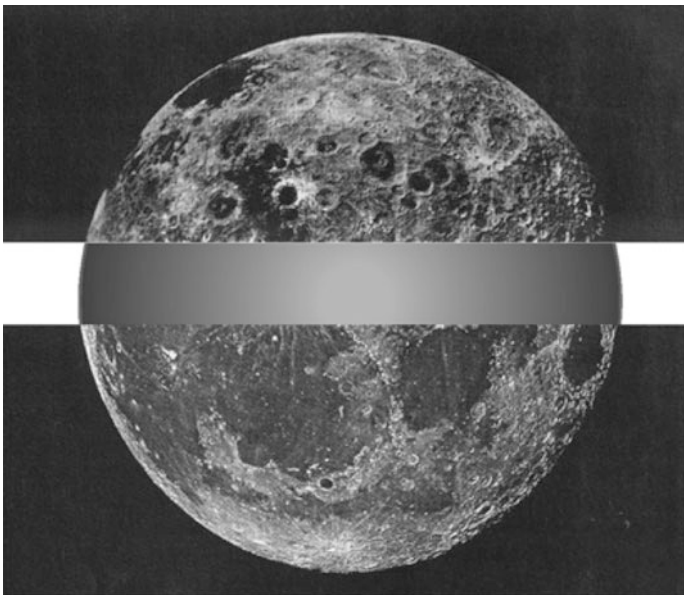

Fig. 6.14 The far side of the Moon from Soviet *Luna 3* spacecraft (*top*) compared with the near side (*bottom*) [from *Discovery Magazine* (Berman 2003)]

There are many anomalies that remain unexplained on the surface. The Apollo 11 astronauts returned a very high density, titanium-rich magma from the *mare basalts*. *Clementine* and the *Lunar Prospector* have identified areas with iron-rich soils in the maria on the near side and in the center of the South Pole-Aitken basin. Locations rich in thorium and KREEP (K = potassium, REE = rare Earth elements, and P = phosphorus) also are known. This indicates that the early Moon underwent intense melting and differentiation in which incompatible elements were concentrated in the molten part of an increasingly solid, crystallized system. The highest levels of thorium, a potential fission fuel, are in the upper left-hand part of the left image in Fig. 6.15, in the Oceanus Procellarum, but the reason, again, is not clear. The *Lunar Prospector* also discovered evidence of water ice at the Moon's north and south poles. The Moon's highlands are dominated by rocks primarily composed of the mineral feldspar. Feldspar is rich in calcium and aluminum. *Clementine* and the *Lunar Prospector* came as close as 7 km (4.3 st. mi) altitude and were able to precisely measure the variations in the Moon's gravity. The result was concentrations of mass ('mascons') higher than the average predicted by gravitational measurements in some of the youngest impact basins.

Clearly, there are wide variations of the Moon's physical and geological characteristics, and there is hardly any symmetry between the near and the far side of the Moon. A great deal of research is necessary to discover how the Moon was formed, what its structure is, and why. Understanding how the Moon was formed may provide insight as to how the inner planets of our Solar System were formed and some of the history of the Earth's development. Because of this diversity in the Moon's geology, there are many opportunities to produce engineering materials and possibly propellants in situ, as the resources on the Moon are developed. The Moon provides the opportunity to create an independent operational base that supports exploration of our Solar System.

The Moon has been also proposed as an astronomical observation site. The Hubble Space Telescope is a tremendous astronomical asset in understanding the development of the universe and in progressing toward resolution of the many uncertainties concerning star formation, quasars, visible and dark matter, and the early time in the universe after the spatial matter became transparent. However, Hubble is a high-maintenance item. Not because of its design or manufacture, but because of the way it must be maintained in Earth orbit. If the US Space Shuttle is not available to transport both crew and materials to Hubble, there is no crewed system that will permit Hubble to be maintained or repaired. If Hubble or its future replacement, the James Webb Space Telescope (JWST) planned to be orbited in 2018, was located on the surface of the Moon, then accessibility to re-supply from Earth and availability of a human repair crew would not require flying to an orbital location and working in zero gravity. If there is something that does not fit or is broken, the mission to the Hubble orbit is aborted, because there are no spares or repair facilities available nearby. On the surface of the Moon instead, all of the necessary facilities could be available for spare parts, parts repair, or part manufacture via possibly 3D printing utilizing Moon harvested materials. The location would have to be chosen on the Moon to enable maximum visibility of the space horizon of interest. A lunar surface telescope could

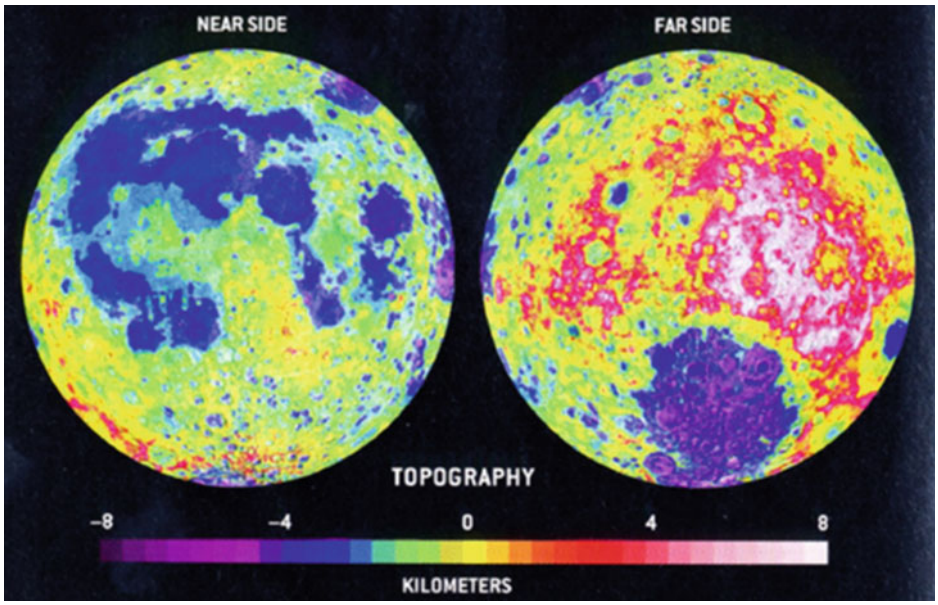

Fig. 6.15 Moon topography from the laser ranger measurements by *Clementine* and *Lunar Prospector* spacecraft [from *Scientific American* (Spudis 2003)]

Fig. 6.16 Photograph of Earth-rise from Apollo 10 command module in lunar orbit (Stafford 1991)

supplement Hubble and replace it when Hubble or the JWST is no longer maintained in orbit.

6.5.3 Manufacturing and Production Site

Given the Moon's wide variations in physical and geological characteristics, the opportunity exists to refine in situ critical spacecraft structural materials, that is, aluminum, titanium, and iron. A recent proposal by one of the authors (C. Bruno) is to use lunar dust to build structural materials using additive manufacturing and plasma torches powered by nuclear or solar power. With the gradual establishment of an infrastructure, Moon-based repair and maintenance facilities could be a part of the total system that enables the traffic and infrastructure envisioned in Chaps. 2 and 5 to become reality.

As the view of the Earth from the Moon is shown in Fig. 6.16, one should keep in mind that the Earth and the Moon are the closest natural Solar System objects locally available, and the infrastructure that permits the expansion of our exploration of the Solar System *needs to be established and maintained using these two initial elements as its foundation.*

Bibliography

Anon. (1984a) "Manned Lunar, Asteroid, and Mars Missions; Visions of Space Flight", Report No. SAIC/84-1448. SAIC, Schaumburg, IL, 1984, 82 pp.

Anon. (1984b) "A Manned Lunar Base: An Alternative to Space Station Science?", Report No. SAIC/84- 1502, SAIC, Schaumburg, IL, 1984, 31 pp.

Anon. (2015) "Declassified Manned Orbiting Laboratory (MOL) Records", National Reconnaissance Office, October 2015.

Batenin, V.M., Bityurin, V.A., Ivanov, G.S., Inozemzev, N.N. and Gorozhankin, P.A. (1997) "Electromagnetic Complex Concept for the Horizontal Start and Landing of a Reusable Air-Space Aircraft", IAC Paper IAF-97-V.5.10, *48th International Astronautical Congress*, Turin, Italy, 6–10 October 1997.

Bayón-Perez, S. (2002) "Design, Transportation, and Operation of a Food Supply Unit for the First Manned Mission to Mars", Master of Science thesis, Saint Louis University, St. Louis, MO.

Berman, B. (2003) "The World's Out of Balance", *Discovery Magazine,* Vol. 24, No. 12, 2003, p. 38.

Brown, C.D. (1998) *Spacecraft Mission Design,* Second Edition, AIAA, Reston, VA., January 1998

Brown, L. (2016) "Moon Express Payload Review Determination", Fact Sheet, FAA, 03 August 2016.

Bruno, C. (2008) "Mass Accelerators: Maglev and Railguns", in: *Advanced Propulsion Systems and Technologies: Today to 2020,* edited by C. Bruno and A. Accettura, AIAA, Reston, VA, Chapter 15, Section VI., 15 March 2008.

Bryce, I. (2001) "Deorbiting a Space Station Without Hitting Anyone", Space Travel, Space Daily, 13 March 2001.

Bussey, D.B.J., Fristrad, K.E., Schenk, P.M., Robinson, M.S. and Spudis, P.D. (2005) "Constant Illumination at the Lunar North Pole", *Nature,* Vol. 434, 13 April 2005, p. 842.

Covault, C. (2008) "Alternate Vision", *Aviation Week and Space Technology,* 17 November 2008, p. 29.

Eckel, H.A. and Schall, W. (2008) "Laser Propulsion Systems", in: *Advanced Propulsion Systems and Technologies: Today to 2020,* edited by C. Bruno and A. Accettura, AIAA, Reston, VA, 15 March 2008, pp. 370–372.

Gubanov, V. (1984) Private communication, European Space Conference, Bonn, Germany, 1984.

Hoffman, S.J and Niehoff, J.C. (1985) "Preliminary Design of a Lunar Surface Research Base", in: *Lunar Bases and Space Activities of the 21st Century,* ed. by W.W. Mendell, The Lunar Planetary Institute, Houston TX, 29–31 October 1985, p. 69.

Loftus, D. (1999) "Final Report on the MSE Technology Applications, Inc. MAGLIFT Project", MSE-TA Report NASA-28, September 1999

Marshall, T.C. (1985) *Free Electron Lasers*, MacMillan Publishing Company, 1985.

Martin, P.K. (2016) "NASA's International Partnerships: Capabilities, Benefits, and Challenges", IG-16-020, NASA Office of Inspector General, NASA, 05 May 2016.

Myrabo, L.N. (1982) "A Concept for Light-Powered Flight", AIAA 82-1214, presented at the *18th Joint AIAA/ASME/SAE/ASEE Joint Propulsion Conference*, Cleveland, OH, June 1982.

Myrabo, L.N. (1983) "Advanced Beamed-Energy and Field Propulsion Concepts", BDM Corporation publication BDM/W-83-225-TR, Final report for the California Institute of Technology and Jet Propulsion Laboratory under NASA contract NAS7-1000, Task Order RE-156, 31 May 1983.

Myrabo, L.N. (2001) "World Record Flights of Beam-Riding Rocket Lightcraft: Demonstration of 'Disruptive' Propulsion Technology", AIAA 2001-3798, presented at the *37th AIAA Joint AIAA/ASME/SAE/ASEE Propulsion Conference*, Salt Lake City, UT, July 2001.

Myrabo, L.N. et al. (1987) "Apollo Lightcraft Project", Final Report, in NASA/USRA Advanced Design Program, 3rd Annual Summer Conference Report, Washington, DC, June 1987, pp. 47–53.

Myrabo, L.N., Messit, D.G. and Mead, F.B. (1998) "Flight and Ground Tests of a Laser- Boosted Vehicle", AIAA 98-3735, presented at the *34th AIAA/ASME/SAE/ASEE Joint Propulsion Conference and Exhibit,* Cleveland, OH, July 1998.

Post, R.F. (1998) "Inductrack Demonstration Model", Report UCRL-ID-129664, Lawrence Livermore National Laboratories, 3 February 1998.

Post, R.F. (2000) "MAGLEV: A New Approach", *Scientific American,* Vol. 282, No. 1, 01 January 2000, pp. 64–69.

Spudis, P.D. (2003) "The New Moon", *Scientific American,* Vol. 289, No. 6, 01 December 2003, pp. 86–93.

Stafford, T. (1991) Editor "America on the Threshold – America's Space Exploration Initiative", Synthesis Group, Space Exploration Initiative, Chairman's Report to Congress, United States Government Printing, Washington DC, June 1991.

Sutter, J.D. (2010) "Obama Budget would Cut Moon Exploration Program", CNN, 15 March 2010.

Patent literature on MagLev

US4709883, Giuliani et al.
US5722326, Post.
US5652472, Tozoni.
US5565763, Arrendale et al.
DE3608499, Schmid.
DE3402755, Theurer.
WO8801245, Newman.

Exploration of Our Solar System

7

7.1 Review of Our Solar System Distances, Speeds, and Propulsion Requirements

Distances to places within our Solar System in Chap. 1 provided a yardstick to measure human ambition. The time for light, traveling at about 300,000 km/s, to cover the average distance Earth to Pluto is 5.45 h. The highest speed reached by a human object is probably the Cassini-Huygens probe, traveling to Saturn in 2004 at about 44 km/s, or 7500 times less than the speed of light. The minimum ΔV needed to reach Mars and destinations in the Earth neighborhood are extremely small compared with the speed of light (see Fig. 7.1).

However, because of the very low I_{sp} available with chemical propulsion, the mass that must be accelerated and ejected to produce thrust and ΔV is a large fraction of the total mass of a spacecraft, as stated by *Newton's second law* written in the form of Tsiolkovsky's equation. This law is a fact of life in our Universe. Thus, with technology based on chemical rockets, the only affordable strategy to explore planetary destinations is to accelerate spacecraft to no more than the minimum ΔV. That means acceleration lasting only minutes, followed by coasting (at zero acceleration) toward the destination. The simplest trajectory embodying this strategy is the Hohmann ellipse or combination of ellipses. Because the Hohmann ΔV are modest, the coasting speed will be similarly modest and equal to the sum of the ΔV to reach first LEO, and then, for instance, Lunar and Martian destination, see Fig. 7.1. Consequently, mission times are of order months and years.

A sense of the times needed to travel within our Solar System using chemical propulsion may be gained by imagining a hypothetical mission to one of the external planets, for instance to Neptune. The average distance, S, of Neptune from Earth is 30 AU, which translates into approximately 4.5 billion km. Table 7.1 shows that a rocket leaving Earth at escape speed (about 11.2 km/s) would reach Neptune in about 11.7 years, actually longer since Hohmann trajectories are not straight lines. A round-trip would last more than 23 years. For manned missions, these times are impractical not only because of the required propellant mass, but also of radiation dose exposure. Dose accrues with transit time, and the spectrum of solar and galactic radiation includes very high energies requiring massive shielding of crewed spacecraft and electronic equipment. Particle fluxes are especially intense near bodies possessing a magnetic field, like the giant planets (and Earth!) (Garrett 2010). It does not take long to conclude that traveling in the Solar System becomes feasible only if trajectories are faster at least by a factor ten, or if they proceed at nearly *constant acceleration*, rather than nearly constant speed. In both cases, the spacecraft must be accelerated far more economically than feasible today with chemical propulsion.

Let us consider a hypothetical trajectory to Neptune based on constant acceleration, a, until mid-course, followed by an equal deceleration to Neptune. Classical mechanics predicts a one-way time given by Eq. (7.1), where S and $S_{1/2}$ are distance and midway distance to Neptune, respectively. For a = 1 g (the Earth gravitational acceleration = 9.81 m/s^2), the round-trip to Neptune would take 15.5 days, not 23 years. Such acceleration would free a crew from all undesirable effects of microgravity or "weightlessness." Reducing a to 1/10 g would make the round-trip last a factor $\sqrt{10}$ longer, or about 46 days.

$$t = \sqrt{\frac{2 \cdot S_{1/2}}{+a}} + \sqrt{\frac{2 \cdot (S_{1/2} - S)}{-a}} = 2 \cdot \sqrt{\frac{S}{a}} \qquad (7.1)$$

These are attractive travel times, but can a spacecraft actually keep accelerating for two weeks or a month? The higher the acceleration, the shorter the trip time, but also the higher the thrust F and the propellant consumption rate $dm/dt = F/I_{sp}$. Since the vehicle initial mass must include the mass of all propellants needed by the propulsion system, and with a = thrust/vehicle mass, the answer can be found from

P.A. Czysz et al., *Future Spacecraft Propulsion Systems and Integration*,
Springer Praxis Books, DOI 10.1007/978-3-662-54744-1_7

the rocket equation and Newtonian mechanics. For a notional (straight) trajectory, Equation set (7.2a–7.2c) governs this problem:

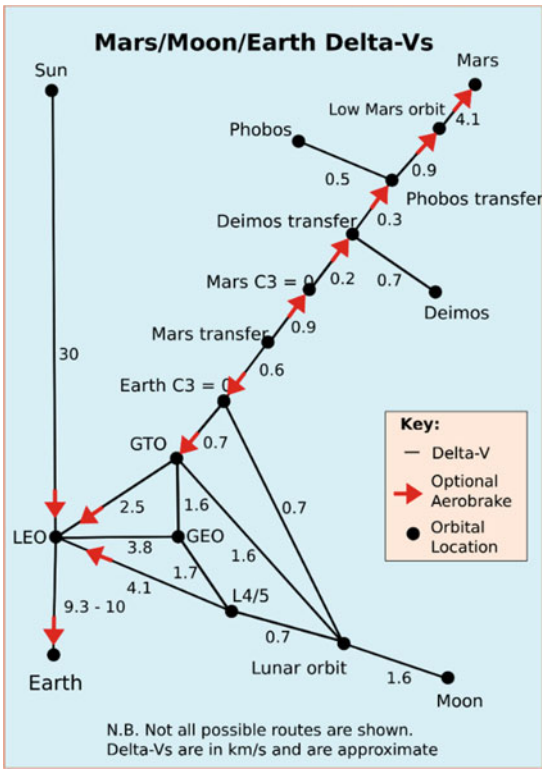

Fig. 7.1 Minimum ΔV to reach circumlunar and circum-Martian destinations with Hohmann trajectories in the inner Solar System (*Courtesy* Wikimedia Commons)

$$t_{1/2} = \sqrt{\frac{2 \cdot S_{1/2}}{a}} \tag{7.2a}$$

$$V_{1/2} = a \cdot t_{1/2} = a \cdot \sqrt{\frac{2 \cdot S_{1/2}}{a}} \tag{7.2b}$$

$$W_{\mathrm{R1/2}} = \exp\left(\frac{V_{1/2} - V_{\mathrm{orbit}}}{g \cdot I_{\mathrm{sp}}}\right) \tag{7.2c}$$

We obtain the gross weights for the flyby mission and the rendezvous mission as follows:

$$(W_{\mathrm{GW}})_{\mathrm{Flyby}} = W_{\mathrm{OWE}} \cdot (W_{\mathrm{R1/2}})_{\mathrm{from\,Earth}} \tag{7.3a}$$

$$(W_{\mathrm{GW}})_{\mathrm{Rendezvous}} = [W_{\mathrm{OWE}} \cdot (W_{\mathrm{R1/2}})_{\mathrm{to\,planet}}] \cdot (W_{\mathrm{R1/2}})_{\mathrm{from\,Earth}} \tag{7.3b}$$

In Eqs. (7.2a–c), the I_{sp} is in seconds. The $W_{\mathrm{R1/2}}$ is the weight or mass ratio either from Earth to the midpoint or from the midpoint to Neptune orbit. Assuming the best chemical I_{sp} = 459 s (≈4500 m/s), Table 7.2 reports results for two constant accelerations (10^{-2} and 10^{-4} g) and for boost-coast trajectories. If the mission is a flyby mission only, the weight ratio for departing Earth applies. If the mission is a rendezvous mission (that is, including orbit capturing), then the product or the two weight ratios (Earth → orbit and orbit → Neptune) apply, since slowing down and orbit capture requires a ΔV specific to the target. A rendezvous *boost-coast* mission to Neptune would have a total weight ratio about 15.5.

Consequently, flybys to Neptune with a 5000 kg spacecraft at 10^{-2}, 10^{-4} g, or a Hohmann boost-coast trajectory

Table 7.1 Our planetary system and its distances are very large on a human scale

Object	Mass (%)	Diameter (%)	Distance (%)	Time at c (min, h, day)	Time at escape V (day, year)
Sun	332,946	109.0	0.00	N/A	N/A
Mercury	0.060	0.38	0.30	2.493 min	132.018 days
Venus	0.082	0.95	0.72	5.984 min	142.018 days
EARTH	**1.000**	**1.00**	**1.00**	8.311 min	0.000 days
Mars	0.110	0.53	1.52	12.633 min	215.87 days
Asteroids			2.70	22.440 min	1.050 year
Jupiter	317.80	11.20	5.20	43.218 min	2.022 year
Saturn	95.17	9.40	9.54	1.321 h	3.709 year
Uranus	14.60	4.20	19.18	2.657 h	7.458 year
Neptune	17.25	4.00	30.05	4.162 h	11.684 year
Pluto	0.100	0.50	39.40	5.458 h	15.320 year
Kuiper Belt	40.0		30–50	5.541 h	15.553 year
Heliopause			100.00	254.0 days	38.883 year

Note 1 AU = $1.496 \cdot 10^8$ km. 1 AU is the average distance between the Earth and the Sun

Table 7.2 Neptune mission time and propellants are a function of acceleration

a (g)	1/100	1/10,000	Boost-coast
d (miles)	4.05E + 09	4.05E + 09	4.05E + 09
1/2 d (miles)	2.02E + 09	2.02E + 09	2.02E + 09
t (yr)	0.258	2.582	11.284
t (days)	94.31	943.14	4121
$V_{1/2}$ (km/s)	799.13	79.91	18.29
$V_{1/2}/c$ (%)	0.43	0.043	0.010
$W_{R1/2}$ (–)	7.52E + 77	1.25E + 07	10.28

imply lifting masses to Earth orbit equal to $3.76 \cdot 10^{78}$, $6.25 \cdot 10^{7}$ and 51.4 t, respectively. A rendezvous boost-coast mission with Neptune would require a departing mass of 77.5 t. A return to Earth for the boost-coast mission would have an Earth-departing mass of 797 t and require about 24 years. For comparison, the Saturn V rocket weighed about 2800 t at lift-off, but only about 5% of that mass reached Earth orbit. Thus, missions within our Solar System along Hohmann trajectories are cheap in terms of mass, but take lifetimes. With constant acceleration they would take only months or a few years at most, but would need an astronomical amount of propellant mass.

That explains why interplanetary spacecraft are low-mass, unmanned, and fly Hohmann trajectories achieved by short acceleration bursts. Hence, the constant search for propellants capable of higher I_{sp} since the dawn of the rocket age. In fact, hundreds of propellant combinations were tested to improve the liquid oxygen/alcohol/water combination the Germans used in their guided ballistic missile V-2 rocket (I_{sp} = 290 s). We know now that the I_{sp} of chemical propellants is limited by thermochemistry and that thermochemistry predicts that in space the liquid H_2/O_2 pair produces the highest practical $I_{sp} \approx 450$ s. Slightly higher I_{sp} are possible with propellants that are either too reactive and toxic (e.g., Fluorine), or too toxic and expensive (e.g., Beryllium). Increasing I_{sp} affords more thrust more economically and decreases mission time, see Table 7.2.

In chemical propulsion, I_{sp} is *the* key factor determining the flowrate of propellants burnt and thus launch mass and cost. This is completely different from ground transportation, where mass does not need to be ejected to produce motion; the reaction applied from the road surface to the wheels being sufficient. Power is the figure of merit in ground transportation which drives the cost. In contrast, for space transportation using chemical propellants, power has no interest: power is simply (dm/dt) times the heat of combustion (a constant). For instance, combustion of H_2 and O_2 produces 13.5 MJ per kg of mixture burnt. The 10^6 N thrust assumed in the Neptune mission needs to burn 222 kg/s, and the combustion power is about 3 GW, or that of five or six large utility power plants. Producing any amount of power is no problem in chemical rockets (1970s Rocketdyne brochures advertising the Space Shuttle main engine (SSME) boasted about the tens of *millions* hp developed at lift-off). The real problem is the rate at which mass needs to be ejected to produce reaction motion, and that is limited by I_{sp} equal, at most, to 450 s. Many hundreds or thousands of tons of propellants are burned in the few minutes of operation of the liquid and solid rocket engines of a space launcher such as Atlas 5 or Ariane 5. Table 7.3 shows the dramatic reduction of propellant (weight ratio W_R) and mission time if I_{sp} could be raised by a factor 2.3 and 10 with respect to the best available I_{sp} today with chemical propulsion.

Chemical propulsion is capable of very high thrust but its propellant consumption limits its operation time to minutes. When the Saturn V took off on July 16, 1969 for its manned Moon mission, the thrust of its first stage was about 3,400,000 lb_f, or 15.4 MN, but lasted only for about 10 min. Most of the energy expended was not used to orbit the Lunar Module, crew, and the reentry vehicle: it was spent to lift the very propellants to accelerate to orbit, in other words, to lift and accelerate itself. A 130 hp motorcar traveling at 180 km/h (110 mph) has a specific impulse of about 21,500 s: more than 40 times better. Any gasoline-powered car gets better "mileage" than any chemical rocket engine.

It is for these reasons that almost all interplanetary missions do reach escape speed by short bursts of thrust: short accelerations limit total propellant mass. In practice, since escape speed from Earth is 11.2 km/s, maximum spacecraft speed is not far from that. Higher speeds can be reached more economically only by means of *gravitational assists*, that is, by flying trajectories purposely designed to swing-by planets and gain some of their kinetic energy. For instance, the Cassini-Huygens spacecraft left LEO at about 12 km/s, and four swing-by's later (twice near Venus and once near Earth and Jupiter) approached Saturn at about 40 km/s. Planet swing-by is cheap, but is constrained by planetary positions ('ephemerides'), so mission trajectories may last a decade or more. Typical deep space missions start by an initial high thrust lasting minutes and are followed by either plain coasting or painstakingly planned swing-by(s). When feasible, this strategy saves mass but stretches mission time to years, see Fig. 7.2.

Table 7.3 Increasing I_{sp} reduces transit time and weight ratio

	Year		
Jupiter	2.69	1.70	0.793
Saturn	4.92	3.12	1.45
Uranus	8.14	5.16	2.40
Neptune	11.15	7.07	3.29
Kuiper Belt	11.13	7.06	3.29
Pluto	13.75	8.72	4.06
Kuiper Belt	16.29	10.34	4.81
Heliopause	27.86	17.67	8.22
I_{sp} (s)	459	1100	4590
W_R (–)	10.70	7.23	3.38

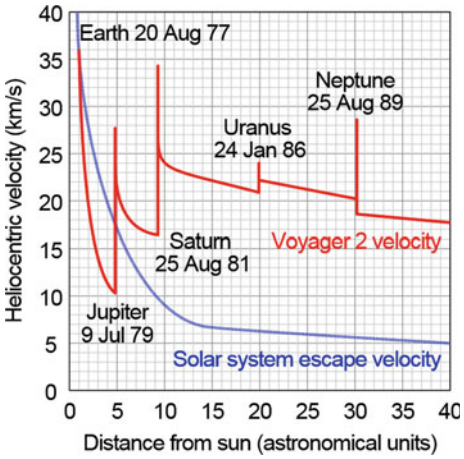

Fig. 7.2 Voyager 2 velocity reboosting used multiple gravity assists (*Courtesy* Wikimedia Commons)

Figure 7.2 plots the Voyager probe speed relative to the Sun. The initial velocity decreased because of Sun attraction so long as it was less than the escape velocity from the Solar System. Near Jupiter, the acceleration boosted the probe above the local escape speed, and from that point on all gravity assists increased its velocity until Voyager left the Solar System for good, more than ten years after launch.

In some instances, a round-trip mission may last almost the professional life of its ground team, and if the ship is manned, a sizable fraction of the crew life. At about constant speed and in absence of specific remedies, the crew would live in microgravity absorbing a steadily growing radiation dose, with irreversible health consequences on bone mass and enzymatic functions. A mission to the far edge of our planetary system, the *Oort Cloud*, believed to be the birthplace of comets (see Chap. 8), entails traveling 50,000 AU. At Earth escape speed, it would take about 17,000 years.

Thus, the so-called *conquest of space*, see the classic literature by Ley and Bonestell (1959), Kaplan et al. (1952), is a meaningless word without ways of shortening travel. Hard as it is to move in the Earth's immediate vicinity, interplanetary travel is much harder, beyond anything that can be reasonably expected of chemical propulsion. No advances can be forecast in chemical propulsion, simply because the energy it can release is limited by thermochemistry to not much more than 10 MJ/kg. Reasonably short interplanetary missions need reasonable initial accelerations. This means thrust maintained for days and weeks, not minutes. This also means substantial power.

Interplanetary and space travel awaits a step change in propulsion: that is, means to raise I_{sp} by at least a factor two. At fixed thrust, doubling I_{sp} halves propellants consumption. However, if thrust is obtained from the thermodynamic expansion of hot products, this also raises the power requirement needed to accelerate and exhaust propellants by a factor 8, since power scales with jet velocity cubed. Propulsion systems with higher I_{sp} must have much higher power adequate to maintain that I_{sp} and the thrust needed.

7.2 Alternative Energy Sources: Nuclear Energy

Making interplanetary travel time practicable for crewed and robotic missions means new propulsion systems and new ways of generating power must be sought. For instance, a worthy goal is to double the I_{sp} of chemical rockets without reducing their range of thrust. To make spaceships reasonably small, that is, to save propellant mass substantially, I_{sp} must at least double.

In textbooks, the I_{sp} in *chemical* rockets usually depends (scales) on combustion temperature T and average molecular weight, MW, according to the one-dimensional rocket equation:

$$I_{sp} \propto \sqrt{\frac{T}{\mathrm{MW}}} \tag{7.4}$$

The I_{sp} of rockets powered by liquid H_2/O_2 is the result of the low molecular weight (about 9–10) of combustion gases,

since they contain not only H_2O (MW = 18), but also excess H_2 (MW = 2). Chamber temperatures drop with excess H_2, but the ratio T/MW keeps growing up to a hydrogen excess fraction of order 30%.

Equation (7.4) shows that increasing I_{sp} in chemical rockets means either raising T or lowering MW, or both. The first choice is constrained by thermochemistry and structural limits: the strength of materials is determined by their chemical bonds and these weaken with increasing temperature. Liquid rocket walls are therefore cooled to less than 1000 K while the gas they confine may reach 3500 K. Thermochemistry limits higher gas temperatures; some solid propellant combinations may include metals and exceed 3500 K, but MW is also higher than 9–10 of the H_2/O_2 pair and I_{sp} is only about 300 s. Similarly, hybrid rockets, where one of the propellant is solid and the other is liquid, like in the Virgin Galactic *SpaceShipOne* and *SpaceShipTwo*, have an I_{sp} less than 300 s. If feasible, higher gas temperatures would be welcome, because they raise I_{sp}. The question is how to reach them.

Taking Eq. (7.4) at face value would beg the question of how to reach higher temperatures. In fact, temperature is really the indicator of internal energy. The one-dimensional conservation of energy equation states that in any process the rate of potential energy E_p decrease must become exactly the rate of kinetic energy E_k increase. Applied to a rocket, at steady state the energy equation becomes:

$$\frac{dE}{dt} = \frac{1}{2}\left(\frac{dm}{dt}\right) \cdot V_e^2 \tag{7.5a}$$

$$V_e = \left(\frac{2 \cdot E}{m}\right)^{\frac{1}{2}} \equiv (2 \cdot J)^{\frac{1}{2}} \tag{7.5b}$$

where J is the potential energy per unit mass and V_e the speed of the mass ejected. With chemical propellants, the internal energy E is that of chemical bonds. Chemical energy is nothing else than the potential energy of the fundamental *electro-weak force*, that is, of the Coulomb forces acting among negative electron shells and positive nuclei of atoms and molecules. The number of fundamental forces in *nature* is just three: (1) *gravitational*, (2) *electro-weak* (including Coulomb), and (3) *nuclear* (also called the "strong force"). Thus, the quest for higher temperatures producing higher I_{sp} should really be a quest for *energy* alternatives, and here, there is not much choice: discarding gravity, the only alternative is the nuclear energy binding neutrons and protons inside the atom nucleus.

Nuclear energy means *fission*, *fusion* (including antimatter annihilation, an extreme form of fusion), or *relaxation* of metastable nuclei. The first suggestion of nuclear fission for interplanetary missions was made in 1946 (Shepherd 1946). By analogy with combustion, matter fissioned, fused, or relaxed is still called "nuclear fuel," or simply fuel; fission fuels are discussed in Sublette (2001). In combustion, what is accelerated and ejected is what has been burnt. In contrast, in nuclear energy the two processes may be separate.

In fission or fusion, the energy release occurs always in the form of kinetic energy of nuclear products, the so-called fission or fusion fragments possessing energies in the range $1–10^2$ MeV. What is meant by fragments is nuclei, particles, or electromagnetic radiation. Their momenta can itself be the thrust source. Alternatively, their energy could be transferred to inert matter. This matter may be a propellant expanding in a nozzle, as in a chemical rocket, or could be a working fluid in a thermodynamic cycle producing electricity fed to an electric thruster; this second option decouples temperature of the power source from I_{sp}. In any event, whether and how to transfer energy from nuclear source to propellant is crucial, shaping different concepts differently (Bruno 2005, 2008, 2014).

This chapter will focus mostly on fission propulsion systems for interplanetary missions; fusion is discussed in Chap. 8 for missions to the far edge of our Solar System and (maybe) beyond.

In fission the nuclei of atoms of nuclear "fuels" such as ^{235}U, ^{239}Pu, ^{233}U, ^{232}Th are split (fissioned) by neutrons. Neutrons are always spontaneously emitted by these fuels (they "decay"); these neutrons can fission other nuclei and release significant energy only if the budget between neutrons produced and neutrons escaping the fuel is positive ($k_{eff} > 1$). In a fission bomb, this criterion defines a "critical" fuel mass. Using the electron-volt (eV) as energy unit ($1\ eV \approx 1.6 \cdot 10^{-5}$ J), fissioning ^{235}U may emit fission fragments with energy up to 160 MeV, to be compared to a fraction of eV typical of combustion products. The fission heat release per unit propellant mass, J, is vastly larger than that released by burning a unit mass of H_2/O_2 in a chemical rocket ($J = 1.35 \cdot 10^7$ J/kg). In fact, any fuel mass is converted into energy according to $E = \Delta m\ c^2$; the energy per unit mass available from ^{235}U fission is approximately $8.2 \cdot 10^{13}$ J/kg, almost 10^7 times larger than in combustion, see Fig. 7.3. This energy must be released in a reactor, where it is converted to kinetic energy of a propellant or to high temperature of a working fluid.

Information on fission is readily available, and a classic primer is Glasstone (1955). Fission physics for propulsion applications can be found in Hill and Peterson (1970), Bussard and DeLauer (1958), Angelo and Buden (1985), Lawrence et al. (1995), Turner (2005). Reactor technology will be discussed only insofar it does impact on propulsion. It is important to emphasize that the release of nuclear energy in a reactor is unlike that by an atomic bomb. No nuclear reactor can explode like an atomic bomb, since the critical mass (a few kilograms of U in a sufficiently small volume) is physically impossible to achieve. In commercial

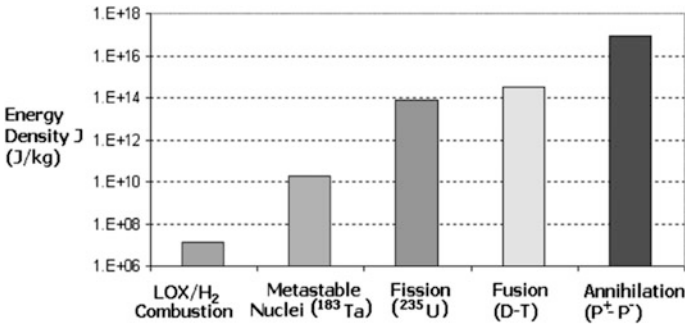

Fig. 7.3 Comparison among chemical and nuclear sources. Note the logarithmic scale

reactors, the most common type, nuclear fuel is always alloyed for structural and neutronics reasons (pure U metal melts at only 1135 °C) and is partitioned into individual modules, called fuel "bars," "rods," or "pins" depending on their shape. Figure 7.4 shows an old fuel bar design from one of the NERVA reactors mentioned in Sect. 7.5. There is literally no way the fuel can reach critical mass when distributed among bars and alloyed with a moderator material.

Because of the Chernobyl "accident" and Fukushima disaster, there persists confusion among the public between a *nuclear* explosion (that of an atomic bomb), and a *thermal* explosion caused by reactor overheating and/or melting down. What happened in Chernobyl was due to overheating following the deliberate, foolhardy shutdown of the cooling system to check the spin down time of the reactor turbine. Overheating caused the graphite moderator to catch fire, not an atomic explosion (Del Rossi and Bruno 2004, 2008). Loss of coolant was also the cause of the disaster at Fukushima, this time due to flooding and breakdown of the cooling pumps by the Great Eastern Japan Earthquake and the following tsunami. In neither case, an atomic explosion occurred.

Nuclear thermal rockets (NTR), one of the two fission-based propulsion modes or strategies, are miniature nuclear power reactors. Standard reactors have a solid "core" made of an assembly of bars containing nuclear "fuel." The most common isotope nuclei capable of fissioning are Uranium and Plutonium, but others exist: these isotopes may be in the form of alloys, of ceramics, in pellets, or in the liquid/gaseous state. For instance, in most commercial reactors, solid ^{235}U-enriched fuel inside bars fissions, releases heat to a coolant flowing through the bar channels and is expanded in a turbine producing electricity. In a space reactor, the coolant (for instance, hydrogen) is ejected from a nozzle; so in a NTR, the coolant is also the propellant. In NTR fission, heat release occurs inside solid bars, limiting temperature to what the bar can tolerate without cracking, corroding, or melting. More advanced concepts to bypass the melting point of Uranium-based fuels include liquid and gaseous fuel cores. The issue of high-temperature materials is critical in all thermal rocket engines, because it controls and limits the I_{sp} that can be obtained.

Until recently, solid fuel temperatures above 2500–3000 K were thought unrealistic: UO_2 melts at 2800 °C, UC at 2400 °C and UN at 2630 °C. In solid-core reactors, fuel inside bars (also called rods or pins depending on their shape) is surrounded by a cladding, e.g., NbC ceramic: this

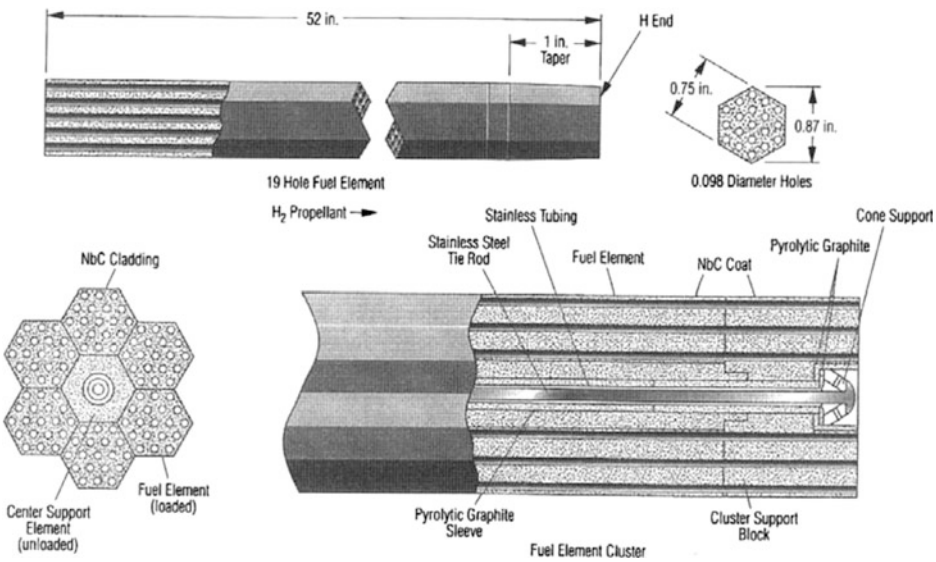

Fig. 7.4 Structural assembly of a NERVA-type fuel bar (Gunn 2001)

may weaken or melt at temperatures much lower than those of the fuel. Progress in additive manufacturing and in superalloys such as PWC-11, containing Nb and Zr carbides, or as T-111, consisting of Ta with small percentages of Hf and W, and with melting temperatures 2700–3200 °C, may eventually raise the operational temperature of future space reactors (Do Nascimento et al. 2015). Binary and ternary ceramics (e.g., Ta_4HfC_5, melting at 4263 K) might enable 4000 K liquid core reactors; hydrogen would be heated close to the same temperature and I_{sp} would reach about 1200 s (Maxwell et al. 2013). The issue of materials for nuclear reactors is complex, involving not only mechanical strength, but also the effect of slow and fast neutrons in creating defects, hot corrosion, fission poisoning due to fission fragments embedding in the original fuel, and the all-important neutron budget controlling criticality. Researchers Nascimento et al. (2015) summarizes these issues.

Besides fission and fusion, the third nuclear energy source is associated with so-called metastable nuclei, also called nuclear "isomers." These are materials in which the atomic nucleus is "strained," that is, where the arrangement of nucleons (neutrons and protons) does not correspond to the minimum energy state (Mukhin 1987, Sect. 2.3.2; Myers and Swiatecki 1966). Such nuclei may be made to "snap back," like a stretched rubber band or a crumpled plastic bottle, reaching their stable configuration and releasing excess energy. Because these nuclei do not split, but simply rearrange their nucleons, the energy release is intermediate between fission and chemical reactions. Generally, neutrons are not emitted and radiation is limited to soft X- and gamma rays; shielding is still necessary, but easier to deal than in fission.

The energy available from metastable nuclei found in nature (e.g., ^{178m}Hf, or ^{180m}Ta) varies from approximately 2.4 MeV (Hafnium) to approximately 75 keV (Tantalum). Per unit mass, these energies are 10^2–10^4 times smaller than in fission, but 1000 times larger than in combustion: a cm^3 of pure ^{180m}Ta holds 300 MJ, or 10,000 times the energy released by the same volume of gasoline burnt in air (Walker and Dracoulis 1999). Natural nuclear isomers are stable but rare, in the case of Tantalum, about 100 ppm compared to the most common tantalum isotope. However, artificial isomers can be "bred" in nuclear reactors.

The main issues of metastable nuclei fuels are their natural scarcity or breeding process, the technology and cost of separating them from their stable brothers, their geographic provenience, and especially how to trigger their energy release in a controlled way. Progress about this last issue seemed or seems at hand (Belic et al. 1999; Kirischuk et al. 2015), but the potential for military applications has made information on this topic very sensitive, scarce, hard to get and/or very controversial. All these problems notwithstanding, this nuclear energy source is of much interest; applications to high-altitude, long-endurance (HALE) UAV have been discussed (Hamilton 2002). Still, much theoretical and experimental work should be carried out before this interesting nuclear energy source can become practical.

7.3 Limits of Chemical Propulsion and Alternatives

Considerations made in the previous sections should convince that chemical propulsion is inadequate for crewed interplanetary missions. With I_{sp} at most of order 450 s (≈4500 m/s), most of the mass of the propellants is spent accelerating the propellants themselves, and payload is 1–3% of the initial launcher mass to low Earth orbit (LEO ΔV of order 8 km/s), the first and costliest step of interplanetary missions. In fact, the Tsiolkovsky relationship

$$\Delta V = g_0 \cdot I_{sp} \cdot \ln\left(\frac{M_{initial}}{M_{final}}\right) \tag{7.6a}$$

$$\frac{M_{initial}}{M_{final}} = \exp\left(\frac{\Delta V}{g_0 \cdot I_{sp}}\right) \tag{7.6b}$$

shows that the argument of the exponential is easily greater than one for chemical propellants, so that $M_{initial} \gg M_{final}$. It just happens that due to Earth's gravitational field, the ΔV to reach low Earth orbit is numerically about twice the best chemical I_{sp}. Hence, a dramatic improvement would follow simply if I_{sp} could be doubled. Yardsticks to measure "advanced" interplanetary propulsion to explore the Solar System might therefore be:

(1) I_{sp} increased by a factor 2 (to lower propellant consumption), and, simultaneously,
(2) thrust "high" enough to ensure acceleration and ΔV reducing Mars transit to less than three months (radiation dose to crew less than 0.3 Sv, see Appendix A).

Meeting these two conditions poses an impossible challenge to chemical propulsion because of fundamental thermochemistry, since power $P \sim (V_e)^2 \sim (I_{sp})^3$. Thermochemistry limits the maximum temperature of exhaust products, that is (Boltzmann) their molecular kinetic energy and thus their bulk velocity V_e, equal to specific impulse in an ideal expansion. Regarding the first limitation of chemical propulsion, if I_{sp} (or V_e) could be doubled for the same thrust F, the propellant consumption $dm/dt \equiv \dot{m}$ (in kg/s) would be halved since at constant thrust

$$\dot{m} = \frac{F}{V_e} = \text{constant} \tag{7.7}$$

but the power demand would increase eight times. So, increasing propulsion efficiency (that is, I_{sp}) means reducing the *mass* flowrate of propellants, *not the power* required to accelerate them. The power will inexorably increase.

In chemical propulsion, jet power

$$P = \frac{1}{2} \cdot \dot{m} \cdot (V_e)^2 \tag{7.8}$$

grows with $(V_e)^3$ if F is not kept constant, but keeping the same thrust F and raising I_{sp} results in

$$P = \frac{1}{2} \cdot \left(\frac{F}{I_{sp}}\right) \cdot (V_e)^2 = \frac{1}{2} \cdot \left(\frac{F}{I_{sp}}\right) \cdot (I_{sp})^2 = \frac{1}{2} \cdot F \cdot I_{sp} \tag{7.9}$$

where P is simply proportional to I_{sp}. Power per se is not an issue in chemical propulsion since it is simply determined by the mass flowrate of propellants consumed: this last is the real issue. Power becomes a concern with propulsion systems other than chemical. For instance, if I_{sp} = 900 s ≅ 9000 m/s and F = 10 t ≅ 10^5 N, the thrust power P = ½ F I_{sp} must be 0.45 GW, and generated without recourse to combustion. In general, increasing propulsion efficiency (that is, I_{sp}) means reducing the *mass* consumption of propellants, but *not necessarily the power* required to accelerate them.

Regarding the second limitation of chemical propulsion (limited ΔV "slowing" interplanetary travel), the yardstick suggested is based on the time for human missions. Outside the Van Allen belt, shielding from cosmic and solar radiation becomes so difficult or impractical that astronaut permanence in space should be limited to at most one year with current technology. Depending on destinations, this translates into ΔV of order many tens or hundreds of km/s. Section 7.1 indicates that to achieve these speeds, the propulsion system must be capable of sustained acceleration for days or weeks, with mass and power consumption unaffordable by chemical means.

Because only three fundamental forces exist in nature, the only alternative to chemical propulsion is propulsion utilizing nuclear power. Nuclear power converts fuel mass into energy according to $E = mc^2$; the energy density J available in fission is about $8.2 \cdot 10^{13}$ J/kg using ^{235}U, almost 10 million times larger than in chemical combustion. This factor alone does justify nuclear propulsion. However, how to exploit such energy is one of the key questions. Section 7.2 pointed out that solid-core nuclear reactors cannot operate for long at temperatures much higher than, say, 2500–3000 K. At a first glance, a clear advantage of the nuclear heating in so-called nuclear thermal rockets (NTR) over H_2/O_2 combustion, characterized by similar temperatures, is not evident. However, in NTR the propellant can be pure hydrogen, and its molecular weight, 2, is much lower than the average 9–10 of the burnt gas produced by H_2/O_2 rocket engines. At the same temperature, an NTR ejecting pure hydrogen will have I_{sp} higher by the square root of the molecular weight ratio, (9 or 10)/2, i.e., by a factor of about 2.2. In fact, in space the best I_{sp} of liquid rocket engines is about 450 s; the I_{sp} of NTR tested in the past was 880–900 s. Furthermore, if a nuclear reactor in space can be operated above 2500 K, a fraction of hydrogen is present as H atoms (MW = 1), so that I_{sp} could be close to 950–1000 s.

I_{sp} in this range is very appealing for interplanetary travel, since the mass ratio is inversely proportional to I_{sp} according to the Tsiolkovsky equation, see Eqs. (7.6a, b). Thus, raising I_{sp} from 450 s of a chemical rocket to 1000 s of an ideal nuclear thermal rocket would reduce the total mass of propellants needed to reach LEO by a factor 2.5. This is as if the lift-off mass of the US Shuttle, about 2800 t, was reduced to 800 t.

In summary, both physics and engineering point to *nuclear propulsion* as the key to practical space exploration (Powell et al. 2004a).

7.3.1 Energy Sources and Specific Impulse

The fundamental limitation of chemical propulsion is "low" I_{sp}. Leaving aside its historical units, in an ideal (complete, isentropic one-dimensional) expansion in a nozzle, I_{sp} coincides with the exhaust velocity, V_e, and for the sake of simplicity in all the following, I_{sp} and V_e will be assumed practically the same. This velocity determines the kinetic energy of the flow, ideally equal to the chemical energy released in the combustion chamber. That is, propellants combustion forms molecules of average mass m, possessing high translational, rotational and vibrational energy E, and very little orderly bulk flow velocity. When the hot gas expands in the nozzle, molecular collisions gradually force all molecules to acquire the same *orderly* bulk flow velocity V at the expense of internal energy E. At the nozzle exit, in the ideal case, this velocity is

$$V_e = \left(2 \cdot \frac{E}{m}\right)^{\frac{1}{2}} \tag{7.10}$$

(we neglect relativistic effects). The ratio E/m is the energy density, J, determined by thermochemistry to be about 10^7 J/kg at most. The limitation on V and I_{sp} is due to the limited potential E of the *electro-weak force* that binds atoms and molecules.

In the previous section, the gain in I_{sp} due to using nuclear energy has been estimated based on the gain in J. In the following, this issue is approached using special relativity.

In all three nuclear processes of Sect. 7.2 energy is released by converting fuel mass into energy. When ^{235}U fissions, the mass of its fission fragments becomes slightly less than the mass of ^{235}U. A certain percentage, α, of the initial mass disappears, converted into kinetic energy (E_k) of the fission fragments, according to

$$E_k = \Delta m \cdot c^2 \tag{7.11}$$

Since c, the speed of light, is $3 \cdot 10^8$ m/s, the energy released is very large on a human scale. To a factor c^2, the mass lost is exactly the decrease of the potential energy of the nuclear force binding neutrons and protons. In Newtonian physics, mass and energy are separate quantities, each separately conserved in any transformation. However, in relativistic physics it is the sum

$$m \cdot c^2 + E_k \tag{7.12}$$

that is conserved. Note that m is the *relativistic* mass given by

$$m = \frac{m_0}{\sqrt{1 - \left(\frac{V}{c}\right)^2}} \tag{7.13}$$

where m_0 is the rest mass (body at rest).

Fission transforms potential energy of the nuclear force in E_k of the fragments, with J of order 10^{13} J/kg. The potential energy of a mass m of fuel that can be converted to E_k is α mc^2, with $\alpha < 1$:

$$\text{Fuel Potential Energy} = \alpha \cdot m_{\text{fuel}} \cdot c^2 \tag{7.14}$$

The effect of fission is to convert the potential energy of the nuclear force binding nucleons together into kinetic energy of nuclear "fragments" (nuclides, neutrons, alpha and beta particles, photons and other nuclear particles). Through collisions with molecules of a propellant present as mass M_p, the E_k of fragments is transferred to propellant molecules and becomes internal energy. To produce thrust, the hot fluid is expanded in a nozzle where internal energy becomes again the kinetic energy of bulk gas ejected at speed V. To calculate the ideal velocity V reached by a mass M_{ppl} of propellant after $\alpha \cdot m$ mass of fuel fissions, a relativistic energy balance must be written. Approximating (for simplicity) E_k with only $\frac{1}{2} \cdot m \cdot V^2$, that is, neglecting neutrino and photon energies, the energy balance becomes (Bruno 2005, 2008)

$$m_0 \cdot c^2 = (1-\alpha) \cdot m_0 \cdot c^2 + \frac{1}{2} \cdot \frac{m_0 \cdot (1-\alpha) \cdot V^2}{\sqrt{1 - \frac{V^2}{c^2}}} + \frac{1}{2} \cdot \frac{M_{ppl_0} \cdot V^2}{\sqrt{1 - \frac{V^2}{c^2}}} \tag{7.15}$$

where m_0 and M_{ppl0} are the fuel and the propellant mass *at rest*. Rewriting this equation, and defining

$$A \equiv \left\{ \frac{\left[(1-\alpha) + \frac{M_{ppl_0}}{m_0}\right]}{2 \cdot \alpha} \right\}^2 > 0 \tag{7.16}$$

the complete solution for the exhaust velocity V (or ideal I_{sp}) $(V/c)^2$ due to relativistic mass conversion into kinetic energy can be found

$$\frac{V^2}{c^2} = \frac{-1 + (1 + 4 \cdot A)^{\frac{1}{2}}}{2 \cdot A} \tag{7.17}$$

showing that in the limit $\alpha \to 1$ (that is, if all fuel is converted into energy, as in matter–antimatter annihilation) and if no inert mass M_{ppl} is added, the velocity V tends to the speed of light c. If inert mass M_{ppl} is added, the limit velocity is less than c.

The normalized exhaust speed V/c is plotted in Fig. 7.5 for three M_{ppl}/m ratios (1000, 10,000 and 100,000) and for the special case $M_{ppl} = 0$. For clarity, the three curves for nonzero M_{ppl} have been plotted after scaling them by 10. Note that V may become comparable to c only for α close to 1. Fission processes occur with much lower mass conversion α, of order 10^{-3}: in ^{235}U fission α is $9.1 \cdot 10^{-4}$. Adding propellant mass M_{ppl} reduces the exhaust velocity V (or I_{sp}) rapidly, but this is necessary not only to keep the reactor at reasonable temperature, but also to produce significant thrust. In fact, the kinetic energy of fission fragments is about 160 MeV/fragment, where 1 eV corresponds to about 11,300 K, and no material would be able to stand fission temperatures. The M_{ppl} constraint explains why past NTR had $I_{sp} < 900$ s. Fusion occurs at α of order 0.003–0.004 (see Chap. 8). Only complete matter–antimatter annihilation proceeds with $\alpha = 1$, and the theoretical speed becomes c.

The special case of $M_{ppl} = 0$ means that all the energy developed by fission ends as kinetic energy of the fragments. Conceptually this means fission products themselves are the propellant, ideally ejected with all their kinetic energy, and perfectly collimated. Such ultimate propulsion has been proposed at the Lawrence Livermore National Laboratories to maximize I_{sp} (Chapline et al. 1988). Thrust would be

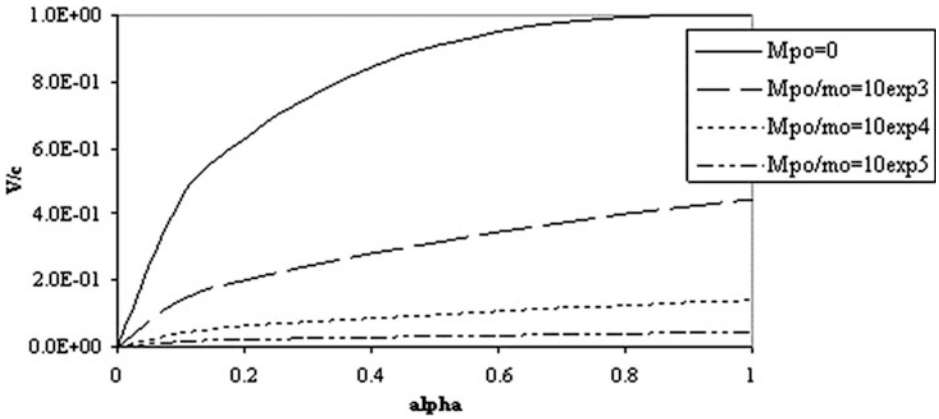

Fig. 7.5 Velocity gained by fuel mass left after fission as a function of percentage α of mass fissioned. The three lower curves are multiplied by a factor 10 for clarity. M_{ppl0} is the rest mass of inert propellant added

extremely modest in this strategy: the mass of fuel fissioning per unit time is naturally low, of order of 0.1 g/s for a 1-GW reactor; a 1-GW rocket with $I_{sp} = 10^5$ s would produce thrust of order 1000 N.

Are there ways to raise I_{sp} above that of NTR? The answer is yes and comes at a price. The alternative is to convert potential energy to electricity powering an electric thruster. Electric thrusters accelerate charged particles by applying a Coulomb or Lorentz force directly to each charged mass particle, not through molecular collisions, see Sect. 7.15. This strategy involves an extra step: fission fragments are first thermalized inside a working fluid. Using a Brayton or Stirling cycle fluid expansion produces mechanical power to drive an electric generator. MHD generators or other direct conversion systems are in principle possible (Bidault et al. 2004). Finally, the generator feeds an electric thruster. The price of this strategy is the low efficiency of converting thermal energy into electricity.

7.3.2 The Need for Nuclear Space Propulsion

The two nuclear propulsion strategies, consisting of either converting fission energy into *kinetic energy of a propellant* (nuclear thermal propulsion, NTP), or into *electricity powering an electric thruster* (nuclear electric propulsion, NEP), have many variants. Historically, nuclear propulsion focused on the first strategy because ICBMs were the original application (see the historical perspective in Sect. 7.5). NTP engines with thrust up to 400 kN and I_{sp} close to 900 s were designed, built, and bench tested in the USA and the Soviet Union for two decades (Gunn 1998). More recently, interest in interplanetary scientific missions to Jupiter's icy moons (JIMO) shifted focus to high-I_{sp} solar-energy propulsion (SEP) and then to NEP, the second strategy. One reason was the I_{sp} in the 1500–4000 s available from off the shelf Hall and gridded ion thrusters. For human missions to Mars, NTP seems best in terms of recurring costs (propellant mass) and, especially, reduced radiation dose due to faster transit (see Appendix A), although the cost of development will be significant compared to well-proven chemical propulsion. For cargo missions, where transit time is less important, SEP and NEP seem more appropriate and less costly.

In the end, which strategy works best depends on the specific mission, not on technology. For the foreseeable future, all missions will leave from LEO, with the possible exception of human Mars missions that NASA might plan to stage from circumlunar orbits. Reaching escape speed is more efficient at high thrust than by using electric thrusters: these force slow spiral trajectories carrying significant gravity losses. On the other hand, once the spacecraft is on a hyperbolic orbit, a constant or even weak thrust can save much propellant and achieve very high transit speed. Combining the two strategies may prove to be the best for human interplanetary missions.

In summary, fundamental physics teaches us that the only non-chemical source of energy for space propulsion is nuclear. Per unit mass, nuclear fuels pack 10^7 times the energy of chemical propellants. Nuclear reactors have been built and tested since the 1950s with no accidents. Fission can meet the two ideal requirements of lowering propellant consumption while still keeping thrust reasonable, that is, comparable to that of conventional rockets. This flexibility, independence from propellant, large I_{sp}, and large power in a compact package suggest nuclear propulsion as the only practical means of reaching the planets of our Solar System (Claybaugh et al. 2004). Thrust and power are no constraints using nuclear propulsion. The problems are engineering and not physics issues, and the technique of using power efficiently, that is, about specific utilization strategies. These are briefly examined below.

7.4 Nuclear Propulsion Strategies

As power scales as the product of thrust T times specific impulse I_{sp}, for a given reactor power the next question is: "How large should I_{sp} be and still produce reasonably high thrust, so that also mission times will be reasonable?" Does it make sense to rebuild GW-class reactors built in the 1960s and 1970s? What are the trade-offs between I_{sp} and thrust?

The answers to all these questions depend on the specific mission. At fixed reactor power most questions can be rephrased as: "For a specific mission, what is the best way to exploit the power available?" Comparing nuclear thermal to nuclear electric strategies helps in making future choices and in steering resources and investments.

Using solid-core reactors, nuclear thermal propulsion can double the I_{sp} of chemical rockets to about 900 s. Solid-core reactors were the first and still the only ones to be developed (see Sect. 7.5). Thrust is obtained as in chemical rockets, by thermodynamically expanding a propellant, typically hydrogen. Specific impulse is limited only by maximum structural temperature.

Acronyms typical of this class of propulsion are nuclear *thermal* propulsion (NTP) and nuclear *thermal* rocket (NTR), since the primary mode of propulsion is based on *thermalizing* fission products. Thermalizing converts the kinetic energy of fission fragments to molecular kinetic energy of the propellant (heat) via collisions; the high temperature and pressure propellant is then expanded in a conventional nozzle. Thus, thrust and I_{sp} depend on the ability to sustain temperature and pressure similar to chemical rockets, but for hours, not minutes.

In a NTR, the temperatures of fuel and structure are limited to about 2500 K. Ongoing research suggests 3000 K may eventually become feasible. Materials capable of 2500 K were tested in the Soviet Union and in the US. Thrust depends on mission, and thermal rockets developing 100,000 lb_f (450 kN) were built and tested in the 1960s. Propellant temperature lower than 2500 K limits I_{sp} to less than 1000 s. However, this is more than twice the I_{sp} of current chemical rockets, and it may enable a human Mars mission faster compared to a Mars mission utilizing chemical propulsion, but it is not enough for enabling a robotic mission to Europa: even a few hours at sustained thrust and I_{sp} = 1000 s would consume too much propellant. The hypothetical Neptune mission used as example in Sect. 7.1 would take much longer than 4 weeks round-trip.

If nuclear thermal rockets are assumed the baseline nuclear propulsion system, what are potential advances capable of raising I_{sp}? Conceptually, to reduce propellant flowrate at fixed power, either structural or thermodynamic limitations must be overcome or bypassed.

One advance led to the so-called Rubbia engine, in which the conventional direction of heat transfer (fission fragments → fuel bars → heat transfer → hot propellant, see Fig. 7.4) is short-circuited by direct injection of fission fragments inside the propellant as it flows. Independently, L. R. Shepherd in 1948 and Y. Ronen in 2000 proposed similar ideas. Another advance would have the fuel fissioning in the gaseous state, that is, at much higher temperature than in solid cores, around 10^3–10^4 K, and heat the propellant via radiation heat transfer. This is the gas-core nuclear rocket concept.

Whether baseline or advanced, NTR schemes convert the kinetic energy of fission fragments directly, or via heat exchange, into hot propellant that expands in a conventional nozzle. Because fission fragments have energy of around 10^2–10^3 keV (approximately 10^6–10^7 K!), the obvious way to moderate temperature is to "dilute" the enormous energy of fission fragments in a much larger mass M_{ppl} of inert propellant as shown in Sect. 7.3.1.

NTR are best suited to fast, high-thrust missions. "Fast" missions may be defined as missions where the spacecraft acceleration is higher than the Sun gravitational acceleration, about 0.0059 m/s^2 at the Earth orbit. Calculations indicate that advanced NTR of the Rubbia-type are capable of I_{sp} of the order (2 to 4) · 10^3 s and thrust approaching 10^3 N. Solid-core reactors tested in the USA and the Soviet Union had lower I_{sp}, of the order 800–900 s, but were capable of thrust in the 10^5 N range. In terms of durability, reactors built and tested at the US Los Alamos Laboratory in the 1950s and 1960s during the US NERVA program demonstrated power in the 1000 MW range for more than 1 h, with $I_{sp} \approx 880$ s. When NERVA was abruptly terminated in the 1970s, the latest generation reactors designed were capable of a thrust/power ratio ≈50 lb_f/MW, and I_{sp} close to 1000s. The Phoebus IIA reactor was tested at 4.2 GW for more than 12 min (Gunn 1998; Dewar 2004), demonstrating this technology was mature. A notional NTR scheme is shown in Fig. 7.6.

The second major advance consists in using the nuclear reactor to power an electric generator. This is nuclear electric propulsion, or NEP. Conversion from thermal to electric power may be by conventional thermodynamic cycles, such Stirling or Brayton, by the thermoelectric effect, by magneto-hydro-dynamics or by more advanced processes (El-Genk 2009). The electric power feeds an *electric thruster* (ET), for instance a gridded ion, Hall, or magneto-plasma-dynamic (MPD) thruster. Coulomb or Lorentz force accelerates the propellant directly, not via thermodynamic expansion, and propellant must be then electrically charged (ionized). Thrust is much lower than in the first strategy, but I_{sp} may reach 10^6 s and more, for instance by using the technology to refuel Tokamak Fusion Reactors with hydrogen isotopes: to refuel tokamak, fuel must be accelerated to speeds of around 10^2 km/s. The issue with NEP is thrust and power, since converting reactor heat

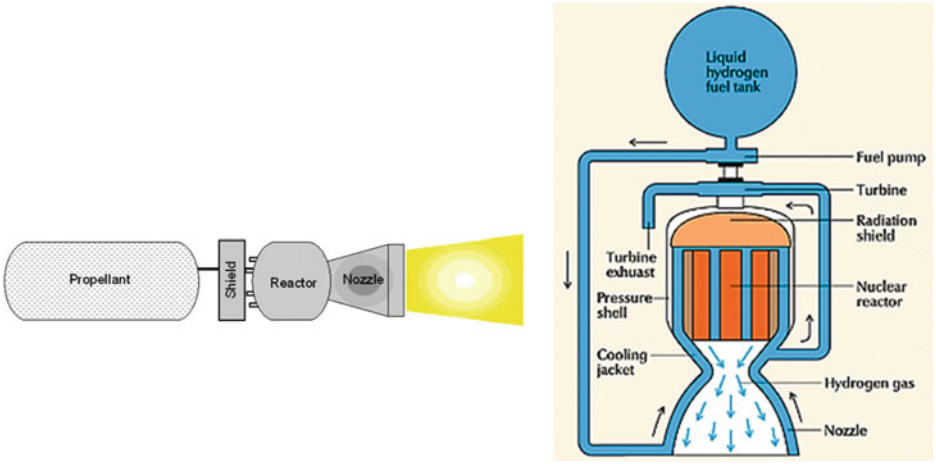

Fig. 7.6 Notional scheme of a nuclear thermal rocket (NTR) using liquid H_2 [Courtesy of Bond 2002 (*left*) and Wikipedia (*right*)]

into electric power has efficiency $\eta \cong 30$–50% (at most). At least half of the reactor power is wasted, more commonly 70% using Brayton (turbine) cycles. The waste must be radiated to space using a bulky and massive space radiator. Thrust scales with power as 2 P_e/I_{sp}, so high-I_{sp} thrusters need correspondingly high electric power. For instance, to produce 100 N thrust, an ion engine with $I_{sp} \approx 5000$ s would need 2.5 MW_e; such thruster does not exist yet. The *thermal* power of the reactor needs to be $1/\eta$ higher.

In this chapter, the question of nuclear electric propulsion for fast human missions will be discussed. Fast NEP-powered missions may need GW power, but this is not outlandish as it sounds. Although designed for a NTR, not for electric propulsion, space reactors capable of power in the GW range were built in the USA under the NERVA program. The issues with high-power NEP are conversion machinery, durability and possibly refueling, since high power implies high nuclear fuel consumption. In space, refueling a fission reactor would pose extraordinary challenges. A notional scheme of a NEP system is shown in Fig. 7.7.

The two propulsion strategies, NTP and NEP, are the two extreme cases of the trade-off between thrust F and I_{sp}. Because thrust power $P \approx 1/2 \cdot F \cdot V_e$, and $V_e = I_{sp}$, at fixed power, the F versus I_{sp} curve is a hyperbola where NTR sits on the left, NEP on the right. The specific mission will tell whether it is better to choose an engine with high F and low I_{sp}, or vice versa. In fact, quick escape from the gravitational attraction of planets requires large thrust; fast interplanetary travel, enabled by constant acceleration, needs very low propellant consumption to be feasible, and suggests high I_{sp}. Any interplanetary mission from Earth includes both these trajectory segments, so ideally one would like to have a propulsion system capable of both propulsion modes. This is the motivation for the VASIMR rocket described later.

There is a third, radical way of exploiting nuclear energy for propulsion: repeated nuclear explosions astern of a spacecraft. This is *pulsed* nuclear propulsion (Schmidt et al. 2002). This strategy was proposed by Dr. S. Ulam (Everett and Ulam 1955) and investigated in the 1950s by Dr. Freeman Dyson (Dyson 1979, 2002) and Dr. Ted Taylor, a fission bomb physicist. History of this project and propulsion aspects are in Schmidt et al. (2002), Flora (2005), Dyson (2002). This unconventional propulsion technique was suggested by the 1950s *Viper* thermonuclear bomb test on Eniwetok. The team examining the ground in the aftermath of the explosions found the two 1-m diameter graphite-coated metal spheres they had hung some ten meters from ground zero, pushed kilometers away but unscathed, with the exception of the coating. Until then it

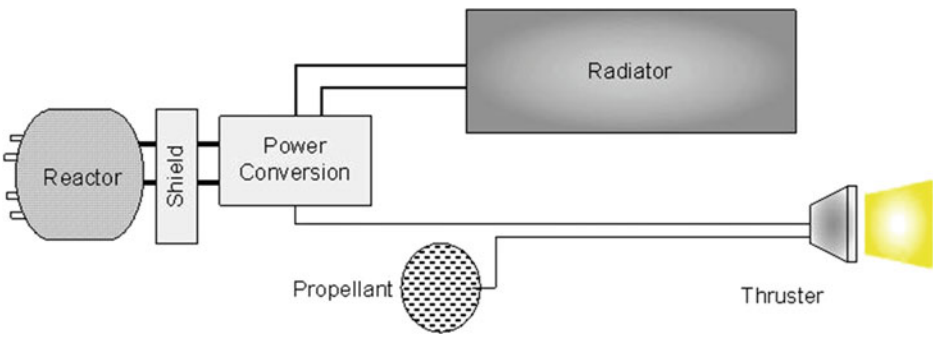

Fig. 7.7 Notional scheme of a nuclear electric rocket. Note the mandatory radiator (Bond 2002)

was assumed that nothing could survive a close nuclear explosion. Later analysis showed that ablation of a plate surface by the intense radiative environment could protect the underlying structure. Suitably sized and reinforced, a so-called thrust plate can indeed receive and survive the momentum due to shocked matter debris and due to radiation impulse. Radiation from the fireball ablates coatings deposited on the thrust plate (polymers or grease) and their gaseous products ejecting from the plate apply thrust in the same way combustion products apply thrust in a rocket. Because the major loss in this concept is due to X-ray and γ-ray emission, to reduce it, to increase thrust, and to reduce plate wear, it was found convenient to add mass that could be converted to plasma at the plate. Much information concerning ablation and its physics is still classified today, but calculations and tests done in 1959 by replacing atomic explosions with high explosives, confirmed the concept was viable provided the spacecraft was massive enough and included shock absorbers to moderate the instantaneous accelerations experienced.

In the 1950s, the nuclear test ban was not in existence, and Dyson and the physicists working on Project Orion envisaged taking off from the ground and accelerating to orbital speeds all by sequential atomic explosions pushing the spacecraft. Orion was eventually designed for a spaceship large enough to do a grand tour of the planets lasting a year. The estimated mass of the spaceship for such a mission was of order 10,000 t, much of it consisting of the pusher plate/shock absorber assembly, see Fig. 7.8. Specific impulse and thrust calculations showed both could be much higher than with chemical propulsion, in particular I_{sp} of the order 10^4–10^6 s were theoretically predicted. Thrust was limited only by the maximum acceleration tolerable by the crew. Some details of Orion propulsion physics are in (Bruno 2012).

Figure 7.8 shows from left to right: crew landing module and propulsion system, crew accommodations (the drum-like structure), intermediate segment, nuclear propellant magazines (hosting the nuclear explosive charges), charge injection system, shock absorbers and pusher plate. Note the nuclear charge in the process of being ejected; the pusher plate has a central channel to allow the passage of charges.

Because of lack of military applications, potential opposition by the public, and certainly by then-Secretary of Defence Robert McNamara, Project Orion was canceled. A similar concept, but using thermonuclear explosions, Project Daedalus, was investigated by the British Interplanetary Society (Bond et al. 1978). The objective was to reach Barnard's Star, 5.9 light-years away, within fifty years (see also Chap. 8).

A revisited Orion project (MagOrion, later Mini-Mag) replaced full size atomic bombs with miniature nuclear explosions using exotic fuels such as ^{244}Cm and ^{247}Cf, therefore reducing the mass of the spacecraft necessary to withstand the periodic bursts of thrust. Ground testing was carried out by mimicking nuclear mini-explosions by means of high intensity electromagnetic pulses (theta pinch-accelerated plasma jets, see Chap. 8). The Andrews Space and Technology Company, Seattle, was the prime contractor. According to its chief scientist, Dr. Dana Andrews, the I_{sp} measured was more than 1000 s (Ewig 2003; Ewig and Andrews 2003). Impulse and thrust are much larger than in any NEP system as instantaneous power is much larger than produced by steady operation of a nuclear reactor.

On paper, microexplosion propulsion releases the largest amount of energy of any device, although in pulse form. The magnetic nozzle converting expanding plasma momentum to thrust via the Lorentz force is the critical component: it must

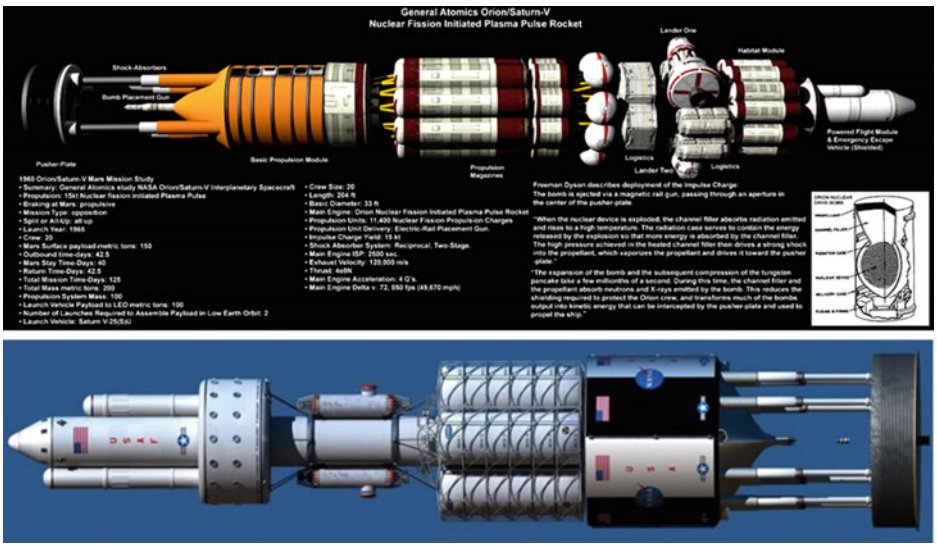

Fig. 7.8 Artist's view of the Orion vehicle planned for the grand tour of the Solar System (*Courtesy* NASA)

capture most of the fission fragments before their charge is neutralized by recombination. To do so, calculations predicted magnetic nozzle sizes of many hundreds of meters. Analyses performed up to 2003 indicated that this was indeed problematic, and a different approach, based on less mass fissioned but higher yield and a tighter magnetic field leaking fragments at one end, was proposed (Andrews and Lenard 2006). Lack of further funding stopped the Mini-Mag Orion at this point.

For sufficient conversion and if enough fuel is available, this mode of propulsion looks suited to power long interplanetary missions, as it combines the large thrust of NTP and the high-I_{sp} of NEP. A similar consideration holds for the pulsed fusion propulsion concepts in Chap. 8. This nuclear strategy could become a major means of future deep space exploration.

7.5 Nuclear Propulsion: A Historical Perspective

The need to carry the heavy atomic bombs of the 1940s motivated the USA and the Soviet Union to explore nuclear propulsion as an alternative to bombers and ballistic rockets. Most of this effort lasted from the late 1940s throughout the 1950s and until the early 1990s. In the USA, the rationale for starting nuclear rockets (by the Atomic Energy Commission, AEC, in 1953, through the program ROVER) was the perceived need for a 75,000 lbf ($3.34 \cdot 10^5$ N) thrust nuclear thermal rocket to power the third stage of US ICBM (intercontinental ballistic missiles). In fact, in 1956 the USAF joined ROVER, but after the Atlas ICBM flew successfully powered by a chemical rocket in 1958, NASA and AEC (at its Los Alamos Science Laboratories, LASL) were charged to replace the USAF as ROVER Program leaders. The focus of ROVER after 1958 was on developing reliable, safe, and efficient nuclear reactors for space applications. In 1961, this effort branched out to Westinghouse and Aerojet General. These contractors were tasked to engineer reactors into rockets. The industrial branch of ROVER was called NERVA (Nuclear Engine for Rocket Vehicle Applications) which started in 1961.

The original organization chart of NERVA is in (Howe 1985). An entertaining history of ROVER/NERVA, focusing mainly on internal US politics, is in (Dewar 2004); technical work can be found in final report form Anon (1972); synopses are Bohl et al. (1989), Howe (1985), Gunn (1998, 2001), Rose (2008). An excellent summary of the technological path of ROVER/NERVA is in Gunn and Ehresman (2003).

After NASA and AEC took over, starting in 1965, the first phase of ROVER progressed at the Los Alamos Science Laboratories (LASL) through a series of proof-of-principle Kiwi reactors (Kiwi-A, Kiwi-B), each with variants testing different fuel bars, geometry, and materials. For instance, in this first phase Kiwi-B4, an advanced design shown schematically in Fig. 7.9, and on its test stand at Los Alamos in Fig. 7.10, was tested at 1030 MW. Program NERVA I started in 1961: its purpose was to engineer Kiwi *reactors* into *rocket* engine prototypes and to test them. NERVA bred the NRX family of "engines" (six in all). For instance, NRX-A3 was derived from Kiwi-B4, and tested at 1,165 MW. The general scheme of all NRX rocket engines is that shown in Fig. 7.11.

The power of the Kiwi reactors was about 1 GW, to support a projected rocket thrust of 50,000 lbf ($2.27 \cdot 10^5$ N). Kiwi, which started in 1965, subsequently evolved at LASL into the Phoebus 1 and 2 reactors. Evolution concerned fuel material technology and reactor diameter; this last was increased from 35-in of Kiwi B4E to 55-in of Phoebus 2, more than quadrupling thermal power. These reactors were considered the precursor of the second phase of NERVA (NERVA II). The Phoebus family of reactors was the most powerful ever. Figure 7.12 shows Phoebus 2 on its test stand at Los Alamos.

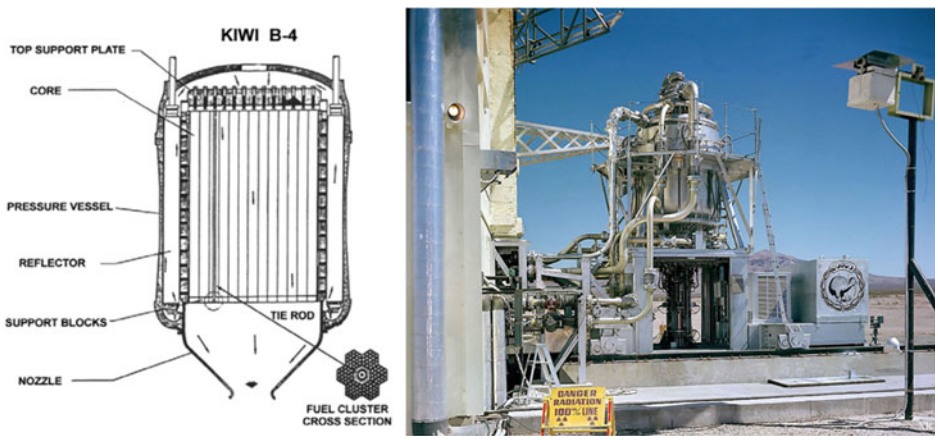

Fig. 7.9 Sketch of the NERVA Kiwi B-4 nuclear reactor (*left*). A cluster of 6 fuel bars cross section is also shown (Gunn 2001, Fig. 2). Picture of an earlier Kiwi reactor on its test stand at LASL is on the *right*

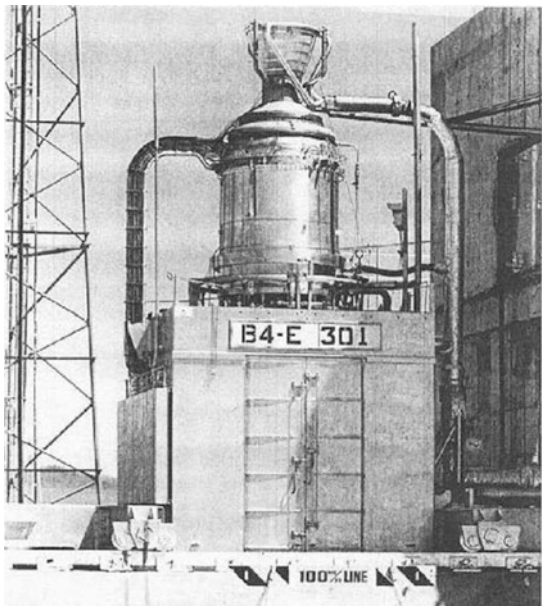

Fig. 7.10 NERVA Kiwi B4-E reactor on its test stand at Los Alamos (Dewar 2004)

In parallel, industry was focusing on increasing rocket engine lifetime, exploring new uranium alloys or compounds. By that time nuclear propulsion was considered essential to manned Mars missions. The NRX-A5 and NRX-A6 engines developed during NERVA I were tested at more than 1 GW for up to 62 min. All space mission plans assumed the engine working for no longer than 1–2 h at most, but also capable of multiple restarts. The NRX family was based on the Kiwi B4E, where fuel was no longer uranium oxide but the much more temperature- and corrosion-resistant uranium carbide. Tests were in fact performed at a steady 2200 K reactor temperature. In fact, the NRX-XE prime design, with its high-temperature UC fuel and compatible ZrC cladding, reduced considerably cracking and the attack of hydrogen on the carbide forming volatile CH_4 gas (Methane). This engine was probably the closest to operate in a flying demonstrator.

At LASL, Phoebus progressed through versions -1A, -1B, and culminated in -2A, tested at 4082 MW for 12.5 min, see Fig. 7.11. At that point, Phoebus funding was suspended, chiefly because the engine that could be derived did not have a specific mission. However, work was continued but on much smaller *research* reactors (e.g., the 500 MW PeeWee) that were less time consuming and less expensive to build, test and operate. Focus was still on fuel rod durability at higher temperature, with industry following suit in the parallel NERVA program. Of note are the neutron fluxes of all NERVA engines, of order $3.2 \cdot 10^{19}$ Hz.

At the end of the program in 1972, the NERVA NRX ETS-1, the last nuclear rocket engine developed, was tested at 1100 MW for a total of 3 h 48 min. ETS-1 was conceived as the direct precursor of the final NERVA I engine shown in Fig. 7.13. The nominal power planned for the final NERVA I rocket was 1500 MW, with I_{sp} = 825 s. As designed, this engine was capable of 10 restarts, for a total 10-h operation time.

Its reliability was projected to be 0.997, that is, more than 10 times better than any current liquid rocket engine. The weight was estimated at 15,000 lb, the thrust $3.34 \cdot 10^5$ N. Power density was ≈2 MW/dm^3 (200 times greater than in gasoline engines). In short-duration bursts, power reached $2 \cdot 10^5$ MW and $8.9 \cdot 10^5$ N thrust (Lawrence et al. 1995). Future upgrades predicted I_{sp} up to 900 s, since progress in high-temperature materials was supposed to enable reactor operation at 2600 K.

The last reactor tested at LASL was PeeWee, in 1968. It demonstrated a 500 MW_{th}, 25,000 lbf engine design capable of I_{sp} = 850 s. Its major feature was a thrust to weight ratio almost 3 (nuclear engines have much lower *T*/*W* than liquid rocket engines due to the dense reactor and shielding). Follow on studies showed that heat recovery could add 25 kW_e to the total power, thus making PeeWee the first dual-mode nuclear thermal engine (Howe and O'Brien 2010). Also in 1972, LASL did a definition study of a 16,000 lbf (71,000 N) thrust rocket engine (the Small Nuclear Reactor Engine, or SNRE) weighing 5890 lb

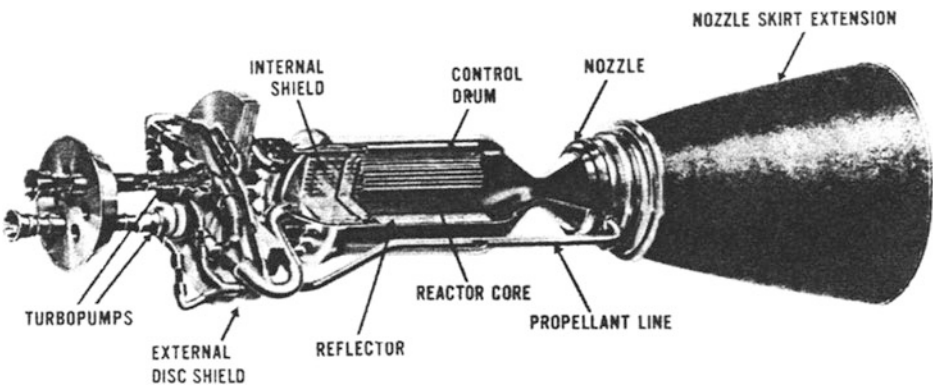

Fig. 7.11 Schematic diagram of the Westinghouse NRX nuclear engine (Dewar 2004)

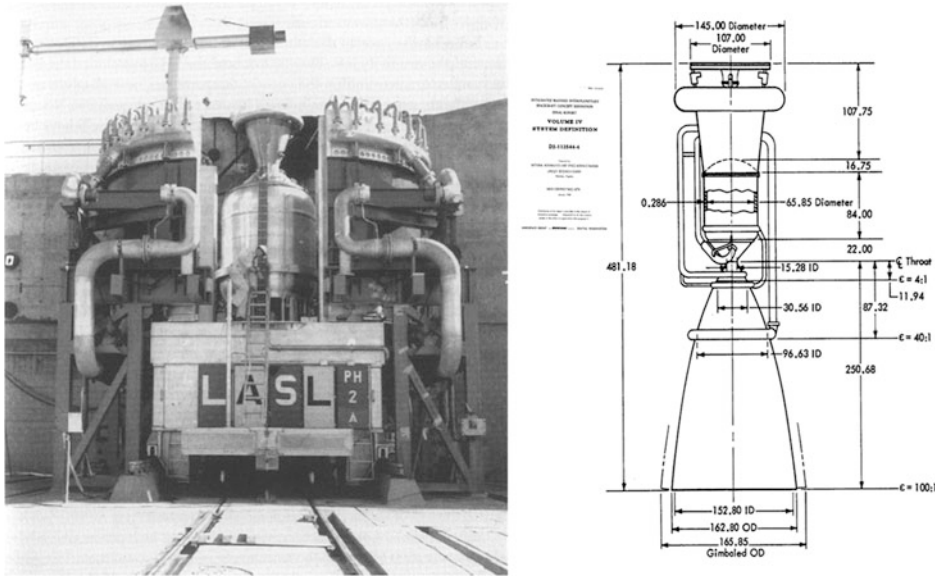

Fig. 7.12 *On left* The 4 GW Phoebus 2 nuclear reactor on its test stand at Los Alamos (Dewar 2004). *On right* A 1963 schematics of the engine based on Phoebus 2 reactor. Sizes are in inches. This is the fly-weight nuclear engine derived from Phoebus reactors (sometimes called "NERVA II") (NASA)

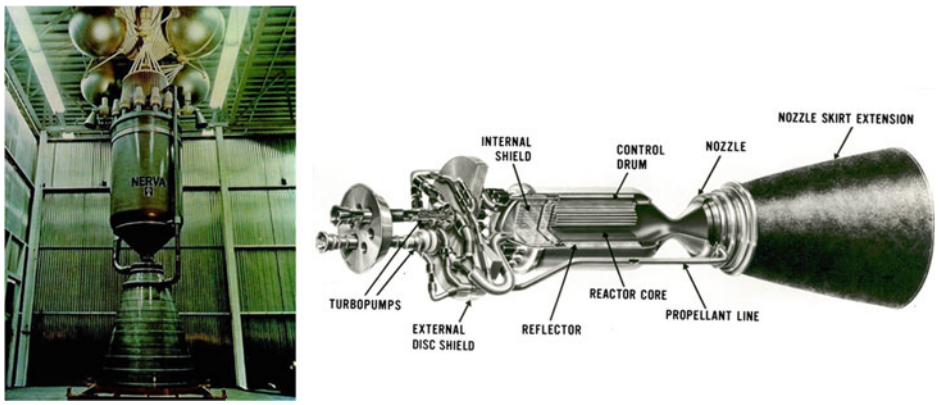

Fig. 7.13 Mock-up of the NERVA 1 on *left* as it stands in the Huntsville Space Park, Alabama (Dewar 2004). Cutaway of the NERVA NTR engine (*Courtesy* NASA)

(2670 kg including the shield) that could be carried to LEO by the US Shuttle, which was at that time in the planning stage. This nuclear engine was proposed to power interplanetary missions and also to drive a "space tug" repositioning payloads from LEO to GEO and other orbits (Gunn and Ehresman 2003). However, because of cost, declining political support, lack of a clearly defined mission, and the Vietnam war, this program was terminated during the Nixon administration. The many lessons learned during the tests, which carried on at Los Alamos for the ROVER program, have been summarized in (Koenig 1986). An extended account of the ROVER/NERVA programs is available in the Encyclopedia of Physical Sciences and Technology (Meyers 2006). Effluents from the reactor tests were continuously monitored locally and by air, and no dangerous radioactive emissions were measured (Friesen 1995).

Sponsored by the USAF, classified work in nuclear propulsion using PBR (Pebble, or Particle Bed Reactor) started in 1983 in the context of the Strategic Defense Initiative (SDI) of President Reagan, dubbed *Star Wars* by the media. The USAF kept working in nuclear propulsion until 1993 (toward the end of SDI), with an annual budget of about $40 million. Much of this work was spent in finding ways to make space nuclear reactors more compact and capable of standing higher operational temperature and/or more power cycles, and resulted in the PBR and CERMET fuel concepts briefly described in Sects. 7.9 and 7.10.

By 1987, the classified part of this program became Project TIMBER WIND (Rose 2008). Its purpose was to design nuclear propulsion (NP) systems to lift nuclear directed-energy weapons (X-ray lasers) to orbit. To improve performance, the propellant was slush-H_2, a solid/liquid 50–50 mixture, where solid H_2 is 16% denser than liquid (Ohira 2004). The combination of a light LiH moderator and PBR produced an engine about half the weight and volume of the last reactors developed under ROVER. The power ramp-up and ramp-down times were also reduced to about 10 s. By 1990, three TIMBER WIND engines, so-called -45, -75, and -250 of sea-level thrust 88-, 147- and 1912 klbf, respectively, were under development, with sea-level I_{sp} ranging

from 890 to 780 s and $T/W = 30$. However, in 1992 this program was allegedly terminated. Because TIMBER WIND is still classified, no other details are available. Based on PBR technology, the USAF expanded this program into the Space Nuclear Thermal Propulsion (SNTP) effort, whilst at the same time restricting applications to second and upper stages of existing military launchers, thus limiting their use to a segment of the ascent in the atmosphere (Haslett 1995). The LEO payload gains predicted varied from 40 to 400%, but ground testing of the engines was an administrative stumbling block, and the program was stopped in 1994.

What is left of NERVA and the USAF work today? A 1999 recognition at LASL discovered more than 1100 documents detailing components of the PeeWee reactor, and more than 150 detailing components of PeeWee, KIWI-B, and Phoebus projects. The amount of information on PeeWee still available lends credence to the feasibility of rebuilding it into an engine with a modest investment (Howe and O'Brien 2010). This seems confirmed by a statement by Dr. Stanley K. Borowski at the AIAA Space conference in August 2015 (Norris 2015). A mock-up of the NERVA ETS engine is still standing in the NASA Space Park in Huntsville, Alabama, see Fig. 7.13. Work on nuclear fuels capable of standing high temperatures, for instance ^{235}UN in a tungsten cermet matrix, is carried on at the Center for Space Nuclear Research in Idaho, in collaboration with the Idaho National Laboratories (INL) nearby. Tungsten matrices would permit higher temperatures than the cermets tested so far by the USAF and would prevent atmospheric dispersion of radioactive fuel in case of catastrophic reentry of a nuclear engine (Smith and Keidar 2015). The INL center is also supporting the SAFE (Subsurface Active Filtering of Exhaust) concept developed to ground test nuclear engines. SAFE is a strategy to exploit the presence of deep holes left at the Nevada nuclear test site from the nuclear weapons experiments of the 1950s and 1960s. Extensive knowledge of Nevada geology gained during that period supports the proposal to develop a safe and economical underground facility.

Conceptual work in NTP is still being carried on at NASA-Glenn Research Center by Dr. Borowski's team who keeps in touch with "old-timers" such as Stan Gunn. The team refines old and new concepts in view of a future manned Mars mission. In one of its latest architecture proposals, the concept has evolved into a NTR working both as a propulsion system and as an electric power generator (≈110 kW). This is the so-called bimodal propulsion concept. Electric power is supposed to be used for instrumentation, support of crew activities, data transmission and refrigeration of the liquid hydrogen propellant during the trans-Mars and trans-Earth (return) stages (Borowski et al. 2000). Later, a trimodal engine concept (TRITON, TRImodal, Thrust Optimized Nuclear) was also proposed (Joyner et al. 2004): this is a small thermal rocket capable of I_{sp} = 911 s and 66.7 kN thrust that can be augmented, for brief periods, by injecting gaseous O_2 past the hydrogen nozzle throat following the LANTR (LOX-Augmented NTR) concept developed and tested at Aerojet Corporation by Dr. M. Bulman and his team, see Sect. 7.23 (Bulman et al. 2004). It includes also an electric generator supplying a maximum 160 kWe. In the LANTR mode, gaseous O_2 is injected just past the throat of the H_2 nozzle where supersonic combustion increases thrust by expanding the hot H_2 and H_2O. Thrust can be augmented by a factor 3 from the 67 kN of the nuclear engine alone, up to 200 kN. TRITON was the result of a collaboration among NASA Glenn Research Center, Pratt and Whitney, RENMAR and Aerojet-Rocketdyne. This last company remains interested in NTP and has proposed to NASA to work on S. Borowski Small Nuclear Engine concept (Palaszewski 2015).

Nuclear Propulsion Work in the Soviet Union and Russia

Russian work, until recently shaded in secrecy, is now partly known, see Goldin et al. (1991), Rachuk et al. (1996), Ponomarev-Stepnoy et al. (1999), Demyanko et al. (2001), Koniukov et al. (2004), Dewar (2004), Koroteev et al. (2007), Rose (2008), Zak (2014), Lanin (2013). The book by Lanin in particular is a trove of technical information of all aspects of Soviet era reactor design, including materials, radiation shielding, and mode of operation (solid or gaseous nuclear fuel). Chapter 1 contains a summary history of the early development of nuclear reactors at the time of the "Three K," see below.

The origins of NP in the SSSR (Soviet Union) go back to Professor M.K. Tikhonravov, at the Soviet Academy of Sciences, working with Korolev's OKB-1 in the early 1950s. Tikhonravov planned a manned Mars mission using chemical propulsion, but his initial calculations indicated a 1600 t mass needed to be lifted to LEO. Even using the giant N-1 launcher, designed for the future Soviet Union manned Moon mission (Godwin 2006), the projected cost of the manned Mars mission was staggering, and this triggered interest in NP. At the same time, just as in the US, the military was looking at propulsion for their ICBM. Calculations in the early 1950s had predicted that a NP-powered single stage missile could reach any target on Earth. It was at that time that Keldysh (the head of the Soviet Academy of Sciences), Korolev (at OKB-1), and Kurchatov (the head of the Soviet nuclear organization) started a collaboration that became known as "the three K." Similarly, to what was taking place in the US, initial work by several institutes focused on fuel, reactor architecture, and materials. A major difference was an early focus on carbides rather than graphite as moderators. Inevitable involvement with ceramics

research institutes produced outstanding fuels: in fact, reactors were planned from the start to eventually operate at temperatures close or slightly above 3000 K (Lanin 2013, Chap. 2). The purpose, as in the US, was to reduce the future weight and maximize thrust of rocket engines powering ballistic missiles. Paralleling reactor development, rocket engine OKB were asked to start planning nuclear rocket missiles. Two ICBM designs by different bureaus followed in the period 1958–1959, one by Glushko and the other by Bondaryuk. Glushko used NH_3 as propellant since it posed fewer logistic problems than liquid hydrogen. His engine had a planned thrust of 1255 kN. Bondaryuk chose a mixture of NH_3 and methyl alcohol.

Rapid progress in rocketry convinced the Soviet military that NP was no longer necessary to power their ICBM. Nevertheless, investing in NP space missions continued, and by 1961 two LH_2-fed NTR engines were designed, one for an upper stage, with thrust of order 30–40 t, the second a much more powerful engine designed by Glushko for Energomash in the 1962–1970 timeframe, the RD-600. This design is especially noteworthy since it was powered by a *gas core*. It used LH_2 as propellant, and could deliver 1960 kN with I_{sp} = 2000 s. It was envisaged as the second stage of an orbital propulsion system for Venus and Mars missions. These two engines continued to be developed until 1971, when all NP work was reassigned to NPO-Luch, in Podolsk, Russia, a company specializing in treating high-risk nuclear fuels and high-temperature materials. The RD-600 was considered so risky that it was not designed at the Energomash's Khimki facility, but at a much more remote OKB-456 Filial 1, near the Semipalatinsk 21 town and nuclear facility now in Kazakhstan. NPO-Luch continued to develop NP for the next 18 years. Their Baikal-1 nuclear thermal engine was designed, assembled, and bench tested at least 30 times, proving the engine was very reliable. Although details remain sketchy, it is known that two more NTR engines were designed in the Chelomei OKB, the small RD-0410 (3.6 t thrust) that was a testing prototype for the full-scale RD-0411 (40 t thrust). Figure 7.14 shows the RD-0410 on display in Russia.

Both solid-core reactors were neutron flux controlled and were extensively tested in "cold" (no fission) and "hot" (fission) mode near the Semipalatinsk-21 facility. A cluster of seven RD-011 should have powered the third stage of UR-700A, the alternative to Korolev's N-1 lunar rocket, and a cluster of four should have powered the last stage, in principle capable of capturing Moon or Martian orbits. According to Zak (2014), Chelomei was planning to develop a UR-700 B variant powered by a liquid core reactor, and a V variant using a gas core. However, after the Academy of Sciences rejected an overly ambitious manned Mars mission project using the UR-700A (the planned Mars spacecraft alone weighed 1100 t), all NP research and development for Moon or Mars missions was terminated in 1972 when it was realized that the USA were stopping all investments in this area as well (Haeseler 2014). At low level, nuclear engine development continued until the collapse of the Soviet Union. It is interesting to note that, as in the US, just when the technology had matured and demonstrated that its performance was much superior to that of chemical rocket engines, it was a political and economic decision—not engineering issues—that terminated all NP work.

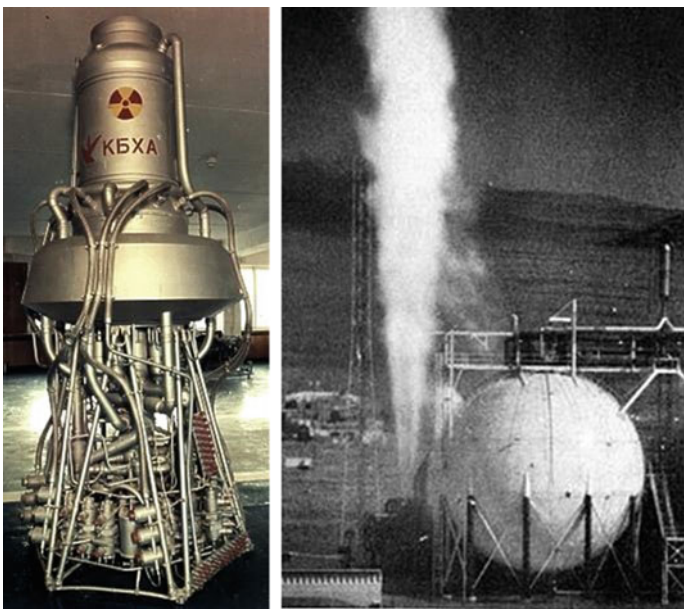

Fig. 7.14 On the *left*, the nuclear rocket engine RD-0410, the prototype for the -0411, developed by the Chelomei OKB; on the *right*, nuclear rocket testing near Semipalatinsk

Roscosmos sources claim to still retain technology and especially testing capabilities. In fact, the Russian NiiCHM organization developed very high-temperature (>3000 K) ceramic fuels that would be invaluable in building future high-performance NTR. Ceramics are brittle, but also very resistant to attack by hot hydrogen, and this strategy was preferred in that it allowed higher operation temperatures. The problems associated with high-temperature gradients and thermal stresses when starting the engine resulted in a long investigation on this issue. The solution found was to use fuel bars composed of twisted two-blade fuel elements (Lanin 2013, Chap. 2).

According to Gafarov et al. (2004), nuclear 1 MW-class reactors for thermal rockets and for NEP are still being investigated and perhaps tested for interplanetary missions. An all-union conference on nuclear propulsion took place in Moscow in May 2005. This conference was the last in a series organized by the N.A. Dollezhal Research and Development Institute of Power Engineering (NIKIET in Russian) and was sponsored by the Russian International Science and Technology Center (ISTC), which also works as a clearinghouse for NP information (Pradas-Poveda 2008). In fact, dual-mode NTR projects (Koroteev et al. 2007) include a nuclear space engine concept in the 340 MW class designed to work at 2900 K using a ternary U/Zr carbide/nitride fuel (some ternary alloys of uranium can stand much higher temperatures than single carbides or nitrides). At 60 bar pressure, vacuum thrust is 68 kN and I_{sp} is close to 960 s. Engine mass (including shielding) is 12.2 t. The level of detail of this project indicates that interest in Russia for NTP technology is still high, and that studies keep being funded. Roscosmos proposed in 2011–2012 to ESA to collaborate on developing NP for a future manned Mars mission. In September 2015, Rosatom (the civilian agency responsible for nuclear reactors) asked Roscosmos 20 billion Russian Rubles to complete in the same year the development of a MW-class reactor for space propulsion started in 2010, readying it for a first flight in 2018 (Smirnov 2015).

This survey shows that NP is alive and is not a new and unproven technology. Work in the 1960s and 1970s at LASL produced NTR reactors capable of 4 GW_{th}. At a conservative I_{sp} = 800 s, this figure would ideally produce thrust of the order $5 \cdot 10^5$ N (≈50 t). The Russians successfully and repeatedly tested the Baikal prototype of RD-410. Reactors and engines were designed and tested with technology and engineering tools that now would be considered obsolete, e.g., with computers orders of magnitude slower than now available. Performance figures and past achievements should have given pause to planners having misgivings in discussing 25- or 50-kW (not MW!) NEP thrusters for the now defunct NASA JIMO (Jupiter's Icy Moons Orbiter) missions.

7.6 Nuclear Propulsion: Current Scenarios

Dormant in the West during the 1970s, renewed attention to nuclear propulsion (NP) for interplanetary missions started in the late 1980s motivated by interest in manned Mars missions. It was and still is clear to the aerospace research community that NP can provide the only practical and safe propulsion system for fast, manned Mars missions (Asker 1991; Merkle 1999). Many cautious articles have appeared in support of high-energy, short missions compared to multi-year missions relying on planetary gravitational assists such as Galileo or Cassini, see e.g., Borowski et al. (1998), Beale and Lawrence (1989), Jones (1992), Asker (1991), Schmidt (1999, 2002), Howe (2001), Lenard (2001), Hrbud (2003). Additionally, the Space Shuttle *Challenger* accident did prove to some that chemical propulsion was not as reliable, and that the cost of orbiting chemical propellants to LEO for Mars missions was staggering. More recently, in-space measurements of Galactic Cosmic Radiation and Solar Radiation (GCR and SR) and especially the Radiation Assessment Detector (RAD) onboard the Mars Science Laboratory probe that brought the Curiosity robot to Mars, measured the radiation dose during the 180-day trip; this was 300 milli-Sievert (Köhler et al. 2014). A Mars round-trip mission would roughly double that, and longer missions would result in a proportionally higher dose. Lacking statistics, excess cancer probability connected with these doses is difficult to quantify. However, estimates suggest between 5 and 30% (Durante and Bruno 2010).

Running against these conclusions is public refusal of anything nuclear. Public acceptance ebbed away in the 1980s and 1990s due to the so-called Chernobyl accident. Until recently, the issue of nuclear propulsion could not even be discussed at the political and decision-making level. Nuclear propulsion and anything nuclear, whether in space or elsewhere, remains to this day a controversial topic (Hagen and Scheffran 2001). The Chernobyl accident in 1987 gave NP a very bad name. A joint JPL-NASA meeting in the spring of 2000 (Sackheim et al. 2000) seemed to indicate the tide was turning toward supporting NP, probably due to increasing public consciousness of the greenhouse effect caused by burning fossil fuels and the rising price of gasoline and heating oil.

After the joint JPL/NASA-Marshall meeting in May 2000, NASA proposed nuclear power as a technology not only for thermal rockets, but also for a broad range of thrusters, including conventional NTR concepts by NASA Glenn Research Center (Borowski et al. 2000), pulsed fission systems, and even some form of fusion rockets (Sackheim et al. 2000). In fact, the name "nuclear propulsion" was replaced by "nuclear-powered thrusters," these being thermal, as at the time of NERVA, electric (ion), or using

magneto-plasma-dynamic acceleration (MPD), such as VASIMR were still in the developmental stage. Sackheim provided a vision and roadmap sketched at NASA and JPL (Sackheim et al. 2000). That effort lasted until January 2004 with the demise of Project Prometheus described later.

Had this roadmap indeed been implemented in the USA (and the publicity given to nuclear propulsion seemed at the time it would have), US investment in nuclear propulsion would have grown rapidly. In juxtaposition, it should be noted that, with the exception of the International Atomic Energy Agency, the EU had and still does not have prior expertise in this area, and this state of affairs will be a major consideration when and if the EU starts investing in the nuclear option for future space missions. The same applies to Japan and China. ESA decided to investigate the issue of NP for manned Mars missions, where architectures based on chemical rockets show all their shortcomings, but still favored chemical propulsion for the Mars probes planned under its Aurora program (Gilles 2004). The USA were interested instead in several NP concepts, among them the Rubbia engine and a reusable nuclear "space tug" to quickly raise satellites from LEO to GEO. The impact of such a system on the commercial GEO satellite market does not need to be emphasized, and economic and technical studies on Orbital Transfer Vehicles (OTV, the official name for the space tug) continued (Ortiz 1993; Ketsdever et al. 2008). The most recent of such proposal is the "Jupiter" space tug by a consortium headed by Lockheed-Martin, the first step toward a future transportation system connecting cislunar space and eventually Mars (Morring 2015a, b). However, at the moment, the Jupiter tug is envisaged using a mix of chemical and solar-electric propulsion.

In 2002, following the Space Exploration Initiative (SEI) of President G.W. Bush at the time, NASA's Nuclear Systems Initiative (NSI) to explore Europa, Callisto, and Ganymede by means of the Jovian Icy Moons Orbiter (JIMO), prepared the public toward nuclear power applications in space. Quoting Sean O'Keefe, NASA Administrator at the time, the purpose was to battle "... *the distance and time dilemma* ..." (David 2002). In 2003, after a budget increase to $1 billion, it became Project Prometheus (Bates 2003).

According to NASA, plans are for now on indefinite hold or are canceled (Berger 2005a, b). Prometheus was to culminate in a "New Frontier" class of unmanned mission to orbit the Jovian satellite Europa to find evidence of liquid water (and possibly life) under its ice crust. The JIMO orbiter was supposed to reach Europa in 2011 (Anon 2003; Prockter 2004; Oleson 2004). JIMO was soon redesigned to orbit also Callisto and Ganymede by 2015, still using NP. A number of NASA in-house or funded studies have analyzed NP issues connected to this mission, e.g., see Oleson and Katz (2003). The consensus was that NEP was preferable to NTR, because the JIMO mission time was not critical. Within Prometheus, NASA established a Nuclear Propulsion Research (NPR) program complementing and supporting JIMO. NPR goals included reaching an I_{sp} up to 9000 s and thruster life of the order of 5–10 years. The initial propulsion system considered was a 25–35 kW gridded ion thruster. Two ion thruster concepts competed for JIMO propulsion: HiPEP and NEXIS. HiPEP was developed at NASA Glenn Research Center in collaboration with Boeing Electron Dynamics Devices, Aerojet, the University of Michigan, and Colorado State University. It was tested in the laboratory up to 40 kW with peak $I_{sp} \approx 9600$ s and 80% efficiency. The grid was made of pyrolytic graphite and was rectangular, saving much space when clustering engine modules to increase total thrust.

The NEXIS thruster, see Fig. 7.15, was developed at CalTech's Jet Propulsion Laboratory with Boeing Electron Dynamics Devices and Aerojet, and had a round carbon/carbon grid (Oleson and Katz 2003). NEXIS was lab tested at 27 kW showing an $I_{sp} = 8700$ s and 81% efficiency (Baggett and Dankanich 2004). Whether voltage

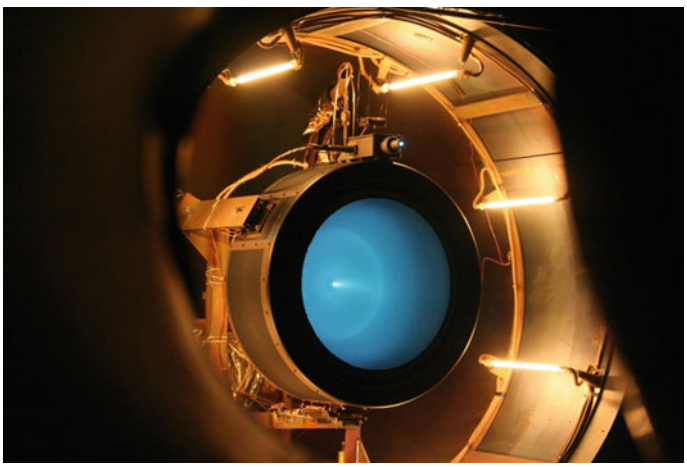

Fig. 7.15 NEXIS gridded ion thruster (Courtesy of NASA)

should be AC or DC and its level, and how to condition power were investigated (Randolph and Polk 2004; Scina et al. 2004). Sustained I_{sp} above 10,000 s without problems was later reported. A peak I_{sp} = 37,000 s was also measured. This technology is obviously mature; the major issue still left is thruster (cathode) life.

If politically supported, JIMO would have had a positive effect on all future NEP technology. At the time, JIMO and Prometheus issues were no longer nuclear "fears" by the public, but finance. The NASA preliminary design of the JIMO spacecraft predicted an astonishing 50 t mass budget; Dr. R. Taylor, head of the Prometheus Project, estimated a $4.5 billion cost to build the 25–50 kW_e nuclear electric engine (Reichardt 2004). These figures raised hard questions, accusations of "gold plating" the mission, and led to the decision to reduce the 2006 NEP budget to $100 million, just short of putting JIMO on hold but not shelving it (Berger 2005a). Michael Griffin, the NASA Administrator at the time, criticized the JIMO mission for being overly ambitious and too costly, and hinted that NEP propulsion should be reserved for a less demanding mission yet to be chosen (Berger 2005b). The speech and executive order by the US President G.W. Bush at the time in January 2006 focusing on Moon and Mars (the SEI, Space Exploration Initiative that spawned the now defunct Project Constellation) effectively axed not only the JIMO mission, but also the entire NP effort since there was insufficient funding for both. Accordingly, NASA concentrated resources on compact nuclear power generators (not nuclear propulsion) supporting manned activities on the surface of the Moon and Mars, for which the technical consensus is that a nuclear power generator is indispensable (Cataldo and Borowski 2004). Building, testing, and orbiting such a generator became the first priority of the NASA nuclear program (Anon 2008a, b). Interestingly, in 2015 ESA with the support of the EU began to plan a mission similar to JIMO, the JUpiter ICy moons Explorer, or JUICE, starting in 2022 and with the objective of visiting Ganymede, Callisto, and Europa, but using conventional chemical propulsion and gravity assists. JUICE should reach Jupiter in 7.5 years.

As much as missions to the outer planets are of interest to scientists (witness the enthusiasm after the Huygens probe landing on Titan and the Pluto/Triton flybys), the public is far more sensitive to Mars exploration, hoping that some form of life may be found. The novel by Weir (2014) and the 2015 blockbuster starring Matt Damon in *The Martian*, the tale of an astronaut stranded on Mars, are still very much resonating with the public. Consequently, the current debate on human Mars missions overshadows any other space initiative. It was apparent that chemical propulsion for a manned mission to Mars would be not just risky, but also extremely expensive (Donahue and Cupples 2000).

For a short period around 1999–2000, solar-electric propulsion (SEP) has been riding high on its high performance in applications to commercial GEO satellites. SEP, although not the favorite propulsion system, has been at least one of the alternatives. However, solar-powered propulsion has inherently low thrust, and is hardly suited to explore the outer planets and their satellites, since solar power scales with the inverse of the squared distance from the Sun. Clearly, SEP thrust would significantly lengthen interplanetary missions (Koppel et al. 2003; Mazanek et al. 2013).

An older synopsis of manned Mars missions proposed in the USA from Von Braun's times and including NTP but also chemical propulsion was in (Donahue and Cupples 2000). This paper documented the evolution of the so-called NASA Design Reference Mission (DRM) up to the 1999 version 4.0. The latest, DRA 5.0, was issued in 2009 (Drake 2009). Propulsion for this mission consists of a cluster of three 25,000 lb_f nuclear thermal engines powering both crewed and cargo spacecraft, the latter deployed in advance of the manned mission. To reduce risk, the heritage of these engines is essentially NERVA's PeeWee or SNRE; accordingly, the I_{sp} is in the 875–950 s range. The crewed vehicle, see Fig. 7.16 on the bottom, is composed, left to right, of the nuclear core stage, the on-line LH_2 tank, a "saddle" tank to be jettisoned when empty to save mass, and the interplanetary habitat and docking vehicles, see also Fig. 7.17.

The engine cluster dry weight is 41 t, the core stage weighs 106 t, and the total weight of the crewed vehicle is 356 t. The lander, sent in advance in the first of the two cargo missions, waits for the astronauts in a Martian orbit. The total IMLEO mass (initial mass in LEO, crewed and cargo missions) is slightly more than 600 t. NASA thought this necessary due to the planned long stay on the Mars surface (DRA 5.0 is a conjunction mission). The Ares launcher was abandoned, but using as a yardstick the 70 t LEO initial payload capability available with NASA's Space Launch System (SLS) (Anon 2016a, b), the current successor to Ares V, 9 or 10 launches would be required. Three missions were envisaged in the DRA 5.0 in the first ten years of the Mars exploration program, their number and schedule completely determined by planetary ephemerides.

The moderate thrust of the NASA DRA.5 nuclear engines would make their ground testing easier. Testing live engines is a sensitive issue with NTP; there are no longer facilities available capable of even simply testing nuclear reactor components (Werner et al. 2010). The SAFE facility is simply a proposal, and at the moment NASA uses the so-called Nuclear Thermal Rocket Element Environmental Simulator (NTREES) at its Marshall Space Flight Center. The dual-mode reactors investigated for many years at NASA Glenn Research Center were judged too complex and unnecessary in DRA.5 because the total engine-on time is

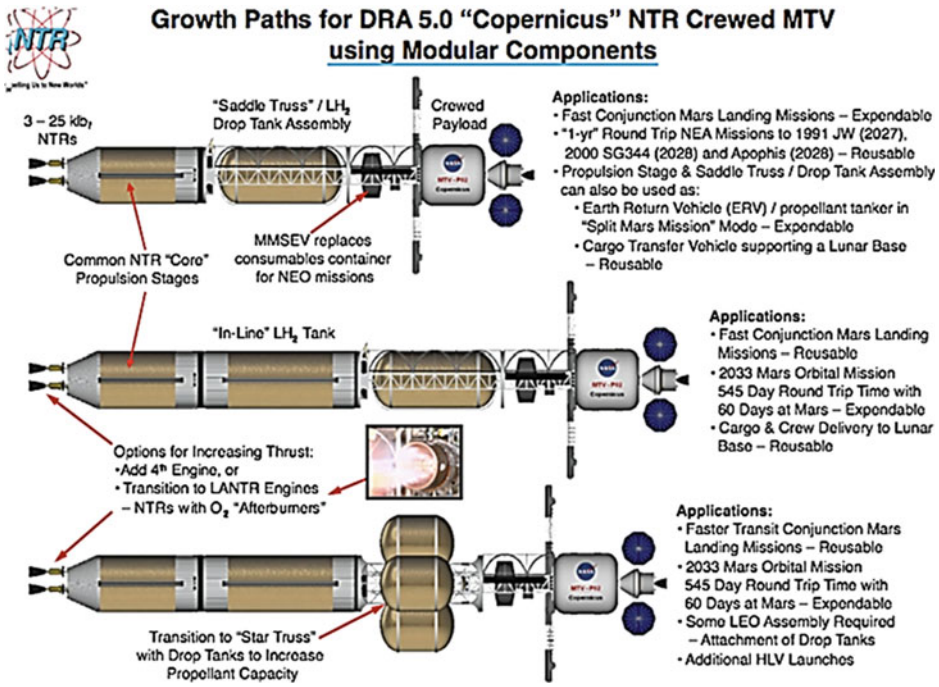

Fig. 7.16 NASA Copernicus spacecraft proposed for the human Mars mission in DRA.5. *Top* cargo ship; *bottom* crewed spacecraft (Drake 2009) (*Courtesy* NASA)

Fig. 7.17 An artist's image of NASA's Copernicus crewed spacecraft in Earth orbit (*Courtesy* NASA)

only 39 min. Thus, electric power is supplied by solar panels (not shown in the figure). Engine technology, based on the last NERVA concepts of 1970–1972, and operational time indicate that NASA wanted to play safe, using the minimum amount of NTP still capable of improving over chemical propulsion but not dramatically so. Really fast (meaning weeks, not months) Mars missions need more than minutes of engine-on time, and that means improving I_{sp} in the first place. At this point in time, NASA has no such intention nor adequate budget.

The mass estimated in the mid-2000s for a human Mars mission was in the many 100 t category and indicated the need for a much heavier launcher than Atlas V or Delta IV Heavy. NASA calculated the payload of this launcher (dubbed "Magnum" at the time) in the 80 t class. Therefore, the effort was comparable to building a Saturn V, but with cost reflecting the twenty-first century rather than the twentieth century. Six launches were planned for a single Mars mission (Donahue and Cupples 2000). The following Space Exploration Initiative (SEI) of President G.W. Bush at the time envisaged a Crew Exploration Module (now Crew Exploration Vehicle, CEV) and a Crew Launcher Vehicle. This became the Ares V heavy lift launcher (Sietzen 2008) powered by liquid and solid Shuttle rocket engines. The Roman numeral "V" was meant to suggest the sequence of Saturn vehicles of the Apollo program. As planned, the 381 ft Ares V was indeed going to be the "Magnum"-lifter wished for by the space industry (Mankins and Mandell 1999). It was going to be powered by six Pratt & Whitney Rocketdyne RS-68B liquid rocket engines, and five and a half-segment Shuttle SRM (solid rocket motor) boosters. Payload was 100–120 t to LEO, and 156,000 lb (70.8 t) to

the Moon (Morring 2008; Coppinger 2008). The RS-68B was to be derived from the LOX/LH_2 650 klb_f-class RS-68 developed by Rocketdyne since 1995 and that is the main engine of the Delta IV launcher. Its I_{sp} is 365 s at sea level and 410 s *in vacuo*.

SEI was totally based on chemical propulsion, excluding from the start any NTP or NEP. Its first objective was the Moon, considered a necessary stepping stone to Mars. This notion is still controversial and has become to some extent an issue with the scientific community that has little interest in the Moon.

Under SEI, a Moon landing was projected in the 2017–2020 timeframe using 1960s and 1970s technology. This technology consisted of modified solid propellant segments, Shuttle Main Engine(s), and a second stage powered by the Pratt & Whitney Rocketdyne J-2X, a new and "thrustier" version of the reliable LH_2/LOX J-2 engine developed during the Apollo program. The J-2X adopts technology from the older Pratt & Whitney Rocketdyne RS-27, from the RS-68, and the XRS-2200 turbopumps tested in the X-33 project. Consistent with this philosophy was the fact that the Ares vehicle, Ares I, was expendable. Stripping Ares of any reusability increased its LEO payload by about 2.5 t (Coppinger 2008).

The Crew Exploration Vehicle (named "Orion" by NASA) is a scaled-up and better-equipped version of the Apollo reentry capsule, with $L/D \approx 0.3$ and very low reentry down- and cross-range. It was designed for parachute and splash-down recovery. Orion is the only element of the SEI plan retained by the Obama administration at the time. It was tested and successfully reentered at speeds close to lunar reentry on December 5, 2014. The heavy lift Ares V of SEI (Anon 2008a, b) was replaced by the Space Launch System, SLS. The SEI philosophy rejected all airbreathing propulsion developed for TSTO concepts and high L/D hypersonic gliders described in the earlier chapters of this book. The reasons for this are many, but the most important are probably lack of understanding of the impact of L/D, mistrust or fear of hypersonics, a technology considered too risky after the two Shuttle accidents, and especially the bias of the historical investment and heritage in standard chemical rocket propulsion and its conservative community. Whether these reasons are justified, or justifiable, however the fact remains that as far as SEI was concerned, space propulsion found a safe haven in the good-old 1960s ICBM rocket-only technology.

In comparison with the return to the Moon mission, the SEI plans for Mars were much less defined. The EU and the USA felt that much more information about the Martian environment was needed; hence the many probes sent and to be sent to explore it. (The presence of water detected by the Phoenix lander now may make a great deal of a difference.) The NASA plans did not go beyond the concept of a manned Mars mission based on the Ares V lift capability. With this completely chemical propulsion scenario, costs estimated in 2008 to prepare for a now defunct Moon landing in 2018 were in the $200–$250 billion range, implying a NASA budget of the order $10 billion/year that never materialized. Under SEI, a Mars mission budget was never attempted.

These figures for chemical propulsion-based estimates worried space agencies. This situation subsequently revived interest into nuclear propulsion. The current state of affairs can be summarized by saying that on purely technical ground, Mars mission planners favor nuclear propulsion since most studies and NASA agree it reduces in-orbit mass to LEO (IMLEO), but its development costs are much feared (Norris 2010). In comparison, chemical propulsion is more mature, but the mass budget is recognized much bigger. Proposals to utilize SEP have lost favor, since low thrust and size of solar panels makes SEP slow and impractical except for cargo transit. Space agencies would use nuclear propulsion immediately if "somebody else" paid the R&D costs.

Because of this technical and financial uncertainty, no government has taken a clear position about a human Mars mission, let alone its propulsion system. The International Space Exploration Coordination Group (ISECG) is the organization with members from most space agencies (but not China) working to draw a common roadmap eventually leading to a Mars mission (Anon 2013). This roadmap is still in a state of flux. In the USA, there are proposals drafted which include the return to the Moon as prelude and testing ground of technologies for Mars; a mission to a still unspecified asteroid to test nuclear propulsion; the Asteroid Redirect Mission (ARM), consisting in moving an entire asteroid to a lunar orbit, downsized recently to capture and moving a single asteroid boulder (Jones 2015; Anon 2014; Mazanek et al 2014); landing on Phobos or Deimos, suggested by The Planetary Society and by a recent NASA presentation at the 2013 Space Challenge (Mazanek et al. 2013), and assembling at Mars a habitat from where robots could be remotely operated and explore Mars before a human landing.

All suggestions include some form of advanced propulsion, often nuclear but also solar-electric. For ARM a 50 kW solar-electric thruster has been proposed and criticized as well (Smith 2015; Morring 2015a, b). NASA has tried to justify asteroid missions and ARM with the need for planetary defence, i.e., to deflect asteroid trajectories found to pose a threat to Earth. However, this reasoning has not found traction with either the public or some of the US House Congressmen on the Space, Science and Technology subcommittee. In fact, in the proposed NASA federal budget for 2017, an item replaces ARM with Restore-L, a mission to test in-space satellite servicing.

In the current world economy, it is difficult to logically reconcile some of these proposals with the Mars objective, in

particular ARM or Restore-L now being defunct (Binzel 2014). The changes in policy since the demise of the SEI/Constellation program coupled with an initial lack of a clear focus by the Obama administration at the time confer a sense of impermanence to any roadmap. This is confirmed by the year by year shifting of key intermediate objectives. A Moon landing was [re]targeted always unofficially, by 2012, 2015, 2018, and 2020s. However, in the USA the Obama administration discouraged NASA from planning or working on Moon missions, while ESA is favoring its Moon Village concept. In fact, among other space agencies, the Moon is retained as the first step toward a human Mars mission. The Planetary Society has proposed installing the Phobos or Deimos habitat in 2033, as a prelude to human landing on Mars in 2039, but a timetable was called premature by NASA (DiMascio 2015). The year 2033 was suggested by S. Borowski (NASA Glenn Research Center) for a crewed Mars mission using NTP (Gray 2015). The reason is that 2033 is the closest year when an opposition-class mission including 60 days on Mars' surface would last the shortest time, about 502 days (Mazanek et al. 2013). This last reference is noteworthy since it accurately documents the options available not only in terms of opposition-class versus conjunction-class missions, but also compares chemical, NTP, NEP, and SEP propulsion systems, including mass budgets and mission lengths.

As it is widely acknowledged, NASA's budget, like that of other space agencies, is totally inadequate to carry on even a return to the Moon mission. No official attempt has been made to build an international operational framework similar to that working for the ISS except through ISECG. This state of affairs is not conducive to bold or new initiatives, including nuclear propulsion.

In Europe, ESA has accepted under the 2008 Aurora program ("*... to formulate and then to implement a European long-term plan for the robotic and human exploration of solar system bodies holding promise for traces of life ...*") that future Mars mission architectures may include NP. The report of the European Working Group on Nuclear Power Sources for Space was approved by the EU Commission in 2005 (Summerer et al. 2007). Small projects aimed at comparing SEP to NEP, or investigating low power NEP have been funded by the EU or by ESA (Bidault et al. 2004; Blott et al. 2012). The main reason is again the potential of NP to reduce IMLEO. Another emerging motivation, this one coming from independent analyses, is to reduce round-trip time and space radiation exposure. In fact, mass budgets and trajectory simulations of NEP-powered Mars missions are indeed encouraging if one is willing to embrace reactors in the many 100s MW class, see Koroteev et al. (2007), Simonetti et al. (2009). How to condition and feed power of such magnitude to electric thrusters would be very challenging, given their very low power per unit volume.

SEP was proposed as an alternative to NP for Mars. Its appeal is lower cost and known, safe solar cell technology. However, the low thrust of SEP is recognized as the major disadvantage. The NASA DRM 4.0 examined both NTP and SEP variants of the Mars transportation system. It envisaged a crewless SEP-powered spacecraft accelerating in a spiral Earth orbit over 9 months to reach escape speed. Close enough to the escape speed, the crew would board the ship by means of a chemical rocket-powered "space taxi." This was criticized by former astronaut Buzz Aldrin as "*... a dumb idea ...*". Adding to this complication, the DRM 4.0 with the SEP option was designed around an 800 kW SEP thruster, requiring at least 4000 m^2 photovoltaics with current technology (Larson and Wertz 1992). In fact, the SEP option for a manned Mars mission would result in the lowest IMLEO, but is out of the question as far as transit time. It is, however, very convenient for cargo transfer missions (Mazanek et al. 2013).

The chemical propulsion option of the SEI treated Mars as the 1960s equivalent of the Moon, and might well be the winner in the years to come. It would consist of landing on Mars as soon as possible to show that "it can be done," leaving to future initiatives and funding to replace it with NTP and, later, with even more advanced NEP thrusters (e.g., the VASIMR concept powered by a nuclear reactor, see Sect. 7.22). The obvious danger of this philosophy is the same as that of the Apollo program: after a number of very expensive Moon shots the public and the US Administration lost interest and terminated it, abandoning the Moon for the next half century. The question is whether this "quick and dirty" chemical propulsion approach, probably financially feasible within an international cooperation agreement, would result in the same disappointing epilogue.

In fact, all analyses so far carried out (e.g., Borowski et al. 1999; Mazanek et al. 2013; Genta and Salotti 2016) concede that the mass of a conventional chemically powered Mars missions would exceed that of spacecraft powered by NTP systems by a factor that depends on the type of mission and on the departure year, but that roughly is between 1.5 and 2. NEP systems promise to be even more efficient in terms of propellant mass, but at the price of much longer mission times. These also depend on the ephemerides of the two planets, but less so for NEP or SEP compared to NTP and chemical propulsion (Mazanek et al. 2013).

Comparisons should also account for the level of sophistication (some say luxury) of accommodations, crew size and components. In 2005, Michael Griffin, newly appointed as NASA Administrator at the time, decided that the estimated mass of the 25 kW-class ion engine vehicle for the JIMO mission was too large, requiring at least two heavy-lift launches (e.g., using Delta IV Heavy, or Atlas 5). Since then, the NEP option for Mars has been given the lowest priority, with surface power generation having the

first, and NTP the second. NASA DRA 5.0 is partly responsible for this. Among technical people and some scientists, the NTP option, the dark horse in the Mars propulsion competition, has regained status lost since the 1970s, also due to the risks posed by long interplanetary transit times inevitable with chemical propulsion. These are the effects on human health of the radiation environment in interplanetary space, see Appendix A. Radiation is a critical issue that bears on arguments pro and contra nuclear propulsion: because solar and galactic energy fluxes cannot be effectively shielded, to reduce dose means logically to reduce exposure time, that is to travel much faster than possible with chemical propulsion and low energy (Hohmann-type) orbits. Doing so also reduces the time in microgravity since it does force the astronauts on the ISS to spend an inordinate amount of awake-time to exercise. Faster travel involves thrust and I_{sp} affordable only with nuclear propulsion.

In July 2015 NASA, probably hurt by criticism concerning lack of specific plans about space exploration, issued a scenario for Mars based on the Block 1 and Block 1B version of the SLS launcher under construction (Harbaugh 2015). In this still current scenario, the Moon is not an intermediate objective, but cargo and crew missions to Mars leave and return from and to a cislunar orbit. An ARM (asteroid redirect mission) is supposed to take place in the same time span. Two propulsion options are proposed. (1) The first uses SEP to deploy in Martian orbit all cargo necessary to a crewed Phobos mission in 2033, and to pre-deploy the cargo for the crewed, long-stay Mars mission in 2039. The total number of flights would be 10 + 12, including that of the crewed Mars spacecraft. This is powered by cryogenic propulsion, limiting transit to about 500 days. (2) In the second option, both cargo and crew spacecraft are powered by a mix of SEP and storable chemical propulsion. The Phobos mission would need only 8 flights but Mars 14 instead of 12, for a total of 26 flights. A rough estimate based on SLS Block 1 capability (70 t to LEO) suggests a total IMLEO of order 1500 t with the first option, and 1800 t with the second.

In fact, the current Mars plan involves using the SLS-1B and eventually scenario (2) but with much higher payload capability, implying significantly larger total mass to be lifted, certainly much larger than in any similar Mars mission based on NTP. Among the plan oddities are the return of storable propellants (presumably NTO and UMDH), no longer mass produced in the US, and of 0.425 MW_e solar-powered electric thrusters.

Although this scenario cannot be afforded within NASA's current funding level, in 2015 the conservative NASA mind-set favoring expendable launchers seemed to have won the debate between nuclear and chemical propulsion. In fact, at the January 2016 AIAA Sciences Technology Conference, NASA announced the intention of orbiting a Moon station. In this scenario, the report by NASA's Office of Inspector General (Martin 2015) surprisingly concluded that NASA has insulated life sciences issues from engineering, and thus has not adequately addressed, among others, radiation effects in Mars missions. To cite the final recommendations: "... *mitigation of the risks for human health posed by long duration missions is a significant undertaking that can only be achieved with effective management and collaboration among the various NASA life sciences offices and technical experts from the engineering and safety disciplines. ...*". It is a good question how NASA plans for Mars by involving multiple year-long missions, architecture plans to be reconciled with these report recommendations.

Predictably, this NASA roadmap focusing on Mars and an asteroid did not sit well with some US Congressmen, who much prefer the return to the Moon as an intermediate step to Mars, and with most other space agencies. ESA is interested in the "Moon Village" concept on the Lunar far side, an outpost away from electromagnetic interference from Earth, to be built by an international partnership facilitated by NASA, but not a NASA objective (Ferrazzani 2016). Russia and China have their own Moon exploration agenda as well. Since there is no chance of the USA alone funding a Mars mission, the desires of other potential partners must be accommodated, similarly to what has been done for the ISS.

Overall, the debate Moon vs. Mars has not been resolved by the NASA scenarios, and should the Moon become a primary or even intermediate goal, it is almost certain propulsion will be, again, chemical, not nuclear, although the need for surface power will see a resurgence of interest in compact space nuclear reactors. In this context, the announcement by NASA of liquid water presence on Mars (Brown et al. 2015) may make a major difference. What has been officially concluded, based on a number of past observations, is that water flows seasonally but is heavily laced with oxidizing chlorinated compounds (perchlorates), an environment unfavorable to life as we know it. This does not rule out the possibility of salt-free underground water.

Note that a nuclear rocket using water as propellant has a theoretical $I_{sp} \approx 300$ s, about 1/3 that of hydrogen, and would be adequate for fast Mars and Moon surface exploration using hoppers, or even for a cislunar transportation infrastructure (Zuppero et al. 1997), since the Clementine lunar probe has shown evidence of water at the lunar south pole. Water ice has been discovered to be a frequent component of many dark comets ('NEO comets') periodically visiting the cisterrestrial space at the rate of 6–7 per year and per AU^2 (Zuppero 2009), see Fig. 7.18.

Cometary water could become the propellant of nuclear thermal engines powering spacecraft exploration of the Solar System (Zuppero and Jacox 1992; Linne and Kleinhenz 2016), freeing the exploration mission from the need for

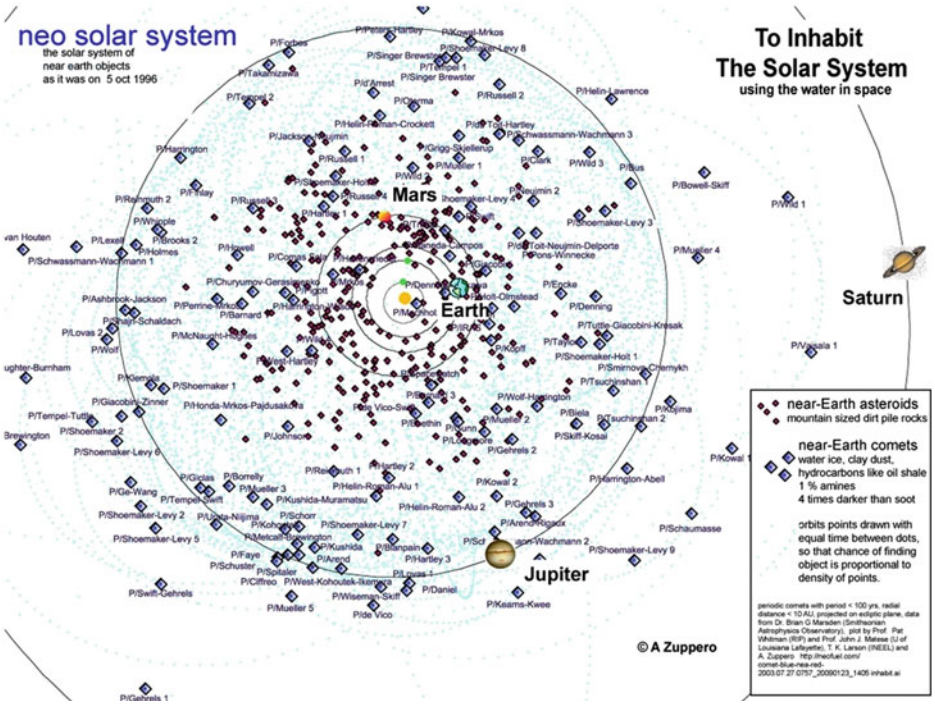

Fig. 7.18 1996 snapshot of NEO comets and NEA between the Sun and Jupiter (Zuppero 2009)

refueling from gravitational wells such as the Earth, planets and satellites. In fact, the *minimum* ΔV to capture a NEO comet orbit from LEO is roughly 3–4 km/s (Zuppero 2009).

Water is also indispensable to grow vegetables hydroponically and to human life in general. Nitrogen has also been discovered to be present in NEO, with significant implications for onboard spaceships food production. Water-rich NEO may in the long term make space exploration independent of Earth resources, and space industry, such as United Launch Alliance (ULA) is beginning to realize their potential usefulness.

A month after NASA Headquarters released its Mars plans in August 2015, Dr. Stanley Borowski announced during the AIAA Space Conference, that NASA Glenn Research Center proposed a small budget nuclear propulsion program with the objective to demonstrate the capability of a nuclear rocket by flying it to the Moon. This demo mission should take place in the 2022–2024 timeframe using engine hardware very similar to the last engine developed under NERVA, the Small Nuclear Rocket Engine, or SNRE. Thrust proposed was either 7500 lbf or 16,700 lbf. The spacecraft powered by the SNRE would "burn" only once, loop around the Moon and head to a deep-space graveyard using a lunar gravity assist manoeuver (Norris 2015). This was the first nuclear propulsion proposal with a chance of being accepted by both, space planners and by the public, and that apparently is also of interest to Aerojet Rocketdyne (Palaszewski 2015). The budgetary go ahead for the demo flight and its time frame is due in 2017.

Mass considerations and space radiation risks clearly point to nuclear propulsion as the only way to power faster and safer human missions. However, conservatism, short term vision by industry, and political hesitancy in the face of the investments that would be required, persist. In the remainder of this chapter, the two classes of nuclear *fission* propulsion systems, NTP and NEP, together with their many variants, will be discussed after outlining nuclear fission reactor technology; Turner (2005) and (Lenard 2008a, b, c) are two references on modern and advanced space reactor concepts.

7.7 Fundamentals of Nuclear Fission

Since it is the oldest nuclear technology, solid-core reactors are often taken as the baseline to gauge the performance of more advanced concepts. Chichester (2012) reports technical details of fuels, fuel elements and reactors. A nuclear propulsion system consists of a nuclear reactor (NR) feeding thermal energy to either a working fluid (NEP) or a propellant (NTP). The entire system is essentially a powered heat exchanger. Heat is produced by the primary fission reaction of a "fuel" consisting of isotopes of U, Pu, Th or other fissionable material. Fuel is always in the form of high melting point ceramics such as oxide (UO_2), carbide (UC), nitride (UN), (U_3Si_2, UAl_x) or alloys (e.g., U–Pu–Zr–Mo) or fine dispersions. The melting point of U is only 1408 K, making U unsuitable to stand solid-core reactor

temperatures. For comparison, UC melts at 2790 K, and from this temperature the coolant can be expanded much more to produce more energy or thrust.

All the fuels mentioned split into two smaller fragments ('fission') when colliding with neutrons of certain energies. In the collision, part of the original nucleus mass is converted into energy of fission fragments (FF), that is, into kinetic energy of the new nuclei, neutrons, alpha and beta particles, and photons. In particular, FF possess very large kinetic energy. In the solid-core NR, most FF are absorbed by the solid-core material encapsulating the fuel. By absorbing it is meant, that the kinetic energy of fragments is deposited and converted to heat during their trajectory inside the reactor core ('thermalization'). Fission produces fragments at a rate of order of kg/h; Sect. 7.2 showed that the heat deposited by fission fragments can be efficiently and safely removed by a much larger mass flowrate of cooling fluid. The temperature of the fluid, typically LH_2, will increase, and in a NTP is responsible for vaporizing and gasifying the fluid that finally expands in a conventional nozzle producing thrust just as in any chemical rocket engine, see Fig. 7.6. In a NEP system, the heated fluid powers a thermodynamic cycle producing mechanical energy and eventually electric power.

The energy deposition rate, or thermal power, of fission fragments in a solid material may be as high as wanted. This concept is behind the application of fission to atomic weapons. Structural material may melt or vaporize if fission is not "moderated" (controlled). This is done in the reactor by inserting or pulling bars, or by rotating drums made of neutron-absorbing material such as graphite or boron. In nuclear physics, energy is conveniently measured in electron-volts (eV) rather than °F, °C or joules (J): 1 eV corresponds to a kinetic temperature of about 11,300 K. For reference, FF released during fission have an energy level of order 10^2 MeV. On a per nucleon (neutron or proton) basis, average binding energy is ≈8 MeV/nucleon (Mukhin 1987), and since the atomic weight of FF emitted from ^{235}U fission is ≈40–140, the energy of fragments may reach a few hundred MeV. Neutrons emitted during fission have spectra typically centered at 5 MeV. For comparison, energy typical of chemical rockets may reach 0.2 or 0.3 eV. To *dissociate* H_2 into two H atoms requires only ≈0.2 eV, and *ionizing* H, that is ejecting its electron and producing H^+, requires just 13.8 eV (eV, not MeV!).

These numbers mean that fission fragments can heat matter to extremely high temperature. If the propellant flowrate is sufficiently large, propellant temperature will be much less than that of the fragments, but still capable, if not properly controlled, of melting or vaporizing any material (reactor "meltdown"). High temperatures are desirable in thermal propulsion, but pose challenges.

The main issue in designing NTP is how to slow down FF by transferring their kinetic energy to a fluid in a gradual manner, that is, without intolerable thermal stresses or temperatures. "Moderators" help in thermalizing FF. The choice of moderators is driven by the need to thermalize neutrons, from their ≈5 MeV energy down to ≈0.1–0.2 eV (1000–2000 °C; see Sect. 7.4).

The maximum temperature the heat exchanger can withstand limits solid-core reactors performance. Thus, fuel composition, structural materials and their reactivity with the propellant at high temperature ('hot corrosion') are paramount problems. During the 1950s and 1960s most of the work in nuclear thermal propulsion at the US Los Alamos Science Laboratory (LASL) focused on how to increase the temperature and to extend the life of fuel elements.

To place solid-core NTP rockets in perspective, recent materials (ternary carbides/nitrides and UZr alloy, for instance) withstand temperatures close to 2800 K. The I_{sp} potentially available with these materials can reach 1000 s, their mass/power ratio 10^{-3} to 10^{-1} kg/kW (a current NASA Glenn Research Center goal for a future 75,000 lb_f thrust engine is 0.08 kg/kW), and their dry thrust/mass ratio 10^{-1} to 1 g_0. In this respect, they are close relatives of chemical rockets, with I_{sp} higher by a factor 2–3 and thrust/mass much lower due to the weight of the solid fuel and to shielding.

The working fluid par excellence is hydrogen, because of molecular weight (MW = 2), thermal conductivity κ and specific heat ratio $\gamma = C_p/C_v$. Helium has a strong point in its lack of reactivity but is much costlier and its higher γ and molecular weight (MW = 4) yield lower I_{sp} than hydrogen.

In the following sections some of the most space-relevant fission NP technologies are presented. They have been selected on the basis of current or recent interest, and on the amount of public domain information available. Some concepts have been omitted because their stage of development is still unknown or because they are simply ideas waiting to be even preliminarily analyzed (Lawrence 2008).

7.8 Solid-Core NTR

Physics of this subject is in Glasstone (1955), Bussard and DeLauer (1958) and engineering literature spans from Glasstone (1955) to Turner (2005). An excellent description of modern reactors and their problems is in an Idaho National Laboratory presentation (Chichester 2012). A conventional solid-core nuclear thermal rocket of the NERVA-type consists of a compact nuclear reactor in which flows a propellant; this cools the reactor and is heated in turn, see Fig. 7.4. Heat is provided by fission taking place inside the solid fuel. The temperature of hydrogen used as coolant/propellant can reach 2000 K and above, depending

on fuel and structural limits. Up to 3000 K seem reachable with advanced materials [e.g., ternary ceramics (Clark 1990; Clark et al. 1993)]. At T ≈ 2500 K, H_2 begins to dissociate into H atoms and the I_{sp} increases slightly. In NERVA-type reactors, pressure (70 atm, about 1000 psia) and temperature are limiting I_{sp} to 880–900 s. Replacing hydrogen with liquid methane to increase density impulse (the product of I_{sp} times propellant density) reduces I_{sp} by a factor about 2. Density impulse is a good index of the volume taken by an energetic material and thus of structural mass per unit energy stored. Water allows a higher density impulse than either hydrogen or methane, but I_{sp} deteriorates even more (it would be a factor 3 lower than hydrogen). Also, since near 2000 K water starts dissociating into oxygen and hydrogen, explosion risks increase. During the NERVA program, water was discarded precisely because of this concern. However, the utilization of water is worth a second look for future missions because of its convenience in optimizing the mass budget. I_{sp} of the order of 300 s would be quite adequate for propulsion in the lower gravity of Moon and Mars, or for trajectories around asteroids, where water is potentially available.

As it (water) flows inside the cooling channels of the rod- or pin-shaped fuel elements, LH_2 gasifies. Its velocity increases and so does the Mach number: this and friction were responsible in NERVA engines for 25–30% pressure drop and thus for reducing ideal thrust. While the first loss is unavoidable (it is called the "fundamental loss" when heating a moving fluid), the second loss can be reduced by optimizing the topology of heat transfer channels. In the end, this led to the Pebble Bed Reactors (PBR) described later.

The thrust/weight ratio of conventional NTR is lower than in chemical propulsion, of order 1/3 or less. This is due to the weight of fuel elements in the reactor and to the radiation shield. Typical fuel elements consist of a fuel core hosted inside a container shaped as "rod," "bar," "pin," or "pebble," preventing fission fragments, especially gaseous Kr and Xe, from escaping. The rod or pin surface is the "cladding." Cladding materials must satisfy specific neutronic properties, in particular should capable of reflecting neutrons rather than absorbing them. Examples are Zr alloys ('Zircaloy'), stainless steels, and refractory alloys for high-temperature reactors. The gap between solid fuel and its cladding is filled with He or liquid Na. Fuel elements or their cluster assembly host channels where the propellant flows. Rods, pins, and pebbles are very expensive to fabricate and must be disposed of at the end of fuel life. Control drums (that can be rotated) or bars (that can be inserted or withdrawn) and the reactor wrap-around reflector prevent neutrons from escaping and slowing down or stopping fission, see Fig. 7.5 (Chichester 2012), and complete a solid-core reactor assembly. Control material should be capable of absorbing neutrons, killing the chain reaction. This assembly must be enclosed in a pressure vessel, see Figs. 7.5 and 7.9.

Conceptually, a nuclear *rocket* reactor may resemble a terrestrial gas-cooled nuclear power reactor, see Lawrence et al. (1995, Fig. 8.4), Chichester (2012), except temperatures and pressures are deliberately higher to produce thrust in a compact package. Some reactors developed under the NERVA program delivered about 1 GW and weighed only about 7500 kg including the 100:1 area ratio nozzle. The neutron shield added between 1000 and 2000 kg. Reactors and complete engines were supposed to last for no longer than 1–2 h, compared to the many thousands of hours of a commercial power utility reactor, for which a mean time between refueling is of order 18 months. The reasons for the short life of the NERVA-type reactors were severe thermal expansion stresses between fuel (UO_2) and cladding, causing cracks and leaks, the attack of hydrogen on the graphite matrix used as moderator, fuel swelling due to gaseous and solid fragments lodging inside both fuel and cladding, and hot corrosion at the interface between fuel and cladding. The need to contain gas and solid fragments led eventually to new concepts as CERMET and pebble bed reactors.

A significant feature of all NTR designed and tested under the NERVA program was that fuel and heat exchanger channels were tightly integrated in the fuel rods design. Compactness minimizes weight, but makes refueling, that is, replacing rods, practically impossible in space operation. The latest NTR tested at Los Alamos were capable of multiple (10–20) restarts, but their operation was assumed to last only until complete fuel burn-out. After that, the entire NTR was to be discarded. The reason for this design philosophy was the gradual and inevitable deterioration of the reactor materials driven by the FF flux, high temperature and pressure causing fuel swelling and leaks. Neutrons do damage materials, including fuel, by dislocating their atoms, and by creating *new* nuclei upon capture. This results in "poisoning" the fuel and reducing or stopping fission kinetics (reactivity). It is a fact that a nuclear reactor keeps changing during its operation, but for many interplanetary missions, NTR thrust sustained for 1–2 h is amply capable to accelerate a spacecraft to many tens of km/s. In the 1960s, when the interplanetary radiation was underestimated or ignored, these ΔV were thought quite adequate. Even in the NASA DRA 5.0 architecture, the nuclear engines are supposed to operate for only 39 min. In designing future reactors for faster missions, the issue of refueling may become a key issue or even a showstopper.

Performance records during the ROVER/NERVA program are:

	Record	Year	Reactor
Power P (GW)	4.2	1968	Phoebus 2A
Thrust T (kN)	930	1968	Phoebus 2A
V_e (m/s)	8280	1968	PeeWee 1
P/W (MW/kg)	0.43	1968	Phoebus 2A
P/V (MW/m^3)	2.34	1972	PeeWee
Reactor on-time (min)	109	1972	NF-1
Restarts (–)	28	1969	XE Prime

NERVA-type engines are still the design philosophy proposed by NASA Glenn Research Center for Mars missions. Given the know-how accumulated in the 1960s and 1970s, this philosophy is understandable but runs contrary to what is ideally desirable: an engine that can be refueled en route by reasonably simple operation. This would allow to reduce maximum reactor temperature whilst extending its life and reliability. The NERVA-type architecture proposed today may be justified on the ground of heritage and know-how. Nevertheless, the risk is to develop a nuclear version of the current disposable chemical launchers, with the same cost (or worse) and additional environmental or political problems. To prevent this, more structurally robust fuels, and refueling, should be priority areas (Howe and O'Brien 2010; Do Nascimento et al. 2015).

Advanced NERVA-type NTR, incorporating modern material technologies and new fuels, have been proposed and discussed for human Mars missions. With NTR based on past NERVA technology missions, transit times are still 2–3 years, too long for the radiation dose the crew could safely stand (Flinn 2004; Zeitlin et al. 2013). It is a fact that the I_{sp} of NERVA-type engines is still too low to drastically cut the mass of an interplanetary ship. Even with I_{sp} of order 800 or 900 s, too much propellant is needed to accelerate and especially *decelerate* a spacecraft for an interplanetary mission. In principle, if the planetary destination has an atmosphere, like Mars, powered deceleration can be replaced by aerobraking.

An aerobraking spacecraft loses speed by capturing an orbit that periodically "dips" inside a planetary atmosphere. The periodic drag rise slows the spacecraft down, thereby enabling to capture the desired altitude orbit. Even with the help of aerobraking, the mass of the Mars *return* vehicle estimated by the NASA Glenn Research Center team for the DR 4 was 169 t (Tauber et al. 1990). Aerobraking increases structural stresses and mass. The Cargo Lander and Habitat Lander, now the Mars Ascent Vehicle, or MAV, must be added to this mass when calculating the total mass to lift to LEO. With I_{sp} of order 900 s, the mass budget of a crewed Mars mission is still very large, and in the 2015 NASA scenario implies 22 SLS launches. The aerobraking option has never been considered for spacecraft in the 100 t class.

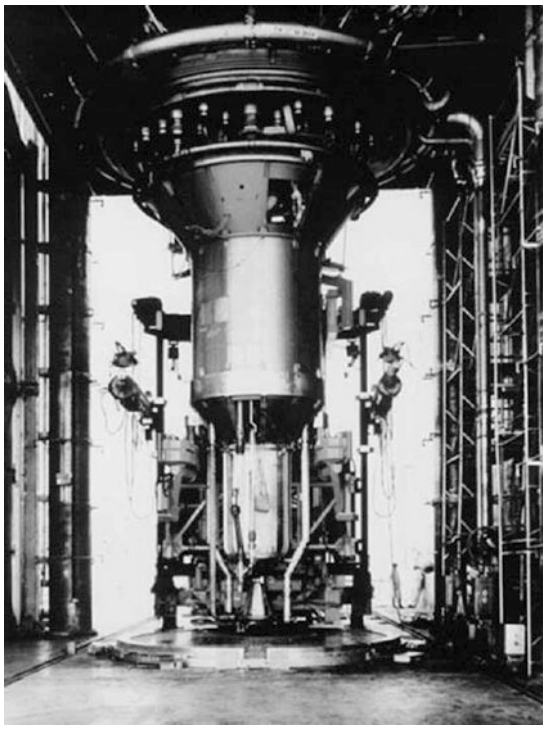

Fig. 7.19 Westinghouse NRX XE experimental nuclear engine on its test stand

To reduce Mars mission mass while avoiding aerobraking, proposals have focused on how to cut NERVA-type engine weight (Mowery and Black 1999). The baseline design was the NRX XE Prime engine built by Westinghouse/Aerojet and tested in the 1970s, see Fig. 7.19. Its core is conceptually replaced by a beryllium "island." The neutronics calculations show this island can replace the NERVA I reflector, reducing the weight of this conceptual engine to about one-tenth of XE Prime. The result of this exercise is a shielded rocket engine concept capable of 20,000 lb_f thrust and weighing about 34,000 lb, including propellant for 20 min of operation, a system with a thrust/weight ratio of order 2/3 of a chemical rocket engine rather than 1/3 common to all NERVA-derived engines. Based on 2500 K reactor temperature achievable, using ternary ceramics or other Russian structural materials, the I_{sp} predicted is about 900 s. The estimated dry engine weight is about 7400 lb. Perhaps the most significant result of such calculations is to show that it is still possible to improve "conventional" NERVA-era designs by using new architectures and materials.

Even with improvements made possible by technology advances since the 1970s, conventional NTR, while more frugal with respect to chemical rockets, still may fall short of enabling truly cheaper manned interplanetary missions. This is not only due to I_{sp} below 1000 s, but also to the mass of the engine and shield. If I_{sp} cannot be raised well above

1000 s, aerobraking would become the only option to avoid a powered Mars orbit capture consuming much propellant. This conclusion must be weighed against the extra mass to orbit due to stronger spacecraft structure. It may sound disappointing, but NERVA-type designs, even improved, might not be "the" final option for interplanetary missions, unless orbited more economically with launch systems utilizing some form of airbreathing propulsion, see Chaps. 1–5.

In fact, were the public to accept nuclear propulsion, NTR could complement and perhaps replace chemical stages in launchers. This was the initial sole motivation for the ROVER program. Assuming ΔV = 8 km/s, typical of LEO insertion, increasing I_{sp} from the 380 s of a LOX/LH_2 rocket engine to the 1000 s achievable by a NTR would reduce the propellant-to-total mass ratio from ≈0.9 to ≈0.5, reducing staging and launch costs. This conclusion is valid provided the overall engine thrust/weight was comparable to that of chemical rockets, an objective still difficult to achieve. NTR for space launchers have been investigated by the US Air Force (Vacca and Johnson 2004) and under Project Timberwind.

A class of missions, where the thrust of NTR would be very convenient or indispensable, is asteroid interception. Even recently, near-Earth objects (Chodas 2016) have been discovered too close and too late for comfort (Jarow 2000). A very large number of asteroids has been catalogued in the Mars-Jupiter belt, see Fig. 7.18. Asteroid 2011 MD was discovered June 23, 2011 when it swung by the Earth at the distance of 7600 km. The small (about 20 m diameter) Chelyabinsk meteoroid that caused damage in Siberia on February 15, 2013 was never detected and luckily burst at the altitude of 29 km. Trajectories of known asteroids might pose a future danger to Earth (Comparetti et al. 2016), to the point that the phrasing of the so-called Torino scale weighing the potential effects of an impacting asteroid has been recently toned down (Anon 2005). If the threat can be detected years ahead of time, SEP- or NEP-powered specialized spacecraft could deviate their trajectory. The issue is with asteroids detected too late to be intercepted by low-power and low-speed missions, since no chemical rocket can economically accelerate to, and match, the many tens of km per second speed seen typical of asteroid orbits (Powell et al. 1997). In fact, if a NEO trajectory would pose a danger to Earth, the last desirable strategy is to destroy it as shown in popular disaster movies: the orbits of its new fragments could be just as dangerous. A more reasonable solution is to nudge the NEO toward a different orbit, overall requiring short reaction time and matching velocity. Nuclear thermal propulsion systems capable of fast acceleration, even at the expense of efficiency, may be mandatory for such missions. Time will tell whether evaluation of the NEO threat may contribute to revive NTR technology.

7.9 Particle Bed Reactor Technology

Following the end of the NERVA program, the USAF took over research in nuclear propulsion under the Department of Defence Space Nuclear Thermal Propulsion (DoD/SNTP) Program (Lawrence 2008). One priority of the effort being a nuclear-powered reusable space tug, more formally the Orbital Transfer Vehicle (OTV). A space tug is a striking alternative to orbit raising chemical stages for commercial satellites. The USAF started in the mid-1970s by modifying the NERVA I reactor, recognizing it as the critical component of the entire propulsion system. The NERVA family of reactors was too massive and too powerful for the missions the USAF had in mind. Beginning in the 1980s, the USAF started exploring a second generation NTP based on the particle/pebble bed reactor (PBR) concept developed in Europe. PBR takes advantage of advances in high-temperature fuels. All NERVA-Kiwi reactors had long fuel bars and long, longitudinal hydrogen channels. Heat exchanging was essentially one-dimensional, heat transfer surface/volume ratio modest and fabrication was complex and expensive.

In PBR the fuel is in the form of tiny 0.5 mm diameter spheres of ^{235}U-rich uranium oxide, UO_2, or more advanced uranium-ceramic compound, see Fig. 7.20. Spheres are coated with layers of hard pyrolytic graphite, sometimes surrounded by a ZrC, SiC or other material capable of standing high temperature and having good neutronics. Many hundreds of these tiny fuel spheres (TRISO, tri-structural isotropic spheres) are packed in a graphite matrix shaped also like larger spheres ('pebbles') the size of billiard or golf balls (Lake et al. 2002; Chichester 2012). The graphite matrix is the moderator. Depending on power requirements, a reactor is sized to reach criticality by hosting the right amount of pebbles. The propellant (H_2) is heated as it flows through the hot pebble bed. In other designs, the particles are packed in between two coaxial cylinders, the hot inner one made of C/C (carbon-carbon) composite and the outer made of aluminum alloy. These fuel elements are clustered in the engine and embedded inside the moderator, for instance beryllium or ^{7}LiH. The hydrogen propellant flows inside the inner cylinders, where it is heated and then expands in a conventional nozzle (Beale and Lawrence 1989). Figure 7.20 shows one PBR scheme proposed for a nuclear thermal rocket. The spherical pebbles occupy the core of the reactor and may be kept moving to "burn" evenly their TRISO fuel (at the same rate). In fact, fission depends on neutronics, and unless recirculated or kept mixing, different pebbles would be exposed to different neutron fluxes. This may not be necessary for a space reactor designed to last only a few hours. Figure 7.20 shows also the cross section of a fuel particle in the SNTP reactor designed for Project Timberwind.

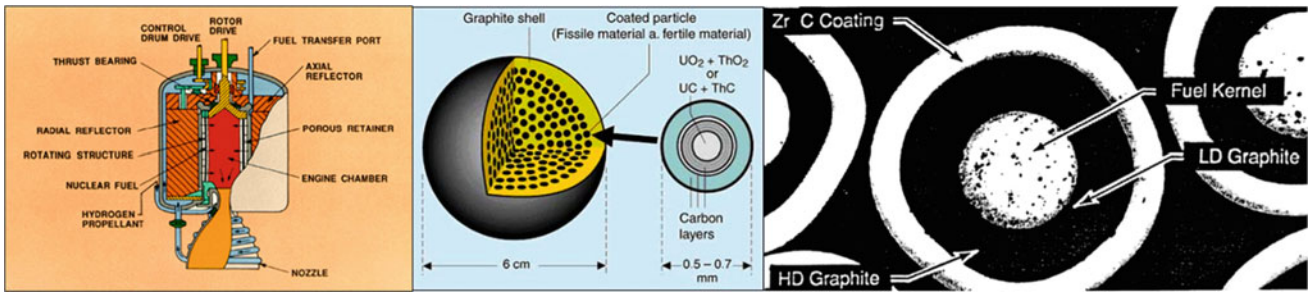

Fig. 7.20 Schematic drawing of a particle (pebble) bed reactor with a drum moderator (*left*). The details of a single pebble matrix are in the *middle*. A micrograph of an actual fuel particle tested in the Space Nuclear Thermal Propulsion (SNTP) reactor is on the *right* (Wikipedia)

Because of 3-D heat transfer, a PBR has a higher volumetric power density compared to conventional fuel rods. The gain in power density may be estimated as a factor of about 10, for a bulk power density of about 10–75 MW/dm^3. At 10 MW/dm^3, a 1-GW reactor could be compacted inside a volume less than that of an oil drum (55 US gallons), although extracting the thermal power from such a volume would be very challenging. The final rocket design when the SNTP program was stopped in 1993 (see Fig. 7.21) had a 30 MW/dm^3 power density, 1 GW thermal power and I_{sp} = 1000 s. Expected thrust was 220 kN with a dry mass 800 kg including turbopumps but without shielding. With a T/W = 2.6, the SNTP engine T/W was much higher compared to the NERVA-derived engines. Russian PBR concepts, using a ternary carbide fuel, claimed to have reached 40 MW/dm^3 or roughly 0.3 MW/kg, with gas exit temperatures ranging from 3100 K for 1-h operation, to 2000 K for 4000 h. The USAF tested individual PBR subcomponents for nearly 20 years, and $T \approx 3000$ K was maintained successfully in a single fuel element. However, the USAF never designed a complete rocket engine. Although nuclear thermal rocket engines have been designed so far to last for a time of order hours, PBR refueling appears easier compared with rods.

In absolute terms, the net gain in I_{sp} foreseeable with this type of NTR propulsion, of order 100–150 s, is significant but still barely a 13% gain over the NERVA I baseline engines. On the mass budget side, however, engine mass for the same thrust ($3.3 \cdot 10^5$ N) was estimated at only 1700 kg, plus some 1500 kg for the shield, a definite improvement. Thus, the thrust/weight of an actual engine without shielding should eventually reach about 20:1 versus the 4:1 ratio obtained by the NERVA I. Part of this improved performance is due to the much lower pressure drop inside the reactor compared to a NERVA-type configuration. Pressure drops of the order 5–6% appear feasible with PBR reactors, given their fuel topology. In comparison, the long narrow channels in NERVA-type fuel bars produced a pressure drop of order 30%.

The major technology problem of PBR engines are the durability of materials at their relatively high design temperatures. At the USAF this was the motivation for investigating CERMET (CERamics-METal) technology for fuel rods. With this technology, shield weight and volume issues are similar to those in NERVA-type engines.

All things considered, a future PBR rocket engine should be much lighter and more compact than a conventional NTR. A fast interplanetary mission to Mars would entail many hours, perhaps a day, of operation at full power. Operation of the engine at 3000 K and, say, 60 atm is probably the single most important consideration in assessing the viability of PBR as a space thruster, while its fuel topology is a major step forward.

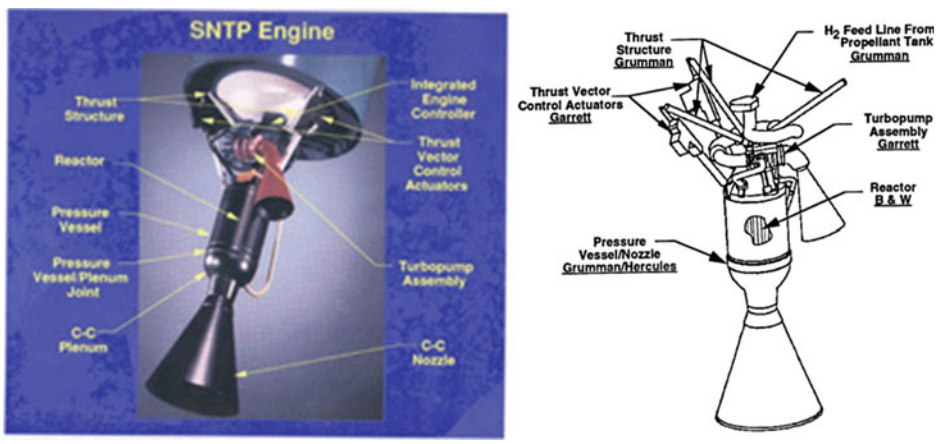

Fig. 7.21 SNTP PBR reactor designed at the time of Project Timberwind

7.10 Cermet Technology

Experience with NERVA I and the work done on PBR indicated the critical issues to be survival of the fuel elements at high temperature and pressure. Driven also by the need to extend the life of fuel elements in the nuclear airplane planned in the 1950s and 1960s (Wendt 1951), the USAF developed the CERMET reactor concept, and tested a single fuel element to check whether working life could be extended (Lawrence 2008).

In the original CERMET NTR, the fuel was stored as ^{235}U-rich UO_2 encapsulated by, or dispersed in, tungsten, molybdenum, or tungsten-rhenium (a notional engine and one of its fuel elements is shown in Fig. 7.22). No moderator (e.g., graphite) is interposed between fuel and metal jacket, so that the energy spectrum of fission fragments is broader. The main task of the refractory metal is to contain fission fragments, including gaseous, better than more conventional ceramic or metal matrices, i.e., with less damaging structural effects. CERMET fuel based on UN has been tested in the USA and the Soviet Union at temperatures of order 1800–1900 K with excellent results (Joyner et al. 2006; Howe and O'Brien 2010). The maximum operating temperature of CERMET fuel elements and their lifetime were demonstrated to be 2500 K for 2–3 h and 19,000 h at 1900 K, respectively. Fuel elements were cycled through many restarts and shutdowns (Lawrence 2008). For this reason, this type of NTR technology is considered best suited to OTV propulsion, where nuclear engines must be turned on and off very reliably for many years.

The spatial density of fuel is not as high as in PBR. In fact, the estimated thrust/weight ratio is only 5–6. Pressure losses of order 30% contribute to the low absolute performance. In fact, the I_{sp} expected from future rocket engines embodying this technology is only about 900 s. The major advantage of this concept is its very attractive and robust fuel elements technology, resulting in the ability of multiple restarts and (presumably) long maintenance-free engine life. The key issue in CERMET fuel for reactor cores is due to the very purpose of its conception, namely swelling due to the containment of fragments and gas. This problem has found, so far, only a partial solution.

7.11 MITEE NTR

The Miniature Reactor Engine (MITEE) is a conceptual nuclear thermal rocket family developed by a group of researchers (Plus Ultra Technologies, Inc.) formerly at or associated with the US Brookhaven National Laboratories. This concept is also based on CERMET technology, dating back when the US Navy formulated a requirement for a fast torpedo propulsion system. Part of the work done at that time has been proposed to power NTR for interplanetary missions including Mars.

Outwardly similar to a conventional NTR, see Fig. 7.23, MITEE designs use fuel elements where hydrogen propellant (introduced at the top of the fuel element shown in the picture) flows radially inwards. The fuel is arranged in multiple sheets, each composed of layers separated by

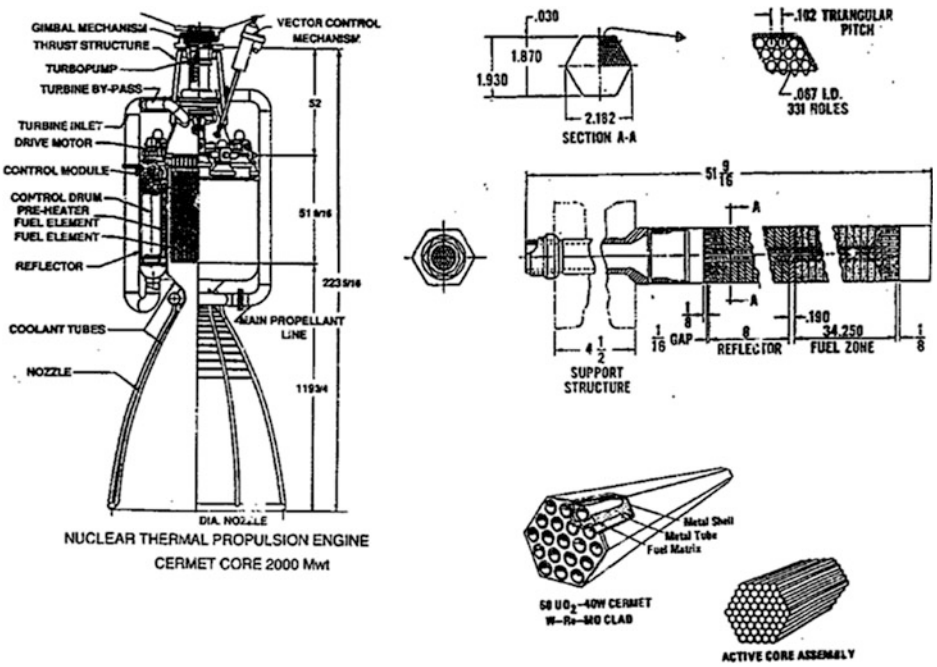

Fig. 7.22 Prismatic CERMET fuel elements (*right*) and a conceptual rocket engine designed at the USAF in the 1970s (*left*)

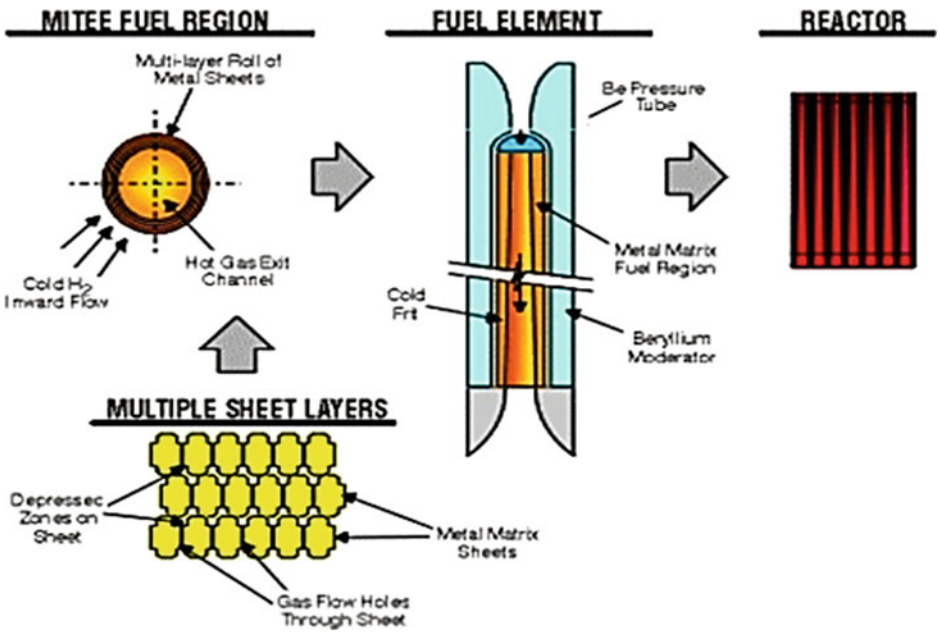

Fig. 7.23 Fuel element structure and assembly inside a MITEE reactor (Maise et al. 1998)

hydrogen channels. Each layer is formed by a metal matrix composite encapsulating the fissioning fuel, as shown in Fig. 7.22. Hydrogen flows radially and is exhausted through a nozzle at the bottom of each element. This flow topology is intermediate between 2-D and 3-D, and does produce a compact NTR. While initial MITEE designs used ^{235}U fuel, later proposals include ^{233}U and ^{242m}Am, since these materials produce even more compact engines (^{242m}Am has a critical mass about a hundred times less than that of ^{235}U).

Published estimates of engine size and mass are surprising. Total engine mass using ^{235}U is 200 kg for a baseline 75-MW engine of 50 cm diameter working at 3000 K, with a power density of about 10 MW/dm^3 and an I_{sp} = 1000. The I_{sp} becomes 1300 s operating the reactor at 3200 K, since above 3000 K molecular hydrogen starts dissociating into H. Even for frozen expansion in the nozzle, thrust is estimated at $\approx 1.4 \cdot 10^4$ N. Total one-time burn is several hours, presumably not at the highest temperature. The engine mass drops to less than 100 kg by replacing ^{235}U with the much scarcer ^{242m}Am metastable isotope (Powell et al. 1998a, b, 1999, 2004a, b; Maise et al. 1998, 2000). These are mass budgets not including the reactor shield.

The MITEE concept kept evolving in three main directions, see Fig. 7.24. A 375 kg nuclear ramjet powered vehicle was proposed to explore the Jovian atmosphere (Powell et al. 1998a, b). (1) The ramjet was the Marquardt MA150-XAA powering the North American MQM-42 Rockwell *Redhead* and *Roadrunner* target missiles of the 1960s and it was capable of accommodating in its internal volume the MITEE nuclear engine. Although the authors did

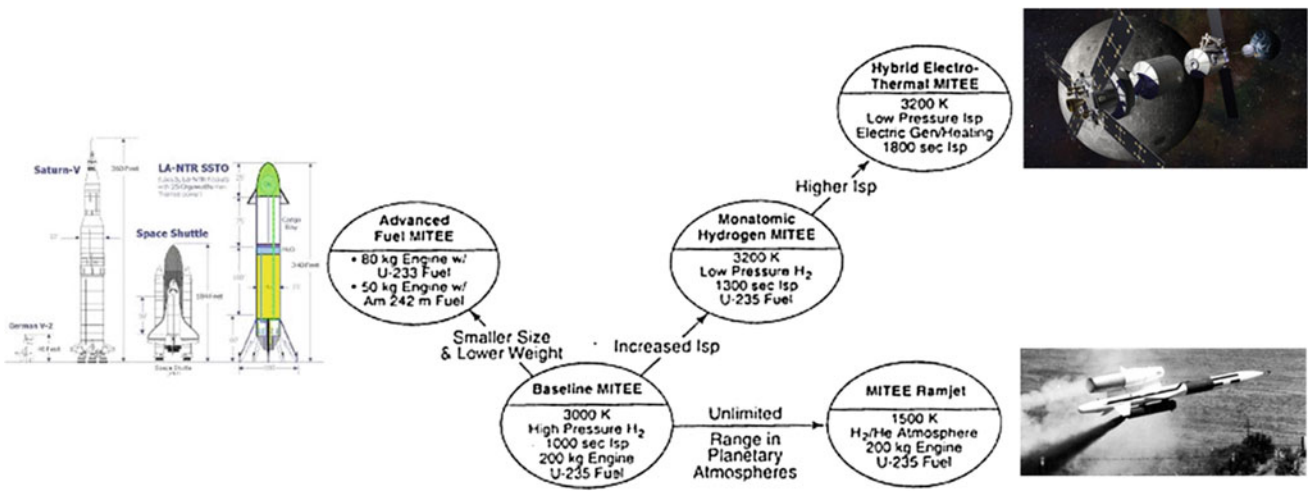

Fig. 7.24 MITEE family of concepts for nuclear thermal rockets [*Courtesy* Paul March (*left*), NASA (*top-right*) and US Army (*bottom-right*)]

not calculate the I_{sp} in the Jovian atmosphere (86% H_2, 14% He), at the same dynamic pressure of the Earth version thrust was predicted about 1500 N. (2) A variant was proposed to shuttle the International Space Station (ISS) back and forth between Earth and Moon orbits (Paniagua et al. 2008). (3) Another variant would use part of the reactor waste heat to reheat hydrogen after expansion, recompressing it and extracting further work from the thermodynamic cycle (Powell et al. 1999, 2004a, b). This cycle is similar to the classic turbine interstage reheating cycle proposed half a century ago by Boveri (1980). Since excess turbine power production is inevitable, hydrogen could also be electrically heated in a combined thermal-electric cycle. According to Powell, multiple cycling can raise hydrogen temperature to ≈3900 K and I_{sp} to ≈1850 s. While interesting, this last development is problematic in terms of the sheer amount of additional machinery and thermomechanical stress. (No turbo-machine power generator has ever been tested in orbit, and no materials capable of sustaining temperatures of order 3000 K have been space qualified.) This last type of NTR is actually a *hybrid* between pure NTR and NEP engines, exploiting the heat otherwise rejected by space radiators.

The family of MITEE concepts is worth of attention because of its compactness. In fact, combining some of the ideas from the MITEE designs with Carlo Rubbia's engine in Sect. 7.13 should result in beneficial synergy.

7.12 Gas-Core NTR

This concept was proposed in 1954 at the Scientific-Research Institute of Thermal Processes (now Keldysh Research Center), in Russia (Koroteev et al. 2002). Somewhat later, NASA Lewis Research Center (now NASA Glenn Research Center) began to investigate this concept as well. The original suggestion for *gas-phase* fission (as opposed to fission in solid fuel) actually goes back to 1949 (Bussard and DeLauer 1958, pp. 322–327), motivated by the need for a Mars mission lasting no longer than 200 days, with no surface stay.

For this mission the I_{sp} and thrust requirements were estimated about 1400 s and 10^5 N, respectively. To make the mass budget viable meant raising I_{sp} without reducing the thrust necessary to obtain significant acceleration. At the time, increasing I_{sp} was conceived possible only by raising the working fluid temperature, which is ultimately limited by the melting point of materials. Note that electric thrusters had not been sufficiently developed at that point in time. Hence, a radical proposal consisting of assuming that the fissioning fuel could not only be allowed to melt, but even to gasify, such that the heat release process could take place at much higher temperatures. The critical issue of this concept has been how to transfer heat from the hot gaseous fuel to the cold propellant, since gas-core temperatures were in the 20,000–50,000 K range.

Two cycles ("open" and "closed") were invented to solve the heat transfer problem. Since a solid heat exchanger was out of the question, radiative heat transfer was the only alternative. In both cycles it was soon found that direct radiation from the fissioning fuel to hydrogen was unfeasible. In fact, at temperatures up to 10,000 K and pressures of the order of a few atmospheres, hydrogen ionizes less than 1% and remains optically thin. For this reason, radiative heat transfer from the uranium plasma was planned as a two-stage process using hydrogen seeded with carbon particles. Hydrogen played the double role of propellant and of seed carrier gas. Fissioning fuel would heat carbon particles directly. In turn, the hot carbon particles would heat the hydrogen carrier to be expanded in a conventional nozzle.

In the "open cycle," the fissioning gas is separated from the propellant by a cooler hydrogen layer (a similar solution was supposed to keep hot hydrogen from touching and destroying the vessel walls confining the reactor). A scheme is shown in Fig. 7.25 on the left. In principle I_{sp} could reach 6000 s using a laminar vortex to keep core plasma and hydrogen propellant separated as much as possible. In order

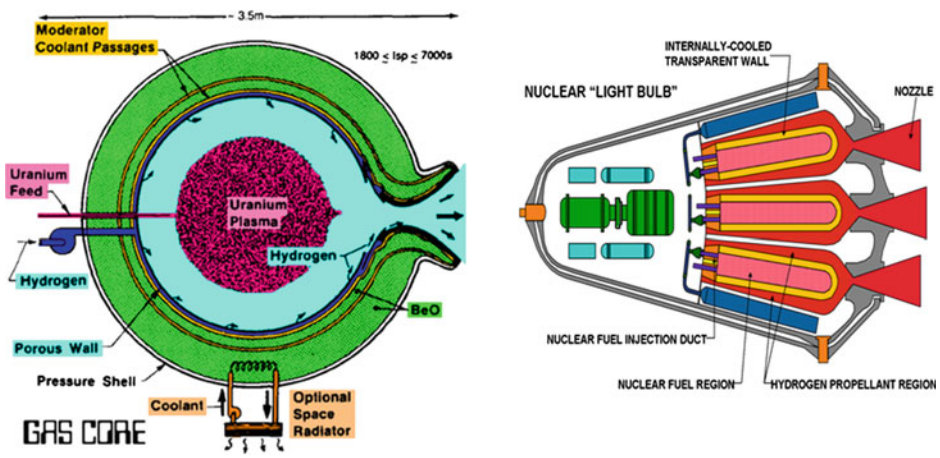

Fig. 7.25 Gas-core reactor concepts: open cycle (*left*) and closed cycle (*right*) (*Courtesy* NASA)

to keep fuel entrainment losses small, the hydrogen-to-core plasma mass ratio was estimated at least 200:1. A large amount of the power produced must be radiated away to space. Thrust available to the Mars mission engine was calculated at $5.0 \cdot 10^5$ N.

In the "closed cycle" or "nuclear light bulb" engine shown conceptually in Fig. 7.25 on the right, in addition to the cooling problems, a second problem was the reprocessing of the buffer gas (with which core plasma tends inevitably to mix). Including a space radiator, the I_{sp} was estimated at 1400–3000 s. Thrust was predicted between $1.5 \cdot 10^5$ and $1.5 \cdot 10^6$ N. This outstanding theoretical performance was matched by complexity resulting in engine mass estimated between 30 and 300 t, depending on thrust. A reference nuclear light bulb design by LASL (Los Alamos Scientific Laboratory) had a nominal thrust of $4.2 \cdot 10^5$ N, I_{sp} = 1870 s, and engine mass of 32 t. Engine sizing predicted a 3.8 m diameter, 6.9 m long cylindrical chamber containing hot plasma. Only the external surface of the optically thick plasma slug radiates a 26 kW/cm^2 flux at a calculated T = 8300 K. (For reference, this is 10–100 times larger than the heat flux over a TPS during reentry from LEO.) The stagnation temperature of the hydrogen propellant, seeded with 1% tungsten in this design, was 6700 K. Testing of this concept actually took place using UF_6 gas instead of seeded hydrogen, and replacing fission heating by radio-frequency heating. In these tests, the UF_6 temperature reached 9000 K and the heat flux measured was 7.6 kW/cm^2; the buffer gas was a fluorine–argon mixture. Deposition of uranium compounds on silica was observed to opacize silica, but this side effect was not considered critical in future engines (Mensing and Latham 1989).

Russian work on the same two cycles is similar to that in the US, but shows also some interesting differences. Among them is the gas maximum temperature below 8000 K. Most of the work at Keldysh Research Center dealt with the open cycle engine; several configurations were investigated, see Koroteev et al. (2002, Chap. 1). This reference summarizes Russian work in gas-core reactors from 1954 to 1975.

Work on gas-core engines for a Mars mission has been presented by LASL researchers (Howe et al. 1998). Emphasis was on ensuring fast round-trip time. While a substantial amount of work is claimed to have taken place toward solving the fluid dynamic problems connected with the core gas and buffer gas interaction (Thode et al. 1997), the estimated total mass budget for a "fast" Mars mission (270 days, including 40 days on the Mars surface) was 582 t. The relatively low I_{sp} = 3,000 s and the heavy engine shielding contributed to this estimate.

The gas-core latest evolution envisions fission taking place inside a recirculation zone driven by a hydrogen jet (Howe 2000). Part of the hydrogen goes directly to the nozzle, but the largest fraction is fluid dynamically forced to recirculate in a toroidal vortex prior to exhausting through the nozzle. The fuel is injected inside this vortex, where the residence time of hydrogen allows to absorb the ^{235}U fission heat. Using its codes, LASL reportedly has solved most of the plasma vortex instabilities expected or observed in the past. There is an analogy between this concept and conventional flame-anchoring in a ramjet or gas turbine combustor. In both cases mixing is slower than heat release, and recirculation must provide enough time for heat transfer.

Some of the critical gas-core technologies appear to be heat transfer and flow control and, in the case of the "nuclear light bulb," silica transparency. In addition, most of the power generated by gas-core reactors must be radiated away, only a small fraction is ending up inside the propellant. This adds the space radiator to an already complex design. On the positive side, gas-core reactors should be relatively compact (if heavy) for their thrust level. In the latest version of their design, LASL researchers seemed to have solved many of the closed cycle problems by doing away entirely with the silica walls, and relying on pure fluid dynamic anchoring, as in many conventional industrial combustion applications. Still, it is apparent that much work is necessary to realize this ambitious concept.

7.13 Rubbia's Engine

This is a concept proposed by the 1984 Nobel Prize in Physics winner Carlo Rubbia in 1998, although the first suggestion of using fission fragments to directly heat rocket propellant was made in 1948, see Shepherd and Cleaver (1948). The same idea was also investigated in Israel by Professor Y. Ronen at Ben-Gurion University (Ronen et al. 2000) and independently analyzed in the 1998–2002 period by a research team led by C. Rubbia and funded by the Italian Space Agency (ASI) as Project 242. A preliminary report described features and performance of this engine (Augelli et al. 1999).

The Rubbia engine differs from all the NTP concepts in that the heat transfer strategy of Sect. 7.5 is reversed. In this engine, it is a thin fuel layer deposited on the inside wall of the reactor chamber that fissions, emitting isotropically fission fragments. Type of fuel (metastable ^{242m}Am) and reactor (essentially a neutronic hohlraum) allow fissioning a thin fuel layer, against the popular belief that a dense mass of fuel is mandatory to reach criticality. In fact, whether or not a fuel may become critical depends on the neutron budget, that is, the difference between neutrons emitted by nuclei and neutrons escaping from the reactor. Dense mass is sufficient but not necessary. About half of the high-energy fragments released isotropically from the fissioning Am layer are injected directly in the hydrogen propellant flowing through the engine. Colliding with hydrogen molecules, the

fission fragments transfer their kinetic energy, up to 200 MeV per fragment, to the gas. Depending on flowrate, the H_2 temperature may reach 8,000 to 15,000 K forming H^+ plasma. Of course, the other half of the fission fragments emitted deposit their energy inside the reactor walls, and cooling is a critical issue.

Provided radiative heat transfer from the hydrogen plasma is moderate, the propellant may become *hotter than the solid walls*, bypassing material temperature restrictions and resulting in a simpler and lighter nuclear propulsion system. The I_{sp} expected of this concept may be much higher than solid-core NTR. Above 3000 K hydrogen starts dissociating into H atoms, lighter than H_2 molecules by a factor 2. As calculated by C. Rubbia, I_{sp} was 2500 s at 8000 K, and 4000 s at 16,000 K.

Such I_{sp} would enable a modest thrust to be maintained for days, not hours, and thus enable faster and lighter human Mars missions. If the propellant temperature could reach 16,000 K, analysis by the ASI team predicted a vehicle for a direct Mars mission could weigh as little as ≈120 t. However, calculations made by C. Rubbia and one of these authors (C. Bruno) indicated that the H^+ plasma would become opaque at about half this temperature and gradually more transparent above (Sibulkin 1968), with destructive impact on the walls. This suggests an operational temperature of ≈8000 K, capable of producing $I_{sp} \approx 2500$ s. With the thrust initially assumed, a Mars conjunction mission would still last slightly more than a year. With hindsight, the GCR (Galactic Cosmic Rays) dose to the crew would still be dangerously high, but lower than that from a standard Hohmann trajectory, including the dose from the engine (Lawrence et al. 1995, Table 8.1). Note that at that time, in 1999, no GCR measurements existed.

According to the information released in the fall of 1998 at CERN, a preliminary estimate for this concept had a mass/power ratio of 1.25 kg/kW, about 10 times larger than conventional NTR. Weight and size, however, are a function of engine operating pressure, which was assumed to be 1 atm as a convenient yardstick at the time. For this engine, ^{242m}Am was the fission material of choice, one of the reasons being that its neutron cross section peaks and then falls quickly with increasing temperature, therefore preventing runaway reaction. This isotope is metastable and must be bred from fast reactors; it can never be weapon material.

Because ^{242m}Am by itself can never become critical, an external neutron source must be used to start its fission. This can be accomplished using a proton (p^+) accelerator and a high Z (atomic mass) target material (e.g., tungsten) where the impacting p^+ beam produces a neutron shower. Neutrons can be produced by the compact neutron sources available in Russia and capable of neutron fluxes $\approx 10^{19}$ s^{-1} (Prelas 1998). The so-called TARC experiment of C. Rubbia at CERN showed that by enclosing the engine inside a graphite "hohlraum" (a cavity behaving as a black body for neutrons), neutron diffusion time and mean free path could be made long enough to sustain steady fission in a thin Am layer without an external source.

A conceptual sketch of this engine, see Fig. 7.26, consists of a chamber where ^{242m}Am is present as a layer coating the walls. Hydrogen is injected inside the chamber, for instance through wall effusion holes distributed on the chamber wall. The Am layer fissions, saturating the chamber with high-energy fission fragments. The chamber is surrounded by a neutron flux reflector, such as graphite or beryllium forming the hohlraum as well as the shield. Hydrogen flowing inside the chamber is heated by the fission

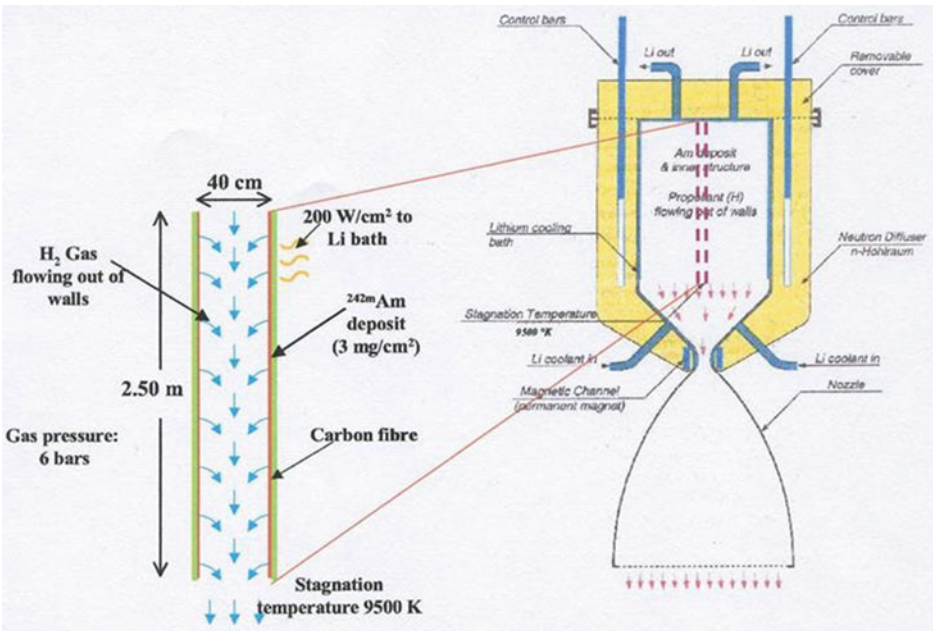

Fig. 7.26 Sketch of a notional fission fragments-heated Rubbia's engine. Details of one of the Am-coated tubes are in the *inset*. The coolant was assumed liquid lithium (*Courtesy* ASI)

fragments, then expands through the nozzle and produces thrust. An actual engine would consist of parallel chamber modules exhausting through a common nozzle. For instance, in one of the designs, modules are tubes 2.5 m long and 0.4 m diameter, coated with 3 microns of ^{242m}Am. Estimated power density was 2 MW/m^2 with fragment energy conversion 20% determined experimentally, although at only 1.2 bar pressure. Light and heavy fragments deposited 100 MeV of their energy within the first 80 mm of their path. Estimated thrust per module at 9000 K and 6 bar was 87 N (Benetti et al. 2006).

The very high temperatures ideally possible by this process are limited by convective and radiative heat losses and by fuel cooling. Thrust depends on chamber pressure, size and neutron fluxes. Thrust needed for a powered Mars mission depends also on the trajectory. A "fast" mission with a single ship was calculated by the ASI research team in 1999 assuming a few kg of ^{242m}Am were available. With 3200 N thrust, a calculated opposition mission took 369 days round-trip, including 41 days on Mars. As for the mass budget, at I_{sp} = 2000 s, the ratio propellant mass/dry spacecraft mass at Earth reentry was 1.75, dropping to less than 1 for I_{sp} = 3000 s (Augelli et al. 2013).

Details of the technical solutions to solve the many physics and engineering problems encountered are still ASI proprietary. In fact, the potential of the Rubbia engine has been only preliminarily investigated. The work done indicates that this novel concept is viable and would bypass many problems associated in the past with conventional NTR, among them their neutron fluxes. The very fact that I_{sp} could be raised to a factor 2–4 above that of other NTR, and a factor 5–8 above that of LOX/LH$_2$ rockets, is still a powerful motivation to pursue this concept further.

Among the critical areas discernible at this early stage of Rubbia's concept are: the radiative heat loss and cooling of the reactor/chamber, the effect of chamber size (diameter) on criticality, nozzle design and engine operation, Americium availability, refueling, and ground testing—the critical issue common to all nuclear propulsion systems. Among the advantages of this novel concept is the fact that Am fission can never runaway, an important factor in public acceptance. The relative simplicity of the reactor design and the potentially large I_{sp} with a reasonably large thrust are probably its most appealing features.

In the US, similar ideas based on carbon filaments coated with 3–5 μm thick fuel, were developed by a team formed by Lawrence Livermore National Laboratories (LLNL) and Idaho National Engineering Laboratories (INEL) (Chapline et al. 1988). Coating fuels considered were ^{242m}Am, ^{243}Cu, ^{239}Pu and ^{235}U (as UC), with critical mass 0.5, 1.1, 5.6 and 11 kg, respectively. At the time the choice focused on ^{242m}Am for reasons of mass, just as in the Rubbia's engine.

This LLNL/INEL concept, promptly dubbed "Chapline's brush," see Fig. 7.27, introduces on the inside conventional fission reactor filaments coated with the fuel of choice. Neutrons from the reactor drive coat fission, and their fragments are ejected with most of their kinetic energy producing thrust. There is no thermalization in a separate propellant (M_p = 0), so ideal exhaust speed should be of order of 10^5–10^7 m/s (I_{sp} in the 10^4–10^6 s range) and higher. However, the fuel consumption in solid-core reactors is very low, and so would be the mass flowrate of fuel ejected as fragments and working as propellant.

Thus while I_{sp} would be in principle very large, thrust would be very low for a given reactor power. This concept eventually evolved into using ^{239}Pu dust as fuel rather than coated filaments, and thrust improved somewhat. In 2005 calculations indicated that a 1 GW reactor could produce 43 N at I_{sp} = 527,000 s with a 0.008 g/s flowrate. Including shielding, the mass budget of the engine alone was 113 t. The low thrust/mass ratio ($\approx 10^{-5}$ m/s^2) for a hypothetical 300 t Jupiter mission spacecraft was responsible for a

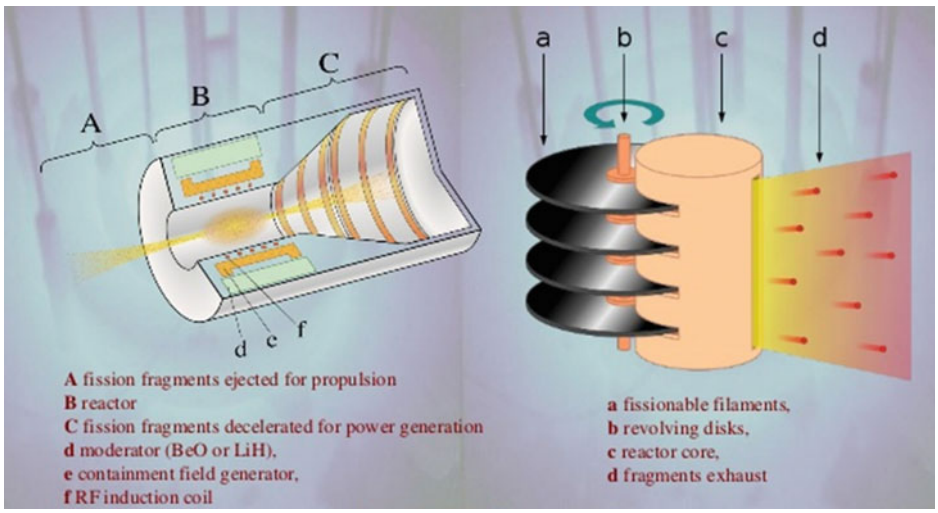

Fig. 7.27 Conceptual view of the "spinning brush" FF (fission fragment) rocket engine (Chapline et al. 1988). **a** Disks made of fuel filaments; **b** spinning assembly; **c** fission reactor; **d** FF emitted producing thrust (*Courtesy* Ian Flower)

round-trip mission close to 16 years. No consideration was given to crew dose due to GCR and to the electromagnetic field created by the Jupiter dynamo (Garrett 2010), both unknown at the time. The synthetic history of this intriguing concept is in a 2012 NASA/NIAC presentation (Werka 2012).

7.14 Considerations About NTR Propulsion

Based on the know-how accumulated since the 1950s, NTP appears viable for certain fast human interplanetary missions and for some fast robotic missions in the outer Earth neighborhood (e.g., for asteroid defence). Although NTP was investigated as a replacement for chemically powered launchers, its acceptance under existing environmental regulations and fears concerning the use of nuclear energy is improbable, and similar considerations hold for its application to OTVs (space tugs). Also of interest to NTP are missions to clean up space debris. Nuclear-powered OTV could tow dead satellites and last stages from LEO and GEO to much more distant "graveyard" orbits, and Lockheed-Martin has just proposed the very similar "Jupiter" concept but powered by chemical rockets (Morring 2015a, b, c). This class of missions could probably become more respectable if instead of NTP the propulsion system was nuclear electric, but the drawback is a much longer towing time. A task NTP can accomplish faster and cheaper is changing the orbital plane of near-Earth spacecraft, a manoeuver very costly in ΔV, as seen in Chap. 5.

While NTP for manned missions is "science" and far in the future (around 2035, according to NASA proposals), orbital transfer missions could have a commercial market right now, if the engine and vehicle existed. The large total impulse of NTP (that is, the product of I_{sp} times the operational lifetime of the engine) makes them ideal for this class of mission. MITEE, or even Rubbia's engine, could power a space tug, with the MITEE engine featuring lower I_{sp} but also lower mass. A major difference between these two concepts is the much prior work already done for the MITEE reactor. Rubbia's engine in comparison, is projected to have a much higher I_{sp}, but is still a concept in the developmental stage (low TRL).

Will the public accept nuclear power in space, including a space tug? The answer to the first part of this question is likely to be a qualified yes, while the answer to the second part is very doubtful. The tug must operate too close to Earth for comfort. In any event, a policy shift toward nuclear propulsion by any US administration should be complemented by an effort to educate the public about the risks and use of nuclear power in space (Smith 2012). No effort has ever been made in this direction. Nevertheless, this is a most important issue in nuclear propulsion and the object of much speculation, see (Anon 2004). In fact, nuclear propulsion systems can be made safer than any chemical rocket. During the NERVA program, no accidents occurred; even a test involving a deliberate thermal explosion of a Kiwi-type reactor to check for radiation effects (the Kiwi-TNT experiment) found them insignificant (Dewar 2004).

Nuclear propulsion in general (not only NTR) is the only alternative to chemical propulsion for many commercial and non-commercial space missions otherwise prohibitively expensive. Under an ideal scenario in which nuclear propulsion would be accepted, an advanced space strategy should include NTR-powered launcher stages, featuring thrust of order 10^5 N/engine with $I_{sp} \approx 950$–1000 s, and crewed spacecraft powered by small engines of thrust $\approx 10^3$ N and with higher $I_{sp} \approx 1500$–2500 s. This was at the core of Project Timberwind and before then at the core of the Soviet Union UR-700 project. Even higher I_{sp} (but low thrust) may become feasible farther in the future using nuclear-powered electric-ion or MPD thrusters such as the VASIMR (Variable Thrust and Specific Impulse Rocket) described later.

7.15 Hybrid Nuclear Rockets

Hybrid engines aim at combining the best features of different propulsion systems. Among those based on nuclear power, a concept by Dr. Melvin J. Bulman at GenCorp Aerojet Corporation of Sacramento, California, is the LOX-Augmented Nuclear Thermal Reactor, or LANTR. The idea is to put to good use the hydrogen exhaust from a nuclear rocket to produce much larger additional chemical thrust. This is achieved by injecting liquid oxygen (LOX) downstream of the engine nozzle throat, where the flow is weakly supersonic and mixing cannot affect the flow going through the nuclear reactor, see Fig. 7.28. Experience in SCRJ injection, and testing with simulating H_2 exhausted from a nuclear reactor, ensured the concept is workable (Bulman and Neill 2000). Its gasdynamics is the reverse of airbreathing supersonic combustion, in that it is the oxidizer that is injected in a pure fuel stream. Depending on the thrust mix of the two propulsion modes (nuclear and chemical), the objective may be to boost thrust for a limited time, in emergencies, or to reduce the size and weight of the nuclear reactor necessary for a mission. For instance, raising thrust by burning the H_2 exhaust enables reaching escape speed earlier with a smaller NTR, or lifting off from a planetary surface.

LANTR has been illustrated several times (Borowski et al. 1994; Glenn and Bulman 1999; Dujarric 1999; Bulman et al. 2004; Joyner et al. 2004). It offers some clear advantages over a pure NTP system, but its acceptance still depends on that of space nuclear propulsion.

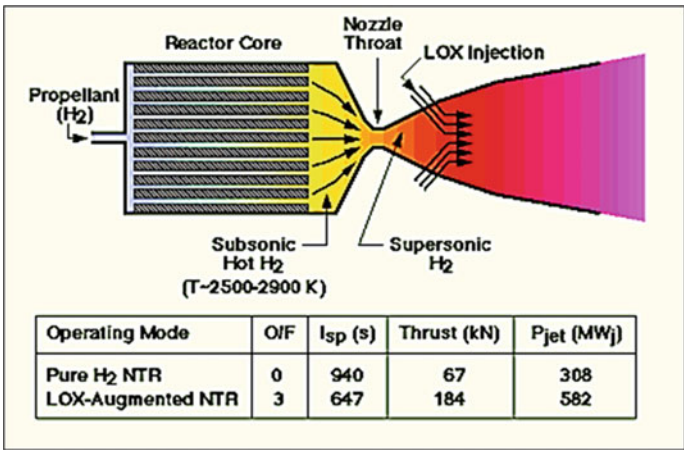

Operating Mode	O/F	Isp (s)	Thrust (kN)	Pjet (MWj)
Pure H_2 NTR	0	940	67	308
LOX-Augmented NTR	3	647	184	582

Fig. 7.28 Notional scheme of hybrid nuclear thermal and chemical (LANTR) engine

The chemical thrust available depends on the flowrate of H_2, thus on the nuclear reactor thermal power; indicatively, possibly in the 10–100 t range. With respect to a chemical rocket burning the same mixture, there is a gain due to the much higher H_2 temperature, about 1000 K downstream of the nozzle in a nuclear thermal rocket versus about 300 K in LOX/LH_2 engines. Calculations with $O/F = 3$ predicted a thrust = 184 kN and I_{sp} = 647 s, see Fig. 7.28 and Table 7.3.

LOX injection downstream of the nozzle throat is necessary not only to avoid interfering with reactor operation, but also to ignite with hot hydrogen the cold subsonic LOX. The nozzle should be designed differently from conventional expansion nozzles because hydrogen and oxygen combustion takes place inside the expanding supersonic hydrogen stream (Stewart et al. 2006). Also, turbulent mixing should be different from that in SCRJ combustors as the momentum flux ratio will not be determined by the fuel but by the LOX jets. The LANTR tested at Aerojet (Bulman and Neill 2000) simulated fission heating of H_2 by using very rich H_2 combustion (mixture ratios up to 7 were simulated, but only up to 1.5 were actually tested). A total of 63 tests were performed at 30–70 atm reactor pressure, showing 40% thrust increase over the standard engine operation reported in Fig. 7.28. In later tests (Bulman et al. 2004), thrust was raised by 55% by increasing the oxygen/hydrogen ratio. This ratio is a key aspect of LANTR that must be tailored to each specific mission. LANTR is also one mode of the "trimodal" strategy (nuclear thermal, electric and chemical) proposed at NASA Glenn Research Center (Joyner et al. 2004).

Because the ideal I_{sp} of LANTR at high thrust is not much higher than 600 s, this concept is promising when thrust must be boosted only for short times. Its applications include emergencies, e.g., when aborting a mission, to speed up injection into interplanetary trajectories, or for interplanetary missions where the mission profile consists of reaching escape speed quickly followed by a much longer segment at lower thrust. Also, when taking off from planetary or satellite surfaces, as suggested also in Dujarric (1999). An example of this profile is the LUNOX mission proposed at NASA Glenn Research Center by S. Borowski. LUNOX envisioned a LANTR-powered craft in the cislunar space, shuttling back and forth between the lunar surface and Earth orbit ferrying liquid oxygen extracted from lunar regoliths. The small NTR was to be based on the last generation of NERVA engines, the LANTR mode adding thrust to that of the nuclear engine when taking off from the lunar surface. LANTR would reduce the nuclear engine-on time and therefore increase its life. The estimated ideal performance of the LUNOX shuttle and propellants consumption as a function of reactor temperature and O/F ratio are given in Table 7.4.

These results are counterintuitive, predicting less propellant necessary when operating in LANTR mode and at high LOX/LH_2. This is due to the fact that the additional consumption of chemical propellants is compensated by a shorter engine-on time. Thus, LANTR may save propellants when tailored to specific missions. In the LUNOX case, performance depends also on the assumption that LOX

Table 7.4 Applying LANTR to the LUNOX mission saves propellants mass

NTR temperature (K)	2,900	2,800	2,600		
Engine life, h	5	10	35	Tank mass ratio:	
LOX/LH_2 ratio (–)	I_{sp} (s)	I_{sp} (s)	I_{sp} (s)	T/W_{engine} (–)	Full/empty (–)
0	941	925	891	3.0	7.1
1.0	772	762	741	4.8	13.5
3.0	647	642	631	8.2	24.3
5.0	576	573	566	11.0	33.3
7.0	514	512	508	13.1	40.0

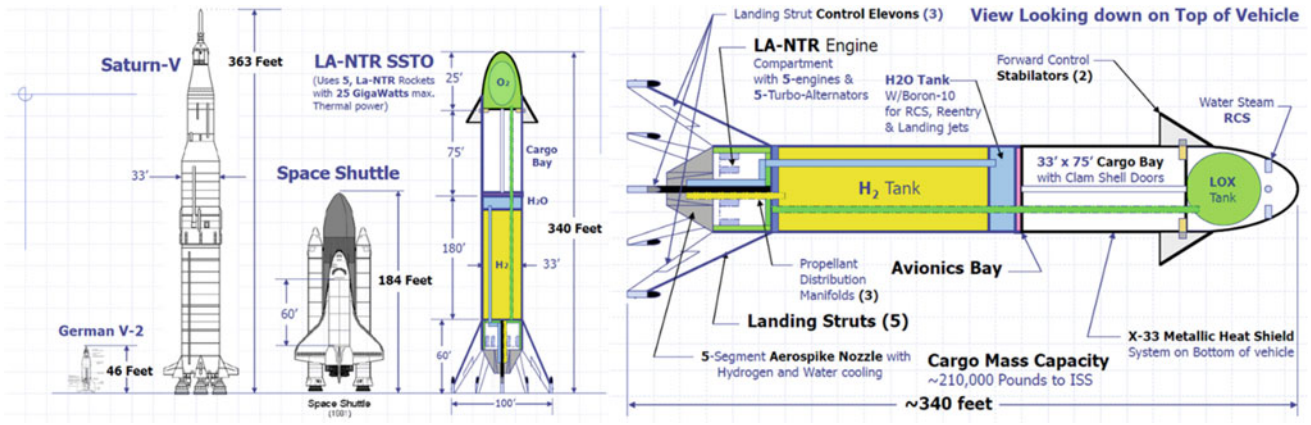

Fig. 7.29 *On left* The LANTR cargo launcher compared to Saturn V and the US Space Shuttle (STS). *On right* Reusable cargo launcher concept powered by LANTR engines (March 2006)

can be extracted economically in situ and ferried to Earth orbit.

The NTR in LANTR engines could be improved replacing the NERVA-type reactor with a PBR. At the time of the still classified US "Project Timberwind" (1992), the thrust/weight ratio of a NTR using a PBR was estimated 25. With this type of reactor and assuming the magnifying effect of LANTR mode on thrust, a PBR-powered LANTR engine could reach T/W ratios of order 75 and still produce I_{sp} much higher than any chemical rocket. This realization motivated in 2001 a very ambitious study by Dr. Paul March, with the ultimate objective to develop the huge SSTO launcher powered by a cluster of five LANTR engines, each in the 5 GW power class and shown in Fig. 7.29 (March 2006; Davis 2004).

The nuclear reactors in this study are a straightforward derivation from the NERVA Phoebus 2A reactors tested at Los Alamos in the 1960s. The thermal power available would also produce electricity using turbo-alternators to power electric thrusters for manoeuvering and for other tasks. The launcher would be completely reusable, reentering from orbit nose-first and landing vertically tail-first, as proved feasible by the McDonnell Douglas DC-X in 1991–1994 (Butrica 2003), and more recently demonstrated successfully, for the first time from orbit, by the Space-X Corporation with its Falcon 9 first-stage booster on December 21, 2015 (Morring 2015c) and in successive flights through 2017.

Its size notwithstanding, the cargo version of this vehicle, at close to 1000 t take off weight, is a factor 3.4 times lighter than the Saturn V. This is made possible by much lighter LANTR engines and the ratio $T/W = 75$ assumed in the calculations, hybrid operation at $LOX/LH_2 = 4$ producing an of $I_{sp} = 600$ s, resulting in the launcher $T/W = 1.7$. The visionary nature of this concept is built on sound understanding of the theoretical performance available from the LANTR engine.

7.16 Nuclear Electric Propulsion (NEP)

Electric propulsion utilizes Coulomb and/or Lorentz forces to accelerate electrically charged (ionized) propellant. Suggestions to this effect were by Konstantin E. Tsiolkovsky in 1911 and Prof. Robert Goddard in 1927. During WW II, while working with Wernher von Braun's team at Peenemunde, Dr. Ernst Stuhlinger started investigating ion thrusters. In the late 1940s, at the time of the first NTR designs, suggestions were made to utilize part of the thermal power of a nuclear reactor to generate electrical energy for tasks such as communications, radar, and eventually for propulsion. Some of the electric propulsion concepts discard thermal propulsion. Others exploit rejected heat from the reactor to generate additional electrical power, and use this power to further accelerate the propellant after nozzle expansion.

In all electric thrusters, whether accelerated by Coulomb or by Lorentz body forces, the propellant must first be charged (ionized). One consequence is that the pressure inside the thruster must be low enough to prevent electrons e^- and ions A^+ from recombining according to the kinetics

$$e^- + A^+ + M \rightarrow A + M \tag{7.18}$$

where A is the propellant molecule (e.g., Xe, Li, Ar or H_2), and M is a generic "third body" (i.e., any molecular species present). The role of M is that of an energy sink. Without M, a collision between electrons and ions accelerated by the Coulomb force and already possessing kinetic energy would typically cause them to "bounce back" without recombining. Only when there is a partner M to the collision between e^- and A^+ can their excess kinetic energy be transferred and a stable bond forms the neutral species A. According to the law of mass action, the rate of recombination between e^- and A^+ is then proportional to the product of the concentrations, or partial pressures, of the three reacting partners (e^-, A^+, and M). Thus, the recombination rate depends on the cube of

pressure. Pressure of order atmospheres means very fast recombination, thus low ionization, less propellant accelerated and very low thrust. In fact, this is the weak point of all electric thrusters: their low pressure/low density operation means that thrust per unit area is orders of magnitude lower than in chemical rockets. For instance, the thrust per nozzle unit area of ion engines is roughly 500 times lower than that of the Rocketdyne F-1 engine powering the Saturn V (Auweter-Kurtz and Kurtz 2008). A survey of the potential and performance expected from electric thrusters can be found in Blott (2008).

A consequence of their low thrust is that most electric- or nuclear electric (EP- or NEP) powered missions must be performed "at constant thrust for long times." With chemical rockets, the ΔV needed by a mission is achieved by accelerating at high thrust for times of order minutes. The least possible expenditure of energy with this maneuver results in a Hohmann orbit: after the initial quick acceleration the spacecraft coasts on an inertial trajectory to its final destination. In contrast, the thrust of electric thrusters is so much lower than that of chemical rockets that to obtain the same ΔV it must be applied continuously for months or years. Reaching escape speed with EP means spiraling many times around a high gravity planetary body; since the thrust vector is no longer normal to the local gravity (that is, tangent to the local trajectory), part of the thrust is not used to produce ΔV but, in astrodynamics parlance, does "gravity work." Thus, thruster life and long-term reliability are two of the key issues in NEP.

What follows is a synthetic description of NEP concepts. All assume the nuclear reactor is just a source of thermal power, to be coupled to an electric generator feeding electricity to a device that produces thrust. There is little conceptual difference between *conventional* satellite electric propulsion (powered by solar cells) and *nuclear* electric propulsion, except in the scale of power available. A review of NP-powered electric thruster types and their performance is in Cassady et al. (2008). Details of current high-power NEP thrusters are in Auweter-Kurtz and Kurtz (2003, 2005, 2008), Fearn (2004, 2005, 2008).

7.17 Nuclear Arcjet Rockets

The simplest NEP engine (Bussard and DeLauer 1958, pp. 328–330) consists of a conventional nuclear reactor and an electric power generator driven by thermodynamic cycle machinery. The generator supports an electric arc converting electric power back to thermal. Propellant is injected in the arc chamber, is heated by the arc and expands in a conventional nozzle, see Fig. 7.30. Estimated ideal I_{sp} is ≈3000–4500 s. In reality, not all propellant going through the arc is effectively heated and in any case is not heated uniformly. Therefore, the practical I_{sp} of arc thrusters is typically a factor 2–3 lower than ideal (Auweter-Kurtz and Kurtz 2003).

Limited experience with arc heaters in the 1–10 kW range indicates that the total mass of the engine system for conventional arcjet thrusters is about 10–100 kg/kW. If the same scaling held also for nuclear-powered arcjets, the thruster would take a substantial fraction of the vehicle mass. However, the thrust density (thrust/unit exit area) is higher than in most other NEP systems, with the exception of Hall ion thrusters, and it might eventually reach ≈3000 N/m^2, a very interesting value.

The arcjet mode of operation may be criticized based on the Second Law, because it is a "back and forth" energy conversion mode: from thermal to electric and then electric to thermal. The fortunes of this concept are tied to a certain simplicity in reaching high temperatures without worrying too much about structural material limits, since the propellant is heated by an arc (mostly by convection and diffusion) and not by a heat exchanger. A serious concern, partly explaining the low I_{sp} of the arcjet, is that much of the heat absorbed by the propellant while traversing the high-temperature arc is stored in non-equilibrium vibrational and electronic excitation modes. In the nozzle expansion, non-equilibrium energy should ideally convert to translation energy, that is, the propellant flow velocity should increase, become uniform and collimated (aligned with the nozzle axis). However, this does not necessarily occur when the expansion is fast and starts from non-equilibrium arc

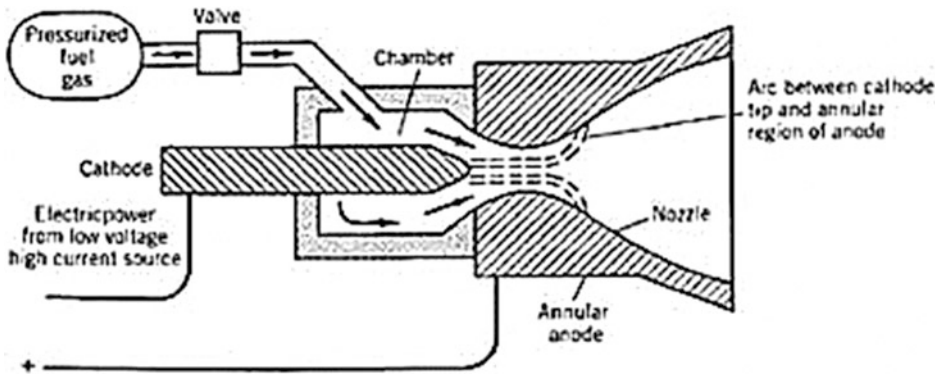

Fig. 7.30 Schematic of uncooled arcjet thruster (Anon 1996)

temperatures that may reach 25,000 K. In practice, part of the thermal energy remains trapped ('frozen') inside the expanding gas.

The difficulty of heating all propellant uniformly, and the fact that a good fraction of the energy taken from the arc has no time to convert to propellant kinetic energy, these facts justify why arcjets have been neglected as propulsion systems. Hybrid arcjets (i.e., arcjets feeding plasma to an induction heating section) look instead promising for high-power (>100 kW) thrusters (Auweter-Kurtz and Kurtz 2005, 2008). Modules assembled together in a power pack (and suitably cooled) could produce thrust of order 0.1 N/kW or higher, with $I_{sp} \approx 1000–2000$ s.

7.18 Nuclear Electric Rockets

If the nuclear reactor powers an electric thruster (ET), the propulsion system becomes a "pure" nuclear electric propulsion (NEP) system. In electric rockets, propellant acceleration is not based on thermodynamic expansion, but on the presence and strength of electric or magnetic fields. In juxtaposition, thermodynamic expansion has an efficiency η depending on the ratio between the maximum and the minimum cycle temperature. The efficiency η can be enhanced only up to a point, because of materials temperature limitations already discussed.

Both magneto-hydro-dynamic (MHD) acceleration based on the *Lorentz force* and electrostatic acceleration based on the *Coulomb force* are thrust-producing physical mechanisms. Both require electricity supplied by an *energy conversion system*. In both, reactor and propulsion system are separate components, see Fig. 7.6, lending themselves to separate optimization.

Thermodynamic conversion is impacted by the η issue associated with thermal to electric energy conversion. Alternatives to thermodynamic generation have been proposed, but the step from physics to engineering is still long, see Bidault et al. (2004), Backhaus et al. (2004), El-Genk (2009), Blott et al. (2012). In this area, Magneto-Hydro-Dynamics (MHD) is a favorite concept, as high-temperature gas available from a nuclear reactor could be ionized by seeding it with metals such as Ba, Na, and K, see Smith and Anghaie (2004). At high temperature, these corrode the structural materials used in making MHD channels. This problem and that of extracting the current from the magnetized channels have stopped all research in MHD for terrestrial applications (Messerle 1995). A promising concept is solid-state Alkali Metal Thermal to Electric Conversion (AMTEC) (Schock et al. 2002). This is a cycle where the reactor power vaporizes an alkali metal, and its vapor expands isothermally inside a ceramic matrix, directly converting expansion work to electric current with an efficiency close to Carnot cycle efficiency, see Fig. 7.31. System studies for power levels from 1 kW to 10 MW_e indicate efficiency improvements exceeding those of machinery, see Cumo et al. (2005). Tests performed at low power (6 kW_e) between 1123 and 650 K have shown the efficiency to range at $\eta \approx 25\%$ (Ferrari and Bruno 2012). This reference reports a comparison among static and dynamic conversion systems for a 100 kW_{th} reactor.

For all these reasons, thermodynamic conversion is still the standard in high-power NEP systems proposed. Using current technology for ground applications, this standard comes with a high price in terms of mass. For instance, stated goals at NASA Glenn Research Center for the JIMO mission were a mass/power ratio less than 40 kg/kW_e (the subscript indicates electric power, not the reactor thermal power). Payload and mission time depend critically on this ratio, see Stuhlinger (1964), Oleson and Katz (2003). This ratio should be compared with NASA's 0.08 kg/kW goal for NTR. This stunning difference is the result of the low

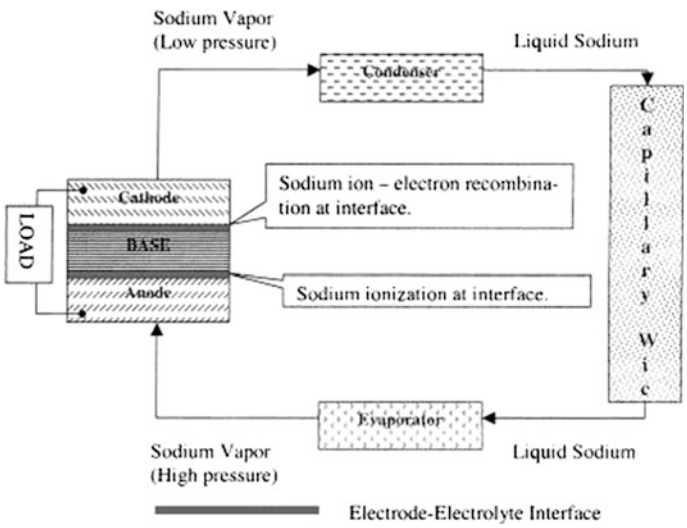

Fig. 7.31 AMTEC power converter schematic (Aubrecht 2005)

efficiency of thermal conversion using turbomachinery and of the mandatory space radiator. NTR does not need either. The extra weight of turbomachinery conversion may be substantially reduced by increasing the rpm, a very promising avenue enabled by near term composite materials and possibly limited by bearing life, see Lenard (2008a, b, c) for a vision in this area.

Low power ion and MHD-based thrusters have been tested for many years and commercialized for satellite applications. Fundamental information can be found in Sutton (1992), Hill and Peterson (1970), Goebel and Katz (2006), Fearn (2008), Auweter-Kurtz and Kurtz (2008), Bruno (2014). Almost invariably, all space electric thrusters have been powered by solar cell arrays. Average power in Earth orbit is of order 300 W/m^2 for high efficiency cells (Patel 2014). What is new in the context of EP is the power available when switching from solar arrays to nuclear reactors. Scaling thruster power from kilowatts to megawatts involves opportunities as well as engineering and technology challenges. These are still far from having been satisfactorily analyzed.

7.19 Electrostatic Ion Thrusters

Commercial ion thrusters installed on satellites produce thrust by electrostatically accelerating ionized propellant (Xenon is a common choice). The Coulomb force acting on ionized propellant is produced by the electric field between high voltage grids. Serially connected solar cells are responsible for the voltage (Bussard and DeLauer 1958, p. 330; Sutton 1992; Goebel and Katz 2006).

The simplest type of ion thruster (often called Gridded Ion Engine, GIE) is schematically illustrated in Fig. 7.32. This scheme was used in the Mu-10 ion thruster powering JAXA's Hayabusa mission (Okada 2010). The grids not only provide the Coulomb force, but also extract and condition the trajectory of Xe^+ ions created in the thruster chamber, where the inevitable space charge in front of the first grid tends to push them back. Similarity with the way optical lenses guide visible light, the grids create the concept of "microwave optics". Different ionization strategies determine different types of GIE; details, differences, and performance of different GIE types are in (Fearn 2008). To further help in guiding the ion current, sometimes magnetic fields are added to places in the chamber or outside. Often GIE take different names based on the specific ionization mechanism used and on the presence of magnetic fields. Finally, to neutralize the negative charging of the spacecraft when the GIE is in operation, the electrons left from the ionization process are cycled back and injected by the charge neutralizer (on the top-right corner of Fig. 7.32) into the ion jet. The ultimate exhaust of a GIE is therefore a very dilute neutral jet of Xenon (as in all ET, ionization can occur only at very low pressure).

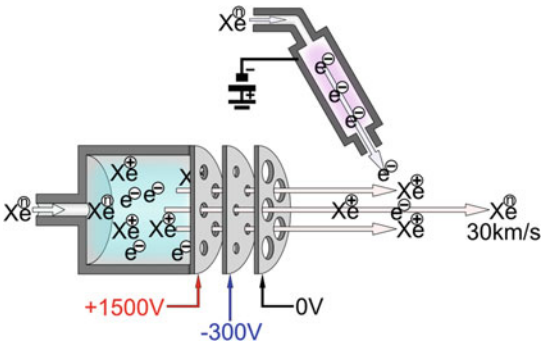

Fig. 7.32 Simplified scheme of the Mu-10 ion thruster and of its operation (Courtesy of JAXA)

Although photovoltaic cell series connection can obtain many or tens of kV, solar power extracted by current photovoltaics in Earth orbit is limited to about 300 W/m^2. Nuclear power may generate larger voltage, ultimately of order 40–50 kV, but whatever the source of power, thrust and I_{sp} are limited by space charge, breakdown voltage, and size of engine exit cross section. In fact, thrust and power densities, in N/m^2 and W/m^2, respectively, are characteristic performance parameters of ion engines. Thrust of commercial ion engines in Earth orbit is about 1–3 N/m^2 with (solar) power in the 1–10 kW. However, 1-MW prototypes have been built and laboratory tested (Fearn 2003). Performance extrapolated to 6 MW with scaling laws derived from lower power engines predict a thrust density that could eventually reach about 300 N/m^2 with I_{sp} of order 30,000 s, and thrust/power ratio about 6 N/MW (Fearn 2004). For comparison, this ratio would still be 10^2–10^3 times smaller than that of NTR, but the I_{sp} would be about 30 times larger. A comprehensive description of this propulsion technology and its scaling is in Fearn (2008), Goebel and Katz (2006). With I_{sp} of order 30,000 s reached in the laboratory, electrical power to feed a 1 kN thruster would need a few hundred megawatts. Reactor power would be $1/\eta$ larger.

Future I_{sp} improvements may come from fusion technology, in particular tokamak reactors (see Chap. 8). Hydrogen or deuterium fusion fuel in the form of H^+ or D^+ ions must be injected in tokamak reactors fast enough to prevent their recombination in the colder gas blanket near the inner wall. Injection speeds of order 4000 km/s have been achieved. Although tokamak injectors are pulsed, such speed corresponds to an *instantaneous* $I_{sp} \approx 400$ ks. In essence, a tokamak fuel injector is a form of ion thruster (Fearn 2008).

An interesting feature of ion engines is that thrust depends in a simple way on the applied voltage. The energy balance for an ion of mass m possessing a charge q (Coulomb) accelerated by an electric field due to a

difference of potential ΔV_{dp} (in volt) between two grids states that the kinetic energy ½ m V_e^2 acquired must be equal to the work done by the field on the charge, $q\Delta V_{dp}$:

$$\frac{1}{2} \cdot m \cdot V_e^2 = q \cdot \Delta V_{dp} \tag{7.19}$$

Thus the exhaust velocity acquired by the ion will be

$$V_e = I_{sp} = \left(2 \cdot q \cdot \frac{\Delta V_{dp}}{m}\right)^{\frac{1}{2}} \text{in [m/s]} \tag{7.20}$$

The thrust is

$$F = \left(\frac{dm}{dt}\right) \cdot V_e \tag{7.21}$$

the ionic current

$$i = q \cdot \frac{\left(\frac{dm}{dt}\right)}{m} \text{ [Ampere]} \tag{7.22}$$

and the power

$$P = I_{sp} \cdot \Delta V_{dp} = \left(\frac{dm}{dt}\right) \cdot \frac{V_e^2}{2} \tag{7.23}$$

As in most electric thrusters, performance parameters are power and current absorbed per unit thrust:

$$\frac{P}{F} = \frac{I_{sp}}{2} \tag{7.24}$$

$$\frac{i}{F} = \frac{q}{m \cdot I_{sp}} \tag{7.25}$$

In principle, ion engines may have a degree of control of thrust and I_{sp} at fixed power by varying the voltage. If this can be achieved in practice, the thrust versus time profile could be optimally tailored to each interplanetary mission.

The main trade-off of all EP thrusters, and of ion engines in particular, is between I_{sp}, mass consumption and thrust. Mass consumption (and thus overall weight) depends on mission time and I_{sp}. Thrust depends on mass flowrate and power. Choosing and designing a propulsion system involves interconnected trade-offs, and in the end becomes a cost-driven exercise.

Because ion engines power already commercial satellites, manned interplanetary missions have been studied or planned around nuclear-powered ion propulsion. This technology is mature and space qualified at power level of $\approx 10^1$ kW. A 100 kW_{th} reactor is within reach (Blott et al. 2012). For the JIMO mission planned by NASA, the nuclear-powered Xenon ion thruster was in fact in the 16–25 kW range (Randolph and Polk 2004; Scina et al. 2004), a practical limit using solar panels in Earth orbit, and hardly achievable near Jupiter. The planned RASC Venus mission (McGuire et al. 2004) also assumed a nuclear ion engine, even though near Venus radiated solar power would be about 2500 W/m^2, twice that available near Earth (1300 W/m^2).

Commercial ion engines use the rare and expensive gas Xenon as propellant, since it is the most economical high molecular weight gas. (Note that, contrary to what happens in thermodynamic expansion, when an external force is available to accelerate a gas, the best propellant to produce thrust is also the heaviest.) Whether enough Xenon will be available for large nuclear engines and long missions must be assessed. The world production of Xenon is about 59 t/year, and its price (in 2015) about $850/kg. At 1 MW power and 70% conversion efficiency, and assuming I_{sp} = 4000 s, the consumption of Xenon per year for a mission would be 13.6 t, or more than one-fourth of the entire world production in a year. Note that operating ion engines continuously for 1 year or more is realistic, since under the same assumptions thrust would be only 17.5 N. In fact, a criticism levelled by then-NASA Administrator M. Griffin to the JIMO mission (including flybys of Callisto and Ganymede) was, that it would consume twice the world's production of Xenon (Berger 2005b). This and other questions concerning the balance between I_{sp} and power in planning interplanetary missions with ET can be understood by looking quantitatively at their effect on propellant mass and ΔV. These questions are not relevant to chemical propulsion, because thrust (applied for a very short time) is the variable controlling acceleration, not power. These are instead *the* issues in electric propulsion, where engines may have to work for months or years. The simplest equations to quantify NEP-powered missions are:

$$\dot{m} = \frac{F}{I_{sp}} \tag{7.26}$$

with $\dot{m}$ is the instantaneous propellant mass. We obtain for the mass of propellant consumed at constant $\dot{m}$ after a time t_{acc}

$$m_{ppl} = F \cdot \frac{t_{acc}}{I_{sp}} \tag{7.27}$$

For the distance travelled at constant acceleration a

$$d_{acc} = 0.5 \cdot a \cdot (t_{acc})^2 \tag{7.28}$$

With ΔV acquired after time t_{acc} at constant acceleration a

$$\Delta V = a \cdot t_{acc} \tag{7.29}$$

and

$$F = M_{spacecraft} \cdot a \tag{7.30}$$

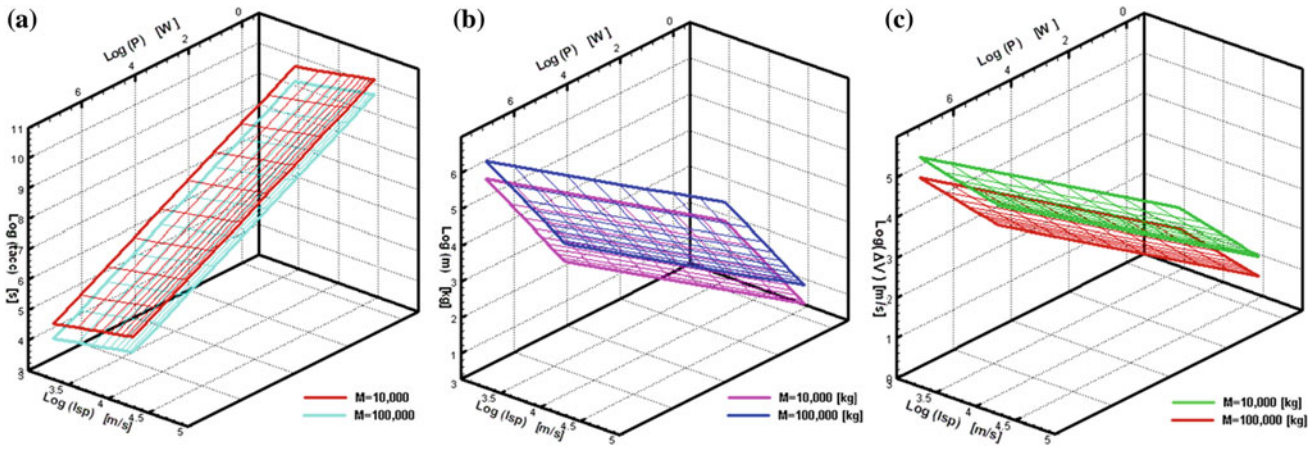

Fig. 7.33 **a** Acceleration time, **b** propellant mass, and **c** ΔV for spacecraft of mass 10,000 and 100,000 kg as a function of power P and I_{sp}

The solution for time, mass m and ΔV is:

$$t_{acc} = \sqrt{\frac{2 \cdot d_{acc} \cdot I_{sp} \cdot M}{P}} \tag{7.31}$$

$$m_{ppl} = \sqrt{\frac{2 \cdot d_{acc} \cdot P \cdot M}{I_{sp}^3}} \tag{7.32}$$

$$\Delta V = \sqrt{\frac{2 \cdot d_{acc} \cdot P}{I_{sp} \cdot M}} \tag{7.33}$$

In this example M, d_{acc} and power P have been assumed as input parameters. The solution set is plotted in Fig. 7.33. Note the favorable effect of I_{sp} on propellant mass and its opposite effect on acceleration time and ΔV. At fixed power, increasing thrust must come at the expense of decreasing I_{sp}, then it takes longer and longer to reach smaller and smaller ΔV.

When planning an interplanetary mission where at least the accelerated part of the trajectory length, d_{acc}, is flown at steady power, one may assume M and P as input. Roughly, d_{acc} should be half the d distance to the final destination. Past that the spacecraft should start decelerating. However, d_{acc} may turn out to be greater than d when the acceleration

$$a = \frac{P}{I_{sp} \cdot M} \tag{7.34}$$

is very small, i.e., for very low thrust and power. If the trajectory is an interplanetary orbit, for instance Earth to Mars, the spacecraft must *spiral* Earth until reaching escape speed. At that point the spacecraft can start accelerating along the trans-Mars trajectory.

As an example of issues in choosing a powered trajectory, consider electric propulsion solutions for a notional Earth to Mars mission ($d = 1.5 \cdot 10^8$ km) using a hypothetical 0.7 MW_e ion engine with $I_{sp} = 4000$ s, and a spacecraft mass $M = 100$ t. Assuming $d_{acc} = 10^7$ km, equations predict $m = 5$ t, $t_{acc} = 1157$ days and $\Delta V = 2$ km/s, clearly insufficient. When stretching to $d_{acc} = 8 \cdot 10^7$ km (about half the Earth–Mars distance), the new solution predicts $m = 15$ t, $t_{acc} = 3450$ days and $\Delta V = 6$ km/s, sufficient in terms of speed but impractical in terms of time. Scaling power by a factor 10 to 70 MW yields $t_{acc} = 33$ days and $\Delta V = 54$ km/s but requires $m = 135$ t, that is violating the $m \ll M$ assumption (and cornering the world Xenon market). Note that $M = 100$ t would be an absolute minimum for a manned Mars spacecraft. In fact, a realistic estimate of time and mass needs trajectory codes and numerical solutions.

From this simple analysis, the conclusion is that for certain crewed missions, present ion engine technology is insufficient to ensure reasonably fast and cheap travel. Only much higher I_{sp}, of order 10 times larger compared to those now available (that is, 40,000 s), can provide a truly satisfactory solution. For a 100 t spacecraft, this requires nuclear reactors in the many 10^2 MW class. Technology developed to inject plasma beams inside tokamak fusion reactors may help in raising specific impulse of gridded ion thrusters, but the power issue and that of the number and size of engines made necessary by low thrust density still remain. With adequate resources, ion engines with power ≈1 MW and thrust of order 20 N may probably become feasible, but for what mission they can be utilized remains unclear. Other solutions may be available by dropping the assumption of continuous thrust, for instance by varying the duration of thrust-on periods in transplanetary and orbit-capturing trajectory segments.

7.20 MPD/MHD Thrusters

High-power magneto-plasma-dynamic (MPD) thrusters (or as well called magneto-hydro-dynamic (MHD) thrusters) exploiting the Lorentz force are somewhat less developed compared to ion engines.

The Lorentz force is the force acting on a charge q moving at velocity $\vec{v}$ and in the presence of a magnetic field $\vec{B}$. The Lorentz force is defined as

$$\vec{f} = q \cdot \vec{v} \times \vec{B} \tag{7.35}$$

and is directed normal to both $\vec{B}$ and $\vec{v}$. Charge motion presumes the charge is moving because of another body or pressure force; note that the Lorentz force is zero if the charge is at rest. How to exploit the Lorentz force to further increase $\vec{v}$ is not immediately obvious. If $\vec{v}$ is directed along a nozzle, and, for instance, $\vec{B}$ is normal to this direction, the Lorentz force will deviate $\vec{v}$ and direct the charge against the nozzle wall.

It is therefore more useful to accelerate charges utilizing both an electric and a magnetic field, not only to accelerate, but also to guide charges. The electric field $\vec{E}$ applies the Coulomb force $q \cdot \vec{E}$ so that the total force applied will be $q \cdot (\vec{E} + \vec{v} \times \vec{B})$. Some physicists call Lorentz force this sum, although $q\,\vec{E}$ is the Coulomb force. MPD thrusters accelerate charges by appropriately shaping $\vec{E}$ and $\vec{B}$ forces by means of electrodes and magnets. If positive (ion) charges ρ^+ are distributed in a gas with density ρ_c (Coulomb/m^3 in the SI system), the total force is

$$\vec{f} = \rho_c \cdot (\vec{E} + \vec{v} \times \vec{B}) \tag{7.36a}$$

$$\vec{f} = \rho_c \cdot \vec{E} + \vec{J} \times \vec{B} \tag{7.36b}$$

where $\vec{J}$ is the current density vector, see Fig. 7.34.

According to Newton's Third Principle, when plasma is accelerated, thrust is applied in the opposite direction. Not all molecules/atoms of a gas need to be ionized to be accelerated by Coulomb or Lorentz forces. At sufficiently high charge density ρ^+, neutrals are also entrained through collisions. Electrons are accelerated in the opposite direction of ions, but their mass is so small that they do not contribute to thrust.

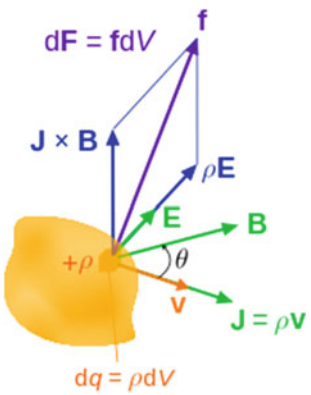

Fig. 7.34 Total force $\vec{f}$ acting on a plasma of charge density ρ and moving at bulk velocity $\vec{v}$ in $\vec{E}$ and $\vec{B}$ fields (*Courtesy* Wikipedia)

The regime of an MPD thruster can be steady in the strict sense, or quasi-steady. The thrust of a quasi-steady MPD may occur in pulses or bursts. When these last long enough, or when the burst repetition rate is high enough, the averaged thrust is said to be quasi-steady. Quasi-steady MPD thrusters have been tested far more than steady MPD, one of the reasons being their lower power demand and their relative simplicity. For high-thrust applications, steady MPD are better. However, without a nuclear generator there is no way they can become effective space engines.

To overcome the problems due to direction of $\vec{B}$, the simplest MPD accelerator may use an axisymmetric $\vec{B}$ field, see Fig. 7.35. The radial component of the Lorentz force generates a magnetic pressure $\sim B^2$ that can accelerate plasma by expanding it thermodynamically. The circumferential velocity must be converted to axial by a magnetic nozzle, and this is a central aspect of all MPD thrusters (Mikellides and Turchi 2000).

On satellites, MPD engines are powered by photovoltaic (solar) cells with an I_{sp} of order 10^3–10^4 s, and their weight and size larger than those of ion engines due to the presence of magnets and their wiring. A laboratory MPD thruster may have a mass/power ratio of order 1–10^3 kg/kW, depending on scale. Replacing copper with superconducting wires, the windings mass could ideally be reduced by 1–2 orders of magnitude (Bruno and Giucci 1999; Casali and Bruno 2008).

Recent advances in MPD technology have brightened the prospective of this type of electric thrusters. High-thrust MPD propulsion has been dormant because the power required to reach acceptable efficiency was too large for commercial satellites and space vehicles (it takes hundreds of kilowatts to achieve efficiencies greater than 30%), and also because such power is unattainable with solar cells or in the laboratory. Historically, MPD propellant acceleration suffers from many losses, for instance: (a) Exhaust composition chemically "frozen" during nozzle expansion, preventing complete conversion of thermal energy to kinetic, just as in arcjets. (b) Plasma instabilities, the bane of all plasma applications, driving unstable currents, increasing plasma resistivity and wasting power. (c) Excess anode heating. (d) Especially cathode erosion/evaporation, overall reducing cathode life. As in all electric thrusters, also a drawback of MPD engines is their low thrust density, a factor 5–10 lower than other electric thrusters (Auweter-Kurtz and Kurtz 2003). The consequence is mass and bulk.

The issue of cathode life is a major issue of MPD thrusters. Because of low thrust, MPD-powered missions may last years (Oleson and Katz 2003). Even tungsten cathodes erode at the rate of approximately 0.2 μg/coulomb (Choueiri 2000). This figure may look small, but a 20 kW

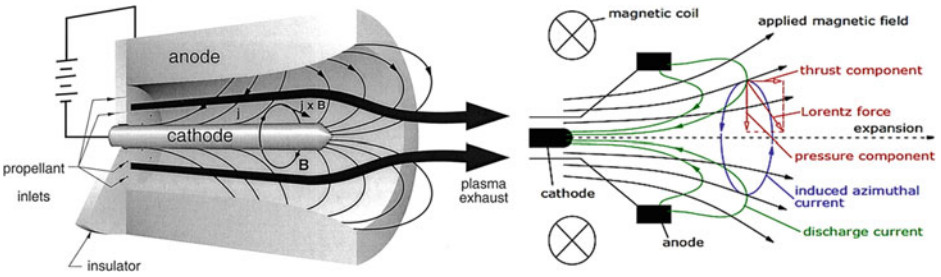

Fig. 7.35 Axisymmetric MPD thruster: the *left* sketch shows propellant injectors and discharge current density $\vec{j}$ (Courtesy of JPL). The *right* sketch shows the electromagnet coil producing the $\vec{B}$ field lines and the radial and axial component of the Lorentz force (Courtesy of M. Auweter-Kurtz)

MPD thruster, like that considered for the JIMO mission, will use 20 A when operated at 1 kV, that is 20 C/s. In a single day, about a third of a gram of tungsten will have been eroded. Progress in this area increased when Russian technology and know-how on steady plasma thrusters became available after the end of the Cold War. Interest by the USAF into a particular type of MPD propulsion (Hall thrusters) has contributed to advance this field.

Hall Thrusters

Hall thrusters were developed in the former Soviet Union at the OKB Fakel starting in the 1960s. A thruster schematic is shown in Fig. 7.36; it uses two axisymmetric coils, one closer to the axis, the other farther away, to produce a $\vec{B}$ field where electrons emitted by a cathode end up being trapped and gyrate along the magnetic force lines.

Xenon propellant injected from the anode region and driven by the Coulomb force collides with the electron cloud and is ionized. The positive ions are attracted toward the negative electron cloud, and because their momentum is orders of magnitude larger than that of electrons, they are accelerated and ejected without recombining. The major advantage of the Hall thruster is its long long operational life, demonstrably in the many thousands of hours and recently reaching close to 10,000 h. In comparison, other MPD thrusters last only weeks. However, the I_{sp} of Hall thrusters is limited to about 3500 s, and their power to 10^1 kW. Because of the particular acceleration mechanism, plasma density tends to be higher than in most ET, and thrust of order of 1–3 N have been produced in the laboratory, for instance during tests of the 50 kW TsNIIMash TM-50 Hall thruster at NASA Glenn Research Center in the 1990s (Dunning and Sankovic 1999).

Hall thrusters do not seem to be the choice for interplanetary human missions, as scaling indicates excessive electromagnet mass at power higher than a few tens of kW (Mikellides and Turchi 2000), but this issue might disappear using superconducting coils. The best application of Hall thrusters is probably in planetary orbits, where they enjoy a decisive thrust advantage over ion engines. SMART-1, the probe ESA sent to a Moon orbit by spiraling Earth for many months was powered by a Hall thruster. So is the 5 kW Aerojet-Rocketdyne XR-5 (now XR-5A) on the USAF

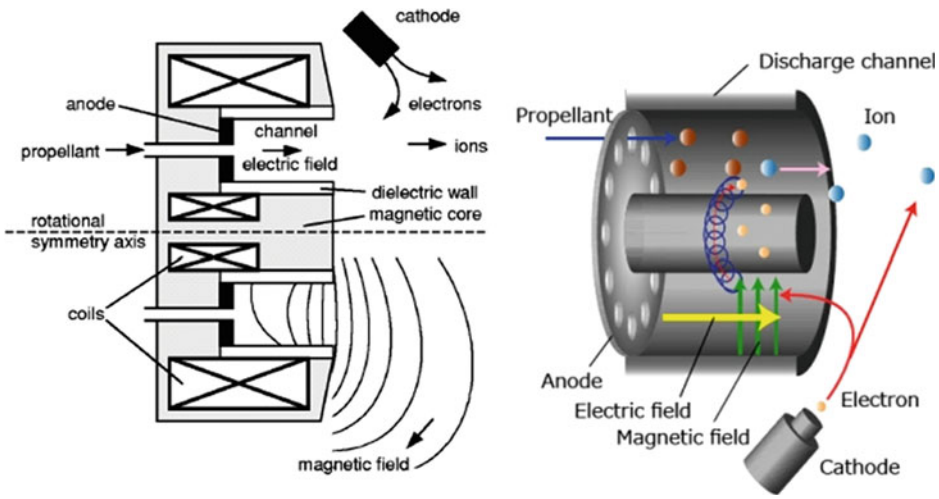

Fig. 7.36 Schematic functioning of Hall thruster (Courtesy of University Toulouse III Paul Sabatier, *left*, and University of Tokyo, *right*)

X-37B spaceplane, presumably used for orbital manoeuvers (Smith-Strickland 2016; David 2015a, b). Certain Hall thruster variants use Bismuth instead of Xenon.

In fact, the most important development in MPD is probably that of propellants. Hydrogen (extraction potential $E_i \approx 13.8$ eV) has been replaced with lithium ($E_i \approx 5.37$ eV). Lithium has been shown to extend cathode life by orders of magnitude (Choueiri 1998; Cassady et al. 2008; Choueiri 2009). RIAME MAI in Moscow, CalTech's Jet Propulsion Laboratory and Princeton University's Plasma and Electric Propulsion Laboratory, these settings collaborated in this area. The Russian company NPO Energia has tested a RIAME-designed 130 kW, 43% efficiency Lorentz force MPD thruster using Lithium, finding very low cathode erosion. Cathode life greater than 1000 h is within reach. Measured I_{sp} was 3460 s with thrust about 3.2 N. Thrust of order 25 N/MW looks achievable. Future plans include a 100 kW and a 120 kW steady MPD thruster.

Before Project Prometheus, NASA was planning improbable 20 MW, *solar*-powered MPD experiments in 2012, and 100 MW in 2024, in view of human or cargo Mars missions. Results suggested to then-NASA Administrator S. O'Keefe to put emphasis on nuclear power. These plans were quickly put on hold and then disappeared. Nevertheless, they indicated that MPD propulsion was considered viable for long missions. Current questions in this context center on the power and type of thruster, that is, below or above 100 kW and whether ion or MPD. Until SEI, mission analysis by NASA was focused on a nuclear powered 25 kW ion engine for the future unmanned JIMO mission to Europa, Callisto, and Ganymede (Bordi and Taylor 2003; Cassady et al. 2008).

In fact, power and type of an electric thruster are issues that could have benefited from Project Prometheus (Iannotta 2004). An advanced electric-propulsion technologies program would have compared MPD and pulsed inductive thrusters, developed at Princeton University and Northrop Grumman, respectively (Braukus 2004). The first used lithium, the second liquid ammonia, a much cheaper propellant. The power was to be about 10 times that for the JIMO mission, about 200 kW. Thrust conversion efficiencies predicted were about 70% for the Northrop thruster and 60% for the lithium MPD thruster of Princeton University.

Assuming cathode life and propellant issues can be solved, MPD thrusters must show they can handle much more than 20 kW. For comparison, the highest ion engine power tested in the laboratory was 1 MW (Fearn 2003). Power is a key element of any NEP trajectory, because it determines thrust and thus mission length. Figure 7.37 (Andrenucci 2004) is indicative of the trade-off between I_{sp} and thrust typical of fixed power propulsion (a thrust conversion efficiency = 0.8 has been assumed in this figure). Because power

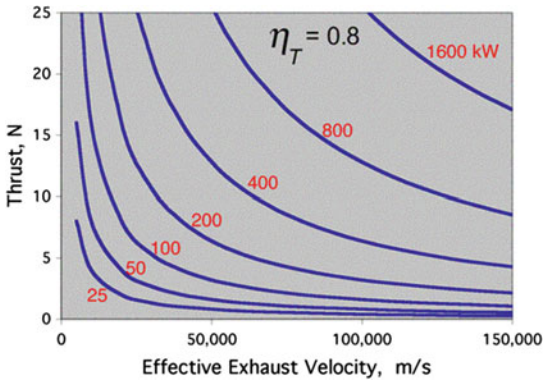

Fig. 7.37 Thrust versus I_{sp} trade-off at fixed power (thrust conversion efficiency assumed to be 0.8) (Andrenucci 2004)

$$P \propto I_{sp} \times \vec{F} \tag{7.37}$$

the curves are hyperbolas, showing the main limitation of electric propulsion is power available.

In this context, it is probably useful to dispel the myth of solar power as a viable energy source for future manned interplanetary missions. To collect 1 MW by solar cells near LEO, one would need 5330 m^2 of cells, an area larger than a football field, assuming an average 15% cell efficiency over the entire mission, or 3320 m^2 at a more optimistic 25%. Even near term, 50% efficient multi-junction cells in development at the US DOE (Anon 2015) would need about 1600 m^2 to produce 1 MW. Furthermore, the solar constant decreases with the square of the distance from the Sun. Near Mars, the solar constant is 2.2 times lower than near Earth. This means that human Mars missions using solar power should be either very long, or use $\approx 10^2$ football fields of solar cell arrays (Simonetti et al. 2009) to produce the 200–500 MW needed by a fast mission minimizing radiation dose. For missions to the outer planets, such as Jupiter, the solar constant decreases so much that a 1 MW power source cannot be solar. A 100 MW thruster for a manned mission would need half a million square meters of solar cells. The sheer weight and cost of orbiting such array would be staggering (Koppel et al. 2003), and in any case, the acceleration tolerated by these flimsy structures would be very low and vibrations/resonance a problem.

Although its TRL currently lags behind ion engines, MPD technology combined with nuclear or solar power seems the more economical way to interplanetary *cargo* missions, the more so because lithium, and its hydride LiH, is a coolant for advanced nuclear reactors (Buffone and Bruno 2002). However, a 100 MW_{th} nuclear reactor is not as significant a challenge as is the electric generator system. There is hardly any known experience of generating 100 kW of electric power in space, let alone 100 MW, and this remains the single most critical NEP technology area.

In order to maximize performance, MPD propulsion should integrate superconductivity, electric thruster, and nuclear reactor in a single electrically and thermodynamically efficient package. A MPD mass reduction by one order of magnitude made possible by future superconducting magnets would drop the MPD accelerator weight to 0.1 kg/kW and the engine mass to 10 t for a 100 MW engine. Scaling laws for high-power MPD thrusters should be derived similarly to what has been done to miniaturize small self-field MPD (Choueiri 1998; Casali and Bruno 2008; Lev and Choueiri 2010) and for ion engines (Fearn 2004, 2008).

Finally, the fraction of thermal power rejected by a thermodynamic cycle to produce electricity is more than half and should be exploited, for instance, to vaporize and perhaps ionize low ionization potential propellants (lithium). This would result in an additional thrust at I_{sp} of order 10^3 s, simultaneously reducing mass and surface of space radiators. The negative aspect of this proposal is a more complex engine. Nevertheless, given their potential higher thrust, hybrid thermal-NEP systems warrant further study and appear to provide a possible solution for interplanetary missions. In fact, still at the conceptual stage, they are the subject of investigation and for this reason are briefly discussed below.

7.21 Hybrid NTR/NER Engines

In this class of proposed concepts, the purpose is to integrate the nuclear reactor, electric propulsion, and superconductivity technologies in a single engine. Except solid-core NTR, all nuclear engines must necessarily reject a large fraction of the heat generated (in Rubbia's engine, this is almost 50%; in other NEP concepts, this fraction is even higher). NTR "reject" most of the heat to the propellant, so a radiator is not needed at all.

To increase efficiency and reduce mass, all other nuclear engines should recycle waste heat to generate electric power. The simplest way is through standard thermodynamics. The electric power recovered could magneto-hydro-dynamically accelerate the exhaust from a nuclear thermal rocket, like for tandem hybrids see Augelli et al. (1999), Dujarric et al. (2000), or feed an ion or MPD thruster (parallel hybrids). Alternatively, power recovered could power optical telecommunication systems, synthetic aperture radars (Gafarov et al. 2004), CO_2, iodine, or diode lasers to melt planetary ice. In any event, even partially recovering waste heat can shrink the size of space radiators, which are massive components in nuclear electric propulsion.

Potential examples of this strategy are the "bimodal" NTR proposed in Borowski et al. (1999), with a modest fraction of the reactor heat converted to electricity to power all onboard systems. This concept was expanded to "trimodal" to include also chemical propulsion (Joyner et al. 2004); the "indirect" nuclear propulsion system in Chew et al. (2004), in which a nuclear reactor heats the propellant via a heat exchanger, uncoupling the reactor power core from the propulsion systems, and the hybrid NTR/NEP described in Powell et al. (2003, 2004), where the waste heat of the MITEE engine (see Sect. 7.11) is converted to electric power and feeds an electric thruster. The more straightforward of such proposals would use waste heat to accelerate the expanded exhaust of a NTR, similarly to what is done by after-burners in jet engines. This is indeed the NTER concept in Sect. 7.22.1.

The appeal of these proposals needs be weighed against their added complexity. Figure 7.38 shows a parallel hybrid concept where part of the waste heat from the nuclear reactor generates electricity powering an ion engine. The many subsystems suggest complexity and mass much higher than a single NTR or NEP system.

On the positive side, hybrids may have decisive advantages. NTR typically offer large thrust and low I_{sp}, while

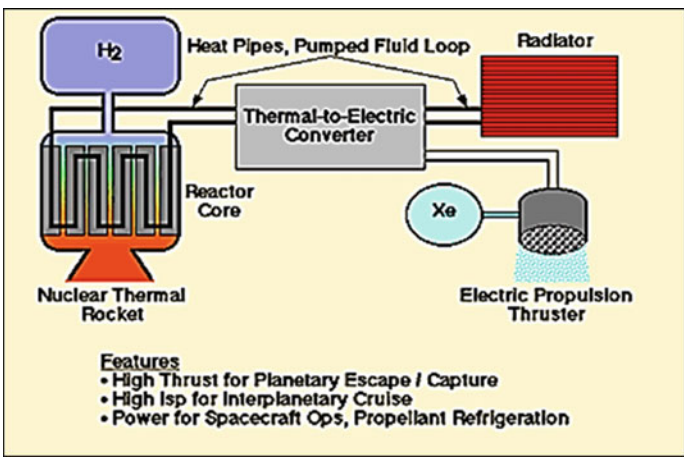

Fig. 7.38 Notional hybrid nuclear thermal/nuclear electric rocket (parallel system)

electric thrusters do just the opposite. In many missions, the two different modes of propulsion may be present to power different segments of the trajectory. How to apportion reactor power between NTR and electric thruster is a paramount question. Different missions may need different NEP to NTR power ratios. For instance, orbiting or deorbiting near planets may demand high thrust to save ascent and descent time of crewed spacecraft.

For planetary missions, the ideal propulsion system should be capable of large thrust at low I_{sp} to reach escape speed quickly, followed by much smaller thrust but much higher I_{sp} to keep accelerating, even at a modest rate, toward its final destination. A hybrid NTR coupled with an electric thruster has such capability by design; a simplified analytical study of this concept is in Bruno et al. (2013), where the initial leg of a notional Earth–Mars trajectory was assumed powered by low thrust, high-I_{sp} electric propulsion, and the second leg to midway by a NTR. Results indicated that this division of tasks is not optimal in terms of propellant and spacecraft mass. In the detailed work of Burke et al. (2013), the opposite strategy (initial segment powered by NTR, followed by electric propulsion) was investigated for a short-stay Mars mission assuming I_{sp} = 3000 s for the ET and I_{sp} = 900 s for the NTR. The thermal engine uses all the reactor thermal power of 545 MW_{th}, and the electric thruster only 1.76 MW_{th}. This bimodal strategy resulted in a 1-year mission with IMLEO about 400 t. General criteria and modes (i.e., tandem or parallel) of apportioning power between two very different propulsion systems, that is, powered trajectory optimization, have not been derived yet. Historically, these questions were raised at the dawn of the jet engine age (1940s), when aircraft manufacturers designed airplanes with both jet *and* piston engines trying to combine the best of the two propulsion systems.

Among the many issues of tandem hybrids is that of ionization that may prove to absorb an excessive fraction of the waste heat recovered. Performance of each engine (NTR and electric) depends on temperature in roughly opposite ways. Ionization of the NTR exhaust should be as low as possible to recover most of the thermal energy; to operate ion or MPD accelerators, ionization should be as high as possible. A tandem NTR + MPD thruster will likely require seeding the exhaust from the NTR with low ionization potential metals, for instance K, Ba, or Li.

In fact, lithium could be *the* propellant for the NTR engine, alone or as LiH. This is much less corrosive than pure Li and conveniently decomposes into Li and H at temperatures of order 970 K. This tandem hybrid concept looks promising in the case of Rubbia-type NTR. MPD acceleration of a Li plasma with I_{sp} = 3000 s has been demonstrated even when the plasma regime was collisional. Although MHD acceleration of H_2 or H_2 + Li exhausted from a NTR has never been tested, it is interesting to estimate its effect on the nominal performance of the Rubbia's engine reported in (Augelli et al. 1999). The efficiency of MPD acceleration (≈40–50%) should raise I_{sp} by 100–200 s, with a simultaneous reduction of the space radiator mass. Assuming I_{sp} = 2500 s as the baseline for the Rubbia's engine, the effect of recovering waste heat would be of order 4–8%.

7.22 Inductively Heated NTR

This hybrid concept is closer to the arcjet of Sect. 7.17. In the first version of this concept, part of the nuclear power heats the coolant/propellant as in NTR. The remainder heats it by means of induction coils surrounding the nozzle. In addition, electrical power is generated by the nuclear reactor waste heat. This concept was proposed mainly to reduce space radiator size and mass. Performance calculations predicted induction heating could raise I_{sp} by 132 s, to a total I_{sp} = 1041 s (Dujarric 1999). An alternative proposal conceived the nuclear reactor generating only electricity to feed the induction loops. This radical option would complicate design, reduce available power due to ohmic losses, and involve a massive radiator.

All propulsion systems producing thrust by means of conventional machinery suffer a substantial η penalty: it is inefficient to generate nuclear thermal power, convert it to electricity (with η no higher than perhaps 50%) and then convert electricity back to heat. The only conceptual advantage seemed to be at the time the ability to control engine power, and especially to distribute and control heating of the propellant *along the engine* more easily. On the downside, the handling of very large currents would produce ohmic and parasitic losses and create unwanted magnetic fields interfering with spacecraft operation.

No estimate of total mass was made for this concept. However, its general philosophy and layout resembles that of so-called clean high enthalpy wind tunnels, for instance, the Plasmatron wind tunnel at the Von Kármán Institute in Belgium (Bottin et al. 1998a, b). A mature Russian technology, Plasmatrons have shown to have good performance and little or no problem in inductively heating air to form plasma at 7000–9000 K. By replacing air with hydrogen at the same temperatures, the I_{sp} should be in the 2000–2500 s range, even including radiation losses. One of the problems in designing induction heaters, besides still incomplete understanding of plasma behavior, is predicting the effect of scaling from relatively small power and size to the power required for deep space and crewed missions. Clustering individual 1–2 MW thrusters appears feasible with adequate cooling, and 1 MW Plasmatrons are an established technology, but too many engines would be necessary for a fast Mars mission, for instance.

In conclusion, inductive NTR heating in combination with conventional nozzle expansion is a dual-mode concept worth investigating further for interplanetary missions. That is probably one of the reasons why ESA acquired the patent rights to this technology. In fact, this concept was further developed in the NTER engine described below.

7.22.1 Nuclear Thermal-Electric Rocket (NTER)

This hybrid nuclear thermal-electric propulsion concept is mostly the creation of Dr. Christian Dujarric, a scientist at the European Space Agency ESA, with the purpose to overcome the problems of induction heating (Dujarric et al. 2013). An engine schematic is shown in Fig. 7.39.

Operation consists of two separate cycles, an open NTR cycle using LH_2 and a closed GHe Brayton cycle. The two cycles have in common a CERMET reactor core chosen for its high-temperature reliability, and the temperature (62 K) of LH_2 pumped from the tank. This is the "cold sink" temperature of the He Brayton cycle ensuring high thermodynamic efficiency. Inside the reactor, H_2 and He are heated by flowing inside separate channels. However, H_2 enters the reactor already preheated to 540 K in the heat exchanger powered by the end temperature of the He cycle (690 K), see upper right of Fig. 7.39. This feature allows the CERMET reactor to work at a relatively conservative 2550 K temperature. The Brayton cycle generates electricity through a proprietary turbo-inductor consisting of a free rotating turbine with contra-rotating blades coated with tungsten. The already hot H_2 flowing downstream of the reactor is convectively reheated to 3250 K by Foucault currents (eddy currents) induced on the tungsten surface when going through the turbine. This reheat temperature is only limited by the melting point of W (wolfram or tungsten).

The purpose of this integrated dual cycle is to limit the temperature of the CERMET reactor to what it can reliably sustain, to about 2,500 K, thus extending its life and number of missions, preventing structural stresses and cracking of fuel rod cladding due to the differential thermal expansion between fuel and ZrC. Cracks would allow fission fragments to mix with the H_2 exhaust and pose unsurmountable environmental problems to ground testing.

Calculations for a notional 0.5 GW reactor indicate 340 MW are available as thermal thrust power, and about 108 MW can be extracted from the Brayton cycle. Instead of using this power to reheat H_2, this power can alternatively be used to power an electric thruster.

An example of a Mars mission trajectory enabled by the two propulsion modes of a NTER is shown in Fig. 7.40. After orbiting cargo and crew spacecraft and the manned habitat outside the Van Allen belt in a high Earth orbit

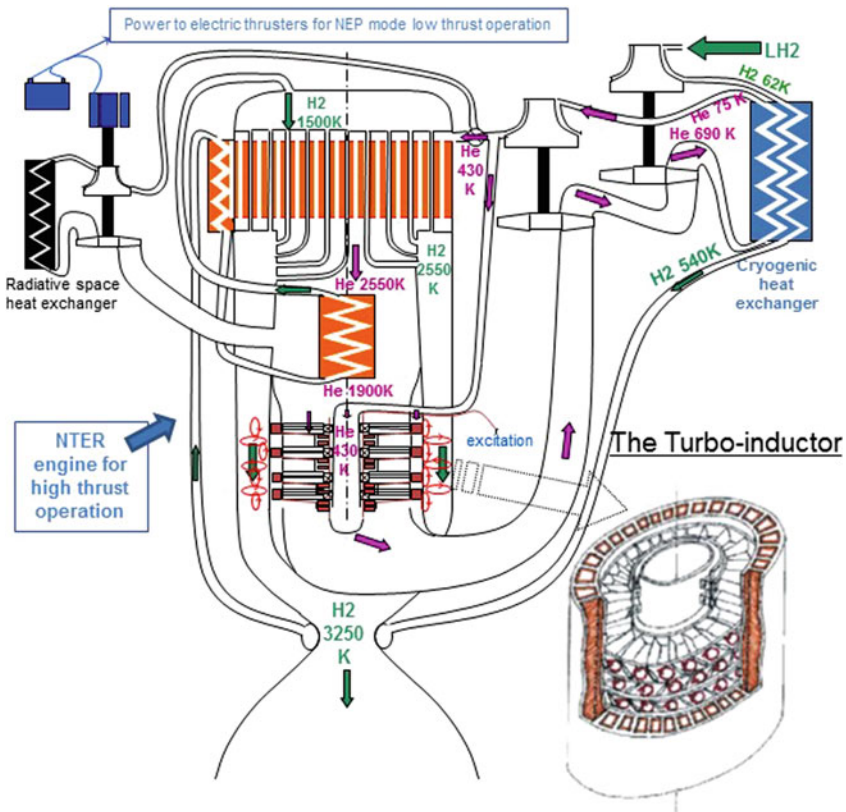

Fig. 7.39 Schematics of the 2013 NTER engine concept (Dujarric et al. 2013)

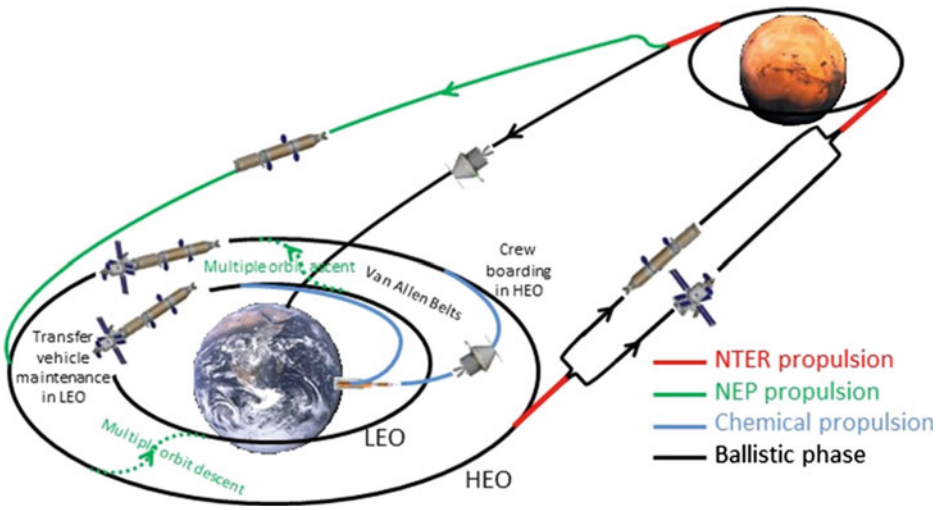

Fig. 7.40 Notional manned Mars mission enabled by the dual-mode NTER engine (*Courtesy* C. Dujarric)

(HEO), the crew spacecraft and manned habitat are mated. Now, in thermal propulsion mode, NTER injects the spacecraft in a trans-Mars trajectory and captures a Mars orbit. The return flight of the crewed habitat is fast, powered by NTER in thermal mode, while the unmanned spacecraft is returned to a HEO in slower electric propulsion mode. Electric propulsion is also used to transfer spacecraft between LEO and HEO parking orbits.

The work by C. Dujarric was proposed to be continued by ESA in collaboration with the French company SNECMA. The proposal included analysis of other hybrid strategies, including LOX augmentation and plasma MHD acceleration (Dujarric et al. 2000, 2013). No action has been taken at the time of this writing, and this project is, for the time being, dormant.

7.23 VASIMR (Variable Specific Impulse Magneto-Plasma-Dynamic Rocket)

VASIMR is a high-power, electro-thermal plasma rocket concept currently under development at Ad Astra Rocket Company, a US-Costa Rican company and a spinoff of NASA's Advanced Space Propulsion Laboratory (ASPL) at Lyndon B. Johnson Space Center. The Ad Astra team is headed by former astronaut Dr. Franklin Chang Diaz (Chang Diaz 2000; Negrotti 2008).

VASIMR technology borrows from fusion research, and especially from the vast experience in plasma heating by radio-frequency (RF) electromagnetic waves used in tokamak fusion machines. Although VASIMR is a MPD thruster, it possesses some unique features worth setting it apart from other MPD propulsion systems. No claim is made by NASA as to the power source of VASIMR, but I_{sp} and thrust imply power large enough that a nuclear reactor appears to be the only practicable source. VASIMR is of great interest because it purposely meets the requirement of the ideal interplanetary propulsion system mentioned in Sect. 7.20, that is, higher thrust at low I_{sp} or lower thrust and high I_{sp}, so that power stays constant, see Fig. 7.37.

Figures 7.41 and 7.42 show the VASIMR system and its operation. It consists of three major magnetic functional blocks, or cells, denoted "forward," "central," and "aft." This configuration is called by plasma fusion physicists an asymmetric mirror, see Chap. 8. The forward cell handles the injection of propellant (Argon, Hydrogen or Deuterium), ionizes it and turns it into plasma. The central cell acts as power amplifier and heats the plasma by beaming radio-frequency electromagnetic energy with a helicon antenna. The energy is captured by plasma via electron cyclotron resonance (ECR) to the level desired to match the magnetic nozzle. Radio-frequency heating exploits the fact that electrons spiraling around magnetic field lines at their cyclotron frequency absorb readily the energy of radio waves beamed at the same frequency (Ilin et al. 2000; Takao et al. 2000). The third, aft-end cell, is the hybrid magnetic-fluid dynamic two-stage nozzle converting plasma energy, including unwanted rotational degrees of freedom, to translational kinetic energy, so that plasma is ejected axially. The nozzle magnetic field keeps plasma away from the walls. Without the aft-end cell, plasma would tend to spiral around the magnetic field lines, and the tangential velocity component of the plasma would be wasted (only the axial component produces thrust). Ad Astra claims plasma produced by VASIMR to be controllable over a wide range of temperatures and densities.

The key feature of VASIMR operation is its purported capability to modulate the plasma exhaust while maintaining constant power, see Fig. 7.43 reporting calculations for a 25 kW VASIMR.

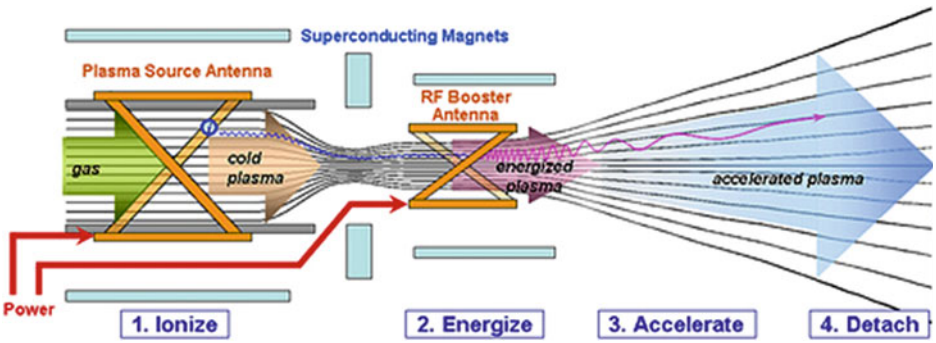

Fig. 7.41 Schematics of the ionization and acceleration of plasma in the VASIMR engine (Courtesy of Ad Astra Corporation)

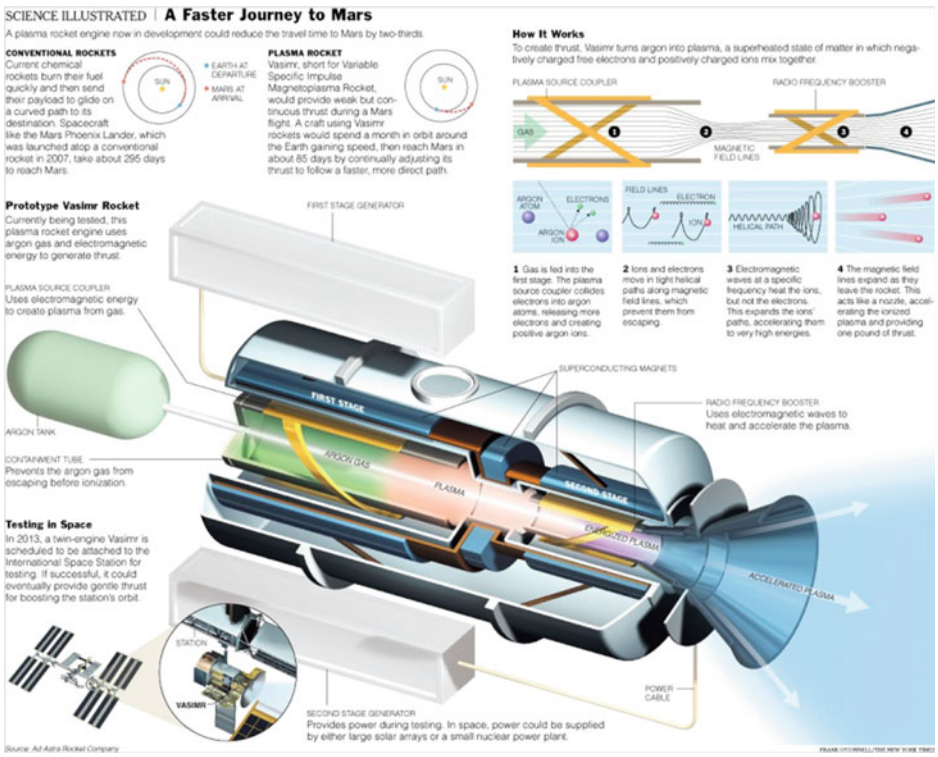

Fig. 7.42 Schematic of the variable specific impulse magnetoplasma rocket (VASIMR) as was initially planned to be tested in 2016 on the International Space Station (*Courtesy* NASA JSC 2000)

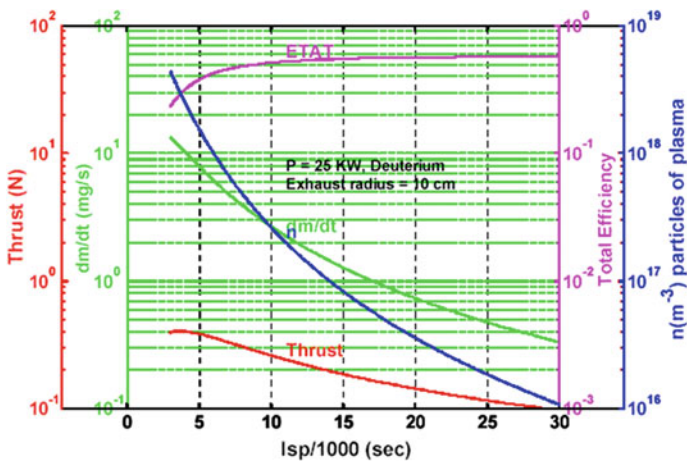

Fig. 7.43 Estimated thrust and propellant flowrate versus specific impulse of a notional 25 kW VASIMR. η_T Total efficiency; dm/dt Propellant flowrate; n Plasma particle density (Courtesy of NASA-ASPL 2000)

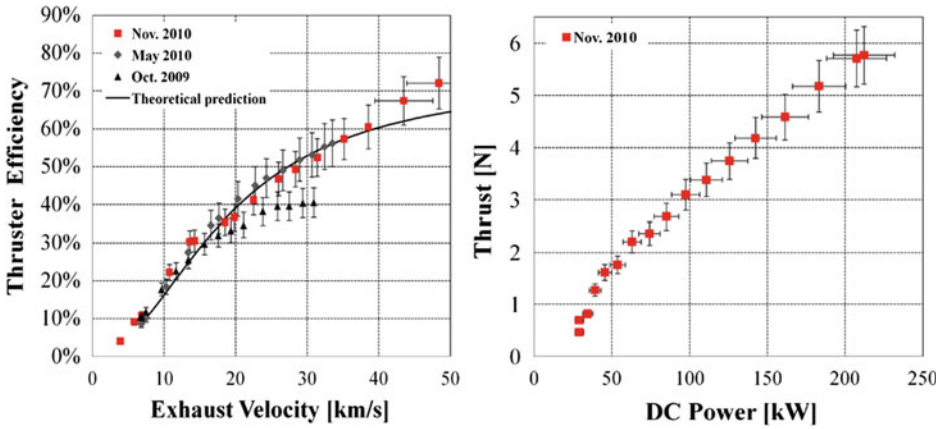

Fig. 7.44 Measured thrust and specific impulse of VASIMR (*Courtesy* Ad Astra Corporation)

Laboratory testing has shown that losses still limit efficiency to 70% at the maximum power tested (about 200 kW). Thrust is of order 3 N/100 kW and scales linearly with power, see Fig. 7.44. If this scaling holds, also at much higher power, it implies 3 kN per 100 MW are available to power lunar and Mars cargo missions, since I_{sp} is more than ten times that of chemical rockets (but still far from that of ion engines).

The fact, that at constant power operation thrust and I_{sp} can be varied while maintaining constant their product, is extremely useful for interplanetary missions where most of the transplanetary trajectory can be flown at small but continuous thrust and high I_{sp}. When the spacecraft must slow down to capture the planetary orbit, thrust can be increased to reduce capture time and radiation dose at the expense of higher propellant consumption (lower I_{sp}). According to the Ad Astra Rocket Company, eventually VASIMR should be capable of producing 1200 N and $I_{sp} = 10^4$ s, increasing to $3 \cdot 10^5$ s with thrust of order 40 N (Chang Diaz et al. 1999, 2000; Ilin et al. 1999, 2000).

Figures 7.45 and 7.46 show notional conjunction-class trajectories for the Mars mission envisaged by Ad Astra Rocket Company with this power outlook presented above. The lengthy time to acquire escape speed from Earth (requiring the spiral trajectory) is noteworthy. For a fast trip, power must be in the 10^2 MW range, a factor 10^3 more than tested so far. This thrust scaling is due to physics and not due to technology. It begs the question of how many engines should be clustered to ensure the thrust of order 1 kN necessary for fast human interplanetary missions (this issue is common to all electric thrusters). The question of engine size and mass for a given power noted, there are theoretical advantages to this propulsion system. One is variable I_{sp} and thrust at constant power. Another is the electrodeless plasma heating doing completely away with cathode erosion. If power density will eventually be as high as envisaged by Ad Astra, the high I_{sp} of this thruster will enable trajectories under weak but continuous acceleration, reducing the damaging effects of microgravity. RF heating has been tested in fusion reactors for 30 years (electrodes are out of the question in fusion machines). It requires high voltage but low current, thus has low ohmic losses. Onboard power available makes possible storing cryogenic propellants (argon, hydrogen or other gas) and operating superconducting magnets to save wiring mass. The high I_{sp} of VASIMR gives it a powered-abort capability, an important point for manned missions.

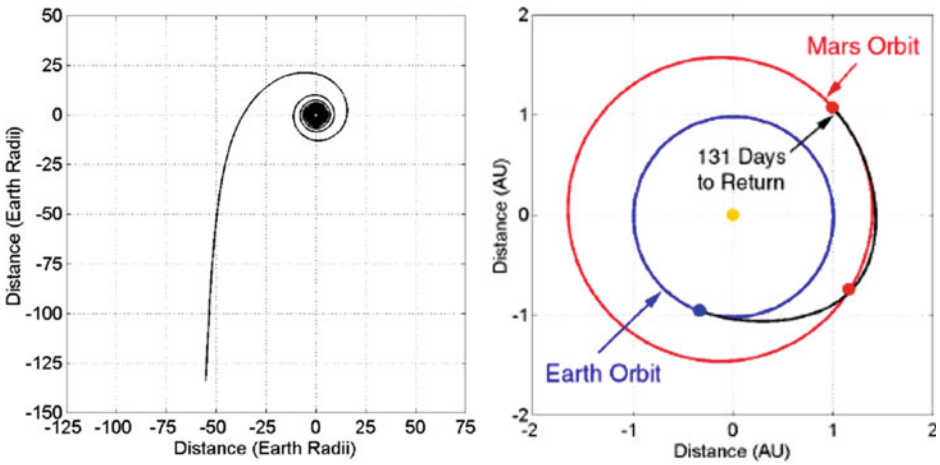

Fig. 7.45 30-day spiral trajectory from Earth and transfer to Mars (Chang Diaz 2000). The scale is in Earth orbit radii

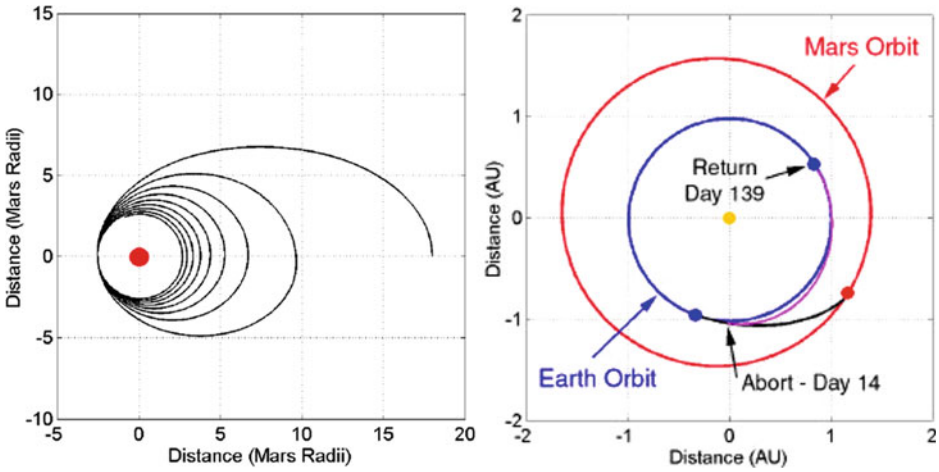

Fig. 7.46 7-day spiral trajectory from Mars and return to Earth (abort on day 14 of the heliocentric trajectory) using VASIMR (Chang Diaz 2000)

Known challenges are engine size, superconducting magnets (NASA experimented with superconducting magnets since the 1970s (Connolly et al. 1971) and more recently in the ASPL context), and the power source. Overall, thermal management is probably the hardest technological hurdle this engine must overcome due to challenges related to (a) a compact and reliable RF heating system, (b) the hybrid magnetic nozzle preventing plasma from heating walls, (c) the cooling and shielding system (plasma radiates over a broad wavelength region), and (d) the inevitable space radiator.

Among factors not initially considered by the VASIMR team is the radiation heat loss from the propellant plasma to the walls. Plasma radiation grows rapidly above 9,000 K and especially at moderate (≈1 atm) pressure. NASA analyses at ASPL indicated these losses can be contained and should not affect performance significantly. A second issue is the effect of pressure on plasma magnetic confinement. In order to ensure full plasma control by the magnetic fields, plasma must be reasonably collisionless. Thus, plasma density should be low, a requirement opposite to that of keeping radiative losses under control and of achieving high-power density. It is practically certain that, for a given thrust, VASIMR engines will be larger compared to other types of electric thrusters, i.e., its thrust per unit exit area will be lower.

The VASIMR concept is envisioned as eventually evolving into a space engine of power in the many 10^2 MW category. In the year 2000, efforts were focused on a 24 kW solar-powered VASIMR demo sponsored by NASA-JSC, NASA-GSFC, and NASA-GRC with the objective to measure space radiation in the Van Allen belt. This mission was scrubbed and redirected toward testing VASIMR on the ISS in 2015 or 2016 to raise periodically its ISS orbit. Figure 7.47 shows how the VASIMR should be installed for testing on the ISS arm.

After Project Prometheus and JIMO were canceled, the development pace of VASIMR slowed down but continued at the laboratory scale at NASA's ASPL. After incorporating Ad Astra, the Chang Diaz team originally at NASA-JSC

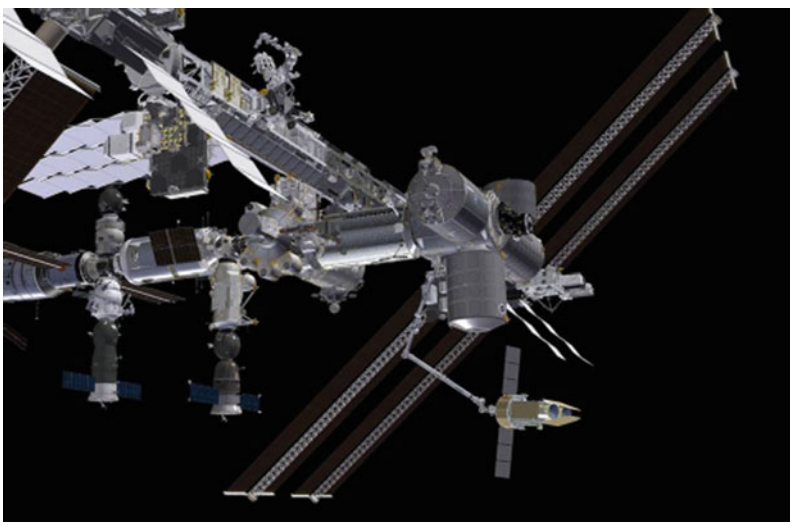

Fig. 7.47 Artist's view of the planned operation of VASIMR VX-200 on the ISS (*Courtesy* Ad Astra Rocket Company)

moved to Costa Rica, but maintained a base in Texas where the high vacuum test facility still is. Experiments investigated power losses (including radiation), the ionization efficiency of the helicon antenna, and magnetic nozzle performance overall confirming that a plasma ion density of order 10^{20} cm^{-3} was achieved at a neutral pressure of order 100 Pa (Negrotti 2008).

In August 2015, Ad Astra announced that an award had been received from NASA on the Next Space Technology Exploration Partnership (NextSTEP). Under the award NASA and Ad Astra will be 50/50 partners to test the advanced version VX-200SS (Steady State) of its 200 kW rocket for a minimum of 100 h at the Ad Astra Texas facility. The test will be carried out at half power (100 kW) to explore reliability and wear. Older VASIMR tests did not last more than a few minutes (David 2015a, b). The three-year program will establish confidence in this class of electrodeless engines, the first step to assess whether VASIMR may indeed be an option to power a mission to Mars, or to enable at least a "dry run" precursor mission such as to a NEO in date still to be determined (Claybaugh et al. 2004).

7.24 Propulsion Strategies Compared

Just as it is a challenging task to compare performance of aircraft propulsion systems, it is also demanding to compare the many ways to use fission energy for space propulsion without assigning a specific task, that is, a mission. In describing propulsion strategies, some general comments have focused on pro and contra of each system, but in the end a fair comparison requires an objective (Braun and Blersch 1991; Griffin et al. 2004).

The human Mars mission still in discussion, after almost a century, seems indeed to provide fair terms for a comparison. Two recent investigations (Mazanek et al. 2013; Guerra et al. 2015) have assumed and analyzed different propulsion means and drawn conclusions about their impact on spacecraft IMLEO and round-trip travel time. The joint NASA study in Mazanek et al. (2013) addresses a short-stay and a long-stay mission. The study accounts for Mars and Earth ephemerids such that the mass versus time is a family of curves, each associated with the year from 2018 to 2045, see Fig. 7.48 taken from the 2013 presentation. Table 7.5

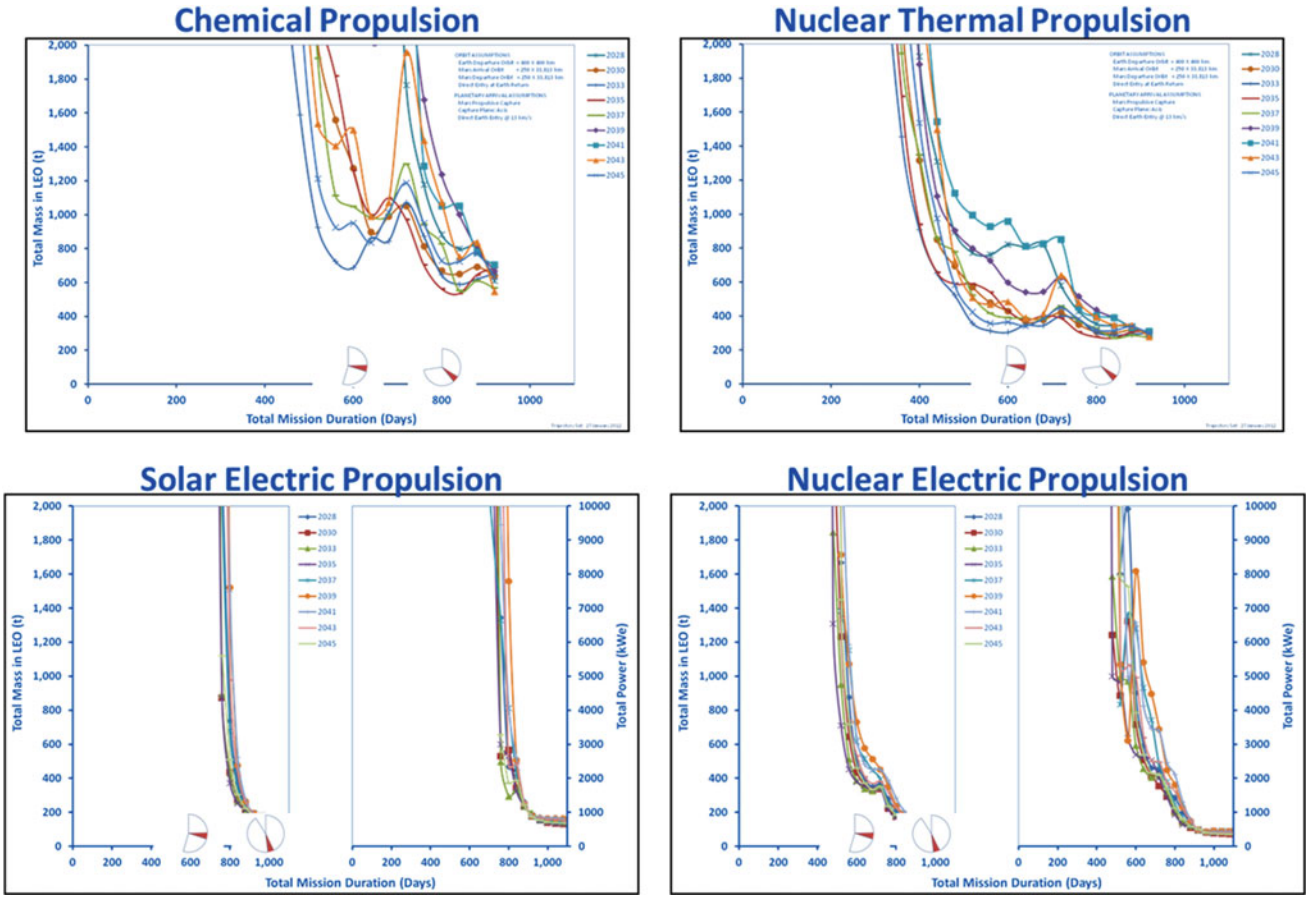

Fig. 7.48 Crewed Mars mission propulsion technologies. IMLEO and round-trip length for the four propulsion systems compared in Mazanek et al. (2013)

Table 7.5 Performance assumed for the four propulsion systems compared in Mazanek et al. (2013). The I_{sp} varies depending on mission

Engine type	LRE-SEP		NEP	NTP
I_{sp} (s)	465	1,800–6,000	1,800–6,000	900
W_{fuel}/TOW (–)	0.23	0.05	0.05	0.27
α* (kg/kW)	N/A	30	20	N/A

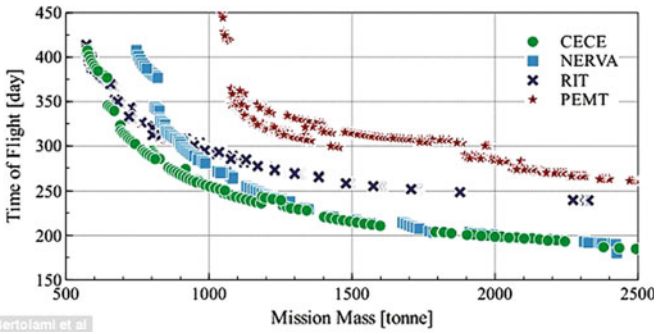

Fig. 7.49 Actual time spent in interplanetary space as a function of IMLEO for the four types of propulsion systems, from Guerra et al. (2015)

reports the performance of the four propulsion systems assumed in the comparison.

Mission times in Fig. 7.48 indicate a mission with chemical propulsion cannot be shorter than about 450 days, and for most years of order 600 days or longer. NTR-powered missions are typically shorter or much shorter, but in both cases the IMLEO is very large, of order 1,500 t or higher. Electric modes lengthen mission substantially but require less IMLEO, even down to 200 t for 900 days round-trips. No amount of electrical power, up to 10 GW_e, can reduce trip time below about 400 days. Note that in (Simonetti et al. 2009) a NEP system was designed capable of a Mars mission in less than a year, provided electric power was in the 400–600 MW_e range. However, the propulsion system (a cluster of many tens of ion thrusters each capable of I_{sp} = 30 ks) would be very bulky. Note that ion thrusters capable of I_{sp} = 30 ks have been demonstrated in the laboratory, but not in space. Therefore, under the assumptions made, the NASA study concludes that no system can ensure a stay in interplanetary space for less than a year, and thus to limit radiation dose to less than 1 Sv as prescribed by most space agencies.

The comparison in Guerra et al. (2015) is more recent, and the propulsion systems chosen (Rocketdyne's CECE as representative of LRE; NERVA II, a conceptual NTR developed during the ROVER/NERVA program; RIT-XT, a low thrust ion thruster for SEP, and the Rubbia's Purely Electromagnetic Thruster, or PEMT, essentially a photon rocket) seem ill matched, characterized by vast differences in TRL. No NEP system was included in this comparison, and few details are offered of spacecraft and crewed modules mass. Also, the effect of ephemerids (departure year) on mass to orbit, although significant, is not accounted for.

The chart in Fig. 7.49 supports the conclusion that none of the four classes of propulsion is capable of significantly lower a round-trip Mars mission below 800 days, thus exposing crews to excessive radiation doses, see Appendix A. This chart is the counterpart of NASA Fig. 7.48, except that the axes are swapped. The trends found in the NASA study are confirmed ('more IMLEO shorten trip time but there is an asymptote'), but the trip time asymptote is about 200–300 days longer. However, when stay-time on Mars is subtracted, and astronauts are assumed protected from radiation on Mars, the effective time in interplanetary space, shown in Fig. 7.49, indicates less than 300 days are feasible both with LRE and NTP systems. Numerical differences with the NASA study are probably due to different assumptions for habitats mass and ephemerides.

In order to prevent discouraging conclusions, note that propulsion strategies, consisting of combining NTP and NEP and using them in different segments of an Earth–Mars trajectory, have been examined only twice (Burke et al. 2013; Bruno et al. Bruno 2014) whilst they promise to be the practical key to shorter and more economical Mars missions.

7.25 Conclusions

The chart in Fig. 7.50 shows the effect of Tsiolkovsky's Law, that is ΔV and mass ratio M_R as function of mission destination and I_{sp} (here correctly replaced by rocket exhaust velocity $I_{sp} = V_{exhaust}/g_0$). For some destinations, constant acceleration trajectories are also reported.

The exponential Tsiolkovsky's Law forces the ΔV versus $V_{exhaust}$ relationship to be cast in log–log form. The many orders of magnitude alone suggest the challenge posed by interplanetary travel. Note that, in terms of sheer energy available, fission-driven nuclear propulsion restricts destinations to not much to the right of $V_{exhaust} \approx 10^5$ m/s. *Travel times*, so critical to human missions, cannot be reported in

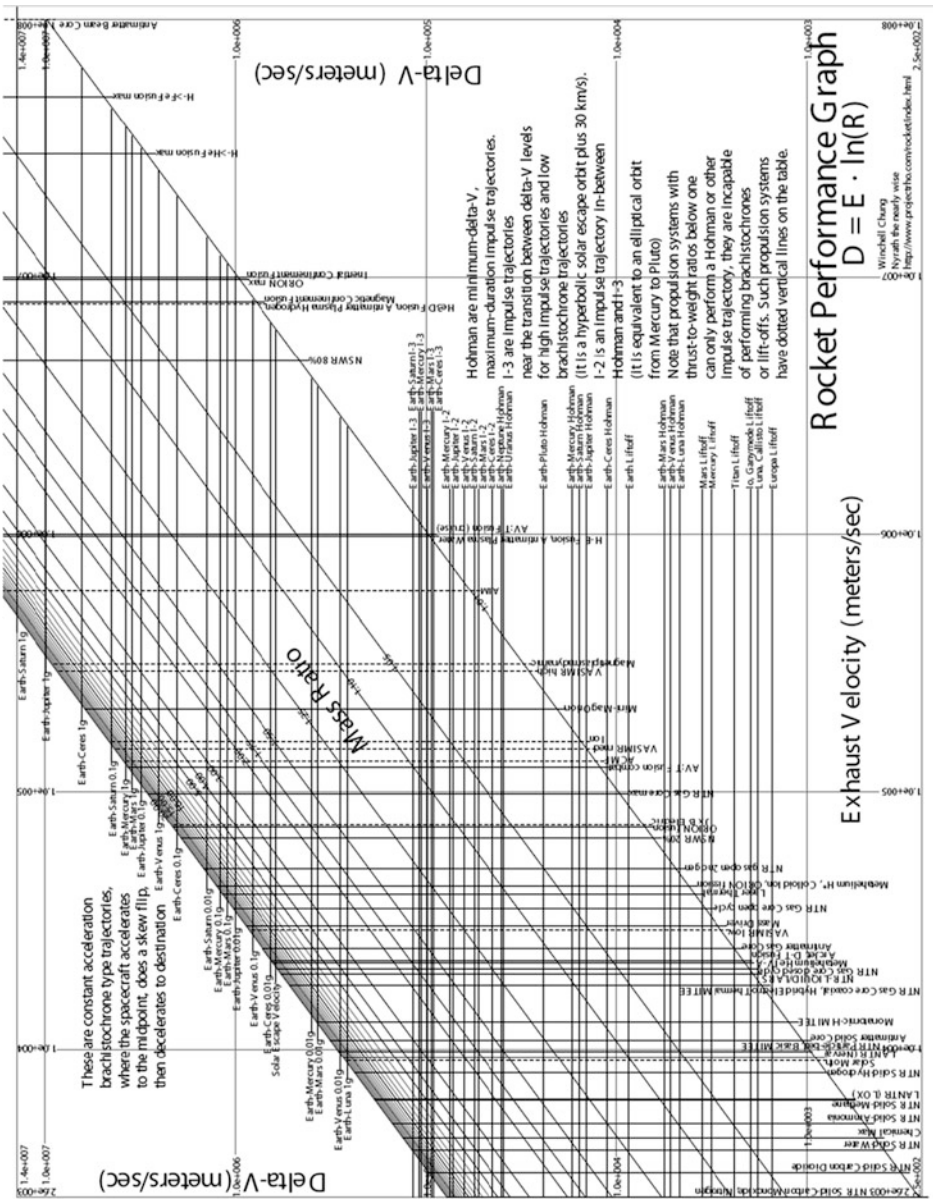

Fig. 7.50 Interplanetary destinations, their ΔV, and mass ratios depend on propulsion system and powered trajectory acceleration (Courtesy of W. Chung)

this chart since they need be explicitly calculated by integrating the spacecraft equation of motion and this requires thrust to be known. Note that time adds another dimension to all technical considerations made so far.

Nearly 50 years have gone by since the Rover Project was started and the NTR engines it spawned were tested. If the vagaries of the US politics, the US agencies, or public opposition do not get in the way, *nuclear propulsion* has a chance of becoming the *centerpiece of manned and unmanned planetary exploration*. No other propulsion technology can do such—not at least within reasonable mission length and budgets.

So far, this chapter has focused on promising concepts and enabling technologies. However, there are other challenges that need to be faced and overcome before nuclear propulsion can succeed.

In these authors' opinion, one of the outstanding issues is public acceptance of orbiting nuclear material—witness the 1997 campaign in the US and Florida in particular against the radioisotope thermoelectric generator power source installed on the Cassini probe (MacAvoy 2004). Fears of anything nuclear have been renewed after the Fukushima disaster on March 11, 2011.

Risks and dangers posed by using nuclear power should be neither ignored nor underestimated, but the public needs to be kept informed and educated, in the sense that nuclear power issues should be compared and put into perspective relative to more conventional energy sources. The response

given by the man in the street to a 2007 EU survey about the so-called Chernobyl accident of 25 years ago was indeed instructive. Most people were convinced that hundreds to hundreds of thousands people had died in Ukraine following the accident. In fact, 31 people among the rescue crew attempting to shutdown the reactor and the firemen putting down the fire were lost within days or weeks due to radiation (Del Rossi and Bruno 2004). The total number of fatalities to date is less than 65, according to UN statistics (Hoffman and Fleming 2005, Kinley 2006, WHO Media Centre, 2015).

This discrepancy between imagined and actual fatalities is telling. Even among educated people, nuclear power is surrounded by the fear and aura of secrecy going back to Hiroshima and Nagasaki. Hardly anybody knows that the Chernobyl accident was no accident at all, but a deliberately authorized foolhardy experiment by a single individual to test the spinning-down time of the power turbines. Likewise, not many people are aware that natural background radiation here on Earth is capable of biological effects at least ten times larger than any existing human-made source.

In this climate, any positive but exclusively technical conclusion regarding future use of nuclear power for space propulsion must be cautiously appraised. On its merit, nuclear propulsion is clearly the *only* practicable technology if fast, safe, human exploration of our planetary system at reasonable cost is a requirement (regrettably, this may be a strong "if"). This can be simply argued on the basis of energy density, ten million times greater than that of the best chemical propellants. By itself, this factor ensures that under proper conditions, nuclear propulsion is the natural prerequisite of human interplanetary space missions. Mass, shielding, and radiation hazards, now assumed as the unavoidable penalties of nuclear propulsion, are evolving issues, and actually benefiting from other, sometimes unrelated, technology areas.

NASA planning before the Space Exploration Initiative (SEI) included NP-powered missions to Europa, Pluto, and Venus, and eventually manned missions to Mars. The implication was that this technology was not only considered realizable, but also safe, although expensive. SEI stopped all progress in NP, but the technical conclusions reached still stand. In particular, a potential application, independent of SEI and worth investigating, is connected to the asteroid threat (Tok 2008). Although risks posed by near-Earth asteroids (NEAs) and near-Earth objects (NEOs) have been assessed as 1/720,000 (Harris 2008), the sheer size of the potential catastrophes should, and do, give cause for concern (Chandler 2008). Whatever the means of deviating their trajectories, dangerous NEAs should be reached as fast as possible after discovery. It should be noted that there is still no specific program to discover NEAs. A NEA threat might be detected "too late" to be intercepted with either conventional or electric propulsion. Chemical rockets would not be capable of the ΔV required, and electric propulsion would be too slow. Only NTR would have the right combination of thrust and specific impulse, especially in the case of a NEA closing at high speed (Powell et al. 1997). Although many scientists would think that a dedicated effort in this area is premature, others suggest that investing in NTR is not (Tok 2008).

After all technical and societal issues are sorted out and solved, the key conditions to transfer nuclear propulsion from technology to space-qualified engines are a steady political will and steady funding. While the US government is on record about supporting development of this technology, ESA in Europe has still to take an official posture. ESA is ruled by most EU member states, so such indecision simply mirrors reluctance from every member state to take a stand, although individual countries may be favorable, e.g., see Blott et al. (2012). Russia has few or no qualms about nuclear power in space: informed sources have claimed some of its reconnaissance KOSMOS satellites orbited in the past were in fact powered by nuclear reactors, and a Roscosmos delegation has offered their NTP technology for a joint ESA-Russian human Mars mission. Japan has no intention of doing so, even though it must develop new strategic surveillance satellites. Because of Hiroshima and Nagasaki and the 2012 Fukushima disaster, Japan still prefers to rely on miniaturization and solar cells, although there have been signs this attitude might change (Nagata et al. 2008). China's intentions in this context have not been made public.

Any effort to develop this propulsion technology, especially under international collaboration, must therefore enjoy a clear and lasting political will. After deciding to go ahead with nuclear power in space, there should not be second thoughts, accepting technical hurdles as part of life. Conflicting roles of agencies, or countries, should be recognized and resolved beforehand. In fact, because nuclear energy was managed by military and civilian organizations well before the space age, nuclear, and space agencies find it in most cases difficult to talk to each other (the Russian nuclear propulsion effort was an exception, but the key people involved, the "three K," were also exceptional). An additional factor in this respect is the fact that a typical aerospace company is smaller, or much smaller, than companies building nuclear reactors, and so are the business prospects of selling space engines. Here, the solution should be to develop dual-mode reactors, capable of applications in space and for ground power generation. But faced with such program, the standard lawmaker committee is tempted to legislate or "suggest" joint teams, where responsibilities are inevitably diluted, rather than clearly assigned. Politically over-cautious management was at the root of some significant project failures, notably that of the US SNAP-100 RTG satellite nuclear power source (Bennett 1998). The opposite

example is the US Navy nuclear reactor program, managed very successfully for 20 years by a single clear-headed individual, Admiral Rickover (1982).

Finally, international treaties on nuclear power in space must be given a second look. The scope and text of the UN principles accepted by the 1992 General Assembly seem, at this time, to be overly restrictive and even preventing in practice the use or deployment of space nuclear propulsion. Born right after the end of the Cold War, during the rush to agree on and to approve what would have been impossible a few years before, the UN principles on nuclear power in space seem now more an obstacle than a tool for protecting humankind from the unwanted effect of nuclear energy. They should be revisited and revised, as others have already suggested (Lenard 2005, 2008a, b, c; El-Genk 2009; Smith 2012).

At this time, humankind is searching for solutions to problems never before so severe or so dramatic: wars, poverty, terrorism, financial crises seem to focus everybody's attention, as if the oldest questions humankind keeps asking "... *Where do we come from? Where are we going? Are we alone in the Universe?* ..." were forgotten.

In fact, these age-old questions have only been put aside, drowned by the sound and fury of here and now. In fact, humankind still wants answers to these questions. After Lise Meitner and Otto Robert Frisch discovered fission in 1939, and some 70 years after its use in war, this technology might provide the sought after *primer* to enable humans to further explore the solar system.

Bibliography

Andrenucci, M. (2004) "Prospective Needs and Technology Options for High Power Devices", Paper presented at the *International Symposium on Energy Conversion Fundamentals*, Istanbul, Turkey, 21–25 June 2004.

Andrews, D.G. and Lenard, R.X. (2006) "Proposed Follow-on Mini-Mag Orion Pulsed Propulsion Concept", Paper AIAA 2006-5223, presented at the 43rd *AIAA/ASME/SAE/ASEE Joint Propulsion Conference,* Sacramento, California, 9–12 July 2006.

Angelo, J.A. and Buden, D. (1985) *Space Nuclear Power*, Orbit Publisher, Melbourne, FL, 1985.

Anon. (1972) "Technical Summary Report of the NERVA Program", Vols. I–VI, Westinghouse Astronuclear Laboratory Publication WANL TNR-230, Pittsburgh, PA, 1972.

Anon. (1996) "Arcjet Thruster Design Considerations for Satellites", Practice No. PD-ED-1253, Page No. 1 OF5, NASA Preferred Reliability Practices, April 1996.

Anon. (2003) "NASA Nuclear Propulsion Targeted for Big Increase", Space News, 20 January 2003, p. 4.

Anon. (2004) Roundtable discussion on NP, Aerospace America, November 2004.

Anon. (2005) "Asteroid Warnings Set to Take Milder Tone", *Nature*, Vol. 434, Issue 7036, 21 April 2005, p. 948.

Anon., (2008a) "STAIF 2008: Space Technology Applications International Forum", papers from Sessions CT-01 and CT-02 contain information about nuclear surface power for lunar outposts, in: *25th Symposium on Space Nuclear Power and Propulsion*, Albuquerque, NM, *AIP Conference Proc.,* ed. by M.S. El-Genk. Vol. 969, American Institute of Physics, Melville, NY, 10–14 February 2008.

Anon. (2008b) "Constellation Program: America's Fleet of Next-Generation Launch Vehicles – The Ares V Cargo Launch Vehicle", NASA Fact Sheet, FS-2008-06-106-MSFC, NASA Facts, NASA, 2008.

Anon. (2013) "The Global Exploration Roadmap", NP-2013-06945-HQ, International Space Exploration Coordination Group (ISECG), published by NASA Headquarters, Washington, DC, August 2013.

Anon. (2014) "Pathways to Exploration: Rationales and Approaches for a US Program of Human Space Exploration", Committee on Human Space Flight, National Research Council (NRC), National Academies Press, Washington, D.C.

Anon. (2015) "Testing Multijunction Solar Cell Efficiency", *Aerospace & Defense Technology*, August 2015, pp. 37–38.

Anon. (2016a) "Nuclear Fuel", Wikipedia, https://en.Wikipedia.org/wiki/Nuclear_fuel, 12 July 2016.

Anon. (2016b) "Space Launch System", NASA Fact Sheet, NASA, FS-2016-02-04-MSFC, 2016.

Asker, J.R. (1991) "Nuclear Rockets Gain Support for Propelling Mars Mission", *Aviation Week & Space Technology*, 18 March 1991, pp. 24–25.

Aubrecht, G.J. (2005) "Energy: Physical, Environmental, and Social Impact", 3rd Edition, Addison-Wesley Educational Publishers Inc., 14 June 2005.

Augelli, M., Bignami, G., Bruno, C., Calligarich, E., De Maria, G., Mulas, M., Musso, C., Pellizzoni, A., Piperno, W., Piva, R., Procacci, B., Rosa-Clot, M. and Rubbia, C. (1999) "Report of the Working Group on a Preliminary Assessment of a New Fission Fragment Heated Propulsion Concept and its Applicability to Manned Missions to the Planet Mars (Project 242)", ASI Internal Report, Roma, 15 March 1999 (proprietary).

Augelli, M., Bignami, G. and Genta, G. (2013) "Project 242: Fission Fragments Direct Heating for Space Propulsion - Programme Synthesis and Applications to Space Exploration", Acta Astronautica, Volume 82, Issue 2, February 2013, pp. 153–158.

Auweter-Kurtz, M. and Kurtz, H. (2003) "High Power and High Thrust Density Electric Propulsion for In-Space Transportation", in *Proceedings of the International Workshop Technology and System Options towards Megawatt Level Electric Propulsion,* Lerici, Italy, 09–10 June 2003.

Auweter-Kurtz, M. and Kurtz, H. (2005) "High Power and High Thrust Density Electric Propulsion for In-Space Transportation", paper IAC-05-C3.5-C4.7.05, presented at the *56th International Astronautical Congress (IAC),* Fukuoka, Japan, 16–21 October 2005. 16–21.

Auweter-Kurtz, M. and Kurtz, H. (2008) "High Power and High Thrust Density Electric Propulsion for In-Space Transportation", in C. Bruno (Ed.), *Nuclear Space Power and Propulsion Systems,* Progress in Aeronautics and Astronautics Series, Vol. 225, AIAA, Reston VA, 15 October 2008, Chapter 4.

Backhaus, S., Tward, E. and Petach, M. (2004) "Traveling-Wave Thermoacoustic Electric Generator", *Applied Physics Letters*, Vol. 85, No. 6, 2004, pp. 1085–1087.

Baggett, R. and Dankanich, J. (2004) "Electric Propulsion", *Aerospace America*, December 2004, pp. 58–59.

Bates, J. (2003) "NASA Science Chief Lays Out Need for New Propulsion System", *Space News*, 09 June 2003, p. 8.

Beale, G.A. and Lawrence, T.J. (1989) "Nuclear propulsion for Orbital Transfer", *Aerospace America*, June, pp. 27–29.

Belic, D., Arlandini, C. et al. (1999) "Photoactivation of $^{180}Ta^{m}$ and its Implications for the Nucleosynthesis of Nature's Rarest Naturally

Occurring Isotope", Physical Review Letters 83(25):5242, 20 December 1999.

Benetti, P., Cesana, A., Cinotti, L. Raselli, G.L. and Terrani, M. (2006) "Americium 242m and its Potential Use in Space Applications", *J. Physics, Conference Series* 41, 2006, pp. 161–168.

Bennett, G.L. (1998) "Lessons of Space Nuclear Power", *Aerospace America*, July, pp. 32–40.

Berger, B. (2005a) "NASA Sacrifices Hubble, JIMO to Focus on Moon-Mars Vision", *Space News*, 14 February 2005, pp. 8–9.

Berger, B. (2005b) "Griffin Praised for Putting Europa Mission Back on the Table", *Space News*, 23 May 2005, p. 6 [see also the Editorial in *Space News* of 30 May 2005, p. 18].

Bidault, C., Bond, R. and Sweet, D. (2004) "Assessment of Electric Propulsion Systems for Exploration Missions: Comparison between Solar-Electric and Nuclear-Electric Propulsion Systems", AURORA Final Report to ESA-ESTEC, July 15, 2004.

Binzel, R.P. (2014) "Human Spaceflight: Find Asteroids to Get to Mars", *Nature*, Vol. 514, Issue 7524, 29 October 2014, pp. 559–561.

Blott, R. (2008) "The Future is Electric", paper IAC-08-C.4.6.03, presented at the *59th International Astronautical Congress,* Glasgow, Scotland, 29 September–3 October 2008.

Blott, R., Koppel, C., Jansen, F., Ferrari, C., Bruno, C., Herdrich, G., Gabrielli, R. and Valentian, D. (2012) "Space Fission Nuclear Power – A Roadmap for Europe", paper IAC-12-C.4.7-C.3.5.3, presented at the *63th International Astronautical Congress*, Naples, Italy, 1–5 October 2012.

Bohl, R.J., Kirk, W.L. and Holman, R.R. (1989) "The Beginnings", *Aerospace America*, June 1989, pp. 18–22.

Bond, R. (2002) "Nuclear Propulsion - Options and Choices", Paper presented at the European Science Foundation Workshop on Nuclear Propulsion, Rome, Italy, 10–11 May 2002.

Bond, A., Martin, A.R., Grant, R.A. and Lawton, T.J. (1978) "Project Daedalus", Supplement to the *J. British Interplanetary Society*, Vol. 31, 1978, pp. S1–S56.

Bordi, F. and Taylor, R. (2003) "The Jupiter Icy Moon Orbiter Mission", in Proceedings of the International Workshop *Technology and System Options towards Megawatt Level Electric Propulsion*, Lerici, Italy, 09–10 June 2003.

Borowski, S.K., Corban, R.R., Culver, D.W., Bulman, M.J. and McIlwain, M.C. (1994) "A Revolutionary Lunar Space Transportation System Architecture Using Extraterrestrial LOX-Augmented NTR Propulsion", AIAA paper 94-3343, presented at the *30th AIAA/ ASME/SAE/ASEE Joint Propulsion Conference*, Indianapolis, IN, 27–29 June 1994.

Borowski, S.K., Dudzinski, L.A. and McGuire, M.L. (1998) "Nuclear Thermal Rocket (NTR) Propulsion for Tomorrow's Moon/Mars Space Transportation Systems - Revolutionary Performance Through Evolutionary Development", Paper IAA-98-IAA.13.1.01, presented at the *49th IAF Congress, Melbourne*, 28 September–02 October 1998. Also: NASA TM 1998-208826, December 1998.

Borowski, S.K., Dudzinski, L.A. and McGuire, M.L. (1999) "Artificial Gravity Vehicle Design Option for NASA's Human Mars Mission Using 'Bimodal' NTR Propulsion", paper AIAA-99-2545, presented at the *35th AIAA/ASME/SAE/ASEE Joint Propulsion Meeting*, Los Angeles, CA, 20–24 June 1999.

Borowski, S.K., Dudzinski, L.A. and McGuire, M.L. (2000) "Artificial Gravity Human Exploration Missions to Mars and Near Earth Asteroids Using 'Bimodal' NTR Propulsion", Paper AIAA 2000-3115, presented at the *36th AIAA/ASME/SAE/ASEE Joint Propulsion Meeting*, Huntsville, AL, 16–19 July 2000.

Bottin, B., Carbonaro, M., Paris, S., Van der Haegen, V., Novelli, A. and Vennemann, D. (1998a) "The VKI 1.2 MW Plasmatron Facility for the Thermal Testing of TPS Materials", Paper presented at the *3rd European Workshop on Thermal Protection Systems*, ESA-ESTEC, Noordwjik, The Netherlands, 25–27 March 1998.

Bottin, B., Carbonaro, M., Van der Haegen and Paris, S. (1998b) "Predicted and Measured Capability of the VKI 1.2 MW Plasmatron Regarding Re-entry Simulation", in *Proceedings of the Third European Symposium on Aerothermodynamics for Space Vehicles*, edited by R.A. Harris, ESA Publication SP-426, Noordwijk, 1998, p. 553.

Boveri, B. (1980) "Gas Turbine Power Plant", Patent Number: 4193266, BBC Brown Boveri & Company Limited, 18 March 1980.

Braukus, M. (2004) "Advanced Electric-Propulsion Technologies R&D Teams Selected", Contract Release c04-p, NASA Headquarters, Washington, 29 July 2004.

Braun, R.D. and Blersch, D.J. (1991) "Propulsive Options for a Manned Mars Transportation System", *Journal of Spacecraft*, Vol. 28, No. 1, January–February 1991.

Brown, D., Cantillo, L. and Webster, G. (2015) "NASA Confirms Evidence That Liquid Water Flows on Today's Mars", Release 15-195, NASA, 28 September 2015.

Bruno, C. (2005) "Physics of Nuclear Propulsion - An Introduction", Paper IAC-05-C3.5- C4.7.01, presented at the *56th International Astronautical Congress (IAC)*, Fukuoka, Japan, 16–21 October 2005.

Bruno, C. (2008) "Nuclear Propulsion: An Introduction", in: C. Bruno (Ed.), *Nuclear Space Power and Propulsion Systems*, Progress in Aeronautics and Astronautics Series, Vol. 225, AIAA, Reston, VA., 15 October 2008.

Bruno, C. (2012) "Nuclear Propulsion", in: *Fluid Dynamics, Computational Modeling and Applications*, ed. by L. Hector Juarez, InTech Books, Rijeka, Croatia, February 2012, pp. 381–402.

Bruno, C. (2014) "Space Propulsion", in: *The International Handbook of Space Technology*, ed. by M. Macdonald and V. Badescu, Springer-Praxis, Chichester, Chapter 11, 08 July 2014.

Bruno, C. and Giucci, S. (1999) "Cryogenic Technology to Improve Electric Thrusters", IAF Paper IAF-99-S.4.04, presented at the *50th IAF Congress*, Amsterdam, Netherlands, 04–08 October 1999, also *Acta Astronautica*, Vol. 51, No. 12, 2002, pp. 855–863.

Bruno, C., Dujarric, C. and Durante, M. (2013) "Propulsion Requirements for a Safe Human Exploration of Mars", paper IAC-13-C47.8, presented at the *64th International Astronautical Congress*, Beijing, China, 23–27 September 2013.

Buffone, C. and Bruno, C. (2002) "Cooling the Rubbia's Engine Nozzle in the Future Test Facility", Paper ISTS 2002-a-22 presented at the *23rd International Science and Technology Space Symposium*, Matsue, Japan, 26 May–02 June 2002.

Bulman, M.J. and Neill, T.M. (2000) "Simulated LOX-Augmented Nuclear Thermal Rocket (LANTR) Testing", Paper AIAA 2000-3897 presented at the *36th AIAA/ ASME/SAE/ASEE Joint Propulsion Conference*, Huntsville AL, 16–19 July 2000.

Bulman, M.J., Neill, T.M. and Borowski, S.K. (2004) "LANTR Engine System Integration", paper AIAA 2004-3864, presented at the *40th AIAA/ASME/SAE/ASEE Joint Propulsion Conference*, Fort Lauderdale, FL, 11–14 July 2004.

Burke, L.M., Borowski, S.K., McCurdy, D.R. and Packard, T.W. (2013) "A One-year, Short-Stay Crewed Mars Mission using Bimodal Nuclear Thermal Electric Propulsion (BNTEP) – A Preliminary Assessment", NASA TM-2013-216566, also paper AIAA 2013-4076, presented at the *49th AIAA/ASME/SAE/ASEE Joint Propulsion Conference,* San Jose, CA, 15–17 July 2013.

Bussard, R.W. and DeLauer, R.D. (1958) *Nuclear Rocket Propulsion*, McGraw-Hill, New York, 1958.

Butrica, A.J. (2003) Single Stage to Orbit – Politics, Space Technology, and the Quest for Reusable Rocketry", The Johns Hopkins University Press, Baltimore and London, 2003.

Casali, D. and Bruno, C. (2008) "Superconductivity", in: *Advanced Propulsion Systems and Technologies: Today to 2020*, edited by C. Bruno and A. Accettura, AIAA Progress in Astronautics and Aeronautics, Vol. 223, AIAA, Reston, VA, 15 March 2008, Chapter 11.

Cassady, R.J., Frisbee, R.H., Gilland, J.H., Houts, M.G., LaPointe, M. R., Maresse-Reading, C.M., Oleson, S.R., Polk, J.E., Russel, D. and Sengupta, A. (2008) "Recent Advances in Nuclear Powered Electric Propulsion for Space Exploration", *Energy Conversion and Management*, Vol. 49, 2008, pp. 412–435.

Cataldo, R.L. and Borowski, S.K. (2004) "Propulsion and Surface Power Systems Commonality Issues for Human Exploration", paper IAC-04-R.4-S.7.03, presented at the *54th International Astronautical Conference (IAC),* Vancouver, Canada, 04–08 October 2004.

Chandler, D. (2008) "The Burger Bar that Saved the World", *Nature*, Vol. 453 No. 7199, 26 June 2008, pp. 1165–1168.

Chang Diaz, F.R. (2000) "The Vasimr Rocket", *Scientific American*, Vol. 283, No. 5, 2000, p. 72.

Chang Diaz, F R., Squire, J.P., Ilin, A.V., McCaskill, G.E., Nguyen, T. X., Winter, D.S., Petro, A.J., Goebel, G.W., Cassady, L., Stokke, K. A., Dexter, C.E., Carter, M.D., Baity, F.W., Barber, G.C., Goulding, R.H., Sparks, D.O., Schwenterly, S.W., Bengtson, R. D., Breizman, B.N., Jacobson, V.T., Sagdeev, R.Z., Karavasilis, K., Novakovski, S.V., Chan, A.A. and Glover, T.W. (1999) "The Development of the VASIMR Engine", *Proceedings of the International Conference on Electromagnetics in Advanced Application,* Torino, Italy, 13–17 September 1999.

Chang Diaz, F.R., Squire, J.P., Bengtson, R., Breizman, B.N., Baity, F. W. and Carter, M.D. (2000) "The Physics and Engineering of the VASIMR Engine", paper AIAA 2000-3756, presented at the *36th AIAA/ASME/SAE/ASEE Joint Propulsion Meeting,* Huntsville, Alabama, 16–19 July 2000.

Chapline, G.F., Dickson, P.W. and Schnitzler, B.G. (1988) "Fission Fragment Rockets: A potential Breakthrough", Paper presented at the International Reactor Physics Conference, Jackson Hole, WY, 11–18 September 1988, DOE/OSTI ID: 6868318.

Chew, G., Pelaccio, D.G., Chiroux, R., Moton, T. and White, C. (2004) "Status and Assessment of the Indirect Nuclear Propulsion Concept", paper AIAA 2004-3868, presented at the *40th AIAA/ASME/SAE/ASEE Joint Propulsion Conference*, Fort Lauderdale, FL, 11–14 July 2004.

Chichester, H.J.M. (2012) "Introduction to Nuclear Reactors, Fuels and Materials", Idaho National Laboratory (INL) presentation INL/MIS-12-24951, 27 February 2012.

Chodas, P.W. (2016) "Asteroid's Chance of Impacting Earth in 2022 Now 43%", Press Conference, International Asteroid Warning Network/JPL, 04 April 2016.

Choueiri, E. (1998) "The Scaling of Thrust in Self-Field MPD Thrusters", *Journal of Propulsion and Power*, Vol. 14, No. 5, 1998, pp. 744–753.

Choueiri, E. (2000) Personal communication with C. Bruno.

Choueiri, E. (2009) "New Dawn for Electric Rockets", *Scientific American*, Vol. 301, No. 2, 2009, pp. 48–55.

Clark, J.S. (1990) Editor, "Proceedings of the NASA/DOE/DOD Nuclear Thermal Propulsion Workshop", held in Cleveland, OH, 10–12 July 1990, NASA CP-10079, 1991.

Clark, J.S., McDaniel, P., Howe, S., Helms, I. and Stanley, M. (1993) "Nuclear Thermal Propulsion Technology: Results of an Interagency Panel in FY 1991", NASA TM 105711, NASA, April 1993.

Claybaugh, W., Garriott, O.W., Garvey, J., Griffin, M., Jones, T.D., Kohlhase, C., McCandless II, B., O'Neil, W. and Penzo, P.A. (2004) "Extending the Human Presence into the Solar System – An Independent Study to The Planetary Society on Strategy for the proposed U.S. Space Exploration Policy", The Planetary Society, July 2004.

Comparetti, A.M. et al. (2016) "Near Earth Objects Dynamic Site – NEODyS-2", University of Pisa, http://newton.dm.unipi.it/neodys/index.php?pc=0, August 2016.

Connolly, D.J., Bishop, A.R. and Seikel, G.R. (1971) "Testing of Permanent Magnet and Superconducting Magnet MPD Thrusters", paper AIAA 71-696, presented at the *7th AIAA/SAE Propulsion Joint Specialist Conference*, Salt Lake City, UT, 14–18 June 1971.

Coppinger, R. (2008) "The Battle Goes on for Ares", *Flight International*, 12–18 August 2008, pp. 22–23.

Cumo, M., Frullini, M., Gandini, A. Naviglio, A. and Sorabella, L. (2005) "MAUS-1,5 Nuclear Reactor for Space Electric Power", paper presented at the *12th International Conference on Emerging Nuclear Energy Systems (ICENES 2005)*, Brussels, Belgium, 21–26 August 2005.

David, L. (2002) "Nuclear Initiative Now Centerpiece of Planetary Effort", *Space News*, 11 February 2002, pp. 8–9.

David, L. (2015a) "US Air Force's Next X-37B Space Plane Mystery Mission to Test Thruster", Space.com, 01 May 2015.

David, L. (2015b) "Plasma Rocket Technology Receives NASA Funding Boost", *Space Insider*, August 24, 2015.

Davis, E.W. (2004) "Advanced Propulsion Study", AFRL-PR-ED-TR-2004-0024, Special Report, AFRL, Edwards AFB, September 2004.

Del Rossi, A. and Bruno, C. (2004) "Safety Aspects in Nuclear Space Propulsion", Paper IAC-04-R.4/S.7.07, presented at the *55th International Astronautical Congress (IAC)*, Vancouver, 4–8 October 2004.

Del Rossi, A. and Bruno, C. (2008) "The Chernobyl Accident: A Detailed Account", in: *Nuclear Space Power and Propulsion Systems*, edited by C. Bruno, AIAA Progress in Astronautics and Aeronautics, Vol. 225, AIAA, Reston, VA, 2008, 15 October 2008, Appendix B.

Demyanko, Y.G, Koniukov, G.V., Koroteev, A.S., Kuz'min, E.P. and Pavel'ev, A. (2001) *Nuclear Rocket Engines*, Norma Inform Publishers, Moscow, 2001 [in Russian; Chapter 1 contains a short history of the nuclear rocket engine ('ARD'). Reactors developed in the Soviet Union are discussed in Chapter 3].

Dewar, J.A. (2004) *To the End of the Solar System: The Story of the Nuclear Rocket*, The University Press of Kentucky, Lexington, KY, 2004.

DiMascio, J. (2015) "When To Go Slow", *Aviation Week & Space Technology*, Vol. 177, No. 7, 2015, p. 24.

Do Nascimento, J.A., Guimaraes, L.N.F. and Ono, S. (2015) "Fuel, Structural Material and Coolant for an Advanced Fast Microreactor", *J. British Interplanetary Society*, Vol. 67, No. 10, 2015, pp. 381–389.

Donahue, B. and Cupples, M. (2000) "Comparative Analysis of Current Human Mars Mission Architectures", paper AIAA 2000-3215, presented at the *36th AIAA/ASME/ SAE/ASEE Joint Propulsion Meeting,* Huntsville, AL, 16–19 July 2000.

Drake, B.G. (editor) (2009) "Human Exploration of Mars Design Reference Architecture DRA 5.0", NASA SP-2009-566, Houston, July 2009.

Dujarric, C. (1999) "An Innovative Hybrid Rocket Propulsion Concept for Take-Off from Planets and Interplanetary Missions", IAF Paper 99-S.6.06, presented at the *50th International Astronautical Federation Congress,* Amsterdam, Netherlands, 04–08 October 1999.

Dujarric, C., Fratacci, G. and Valentian, D. (2000) "Hybridisation of Chemical, Nucleothermal and Electric Rocket Propulsion Principles: A Possible Way to Increase Rocket Specific Impulse?", Paper IAF-00-S.6.02 presented at the *51st International Astronautical Federation Congress,* Rio de Janeiro, 02–06 October 2000.

Dujarric, C., Santovincenzo, A. and Summerer, L. (2013) "The Nuclear Thermal Electric Rocket: A Proposed Innovative Propulsion Concept for Manned Interplanetary Missions", *Progress in Propulsion Physics*, Vol. 4, 2013, pp. 293–312. DOI: 10.1051/eucass/201304293.

Dunning, J. and Sankovic, J. (1999) "NASA's Electric Propulsion Program", paper AIAA 99-2161, presented at the *35th AIAA/ASME/SAE/ASEE Joint Propulsion Conference and Exhibit*, Los Angeles, CA, 20–24 June 1999.

Durante, M. and Bruno, C. (2010) "Impact of Rocket Propulsion Technology on the Radiation Risk in Missions to Mars", European Physical Journal D, published on-line,16 February 2010, DOI: 10.1140/epjd/e2010-00035-6.

Dyson, F. (1979) *Disturbing the Universe*, Harper and Row, New York. 1979, Chapter 10.

Dyson, G. (2002) *Project Orion*, Allen Lane-The Penguin Press, London, 2002.

El-Genk, M. (2009) "Toward Global Standards of Peaceful Uses of Space Nuclear Reactor Power Systems", *J. British Interplanetary Society*, Vol. 62, July 2009, pp. 282–293.

Everett C.J., and Ulam, S.M. (1955) "On a Method of Propulsion of Projectiles by Means of External Nuclear Explosions", Los Alamos National Laboratories Report LAMS-1955, 1955.

Ewig, R. (2003) "Mini-MagOrion Program Document: Final Report", Andrews Space & Technology Report AST-MMO-P-DC-02-2594, Seattle, WA, January 2003.

Ewig, R. and Andrews, D. (2003) "Mini-MagOrion: A Pulsed Nuclear Rocket for Crewed Solar System Exploration", AIAA 2003-4525 presented at the *39th AIAA/ASME/ SAE/ASEE Joint Propulsion Conference*, Huntsville, AL, 20–23 July 2003.

Fearn, D. (2003) "The Prospects of MW Power Level Gridded Ion Thrusters", in Proceedings of the International Workshop "Technology and System Options towards Megawatt Level Electric Propulsion", Lerici, Italy, 9–10 June 2003.

Fearn, D. (2004) "The Application of Gridded Ion Thrusters to High Thrust, High Specific Impulse Nuclear-Electric Missions", Paper IAC-04-R.4/S.7-09, presented at the *55th International Astronautical Congress,* Vancouver, Canada, 02–09 October 2004.

Fearn, D. (2005) "The Application of Ion Thrusters to High Thrust, High Specific Impulse Nuclear-Electric Missions", Paper IAC-05-C3.5-C4.7.04, presented at the *56th International Astronautical Congress (IAC)*, Fukuoka, Japan, 16–21 October 2005.

Fearn, D.G. (2008) "Application of Ion Thrusters to High-Thrust, High-Specific-Impulse Nuclear Electric Missions", in: C. Bruno (Ed.), *Space Nuclear Propulsion and Power*, Progress in Astronautics and Aeronautics Series, Vol. 225, AIAA, Reston, VA, 15 October 2008.

Ferrari, C. and Bruno, C. (2012) "Technical Note D31.2 on 30 kWe Fission Power Source – General Configuration Options", Technical Note D31.2, EU Seventh Framework Programme (FP7/2007-2013), Grant No. 28408, 2012.

Ferrazzani, M. (2016) "Moon Village: From Vision to Reality", Legal Concil, European Space Agency, Brussels, 11 March 2016.

Flinn, E.D. (2004) "Can People Go to Mars?", *Aerospace America*, May 2004, pp. 22–23.

Flora, M. (2005) "Project Orion: Its Life, Death, and Possible Rebirth", www.islandone.org/Propulsion/ProjectOrion.html.

Friesen, H.N. (1995) "Radiological Effluents Released from Nuclear Rocket and Ramjet Engine Tests at the Nevada Test Site 1959 through 1969 Fact Book", US Department of Energy Report DOE/NV-401, June 1995.

Gafarov, A.A., Gorshkov, O.A., Rozhdestvensky, N.M., Kudryashov, V.A., Skryabin, M.I., Bachmanov, M.M., and Fedotov, G.G. (2004) "Conceptual Project of the Interplanetary Spacecraft with Nuclear Power System and Electric Propulsion System for Radar Sounding of Ice Sheet of Europa, Jupiter Satellite", paper IAC-04-R.4-S.7.02, presented at the *55th International Astronautical Congress (IAC)*, Vancouver, Canada, 4–8 October 2004.

Garrett, H.B. (2010) "The Interplanetary and Planetary Environments", in *Encyclopedia of Aerospace Engineering*, by Blockley, R. (editor), John Wiley & Sons, 27 October 2010.

Genta, G. and Salotti, J.M., editor and 29 authors (2016) "Global Human Mars System Missions Exploration Goals, Requirements and Technologies", International Academy of Astronautics, Cosmic Study SG 3.16, IAA, Paris, 2016.

Gilles, J. (2004) "Britain Warms to European Space Exploration Plan", *Nature*, Vol. 431, 07 October 2004, p. 619.

Glasstone, S. (1955) *Principles of Nuclear Reactor Engineering*, Van Nostrand, New York, 1955, Chapter X.

Glenn, D.E. and Bulman, M.J. (1999) "CFD Analysis of the LOX-Augmented Nuclear Thermal Rocket (LANTR)", paper AIAA 99-2546, presented at the *35th AIAA/ ASME/SAE/ASEE Joint Propulsion Meeting*, Los Angeles, CA, 20–24 June 1999.

Godwin, R. (2006) *Russian Spacecraft*, Apogee Books, Burlington, Ontario, Canada, September 2006.

Goebel, D.M. and Katz, I. (2006) "Fundamentals of Electric Propulsion: Ion and Hall Thrusters", JPL Space Science and Technology Series, Pasadena, Ca., 2006.

Goldin, A.Ya., Koroteev, A.S., Semyonov, V.F., Konopatov, A.D., Pavshuk, V.A. and Ponomarev-Stepnoy, N.N. (1991) "Development of Nuclear Rocket Engines in the USSR", paper presented at the *AIAA/NASA/OAI Conference on Advanced Space Exploration Initiative (SEI) Technologies*, 4–6 September 1991, San Diego, CA.

Gray, R. (2015) "Is the Future of Space NUCLEAR? NASA is Developing New Rockets to Send Astronauts to New Corners of the Solar System", *Daily MailOnLine*, 03 February 2015.

Griffin, B., Thomas, B., Vaughan, D. et al. (2004) "A Comparison of Transportation Systems for Human Missions to Mars", AIAA 2004-3834, *40th AIAA/ASME/SAE/ASEE Joint Propulsion Conference and Exhibit*, Fort Lauderdale, FL, 11–14 July 2004.

Guerra, A.G.C., Bertolami, O. and Gil, P.J.S. (2015) "Comparison of Four Space Propulsion Methods for Reducing Transfer Times of Manned Mars Mission", arXiv:1502.05467v.2, physics.pop-ph, 26 November 2015.

Gunn, S.V. (1998) "Nuclear Thermal Rocket – An Established Technology", Paper presented at the Explospace Workshop, Cagliari, Italy, 20–22 October 1998. ESA Publication WPP-151, pp. 3b.3–3b.14.

Gunn, S.V. (2001) "Nuclear Propulsion—a Historical Perspective", *Space Policy*, Vol. 17, No. 4, 2001, pp. 291–298.

Gunn, S.V. and Ehresman, C.M. (2003) "The Space Propulsion Technology Base Established Four Decades Ago for the Thermal Nuclear Rocket is Ready for Current Applications", Paper AIAA 2003-4590 presented at the *39th AIAA/ASME/SAE/ASEE Joint Propulsion Conference*, 20–23 July 2003, Huntsville, AL.

Haeseler, D. (2014) "Soviet Mars Propulsion - Nuclear Thermal", Astronautix, 2016.

Hagen, R. and Scheffran, J. (2001) "Nuclear Space - An Indispensable Option?", *Space Policy*, Vol. 17, No. 4, 2001, pp. 261–264.

Hamilton, C.E. (2002) "Design Study of Triggered Isomer Heat Exchanger-Combustion Hybrid Jet Engine for High Altitude Flight", US Air Force Institute of Technology PhD thesis, released as Report AIT/GAE/ENY/02-6, 2002.

Harbaugh, J. (2015) "NASA's Space Launch System Design 'Right on Track' for Journey to Mars", Space Launch System, NASA, http://www.nasa.gov/sls, 23 July 2015.

Harris, A. (2008) "What Spaceguard Did", *Nature*, Vol. 453 No. 7199, 26 June 2008, pp. 1178–1179.

Haslett, R.A. (1995) "Space Nuclear Thermal Propulsion Program Final Report", Phillips Laboratory Report PL-TR-95-1064, Kirtland Air Force Base, NM 87117-5776, 1995.

Hill, P.G. and Peterson, C.R. (1970) *Mechanics and Thermodynamics of Propulsion*, 1st Edition, Addison-Wesley, Reading, MA, 1970, Chapter 15.

Hoffman, M. and Fleming, M. (2005) "Chernobyl: The True Scale of the Accident", Press Release, International Atomic Energy Agency, World Health Organization, United Nations Development Programme, 05 September 2005.

Howe, S.D. (1985) "Assessment of the Advantages and Feasibility of a Nuclear Rocket for a Manned Mars Mission", Los Alamos National Laboratories Report LA-UR-85-2442, 1985.

Howe, S.D. (2000) "Nuclear Rocket to Mars", *Aerospace America*, August 2000, p. 39.

Howe, S.D. (2001) "High Energy Density Propulsion - Reducing the Risk to Humans in Planetary Exploration", *Space Policy*, Vol. 17, No. 4, 2001, pp. 275–284.

Howe, S.D. and O'Brien, R.C. (2010) "Recent Activities at the Center for Space Nuclear Research for Developing Nuclear Thermal Rockets", Paper IAC-10.C4.7-C3.5.2, presented at the *61st International Astronautical Congress,* Prague, 27 September–01 October 2010.

Howe, S.D., DeVolder, B., Thode, L. and Zerkle, D. (1998) "Reducing the Risk to Mars: The Gas Core Nuclear Rocket", in *Space Technology and Applications International Forum (STAIF-1998*), edited by Mohamed S. El-Genk, Publication CP-420, The American Institute of Physics, New York, 1998, p. 1138.

Hrbud, I. (2003) "Nuclear and Future Flight Propulsion", *Aerospace America*, December, pp. 62–63.

Iannotta, B. (2004) "NASA Funds Research on Very High-Power Electric Thrusters", *Space News*, 16 August 2004, p. 16.

Ilin, A.V., Chang Diaz, F.R., Squire, J.P. and Carter, M.D. (1999) "Monte Carlo Particle Dynamics in a Variable Specific Impulse Magnetoplasma Rocket", in Proceedings of the Open Systems '98 Meeting, Novosibirsk, July 1998; also in *Transactions in Fusion Technology*, Vol. 35, 1999, pp. 330–334.

Ilin, A.V., Chang Diaz, F.R., Squire J.P., Breizman, F.W. and Carter, M.D. (2000) "Particle Simulations of Plasma Heating in VASIMR", paper AIAA 2000-3753, presented at *36th AIAA/ASME/SAE/ASEE Joint Propulsion Conference*, Huntsville, AL, 17–19 July 2000.

Jarow, L. (2000) "Will a Killer Asteroid Hit the Earth?", *Time Magazine*, 10 April 2000, pp. 50–51.

Jones, L.J. (1992) "Nuclear Thermal Propulsion", *Aerospace America*, December, p. 28.

Jones, T.D. (2015) "NASA's Bid to Grab Asteroid – 9 Things to Know", *Aerospace America*, Vol. 53, No. 4, April 2015, pp. 20–23.

Joyner, C. R., Phillips, J.E., Fowler, R.B. and Borowski, S.K. (2004) "TRITON: a TRImodal, Thrust Optimized, Nuclear Propulsion and Power System for Advanced Space Missions", paper AIAA 2004-3863, presented at the *40th AIAA/ASME/SAE/ ASEE Joint Propulsion Conference*, Fort Lauderdale, FL, 11–14 July 2004.

Joyner, C.R., Rowland, R. and Lentati, A. (2006) "Multi-Disciplinary Analysis of CERMET Nuclear Thermal, Bimodal Nuclear Thermal, and Thrust Augmented Nuclear Thermal Propulsion for Human Exploration Missions", paper presented at Session C28, *Space Technology & Applications International Forum (STAIF-2006)*, Albuquerque, NM, 12–16 February 2006.

Kaplan, J., Von Braun, W., Haber, H., Ley, W., Schachter, O., Whipple, F.L. and Ryan, C. (Editor) (1952) *Across the Space Frontier*, 1st edition, September 1952.

Ketsdever, A.D., Young, M.P., Pancotti, A.P. and Mossman, J.B. (2008) "An Overview of Advanced Concepts for Space Access", USAF Research Laboratory Report AFRL-RZ-ED-TP-2008-238, Edwards AFB, CA, 06 June 2008.

Kinley, D. (editor) (2006) "Chernobyl Legacy: Health, Environmental and Socio-Economic Impacts", International Atomic Energy Agency (IAEA), The Chernobyl Forum Report, Vienna, Austria, April 2006.

Kirischuk, V.I., Ageev, V.A., Kandybel, S.S., and Ranyuk, Y.M. (2015) "Induced acceleration of the Decay of the 31-Yr Isomer of ^{178m2}Hf Using Bremsstrahlung", Physics Letters B, Vol. 750, 2015, pp. 89–94.

Koenig, D.R. (1986) "Experience Gained from the Space Nuclear Rocket Program (Rover)", Los Alamos National Laboratories Report LA-10062-H, May 1986.

Köhler, J., Zeitlin, C., Ehresmann, B. et al. (2014) "Measurements of the Neutron Spectrum on the Martian Surface with MSL/RAD", Journal of Geophysical Research, Vol. 119, Issue 3, March 2014, pp. 594–603.

Koniukov, G.V., Petrov, A.I., Popov, S.A., Rachuk, V.S., Belogurov, Y.I., Mamontov, Yu.I., Fedik, I.I., D'yakov, Ye.K., Mogil'ny, I.A., Konovalov, V.A., et al. (2004) "Prototype of Atomic Rocket-IRGIT Reactor", *Atomic Energy*, Vol. 97, No. 3, 2004, pp. 173–177 [in Russian].

Koppel, C.R., Valentian, D., Latham, P.M., Fearn, D., Bruno, C. and Nicolini, D. (2003) "Preliminary Comparison between Nuclear-Electric and Solar-Electric Propulsion Systems for Future Interplanetary Missions", paper AIAA 2003-4689, presented at the *39th AIAA/ASME/SAE/ASEE Joint Propulsion Conference,* Huntsville, AL, 20–23 July 2003.

Koroteev, A.S., Prishletsov, A.B., Martishin, V.M., Pavelyev, A.A., Shcherbinin, V.P., Reshmin, A.I. and Iosilevskii, I.L. (2002) "Rocket Engines and Powerplants Based on Gas-Core Nuclear Reactor", edited by A.S. Koroteev, Mashinostroenie Publisher, Moscow, 2002 [in Russian].

Koroteev, A.S., Akimov, V.N. and Gafarov, A.A. (2007) "Development and Use of Space Nuclear Energetics in Russia", *Polyot (Flight)*, Vol. 7, July 2007, pp. 3–15 [in Russian].

Lake, J.A., Bennett, R.G. and Kotek, J.F. (2002) "Next-Generation Nuclear Power", *Scientific American*, Vol. 286, No. 1, 2002, pp. 70–79.

Lanin, A. (2013) *Nuclear Rocket Engine Reactor*, Springer Verlag, Berlin, October 2012.

Larson, W.J. and Wertz, J.R. (editors) (1992) *Space Mission Analysis and Design*, 2nd Edition, Space Technology Library, Kluwer, Dordrecht, November 1992, Section 11.4.

Lawrence, T.J. (2008) "Nuclear Thermal Rocket Propulsion Systems", in: *Nuclear Space Power and Propulsion Systems*, edited by C. Bruno, Progress in Aeronautics and Astronautics Series Vol. 225, AIAA, Reston, VA, 15 October 2008.

Lawrence, T.J., Witter, J.K. and Humble, R.W. (1995) "Nuclear Rocket Propulsion Systems", in *Space Propulsion Analysis and Design*, edited by R.W. Humble, G.N. Henry and W.J. Larson, McGraw-Hill, New York, Ch. 8, and also as otherwise cited, 1995.

Lenard, R.X. (2001) "Societal Imperatives and the Need for Space Nuclear Power and Propulsion Systems", Space policy, Vol. 17, No. 4, November 2001, pp. 285–290.

Lenard, R.X. (2005) "Nuclear Safety, Legal Aspects and Policy Recommendations", Paper IAC-05-C3.5-C4.7.06, presented at the *56th International Astronautical Congress (IAC)*, Fukuoka, Japan, 16–21 October 2005.

Lenard, R.X. (2008a) "Review of Reactor Configurations for Space Nuclear Electric Propulsion and Surface Power Considerations", in: *Nuclear Space Power and Propulsion Systems*, edited by C. Bruno, AIAA Progress in Astronautics and Aeronautics, Vol. 225, AIAA, Reston, VA, 2008, Ch. 5.

Lenard, R.X. (2008b) "Improving Performance of Near-Term Nuclear Electric Propulsion Systems", paper IAC-08-C4.7-C3.5.4, presented at the *59th International Astronautical Congress*, Glasgow, Scotland, 29 September–03 October 2008.

Lenard, R.X. (2008c) "Nuclear Safety, Legal Aspects and Policy Recommendations", in: *Nuclear Space Power and Propulsion Systems*, edited by C. Bruno, AIAA Progress in Astronautics and Aeronautics, Vol. 225, AIAA, Reston, VA, 2008, Ch. 6.

Lev, D. and Choueiri, E.Y. (2010) "Scaling of Efficiency with Applied Magnetic Field in Magnetoplasmadynamic Thrusters", paper AIAA 2010-7024, presented at the *46th AIAA/ASME/SAE/ASEE Joint Propulsion Conference*, Nashville, TN, 25–28 July 2010.

Ley, W. and Bonestell, C. (1959) *The Conquest of Space*, 10th Printing, The Viking Press, April 1959.

Linne, D. and Kleinhenz, J. (2016) "Extraction and Capture of Water from Martian Regolith Experimental Proof-of-Concept", paper AIAA-2016-0226, presented at the 54th Aerospace Sciences Meeting, San Diego, CA, 3–8 January 2016.

MacAvoy, J.J. (2004) "Nuclear Space and the Earth Environment: The Benefits, Dangers, and Legality of Nuclear Power and Propulsion in Outer Space", William & Mary Environmental Law and Policy Review, Vol. 29, Issue 1, Article 6, Rev. 191, 2004.

Maise, G., Powell, J.R., Paniagua, J., Ludewig, H. and Todosow, M. (1998) "Exploration of Jovian Atmosphere Using Nuclear Ramjet Flyer", paper IAF-98-S.6.08, presented at the *49th International Astronautical Congress (IAC)*, Melbourne, Australia, 28 September–02 October 1998.

Maise, G., Powell, J.R., Paniagua, J., Ludewig, H. and Todosow, M. (2000) "Compact Ultra Lightweight Nuclear Thermal Propulsion Systems for Interplanetary Space Missions", IAC paper presented at the *51st International Astronautical Congress (IAC),* Houston, TX, 02–06 October 2000.

Mankins, J. and Mandell, H. (1999) "NASA's Integrated Mars Reference Missions", paper IAA-99-IAA.13.3.01 presented at the *50th International Astronautical Congress (IAC)*, Amsterdam, The Netherlands, 04–08 October 1999.

March, P. (2006) "Low Cost Access to Space", Revision H, presentation, 15 April 2016.

Martin, P.K. (2015) "NASA's Efforts to Manage Health and Human Performance Risks for Space Exploration", Office of Inspector General, Report IG-16-003, 15 October 2015.

Maxwell, J.L., Webb, N.D., Espinoza, M., Cook, S., Houts, M., and Kim, T. (2013) "High-Temperature Nanocomposites for Nuclear Thermal Propulsion and In-Space Fabrication by Hyperbaric Pressure Laser Chemical Vapor Deposition", *J. British Interplanetary Society*, Vol. 66, No. 10–11, 2013, pp. 328–333.

Mazanek, D.D, Abell, P., Antol, J., Barbee., Beaty, D., Bass, D., Castillo-Rogez, J., Coan, D., Colaprete, A., Daugherty, K., Drake, B., Earle, K., Graham, L., Hambree, M., Hoffman, S., Jefferies, S., Lewis, R., Lupisella, M. and Reeves. D. (2013) "Considerations for Designing a Human Mission to the Martian Moons", 2013 Space Challenge, NASA, California institute of Technology, 25–29 March 2013.

Mazanek, D.D., Merrill, R.G., Brophy, J.R. and Mueller, R. P. (2014) "Asteroid Redirect Mission Concept: a Bold Approach for Utilizing Space Resources", Paper IAC-14-D.3.1.8, presented at the *65th International Astronautical Congress*, Toronto, Canada, 29 September–03 October 2014.

McGuire, M.L., Borowski, S.K. and Packard, T.W. (2004) "Nuclear Electric Propulsion Application: RASC Mission Robotic Exploration of Venus", paper AIAA 2004-3891, presented at the *40th AIAA/ASME/SAE/ASEE Joint Propulsion Conference,* Fort Lauderdale, FL, 11–14 July 2004.

Mensing, A.E. and Latham, T.S. (1989) "Gas-Core Technology", *Aerospace America*, June 1989, p. 25.

Merkle, C.L. (editor) (1999) "Ad Astra per Aspera: Reaching for the Stars", Report of the Independent Review Panel of the NASA Space Transportation Research Program, Washington, DC, January 1999.

Messerle, H.K. (1995) *"Magneto-Hydro-Dynamic Electrical Power Generation"*, J. Wiley and Sons, Chichester.

Meyers, R. (editor) (2006) *Encyclopedia of Physical Science and Technology*, 3rd Edition, Vol. 15, Elsevier, Amsterdam, 2006, pp. 555–575.

Mikellides, P.G. and Turchi, P.J. (2000) "Applied Field Magnetoplasmadynamic Thrusters, Part 1: Numerical Simulations using the MACH2 Code", *J. Propulsion and Power*, Vol. 16, No. 6, 2000, pp. 887–901.

Morring, F. (2008) "NASA Raises Ares V Lift", Aviation Week Aerospace Daily & Defense Report, 28 June 2008.

Morring, F. (2015a) "Jupiter's Space Tug Could Deliver Cargo To The Moon", *Aviation Week*, Intelligence Network on-line, 12 March 2015.

Morring, F. (2015b) "Affordable Mars", *Aviation Week & Space Technology,* Vol. 177, No. 7, 2015, p. 22.

Morring, F. (2015c) "SpaceX Nails Falcon 9 First-Stage Landing", Aviation week Network, AW&ST, 21 December 2015.

Mowery, A.L. and Black, D.L. (1999) "Space Propulsion Annular Compact Engine (SPACE) - A NERVA Technology Compact Nuclear Rocket", AIAA Paper 99-2548, presented at the *35th AIAA/ASME/SAE/ASEE Joint Propulsion Conference*, Los Angeles, CA, 20–24 June 1999.

Mukhin, K.N. (1987) *Experimental Nuclear Physics*, Vol. I: *Physics of Atomic Nucleus*, Mir Publishers, Moscow, 1987, Chapter 1, p. 50; and Section 2.3.2, pp. 138 et seq.

Myers, W.D., and Swiatecki, W.J. (1966) "Nuclear Masses and Deformations", *Nuclear Physics*, Vol. 81, 1966, pp. 1–60.

Nagata, H., Miyoshi, M., Kotani, Y., Yamamoto, N., Kajimura, Y. and Nakashima, H. (2008) "Proposal of Nuclear Electric Propulsion System: Twin Star", paper ISTS-b-08, presented at the *Int. Symposium on Space Technology and Science (ISTS),* Hamamatsu, Japan, 01–08 June 2008.

Negrotti, A. (2008) "VASIMR Prefeasibility Analysis", in: *Advanced Propulsion Systems and Technology: Today to 2020*, edited by C. Bruno and A. Accettura, Progress in Astronautics and Aeronautics Vol. 223, AIAA, Reston, VA, 15 March 2008, Ch. 13.

Norris, G. (2010) "Power Options", *Aviation Week,* Vol. 172, 04 October 2010, pp. 48–50.

Norris, G. (2015) "NASA's Road Map Toward Possible Nuclear Rocket Flight Demo", Aviation Week & Space Technology, AviationWeek.com, 21 September 2015.

Ohira, K. (2004) "Development of Density and Mass Flowrate Measurement Technologies for Slush Hydrogen", *Cryogenics*, Vol. 44, No. 1, 2004, pp. 59–68.

Okada, T. (2010) "The Hayabusa Mission: Challenge to Near-Earth Asteroid Sample-Return and New insights into Solar System Origin", *47th Meeting of Scientific and Technical Subcommittee*, UN COPUOS, Vienna International Center, 16 February 2010.

Oleson, S.R. (2004) "Electric Propulsion Technology Development for the Jupiter Icy Moons Orbiter Project", AIAA Paper 2004-3453, American Institute of Aeronautics and Astronautics, Washington, D.C., July 2004.

Oleson, S. and Katz, I. (2003) "Electric Propulsion for Project Prometheus", paper AIAA 2003-5279, presented at the *39th AIAA/ASME/SAE/ASEE Joint Propulsion Conference,* Huntsville, AL, 20–23 July 2003.

Ortiz, L. (1993) "A Cost Analysis for a Nuclear Space Tug", *Adv. Astron. Sci*., Vol. 82, 1993, pp. 1361–1374.

Palaszewski, B. (2015) "Initial steps for Nuclear Thermal Rocket Design", *Aerospace America*, Vol. 53, No. 11, December 2015, p. 56.

Paniagua, J., Maise, G. and Powell, J. (2008) "Converting the ISS to an Earth-Moon Transport System Using Nuclear Thermal Propulsion", in *Proceedings of STAIF-2008,* AIP Conf. Proc. 969, American Institute of Physics, Melville, NY, 2008.

Patel, M.R. (2014) "Electrical Power", in: *The International Handbook of Space Technology*, ed. by M. Macdonald and V. Badescu, Springer-Praxis, Chichester, UK, 2014, Chapter 10.

Ponomarev-Stepnoy, N.N., Talyzin, V.M., Pavshuk, V.A., Putko, V. Ya., Konovalov, V.A., Raskach, F.L., Ulasevich, V.K., Smetannukov, V.P., Kolganov, V.D., Fedik, I.I., et al. (1999) "Rabotyi po Otiechiestvennogo ARD", *Atomic Energy*, Vol. 86, No. 4, 1999, pp.296–302 [in Russian; this paper has a picture of the "three Ks" (Korolev, Kurchatov and Keldysh) together].

Powell, J. (1999) "Compact Nuclear Rockets", *Scientific American*, February 1999, p. 72.

Powell, J., Maise, G., Ludewig, H. and Todosow, M. (1997) "High-Performance Ultra-Light Nuclear Rockets for Near-Earth Objects Interactions Missions" *Ann. New York Academy of Science*, Vol. 822, Part 1, May, pp. 447–467.

Powell, J., Paniagua, J., Ludewig, H., Maise, G. and Todosow, M. (1998a) "MITEE: A New Nuclear Engine Concept for Ultra-Fast, Lightweight Solar System Exploration Missions", in *Space Technology and Applications International Forum (STAIF) - 1998*, edited by Mohamed S. El-Genk, Publication CP-420, The American Institute of Physics, New York, 1998, p. 1131.

Powell, J., Paniagua, J., Ludewig, H., Maise, G. and Todosow, M. (1998b) "MITEE: An Ultra Lightweight Nuclear Engine for New and Unique Planetary Science and Exploration Missions", Paper IAF-98-R.1.01, presented at the *49th International Astronautical Congress (IAC)*, Melbourne, Australia, 28 September–02 October 1998.

Powell, J., Maise, G., Paniagua, J., Ludewig, H. and Todosow, M. (1999) "The MITEE Family of Compact, Ultra Lightweight Nuclear Thermal Propulsion Engines for Planetary Exploration Missions", Paper IAF-99-S.6.03 presented at the *50th International Astronautical Congress (IAC)*, Amsterdam, Netherlands, 04–08 October 1999.

Powell, J., Maise, G. and Paniagua, J. (2003) "HIP: A Hybrid NTP/NEP Propulsion System for Ultra-Fast Robotic Orbiter/Lander Missions to the Outer Solar System", Paper IAC-03-S.P.02, presented at the *54th International Astronautical Congress (IAC)*, Bremen, Germany, 29 September–3 October, 2003.

Powell, J., Maise, G. and Paniagua, J. (2004a) "Is NTP the Key to Exploring Space?", *Aerospace America*, Vol. 42, No. 1, January 2004, pp. 36–42.

Powell, J.R., Maise, G. and Paniagua, J. (2004b) "MITEE and SUSEE: Compact Ultra Lightweight Nuclear Power Systems for Robotic and Human Space Exploration Missions", Paper IAC-04-IAA-R.4/S.7-04 presented at the *55th International Astronautical Congress (IAC)*, Vancouver, Canada, 02–08 October 2004.

Pradas-Poveda, I. (2008) Personal communication C. Bruno.

Prelas, A. (1998) Personal communication with C. Bruno.

Prockter, L. (2004) "The Jupiter Icy Moons Orbiter: An Opportunity for Unprecedented Exploration of the Galilean Satellites", paper IAC-04-IAA.3.6.4.02, presented at the *54th Int. Astronautical Congress (IAC),* Vancouver, Canada, 04–08 October 2004.

Rachuk, V.S., Belogurov, A.I., Grigorenko, L.N. and Mamontov, Yu.I. (1996) "Russian Investigations in the Area of Nuclear Rocket Engines (NRE) Research International Programs", paper presented at the *5th International Symposium on Propulsion for Space Transportation*, 22–24 May 1996, Paris.

Randolph, T.M. and Polk Jr., J.E. (2004) "An Overview of the Nuclear Electric Xenon Ion System (NEXIS) Activity", paper AIAA 2004-3450, presented at the *40th AIAA/ASME/ SAE/ASEE Joint Propulsion Conference*, Fort Lauderdale, FL, 11–14 July 2004.

Reichardt, T. (2004) "Reviewers Caution NASA Over Plans for Nuclear-powered Craft", *Nature*, Vol. 431, 2004, p. 113.

Rickover, H.G. (1982) "Doing a Job", speech at Columbia University, GovLeaders.org, 1982.

Ronen, Y., Aboudy, M. and Regev, D. (2000) "A Nuclear Engine with ^{242m}Am as a Nuclear Fuel", *Ann. Nucl. Energy*, Vol. 27, 2000, p. 85.

Rose, B. (2008) *Military Space Technology*, Ian Allen, Horsham, UK, September 2008, Ch. 4.

Sackheim, R., Van Dyke, M., Houts, M, Poston, D., Lipinski, R., Polk, J. and Frisbee, R. (2000) "In-Space Nuclear Power as an Enabling Technology for Deep Space Exploration", AIAA Paper 2000-3881, presented at the *36th AIAA/ASME/SAE/ASEE Joint Propulsion Conference*, 16–19 July 2000, Huntsville, AL.

Schmidt, G.R. (1999) "Nuclear and Future Flight Propulsion", *Aerospace America*, December 1999, p. 66.

Schmidt, G.R., Bonometti, J.A. and Irvine, C.A. (2002) "Project Orion and Future Prospects for Nuclear Pulsed Propulsion", *J. Propulsion and Power*, Vol. 18, No. 3, May–June 2002, 497–504.

Schock, A., Noravian, H., Or, C. and Kumar, V. (2002) "Design, Analysis and Fabrication Procedure of AMTEC Cell, Test Assembly, and Radioisotope Power System for Outer-Planet Missions", *Acta Astronautica*, Vol. 50, No. 8, 2002, pp. 471–510.

Scina, J.E., Aulisio, M., Gerber, S.S., Hewitt, F., Miller, L. and Elbuluk, M. (2004) "Power Processing for a Conceptual Prometheus Electric Propulsion System", paper AIAA 2004-3452, presented at the *40th AIAA/ASME/SAE/ASEE Joint Propulsion Conference,* Fort Lauderdale, FL, 11–14 July 2004.

Shepherd, L.R. (1946) "The Problem of Interstellar Propulsion", *J. British Interplanetary Society*, Vol. 1, 1946, pp. 55–65.

Shepherd, L.R. and Cleaver, A.V. (1948) "The Atomic Rocket – 1 and 2", *J. British Interplanetary Society*, Vol. 7, No. 6, pp. 237–240; and Vol. 8, No. 1, p. 30, January 1949. Cited also in [Bussard and DeLauer (1958) p. 319].

Sibulkin, M. (1968) "Radiative Properties of Model Gases for Application in Radiative Energy Transfer", *J. Quantitative Spectroscopy & Radiative Transfer,* Vol. 8, No. 1, 1968, pp. 451–470.

Sietzen, F. (2008) "Reinventing Heavy Lift", *Aerospace America*, Vol. 46, No. 8, August, pp. 38–42.

Simonetti, A., Ferraro, F., D'Elia, R., Paternostro, S., and Bruno, C. (2009) "Analysis of a Manned Mars Mission with Nuclear Electric Propulsion (NEP) System", paper IAC C4.7.- C3.5 presented at the *60th International Astronautical Congress*, Daejeon, Korea, 12–16 October 2009.

Smirnov, V. (2015) "Rosatom to develop nuclear reactor for long-range space missions", TASS Russian News Agency, 14 September 2015.

Smith, T.E.R. (2012) "Review, Analyses, and Recommendations Related to Modern International Use of Nuclear Space Technologies with Focus on United States and Russia", *J. British Interplanetary Society,* Vol. 65, No. 11–12, 2012, pp. 360–372.

Smith, M. (2015) "Let's Fix the Asteroid Redirect Mission", *Aviation Week & Space Technology*, 23 February 2015.

Smith, B. and Anghaie, S. (2004) "Gas Core Reactor with Magneto-hydrodynamic Power System and Cascading Power Cycle", *Nuclear Technology*, Vol. 145, No. 3, 2004, pp. 311–318.

Smith, T.E.R. and Keidar, M. (2015) "Arcjet Ablation of Tungsten-based Nuclear Rocket Fuel", *J. Spacecraft and Rockets,* Vol. 52, No. 3, 2015, pp. 1003–1008.

Smith-Strickland, K. (2016) "What's the X-37 Doing Up There?", Air & Space Magazine, Air&Space Smithsonian, February 2016.

Stewart, M.E.M., Krivanek, T.M., Hemminger, J.A. and Bulman, M. J. (2006) "3D Reacting Flow Analysis of LANTR Nozzles", in STAIF 2006, *23rd Symposium on Space Nuclear Power and Propulsion*, Albuquerque, NM, 12–16 February 2006.

Stuhlinger, E. (1964) *Ion Propulsion for Space Flight*, McGraw-Hill Book Company, New York, 1964.

Sublette, C. (2001) "Section 6.0 Nuclear Materials", in "Nuclear Weapons Frequently Asked Questions", Version 2.25, 09 August 2001 (http://www.nuclearweaponarchive.org/Nwfaq/Nfaq6.html).

Summerer, L., Gardini, B. and Gianfiglio, G. (2007) "ESA's Approach to Nuclear Power Sources for Space Applications", Paper 7325, Proceedings of ICAPP 2007, Nice, France, 13–18 May 2007.

Sutton, G.P. (1992) *Rocket Propulsion Elements*, 6th Edition, Wiley Interscience, New York, 1992, Chapter 19.

Takao, Y., Noutsuka, T., Mori, Y., Uemura, K., Sou, H. and Nakashima, H. (2000) "Electron Cyclotron Resonance (ECR) Plasma Thruster Research", Paper ISTS 2000-b-32, presented at the *22nd International Symposium on Space Technology and Science*, Morioka, Japan, 28 May–04 June 2000.

Tauber, M.E., Bowles, J.V. and Yang, L. (1990) "Use of Atmospheric Braking During Mars Missions", *Journal of Spacecraft and Rockets*, Vol. 27, No. 3, 1990, p. 514.

Thode, L.E., Cline, M.C. and Howe, S.D. (1997) "Vortex Formation and Stability in a Scaled Gas Core Nuclear Rocket Configuration", paper AIAA 97-2955, presented at the *33rd AIAA/ASME/SAE/ASEE Joint Propulsion Conference*, Seattle, Washington, 11–15 July 1997.

Tok, J. (editor) (2008) "Asteroid Threats: A Call for Global Response", Association of Space Explorers, Washington, DC, 25 September 2008.

Turner, M.J.L. (2005) *Rocket and Space Propulsion*, Springer-Praxis, Chichester, UK, 2005, Ch. 7.

Vacca, K. and Johnson, A. (2004) "Feasibility of a Nuclear Single Stage to Orbit Reusable Vehicle", Paper IAC-04-IAF-R.4/S.7-06, presented at the *55th International Astronautical Congress (IAC)*, Vancouver, Canada, 4–8 October 2004.

Walker, P. and Dracoulis, G. (1999) "Energy Traps in Atomic Nuclei", *Nature*, Vol. 399, 1999, pp. 35–40.

Weir, A. (2014) *The Martian*, Crown Publishers, NY, 28 October 2014.

Wendt, G. (1951) "A Scientist Previews The First Atomic Airplane", Popular Science, October 1951, pp. 98–102.

Werka, R. (2012) "FFRE Powered Spacecraft" NIAC Presentation, NIAC Spring Symposium, 27 March 2012.

Werner, J., Bhattacharyya, S. and Houts, M. (2010) "An Overview of Facilities and Capabilities to Support the Development of Nuclear Thermal Propulsion", *J. British Interplanetary Society*, Vol. 63, No. 9/10, 2010, pp. 323–329 [this issue includes eleven articles from the AIAA NETS-2011, Nuclear and Emerging Technologies for Space Conference, Albuquerque, NM, 07–01 February 2011].

WHO Media, (2015) www.WHO.INT/mediacentre/news/releases/2005/pr38/en/

Zak, A. (2014) "Russia in Space – The Past Explained, The Future Explored", 1st Edition, Apogee Prime, 2014.

Zeitlin, C., Hassler, D.M., Cucinotta, F.A. et al. (2013) "Measurements of Energetic Particle Radiation in Transit to Mars on the Mars Science Laboratory", Vol. 340, Issue 6136, *Science*, 31 May 2013, pp. 1080–1084.

Zuppero, A.C. (2009) "To Inhabit The Solar System – Using the Water in Space", 2009, p. 318, 284.

Zuppero, A.C. and Jacox, M.G. (1992) "Near Earth Object Fuels (Neo-Fuels): Discovery, Prospecting and Use", Paper IAA-p2-0159, presented at the *43rd Congress of the International Astronautical Federation (IAF)*, Washington, DC, 28 August–05 September 1992.

Zuppero, A.C., Schnitzler, B.G. and Larson, T.K. (1997) "Nuclear Heated Steam Rocket Using Lunar Ice", paper AIAA 97-3172, presented at the *33rd AIAA/ASME/SAE/ASEE Joint Propulsion Conference*, Seattle, WA, 6–9 July 1997.

Stellar and Interstellar Precursor Missions

8

8.1 Introduction

Staggering as they may seem to us, interplanetary distances are puny compared to those to reach stars. Our Solar System is located about two-thirds of the way from the center of our Milky Way Galaxy to the rim, about 25,000 light-years from the galactic center on the inner edge of the Orion arm, see Fig. 8.1. Our Galaxy has a diameter of approximately 100,000 light-years and is roughly shaped as a luminous disk 12,000 light-years thick near its hub, decreasing to about 1,000 light-years near its "arms." The presence of a black hole of mass corresponding to 2 to 3 million Sun masses, and long believed to be at its center (Cohen et al. 2003), seems confirmed by recent radiowave measurements using very long baseline interferometry (Reynolds 2008; Hartnett et al. 2009).

Astrophysicists mapping the 21-cm hydrogen radiation line had previously thought that our Galaxy was a spiral galaxy with five major arms or spokes (Centaurus, Sagittarius, Orion, Perseus, and Cygnus). In fact, recent data from the NASA Spitzer Telescope seems to indicate that our Galaxy has only two major arms, Perseus and Centaur. The density of stars in the other three regions was found lower than estimated in the past, and definitely lower than in the two major arms.

Using as yardstick the distance of our Earth to the Sun, the astronomical unit AU = $1.496 \cdot 10^8$ km, one light-year ($9.46 \cdot 10^{12}$ km) is approximately equal to 63,200 AU. Our Galaxy comprises some 250 million stars. Their density decreases from the Galactic center toward the arms end, where average interstellar distances are of the order of many light-years, see Chap. 1. The spiral structure of the Galaxy is such that the average distance between stars, were it a true homogeneous disk, would be about 50 light-years. In fact, stars are not uniformly distributed. Their density increases going toward the galactic center and inside its major arms. This explains why the Sun's nearest neighbor is only a few light-years away, see Table 8.1.

In this table, the basic unit of distance is no longer the size of our Solar System, or the AU, but rather 1 light-year. For comparison, Proxima Centauri, the star closest to our Sun, is 4.2 light-years away, or 4000 times the diameter of our solar system measured at Pluto's orbit. If we had means to reach Pluto in a few months, reaching Proxima Centauri at the same speed would take of the order of a millennium.

Given these immense distances, one might wonder why we should desire to cross them. At its heart, this is a philosophical question that has accompanied all old and new human endeavors, e.g., see (Mazlish 1985; Ashworth 2014). Most scientists would agree that the answer is the hope of finding life, and maybe intelligent life. Whether this is a well-founded hope is still being debated (e.g., Morrison et al. 1977; Crawford 2000; Davies 2010; Wheeler 2014). The closest star to our Sun, Proxima Centauri, a star of spectral type M5e, is very different from our Sun (its type is G2V). The symbols identifying the star type were devised to classify the star's electromagnetic spectrum, which may give an idea of what sort of light one would see on a hypothetical planet orbiting a star. For instance, the Sun "surface," or disk, we see emits light as a black body radiating at 5800 K, the yellow-green peak of its spectrum imparting that warm quality humans associate to its light. An M-type star such as Proxima Centauri would have a cooler surface temperature, about 3600 K, its hue shifted toward the red-yellow, and having probably a fascinatingly unknown effect on life-forms (Kiang 2008). In fact, a planet roughly 30% larger than Earth and at "goldilocks" distance from Proxima B was discovered orbiting this star in August 2016. In this context, another fundamental question is whether life as we see it on Earth is the only possible type of life (Asimov 1979). Common agreement is that organic life must be based on water and if we believe it, this may set limits to temperature excursions. However, ultimate constraints (the so-called goldilocks environmental conditions) are still vague (Baross et al. 2007). This question may be extended to the search of life in the most general sense, e.g., "growing and adapting" according to Jacques Loeb's definition (Loeb 1918), and much hay has been made in this context by science fiction writers.

P.A. Czysz et al., *Future Spacecraft Propulsion Systems and Integration*,
Springer Praxis Books, DOI 10.1007/978-3-662-54744-1_8

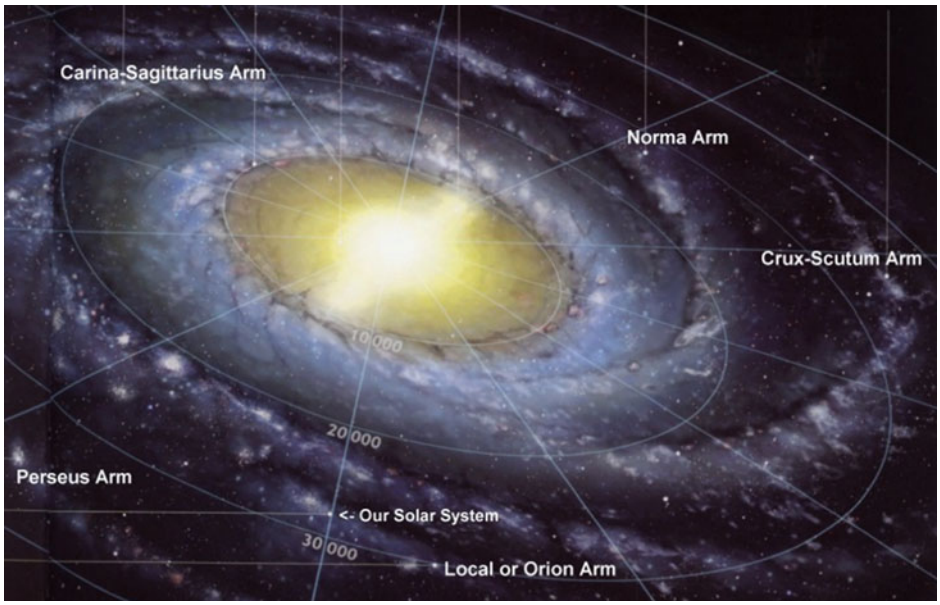

Fig. 8.1 Artist's view from astronomical measurements of our Galaxy and its arms (*Courtesy* Astronomy Trek)

Table 8.1 Stars nearest to the Sun

Name	Distance (ly)	Spectral type (−)	Radial velocity (km/s)	Apparent magnitude (−)	Luminosity (Sun = 1.00) (%)
Sun		G2V		−26.7	1.0
Proxima Centauri	4.2	M5E	−16	11.05	0.00006
a-Centauri A	4.3	G2V	−22	−0.01	1.6
a-Centauri B		K0V		1.33	0.45
Barnard Star	5.9	M5V	−108	9.54	0.00045
Wolf 359	7.6	M8E	+113	13.53	0.00002
BD + 36°2147	8.1	M2V	+84	7.50	0.0055
Luyten 726-8A	8.4	M6e	+29	12.52	0.00006
Luyten 726-8B		M6e	+32	13.02	0.00004
(UV Ceti)					
Sirius A	8.6	A1V	−8	−1.46	23.5
Sirius B		A1V		8.3	0.003

Note for historical reasons, between one magnitude and the next the light ratio is 2.512. The more negative the magnitude, the larger the apparent star diameter

However, if there are no planets to orbit around or to land on, it is hard to conceive the motivation of such immensely long and expensive journeys. The volume of space grows with the cube of the distance from our Sun; the farther we travel, the more rapidly the rate at which unknown "things" may exist. This is completely unlike the era of sea voyages on Earth, where traveling in the same direction eventually brought one back to the port of departure. By crisscrossing sea and land, explorers discovered and mapped Earth's surface. In contrast, similar linear trajectories in space would map and reveal less and less as the distance traveled increased. In essence, humankind will be limited to explore single points inside a gigantic sphere.

Human beings have always been driven to explore far-away places by the hope of finding new life-forms and scenery, not just light. The star to reach and the distance to cross will in the end be chosen on the basis of information about the existence of planets, rather than solely by scientific curiosity about stars (Lissauer 1999). In fact, the number of exoplanets discovered by the orbiting Kepler telescope is steadily growing. Their size varies from twice to twenty times that of Earth, although the vast majority belongs to gas giants similar to Jupiter or Saturn (Schneider 2005; Encrenaz et al. 2004; Mecham 2011). According to the Extrasolar Planets Encyclopedia (Schneider 2005), as to this writing this number is at 3610 (as of 01 June 2017) and is bound to

grow rapidly after 2017 when NASA will orbit Kepler telescope's successor, the Transiting Exoplanet Survey Satellite or TESS (Anon. 2014). Kepler can image planets orbiting stars at up to 2000 light-years from the Sun, at distances even greater than those in Table 8.1.

The thought of finding not just life, but also intelligent life might be a powerful motivation if people were actually convinced of the likelihood of its existence. This fascinating topic is the subject of much discussion (Crawford 2000; Webb 2002). Although galactic distances should give pause to the discussion of propulsion systems for stellar missions, this has not discouraged even earlier proposals, e.g., Shepherd (1952) and Dyson (1968).

Limiting this discussion to scientific goals, however, there are objects and regions of space much farther than our known planetary system, and they are much closer than stars and at the same time of great interest. Perhaps with some exaggeration, these are exploration targets that have been named quasi-interstellar (QI) destinations. Among them, and in order of their known distance from Earth, are the Kuiper Belt, the Heliopause, the gravitational Sun lens region, and the Oort Cloud. Quasi-interstellar precursor missions to these regions are very attractive; the reasons are given briefly below.

8.1.1 Quasi-Interstellar Destinations

Loosely speaking, the Kuiper Belt is the region of space beyond the orbit of Neptune or Pluto and conventionally extending up to 100 AU from our Sun. Until the 1950s, astronomers thought Pluto was more or less the farthest and last "planet." With the exception of comets, perhaps only one or two other objects might be lying beyond its orbit. In 1951, the Dutch astronomer Gerard Kuiper started wondering about the place of birth of *short-period* comets, since each of their passes near the Sun subtracts 0.01% of their mass. As a consequence, their lifetime should be short, some 10,000 passes, or only half a million years (Luu and Jewitt 1996). Since the Solar System is more than 4.5 billion years old, no comet should have survived ever since.

After discovering "planetoids," bodies orbiting the Sun larger than Pluto's moon Charon and with extremely long orbital periods, we know now that the space beyond Neptune and Pluto is in fact quite populated. The number density of objects there is much too low to form larger bodies by mutual gravitational attraction. However, attraction by the large planets (Jupiter, Saturn, and especially Neptune) can draw and pull these objects toward the Sun along highly elliptic orbits. If, as it seems, this is a realistic picture, the Kuiper Belt is a reasonably close region of space where we could find objects (KBO—Kuiper Belt Objects, or TNO—Trans Neptunian Objects) dating back to the formation of the Solar System, including most short-period comets (Hahn 2005).

In fact, during its Saturn flyby, the Cassini spacecraft took close pictures of one of the Saturn satellites, Phoebe. Phoebe has a retrograde orbit and an average diameter of 220 km. The pictures were fairly good, and indicated the presence of water (Porco 2004). The inference is that Phoebe did not come from the rocky "dry" asteroid belt between Mars and Jupiter, but rather from the Kuiper Belt, the birthplace of most short-period and water-rich comets. This fact, and the peculiar retrograde orbit, hints that Phoebe is likely a KBO captured by Saturn. Similarly rich in water is the KBO Quaoar (Jewitt and Luu 2004). In contrast, the most recent evidence of water on closer objects is that on Ganymede in 2015. Water is a synonimous of life.

Some of the planetoids observed have fascinating features. Table 8.2 compares Pluto to Sedna and one of the largest objects recently discovered, DW2004. Sedna shuttles back and forth from beyond the Kuiper Belt (in fact, near the edge of the Oort Cloud) to the Sun. Its extremely eccentric orbit might be explained by an encounter with a star (Kenyon and Bromley 2004). A reasonable conjecture is that Sedna must carry on its surface traces of its immense journeys, making it a very desirable scientific target. Some comets may travel even farther, but are not as large, which poses the question of how Sedna and other planetoids were formed. Another interesting body is 2003 UB313, a KBO bigger than Pluto (Brown et al. 2005; Anon 2006a, b). Its orbit is inside that of Pluto and is tilted 45° with respect to the ecliptic.

The tentative budget of the "New Frontiers" NASA program (Weaver and Stern 2008) did include a "New Horizons 2" (NH 2) mission to explore nearby KBO (Spencer et al. 2003). One of the candidate objects was 1999 TC36, a twin system, each body about 400 km across. 1999 TC36 is similar to the Pluto-Charon system, albeit smaller. This NH 2 mission was to start in 2008, utilize gravity assists from Jupiter and Uranus, and reach TC36 in 2014, and was considered a "very fast" mission. (NASA

Table 8.2 Comparing orbits of Pluto and of some KBO (Kuiper Belt Object)

	Diameter (km)	Distance from the Sun (10^9 km)	Orbital period (year)
Pluto	2300	4.4–7.4	248
Sedna	1280–1760	11–113	10,500
DW2004	1610	4.6–7.1	250

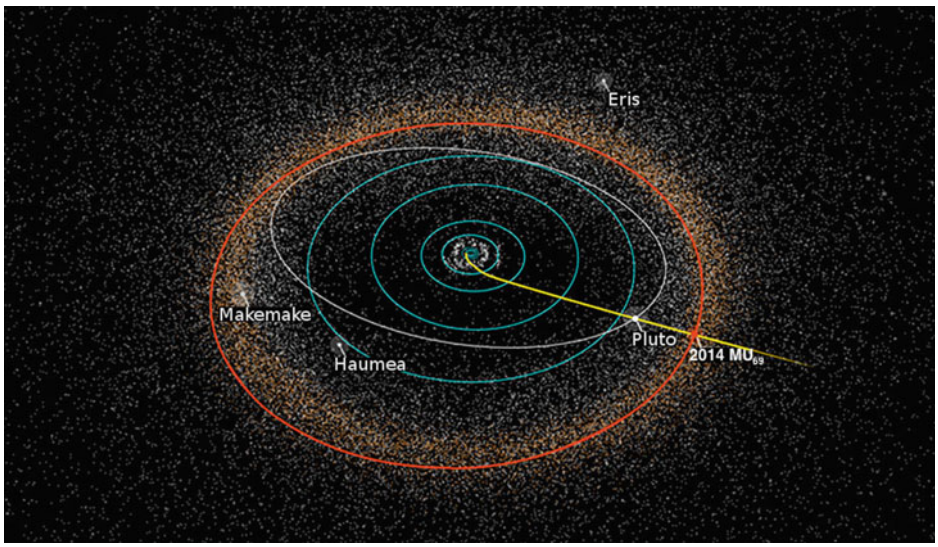

Fig. 8.2 Trajectory of the Pluto New Horizons spacecraft and that of the Kuiper Belt Object PT1/MU69 (*Courtesy* NASA)

eventually scrubbed this mission.) Meanwhile, the first New Horizons mission to Pluto (Anon. 2015a, b) launched on January 16, 2006, crossed Saturn's orbit and, at a leisurely 18.2 km/s, that of Uranus in 2011, reaching the closest distance to Pluto on July 15, 2015, nearly ten years after launch. Such is the pace of missions powered by chemical propulsion. After passing Pluto, NASA planners modified the trajectory of the spacecraft so as to enable a flyby of the KBO named 2014 PT1/MU69 in January 2019, see Fig. 8.2. Makemake, Haumea, and Eris are other KBO recently discovered.

The interest in KBO is not only due to their status as "remnants" of planetary formation, but also due to their odd orbits. These might be explained by the existence of a planet bigger than Pluto and much farther away. This so-called plutoid has been postulated by astronomers P. Likawka and T. Mukai (Than 2008; Hand 2016). Beside being a new and exciting research area, KBO study is stimulating novel ideas related to the origin and formation of our Solar System.

A second quasi-interstellar (QI) target is the Heliopause, the region of space directly influenced by the Sun and extending much farther than the Kuiper Belt. The solar wind is a flow of plasma (mostly protons) emitted isotropically by the Sun at speeds between 300 and 700 km/s. These are supersonic speeds with respect to plasma acoustic speed. In the *interstellar* plasma, crossed by the Sun with all its planets, the supersonic plasma flow creates a shock that has been detected by its radio emission (Gurnett et al. 1993). This immense shock separates the Solar System from interstellar space and bounds the bubble-like region called heliosphere, of size 100–150 AU. In fact, the actual size of the heliosphere depends on the Sun cycle, the magnetic field of interstellar space, and the presence of neutral particles (Encrenaz et al. 2004, Sect. 5.1.5). The entire Solar System moves inside our Galaxy inside the heliosphere bubble and has no contact with true interstellar space. From Earth, as well as from all other planets, we are looking at "space" like fish from inside a glass bowl. There is keen interest among scientists in investigating the properties of "true" space, i.e., space outside the heliosphere, far from the influence of our Sun.

As the density of solar wind plasma decreases with the cube of distance from the Sun, so does the strength of the shock separating the heliosphere from the true space environment. Thus the solar wind eventually becomes subsonic, slowing down abruptly. The region where this occurs is called the heliosheath. The heliosheath is of great scientific interest as well, because this is where the solar wind starts interacting with the true interstellar plasma and where it gets hotter. A sign of this interaction is the increasing magnetic field recorded by the Voyager 1 probe after reaching the heliosheath a few years ago (Hamilton 2004; Britt 2005).

Still farther away from the Sun, even the heliosheath ends at the so-called Heliopause, beyond which lies true "pristine" interstellar space. The Heliopause is a peculiar environment, characterized by hydrogen plasma (protons and electrons) with density of the order of 1 particle per cubic centimeter and immersed in a weak magnetic field. The Voyager 2 probe (Anon. 2013), launched by NASA in 1977, has crossed the heliosheath (Jokipii 2008) and should reach the Heliopause around 2018. By then it will have taken more than *30 years* for a man-made object to reach interstellar space. There is indeed no way to simulate in a laboratory the conditions near the Heliopause or in true space.

A third QI deep-space target of great interest to astrophysics is associated with the relativistic effects of massive bodies on starlight propagation. This is called gravitational "lensing" (Wambsganss 2001). The General Theory of Relativity predicts that a gravitational field bends light. Our Sun does that with the light of every star grazing its apparent

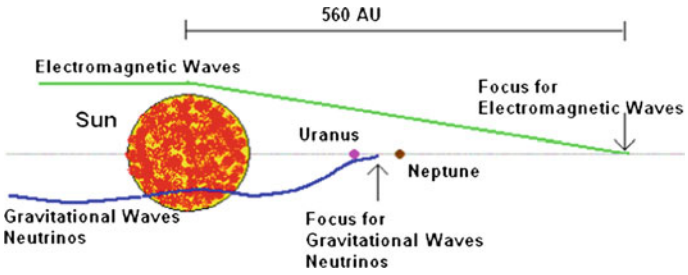

Fig. 8.3 Sun gravitation acts as a lens and bends light (*Courtesy* C. Maccone)

disk. Simple theory predicts that rays of parallel light from such stars are deflected by an angle ε (deflection of the electromagnetic wave) given by

$$\varepsilon = 4 \cdot \frac{G \cdot M_{\text{Sun}}}{r \cdot c^2} \tag{8.1}$$

where G is the universal gravitational constant, M_{Sun} is the mass of the Sun, c is the speed of light, and r is the distance of the parallel rays from the Sun center. The nearer the light rays to the solar disk, the sharper the bending angle ε, see Fig. 8.3. The Sun acts as a lens not just for visible starlight, but for all electromagnetic waves.

Viewed from Earth, the rays focus at a point that depends on r and "behind our back" when looking straight at the Sun. The minimum r is of course the Sun radius. When r is equal to the Sun radius, starlight rays focus at the point closest to Earth. This minimum focus is located at a distance about 542 AU (the exact focus distance depends on the light wavelength).

Calculations show that the angular and spatial resolution made possible by observing objects through this powerful "lens" are impressive. The resolution is a function not only of the gain due to the lensing effect of the Sun, but also of the gain of the spacecraft antenna, proportional to its dish radius, r_{antenna}. The total gain is the product of the two (Maccone 2009):

$$\text{Total Gain} = 16 \cdot \pi \cdot G \cdot M_{\text{Sun}} \cdot (r_{\text{antenna}})^2 \cdot \frac{v^3}{c^5} \tag{8.2}$$

The dependence on the cube of light frequency, v, tells that, by choosing it well, angular resolution may become from two to four orders of magnitude better than the most accurate optical instrument ever used, for instance, that of the star-mapping Hipparcos satellite launched in 1989. Theoretically, the resolution with a modest 12-m antenna dish positioned at the Sun lens focus could tell details of objects in the Oort Cloud 145 km apart at the frequency of neutral H_2 (1420 MHz), and 9 km apart at the higher emission frequency of water, 22 GHz. The Alpha Centauri star could be resolved at 1250 and 80 km at the same two frequencies. Note that we are talking of telling features 80 km apart on a star some 4.3 light-years from Earth.

This nearly unbelievable performance has motivated conceptual planning of missions to the nearest Sun gravitational focus, that is, at ≈542 AU from the Sun. Such is the FOCAL mission proposed in (Maccone 2009). In fact, if looking for habitable planets is a long-term objective of human exploration, this mission would be mandatory as there are no other means to determine which of the many extrasolar planets being steadily discovered would be a suitable candidate. In this sense, a FOCAL-type mission is the prerequisite to plan stellar missions.

Much farther, by about half a light-year, is the so-called Oort Cloud. Long ago astronomers started to suspect that *long-period* comets with extremely eccentric orbits spent most of their time at a distance from the Sun between 10^4 and 10^5 AU. The Oort Cloud is the farthest known region of the Solar System (Weissman 1998). Its distance from the Sun is between 1000 and 60,000 AU, but some astronomers push these boundaries farther, between 20,000 and 200,000 AU. It is named after the Dutch astronomer J. Oort, who conjectured that this region of space must contain millions, or even billions of comets (the current estimate is in fact 10^{11}). Present understanding of the Oort Cloud is that it consists of stably orbiting matter that did not participate in the formation of the Solar System, because the mutual distance between objects was, and is, too large for gravitational interaction to take place. Similarly to the Kuiper Belt, the Oort Cloud is interesting because it may contain intact relics of the formation of our planetary system. Gravitational interaction with stars during their infrequent approach to the Sun (events occurring every million years or so (Cesarone et al. 1984)) may draw Oort Cloud bodies toward the Sun in very elliptic orbits. Some become comets (Encrenaz et al. 2004, Sect. 11.2), and others may be too "dry" and do not form plumes at all (e.g., Sedna, with a 75 AU aphelion).

According to the late Carl Sagan, comets are "dirty snowballs," their dirt being probably the original material that the planetesimals were made of. Besides minerals, composition includes, surprisingly, water ice and many organic compounds. The Rosetta mission to comet 67P/Churyumov-Gerasimenko, see Fig. 8.4, the first to a comet, has begun to shed some light on cometary composition (Hand 2014, 2015; Quirico et al. 2015). Many organic

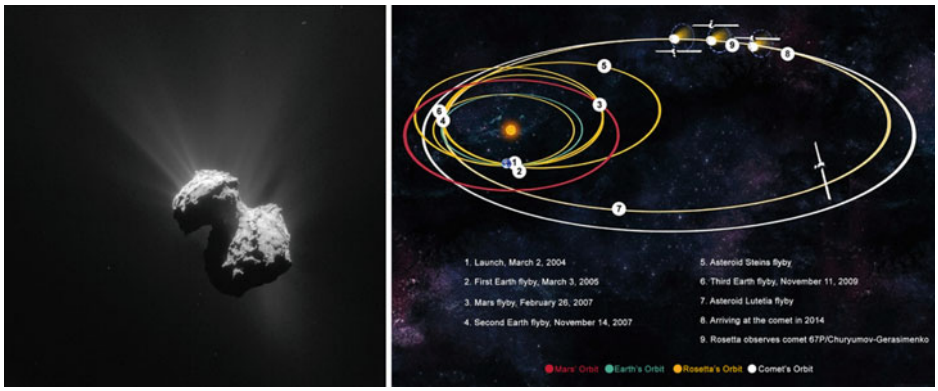

Fig. 8.4 View of comet 67/P on the *left* taken by the Rosetta probe on July 07, 2015 (*Courtesy* ESA). The schematic on the *right* shows Rosetta's trajectory to reach comet 67P (follow the *yellow* trajectory) (Anthony 2014)

compounds were detected (Capaccioni et al. 2015). Mineral composition may help to understand the mechanism of planetesimal accretion, since the distribution of elements in the Solar System is known (Sciama 1971). Gravity and other data from Rosetta's Philae lander, for instance, indicate the 67/P density is only 470 kg/m^3, porosity 80–90%, and its structure crumbly. The type and abundance of elements depend on the supernova explosion that created in our Galactic region what astrophysicists call "heavy matter" or "metals" (i.e., any element heavier than helium). In the Kuiper Belt, matter underwent frequent collisions and mixing, unlike what has happened in the Oort Cloud, where the much lower number density of objects should ensure finding matter in its original state.

Not all Oort Cloud matter is cometary. Sedna is a case in point, but others have been observed, e.g., 2006 SQ372, an Oort Cloud object in an elliptic orbit with semiaxes about 1000 and 24 AU, and a period estimated at 22,500 years (Hecht 2008). These are QI messengers shuttling back and forth from the outer reaches of the Solar System to the vicinity of the Sun. They are of great interest not only as objects of investigation, but also as potential instrumented platforms. Traveling beyond the Heliopause they could collect and send data (Dinerman 2008), albeit over timescales of months. A similar concept has been proposed by Dr. Masahiro Ono at NSA-JPL for comets. The "Comet Hitchhiker" spacecraft would harpoon a comet and rely on extremely high tensile strength cable to zero the ΔV and allow the spacecraft to land (Ono et al. 2015). Whether or not this is feasible, boarding these objects and installing instrumentation when they move close to the Sun would require engineering and propulsion systems with unprecedent performance and autonomy. In the case of many comets, lack of structural strength would add to the complexity of such missions.

The QI scientific missions just mentioned are still far from involving stellar distances. FOCAL would travel about 5% of a light-year; the Oort Cloud extends at most to 0.5 light-years from Earth. Nevertheless, these are extremely far targets compared to what has been achieved so far. As of August 2016, Voyager 1 and 2, the probes farthest from Earth, are at about 136 AU from us, and Pioneer 10 at 114 AU. In order to reach QI destinations in times compatible with the lifetimes of crew and ground teams, new propulsion means need to be developed (Bruno et al. 2013).

8.1.2 Time and Distance

At constant speed, crossing times to nearby stars, or even to the Oort Cloud, takes too long. In the hypothetical mission to Neptune at 1 g acceleration, used as an example in Chap. 7, the flyby speed reached at Neptune was 6700 km/s. Assuming the engine turned off there, coasting from Neptune to Proxima Centauri would take another 188 years. Such an engine would have to produce sufficient thrust to sustain 1 g acceleration for 7.75 days. Tsiolkovsky's equation for an advanced nuclear thermal rocket (I_{sp} = 1000 s) predicts the mass ratio $M_{ppl}/M_{initial}$

$$M_{ppl} = \exp\left(\frac{\Delta V}{g \cdot I_{sp}}\right) = \exp(683.2) = 5.131 \cdot 10^{296} \quad (8.3)$$

a truly astronomical number. Unless the I_{sp} of the propulsion system can be drastically raised, the initial mass of the ship would be unrealistically large and completely dominated by propellant mass, so that the thrust requirement to maintain 1 g acceleration would be unfeasible large. Stellar or quasi-interstellar missions using Newton's Third Law are doubly constrained. At constant speed, they take too long, and at constant acceleration, thrust consumes too much mass.

In principle, bypassing the second constraint is possible by collecting in flight interplanetary/interstellar mass to utilize for propulsion, just as the airbreathing engines in Chap. 4 collect air. Interstellar space is not a mathematical void. In the disk of our Galaxy, the average mass density of interstellar hydrogen, ρ_H, is of order 10^{-27} kg/m^3 (Sciama 1971, p. 25). Since a hydrogen atom weighs about $1.67 \cdot 10^{-27}$ kg, this density corresponds to about one

Table 8.3 Chemical, fission, and fusion energy release and their relativistic mass conversion fractions, adapted from (Kammash 1995)

Fuels (fuel ratios) (−)	Products	Energy density, $E/m = \alpha c^2$ (J/kg)	Converted mass fraction $\alpha = \Delta m/m$ (−)
Chemical			
Conventional: LO_2/LH_2	Water, hydrogen	$1.35 \cdot 10^7$	$1.5 \cdot 10^{-10}$
Nuclear fission			
^{233}U, ^{235}U, ^{239}Pu	Fission fragments,	$8.2 \cdot 10^{13}$	$9.1 \cdot 10^{-4}$
(~200 MeV/^{235}U fission)	Neutrons, γ-rays		
Nuclear fusion			
D–T (0.4/0.6)	Helium, neutrons	$3.38 \cdot 10^{14}$	$3.75 \cdot 10^{-3}$
Catalized D–D (1.0)	Hydrogen, helium,	$3.45 \cdot 10^{14}$	$3.84 \cdot 10^{-3}$
	Neutrons		
D–^{3}He (0.4/0.6)	Hydrogen, helium	$3.52 \cdot 10^{14}$	$3.9 \cdot 10^{-3}$
p–^{11}B (0.1/0.9)	Helium	$7.32 \cdot 10^{13}$	$8.1 \cdot 10^{-4}$
Matter plus antimatter			
p–p^- (0.5/0.5)	Pions, muons,	$9 \cdot 10^{16}$	1.0
	Electrons, positrons,		
	Neutrons, and γ-rays		

hydrogen atom per cubic meter. In the Galactic mid-plane, H_2 particle density is ≈200 cm^{-3} (Reynolds 2002). Atoms can be captured at "sufficient speed" by an appropriately designed scoop or inlet. This is the "interstellar ramjet" concept (Bussard 1960; Cassenti and Coreano 2004). The hydrogen collected could be fused to generate power and thrust. The power, P, is a function of speed, V, and inlet area, A. The mass flow of H atoms collected while flying is

$$\dot{m} = \rho_H \cdot A \cdot V \tag{8.4}$$

and the power generated by fusing them is

$$P = \dot{m} \cdot \alpha \cdot c^2 \tag{8.5a}$$

$$P = \rho_H \cdot A \cdot V \cdot \alpha \cdot c^2 \tag{8.5b}$$

where α is the mass fraction of captured H atoms actually fused, of order (3–4) · 10^{-3} (see Table 8.3). Hence, the minimum inlet area to ensure a given P is

$$A = \frac{P}{\rho_H \cdot A \cdot \alpha \cdot c^2} \tag{8.6}$$

When entering numbers in Eq. (8.6), and even assuming V of the order of the speed of light c, the scooping area to collect 1 GW is of order of 10^{12} m^2, a square $10^3 \cdot 10^3$ km. In fact, our Sun is in a region of our Galaxy where ρ_H may be even lower than assumed in this estimate, about 0.04 atoms/cm^3 (Cassenti and Coreano 2004).

Besides, scoop drag may easily be larger than thrust. If relativity holds, interstellar ramjets are unfeasible for the foreseeable future. In any event, the interstellar ramjet still depends on a "booster" capable of accelerating the ramjet to that "sufficient speed" V and thus requires onboard propellant.

8.2 Propulsion for Quasi-Interstellar and Stellar Missions

In the following, the focus is on human missions where time and payload are of essence. Intriguing propulsion means, such as solar and magnetic sails and other technologies that, promising as they may be, are either still unsuited to carry substantial payload or do not produce enough thrust, are presented in (Bruno and Accettura 2008; Bruno et al. 2013). Laser-driven propulsion has been discussed in Chap. 4 and will be mentioned again later.

Distances and times discussed in Chaps. 1 and 7 are much magnified when applied to QI missions. The key propulsion issues are still the same: I_{sp} (determining the total mass of propellant), thrust (determining mission time), and therefore power (to sustain thrust). A difference is the extreme influence these three factors have on QI and interstellar precursor missions. Momentum change and thrust may be realized by thermodynamic expansion or by direct application of a force. In chemical and thermal fission or fusion rockets, exhaust gas is accelerated by thermodynamic expansion of matter.

At the microscopic scale, *thermal thrust* is the result of a three-stage energy conversion process. (1) In stage one,

energy is simply stored as potential energy $m \cdot c^2$ associated to rest mass. (2) When some fraction $\alpha < 1$ is released in the second stage, this potential energy becomes the microscopic kinetic energy of particles. Particles may be molecules of products and unburnt propellants, neutrons, alpha and beta particles, and photons of energy $h \cdot \nu$. (3) In stage three, collisions and the confinement effect of a thermodynamic or magnetic nozzle convert microscopic kinetic energy into bulk kinetic power $1/2\ (\mathrm{d}m/\mathrm{d}t) \cdot V_e^2$ of a material jet exhausting at velocity V_e. It is this third and last stage that is responsible for momentum change (thrust) in any thermal rocket. In the thermal rocket, the bulk V_e cannot exceed that of the microscopic particles since energy is conserved.

Thrust by direct application of force to the matter to be accelerated is realized in electric rockets or thrusters (ET), see the discussion in Chap. 7. External electric or electromagnetic fields are applied to charged particles (ions or colloids), and Coulomb or Lorentz forces accelerate those particles. Electric thrusters convert potential energy to bulk kinetic energy in a single stage. Thus, I_{sp} is not limited by thermodynamics, but only by the intensity of the electromagnetic fields that can be applied, and ultimately by the power generator supplying current and voltage.

At this point, it is useful to review the scaling of thrust, F, and I_{sp} already defined. Thrust, F, is assumed still based on Newton's Third Law, the result of change in bulk momentum of propellants. The concept of propellant is now broadened to include whatever mass is accelerated by the propulsion system. Neglecting the momentum possessed by the propellant prior to its acceleration, the thrust $F = (\mathrm{d}m/\mathrm{d}t) \cdot V_e$, where V_e is the velocity of the mass ejected from the rocket, and $(\mathrm{d}m/\mathrm{d}t)$ is the mass flowrate. *If gas is what is ejected*, there is a contribution to thrust due to the difference between exhaust pressure and external pressure (zero in vacuo), but for scaling purpose this is typically small and will be neglected. Then, by definition

$$I_{sp} = V_e \tag{8.7}$$

The specific impulse is ideally the mass ejection velocity and has dimensions of velocity. The customary units of seconds for I_{sp} go back to the time engineers used weight instead of mass to define mass flowrates.

In a steady *gaseous* exhaust, the mass flowrate $\mathrm{d}m/\mathrm{d}t$ is proportional to the ejection velocity:

$$\frac{\mathrm{d}m}{\mathrm{d}t} = p_e \cdot A_e \cdot V_e \tag{8.8}$$

with ρ the density and A the area of the exhaust section, so that

$$F = p_e \cdot A_e \cdot (V_e)^2 \tag{8.9}$$

The power P to sustain thrust is the kinetic power of the mass ejected

$$P = \frac{1}{2} \cdot \left(\frac{\mathrm{d}m}{\mathrm{d}t}\right) \cdot (V_e)^2 \tag{8.10a}$$

$$P = \frac{1}{2} \cdot F \cdot V_e \tag{8.10b}$$

$$P = \frac{1}{2} \cdot F \cdot I_{sp} \tag{8.10c}$$

Thus propulsion scales as follows when thrust is due to gas thermodynamic expansion:

$V_e \sim I_{sp}$	determines mass consumption
$F \sim (I_{sp})^2$	determines acceleration and mission time
$P \sim (I_{sp})^3$	determines size of engine

In propulsion systems where momentum change is not due to gas expansion but by direct application of a Lorentz or Coulomb force (electric thrusters, ET), the flowrate is not coupled to $\mathrm{d}m/\mathrm{d}t$, but may be subject to other constraints. Thus for ET propulsion scales as follows:

$$V_e \sim I_{sp}$$
$$F \sim (\mathrm{d}m/\mathrm{d}t) V_e$$
$$P \sim 1/2(\mathrm{d}m/\mathrm{d}t)(V_e)^2 = 1/2\, F\, V_e = 1/2\, F\, I_{sp}$$

Independent of the acceleration mechanism, whether thermal or direct, at constant power there is an inverse relationship between F and I_{sp}. The product of the two is a hyperbola in the F and I_{sp} plane, and increasing I_{sp} to reduce propellant consumption must be paid in terms of lower thrust and longer mission time. Thus, the choice of F and I_{sp} is a balance, or trade-off, depending on the specific mission.

In addition, *electric* thrusters suffer from a major constraint: the maximum density of ionized propellant. Ions (+) and electrons e^- tend to recombine to form neutral atoms or molecules with a rate proportional to the cube of concentration (or pressure). Since neutral atoms cannot be accelerated, the density of the ionized propellant must be low, and so are $(\mathrm{d}m/\mathrm{d}t)$ and thrust. While ion thrusters may reach a specific impulse ranging from 10^5 to 10^6 s, their thrust is of order 0.01–0.1 mN/kW, or in terms of thrust density, a few N/m^2 (Fearn 2008). MPD thrusters may have a thrust density a factor of 100 higher, but the ratio F/P is not much different. In practice, a high-I_{sp} electric thruster comparable to that of a small chemical rocket would mean very large and impractical clusters of many tens or even hundreds of individual ET modules.

Whatever the thrust mode, and neglecting relativistic effects, energy conservation between stage one (1) and three

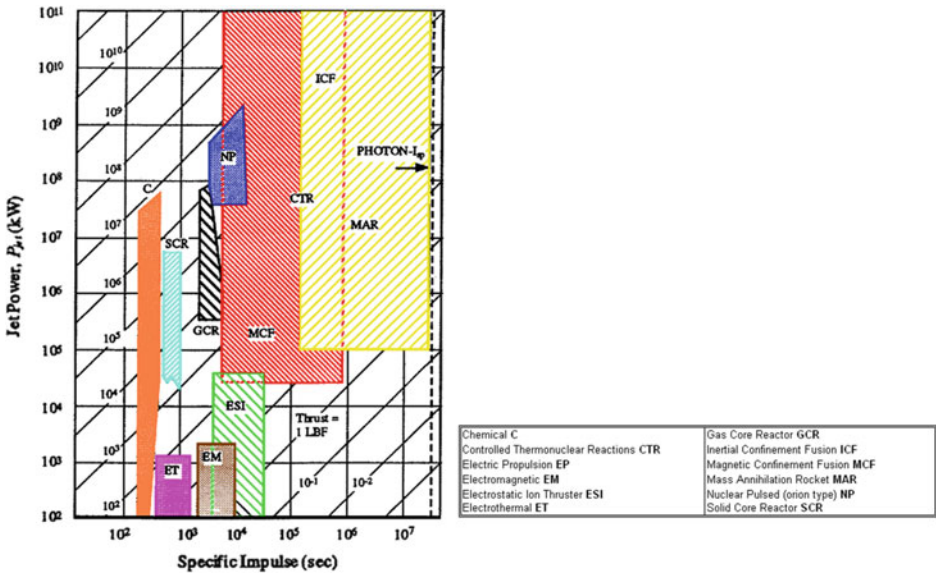

Fig. 8.5 Jet power, thrust, and I_{sp} of space propulsion systems, adapted from (Kammash 1995)

(3) states that potential energy per unit mass, J, must be equal to 1/2 $(V_e)^2$, the kinetic energy acquired by that unit mass during conversion. Here J is the microscopic kinetic energy per unit mass of the medium where potential energy has been released. In nuclear fission propulsion, the medium is an inert gas (hydrogen, for instance), but could be also the very fission fragments mentioned in Chap. 7, as they possess kinetic energy of order 167 MeV when the fuel is ^{238}U (Hill and Peterson 1970, p. 475). Similarly, in hydrogen fusion, the medium could be the fusion products themselves, that is, He nuclei possessing energy in the 4–40 MeV range (see Table 8.3). Because He nuclei are much lighter than average *fission* fragments, their energy density, , is larger. Thus, the more general definition of the ideal specific impulse is$J$

$$V_e = I_{sp} = (J)^{1/2} \tag{8.11}$$

Table 8.3 and Fig. 8.5 show the gain in performance when transitioning from chemical ($J \approx 10^7$ J/kg) to fusion ($J \approx 10^{14}$ J/kg) propulsion.

Fusion has a higher conversion $\alpha \approx (3\text{–}4) \cdot 10^{-3}$ (depending on fuels) compared to fission, where $\alpha \approx 9.1\ 10^{-4}$ using ^{235}U fuel. Therefore, the energy density in fusion is higher by a factor 4 to 5, see Table 8.3. Similarly to what was noted in Chap. 7 for fission rockets, if the kinetic energy of He nuclei released by fusion is not utilized directly for propulsion in the form of momentum, but is thermalized in an inert propellant, I_{sp} may be limited by the melting point of materials and will be no different from that of a nuclear thermal rocket. The gas core and Rubbia's concept in Chap. 7 circumvent somewhat the limitation imposed by the material melting point, so their I_{sp} is higher by a factor 2–3 compared to the I_{sp} of NERVA-type rockets. The same strategy might be possible also in fusion rockets, and the I_{sp} gain with respect to similar fission rockets would also be a factor 2–3. Much higher I_{sp} is available with fusion-powered *electric* thrusters, at the price of much lower thrust, lower thermal to electric conversion efficiency, and higher weight.

In *thermal* fusion propulsion, I_{sp} may be made very high if He nuclei are themselves the propellant and are ejected at the speed of their microscopic kinetic energy. In this case, there is indeed a significant difference between fission and fusion thermal rockets. Fission fragments from ^{235}U fall into two families centered around 40 and 160 atomic mass units, so they are "heavy." If the fusion fragments consist mainly of ^{4}He, their mass is a factor 10–40 times lighter. Everything else being equal, the I_{sp} potentially available will be higher than fission by the square root of the same factor, times the square root of the energy conversion α, because the specific energy of hydrogen fusion is about five times higher than fission. The *ideal* I_{sp} calculated for different fusion rocket concepts is given in Fig. 8.5 (Kammash 1995). This figure shows that the I_{sp} of a magnetic confinement fusion (MCF) rocket may be 10^2–10^3 times higher than in fission concepts. Similar data is in (Lawrence 2008). Even higher I_{sp} is predicted for a mass annihilation rocket (MAR), the extreme form of fusion where *all* mass is converted into energy ($\alpha = 1$) (Morgan 1982; Forward 1985). The last vertical line on the right of Fig. 8.5 is the theoretical I_{sp} of the Sänger/Rubbia photonic rocket concept of Chap. 7. Its I_{sp} is exactly equal to c, *if* fuel mass is not accounted for in the mass consumption rate.

If the energy of fused particles at stage two is *thermalized* in a larger flow of an inert propellant, J decreases and so will temperature, a positive aspect in designing the engine. Just as in the fission propulsion systems described in Chap. 7, I_{sp}

will decrease as well, but less than J because of the square root relationship in Eq. (8.11). The heated inert propellant can be expanded in a conventional nozzle where the I_{sp} will be similar to that of solid-core nuclear thermal rockets (about 1000 s), but thrust will be proportionately much higher.

Considering the *electric* option, fusion products may be thermalized in a working fluid when the purpose is to generate electricity via conventional thermodynamic cycles. The electricity is fed to a cluster of ion or MPD rockets capable of I_{sp} much higher than NTR. However, at fixed power, if I_{sp} can be made higher, the thrust F must decrease accordingly:

$$\text{Thrust Power} \approx F \cdot V_e = F \cdot I_{sp} \tag{8.12}$$

The trade-off in all *electric* thrusters working at fixed power has been discussed in Chap. 7. This is between high I_{sp} (low propellant consumption) with low F (low acceleration = longer mission time) and its reciprocal, that is lower I_{sp} with high F (fast acceleration = shorter mission). Figure 8.5 shows indirectly this trade-off, since for a fixed power a number of propulsion systems exist, each with its own specific impulse. The final choice depends on the particular mission. Then, raising I_{sp} via electric propulsion comes at the penalty of lower thrust, low overall conversion efficiency (perhaps 30–50%) and a substantial space radiator needed to dissipate the 70–50% of reactor heat that must be rejected at the bottom temperature of the cycle.

In Chap. 7 it was seen that increasing I_{sp} by means of electric propulsion does not pose insurmountable problems. For electric propulsion applications, an I_{sp} in the 10^5 s range is assumed feasible in NASA studies (Choueiri 2002; Mikellides 2004; Cassady et al. 2008). By applying the Coulomb or Lorentz force to ionized matter, the jet speed is no longer tied to thermodynamics. *Powering* an electromagnetic system producing large I_{sp} is instead the challenge, since the exhaust jet power scales as

$$P = \frac{1}{2} \cdot \left(\frac{dm}{dt}\right) \cdot (V_e)^2 \propto (I_{sp})^2 \tag{8.13}$$

and much of the onboard electric power is not converted to the kinetic energy of ions, but to waste heat. More efficient ways to accelerate ions might change this picture. Among them are picosecond pulsed lasers producing intense electric fields and relativistic electron beams. Impinging on thin foils they produce ion beams in the many MeV energy range (Hegelich et al. 2006). Carbon beam of energy 30–40 MeV ($I_{sp} \approx 10^7$ m/s) have been demonstrated. Very similar is ion acceleration using the so-called Wakefields, also driven by electron beams or lasers (Joshi 2006). This approach could potentially revolutionize particle accelerators, since it takes a fraction of the space of the magnetic machines at CERN or Brookhaven, and might also have a large impact on electric propulsion. In essence, the Coulomb force to accelerate ions is applied at the microscopic level and by fields that in picosecond (ps) times reach 1–2 TV (teravolt).

8.2.1 Fusion Requirements and Impact on Propulsion

The energy density arguments in favor of fusion propulsion are solid, but assume feasibility of fusion engines. Fusion is the process powering stars. In order to fuse, nucleons must be brought close enough for the attractive nuclear force to overcome the Coulombic repulsion among protons. This requires either density to be much higher than in ordinary matter, or extremely high kinetic energy to be converted to work against the Coulomb force repelling like charges, or both. In stars, both requirements are satisfied. The mechanism responsible for fusion is gravitational compression of very hot plasma, always in competition with plasma radiation pressure. Reproducing this process in the laboratory is impossible, thus gravitational compression must be replaced by other mechanisms, increasing either density or kinetic energy (temperature).

Hence the effort since the 1950s to devise practical "plasma reactors (machines)" striving to reach temperatures $\approx 10^1$–10^2 keV or pressures of 10^1–10^2 GPa or, even better, both simultaneously, and for times $\approx 10^1$–10^2 ns. Once these conditions are realized, theory indicates fusion may continue unaided and with energy gain $Q > 1$. The quest for fusion since the 1950s has proceeded along these two main directions. More recently, efforts are underway trying to combine both in smaller and less expensive facilities. This challenge is much harder when the purpose is to realize the enormous energy potential of fusion in a spacecraft, that first must be lifted to a planetary orbit (while taking weight and cost constraints into account).

In this context, a misconception in imagining QI or interstellar missions is that the ideal propulsion system should have the highest possible I_{sp}. While true for chemical propulsion, this goal is not valid for propulsion where the power source is separated from the thruster, as is the case of fission- or fusion-powered electric propulsion. Dr. Ernst Stuhlinger developed the fundamental understanding of electric propulsion capability during WW II, while working at Peenemünde in von Braun's team (Stuhlinger and Ordway 1994). The concept of electric propulsion had been invented independently by Robert Goddard (in 1906) and Tsiolkovsky (in 1911). However, Stuhlinger was the first to realize the potential of electrically-driven propulsion using small but sustained thrust, and to develop the mathematical theory of space missions at constant thrust (Stuhlinger 1964). For fixed mission distance, his work shows that there is an optimum I_{sp} associated to each destination, payload and mission time. Of special importance in this analysis is the

ratio α between engine power and mass. Note that this α is different from the matter to energy conversion fraction α. Using the Tsiolkovsky relationship, the payload ratio μ (payload mass/initial spacecraft mass) can be found analytically as a function of mission end time τ and I_{sp} for any assigned engine α:

$$\frac{(W_{OEW} - W_{powerplant})}{W_{TOGW}} = \exp\left[\frac{-u_\tau}{I_{sp}}\right] - \left[\frac{I_{sp}^2}{2 \cdot \alpha \cdot \tau}\right] \cdot \left[1 - \exp\left[\frac{-u_\tau}{I_{sp}}\right]\right] \tag{8.14}$$

Here

$$W_{TOGW} = (W_{OEW} - W_{powerplant}) + W_{ppl} + W_{powerplant} \tag{8.15}$$

where u_τ is the velocity acquired at time τ under constant thrust. The dependence of the payload ratio on I_{sp} is not monotonous. In fact, defining

$$V_c \equiv (2 \cdot \alpha \cdot \tau)^{\frac{1}{2}} \tag{8.16}$$

the mass ratio can be rewritten

$$\frac{(W_{OEW} - W_{powerplant})}{W_{TOGW}} \equiv \mu = \exp\left[\frac{-u_\tau}{I_{sp}}\right] - \left(\frac{I_{sp}}{V_c}\right)^2 \cdot \left[1 - \exp\left[\frac{-u_\tau}{I_{sp}}\right]\right] \tag{8.17}$$

where V_c is the characteristic velocity associated to the mission, defined simply by its propulsion system α and duration τ (the characteristic velocity is associated to each mission, that is to each τ, and to each propulsion system, that is to each α). The I_{sp}/V_c ratio is a "normalized" specific impulse. The payload fraction $(W_{OEW} - W_{powerplant})/W_{TOGW}$ is plotted in Fig. 8.6 (also reported in Appendix B), showing that for each normalized final velocity u_τ there exist an optimum normalized I_{sp} maximizing the payload. Higher I_{sp} should therefore be combined with the thrust that optimizes τ.

Note that α varies by orders of magnitude, from 10^5 W/kg (for NTP) to 10 W/kg for NEP systems. For each $V(\tau)$, the payload ratio peaks at roughly $I_{sp}/V_c \approx 1$. Stuhlinger assumed this ratio exactly unity to obtain an approximate analytical solution for the mission time τ as a function of the distance $S(\tau)$ covered and of the payload ratio μ:

$$\tau = \left[\frac{S^2(\tau)}{\alpha}\right]^{\frac{1}{3}} \cdot \left[1 - \frac{\left(\frac{1}{2} + \mu\right)}{(1 - \mu)}\right] \cdot \ln\left[\frac{3}{1 + 2 \cdot \mu}\right]^{-\frac{2}{3}} \tag{8.18}$$

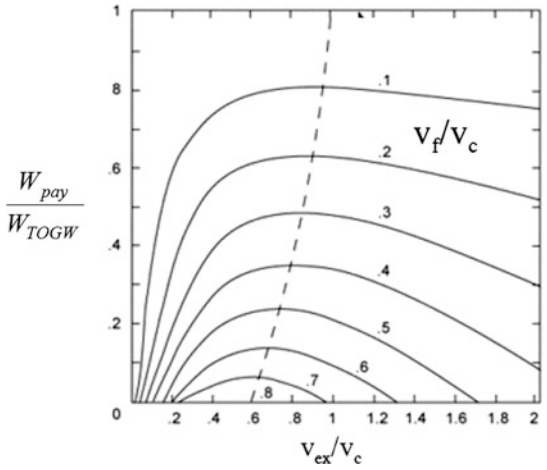

Fig. 8.6 Payload fraction as a function of I_{sp}/V_c and final velocity (Bruno and Simone 2009a, b)

This relationship is valid only in the approximation

$$\frac{I_{sp}}{V_c} \approx 1 \tag{8.19}$$

which is satisfied only by selected combinations of τ, α and I_{sp}. When the payload ratio $\mu << 1$, the engine α to reach a distance S (in AU) in a time τ (in years) can be further approximated by

$$\alpha = 10^{-3} \cdot \frac{S^2}{\tau} \text{ (kW/kg)} \tag{8.20}$$

While Stuhlinger found this exact solution for the payload ratio, none does exist for any other parameter α, τ, $S(\tau)$. In order to generalize Stuhlinger's results, the relationships for the other parameters must be obtained numerically, by finding the zeroes of the implicit nonlinear expression for the distance $S(\tau)$ (Bruno and Simone 2009a, b):

$$S(\tau) - I_{sp} \cdot \tau \cdot \left\{\left[1 - \frac{\left(\frac{I_{sp}}{V_c}\right)^2 + \mu}{1 - \mu}\right] \cdot \ln\left\{\frac{\left(\frac{I_{sp}}{V_c}\right)^2 + 1}{\left(\frac{I_{sp}}{V_c}\right)^2 + \mu}\right\}\right\} = 0 \tag{8.21}$$

In this expression the term $S(\tau)$, I_{sp}, α, μ and τ are parameters. Focusing on one at a time and holding all others constant allows to find the trends shown in Figs. 8.7, 8.8, 8.9 and 8.10.

These charts report the performance of electric thrusters (characterized only by the α parameter) for flybys varying from Sedna at aphelion (73 AU), to the FOCAL mission at 540 AU from the Sun, and to the edge of the Oort Cloud at 730 AU. For instance, Fig. 8.7 confirms that there is an optimum I_{sp} maximizing the payload ratio to the FOCAL

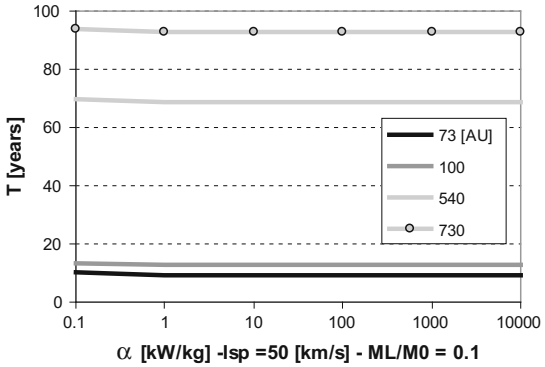

Fig. 8.8 At much lower I_{sp} = 50 km/s, mission time to four QI destinations does not depend on α anymore. Payload ratio = 0.1

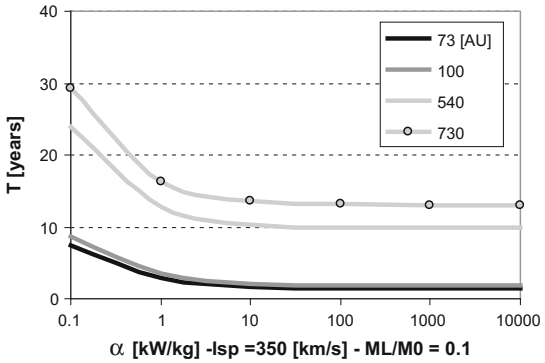

Fig. 8.9 Mission time decreases with α(<10 kW/kg) at high I_{sp} = 350 km/s. Payload ratio = 0.1

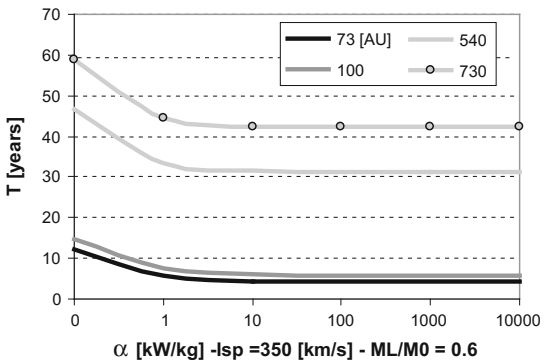

Fig. 8.10 Missions last very long at high payload ratio (0.6) even with high I_{sp} = 350 km/s

destination and that increasing I_{sp} reduces the payload ratio significantly. Comparing Figs. 8.7 and 8.8 indicates that any technology raising α even to values >> 1 kW/kg has little effect on mission time if I_{sp} is in the "low" range (that is, for I_{sp} = 50 km/s, quite feasible with current gridded ion technology). However, it can be decreased by a factor of 3 or more if I_{sp} can be raised to 350 km/s (demonstrated in the laboratory at NASA-Glenn).

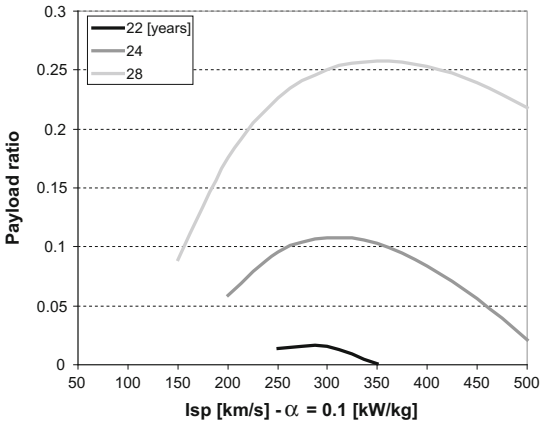

Fig. 8.7 I_{sp} (km/s) optimizes payload ratio and depends on mission time (years). Note the very high I_{sp} for α = 0.1 kW/kg and S = 540 AU

Comparing Figs. 8.9 and 8.10 shows that increasing the payload fraction by a factor 6 doubles mission time, even at I_{sp} = 350 km/s. The ideal (electric) power required, see Fig. 8.11, is surprisingly modest given the target destination and the range of spacecraft mass. This is also due to the fact that all missions considered are flybys, with no orbit capturing or manoeuvering. Note that the nuclear reactor thermal power should be at least a factor of 2–3 larger than the thruster power due to energy conversion inefficiency.

This same approach enables estimating payload and times of orbit-capturing missions (e.g., around Sedna or OCOs) by first assuming the half-way distance to the target, $S_{1/2}$, and then repeating the calculations for the deceleration phase to the correct speed for capturing the desired target orbit. Note that sizing thrust and I_{sp} in such way does not apply only to NEP, but in general to any propulsion system capable of continuous rather than impulsive thrust.

One critical issue about NEP or continuously powered QI missions is that for low thrust levels mission times may last longer than any commercial reactor mean time between maintenance (MTBM) (about 18 months). This is one of the many challenges associated to QI missions. This fact tends to be often overlooked, and it does suggest investigating fusion propulsion concepts that may combine high I_{sp} with high thrust.

8.3 Traveling at Relativistic Speeds

Planning QI or interstellar precursor missions must eventually include relativistic effects if the target is to be reached in times of the order of human lives. In Chap. 7, exploration of the Solar System was proposed using constant acceleration a for a sizeable portion of the trip. One may think this strategy could work also for interstellar missions. Consider, for instance, a hypothetical orbit to Proxima Centauri at

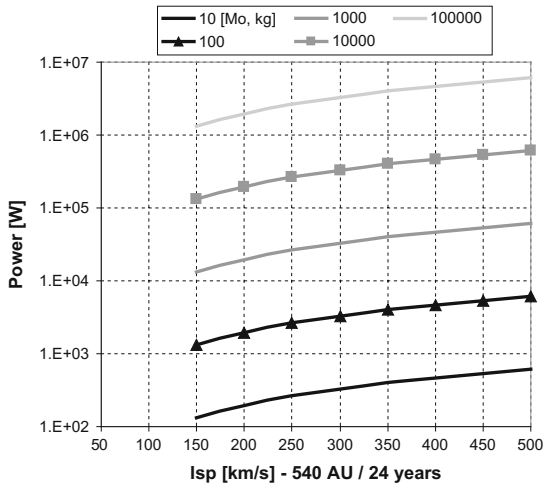

Fig. 8.11 Electric power grows with spacecraft mass M_0 but stays below 10 MWe. Distance S for τ = 24 years equates to 540 AU (FOCAL mission distance)

constant a = 1 g acceleration (g = 9.807 m/s^2) to the mid-point distance, $S_{1/2} \approx 2$ light-years. After reaching the mid-point, the spacecraft is assumed to decelerate at $a = -1$ g to the star. Note that 1 g acceleration is often used in examples because it generates the same effect of weight on Earth. *Newtonian* mechanics predicts a trip time

$$\text{Trip Time} = 2 \cdot \sqrt{\frac{2 \cdot S_{1/2}}{a}} \tag{8.22}$$

with the mid-course speed, $V_{1/2}$, given with

$$V_{1/2} = \sqrt{2 \cdot a \cdot S_{1/2}} \tag{8.23}$$

and in this particular case $V_{1/2} = 6.3 \cdot 10^8$ m/s, or 2.1 times the speed of light! According to Special Relativity, this is impossible, and so is the acceleration a = 1 g assumed. Thus, beyond the issue of power needed to keep accelerating for long times, there are issues associated to physics itself when spacecraft speed starts approaching the speed of light. Newtonian mechanics is insufficient to calculate or plan trips over distances where spacecraft speed may approach the speed of light.

Note also that in the 1916 version of the Theory of Special Relativity (Einstein 1916) mass "at rest," m_0 (that is, when its velocity $V = 0$), is different from the same mass, m, in motion:

$$m = \frac{m_0}{\sqrt{1 - \left(\frac{V}{c}\right)^2}} \tag{8.24}$$

The energy

$$E = m \cdot c^2 \tag{8.25}$$

must therefore be redefined as

$$E = \frac{m_0 \cdot c^2}{\sqrt{1 - \left(\frac{V}{c}\right)^2}} \tag{8.26}$$

These expressions are the result of the Lorentz transformations (Einstein 1916; Froning 1983; Lang 1999) that Einstein used to render both mechanics *and* electromagnetism invariant when changing inertial frame of reference (Harwit 1973; Chap. 5). Unlike the laws of dynamics, the Maxwell equations of electromagnetism, including the Lorentz force, change when classical Galilean transformations are used to correlate inertial frames. Albert Einstein discarded in 1948 the concept of relativistic mass defined by Eq. (8.24) in favor of relativistic energy, see Eq. (8.26), which is completely consistent with the four-dimensional momentum formulation of his original theory, see (Miller 1981) for details.

Inspection of Eq. (8.26) shows that for a mission segment at sustained power, enabling the spacecraft's speed to approach the speed of light, there appears a problem. In Newtonian mechanics, a thrust F applied to a mass M results in an acceleration

$$a = \frac{F}{M} \tag{8.27}$$

The thrust power needed scales with $1/2 \cdot F \cdot V$ and grows with $1/2 \cdot (\mathrm{d}m/\mathrm{d}t) \cdot V^2$ if V is the velocity of the mass ejected. Power stays always finite. Instead, the relativistic Eq. (8.26) predicts that energy grows faster than V^2 as V/c grows, and tends to infinity as V approaches light speed. Because energy can be produced only by mass conversion, the implication is that to reach higher and higher speed, the fuel or inert mass carried must also be larger and larger. In

order to achieve light speed, mass and energy become infinite. Thus, the second issue is the mass needed to accelerate an hypothetical spacecraft when its speed nears c. This question can be better posed in terms of the mass ratio M_R, the ratio between initial and final spacecraft mass. In order to keep M_R reasonable, Tsiolkovsky's law suggests that the propulsion system must be capable of I_{sp} much higher than conceived today, perhaps by a factor 10^2–10^4.

Figure 8.5 suggests that fusion or annihilation rockets might theoretically reach such I_{sp}. For the 10 t spacecraft considered in Chap. 1, the LEO mass (IMLEO) is 1000 t (2,205,000 lb). That is less than some large vertical launch rocket launchers, that have a lift-off mass of order 2000 t (4,410,000 lb). The cost of orbiting such mass is challenging, but five Roscosmos Energia-class launchers with a 230 t cargo capability could lift the spacecraft in five launches. If the 300 t configuration were used with a tandem payload section, instead of a laterally mounted cargo container, then only four launches would be necessary. The NASA designed SLS launcher under development in the US would require more launches, since the initial configuration is scheduled to orbit 70 t, and up to 130 t in the Block 2 future configuration (Anon. 2016a, b).

In reality, a 10 t payload is insufficient for such mission. For long crewed missions, at least a 100 t spacecraft is necessary and the total mass to be lifted to LEO (for a *one-way* mission) is now 10,000 t (22,050,000 lb). The results would be a massive vehicle in LEO, perhaps such as that depicted in Fig. 8.12. As propellant tanks empty, they would be discarded to reduce the empty weight of the spacecraft and therefore the propellant consumed. For interstellar or QI missions, the ship's energy source capable of sustained thrust and high I_{sp} over the duration required must be based on fusion or antimatter annihilation, and the ideal mission time, $t_{mission}$, would be determined by the fact that the average thrust power P

$$P = \frac{1}{2} \cdot F \cdot I_{sp} \tag{8.28}$$

is related to the potential energy available onboard

$$E = \alpha \cdot m_{fuel} \cdot c^2 \tag{8.29}$$

by the constraint on average power

$$P = \frac{E}{t_{mission}} \tag{8.30}$$

Time and distance permitted by a particular propulsion system and mass ratio are not strictly related to whether the spacecraft is manned or robotic. But the assets required to sustain conscious human beings over durations of order 10–20 years with current technology result in a prohibitive weight and volume penalty. For such missions, spacecraft with propulsion based on Newton's Third Principle should be self-sufficient, resembling integrated ecological systems. Such hypothetical spacecraft have been called "Multi-Generational Space Ships" (Kondo et al. 2003). The complexity of such enterprise would be immense. Despite this challenge, several detailed conceptual studies have been and still are carried out. Examples are the crewed Daedalus mission (Bond et al. 1978), and more recently Project Icarus for an unmanned interstellar probe, see (Long et al. 2009; Crawford 2010; Baxter 2010; Millis 2010; Baxter 2010, 2013), and the ongoing "The 100-Year StarShip Study" or 100YSS by DARPA/NASA (Anon. 2011a, b). "The 100-Year StarShip Study" holds Symposia every year since 2011 and deals with a broad variety

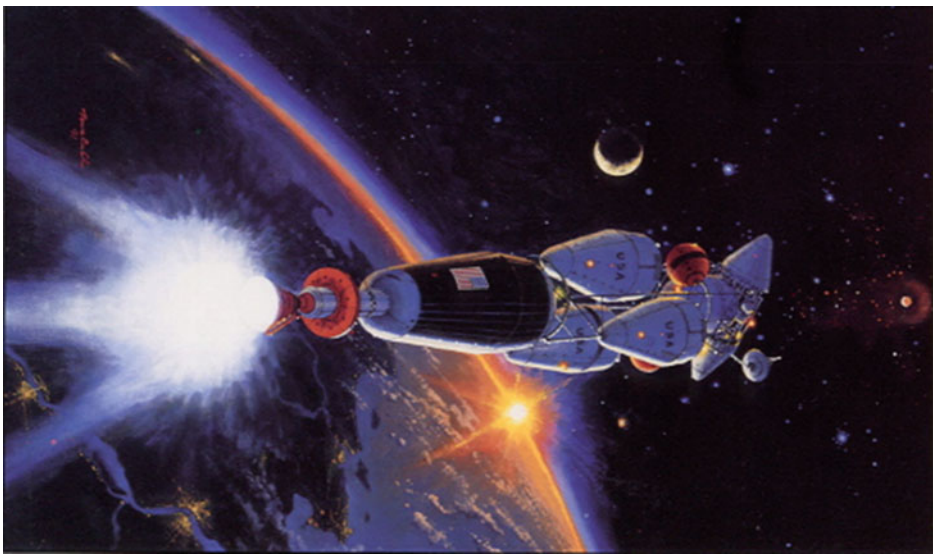

Fig. 8.12 Artist's view of a future heavy-lift vehicle in LEO

of social, economic and philosophical issues besides strictly technical ones (Barnhart et al. 2014). Although these are topics beyond the scope of this chapter, these imaginative studies often open new vistas and suggest possibilities ignored by more conventional approaches (Gilster 2012).

In order to operate a propulsion system when speed approaches a significant fraction of the speed of light, energy and mass should be treated relativistically. Under those conditions, the constant acceleration strategy mentioned for exploring the Solar System may no longer be a template for stellar trips. The constraint $V/c < 1$ affects all aspects of spacecraft, including that of its propulsion system. For fast QI and interstellar travel, the I_{sp} (or, exhaust V_e) may become no longer negligible with respect to c. Then gas-dynamics and magneto-hydro-dynamics (MHD) should be reformulated to account for relativistic effects in the propulsion system itself. Although relativistic equations of motion for gases and plasmas have been developed, they are far from having been universally accepted, let alone understood, for application to realizable propulsion systems (Anile and Choquet-Bruhat 1989).

This caveat suggests that, for the time being, issues associated with relativistic propulsion systems should be left aside, at least insofar as they are based on the Third Principle of Motion. What follows assumes V_e/c sufficiently small that relativistic effects may be neglected. In fact, relativistic effects become greater than 10% only at $V \geq 0.98 \cdot c$; so this assumption is not too restrictive. What propulsion systems, if any, are likely to work over interstellar or quasi-interstellar distances will be discussed next, keeping in mind that energy density J and power P are key aspects in addressing these questions. It is also understood that theoretical considerations about fusion and its implementation in a rocket are grounded in established physics, but that such propulsion systems and their application do not yet exist. Therefore, many if not all of the systems discussed or outlined, and all of the most innovative concepts, are speculative at this point in time.

8.4 Power for Quasi-Interstellar and Stellar Propulsion

The physics at our disposal to discuss QI and stellar propulsion is still based on that developed up to the late 1920s, that is special relativity and quantum mechanics, besides Newton's Third Principle. Within its formulation, energy and mass are interchangeable. Einstein's

$$E = m \cdot c^2 \tag{8.31}$$

holds the only key to *new* power sources. In fact, the question is not of finding *new* power sources, but that of finding new and efficient ways to *exploit* Einstein's theory of special relativity given by Eq. (8.31).

In this context the heat of combustion (e.g., $J = 1.3 \cdot 10^7$ J/kg when burning hydrogen and oxygen in stoichiometric proportions) is predicted by Einstein's formula. In the rearrangement of electronic orbitals occurring in chemical reactions, what is called "combustion heat" is actually due to a very slight mass decrease, or mass "defect" Δm, of the mass of products with respect to that of the reactants. This Δm is of order $1.5 \cdot 10^{-10}$% (Harwit 1973; Kammash 1995, p. 6). The sum of the change of potential energy $\Delta m \cdot c^2$ and of the microscopic kinetic energy produced is of course constant. Then, no matter what the process, a mass "defect" must correspond to an "excess" of kinetic energy. In engineering it is more practical to keep track of (i.e., "conserve") macroscale Gibbs' energy, enthalpy or internal energy, rather than accounting for the exceedingly small mass defect of products with respect to the reactants. Although perfectly valid, Einstein's theory of special relativity given with Eq. (8.31) is never used in thermochemistry, because classical mass would not be conserved, and the energy equation would have to contain additional terms involving $m \cdot c^2$. In fact, dynamics itself would have to be rewritten, using space–time (not space and time separately) and the 4-vector, or tensor, $\vec{p}$ (Harwit 1973; Chap. 5; Miller 1981).

Fission was the first example of deliberate searching for processes where mass could be converted into energy. The binding energy curve, see Fig. 8.13 (Mukhin 1987), indicates that ^{235}U (as well as other actinides) is a good candidate nuclear fuel, with about 200 MeV released per nucleus, yielding $8.2 \cdot 10^{13}$ J/kg. The fraction α of mass converted is $9.1 \cdot 10^{-4}$.

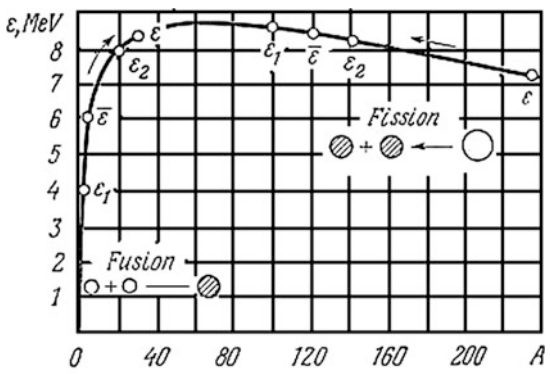

Fig. 8.13 Binding energy per nucleon as a function of mass number A (Mukhin 1987)

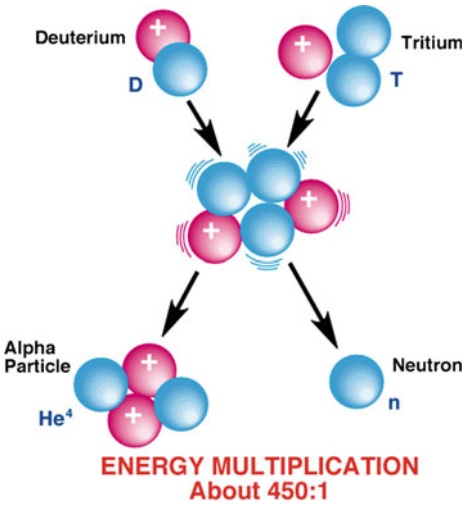

Fig. 8.14 Deuterium-Tritium (D–T) fusion reaction is the most efficient reaction known in terms of energy released (*Courtesy* Princeton Plasma Physics Laboratory)

8.5 Fusion Propulsion

Figure 8.13 shows that, at the left end of the atomic number spectrum, Hydrogen is also a good candidate fuel. Obviously ^{1}H cannot be fissioned. Instead, four of its nuclei can be "fused" to form a heavier nucleus (^{4}He), because the binding force among the four nucleons of ^{4}He is stronger than among four separate ^{1}H nuclei. This is indeed the goal of fusion research, and in this respect the two hydrogen isotopes, deuterium (^{2}H ≡ D), and tritium (^{3}H ≡ T) are better than common hydrogen. Figure 8.14 is a sketch of how D and T fuse and form a ^{4}He nucleus (an alpha particle) plus a neutron. Other light nuclei may be fused to form a heavier nucleus, but nearly all fusion research is focused on hydrogen, because theoretically its nuclear kinetics is easier to start (Chen 1985).

For illustration only, a hydrogen fusion reaction, and its mass (kilogram) and energy (joule) budgets could be simplified as follows (see also Table 8.3).

Reaction:	4H	→	He	+	Energy
Mass:	$4\ (1.6725 \cdot 10^{-27})$	→	$6.645 \cdot 10^{-27}$	−	$0.045 \cdot 10^{-27}$
Energy:	$6.69 \cdot 10^{-27}c^2$	→	$6.645 \cdot 10^{-27}c^2$	+	$0.045 \cdot 10^{-27}c^2$

where the mass defect is $0.045 \cdot 10^{-27}$ kg per each He atom formed, converting about 0.67% into energy with yield $J = 3.45 \cdot 10^{14}$ J/kg. Note that to fuse hydrogen atoms, the Coulomb repulsion among electron shells and that between nuclei must be overcome. The work done against repulsion is at the expense of the nuclei kinetic energy, and this needs strong collisions, that is, "high" temperature. Then, the energy available from fusion is the difference between the energy released and that necessary to force hydrogen atoms together. The energy gain Q is the ratio between net energy released and energy used to force fusion to occur, and it should be >1. Note also that only about 0.38% of the mass of the hydrogen isotopes is converted into energy. This number depends on the specific fusion reaction, see Table 8.3. Per unit mass, fusion yields more than 10^8 times the energy of gasoline burning with air.

These numbers, and the relative abundance of hydrogen and deuterium on Earth, $\approx 2 \cdot 10^{-4}$ of all terrestrial hydrogen atoms (Harwit 1973, p. 257), have motivated fusion research since the Soviet Union and the US Project Matterhorn of the 1950s. The mass defect in fusing hydrogen is still minuscule, but greater by a factor 4–5 than in uranium or plutonium fission. Funding fusion research for power generation rides on the hope to extract this energy from the huge amount of deuterium present in seawater (0.016%). The International Thermonuclear Experimental Reactor (ITER) project is the most recent collaboration effort to build a fusion reactor capable of producing a steady net gain of energy (Khatchadourlan 2014).

Table 8.3 also shows that the ultimate energy source is annihilation; that converts 100% of the mass of matter and antimatter into energy (Morgan 1982; Forward 1985). Annihilating a proton, p, and an antiproton, p^-, converts 100% of the mass of both particles, releasing c^2 energy per kg, or $J \approx 9 \cdot 10^{16}$ J/kg. However, the energy is not released in the most convenient form for propulsion or power. Annihilation produces mostly energetic particles such neutrinos and gamma rays, for instance. Thrust produced by their momenta would be very small, not just because products have low (or virtual) mass, but also because they would have to be collimated. Conceptually, a magnetic nozzle such as that of the pulsed MiniMag Orion rocket (Ewig and Andrews 2003) might achieve this objective, but the difficulties are daunting. The standard alternative is to thermalize the kinetic energy of products inside a propellant and let it expand in a conventional nozzle, still a major technology problem.

Based on these considerations and assuming the theoretical I_{sp} discussed in research papers will become reality in a not so distant future, it is worth estimating the effect of fusion propulsion on stellar or QI missions times. In such estimates, the trade-off between I_{sp}, F, and the overall power and mass demand of the propulsion system are central issues.

8.5.1 Mission Length Enabled by Fusion and Annihilation Propulsion

The effect of fusion-enabled performance on stellar trips has been estimated. In (Borowski 1987) missions at *constant thrust* gauge these effects. A constant thrust mission is different from a mission at constant acceleration, because the mass of the ship decreases with time; its convenience as a yardstick lies in the fact that solutions are analytical. Using constant thrust F, the round-trip time t_{ES} from Earth to Proxima Centauri, assuming a notional straight trajectory for simplicity, is

$$t_{\mathrm{ES}} = \frac{4 \cdot D}{g \cdot I_{\mathrm{sp}}} + \sqrt{\frac{D \cdot M_{\mathrm{f}}}{F}} \tag{8.32}$$

where D is distance, about 4.3 light-years or $4 \cdot 10^{16}$ m, and M_{f} is the final mass of the ship at destination. The ratio F/M_{f} is an acceleration, precisely that *at the trip end* (not during the trip) and for the present purpose it is assumed a constant (for instance, 1 g).

The inverse dependence of trip time on I_{sp} on Eq. (8.32) is striking. The inverse dependence on F is tempered by the square root. For I_{sp} in the upper range of fusion propulsion modes (10^6–10^7 s, see Fig. 8.5), the first term is much smaller than the second and can be neglected.

These results, see also (Bruno and Simone 2009a, b) and in analytical form also in (Stuhlinger 1964), indicate that there is an optimum I_{sp} for each mission defined in terms of payload and distance. For round-trips to Proxima Centauri, actual numbers in Eq. (8.32) predict 508 years at $I_{\mathrm{sp}} = 10^6$ s, and 51 years at $I_{\mathrm{sp}} = 10^7$ s, respectively. The *average* speed, V_{av}, is

$$V_{\mathrm{av}} = \frac{D}{t_{\mathrm{ES}}} = \frac{g \cdot I_{\mathrm{sp}}}{4} \tag{8.33}$$

With the approximation made, this average velocity depends only on I_{sp} (here in seconds) and is of order 10^6 or 10^7 m/s, respectively. This means Newtonian mechanics can still be used if I_{sp} is in the low range, but would need a relativistic correction if the *instantaneous* velocity reached more than $0.98 \cdot c$. Since even in relativistic physics I_{sp} must be less than $c = 3 \cdot 10^8$ m/s, the very long mission times found show that a mission at constant thrust is still not the fastest strategy to reach our closest star.

To reduce QI and interstellar mission times, it appears inevitable that spacecraft speed should be close to c. At the speed of light, the round-trip would take 8.4 years, and at an average $V = 0.5 \cdot c$ nearly 17 years, not accounting for acceleration and deceleration (this last not necessary if the mission is a flyby). The thrust profile versus time should show a ramp, followed by a plateau until V reaches a significant fraction of c. In order to orbit near the star or planet, a nearly symmetric deceleration is necessary. For a given final mass, this strategy implies very high thrust power $P \sim F \cdot I_{\mathrm{sp}}$ during acceleration or deceleration, when F is increased or is constant. Once the ship reaches the planned fraction of c, power is turned off ($F = 0$), and the ship coasts.

As an example, if the time-averaged ship mass is of order 100 t (metric tons), and $a = 3 \cdot g$ (barely tolerable for long by trained fighter pilots), $F = 3 \cdot 10^6$ N, and at an optimistic $I_{\mathrm{sp}} = 10^7$ m/s power would exceed 10^4 GW. Fusion energy release is of order $3 \cdot 10^{14}$ J/kg, and because the conversion rate α is 0.3–0.4%, about 33 kg/s of D–T fuel (see Sect. 8.6) would have to be fused. During only one day, the total mass of fuel "burned" would be of order 2850 t, two orders of magnitude greater than the assumed mass of the ship. Working close to the theoretical I_{sp}, say 10^8 m/s, the fuel consumption would reduce to 285 t/day, still unaffordable. In the limit of annihilation, that is, fusing protons and antiprotons with 100% conversion efficiency, mass consumption would drop to 9.6 kg/day, and after a day the speed would be of order 10^6 m/s, or $0.01 \cdot c$. All assumptions and simplifications notwithstanding, these numbers point at mass annihilation as the [still] conceptual solution to interstellar or QI missions (Borowski 1995).

No nuclear process exists with yield between that of fusion and that of annihilation. Percent mass conversion is either in the few parts per thousand (using D, T or H fuels) of 100% annihilation. The reason is the nuclear binding energy, see Fig. 8.13, is limited to about 8 MeV per nucleon. Until annihilation becomes a realistic means of propulsion, and provided relativistic effects can be dealt with, QI and stellar travel with a ship mass below $\approx 10^3$ t will be constrained not only by distance but also, more significantly, by how long acceleration or thrust can be maintained to reach a substantial fraction of the speed of light. In practice, QI and stellar travel will be constrained by mass.

Before examining the details of high energy density propulsion based on fusion, an intriguing aspect of QI and stellar missions carried out at relativistic speed is that spacecraft clock time will differ from the ground team Earth time. This aspect is discussed in Chap. 9.

The considerations made about times and mass in this chapter should warn about presuming too much from propulsion as we know it, that is, based on Newton's Third Principle. Power and mass consumption, together with distances and mission times, are formidable hurdles, even though mastering mass annihilation may overcome the first two. This tentative conclusion does not prevent investing in and discussing fusion propulsion, as it seems viable for future less ambitious QI and interplanetary missions. Accordingly, what follows deals with how fusion energy can actually be harnessed for a space propulsion system, with emphasis on the different technologies proposed (Leifer 1999; Cassibry et al. 2015).

8.6 Fusion Fuels and Their Kinetics

The first proposals to utilize fusion in rockets and space propulsion were in (Maslen 1959; Englert 1962). NASA recognized the potential of fusion much later (Schulze and Roth 1990). Studies of generic fusion propulsion concepts (Santarius and Logan 1998) did focus on power available per unit mass of the reactor, α^*, not per unit propellant or fuel mass. This is the same parameter used by Stuhlinger in the 1960s in his pioneering analysis of the effect of engine on mission payload and time, and in fact this is *the* key parameter of a practical reactor (Stuhlinger 1964). The appeal of fusion propulsion is the fact that estimates of α^* may be in the range of a few kilowatts per kilogram compared with 0.01–0.16 for tested NEP systems, and 20–30 for NTP systems (Bruno et al. 2009a, b).

The starting point in attempting to conceptually design a fusion propulsion system is the choice of fusion fuel. The kinetics of candidate fuels is in Fig. 8.15. As in combustion chemistry, fusion reactions may start after overcoming an activation energy barrier. They "ignite" when the kinetic energy of the reactants is brought above a threshold. The reason is the same of combustion, that is, Coulomb repulsion among like-charged orbitals in chemistry, and among protons in fusion. Coulomb repulsion competes with attraction by the "strong" nuclear force acting between all nucleons. Since the nuclear force has the shortest range of all three elementary forces, its attraction is felt by nuclei only when they can be "shoved" very close. Therefore, much kinetic energy must be given or transferred to nuclei to overcome Coulomb repulsion. Depending on reactants, threshold temperatures triggering fusion among nuclei may be from tens to hundreds of million °C or K. In eV units, this means that D, T, and other potential reactants must be injected in the fusion reactor with energy 10–100 keV. At these temperatures, electrons are no longer attached to atoms, and matter is in the plasma state, where positive nuclei and negative electrons have kinetic energy so large that Coulomb attraction cannot form again the original neutral atoms.

Fusing together nuclei of D or T may occur *only* at these kinetic energies. In fact, the key issue in fusion is reaching sufficiently high reactants temperatures for sufficient "confinement" time τ (Lawson 1957). The Lawson breakeven criterion states

$$n_1 \cdot n_2 \langle \sigma v \rangle \cdot \tau \cdot E_f - \tau \cdot (P_B + P_S) = \frac{3}{2} \cdot (n_1 \cdot k \cdot T_1 + n_2 \cdot k \cdot T_2) \tag{8.34}$$

where $\sigma \cdot v$ is the kinetic rate parameter, E_f is the fusion heat release, and P_B, and P_S are losses due to bremsstrahlung and synchrotron radiation, respectively. The terms n_1 and n_2 are the particle number densities of the two reactants, see Fig. 8.15, in general at different temperatures T_1 and T_2, respectively. The term k is the Boltzmann constant. Rate parameters and energy losses are in (Huba 2016). Equation (8.34) shows the importance of plasma temperature and density, and is an ignition criterion based on a *steady-state* ignition power budget. It says essentially that the net rate of fusion energy generation, that is, fusion rate times energy released per fusion event, minus power lost by radiation, must be equal to the kinetic energy absorbed by the reactants. Thus the kinetic energy of reactants, on the right-hand side of Eq. (8.34), not only must be high enough to support the fusion heat release (first term on the left-hand side), but

Reaction	Yield (%) and products (MeV)	$T_{ignition}$, K
1a	$D + D \xrightarrow{50\%} T(1.01) + p(3.02)$	$300 \cdot 10^6$
1b	$\xrightarrow{50\%} He^3(0.82) + n(2.45)$	
2	$D + T \longrightarrow He^4(3.5) + n(14.1)$	$50 \cdot 10^6$
3	$D + He^3 \longrightarrow He^4(3.6) + p(14.7)$	$500 \cdot 10^6$
4	$T + T \longrightarrow He^4 + 2n + 11.3$	
5a	$He^3 + T \xrightarrow{51\%} He^4 + p + n + 12.1$	
5b	$\xrightarrow{43\%} He^4(4.8) + D(9.5)$	
5c	$\xrightarrow{6\%} He^3(2.4) + p(11.9)$	
6	$p + Li^6 \longrightarrow He^4(1.7) + He^3(2.3)$	
7a	$p + Li^7 \xrightarrow{-20\%} 2He^4 + 17.3$	
7b	$\xrightarrow{-80\%} Be^3 + n - 1.6$	
8	$D + Li^6 \longrightarrow 3He^2 + 22.4$	
9	$p + B^{11} \longrightarrow 3He^4 + 8.7$	
10	$n + Li^6 \longrightarrow T + He^4 + 4.8$	
11	$n + Li^7 \longrightarrow T + He^4 - 2.5$	

Fig. 8.15 Fusion kinetics (T = tritium; D = deuterium; p = proton; n = neutron. Energies released are in MeV [adapted from (Huba 2016)]

must also compensate for the radiative heat loss (second term on the left-hand side). This condition is similar to the condition for flame anchoring inside a combustor; the difference is that the main power loss is due to convection, not radiation and that the confinement time τ is replaced by a similar fluid dynamic residence time inside the combustor.

The Lawson condition is an energy "breakeven" condition linking temperature, particle density, and confinement time. Notwithstanding its difficulty, fusion per se has already been demonstrated since 1968, but not for a time sufficient to be a self-sustaining steady process in a practical device and for long periods of time. The difficulty is the fact that fusion is not a natural event on a human or even planetary scale. Fusion is the power source of stars (Kaufmann 1993; Chap. 3). In stars, it is gravitation that compresses and heats matter until temperatures become high enough to start fusing. In a reactor, gravitational effects are negligible, and fuel must be heated to ignition temperatures by an external power source, for instance, by radio-frequency electromagnetic heating. Then temperatures must be about *10 times higher* than in our Sun as Eq. (8.34) shows. In the energy source term on the right-hand side, if the particle number densities of the two reactants, n_1 or n_2, are lower compared to the conditions in the Sun, the temperature must be higher to compensate.

By substituting into Lawson's criterion known experimental values, and simplifying the mathematical form of the power losses, the compact expression for the breakeven condition becomes:

$$n \cdot \tau \approx 10^{14} \frac{\mathrm{s}}{\mathrm{cm}^3} \tag{8.35}$$

This is a hyperbola in the (n, τ) plane. Equation (8.35) still quantifies in extremely simplified form the balance between source and sink in Eq. (8.34). Plasma at moderate density may ignite, but only if confined for a sufficient time. This is a severe constraint; for instance, for $n \approx 10^{14}$ cm^{-3} (incidentally, a value typical of alpha particles emitted by smoke detectors) the confinement time is about 1 s, still a factor three or so longer than ever obtained in steady-state fusion reactors so far. The Lawson criterion has focused fusion research on confinement techniques and fuels, requiring low ignition temperature even though their energy yield may be smaller.

After ignition, fuel must be kept supplied to the reactor to maintain fusion. This process may be steady-state or pulsed. The fraction of energy released by fusion relative to that necessary to heat the fuel is the "energy gain" Q, the ratio between energy output and energy used to ignite. This number quantifies the overall efficiency of a fusion reactor.

A second issue in choosing fuels is the type of particles produced (Santarius and Logan 1998). Most fusion kinetics releases high-energy neutrons, see Fig. 8.15. In order to extract their kinetic energy, neutrons must be thermalized, i.e., stopped. This is difficult (see Appendix A) since neutrons are not charged particles, thus are not subject to the Coulomb force, and slowing them can be done only through collision with nuclei. This requires matter (shielding) and increases reactor mass. Besides, collisions modify microscopic lattices causing eventually structural damages. In choosing fuels, there is a trade-off between ignition quality and neutronics. For instance, reaction (2) in Fig. 8.15 is the easiest to ignite at a nominal 50 MK (million degrees Kelvin; actually this temperature can be higher depending on its spatial profile and on heat losses). It is also very "dirty," in the sense that 80% of the total energy released is in the form of neutrons of 14.1 MeV. Recovering the kinetic energy of neutrons by thermalizing them is critical for efficiency. The standard recovery strategy consists of surrounding the fusion reactor with one or more "blankets" containing lithium and using the high-energy of neutrons crossing the lithium blanket to breed the tritium necessary to maintain D–T kinetics. Lithium works as the reactor coolant, collecting and thermalizing the neutron kinetic energy. The thickness of the blanket contributes significantly to the overall reactor mass.

Inspection of Fig. 8.15 suggests reaction (1a) has better kinetics: it needs only D (not T), a fuel that can be extracted from seawater for about $1000/kg. D abundance in seawater is estimated at 0.016% or 10^{13} t. However, reaction (1a) has a low energy yield, and its ignition at 300 MK is much harder than for reaction (2). In reality, when fusing D–D, all three reactions (1a), (1b), and (2) may take place simultaneously. Their combined kinetics is convenient, because of the "low" ignition temperature and because of high overall energy yield, but produces unfortunately fast neutrons.

Because tritium does not exist in nature, it must be "fabricated" by nuclear processes such as reactions (10) and (11). Neutron fluxes must be of order 10^{14} cm^{-2}s^{-1} inside the lithium blanket surrounding the reactor (Metz 1976). A still untried alternative to breed tritium is by using fission, in combined fusion–fission cycles. Another is to exploit the large neutron flux from D–T fusion to breed ^{233}U from a ^{232}Th (Thorium) blanket surrounding the fusion reactor, and fission it immediately to produce thermal power (Kammash 2010). Combining fusion and fission originated in the aftermath of the 1954 Bikini thermonuclear bomb test. Debris from the test reached Japanese fishermen on their *Lucky Dragon 5* boat 90 miles away and was discovered to contain fission fragments. Scientists did not expect the ^{238}U layer surrounding the fusion core to fission, but it did because of the intense neutron flux (Heckstall-Smith 1958).

Reaction (3) needs ^{3}He, a rare isotope. Naturally available Helium, itself scarce, is ^{4}He. ^{3}He could be mined on the lunar surface where it is produced by the solar wind. Lunar soil abundance has been estimated at 10^9 kg (Wittenberg et al. 1986). In case ^{3}He would become available, reaction

(3) would become very attractive, its high ignition temperature notwithstanding, because of high-energy yield and because it does not produce neutrons. Calculations (Shmatov 2006) indicate that, contrary to what has been assumed in the past, fusion efficiency of order 20% is feasible with D + ^{3}He if they can be compressed to a density of the order of 300 g/cm^3. This density can be reached in inertial confinement, see Sect. 8.11.

The most attractive "clean" or "aneutronic" kinetics is reaction (9) between a proton and a boron isotope. It produces only high-energy helium and no other "dirty" particles. However, its ignition temperature is theoretically infinite because of excessive bremsstrahlung losses. Its practical implementation (for instance, by differential reactants heating) is probably far in the future and might require a nuclear catalyst.

Just as in chemistry, the choice of reactants does not necessarily produce only the desired products. Many pathways are open to an initial reactants set, and they may form different products. For instance, reactants D and ^{3}He in reaction (3) may also drive reactions (1) and (2), with rates and final products determined by their respective collision cross sections depending on temperature and number densities. This means that reaction (3) can produce neutrons indirectly. Only reaction (9) would be truly aneutronic. Radioactivity, although a milder concern than in fission, does remain a fusion issue.

8.7 Fusion Propulsion Strategies

Fusion occurs when two different nuclei have sufficient energy to be mutually attracted by the nuclear force for a sufficient time. The main drivers are, therefore, temperature and time, and many recipes have been tried to achieve their successful combination. Following the classification of (Cassibry et al. 2015), these have produced fusion devices belonging to one of four main confinement classes: *magnetic*, *inertial*, *electrostatic-inertial,* or *magnetic-inertial*. Since fusion with gain $Q > 1$ has not yet been achieved, strategies and devices are still at a preliminary or proof of concept stage. None has been specifically designed for application to propulsion.

Magnetic confinement fusion (MCF, MFE) relies on steady magnetic fields $\vec{B}$ to confine fuel plasma at low density (10^{23} m^{-3}) in a reactor volume $\approx 10^1$–10^2 m^3. Because of thermal conduction (see below), their minimum size is of the order of 2–3 m. At typical plasma density, the energy stored in plasma is about 1 GJ. Tokamak and their variants (spheromak, stellarator, reversed field pinch machines, and others) are examples. This technology has received most funding, not a minor reason being the fact that tokamak are large and involve tens or hundreds of technical people. The ITER reactor being built in France by an international consortium is the best-known representative. It is hoped ITER will reach $Q > 1$ in the 2010–2020 decade.

Inertial confinement fusion (ICF) relies on high-power pulsed lasers to ablate the outer shell of pellets encasing fuel, resulting in the implosion, compression, and subsequent heating of the center by the shock traveling radially inwards. The initial outer shell pressure due to the sudden pulse ($\approx$20 ns) may reach 100 Mbar. The shock travels toward the pellet center at 300–400 km/s, where ideally adiabatic compression produces 200–300 Gbar and $\approx$10 keV (10 MK) for $\approx$20 ps and can ignite fuel. The extremely high density puts ICF at the opposite end of the spectrum with respect to MCF. The 10^{-1}–10^1 mm pellet is the actual reactor. Each plasma energy pulse is $\approx$1 MJ, but due to low laser efficiency, the laser energy storage system may have to accommodate about ten times that, resulting in an instantaneous power of $\approx 10^4$ TW. The bank of lasers, their electric feeding, and power switching drive the bulk and cost of ICF facilities. A steady injection sequence of pellets is necessary for quasi-steady energy release, and this implies quick acting energy storage and discharge. The best-funded US facility using this strategy is the National Ignition Facility (NIF) at the Sandia National Laboratories (Anon. 2016).

Electrostatic-inertial confinement (IEC) in its simplest form relies on a radial electrostatic field $\vec{E}$ imposed, for instance, by a spherical wire cage; this field accelerates D^+ and T^+ ions toward the sphere center where ideally they collide at very high speed and ignite. The voltage producing $\vec{E}$ may reach $\approx 10^2$ kV. Experimental setups are typically orders of magnitude smaller than MCF, so testing is relatively inexpensive. However, emphasis on the first two strategies and unresolved issues has prevented adequate funding to prove its merits.

Magnetic-inertial fusion (MIF $\approx$ MIC) uses a pulsed magnetic field $\vec{B}$ to implode a liner that compresses ("squeezes" or "pinches") axisymmetrically D–T fuel until it ignites. Compared with inertial confinement, MIC produces much higher density per unit area, a critical quantity in plasma ignition. The confinement time is longer ($\approx$100 ns–1 μs) and energy is small, about 1 MJ. Besides, no large assemblies of lasers or plasma guns are needed, only current pulses $\approx 10^1$–10^2 MA. Simulations predict $Q \approx 10^2$–10^3. Variants include pulsed θ-pinch (magnetic field runs down the axis of the cylinder, while the electric field is in the azimuthal direction) and Z-pinch (current runs down the axis (or walls) of the cylinder while the magnetic field is azimuthal), both promising for propulsion applications. This confinement strategy is attracting attention because of reduced investment and operating costs compared to other fusion strategies.

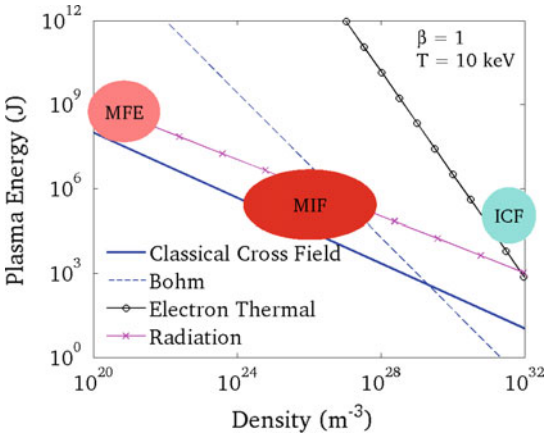

Fig. 8.16 Plasma energy and reactor size (i.e., plasma number density) are a function of energy losses specific to different fusion strategies (Cassibry et al. 2015)

The lines in Fig. 8.16 provide an idea of the size of the reactor in terms of energy and of the losses characteristic of different fusion modes. They are drawn for a representative temperature (10 keV) and predict minimum reactor energy content as a function of the plasma density still allowing fusion of D–T fuel. Losses specific to each fusion strategy (the lines in the chart) show minimum reactor energy. For instance, MFE and MIF losses are due to thermal (solid blue line) and turbulent conduction (crossed blue line), the latter the bane of all tokamak reactors. For a given plasma density, the minimum reactor energy must be equal or larger than that of the blue line. The black line applies to ICF reactors. In order to ignite, plasma must be adiabatically imploded to density orders of magnitude higher than those in magnetic confinement. The "reactor" is the fuel pellet itself, and its density is a compromise: too low prevents ignition and too high drives excessive conductive losses by electrons. The population density of the conduction electrons is proportional to that of the plasma. Laser power deposition is limited by low lasing efficiency and by the energy storage system (e.g., capacitors) that must be recharged after each "shot." Together with losses, these two factors limit the quantity of matter that can be fused, in practice, a pellet of about 1 mm in size (Winterberg 1971). Much higher energy per "shot" is not available from current lasers; much lower is quickly dissipated.

Hybrid fusion concepts combining fission with fusion have been proposed or investigated to overcome the problems specific to each strategy. Some use neutrons, escaping from partial fusion of D–T, to trigger fission in U or Th isotopes that would normally not fission. These schemes look promising but further complicate reactor design, adding the problems of nuclear poisoning and refueling to that of stopping fusion-produced neutrons. In fact, no hybrid system is on the agenda of energy R&D agencies (Cassibry et al. 2015).

8.7.1 Thermal Versus Electric Fusion Propulsion

Just as in fission, the next question in applying fission to propulsion is how to produce thrust, since power may be available in the undesirable form of high-energy neutron and gamma ray fluxes.

Fusion produces high kinetic energy He^{++}, H^+, electrons, and neutrons, see Fig. 8.15. One strategy is to exploit the momentum of these particles "as is," by letting them free to leave the reactor. Their recoil produces usable thrust if their momenta are aligned in the same direction. H^+ and alpha particles can be collimated by a magnetic field (Metz 1976). This propulsion mode is the same as that of chemical or fission fragment rockets (see "thermal fusion propulsion" in Sect. 7.15), with the "propellant" being the fusion products themselves. In fact, the temperature of fusion products (10–40 MeV per He nucleus) results in a velocity (I_{sp}) in the 10^6–10^7 m/s range. Thrust will depend on the rate of mass fused and ejected, i.e., on reactor power. Figure 8.5 shows that thrust $F = 100$ t with $I_{sp} = 10^5$ s requires 1000 GW, thus a fusing rate of order 1 kg/s. With $\alpha \approx 3.5 \cdot 10^{-3}$, see Table 8.3, the actual D − T fuel mass injected into the reactor must be $1/\alpha$ larger, or about 300 kg/s. Such thrust cannot be sustained for long. Ultimately, not even a one-way stellar mission would be feasible within a 20-year time span. However, quasi-interstellar robotic missions might be feasible, while being very expensive.

The alternative mode is fusion-powered NEP, or "fusion-electric" propulsion. The reactor powers a generator feeding electricity to an electric thruster. All fusion products must be thermalized inside a working fluid (e.g., lithium) that produces energy by thermodynamic or other direct conversion scheme. Thermodynamic conversion as we know it is at most 30–50% efficient. Waste heat must be radiated away by space radiators, where the working fluid at the cycle "cold end" transfers heat to space. The temperature of free space is the 2.72 K of the cosmic background radiation discovered by Wilson and Penzias (Assis and Neves 1995). As a yardstick, the areal mass of the ISS radiator is 8 kg/m^2. It could be halved by using carbon/carbon fibers and in the future may drop to 0.25 kg/m^2 by thin film fabrication and using H_2 coolant rather than lithium (Lenard 2008). Radiator mass is the major disadvantage of NEP.

At present, most fusion concepts generate electric power from thermodynamic cycles based on the heat extracted from the reactor lithium blanket (Polsgrove et al. 2010; Cassibry et al. 2015), but MHD conversion has also been proposed (Adams et al. 2003). One positive aspect of NEP is that it uncouples the propulsion system from the power generator, a better choice when thrust and I_{sp} need to be modulated. For instance, maneuvering near strong gravitational fields requires large thrust even if at the price of lower I_{sp}, while much smaller thrust at a much higher I_{sp} is better when

cruising. Electric thrusters lend themselves to such trade-offs in operating mode far more easily compared to thermal fusion rockets. Compared to chemical or fission rockets, where inert matter can be added to increase thrust at the expense of I_{sp}, MCF fusion reactors are intolerant of inert (non-fusing) matter addition, since it can quench fusion kinetics immediately.

All these considerations are tentative. At the present stage of fusion research, it would be premature to assign a priority to the first or to the second strategy that, in any case, would depend on the specific mission and on factors which are at present beyond our knowledge. As progress toward commercial fusion continues, future questions will center on the type of fusion reactor and energy extraction technology. Work in this area began in the 1950s and is still continuing. Because fundamental information is available (e.g., Kammash 1995; Anon. 2006b; Cassibry et al. 2015), the following sections focus on elementary physics rather than still immature engineering. No experience exists in fusion propulsion, and the authors will feel satisfied if at least the main advantages and disadvantages of proposed fusion and energy conversion strategies are made clear.

8.8 Fusion Propulsion Reactor Concepts

The history of fusion concepts for space propulsion goes back to the very beginning of the SSSR (Soviet Union's history of nuclear propulsion remains unclear) and US (Project Matterhorn 1961) fusion programs. At that time, hydrogen plasma to be fused was conceived confined inside a "magnetic bottle" by means of a magnetic field shaped by electrical coils. Ionized hydrogen isotopes were supposed to fuse while traveling back and forth between the two ends of the bottle. More than sixty years later, plasma physicists are still struggling with the many facets of magnetic confinement (Miyamoto 2006). Progress has enabled plasma technology to achieve fusion (the first evidence of fusion was obtained in 1968 in the Soviet Union), albeit only by injecting inside the plasma more energy than that released by the fusion process itself. This has not deterred researchers, quite few of them visionary, from proposing fusion *propulsion* concepts. (Cassibry et al. 2015) is an excellent synthetic review of the prospectives of fusion propulsion. The most intriguing concepts are not based on electric but rather on thermal strategies, allowing fusion products to be ejected at the velocity corresponding to their kinetic energy, and therefore with thrust depending on the rate of fused fuel. In some concepts, inert propellant is added downstream of the reactor to increase thrust. Thermal propulsion devices in this class are called open magnetic confinement (OMC) reactors, an oximoron, and are discussed in Sect. 8.10. Their application to propulsion is in (Romanelli and Bruno 2005) and Appendix B.

In the following discussion of fusion propulsion systems, the level of detail is purposely kept modest, with emphasis on propulsion rather than on the specifics of the reactors. According to the NASA's technology readiness level (TRL) scale (Anon. 2011b), all these concepts would be given TRL = 1 at most.

8.8.1 Confinement Strategies

By far, the best-known and best-tested fusion reactor is the tokamak [**to** (roidal) **ka** (chamber) **mak** (machine)], originally proposed and built in the former SSSR (Smirnov 2010). Tokamak solves the difficulty of confining plasma in a bottle by turning the bottle onto itself, therefore morphing it into a toroid (a donut). Plasma is confined and prevented from quenching on the cold reactor walls via multiple electromagnetic fields: (a) a field with field lines following the larger torus circumference; (b) a poloidal field with lines trying to "squeeze" the smaller torus diameter and periodic in time, and (c) a field directed as the symmetry axis of the torus, see Fig. 8.17.

Moving plasma is an electric current which itself creates a magnetic field that adds to those imposed from the outside. Properly sized, the three fields combine to ensure low plasma drift and thus better confinement. An excellent

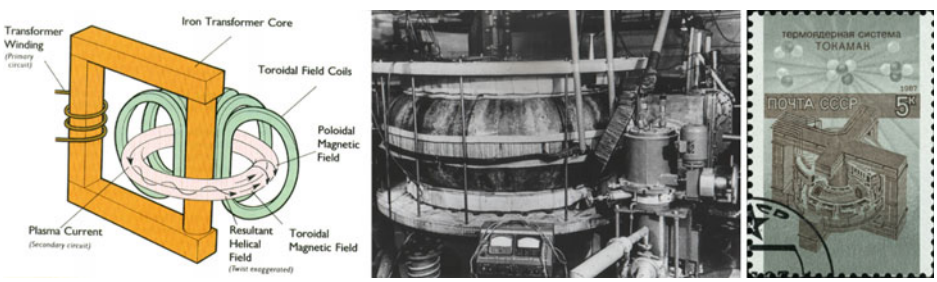

Fig. 8.17 Tokamak schematic (*left*), the world's first tokamak T-1 at the Kurchatov Institute Moscow in 1958 (*middle*) (Smirnov 2010), and a USSR stamp from 1987 showing a tokamak thermonuclear system (*Courtesy* Wikipedia on *right*)

introduction to tokamak and their issues is by (Kikuchi and Azumi 2015; Balshaw 2015). This class of fusion reactors is called magnetic confinement reactors, or MCR. Plasma moves along spirals, see Fig. 8.17. Conceptual operation of MCR is steady, but the actual mode may depend on the transformers feeding current to the electromagnets producing the magnetic field. The transformers link the plasma, viewed as a classic secondary electric circuit, to the external power supply. If electromagnets are not superconducting, ohmic heating forces reactor operation to be intermittent, for instance to stop once per hour to cool down wiring. In any event, slow plasma contamination by unwanted matter, e.g., due to metal particles extracted from the reactor walls by plasma impingement, makes periodic shutdown and cleaning inevitable on MCR conceived for *ground power generation*.

In *space operations*, regularly scheduled maintenance may be impracticable or impossible because of environmental, safety, and radiation hazards and is a major issue. If feasible, space-qualified MCR will probably have to meet much more stringent reliability requirements than those envisaged at the moment for ground fusion power plants. Note that experience in MCR comes from ground fusion *short tests* (single "shots"). We are very far from steady energy or thrust production.

Other reactor configurations, embodying different fusion plasma confinement strategies, have been proposed and tested or are still at the stage of suggestions. As already mentioned, the second most investigated is inertial confinement fusion reactors (ICR) in which GW-class lasers pulse a small (≈1 mm) pellet encasing fuel within a metal jacket. The energy pulse ablates the external jacket, raising the pellet temperature and gasifying the metal case. This gas becomes a radiating plasma, and its radiation pressure compresses ('implodes') the fuel to the density and temperature needed to ignite. Radiative compression may reach hundreds of Gbar ($\approx 10^{11}$ atm) for a few tens of ps.

For steady power generation, ICR need to be fed a stream of pellets. Each pellet is "lased," fused, and releases power of order 1 MJ. ICR operation is necessarily always pulsed, with the repetition rate determined by the power demand and constrained by lasers recharging rate. Pulsed operation may seem awkward to chemical rocket engineers, but is advantageous or convenient when releasing destructive energy levels. For instance, automotive engines reach *instantaneous* in-cylinder temperatures of order 2500 K, much higher than the melting point of steel. However, its pulsed operation reduces the average heat transfer and temperatures to quite acceptable values. In contrast, commercial gas turbine engines are limited to 1800–1900 K precisely by their steady combustion and heat transfer mode. The Project Orion concept (Dyson 2002), in which pulsed nuclear explosions were proposed to push a spaceship, shares similarities with an ICR, particularly in terms of ablation physics (but not of scale).

In what follows, both MCR and ICR will be briefly described and their *known* issues and shortcoming discussed.

8.9 Magnetic Confinement Reactors (MCR)

MCR go back to the very beginning of fusion studies, when confining high-temperature plasma was thought feasible only by means of a steady magnetic field preventing interaction with cold reactor walls. Plasma can be magnetically confined when the magnetic pressure applied by the total magnetic field $\vec{B}$, proportional to B^2, is larger than the thermodynamic pressure $n \cdot k \cdot T$, with n the number density and k the Boltzmann constant. That means that the "beta" ratio between thermodynamic and magnetic pressure, using c.g.s. units, is

$$\beta = \frac{8 \cdot \pi \cdot n \cdot k \cdot T}{B^2} \tag{8.36}$$

The ratio must be close to unity to guide and confine the plasma, but no higher to prevent plasma from collapsing. In fact, plasma instabilities and other factors limit beta to about 5–10% in most tokamak. The maximum beta, $\beta_{\max}$, was found to depend on plasma current I and externally imposed $\vec{B}_{\text{ext}}$ field as

$$\beta_{\max} = \frac{\beta_{\text{ext}} \cdot I}{r \cdot B_{\text{ext}}} \tag{8.37}$$

where r is the smaller of the two torus radii.

Since n and T are very large (n must meet the Lawson ignition criterion, see below), so must be $\vec{B}$. The confinement mechanism of charged plasma particles (H^+, He^{++}, D^+, T^+, e^-) is the Lorentz force. In a magnetic field of induction $\vec{B}$, this force makes species possessing an electric charge q gyrate (that is, spiral) around the $\vec{B}$ field lines. The gyration, or cyclotron, frequency Ω is proportional to $\vec{B}$ and inversely proportional to the mass of the charged particle, m. The gyration radius, ρ, of the helix followed by the charge is proportional to the velocity component $v_\perp$ normal to $\vec{B}$ divided by Ω, that is

$$\Omega = \frac{q \cdot B}{m} \tag{8.38}$$

$$\rho = \frac{v_\perp \cdot m}{q \cdot B} \tag{8.39}$$

The gyration frequency and radius are important for two reasons: Ω must be higher than the plasma collision frequency, otherwise trajectories will not be guided and confined by the field $\vec{B}$ but will change randomly after each collision. Second, the volume of the reactor where plasma is confined must be large enough to host the charges gyrating

around field lines with spiral radius ρ, so the size of the reactor depends on plasma density and on ρ. Equations (8.38)–(8.39) tell that ρ and thus reactor size scale as $1/B$. To increase beta and to reduce reactor size, B must be made as high as feasible.

In fact, using electrons as an example of charged species, assume a field of 1 T (1 T = 10^4 gauss). This is an intense field: for comparison, at sea level the Earth's magnetic field is 0.3 gauss and 1 T is some 33,000 times more intense than the Earth's magnetic field, but still manageable. At 1 T, the gyration radius of a single electron around a $\vec{B}$ line may be of order 0.1 mm for electron velocities of order 10^6 m/s. Ions such as H^+, about 1840 times heavier than electrons, at 1 T field are confined within a gyration radius of maybe 1 cm. Permanent magnets can produce 1-T fields, but only within short distances. The actual size of a fusion reactor for thermal space propulsion is dictated not only by the gyration radius of a single charge, but also by the total flow of plasma present and to be ejected to produce thrust. Plasma density and exhaust velocity, V_e, determine the actual cross section, A, of the reactor. Small gyration radii reduce the volume of plasma taken by spiraling charges, and the more intense the $\vec{B}$ field, the more manageable the size of a MCR.

Magnetic fields of order 1–10 T are feasible with conventional electromagnets, but copper coils are heavy, take space, and need cooling. Until the so-called superconducting wires became commercially available (Dew-Hughes 2001), imposing $\vec{B} \approx 1$ T in a sizeable volume was very expensive. Superconducting cables can carry current densities about three orders of magnitude higher compared to copper ($\approx 10^3$ A/mm^2) with practically no electric resistance at all, and thus no ohmic power losses, but do require cryo-cooling to maintain superconductivity. Superconducting cables power the giant magnets enabling particle accelerators and fusion ignition experiments worldwide.

Much superconducting technology is based on the so-called low-temperature superconductors (LTSC), made of alloys such as Nb_3Ti. They are kept at ≈20 K by liquid helium cooling. The LTSC wires in fusion tokamak are hosted inside stainless steel jackets, thermally insulated and drenched in circulating liquid helium. As an added precaution to avoid destructive damage, a thick copper sheath surrounds the insulation. Its purpose is to carry the high current normally transported by the superconducting wires should the LTSC material suddenly lose its superconducting properties.

This type of construction means also expensive, large, and massive cables, unsuitable for space applications. The realistic alternative is high-temperature superconducting (HTSC) materials, capable of staying superconducting at or above the temperature of liquid nitrogen, 77.4 K, rather than that of liquid He, (about 4 K). These materials (e.g., YBCO, MgB_2, and others) are more fragile than LTSC, but are more practical and they are moving toward commercialization. They can carry almost the same current density of LTSC, but with far less demanding cryogenic technology (Casali and Bruno 2004). With HTSC technology, magnetic fields are practically limited only by the Meissner effect, the maximum $\vec{B}$ intensity that the superconductor can tolerate before losing its SC properties. In practice, up to 10–15 T are feasible with HTSC. Superconductivity can shrink and lighten the tokamak.

A more recent MCR concept from the 1970s, the spheromak (Jarboe 1994; El-Guebaly 2010), see Fig. 8.18, compacts the toroidal topology into a sphere-like surface (spheroid). In spheromak, the magnetic field is generated by the plasma currents themselves. Poloidal and toroidal fields are approximately of equal strength since spheromak plasma creates its own toroidal $\vec{B}$ field. Note that its symmetry axis is coinciding with that of the spheroid. The mechanism of plasma generation is that of the turbulent dynamo. This concept is similar, as far as it is known, to the mechanism responsible for the terrestrial magnetic field. The magneto-hydro-dynamic regime of plasma in all MCF reactors is turbulent. However, in spheromak confinement, sustained fusion was found more sensitive to turbulence than in the tokamak. For this reason, interest in spheromak waxed and waned, but this machine has been reinvestigated at the Lawrence Livermore National Laboratories in their Sustained Spheromak Physics Experiment (SSPX), at the ENEA Laboratories in Italy (Alladio et al. 2000), and elsewhere. For space propulsion, its appeal is compactness when compared to that of the tokamak. A propulsion system based on the spheromak was indeed proposed (Williams et al. 1998).

The most recent MCF machine is the compact fusion reactor (CFR) being built at Lockheed Martin (Norris 2014; Mehta 2016). According to company information (Rickard Hedden 2014; McGuire 2007), in 2–3 years, this experimental reactor should result in a prototype burning D–T fuel and capable of producing 100 MW in a 6 m · 12 m package. The novelty of CFR is the magnetic field topology, deliberately simplified by Lockheed-Martin in the schematic of Fig. 8.19. Superconducting multiple coil geometry creates high intensity $\vec{B}$ cusps and should eventually raise β much closer to unity than in the conventional tokamak. As a consequence the plasma should be much denser, confined in a volume estimated by Lockheed Martin ten times smaller than in the tokamak. The thickness of the neutron absorbing blanket should stay the same compared to the larger tokamak, but the reduced size of the reactor should result in a much more compact machine, with reduced development and recurring costs.

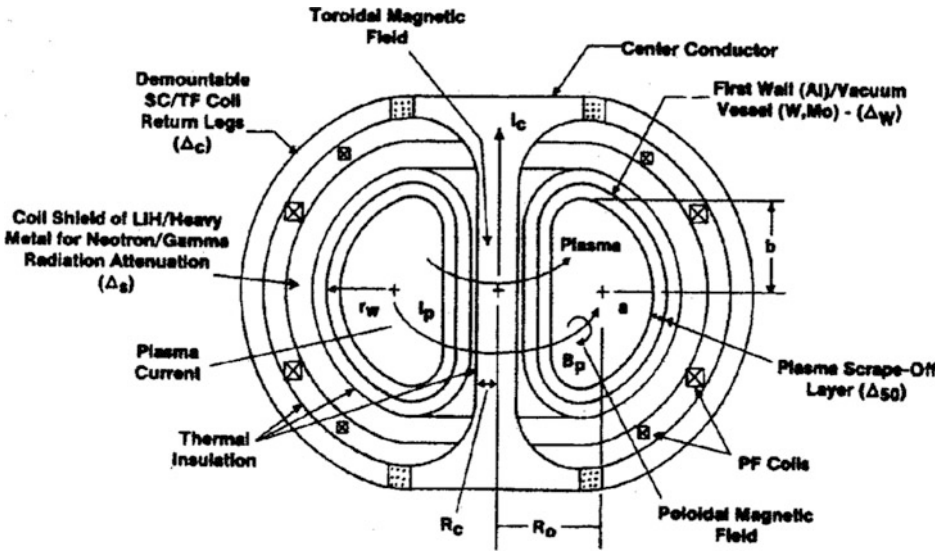

Fig. 8.18 Schematic of an advanced (spherical torus) tokamak reactor (spheromak) showing first wall and thermal blanket. As depicted, the spheromak can generate energy but not thrust

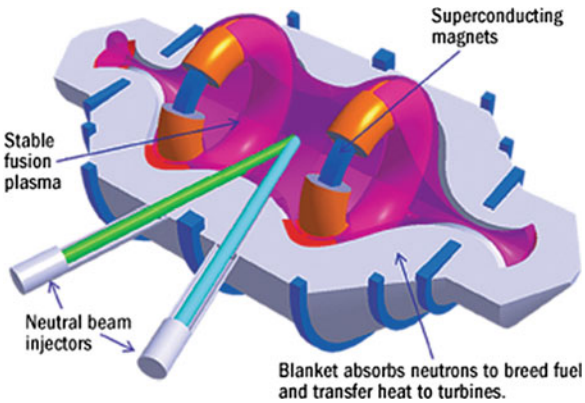

Fig. 8.19 Artist's view of the MCF compact reactor investigated by Lockheed-Martin (Rickard Hedden 2014)

8.10 Mirror Magnetic Confinement Rockets (Mirror MCR)

At the beginning of fusion research, plasma was confined between two symmetrical high $\vec{B}$ regions (the "bottle"). In between these two regions, diverging $\vec{B}$ field lines shape a sort of magnetic "sausage" pinched at the two ends by stronger $\vec{B}$ fields, see Fig. B.6. Plasma particles spiral along the $\vec{B}$ field lines, moving either way toward the two ends depending on charge. Under the right conditions, in their back and forth motion they periodically convert translation to spin (gyration) energy. Ideally, they should reach either end with very high gyration frequency and no translational energy at all, thus preventing their escape. It is the zero-translation condition at either end that forces particles to turn back. In this type of reactor, the two high $\vec{B}$ end regions act as "mirrors" reflecting charged particles. By properly shaping the $\vec{B}$ field, plasma can be confined long enough to absorb energy injected from the outside and to ignite. Once ignited, feeding the reactor with fuel will keep it working steadily.

This simple picture is actually far richer in detail. For instance, electrons are lighter than ions and tend to leak at both mirror ends. The ratio between the low and the high $\vec{B}$ in the "sausage" is critical and must be kept above a certain value. Plasma turbulence disrupts ion motion and much more, see Appendix B. A comprehensive review of mirror fusion devices and their features can be found in (Post 1987). This review is three decades old because interest in this approach has not been as great as that in the tokamak and other concepts. Nevertheless, this seems to be the most practical reactor for rocket propulsion.

A mirror MC reactor becomes a *fusion rocket* by "leaking" plasma from one of the mirror ends and letting it escape and accelerate in a magnetic nozzle, see Fig. 8.20. In other words, $\vec{B}$ must be made asymmetrical. Then, if the plasma residence time allows the fuel enough time to fuse,

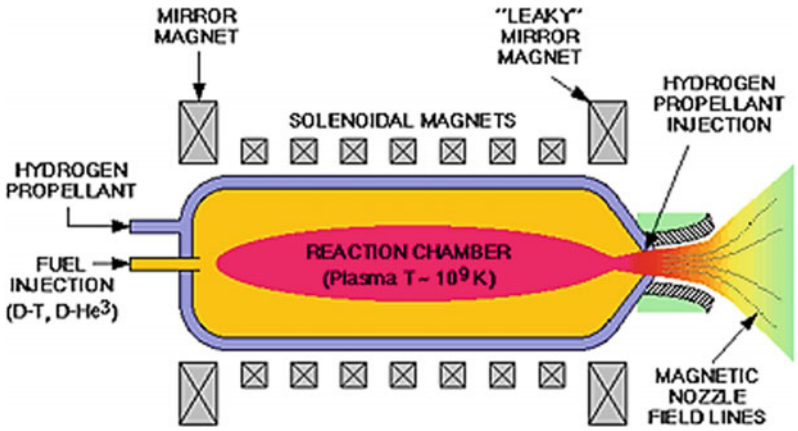

Fig. 8.20 Schematic illustration of a cylindrical geometry mirror magnetic confinement rocket (*MCR*)

by adjusting $\vec{B}$ at one end, the plasma can escape at a controlled rate with all its kinetic energy and momentum to produce thrust. Inert propellant may be added to increase thrust, but not inside the reactor because of quenching. Inert matter must be injected just upstream or inside a magnetic nozzle.

The $\vec{B}$ field in a properly designed magnetic nozzle confines and guides the plasma just as solid walls confine hot gas in a conventional rocket nozzle. There is, however, a major difference. The plasma particle gyration velocity must be converted to axial velocity since the tangential velocity component does not produce thrust. Efficient conversion is one of the issues in designing magnetic nozzles.

This schematic description suggests mirror MCR may become the core of steady thermal fusion propulsion, where fusion products (ionized He, but also D, T, and H not fused, and electrons) are the sole propellants, see (Carpenter and Brennan 1999).

Figure 8.5 shows that I_{sp} can reach 10^5–10^6 m/s, higher than with nuclear thermal fission or some NEP concepts. A mirror fusion thruster is similar to a chemical rocket engine, with combustion of propellants replaced by thermonuclear burning of D and T. The analogy with air-breathing propulsion has motivated investigations of combined MHD airbreathing and fusion propulsion for atmospheric flight (Murthy and Froning 1991; Froning et al. 2005). As already discussed, thrust from direct thermal propulsion may be modest, thus the problems posed by interstellar or QI travel in Sects. 8.1–8.5 are still unsolved. The much larger I_{sp} possible with fusion rockets implies that any acceleration to shorten missions will demand large thrust and even larger power. For instance, supporting 50 t thrust (≈500 kN) at $I_{sp} = 10^6$ m/s requires a 500 GW reactor. Since plasma density is orders of magnitude lower than in chemical rockets, high I_{sp} and high thrust MCR engines should be enormous. Nevertheless, their inherent simplicity is appealing to many fusion specialists who think it is the natural way of converting fusion power to propulsion. Analysis of OMC (open magnetic confinement) theory, issues, and work in progress is the subject of Appendix B.

8.10.1 Tokamak MCF Rockets

After the magnetic bottle, the next stage of *power* fusion research took place in the 1960s and focused on curing the unwanted "leaking" plasma problem at the two mirror ends. As mentioned, the plasma "sausage" was morphed into a donut or torus in which $\vec{B}$ has two components: One toroidal component where its field lines are following the torus walls, and one poloidal component, where the field is "wrapping" them variable in time. This is the tokamak in Figs. 8.21 and 8.22.

The tokamak configuration is currently being experimented with in most fusion research centers and by the ITER consortium (Anon. 2014b). However, pure tokamak does not lend themselves to propulsion, since their topology is closed. The tokamak was conceived for power generation. Nevertheless, just as in mirror MCF machines, a high-energy plasma jet might be allowed to escape without quenching taking place in the reactor, for instance, from the region near the axis of the torus. This concept becomes the reverse field configuration (RFC) rocket described later.

Alternatively, products might be ejected via a duct *tangential* to the tokamak torus called a "divertor," see Fig. 8.23. Dr. Robert Bussard was the first to propose this solution (Bussard 1990). Both architectures are problematic, since plasma needs to simultaneously stay confined and escape, all this at a controlled rate and while being ignited and fusing.

A cross section of an advanced tokamak reactor with similar poloidal and toroidal dimensions (that is, a spheromak) has been shown before in Fig. 8.18. It shows the plasma current and its direction, with the imposed poloidal and toroidal $\vec{B}$ fields. These two fields complement each other, in the sense that a purely toroidal field would not by itself confine plasma, as drift currents would separate ions

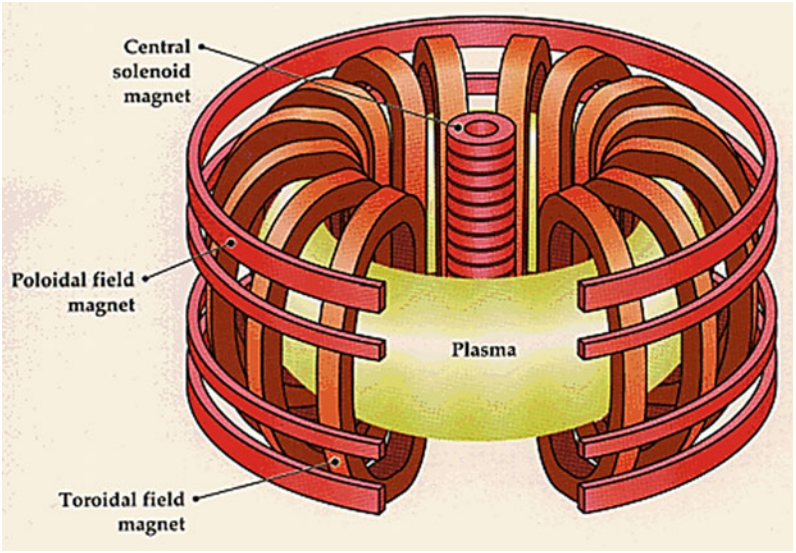

Fig. 8.21 Tokamak coils produce the poloidal and toroidal magnetic fields

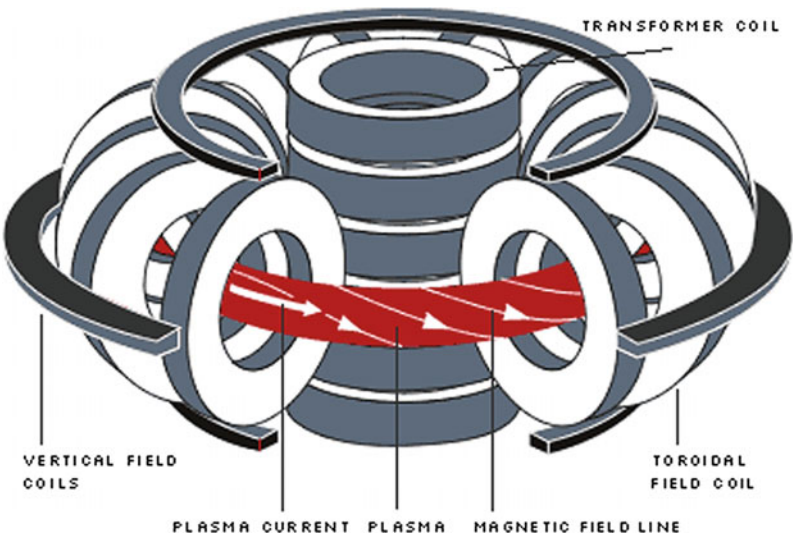

Fig. 8.22 Three external $\vec{B}$ fields and the field induced by plasma currents guide and confine the plasma in the tokamak

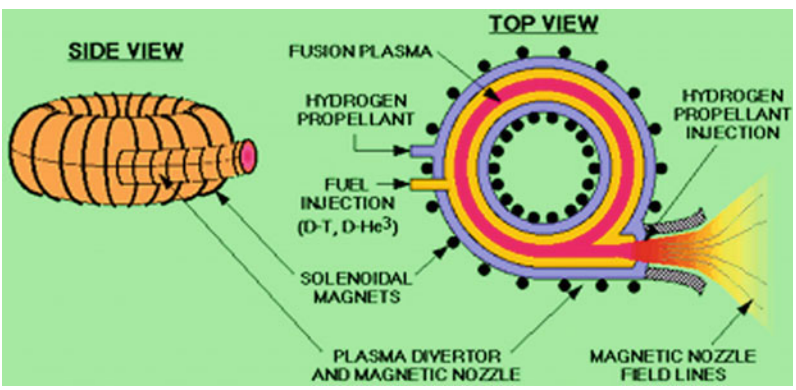

Fig. 8.23 Schematic view of a "donut"-shaped geometry plasma divertor to produce thrust from tokamak

from electrons, thereby creating de facto an unwelcome electric field. The poloidal field opposes this separation effect and allows plasma to be reasonably well confined. The same figure shows also the so-called first wall of the confinement structure, that is, the structure enclosing plasma and separating it from the coolant blanket. This last is the volume occupied by molten lithium that cools and at the same time absorbs the high-energy neutrons breeding tritium. The blanket is followed by the radiation shield and the magnets. Thermal energy extracted from the blanket can produce electric power through conventional thermodynamic cycles.

Together with other minor factors, it is tokamak fuel kinetics that determines the fraction of fusion energy released as kinetic energy usable as thrust, and that in the undesirable form of radiation. Among the many technical issues associated with fusion propulsion, that of radiation and its shielding occupies a special place. Neutrons produced by D–T fusion are indispensable to convert the liquid lithium coolant blanket behind the first wall into tritium necessary to drive reactions (2), (4), or (5a) in Fig. 8.15. Burning D–T releases most of the energy inside the lithium blanket in the form of fast neutrons; their flux of kinetic energy is of order MW/m^2. At the same time, this flux tends to damage structural materials and is deadly if not shielded, see Appendix A. The task of shielding is to slow down and stop *unwanted* neutrons, those that are not stopped by the mechanisms are forming tritium inside the blanket.

Any particle emitted by nuclear processes, but especially neutrons and gamma photons, carries enough energy to penetrate solid material and dislodge atoms from their crystal lattices. With respect to fission, fusion kinetics produces neutrons with higher average energies, see Fig. 8.15. Some of these interact with matter forming He or H atoms inside microcrystalline lattices and embrittling the material. This was the reason for the limited life of fission reactors tested in the 1960s and 1970s. The effect of high-energy neutrons on stainless steel used for the first wall is to reduce ductility to about 1% of the original after two years (Kulcinski and Conn 1974). This occurs because inside steel radiation forms about 1,000 atoms of helium and hydrogen per million structural atoms. Correspondingly, conventional stainless steel tends to swell by about 7–9%, if untreated. Apparently, cold working steel tends to reduce swelling to below 1%, but these numbers remain worrysome and the target of structural and material research.

Shielding technology has continuously been improved. There are promising and light materials based on C/C (carbon/carbon) composites, for instance, but experience with them is still scarce. Traditional shielding still must rely on interposing sufficient matter (in terms of thickness and/or density) to stop radiation. This adds bulk and mass to fusion engines and does not prevent radiation damage to the shield itself. Figure 8.24 shows, from left to right and to scale, the layers of matter interposed between the hot plasma and the reactor external wall (Kulcinski and Conn 1974). Although dated, this layered structure is representative of MCR designs. It may be divided into three main zones: (1) the inner torus confining plasma, (2) the blanket, and (3) the shield. Magnetic coils shape the $\vec{B}$ field permeating the torus and keep plasma about 50 cm away from the first wall that in this example is made of 0.4 cm thick stainless steel. Ideally, nothing should exist between the edge of plasma and the first wall. Beyond the wall is the lithium blanket and its recirculating lithium system, extracting most of the neutron's energy as a hot lithium flow. Note that lithium corrodes metals. Tritium is bred by neutrons deposited inside the lithium blanket and is extracted (in this particular scheme) by two independent circuits, so that one may be closed while the second is in service. A thermal insulation vacuum gap separates the blanket from the shield, made of boron carbide and lead. The carbide slows down and thermalizes neutrons that have not been stopped by the blanket, while lead absorbs gamma rays. In this design, helium is used to cool the shield assembly. A final vacuum gap insulates the reactor from the low-temperature superconducting magnet. The shield concept shown was designed for a 5 GW_{th} tokamak.

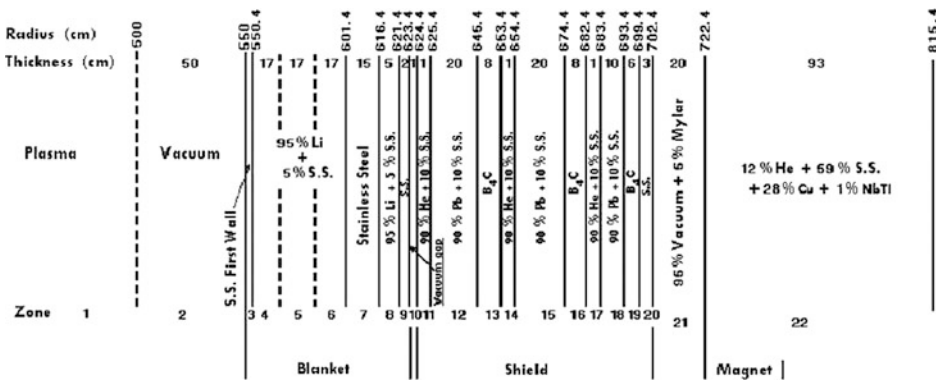

Fig. 8.24 Schematics of a shield system for a tokamak reactor, including the lithium cooling system necessary to tritium breeding, adapted from (Kulcinski and Conn 1974)

Overall, the blanket plus shield structure is about 172 cm thick, and it may weigh in large tokamaks $\approx 10^4$ t.

A way around the radiation problem is to look for a fusion kinetics that does not release neutrons, the particles which are more difficult to stop and thermalize. Protons carry the same average momentum as neutrons, but because they are ionized they can be stopped by matter (or by an external electromagnetic field) far more easily and require much less shielding mass. It was already noted that "aneutronic" kinetics yields less energy than D–T, see Fig. 8.15, and its ignition temperature is ten times higher.

The cooling system integral to a tokamak for power generation constitutes also the heat exchanger extracting the fusion energy deposited in the coolant by high-energy particles and thermalized as heat. In fusion propulsion systems which are producing the electricity to power electric thrusters, direct conversion systems are sought that could be more efficient and compact than thermodynamic conversion machinery based on Rankine, Brayton, or Stirling cycles.

8.10.2 Comparing Thermal and Electric MCF Rockets

Description and operation of mirror MCF reactors suggest them as the core of *thermal* rockets. The closed topology of the tokamak lends itself to power *electric* thrusters. Just as outlined in Chap. 7, a propulsion system constituted by separate energy and thrust generators does have merits, the main being that each component may be optimized to some extent independently. The drawback of electric fusion propulsion is machinery for energy conversion and the radiator. Thermal energy must be converted into electricity, and at the current state of technology this may be done in the simplest way only via a low efficiency thermodynamic cycle. A sequence of two cycles (Brayton and Rankine, for instance) may increase conversion efficiency by a few percentage points, but combined power generation further complicates an already complex conversion scheme. In the end, the efficiency of conventional cycles may reach at most 50%. The remaining thermal energy may be partly converted for other tasks (radar, laser telecommunications, and cryogenics are the ones that come to mind), but the greatest fraction would have to be rejected to the "cold" or "bottom" sink. That means a space radiator is adding to the total spacecraft mass. Space radiators weigh 0.02–0.8 kg/kW of heat dissipated, depending on technology. At an optimistic 0.1 kg/kW, radiator mass is about 100 t per gigawatt of thermal power.

The electric power extracted feeds magneto-plasma-dynamic or ion thrusters capable of I_{sp} in the 10^4–10^5 m/s ten or twenty years from now. MPD rockets have higher thrust per unit area than ion thrusters, but their I_{sp} is lower, see Chap. 7. Combining MCF reactors and MPD rockets will result in a massive propulsion system. Power switching and conditioning for GW-class thruster clusters operated at high currents or high voltage, or both, would certainly be an extraordinary technology challenge. Even when spreading power across engine clusters, mass and bulk would remain problematic. It is possible that fusion-powered electric thrusters, as conceived now, may never be a workable propulsion system.

This said, *direct conversion* (i.e., not based on thermodynamic cycles) is a technology with potential impact on these considerations. Direct conversion has a relatively short history and has been limited to very low-power (<1 kW) applications. The RTG (radioisotope thermoelectric generator), built for the Galileo and Cassini missions, exploits the emission of charged particles from high-temperature solid materials to produce electrical power. The appeal of RTG is that they have no moving parts, but their efficiency is even less than thermodynamic conversion, in the 5–15% range at the very best. Historically, the most investigated type of direct conversion was based on magnetohydrodynamics (MHD), a technology developed and tested for more than 20 years in the EU, the Soviet Union and the US (Messerle 1995). It consists of flowing a hot ionized gas in a duct crossed by a magnetic field $\vec{B}$. If the $\vec{B}$ vector is normal to the gas velocity $\vec{u}$, an electric field $\vec{E}$ normal to both is generated by the motion of ions, and energy can be extracted by the voltage difference. This class of generators is the exact reverse of MPD electric thrusters described in Chap. 7. MPD thrusters apply external $\vec{E}$ and $\vec{B}$ fields that create an accelerating Lorentz force $\vec{F}$. In MHD generation, slowing down $\vec{u}$ in a field $\vec{B}$ creates an electric field $\vec{E}$ and thus a voltage.

MHD generators are inherently suited to extract energy from fusion, in that fusion products move at high speed and are ionized. Any fusion kinetics producing few or no neutrons, e.g., reactions (6), (8) or (9) in Fig. 8.15, would be ideal in this context. Handling such energetic particles in an MHD generator would pose enormous problems, but energy extraction would, in principle, be much more efficient than based on thermodynamic cycles or thermionics. Industrial MHD generation was abandoned in the mid-1980s, mainly because of the difficult engineering problems posed by working with high-temperature ionized gas. At the time, this gas was the particle-laden exhaust of coal burners, at temperatures of order 1800 K. Since spontaneous ionization at this temperature was negligible (ionizing air nitrogen needs about 15 eV), the coal combustion products were seeded with alkaline metals (K, Ba, or Na) that ionize at energies of order 3–4 eV. These metals are extremely corrosive and damaged MHD duct sections very rapidly.

Revisiting this technology is probably mandatory for direct conversion of heat into electricity. In fusion propulsion, the problem is not ionization but it is the high plasma energy, see (Adams et al. 2003).

A different method, based on solid state electrolytes, reaches 25% efficiency but has been tested so far at no more than a few tens of kW. This is the AMTEC technology described in Sect. 7.18. It could become a viable option if scalable to the thermal power of fusion reactors. Consequently, a tokamak reactor is naturally suited for *electric* fusion propulsion.

Are there new ideas in direct energy conversion? These ideas are, however, mostly at the stage of just ideas. For instance, interesting work has been carried on since the 1980s in converting energy from radioactive decay of radio-nuclides producing alpha and beta particles into electricity (Brown 1989). This may seem identical to RTG, where the energy of alphas and betas is thermalized and the heat released produces electrons; in fact, this is not so. This novel concept is based on the fact that the energy of particles, emitted by radio-nuclides, also includes that of the electromagnetic field they generate due to their charge and motion. The fraction of energy in the form of the electromagnetic field is much greater compared to that present as kinetic energy captured by RTG. Time will tell whether this concept can be scaled up and engineered. Success in this area hinges on the chances of fusion propulsion to be investigated with significant resources. At the moment, these are slight, but continuing interest by Japan in the GAMMA-10 mirror machine (at the Tsukuba research center), by Russia in the GOL-3 gas-dynamic mirror reactor at Novosibirsk, and by ESA, e.g., see (Romanelli and Bruno 2005), may be positive signs. Impulsive thrust as in the case of Project Orion and Project Daedalus may completely bypass thermodynamic conversion. However, whilst thrust produced may be large, so seems to be the magnetic nozzle to capture it (Adams et al. 2003; Polsgrove et al. 2010).

To conclude this section, at the stage of our knowledge today, substantial work is needed to decide on a strategy to convert MCF energy into thrust. An educated guess is that although *electric* fusion propulsion is probably the only way to convert MCF power to thrust, low energy/unit volume, still bulk, and mass are too large to be adapted to space propulsion. This preliminary conclusion is quantified later in Sect. 8.13.

8.11 Inertial Confinement Fusion

This strategy for confining and fusing plasma was proposed about ten years after the beginning of US and Russian fusion research (Basov and Krokhin 1964). Two factors contributed to start work on inertial confinement: the realization that MCR presented problems more difficult than initially thought, and the availability of pulsed lasers in the GW-class. This second factor suggested the possibility of igniting fusion reactions with power bursts. Note that the Lawson condition for ignition, Eq. (8.34), is a steady-state energy balance linking plasma particle density n to confinement time τ. Density in MCR must be low, least the plasma becomes collisional and the magnetic field ineffective. Accordingly, the beta factor in a tokamak is also low, of order 5%. Inevitably, the only way to compensate for low n is to heat the plasma to higher temperatures and for longer time τ. During this time, plasma instabilities, radiation losses, and other factors tend to reduce substantially the effective amount of heating that the plasma can theoretically absorb. On the $n - \tau$ plane, the MCR strategy occupies the rightmost end of the hyperbola.

In inertial confinement fusion (ICF), these problems may be bypassed by striking a solid fuel pellet (not plasma) with high-power lasers. Interaction between electromagnetic energy and matter involves two fundamental areas of physics and has been investigated since the laser has been invented. This interaction ensures not only heating but also compression. The pellet may be frozen D–T fuel encapsulated in a metal and/or polymeric case. Proponents of inertial confinement fusion envisaged a cluster of lasers (e.g., the Los Alamos "SHIVA" laser assembly, now at the National Ignition Facility at the US Lawrence Livermore National Laboratory), simultaneously delivering an energy pulse to a single fuel pellet from many directions. Figure 8.25 positions the NIF capability in the ranges of temperature and density occurring in natural environment or phenomena. What is missing in Fig. 8.25 is event or experiment duration, but the chart gives an idea of progress made in this type of confinement.

At the US National Ignition Facility, energy of order 2 MJ can be deposited by 192 lasers firing simultaneously for 10^{-10}–10^{-9} s, corresponding to an instantaneous power of 450 TW (1 TW = 1 Terawatt = 10^3 GW = 10^6 MW). The energy deposited ablates the surface, creating a quasi-spherically symmetric high-speed jet that compresses the pellet uniformly (NAP Report 2003; Chap. 4). As the pellet implodes, it reaches the density required for fusion ignition on a timescale of order 10^1 ps, more than a billion times shorter than the ≈1 s confinement time of tokamak (Daiber et al. 1966; Nakai and Mima 2007). Theoretically, there should be hardly any time for plasma instabilities and other unwanted effects to develop and prevent ignition. Unlike MCF, ICF heating is totally unsteady, but a mental picture of this strategy still based on the $n{\cdot}\tau$ scaling of Eq. (8.35) would indicate it occupies the *leftmost end* of the hyperbola. A graphic of the ICF is shown in Fig. 8.26. Features of pulsed lasers are in (Huba 2016).

In the simplest ICF rocket concept, a stream of fuel pellets is injected inside the fusion chamber and fused by laser(s) one

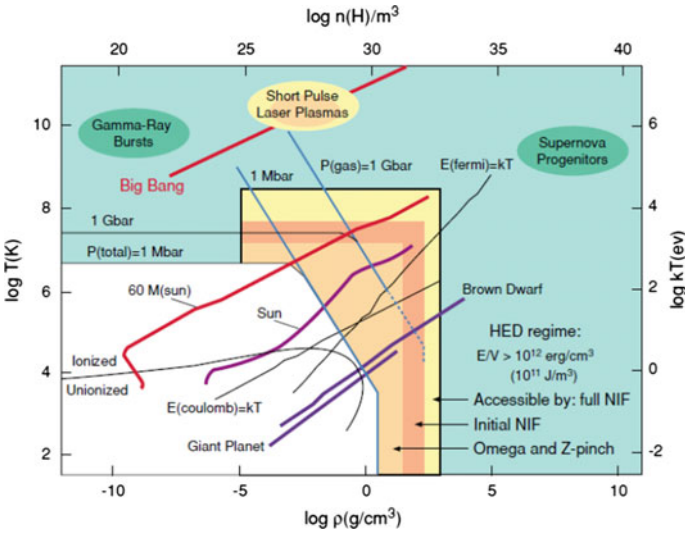

Fig. 8.25 Temperature and density realizable in the US NIF (*light rectangles*) compared to those in nature (*Courtesy* LLNL)

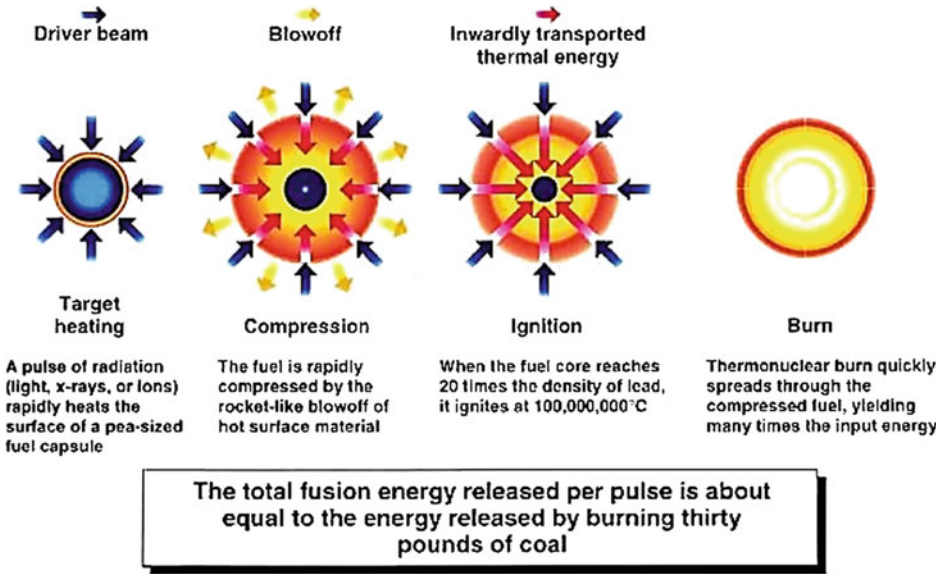

Fig. 8.26 Schematic sequence of events in inertial confinement fusion of a fuel pellet struck by multiple laser beams (*Courtesy* Virtual National Laboratory)

by one. The hot plasma expands in a nozzle and produces thrust. How much thrust is produced depends on the mass fused, that is, on the pellet injection repetition rate. The nozzle should be a magnetic nozzle, where an external magnetic field not only limits the heat transferred from the plasma to the nozzle, but also guides and accelerates it. Figure 8.27 shows a notional ICF rocket using multiple laser beams.

To predict ignition conditions in ICF reactors, the steady state Lawson's criterion cannot be applied, since the ICF process is deliberately *unsteady*. The correct criterion must be based on characteristic times. In (Kammash 1995, p. 17), this criterion can be cast in simple terms by introducing just two characteristic times, $t_d = R/c_s$, the destruction time of a pellet of radius R by pressure waves generated by the laser pulse in the fuel plasma, traveling at plasma sound speed, c_s, and the time t_b for fuel burning (fusing). The time for fuel burning t_b may be estimated by imposing that the burning rate of plasma scales as in all collision processes, that is, $\approx(\rho/m_i)/t_b$, the number density per unit time. This burn rate must be proportional to the collision cross section among plasma particles. Here ρ is the plasma density and m_i is the mass of the plasma ion, He^{++}, T^+, D^+, or H^+. In essence, t_d is a residence or transport time, and t_b is a kinetic time.

The ratio f_b between these two times

$$f_b = \frac{t_d}{t_b} \tag{8.40}$$

is a measure of the fuel burn fraction. If $f_b < 1$, during the pellet implosion the pressure wave travels too fast and destroys the pellet *before* fuel ignites. For fusion to occur, burn time should be much faster than destruction time, requiring $f_b >> 1$. By expressing sound speed and collision

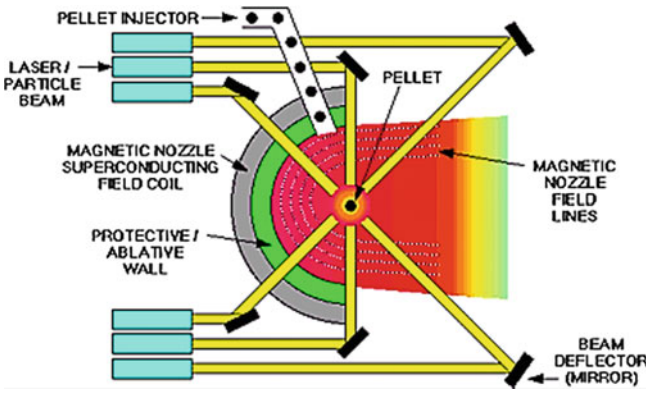

Fig. 8.27 Conceptual scheme of an inertial confinement fusion (*ICF*) rocket and its magnetic nozzle

cross section as a function of temperature, it can be shown that the burn fraction is essentially proportional to the product $\rho \cdot R$:

$$f_b \propto \rho \cdot R \tag{8.41}$$

To an order of magnitude, this scaling is also the simplest condition ensuring high efficiency of inertial fusion ignition and can be written (in the c.g.s. units still preferred by physicists) as

$$\rho \cdot R \gg 1 \left(\frac{\mathrm{g}}{\mathrm{cm}^2}, \text{ a surface density}\right) \tag{8.42}$$

The meaning of Eq. (8.42) is that for fusion to occur, the energy deposited on the fuel pellet surface must compress the pellet and densify it to the point that the strong nuclear force can overcome Coulombic repulsion among D and T protons. What matters is the density of the thin surface layer where energy is deposited, not the bulk pellet density. Consequently, the smaller the pellet, the higher the density ρ that must be reached.

One may conclude that by using large enough pellets, fusion will start without any problem. In fact, raising R does not automatically ensure the right density. Bigger pellets need more energy and larger lasers to achieve the same energy per unit area. Consequently, the ICF ignition condition of Eq. (8.42) hints obliquely at the energy budget. The net energy available from ICF will be that released by fusion *minus* that used up by the laser beams to compress the pellet. Their ratio Q is the "gain" of ICF systems, and a major subject of investigation in inertial fusion.

By further manipulating the expression for $\rho \cdot R$, it is possible to recast it in terms of the n and τ appearing in the Lawson's criterion for magnetic confinement, obtaining for ICF ignition the condition

$$n \cdot \tau \approx \frac{\rho \cdot R}{m_i \cdot c_s} \left(\frac{\mathrm{s}}{\mathrm{cm}^3}\right) \tag{8.43}$$

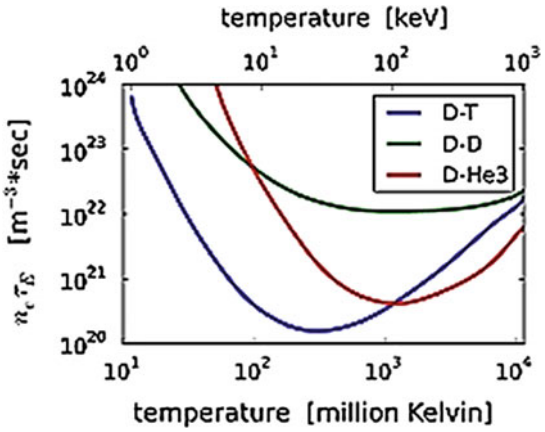

Fig. 8.28 Minimum value of the $n \cdot \tau$ product as a function of temperature and fusion fuel combinations (*Courtesy* Wikipedia)

Figure 8.28 shows the dependence of the $n \cdot \tau$ product on temperature for reactions (1)–(3) in Fig. 8.15.

If we assume $\rho \cdot R = 3$ g/cm^2, a numerical value considered adequate by the ICF community for D–T fuel, Eq. (8.43) becomes numerically

$$n \cdot \tau \approx 1.5 \cdot 10^{20} \left(\frac{\mathrm{s}}{\mathrm{cm}^3}\right) \tag{8.44}$$

Comparing the breakeven/ignition criteria for MCF and for ICF, the second appears ten times harder to meet. This is not completely true, since MCR systems barely meet the Lawson criterion and burn less fuel than ICF systems under these same critical conditions. The theoretical advantage of ICF over MCF is actually that ICF does not need externally applied magnetic fields. This fact makes it attractive for propulsion, because ideally it does away with large magnets, superconducting or not, and their associated mass and complexity. On the other hand, ICF propulsion needs very large and powerful laser or particle beam facilities. These tend to be bulky and massive. Even so, ICF is considered an alternative to MCR-based propulsion systems.

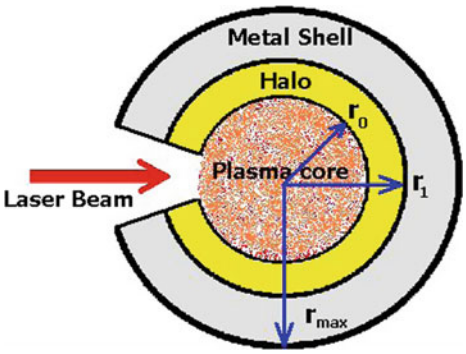

Fig. 8.29 Cross section of a fuel pellet inside its metal casing (not to scale)

ICF, based on energy deposition on the external pellet surface, evolved to injecting a single laser through a hole reaching to the hollow center of the fuel pellet. Compression still occurs via ablation, but this takes place on the inside surface, see Fig. 8.29.

In addition, plasma generated by the single laser pulse forms its own magnetic field in a time of the order of tens of picoseconds. Accordingly, Maxwell equations predict $\vec{B}$ should be sufficiently intense to confine plasma, provided energy losses are moderate (ICF losses are mostly due to conduction electrons carrying away thermal energy from the extremely dense plasma). Besides the short timescale, the other key difference between ICF and MCF is the much smaller spatial scale, of the order of the pellet size (≈1 mm). Impulsive confinement prevents the just forming plasma from bursting immediately through the pellet case. In fact, this strategy could be classified among the many variants of magnetic inertial confinement fusion (MICF).

Partly reverting to the original ICF concept, compression of the fuel pellet in the US NIF (National Ignition Facility) was planned by surrounding it with simultaneously firing laser beams, see Fig. 8.30. The frozen D–T fuel is deposited as a thin layer inside a 2.2 mm diameter metal capsule. This capsule is suspended in a hohlraum (a small cylindrical case) open at both ends to allow laser beams to enter. As tested in 2013–2014, nominal power and energy per shot were 500 TW and 1.8 MJ, respectively, ensuring the Lawson criterion to be met by a factor two in density and containment time and thus, within ample margins, ignition. When lasers fire at the inner wall of the hohlraum, it reaches instantaneous temperatures high enough to emit X-rays in all directions. This X-ray bath ablates the case metal, and this compresses adiabatically both, the capsule and fuel. Theoretically, fuel should reach ≈300 eV (100 MK), at the same time densify by a factor >> 10^3, and consequently ignite. This approach to inertial fusion is based on US weapon work from the 1970s and 1980s to produce X-ray lasers.

In fact, after delays due to using the NIF for the Stockpile Stewardship Program (Anon. 2015b), the NIF testing campaign showed a gain $Q \approx 3$. This should have ensured ignition, but plasma losses due to Rayleigh-Taylor instability increased just as much. The losses were due to Rayleigh-Taylor waves mixing the ablating metal of the capsule with the inner fuel layer during the compression/ablation phase, and therefore interfering with fusion kinetics and radiation. These waves were found to grow with the square root of ablation acceleration. Thus, while fast ablation ensures fast compression, at the same time it destabilizes it by distorting the shape of the pellet surface and "scrambling" together metal and fuel. In practice, the NIF was still a factor ≈3 short of achieving the Lawson criterion. Improving the NIF is being planned (Kramer 2015).

Fast ignition of pellets has also been proposed by hitting with a high-energy laser a fuel pellet coated with a deuteron D^+ rich material. Interaction between laser and D^+ coating forms a D^+ beam entering the pellet and triggering ignition. Calculations indicate that if the fuel pellet has already been sufficiently laser-compressed, ignition should be easier, require less energy, and result in higher gain. The advantage of this two-stage technique is that it does not need radially symmetrical compression by a laser cluster. A review of the physics leading to this concept is in (Miley et al. 2010), where theory predicts gains of up to 10^3. This was applied in the US Lawrence Livermore Laboratory designed VISTA spacecraft for exploring the Solar System (Orth 2003); the concept is described later.

Another variant of ICF, specifically proposed for application to propulsion, replaces laser beams with plasma guns (Adams et al. 2003). In this concept, the fuel is D

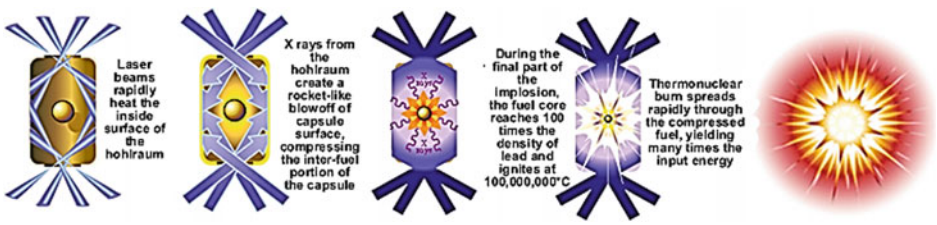

Fig. 8.30 Schematic view of inertial "indirect drive" fusion (*Courtesy* of Lawrence Livermore National Laboratory)

(Deuterium), which is much more abundant and thus available compared to T (Tritium). However, because of the high activation energy of the D–D reaction, ignition is triggered by D–T pellets. Each D–T pellet is the focus of 48 plasma guns, each simultaneously firing a slug composed of two D and H slugs in tandem. Ideally, the instantaneous structure of the new pellet formed by the impact of the two slugs should be composed of the D–T core, a thicker D layer, and a much thicker H skin. In this concept, fusion is triggered by the ignition of the D–T core, but the main fuel and fusion reaction is D–D. The role of hydrogen is to add unreacting mass and augment thrust. This ICF variant hinges on the feasibility of forming pellets with the structure just described, which still requires an assembly of plasma guns, fewer than the lasers in the NIF, but still bulky and complex. As in all fusion concepts, the ^{4}He produced is too energetic to be expanded in a conventional nozzle. In its place, there must be instead a magnetic nozzle (see later). The example in (Adams et al. 2003) shows the capability of this fusion propulsion concept in a mission to Jupiter's moon Callisto. With 1 GW and $1/\alpha = 0.022$ kg/kW, the calculated $I_{sp} =$ 70,400 s and the thrust ≈3000 N predicted a 654-day round-trip mission was feasible. This was assumed to start in 2045 at a total gross weight of 650 t from the L_1 Lagrangian point (not LEO) and included a 30-day stay on Callisto's surface. The total consumption of D, T, and Hydrogen was 220 t. The massive spaceship could initially accelerate at $5 \cdot 10^{-4}$ g, increasing slightly to $7 \cdot 10^{-4}$ g at the end of the mission.

8.11.1 Fusion Ignition

Because the conditions allowing fusion are very restrictive, *nuclear catalysts* playing a role similar to what ordinary catalysts can do in chemistry have been proposed to lower ignition temperature. For instance, in D + D or D + T kinetics, theoretical predictions suggest muons as catalysts. Provided target density is sufficiently high, the presence of muons and their collisional interaction with the fuel increase the rate of fusion events (Takahashi and Yu 1998). Muons are produced by pion decay when p and p^- annihilate. Thus, a truly advanced, if speculative, fusion concept should consider combining ICF and antimatter kinetics in the same system (Gaidos et al. 1998). Also, laser microexplosions have been proposed to accelerate ignition. Igniting fusion presents the same challenges of igniting high explosives, solid rocket propellants, or fires. An energy barrier, whether quantitative (amount of energy) or qualitative (temperature), must be overcome, and the practical way to do so is an "ignition chain." Small explosions trigger bigger ones in sequence until the entire mass of reactants burns or detonates. In the solid boosters of space launchers, this chain comprises two or three rocket engines of increasing size, each igniting the next, the last and larger capable of starting uniform burning everywhere in the port of the main grain (Bruno 2014).

In fusion ignition, microexplosions, catalysts, annihilation, or even D–T may trigger much higher activation energy reactions such as D–D and eventually D–^{3}He. Controlling these high-energy processes is tricky (Shmatov 2000, 2004). The p–p^- annihilation reaction has been suggested as the "simplest" way to start ignition of ICF rockets (Shmatov 2005). An intriguing fluid dynamic ignition chain has been proposed by Winterberg (2014a, b). In this method, a conventional explosive shocks liquid hydrogen. The shock wave is made to converge forming a high pressure, transient superexplosive with energy in the keV range and capable of triggering reaction (8) in Fig. 8.15 between D and ^{6}Li.

8.12 Inertial Electrostatic Confinement (IEC) Fusion

Among the ICF concepts, this is one of the simplest and most esthetically appealing. Nevertheless, it has been investigated much less than MCF, probably due to its competition with the well-established US and ITER (International Thermonuclear Experimental Reactor) tokamak research programs and because its initial champion, Dr. Robert Bussard, passed away in 2007. This concept was originally proposed by R. L. Hirsch in 1967 (Hirsch 1967). It was later called "charged-particle-electric-discharge-engine" and more recently the "quiet energy discharge", or QED (Bussard 1990).

In the QED reactor concept, ionized D–T fuel is injected isotropically toward the center of a spherical wire mesh of radius r (the anode) kept at a potential −100 kV. The D–T ions accelerated by the Coulomb force travel toward the anode (the spherical mesh center) and are compressed by the density increasing as $1/r^3$, see Fig. 8.31. For sufficiently negative anode voltage, at some distance r from the center the fuel should satisfy the Lawson criterion and ignite. An apparent difficulty with engineering a QED reactor into an engine is how to collimate all isotropically emitted fusion products to obtain one-directional thrust. This concept was investigated also at the University of Illinois (Miley et al. 1995, 1998) and in Japan for application to a compact neutron source (Ohnishi et al. 1998). Bussard devised a range of applications for QED, from airbreathing engines to thermal rockets capable of QI missions (Bussard and Jameson 1995). They include the all regeneratively cooled

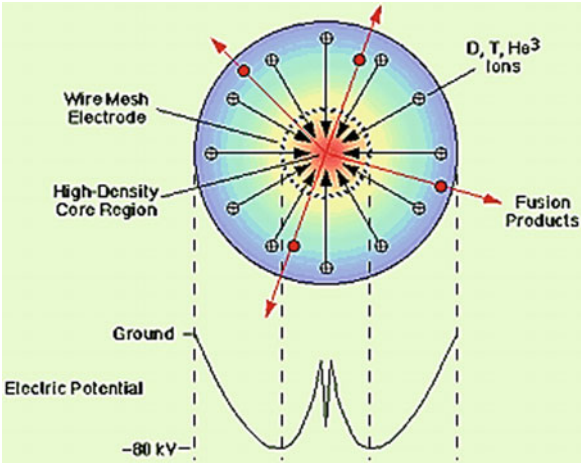

Fig. 8.31 Conceptual scheme of inertial confinement fusion (*ICF*) reactor. The *line* plot shows the electrostatic potential accelerating D^+ and T^+ radially inwards

(ARC) rocket where H_2, H_2O, or NH_3 propellant is heated by a fusion-driven relativistic electron beam, and a diluted fusion products (DFP) rocket where fusion products are mixed with a propellant to increase thrust. In both cases, the exhaust is passed through a magnetically-insulated nozzle. Estimating performance indicated I_{sp} of order 5000–8000 s and thrust of order 20–50 t ($\approx 2–5 \cdot 10^5$ N) were feasible for Mars conjunction missions, where H_2O propellant would reduce the LEO spacecraft mass to about 500 t, and transit time to 40–50 days. For QI missions, the I_{sp} in DFP mode was estimated up to 10^6 s with a correspondingly lower thrust ≈ 0.1 t ($\approx 10^3$ N).

In essence, this theoretical performance, three orders of magnitude better than any NEP system, is the result of assuming nearly total conversion of electron beam energy to very high-temperature plasma via the well-known exchange between electronic translational energy and propellant molecular (vibrational) degrees of freedom (Gorse et al. 1985). The ICF/QED reactor concept is attractive because a proof of principle demonstration should be feasible at the laboratory scale. Engineering the ARC or DPF fusion/propulsion system would be challenging, but the theoretical analysis of their physics was encouraging (Bussard and Jameson 1993; Bussard et al. 1993; Bussard and Jameson 1995; Miley et al. 1998; Froning and Bussard 1998). NASA-Marshall took note of QED and funded Froning and Bussard a single year (1997). Afterward, QED fusion could not find support from either US DOE or NIST (March 2004), and it is very doubtful any initiative dealing with propulsion application could be sustained before proving IEC is indeed feasible.

After 1997, ill health forced Dr. Bussard to reduce his research activity and to focus on publicizing his original ideas until he passed away in 2007. Research continued in the US at the University of Illinois, motivated by the fact that theoretically the reactor can be contained in a small volume, fuel density, and plasma temperature can be moderate (e.g., temperature needs to reach only about 100 eV rather than keV as in inertial confinement), and so are the bremsstrahlung losses and neutron fluxes. In principle, IEC could achieve ignition of the attractive aneutronic reaction $p^+–^{11}B$ fuel. The state of the art of this fusion strategy is described in (Miley and Krupakar Muraly 2014). Although promising and seemingly orders of magnitude less expensive than MCF or ICF, unresolved problems remain and IEC continues to be poorly funded.

8.13 MCF and ICF Fusion: A Comparison

In this section, the two fusion approaches that have received most attention and investments are compared. A logistic and cost issue in comparing merits of hypothetical MCF and ICF propulsion systems stems from the mass and bulk of a fusion-powered spacecraft to be orbited. In mirror MCF rockets, the plasma responsible for thrust is controlled by $\vec{B}$ fields, see Sect. 8.9. With $\vec{B}$ of the order of a few Tesla, the gyration radius is of order 1 cm, and the plasma cross section (the "bottle" cross section) is fixed by the mass flow-rate necessary to obtain the design thrust. In sizing an MCR fusion chamber, the other key size is the length L of the "bottle." An order of magnitude for L, or even the torus radius in the case of a tokamak, can be estimated by realizing that it must contain plasma long enough for fusion to start and self-sustain. A simple kinematic criterion can, therefore, be derived. For a more detailed analysis of this problem, see Appendix B.

This criterion states that the average distance traveled by the average hydrogen ion, while fusing, must be shorter than L. The ion distance traveled is proportional to ion velocity, scaling with the square root of E or the square root of T times the residence time τ in the bottle. The shape of gyrating ion trajectories depends on the shape of the magnetic bottle, and to account for them L is weighted with the ratio $\beta_{max} > 1$

between peak and mean $\vec{B}$ field inside the bottle. In essence, if τ is the residence time of the fusing plasma, and if

$$\sqrt{E} \approx \frac{V}{m} \approx \frac{3}{2} \cdot \sqrt{T} \tag{8.45}$$

is the average ion energy, or temperature, or velocity per unit ion mass, and

$$\beta_{\max} = \frac{B_{\max}}{B_0} \tag{8.46}$$

where $B_{\max}$ is the peak magnetic field within the bottle, and B_0 is the mean magnetic field within the bottle, the condition for fusion becomes:

$$\tau \cdot \sqrt{E} \approx \beta_{\max} \cdot L \tag{8.47}$$

This criterion states that the effective length of the reactor to accommodate fusing particles in a particularly shaped $\vec{B}$ field must be equal to the length traveled by ions. Since the product $n{\cdot}\tau$ must satisfy the Lawson criterion for ignition, coupling together Eqs. (8.34) and (8.46) constrains the actual length of the fusion chamber in MCF rockets.

Not surprisingly, the major factor in scaling L is the extremely high fusion ion energy. Because of high ion speed, even short ignition/residence times τ mean very long distances traveled. Calculations show that a mirror MCR propulsion system must have a length many orders of magnitude greater than the bottle cross section, in practice 10^1–10^2 m. The physics of mirror MCF propulsion seems to dictate very thin and long engine shapes, although the Lockheed-Martin corporation claims this can be changed by appropriately shaping the $\vec{B}$ field. Electromagnets capable of imposing $\vec{B}$ fields of the order of a few Tesla over distances of tens of meters are massive. Consequently, mastering the technology of superconducting magnets may be a critical step toward designing mirror fusion rockets of practical size.

As realized early in fusion research, magnetic confinement may be compacted by switching from a mirror to a tokamak topology. The length of the bottle decreases by roughly a factor π. However, at our stage of knowledge, it is hard to conceive *practical* ways of producing thermal thrust from a standard tokamak, but divertors and field reversed configuration (FRC) reactors have been proposed, see Fig. 8.31. These can embed a tokamak within a mirror propulsion configuration (Taccetti 2002; Taccetti et al. 2003). Ideally, combining the best of two worlds, FRC reactors could fuse plasma while letting it escape at one end (i.e., to the right in Fig. 8.32) to produce thrust. The presumed advantage of FRC reactors is their compactness, similar to that of spheromaks but differing in that the poloidal magnetic field is more intense than the toroidal

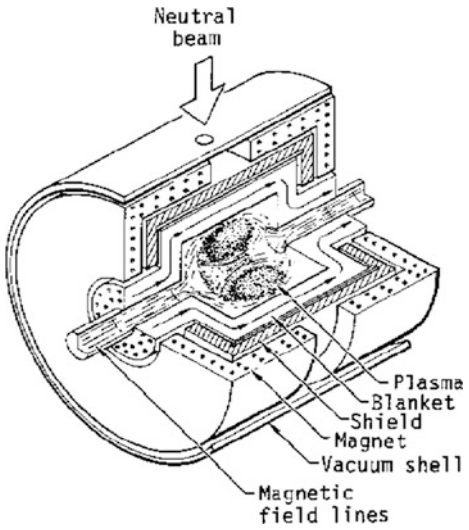

Fig. 8.32 Sketch of an FRC reactor with neutral beam port (Chapman et al. 1989)

(in spheromaks the two are comparable). The FRC concept is relatively new, so not much work has been done to predict its performance, and especially to estimate its overall size and mass, see Appendix B.

If FRC reactors cannot be made to work as practical thermal rockets, tokamak engines might be restricted to the role of electric power sources of relatively low efficiency. Onboard power generation is necessary in any case, but direct propulsion via a mirror bottle looks conceptually simpler than a tokamak power system producing electrical power.

In terms of size, at first glance ICF propulsion systems seem to scale with pellet diameter (≈1 mm). This is orders of magnitude smaller than mirror rocket fusion chambers, see Fig. 8.16. An ICF reactor might be visualized as a channel where encapsulated fuel pellets are injected, hit one by one by multiple lasers or particle beams, and ignite.

However, the energy released during a single pellet fusion event, of order of 1 MJ, can damage reactor walls. Damage is due to radiative heat transfer from the plasma, electron heat conduction, and to plasma impinging on walls. Unlike steady-state fusion, however, the time over which energy release occurs is very short. This situation is similar to that already mentioned of an automotive engine, where instantaneous temperatures may exceed 2500 K, but the confinement time is short enough that cylinder walls may be made of aluminum and may be water cooled.

To prevent wall damage, the standard remedy is to use a magnetic field. Magnetic confinement appears necessary for the engineering of ICF propulsion systems, although the volume of space where $\vec{B}$ must compress the hot plasma

formed by the fusing and exploding pellet is about two orders of magnitude smaller than in MCR. Calculating the magnetic field $\vec{B}_0$ necessary to stop pellet debris at a safe distance d from the wall itself is tedious. To first order, $\vec{B}_0$ is given by:

$$(B_0)^2 = \frac{8 \cdot KE \cdot \frac{d}{R_c^3}}{R_c - d \cdot \ln\left(\frac{R_c}{d}\right)} \tag{8.48}$$

where R_c is the radius of the reactor channel, and KE is the initial kinetic energy of the fusing pellet. The spatial distribution of $\vec{B}$ may be found by noting that the flux of $\vec{B}$ must be conserved, so that in a cylindrical channel $\vec{B}$ must scale with the channel surface, i.e., with R^2:

$$\frac{B}{B_0} = 1 - \left(\frac{R}{R_c}\right)^2 \tag{8.49}$$

Since d is presumably much smaller than R_c, the $\vec{B}_0$ field depends mostly on the channel size R_c and on the kinetic energy of the exploding pellet plasma. Typical pellet mass ranges from 0.25–1.00 g for D–T and energies which predict for $\vec{B}$ to range between 0.3–0.4 T. Such $\vec{B}$ is quite realizable. To an engineer, confining a miniature thermonuclear explosion inside a channel of a few centimeters diameter sounds very unlikely. In fact, the mass of pellets considered for controlled ICF is a minute fraction of that in a thermonuclear warhead, and the scaling of potentially damaging heat transfer is nonlinear with channel radius. In the end, fundamental physics shows ICF rockets may work with existing technology. On a much grander scale, that was also the conclusion of Project Orion in the 1950s. The goal of Project Orion was to drive a spaceship by repeatedly exploding fission bombs at a certain distance from a "pusher plate" attached to its stern and designed to stand the periodic recoil (Dyson 2002). This project was briefly resurrected (Orth 2003) using nuclear microexplosions, simulated by the DPF reactor in Fig. 8.33.

In summary, aside from the laser assembly, ICF propulsion seems to imply smaller engines compared to magnetic confinement, with power and thrust linearly dependent on pellet injection rate. However, total mass and bulk depend not just on the engine but on the laser or particle beam assembly which is the single most critical component of ICF propulsion. In comparison, mirror MCF rockets may need very long reactors, perhaps made more compact by a factor 3–4 when using FRC concepts. Replacing thermal fusion rockets with electric rockets adds energy conversion machinery to both MCR and ICF systems, and the reactor power output must be a factor 2–3 larger than pure thrust power.

Based on current understanding of fusion engineering, MCF-based rockets may be very large, in any case an order of magnitude larger than ICF propulsion systems. Table 8.4 reports size, mass, performance, and other critical parameters of two mirror MCR rockets designed in the mid-1990 s using D–T and D-He^3 fuel (Kammash 1995). Similar estimates are in (Williams 2004), together with design criteria for a reference mission to Mars and Europa. Even for less ambitious interplanetary missions, the estimated total mass

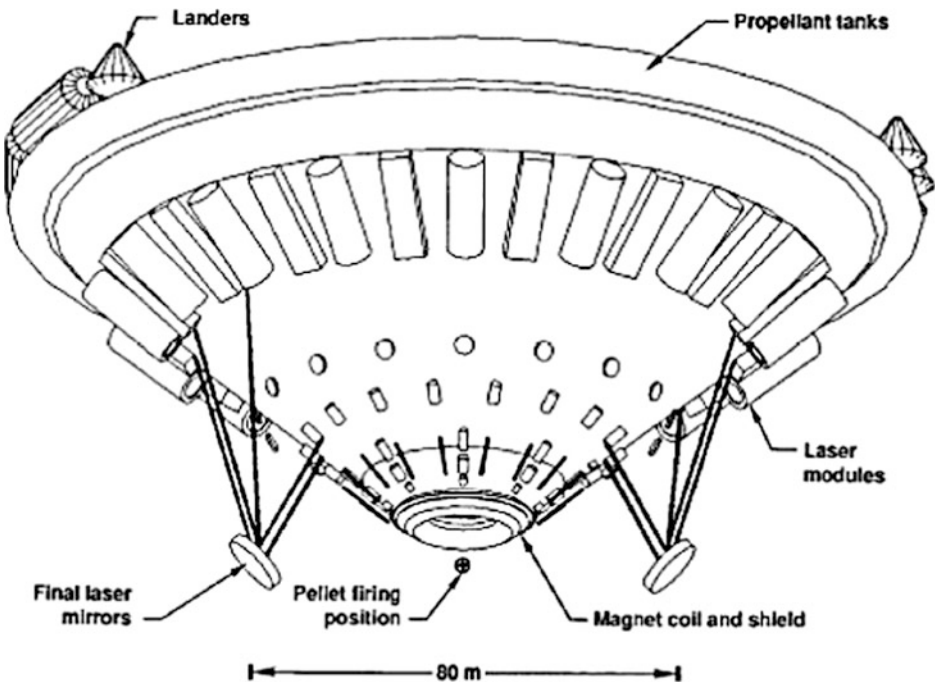

Fig. 8.33 Sketch of VISTA ICF-powered spacecraft and its main components (Orth 2003)

Table 8.4 Mass budget for two MCF gas-dynamic mirror propulsion systems (adapted from Kammash 1995)

Parameter	D–T rocket	D–He^3 rocket
Gain factor Q	1	1
Mirror ratio R	50	50
Plasma β	0.95	0.95
Vacuum magnetic field B_{r0}	15.846	184.81
Plasma length L (m)	50	50
Plasma radius r_p (cm)	7.071	7.071
Injection energy E_{in} (keV)	20	200.0
Ratio of D and He^3 densities D:He^3		6:4
Equilibrium fuel ion density n_i (cm^{-3})	$4.728 \cdot 10^{16}$	$4.359 \cdot 10^{17}$
Equilibrium fuel ion temperature T_i (keV)	6.555	84.629
Fuel ion confinement time τ_i (s)	$2.862 \cdot 10^{-3}$	$7.859 \cdot 10^{-4}$
Reflectivity R_e (%)	90	90
Fusion power P_f (MW)	$4.171 \cdot 10^{4}$	$1.429 \cdot 10^{7}$
Neutron power P_n (MW)	$3.336 \cdot 10^{4}$	$2.061 \cdot 10^{4}$
Bremsstrahlung radiation power P_b (MW)	$2.281 \cdot 10^{3}$	$1.757 \cdot 10^{6}$
Synchrotron radiation power P_S (MW)	$3.465 \cdot 10^{2}$	$7.478 \cdot 10^{6}$
Neutron wall loading W_n (MW/m^2)	622.039	384.2
Surface heat flux (MW/m^2)	42.526	32,758.3
Thrust F (N)	$4.970 \cdot 10^{4}$	$6.760 \cdot 10^{6}$
Thrust power P_F (MW)	$5.503 \cdot 10^{4}$	$2.773 \cdot 10^{7}$
Magnet mass[c] M_m (Mg)	37.4	2265.5
Radiator mass M_{rad} (Mg)	7128.2	$3.555 \cdot 10^{5}$
Refrigerator mass[c] M_{ref} (Mg)	12.5	755.2
Shield mass M_S (Mg)	50.2	15.9
Total mass[c] M_{tot} (Mg)	7228.3	$3.585 \cdot 10^{5}$
Specific power[a] α (kW/kg)	7.087	74.374
Specific power[b] α (kW/kg)	7.559	77.718
Specific power[c] α (kW/kg)	7.613	77.343
Specific impulse I_{sp} (s)	$1.129 \cdot 10^{5}$	$4.183 \cdot 10^{5}$

of the fusion power system is more than 7000 t, a figure that, if realistic, would probably prevent any such engine from being built. Some of the parameters used in (Kammash 1995) and adapted in Table 8.4, for instance the neutron fluxes cited, are up to two orders of magnitude higher than in tested experimental fusion reactors, see Appendix B.

In fact, the power to mass ratio was later modified upward after realizing that leaking electrons did contribute to thrust and I_{sp} (Kammash and Galbraith 1998). This shows that our understanding of how to engineer a fusion propulsion system is so incomplete that designs must be considered attempts, rather than steps, toward a solution concept.

In comparison, laser-driven ICF propulsion systems have been proposed more recently and have received less attention, so their details and analyses are even sketchier, see for example the mass budget for an ICF rocket in Table 8.5.

Similar estimates need to be taken with many grains of salt (Williams 2004). Until fusion becomes industry capability, all these estimates may not be considered realistic. For instance, the total length of the mirror MCF engine (of order 50 m) in Table 8.4 is reasonable for a plasma density about 10^{22} cm^{-3}. However, in the most advanced *ground* tokamak designed, the International Thermonuclear Experimental Reactor (ITER) under construction in France, the plasma density is an order of magnitude lower due to instabilities. Since the size of the mirror engine scales almost linearly with density, a more conservative estimate, while assuming the same density of $\approx 10^{21}$ cm^{-3}, would predict a reactor mirror close to 500 m. Notice also that the D–^{3}He engine in Table 8.4 has $Q = 1$, meaning a neutral energy budget (power obtained equal to auxiliary power to create plasma), leaving no net power generation. The neutron flux (of order

Table 8.5 Mass budget for an inertial confinement fusion (ICF) rocket [adapted from (Kammash 1995)]

Driver:	Mass, metric ton
Lasers	110
Radiators	92
Optics, structure	18
Energy handling	42
	262
Thrust chamber:	
Shield coil	126
Heat rejection	40
	166
Overhead:	
Payload shield	17
Fuel tank	16
Reactors	5
Truss	20
	58
Total	436

600 MW/m^2) is, optimistically, more than 10 times that in any tokamak reactor. Controlling radiation damage would pose quite a challenge. In essence, our understanding of how fusion propulsion will eventually evolve is far more limited than that of jet engines in the 1940s, see the famous picture of Whittle's 1937 WU jet engine prototype (Gunston 2006).

Probably consistent with the engineering of space radiators in the 1990s, Table 8.4 shows that MCF mass budgets are dominated by the space radiator. Unlike fission thermal rockets, where energy release is completely converted to thrust power, a thermal fusion rocket produces power mainly in the form of kinetic energy of neutrons and radiation, neither immediately usable for thrust. The power fraction thermalized within the reactor structure must be disposed by a space radiator. In the D–T powered rocket of Table 8.4, the radiator mass is about 98% of the total. This effect is due to having assumed for the radiator mass 1 kg per unit kW radiated to space, and a maximum radiator temperature of only 600 K. In fact, NASA estimates the weight of space radiators at 0.015–0.200 kg/kW in future nuclear electric propulsion systems. At 0.1 kg/kW, the radiator mass would drastically reduce to about 700 t, but would be still very large. Cooling and size (length) are major issues in MCR mirror rocket concepts. Recovering heat radiated to space to produce electric power (e.g., for electric thrusters) may turn out to be indispensable to reduce total mass. The resulting propulsion system would be a hybrid, the thrust being partly thermal and partly electric.

Cooling of ICF rockets appears less demanding, see Table 8.5, because the heat loss due to bremsstrahlung is relatively small in pulsed fusion. Accordingly, the estimated radiator mass is less than 10% of the total engine mass, compared to more than 90% for the MCR concepts in Table 8.4. The most massive items in the ICF rocket are the laser assembly and the electromagnets. Their mass fraction is 50% of the total. Superconducting coils could reduce mass by at least one order of magnitude. The critical mass component of ICF rockets would then become the laser assembly. In addition to their mass penalty, lasers absorb a good fraction of the fusion power. Compared to MCF, ICF propulsion appears to lead to more compact but less performing systems. The mass budget of ICF and its technical challenges are indeed formidable (Cassenti 2004; Winterberg 2010).

Figure 8.33 is an artist's view of an ICF-powered spacecraft conceptually designed at the US Lawrence Livermore National Laboratory (LLNL) and called VISTA (Vehicle for Interplanetary Space Transport Applications) (Orth 2003).

VISTA was designed in view of crewed Mars and QI missions and was deemed feasible in the 2050. VISTA uses multiple pulsed laser beams to fuse a steady stream of fuel pellets. The top part of the craft contains the liquid D–T fuel, to be transformed en route into marble-size pellets by encapsulating it inside a "converter" foil made by 50 g of a D-rich material. As mentioned, the purpose of this foil is to form the D^+ beam, enabling ignition when hit by the external lasers. For radiation protection, the crew habitat is inside the pancake-shaped fuel tank. The core of the fusion engine is a 26-m-diameter superconducting magnet inducing 12 T and performing also the role of the magnetic nozzle where thrust is applied by fusing pellet plasma. When a fuel pellet is hit

by laser pulses and fuses, fusion fragments expand, and plasma pressure drops with radial distance until below the magnetic pressure $\approx B^2$ created by the magnet. The 50° conical shape ensures that the plasma, guided by the $\vec{B}$ field, applies its momentum to the *external* spacecraft surface. Accordingly, a thermal protection system capable of stopping neutrons and gammas coats the lower surface of the spacecraft. Each fusing pellet releases 5 MJ with 6% efficiency, and at a firing rate of 30 Hz, calculations indicated $\alpha \approx 20$ kW/kg and a maximum $I_{sp} \approx 20{,}000$ s.

VISTA has a diameter of about 100 m and a mass estimated at 5800 t, including a 100 t payload for a 60 day Mars round-trip. In order to augment the thrust produced by ^{4}He plasma, inert hydrogen propellant is fed to the engine. Most of the spacecraft mass (4100 t) is in fact inert hydrogen propellant, while D–T fuel is only about 40 t, or only 10% of the hydrogen mass. At pellet injection frequency of 30 Hz, total thrust power is 30 GW. For the Mars mission, the I_{sp} estimated with inert hydrogen mass addition is ≈17,000 s. Performance figures depend critically on the expansion of the plasma cloud formed after the laser system strikes the fuel pellets, and on the shape of the superconductive magnetic field. To reduce design uncertainty, experiments to test thrust efficiency were carried out and compared with CFD simulations, convincing researchers that in the laboratory model 60% of fusion power was converted to thrust power. If laser energy could be reduced, VISTA may eventually weigh only 1/7 of the original. The VISTA concept has been revisited taking advantage of the so-called fast ignition pellet heating (Vchivkov et al. 2003; Nakashima et al. 2005; Miley et al. 2010). Work on "fast ignition" heating is continuing also in Japan and Russia using the magnetic-inertial confinement approach and particle beams. The 100 km/s cruise speed limits VISTA performance to near QI missions. For instance, reaching 104 AU was estimated to take 20 years, essentially a lifetime round–trip mission.

The conclusion of the exercises documented here and in Tables 8.4 and 8.5 is that spacecraft powered by MCF and ICF reactors designed with our current status of understanding of fusion is still too massive to be feasible.

8.14 Magnetic-Inertial Confinement (MIC) Fusion

The cost, mass, and complexity of fusion based on magnetic and on inertial confinement have driven efforts toward simpler and more manageable concepts. MIC tries to combine the best of the two approaches into a workable fusion reactor. MIC is based on transient magnetic fields that "squeeze" or "pinch" plasma, compressing it until ignition occurs. Doing so focuses plasma into a narrow region, hence the dense plasma focus (DPF) characterization. Both aspects of MCF and ICF are present in MIC: high density to facilitate ignition and confinement by an intense but transient $\vec{B}$ field requiring modest facilities for testing and evaluation.

Conceptual working of a θ-pinch DPF rocket is shown on the left of Fig. 8.34. Note that θ is the azimuthal (circumferential) coordinate. Fuel injected inside the reactor is ionized by the voltage between anode and central cathode. The resulting plasma current $\vec{j}$ is directed radially, so the $\vec{B}$ field it

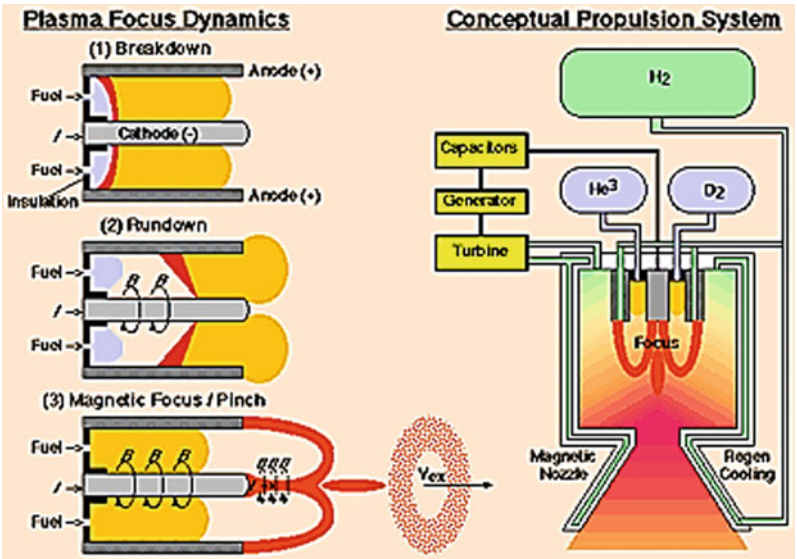

Fig. 8.34 θ-pinch dense plasma focus (DPF) dynamics (*left*); a view of a notional DPF rocket (*right*)

induces must be normal to $\vec{j}$, that is, is azimuthal. This field "pinches" or "squeezes" the plasma current $\vec{j}$, and if that is composed of D–T plasma, the (ideally) adiabatic increase in density and temperature may ignite it. There is some experimental evidence that in unsteady mode plasma, ignition may be achieved with reactors much smaller than steady-state MCF or ICF reactors. According to the Maxwell equations, the Lorentz force $\vec{j} \times \vec{B}$ is normal with respect to both instantaneous current and $\vec{B}$ and therefore accelerates the just-fused ^{4}He plasma in the axial direction producing thrust.

In DPF rockets, plasma may be periodically formed and ejected ('pulsed') as the sole propellant, but it can also be thermalized by mixing it with inert H_2. This lowers I_{sp} but increases thrust. Acceleration of the mixture formed by plasma and inert may take place in a conventional or magnetic nozzle, depending on the energy of the ^{4}He plasma produced. Also depending on whether inert H_2 is added or not, the ideal I_{sp} has been estimated in the range 4000–10^6 s. Calculations of power output from DPF reactors indicate low Q gain. The output energy is almost equal to that necessary to ignite. However DPF rockets could be very compact. This, and the fact that experiments with DPF are relatively inexpensive compared to those with steady MCR, explains past and current interest in this type of reactor at US universities but also in industry (Lerner 1992).

Pulsed Z-pinch fusion uses a similar strategy, only the directions of $\vec{B}$ and current $\vec{I}$ are swapped. A survey of Z-pinch architectures can be found in (Stygar et al. 2007). A transient ($\approx 10^1$ ns) current of intensity $I \approx 10^0$–10^1 MA is directed along z, the axial direction of the reactor in Fig. 8.35, and induces a radial $\vec{B}$ field. As in the θ-pinch mechanism, the Lorentz force "squeezes" or "pinches" plasma by increasing magnetic pressure B^2/μ_0 uniformly in the radial direction. Consequently, plasma accelerates in the axial direction z just like toothpaste is squeezed from a tube. Periodically discharging a capacitor bank supplies the intense current needed to produce $\vec{B}$.

In essence, pinching replaces lasers with much less expensive and less bulky capacitors, and it can be adapted to propulsion as illustrated schematically in Fig. 8.35.

In this figure, D–T fuel is injected from the reactor left wall, the anode of the circuit. The D–T jet is surrounded by an annular jet of ^{6}Li and/or ^{7}Li (green in the figure). A transient pulse of current $I \approx 10^2$ MA raises the D–T temperature to 2–3 GK and creates, at the same time, the magnetic field $\vec{B}$ pinching adiabatically the D–T jet. At these temperatures, plasma emits X-rays. These help to compress both D–T and Lithium and initiate fusion. The Lithium and D–T jets meet at the focus of the pinch. The Lithium plasma conducts the current from cathode to anode, and it closes the circuit and improves the stability of the current during the pulse (Davies 2006). The plasma cathode was suggested in (Winterberg 1980). The coaxial ^{6}Li or ^{7}Li plasma absorbs neutrons from the fusing D–T, fuses and produces Tritium, working at the same time as a neutron shield and as energy booster. The reactions are (1), (2), (8), and (10) in Fig. 8.15, with fuel and energy release given by

Fuel pair	Energy (MeV)	Reaction
D–T	17	(1a)
D–D	4	(2)
^{6}Li–D	22.4	(8)
^{6}Li–n	4.8	(10)

If Lithium is completely reacted, the propellant ejected from the reactor is ^{4}He (alpha particles). The ^{4}He plasma ejected expands as a bubble (a "plasmoid") inside the magnetic nozzle after each Z-pinch pulse and produces thrust. (Polsgrove et al. 2010) proposed a Z-pinch propulsion system for crewed Mars and Jupiter missions. No details of the reactor are provided, since the focus is on optimizing thrust and specific impulse and on sizing of the magnetic nozzle, shown schematically in Fig. 8.36. It is useful at this point to describe a magnetic nozzle operation.

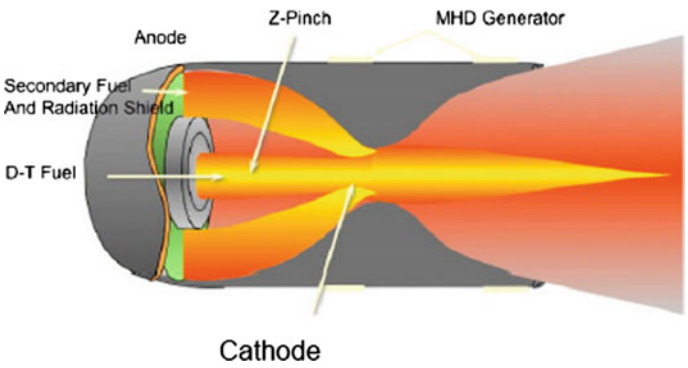

Fig. 8.35 Schematics of a fusion reactor (and propulsion system) using D–T (primary fuel) and Lithium (secondary fuel, in *green*) to close the electrical circuit (not shown)

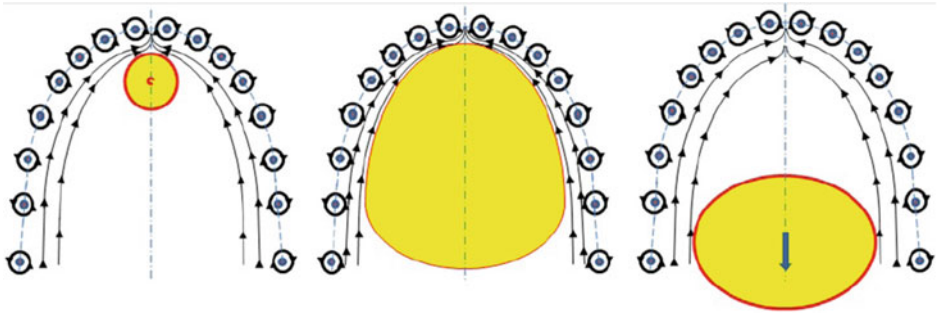

Fig. 8.36 Sequence of images on the meridian plane of the magnetic nozzle showing evolution of the plasma bubble ejected after each pinch (Polsgrove et al. 2010). From *left* to *right*: ^{4}He plasma (*yellow bubble*) ejected from the fusion reactor (not shown) expands, compresses the magnetic field $\vec{B}$, and is ejected by the magnetic pressure $B^2/2 \cdot \mu$ in the nozzle. The *dark dots* are cross sections of the electromagnetic hoop conductors producing the $\vec{B}$ field shown (*Courtesy* NASA MSFC)

A magnetic nozzle is constituted of an electrified series of conducting hoops, or coil, spatially shaping a 3-D paraboloid-like $\vec{B}$ field. This field defines the magnetic nozzle contour. Except for hoops and coil, the nozzle has no solid walls. The ^{4}He plasma bubble ejected from the reactor after each pinch tends to expand isotropically and, being electrically conductive, interacts with the $\vec{B}$ field. As plasma ejected from the reactor enters the nozzle, $\vec{B}$ must adapt to the moving plasma charge in a time scaling as $1/\sigma$, the inverse of the electric conductivity. However, the expansion time is much shorter than this conduction time, and $\vec{B}$ has no time to adjust and is "pushed back" (compressed). During this compression, the magnetic field forming inside the plasma cancels out the external $\vec{B}$ field, and the kinetic energy of expanding plasma is converted to magnetic energy, scaling as B^2. As the plasma expands, it cools and its expansion slows down. The compressed $\vec{B}$ field springs back and accelerates the still expanding bubble out of the nozzle. Either in terms of magnetic pressure $B^2/2 \cdot \mu$ or in terms of the Lorentz force (applied to the hoops), a reaction force, that is, thrust is produced. In essence, the magnetic nozzle converts a significant fraction of the radial momentum of isotropically expanding plasma to axially directed momentum and therefore maximizes thrust.

Sizing a *Z*-pinch powered spacecraft as a function of thrust and I_{sp} shows that the Li/H mass ratio is a critical parameter determining mission time and IMLEO. For instance, a Mars mission requires this ratio to be about 200. Higher ratios increase thrust but lower I_{sp} too much and vice versa if this ratio is much below 200. A simplified Earth–Mars trajectory calculation with this ratio indicates a "good" thrust and I_{sp} combination, ensuring a 177-day round-trip and consuming 87 t of propellants to generate $3.8 \cdot 10^4$ N and $1.9 \cdot 10^4$ s, respectively. With the same combination, a 72-day mission has also been calculated, but the propellant mass jumps to 350 t. With the same assumptions, a slower one-way FOCAL mission would last about 3.5 years and would need 195 t of propellants. These are numbers of interest to interplanetary missions, but they show that QI missions, even with advanced fusion propulsion concepts, are still beyond reach.

8.15 Fusion Propulsion Summary

After all investigations of fusion propulsion, including the very detailed VISTA, performance remains a matter of speculation, because net energy gain and self-sustaining steady fusion have yet to be demonstrated. Simply calculating energies of fusion products, I_{sp} of order 10^5–10^6 s can be predicted for D–T and D-He^3 fueled MCF rockets. An ICF rocket may be ideally capable of similar I_{sp} during a single pulse, but the spherical titanium or tungsten metal case is a significant fraction of the pellet mass, and specific impulse will be less than expected. The pulsed thrust mode will contribute to lower the average thrust. The ICF mass budget, shown in Table 8.5, was estimated by calculating the He exhaust speed equal to $3.75 \cdot 10^5$ m/s, and the tungsten velocity equal to $4.4 \cdot 10^4$ m/s, consistent with its much higher molecular weight. The effective I_{sp} is weighted by the speed of the heavy tungsten ions, rather than by that of the He nuclei.

Comparison between *thrust* available from either MCF or ICF depends on the onboard power assumed for a specific mission. A better comparison is in term of thrust per unit mass of the engine. For magnetic confinement rockets using D-He^3 fuel, calculations predict about $2 \cdot 10^{-2}$ N/kg, and about $0.7 \cdot 10^{-2}$ N/kg for the more practical D–T combination. While the ratio thrust/mass is acceptable, the mass of the engines is not. Superconducting technology may eventually help to shed weight, but is unproven in space at the power level desired. Current MCF rocket concepts should be revisited by including ways of reducing or exploiting the large waste heat dictating massive space radiators.

Magnetic-inertial confinement (MIC) concepts, as the θ-pinch and *Z*-pinch in Sect. 8.14, are less developed (that is,

less funded), but seem much more promising in terms of lower bulk, mass, and complexity. This is because they need only capacitors, not lasers nor plasma guns or large continuously operated electromagnets.

8.16 Antimatter Propulsion

All concepts described so far are based on fusion triggered by energy deposition (either directly in a plasma or on a pellet forming plasma or in the form of magnetic pressure). Triggering implies that to overcome Coulomb repulsion between D^+ and T^+, kinetic energy must be supplied to the plasma. The process is, therefore, not spontaneous, even though its ΔG is $<< 0$, which is entropically more likely. Propulsion concepts have been proposed where fuel pellets are ignited by microexplosions compressing pellets to the right density and temperature and driven by annihilating antimatter, antiprotons p^-, or by neighboring pellets undergoing fusion themselves. This has suggested matter-antimatter as the nuclear fuel.

Antimatter propulsion may be seen as an extreme form of fusion. The fuel is made of matter and antimatter that annihilate on contact and become kinetic energy of pions. This very special type of fusion does not have to meet density or temperature constraints—it is totally spontaneous. This idea was originally proposed by *E.* Sänger (Sänger 1953), but it was not pursued for lack of physical understanding of how to store and prevent p^- from recombining with ordinary matter (Kerstein and Matko 2007). At least in the laboratory, this is no longer an issue. At sufficiently high energies, antiprotons can be routinely produced by particle accelerators such as the US Fermilab and that at CERN (Forward 1985; Holzscheiter et al. 1996). The question is availability and the cost of making and storing sufficient amount of p^- to power a practical propulsion system (the estimated cost of p^- in 1984 was of order M$10/mg). The chart in Fig. 8.2 of (Schmidt et al. 2000) reports that in 2000, the Fermilab was capable of producing 10^{-8} g/year of p^-, with a 10^{-6} g/year future capability. At this rate, the cost of electricity alone would be $\$62 \cdot 10^{12}$/g. Antiproton storage is routine by means of a Penning trap, a cryogenic container kept at 4 K and holding p^- by means of an intense, 6 T magnetic field. As a side note, this is the "bottle" described in the opening chapter of the *Angels and Demons* novel by Brown (2006). Storing up to 10^9 antiprotons per trap has been demonstrated at Penn State, and 10^{14} appears feasible (Holzscheiter et al. 1996). At $1.6 \cdot 10^{-27}$ g/proton, a single Penning trap could store $\approx 10^{-13}$ kg of antimatter, and the potential energy released by annihilation ($\alpha = 1$, see Fig. 8.5) would be of order 10^4 J. Standard Penning traps weigh now ≈50 kg, but storing technology is still in its infancy. Recently, 10-cm long, 100-μm-diameter nanotubes have demonstrated storage of up to 10^{10} p^- for a few days (Weber et al. 2014).

The theoretical I_{sp} of antimatter rockets is the highest possible, since the energy per unit mass J in any annihilation process is exactly c^2. Measured pions energy is in the 250 MeV range (i.e., pion speed $\approx 0.94 \cdot c$). The performance of antimatter as energy source has been calculated for interstellar and precursor missions in (Schmidt et al. 2000). Their Fig. 8.1 chart lists the mass of antiprotons needed as a function of spacecraft mass and engine technology. Annihilation may take place in a solid or gas mass, or it may accelerate only the annihilation products.

The extraordinary cost of antimatter may be minimized by using it only to *catalyze* fusion reactions, e.g., the aneutronic reaction D + ^{3}He. Depending on fusion strategy and mission, the mass of antimatter needed to power spacecraft may vary literally by orders of magnitude, from 10^{-9} g simply used as catalyst, to 10^9 g when annihilation products are the only propellant. As an example of the former, by using a solid core to absorb the energy released and then using it to heat Helium propellant, the mass of antiprotons necessary for a 100-kg probe to reach 10^3 AU in the Oort Cloud (a 50-year mission) is estimated of order 10–100 mg (ΔV is of order 10^3 km/s in this case). However, for the same 50-year mission, a 100-t spacecraft would require 100 kg of antiprotons. These numbers must be kept in mind when discussing antimatter propulsion. As with any high I_{sp} propulsion systems, the I_{sp} versus thrust trade-off means, that the thrust desired for fast space travel must be paid in terms of power, that is, the rate of consumption of antimass. Adding inert mass to the annihilation process is the standard way to increase thrust. However, here the problem is complicated by the very short timescale of p^-–p^+ kinetics. This question is one of many in assessing the merits of antimatter versus "conventional" fusion propulsion (Borowski 1987). Borowski concluded that advanced ICF, using for instance D +^{3}He or catalyzed D+D fusion, is preferable to annihilation.

In 2003, Dr. Frisbee (2003) proposed to produce antiprotons "on the fly" by focusing a 2-ps pulsed laser beam in the same class of the Lawrence Livermore "Titan" laser (1020 W/cm^2) on a gold foil. Annihilation with ordinary matter would release energy to power a pulsed hydrogen thruster. Calculations indicated that ≈90% of antimatter can be made to emit energy in a preferential direction, and this concept could do away with bulky and heavy paraboloid mirrors. The focus of this discussion has been on the detailed physics of the interaction laser–matter rather than on propulsion. The notorious inefficiency of lasers combined with the double energy conversion process does not leave much hope that this system could improve on more conventional fission or fusion propulsion.

An even more advanced form of propulsion, still based on annihilation, envisages photons as the propellant. Energy

and virtual momentum of photons are so small that to produce reasonable thrust, radiance must be very intense and light collimated. The original idea is attributed to Sänger (Sänger 1953, 1959, 1965a, b), who conceived a perfectly reflecting paraboloid with fission or fusion nuclear heat source in its focus. All photons emitted would be collimated along the paraboloid axis. C. Rubbia reproposed the same concept and calculated that to produce a 3-N thrust, the thermal power of an ideally reflecting paraboloid should be about 1 GW. In all applications, the attractive feature of photonic rockets is their I_{sp} coinciding with c, the speed of light. Winterberg presented in 2012 an even more speculative concept based on harnessing annihilation directly to produce a gamma ray lasing effect, but did not estimate performance (Winterberg 2012).

8.17 Impulsive Propulsion

Confinement and ignition studies have suggested radical solutions to the problem of fast space flight that are alternatives to MCF and ICF. These are fusion micro- or macro-explosion concepts, starting with Project Orion (1960s) and Project Daedalus (1973–1978). The pulsed propulsion concepts in Sect. 8.14 may be seen as the low end of the energy spectrum of these proposals. At their heart is the fact that nuclear explosions produce light particles such as H or He with energies in the tens of keV, corresponding to velocities of order 10^5–10^6 m/s. Thermalizing this energy in fission or fusion reactors reduces the temperatures to manageable values, but it limits efficiency and reduces the potential I_{sp} as well. Exploding full-size fission or fusion bombs astern of a pusher plate wastes at least half of the energy. In fact, the I_{sp} of Orion was found to be approximately $I_{sp} = C_0 V_e$, where V_e is the debris velocity following the nuclear explosion and C_0 is a collimation or coupling factor <1 empirically accounting for the fraction of the impulse transmitted to the thrust plate by the debris (Bruno 2012). For well-matched fireball and thrust plate diameters (this depends on yield, plate diameter, and distance between plate and exploding fuel), C_0 is of order 0.5 for a 1-Mt yield thermonuclear bomb, which may produce V_e of order 10^4 km/s and a fireball of about 1 km size. Good matching, that is, collecting as much as possible of the impulse, would require thrust plates, if not of the same, at least of similar size. A mid-sized Orion spacecraft designed at General Atomic (Nance 1964) had a 40-m diameter and a mass 1000–2000 t. In order to reach approximately 10% of the light speed required 1080 fission bombs, each weighing between 370 and 750 kg. A good guess for its I_{sp} would be much less than 10^7 s, perhaps 10^5 s, given the size of the thrust plate. The number and mass of the bombs necessary for a single mission suggests that this mode of propulsion will never be practical.

The second historical study of impulsive, large scale fusion propulsion is the cited Project Daedalus (Bond et al. 1978). This five-year study by the British Interplanetary Society envisaged detonating D + ^{3}He pellets at the rate of 250 Hz by electron beam pulses, not lasers, since the former can be produced with much higher efficiency. ^{3}He does not exist on Earth and was supposed to be harvested in the Jovian atmosphere before starting the interstellar leg of the mission. Thrust was collected as Lorentz force by means of an electromagnetic nozzle (see Fig. 8.36) contributing to the astounding mass of the ship, about 54,000 t. In fact, the nozzle must be large enough to capture most of the expanding plasma and converting it via a $\vec{B}$ field to magnetic pressure $B^2/2 \cdot \mu$. The Project Daedalus spacecraft was assumed to accelerate over four years to its 36,000 km/s cruise speed ($0.071 \cdot c$), reaching Barnard's Star, at a distance of 5.9 light-years from the Sun, within the useful 50-year life of a human being. This star was chosen since at the time it was believed to have a planet. The spacecraft was a two-stage vehicle equipped with optical and radio telescopes to investigate Barnard's Star planet during a flyby. No return was planned. To date, this remains the most detailed study of a manned interstellar mission using pulsed macro-explosions.

Dr. F. Winterberg started investigating impulsive propulsion in the 1960s aiming at bringing down the energy of each pulse to a reasonable level and at increasing the efficiency of energy conversion. Winterberg (Winterberg 1971) set the stage for the development of concepts utilizing the so-called microbombs or microexplosions, defined as of order 1 kiloton. In this context, the concept of the magnetic nozzle was also introduced to prevent destruction of the propulsion system. His energy balance calculations indicated that a 1–2-mm-diameter pellet consisting of a D–T core surrounded by a ^{235}U layer could ignite and release neutrons activating U fission when "hit" with an e-beam of current and energy in the MA and MeV range. Pellets were supposed to explode sequentially at frequency of a few Hz in the focus of a paraboloid-like magnetic nozzle, see Fig. 8.36, of approximate radius R scaling with the pellet energy release E_B and magnetic field intensity H as

$$R = (12 \cdot E_B)^{\frac{1}{3}} \cdot H^{-\frac{2}{3}} \tag{8.50}$$

The pulse of the current was assumed to be produced by the discharge of a capacitor bank, at the time (1971) limited to an energy density $\approx 10^{-2}$ J/cm^3 and bulk weight 2 g/cm^3, therefore contributing significantly to the mass of the propulsion system. Performance calculations were similar to the approach in (Stuhlinger 1964), that is, based on finding an optimum ratio between the end of the acceleration phase and exhaust velocity (in practice, this ratio is about 1.6). In

the 1971 article, inert hydrogen is assumed to be added to the nuclear fuel to increase thrust. At a pulse rate of 3 Hz and 1 kt energy/pulse, a 1500 t spaceship including 1200 t of hydrogen and 4.7 t of fuel was predicted capable of reaching 100 km/s in a day and 300 km/s in 8 days.

This seminal work evolved by replacing e-beams with ion beams to overcome the Alfven limit on the current necessary to ignite. The current is limited by the self-pinching effect of the magnetic field associated with the current (Winterberg 1980; Davies 2006). Because the Alfven limit scales with the particle mass, ions (e.g., H^+) can transport more than 10^3 times the e-beam current. This research also suggested the energy yield of each microexplosion could be raised by transitioning the explosion to a detonation. In fact, the products of D–T fusion, for instance p^+ and ^{3}He, can again react with D or with additional fuels such as ^{11}B, see Fig. 8.15. In fact, this opens the theoretical possibility of higher-yield multi-stage fusion, and of detonating fusion products, for instance ^{3}He–D. In order to detonate any fuel, the necessary pre-compression was envisaged to be driven by X-ray emission from a heavy metal reactor liner heated impulsively by the first-stage D–T burn. The increased yield due to detonating ^{3}He-D increases the X-rays flux and the process repeats itself, hence the term "autocatalytic" used in this context in analogy with a similar effect described in (Condon 1943).

In a series of follow-on papers (Winterberg 2009a, b, 2010, 2013), Winterberg refined the microexplosion propulsion concept replacing D–T fuel with more available and less neutronically "dirty" D–D. This fuel has a much higher activation energy, but calculations indicated ignition is still feasible with a $\approx 10^0$ MA proton beam of energy in the GeV range, provided that, instead of a pellet, the fuel is a solid D–D bar where the requirement for compression, $\rho \cdot z > 10$ g/cm^2, can be obtained more easily than in a spherically symmetric pellet limited in diameter to 1–2 mm (for comparison, D–T ignition needs $\rho z > 1$ g/cm^2, see Eq. 8.42). The means proposed to reach GV-class voltages consisted in charging the entire spacecraft in the vacuum of space, replacing bulky and massive capacitors supplying MA-class beams.

Lifting payloads to orbit using microbombs in the atmosphere is also tentatively discussed in the 2010 paper. In air, charging the spacecraft can no longer replace the capacitor bank, and HMX (octogen) solid propellant is assumed to compress and heat Argon, triggering a photon avalanche that should ignite a small amount of first-stage D–T, followed by ignition and burn of the theoretically aneutronic D–D fuel. These two conceptual propulsion systems, the first for a Mars mission and the second for high lift to orbit, are further presented and discussed in (Winterberg 2014b, 2015).

Proposing fission or fusion explosions for propulsion leads to criticism not because of unsound physics, but because engineering and technological understanding of the many details are still immature. Nevertheless, they focus on interstellar travel, a topic so far considered pure science fiction while being very imaginative by exploiting technologies associated to thermonuclear explosions considered exclusively military, destructive and thus scientifically unproductive.

In fact, interest in *efficient* pulsed propulsion has been on the rise for some time, even though public domain information of aspects directly connected with past weapon work is scarce. Much has been declassified recently. Common to all recent proposed concepts producing thrust is the adoption of magnetic nozzles and of the Lorentz force rather than mechanical pressure to transform energy yield into thrust. MagOrion and MiniMagOrion (MMO) (Lawrence 2008; Ewig and Andrews 2003) are concepts similar to those proposed by Winterberg, but were originally classified and public information now available lacks details. These concepts yield theoretical I_{sp} of order 10^4 s, thus are considered "moderate." Their most appealing feature, however, is not I_{sp} but thrust, in the range 10^4–10^6 N, enabling substantial acceleration and fast travel. The price of "moderate" I_{sp} is, of course, high fuel consumption.

A significant aspect of impulsive propulsion is that thrust and momentum pulses are assumed to be applied via an external magnetic nozzle, similar to what is done in a chemical rocket. Consequently, energy is not deposited inside the spacecraft and no radiator is necessary. Allegedly, these concepts and their engineering have been analyzed under Project Orion and Mag Orion, but some areas are still classified preventing from drawing substantive conclusions as to feasibility and merit. In any case, the I_{sp} reported imply that interstellar and QI missions would still need too much mass.

Work in fusion propulsion continues at low level in the US (e.g., at the University of Michigan, Penn State, University of Alabama, University of Nevada, NASA-Marshall, LASL, INEL and others) and in Russia (e.g., at the Ioffe Physical Technical Institute). However, modest funding and the many engineering problems to solve suggest no breakthrough or testing is forthcoming anytime soon.

8.18 Photonic Propulsion

Recent developments from the defense world in phase-lock lasers, e.g., see (Lubin et al. 2014), have resurrected in modified form an original idea by E. Sänger (Sänger 1965a, b), consisting in using light pressure to push a spacecraft to relativistic velocity. Sänger visualized a spacecraft using photons as propellant. A light source produces photons of virtual mass $h \cdot \nu/c$, where h is the Planck constant and ν the

light frequency. The recoil of photons is the reaction force applied to the source. It was mentioned that this concept was reinvented by C. Rubbia in the 1990s, assuming a high-temperature and a perfectly reflecting parabolic mirror of all photons of all wavelengths and radiatively heated by a nuclear reactor. The appeal of this concept is the speed of light of photons. If one neglects the relativistic mass to be converted into the energy to produce light, the ideal I_{sp} is exactly equal to c. Including in I_{sp} is the reactor mass consumption, for the fissioned mass the actual I_{sp} is lower but still orders of magnitude higher compared to chemical or electric rockets. The drawback of the photonic rocket is of course low thrust. For instance, a 1 GW photonic rocket is capable of only 3 N thrust.

The new concept due to Professor Philip Lubin merges photonic thrust and the laser propulsion tested by Leik Myrabo, see Chap. 4. The ground-based laser beam is not ablating or energizing inert matter, but simply accelerates a spacecraft by photon thrust applied to its external surface (Lubin 2016). The power to provide a reasonable thrust and acceleration rises with the cube of speed and would be unrealistically high for a single laser. However, work on laser weapons has made possible to combine in a single optical phase the output of many laser beams with efficiency of order 0.6 and higher. This fact opens up the possibility of pushing objects to quasi-stellar and stellar distances. The spacecraft must have a sufficiently large reflecting mirror to still capture the expanding beam as the distance increases with time. Thus, mirror size scales with mission distance and may be very large. For instance, a 100 kg probe fully illuminated by a laser farm can travel to ≈6 AU at 0.237 g in around 1 day, before beam diffraction starts lowering the flux captured. But in order to reach 6 AU, the mirror diameter must be 270 m, and total laser power must be 70 GW. The laser farm to produce this flux can be estimated to occupy 10 km^2.

Thus, the key to this concept is size and mass of the mirror and power. Contrary to the case of light sails, laser power does not decay as fast with distance (light sails depend on solar flux, scaling with the inverse of the square of distance from the Sun). It is safe to conclude that the scale of power required is staggering, as expected. The physics of this concept has been thoroughly examined, and the conclusion is that the concept is credible and very expensive. At the same time, it seems this propulsion concept is the only possible way to send probes to (reach) the stars.

8.19 Conclusions: Can We Reach the Stars?

The focus of this chapter is on giving a technology answer to questions going back to the first time men gazed at stars: *What are they? Are there beings like us? Can we go there?* In order to answer the last question, in this chapter we enrolled the ultimate known power source, fusion. Calculations, analyses, and outlooks presented leave the question still without a clear answer. Within the constraints posed by the physics we know, chances of reaching stars using fusion propulsion are limited.

Stripping fusion rocket concepts of their mystique leads to a rather disappointing conclusion: thrust may even be in the 10^5 N range and I_{sp} in the 10^7 s, but combining the two *with current or near technology* into an engine would require giant spacecraft and unaffordable mass consumption. The I_{sp} potentially achievable is infinitely better than those of chemical propulsion, but still insufficient to carry humans on interstellar exploration within reasonable timescales. The first fundamental limitation in traveling over quasi-interstellar and stellar distances is mass fraction converted to energy. In fusion, it is a factor five larger than in fission, but still limited to fractions of a percent. Fusion propulsion, as we can conceive it now, will probably enable us to travel beyond our Solar System, but only to destinations much closer than the nearest star. Even the Oort Cloud is probably too far away to be explored by a crewed vehicle. The mass of a spacecraft bound for Proxima Centauri would be so large, and the time to cross the gulf in between would be so long, as to effectively make human exploration practically, although not physically, impossible.

Only matter annihilation may lower mass consumption to the point of enabling near interstellar missions by robotic spacecraft and (perhaps) crewed ships. Matter-antimatter "fusion" is still a concept. However, its energy is released in the form of radiation which is not easily convertible to thrust. Among the points made in (Lubin 2016) is the fact that external photonic propulsion does not require to produce unrealistic amounts of antimatter; thus, it is more realizable than antimatter propulsion for sending probes of limited mass. For human travel where spacecraft mass is necessarily large and maneuvrability is important, harnessing antimatter seems the only means of travel. Although its scientific and engineering challenges are formidable, its theoretical performance holds the promise of reaching speeds close to light speed.

At these speeds, there are fundamental limitations due to relativity. Except in science fiction novels, it is difficult to envisage a ship where crews lead self-contained lives, work with little or no external support for years, knowing that any form of communication takes also years and that, upon returning to Earth, they would find a different place and not many friends, family and colleagues alive (see Sect. 9.2 for this aspect of space travel). Robotic interstellar missions are at least easier to imagine since radiation, shielding, and the environmental control system would be less critical or unnecessary, acceleration could be much higher than the

1 *g* human beings can tolerate, and no psychological or physiological problems would complicate travel.

There are indeed space exploration visions based on robots capable of autonomous operation, from orbit capturing around a planet to descent and exploration. For instance, Dr. W. Fink at CalTech has been developing robotics incorporating decision-making software based on sensor integration, see (Hsu 2008), and has proposed testing such technology on future Europa or Titan missions. Right now, it is doubtful that even Mars could be explored robotically since the telecommunication time lag prevents real time response to specific situations. Any robotic crew, designed to carry-on stellar or quasi-stellar exploration, will have to be endowed with such sophisticated autonomy and artificial intelligence the likes of which we cannot even imagine at present (Grappone 2013). Note that because of time and relativistic physics, results of such explorations would reach Earth years or tens of years after being obtained.

The will and resources to invest into interstellar travel, whether robotic or human, is comparable to the Middle Ages cathedral building. That is, it should involve financial and technological efforts carried on over one or more generations. Short of breakthroughs in physics, like, for instance the control of inertia and mass, interstellar missions will be realized only when trip times of the order of decades become not only feasible and affordable, but also psychologically acceptable.

In these rather sobering (or realistic) conclusions, there may be the ultimate key to stellar travel. If no breakthrough in physics ever occurs, at a certain point in its history, humankind will accept that stars cannot be "visited" but only reached, that is, maybe once in a lifetime. As it happened on Earth in the past, humans will choose to leave their cradle for good. When this happens, fusion may be the means of propulsion.

Bibliography

Adams, R.B., Alexander, R.A., Fincher, S.S., Hopkins, R.C., Philips, A.D., Polsgrove, T.T, Lichtford, R.J., Patton, B.W., Statham, G., White, P.S. and Thio, Y.C.F. (2003) "Conceptual Design of In-Space Vehicles for Human Exploration of the Outer Planets", NASA Report TP-2003-212691, NASA, Marshall Space Flight Center, Alabama, November 2003.

Alladio, F., Grosso, L.A., et al. (2000) "Results of Proto-Pinch Testbench for the Proto-Sphera Experiment", *27th EPS Conference on Controlled Fusion and Plasma Physics*, Budapest, Hungary, 12–16 June 2000.

Anile, A. and Choquet-Bruhat, Y. (Editors) (1989) *Relativistic Fluid Dynamics,* Springer-Verlag, Berlin, August 1989.

Anon. (2003) "Frontiers in High Energy Density Physics: The X-Games of Contemporary Science", Committee on High Energy Density Plasma Physics, Plasma Science Committee, National Research Council, National Academic Press, Washington, DC, 2003.

Anon. (2006a) "New 'Planet' Is Larger than Pluto", News/SP/2006 (10), Press Release, 02 February 2006.

Anon. (2006b) "(Em)powering the Next Generation", UNM Engineering Magazine, School of Engineering, The University of New Mexico, Spring 2006, pp. 10-11. STAIF: the Institute for Space and Nuclear Power Studies, MSC01-1120, University of New Mexico, Albuquerque, NM 87131-0001, hosts a *Space Technology and Applications International Forum (STAIF)* every year. See the American Institute of Physics (AIP) site for STAIF Proceedings, containing papers dealing with advanced fission, fusion and antimatter propulsion.

Anon. (2011a) "Request For Information (RFI) – 100 Year Starship Study", Solicitation Number: DARPA-SN-11-41, DARPA/TTO, 03 May 2011.

Anon. (2011b) "Technology Readiness Assessment Guide", DOE G 413.3-4A, U.S. Department of Energy, 15 September 2011.

Anon. (2013) "Voyager to the Outer Planets and Into Interstellar Space", JPL 400-1538, NASA Facts, NASA, September 2013.

Anon. (2014a) "TESS – Transiting Exoplanet Survey Satellite", FS-2014-1-120-GSFC, NASA Facts, Goddard Space Flight Center, NASA, 2014.

Anon. (2014b) "WS Atkins plc – Analyst and Investor Visit to ITER", Plan Design Enable, Presentation, ATKINS, 02 October 2014.

Anon. (2015a) "New Horizons Pluto Flyby", Press Kit, NASA Headquarters, NASA, July 2015.

Anon. (2015b) "Fiscal Year 2016 Stockpile Stewardship and Management Plan", DOE/NA-0029, Report to Congress, National Nuclear Security Administration, US Department of Energy, March 2015.

Anon. (2016a) "Space Launch System", FS-2016-02-04-MSFC, NASA Facts, NASA, 2016.

Anon. (2016b) "National Ignition Facility – User Guide 2016", LLNL-TM-681123_P2103437_ WO15466_NUG, Lawrence Livermore National Laboratory, 2016.

Anthony, S. (2014) "Europe's Rosetta Becomes the First Spacecraft to Orbit a Real, Live Comet", ExtremeTech, 06 August 2014.

Ashworth, S. (2014) "The Starship Philosophy: Its Heritage and Competitors", *J. British Interplanetary Society*, Vol. 67, No. 11-12, pp. 447–459.

Asimov, I. (1979) *Extraterrestrial Civilizations*, Crown Publisher, New York, April 1979.

Assis, A.K.T and Neves, M.C.D. (1995) "History of the 2.7 K Temperature Prior to Penzias and Wilson", APEIRON, Vol. 2, Nr. 3, 03 July 1995.

Balshaw, N. (2015) "All-The-World's Tokamaks", www.tokamak.info, last updated 26 September 2015.

Barnhart, D., Garretson, P. and Will, P. (Editors) (2014) "100 Year Starship Study 2011: Time Distance Solutions". Papers are in: *Journal of the British Interplanetary Soc*iety, Vol. 67, No. 4 and 5, April and May 2014.

Baross, J.A. et al. (Editors.) (2007), *The Limits of Organic Life in Planetary Systems,* National Research Council of the National Academies, National Academies Press, Washington, DC, 2007.

Basov, N.G. and Krokhin, O.N. (1964) "Laser-Initiated Thermonuclear Fusion" (in Russian), *Sov. Phys. JETP.,* Vol. 19, No. 123, 1964 [also in English in IEEE (1968), *J. Quantum Elect.,* Vol. 4, p. 864].

Baxter, S. (2010) "Project Icarus: The Challenge of Mission Longevity", *Journal of the British Interplanetary Society*, Vol. 63, No. 11/12, pp. 426-433. Also in the same issue: "Project Icarus: Three Roads to the Stars", pp. 444–448.

Baxter, S. (2013) "Project Icarus: Interstellar Spaceprobes and Encounters with Extraterrestrial Intelligence", *Journal of the British Interplanetary Society (JBIS)*, Vol. 66, 2013, pp. 51–60.

Bond, A., Martin, A.R., Buckland, R.A., Grant, T.J., Lawton, A.T., Mattison, H.R., Parfitt, J.A., Parkinson, R.C., Richards, G.R., Strong, J.G., Webb, G.M., White, A.G.A. and Wright, P.P. (1978)

"Project Daedalus: The Final Report on the BIS Starship Study", *J. British Interplanetary Society (JBIS) Supplement,* Vol. 31, 1978, pp. S1-S192

Borowski, S.K. (1987) "A Comparison of Fusion/Antiproton Propulsion Systems for Interplanetary Travel", AIAA Paper 87-1814, *23rd Joint Propulsion Conference*, San Diego, CA, 29 June–02 July 1987.

Borowski, S.K. (1995) "Comparison of Fusion/Antiproton Propulsion Systems for Interplanetary Travel", in *Fusion Energy for Space Propulsion,* edited by T. Kammash, Progress in Astronautics and Aeronautics Series, Vol. 167, AIAA, Reston, VA, 1995.

Britt, R.R. (2005) "NASA Voyager 1 Team Says Spacecraft Has Reached Solar System's Outer Layer", *Space News,* 30 May 2005, p. 17.

Brown, D. (2006) *Angels & Demons: A Novel*, Washington Square Press, 2006.

Brown, M.E., Trujillo, C.A. and Rabinowitz, D.L. (2005) "Discovery of a Planet-Sized Object in the Scattered Kuiper Belt", *The Astrophysical Journal*, Vol. 635, No. 110, December 2005.

Brown, P. (1989) "Apparatus for Direct Conversion of Radioactive Decay Energy to Electrical Energy", US Patent No. 4,835,433, 1989.

Bruno, C. and Accettura, A. (Eds.) (2008) *Advanced Propulsion Systems and Technologies: Today to 2020,* Progress in Aeronautics and Astronautics Series Vol. 223, AIAA, Reston, VA, 2008.

Bruno, C. and Simone, D. (2009) "Nuclear Electric Propulsion for Interstellar Precursor Missions". Paper presented at the *6th IAA Symposium on Realistic Near-Term Advanced Scientific Missions*, Aosta, Italy, 6–9 July 2009.

Bruno, C., Simone, D. and Czysz P.A. (2009) "Investigation of Nuclear Elecric Powered Interstellar Precursor Missions", IAC paper IAC-09-D4.1-D4.3.7, presented at the *61st International Astronautical Congress (IAC),* Prague, 27 September–01 October 2009.

Bruno, C. (2012) "Nuclear Propulsion" in *Fluid Dynamics, Computational Modeling and Applications*, edited by L. Hector Juarez, InTech Editions, Rijeka, Croatia, Chapter 16. ISBN 978-953-51-0052-2.

Bruno, C. et al. (2013) "Key Technologies to Enable Near-Term Interstellar Scientific Precursor Missions", International Academy of Astronautics, Study Group SG III-10, Paris, 2013, Section 5.1.

Bruno, C. (2014) "In-Space Propulsion" in The International Handbook of Space Technology, edited by M. Macdonald, and V. Badescu, Springer-Praxis Books, Springer, London, February 2014, Chapter 11.

Bussard, R.W. (1960) "Galactic Matter and Interstellar Flight", *Acta Astronautica,* Vol. 6, 1960, pp. 179–195.

Bussard, R.W. (1990) "Fusion as Electric Propulsion", *Journal of Propulsion,* Vol. 6, No. 5, September–October 1990, pp. 567–574.

Bussard, R.W. and Jameson, L.W. (1993) "The QED Engine Spectrum: Fusion-Electric Propulsion for Airbreathing to Interstellar Flight", paper AIAA 93-2006, presented at the *29th Joint Propulsion Conference,* Monterey, CA, 28–30 June 1993.

Bussard, R.W., Jameson, L.W. and Froning, H.D. (1993) "The QED Engine: Fusion-Electric Propulsion for CIS-Oort/Quasi-Interstellar (QIS) Flight", paper IAF.4.1-93-708, presented at the *44th IAF Congress*, Graz, Austria, 16–22 October 1993.

Bussard, R.W. and Jameson, L.W. (1995) "Inertial-Electrostatic-Fusion Propulsion Spectrum: Air-Breathing to Interstellar Flight", *Journal of Propulsion and Power*, Vol. 11, No. 2, 1995, pp. 365–372.

Capaccioni, F. et al. (2015) "The Organic-Rich Surface of Comet 67P/Churyumov-Gerasimenko as seen by VIRTIS/Rosetta", *Science,* Vol. 347, No. 6220, 23 January 2015.

Carpenter, S.A. and Brennan, K.M. (1999) "Overview and Status of a Mirror Fusion Propulsion System Design Study", *Acta Astronautica,* Vol. 44, No. 7-12, April to June 1999, pp. 471–506.

Casali, D. and Bruno, C. (2004) "Superconducting Materials Applied to Electric Propulsion", AIAA *Journal of Spacecrafts and Rockets,* Vol. 41, No. 4, July to August 2004, pp. 671–676.

Cassady, R.J., Frisbee, R.H., Gilland, J.H., Houts, M.G., LaPointe, M. R., Maresse-Reading, C.M., Oleson, S.R., Polk, J.E., Russel, D. and Sengupta, A. (2008) "Recent Advances in Nuclear Powered Electric Propulsion for Space Exploration", *Energy Conversion and Management*, Vol. 49, Issue 3, March 2008, pp. 412–435.

Cassenti, B.N. (2004) "Engineering Challenges in Inertial Confinement Fusion Propulsion", AIAA Paper 2004-3533, presented at the *40th AIAA/ASME/SAE/ASEE Joint Propulsion Conference,* Fort Lauderdale, FL, 11–14 July 2004.

Cassenti, B.N. and Coreano, L. (2004) "The Interstellar Ramjet", Paper AIAA 2004-3568, presented at the *40th AIAA/ASME/SAE/ASEE Joint Propulsion Conference*, Fort Lauderdale, FL, 11–14 July 2004.

Cassibry, J., Cortez, R., Stanic, M., Watts, A., Seidler, W., Adams, R., Statham, G. and Fabisinski, L. (2015) "Case and Development Path for Fusion Propulsion", *Journal of Spacecraft and Rockets,* Vol. 52, No. 2, 2015, pp. 595–612.

Cesarone, R.J., Sergeyevsky, A.B. and Kerridge, S.J. (1984) "Prospects for the Voyager Extra-Planetary and Interstellar Mission", *J. British Interplanetary Society (JBIS),* Vol. 37, No. 3, 1984 pp. 99–116.

Chapman, R., Miley, G.H. and Kernbichler, W. (1989) "Fusion Space Propulsion With a Field Reversed Configuration", *Fusion Technology*, Vol. 15, p. 1154.

Chen, F.F. (1985) *Introduction to Plasma Physics and Controlled Fusion*, Vol. I and II, Plenum Press, New York, 1985.

Choueiri, E.Y. (2004) "A Critical History of Electric Propulsion: The First Fifty Years (1906-1956)", Paper AIAA-2004-3334, presented at the *40th AIAA/ASME/SAE/ASEE Joint Propulsion Conference*, Fort Lauderdale, Florida, 11–14 July 2004.

Choueiri, E.Y. (2002) Personal communication with C. Bruno.

Cohen, E.R., Lide, D.R. and Trigg, G.L. (2003) *AIP Physics Desk Reference,* 3rd Edition, Springer Publisher, New York, January 2003, p. 130.

Condon, E.U. (1943) "Los Alamos Primer Notes", based on a set of five lectures given by R. Serber during the first two UIFIB weeks of April 1943, as an 'indoctrination course' in connection with the starting of the Las Alamos Project, 1943 [see http://www.fas.org/sgp/othergov/doe/lanl/docs1/00349710.pdf].

Crawford, I. (2000) "Where Are They?" *Scientific American,* Vol. 283, No. 7, 2000, pp. 28–33.

Crawford, I.A. (2010) "Project Icarus: Astronomical Considerations Relating to the Choice of Target Star", *Journal of the British Interplanetary Society (JBIS)*, Vol 63, No. 11/12, 2010, pp. 419–425.

Daiber, J.W., Hertzberg, A. and Wittliff, C.E. (1966) "Laser-Generated Implosions", *Physics of Fluids,* Vol. 9, Issue. 3, 1966, pp. 617–619.

Davies, J.R. (2006) "The Alfven Limit Revisited and its Relevance to Laser-Plasma Interactions", *Laser and Particle Beams*, Vol. 24, No. 2, June 2006, pp. 299–310.

Davies, P. (2010) *The Eerie Silence: Are We Alone in the Universe?* Allen Lane/Penguin Press, London, 2010.

Dew-Hughes, D. (2001) "The Critical Current of Superconductors: An Historical Review", *Low Temperature Physics*, Vol. 27, No. 9–10, September to October 2001.

Dinerman, T. (2008) "Hitching a Ride to the Oort Cloud" *The Space Review,* 18 August 2008.

Dyson, F. (1968) "Interstellar Transport", *Physics Today*, Vol. 21, 1968. pp. 41–45.

Dyson, G. (2002) *Project Orion: The True Story of the Atomic Spaceship,* Henry Holt and Co., 16 April 2002.

Einstein, A. (1916) *Über die spezielle und allgemeine Relativitaetstheorie (Gemeinvestaendlich)* Heft 38, No. 2677, Vol. 106, Friedrich Vieweg & Sohn, Braunschweig, 1916.

El-Guebaly, L.A. (2010) "Fifty Years of Magnetic Fusion Research (1958-2008): Brief Historical Overview and Discussion of Future Trends", *Energies*, Vol. 3, 2010, pp. 1067-1086

Encrenaz, T., Bribing, J.P., Blanc, M., Barucci, M.A., Roques, F. and Zoucka, P.H. (2004) *The Solar System*, Chapter 14, Table 14.1, Springer, Berlin, 2004.

Englert, G.W. (1962) "Toward Thermonuclear Rocket Propulsion", *New Scientist,* Vol. 16, No. 307, 1962, pp. 16–18.

Ewig. R. and Andrews, D. (2003) "MiniMagOrion: A Pulsed Nuclear Rocket for Crewed Solar System Exploration", AIAA 2003-4525, presented at the *39th AIAA/ASME/SAE/ASEE Joint Propulsion Conference,* Huntsville, AL, July 2003.

Fearn, D.G. (2008) "Application of Ion Thrusters to High-Thrust, High-Specific Impulse Nuclear Electric Missions", *Nuclear Space Power and Propulsion Systems*, ed. by C. Bruno, AIAA, Reston VA, 2008, Chapter 3, p.68.

Forward, R.L. (1985) "Antiproton Annihilation Propulsion", *J. Propulsion,* Vol. 1, No. 5, 1985, pp. 570–374.

Frisbee, R.H. (2003) "Advanced Propulsion for the XXI Century", paper AIAA-2003-4676, presented at the *39th AIAA/ASME/SAE/ASEE Joint Propulsion Conference*, Huntsville, AL, 20–23 July 2003.

Froning, H.D. (1983) "Requirements for Rapid Transport to the Further Stars", *Journal of the British Interplanetary Society*, Vol. 36, May 1983, pp. 227–230.

Froning, H.D. and Bussard, R.W. (1998) "Aneutronic Fusion Propulsion for Earth-to-Orbit and Beyond", in *Proc. STAIF 1998,* AIP Publication CP-420, American Institute of Physics, Melville, NY, January 1998, pp. 1289–1294.

Froning, H.D., Miley, G.H., Luo, N., Yang, Y., Y., Momota, H. and Burton, E. (2005), "Combining MHD Airbreathing and Fusion Rocket Propulsion for Earth-to-Orbit Flight", in *Proc. STAIF 2005,* AIP Conference Proceedings, Vol. 746, Albuquerque, New Mexico, 13–17 February 2005, pp. 1339–1344.

Gaidos, G., Lahio, J., Lewis, R.A., Dundore, B., Fulmer, J. and Chakrabarthi, S. (1998) "Antiproton-Catalyzed Microfission/Fusion Propulsion Systems for Exploration of the Outer Solar System and Beyond", in *Proc. STAIF 1998,* AIP publication CP-420, American Institute of Physics, Melville, NY, January 1998, pp. 1365–1372.

Gilster, P. (2012) "100 Year Starship Public Symposium", Centauri Dreams, 15 August 2012.

Gorse, C., Capitelli, M. and Ricard A. (1985) "On the Coupling of Electron and Vibrational Energy Distribution in H_2, N_2 and CO Post Discharges", *Journal of Chemical Physics,* Vol. 82, Issue 4, February 1985, p. 1900.

Grappone, A.G. (2013) "Conceptual Design for an Autonomous Interstellar Probe", in: C. Bruno editor, "Key Technologies to Enable Near-Term Interstellar Scientific Precursor Missions", International Academy of Astronautics, Paris, 2013, Section 5.1.

Gunston, B. (2006) *The Development of Jet and Turbine Aero Engines*, Haynes Publishing, Sparkford, UK, October 2006.

Gurnett, D.A., Kurth, W.S., Allendorf, S.C. and Poynter, R.L. (1993) "Radio Emission from the Heliopause Triggered by an Interplanetary Shock", *Science,* Vol. 262, 1993, pp. 198–203.

Hahn, J. (2005) "When Giants Roamed", *Nature,* Vol. 435, pp. 432-433. Complete articles on early Solar System formation and the role of the Kuiper belt can be found in the three papers by Tsiganis et al., Morbidelli et al., and Gomes et al. in the same issue, pp. 459–469.

Hamilton, D. (2004) "After a 27-Year journey, Voyager 1 Enters Heliosheath", The Photon Online, Research Spotlight, Vol. 45, University of Maryland-Physics Online Newsletter, 2004.

Hand, E. (2016) "Astronomers Say a Neptune-Sized Planet Lurks Beyond Pluto", sciencemag.org, Science/AAAS, 20 January 2016.

Hand, E. (2015) "Comet Close-Up Reveals a World of Surprises", *Science,* Vol. 347, No. 6220, 23 January 2015, pp. 358–359.

Hand, E. (2014) "Comet Rendezvous", *Science,* Vol. 346, No. 6216, 2014, pp. 1442–1443.

Hartnett, K. (Editor in Chief) et al. (2009) *Hubble 2009 – Science Year in Review*, NASA Publication 2010-1-120-GSFC, NASA Goddard Space Flight Center, Greenbelt, Maryland, 2010.

Harwit, M. (1973) *Astrophysical Concepts,* Wiley, New York, 1973.

Hecht, J. (2008) "First Object Seen from Solar System's Inner Oort Cloud", *New Scientist*, Daily News, NewScientist.com news service, 18 August 2008.

Hegelich, B.M., Albright, B.J., Cobble, J., Flippo, K., Letzring, S., Paffett, M., Schreiber, J., Schultze, R.K. and Fernández, J.C. (2006) "Laser Acceleration of Quasi-Monoenergetic MeV Ion Beams", *Nature*, Vol. 439, 26 January 2006, pp. 441–448.

Heckstall-Smith, H.W. (1958) *Atomic Radiation Dangers and What They Mean to You*, J.M. Dent & Sons, London, 1958, pp. 46–47.

Hill, P.G. and Peterson, C.R. (1970) *Mechanics and Thermodynamics of Propulsion*, Addison-Wesley, Reading, MA, 1970, Chapter 15, p. 471.

Hirsch, R.L. (1967) "Inertial Electrostatic Confinement of Ionized Fusion Gases", *Journal of Applied Physics*, Vol. 38, Issue 7, 1967, p. 4522.

Holzscheiter, M.H., Lewis, R.A., Rochet, J. and Smith, G.A. (1996) "Production and Trapping of Antimatter for Space Propulsion Applications", AIAA Paper 96-2786, presented at the *32nd AIAA/ASME/SAE/ASEE Joint Propulsion Conference*, Lake Buena Vista, FL, 1–3 July 1996.

Hsu, J. (2008) "The Future of Space Robots", *Space.Com,* 02 July 2008.

Huba, J.D. (2016) *"NRL Plasma Formulary"*, Report NRL/PU/6790-16-614, Naval Research Laboratory, The Office of Naval Research, Washington, DC, p. 44.

Jarboe, T.R. (1994) "Review of Spheromak Research", *Plasma Physics Controlled Fusion,* Vol. 36, No. 6, pp. 945–990.

Jewitt, D.C. and Luu, J. (2004) "Crystalline Water Ice on the Kuiper Belt Object (50000) Quaoar", *Nature,* Vol. 432, 9 December 2004, pp. 731–733.

Jokipii, J.R. (2008) "A Shock for Voyager 2", *Nature,* Vol. 454, No. 7200, 3 July 2008, pp. 38–39. [This issue also contains five scientific articles on this subject.].

Joshi, C. (2006) "Plasma Accelerators", *Scientific American*, Vol. 294, February 2006, pp. 40–47.

Kammash, T. (1995) "Principles of Fusion Energy Utilization in Space Propulsion", in *Fusion Energy Space Propulsion*, edited by T. Kammash, Progress in Astronautics and Aeronautics Series, Vol. 167, AIAA, Reston, VA, January 1995.

Kammash, T and Galbraith, D.L. (1998) "Improved Physics Model of the Gasdynamic Mirror Fusion Propulsion System", *Journal of Propulsion and Power*, Vol. 14, No. 1, 1998, pp. 24–28.

Kammash, T. (2010) "Self-Fueling Fusion Hybrid Reactor For Space Power and Propulsion", *Journal of the British Interplanetary Society (JBIS)*, Vol. 63, No. 10, 2010, pp. 384–386.

Kaufmann, W.J. (1993) *Discovering the Universe,* 3rd Edition, W.H. Freeman, New York, Chapter 17 and Appendix 4.

Kenyon, S.J. and Bromley, B.C. (2004) "Stellar Encounters as the Origin of Distant Solar System Objects in Highly Eccentric Orbits", *Nature,* Vol. 432, 02 December 2004, pp. 598–602.

Kerstein, A. and Matko, D. (2007) "Eugen Sänger: Eminent Space Pioneer", *Acta Astronautica*, Vol. 61, Pergamon Publisher, May 2007, pp. 1085–1092.

Khatchadourlan (2014) "How to Fix ITER", The New Yorker, Daily Comment, 28 February 2014.

Kiang, N.Y. (2008) "The Color of Plants on Other Worlds", *Scientific American,* Vol. 298, No. 4, April 2008, pp. 28–35.

Kikuchi, M. and Azumi, M. (2015) *Frontiers in Fusion Research II – Introduction to Modern Tokamak Physics*. Springer, Heidelberg, 2015. Chapter 1.

Kondo, Y., Bruhweiler, F., Moore, J. and Sheffield, C. (Editors) (2003) *Interstellar Travel and Multi-Generational Space Ships*, Apogee Books Space Series, Apogee Books, June 2003. [For a bibliography on this subject, see http://www.ibiblio.org/lunar/school/library/bib.html].

Kramer, D. (2015) "Taking the Next Steps in Fusion Ignition Quest", *Physics Today,* Vol. 68, No. 2, February 2015, p. 24.

Kulcinski, G.L. and Conn, R.W. (1974) "The Conceptual Design of a Tokamak Fusion Power Reactor, UWFMAK-1", UWFDM-90, Fusion Technology Institute, University of Wisconsin, Madison Wisconsin, April 1974.

Lang, K.R. (1999) *Astrophysical Formulae – A Compendium for the Physicist and Astrophysicist,* Third Edition, Series: Astronomy and Astrophysics Library, Springer Verlag, Berlin, June 1999, p. 145 et seq.

Lawrence, T.J. (2008) "Nuclear-Thermal-Rocket Propulsion Systems", in: *Nuclear Space Power and Propulsion Systems,* edited by C. Bruno, AIAA, Reston, VA, October 2008, Chapter 2.

Lawson, J.D. (1957) "Some Criteria for Power Producing Thermonuclear Reactions" in: *Proceedings of the Royal Society of London, Section B,* Vol. 70, No. 1, 1957, pp. 1–6.

Leifer, S.D. (1999) "Reaching for the Stars", *Scientific American,* Vol. 232, No. 2, 01 February 1999, pp. 74–75.

Lenard, R.X. (2008) "Near-Term Nuclear Electric Propulsion Power System Performance Capabilities", Paper IAC-08 C4.7-C3.5.4, presented at the *57th International Astronautics Conference,* Glasgow, 29 September–04 October 2008.

Lerner, E.J. (1992) "The Big Bang Never Happened: A Startling Refutation of the Dominant Theory of the Origin of the Universe", Vintage Publisher, October 1992.

Lissauer, J. (1999) "How Common are Habitable Planets?", *Nature,* Vol. 402 Supplement, No. 6761, 1999, pp. C11–C14.

Loeb, J. (1918) *The Mechanistic Conception of Life: Biological Essays*, The University of Chicago Press, 1918.

Long, K., Obousy, R.K., Tziolas, A.C., Mann, A., Osborne, R., Presby, A. and Fogg, M. (2009) "Project Icarus: Son of Daedalus – Flying Closer to Another Star", *Journal of the British Interplanetary Society (JBIS),* Vol. 62, No. 11/12, 2009, pp. 403–414.

Lubin, P., Hughes, G.B., Bible, J., Bublitz, J., Arriola, J., Motta, C., Suen, J. Johansson, I., Riley, J., Sarvian, N., Clayton-Warwick., D., Wu, J., Milich, A., Oleson, M., Pryor, M., Krogen, P., Kangas, M. and O'Neill, H. (2014) "Toward Directed Energy Planetary Defense", *Optical Engineering*, Vol. 53, No. 2, February 2014, pp. 025103–1 to 025103–18.

Lubin, P. (2016) "A Roadmap to Interstellar Flight", *J. British Interplanetary Society (JBIS)*, in press, last revised 2 September 2016.

Luu, J.X. and Jewitt, D.C. (1996) "The Kuiper Belt", in *Scientific American,* Vol. 274, No. 5, 1996, pp. 32–39.

Maccone, C. (2009) *Deep Space Flight and Communications: Exploiting the Sun as a Gravitational Lens*, Springer Praxis Books, Springer, Berlin, April 2009.

March, P. (2004) Personal communication (email, November 4, 2004).

Maslen, S.H. (1959) "Fusion for Space Propulsion", *Institute of Radio Engineers Transactions on Military Electronics,* Vol. MIL-3, No. 2, April 1959, pp. 52–57.

Mazlish, B. (1985) "The Idea of Space Exploration", in: Roland, A. (Editor) *A Spacefairing People – Perspectives on Early Spaceflight*, NASA SP-4405, The NASA History Series, NASA, Washington, DC, 1985.

McGuire, T.J. (2007) "Improved Lifetimes and Synchronization Behavior in Multi-Grid Inertial Electrostatic Confinement Fusion Devices", PhD Thesis, Department of Aeronautics and Astronautics, MIT, February 2007.

Mecham, M. (2011) "Exoplanet Extras", *Aviation Week and Space Technology*, Vol. 173, No. 5, 07 February 2011, p. 38.

Mehta, A. (2016) "Lockheed Still Supporting Portable Nuclear Generator", DefenseNews, 03 May 2016.

Messerle, H.K. (1995) *Magnetohydrodynamic Electrical Power Generation*, J. Wiley & Sons, Chichester, UK, August 1995.

Metz, W.D. (1976) "Fusion Research (II): Detailed Reactor Studies Identify More Problems", *Science,* Vol. 193, 02 July 1976, pp. 38–40 and p. 76.

Mikellides, P.G. (2004) "Modeling and Analysis of a Megawatt-Class Magnetoplasmadynamic Thruster", *Journal of Propulsion and Power,* Vol. 20, No. 21, 2004, pp. 204–210. See also the Proceedings of the "Technology and System Options towards Megawatt Level Electric Propulsion" Workshop, Lerici, Italy, 9–10 June 2003.

Miley, G.H., Satsangi, A.J., DeMora, J., Javedani, J.B., Gu, Y., Burton, R.L. and Nakashima, H. (1995) "Innovative Technology for an Inertial Electrostatic Confinement Fusion Propulsion Unit", in *Fusion Energy for Space Propulsion,* edited by T. Kammash, Progress in Astronautics and Aeronautics Series, Vol. 167, AIAA, Reston, VA, January 1995, pp. 161–178.

Miley, G., Bromley, B., Jurczyk, B., Stubbers, R., DeMora, J., Chacon, L. and Gu, Y. (1998) "Scaling of the Inertial Electrostatic Confinement (IEC) for Near-term Thrusters and Future Fusion Propulsion", in *Proc. STAIF 1998,* AIP publication CP-420, American Institute of Physics, Melville, NY, January 1998, pp. 1373–1375.

Miley, G.H., Yang, X., Flippo, K.A. and Hora, H. (2010) "Fusion Space Propulsion Using Fast-Ignition Inertial Confinement Fusion (FI-ICF)", *J. British Interplanetary Society,* Vol. 63, No. 9/10, September 2010, pp. 387–390.

Miley, G.H. and Krupakar Muraly, S. (2014) Inertial Electrostatic Confinement (IEC) Fusion: Fundamentals and Applications, Springer, New York, 2014.

Miller, A.I. (1981) *Albert Einstein Special Theory of Relativity: Emergence (1905) and Early Interpretation (1905-1911),* Addison-Wesley, Reading, MA, 1981.

Millis, M.G. (2010) Progress in Revolutionary Propulsion Physics. In: IAC-10-C4.8.7, IAC 2010, presented at the 61st International Astronautical Congress 2010, Prague, Czech Republic, 27 Sept–01 Oct 2010.

Miyamoto, K. (2006) *Controlled Fusion and Plasma Physics,* CRC Press, 23 October 2006.

Morgan, D.L. (1982) "Concepts for the Design of an Antimatter Annihilation Rocket", *J. British Interplanetary Society*, Vol. 135, 1982, pp. 405–408.

Morrison, P., Billingham, J. and Wolfe, J. (Editors) (1977) "The Search for Extraterrestrial Intelligence, SETI", NASA SP-419, NASA, 1977.

Mukhin, K.N. (1987) *Experimental Nuclear Physics, Volume 1: Physics of Atomic Nucleus*, MIR Publishers, Moscow, 1987, p. 50.

Murthy, S.N.B. and Froning, H.D. (1991) "Combining Chemical and Electric-Nuclear Propulsion for High Speed Flight", in: *Proceedings of the 10th International Symposium on Airbreathing Engines (ISABE)*, Nottingham, UK, 01 - 06 September 1991, edited by F.S. Billig, American Institute of Aeronautics and Astronautics, Reston, VA, Vol. 2, pp. 1319–1326.

Nakai, S., and Mima, K. (2007) "Development of Inertial Fusion Energy by Laser", in: *Laser Ablation and its Applications*, edited by C.R. Phipps, Springer, New York, 2007, Chapter 15.

Nakashima, H. Kajimura, Y., Kozaki, Y. and Zacharov, Y.P. (2005) "A Laser Fusion Rocket Based on Fast Ignition Concept", Paper IAC-05-C3.5-C4.7.07, presented at the *56th International Astronautical Congress (IAC)*, Fukuoka, Japan, 16–21 October 2005.

Nance, J.C. (Project Manager) (1964) "Nuclear Pulse Propulsion (Project Orion) - Technical Summary Report", General Atomic Report GA-4805, San Diego, CA., Vol 1, the Technical Summary is General Atomic GA-5009, released by NASA, George Marshall Flight Center, Huntsville, AL, 19 September 1964.

Norris, G. (2014) "Fusion Frontier", *Aviation Week & Space Technology*, Vol. 176, No. 37, 20 October 2014, pp. 42–43.

Ohnishi, M., Yamamoto, Y., Hasegawa, M., Yoshikawa, Y. and Miley, G.H. (1998) "Study on an Inertial Electrostatic Confinement Fusion as a Portable Neutron Source", *Fusion Engineering and Design,* Vol. 42, Issues 1-4, September 1998, pp. 207–211.

Ono, M., Quadrelli, M. et al. (2015) "Comet Hitchhiker", NASA, NIAC Phase I Final Report, 30 June 2015.

Orth, C.D. (2003) "VISTA – A Vehicle for Interplanetary Space Transport Application Powered by Inertial Confinement Fusion", Lawrence Livermore National Laboratory Report UCRL-TR-110500, Lawrence Livermore National Laboratory, 16 May 2003.

Polsgrove, T.T., Fabisinski, L., Fincher, S., Qualis, C.D.M., Miernik, J., Percy, T., Statham, G., Turner, M., Cassibry, J., Cortez, R. and Santarius, J. (2010), "Z-Pinch/Dense Plasma Focus Thermo-Nuclear Propulsion System" Final Report, Advanced Concept Office (ED04), NASA Marshall Space Flight Center, Alabama 35812, 08 October 2010.

Porco, C. (2004) "Cassini Captain's Log: 2004.184", *The Planetary Report - A Halo of Moons,* Vol. XXIV, No. 5, September-October 2004, pp. 12–18.

Post, R.F. (1987) "The Magnetic Mirror Approach to Fusion", *Nuclear Fusion,* Vol. 27, No. 10, pp. 1579–1739.

Quirico, E. et al. (2015) "Composition of Comet 67P/Churyumov-Gerasimenko Refractory Crust as Inferred From VIRTIS-M/Rosetta Spectro-Imager", Paper EPSC2015-621,, Proceedings of the *European Planetary Science Congress*, EPSC Abstracts, Vol. 10, 2015.

Reynolds, C.S. (2008) "Bringing Black Holes into Focus", *Nature,* Vol. 455, No. 7208, 04 September 2008, pp. 39–40.

Reynolds, R.J. (2002) "The Gas Between the Stars", *Scientific American*, Vol. 286, No. 1, 2002, pp. 32–41.

Rickard Hedden, C. (2014) "Meet The Leader of Skunk Works' Compact Fusion Reactor Team", *Aviation Week & Space Technology*, 20 October 2014.

Romanelli, F. and Bruno, C. (2005) "Assessment of Open Magnetic Fusion for Space Propulsion", ESA-ESTEC Final Report, ESA-ARIADNA Contract 18853/05/NL/MV, Noordwijk, 2005.

Sänger, E. (1953) "The Theory of Photon Rockets", *Ingenieur Archiv,* Vol. 21, 1953, pp. 213–219.

Sänger, E. (1956) "Die Erreichbarkeit der Fixsterne", in *Rendiconti del VII Congresso Internazionale Astronautico,* Associazione Italiana Razzi *(Proceedings of the VII International Astronautical Congress)*, Rome, 1956, pp. 97-113. Also in: Mitteilungen der Landesgruppe Nordbayern der DGRR vom 13.05.1958.

Sänger, E. (1965a) *Space Flight*, Mc Graw-Hill, New York, 1965, pp. 187–215.

Sänger, E. (1965b) "Rocket Flight Engineering", NASA TT F-223, NASA Technical Translation, NASA, 1965.

Santarius, J.F. and Logan, B.G. (1998) "Generic Magnetic Fusion Rocket", *Journal of Propulsion and Power,* Vol. 14, No. 4, 1998, pp. 519–524.

Schmidt, G.R., Gerrish, H.P., Martin, J.J., Smith, G.A. and Meyer, K. J. (1999) "Antimatter Production for Near-Term Propulsion Applications", *Journal of Propulsion and Power*, Vol. 16, No. 5, 2000, pp. 923-928 [also AIAA 1999-2691, presented at the *35th AIAA/ASME/SAE/ASEE Joint Propulsion Conference*, Los Angeles, CA, June 1999].

Schneider, J. (2005) "The Extrasolar Planets Encyclopedia", www.exoplanet.eu, 19 August 2016.

Schulze, N.R. and Roth, J.R. (1990) "The NASA-Lewis Program on Fusion Energy for Space Power and Propulsion, 1958–1978", *Fusion Technology,* Vol. 19, No. 1, April 1990, pp. 11–28.

Shepherd, L.R. (1952) "Interstellar Flight", *J. British Interplanetary Society. (JBIS)*, Vol. 11, 1952, pp. 149–167.

Sciama, D.W. (1971) *Modern Cosmology,* Cambridge University Press, London, 1971, p. 71.

Shmatov, M.L. (2000) "Space Propulsion Systems Utilizing Ignition of Microexplosions by Distant Microexplosion and Some Problems Related to Ignition of Microexplosions by Microexplosions", *J. British Interplanetary Society,* Vol. 53, No. 2, 2000, pp. 62–72.

Shmatov, M.L. (2004) "Creation of the Directed Plasma Fluxes with Ignition of Microexplosions by and with the Use of Distant Microexplosions", *J. British Interplanetary Society,* Vol. 57, No. 10, 2004, pp. 362–378.

Shmatov, M.L. (2005) "The Typical Number of Antiprotons Necessary to Heat the Hot Spot in the D-T Fuel Doped with U, *J. British Interplanetary Society,* Vol. 58, No. 2, 2005, pp. 7481.

Shmatov, M.L. (2006) "The Expected Efficiency of Burning of the D-^{3}He Fuel in Space Propulsion Systems", *Journal of the British Interplanetary Society,* Vol. 59, No. 1, January 2006, pp. 35–38.

Smirnov, V.P. (2010) "Tokamak Foundation in USSR/Russia – 1950-1990", *Nuclear Fusion*, Vol. 50, Issue 1, *Nuclear Fusion*, IOP Publishing and International Atomic Energy Agency, January 2010.

Spencer, J., Buie, M., Young, L., Guo, Y. and Stern, A. (2003) "Finding KBO Flyby Targets for New Horizons" *Earth, Moon, and Planets,* Vol. 92, Nos. 1–4, June 2003, pp. 483–491.

Stuhlinger, E. (1964) "Ion Propulsion for Space Flight", McGraw-Hill, New York, January 1964.

Stuhlinger, E. and Ordway, F.I. (1994) *Wernher Von Braun Crusader for Space: A Biographical Memoir*, Krieger Publisher, April 1994.

Stygar, W.A., Cuneo, M.E., Headley, D.I., Ives, H.C., Leeper, R.J., Mazarakis, M.G., Olson, C.L., Porter, J.L., Wagoner, T.C. and Woodworth J.R. (2007) "Architecture of Petawatt-Class Z-Pinch Accelerators", *Phys. Rev. Special Topics*, Vol. 10, No. 3, March 2007, pp. 3401–3424.

Taccetti, J.M. (2002) "Overview of High-Density FRC Research on FRX-L at Los Alamos National Laboratory", LASL Report LA-UR-02-6305, September 2002.

Taccetti, J.M. et al. (2003) "FRX-L: A Field-Reversed Configuration Plasma Injector for Magnetized Target Fusion", *Review of Scientific Instruments*, Vol. 74, No. 10, pp. 4314–4323.

Takahashi, H. and Yu, A. (1998) "Muon-Catalyzed Fusion for Space Propulsion, and a Compressed Target for Producing and Collecting Anti-Protons", in *Proc. STAIF 1998,* AIP publication CP-420, American Institute of Physics, Melville, NY, January 1998, pp. 1359–1364.

Than, K. (2008), "Large 'Planet X' May Lurk Beyond Pluto", *Space.com*, June 18, 2008..

Vchivkov, K.V., Nakashima, H., Zacharov, Y.P., Esaki, T. Kawano, T. and Muranaka, T. (2003) "Laser-Produced Plasma Experiments and Particles in Cell Simulation to Study Thrust Conversion Processes in Laser Fusion Rocket", *Japanese Journal of Applied Physics,* Vol. 42, Part 1, No. 10, October 2003, pp. 6590–6597.

Wambsganns, J. (2001) "Gravity's Kaleidoscope', *Scientific American,* Vol. 284, No. 11, 2001, pp. 52–59.

Weaver, H.A. and Stern, S.A. (2008) "New Horizons: NASA's Pluto-Kuiper Belt Mission", in *The Solar System Beyond Neptune*, Edited by Barucci, M.A., Boehnhardt, H., Cruikshank, D.P., Morbidelli, A. and Dotson, R., The University of Arizona Press, 2008, pp. 557–571.

Webb, S. (2002) *If the Universe is Teeming With Aliens ... Where Is Everybody?*, Copernicus Books, Praxis Publishing, 2002.

Weber, M.H., Lynn, K.G., Jennings, J., Lund, K. and Minnal, C. (2014) "A Novel Method to Store Charged Antimatter Particles", in: 100 Year Starship 2014 Public Symposium Conference Proceedings, Pathway to the Starts - Footprints on Earth, M. Jamison editor, 100 Year Starship Store, 18–21 September 2014.

Weissman, P.R. (1998) "The Oort Cloud", *Scientific American,* Vol. 279, No. 3, September 1998, pp. 62–67.

Wheeler, E. (2014) "The 'Wow' Signal, Drake Equation and Exoplanet Considerations", *J. British Interplanetary Society*, Vol. 67, No. 11–12, 2014, pp. 412–417

Williams, C.H., Borowski, S.K., Dudzinski, L.A. and Juhasz, A. J. (1998) "A Spherical Torus Nuclear Fusion Reactor Space Propulsion Vehicle Concept for Fast Interplanetary Travel", NASA TM 1998-208831/AIAA-98-3591, NASA, December 1998.

Williams, C.H. (2004) "Application of Recommended Design Practices for Conceptual Nuclear Fusion Space Propulsion Systems", Paper AIAA 2004-3534, presented at the *40th AIAA/ASME/SAE/ASEE Joint Propulsion Conference,* Fort Lauderdale, FL, 11–14 July 2004 [also published as: "Special Project Report - Recommended Designed Practices for Conceptual Nuclear Fusion Space Propulsion Systems", Special Publication SP-108-2004, AIAA, Reston, VA, 2004.

Winterberg, F. (1971) "Rocket Propulsion by Thermonuclear Micro-Bombs Ignited with Intense Relativistic Electron Beams", *Raumfahrtforschung,* Vol. 15, No. 5, September to October 1971, pp. 208–217.

Winterberg, F. (1980) "Super-Ion-Beams and Advanced Target Concepts for Thermonuclear Microbomb Rocket Propulsion", *Acta Astronautica*, Vol. 7, Issue 7, 1980, pp.825–837.

Winterberg, F. (2009a) "Ignition of a Deuterium Micro-Detonation with a Gigavolt Super Marx generator", *J. Fusion Energy*, Vol. 28, 2009, pp. 290–295.

Winterberg, F. (2009b) "Advanced Deuterium Fusion Rocket Propulsion for Manned Deep Space Missions", *J. British Astronautical Society*, Vol. 2, 2009, pp. 286–307.

Winterberg, F. (2010) *The Release of Thermonuclear Energy by Inertial Confinement: Ways Towards Ignition*, World Scientific, Singapore, 2010, Chapters 7 and 8.

Winterberg, F. (2012) "Matter-Antimatter Gigaelectronvolt Gamma Ray Laser Rocket Propulsion", *Acta Astronautica*, Vol. 81, Issue 1, December 2012, pp. 34–39.

Winterberg, F. (2013) "Deuterium-Tritium Pulse Propulsion with Hydrogen as Propellant and the Entire Spacecraft as a Gigavolt Capacitor for Ignition", *Acta Astronautica*, Vol. 89, 2013, pp. 126–129.

Winterberg, F. (2014a) "To Mars in Weeks by Thermonuclear Microbomb Propulsion", *Journal of Propulsion and Power,* Vol. 30, No. 6, 2014, pp. 1480–1484.

Winterberg, F. (2014b) "Thermonuclear Operation Space Lift" in: 100 Year Starship 2014 Public Symposium Conference Proceedings, M. Jamison editor, 100 Year Starship Store, 2014 [see www,100yss.org].

Winterberg F. (2015) "Thermonuclear Operation Space Lift", *Journal of Spacecraft and Rockets*, Vol. 52, No. 2, 2015, pp. 613–618.

Wittenberg, L.J., Santarius, J.F. and Kulcinski, G.L. (1986) "Lunar Source of He^3 for Commercial Fusion Power', *Fusion Technology,* Vol. 10, No. 2, September 1986, pp. 167–178.

View to the Future and Exploration of Our Galaxy

9

9.1 Introduction

The Andromeda Galaxy (Messier 31 or M31), see Fig. 9.1, is the nearest galaxy to the Milky Way, our galaxy. Both are residing within the neighborhood of the galactic cluster, which consists of an assembly of galaxies that are bound together by gravity. The Milky Way Galaxy contains our Solar System. The Milky Way is some 100,000 light-years in diameter, with its central bulge about 20,000 light-years in depth. That central bulge contains the very massive black hole that drives the kinetics of the Milky Way Galaxy (Smith et al. 2012).

In Chap. 8, we have seen that our Solar System is on one of the spiral arms some 32,000 light-years from the galaxy center, and there is a group of stars (about seven) that are within 10 light-years of our Sun. Beyond that local group, our galactic stars are much more distant. Even if we travel at the speed of light, our nearby star neighbors are up to a 20-year round-trip away. Can we overcome such distances, or are we bound to our Solar System, or at most our nearby stars? That is the question that dominates our view to the future, after the sobering conclusions in Chap. 8.

Using General Relativity, researchers can theorize approaches to traveling at fractional light speed, and even at greater than light (superluminal) speed. The validity of some of these theories has being investigated by NASA Glenn Research Center (Millis 2004, 2005). The Earth's Milky Way Galaxy contains up to 100,000 million stars. The Earth is about 32,000 light-years from the center. Without super light speed, the Galaxy is isolated from our ability to explore it in any realistic time frame, except perhaps for our very nearby galactic neighbors. The distances are almost not comprehensible. At 1000 times the speed of light, it would take 32 years for us to reach the Galactic center. Yet, some researchers think that to consider superluminal speed is no more daunting than the past century's researchers considering supersonic travel. Although thinkable scenarios need to be sifted, there are indeed concepts that appear to be based on solid physics.

Many of these are presented at the annual International Astronautical Federation (IAF) Congress. Some will be discussed in terms of what might be possible. As already pointed out in Chap. 8, and shown in Fig. 9.2, we are nowhere near having the capability to reach the nearest star in our current projection of future systems for this century. Nevertheless, the number of research or speculative papers and books describing means of achieving interstellar travel is quite large, see for instance (Mallove and Matloff 1989; Woodward 2013; Cook 2002; Rodrigo 2010; LaViolette 2008), containing a compendium of scientific, engineering, and, sometimes, hypothetical knowledge about interstellar travel, overall underscoring the continuing appeal of this topic. But what are the possibilities, or at least the potential?

As done in research papers, we can indeed marshal and calculate numbers, but achieving the conditions computed remains questionable. Again, our foes are inertia and mass. Dr. David Froning states in 1991:

> … It is well known that enormous amounts of rocket propellant are required to overcome gravitational and inertial resistance to Earth-to-orbit flight. Here, overcoming gravitational and inertial resistance to upward and forward flight requires impartation [imparting] of about 7.5 km/s velocity to Earth-to-orbit rocket ships, and this requires that about 90 percent of single-stage-to-orbit (SSTO) rocket ship weight be propellant. Thus, if field actions and reactions of field propulsion could significantly reduce gravitational and inertial resistance, rocket thrust and propellant needs would be significantly reduced. But a major obstacle to reducing such resistance by field propulsion is current lack of understanding as to the origins of gravitation and inertia - of why and how they instantly arise to resist vehicle acceleration (or deceleration) and the vehicle's upward flight. Although the relation of gravity and inertia to parameters such as motions, distances, and ponderosities of material bodies are well known, there is no consensus whatsoever as to the origins of gravity and inertia … (Froning 1991)

Froning discusses three possible origins of mass and three possible origins of inertia. None of the six possibilities have been confirmed. Then, until a new understanding such as quantum gravitation can change the situation, we are confined, optimistically, to about 10 light-years from our Sun.

P.A. Czysz et al., *Future Spacecraft Propulsion Systems and Integration*,
Springer Praxis Books, DOI 10.1007/978-3-662-54744-1_9

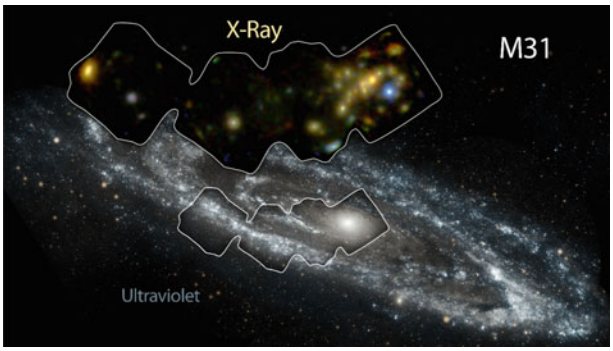

Fig. 9.1 Andromeda galaxy in high-energy X-rays imaged with NASA's nuclear spectroscope telescope array (NuSTAR). *Courtesy* NASA/JPL-Caltech/GSFC

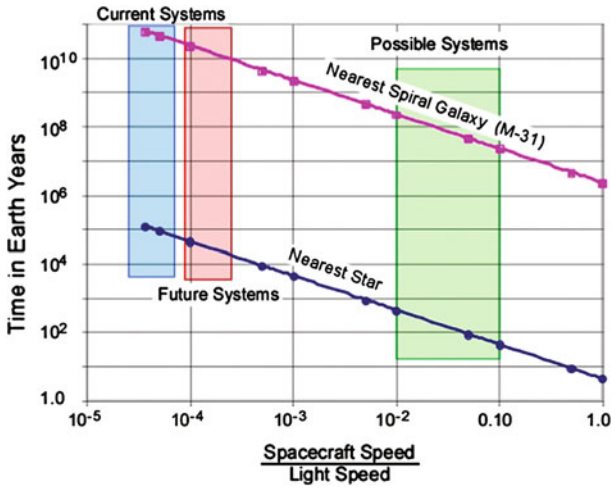

Fig. 9.2 Journey time as a function of spacecraft speed

The speed at which we can reach destinations within this sphere is wholly dependent on the specific impulse and thrust of the propulsion systems we can create. Today, we are limited to the leading edge of this sphere, that is the Oort Cloud. If practical fusion rockets become a reality, we could probably get a little farther, but to reach even the trailing edge of the Oort Cloud, we need a factor of ten increases in specific impulse. In order to reach 10 light-years requires a 10,000-fold increase in specific impulse, simply to limit mass consumption, that is, not considering the thrust required to limit travel time.

Then, what we need to do now is concentrate on getting from the surface of the Earth to orbit and to maneuver efficiently while in orbit. When these far-in-the-future propulsion advances are made, we will have the Earth-orbit-Moon infrastructure to take advantage of these developments.

9.2 Issues in Developing Near- and Far-Galactic Space Exploration

Reaching speeds close to that of light (relativistic speeds) in traveling through space is predicted to have major effects. Some of these effects have been mentioned in Chap. 8, see Stuhlinger (1964). They are the physical result embodied in the *Theory of Special Relativity* created by Einstein (1905). According to this theory, there are no privileged frames of reference such as the famed "absolute inertial frame" of classical physics. It is fact that the laws of dynamics appear the same in all frames of reference moving at constant velocity relative to each other (inertial but not absolute frames). This statement can be rephrased by saying that the laws of dynamics are "invariant" with respect to Galilean transformations, i.e., they remain the same in two frames of references in uniform motion (*constant* velocity) relative to each other. Experiments by Michelson and Morley (Rahaman 2014), repeated and validated for over a century, also showed the speed of light is invariant with the frame of reference, i.e., it does *not* increase or decrease due to the relative velocity between two inertial frames. This has been a disconcerting and counter-intuitive result that troubled many physicists. These two facts ultimately resulted in Einstein's intuition that simultaneous events cannot exist.

The second motivation for abandoning absolute frames of references and Galilean transformations was the need to make invariant not only the laws of dynamics, but also the laws of electromagnetism when changing frames of reference. In fact, contrary to the laws of dynamics, Maxwell equations change in a Galilean transformation. For instance, because the Lorentz force on a charge depends on its velocity, it would differ in different Galilean reference systems. This mathematical result was unacceptable, amounting to the existence of different electromagnetism "physics" in different inertial frames. The work done by Larmor, Lorentz, and Einstein himself convinced Lorentz that the Galilean transformations had to be replaced by the Lorentz transformations (Faraoni 2014), in which the characteristic ratio between frame speed and the speed of light appears. It is because of these new relationships between two inertial frames of reference that a clock on a spacecraft moving at constant velocity with respect to an Earth's observer would appear to him/her to run at a different speed than a clock on Earth. In other words, Earth time is *not* spaceship time.

The revolutionary character of *Special Relativity* stems from the fact that there cannot be a "third" or "impartial" observer capable of judging the "right" time between the two. The two frames in relative inertial motion are equally "right," each in its own frame, a consequence that alone can "explain" the *twin paradox* so often cited in connection to

relativity (Unnikrishnan 2005). Then, Earth time and ship time are different, but it is Earth time we must be concerned with because that is the time in which the project team is living. H. David Froning has spent a career investigating deep-space travel possibilities, and the authors wish to acknowledge his contribution to this section (Froning 1980, 1981, 1983, 1985, 1986, 1987, 1989, 1991, 2003; Froning et al. 1998; Froning and Barrett 1997, 1998; Froning and Roach 2000, 2002, 2007; Froning and Metholic 2008).

To recall, the Lorentz transformation of Special Relativity (Einstein 1915; Lang 1999) results in a time relationship for the Earth observer and for the spacecraft traveler as follows:

$$t_{\text{Earth}} = \frac{t_{\text{spacecraft}}}{\sqrt{1 - \left(\frac{V}{c}\right)^2}} \tag{9.1a}$$

$$t_{\text{spacecraft}} = t_{\text{Earth}} \cdot \sqrt{1 - \left(\frac{V}{c}\right)^2} \tag{9.1b}$$

Note that in Galilean transformations (in classical physics), the two times are assumed identical, that is,

$$t_{\text{Earth}} = t_{\text{spacecraft}} \tag{9.2}$$

because the speed of light seemed at that time infinite. This classical result is in fact predicted by the Lorentz transformations in the limit $c \to \infty$.

Then, as the spacecraft approaches the speed of light, the crew's apparent time is shorter than the observer's apparent time on Earth. Both perceive that the event or journey has occurred over an equal duration. It is not until the spacecraft crew returns to Earth that the discrepancy in perceived times becomes apparent. Researchers have derived the relativistically correct equations for a spacecraft journey's duration (t_e) in an Earth-bound observer frame of reference, and for the journey duration (t_{sc}) of that same spacecraft in its own moving reference (Froning 1980). For the simple case of one-dimensional *rectilinear* motion, Krause has derived the expressions for (t_e) and (t_{sc}) for a spacecraft acceleration (a_{sc}) in its own moving frame during the initial half of the total journey distance (S) followed by a constant spacecraft deceleration ($-a_{sc}$) during the final half of the total journey (Krause 1960; Maccone 2008a).

The reader is warned that the relationships below can be derived and are valid only when the motion is rectilinear, i.e., when the space–time continuum is the so-called Rindler space–time (only two-dimensional). This is not a very realistic assumption but one that simplifies this problem. In the fully four-dimensional space–time, or Minkowski's space, the effect of changing velocity (acceleration) is much more complex. There is, in fact, an important consequence with respect to changing velocity, because velocity is a vector. Even simply inverting direction invalidates the consequences of the Lorentz transformations that are strictly valid among *inertial* frames, that is, with constant relative velocity. Because velocity is defined by a magnitude (speed) and a direction, if either changes, then it has to be the result of acceleration. The most common effect of acceleration is a change in the magnitude of the speed. However, a constant speed turn is in fact an acceleration from a continuously varying direction. The direction of the acceleration is perpendicular to the flight path, and pointed at the center of the (instantaneous) rotation. This is the acceleration, the result of any rotation of the velocity vector. Thus, in the spacecraft reference frame, a spacecraft crew in orbit is under a constant acceleration, balanced of course by their gravitational weight. In space, the thrust from a propulsion system is necessary to initiate any acceleration, whether positive or negative. Because there are no aerodynamic forces in space, any motion initiated will continue until it is decelerated by a propulsion force of equal magnitude and opposite direction.

In the two-dimensional continuum assumed in the example by Krause, the two times, crew time and Earth time, are given by the following equations:

$$t_e = 2 \cdot \sqrt{\frac{S}{a_{sc}} \cdot \left(1 + \frac{a_{sc} \cdot S}{4 \cdot c^2}\right)} \tag{9.3}$$

With

$$t_{sc} = \frac{2 \cdot c}{a_{sc}} \cdot \cosh^{-1}\left(1 + \frac{a_{sc} \cdot S}{2 \cdot c^2}\right) \tag{9.4}$$

These equations can be solved for a number of different destinations as a function of spacecraft acceleration and their times compared. The life of a deep-space mission management team (ground team) is probably about 20–30 Earth years. If we wish to travel farther into space, that is, faster relative to the Earth time frame of reference, then we must travel faster.

We have seen in Chap. 8 that accelerated trajectories need tremendous amounts of propellant mass and appear unfeasible at the present state of our knowledge. However, it is interesting to see the consequences of acceleration on travel time if, at some point in the future, propulsion systems other than based on Newton's Third Principle will be discovered.

Before discussing travel times, we need to establish the *absolute limit,* or boundary, posed by Special Relativity, that is, when spacecraft speed equals light speed. For such a flight profile, the maximum spacecraft velocity will be assumed to be reached at the journey midpoint only, see Fig. 9.3. From the starting point to the midpoint, the spacecraft has a continuous and constant positive acceleration. From the midpoint to the end point, the spacecraft has a

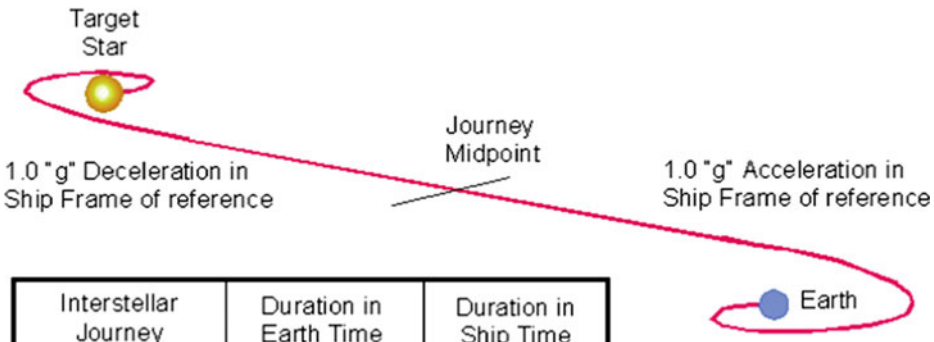

Interstellar Journey	Duration in Earth Time	Duration in Ship Time
Earth to Nearest star	4.53 years	2.86 years
Earth to Galaxy Center	33,000 years	24.7 years
Earth to Nearest Spiral Galaxy	2.2 million years	28.3 years

Fig. 9.3 Specific examples of Earth versus ship times

continuous and constant negative acceleration. Eugen Sänger derived the ratio of the spacecraft velocity (V) to light speed (c) at the journey midpoint, as given in Eq. (9.5) (Sänger 1956).

$$\frac{V}{c} = \tanh\left[\cosh^{-1}\left(1 + \frac{a_{sc} \cdot S}{2 \cdot c^2}\right)\right] \tag{9.5}$$

In Eq. (9.5), the value of the hyperbolic tangent approaches 1 as the value of the hyperbolic arc cosine approaches infinity. So, this solution tells that objects *never reach light speed* unless their acceleration is also infinite. Said otherwise, reaching light speed requires reaching also infinitely large kinetic energy, because V/c tends to 1 and the Lorentz transformation factor (the square root at the denominator) tends to infinity. In Sect. 8.3, we have seen that this is the result of the fact that *potential* energy grows with the Lorentz transformation factor $(1 - V^2/c^2)^{-1/2}$, see Eq. (8.26). However, the hyperbolic tangent has a value of 0.9999, or V is only 0.01% less (30 km/s less) than light speed when the value of the hyperbolic arc cosine function is 70.7. As a consequence, the ($V/c \approx 1$) curve on Fig. 9.4 represents actually 0.9999% of light speed.

Equations (9.3) and (9.4) for Earth time and spacecraft crew time can be solved, for instance, for three sample destinations: (1) For one of the nearest stars, *Proxima Centauri*, 4.24 light-years distant; (2) For the *Galactic Center*, 33,000 light-years away: and (3) For the nearest spiral galaxy, *Andromeda*, 2,200,000 light-years away. Figure 9.4 shows that with the flight profile just assumed for a hypothetical Earth observer, the spacecraft time seems to flow more slowly than Earth time. In terms of spacecraft time, the mission time appears to be approaching a constant value. In the spacecraft, the clock onboard would appear to run slower and slower as the acceleration is increased. To *the crew*, the transit time to final destination continuously decreases as the constant acceleration, a_{sc}, increases, just as expected. Remember, in this discussion, these are one-way missions. However, if the spacecraft were to return to Earth, both the Earth observer's time and spacecraft's crew time would double. These results are shown in Fig. 9.4 on the right, where solid lines are Earth time and broken lines are crew or spaceship time. Each of the Earth observer time curves (solid lines) approaches asymptotically the time corresponding to the distance from Earth, *measured in light-years,* as the spacecraft velocity approaches light speed.

The spacecraft crew time (broken line) breaks away from the Earth observer line above some acceleration threshold. The greater the distance, the lower the value where the spacecraft/crew-perceived acceleration curve breaks away from the Earth observer line. For the nearby Proxima Centauri star, the observer and the spacecraft crew time curves are relatively close until almost $1g$ acceleration (9.8067 m/s^2). For the two more distant destinations, and for practical accelerations, there are orders-of-magnitude differences between Earth and crew times. In fact, one of the many problems with interstellar travel is the different times predicted by Special Relativity between non-inertial frames. Note again that in these calculations the effect on time due to the non-inertial frames of reference, when the ship accelerates and even inverts its velocity, has been neglected, see Boniolo (1997).

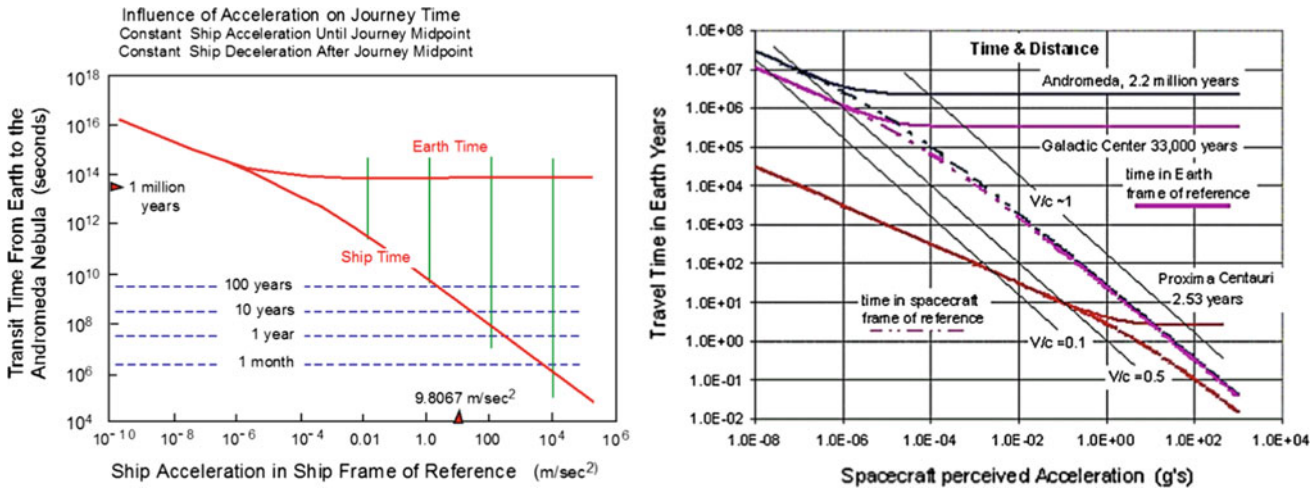

Fig. 9.4 Flight profile and differences between crew and Earth times. Influence of acceleration on journey time (*left*) and the interaction with the three destinations such as the Proxima Centauri, the Galactic Center, and the Andromeda spiral galaxy (*right*)

The ship time to the nearest star *Proxima Centauri* (4.24 light-years) is about 58% of Earth time. The difference is not sufficient to terribly disconcert the arriving crew: The Earth team perceives the trip as 1.86 years longer than the crew. However, as the distance and acceleration increase to reach the *Galactic Center* (center of the Milky Way about 33,000 light-years), the discrepancy in clocks is startling. The ship clock has only registered 24.7 years, while on Earth 30,000 years have gone by. That is more distant to the future than the past Ice Age is to the present! The crew would have no concept of what to expect when returning, and there would be probably no chance of any communication with anything or anyone on Earth. Moving to the nearest spiral galaxy *Andromeda* (2.2 million light-years), the clock on the spacecraft would have only registered 28.3 years, while the Earth clock would have registered 2.2 million years. That is about the time in the past when the first human-like beings appeared on Earth. Then, how do we address the different clock rates so that deep-space exploration can be managed by Earth-based mission teams within their 20 years or so of professional life? This is a very good question for long interstellar travel and it may have become moot by the time such travel is feasible. Whether the spacecraft is manned or robotic, for distant space destinations, there would be no one on Earth that knew *what* was returning to Earth, or *why*.

Putting aside the effects of the Theory of Special Relativity on clocks, it is *time* to discuss the root of the problem, that is, the definition of time or, more correctly, the passing of time. Humans perceive the present moment as having special significance. As the clock ticks, one moment passes and another comes into existence, and we call the process "the flow of time." Physicists, however, argue that no moment, not even the "present," is more special than any other moment. Objectively, the past, present, and future must be equally real. Physicists talk about "absolute past" and "absolute future" in Minkowski's space–time, see Miller (2008), Boniolo (1997), Boniolo and Budinich (2010). That is, all of eternity is laid out in a four-dimensional domain composed of time and three spatial dimensions. What is observed as the *passage of time* is actually that earlier states of the world are different from earlier states of the world we remember. "… *The fact that we remember the past, rather than the future, is an observation not of the passage of time but of the asymmetry of time—a clock measures duration between events much as a measuring tape measures distances between places; it does not measure the 'speed' with which one moment succeeds another. Therefore, it appears that the flow of time is subjective, not objective* …" (Davies 2002). In fact, clocks do not measure time. They only measure the different position of the clock hands. In this view, it is us who connect their positions as a flowing continuum.

The existence of a time arrow is a major question which was first posed by the British Astronomer Arthur Stanley Eddington in 1927 (Weinert 2004). The time arrow is related to the fact that in any isolated system, entropy cannot decrease (Mackey 1991; Layzer 1975). All the fundamental equations of physics hold irrespective of the time direction, but, in our Universe at least, time seems to be flowing only in one. This troubling issue might be resolved by admitting the existence of a "multiverse," a structure composed of many universes, where each has its own time arrow (Carroll 2008). In such a multiverse, time may flow statistically either way, so that there is no preferential direction. Note that no evidence of multiverses has been found so far. In a special issue of *Scientific American,* the main topic was "A Matter of Time." Davies provides an example of that in his article "That Mysterious Flow" (Davies 2002). An Earthling in

Houston and a person on a spacecraft crossing our Solar System at 80% of the speed of light attempt to answer the question: *"What is happening on Mars right now?"* A resident of Mars has agreed to eat lunch when the clock on Mars reads 12:00 P.M. and transmit a signal at the same time.

The puzzling comparison among times of the events between the Earthling, Martian, and Spaceman is shown in Table 9.1. The real difficulty is that, surprisingly, we really do not have a real definition of time! Astounding as it sounds, we have developed physics over centuries using an undefined quantity. Quoting again from *Scientific American*, *"... Neither scientists nor philosophers know what time is or why it exists. The best thing they can say is that time is an extra dimension akin, but not identical, to space. ..."* The physicist Bryce DeWitt has obtained a theory of quantum mechanical gravitation (still the Holy Grail of physics) by eliminating time from the theory itself, as if time was not a physical variable of interest (DeWitt 2003). This is also the opinion of the physicist Julian Barbour (Lemonick 2001), who is convinced that time is an illusion created by our brain, an idea put forward also by Fred Hoyle in the 1960s in one of his fiction books (Hoyle 1957) and mentioned by Gribbin (1992, Ch. 7).

The search for a *quantum gravitation theory* may have a profound influence not only on understanding our Universe's architecture, but also on space travel. A recent suggestion by Ambjørn et al. (2008) postulates that the structure of the Universe may be constructed with simple building blocks or elements, the so-called simplices, using what we already know (gravitation, quantum mechanics, and the principle of superposition), *provided* the principle of causality is added. This elegant constraint, or way out, means time must flow in the same direction for neighbor simplices.

This suggestion is being implemented by its authors in a comprehensive theory that allegedly predicts some of the key features of our Universe, including Einstein's cosmological constant now back in fashion to explain dark energy. If this theory can be validated, a consequence is that wormholes (one of the most used travel devices invented by science fiction writers) may *not* exist. The structure of our Universe would in fact be very smooth (i.e., maintaining the same concept of distance between two points we are familiar with, with no "wormhole shortcuts"). As we shall see, another way out of the time quandary is to travel in another non-time dimension, if such a postulated dimension exists. *If* the space–time continuum is more than four-dimensional (i.e., made of three space coordinates and time), there is a way to reach the most distant star and galaxies in less than human lifetimes.

As we approach the speed of light, another problem is the propellant mass anticipated in Chap. 8. As spacecraft speed increases toward the speed of light, its kinetic energy increases. This is predicted by the Einstein relationships, see Eq. (8.25), and for all practical purposes, it is as if to an observer the vehicle mass becomes infinite at the speed of light. One wonders what is a reasonable mass ratio, M_R, for a long mission carried out at speeds close to that of light. By including relativistic physics, a *minimum* mass ratio needed

Table 9.1 What time is it on Mars?

Time	Observer	Event
Before noon	Earth	Earthling and Martian exchange light signals and determine the distance between them is 20 light-minutes and synchronize clocks
Before noon	Spacecraft	Spaceman and Martian exchange light signals and determine the distance between them is 12 light-minutes and synchronize clocks
12:00 p.m.	Earth	Earthling assumes Martian has begun to eat lunch, and prepares to wait 20 min for verification
12:00 p.m.	Spacecraft	Spaceman hypothesizes Martian has begun to eat lunch, and prepares to wait 12 min for verification
12:07 p.m.	Spacecraft	Signal arrives disproving hypothesis; spaceman infers Martian began eating lunch before noon
12:11 p.m.	Earth	Knowing spacecraft's speed, Earthling deduces spaceman has encountered the light signal on its way to Mars
12:15 p.m.	Spacecraft	Spaceship arrives at Mars and spaceman and Martian notice that their two clocks are out of synchronization, but disagree as whose is correct
12:20 p.m.	Earth	Signal arrives at Earth. The Earthling has confirmed the hypothesis that noon on Mars is noon on Earth
12:25 p.m.	Earth	Ship arrives at Mars
12:33 p.m.	Spacecraft	Signal arrives at Earth. The clock discrepancies demonstrate that there is no universal present moment

Adapted from Davies (2002)

by a very efficient propulsion system (that is, with the highest specific impulse, I_{sp}) can be estimated. The most efficient interstellar rocket ever considered was the photon rocket (Sänger 1956). A photon rocket converts all of its onboard propellant into a perfectly collimated photon (light) beam. Thrust is the recoil due to momentum applied by photons to the spacecraft. The ideal photon rocket has the highest possible $I_{sp} = c$ if the mass consumed to generate light is neglected. Of course photon thrust is tiny. Eugen Sänger (see Sect. 9.2) calculated the mass ratio M_R of this ideal spacecraft performance assuming a trajectory where the spacecraft accelerates at constant a_{sc} until *reaching the speed of light* at the mid-distance $S_{1/2}$ and then decelerates at the same rate $-a_{sc}$ to its final destination:

$$M_R = \exp\left(2 \cdot \cosh^{-1}\left(1 + \frac{a_{sc} \cdot S}{2 \cdot c^2}\right)\right) \tag{9.6}$$

This equation incorporates Einstein's relativistic effects, so the mass ratio approaches infinity as the spacecraft speed approaches light speed. In this trajectory, the mathematical expression calculated by Sänger for the midpoint velocity is as given before by Eq. (9.5). These equations are intriguingly similar to those developed in aerodynamics used to calculate transonic drag, predicting infinite drag at Mach = 1. After WWII this arresting result worried physicists planning to break the "sound barrier," but this "barrier" was in fact due to the linearization of drag by aerodynamicists in order to obtain an analytical solution (Anderson 1997). Therefore, some may doubt whether relativistic effects near $V = c$ are due to a hidden assumption in developing Special Relativity thereby producing a similar mathematical result, or if they are a true physical singularity. The calculation of the mass ratio needed to accelerate to speeds close to the speed of light yields inordinately high values for the mass ratio, just as evaluating aerodynamic drag with linearized aerodynamics near sonic velocity (Mach $\rightarrow$ 1) yields unrealistically high drag. For most physicists, there is no question: because of the Michelson-Morley experiment in 1887 and accurate measurements of time differences between satellite and Earth clocks, Special Relativity has been validated for good. However, some keep doubting, because the discontinuity when $V = c$ seems a pure mathematical artifact, that is, the effect of the Lorentz transformations based on the invariance of c. Still, almost all physicists are convinced of the validity of Special Relativity.

Combining Tsiolkovsky's rocket equation (Tsiolkovsky 2004) and the M_R equations, one can estimate the average I_{sp} needed for a specific mission, as given below. In the simple flight profile chosen by Sänger, for example, when the mass ratio approaches infinity, the specific impulse I_{sp} approaches zero. For speeds less than 91% of the speed of light, the limit M_R and I_{sp} (here in seconds) are given by

$$M_R = \exp\left(2 \cdot \cosh^{-1}\left(1 + \frac{a_{sc} \cdot S}{2 \cdot c^2}\right)\right) = \exp\left(\frac{\Delta V}{g_0 \cdot I_{sp}}\right) \tag{9.7}$$

$$I_{sp} = \frac{\frac{\Delta V}{g_0}}{2 \cdot \cosh^{-1}\left(1 + \frac{a_{sc} \cdot S}{2 \cdot c^2}\right)} \text{(s)} \tag{9.8}$$

When the spacecraft speed is in the vicinity of light speed, as measured by the difference

$$\Delta c = c - V_{sc} \tag{9.9}$$

an approximation for the mass ratio M_R and I_{sp} is:

$$M_R = \frac{599{,}475}{\Delta c} \tag{9.10}$$

$$I_{sp} = 1{,}373{,}120 \cdot \Delta c^{0.076744} \text{ (s)} \tag{9.11}$$

with

$$\Delta c = 299{,}796 - V_{sc} \tag{9.12}$$

A value Δc = 5994.75 km/s makes the absolute speed 97.85% of light speed, and the mass ratio to achieve that, M_R = 100, may be tractable. The corresponding I_{sp} is 2,676,900 s. That is about three orders of magnitude greater than the best (electric) space engines can provide today.

Traveling close to light speed, even with reasonable M_R, requires either dramatic improvements in propulsion or radically new ways of conceiving propulsion and space travel. Some are discussed below.

9.3 Black Holes and Galactic Travel

The time, energy, and logistic limits posed by traveling in reasonable times to our closest stars (let alone to Galactic destinations) motivate the search for propulsion means alternative to those based on current physics (Newton's Third Principle). This is an endeavor common to science fiction writers and scientists alike.

The measurements taken from scientific satellites indicate that the space–time continuum of the Theory of General Relativity (Minkowski space–time) is nearly flat. If space–time were "warped," that is curved, the force and energy available from gravitation would be much larger than predicted by the simple Newton's Law. Then a new propulsion system would, in principle, be possible (Alcubierre 1994; Obousy and Cleaver 2008). Such a system has been

proposed by Millis (1996) and is examined in Ford and Roman (2000), Minami (2008). Feasibility is for the moment speculative, due to the mathematical complexity of the tensor calculus required when manipulating General Relativity equations (Maccone 2008b), but at least Relativity or any other basic physical principle does not appear violated. Contrary to popular belief, General Relativity allows for a number of effects that are positively unexpected or "strange," some far stranger than fiction. The fundamental equations of physics, including General Relativity, tell what cannot be achieved or done (i.e., all that is forbidden). They do not tell us anything about what is actually possible to do. They behave like the old joke about what is lawful and what is not in England, Germany, Russia, and Italy: *"In England all is permitted, except what is explicitly forbidden. In Germany all is forbidden, except what is explicitly permitted. In Russia all is forbidden, even what is explicitly permitted. In Italy all is permitted, even what is explicitly forbidden."* General Relativity would then be an English Law. Solving the General Relativity equations is difficult, and obtaining results (some quite unexpected) has been and still is a step-by-step process, each sometimes correcting or modifying the previous one.

Among the most interesting of these results are those concerning black holes. By now, the work of Stephen Hawking and Roger Penrose, publicized by books, movies, and the popular press, has made black holes a well-known term and even a metaphor (deGrasse Tyson 2007). Its "strange" and disconcerting properties are still being investigated by theoreticians, and they are far from having been completely explored. Their relevance to propulsion is that they carry significant implications for space travel. In some far future, the physics of black holes may conceivably result in replacing the very idea of *space travel* with the more physically consistent idea of *space–time travel* (Gribbin 1992). Note that the number of "primordial black holes" (those created by the big bang) is estimated in the trillions, their average mass of order 10^{12} kg. They are theorized to evaporate in a process called "Hawking radiation" producing antimatter (mostly positive electrons). This process might explain the so-called dark matter invoked to justify the missing mass of our Universe.

A black hole is a true discontinuity in the space–time continuum. A black hole is not "made" out of matter, although it attracts and collects matter. Then it is not another exotic star such as a neutron stars or pulsar either. It may be defined simply in terms of four-dimensional space–time topology as a purely geometric concept, characterized by a center and a surface (Kaufmann 1992). It is theorized that black holes are the final products of massive stars at the end of their life cycle. If their mass is too big to end as a white dwarf or neutron star, the gravitational force compressing a spent star matter is no longer compensated by the pressure developed by thermonuclear reactions. Then, mass keeps compressing and shrinking, density increases, and so does gravitation, until not even light may escape. The radius of the collapsing star at this point is called the Schwarzschild radius, and defines the so-called event horizon. The German astronomer Karl Schwarzschild was the first to discover this effect when solving Einstein field equations of General Relativity in 1916 (Schwarzschild 1916). Beyond this distance, an external observer cannot see any longer inside the collapsing star, and optically speaking the star disappears. Most recently, in August 2016, Jeff Steinhauer, from the Technion Department of Physics, announced results of an experiment where laboratory-sized black holes may have been generated, results finally proving that the Hawking radiation exists (Weiner 2016).

Inside the collapsing star, gravitation curves space–time more and more till a "hole" is punched in its fabric. The star matter is swallowed by this singularity, as (for a *static* hole at least) density and gravitational force become infinitely large. The sharply increasing curvature of space–time when nearing a black hole is perfectly equivalent to that created by mass gravitation. For this reason, a black hole is also characterized by a mass, that is, the *equivalent* mass that would have the same gravitational effect. Inside the event horizon, the pull of the black hole singularity cannot be overcome by any force or thrust, and gravitation bends even photon trajectories. Outside the event horizon, space–time tends to become gradually flatter, and the pull decreases, tending to that of an equivalent ordinary mass. For instance, a black hole with mass equal to that of ten times our Sun would start behaving like a star of that mass from a distance of order three or four AU (Kaufmann 1992).

In 1939, Oppenheimer and Volkoff (1939) calculated the limit mass of a star beyond which the star would collapse into a singularity. In 1971, the Uhuru satellite, designed to monitor space X-ray emissions, was launched from the Italian "San Marco" platform off the Kenyan coast. This X-ray astronomy satellite observed a strong source of X-rays from a supergiant blue star in the Cygnus constellation, later found in fact to be a binary system. The other star, named Cygnus X-1, had a mass estimated at more than ten times that of our Sun, but compressed within a 300 km diameter, was (and still is) invisible. In the Harvard College Observatory, the giant star took the catalog name HDE 226868. We do know now its companion, Cygnus X-1, is very likely a black hole. Much progress in this field has been made since the 1970s. At present, black holes are considered the natural final evolution of massive stars and their estimated average distribution density is significant. For instance, statistically, there should be a black hole within 15 light-years from our Sun, although it cannot be observed directly (DeWitt and DeWitt 1973; Lasota 1999).

Meanwhile in 1963, Kerr had already calculated some properties of a *rotating* black hole, and the work by Newman

in 1965 had explored the properties of *charged* black holes. Their joint solutions of the theory of General Relativity are called now the Kerr–Newman solution, to which theoretician Paul Davies added later quantum mechanics effects. So far, all these results were obtained by solving Einstein's field equations. No rotating black holes has been deduced from observational astrophysics yet. However, this fact has not deterred theoreticians from investigating more and more features of these objects. For instance, when Carl Sagan decided to write his novel *Contact* (Sagan 1985), he asked Kip Thorne, the leading gravitation physicist at CalTech, to help him in checking mathematically whether black holes could be exploited for space–time travel (Gribbin 1992). The answer was positive (Thorne 1995).

In fact, General Relativity solutions for static black holes had already shown the existence of channels ("wormholes" is their popular name) punched by black holes between different regions of space–time. This means that black holes may be the entrance into channels leading to places in our universe, or even to a *different* universe. These General Relativity solutions are the so-called Rosen-Einstein bridge solutions and, if confirmed by observation, would imply interstellar travel may be possible. This same class of solutions, however, predict that *neutral* and *static* black holes must evolve and last only for an instant, while space–time inside shrinks to a mathematical point. The difference between *rotating* or *charged* Kerr–Newman black holes is that the latter allow finite size and duration of wormholes. The singularity predicted at the center of Kerr–Newman black holes is not a point but rather a ring. If the black hole is sufficiently large and massive, objects of finite size may enter and travel without being torn apart by the gravitational tidal forces associated to smaller black holes inherently possessing sharper space–time curvature (Gribbin 1992). In principle, these General Relativity solutions suggest a spaceship may go through a massive black hole and emerge in a different part of our universe in a transit time much shorter than covering the same distance along the ordinary (nearly flat) space–time continuum while not exceeding light speed. In other words, the transfer from one part of the universe to another does not violate the light "speed limit." The ship would simply take a shortcut (the wormhole) created by the intense curvature of space–time near a singularity.

However, there are caveat associated with this. The trip through a rotating or a charged black hole is one-way, unless the charge (or angular velocity) of the black hole is so large that the singularity at its center, still annular, becomes in the language of gravitation "naked." Naked singularities are predicted by General Relativity and are singularities where the event horizon does not exist. By using this class of black holes, traveling both ways becomes possible in space but not in time. Then, the spaceship would be able to return to its point of departure, but the time would precede departure time! This disconcerting fact can be shown using the so-called Penrose diagrams, and it is due to the extreme effects typical of singularities in space–time. Space and time can no longer be kept separate as in our ordinary, locally nearly flat space–time (Kaufmann 1992; Thorne 1995).

Are there such rotating or charged black holes? As said, none has been "observed." An inference shared by many astrophysicists, however, is that quasars *may* be such objects. Quasars are indeed massive, a fact that can be deduced by their enormous rate of electromagnetic energy release, and they rotate. If this is indeed so, quasars are natural connections to other space–time regions.

A second caveat about using black holes as shortcut entrances between regions of space–time is the fact that any material object must have a speed less than that of light. When the spaceship enters a black hole it is preceded by the isotropically emitted gravitational waves traveling at light speed. This gravitational radiation may be amplified by the black hole to the point of perturbing the space–time curvature in front of the ship itself, thus preventing entrance. Phrasing this problem differently, the question is how sensitive, or stable, a black hole is to external perturbations? Indeed, the exact Kerr solution does show the solution is sensitive. However, it is precisely this solution "weakness" when facing any practical application that presents an opportunity. If the black hole is unstable, its equilibrium may be in some way altered in the direction of favoring entrance, not exclusively preventing it. This viewpoint looks at black holes as the next major step in space travel.

In fact, work on the ship mass effect on the Kerr–Newman black hole, spurred by C. Sagan's questions to Kip Thorne, showed that black holes may be born naturally (and are therefore common), so that, in some way, perturbations must either dissipate or be insufficient to "close" a black hole. Researchers working with Kip Thorne aimed at finding answers to C. Sagan's questions decided to engineer black holes to meet the objectives of the plot in *Contact,* an instance of fiction motivating a theory (Morris et al. 1989). The team at CalTech did what is called "reverse engineering" of a black hole. In other words, they assumed the features such a wormhole should have in order to be a practical means of transportation, and then set out to find what was necessary to make it based on what is known from General Relativity (Morris et al. 1988; Morris and Thorne 1988). Perhaps, the most important result they obtained is, that matter inside the black hole must be capable of exotic properties (either anti-gravity or negative pressure) in order to keep the wormhole steady and to prevent it from contracting during the spaceship transit. Such exotic matter may, for instance, consist of cosmic strings. All these properties, hard to even conceive in ordinary matter, are nothing radically new. The Casimir effect indicates such exotic properties are not only theoretically possible, but can be also

theoretically observed. String theories have been investigated since the 1980s (Greene 1999).

An intriguing proposal in this quest was advanced by Visser (1989). Visser proposed a space-gate unlike the ones discussed so far. The major problem with conventional black holes is the distortion of space–time, subjecting travelers and their ships to intense gravitational tidal forces. These forces become moderate only for very large (massive) black holes, where gravitation is distributed over a vast enough portion of space, overall resulting in a mild space–time curvature. Relaxing the assumption of rotating or charged holes, where exotic matter would prevent the ring inside from closing due to the gravitational disturbance generated by the transiting ship, Visser envisaged a star-gate in the shape of a flat-faced cube. A spaceship can cross such gate without feeling any force induced by space–time, and without touching the matter holding the gate together. This solution is predicated on the ability to keep the space–time cube flat by using exotic matter to delimit its edges. Note that all the associated complex physics is still the outcome of solutions of the field equations developed by Einstein in his General Relativity theory, indicating that his theory is reliable. In fact, after much mathematical and experimental testing, nothing has been found to challenge this theory to this day.

9.4 Breakthrough Physics and Propulsion

In juxtaposition, efforts are under way to find *new* physics, physics that would enable us to bypass limitations such as the speed of light. It is this limit that is assumed to be the main issue blocking our path toward the exploration of stars and of our Galaxy. In this context, it must be said that certainly we have *not* explored all there is to know in our understanding of physical laws. After all, what we know has been found by looking at a very small portion of our universe. Are the laws we know everywhere the same? Do they change with time? Some physicists think so (Smolin 2013).

After the two probes, *Pioneer 10* and *Pioneer 11* (also *Galileo* and *Ulysses*, as found later), showed a tiny but measurable deceleration, the so-called Pioneer Anomaly, that could not be explained by any of the mechanisms proposed, some physicists began to conjecture that gravitation, or inertia, was changing with distance (in this case, from the Sun) (Anderson et al. 1998). However, the painstaking analysis of all Pioneer data by S. Turyshev's team at the Jet Propulsion Laboratory in 2012 showed that the effect could be explained by photon thrust due to the dish antenna heated by the RTG nuclear generator (Turyshev et al. 2012). Similarly, many physicists thought that the experiments in the Large Hadron Collider (LHC) at CERN (Anon. 2008) would result in changing our current understanding of physical laws and trigger another revolution (Quigg 2008). In fact, the sought-for Higgs particle (Higgs boson) was indeed detected in 2013, but not its wished for "twin," so that no revolution appears likely any time soon. This dampened hopes, for the time being, for new physics that could broaden the understanding of the Universe and weaken or remove existing limits.

Nevertheless, the fact is that we have barely scratched the prediction potential of the General Relativity equations. Dark matter, dark energy, inertia, the equivalence between inertial and gravitational mass, quantum entanglement, and the relationship between quantum mechanics and gravitation —these aspects are still unexplained by the Standard Model ('t Hooft 2007). New quantum gravity theories are frequently proposed, e.g., Kane (2003), Smolin (2004), Barceló et al. (2009), Lisi and Weatherall (2010). Hopes to circumvent inertia or gravitation remain.

Probably, the single most severe shortcoming in efforts to exploit the potential of General Relativity is our limited conception of space and time. In particular, time is more and more frequently questioned or questionable; we still are at loss to *define* time. As mentioned, we should abandon our concept of space travel in favor of space–time travel. Besides the questions above, related to the very fabric of the Universe we know, there are also more mundane problems connected with the energy needed for such travel. These questions and attitudes motivate the search for still undiscovered laws, or connections between laws, constituting what has been given the catchy name of "breakthrough physics" (Hamilton 2000) and "breakthrough propulsion" (Millis 1996, 1998). These are nicknames given by scientists and engineers frustrated by the constraints posed by "known" physics, and should be understood to mean "physical principles beyond the ones we know"; they might be part of currently unknown physics, or developments from General Relativity, or from the Standard Model, that we still have not explored.

"Breakthrough" physics sometimes adopts General Relativity equations, and sometimes modifies them to suit a particular goal, or replaces them with something else that often does not stand the test of time and peer reviews. It is hard to judge the merits of ideas or models based on completely "new" physics that should, in the best intentions of the authors, suggest new means of propulsion, e.g., see Puthoff (2010). As for alternative energy sources, much has been made of the zero-point energy (*ZPE*) discovered by Einstein and Stern. This energy is often associated with Planck's length (a scale arbitrarily formed by using three fundamental physical constants). The zero-point energy field is tied to so-called quantum mechanical vacuum energy fluctuations. The existence of quantized energy fluctuations is responsible for the experimentally proven Casimir force (Casimir 1948; Ball 2007).

The consequences of zero-point energy have been investigated for several years. In propulsion its appeal

derives from the fact that, while its absolute magnitude is extremely small, its scale should be just as small (e.g., the Planck's length just defined is of the order of 10^{-36} m). By implication, the estimate for the zero-point energy associated with a sizable volume yields extremely large values, in fact so large as to curve space, a fact not observed and theoretically obscure (Garattini 2008). Besides, nobody would know how to extract this energy (Yam 1997), but myths abound. This difficulty has not discouraged suggestions to use it for a propulsion device of some sort.

An example is the so-called EmDrive, Q Drive, RF Resonant Cavity Drive, or Cannae Drive, depending on the groups that built and tested the concept. This was conceived in the UK by R. Shawyer in 2008–2009 and tested at his SPR Ltd company, at NASA Johnson Research Center (Eagleworks Laboratories), by chemical engineer Dr. Guido Fetta in the USA, and at China's Northwestern Polytechnic University. A chronology and downloadable papers are available from SPR Ltd. An early picture of the device, as built by SPR Ltd, is shown in Fig. 9.5. It consists of a cone frustum where a standing EM wave of frequency in the MHz range is introduced. No mass and (apparently) no radiation is released by the device, but thrust may have been measured varying between micro-N and milli-N, depending on radio frequency (RF) power applied at the experimental facility. All explanations provided so far fail to satisfy fundamental physics, such as conservation of momentum and energy, but the initial observation that thrust was measured appears inconclusive (Tajmar and Fiedler 2015). Tajmar and Fiedler conclude: *"... To this end it was successful in that we identified experimental areas needing additional attention before any firm conclusions concerning the EMDrive claims could be made. Our test campaign therefore cannot confirm or refute the claims of the EMDrive but intends to independently assess possible side-effects in the measurement methods used so far. …"* Whether or not thrust has been measured, the EmDrive experiments have made researchers invoke zero-point energy or inertia reduction for possible explanations. In an article by MacDonald (2015), Eric W. Davies, physicist at the Institute for Advanced Studies at Austin, pointed to a possible flaw in the experimental setup.

A second aspect of the existence of zero-point energy is its postulated association with gravitation. As shown in the definition of the Planck length, theories of inertia and presumed ways of reducing inertia, and of shielding or altering gravity go under the name of "electro-gravitics" breakthrough physics. In this case, the claims tend to be experimental, but most such experiments have not been independently reproduced, casting doubts on their accuracy. In this context, skepticism is in order, mainly because understanding of gravitation is incomplete (Maggiore 2007; Cook 2002; Thorne 1995). This said, the detection of gravitational waves by the team of scientists that designed and built the LIGO Laser Interferometer Gravitational-Wave Observatory) project (Overbye 2016) not only confirms the dynamic nature of space–time as postulated by Einstein, but may contribute to explain the relationship between gravitational and inertial mass. Note that no inertia "constant" exists in physics except through the puzzling equivalence between gravitational and inertial mass. As defined, the Planck length does not involve inertia.

Other energy sources have been derived by either postulating or deriving new relationships from the equations of General Relativity. To date, however, it is very difficult to check the consistency and validity of any of these developments, as they are couched in often abstruse mathematics that in most cases requires considerable analytical skills to be manipulated (if understood). Some of these predictions, if verified by experiments, would have dramatic implications not only for propulsion and space travel, but also for power generation in general. In this context, there is much anecdotal but hard-to-substantiate "evidence" on the Internet. Dr.

Fig. 9.5 EmDrive tested at SPR Ltd. *Courtesy* SPR on *left* and kindle e-book by R. Walker *right*

Martin Tajmar, now at TU Dresden (Germany), and Dr. Marc Millis, formerly at NASA, have done much to debunk the mystique and the exoteric claims of proposals to exploit breakthrough physics concepts (Tajmar 2003; Millis and Davis 2009). The effect of hypothetical gravity and inertia shielding on specific impulse of chemical rockets has also been studied (Bertolami and Tajmar 2005; Tajmar and Bertolami 2005). Curiously, in this last case, the effect has been investigated only insofar the molecular weight of the exhaust from a rocket is concerned, not the spacecraft mass itself; predictably, the impact on I_{sp} was found negligible. Nevertheless, these two references are very useful to assess the state of breakthrough physics, containing a wealth of citations of recent work on this subject. Even after much sifting, one or two experiments are still baffling, resisting explanations based on standard physics. Experimental and theoretical evidence is suggesting a fourth force, e.g., see Tajmar et al. (2008a, b). Millis and Davies (2009) critically analyze many recent theories and experiments allegedly supporting conceptual revolutionary propulsion.

Dark matter and dark energy are another source of inspiration when looking for unconventional energy. Dark matter is believed to make up to 85% of all matter in our Universe, and it is possible to conceive it as a means of propulsion. In fact, the existence of dark matter is so far presumptive, and most physicists think it is not ordinary matter at all (Hogan 2007). Dr. Marla Geha, at Yale Observatory, identified the Segue-1 dwarf spheroidal galaxy. Segue-1 has the same mass of 450,000 Suns, but is extremely dim, some 350 times less than expected, suggesting it is mostly composed of dark matter (Courtland 2008). Supersymmetry theory predicts that each particle known in the Standard Model must have a non-standard and heavier counterpart. The lightest counterpart has been named "neutralino." When two neutralinos collide they annihilate and the decay products eventually produce high-energy electrons and positrons. Preliminary data from the European PAMELA satellite showed the ratio p^-/p^+ reaching a peak 0.0002 at about 10 GeV, then declining to 0 at higher energies. One explanation was initially based on collisions between dark matter particles predicted by supersymmetry (Brumfiel 2008a, b), but the decay at high GeV eventually provided conventional explanations.

A new area of investigation in physics, negative matter, may be utilized to construct propulsion machines. Negative matter was proved to be compatible with General Relativity by Bondi (1957). That inertial matter may behave as a negative quantity, therefore accelerating in the direction opposite to applied force, has been observed for neutrons in crystals, e.g., see Raum et al. (1995). The original suggestion to build a self-accelerating mass dipole (Forward 1990) has been further developed recently by Tajmar (2014). The mass dipole consists of an ordinary (+) mass, also positively charged, and of a *negative* mass, negatively charged, connected by a spring. The Coulomb force between the two charges attracts the two masses, but because one is negative, they both accelerate in the same direction, that is, the direction going from the positive to the negative mass. If negative mass can be produced in some way, the magnitude of the effect should be quite significant, because the forces are electrostatic, not gravitational. This investigation is continuing.

Other attempts to provide solutions, or at least suggestions on how interstellar and galactic travel could be realized, consist in simplifying or modeling in a simpler way some of the results that have been extracted from General Relativity. Although the language may not be rigorous, or the description not completely consistent with the formalism of General Relativity and in any case highly speculative, these attempts are often useful as they may make easier to understand what the equations predict while possibly suggesting further avenues of investigation. For instance, the complexity of describing the Kerr–Newman solution may be simulated (albeit in one dimension) by introducing a "hyperspace," replacing the four-dimensional metric of the field equations. This is the attempt D. Froning made in using his *K*-tau hyperspace in Sect. 9.5

9.5 Superluminal Speed: Is It Required?

At subluminal speeds (based on Newton's Third Principle), we have shown that round-trip travel to distant galactic destinations cannot be accomplished within the lifespan of an Earth-bound project team. But what if the spacecraft can exceed the speed of light? Some investigators have postulated the possible existence of faster-than-light (superluminal) entities (Tanka 1960; Bilaniuk 1962). There is a mathematical approach to the Lorentz transformations that avoids violating Einstein's Special Relativity and that involves introducing the imaginary square root of minus one (i is its mathematical symbol). The consequence is that all results become real numbers (and not complex in the mathematical sense) only if the speed of the spacecraft is *greater* than the speed of light.

If the spacecraft speed could be much greater than the speed of light, then time, the distance divided by speed, becomes vanishingly small, even over enormous distances. Thus, destinations that are millions of light-years distant from Earth could be reached in short intervals of time if the ship acceleration could be quite large and the speed of the spacecraft many times the speed of light. But even if the ship speed is many multiples of the speed of light, the duration in spacecraft time is the distance divided by the speed of light, and that determines the spacecraft time elapsed during the mission and the physical aging of the crew (Jones 1982).

Thus, even with an 80-year lifespan of the spacecraft crew, the crew could only reach and return from stars that are less than 40 light-years distant from Earth.

Then, for *less-than-light-speed* (subluminal) travel, it is the lifespan of the Earth-bound observers that is the limitation. For *greater-than-light-speed* (superluminal) travel, it is the lifespan of the spacecraft crew that is the limitation. In both cases, the limitations are equally severe. If we assume round-trip travel without a radically different approach to propulsion or to the concept of spacecraft, we are confined to the region around our Solar System. This would change drastically if interstellar travel were to be considered in the context of colonization, where trips may become one-way missions.

The passing of time within a spacecraft will appear to slow down to zero to a hypothetical "inertial" observer of the spacecraft as it reaches the speed of light. Thus, in effect, all sense of time will seem to the observer to vanish when looking at beings that reach the speed of light. But let us imagine that this vanished sense of something is replaced with something that has nothing to do with either time or distance. Although the essence of this something is as yet a postulate unknown, it has been given the designation tau (τ) (Froning 1983). Tau has no correspondence with time or distance; its essence cannot be measured in terms of spatial or temporal separations. It is a dimensionless quantity devoid of any units involving distance or time. Just as it is possible to multiply a time by a constant (such as $c \cdot t$) that gives it the unit of distance, it is also possible to multiply tau (τ) by a constant K that results in a term ($K \cdot \tau$) that is also in distance units. Although the metric of $K \cdot \tau$ can be made the same as $c \cdot t$, it must be measured along an axis that is perpendicular to the (x-$c \cdot t$)-plane, as tau represents something that is neither time nor distance, as shown notionally in Fig. 9.6.

In a sense, devising such τ is akin to simplifying the field equations of General Relativity for illustration purposes, as they cannot yet predict what really happens when a spacecraft enters and passes through the wormholes in Sect. 9.3. Since when traveling at the speed of light no apparent time elapses, the spacecraft would arrive instantly and simultaneously at all locations along the flight path. Along this path of flight, to the crew on the spacecraft all spatial separations would collapse to zero without relativistic time dilatation, as all spatial separations are transverse to the light-speed spacecraft flight. The spacecraft in effect "jumps" into a dimension "perpendicular" to the normal three spatial dimensions and time. In order to accomplish this jump, the spacecraft must achieve light speed and fly a specific flight path. There is a specific trajectory that can be determined to accomplish the jump (Froning 2003).

Thus, the first constraint to travel in this way is that the spacecraft must achieve light speed and fly a specific trajectory. In a sense, the spacecraft "soars" over space and time of the x-ct plane. The flight segment in this hyperspace can be represented as a parabolic-like trajectory over the x-ct plane and in the x-$K\tau$ plane, see Fig. 9.6. The spacecraft then returns to light speed and an inverse trajectory returns the spacecraft to the physical x-ct plane. There is no material motion associated with the spacecraft travel in the x-$K\tau$ plane, because the plane contains no time. The spacecraft travel along the x-$K\tau$ plane would be imperceptible to the slower-than-light-speed observers as the travel occurs within a plane of event/existence that is at a "right angle" to the x-ct plane. Thus, the spacecraft would disappear after reaching light speed, followed immediately by its reappearance trillions of miles away in the proximity of the target star, when the spacecraft returns to sub-light speed. As the spaceship travels in the x-$K\tau$ plane, the "unfolding of tau" is not the same as the "passage of time" in the x-ct plane. Here, our classical concept of time is perceived as an inexorable movement toward the "future" from the "past." As cited from Davies (2002), this perception has no mathematical or

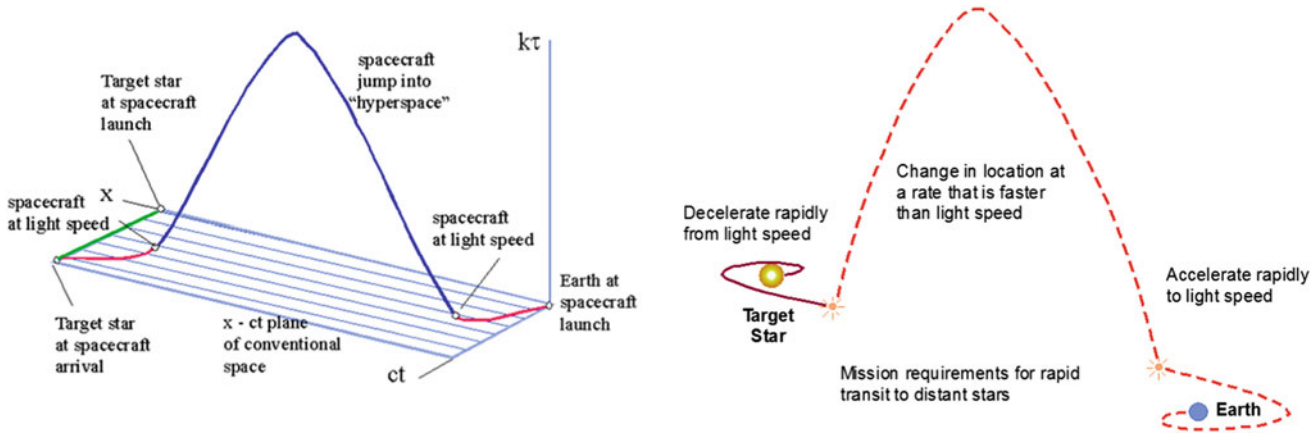

Fig. 9.6 Ship jumps out of conventional space into Einstein space–time

physically based reality. By contrast, the essence of tau must be such that $K\tau$ both increases and decreases during the spacecraft's travel in the x-$K\tau$ plane. Of course, spacecraft navigation in the x-$K\tau$ plane is impossible unless position and direction can be determined for each increment of tau, as tau unfolds with the spacecraft. Froning (1983) gives the details of the mathematical derivation of this strange journey.

With more conventional propulsion, the solution to the aging of the crew problem is to accelerate at very high rates. That, of course, would crush occupants and equipment. Trained pilots can stand a 3g acceleration for only ten or fifteen minutes (this was the time and acceleration sustained to orbit by the Space Shuttle during the ascent). Then, the underlying discovery that could enable deep-space exploration by both humans and machines is an anti-inertia shield, something that would reduce the inertial mass opposing acceleration. Clearly, the accelerations required to explore the Galaxy are significant. Figure 9.7 shows the effect of increasing the acceleration of the spacecraft with respect to the Earth frame of reference. A nominal 2-year trip at conventional 1g acceleration shrinks to a 1.7-h trip at 10,000g, i.e., a reduction to one ten-millionth of the 2-year mission. With that shrinkage, the 30-year mission to the Galaxy center would take just 2.9 years! Then, the key to rapid travel to distant destination is not super light speed, but super-fast or steady accelerations (Long 2009). That requires the discovery of an anti-inertia/anti-mass system to permit the human body and physical structures to withstand such accelerations and loads.

At this point in time, no one appears to have the energy source nor the anti-inertia or anti-gravity approach that would permit such accelerations or the flight speeds that approach light speed. According to physicist and philosopher Ernst Mach's conjecture, inertia is due to the mass present in the Universe (this is *Mach's principle*). Accelerating a mass would affect all other masses via changes in gravitational forces. If so, an inertial time lag should in principle be detected moving a mass fast enough for relativistic effects to take place. Such an experiment would be hard to perform, and, if successful, would rule out any chance of finding anti-inertia or inertia-less propulsion systems. Experiments to check the Mach principle and a theory for the origin of inertia have been proposed by Woodward (2001, 2004). Other theories have proposed that inertia is due to the interaction of an accelerating mass with vacuum energy (Yam 1997; Rueda and Haisch 1998). An explanation of the *Pioneer anomaly* based on inertia modification at large scales was tested and seemed to work (McCulloch 2008) before being replaced by the more prosaic one based on the thrust due to heat radiation (Betts 2012; ten Boom 2012). Results by Woodward seem to indicate that his theoretical explanation of inertia may be right. Since it uses electromagnetism, it would open the door to anti-inertia devices based on manipulating magnetic fields.

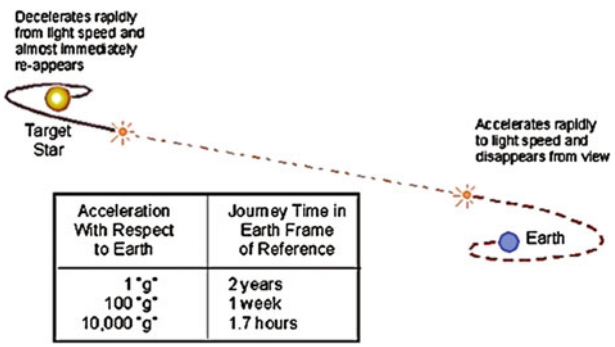

Fig. 9.7 High acceleration shortens Galactic travel times

In summary, rapid transit to distant stars and galaxies would involve the spacecraft accelerating to light speed at rates quite beyond present human or material limitations. It would require the understanding of, and then the ability to control, inertial mass. When so, the spacecraft would be disappearing from human sight. Almost "immediately," in terms of spacecraft clock, the spacecraft would reappear billions of kilometers away close to the target star or galaxy. During those moments when the spacecraft disappears, the spacecraft would have "jumped" over the so-called space–time continuum in an "arching" flight path. If theories and postulates are correct, the maximum speed necessary to achieve is, at most, light speed, and *superluminal speeds would be of no time benefit.*

If our Cosmos possess a greater spatial dimensionality than three (length, height, and width) and one-dimensional time, then a spacecraft may be able to "soar" above the time and space realm of existence and travel great distances in only the time required to accelerate to light speed and then decelerate from light speed to the target destination. The key requirement is to be able to achieve light speed and *no greater*. Clearly, there is hope that in some future time and place, a space-faring civilization might learn to journey round-trip through space to further stars.

In a similar vein, if our Universe has extra dimensions, as posited by string theory, Richard K. Obousy and Gerald B. Cleaver at Baylor University, Texas, claim that manipulating the 11th dimension in the so-called m-theory (a development of string theory), the cosmological constant could be made to change *locally* by using the Casimir effect, forcing space to "warp" (i.e., to contract) in front of a spaceship and expand behind it (Obousy and Cleaver 2008). Warping was originally put forward by the physicist Alcubierre (1994). A ship inside the warped space "bubble" would not move and would not violate the c limit. Instead, space would stream by at a speed depending on "warp" intensity. Since there is no relativistic constraint on the expansion speed of space–time, a spacecraft could arrive at its destination much faster than a

light beam connecting the departure and arrival points. Calculations indicate that a 1000 m^3 warp bubble would need about 10^{28} kg of annihilating matter-antimatter to form. At the same time, the space-streaming speed would be orders of magnitude larger than *c*. In fact, choosing the limit value estimated for the cosmological constant (10^{40} Hz), the energy required to form the bubble would increase to 10^{99} kg of matter-antimatter, but the space-streaming speed would become $10^{32}c$. This would mean that the entire Universe could be crossed in 10^{-15} s.

If these numbers can be taken seriously, in the far future the higher dimensionality of space–time may be the true key to fast interstellar travel. If this higher dimensionality does not exist, the stupendous gulf of cosmic space appears to be an insurmountable barrier.

There is a final question that may leave a little room for doubting this pessimistic remark. Quantum mechanics *entanglement* is an *"... observed phenomenon where a physical property of a particle (or even a larger system) becomes instantly dependent on the properties that are being measured on another particle, regardless of how far apart the particles are ..."* (Rudolph 2008; Albert and Galchen 2009). While entanglement does not involve matter motion, it still seems to violate the spirit of the relativistic *c* limit. The lower bound for the speed at which this phenomenon occurs has been estimated to be *at least* of the order of 10^4 to 10^5 *c* (Salart et al. 2008). Entanglement of two electrons has been experimentally confirmed at Delft University (Hensen et al. 2015). What is at the heart of this, *"... spooky action at a distance ..."* as Einstein called it (Friedman 2014), is a mystery fostering hope that, at some point, the *c* barrier may be overcome.

9.6 Conclusions

A legitimate question is whether the ideas for traveling to destinations in our Galaxy discussed in this chapter may be considered even remotely practicable. Among facts that may give some hope, in the sense that they are promising and based on established physics, are the possible existence of wormholes and quantum entanglement, enabling intra-galactic or extra-galactic travel. Wormholes are predictable from General Relativity, and quantum entanglement has been demonstrated and is the foundation of current work on quantum computing. Furthermore, subject to progress in the physics we already have at our disposal, wormholes may be designed by again using General Relativity. As wormholes depend on the existence of black holes, they appear at the moment impossible to build in an engineering sense. However, the relative abundance of them in our Sun's immediate neighborhood gives hope appropriate ones may be found.

Skepticism concerning these concepts is justified, and this was also the case with learned savants that in the 1500s were exposed to the drawings of parachutes and flying machines by Leonardo da Vinci. Much more recently, on January 13, 1920, Robert Goddard was ridiculed by the "New York Times" when he proposed to reach the Moon using rockets (Kuntz 2001). In this age today "we know better," admire Leonardo's farsightedness, pity his naiveté, and shy away not only from his boldness, but also that prevalent in the 1950s and 1960s. With future hindsight, some of the ideas discussed about using gravitation, space–time curvature, and topology, space travel may eventually become practical. Certainly, they form the only established body of physics we can use now and for the predictable future, and they solve or bypass questions connected with time paradoxes and causality. Backed by General Relativity, it appears the precautions time travelers must take to avoid accidentally killing one's ancestors may be unnecessary. Rather than travelling in space and then putting up with, or fixing, the many problems caused by time, understanding Einstein's space–time may provide ways of reaching stars. So, the answer to the question opening this chapter and this section is, literally, *Time will tell*.

Bibliography

Albert, D.Z. and Galchen, R. (2009) "Was Einstein Wrong? A Quantum Threat", *Scientific American*, Vol. 300, No. 3, March 2009, pp. 32–39.

Alcubierre, M. (1994) "The Warp Drive: Hyper-Fast Travel within General Relativity", *Classic and Quantum Gravity,* Vol. 11, L73–L77, February 1994.

Ambjørn, J., Jurkiewicz, J. and Loll, R. (2008) "The Self-Organizing Quantum Universe", *Scientific American,* Vol. 299, No. 1, July 2008, pp. 42–49.

Anderson, J.D. (1997) *A History of Aerodynamics—and its Impact on Flying Machines*, Cambridge Aerospace Series, Cambridge University Press, 1997.

Anderson, J.D., Laing, E.L., Liu, E.L., Nieto, M.M. and Turyshev, S.G. (1998) "Indication, from Pioneer 10/11, Galileo, and Ulysses Data, of an Apparent Anomalous, Weak, Long-Range Acceleration", *Phys. Review Letters,* Vol. 81, 1998, pp. 2858–2861.

Anon. (2008) "CERN LHC: The Guide", CERN-Brochure-2008-001-Eng, January 2008.

Ball, P. (2007) "Fundamental Physics: Feel the Force", *Nature,* Vol. 447, No. 7146, 14 June 2007, pp. 772–774.

Barceló, C., Liberati, S., Sonego, S. and Visser, M. (2009) "Black Stars, Not Holes", *Scientific American*, Vol. 301, No. 4, October 2009, pp. 38–45.

Bertolami, O. and Tajmar, M. (2005) "Hypothetical Gravity Control and Implications for Spacecraft Propulsion", *J. Propulsion* Power, Vol. 21, July 2005, pp. 692–696.

Betts, B. (2012) "Pioneer Anomaly Solved!", *The Planetary Society*, 19 April 2012.

Bilaniuk, Jeff (1962) Personal communication.

Bondi, H. (1957) "Negative Mass in General Relativity", *Review of Modern Physics*, Vol. 29, No. 3, 01 July 1957, pp. 423–428.

Boniolo, G. (ed.) (1997) *Filosofia della Fisica* (Philosophy of Physics), Mondadori, Milan, Chapter 1 (in Italian) 1997 [this textbook covers from relativity to logical quantum mechanics. Chapter 1 (pp. 1–167) deals with the principle of special relativity and its 'paradoxes' in detail; in N. Falletta's *Paradoxicon,* the 'twins paradox' is explained for the general public in Chapter 20].

Boniolo, G. and Budinich, P. (2010) *The Role of Mathematics in Physical Sciences*, Springer Publisher, softcover reprint of 1st edition 2005 edition, February 2010.

Brumfiel, G. (2008a) "Physicists Await Dark Matter Confirmation", *Nature,* International Weekly Journal of Science, Vol. 454, No. 7206, 13 August 2008, pp. 808–809.

Brumfiel, G. (2008b) "Particle Physics: The Race to Break the Standard Model", *Nature,* Vol. 455, No. 7210, 10 September 2008, pp. 156–159.

Carroll, S.M. (2008) "The Cosmic Origin of Time's Arrow", *Scientific American,* Vol. 298, No. 6, June 2008, pp. 48–57.

Casimir, H.B.G. (1948) "On the Attraction Between Two Perfectly Conducting Plates", *Proc. Koninklijke Nederlandse Akademie Wetenschappen,* Vol. 51, 1948, pp. 793-795.

Cook, N. (2002) *The Hunt for Zero Point: Inside the Classified World of Antigravity Technology*, Broadway Publisher, New York, August 2002.

Courtland, R. (2008) "Astronomers Find Universe's Dimmest Known Galaxy", *New Scientist*, Daily News, 18 September 2008.

Davies, P. (2002) "That Mysterious Flow", *Scientific American,* Vol. 287, No. 3, October 2002, pp. 24–29.

deGrasse Tyson, N. (2007) *Death by Black Hole: and other Cosmic Quandaries*, W.W. Norton & Company, January 2007.

DeWitt, B.S. (2003) *The Global Approach to Quantum Field Theory,* Vol. 1 and 2, Oxford University Press, New York, 2003.

DeWitt, C. and DeWitt, B.C. (editors) (1973) *Black Holes,* Gordon & Breach, London, 1973 [this is a collection of chapters by Hawking, Carter, Bardeen, Gursky, Novikov, Thorne and Ruffini on black holes theory and data; it is a good snapshot of the initial stage of research on this topic].

Einstein, A. (1905) "Zur Elektrodynamik bewegter Körper", Annalen der Physik, Vol. 17, Issue 10, 30 June 1905, pp. 891–921.

Einstein, A. (1915) "Zur allgemeinen Relativitätstheorie", *Königlich Preußische Akademie der Wissenschaften*, Sitzungsberichte: 778–786, Vol. 6, 21 December 1915, pp. 214–224.

Faraoni, V. (2014) *Special Relativity—Undergraduate Lecture Notes in Physics*, Springer Publisher, 2014, Berlin, Chapter 2.

Ford, L.H. and Roman, T.A. (2000) "Negative Energy, Wormholes and Warp Drive", *Scientific American,* Vol. 282, No. 1, January 2000, pp. 46–53.

Forward, R. L. (1990) "Negative Matter Propulsion", *J. Propulsion and Power*, Vol. 6, No. 1, 1990, pp. 28–37.

Friedman, A. (2014) "Can the Cosmos Test Quantum Entanglement?", *AstronomyMagazine*, Kalmbach Publishing Co., 2014, pp. 28–33.

Froning, H.D., Jr. (1980) "Propulsion Requirements for a Quantum Interstellar Ramjet", *J. British Interplanetary Society,* Vol. 33, No. 7, 1980, pp. 265–270.

Froning, H.D., Jr. (1981) "Investigation of a Quantum Ramjet for Interstellar Flight", MDC paper G7887, *AIAA/SAE/ASME 17th Joint Propulsion Conference, Colorado Springs, 27–29 July 1981.*

Froning, H.D., Jr. (1983) "Requirements for Rapid Transport to the Further Stars", *J. British Interplanetary Society,* Vol. 36, May 1983, pp. 227–230.

Froning, H.D., Jr. (1985) "Use of Vacuum Energies for Interstellar Flight", MDC paper H1496, presented at the *36th Congress of the International Astronautical Federation, Stockholm, Sweden, 7–12 October 1985.*

Froning, H.D., Jr. (1986) "Investigation of Very High Energy Rockets for Future SSTO Vehicles", MDC paper H1496, *37th Congress of the International Astronautical Federation, Innsbruck, Austria, 4–11 October 1986.*

Froning, H.D., Jr. (1987) "Investigation of Antimatter Airbreathing Propulsion for Single-Stage-To-Orbit Ships", MDC paper H2618, *presented at the 38th Congress of the International Astronautical Federation, Brighton, UK, 10–17 October 1987.*

Froning, H.D., Jr. (1989) "Interstellar Studies—Their Role in Astronautical Progress and the Future of Flight", MDC paper H5276, *40th Congress of the International Astronautical Federation, Malaga, Spain, 7–12 October 1989.*

Froning, H.D. Jr. (1991) "Field Propulsion for Future Flight", paper AIAA-1991-1990-CP, *27th AIAA/ASME/SAE/ASEE Joint Propulsion Conference, Sacramento, CA,* 24–26 June 1991.

Froning. H.D. Jr. (1997) "Experiments to Explore Space Coupling by Specially Conditioned Electromagnetic Fields", NASA/CP-1999-208694, NASA Breakthrough Propulsion Physics Workshop Proceedings, 1999, pp. 207–215.

't Hooft, G. (2007) "Perspective The Making of the Standard Model", *Nature*, Vol 448, 19 July 2007, pp. 271–273.

Froning, H.D. Jr. (1999) "Fast Space Travel by Vacuum Zero-Point Field Perturbations", AIP Conference Proceedings, Vol. 458, Issue 920, 1999, pp. 920–925.

Froning, H.D. Jr. (2003) "Study to Determine the Effectiveness and Cost of a Laser-Propelled 'Lightcraft' Vehicle System, AFRL-PR-ED-TR-2003-0033, Special Report, AFRL, Air Force Materiel Command, Edwards AFB, CA, 2003.

Froning, H.D., Jr. and Barrett, T.W. (1997) "Inertia Reduction—and Possibly Impulsion—by Conditioning Electromagnetic Fields", AIAA-97-3170, *33rd AIAA/ASME/SAE/ASEE Joint Propulsion Conference and Exhibit*, Seattle Washington, 6–9 July 1997.

Froning, H.D., Jr. and Barrett, T.W. (1998) "Space Coupling by Specially Conditioned Electromagnetic Fields", AIP Conference Proceedings, Vol. 420, Issue 1449, 1998.

Froning, H.D. and Metholic, G.V. (2008) "Unlabored Transitions between Subluminal and Superluminal Speeds in a Higher Dimensional Tri-Space", AIP Conference Proceedings, Vol. 969, Issue 1, 21 January 2008.

Froning, H.D., Jr. and Roach, R.L. (2000) "Preliminary Simulations of Vehicle Interactions with the Zero-Point Vacuum by Fluid-Dynamic Approximations", paper AIAA-2000-3478, *36th AIAA/ASME/SAE/ASEE Joint Propulsion Conference and Exhibit*, Huntsville, AL, 17–19 July 2000.

Froning, H.D., Jr. and Roach, R.L. (2002) "Preliminary Simulations of Vehicle Interactions with the Quantum Vacuum by Fluid Dynamic Approximations", paper AIAA-2002-3925, *38th AIAA/ASME/SAE/ASEE Joint Propulsion Conference and Exhibit*, Indianapolis, IN, 7–10 July 2002.

Froning, H.D., Jr. and Roach, R.L. (2007) "Fluid Dynamic Simulations of Warp Drive Flight Through Negative Pressure Zero-Point Vacuum", AIP Conference Proceedings, Vol. 880, Issue 1125, 2007.

Froning, H.D., Jr., Barrett, T.W. and Hathaway, G. (1998) "Experiments Involving Specially Conditioned EM Radiation, Gravitation and Matter", AIAA paper AIAA-98-3138, *34th AIAA/ASME/SAE/ASEE Joint Propulsion Conference and Exhibit*, Cleveland, OH, 13–15 July 1998.

Garattini, R. (2008) "Casimir Energy: A Fuel for Traversable Wormholes", *J. British Interplanetary Society,* Vol. 61, No. 9, 2008, pp. 370–372.

Greene, B. (1999) *The Elegant Universe: Superstrings, Hidden Dimensions, and the Quest for the Ultimate Theory*, W.W. Norton Publisher, 1999.

Gribbin, J. (1992) *In Search for the Edge of Time,* Bantam Books, Transworld Publishers, London, April 1992.

Hamilton D.B. (Ed.) (2000) "Breakthrough Energy Physics Research (BEPR) Program Plan", US Department of Energy, Office of Energy Efficiency & Renewable Energy, Washington, DC, October 2000.

Hensen, B, Bernien, H., Dréau, A.E., Reiserer, A., Kalb, N., Blok, M. S., Ruitenberg, J., Vermeulen, R.F.L, Schouten, R.N., Abellán, C., Amaya, W., Pruneri, V., Mitchell, M.W., Markham, M., Twitchen, D.J., Elkouss, D., Wehner, S., Taminiau, T.H. and Hanson, R. (2015) "Loophole-Free Bell Inequality Violation Using Electron Spins Separated by 1.3 Kilometres", *Nature* online, Vol. 526, 29 October 2015, pp. 682–686.

Hogan, J. (2007) "Unseen Universe: Welcome to the Dark Side", *Nature,* Vol. 448, No. 7151, July 2007, pp. 240–245.

Hoyle, F. (1957) *The Black Cloud*, Easton Press, 1957.

Jones (1982) Personal communication.

Kane, G. (2003) "The Dawn of Physics Beyond the Standard Model", *Scientific American*, Vol. 288, No. 6, June 2003, pp. 68–75.

Kaufmann, W.J. (1992) *Discovering the Universe,* W.H. Freeman & Company, October 1992.

Krause, H.G.L. (1960) "Relativistic Rocket Mechanics", NASA Report TT F-36, Technical Translation from Astronautica Acta, Vol. II, No. 1, 1956, Washington, DC, 01 October 1960.

Kuntz, T. (2001) "150th Anniversary: 1851-2001; The Facts That Got Away", *The New York Times*, World, 14 November 2001.

Lang, K.R. (1999) *Astrophysical Formulae: Radiation, Gas Processes, and High Energy Physics (Volume 1)*, 3rd Edition, Springer Publisher, June 1999.

Lasota, J.P. (1999) "Unmasking Black Holes", *Scientific American,* Vol. 280, No. 5. 1999, pp. 40–47.

LaViolette, P.A. (2008) *Secrets of Antigravity Propulsion—Tesla, UFOs, and Classified Aerospace Technology*, Bear & Company Publisher, 2008.

Layzer, D. (1975) "The Arrow of Time", Scientific American, 1975, pp. 56–69.

Lemonick, M.D. (2001) "No Time Like The Present", Time International (South Pacific Edition), Issue 50, 17 December 2001.

Lisi, A.G. and Weatherall, J.O. (2010) "A Geometric Theory of Everything", *Scientific American*, Vol. 303, No. 6, December 2010, pp. 54–61.

Long, K.F. (2009) "Fusion, Antimatter & the Space Drive: Charting a Path to the Stars", *J. British Interplanetary Society*, Vol. 62, No. 3, March 2009, pp. 89–98.

Maccone, C. (2008a) "Focal Probe to 550 or 1000 AU: A Status Review", *J. British Interplanetary Society,* Vol. 61, No. 8, 2008, pp. 310–314.

Maccone, C. (2008b) "Computer Tensor Codes to Design the Warp Drive", *J. British Interplanetary Society,* Vol. 61, No. 9, 2008, pp. 358–363.

MacDonald, F. (2015) "Independent Expert Confirms That the 'Impossible' EM Drive Actually Works", sciencealert.com, 28 July 2015.

Mackey, M.C. (1991) *Time's Arrow: The Origins of Thermodynamic Behavior*, Springer Publisher, December 1991.

Maggiore, M., (2007), *Gravitational Waves: Vol. 1: Theory and Experiments,* Oxford University Press, Oxford, UK, 2007.

Mallove, E.F. and Matloff, G.L. (1989) *The Starflight Handbook: A Pioneer's Guide to Interstellar Travel*, John Wiley & Sons, June 1989.

McCulloch, M.E. (2008) "Can the Flyby Anomalies Be Explained by a Modification of Inertia?", *J. British Interplanetary Society,* Vol. 61, No. 9, 2008, pp. 373-378.

Miller, A.L. (2008) *Albert Einstein's Special Theory of Relativity: Emergence (1905) and Early Interpretation (1905–1911),* Springer Publisher, 1998 Edition, June 2008.

Millis, M.G. (1996) "Challenge to Create the Space Drive", NASA TM 107289, NASA Lewis Research Center, Cleveland, Ohio, prepared for the *Interstellar Flight Symposium of the 15th Annual International Space Development Conference* sponsored by the National Space Society York, New York, 23–24 May 1996.

Millis, M.G. (1998) "NASA Breakthrough Propulsion Physics Program", NASA TM-1998-208400, NASA Lewis Research Center, June 1998.

Millis, M.G. (2004) "Prospects for Breakthrough Propulsion From Physics", NASA/TM-2004-213082, NASA Glenn Research Center, Cleveland, Ohio, May 2004.

Millis, M.G. (2005) "Assessing Potential Propulsion Breakthroughs", NASA/TM-2005-213998, NASA Glenn Research Center, Cleveland, Ohio, December 2005.

Millis, M.G. and Davis, E.W. (editors) (2009) *Frontiers of Propulsion Sciences,* AIAA Progress in Astronautics and Aeronautics, Vol. 227, AIAA, Reston, VA, January 2009.

Minami, Y. (2008) "Preliminary Theoretical Considerations for Getting Thrust via Squeezed Vacuum", *J. British Interplanetary Society,* Vol. 61, No. 8, 2008, pp. 315–321.

Morris, M.S. and Thorne, K.S. (1988) "Wormholes in Spacetime and Their Use for Interstellar Travel: A Tool for Teaching General Relativity", *Am. J. of Physics,* Vol. 56, No. 5, May 1988, pp. 395–412.

Morris, M.S., Yurtsever, U. and Thorne, K.S. (1989) *Traversible Wormholes, Closed Timelike Curves, and the Averaged Weak Energy Condition*, Abstracts of Contributed Papers, Twelfth International Conference on General Relativity and Gravitation (GR12), Boulder, Colorado, 02-07 July 1989, p. 247.

Morris, M.S., Thorne, K.S. and Yurtsever, U. (1988) "Wormholes, Time Machines, and the Weak Energy Conditions", *Phys. Review Letters,* Vol. 61, No. 13, 26 September 1988, pp. 1446–1449.

Obousy, R.K. and Cleaver, G.B. (2008) "Warp Drive: A New Approach", *Journal of the British Interplanetary Society,* Vol. 61, No. 9, January 2008, pp. 364–369.

Oppenheimer, J.R. and Volkoff, G.M. (1939) "On Massive Neutron Cores", *Physical Review,* Vol. 55, No. 374, 15 February 1939, p. 374.

Overbye, D. (2016) "Gravitational Waves Detected, Confirming Einstein's Theory", The New York Times, 11 February 2016.

Puthoff, H.E. (2010) "Advanced Space Propulsion Based on Vacuum (Spacetime Metric) Energy" *Journal of the British Interplanetary Society*, Vol. 63, No. 3, 2010, pp. 82–89.

Quigg, C. (2008) "The Coming Revolutions in Particle Physics", *Scientific American,* Vol. 298, No. 2, February 2008, pp. 46–53.

Rahaman, F. (2014) *The Special Theory of Relativity: A Mathematical Approach*, Springer Publisher, 2014, Chapter 2.

Raum, K., Koellner, M. Zeilinger, A., Arif, M. and Gähler, R. (1995) "Effective-Mass Enhanced Deflection of Neutrons in Noninertial Frames", *Phys. Rev. Letters,* Vol. 74, No. 15, 10 April 1995, pp. 2859–2862.

Rodrigo, E. (2010) *The Physics of Stargates: Parallel Universes, Time Travel, and the Enigma of Wormhole Physics*, Eridanus Press, September 2010.

Rudolph, T.G. (2008) "Quantum Mechanics: The Speed of Instantly", *Nature,* Vol. 454, No. 7206, 14 August 2008, pp. 831–832.

Rueda, A. and Haisch, B. (1998) "Contribution to Inertial Mass by Reaction of the Vacuum Accelerated Motion", *Foundations of Physics,* Vol. 28, No. 7, July 1998, pp. 1057–1108.

Sagan, C. (1985) *Contact*, Simon & Schuster, October 1985.

Salart, D., Baas, A., Branciard, C., Gisin, N. and Zbinden, H. (2008) "Testing the Speed of Spooky Action at a Distance", *Nature,* Vol. 454, No. 7206, 25 August 2008, pp. 861–864.

Sänger, E. (1956) "Die Erreichbarkeit der Fixsterne", in Rendiconti del VII Congresso Internazionale Astronautico, Associazione

Italiana Razzi (Proceedings of the VII International Astronautical Congress), Rome, 1956 [*also in Mitteilungen der Landesgruppe Nordbayern der DGRR*, pp. 97–113, 13 May 1958]

Schwarzschild, K. (1916) "Über das Gravitationsfeld eines Massenpunktes nach der Einsteinschen Theorie", Sitzungsberichte der Deutschen Akademie der Wissenschaften zu Berlin, Klasse für Mathematik, Physik, und Technik, 1916, pp. 189.

Smith, M.C., Okamoto, S., Yuan, H.B. and Liu, X.W. (2012) "The Assembly of the Milky Way and its Satellite Galaxies", *Research in Astronomy and Astrophysics*, Vol. 12, No. 8, 2012, pp. 1021–1043.

Smolin, L. (2004) "Atoms of Space and Time", *Scientific American*, Vol. 290, No. 1, January 2004, pp. 66–75.

Smolin, L. (2013) *Time Reborn: From the Crisis in Physics to the Future of the Universe, Houghton Mifflin and Harcourt*, New York, April 2013.

Stuhlinger, E. (1964) *Ion Propulsion for Space Flight*, McGraw-Hill, New York, 1964.

Tajmar, M. (2003) *Advanced Space Propulsion Systems,* Springer Publisher, New York, 2003.

Tajmar, M. (2014) "Propellantless Propulsion with Negative Matter Generated by Electric Charges" AIAA Paper 2013-3913, presented at the *50th AIAA/ASME/SAE Joint Propulsion Conference*, San Jose, CA, 14–17 July 2013.

Tajmar, M. and Bertolami, O. (2005) "Hypothetical Gravity Control and Possible Influence on Space Propulsion", *J. Propulsion and Power,* Vol. 21, No. 4, 2005, pp. 692–696.

Tajmar, M. and Fiedler, G. (2015) "Direct Thrust Measurements of an EM Drive and Evaluation of Possible Side-Effects," AIAA 2015-4083, 51st AIAA/SAE/ASEE Joint Propulsion Conference, AIAA Propulsion and Energy Forum, Orlando, Florida, 27–29 July 2015.

Tajmar, M., Plesescu, F., Seifert, B., Schnitzer, R. and Vasilijevich, I. (2008a) "Search for Frame-Dragging-Like Signals Close to Spinning Superconductors", in: *Proc. 2nd Internat. Conf. on Time and Matter,* edited by M.J. O'Loughlin, University of Nova Gorica Press, Nova Gorica, Slovenia, 2008, pp. 49–74.

Tajmar, M., Plesescu, F., Seifert, B., Schnitzer, R., and Vasilijevich, I. (2008b) "Investigation of Frame-Dragging-Like Signals from Spinning Superconductors Using Laser Gyroscopes", in: *Proceedings of STAIF 2008,* AIP Conference Proceedings CP 969, Albuquerque, New Mexico, 10–14 February 2008, pp. 1080–1090.

Tanka, S. (1960) Personal communication.

ten Boom, P.G. (2012) "The Pioneer Anomaly: An Inconvenient Reality or NASA's 12 Year Misconception?", Proceedings of the *12th Australian Space Science Conference*, Melbourne, 24–26 September 2012.

Thorne, K.S. (1995) *Black Holes and Time Warp: Einstein's Outrageous Legacy,* Norton & Company, January 1995.

Tsiolkovsky, K.E. (2004) *Selected Works of Konstantin E. Tsiolkovsky*, University Press of the Pacific, November 2004.

Turyshev, S.G., Toth, V.T., Kinsella, G., Lee, S.C., Lok, S.M. and Ellis, J. (2012) "Support for the Thermal Origin of the Pioneer Anomaly", *Phys. Rev. Letter*, Vol. 108, Issue 241101, 12 June 2012.

Unnikrishnan, C.S. (2005) "On Einstein's Resolution of the Twin Clock Paradox", *Current Science*, Vol. 89, No. 12, 25 December 2005.

Visser, M. (1989) "Traversable Wormholes: Some Simple Examples", *Physical Review D,* Vol. 39, Issue 10, May 1989, pp. 3182–3184.

Weiner, S. (2016) "Physicist Creates Lab-Sized 'Black Hole': The Experiment's Results May Finally Prove that Hawking Radiation Exists", *Popular Mechanics*, 26 August 2016.

Weinert, F. (2004) *The Scientist as Philosopher: Philosophical Consequences of Great Discoveries*, Springer Science & Business Media, November 2004.

Woodward, J.F. (2001) "Gravity, Inertia and Quantum Vacuum Zero Point Fields", *Foundations of Physics,* Vol. 31, No. 5, May 2001, pp. 819–835.

Woodward, J.F. (2004) "Flux Capacitors and the Origin of Inertia", *Foundations of Physics,* Vol. 34, No. 10, October 2004, pp. 1475–1514.

Woodward, J.F. (2013) *Making Starships and Stargates—The Science of Interstellar Transport and Absurdly Benign Wormholes*, Springer Publisher, New York, 2013.

Yam, P. (1997) "Exploiting Zero-Point Energy", *Scientific American*, Vol. 277, No. 6, December 1997, pp. 54–57.

Appendix A: Radiation—Risks, Dose Assessment, and Shielding

A.1 Introduction

"Radiation" and "nuclear" are words feared by people. Even in technologically developed countries, the public has little or no knowledge of radiation, and when they do, they associate them with weapons, accidents, fallout, and cancer. Only a few know that about half of the Earth heating is due to spontaneous fission of radioactive elements present in the crust and mantle. Without this steady radioactive decay, the Earth would be a far colder place (Gando et al. 2011). The radiation flux emerging from the crust is responsible for the so-called background radiation permeating our environment since Earth was formed. Also, for the same amount of power generation, coal combustion spreads far more ash radioactivity than nuclear waste (McBride et al. 1978; Hvistendahl 2007). Because only specialists (and not necessarily physicians) know about natural background exposure or medical use of radiation, proposals to use nuclear energy, in particular on or for rockets, have always encountered strong resistance from policymakers and the public.

The purpose of this appendix is to inform the non-specialist about what radiation and its dose are, about effects of radiation on humans, and about sources of radiation, including estimates of the dose from nuclear propulsion systems, its shielding, and impact on interplanetary travel.

A.2 Radioactivity

Radioactivity is the process undergone by unstable nuclei (radionuclides), as well as nuclei in excited states, causing spontaneous changes, or transformations, in composition and/or internal energy of the nucleus. This means that radioactivity may change a chemical element into another, releasing or absorbing energy in the process. The most common transformations are as follows: alpha decay, beta decay, and gamma decay. A material that spontaneously emits such radiation due to decay is said radioactive.

A.2.1 Alpha Decay

In alpha decay, the nucleus of an element with mass number A_1 and atomic number Z_1 emits an alpha particle. Alpha particles are made of two protons and two neutrons, that is, they are helium nuclei. Nucleus 1 (the "parent") is replaced by a new nucleus 2 (the "daughter") whose mass number A_2 is equal to A_1—4 and whose atomic number Z_2 is Z_1—2, and an alpha particle is emitted. For instance, ^{222}Rn, $A_{Rn} = 222$, $Z_{Rn} = 86$, decays into ^{218}Po (Polonium 218), meaning that the nucleus of ^{222}Rn emits an alpha particle ($A_\alpha = 4$, $Z_\alpha = 2$), leaving behind a nucleus whose mass number is $(222 - 4) = 218$ and atomic number $(86 - 2) = 84$, that is, ^{218}Po.

The mass (energy) of the parent nucleus must exceed the sum of the masses (energies) of the daughter nucleus and of the alpha particle emitted. This decay constraint can be expressed as follows (Mukhin 1987):

$$M(A,Z) > M(A-4,Z-2) + M(\mathrm{H}_\mathrm{e}^4) \qquad (A.1)$$

A.2.2 Beta Decay

Beta decay is the spontaneous transformation of an unstable nucleus into a new nucleus with charge differing by $\Delta Z = \pm 1$ due to the emission of an electron (β^- decay) or a positron (β^+ decay) or due to the capture of an electron (e-capture).

In the β^- decay, one of the neutrons of the nucleus becomes a proton after emitting an electron. The mass number A does not change, while the new nucleus has an atomic number higher by 1.

Tritium (^{3}H, often symbolized by the symbol T), $A_T = 3$ and $Z_T = 1$, β^- decays into ^{3}He, $A_{He} = 3$ and $Z_{He} = 2$, meaning that one of the two neutrons of the tritium nucleus emits an electron and becomes a proton. The mass number does not change, i.e., $A_T = A_{He}$, while the positive charge of the new nucleus increases by 1 unit:

P.A. Czysz et al., *Future Spacecraft Propulsion Systems and Integration*,
Springer Praxis Books, DOI 10.1007/978-3-662-54,744-1

$$Z_{He} = Z_T + 1 \tag{A.2}$$

The energy constraint specifies that the mass (energy) of the parent nucleus must be larger than the sum of the masses (energies) of the daughter nucleus and of the electron, as expressed by the following (Mukhin 1987):

$$M(A,Z) > M(A,Z+1) + m_e \tag{A.3}$$

In the β^+ decay, the unstable nucleus emits a positron (a positive electron). The β^+ decay can be treated as the transformation of a proton into a neutron, because also in this case, the parent and the daughter nuclei have the same mass number A, while the atomic number Z of the daughter is lower by 1. The proton mass is lower than the neutron mass (energy). The transformation of the proton into a neutron is possible since the proton is bonded to a nucleus and the excess energy to become a neutron is extracted from the nucleus itself. The energy constraint can be expressed in analogy with the β^- case as follows (Mukhin 1987):

$$M(A,Z) > M(A,Z-1) + m_e \tag{A.4}$$

For instance, C^{11}, $A_C = 11$ and $Z_C = 6$, β^+ decays into B^{11}, $A_B = 11$ and $Z_B = 5$, and the missing charge of Boron 11 is that of the positron emitted.

The third type of beta decay is electron capture. It consists of the capture of an electron by a nucleus from its own electron shell. For heavy nuclei, where the K shell is close to the nucleus, this phenomenon, also called K-capture, is quite common. Captures from L shell (L-capture), M shell (M-capture), etc. have also been observed. After the capture, the nucleus has the same mass number A, but its atomic number Z decreases by 1. The electron captured and one of the protons of the nucleus become a neutron in the daughter nucleus. For instance, Be^7, $A_{Be} = 7$, $Z_{Be} = 4$, after capturing an electron from its K shell, becomes Li^7, $A_{Li} = 7$, $Z_{Li} = 3$. The mass number does not change: $A_{Be} = A_{Li} = 7$, while the atomic number Z of the lithium is lower by 1. The mass (energy) constraint is that the sum of the masses (energies) of the captured electron and the parent nucleus must be larger than the mass (energy) of the daughter nucleus (Mukhin 1987):

$$M(A,Z) > M(A,Z-1) + m_e \tag{A.5}$$

Because of the vacancy created in the electron shell, the transition of one of the shell electrons to that vacancy is accompanied by the emission of X-rays.

A.2.3 Gamma Rays

Unstable nuclei going from a higher ("excited") energy state down to a less energetic, and eventually stable, state can emit energy quanta in the γ-ray wavelength ($10^{-8} \geq \lambda \geq 2.0 \cdot 10^{-11}$ cm). There may be single transitions, where the nucleus goes directly from an excited to the ground (stable) state following the emission of a single γ quantum, or there may be multiple transitions, i.e., a cascade, bringing the nucleus to the ground state and involving multiple emissions of γ quanta. The energy of the γ quantum emitted is determined by the energy difference between the two energy levels of the transition.

Many mechanisms can excite nuclei and lead to gamma radiation. Quite commonly, alpha and beta decays can leave the nucleus in an excited state. An alpha decay is usually followed by the emission of low-energy (<0.5 MeV) γ quanta, while after a beta decay, the γ quanta emitted may have energy up to 2.0–2.5 MeV (Mukhin 1987).

A.3 Radiation, Dose Quantities and Units

An ad hoc set of quantities and related units required to describe radiation decay and its effects have been developed since the effects of nuclear radiation were discovered and gradually understood (Klein 1988; US Nuclear Regulatory Commission 2008; Petrangeli 2006). A list of them follows.

A.3.1 Activity (Bq)

Given any radiation decay (α, β, γ, etc.), the *activity* of an element is the rate at which any and all transitions (i.e., emissions of α, β, and γ rays) occur. A radionuclide has an activity of 1 *becquerel* (Bq), when it undergoes one transition per second. An older unit is the curie (Ci), equivalent to $3.7 \cdot 10^{10}$ transitions per second. Mme Curie defined it as "... *la quantité d'émanation en équilibre avec un gramme de radium* ...," that is that quantity of radon-222 in equilibrium with 1 g of its parent radium-226 (Anon 2016a). It is worth noting here that both SI units and old ones, partly deriving from the c.g.s. (cm, gram, second) system, are currently used to define not only activity, but also most other radiation units. Units of activity and symbols are

$$1 \cdot \text{Bq} = 1 \frac{\text{transition}}{\text{second}} \tag{A.6a}$$

$$1 \cdot \text{Ci} = 3.7 \cdot 10^{10} \text{Bq} \tag{A.6b}$$

Activity is *not* a synonym of power or energy; thus, it has *nothing to do with* the effects of radiation on matter, living or not.

A.3.2 Half-Life, $T_{1/2}$ (s)

The *half-life* is the time over which half the nuclei of a given radionuclide decay. Depending on the radionuclide

considered, the half-life varies from billions of years (i.e., U^{238} has a half-life of $4.468 \cdot 10^9$ years) down to small fractions of seconds (i.e., that of Po^{214} is 164 ms). As an example, Pb^{214} has a half-life of 26.8 min; this means that N nuclei of Pb^{214} after 26.8 min become $N/2$ nuclei, the other $N/2$ having become Bi^{214} because of beta decay; and after 53.6 min, only $N/4$ nuclei of Pb^{214} will exist, since 3/4 N have become Bi^{214}, and so on.

A.3.3 Absorbed Dose, *D* (Gy)

Radiation going through matter releases energy. The *absorbed dose* is the *energy* deposited by radiation inside matter per mass unit. Its SI unit is the *gray* (Gy), equivalent to 1 J deposited per *kilogram* of absorbing target material (1 J/kg). The older unit is the rad (radiation absorbed dose), defined as the deposition of 100 ergs per *gram* (Anon 2016a), and the conversion factor is

$$\text{Gy} = 100 \text{ rad} \tag{A.7}$$

A.3.4 Equivalent Dose, *H* (Sv)

Biological effects caused by radiation are dependent not only upon the dose absorbed (in Gy) but also, and above all, upon the *kind* of radiation. "Sparsely" ionizing radiations such as gamma rays, X-rays, or beta rays are less effective in damaging compared to "densely" ionizing radiation such as the much heavier alpha particles or fission fragments. To account for this difference, a corrective weighting factor dependent on the kind of radiation and energy was introduced. Weighting factors w_r range from 1 (for photons or electrons) up to 20 (for alpha particles), and they are dimensionless, see Table A.1. Those specific to neutrons are given in Table A.1 and Fig. A.1 (Anon 1990).

Table A.1 Weighting factors for different types of radiation

Radiation and energy (keV, MeV)	Weighting factor, w_r (−)
Photons, all energy	1
Electrons, all energy	1
Neutrons, <10 keV	5
10–100 keV	10
100 keV–2 MeV	20
2 MeV–20 MeV	10
>20 MeV	5
Protons, all	1
Protons, (not recoil) >2 MeV	5
Alpha particles, all energy	20
Fission fragment, all energy	20
Heavy nuclei, all energy	20

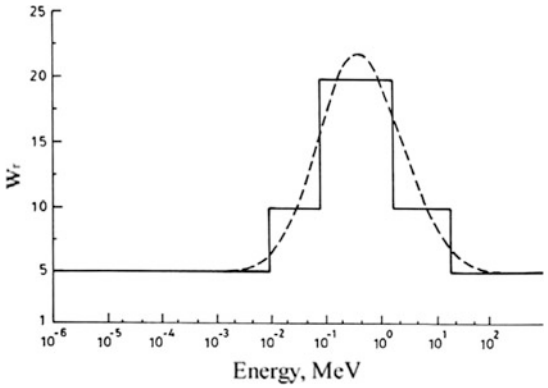

Fig. A.1 Weighting factors for neutrons

The sum of the total radiation doses, D, combined with the proper weighting factor w_r gives the *equivalent dose*, H (Anon 1990):

$$H = \sum w_r \cdot D \tag{A.8}$$

Since w_r is dimensionless, the equivalent dose H has the same dimension as the absorbed dose D, i.e., joules per kilogram. Its SI unit is the *sievert* (Sv). The older unit is the *rem* (roentgen equivalent in man), whereby

$$1 \text{ Sv} = 100 \text{ rem} \tag{A.9}$$

A.3.5 Effective Dose, *E* (Sv)

Consequences of radiation on the human body depend on the particular organ or tissue hit by radiation, as different organs have different responses to radiation exposure. This is the reason why another weighting factor (w_T) must be introduced, see Table A.2 (Anon 1990).

The sum of the equivalent dose, D, with the tissue weighting factor gives the *effective dose*, E (Anon 1990). The dimensions of the effective dose are *the same as* absorbed dose and equivalent dose, joules per kilogram. Its SI unit is the same as that of the equivalent dose, that is, *sievert.*

$$E = \sum w_T \cdot H \tag{A.10}$$

A.3.6 Collective Dose (man-Sv)

Absorbed, equivalent, and effective doses apply to *individuals* or average individuals. In order to assess the dose received by a *group* or *population,* it is useful to introduce the *collective dose.* It is obtained by summing up the individual doses of each person of the group considered. Its SI unit is man-Sv. A collective dose of 1000 mSv corresponds to 1000 people receiving each 1 mSv or 10 people 100 mSv.

Table A.2 Weighting factors for tissues/organs

Organ or tissue	Weighting factor, w_T (−)
Gonads	0.20
Red bone marrow	0.12
Colon	0.12
Lung	0.12
Stomach	0.12
Bladder	0.05
Breast	0.05
Liver	0.05
Esophagus	0.05
Thyroid	0.05
Skin	0.01
Bone surfaces	0.01
Remainder	0.05

This quantity is defined for a specific source of radiation or for a specific practice causing exposure, and is a convenient measure when assessing the consequences of nuclear accidents (Anon 2010).

A.3.7 Dose Commitment (Sv)

Some events, such as weapon tests, release radioactivity in the environment and cause continuous exposure over a long time period that may include several generations. In order to account for the dose committed to a typical hypothetical individual at the moment and in the future, the so-called dose commitment is used. This is the integral, over a specified time period after the event, of the average dose rate per person (typically 250 or 10,000 years), to a specified group (even the whole world population). Its SI unit is still the sievert (Sv) (Anon 2010). If an event delivers a dose commitment of 1.4 mSv for 250 years, a hypothetical individual, born at the moment of the event and died 250 years old, would receive a dose of 1.4 mSv during his entire life.

A.4 Effects of Ionizing Radiation

Ionizing radiation interacts with matter changing the state of atoms and molecules. In cells, there are two types of consequences after radiation deposition: The cell may die or it may be modified. These two different consequences give rise to different implications for the whole body. There can be deterministic and stochastic effects.

A.4.1 Deterministic Effects

Radiation may kill cells of a tissue/organ. If the number of cells killed is low, the tissue keeps on functioning without any serious consequence. With increasing number of cells killed, the tissue is harmed and loses its function, possibly resulting in tissue or even organ death. It is clear that an increasing number of dead cells cause more and more serious damage to the tissue. This depends on the fact that cell depletion is a dynamic process in competition with proliferation of unaffected cells. If the loss of cell is low, it can be quickly compensated by repopulation resulting in no damage or short time effects. If the loss is high, the number of tissue cells decreases, thereby causing serious damage and/or death. The proportion of cells killed depends on the dose exposure. Consequently, the severity of effects depend on dose as well. These effects are defined as deterministic and have dose thresholds.

Table A.3 Threshold for some deterministic effects

Deterministic effect	Threshold (Gy)
Male temporary sterility	
Acute exposure	0.15
Chronic exposure (per year)	0.4
Male permanent sterility	
Acute exposure	3.5–6
Chronic exposure (per year)	2
Female permanent sterility	
Single exposure	2.5–6
Chronic exposure (per year)	0.2
Depression of blood formation	
Acute bone marrow exposure	0.5
Long-term exposure (per year)	0.4
Lens opacities (sparsely ionizing radiation)	2–10
Lens opacities (densely ionizing radiation)	1–2
Lens opacities (chronic exposure to sparsely ionization radiation per year)	0.15
Dry skin desquamation (3 weeks after exposure)	3–5
Moist desquamation (blistering after 1 month)	20
Tissue necrosis	50

Some deterministic effects are as follows: temporary or permanent sterility, depression of the blood-forming system, skin reddening, desquamation, skin loss, lens inflammation, and cataract. A peculiar case of deterministic effect is the radiation syndrome from acute and whole body irradiation. If the dose is high enough, the strong cell depletion in vital organs (blood-forming organs, gastrointestinal tract, etc.) causes death. An acute whole body exposure dose between 3 and 5 Gy, without any specific medical treatment, causes the death of 50% of the population exposed.

Table A.3 gives some thresholds for deterministic effects shown. The thresholds, like all thresholds for deterministic effects, apply to healthy people (Anon 2010).

A.4.2 Stochastic Effects

If a cell is not directly killed by radiation but somehow modified, the outcome will be different from deterministic effects. In vitro cellular research shows that damage from

radiation to deoxyribonucleic acid (DNA) gives rise to most of the detrimental effects. There are two mechanisms by which radiation may damage DNA: direct or indirect interaction. In the direct interaction case, ionizing radiation directly damages a gene. In the indirect interaction case, radiation produces active chemical radicals near the DNA. The diffusing radicals may interact with DNA and induce chemical changes.

Very efficient mechanisms exist (enzyme actions) to repair DNA, whatever the cause of harm. If only one of the two symmetric strands forming the DNA is damaged, the use of information on the other strand makes the repair process highly probable and successful, though it is *not always error-free*. If both strands are damaged at the same location, the *information is lost forever*. The repair process is more difficult, and genetic changes are likely. Such changes are defined as genetic mutations. The very nature of this process of damage and repair gives rise to effects that are random and statistical and therefore are defined as stochastic. Stochastic effects can be somatic (i.e., cancer-inducing), that is, they occur on the exposed individual, or hereditary. Damaged cells are those whose function is to transmit genetic information to offspring. As it cannot be proven that below a certain dose the repair process is totally effective, differently from deterministic effects, there is no threshold in this case (Anon 2010). This is the so-called "linear hypothesis".

A.4.2.1 Radiation-Induced Cancer

There is substantive evidence that almost all cancers originate from a single cell. However, single changes in the cell genetic code are usually insufficient to initiate a cancer. Several cell mutations (2–7) are required in the carcinogenesis process from pre-neoplasia to cancer. Radiation may act at several stages of the process, but it seems to have a major role in the initial conversion of the cell to a pre-neoplastic state. A pre-neoplastic cell is immersed in an environment of normal cells, which tend to suppress and constrain pre-neoplastic properties. Overcoming these constraints results in a cancer.

Cancer may be triggered by many factors such as smoke and chemical agents. It is therefore impossible to determine whether radiation is the cause of a particular type of cancer or not. The only way to ascertain a correlation between radiation and cancer induction is statistical. Epidemiology is the study of the distribution of diseases among people, and it is still an observational rather than experimental science. Therefore, bias or confounding factors are highly probable. In the present context, the so-called Life Span Study (LSS) is an ad hoc study on survivors of Hiroshima and Nagasaki which has produced a significant amount of data on effects of exposure to radiation on humans (Anon 2016b). Studies of people partially exposed to radiation due to medical investigations or treatments are another source of data, together with information available from studies of occupational exposures, i.e., in the Mayak Production Association facility in Russia, and the Chernobyl accident (Anon 2010). In the case of the Fukushima accident in Japan, the study started almost immediately (Anspaugh et al. 2012) and is still continuing.

From a general point of view, linear (or linear-quadratic) no-threshold dose response is to be expected, even though for certain cancers and especially at low doses, correlations are less precise. Some interesting results are those for solid cancers obtained by the Life Span Study (LSS) (Anon 2010), where ERR (excess relative risk) (Fig. A.2) and EAR (excess absolute risk) (Fig. A.3) were estimated. ERR and EAR represent the increased cancer rate in an exposed group relative to an unexposed group, measured on relative and absolute scales. An ERR of 1 corresponds to a doubling of the cancer rate. EAR may be expressed as the number of excess cases of cancers, for example, per 10,000 persons and per unit dose (i.e., 1 Sv) or per a specified dose (Anon 2010).

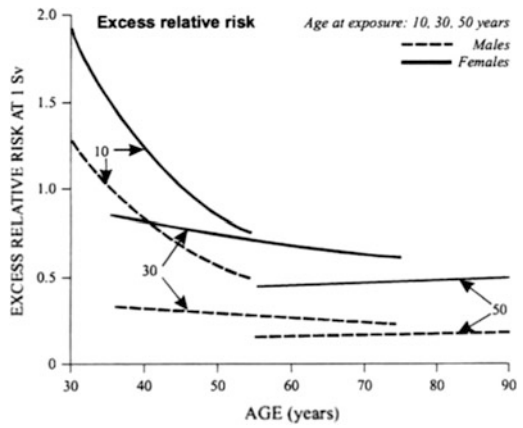

Fig. A.2 Excess relative risk at 1 Sv

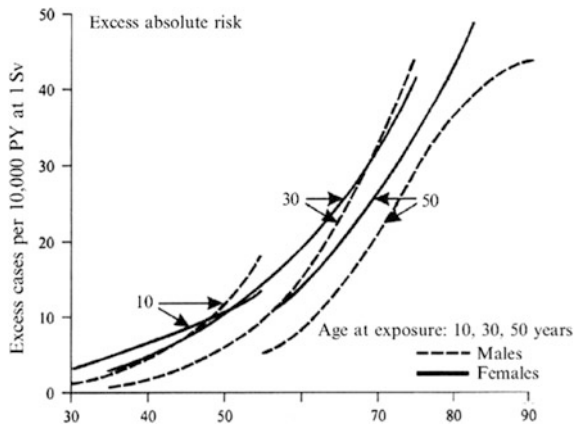

Fig. A.3 Excess absolute risk at 1 Sv

A.4.2.2 Hereditary Effects

No radiation-induced hereditary disease has been demonstrated in humans so far. However, ionizing radiation is recognized as mutagenic and experiments on plants and animals have clearly shown that radiation may cause genetic effects, and there is no reason to believe that humans are an exception.

It has been estimated that for a population exposed to radiation in one generation, the risk, expressed as number of cases per million persons per gray (Gy), in the progeny of the first post-radiation generation is as follows: 750–1500 autosomal dominant and X-linked diseases; 250–1200 chronic multifactorial diseases; and 2000 congenital abnormalities. The total radiation-induced cases are 3000–4700 per gray (Gy) and per million and represent 0.41–0.67% of the total 738,000 cases per million (Anon 1959).

A.5 Sources of Radiation Exposure

The radiation to which humans are exposed originates from various sources. It can be natural radiation or can be produced by human activities (anthropogenic).

A.5.1 Natural Radiation Exposure

Natural radiation, also defined as *background radiation,* has always existed in nature, and life has developed and keeps on proliferating on Earth in a naturally radioactive environment. There are different sources of background radiation, and they can be responsible for either internal or external exposure. Doses from natural sources are summarized in Table A.4 and vary from 1 to 10 mSv/year. The *worldwide annual effective dose* is 2.4 mSv, and for a world population of 7.5 billion people, the *collective dose* is $18 \cdot 10^6$ mSv (Anon 2010).

A.5.1.1 Cosmic Rays

Cosmic rays are a source of external exposure. They can be divided into primary and secondary radiation. Primary radiation can be further divided, depending on its origin, into galactic and solar, the second being less significant. Outside the Earth atmosphere, the main component of cosmic radiation is positively charged particles of energy between 10^2 and 10^5 MeV. They constitute the so-called primary radiation (galactic and solar). When these particles approach Earth, they are deflected by the terrestrial magnetic field (the Van Allen belt) according to their momentum. Those particles entering the Earth's atmosphere and while traveling toward the surface are defined primary radiation and interact with the atmosphere, producing many particles such as electrons, photons, mesons, protons, and neutrons. These are grouped under the name of secondary radiation.

Table A.4 Mean dose value for natural background radiation

Source	Worldwide average annual effective dose (mSv)	Typical range (mSv)
External exposure		
Cosmic rays	0.4	0.3–1.0
Terrestrial gamma rays	0.5	0.3–0.6
Internal exposure		
Inhalation (mainly radon)	1.2	0.2–10.0
Ingestion	0.3	0.2–0.8
Total	2.4	1.0–10.0

Secondary radiation particles themselves can interact with the atmosphere or decay, producing so-called avalanche ionization. From a single starting event up to 10^8 particles can be generated. At about 20 km from sea level (SL), cosmic radiation is constituted almost exclusively of its secondary component (Galli and Mancini 1996). The typical range of effective dose per person per year is 0.3–1.0 mSv, with average effective dose ≈0.4 mSv (Anon 2010). For locations high above sea level, very large doses are received, i.e., in La Paz, Bolivia (3600 m above sea level), the average dose due to cosmic rays is 2.02 mSv per year. A flight at an altitude of 8 km causes a dose rate of 2.8 mSv/h (Galli and Mancini 1996).

A.5.1.2 Terrestrial Radiation

Inside the Earth crust, there are radionuclides whose half-life ($T_{1/2}$) is comparable with the Earth's age. *In fact, the Earth's core is still hot thanks to the energy released by radionuclides in their decay processes.* The most significant for dose computation are K^{40} ($T_{1/2} = 1.28 \cdot 10^9$ year), Th^{232} ($T_{1/2} = 1.41 \cdot 10^{10}$ year), and U^{238} ($T_{1/2} = 4.47 \cdot 10^9$ year). Of secondary importance are Rb^{87} ($T_{1/2} = 4.7 \cdot 10$ year) and U^{235} ($T_{1/2} = 7.04 \cdot 10^8$ year). Most radionuclides belong to one of the three families of uranium, thorium, and actinium, see Fig. A.4 (Galli and Mancini 1996). In all three families, radon (Rn) appears. Radon appearance is the clearest evidence that the Earth's crust is radioactive. Terrestrial radiation can be responsible for internal or external exposure.

External exposure from terrestrial radiation

External exposure to gamma rays from natural radionuclides can occur both outdoors, since radionuclides are present in the Earth's crust, and indoors, as they may be present in construction material. Combining outdoor and indoor exposure, for a person spending 80% of time indoors, a range of 0.3–0.6 mSv per person per year is typical. Worldwide-averaged annual effective exposure is estimated at ≈0.5 mSv (Anon 2010).

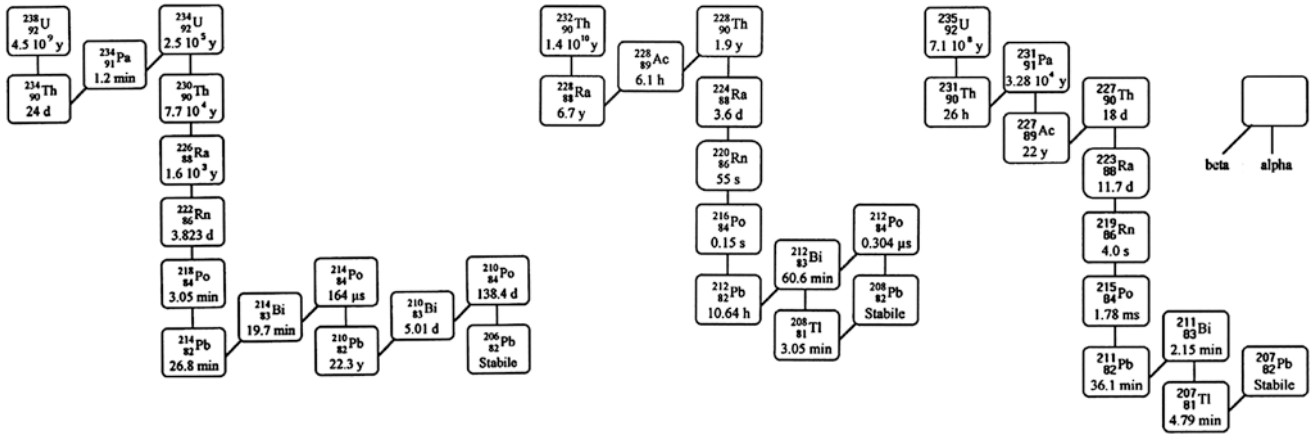

Fig. A.4 Decay chains. From *left to right* Uranium-238; Thorium-232; Uranium-235

Internal exposure from terrestrial radiation

Potassium isotopes are present in the human body with a weight percentage of 0.18%. The isotope K^{40} has an isotopic abundance of $1.18 \cdot 10^{-4}$, and its main decay mechanism is beta. The annual dose from K^{40} is estimated to be 0.165 mSv. Some isotopes (the most significant being Pb^{210} and Po^{210}) can be ingested through food and water or, in the case of Po^{210}, also by smoking. The typical range of the annual effective dose is 0.2–0.8 mSv, but higher values are detected in South America (due to Po^{210} present in "Yerba Mate" drinks) and arctic and subarctic areas, where Po^{210} and Pb^{210} tend to accumulate in moose meat. Worldwide-averaged annual effective dose is 0.3 mSv.

Some radioisotopes may be inhaled, the most significant radioisotope in this case being Rn^{222} and, less importantly, Po^{210} (smoking 10 cigarettes a day doubles Po^{210} introduction). Typical range of inhaled dose is 0.2–10 mSv. The range is so wide because the contribution is mainly given by radon and its intensity depends on its indoor accumulation. The worldwide-averaged annual effective dose due to inhalation is 1.2 mSv. A summary of background radiation sources is given in Table A.4 (Anon 2010).

A.5.2 Medical Radiation Exposure

Ionizing radiation for medical purposes, both in diagnosis and in treatment, is widely used. It must be noted that most of these procedures are carried out in countries where only one-quarter of the world population lives. In fact, world health care has been divided into four qualitative levels, depending on the number of physicians available, see Table A.5.

Diagnostic exposures are characterized by low doses to individuals, while therapeutic exposure is usually much larger. High doses are used to treat diseases, especially cancer. The number of diagnostic procedures is much larger than treatment procedures (the ratio is about 450 to 1). This is due to the widespread use of X-rays, contributing to 78% of collective dose.

The worldwide-averaged annual effective dose is 0.4 mSv, and the total collective dose estimated is $2500 \cdot 10^6$ mSv. Table A.5 shows effective doses reported for each healthcare level (Anon 2010). Table A.6 (Galli and Mancini 1996) shows the effective dose for some diagnostic examinations.

A.5.3 Exposure from Atmospheric Nuclear Testing

Until the "Treaty Banning Nuclear Weapon Tests in the Atmosphere, in Outer Space, and Under Water," signed in Moscow on August 05, 1963 (Bechhoefer 1973), almost all nuclear explosions to test fission and fusion weapons were carried out in the atmosphere, mostly in the Northern

Table A.5 Average dose from medical use

Healthcare level	Population per physician (−)	Annual number of examinations per 1000 persons (−)	Average annual effective dose to population (mSv)
I	<1000	920	1.2
II	1000–3000	150	0.14
III	3000–10,000	20	0.02
IV	>10,000	<20	<0.02
Worldwide average		330	0.4

Table A.6 Doses from some medical examinations

Examination	Effective dose per examination (mSv)
Chest radiography	0.14
Mammography	0.5
Angiography	12
Urography	3.7
Dental	0.03

Hemisphere. For instance, the former Soviet Union carried out 456 tests at Semipalatinsk (Kazakhstan) between 1949 and 1989 (Mikhailov 1996). After the treaty, almost all nuclear testings have taken place underground. The two time periods of most intense atmosphere tests were 1952–1958 and 1961–1962, see Fig. A.5. The total number of atmospheric tests was 543, and the estimated total yield is 440 megatons (189 megatons from fission) (Bergkvist 2000).

The total collective effective dose resulting from weapon tests to date is $3.0 \cdot 10^7$ mSv. About $7.0 \cdot 10^6$ mSv will be delivered within the first 250 years (i.e., until 2200). The remainder, due to the long life of the C^{14} radionuclide produced, within the next 10,000 years. The annual average effective dose varies both with time (decreasing, thanks to the ban treaty), and with location. In the Northern Hemisphere, the dose is higher than in the Southern Hemisphere. For instance, the average effective dose estimated for the year 1999 was 5.87 μSv in the Northern Hemisphere, 2.68 μSv in the Southern Hemisphere, and 5.51 μSv globally, see Table A.7.

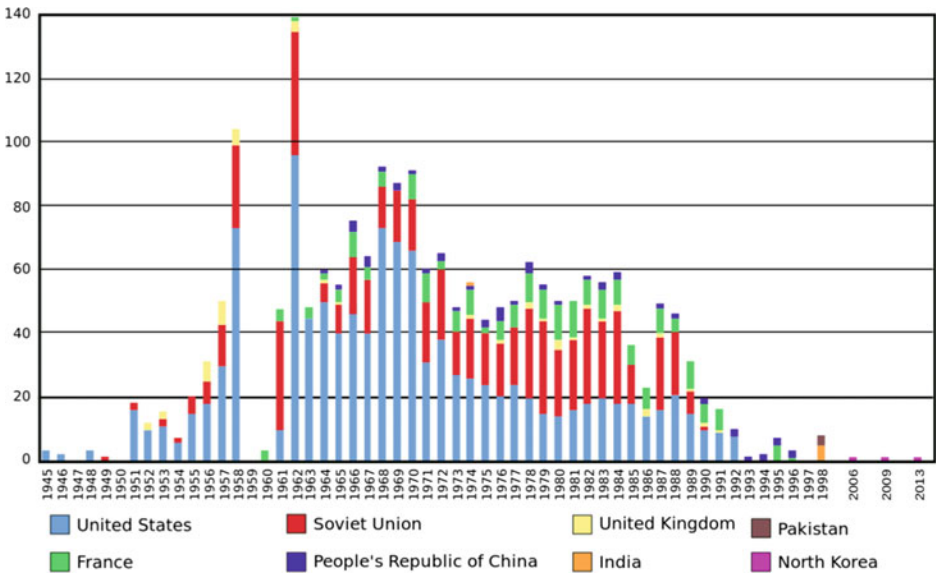

Fig. A.5 Number of weapon tests per year worldwide (1945–2013) [*Courtesy* Wikimedia Commons]

Table A.7 Doses from weapon tests

Year	Average annual effective dose		
	Northern hemisphere (μSv)	Southern hemisphere (μSv)	World (μSv)
1945	0.64		0.57
1955	16.8	3.34	15.4
1965	48.7	11.7	44.6
1975	14.8	5.01	13.7
1985	8.98	2.78	8.30
1995	6.61	2.55	6.20
1996	6.42	2.57	5.97
1997	6.23	2.59	5.85
1998	6.05	2.63	5.63
1999	5.87	2.68	5.51
1945–1999	1076	328	994
1999–2099	264	157	253
2099–2199	63	53	62
2200–	2181	2180	2181
1945–	3580	2720	3490

A.5.4 Exposure from Nuclear Power Production

Today, about 17% of electricity produced worldwide, i.e., about 250 GW, is nuclear. Assuming that this practice continues over the next 100 years, the maximum collective dose can be estimated from the cumulative dose over the period of practice. The normalized 100-year collective dose is 6 mSv per gigawatt and per year. The annual dose is 1500 mSv ($6 \cdot 250$), resulting in a maximum annual dose per person of 0.2 μSv (Anon 2010).

A.5.5 Exposure from Major Accidents

There have been accidents in using nuclear energy or radioactive elements. In medical and diagnostic practice, accidents may occur (a few hundreds of all types each year), which usually carry a serious consequence. The probability that any member of the public be involved is, however, very small, and, by and large, the consequences do not affect it.

Weapons production and transportation have resulted in several accidents, but the collective dose committed is small. The two most serious accidents in nuclear weapons production were at Kyshtym in the former USSR (Anon 2007) and at the Windscale plant at Sellafield (UK) (Anon 1996), both in 1957. The first accident caused a collective dose of 2500 mSv over the next 30 years. The Sellafield accident caused a total collective dose in Europe (including England) of about 2000 mSv.

The three most important accidents in power plants were those at Three Mile Island (Kemeny 1979), Chernobyl (Anon 2006, 2010), and Fukushima (Anon 2015). Note that the Chernobyl installation produced energy only as a by-product, the plant being chiefly a plutonium-producing facility; thus, what happened can hardly be defined as an accident. At Three Mile Island, the containment system, missing in the Chernobyl plant, prevented a large amount of fission fragments from spreading in the environment. Here, the total collective effective dose was ≤ 40 person Sv, with the maximum dose to nearby individuals ≤ 1 mSv. The Chernobyl accident had much more serious consequences. It caused the death of 30 people among the rescue workers within a few weeks (less than 60 to date), and 1800 cases of thyroid cancer in the children exposed (all continuing to be treated). No other health impact has been reported by the World Health Organization up to the year 2008. The worldwide average annual effective dose per person due to the Chernobyl accident, estimated for the year 2000, is 0.002 mSv, down from its peak 0.04 mSv in 1986 (Anon 2010). Note that cancer rates went up by 3% in the affected area, but the children who contracted thyroid cancer have now a 99% survival rate rather than 80–85% previously estimated (Stephan 2005; Mousseau et al. 2005). In fact, according to a report by the Chernobyl Forum released in 2006, poverty and mental-health problems pose a much greater threat to the local community than radiation, see also (Del Rossi and Bruno 2008).

The Fukushima accident was triggered by the Great East Japan Earthquake of March 11, 2011. Poor engineering practice stopped the cooling water flow to the three TEPCO Fukushima Daiichi reactors; they melted within the first three days. The accident was far more covered and documented than Chernobyl and a large amount of data is available, e.g., (Anspaugh et al. 2012; Anon 2015). Although no fatality or acute radiation sickness occurred, a large amount of radioactivity, estimated in 940 PetaBq of Iodine-131 equivalent, was spread in a large area around Fukushima. A few thousand workers and resident people received doses between 10 and 100 mSv, where the average dose for two-thirds of the residents was slightly above 1 mSv. Twenty-five thousands of TEPCO workers participated in the cleanup after the accident; 95% received doses less than 50 mSv during the next 25 months. Both, extension of the area and radioactivity levels, are believed to be a factor 10 lower compared to Chernobyl, as documented in the WHO report by Anspaugh et al. (2012). As in the case of Chernobyl, Japanese researchers concluded that disruption due to the evacuation of some 100,000 local residents caused more harm, mostly in terms of depression, anxiety, and suicide rate.

A different type of accident occurred about 25 years ago in Taiwan. Recycled steel, accidentally contaminated with radioactive ^{60}Co, ended up in construction work, exposing to radiation more than 10,000 inhabitants in 180 buildings over periods ranging from 9 to 20 years (McDonald 1994). The radiation dose received averaged about 0.4 Sv, for a total collective dose of 4000 person Sv. The observed cancer rate was 3.5 per 10^5 person-year; congenital heart malformations among children during the same period were $1.5 \cdot 10^{-3}$. These figures were recently compared with the averages over Taiwan's general population, which are 116 cancers per 10^5 person-year and $23.0 \cdot 10^{-3}$ malformations. This seems to indicate that a "moderate" dose of radiation is beneficial (Chen et al. 2004; Renner 2003). This finding should be, and probably will be, evaluated again with tests on animals in order to corroborate or disprove it. In any event, it seems to agree with a similar finding in laboratory mice and among workers in the General Dynamics Electric Boat nuclear submarine shipyard in Groton, CT. A comprehensive description of this effect, called "hormesis," is in (Prekeges 2003). A possible explanation is the so-called theory of radiative hormesis. According to this theory, a "low" level of stress prepares biological organisms to face and overcome larger disruptions, either internal or external. The Taiwan study hints this level could be of the order of 50 mSv per

year in the case of cancers. If confirmed, this effect would force to reconsider the linear hypothesis.

A.5.6 Occupational Exposure

There are jobs in which workers are routinely exposed to radiation, both because of man-made sources (i.e., medical X-rays, nuclear fuel cycle facilities, etc.) and because of enhanced levels of natural radiation (i.e., airplane crews flying at a height of 8 km receive a dose of 2.8 μSv per hour). This kind of exposure does not affect other members of the public, but it is important to realize the dose these workers receive, see Table A.8, in order to have a better understanding of the issue (Anon 2010).

A synthesis of radiation used in medical practice,diagnostics due to natural sources and of its effects on health is shown in Fig. A.6.

A.5.7 Exposure from Nuclear Propulsion Systems

A new source of dose could in principle result from future space nuclear propulsion systems (none exists at this time). NERVA-type rockets (Chap. 7), Rubbia's engine (Sect. 7.13), and MITEE (Sect. 7.11) (Rubbia 2000; Augelli et al. 2013; Powell et al. 1998, 1999; Maise et al. 2000, personal communication) are among the systems considered. An assessment of the dose committed to the public arising from their use is necessary in order to show their potential impact.

In order to set to rest a hard to die misconception, there is literally no way a nuclear reactor, whether for power generation or propulsion, could trigger a nuclear explosion. The reason is the impossibility of reaching the proper conditions of confinement time and critical mass.

However, what could happen is that, because of malfunction of the reactor cooling/moderating system, fission "runaway" could overheat and even melt down the core. This is called a loss of coolant accident, or LOCA (Anon 2009a). When this happens (it did in the case of Chernobyl and Fukushima), high-temperature chemical reactions can occur, especially if water or graphite is the moderator. Water dissociates into hydrogen and oxygen at high temperature, and they can burn or explode. Graphite burns with air and oxygen and tends to combine with hydrogen. Core overheating may also cause explosions simply due to rapid thermal expansion of the nuclear fuel or other reactor materials. LOCAs are most serious accidents in nuclear reactors. In the absence of a containment structure, radionuclides from the core can be ejected by the chemical or thermal explosion and contaminate the nearby environment.

This said, it should be clear that this class of accidents is in fact due to chemistry, not fission, and the use by the popular press of the term "nuclear explosion" in this context is due to misinformation.

In order to test the effects of an actual meltdown due to runaway fission, during the NERVA program, a test was performed at Los Alamos in which a Kiwi nuclear reactor was deliberately allowed to explode by excluding the cooling system (this was the so-called Kiwi TNT test) (Fultyn 1968). Results are reported in (Dewar 2002, 2004). The reactor was totally destroyed, but contamination was limited to a relatively small area with radius of order 100 m. After clearing the site of debris, activities were resumed. This test did much to allay fears that a NERVA-type core meltdown and explosion could in any way produce a large-scale catastrophe. In comparison, a nuclear rocket reactor is inherently smaller than a power plant reactor, so the outcome of the Kiwi TNT test is encouraging the understanding toward practical implementation of future nuclear rocket reactors.

There is a specific and more serious concern in propulsion applications since such a nuclear reactor must be (a) orbited, i.e., lifted through the Earth atmosphere, (b) perform its interplanetary mission starting from LEO or MEO, and (c) possibly be parked again in Earth orbit at the end of its mission. The question is what could happen during each of these three mission segments. UN and US legislation

Table A.8 Annual *pro capite* doses in the year 2000

Source	Worldwide annual *pro capite* dose (mSv)	Range or trend
Natural background	2.4	Typical range 1–10 mSv. Sizeable population also 10–20 mSv
Diagnostic medical use	0.4	Typical range 0.04–1.0 mSv at lowest and highest level of health care
Atmospheric nuclear testing	0.005	Has decreased from a maximum of 0.15 mSv in 1963. Higher in northern hemisphere and lower in southern hemisphere
Chernobyl accident	0.002	Has decreased from a maximum of 0.04 mSv in 1986. Higher in locations near the accident area
Nuclear power production	0.0002	Has increased with the expansion of plants but decreased thanks to improved practice

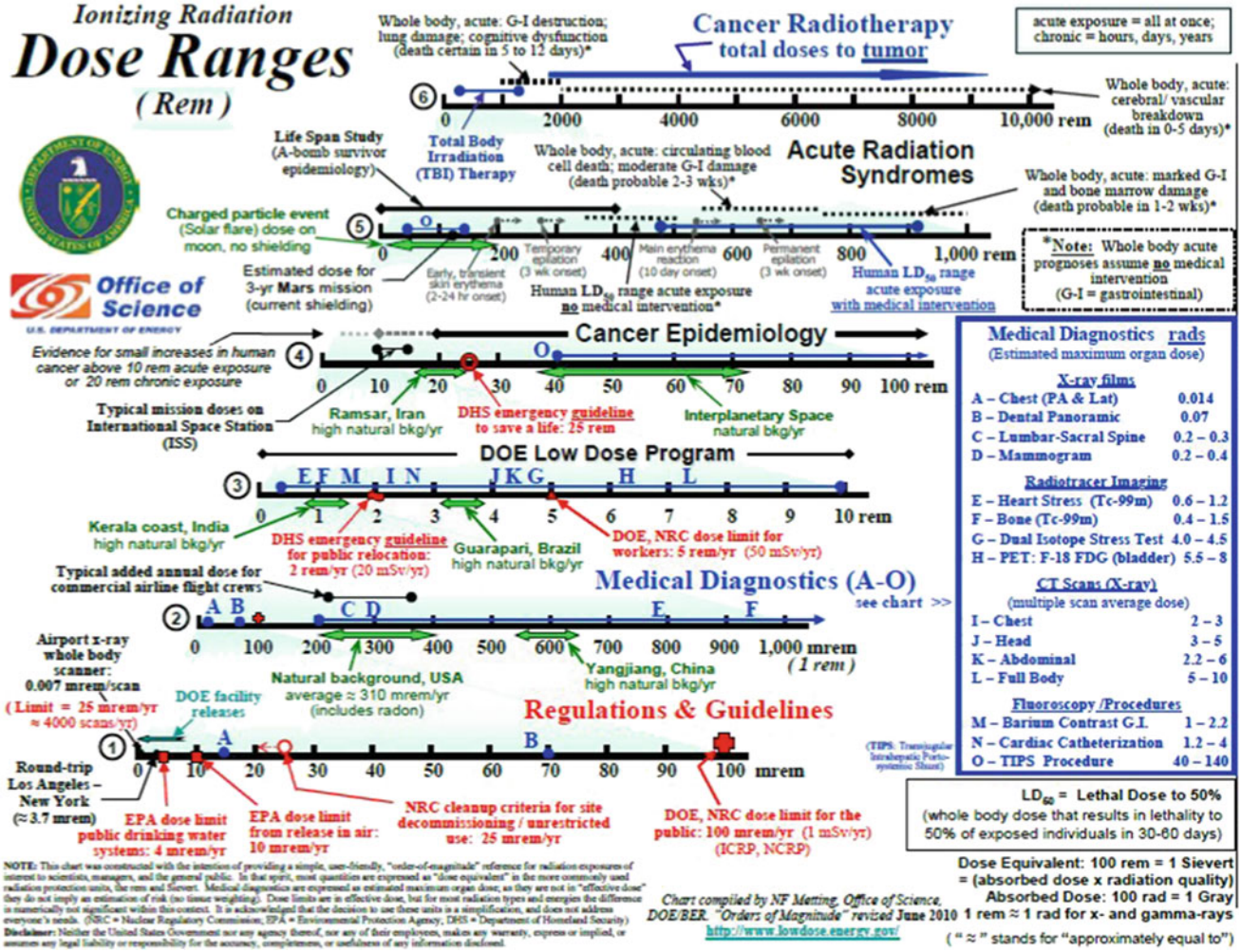

Fig. A.6 Radiation dose ranges: limits, natural, anthropogenic sources, and health effects (*Courtesy* US DOE, Office of Science)

addressed this question in depth (Lenard 2008), and the interested reader should refer to it for details. In the present context, this issue is briefly discussed from a technical viewpoint.

Any reactor will contain elemental fissile material fuel inside its rods of order 1–10 kg depending on fuel type. It is assumed that the reactor is *not* working while lifted to orbit. However, during the critical ascent phase, the danger is an accident, such as that of the 1986 *Challenger* Space Shuttle (McDonald and Hansen 2009), in which a chemically powered launcher could explode. Such accident could damage the reactor to be orbited, and the damage could spread fissile material from the compromised reactor stored in the payload bay either into the atmosphere or on the ground as solid debris. In retrospect, an accident during any interplanetary trajectory would *not* affect Earth. Considering the worst-case scenario, the most dangerous occurrence would be if the reactor, containing all the radionuclides produced during a mission, were for some reason to *reenter* Earth's atmosphere accidentally. Since no space agency is considering deliberate reentering of nuclear reactors, such event would be indeed accidental.

The consequences would be the spreading of many families of radionuclides in the atmosphere, at a height likely to coincide with the peak of aerodynamic heating, roughly between 40 and 10 km. The total mass of radionuclides spread would be approximately the same as that of the original fuel, of order 1–10 kg. Additional contamination would come from secondary radioactivity induced in the reactor structural materials. This accident would be similar to the effect of an atomic explosion in the atmosphere, where fissionable material and bomb structure are vaporized and released. Data from atmospheric atomic tests exists that can be effectively used to estimate these effects. In any event, the quantity of radionuclides in an atomic explosion is many times larger than in any nuclear reactor at this time envisaged for space missions. Accordingly, radioactive contamination is expected to be smaller (Lenard 2008).

A.5.7.1 Nuclear Accidents in the Rubbia Engine

In order to evaluate the impact of accidents due to nuclear space reactors, Rubbia and MITEE engines have been chosen as representative of modern nuclear propulsion technology, although their actual use in space missions seems far in the future. Like all nuclear propulsion concepts, the Rubbia engine (see Chap. 7) is totally inert while in the atmosphere. The dose to the public would be the highest in a hypothetical accidental reentry, for instance at the end of a Mars mission. For each kilogram of Am^{242m} loaded, the total collective dose committed for the following 250 years is estimated at 9.5 mSv. The individual dose commitment over the following 250 years would be $1.8 \cdot 10^{-6}$ mSv. In the case of an americium stockpile of 15 kg, representative of a manned Mars mission using the Rubbia engine, the total collective dose committed for the first 250 years would be 140 mSv, while the individual value would be $3.0 \cdot 10^{-5}$ mSv (Rubbia 2000).

In addition, the Am^{242m} fuel was purposely chosen because of its neutron cross section sharply decreasing with temperature. This feature means that any runaway fission in Am^{242m} would automatically stop above a certain temperature, and the reactor regime would be brought back to a stable state.

A.5.7.2 Nuclear Accidents in a MITEE Engine

Also in the case of MITEE (see Chap. 7), the most catastrophic accident would be the total destruction of the vehicle accidentally reentering the atmosphere after a mission. Like Rubbia's engine, MITEE is planned not to fission while in the Earth atmosphere, so that a prompt criticality accident (explosion caused by overheating) would have less considerable consequences than the total destruction of a chemical explosion or unwanted reentry in the atmosphere after returning from a Mars mission. The average dose commitment over the following 250 years would be about $1.6 \cdot 10^{-8}$ mSv for each kilogram of uranium loaded, and for a typical MITEE configuration, the average dose commitment for 250 years would therefore be about $4.0 \cdot 10^{-7}$ mSv (Anon 2010; Powell et al. 1998, 1999; Maise et al. 2000, personal communication).

A.5.7.3 Safe Ground Testing of Future Nuclear Rockets

A key issue in planning nuclear propulsion is ground testing. During the ROVER project, Kiwi and Phoebus reactors were tested at Los Alamos in the open air. The book by Dewar recounts details of those tests and the safety measures employed. It suffices to say here that no accident involving loss of life or damage to people took place during the entire US program (Dewar 2002, 2004). The paper by (Dewar 2002), for instance, documents how effluents from the nuclear furnace test reactor were treated at LASL (Los Alamos Scientific Laboratory) during the last period of the ROVER program.

Nevertheless, planning future ground tests is a definite concern. However, at least in the case of the type of reactor envisaged by C. Rubbia and investigated by the Italian Space Agency (ASI) under Project P 242 (Augelli et al. 2013), the following considerations apply.

The Rubbia engine is modular, each module being a self-standing generator of hot hydrogen gas. About 30–40 modules compose the engine. For a manned Mars mission, the thrust F required is of order 10^3 N, while the specific impulse I_{sp} is of order 2500 s. Comparison with the NERVA Phoebus 2A engine tested at Los Alamos (F = 334,000 N, I_{sp} = 825 s, mass flow rate = 40 kg/s) shows that the single module of the Rubbia engine to be tested in an appropriate test facility will process a mass flow rate of hydrogen of order 2.5 g/s. So, the scale factor between a module of the Rubbia engine and NERVA is about 16,000. The amount of hydrogen, and therefore of fission fragments deposited inside the hydrogen used as propellant, will be exceedingly small.

As a consequence, testing a single module of the Rubbia engine may be performed in a closed loop, and this appears feasible for all nuclear rockets of comparable thrust, and built following a modular philosophy, therefore also MITEE. Ways of efficiently separating fission fragments from hydrogen have already been described in the final report of ASI on the Rubbia engine (Augelli et al. 1999). Closed-loop tests of bars or rods can be performed in any reasonably self-contained facility and building, thus ensuring that no radiation may escape. In the USA, the SAFE (Subsurface Active Filtering of the Exhaust) testing concept developed at INL (Idaho National Laboratory) (Howe et al. 2003) addressed the testing issue by basing it deep underground in the caverns produced by the Nevada tests in the 1950s and 1960s, see Sect. 7.5, and by filtering all effluents so they stay sequestered there (Werner 2011).

A.5.8 Comparison of Exposures

The doses received by an individual from all main sources for the year 2000 are summarized in Table A.9. Their values are given in *annual* per caput effective dose (mSv). The values are averaged, meaning that there are significant variations in exposure to individuals, depending on location, diet, personal habits, and so forth.

The largest contribution to total dose is from the natural background, 2.4 mSv, but typical values may range from 1 up to 10 mSv, with large groups of population receiving a dose of 10–20 mSv.

The second most important source, 0.4 mSv, is from the medical use of radiation. This has a rising trend, thanks to increasingly available medical radiation facilities. The third

Table A.9 Comparison of annual doses from different sources

Source	Effective dose/dose commitment (mSv)	Comment
Rubbia's engine accident → catastrophic LEO reentry	$1.8 \cdot 10^{-6}$	Dose committed for 250 years (per kg fuel)
MITEE accident → catastrophic LEO Reentry	$1.6 \cdot 10^{-8}$	Dose committed for 250 years (per kg fuel)
Natural background	2.4	Average effective dose in 1 year
Dental X-ray examination	0.03	Average effective dose from a single examination
Flying at 8 km for 10 h	$2.8 \cdot 10^{-8}$	1 h gives $2.8 \cdot 10$ μSv

cause is the fallout from past weapon tests, i.e., 0.005 mSv. This value has been decreasing thanks to the 1963 partial Nuclear Test Ban Treaty, the maximum value being reached in 1963, when it was 7% of the natural background. Other man-made sources, such as the Chernobyl and Fukushima accidents and nuclear power production activities, are much smaller, about 0.002 and 0.0002 mSv, respectively.

A.5.9 Radiation from Reactors—Conclusions

The individual dose commitments for 250 years arising from a rather improbable total "crash" of Rubbia's engine ($1.8 \cdot 10^{-6}$ mSv) and MITEE ($1.6 \cdot 10^{-8}$ mSv) are both insignificant compared to other sources of exposure. Should the Rubbia engine crash, a hypothetical individual born in the year of the crash and dying at age 250, would have received all along his life a $3.0 \cdot 10^{-5}$ mSv dose, much lower than the dose imparted by a dental examination (0.03 mSv). The same would be true for a MITEE accident of the same type. The average dose from natural background to each individual is 2.4 mSv in one single year. Table A.9 compares contributions of various sources.

Therefore, the contribution to the individual average dose from the crash of a spacecraft, powered by nuclear reactors, seem not a reason of concern to public health.

A.6 Reactor Shielding

The Hiroshima cloud and the Chernobyl and Fukushima accidents with all their horrific effects still cast a pall over anything nuclear. Therefore, living in a spacecraft close to a nuclear engine raises immediate safety questions. It is a fact that in interplanetary space, galactic cosmic radiation (GCR) and solar radiation (SR) do pose a much more severe danger to crew health, see Sect. A.7.

Radiation from fission is a catch-all name including, in general, electromagnetic photons and particles with mass, including neutrinos (Chichester 2012). Fission fragments, neutrons, electrons (beta rays), and photons (in the X-ray and gamma bands), with energy in the keV to MeV range, are emitted by fissioning nuclei. From a distance, a reactor may be assumed to be a point source radiating isotropically, so the intensity of radiation, defined in terms of flux of particles (number of particles emitted per unit area and unit time), will attenuate with distance d as $1/d^2$. At sufficient distance, shielding may not be needed to protect crew and equipment of a nuclear-powered spacecraft. However, d is typically large and a material shield is always included in designing a nuclear propulsion system. Crew must live within the shadow cast by the shield.

Radiation may be roughly divided into primary and secondary. *Primary radiation* is the immediate result of nuclei fission, and it includes the fission fragments (FF) themselves. *Secondary radiation* is the effect of radioactive decay of FF and of the interaction of primary radiation with matter or with itself. The conceptual sketch of Fig. A.7 shows the many facets of radiation. This section will only outline main radiation features involved in designing shields.

An ideal shield should slow down fast *neutrons* so they can be captured by its nuclei, and absorb the energy of all *gamma* photons (Glasstone 1955). Gamma rays and neutrons are the most dangerous constituents of radiation, because they penetrate matter farthest. A shield dimensioned for these particles can stop everything else. A shield needs not to be thought of as necessarily separate from the engine. In nuclear space engines, part of the shield may be the propellant in tanks interposed between reactor and crew quarters.

In what follows, CGS units (centimeter, gram, second) may be used, as nuclear physicists still prefer and use them.

A.6.1 Absorption

The simplest model to describe absorption of radiation in a continuous medium with uniform properties assumes that the change of radiation intensity, $\mathrm{d}I$, crossing a distance $\mathrm{d}x$ is linearly proportional to the local intensity, $I(x)$:

$$\mathrm{d}I(x) = \mu \cdot I(x)\mathrm{d}x \tag{A.11}$$

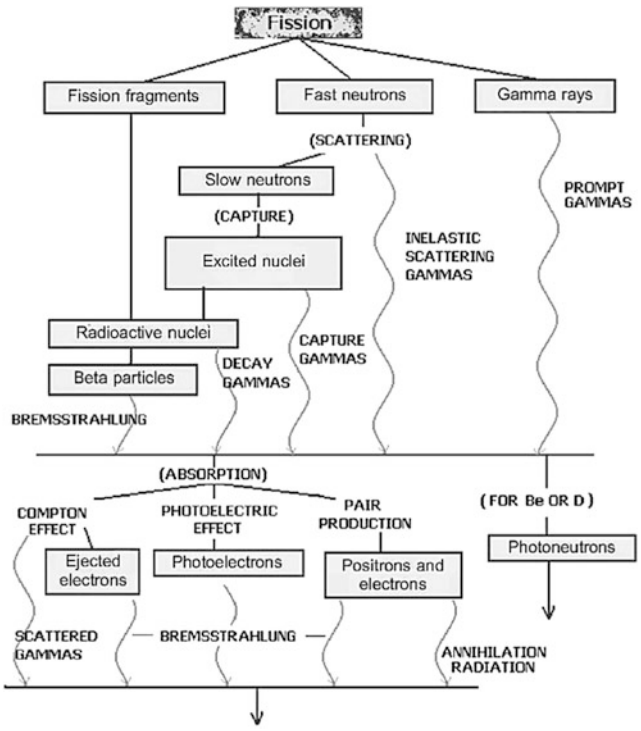

Fig. A.7 Types of primary and secondary radiation emitted from a fission reactor

where μ is the *line* absorption coefficient, its dimensions the inverse of a length. Thus, $I(x) = I(0)\exp(-\mu \cdot x)$, meaning that the flux of particles from a source decreases exponentially along the x direction. At a distance $1/\mu$ from the origin, I becomes e-times smaller.

A.6.1.1 α Particles ("Alphas")

Because of their charge, alphas are readily stopped by matter. The energy deposited during absorption ionizes materials producing ion pairs. Penetration by alphas is quantified by their range, R, the distance travelled in a medium. Using the $I(x)$ law, the μ of alphas is large (fast attenuation). The range scales with $1/\rho$, so in standard air, the range R of many isotope-emitted alphas (energy $\approx$ 5 MeV) is ≈2.5–3.0 cm. In aluminum, the range decreases by the factor $\rho_{Al}/\rho_{air} \approx 1600$, and in lead, this factor is ≈5000. Aluminum foil stops alphas very effectively (Anon 1993). Alphas emitted by ^{241}Am (the americium isotope present in most smoke detectors) do not pose any danger, because they are stopped by air a few cm from the ceiling or wall.

A.6.1.2 β Particles ("Betas")

Betas (electrons) are about 3880 times lighter than alphas. Their momentum, size, and cross section are much lower than alphas. In the 0.1–3 MeV energy spectrum, their range, R, in air varies between 11 cm and 13 m. Scaling with density is similar to that of alphas and is a linear function of their maximum energy E_{max}. For instance, between 0.8 and 3 MeV, an experimental fit for R is

$$R_\rho = 0.54 \cdot E_{max} - 0.15\,(\mathrm{g/cm^2}) \qquad (A.12)$$

A.6.1.3 γ Rays ("Gammas")

Fission gamma rays are photons of wavelength 10^{-8}–10^{-11} cm. They are emitted by nuclei excited by collisions with fission neutrons or decaying. Their energies may be of order several MeV. Gammas penetrate deeply inorganic and living matter, and shielding must stop them completely.

The line absorption of gammas follows the $I(x)$ law, but μ is a function of $I(x)$. Gammas of 0.1 MeV energy crossing standard air have $\mu = 2.0 \cdot 10^{-4}$ cm^{-1} (very small, implying small attenuation or longer penetration distance); μ decreases exponentially to $0.4 \cdot 10^{-4}$ at 5.0 MeV. The reason is the inverse dependence of the cross section σ on the kinetic energy of the traveling photons. Lead has $\mu = 5.0$ cm^{-1} at 0.25 MeV, exponentially decreasing to 0.5 cm^{-1} at 5.0 MeV. The ratio between lead and air in attenuating gamma radiation is a factor 10^4, see Table A.10.

In designing shields, it was found that for almost all materials, the ratio μ/ρ is about constant at a given energy, decreasing only with decreasing energy. For instance, μ/ρ at 0.5 MeV is 0.08 cm^2/g, while at 5.0 MeV, it becomes 0.03 cm^2/g. This result equally applies to H_2O, Al, Fe, and Pb, see Table A.11. For this reason, it is convenient to rewrite $I(x)$ as

Table A.10 Gamma ray absorption coefficient for some shield materials

Energy (MeV)	Water (−)	Aluminum (−)	Iron (−)	Lead (−)
0.5	0.090	0.230	0.63	1.70
1.0	0.060	0.160	0.44	0.77
1.5	0.057	0.140	0.40	0.57
2.0	0.048	0.120	0.33	0.51
3.0	0.038	0.090	0.30	0.47
4.0	0.033	0.082	0.27	0.48
5.0	0.030	0.074	0.24	0.48

Table A.11 Absorption coefficients μ and μ/ρ of 4 MeV gamma rays in some materials

Material	M (cm^{-1})	P (g/cm^3)	μ/ρ (cm^2/g)
Uranium	0.720	18.70	0.038
Tungsten	0.680	19.30	0.035
Lead	0.480	11.30	0.042
Iron	0.270	7.80	0.034
Beryllium oxide	0.076	2.30	0.033
Boron carbide	0.072	2.50	0.029
Beryllium	0.053	1.85	0.029
Graphite	0.052	1.62	0.032
Water	0.033	1.00	0.033
Sodium	0.030	0.93	0.032

$$I(x) = I(0)\exp\left[\left(\frac{\mu}{\rho}\right)\rho x\right] \tag{A.13a}$$

$$I(x) = I(0)\exp\left[\left(\rho x/\left(\frac{\mu}{\rho}\right)\right)\right] \tag{A.13b}$$

This means that the scaling of gammas is still of the type "density times distance," but where the volumetric density ρ is replaced by the areal density ρ/μ (mass/unit area). Then, ρ/μ can be interpreted as the mass that must "sit" over a unit area to absorb the flux of gammas. Conversely, the greater μ/ρ, the larger the distance gammas can cross before being absorbed by matter.

A.6.1.4 Neutrons

Neutrons are the hardest particles to stop, because they possess mass but not charge, and therefore are not slowed down by the Coulomb force from electron shells or nuclei. Similarly to alphas and betas, their (weak) interaction with nuclei occurs only in collisions. The neutron cross section σ depends on energy and type of nucleus. The key concept of cross section can be understood using simplified modeling. The number d C of neutrons *captured* by a nucleus (thus effectively stopped) per unit time when crossing a distance d x is assumed to be

$$\mathrm{d}C = I \cdot (N \cdot \mathrm{d}x) \cdot \sigma \tag{A.14}$$

where I is the neutron flux (cm^{-2}) and N the volumetric density of nuclei (cm^{-3}) so that N d x is the *areal* density of nuclei. Then, σ can be interpreted as the effective rate of capture per unit flux and unit nuclei surface density. Note that the effect of *scattering* is not included in this simple model. This model predicts that the flux $I(x)$ is a function of penetration x according to

$$I(x) = I(0)\exp[N \cdot \sigma \cdot x] \tag{A.15}$$

The product $N{\bullet}\sigma$ plays the same role of the absorption coefficient of alphas and betas. As for gamma rays, the difference is that σ is a function of energy and type of nucleus. N depends on the shield material and is easily determined. The cross section is a much more difficult quantity to measure (or predict), and, in the end, is what controls shielding properties. Next, we consider neutrons produced by fission which are classified according to their energy.

Fast neutrons are those with energy above 0.1 MeV and up to 10 MeV (this energy corresponds to 15% of the speed of light). All neutrons promptly emitted by a fissioning nucleus are fast. Fast neutrons can be stopped only by forcing them to interact with as many nuclei as possible. This means a shield very thick or very dense. In either case, it is the quantity of matter that determines neutron-stopping capability.

Slow neutrons (below 1 MeV) are neutrons that have already collided with nuclei and have been scattered. Scattering may be elastic (momentum and KE are conserved) or inelastic (only momentum is conserved). Elastic scattering is typical of low-energy neutrons and takes place when they collide with light nuclei (e.g., hydrogen or lithium). In inelastic scattering collisions, neutrons transfer part of their

KE to nuclei and excite them. Inelastic scattering is nucleus-specific. Much work has gone into calculating or measuring scatter by different materials, because this knowledge is critical to solid core reactor design. In order to excite nuclei, neutrons must have sufficient energy, say, >0.1 MeV. The process of transferring KE from a neutron to a nucleus may be visualized as similar to that when a liquid droplet hits a larger drop with a higher surface tension. In this analogy, surface tension mimics the strong nuclear force. Nuclei "vibrate" after the collision, that is, the bonds among protons and neutrons stretch and relax at a frequency of order 10^{21} Hz. Eventually, in times of order 10^{-3} s, nuclei reach their stable state by releasing energy (photons), so the ultimate effect of inelastic collisions is to heat the material. This is desirable if the ultimate purpose is to heat the propellant in a NTR (nuclear thermal rocket). However, it is quite undesirable if the material is the shield or structural parts of a nuclear engine.

Both types of scattering slow down neutrons. They eventually become "thermal neutrons," that is, neutrons in thermal equilibrium with the shield material. At room temperature, the thermal speed of neutrons in matter is about 2200 m/s.

A.6.2 Reactor Shielding Practice

The basic shielding strategy is to stop neutrons and gammas. Neutrons must be captured, while gammas must be absorbed; their energies must be thermalized.

Slowing down fast neutrons is called "moderating" in reactor physics. The slowing down is preliminary to final capture of neutrons (note that fuels such as ^{235}U use slow neutrons to fission). No matter whether slow or fast, shield design depends on σ. In many high-energy collisions, the cross section shrinks with energy (speed), making interaction less likely. For low-energy collisions, there are instead interactions where the collision cross section increases by many orders of magnitude at very specific energies. These are called resonant collisions/cross sections and are very important in reactor safety and shielding.

In order to give an example of questions arising in shield design, an obvious strategy for slowing down neutrons would be to surround the reactor with LH_2, because hydrogen is a good moderator. Neutrons and hydrogen nuclei have masses of the same order, making it easier to transfer the kinetic energy of neutrons to H nuclei. Unfortunately, the neutron-H cross section at high energy becomes small. Lower energy neutrons are slowed down efficiently by H, but those with high energy are not. Only high mass number elements, such as Pb, Ba, and W, slow down neutrons through inelastic collisions. These elements are poor moderators of neutrons, that is, at lower energy, deceleration via elastic collisions is inefficient. The solution to this quandary is to combine *both* families of materials in the shield construction.

Capture is the final step in stopping neutrons and the final goal of the shield. Capture occurs when a slow neutron has lost so much energy through scattering that it may end up *inside* a nucleus. This nucleus might still be stable after capturing a neutron, but more often turns unstable and decays, producing a new nucleus and emitting secondary radiation This radiation may last several minutes or hours after the reactor has been shut down, i.e., after the initial fission neutrons have stopped for good. If a fast neutron has been scattered inelastically, chances are the next few elastic collisions will result in its capture.

Stopping neutrons (capture) comes at a price. Their loss of kinetic energy is emitted as gamma rays. For instance, Cd (cadmium) is a good neutron capturer, but the gamma photon emitted after capture has an energy of order 7.5 MeV! Then, choosing a neutron "absorber" material needs careful calculations. Note that capture modifies the nature and structure of the nucleus. Through secondary radiation, new elements may form *inside* the shield. In general, all types of radiation interacting with matter, whether shield, propellant, or the fuel itself, may form new elements which can greatly change structural, thermal, and state properties, as mentioned in Chap. 7.

By and large, such changes are undesirable. For instance, radiation tends to gasify liquid hydrogen. In fuels, this phenomenon reduces the ability of fuel to fission. In the case of ^{235}U, about 1% of new elements formed inside a low-enriched fuel matrix may stop fission altogether, a phenomenon being called "fuel poisoning." In commercial nuclear reactors, where enrichment is moderate, the fuel bars are poisoned roughly after 12–18 months of operation and need to be replaced.

In an engineering sense, as far as the stopping ability of materials, gammas and neutrons behave similarly. In fact, it is common to replace the $I(x)$ equations by a compound expression accounting for both absorption and scattering:

$$I(x) = B(x) \cdot I(0) \exp\left[-\frac{x}{\lambda}\right] \qquad \text{(A.16)}$$

where λ is the relaxation length, replacing $1/\mu$, and $B(x)$ is the so-called buildup factor (Glasstone 1955, p. 595). This expression tells that gamma and neutron fluxes crossing a distance λ are reduced by a factor e. After much simplifying, at "short" distances ($x/\lambda < 1$), B is of order 1. When the distance (or shield thickness) is much larger than λ, the factor B is of order $x = \lambda$ for gammas and somewhat smaller for fast neutrons. Table A.12 shows the relaxation length of some common materials, the starting step toward shield design.

Table A.12 Relaxation length of 5 MeV neutron and gamma ray for some materials

Material	Density (g/cm^3)	Relaxation length	
		Fast neutrons (cm)	Gamma rays (cm)
Water	1.00	~10	30
Graphite	1.62	~9	19
Beryllium	1.85	~9	18
Beryllium oxide	2.30	~9	14
Aluminum	2.70	~10	13
Iron	7.80	~6	3.7
Lead	11.30	~9	2.5

In extreme synthesis, shielding is mostly dependent on mass, not on the type of material or its thickness. However, the different requirements to stop different types of radiation may temper this conclusion, and it was mentioned that a "sandwich" of different materials is the current solution. A standard shielding used in the SP-100 space power reactor (Sovie 1987) is still considered valid today. It includes 15 cm of hydrogen-rich LiH_2, followed by 2–4 cm of tungsten, and again 58–64 cm of LiH_2. This is an example of so-called graded- Z shielding, where materials of decreasing atomic number Z are interposed between the radiation source and astronauts or equipment. For instance, starting from the reactor solid core, a high- Z tantalum or tungsten layer scatters electrons and protons and stops gammas. These nuclei emit hard X-rays, which in turn are absorbed by the next layer and emit softer X-rays, and so on, until a simple aluminum or a polymer layer stops whatever low-energy radiation is left. Nonlinear absorption by graded- Z layers may reduce the total shielding weight by up to 60%. Shielding requirements for a high-energy density PBR (particle bed reactor) are in (Gruneisen 1991).

Shielding is the price of fission-based propulsion. It drives the overall thrust/mass ratio of NTR (nuclear thermal rocket) and contributes substantially to that of NEP (nuclear electric propulsion) while the other mass contribution is that of the space radiator. However, this conclusion, dating back to the work done during the Manhattan Project (Gosling 2010), does not rule out that certain fuels or material structures may reduce the weight of shields as we conceive them now. For instance, unconventional fuels with very low critical mass, of the order of grams, may fission in a reactor of size much smaller than conventional reactors, e.g., by a factor $q > 1$. Even though the overall shield *thickness* may remain unaltered, the total shield *mass* would decrease roughly by the factor $(q)^3$. This fact does not change the fuel inventory that a reactor must host to complete the mission, and if the reactor cannot be refueled en route, the fuel mass volume still determines the mass of the shield.

NASA work by (Barghouty and Thibeault 2006)on a polyethylene-based plastic called RFX-1 has raised expectations that also materials with lighter atom structures may be effective shields (Barry 2005).

A.6.3 Residual Radioactivity

After a fission reactor has been switched off, it keeps emitting secondary radiation from decaying nuclei, see Table A.12. The intensity decreases with time t (of order days) and is a function of the length of time t_0 the reactor has been in operation. A semiempirical relationship valid for ^{235}U fuel predicts the residual power emitted (Glasstone 1955, p. 119) to be approximated by

$$P_{\gamma+\beta} = 5.9 \cdot 10^{-3} \cdot P((t - t_0)^{-0.2} - t) \text{ (W)} \qquad \text{(A.17)}$$

where $P_{\gamma+\beta}$ is the residual power of the combined gamma and beta particles, and P is that of the fission reactor. Equation (A.17) shows that the decay is not exponential, but that it follows a weak power law. For instance, after 30 days of operation (a time representative of interplanetary missions), it takes about 30 days for "cooling off" to have the residual radiation down to 0.01% of the reactor power. A 1-MW reactor would still release 100 W radiation after one month from shutdown.

The *activity*, measured in curie, is proportional to power. Thus, the *activity* follows the same power law

$$P_{\gamma+\beta} = 1.4 \cdot P((t - t_0)^{-0.2} - t) \text{ (W)} \qquad \text{(A.18)}$$

A.7 Interplanetary Radiation

Interplanetary radiation is a catch-all name including photon energy as well as kinetic energy of particles. Although some interplanetary radiation is originating from both photon and particle energy, this radiation is therefore very different in composition and energy levels when compared to radiation emitted from fission or fusion reactors (an example are neutrons, which are absent from cosmic radiation). When

considering life on Earth, our galaxy and the Sun are the major sources. However, radiation is also created near the planets possessing an electromagnetic field, such as the giant planets and of course around Earth. Consequently, crossing the Van Allen belt into the solar wind is dangerous (Garrett et al. 2010). Galactic and extra-galactic sources are responsible for the so-called galactic cosmic radiation (GCR). The Sun emits the solar wind (mostly high-energy protons) and, occasionally, intense and still unpredictable solar flares. This is solar radiation (SR).

Cosmic (and galactic) rays are mainly protons and heavier nuclei with extremely high energies. Their velocity may reach >0.999 *c*. Gamma ray bursts also occur. Their energy spectrum follows a power law shown in Fig. A.8 and cannot be simulated by any particle accelerator. The highest energies have very small fluxes believed to be associated with radiation from faraway galaxies. The mechanism creating galactic rays and gamma bursts is still a subject of investigation (Cronin et al. 1997; Plaga 2008).

Of much concern to space travel is the fact that, because of their energy, both cosmic rays and solar protons are harmful to life and equipment. However, reaching up to roughly 2000 km from our planet surface, the Van Allen belts are an effective electromagnetic shield. Above and away from Earth, radiation poses risks to humans not only during travel, but also while on planetary surfaces and inside habitats if not properly protected. In-space radiation protection is further complicated by solar flares raising the flux of solar protons by orders of magnitude, depending on how close the spacecraft is to the Sun. A telling comparison between the energy spectra during a solar event and the (steady) galactic radiation (at 1 AU) is in (Hayatsu et al. 2008). For instance, the dose equivalent from the solar event of January 20, 2005 (Miyasaka et al. 2005) was 220 mSv, to be compared with the 2.4 mSv of the average natural background dose accumulated *over 1 year* on Earth.

The galactic radiation contribution is smaller by a factor of 10^2–10^8, depending on the energy spectrum, but may be still tens times larger than the natural background dose. The experience gained by Soviet cosmonauts on Mir indicates that radiation and microgravity have other, subtler effects besides the loss of bone and muscle mass, in particular referring to cell damage and enzymatic changes.

Thus, an open question in interplanetary space travel is how to shield a spacecraft from solar and galactic radiation. So far, this section has provided information on shielding a *nuclear reactor*, an easier task. While the same physics applies, the difference is the magnitude of the energy involved. Work is in progress in this area; see, for example, (Atwell et al. 2006; Tripathi et al. 2008; Destefanis 2008). The radiation problems faced by the crew during a Mars expedition have been examined in great detail in Russia (Tocheny 2000), by NASA (Davison 2015) and others. However, a "magic bullet" capable of solving the radiation problem still has not been found. In fact, although the fluxes at the high-energy end of the spectrum are very low, there are galactic protons at energy levels reaching 10^{20} eV, see Fig. A.9. Nothing comparable has ever been produced by any particle accelerators. Note that the Large Hadron Collider (LHC) at CERN accelerates particles to a few TeV; the energy of neutrons or gammas in nuclear reactors is limited to perhaps 10 MeV.

These facts are known to physicists, but they have not been sufficiently appreciated by aerospace engineers until

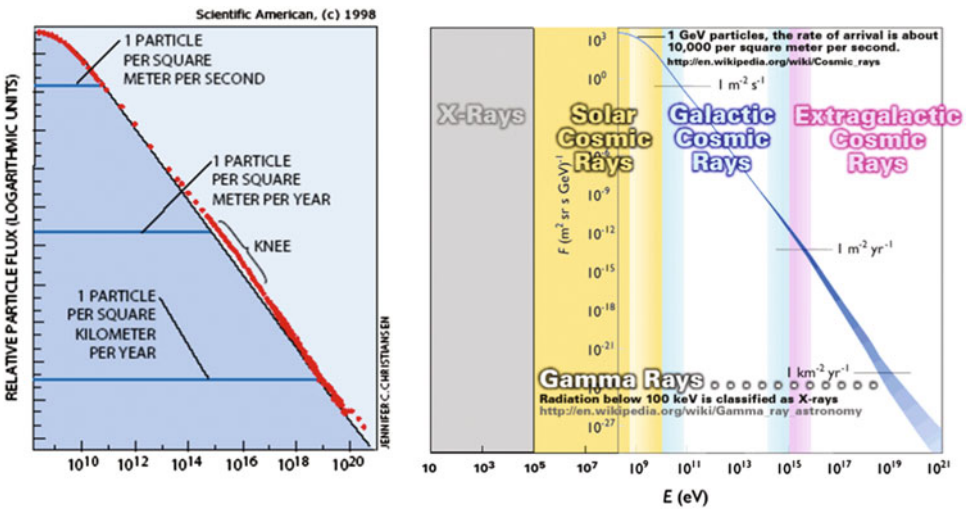

Fig. A.8 Energy spectrum of cosmic rays at the top of Earth's atmosphere [Courtesy of Scientific American (*left*), and Malaga Bay (*right*)]

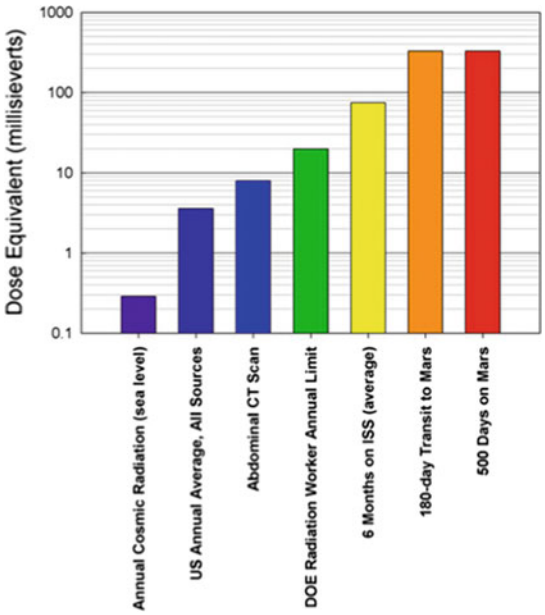

Fig. A.9 Space radiation doses compared to terrestrial sources [*Courtesy* NASA/JPL-Caltech]

recently (witness the scarce attention to this issue in papers proposing interplanetary missions). Radiation and shielding began to emerge as major challenges to human missions only recently (Werner 2015). In fact, space radiation may very well be *the* showstopper of future crewed expeditions traveling on (slow) Hohmann transfer orbits. Parker argues that based on *what we know*, no practical shielding, either passive or active, can safely protect humans during a Mars trip (Parker 2006). Similar pessimistic views are also expressed by (Choi 2008; Rapp 2006) and others.

Most space agencies limit the radiation dose over an entire astronaut career. NASA limits the dose to 0.8–1.2 Sv for non-smoker 30- to 60-year-old males. For females, the same limits are 0.6–1.0 Sv. These doses are believed to keep the excess probability of getting a form of cancer below 5%. Even before the beginning of the space age, because of the atomic bomb effects, these statistics were and are known to biophysicists and physicians (Heckstall-Smith 1958; Wilson et al. 2001; Cucinotta et al. 2001, 2011; Anon 2008; Kim et al. 2009; Schwadron et al. 2013). Space planners started paying attention to this issue after the Augustine Commission in 2009 explicitly identified GCR (galactic cosmic radiation) as one of the high priority challenges facing any deep space program (Anon 2009b).

This unsatisfactory situation has been significantly altered after the in-space measurements taken by the Radiation Assessment Detector (RAD) on the Curiosity rover flown to Mars on a "fast" Hohmann orbit by the Mars Science Laboratory (MSL) probe (Hassler et al. 2014). It is of interest to note that the RAD was primarily designed to measure radiation on Mars, not in space. However, the RAD took measurements during the Earth-Mars transit. It is of interest to note that the measurements were taken inside the probe, i.e., in an environment similar to that astronauts would inhabit during a human Mars mission. The MSL, launched on August 06, 2012, spent 253 days in space and recorded a dose of 1.8 mSv/day. This should be compared to an average background dose on Earth from all sources of 2 to 3 mSv *per year* and 3–6 mSv if medical diagnostic procedures are included. Consequently, the dose to an astronaut after a single Mars round-trip lasting the same time would be 0.66 ± 12 Sv, near that allowed in his/her lifetime (Zeitlin et al. 2013). The Curiosity RAD went on measuring radiation on Mars. This radiation contribution over about 300 days of observation was estimated from 0.26–0.30 Sv/year depending on altitude, i.e., on the local thickness of Mars' atmosphere (Hassler et al. 2014). A comparison of doses on a log scale is shown in Fig. A.9.

Probably because of these measurements, NASA included in the Orion crew capsule a temporary shelter in case of unexpected solar events. The shelter has aluminum enclosures for all astronauts and is located in the aft bay, close to the thick heat shield used during the reentry phase. Astronauts are supposed to interpose as much matter as they have available between them and the outside. Although this seems to be not a long-term solution, it shows that this issue is finally beginning to be recognized. In fact, individual radiation vests (AstroRad, by the Israeli StemRad company) have been proposed (Boucher 2015). The vest protects the torso, where lung and bone marrow cells are especially susceptible to damage by SR and GCR (Williamson 2016).

In fact, radiation is a key issue in lunar or planetary colonization. The GCR and SR energy spectra are so high as to demand impractically massive shielding, at least as we conceive it now. Even if shielding can stop primary GCR and SR, their interaction with the shield matter may produce secondary radiation penetrating a spacecraft. Applying electrostatic or electromagnetic fields to the spacecraft can stop part of the energetic particles, but, aside from the impact on shield weight, the question becomes of how to protect astronauts from the very fields used (Parker 2006; Durante 2014). This said, it is worth citing a suggestion from Professor George Hitt, of Khalifa University, United Arab Emirates, the winner of the NASA competition, to solve the problem posed by radiation dose to crew in Mars missions (Bardsley 2015). Professor Hitt suggests building a single massively shielded space "bus" able to shuttle back and forth on an orbit osculating those of Earth and Mars. The exposure time of astronauts would be only that between the two planetary surfaces and the respective low orbits. Although original, this proposal would not solve the secondary

radiation problem while further limiting the choice and duration of Earth–Mars transits.

In addition to undesirable health effects caused by radiation, many other effects have been experienced by astronauts such as lack of sleep, eye problems such as fatigue, scotoma, edema of the optic nerve, and "cotton wool" spots. Astronaut Scott Kelley has specifically complained of reduced vision due to increased intraocular pressure (Hardwood 2015). Cognitive impairment in laboratory testing of animals is also emerging and is especially worrisome, as reported by researchers at Johns Hopkins University (Anon 2014; Davies et al. 2014) and NASA (Parihar et al. 2015, 2016; Mironova 2015), showing charged particles reduce the brain dendritic complexity in mice, suggesting diminished attention and memory in future interplanetary astronauts. It is a fact that practical space travel demands interdisciplinary collaboration among aerospace engineers, biologists, and physicists, something still far from being common, as explicitly mentioned in the report from the NASA Office of the Inspector General report (Martin 2015) that invited NASA mission planners to pay attention to the impact of health and risk to future manned interplanetary missions.

At this stage of our present industry capability and technology understanding, shielding from GCR and SR appears still unfeasible rather than just problematic, because of astrophysics and of engineering challenges. Thus, if solar cosmic particle energy and fluxes are outside our control and shielding is a problem, the obvious way to reduce dose is to reduce time of exposure. In considering interplanetary manned missions, all information therefore argues strongly for shortening trip duration as much as possible. That requires much larger energies than have been used so far, in order to obtain higher transit velocities. Consequently, one primary conclusion is that some form of nuclear propulsion is required to increase transit velocity much above what is available from chemical propulsion to reduce radiation exposure duration (Penn 2010; Durante 2014).

Bibliography

Anon. (1959) "Effect of Radiation on Human Heredity", Second Impression, Report of a Study Group, World Health Organization, Geneva, Switzerland, 1959.

Anon. (1990), "The 2007 Recommendations of the International Commission on Radiological Protection".*Annals of the ICRP,* ICRP publication 103, Elsevier Publication, March 2007.

Anon. (1993) "Stopping Powers and Ranges of Protons and Alpha Particles with Data Disk" ICRU Report 49, International Commission on Radiation Unit and Measurements, Bethesda, Maryland, 1993.

Anon. (1996) "Significant Incidents in Nuclear Fuel Cycle Facilities", IAEA-TECDOC-867, International Atomic Energy Agency, Vienna, Austria, 1996.

Anon. (2006) "Environmental Consequences of the Chernobyl Accident and Their Remediation: Twenty Years Of Experience", Report of the Chernobyl Forum Expert Group 'Environment', Radiological Assessment Reports Series, International Atomic Energy Agency, Vienna, Austria, 2006.

Anon. (2007) "The Kyshtum Accident, 29th September 1957", NRPA Bulletin, ISSN 0806-895x, 28 September 2007.

Anon. (2008) "Managing Space Radiation Risk in the New Era of Space Exploration", The National Academies Press, Washington, DC, 2008.

Anon. (2009a) "Nuclear Fuel Behaviour in Loss-of-coolant Accident (LOCA) Conditions – State-of-the-Art Report", NEA No. 6846, Nuclear Energy Agency, Organisation for Economic Co-Operation and Development (OECD), 2009.

Anon. (2009b) "Seeking A Human Spaceflight Program Worthy of a Great Nation", Review of U.S. Human Spaceflight Plans Committee, Augustine Commission, White House Office of Science and Technology Policy (OSTP) and NASA Administrator, October 2009.

Anon. (2010) "Sources and Effects of Ionizing Radiation" Volume I, United Nations Scientific Committee on the Effects of Atomic Radiation, Report to the General Assembly with Scientific Annexes, UNSCEAR 2008, E.10.XI.3, United Nations, New York, 2010.

Anon. (2014) "Some Astronauts at Risk for Cognitive Impairment, Animal Studies Suggest", New Releases,*John Hopkins Medicine*, 23 April 2014.

Anon. (2015) "The Fukushima Daiichi Accident", GC(59)/14, Report by the Director General, International Atomic Energy Agency, IAEA Austria, August 2015.

Anon. (2016a) "1913: The U.S. Curie Standard", National Institute of Standards and Technology (NIST), U.S. Department of Commerce, 26 September 2016.

Anon. (2016b) "A Brief Description", Radiation Effects Research Foundation, A Japan-US Cooperative Research Organization, RERF Publisher, First Revision April 2016.

Anspaugh, L. et al. (2012) "Preliminary Dose Estimation from the Nuclear Accident after the 2011 Great East Japan Earthquake and Tsunami", World Health Organization, Geneva, Switzerland, 2012.

Atwell, W., Nealy, J. and Clowdsley, M. (2006) "Space Radiation Exposure Mitigation: Study of Selected Materials", SAE 2006-01-2103,*Transactions Journal of Aerospace*, Vol. 115-1, July 2006, pp. 226–236.

Augelli, M., Bignami, G., Bruno, C., Calligarich, E., De Maria, G., Mulas, M., Musso, C., Pellizzoni, A., Piperno, W., Piva, R., et al. (1999) "Report of the Working Group on a Preliminary Assessment of a New Fission Fragments Heated Propulsion Concept and its Applicability to Manned Missions to the Planet Mars (Project 242)", ASI Internal Report, Roma, 15 March 1999.

Augelli, M., Bignami, G. and Genta, G. (2013) "Project 242: Fission Fragments Direct Heating for Space Propulsion - Programme Synthesis and Applications to Space Exploration", Acta Astronautica, Volume 82, Issue 2, February 2013, pp. 153–158.

Bardsley, D. (2015) "Abu Dhabi Professor Wins NASA Award for Mars Shield Idea",*The National*, Abu Dhabi Media, 22 April 2015.

Barry, P.L. (2005) "Plastic Spaceships",*NASA Science News*, 25 August 2005.

Bechhoefer, B.G. (1973) "The Nuclear Test Ban Treaty in Retrospect", Vol. 5, Issue 2,*Case Western Reserve Journal of International Law*, School of Law, Case Western Reserve University, 1973.

Bergkvist, N.O. (2000) "Nuclear Explosions 1945-1998", FOA-R–00-01572-180-SE, Defence Research Establishment, Division of Systems and Underwater Technology, Stockholm, Sweden, July 2000.

Boucher, M. (2015) "StemRad and Lockheed Martin Working on AstroRad to Protect Astronauts",*SpaceRef.com*, 16 October 2015.

Chen, W.L. et al. (2004) "Is Chronic Radiation an Effective Prophylaxis Against Cancer?",*Journal of American Physicians and Surgeons,* Vol. 9, No. 1, pp. 6–10.

Chichester, H.J.M. (2012) "Introduction to Nuclear Reactors, Fuels, and Materials", Idaho National Laboratory (INL) presentation INL/MIS-12-24951, Nanotechnology in Nuclear Fuels and Materials R&D, Rice University, 27 February 2012.

Choi, C.Q. (2008) "Space Radiation Too Deadly for Mars Mission", *Space.com*, 31 March 2008.

Cronin, J.W., Gaisser, T.K. and Swordy, S.P. (1997) "Cosmic Rays at the Energy Frontier",*Scientific American*, Vol. 276, No. 7, January 1997, pp. 32–37.

Cucinotta, F.A., Schimmerling, W., Wilson, J.W., Peterson, L.E., Badwahr, G.D., Saganti, P.B. and Dicello, J.F. (2001) "Space Radiation Cancer Risk Projections for Exploration Missions: Uncertainty Reduction and Mitigation", NASA Johnson Space Center Report JSC-29295, January 2001.

Cucinotta, F.A., Kim, M.H.Y and Chappell, L.J. (2011) "Space Radiation Cancer Risk Projections and Uncertainties", NASA/TP-2011-216155, NASA, July 2011.

Davies, C.M., DeCicco-Skinner, K.L., Roma, P.G. and Hienz, R.D. (2014) "Individual Differences in Attentional Deficits and Dopaminergic Protein Levels following Exposure to Proton Radiation", *Radiation Research,* Vol. 181, No. 3, March 2014, pp. 258–271.

Davison, S. (2015) "Mars Mission and Space Radiation Risks Overview", Briefing to NAC HEOMD/SMD Joint Committee, NASA Headquarters, 07 April 2015.

Del Rossi, A. and Bruno, C. (2008) "The Chernobyl Accident: A Detailed Account", in:*Nuclear Space Power and Propulsion Systems*, edited by C. Bruno, Vol. 225, AIAA Progress in Astronautics and Aeronautics, AIAA, Reston, VA, 15 October 2008, App. B.

Destefanis, R., Briccarello, M. et al. (2008) "Radiation Shielding for Space Exploration: the MoMa - COUNT Programme", SAE Paper 2008-01-2161, presented at the*38th International Conference on Environmental Systems (ICES)*, San Francisco, CA, 29 June–02 July 2008.

Dewar, J.A. (2002) "The Story of the Nuclear Rocket: Lessons for the Future", IAC paper IAC-02-IAA.2.4.06, presented at the*53rd International Astronautical Congress - The World Space Congress*, Houston, Texas, 10–19 October 2002.

Dewar, J.A. (2004)*To the End of the Solar System: The Story of the Nuclear Rocket*, The University Press of Kentucky, Lexington, KY, 2004.

Durante, M. (2014) "Space Radiation Protection: Destination Mars", *Life Science in Space Research*, Vol. 1, April 2014, pp. 2–9.

Fultyn, R.V. (1968) "Environmental Effects of the Kiwi-TNT Effluent: A Review and Evaluation", LA-3449, UC-41, Health and Safety, Los Alamos Scientific Laboratory of the University of California, Los Alamos, New Mexico, April 1968.

Galli, G. and Mancini, C. (1996) "Esposizione alla Radioattività Ambientale",*Ingegneria Nucleare e Tecnologie Energetiche,* Vol. 38, No. 1–4, January–August 1996.

Gando, A. et al. (2011) "Partial Radiogenic Heat Model for Earth Revealed by Geoneutrino Measurements",*Nature Geoscience*, Vol. 4, 17 July 2011, pp. 647–651.

Garrett, H.B., Kokorowski, M. and Evans, R.W. (2010) "Comparison of Planetary Space Radiation Environments and Effects",*J. British Interplanetary Society*, Vol. 63, No. 9/10, 2010, pp. 363-369.

Glasstone, S. (1955)*Principles of Nuclear Reactor Engineering*, Van Nostrand, New York, 1955, Chapter X.

Gosling, F.G. (2010) "The Manhattan Project – Making the Atomic Bomb", DOE/MA-0002 Revised, National Security History Series, US Department of Energy, January 2010.

Gruneisen, S.J. (1991) "Shielding Requirements for Particle Bed Propulsion Systems", Phillips Laboratory Report PL-TR-91-3018, Edwards Air Force Base, CA 93523-5000, 1991.

Hardwood, W. (2015) "NASA Astronaut Scott Kelly on Life Aboard the Space Station",*CBS News*, 23 June 2015.

Hassler, D.M., Zeitlin, C., Wimmer-Schweinbruber, R.F., Ehresmann, B., Rafkin, S., Eigenbrode, J.L., Brinza, D.E., Weigle, G., Boettcher, S., Boehm, E., Burmeister, S., Guo, J., Koehler, J., Martin, C., Reitz, G., Cucinotta, F.A., Kim, M.-H., Grinspoon, D., Bullock, M.A., Posner, A., Gomez-Elvira, J., Vasavada, A., Grotzinger, J.P., and MSL Science Team (2014) "Mars' Surface Radiation Environment Measured with the Mars Science Laboratory's Curiosity Rover", *Science*, Vol. 343, No. 6169, 24 January 2014.

Hayatsu, K., Kobayashi, S., Hareyama, M., Yamashita, N., Sakurai, K. and Hasebe, N. (2008) "Radiation Dose Estimated in the Lunar Environment", Paper ISTS 2008-p-08, presented at the*26th International Symposium on Space Technology and Science (ISTS),* Hamamatsu, Japan, 01–08 June 2008.

Heckstall-Smith, H.W. (1958)*Atomic Radiation Dangers – And What They Mean to You,* J.M. Dent & Sons, London, 1958.

Howe, S.D., Travis, B. and Zerkle, D.K. (2003) "SAFE Testing Nuclear Rockets Economically", LA-UR-02-7382,*Space Technology and Applications International Forum*, STAIF, 2003.

Hvistendahl, M. (2007) "Coal Ash is More Radioactive than Nuclear Waste",*ScientificAmerican.com*, 13 December 2007.

Kemeny, J.G. et al. (1979) "President's Commission on The Accident at Three Mile Island – The Need for Change: The Legacy of TMI", Report of the President's Commission, Washington, D.C., October 1979.

Kim, M.H.Y., De Angelis, G. and Cucinotta, F.A. (2009) "Probabilistic Assessment of Radiation Risk for Astronauts in Space Missions", IAF Paper IAC-09-A1.4.09, presented at the*60th International Astronautical Congress (IAC)*, Daejeon, South Korea, 12–16 October 2009.

Lenard, R.X. (2008) "Nuclear Safety, Legal Aspects and Policy Recommendations", in:*Nuclear Space Power and Propulsion Systems*, edited by C. Bruno, AIAA Progress in Astronautics and Aeronautics, Vol. 225, AIAA, Reston, VA, 2008, Ch. 6.

Maise, G., Powell, J.R., Paniagua, J., Ludewig, H. and Todosow, M. (2000) "Compact Ultra Lightweight Nuclear Thermal Propulsion Systems for Interplanetary Space Missions", IAC paper presented at the*51st International Astronautical Congress (IAC),* Houston, TX, 02-06 October 2000.

Martin, P.K. (2015) "NASA's Efforts to Manage Health and Human Performance Risks for Space Exploration", Office of Inspector General, Office of Audits, Report No. IG-16-003, NASA, 29 October 2015.

McBride, J.P., Moore, R.E., Witherspoon, J.P. and Blanco, R.E. (1978) "Radiological Impact of Airborne Effluents of Coal and Nuclear Plants",*Science,* Vol. 202, No. 4372, 08 December 2008, pp. 1045–1050.

McDonald, S. (1994) "Taiwan Hunts for Radioactive Apartments",*Los Angeles Times*, Reuters, 12 June 1994.

McDonald, A.J. and Hansen, J.R. (2009)*Truth, Lies, and O-Rings – Inside the Space Shuttle Challenger Disaster*, University Press of Florida, 2009.

Mikhailov, V.N. (editor) (1996) "USSR Nuclear Weapons Tests and Peaceful Nuclear Explosions: 1949 through 1990", The Ministry of the Russian Federation for Atomic Energy, and Ministry of Defense of the Russian Federation, 1996.

Mironova, N. (2015) "Addressing Risk of Brain Damage in Spaceflight",*Aerospace America,* Vol. 53, No. 7, July–August 2015, p. 7.

Miyasaka, H., Takahashi, E. et al. (2005) "The Solar Event on 20 January 2005 Observed With the Tibet YBJ Neutron Monitor Observatory",*29th International Cosmic Ray Conference*, Pune, India, 03–10 August 2005.

Mousseau, T.A., Nelson, N. and Shestopalov, V. (2005) "Don't Underestimate the Death Rate from Chernobyl", Correspondence, *Nature*, Vol. 437, 20 October 2005, p. 1089.

Mukhin, K.N. (1987)*Experimental Nuclear Physics - Physics of Atomic Nucleus*, Vol. I, MIR Publishers, Moscow, 1987.

Parihar, V.K., Barrett, A., Tran, K.K., Macaraeg, T.G., Chu, E.M., Kwok, S.F., Chmielewski, N.N., Craver, B.M., Baulch, J.E., Acharya, M.M., Cucinotta, F.A. and Limoli, C.L. (2015) "What Happens to Your Brain on the Way to Mars",*Science Advances*, Vol. 1, No. 4, 01 May 2015.

Parihar, V.K., Allen, B.D., Caressi, C., Kwok, S., Chu, E., Tran, K.K., Chmielewski, N.N., Giedzinski, E., Acharuya, M.M., Vritten, R.A, Baulch, J.F. and Limoli, C.L. (2016) "Cosmic Radiation Exposure and Persistent Cognitive Dysfunction",*Scientific Reports*, Vol. 6, No. 34774, October 2016.

Parker, E.N. (2006) "Shielding Space Travelers",*Scientific American*, Vol. 294, No. 9, March 2006, pp. 22–29.

Penn, J. (2010) "NASA's Plan Is Not Sustainable",*Aviation Week & Space Technology*, Vol. 172, No. 44, 06 December 2010, p. 74.

Plaga, R. (2008) "Rays from the Dark",*Nature,* Vol. 453, No. 7191, 01 May 2008, pp. 48–49.

Powell, J., Paniagua, J., Ludewig, H., Maise, G. and Todosow, M. (1998) "MITEE: An Ultra Lightweight Nuclear Engine for New and Unique Planetary Science and Exploration Missions", Paper IAF-98-R.1.01, presented at the*49th International Astronautical Congress (IAC)*, Melbourne, Australia, 28 September–02 October 1998.

Powell, J., Maise, G., Paniagua, J., Ludewig, H. and Todosow, M. (1999) "The MITEE Family of Compact, Ultra Lightweight Nuclear Thermal Propulsion Engines for Planetary Exploration Missions", Paper IAF-99-S.6.03 presented at the*50th International Astronautical Congress (IAC)*, Amsterdam, Netherlands, 04–08 October 1999.

Prekeges, J.L. (2003) "Radiation Hormesis, or, Could All That Radiation Be Good for Us?",*Journal Of Nuclear Medicine Technology*, Special Contributions, Vol. 31, No 1, March 2003, pp. 11–17.

Rapp, D. (2006) "Radiation Effects and Shielding Requirements in Human Missions to the Moon and Mars",*Mars Journal*,*The International Journal of Mars Science and Exploration*, Vol. 2, 29 September 2006, pp. 46–71.

Renner, R. (2003) "Nietzsche's Toxicology",*Scientific American*, Vol. 289, No. 3, 18 September 2003, pp. 28–30.

Rubbia, C. (2000) "Fission Fragments Heating for Space Propulsion", CERN SL-Note 2000-036 EET, European Organization for Nuclear Research (CERN), Geneva, 2000.

Schwadron, N.A., Smith, S. and Spence, H.E. (2013) "The CRaTER Special Issue of*Space Weather*: Building the Observational Foundation to Deduce Biological Effects of Space Radiation",*Space Weather,* No. 11, 26 February 2013, pp. 47–48.

Sovie, R.J. (1987) "SP-100 Advanced Technology Program", AIAA Paper AIAA-87-9232,*22nd Intersociety Energy Conversion Engineering Conference*, Philadelphia, Pennsylvania, 10-14 August 1987, also published as NASA TM-89888.

Stephan, V. (2005) "Chernobyl: Poverty and Stress Pose 'Bigger Threat' than Radiation",*Nature*, Vol. 437, Issue 181, 08 September 2005.

Tocheny, L. (2000) "Radiation Safety of Mars Expedition",*Mars Mission*, Vol. 12, Section 4, ISTC Project 1172, International Science and Technology Center, Moscow, 2000.

Tripathi, R.K. and Nealy, J.E. (2008) "Mars Radiation Risk Assessment and Shielding Design for Long-Term Exposure to Ionizing Space Radiation", IEEEAC Paper 1291,*IEEE Aerospace Conference*, MT, 01–08 March 2008.

Werner, J. (2011) "An Overview of Facilities and Capabilities to Support the Development of Nuclear Thermal Propulsion", Paper 3309, INL/CON-10-20537,*Proceedings of Nuclear and Emerging Technologies for Space 2011*, Albuquerque, NM, 7–10 February 2011.

Werner, D. (2015) "The Human Factor",*Aerospace America*, April 2015, pp. 26–36.

Williamson, M. (2016) "Anti-Radiation Vest Eyed for Orion Crew", *Aerospace America*, Vol. 54, No. 3, March 2016, p. 7.

Wilson, J.W., Cucinotta, F.A., Kim, M.H.Y. and Schimmerling, W. (2001) "Optimized Shielding for Space Radiation Protection", *Physica Medica*, Vol. XVII, Supplement 1, 2001, pp. 67–71.

Zeitlin,C., Hassler, D.M., Cucinotta, F.A., Wimmer-Schweingruber, R. F., Brinza, D.E., Kang, S., Weigle, G., Bloettcher, S., Boehm, S., Guo, J., Koehler, J., Martin, C., Posner, A., Rafkin, S. and Reitz, G. (2013) "Measurements of Energetic Particle Radiation in Transit to Mars on the Mars Science Laboratory",*Science,* Vol. 340, No. 6136, 31 May 2013, pp. 1080–1084.

Appendix B: Assessment of Open Magnetic Fusion for Space Propulsion

B.1 Introduction

Chapter 8 introduced fusion as the ultimate power source and discussed its propulsion application in a broad sense, including magnetic and inertial confinement fusion, their combination in hybrid systems, and impulsive modes of energy release to produce thrust. Because magnetic confinement fusion is probably the most advanced of all fusion strategies, this appendix focuses on reactors using magnetically confined fusion and proposals on how they could be made into space propulsion systems.

Exploring the solar system and beyond requires the development of adequate propulsion. Reasonable mass consumption implies, as seen in Chap. 7, very large power. Here, a rough but simple estimate can help in understanding the problem. In order to accelerate a mass M_w up to a velocity v_c in a time T requires an average thrust power P (kinetic energy of the mass accelerated divided by time) given by

$$P = \frac{\left(\frac{M_w \cdot v_c^2}{2}\right)}{T} \tag{B.1}$$

This condition defines a characteristic velocity v_c given by

$$v_c \equiv (2 \cdot \alpha \cdot T)^{\frac{1}{2}} \tag{B.2}$$

where

$$\alpha \equiv \frac{P}{M_{\text{powerplant}}} \tag{B.3}$$

the so-called specific power (thrust power per unit mass), defined here in relation to the mass of the propulsion system. Representing a constant factor, α can be redefined in terms of power per unit mass of the propulsion system, and this is the approach in (Stuhlinger 1964) already used in Chap. 7. Note that mass consumption, while power is "on," has been neglected, similarly to what has been done in Sect. 7.18. Then, this first-order analysis is restricted to the case of small mass consumption.

The trajectory distance or length L is approximated by

$$L = k_0 \cdot v_c \cdot T \tag{B.4}$$

with k_0 being a constant of order unity that depends on the details of the trajectory. Upon combining the previous conditions and taking, for instance, $k_0 = 1/3$, it follows that the specific power α is related to L and T by the condition

$$\alpha \approx 10^{-3} \cdot \frac{L^2}{T^3} \tag{B.5}$$

where, from now on, α is in kW/kg, L in astronomical units (1 AU $\approx 150 \cdot 10^6$ km) and T in years.

Thus, once the distance L is assigned, the request of a reasonable flight duration T sets a limit on the specific power α. As an example, a mission to Mars ($L \approx 1$•AU) over one month requires a specific power in the range $\alpha \approx 1.7$ kW/kg. A mission to the Oort Cloud ($L \approx 10^4$ AU) lasting 20 years requires a specific power $\alpha \approx 12$ kW/kg. Thus, specific power in the range from 1 to 10 kW/kg is a rough estimate of α needed to explore the solar system. Note also that a mission to Proxima Centauri ($L \approx 2.5 \cdot 10^5$ AU), lasting less than 10 years, would require (neglecting relativistic corrections) specific power in excess of $6.0 \cdot 10^4$ kW/kg, an extremely large value. However, for increasingly large L, the simplifying assumption of constant $M_{\text{powerplant}}$ is no longer valid.

In assessing propulsion system performance, a second figure of merit, besides specific power, is the payload fraction $M_{\text{pay}}/M_{\text{TOGW}}$. Following (Stuhlinger 1964), the payload fraction can be cast in terms of the characteristic velocity v_c defined in Eq. (B.2) from the Tsiolkovsky's equation. Upon defining

P.A. Czysz et al., *Future Spacecraft Propulsion Systems and Integration*,
Springer Praxis Books, DOI 10.1007/978-3-662-54,744-1

$$M_{\mathrm{TOGW}} = (M_{\mathrm{OEW}} - M_{\mathrm{powerplant}}) + M_{\mathrm{ppl}} + M_{\mathrm{powerplant}} + M_{\mathrm{pay}} \tag{B.6}$$

with M_{TOGW}, $M_{\mathrm{OEW}} - M_{\mathrm{powerplant}}$, M_{ppl}, $M_{\mathrm{powerplant}}$, and M_{pay} being the initial, airframe minus propulsion system, propellant, propulsion system, and payload mass, respectively, and expressing $M_{\mathrm{powerplant}}$ in terms of the specific power

$$M_{\mathrm{powerplant}} = \frac{P}{\alpha} \tag{B.7}$$

it is possible to show that

$$\frac{M_{\mathrm{ppl}}}{M_{\mathrm{TOGW}}} = \exp\left[\frac{-v_{\mathrm{f}}}{v_{\mathrm{ex}}}\right] - \left(\frac{v_{\mathrm{ex}}}{v_{\mathrm{c}}}\right)^2 \cdot \left(1 - \exp\left[\frac{-v_{\mathrm{f}}}{v_{\mathrm{ex}}}\right]\right) \tag{B.8}$$

with v_{f} the final velocity and v_{ex} the exhaust velocity of the propellant being ejected related to the specific impulse

$$I_{\mathrm{sp}} = \frac{v_{\mathrm{ex}}}{g}(\mathrm{s}) \tag{B.9}$$

Equation (B.8) shows that a positive payload fraction can be obtained only for

$$\frac{v_{\mathrm{f}}}{v_{\mathrm{c}}} = \frac{v_{\mathrm{f}}}{\sqrt{2 \cdot \alpha \cdot T}} \leq 0.8 \tag{B.10}$$

within a finite domain of $v_{\mathrm{ex}}/v_{\mathrm{c}}$ that increases as $v_{\mathrm{f}}/v_{\mathrm{c}}$ decreases. The optimal payload fraction is obtained for

$$v_{\mathrm{c}} \approx \sqrt{2} \cdot v_{\mathrm{ex}} \tag{B.11}$$

see Fig. B.1.

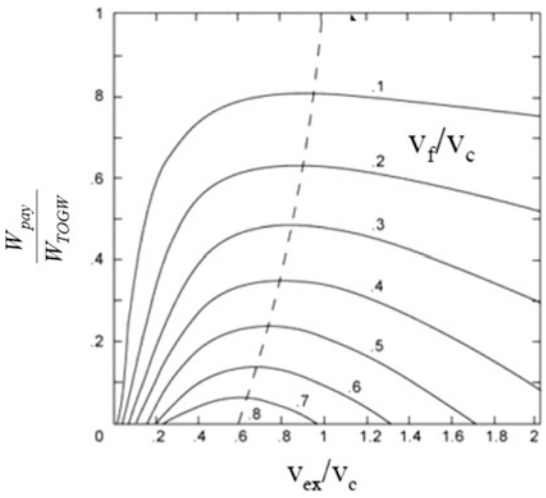

Fig. B.1 Payload fraction versus velocity ratio

Figure B.1 confirms that reasonable performance demands high specific impulse. For instance, taking the optimal payload condition as given by Eq. (B.11), in order to reach 1 AU in one month with a specific power of 3.5 kW/kg and payload fraction of ≈0.1 ($v_{\mathrm{f}}/v_{\mathrm{c}} \approx 0.7$), requires a specific impulse of the order 10^4 s, well beyond the capabilities of chemical propulsion systems.

Note that the above conditions determine also the thrust per unit mass, F/M, (i.e., average acceleration). Since

$$P \approx F \cdot v_{\mathrm{ex}} \tag{B.12}$$

it follows for the thrust per unit mass

$$\frac{F}{M} \approx 10 \cdot \frac{g \cdot \alpha}{I_{\mathrm{sp}}}\left(\frac{\mathrm{kW/kg}}{\mathrm{s}}\right) \tag{B.13}$$

For values of the specific power larger than 6 kW/kg and an $I_{\mathrm{sp}} = 10^5$ s, the acceleration F/M is larger than that in the Sun gravitational field (≈$6.0 \cdot 10^{-4}$ g at the Earth radius). That defines "high thrust" missions that are therefore possible in such a parameter range.

In order to reach high specific impulse, fusion propulsion was originally proposed. Indeed:

- Fusion reactions produce low-mass (atomic number A = 1 − 4), high-energy (up to 14 MeV) fusion products with specific impulse of the particles ejected in the range $I_{\mathrm{sp}} = 4.0 \cdot 10^6$ s.
- The reacting ("fusing") mixture is typically composed by H or He isotopes with average energy between 10 keV and 100 keV. If part of such mixture is used for propulsion, rather than the faster reaction products, specific impulse in the range $(0.5–2.0) \cdot 10^5$ s can still be obtained.
- Even the low-temperature plasma flowing in the region surrounding the reacting core (in a fusion reactor the so-called scrape-off region) can have temperatures in the range of 100 eV corresponding to a specific impulse ≈$5.0 \cdot 10^3$ s.

Chapter 8 discussed the two modes of using the fusion process for space propulsion:

- *Fusion electric propulsion*: Similarly to NEP in Chap. 7, fusion power is converted to electric power either through a conventional thermodynamic cycle (in this case, the power rejected must be radiated in space) or through direct conversion. The main disadvantages of this scheme are the presence of a radiator, of all the items needed for the electricity conversion (e.g., turbines or other machinery), the large mass of the electric propulsion system, and especially the overall conversion efficiency (thermal power into thrust power).

– *Direct (thermal) propulsion*: The un-reacted fuel and the fusion products are expanded in a magnetic nozzle, possibly mixed with cold (inert) propellant for thermo-structural reasons, and to achieve a unidirectional jet, with an optimal combination of specific impulse and thrust that will depend on the specific mission. Note that some electricity production is needed for control and auxiliary heating. In addition, the ejection of un-reacted propellant (e.g., fuel itself) requires lifting to space (to LEO) substantial mass, and must be taken into account in evaluating overall performance.

Since fusion has the capability of producing high I_{sp}, the possibility of its application for space propulsion depends on the feasibility of building systems with specific power in the range from 1 to 10 kW/kg (Schulze 1994). For the reasons mentioned in Sect. 8.10, the most natural continuous fusion rocket architecture must be of the mirror type, as sketched in Fig. 8.20. Nevertheless, other potentially interesting architectures are of interest and should be investigated.

The aim of this appendix is thus to assess the potential of open magnetic field configurations in a broad sense, i.e., configurations capable of ejecting propellant while fusing. An example of a Mars mission trajectory is presented at the end of this appendix, showing the potential of fusion propulsion with the aim of shortening transit time.

Historically, spatial applications of steady-state fusion reactors were investigated by NASA between 1958 and 1978 (Schulze and Roth 1990). The application was in-space electrical power generation as well as propulsion. These two applications are somewhat orthogonal, though the underlying plasma and fusion science are similar. The NASA-Lewis program focused on the simple mirror and on the electric field bumpy torus, both representing steady-state magnetic fusion energy approaches at the time. The program was canceled in 1978 for budgetary reasons, as NASA was preparing to embark on the Space Shuttle program. During the 1980s, attention focused on the possibility of electric power generation in space over periods of time >1 day and at the multimegawatt level. These studies, see (Roth 1989) for a review, predicted low specific power.

The studies carried out since the late 1980s have therefore tried to optimize fusion performance in order to maximize specific power. Several concepts have been considered: the

Table B.1 Fusion space propulsion system studies

Reference	Configuration	α (kW/kg)	P (MW)	W_{pay} (t)	W_{str}/W_{tank} (t/t), (−)	W_{fuel} (t)	$W_{radiator}$ (t)	$W_{generator}$ (t)	$W_{reactor}$ (t)	I_{sp} (s)
Borowski (1995)	Spheromak	10.5								
Borowski (1995)	Spherical torus	5.8								
Santarius (1988)	Tandem mirror	2	1000					25	420	
Bussard (1990)	Tokamak	3.7	3925	1900	220/570	6310	760	170	70	$5 - 7 \cdot 10^3$
Teller (1991)	Dipole	1.0	1250						1180	$10^4 - 3 \cdot 10^5$
Nakashima (1994)	FRC	1.0								$10^3 - 10^6$
Williams (1998)	Spherical torus	5.4	6145	108	/131	45 + 1292	236	145	624	$4 \cdot 10^4$
Thio (1999)	MTF	400	25,000				17		41	$7.7 \cdot 10^4$
Kammash (1995b)	Gasdynamic trap	7.5	55,000				7128		100	$1.1 \cdot 10^5$
Cheung (2004)	Colliding beam FRC	3	100		1.4		6	18 + 2.1	5.5	$1.4 \cdot 10^6$
Santarius (1998)	Generic DT	0.6	600				642		357	
Santarius (1998)	Generic D-^{3}He	5.3	600				48		63.6	
Santarius (1998)	Generic D-^{3}He	10.1	600				44		15.8	

In calculating specific power, payload and fuel are not included. Reactor includes auxiliary power, batteries, cooling system, and magnetic nozzle

high-field tokamak (Bussard 1990), the spherical torus (Borowski 1995; Williams 1998), mirror systems (Kulcinski et al. 1987; Santarius et al. 1989; Carpenter and Deveny 1992, 1993; Kammash et al. 1995), field reversed configuration (Chapman et al. 1989; Cheung et al. 2004), and magnetic dipole (Teller et al. 1992). These configurations will be reviewed in the context of confinement systems. They are summarized in Table B.1, which also shows the specific power, thrust power, and, when available, the mass of various components.

This appendix is organized as follows: Sect. B.2 discusses issues related to magnetic confinement fusion for space propulsion applications. In Sect. B.3, the present status of research on open magnetic field configurations is reviewed. Sect. B.4 lists issues where R&D activities should focus for specific application of fusion to space propulsion. Sect. B.5 examines the performance potential possible with fusion propulsion, specifically for a manned Mars mission. Conclusions are reported in Sect. B.6.

B.2 Space Fusion Power: General Issues

In this section, we first review the kinetics of the most important fusion reactions and the conditions for achieving energy amplification. In the last part, a simple model for a fusion rocket is considered and a parametric expression for the specific power α is derived and discussed.

B.2.1 Application of Fusion for Space Propulsion

The starting point is the choice of fuel fusion cycles (Miley 1987). The kinetics of candidate fuels is shown in Table B.2, see also (Cox et al. 1990).

The D–T reaction has the largest reactivity and lowest ignition temperature (≈20 keV). However, it has two main problems:

- 80% of the energy is produced as high-energy (14 MeV) neutrons. They require heavy shielding and result in intermediate production of heat, therefore requiring a radiator.
- In order to avoid (for security reasons) large tritium inventories, tritium must be produced in space through the conventional D-T fuel cycle.

The D–D reaction involves deuterium, a very common hydrogen isotope (there are 33 mg of deuterium in each liter of water). It produces 33% of energy in the form of 2.45 MeV neutrons. Neutrons are produced in the secondary reactions involving D and T. Although the neutron problem is somewhat alleviated, energies of the reactants in the 10^2 keV range must be achieved for ignition.

The D–^{3}He reaction needs reactant energies in the same range as the D–D reaction, but has the advantage of producing fewer neutrons ($\leq 15\%$) through D–D and secondary D–T reactions. Furthermore, the charged reaction products can be used for direct electricity conversion. Its main problem is lack of ^{3}He on Earth. ^{3}He could be extracted by mining lunar dust, where it is deposited by the solar wind; its inventory is estimated $\approx 10^6$ t (Kulcinski et al. 2000). Cost would be in the range from $400 to $1000/g. For a recent survey of the abundance of noble gases on the Moon, see (Ozima et al. 2005). In perspective, ^{3}He is considered the most promising fuel for space propulsion.

The p-^{6}Li and p-^{11}B reactions have even lower neutron production (≈5 and ≈1%, respectively) and are conventionally defined "aneutronic," although the only truly aneutronic reaction is the ^{3}He–^{3}He reaction. Their main problem is the very stringent requirements to achieve a positive fusion gain. Indeed, in a system with equal electron and ion temperature, the fusion power output never exceeds power lost via bremsstrahlung. Thus, even in the ideal case of no energy conduction losses, the system cannot achieve positive fusion gain Q, except when far from thermal equilibrium (i.e., for different electron and ion temperatures).

Finally, it should be mentioned that the possibility of fusion reactions catalyzed by matter-antimatter reaction has been considered for fusion propulsion systems based on inertial confinement, see Sect. 8.16.

B.2.2 Achieving Self-sustained Fusion

In order to achieve ignition, reactants must be heated at temperature ≈10–100 keV to overcome the Coulomb repulsion between positively charged nuclei. At these temperatures, electrons are no longer attached to atoms, and the state of matter is called "plasma." Since plasma is composed of free charged particles, it can be confined by magnetic fields.

Conditions to achieve significant fusion power have been discussed in (Lawson 1957) and are briefly reviewed in the following. The fusion gain Q

$$Q = \frac{P_{\text{fusion}}}{P_{\text{auxiliary}}} \tag{B.14}$$

is defined as the ratio between the fusion power output P_{fusion} and the auxiliary power $P_{\text{auxiliary}}$ needed to heat plasma. It depends on the amount of energy lost through

Table B.2 Fusion reactions

Reaction	Fusion fuel cycles (MeV)	Ignition temperature (°C)
1a	$D + D \xrightarrow{50\%} T(1.01) + p(3.02)$	$300 \cdot 10^6$
1b	$\xrightarrow{50\%} He^3(0.82) + n(2.45)$	
2	$D + T \rightarrow He^4(3.5) + n(14.1)$	$50 \cdot 10^6$
3	$D + He^3 \rightarrow He^4(3.6) + p(14.7)$	$500 \cdot 10^6$
4	$T + T \rightarrow He^4 + 2n + 11.3$	
5a	$He^3 + T \xrightarrow{51\%} He^4 + p + n + 12.1$	
5b	$\xrightarrow{43\%} He^4(4.8) + D(9.5)$	
5c	$\xrightarrow{6\%} He^3(2.4) + p(11.9)$	
6	$p + Li^6 \rightarrow He^4(1.7) + He^3(2.3)$	
7a	$p + Li^7 \xrightarrow{-20\%} 2He^4 + 17.3$	
7b	$\xrightarrow{-80\%} Be^3 + n - 1.6$	
8	$D + Li^6 \rightarrow 3He^2 + 22.4$	
9	$p + B^{11} \rightarrow 3He^2 + 8.7$	
10	$n + Li^6 \rightarrow T + He^4 + 4.8$	
11		

radiation (in the following, we will consider only bremsstrahlung) and thermal conduction. This is usually quantified in terms of so-called energy confinement time τ_E, defined, in steady-state conditions, as the ratio between the energy content of the plasma and the heating power. Self-sustained conditions ($Q = \infty$) are achieved when the fusion power released as kinetic energy of charged particles confined by the magnetic field balances the energy losses of the configuration and no auxiliary power is necessary, that is, $P_{auxiliary} = 0$. Driven-fusion operation (achieved in many fusion facilities) is instead associated with a finite value of the auxiliary power and therefore of the fusion gain Q.

Equilibrium between plasma heat release rate and energy losses determines the operating point of the reacting plasma. This can be written as follows:

$$\left(\frac{1}{2}\right) \cdot \sum_{ij} n_i \cdot n_j \cdot \langle \sigma \cdot v \rangle_{ij} \cdot E_{fus,ij} \cdot \left(f_{ij} + \frac{1}{Q}\right) = n_e^2 \cdot Z_{eff} \cdot k_B \cdot T_e^{1/2} + \left(\frac{3}{2}\right) \cdot \sum_i n_i \cdot \frac{T_i}{\tau} \qquad \text{(B.15)}$$

The electron density n_e is determined by the charge neutrality condition

$$n_e = \sum_j n_j \cdot Z_j \qquad \text{(B.16)}$$

In the above expressions, n_j and Z_j are the reacting ion species density and charge, respectively, $(\sigma \bullet v)_{ij}$ is the reactivity (to be evaluated with the actual distribution function of the ions), $E_{fus,\ ij}$ is the energy released in the reaction, f_{ij} is the fraction of the fusion energy transferred to the plasma, $Z_{eff} \equiv \Sigma_j\, n_j \bullet Z_j^2/n_e$ is the effective charge, T_j is the temperature of the j-th species, $k_B = 1.69 \cdot 10^{-24}$ MW(eV)$^{-1/2}$, and τ is the energy confinement time. The above conditions define the value of $n_e \bullet \tau$ as a function of temperature associated with a given fusion gain Q. In general, optimal values of the concentrations n_j/n_e can be found that minimize the $n_e \bullet \tau$ value. Note that the values of the fraction f_{ij} depend both on the fraction of fusion energy released in the form of charged particles and on the capability of the configuration to confine them in the region where fusion reaction occurs.

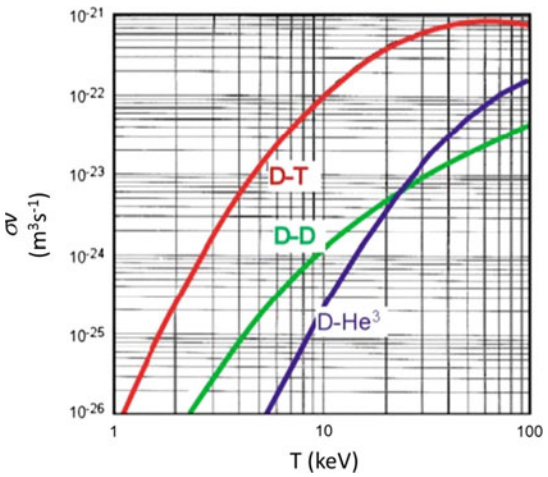

Fig. B.2 Fusion: Maxwellian reactivity

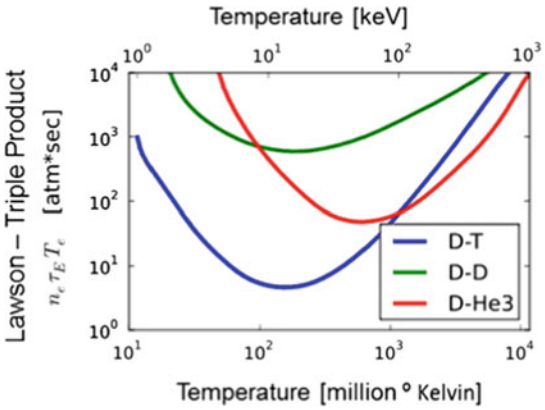

Fig. B.3 Lawson criterion for different fuel pairs

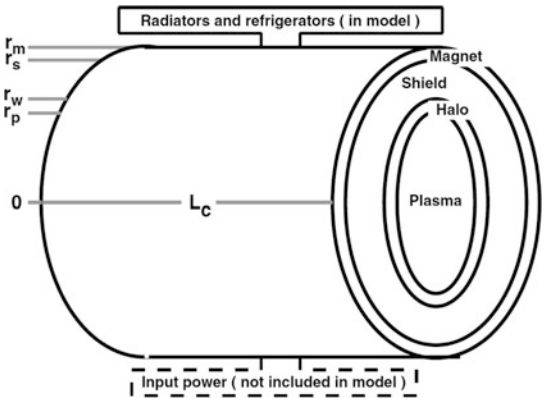

Fig. B.4 Generic fusion rocket geometry, from Santarius and Logan (1998)

Equations (B.15) and (B.16) determine the $n_e \bullet \tau$ product only for the case of thermal equilibrium among all species, when all electrons and ions relax to a Maxwellian distribution function with the same temperature T shown in Figs.B.2 and B.3. The $n_e \bullet \tau$ values as a function of temperature are shown in Fig. B.3 for different reactions. The curves show a vertical asymptote for $T = T_{ideal}$, the ideal ignition temperature below which fusion power output is lower than power lost by bremsstrahlung. A broad $n_e \bullet \tau$ minimum is achieved for optimal values of the temperature, T_{opt}, see Fig. B.3. For $T \gg T_{opt}$, reactivity decreases and $n_e \bullet \tau$ must be raised. The case of fully thermalized plasma ($T_e = T_i$) allows self-sustained operation only for the D–T, D–^{3}He, and D–D reactions. In addition to the pure D–D cycle, the so-called catalyzed D–D cycle, in which a small amount of T is added to the D fuel and then recovered through the D–D cycle, is often considered.

In some confinement scheme, especially in conjunction with the use of unconventional fuels (Rostoker 1993), the condition of thermal equilibrium does not apply and Eq. (B.15) should be replaced by separate equations for the power balance of each species. In these schemes, the electrons act only as a "cold" neutralizer and bremsstrahlung is reduced to a level that allows a positive Q gain. Auxiliary power is usually supplied in the form of energetic ion beams, and the beam-beam and beam-target reactions must be accounted for. The following points must be strongly emphasized:

- The electron temperature cannot be arbitrarily small since energetic particles (injected by external methods or produced by fusion reactions) would be rapidly slowed down by collisions with low-energy electrons.
- The fusion reactivity must be evaluated with the appropriate distribution functions for the reacting species (typically, a slowing down distribution function for externally injected beams).

B.2.3 Design of a Generic Fusion Propulsion System

After having summarized the condition for achieving fusion gain $Q > 1$, we now discuss the trade-off between the pluses and minuses of various fusion systems in optimizing the specific power α.

Following (Santarius and Logan 1998), it is useful to determine the requirements for a generic fusion propulsion system based on magnetic confinement without making reference to any *specific* magnetic confinement concept. In the following, the system will be assumed equivalent to a cylindrical solenoid of radius r_m and volume V inducing a magnetic field$\vec{B}$ (see Fig. B.4). The plasma is assumed to have a radius r_p. A scrape-off layer of width much lower than r_p separates the plasma from the first wall (radius $r_w \approx r_p$). The magnet is shielded by a blanket of radius $r_s \approx r_m$.

The assumed (idealized) power flow is shown in Fig. B.5. The power that flows out of the reaction chamber is the sum of the fusion power plus the auxiliary power. A fraction f_T is used directly for thrust (direct propulsion or fusion electric propulsion can be simulated by a coefficient $f_T = 1$ or $f_T = 0$, respectively). The remaining fraction is converted either by

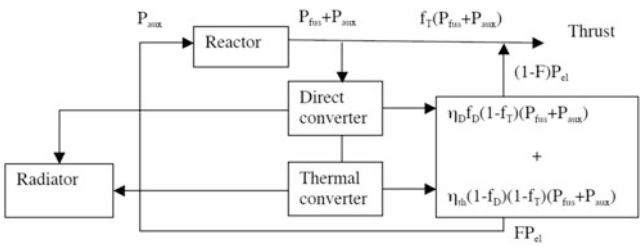

Fig. B.5 Ideal power flow in a notional fusion rocket

direct conversion (for a fraction f_D with efficiency η_D) or by thermal conversion (for the remaining part) into electrical power with an efficiency η_{th}:

$$P_{el} = [\eta_D \cdot f_D + \eta_{th} \cdot (1 - f_D)] \cdot (1 - f_T) \cdot (P_{fus} + P_{aux}) \tag{B.17}$$

A certain fraction of this power must be used for the spacecraft ancillary systems. If the efficiency for auxiliary power generation is η_{aux}, such a fraction is given by

$$\frac{P_{aux}}{\eta_{aux}} \equiv F \cdot P_{el} \tag{B.18}$$

where now the symbol F indicates the re-circulating power fraction. The fusion gain Q can then be related to F, η_{th}, and η_{aux} by

$$Q = \frac{1}{F \cdot \eta_{aux} \cdot [\eta_D \cdot f_D + \eta_{th} \cdot (1 - f_D)] \cdot (1 - f_T)} - 1 \tag{B.19}$$

The waste power to be radiated into space is therefore

$$P_{rad} = [f_D \cdot (1 - \eta_D) + (1 - \eta_{th}) \cdot (1 - f_D)] \cdot (1 - f_T) \cdot (P_{fus} + P_{aux}) + (1 - \eta_{aux}) \cdot \frac{P_{aux}}{\eta_{aux}} \tag{B.20}$$

B.2.4.1 Radiator

Waste power is produced by the neutron power deposited in the blanket, by radiation and by the auxiliary systems. Energy is radiated into space following the Stefan–Boltzmann law

$$P_{rad} = \varepsilon \cdot \sigma \cdot T_R^4 \cdot S_{rad} \tag{B.22}$$

with ε the radiator emissivity, σ the Stefan–Boltzmann constant, T_R the radiator temperature, and S_{rad} the radiator surface. At fixed P_{rad}, the radiator surface decreases as the radiator temperature increases. As shown in (Roth 1989), the radiator temperature that minimizes the radiator mass in the limiting case of an ideal Carnot efficiency ($\eta = 1 - T_R/T_H$) corresponds to 3/4 of the temperature T_H in the blanket/exhaust system. This estimate yields low values of the conversion efficiency ($\eta = 25\%$). Conventional structural material limits do not allow to go beyond $T_H \approx 300$ °C (advanced materials, e.g., SiC/SiC, could achieve $T_H \approx 1000$ °C). If ρ_{rad} is the mass per unit surface of the radiator (in kg/m^2), the radiator mass M_{rad} is linked to fusion power by the following expression, obtained by combining Eqs. (B.20) and (B.22) and using the Carnot expression for the efficiency:

$$M_{rad} = \rho_{rad} \cdot \left\{ \left[f_D \cdot (1 - \eta_D) + \left(\frac{T_R}{T_H} \right) \cdot (1 - f_D) \right] \cdot (1 - f_T) \cdot \left(1 + \frac{1}{Q}\right) + \frac{(1 - \eta_{aux})}{(Q \cdot \eta_{aux})} \right\} \cdot \frac{P_{fus}}{\varepsilon} \cdot \sigma \cdot T_R^4 \equiv \frac{P_{fus}}{\alpha_{rad}} \tag{B.23}$$

If the reactor is self-sustained ($P_{aux} = 0$), then the re-circulating fraction vanishes. In practice, this does not even occur for $P_{aux} = 0$, since part of the electric power must feed the control system, the cryogenic system, etc. Assuming realistic values $F = 20$ and 50% for both efficiencies, values for $Q \approx 20$–30 are necessary for efficient energy production.

From the above expressions, the power available for thrust is finally as follows:

$$P_{thrust} = [(1 - F) \cdot [\eta_D \cdot f_D + \eta_{th} \cdot (1 - f_D)] \cdot (1 - f_T) + f_T] \cdot \left(1 + \frac{1}{Q}\right) \cdot P_{fus} \tag{B.21}$$

B.2.4 Mass Budget

In the following, we consider only contributions to mass due to fusion reactor components.

Equation (B.23) determines the specific power associated with the radiator. A "reasonable" value is 5 kW of rejected power for each kg of radiator mass, corresponding to $\rho_{rad} = 1.5$ kg/m^2 at 600 K radiating temperature. These numbers tend to be on the conservative side, as modern heat exchangers can be built that have specific weights of order 0.01–0.15 kg/kW.

B.2.4.2 Magnet

Present magnetic confinement concepts require the generation of magnetic fields in plasma of order 1–10 T (Tesla). Two technologies are considered here. (1) Low-temperature superconductors and (2) actively cooled copper. High-temperature superconductors are promising, especially using MgB_2, but are still at a too preliminary stage for sizing a fusion-relevant system, see (Casali and Bruno 2005, 2008). A cryoplant receiving power from the reactor must keep all wiring at the superconductive state.

Superconductor technology: The development of Nb_3Sn low-temperature superconductors for the International Tokamak Experimental Reactor (ITER) (Lane 2012) being built in France has currently produced cables that can carry a current density of order 50 MA/m^2 at a magnetic field of 12.5 T (Huguet et al. 2003). The current density in cables depends on individual cable strand performance (in the case of ITER, single strands may carry 650 A/mm^2), but also on other parameters such as the Cu/non-Cu ratio, the void fraction, and the amount of space needed for the cooling channel, jacket, and insulator. All of these aspects are typically reducing the strand performance by an order of magnitude. Note, however, that Nb_3Sn strands with a critical current density of 2000 A/mm^2 have been produced. Strands with a critical current density in the range of 3000 A/mm^2, about a factor five larger than the ITER requirements, are expected in the near future.

Note also that the numbers above refer to a 12.5 T magnetic field in the conductor. Higher values of the critical current can be achieved at lower magnetic fields. Thus, values up to 250 MA/m^2, envisaged in some studies, can be considered realistic. The cable specific weight assumed here is 6 t/m^3 (using current conservative and ground-based tokamak magnet practice and technology). A cylindrical solenoid with a radial width of 0.2 m can therefore produce a 12.5 T magnetic field. If r_m and V are the radius of the solenoid and the internal volume, the mass of the magnet (neglecting the supporting structure) is approximately given by

$$M_{mag} \approx 2.4 \cdot \frac{B}{12.5} \cdot \frac{V}{r_m} \left(\frac{\mathrm{T} \cdot \mathrm{m}^3}{\mathrm{m}} = \mathrm{ton} \right) \tag{B.24}$$

Actively cooled copper magnet technology: Copper magnet technology is capable of inducing larger magnetic fields and thus higher fusion power density. An upper bound to magnet mass is estimated using the virial theorem

$$M_{mag} \approx 2 \cdot \rho_{mag} \cdot \frac{B^2}{2 \cdot \mu_0} \cdot \frac{V}{\sigma_{stress}} \tag{B.25}$$

with $\sigma_{stress} \approx 1$ GPa. For $\rho_{mag} = 2.5$ t/m^3, the above estimate yields about 600 t for an ITER-size magnet.

The magnet mass is proportional to the volume of the solenoid. Since within the present model the plasma volume V_p is a factor $(r_p/r_m)^2$ smaller than the magnet volume, and since the plasma volume is related to the fusion power by

$$P_{fus} = P_{spec} \cdot V_p \tag{B.26}$$

with P_{spec} the fusion power density in the reaction chamber, the magnet mass can be written

$$M_{mag} = k_m \cdot V = k_m \cdot \left(\frac{r_m}{r_p} \right)^2 \cdot \frac{P_{fus}}{P_{spec}} \equiv \frac{P_{fus}}{\alpha_{mag}} \tag{B.27}$$

with k_m given by Eq. (B.24) or (B.25).

Comparison between superconducting and copper magnet for fusion applications shows that superconductors have always advantages over copper magnets in terms of the magnet mass, unless extremely high magnetic fields are desired.

B.2.4.3 Cryoplant

Following (Santarius 1998), a value 1000 kg/kW for the mass per unit heat extracted is assumed (this value is actually one order of magnitude lower than available with present systems). This value shows the importance of thermal insulation. The cryoplant power is determined by the nuclear heating of the magnet:

$$P_{cryo} = f_n \cdot P_{fus} \cdot \left(\frac{r_p}{r_m} \right) \cdot \exp\left(-\frac{r_m - r_p}{\lambda_n} \right) \tag{B.28}$$

where $\lambda_n \approx 0.13$ m is the neutron mean free path in the blanket and f_n the fraction of fusion energy associated with neutrons. The cryoplant mass is therefore given by

$$M_{cryo} = f_n \cdot P_{fus} \cdot \left(\frac{r_p}{r_m} \right) \cdot \exp\left[-\frac{r_m - r_p}{\lambda_n} \right] \cdot 1000 \ \frac{\mathrm{kg}}{\mathrm{kW}} \tag{B.29}$$

And, synthetically,

$$M_{cryo} = \frac{P_{fus}}{\alpha_{cryo}} \tag{B.30}$$

B.2.4.4 Blanket

An optimized blanket made by LiH has been proposed in (Kulcinski et al. 1987) with a density ρ_s in the 10^3 kg/m^3 range (Santarius and Logan 1998), much less than the value $\approx 10^4$ kg/m^3 for the solid and liquid blankets envisaged in a fusion reactor. The blanket mass is given by

$$M_s = \rho_s \cdot \left(1 - \frac{r_p^2}{r_m^2} \right) \cdot V \tag{B.31}$$

$$M_s = \rho_s \cdot \left(\frac{r_m^2}{r_p^2} - 1 \right) \cdot \frac{P_{fus}}{P_{spec}} \tag{B.32}$$

$$M_s = \frac{P_{fus}}{\alpha_s} \tag{B.33}$$

B.2.4.5 Auxiliary Systems

The estimate used in (Williams et al. 1998) for the negative neutral beam system corresponds to an efficiency of 29% (108 MW beam power out of 367 MW input power). The total mass is dominated by the 20 sources (2.5 t each), which include the filament source, the three-stage accelerator, and the neutralizer. These assumptions correspond to a hoped-for reduction by about an order of magnitude of existing

systems. Much lower mass estimates have been used in (Cheung et al. 2004). We assume here a figure of 2.5 kg/kW of injected power. The mass of the auxiliary system is given by

$$M_{\text{aux}} = 2.5\frac{\text{kg}}{\text{kW}} \cdot \frac{P_{\text{fus}}}{Q} \tag{B.34}$$

Since $Q \approx 20$, we neglect this contribution in the following.

B.2.4.6 Conversion

A conventional closed Brayton cycle is assumed for practicality. The cycle working fluid is typically He. The mass budget for a 400 MWe system (at 20% efficiency), operating with inlet temperature 1700 K and outlet temperature 1300 K (Williams et al. 1998), is about 145 t. Note (Cheung et al. 2004) assume 40% efficiency (7 MW produced out of an input of 18 MW). The mass was calculated assuming 3 kg/kWe for the conversion system (excluding the radiator). As is the case of other figures cited in such calculations, at times, these are either strongly underestimated or, as in this particular case, broadly overestimated. For instance, at 3 kg/kWe, the mass of the 400 MWe system would be 1200 t. For comparison, a similar power gas turbine-powered system would weigh about ten times less. In the present simplified analysis, we neglect this component.

B.2.5 Specific Power

By adding all contributions from the estimates above, the total mass M and thus the specific power α are predicted as

$$M \equiv \frac{P_{\text{thrust}}}{\alpha} = P_{\text{fus}}\left(\frac{1}{\alpha_{\text{mag}}} + \frac{1}{\alpha_{\text{s}}} + \frac{1}{\alpha_{\text{cryo}}} + \frac{1}{\alpha_{\text{rad}}}\right) \tag{B.35}$$

Upon substituting all expressions found, the following is obtained with $k_{\text{m}} = 2.4\ (B(T)/12.5)\ r_{\text{m}}\ (\text{m})^{-1}$ using superconducting magnets and $k_{\text{m}} = 2.0 \cdot 10^{-3}\ B(T)^2$ using copper conductors.

The *simplest* limiting case for the above expression is $f_{\text{n}} = 0$ (aneutronic reactions) and $f_{\text{T}} = 1$ (direct thermal propulsion) which yields (with $r_{\text{p}} = r_{\text{m}}$, i.e., no shield)

$$\alpha\left(\frac{\text{kW}}{\text{kg}}\right) \approx \frac{P_{\text{spec}}\left(\frac{\text{MW}}{\text{m}^3}\right)}{k_{\text{m}}} \tag{B.37}$$

Thus, to obtain specific power in the range from 1 to 10 kW/kg, the fusion power density for aneutronic reactions must be in the range from 1 to 10 MW/m^3 times the constant $k_{\text{m}} \approx 1$.

In the case of neutron-producing reactions, it is convenient first to maximize Eq. (B.35) with respect to the ratio $r_{\text{p}}/r_{\text{m}}$ at fixed r_{m} (i.e., to minimize the cryoplant plus blanket mass) and then with respect to the ratio $T_{\text{R}}/T_{\text{H}}$ (assuming the Carnot expression for the efficiency η) at the fixed T_{H}, determined by thermos-structural material limitations.

Two limiting cases can be singled out, depending on whether (a) the radiator mass, or (b) the fusion system mass, tends to dominate.

Case (a) for large radiator mass, that is,

$$\frac{\varepsilon \cdot \sigma \cdot T_{\text{R}}^4}{\rho_{\text{rad}}} \ll \left(\frac{r_{\text{p}}}{r_{\text{m}}}\right)^2 \cdot \frac{P_{\text{spec}}\left(\frac{\text{MW}}{\text{m}^3}\right)}{k_{\text{m}} + \rho_{\text{s}}\left(\frac{\text{t}}{\text{m}^3}\right)} \tag{B.38}$$

In this limit, the mass budget is dominated by the radiator, and the specific power α is independent of fusion power density:

$$\begin{aligned}\alpha\left(\frac{\text{kW}}{\text{kg}}\right) \approx\ & \frac{\varepsilon \cdot \sigma \cdot T_{\text{R}}^4}{10^3 \cdot \rho_{\text{rad}}} \\ & \cdot [(1-F) \cdot [\eta_{\text{D}} \cdot f_{\text{D}} + \eta_{\text{th}} \cdot (1-f_{\text{D}})] \cdot (1-f_{\text{T}}) + f_{\text{T}}] \cdot \left(1 + \frac{1}{Q}\right) \\ & \cdot \left[[f_{\text{D}}(1-\eta_{\text{D}}) + (1-\eta_{\text{th}}) \cdot (1-f_{\text{D}})] \cdot (1-f_{\text{T}}) \cdot \left(1 + \frac{1}{Q}\right) + \frac{(1-\eta_{\text{aux}})}{(Q \cdot \eta_{\text{aux}})}\right]^{-1}\end{aligned} \tag{B.39}$$

$$\begin{aligned}\alpha\left(\frac{\text{kW}}{\text{kg}}\right) =\ & [(1-F) \cdot [\eta_{\text{D}} \cdot f_{\text{D}} + \eta_{\text{th}} \cdot (1-f_{\text{D}})](1-f_{\text{T}}) + f_{\text{T}}] \cdot \left(1 + \frac{1}{Q}\right) \\ & \times \left\{ \begin{array}{r} \left(\frac{r_{\text{m}}}{r_{\text{p}}}\right)^2 \cdot P_{\text{spec}}\left(\frac{\text{MW}}{\text{m}^3}\right)^{-1} \cdot \left[k_{\text{m}} + \left(1 - \frac{r_{\text{p}}^2}{r_{\text{m}}^2}\right) \cdot \rho_{\text{s}}\left(\frac{\text{t}}{\text{m}^3}\right)\right] + \\ + f_{\text{n}} \cdot 10^3 \cdot \left(\frac{r_{\text{p}}}{r_{\text{m}}}\right) \cdot \exp\left[-\frac{(r_{\text{m}} - r_{\text{p}})}{\lambda_{\text{n}}}\right] + \\ + [f_{\text{D}} \cdot (1-\eta_{\text{D}}) + (1-\eta_{\text{th}}) \cdot (1-f_{\text{D}})] \cdot (1-f_{\text{T}}) \cdot \left(1 + \frac{1}{Q}\right) + \frac{(1-\eta_{\text{aux}})}{(Q \cdot \eta_{\text{aux}})} \cdot \\ \cdot 10^3 \cdot \rho_{\text{rad}} \cdot \frac{1}{\varepsilon \cdot \sigma \cdot T_{\text{R}}^4} \end{array} \right\}^{-1}\end{aligned} \tag{B.36}$$

The radiator temperature reduces to

$$T_R = \frac{3}{4} \cdot T_H \tag{B.40}$$

in the limit $f_D \ll 1$, $f_T \ll 1$ (Roth 1989). Note that the radiator temperature can become larger than the blanket temperature T_H for finite values of f_T and f_D. This result simply means that if the fraction of energy going directly to thrust or which is recovered by direct electricity conversion is large, there is no need to have thermal electricity conversion and the remaining fraction must be radiated at the highest possible temperature. For a radiator radiating at 5 kW/kg, Eq. (B.39) predicts specific power in the range from 1 kW/kg (for $f_D = f_T = 0$, i.e., fusion electric propulsion) to 9 kW/kg (for $f_D = f_T = 0.5$, in which only 25% of the power must be radiated). Specific power increases very rapidly with f_D and f_T. *It is thus apparent that fusion electric propulsion is marginal in terms of specific power.* Note that Eq. (B.39) is independent of any parameter related to plasma behavior.

Case (b) for small radiator mass, that is,

$$\frac{\varepsilon \cdot \sigma \cdot T_R^4}{\rho_{rad}} \gg \left(\frac{r_p}{r_m}\right)^2 \cdot \frac{P_{spec}\left(\frac{MW}{m^3}\right)}{k_m + \rho_s\left(\frac{t}{m^3}\right)} \tag{B.41}$$

In this limit, radiator mass is negligible with respect to reactor mass

$$\alpha\left(\frac{kW}{kg}\right) \approx [(1-F)\cdot[\eta_D \cdot f_D + \eta_{th}\cdot(1-f_D)]\cdot(1-f_T)+f_T]\cdot\left(1+\frac{1}{Q}\right)\cdot\left(\frac{r_p}{r_m}\right)^2 \cdot \frac{P_{spec}\left(\frac{MW}{m^3}\right)}{k_m + \rho_s\left(\frac{t}{m^3}\right)} \tag{B.42}$$

where

$$r_m = r_p + 3\cdot\lambda_n \cdot \ln 10 - \lambda_n \cdot \ln\left\{2\cdot\left(\frac{r_m}{r_p}\right)^3 \cdot \frac{k_m + \rho_s}{f_n \cdot P_{spec}\left(\frac{MW}{m^3}\right)\cdot\left(\frac{r_p}{\lambda_n}+1\right)}\right\} \tag{B.43}$$

This solution generalizes Eq. (B.37) to include the blanket mass. The radiator temperature can be substantially lower than T_H, and high efficiency η can be obtained. For a radiator radiating 5 kW/kg (as noted, a conservative value), Eq. (B.42) becomes valid for

$$\left\{[f_D(1-\eta_D)+(1-\eta_{th})\cdot(1-f_D)]\cdot(1-f_T)\cdot\left(1+\frac{1}{Q}\right)+\frac{(1-\eta_{aux})}{(Q\cdot\eta_{aux})}\right\}\cdot P_{spec}\left(\frac{MW}{m^3}\right) < 5\cdot\left(\frac{r_m}{r_p}\right)^2\left[k_m+\rho_s\left(\frac{t}{m^3}\right)\right] \tag{B.44}$$

B.2.6 Fusion Power Density

In order to understand what specific power can be expected from a fusion reactor and how it is related to plasma parameters, it is convenient to assume that the operating temperature is close to the optimal temperature T_{opt} (i.e., the temperature corresponding to the minimum of the $n \bullet \tau$ vs. T curve).

The optimal temperature depends on the choice of reactants, on the gain Q, and on the radial profile factors. The electron density n_e can be expressed in terms of the parameter β

$$\beta \equiv 2\cdot\mu_0\cdot f_1 \cdot n_e \cdot \frac{T}{B^2} \tag{B.45}$$

where

$$f_1 \equiv 1 + \sum_i \frac{n_i}{n_e} \tag{B.46}$$

is a factor of order unity depending on the fuel composition, and

$$n_e = \beta \cdot \frac{B^2}{2\cdot\mu_0\cdot f_1 \cdot T_{opt}} \tag{B.47}$$

The achievable values of β depend on the stability properties of the specific magnetic configuration considered and are discussed in the next section. Note that expressing plasma density in terms of β is correct as long as no more stringent limits on the plasma density are discovered (e.g., in tokamak operation density is experimentally observed to reach a maximum proportional to the average plasma current density).

From the above conditions, it is possible to determine the fusion power per unit volume that can be produced in the form of neutrons and charged particles:

$$P_{spec} = n^2 \cdot f_2 \cdot (\sigma\cdot v)\cdot E_{fus} \tag{B.48}$$

$$P_{\text{spec}} = \left[\frac{\beta \cdot B^2}{2 \cdot \mu_0 \cdot f_1 \cdot T_{\text{opt}}}\right]^2 \cdot f_2 \cdot (\sigma \cdot v) \cdot E_{\text{fus}} \tag{B.49}$$

with

$$f_2 \equiv \left(\frac{n_{\text{i}}}{n_{\text{e}}}\right) \cdot \left(\frac{n_{\text{j}}}{n_{\text{e}}}\right) \tag{B.50}$$

a coefficient related to the fuel composition and E_{fus} the energy released in a fusion reaction. It is apparent that in order to maximize the fusion power density for a given reaction, *plasma must be as dense as possible*. From Eq. (B.49), this can be accomplished both by maximizing the value of β and by operating at large$\vec{B}$.

For the sake of illustration, the values of P_{spec} achievable with D–T and D–^{3}He reactions are shown in Table B.3 for three values of β and for B = 10 T.

Comparing D–T and the D–^{3}He reactions at the same value of (β B^2) shows that the D–^{3}He reaction has specific power about two orders of magnitude lower than that of the D–T reaction. The conclusion from Table B.3 is that the D–^{3}He reaction becomes interesting only if β can be made larger than 10%.

Note that the neutron power P_{n} per unit surface that can be tolerated by the first wall before serious structural degradation occurs is limited. The target specific fluence is

$$P_{\text{n}} \cdot \frac{\Delta T}{S} \approx 10 \text{ to } 15 \frac{\text{MWyear}}{\text{m}^2} \tag{B.51}$$

This value depends on the neutron energy (the 14 MeV of the D–T reaction is the worse situation). The target for first wall replacement in ground systems is 5 years at full power. This sets a limit of ≈2–3 MW/m^2 for the specific neutron power. This latter depends on the shape of the reaction chamber. In the simple case of a spherical chamber of radius r_{w}, it is given by

$$\frac{P_{\text{n}}}{S} = f_{\text{n}} \cdot P_{\text{spec}} \cdot \frac{r_{\text{w}}}{3} \tag{B.52}$$

In the case of a cylindrical chamber of radius r_{w} and length L, it is given by

$$\frac{P_{\text{n}}}{S} = f_{\text{n}} \cdot P_{\text{spec}} \cdot \frac{r_{\text{w}}}{2} \tag{B.53}$$

Thus, the limit on the neutron wall load imposes a limit on specific power that is more stringent for large chamber radii. Taking as an example 1 year of full power operation, the specific power would be limited by

$$P_{\text{spec}} \left(\frac{\text{MW}}{\text{m}^3}\right) < \frac{20 \text{ to } 45}{f_{\text{n}} \cdot r_{\text{w}} \text{ (m)}} \tag{B.54}$$

Table B.3 Fusion power per unit volume as function of β

%	D–T (MW/m^3)	D–^{3}He (MW/m^3)
β = 100	10^4	123
β = 10	10^2	1.2
β = 1	1	0.01

B.2.7 Summary

In order to summarize, the key results of this analysis at the current status of fusion technology are as follows:

- If the system mass is dominated by the radiator, the specific power α does not depend on the fusion power per unit volume and, using a conservative 5 kW radiated per each kg of radiator mass, α can vary from 1 kW/kg, in the case of pure fusion electric propulsion, to 10 kW/kg, if fuel kinetics allows converting 50% of fusion power to thrust power. Based on these values of α, interstellar or QI missions are unfeasible with fusion electric propulsion.
- If the reactor mass dominates, the specific power increases linearly with fusion power density. Fusion power density in excess of 1 MW/m^3 is needed. This figure is compatible with advanced fuels such as D–^{3}He only if values of β above 10% can be achieved.
- Fusion power density cannot exceed the value given in Eq. (B.54) (which assumes one-year full power operation) due to the constraint on the neutron wall load.

B.3 Status of Open Magnetic Field Configuration Research

B.3.1 Classification and Present Status of Open Magnetic Field Configurations

It has been shown in the previous section that in order to achieve large specific power, it is necessary to use to the largest possible extent fusion in the form of *direct* (thermal) *propulsion*, with some optional direct electricity conversion. This is not easy to achieve in equilibrium configurations, such as conventional tokamaks, where plasma cannot escape from the reactor, but could be achieved by *open magnetic field* (OMF) configurations.

The topology of OMF configurations may vary. The simplest mirror topology is cylindrical, as shown in Fig. 8.20, but field reversed configurations and spheromaks transitioning to a torus in the confinement region may be viable. Nevertheless, the common feature of the open magnetic field

configuration is that the magnetic field lines escape from the plasma confinement zone without intercepting any wall. It is this feature that enables using the fusion plasma both for direct propulsion and direct conversion. Note that such a feature may be common also to other systems, such as the very low aspect ratio (spherical) tokamak, not considered here but already proposed for propulsion applications.

The best plasma fusion performance achieved so far has been obtained in *closed* magnetic field configurations (specifically, in tokamaks). However, for propulsion, *open* magnetic field configurations have intrinsic advantages:

- easier steady-state operation;
- natural particle exhaust;
- high β ($\equiv$thermal pressure/magnetic pressure);
- simple design;
- direct conversion of fusion power into mechanical thrust.

In the following, we consider three main classes of OMF configurations:

- open-ended systems, such as mirrors;
- closed field line systems, such as field reversed configurations (FRC) and spheromaks;
- levitated dipoles.

The analysis below addresses the potential of these configurations to achieve high β, which is mandatory for the use of advanced fuels, and good confinement (i.e., large $n \bullet \tau$ values and reasonable fusion gain) under conditions typical of sustained thrust. In order to fully assess the potential of a configuration, a good theoretical understanding of the underlying physical processes is mandatory. Unfortunately, such required theoretical understanding is not yet available for all configurations of interest. In some limiting cases, the answer provided by experimental evidence obtained so far may be enough to draw conclusions about extrapolating results to a range of parameters relevant to a burning plasma. This is the case of ideal plasma MHD, where the stability of magnetic configurations depends only on $\vec{B}$ shape and on β. However, weaker MHD modes are heavily affected by kinetic effects related, for instance, to finite particle orbit width. In some cases, even the application of the ideal MHD model is questionable, due to the large orbit size in some of the configurations examined below.

In order to understand the gap between the configuration proposed and existing or future devices, we consider only three dimensionless parameters which are as follows:

- the ratio β between plasma pressure and magnetic pressure;
- the collisional parameter (usually indicated by ν^*) defined as the ratio between the typical scale length along the magnetic field and the mean free path of Coulomb-driven collision;
- the normalized Larmor radius ρ^* defined as the ratio between the ion Larmor radius and the typical scale length transversal to the magnetic field.

It can indeed be easily shown, see, e.g., (Kadomtsev 1975, 1992), that the plasma physics equations (i.e., Boltzmann plus Maxwell equations) can be cast in dimensionless form. It also can be shown, in case the Debye length (also called Debye radius) does not play any role in the processes underlying stability and transport (which is always the case), full similarity among plasma behavior is assured by identical values of the three dimensionless parameters defined above. For comparison, present tokamak experiments have achieved values of β and ν^* similar to those of interest for ITER and ρ^* still differing by about a factor 3.

B.3.2 Mirror Configurations

Mirror configurations confine the plasma in a solenoidal magnetic "bottle". They are natural candidates for fusion propulsion since they allow the plasma to exhaust at one end of the "bottle", producing thrust and, simultaneously, direct energy conversion (Kammash 1995). The key question is: Can mirror configurations achieve the fusion power density needed for space propulsion as defined in Sect. B.3.1? In this context, the most recent and detailed review of the status of mirror research is still that in (Post 1987).

B.3.2.1 Simple Mirror Configuration

At the simplest level, a mirror configuration consists of a pair of Helmholtz coils with currents flowing in the same direction, as shown in Fig. B.6.

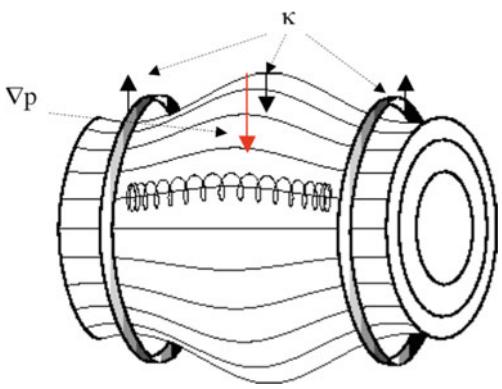

Fig. B.6 Simple mirror field configurations. The direction of the magnetic field curvature κ is also shown

The magnetic field intensity varies along $\vec{B}$, with a minimum value $\vec{B}_{\min}$ in the middle and a maximum value $\vec{B}_{\max}$ at the coil location. Confinement in the simplest mirror configuration is described by the conservation of kinetic energy of plasma particles

$$E = \frac{m \cdot v^2}{2} \tag{B.55}$$

and of the first adiabatic invariant, which is the magnetic moment μ

$$\mu = \frac{m \cdot v_{\perp}^2}{2 \cdot B} \tag{B.56}$$

where $v_{\perp}$ is the particle velocity perpendicular to $\vec{B}$, of a particle of mass m moving in a weakly inhomogeneous magnetic field $\vec{B}$. Charged particles spiral around the $\vec{B}$ field lines at a distance called the Larmor radius. These conservation laws imply that a particle moving along the field (with velocity $v_{\|}$) is reflected at the plasma location where

$$\frac{m \cdot v_{\|}^2}{2} \equiv E - \mu \cdot B = 0 \tag{B.57}$$

Therefore, upon producing a magnetic field configuration such as that shown in Fig. B.6, particles will be *trapped* provided that the ratio μ/E is larger than $1/B_{\max}$.

It can be shown that in the case of an isotropic particle distribution in the velocity space, the fraction f_T of plasma particles satisfying the trapping condition is given by

$$f_T \approx \sqrt{1 - \frac{1}{R}} \tag{B.58}$$

with

$$R \equiv \frac{B_{\max}}{B_{\min}} \tag{B.59}$$

the so-called mirror ratio. Particles not satisfying this condition will be promptly lost, with the result of producing an anisotropic distribution function characterized by a "loss cone" in the velocity space. For large values of the mirror ratio, the fraction of unconfined particles is

$$1 - f_T \approx \frac{R}{2} \tag{B.60}$$

Obviously, the fraction of unconfined particles can be made smaller if they are injected in the configurations with small parallel velocity, e.g., by perpendicular neutral beam injection. On the other hand, collisions tend to restore isotropy and the loss cone is continuously populated by scattering in velocity space.

Since the electrons have higher collision frequency than ions, they are scattered in the loss cone (and therefore lost) at a higher rate. As a consequence, plasma tends to be positively charged. Its potential ϕ is determined by the condition that transport must be *ambipolar*, i.e., that overall charge neutrality must be maintained, yielding values in the range

$$e \cdot \phi \approx (4 \text{ to } 8) \cdot T_e \tag{B.61}$$

where T_e is the electron temperature. The effect of the ambipolar potential is that it is decreasing the loss of low-energy electrons while increasing the ion loss.

As a result, in such a simple configuration, confinement is maintained on the ion–ion collision timescale τ_{ii} (the timescale for the scattering of a trapped ion into the loss cone). The ion–ion collision time is proportional to $(E_i)^{3/2}$, with E_i representing the ion energy. Therefore, higher values of the confinement are achieved by increasing E_i. On the other hand, fast ions tend to preferentially transfer their energy to electrons by Coulomb-driven collisions if

$$E_i > 15 \cdot T_e \tag{B.62}$$

If the electron temperature T_e is too low, slowing down of the injected ions by electrons (so-called electron drag) occurs on a fast timescale

$$\tau_{SD} \propto \frac{T_e^{\frac{3}{2}}}{n_e} \tag{B.63}$$

Thus, electrons must be kept at sufficiently high temperature.

At first sight, maintaining high electron temperature in an open-ended configuration might appear difficult. Classical fluid transport theory would predict very large electron thermal conduction (and therefore, high-energy losses and very high heating power to keep the electrons at sufficiently high temperature). However, in experiments characterized by low collision rate (i.e., when the mean free path is longer than the mirror distance), the electron thermal conductivity along the magnetic field is much lower than the classical estimate. This result is a consequence of the presence of the ambipolar potential ϕ that confines electrons inside the mirror. Only supra-thermal (non-equilibrium) electrons can escape the ϕ barrier and contribute to thermal conduction loss. This effect dramatically reduces electron thermal conductivity, at the expense of low plasma density, and thus *enlarges the device* at fixed power. This was already noted in Chap. 8 and quantified in Fig. 8.16.

The $n \bullet \tau$ parameter can be estimated by solving the Fokker–Planck equation accounting for the presence of the ambipolar potential and electron drag. It can be shown (Post 1987) that the confinement parameter is approximately given by

$$n \cdot \tau \approx 2.5 \cdot 10^{16} \cdot E_i \ (\mathrm{keV})^{\frac{3}{2}} \cdot \log_{10}(R) \ (\mathrm{m}^{-3} \cdot s) \quad \text{(B.64)}$$

Note that the dependence on the mirror ratio R is only logarithmic and that the above expression is independent of size and magnetic field. In order to obtain a significant gain, E_i should be of order 10^2 keV. However, above a certain kinetic energy, the fusion cross sections tend to decrease. This happens above 100 keV for D–T and 400 keV for D–^{3}He (when measured in the center of mass frame of reference). Therefore, an optimal value exists for ion energy.

All these constraints limit efficient energy production by the simple mirror. Indeed, at the simplest level, a mirror reactor works as an energy amplifier. Power is injected through high-energy neutral beams and fusion power is recovered with a gain

$$Q \equiv \frac{P_\mathrm{fus}}{P_\mathrm{inj}} \quad \text{(B.65)}$$

with Q given by

$$Q \approx \frac{n \cdot \tau}{4} \cdot [\sigma \cdot v] \cdot \frac{E_\mathrm{fus}}{E_\mathrm{i}} \quad \text{(B.66)}$$

where E_fus is the energy released by the fusion reaction. The $n \bullet \tau$ scaling in Eq. (B.66) for a simple mirror configuration (D–T, $R = 10$, $E_i \approx 300$ keV) implies values of $Q \approx 1$, too low even for producing electricity by direct conversion. Even lower values ($Q \approx 0.3$) are predicted for the D–^{3}He reaction.

In addition to low gain, the simple mirror configuration has limited MHD stability due to the presence of "interchange" instabilities in the region between the mirrors. Indeed, the exchange of a plasma flux tube with a vacuum flux tube is energetically favorable if the local magnetic field curvature $\vec{\kappa}$ ($\vec{\kappa} \equiv B \bullet \nabla \vec{b}$, with $\vec{b} \equiv \vec{B}/B$) is parallel to the pressure gradient, as in the central part of the mirror cell (the opposite occurs near the mirror locations), see Fig. B.6. The instability is suppressed by superimposing a multipolar field to produce a so-called minimum- B configuration in which a "magnetic well" is formed around the symmetry axis. The demonstration of the stability of minimum- B configurations was achieved in modified mirror systems called "baseball," or Ying-Yang, coils shown in Fig. B.7. Unfortunately, when a multipolar component is superimposed to the axisymmetric mirror field, the axial symmetry breaks down with a detrimental effect on the radial particle transport. Radial drifting away of particles causes transport losses either by collisions, as in closed toroidal magnetic configurations, or by resonant processes.

Small-scale instabilities can be also generated by anisotropy in the velocity space and in particular in the loss cone. These instabilities have been shown to be much less deleterious than theoretically predicted, provided warm plasma is injected into the mirror, and will not be considered further in this context. For a discussion of the many micro-instabilities in mirrors, see (Post 1987).

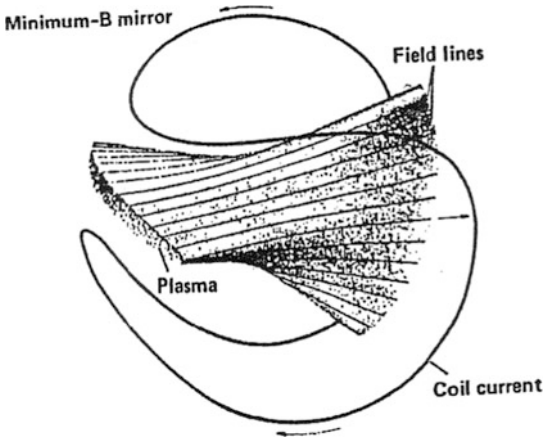

Fig. B.7 Baseball coils (Post 1987)

To overcome all these problems, advanced mirror concepts have been proposed and are briefly reviewed in the rest of this section.

B.3.2.2 Tandem Mirror

The idea behind the tandem mirror (TM) is to modify the shape of the electrostatic potential along $\vec{B}$ in such a way as to confine both escaping ions and electrons. In the tandem mirror arrangement, see Fig. B.8, two smaller mirror cells are added at each end of the larger central cell where fusion reactions are supposed to take place.

By using external inputs, such as radio frequency heating and neutral beam injection, the axial profiles of density and temperature in the two end cells are tailored so as to

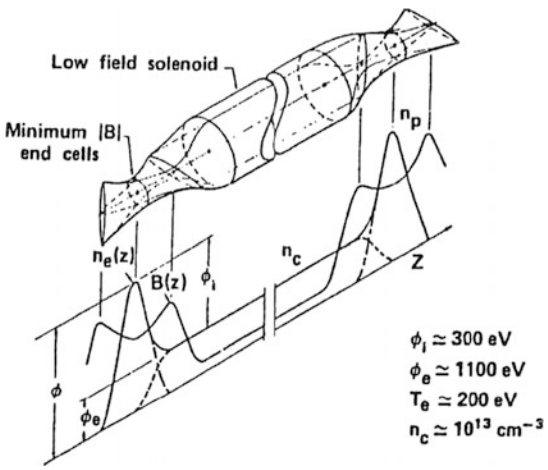

Fig. B.8 Tandem mirror schematic (Post 1987)

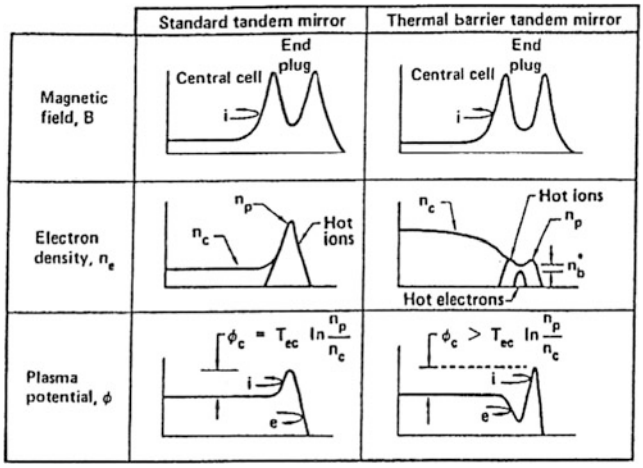

Fig. B.9 Axial profiles in a tandem mirror. This schematic illustration from (Post 1987) compares density and electrostatic potential profiles in a standard tandem mirror and in a tandem mirror with thermal barrier

transform them into electrostatic "plugs" at a positive potential, thus reducing the loss of positive ions from the central cell. The axial profiles of density, temperature, and electrostatic potential are shown in Fig. B.9.

Plasma potential, electron density, and electron temperature are related by the condition that the highly mobile electrons relax to a Boltzmann distribution, yielding

$$\phi(z) = \phi(z_0) + T_e \ln\left[\frac{n(z)}{n(z_0)}\right] \tag{B.67}$$

with z the axial coordinate and z_0 corresponding to the midplane. Equation (B.67) suggests two possible schemes for tailoring the plasma potential:

(a) First, the conventional TM scheme, in which higher potential in the plug cells is achieved by increasing the plug density with respect to the central cell density. Such increase is obtained by injecting energetic ions in the plug. The axial profiles of the magnetic field, density, and plasma potential are shown in Fig. B.9. Since the density in the central cell must be sufficiently high (fusion power output P_{fus} scales as n^2), very high values of plug density (or pressure) are in order, and this implies very high B (≈15 T) in the end cells and high-energy neutral beams ($E \approx 1$ MeV). Note that the electrons in this configuration are reflected at the two plug-cell ends. Therefore, electrons in the plug are in thermal contact with electrons in the central cell. Any attempt to increase the temperature in the plugs will also increase the temperature in the central cell while demanding more power.

(b) Second, the thermal barrier scheme, in which electrons are reflected *before* reaching the central cell. This scheme thermally insulates (hot) electrons in the plugs from (colder) electrons in the central cell, so only the former needs to be heated. If a thermal barrier is established, electron temperature in the plugs can be kept higher than in the central cell, and high electrostatic potential can be maintained in the plug to confine ions. In order to establish a barrier, ions are removed by the thermal barrier region by charge exchange with a neutral beam injected almost parallel to $\vec{B}$. The negative charge difference creates the electrostatic potential hump (the barrier).

Between the two, the second scheme is more practical, since it puts less stringent conditions on the two main engineering parameters, the magnetic field and the energy of injected ions, in the two end plugs.

In order to maintain this configuration, external power must be injected into the two end cells. However, if the end cell volumes are sufficiently smaller than those of the central cell, their power consumption is negligible and large Q becomes feasible.

Detailed calculations of the ion confinement in the central cell show that manipulation of the plug potential can enhance the $n \bullet \tau$ product by a significant factor. Estimates yield enhancement factors roughly given by

$$e \cdot \frac{\phi}{T_i} \cdot \exp\left[e \cdot \frac{\phi}{T_i}\right] \tag{B.68}$$

This has been experimentally confirmed in the first generation of TM experiments, e.g., TMX (tandem mirror experiment) at Livermore, see (Post 1987) for details, where ion and electron confinement have been enhanced by an order of magnitude. However, it is already apparent from Fig. B.9 that maintaining the desired shape of the electrostatic potential requires very sophisticated tools that must work over a broad range of parameters, especially at the density necessary to achieve ignition and high power.

An important aspect of the TM is its stability against flute-like interchange modes, i.e., pressure-driven modes with very little variation along magnetic field lines. The TM configuration is stable, even in the absence of an additional multipolar field in the central cell, due to the connection between plasma in the central cell and plasma in the end cells (typically made by baseball or Ying-Yang coils and therefore MHD stable). However, other MHD instabilities exist such as ballooning instability modes. These are localized in the regions of unfavorable magnetic field line curvature inside the central cell, and therefore do not feel the stabilizing

influence of the end cells but produce a substantial line bending of the magnetic field lines. Ballooning lowers β typically by a factor two with respect to flute-like modes (Post 1987, and references therein). However, kinetic effects, such as finite particle orbit width, can significantly increase the stability threshold (note that in the old tandem mirror 2XIIB experiment, β values larger than 200% were achieved in regimes with large particle orbits). In summary, β values above 20% might be achieved by tandem mirrors (TM).

The possibility of MHD stabilizing the central cell without superposing a multipolar field has the important consequence of reducing radial transport. In conventional mirrors, radial transport is negligible with respect to axial transport, but becomes significant in tandem mirrors due to the enhancement of axial transport by the plug potential.

Note an important difference between radial transport in mirrors and in toroidal (tokamak) systems. In the tokamak system, radial transport is purposely made ambipolar. Any mechanism enhancing losses of one species produces a situation where the loss rate of the other species is also enhanced. This is not the case in mirrors. Since there are two loss channels (axial and radial), radial ion losses can be balanced, for instance, by axial electron losses without the need to increase the cross-field electron diffusion. This observation is the basis for controlling radial transport by dialing the end plate potential. Electrons lost by axial transport are collected on an end plate that becomes charged negatively while also driving the plasma to a negative potential. When inserting and varying a resistance between end plate and wall, this also varies the radial potential difference between the plasma and wall, and thus, radial transport can be controlled and reduced.

The first generation of TM experiments (TMX at the Lawrence Livermore National Laboratory from 1979 to 1987, and GAMMA-6 at the University of Tsukuba, Japan, since 1978) produced architectures and achievements including the following:

- The GAMMA-10 reactor, with an axisymmetric central cell minimizing radial transport and stabilized by quadrupolar magnetic wells coupled to the central cell by "axisymmetrizing" transition coils, see Fig. B.10. Outside these "anchor" cells, there are axisymmetric mirror cells where the thermal barrier and plugging potential are generated (Cho et al. 2004). GAMMA-10 is 27 m long. The volume of the vacuum vessel is 150 m^3. The central cell is 6 m long and has a fixed limiter with a diameter of 0.36 m. The magnetic field intensity B_m at the midplane is 0.405 T with a mirror ratio R = 5.2. Ion cyclotron heating with 200 kW at 4.47 or 6.36 MHz, and 100 kW at 9.9 or 10.3 MHz produces hot ions in the central cell, and anchors and stabilizes plasma, respectively. The axisymmetric end cells are 2.5 m long, with B_m = 0.497 T and R_m = 6.2.

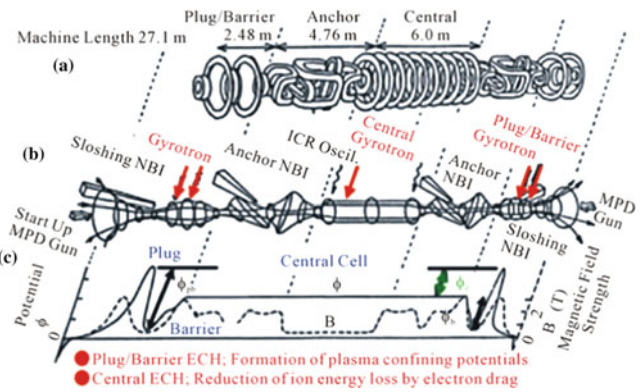

Fig. B.10 Schematic view of the GAMMA-10 tandem mirror (Cho et al. 2004):**a** magnetic coil set,**b** magnetic flux tube with heating systems, as well as**c** axial magnetic field (*dashed curve*) and potential profiles (*solid curve*)

- The tandem mirror Experiment (TMX-U) at Livermore (Simonen 1988) employed quadrupolar mirrors at the end of the central cell. These were connected to quadrupolar (MHD-stable) magnetic wells where thermal barrier and plugging potential were formed. Before its decommissioning, TMX-U was able to demonstrate the thermal barrier concept at modest particle number densities $\approx(1–3) \cdot 10^{18}$ m^{-3}. According to the Livermore team, the theoretical design limit ($\approx 10^{19}$ m^{-3}) was never reached due to insufficient power. The experiment also confirmed theoretical expectations about the stabilizing effects of a population of "sloshing ions" produced by oblique injection of neutral beams.
- The TARA experiment at MIT (Guss et al. 1988): This experiment aimed at testing the possible use of axisymmetric central and plug cells (to reduce radial transport) with MHD stabilization provided by two quadrupolar anchor cell located at each end, outside the region where plugging occurs.

Research is being carried out at present also on the AMBAL-M device at the Budker Institute in Novosibirsk (Annenkov et al. 2016) and on the HANBIT device in Korea (Lee et al. 2007). The large MFTF-B tandem mirror facility at Livermore was mothballed right after the test of various systems in 1986, due to budgetary constraints (Armentrout 2013).

All the experiments above have successfully demonstrated the validity of the TM concept (using both conventional and thermal barrier configurations) and, in particular:

- The effectiveness of electrostatic plugs in suppressing ion end losses (axial confinement time up to 0.7 s was demonstrated in GAMMA-10); detailed measurements performed in TMX-U show very good agreement between experimentally measured electrostatic potential and theoretical predictions;
- At low density, the feasibility of thermal barriers; at high density maintaining a steady-state thermal barrier has not yet been proven;
- The ability to control radial transport by controlling the radial electric field in the central cell; radial ion confinement times >1 s have been demonstrated in GAMMA-10 (with an axisymmetric central cell) and about 0.1 s in TMX-U (with non-axisymmetric central cell);
- The effectiveness of the ambipolar potential to isolate electrons from thermal contact with the outside region, reducing the effective electron parallel thermal conductivity loss; the electron temperature reached values ≈300 eV;
- Maintaining MHD stability by using minimum-B anchor cells;
- Suppressing high-frequency micro-instabilities using sloshing ions and trapped warm plasma.

Encouraging as this may sound, scaling those results to plasma at density and potential ten times higher remains a question mark. Compared with fusion reactors (and taking the central cell parameters), these results still need substantial scaling both in terms of ρ^* (by about a factor 10) and of β (by about a factor 5), whereas the values of the collision parameter ν^* would be similar to those obtained in present devices.

B.3.2.3 Field Reversed Mirror

In a field reversed mirror, see Fig. B.11, the plasma is confined by a ring current of energetic particles (typically induced by injecting neutral beams). If the current in the ring is large enough, field reversal occurs and a "napkin-ring"-shaped configuration is produced where closed magnetic field lines confine plasma. This concept was pioneered by the ASTRON machine (Gormezano 1979), where field reversal was attempted with a beam of particles characterized by orbits of size comparable with the experimental device.

The field reversed mirror has much in common with "compact tori" configurations and will be discussed later.

B.3.2.4 Gasdynamic Mirror

A gasdynamic mirror (Mirnov et al. 1979; Kammash and Emrich 1998), see Fig. B.12, is a mirror configuration

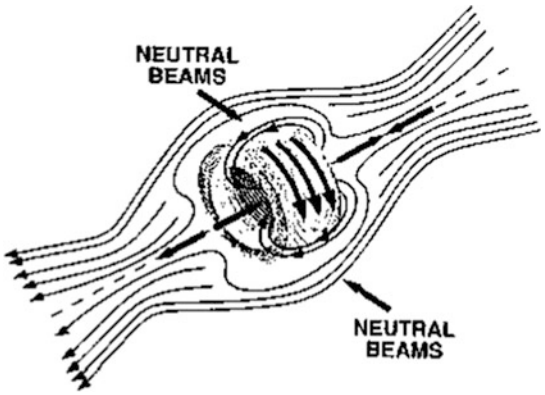

Fig. B.11 Field reversed mirror schematic (Schulze et al. 1990)

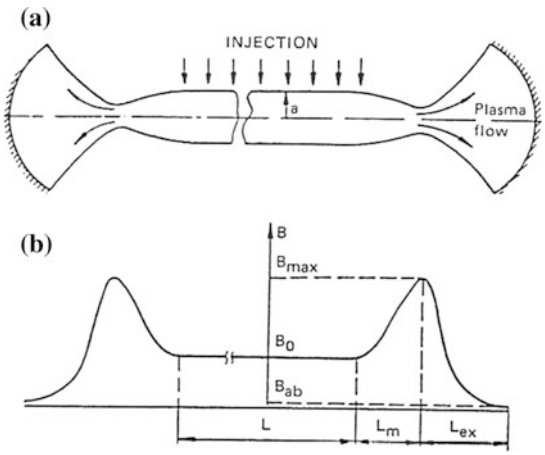

Fig. B.12 Layout of a gasdynamic mirror (Nagornyj 1984) showing **a** magnetic field lines; **b** magnetic field strength on the axis. B_{max}, B_0, and B_{ab} stand for the magnetic field value in the mirror, the solenoid, and the absorber. The parameters L, L_m, and L_{ex} are the lengths of the solenoid, of the mirror, and of the expander, respectively. The parameter a is the plasma radius in the solenoid

characterized by a mean free path shorter than the mirror longitudinal dimension L and by a high mirror ratio ($R > 10$). Due to collision frequency, plasma confined in the trap is very close to an isotropic Maxwellian state. As a consequence, many instabilities, potentially dangerous in classical magnetic mirrors with a collisionless plasma, generally cannot be excited. Moreover, unlike conventional mirrors, longitudinal plasma losses are insensitive to the ion angular scattering rate that might be enhanced by micro-instabilities. Minimizing the curvature of magnetic field lines, that drive plasma instabilities, enables large β. In a gasdynamic mirror, the confinement time τ scales as

$$\tau \approx \frac{L \cdot R}{v_{ti}} \tag{B.69}$$

where v_{ti} is the ion thermal velocity, showing much stronger dependence on the mirror ratio compared to conventional mirrors. Furthermore, confinement time depends on the system size, unlike ordinary mirrors.

The short mean free path constraint can be expressed as

$$v_{ti} \cdot \tau_{ii} \ll L \cdot R \tag{B.70}$$

(note the presence of the factor R). Therefore, short mean free path and high confinement require *long* configurations and *large* mirror ratio. It can indeed be shown that for energy production using D–T, the mirror length should be in the range of 10 km at plasma densities around 10^{21} m^{-3} and mirror ratio $R = 50$. Since the Lawson parameter is proportional to $n \bullet L$, shorter configurations can be achieved only with much higher density. With plasma radius ≈0.1 m, such device would produce power of order 10^1 GW. The neutron power density would be around 10 MW/m^2. Even higher density would reduce size, but would also increase neutron fluence at the wall above currently assumed realistic limits.

At present, the only known gasdynamic mirror in operation is at the Budker Institute in Novosibirsk (Kruglyakov 2002). It consists of a device with a mirror-to-mirror distance of 7 m, magnetic field up to 0.3 T in the midplane and up to 15 T at the mirrors, with a midplane radius of ≈8–15 cm. Oblique neutral beam injection at 15 keV is used for plasma heating up to 4 MW. Fast ions are reflected inside the mirror and density peaks in the outer part of the central cell, where fast ion densities up to 10^{19} m^{-3} have been measured. Target plasma density in the range of (3–20) $\cdot$ 10^{19} m^{-3} has been produced with electron temperature up to 130 eV.

This device demonstrated that MHD plasma can be stabilized in axially symmetric magnetic fields. Flute modes were stabilized by using external axisymmetric anchor cells, where field line curvature was favorable for stability. On-axis β values exceeding 40% were almost entirely associated with the fast ion population.

The gasdynamic mirror has been proposed as a potential volumetric neutron source. When compared with power fusion reactors and assuming the parameters of the central cell, the present results need to be extrapolated (scaled) by about a factor 5 in ρ^*, and 2.5 in ν^*, whereas the values of β would be within 50% of those obtained in the present device.

A second gasdynamic mirror experiment was carried on at the NASA Marshall Space Flight Center (Emrich 2002) to investigate stability limits of this configuration.

B.3.2.5 Other Mirror Concepts

Other mirror concepts have been proposed over the years, such as multiple mirrors (a configuration with many identical mirror cells linked together) and the rotating mirrors (where plasma rotates around the symmetry axis subject to a radial electric field that induces an $\vec{E} \times \vec{B}$ drift in the poloidal direction). These concepts, that are still in a preliminary stage of development but are grounded on physics to a large extent similar to the mirror concepts discussed, will not be further considered here.

Experiments with multiple mirrors were carried on at the GOL-3 facility in Novosibirsk (Kruglyakov et al. 2002).

B.3.2.6 Mirror Studies for Space Propulsion

The tandem mirror has been investigated as a space propulsion system. Here, we consider the study in Kulcinski et al. (1987) for a Space Orbiting Advanced Fusion Power Reactor (SOAR), see Fig. B.13. Although the system was originally proposed only for energy production, its features are similar to those of a propulsion system. Electric power assumed is 1 GW, produced by the D-^{3}He reaction through direct conversion (at 80% efficiency). Power output is 1.9 GW with 70 MW in the form of neutrons. About 470 MW are lost through radiation. The shield is an optimized LiH blanket weighing 300 t and designed to absorb all the rejected heat. The central cell is 73 m long with radius 0.55 m. The estimated total mass is 500 t with $\alpha = 2$ kW/kg. The magnet is axisymmetric and uses NbTi superconducting coils inducing 7.7 T in the central cell, and Nb_3Sn coils inducing 18 T at the choke and 12 T at the end coils. The auxiliary heating power is 70 MW produced with 75% efficiency. Inert mass, added downstream of the reactor which is heated by waste heat, can be expanded to produce additional thrust, see Fig. B.13.

A gasdynamic mirror propulsion system was considered also in Kammash et al. (1995). The reactor has a central cell 50 m long with a radius of 7 cm and a magnetic field of 15 T. The high-density (≈5 $\cdot$ 10^{22} m^{-3}), low-temperature ($T \approx 6.5$ keV) D–T plasma is sustained by the injection of 40 GW of neutral beams with energy 20 keV. The energy confinement time is about 3 ms. The fusion gain is only $Q = 1$. The plasma density produces an extremely high neutron heat load (≈622 MW/m^2), well above values considered for terrestrial fusion power plants (<5 MW/m^2). Taking the already mentioned fluence limit of 15 MW year/m^2, such neutron wall load would limit the duration of full power operation to about 9 days. No reactor layout is provided. The thrust power predicted is 55 GW. The rest of the power (≈36 GW) must be radiated into space; this is the reason for the large radiator mass (≈7200 t), which is the dominant component. For a radiator capable of radiating 5 kW per each kg of mass, the resulting specific power is of order 7 kW/kg. The possibility of using D-^{3}He was also considered in the

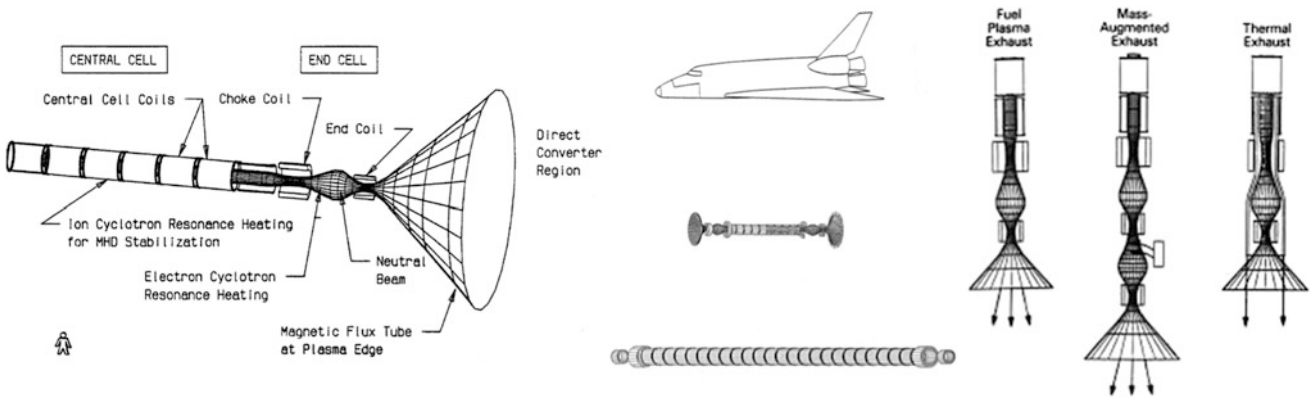

Fig. B.13 SOAR (*left*): conceptual tandem mirror; (*middle*): general configuration of 250 and 1000 MWe versions of SOAR compared to Space Shuttle Orbiter; (*right*): from left to right: ejecting plasma only, adding mass to increase thrust, adding thermal thrust by expanding reactor cooling fluid (Kulcinski et al. 1987)

same study. With the same dimensions and the same gain factor, the magnetic field must be increased up to 18.5 T, the injection energy up to 200 keV, and fusion power to 147 GW. The increase in volume significantly raises the radiator mass (>300,000 t), but specific power is also increased (≈80 kW/kg). Power for the neutral beam is not discussed.

All these figures, and especially those associated with the energy budget, are somewhat inconsistent and, as noted in Chap. 8, should be taken with the benefit of doubt. Certainly, they would deny any chance of funding.

B.3.3 Field Reversed Configurations (FRC)

Compact toroids are configurations characterized by the absence of a mechanical structure shaping plasma. The configuration is "compact" in the sense that plasma extends to the geometrical axis, and the configuration is "toroidal" in the sense that the topology of the closed magnetic surfaces is similar to that of a torus, see Fig. B.14. Ideally, compact toroids combine the good confinement properties of closed toroidal configurations with the simple topology of open magnetic field systems.

Compact toroids consist of two distinct regions:

- A closed field line region inside a magnetic separatrix, with radius r_s,
- An open field line sheath outside the separatrix.

Plasma is confined inside the separatrix surface and exhausted through the open field line region.

Compact toroids can be classified according to two parameters, see Table B.4.

- The ratio between the poloidal magnetic field $\vec{B}$ in the (r– z) plane and the toroidal magnetic field B_θ (along θ);
- the parameter (usually denoted with S) corresponding to the number of ion gyro-radii between the field null and the separatrix; this parameter is related to the inverse of the ρ^* parameter.

Table B.4 shows such classification.

This section describes the field reversed configurations (FRC); the next section is devoted to spheromaks.

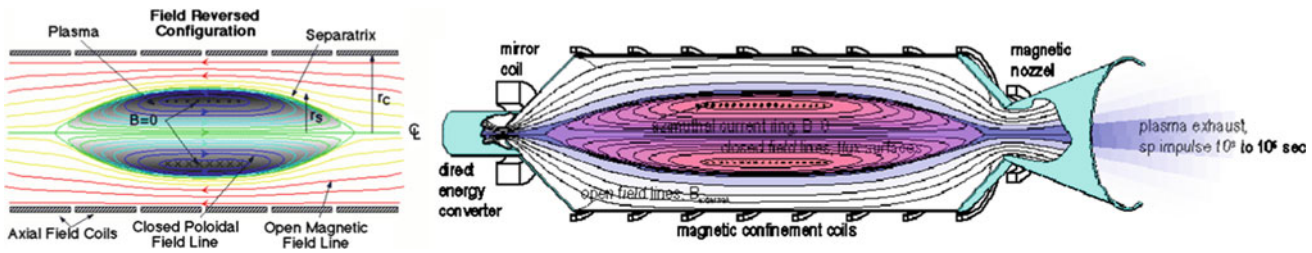

Fig. B.14 Field reversed configuration: a toroidal electric current is induced inside a cylindrical plasma, making a poloidal magnetic field, reversed with respect to the direction of an externally applied magnetic field (*Courtesy* The University of Washington)

Table B.4 Compact toroid classification

	S > 1 (−)	S < 1 (−)
$B \gg B_\theta$	Field reversed configuration (FRC) Field reversed mirror (FRM)	ASTRON
$B \approx B_\theta$	Spheromak Field reversed mirror (FRM)	

B.3.3.1 FRC Formation and Equilibrium

The FRC is a variety of compact toroids with the following characteristics: no appreciable toroidal field, values of β of order unity, no rotational transform, all equilibrium current maintained by diamagnetism, and a scrape-off layer exhausting heat and particles outside the coil system. FRC were reviewed in (Tuszewski 1988).

FRCs were accidentally discovered in the 1960s in θ-pinches. In order to understand the main features of this configuration, it is useful to consider the main formation scheme (the θ-pinch formation), which is illustrated in Fig. B.15:

a. The discharge tube is filled with neutral gas and a bias magnetic field is applied; the gas is pre-ionized freezing the magnetic field in the plasma with a temperature of a few eV.
b. The current in the theta-pinch coils is reversed on a fast timescale, inducing a plasma current along θ (and an axial field *opposite* to the bias field) that causes the plasma and bias field to implode radially.
c. Oppositely directed magnetic field lines reconnect near the end of the θ-pinch coil, forming a closed magnetic field configuration.
d. Large magnetic tension at the reconnection region causes the FRC to contract in the axial direction until an equilibrium configuration is achieved.

During phase (b), plasma heating occurs through a shock followed by slow compression. Ohmic heating also occurs during the annihilation of the bias field and is characterized by resistive dissipation much higher than classical.

The main feature of interest related to FRC is the fact that in order to achieve an equilibrium configuration, the average β of plasma must be high. Simple analytical models (confirmed by detailed numerical simulations) show that

$$\beta = 1 - \frac{r_s^2}{2 \cdot r_c^2} \tag{B.71}$$

with r_s and r_c the separatrix radius and the flux conserver radius, respectively. Since $r_s \leq r_c$, this implies $\beta > 50\%$. Nevertheless, the plasma remains remarkably stable.

The flux ϕ of the axial magnetic field between the null point and the separatrix can be shown to be bound by the two values $k = 0$ and $k = 1$ in the expression for ϕ

$$\phi \equiv \int_R^{r_s} (B \cdot 2 \cdot \pi \cdot r) dr = \pi \cdot r_c^2 \cdot B_e \cdot \left(\frac{r_s^2}{2 \cdot r_c^2} \right)^{\frac{3+k}{2}} \tag{B.72}$$

where B_e is the magnetic field outside the separatrix (determined by the poloidal coil current). From Eq. (B.72), an expression for the parameter S is as follows:

$$S = \frac{\phi}{2 \cdot \pi \cdot r_s \cdot \rho_{ie} \cdot B_e} \tag{B.73a}$$

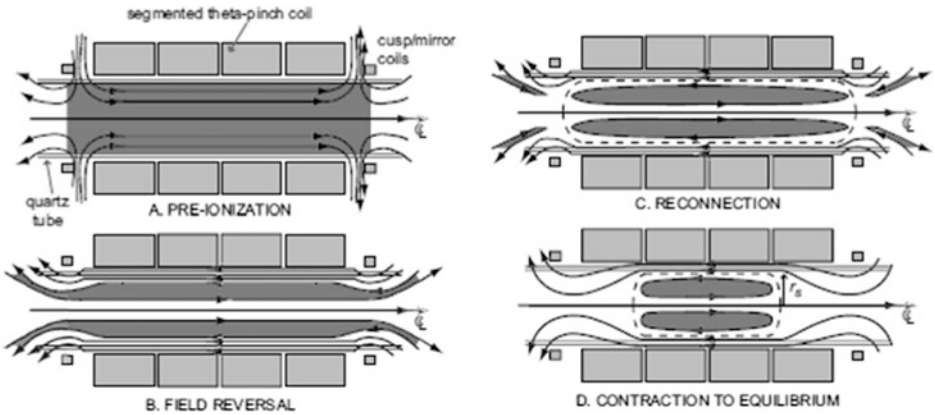

Fig. B.15 FRC formation sequence:**a** Chamber is filled with neutral gas, bias magnetic field is applied, and gas is ionized.**b** Current in θ-pinch coil is rapidly reversed, plasma implodes.**c** Magnetic field lines reconnect.**d** FRC contracts axially to equilibrium configuration (the separatrix radius r_s is shown) (Taccetti et al. 2003)

$$S = 2^{-\frac{3}{2}} \cdot \left(\frac{r_c}{\rho_{ie}}\right) \cdot \left(\frac{r_s^2}{2 \cdot r_c^2}\right)^{\frac{2+k}{2}} \quad \text{(B.73b)}$$

with ρ_{ie} the ion gyration radius ("gyroradius") in the outer magnetic field. Therefore, the parameter S is always lower than the value obtained for $r_s = r_c$ ($\beta = 0.5$ or 50%) and $k = 0$, i.e.,

$$S < \frac{r_c}{5 \cdot \rho_{ie}} \quad \text{(B.74)}$$

B.3.3.2 Open Issues in FRC Research

The main issues of FRC can be synthetically grouped under *stability*, *formation*, *steady operation*, *transport*, and *technology development*. For details, see (Steinhauer 1996).

Stability: FRCs are high- β configurations and might be expected to be MHD unstable. Indeed, a FRC is the toroidal version of the *Z*-pinch that is well known to be unstable for sausage and kink modes in the absence of a longitudinal magnetic field (toroidal in the case of FRC). Contrary to these expectations, current FRC experiments are not limited by known instabilities. Specifically:

- Ideal MHD modes: The most serious instability predicted in FRC is the internal tilt mode which breaks the toroidal flux surfaces and corresponds to the kink mode in a *Z*-pinch (for small plasma elongation, the external tilt mode, which produces a plasma axis "flip" may be unstable). No observation of the internal mode has been reported so far.
- Tearing modes: Tearing modes are observed during the formation phase, but the subsequent equilibria appear to be stable.
- Rotational modes: Following the formation phase, plasma starts to rotate in the ion diamagnetic direction. Although the origin of this plasma rotation is not fully understood, rotation causes new instabilities. The most dangerous is the $n = 2$ rotational instability that can destroy the configuration. A threshold in the ratio $\alpha \equiv \Omega/\Omega_{Di}$ (with Ω the rotation frequency and Ω_{Di} the ion diamagnetic rotation frequency) in the range $\alpha \approx 1.5$ is predicted by theory. The mode is suppressed by applying a multipolar field by external coils with straight or helical windings.

The fact that many instabilities in FRC are predicted, but not actually observed, is not surprising. Several effects can play a stabilizing role:

- The parameter S (the number of ion gyro-radii between the field null and the separatrix) is of order ≈1–2 in current experiments. Under these conditions, several kinetic effects can play a stabilizing role: orbit width comparable with the perpendicular mode wavelength, diamagnetic frequency comparable with the Alfvén growth rate, and finite plasma compressibility. Note also that the MHD model is not adequate in this limit. Thus, the most important question is whether FRC will remain stable also in reactor-relevant conditions, when projected values of S are in the range from 30 to 40.
- The low-beta open field region is MHD stable because of the favorable curvature of the magnetic field lines at the end of the configuration. This effect can help in stabilizing the FRC core.
- The presence of a conducting boundary and of toroidal rotation may also be stabilizing factors.

Although the role of kinetic effects is widely recognized, there is not yet quantitative agreement between experimental results on FRC stability and theoretical analyses. Thus, extrapolating to a next generation of FRC experiments, or scaling, is not yet possible. Since the requirement of larger S (for better confinement) is conflicting with the requirement of bulk plasma stability, it is clear that additional stabilizing mechanisms should be investigated. For example, it has been suggested to produce an energetic ion ring by injecting energetic ions. They would carry most of the equilibrium current and, at the same time, would provide both a stabilizing mechanism and a means to sustain a steady-state configuration. This approach has been already used in the ASTRON device and in field reversed mirror (FRM) experiments and was proposed for the colliding beam fusion reactor (CBFR) discussed below (Rostoker 1993).

Formation: The theta-pinch formation sequence produces FRC on a timescale of a few Alfvén times and would imply large pulsed power when extrapolated to a reactor. Slow FRC formation schemes aim at formation over the resistive timescale (a few orders of magnitude longer) by the Coaxial Slow Source (CSS), the rotamak, the extrap, and the field reversed mirror. These methods are described in Tuszewski (1988). The ability to extrapolate these methods to reactor conditions must still be proven.

An interesting feature of FRC related to their stability is the possibility of translating the configuration along the symmetry axis away from the formation region through a weak gradient in the axial field. This property allows better adiabatic compression heating and physical separation of the high technology formation chamber, from the burn and quench chambers. This is particularly interesting in the context of the so-called magnetized target fusion (MTF) approach (Siemon et al. 1999). The FRC is translated inside a metallic liner which is then imploded on a microsecond timescale (Taccetti et al. 2003). This approach is

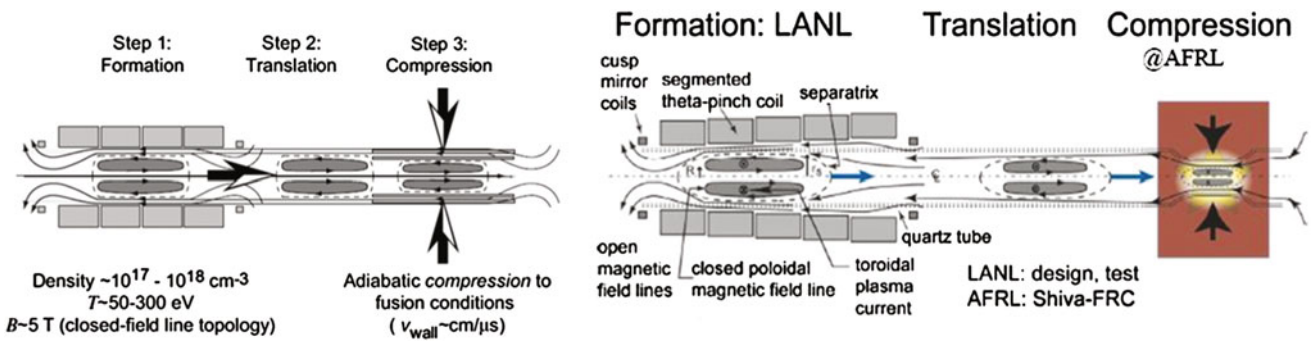

Fig. B.16 Three steps of FRC-based MTF approach (*left*) from Taccetti et al. (2003) and (*right*) (Courtesy of LANL)

intermediate between magnetic and inertial confinement schemes and illustrated in Fig. 3.11 (Fig. B.16).

Steady operation: Present experiments demonstrate that the lifetime of the configuration depends on the rate at which the magnetic flux ϕ initially trapped is dissipated. In order to maintain the configuration in steady-state conditions, several methods have been proposed that need to be tested: (a) rotating magnetic fields (tested only in cold plasmas), (b) neutral beam current drive, and (c) spheromak merging.

(a) In the case of rotating magnetic field (RMF) approach, a current driving a small rotating transverse field component is generated by oscillating currents driven in longitudinal conductors located near the wall. Under certain frequency and collision conditions, the transverse field penetrates the plasma and drives an electron current in a manner similar to an induction motor. This method has been proven only in cold devices called rotamaks. Experiments are ongoing to demonstrate its applicability to hot plasmas.
(b) Neutral beam injection experiments could sustain the configuration for times much longer than 1 ms. Injection of 100 A, 30–60 kV beams would also induce plasma rotation with velocities of the order of the Alfvén velocity, the velocity of propagation of magnetohydrodynamic waves in plasma and equal to $B/(\mu_0 \cdot \rho)^{1/2}$. As already noted, beam particles could also play a stabilizing role. This approach, also used in the CBFR, has been used in field reversed mirrors (FRMs).
(c) Spheromak merging has been shown in the TS3 device to produce a FRC configuration if the two spheromaks have opposite helicity (see later).

Transport: Turbulent transport has been observed in FRC. Turbulence affects not only the cross-field particle and energy transport, as in the tokamak, but also the decay of the poloidal magnetic flux (attributed to anomalous resistivity). In the scrape-off layer, anomalously slow particle outflow has been also detected.

Some basic understanding exists only for the cross-field particle/energy transport, which is consistent with the expectation of low-frequency drift-wave turbulence. Several small-scale instabilities have been proposed as explanations: (a) the lower hybrid drift instability, (b) micro-tearing modes driven by electron temperature gradient, and (c) Kelvin–Helmholtz instability driven by shear. Classical losses associated with unconfined particles in velocity space (similar to those in the simple mirror configuration) in the region close to the separatrix have been also proposed. Current diagnostic capabilities can determine, with reasonable accuracy, the particle confinement time τ_N. Particle losses appear to account for 60–80% of the energy losses, the remainder being associated with radiation and thermal conduction. Measured τ_N is in the range from 10 to 200 μs, scaling linearly with the parameter $R^2/\rho_{i.e.}$, as shown in Fig. B.17, with

$$r_s = \sqrt{2} \cdot R \tag{B.75}$$

This empirical scaling is more or less consistent with theoretical scaling derived from quasi-linear estimates of the turbulent transport and clearly shows the apparently conflicting requirements of stability (low S) and good confinement (high S). Classical transport is not consistent with the observed trends, although the ratio between experimental and classical value of confinement time can be as low as 3. As to the characteristic decay time of the poloidal flux, the comparison between the experimental value and that derived

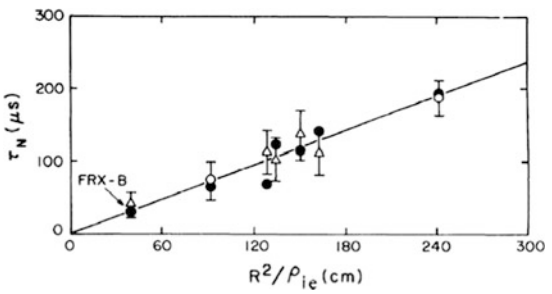

Fig. B.17 Scaling of particle confinement time

from the classical Spitzer resistivity shows a discrepancy ranging between 2 and 20, suggesting the presence of substantial turbulence effects. Finally, we note that changes in the turbulence regimes (and therefore in global transport) may be expected for larger values of S.

Technology development: A research program pursued as a joint effort between the University of Washington (UW) and Los Alamos National Laboratory (LANL), aimed at developing the best method to generate rotating magnetic fields, included the following: (1) design and construction of a suitable high-power RF source and drive coils capable of a pulse longer than 1 ms; (2) demonstration of the RMF technique in a plasma column of moderate size (0.5 m diameter and 1.5 m length); (3) investigation of alternate and more efficient methods for generating higher power RMF.

B.3.3.3 Present FRC Experiments

Parameter ranges achieved so far in the various FRC facilities range from $5 \cdot 10^{19}$ to $5 \cdot 10^{21}$ m^{-3} in plasma density, 3 keV ion temperature and 0.5 keV electron temperature, and β in the range from 0.75 to 0.95. The high values of plasma density are particularly remarkable, although obtained in first-generation and short duration experiments. As the configuration lifetime increases, the trend is toward lower density. Typical values of r_s/r_c are in the range from 0.4 to 0.6, although values up to 0.9 have been achieved. Elongations in the range from 3 to 10 have been obtained. Values of the Lawson parameter $n \bullet \tau$ as large as 10^{17} m^{-3} s have been obtained.

Research in FRC is carried out mainly in the USA, Russia, and Japan. The main facilities are listed below:

BN (TRINITI Research Center, Troitsk, Russia): This facility (L = 0.9 m, r_c = 0.21 m, B = 0.45 T, τ = 50 μs) has investigated improved control techniques, internal magnetic field structure, and electron energy distribution. It has been used also to form different magnetic configurations (spheromak and tokamak).

TL (TRINITI Research Center, Troitsk, Russia): This facility uses independent active end-control coils for dynamic formation and has investigated start-up methods with different timescales.

TOR (TRINITI Research Center, Troitsk, Russia): This facility (L = 1.5 m, r_c = 0.3 m, B = 1 T, τ = 100 μs) has investigated the intense heating taking place at start-up.

NUCTE-3 (Nihon University, Japan): This facility (L = 2 m, r_c = 0.16 m, B = 1 T, τ = 60 μs) has investigated global modes dynamics and control of the separatrix shape by auxiliary coils. The effect of a multipolar field on stability and confinement has also been investigated.

FIX (Osaka University, Japan): By using a theta-pinch source, this facility generates FRCs that are then translated to a large chamber where they expand. The density drop following expansion (to $5 \cdot 10^{19}$ m^{-3}) enables neutral beam injection (Okada et al. 2005).

TS-3/TS-4 (Tokyo University, Japan): The TS-3 facility has been employed for the formation of a variety of magnetic configurations (FRC, spheromaks and ultra-low aspect ratio tokamak). The FRCs have been formed by counter-helicity merging of two spheromaks (see below about helicity). TS-3 was later upgraded to the TS-4 facility (Kawamori et al. 2005).

LSX/mod (The University of Washington, USA): This is the largest FRC facility in the world (L = 5 m, r_c = 0.9 m, B = 0.8 T). It was converted to the TCS facility (with a confinement chamber at the end of the translation section) to perform experiments on controlling the separatrix shape and to start up and sustain rotating magnetic fields (Hoffman et al. 2005). This facility should provide information on MHD stability at larger S (lower ρ^*). The STX facility at the University of Washington, USA (L = 3 m, r_c = 0.4 m, B = 0.2 T), also renamed the Star Thrust Experiment (Miller et al. 1998), was partially funded by NASA to investigate applications to space propulsion such as with rotating magnetic fields. Very powerful (but short-lived) rotating magnetic fields were used to overcome ionization and radiation barriers that have, so far, limited the use of this technique to low-temperature plasmas.

MRX/SPIRIT (Princeton, USA): The Magnetic Reconnection Experiment (MRX) can generate spheromaks, low aspect ratio tokamak, and FRC. SPIRIT is a proposal to investigate MHD stability and confinement over a wide range of S (1–15) and elongation ($0.5 < 0.5\ r_s < 4$). In the future, neutral beam injection could be tested.

FIREX (Cornell University, USA): The Field-reversed ion ring experiment injects an ion beam from a diode through a magnetic cusp, which forms an ion ring that should carry a large fraction of azimuthal current and provide stability.

ROTAMAK (Flinders University, South Australia): In this facility, spherical FRCs have been produced and sustained for up to 40 ms using up to 200 kW of rotating magnetic field power. The amount of drive current is limited by available power.

FRX-L (Los Alamos) is a compact plasma injector to study high-density FRC formation, stability, and translation physics. This facility is preparing for its eventual use to demonstrate the physics of magnetized target fusion. Very high average densities (up to $4 \cdot 10^{22}$ m^{-3}) have been achieved with a (ion plus electron) temperature of 500 eV. Liner implosion tests have been carried out without plasma (Taccetti et al. 2003).

This short survey shows the variety of problems that have emerged in attempting to exploit fusion power. It is, at the

same time, daunting and indicative of the magnitude of future efforts still required in the future.

B.3.3.4 FRC for Space Propulsion

FRC reactors for space propulsion have been first proposed in Chapman et al. (1989) using D–^{3}He fuel. Thrust is assumed to be obtained by using a magnetic nozzle, where plasma is flowing along the open field lines while being mixed with inert propellant, see Fig. B.18. The design was largely based on the conceptual design of the land-based power plant SAFFIRE (Miley et al. 1978).

The example considered in Chapman et al. (1989) foresees the use of a 5 T magnet confining plasma in an 80 m^3 volume with a plasma radius of 1.5 m. With 2 s confinement time and $\beta \approx 76\%$, power is ≈0.5 GW. Note that the parameter S for such a configuration would be around 50, well above present values.

More recently, a colliding beam fusion reactor (CBFR) space propulsion system has been proposed (Cheung et al. 2004), which is shown in Fig. B.19.

The reaction is p–^{11}B (although also D–T and D–^{3}He reactions have been considered). The CBFR (Rostoker et al. 2003) is an evolution of the ion ring concept already introduced. Neutral beams are injected to produce a current that sustains the configuration. Electrons are confined by the radial electric field determined by the plasma-fluid radial force balance. Fusion products escape confinement and, to maintain charge neutrality, extract electrons with sufficiently high energy to climb the electrostatic potential well. This cools the electrons and reduces bremsstrahlung. The beams tend to thermalize, and this effect must be compensated for by continuous injection which requires a significant amount of re-circulating power (around 50% for p–^{11}B fuel).

The CBFR for space propulsion has a chamber 6.9 m long with a 0.6 m radius. The external magnetic field is about 0.5 T. The reactor generates about 77 MW of fusion power ($P_{spec} \approx 20$ MW/m^3) and needs 50 MW of injected power for steady-state operation. A direct energy converter intercepts

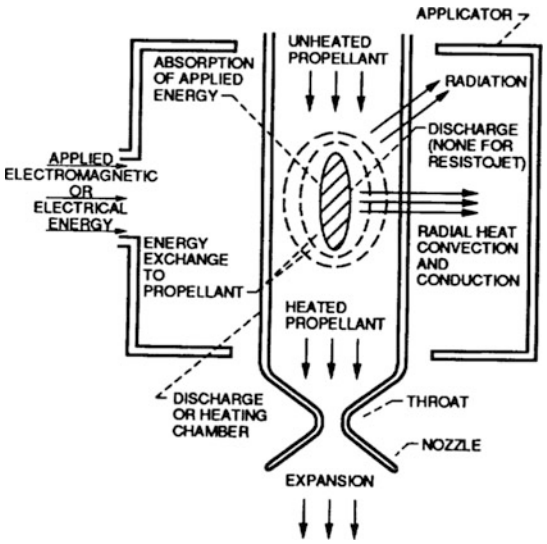

Fig. B.18 FRC propulsion concept from Power and Chapman (1989)

approximately half of the alpha particles, decelerates them by an inverse cyclotron process, and converts directly their energy to electricity. The remaining alpha particles are ejected as propellant and produce thrust. Direct energy conversion yields about 38.5 MW of electrical power. The remaining 11.5 MW are produced from bremsstrahlung losses by a thermoelectric converter (4.6 MWe out of 23 MW). The fraction not converted is fed to a Brayton cycle heat engine that supplies the remaining 7 MW. Waste heat (11 MW) is rejected to space. The mass budget is shown in Table B.1. The resulting specific power α is about 3 kW/kg.

A propulsion system based on the magnetized target fusion (MTF) approach has been proposed in Thio et al. (1999). A pair of conical theta-pinches produce a compact torus (either a FRC or a spheromak) that is imploded by a spherically converging plasma liner deposited by a number of plasma jets. The liner is compressed to very high density and forms an inner fusion fuel layer responsible for the main fusion yield, and an external layer, made of hydrogen, that

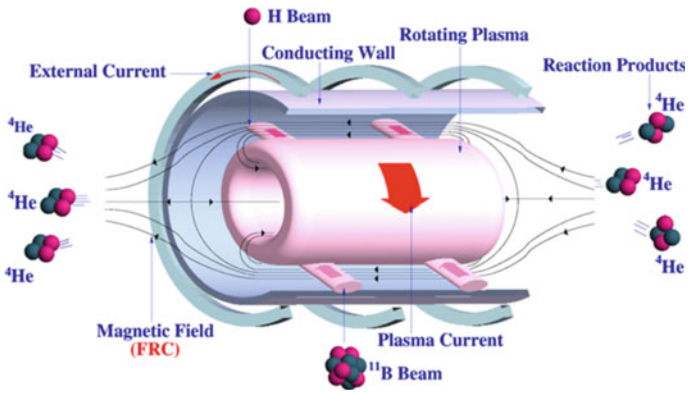

Fig. B.19 Colliding beam fusion reactor (CBFR) space propulsion system (Cheung et al. 2004)

slows down the neutrons, absorbing and converting 95% of their energy in charged particle energy. The spherically expanding plasma produced in this way is squeezed into an axial jet by a pulsed magnetic field. High conversion efficiency to direct thrust was foreseen, but no actual test was attempted. This system evolved into architectures already discussed in Chap. 8.

At least on paper, this is a compact system. Higher radiator efficiencies, up to about 50 kW/kg, were assumed in this study and explain the reasonable radiator mass. Reactor weight was estimated to be only 41 kg for 25 MW power output. Therefore, the resulting specific power is astonishingly high, about 400 kW/kg, dropping to about 100 kW/kg using more conventional figures for the radiator mass. The key to such a result is the *assumed* high fusion power density typical of the MTF approach, and the percentage of conversion of neutron power to charged particle power in the liner, that reduces the power to be radiated away. Such proposal was and still is at the conceptual stage, and its feasibility can only be assessed after evaluating future experimental results coming from other magnetize target fusion (MTF) facilities, such as FRX-L.

B.3.4 Spheromaks

A spheromak reactor has a toroidal configuration not shaped by either solid walls or magnetic field. In this respect, a spheromak is similar to the FRC. Unlike the FRC, poloidal and toroidal field strengths are approximately equal. Spheromak research has been reviewed in Jarboe (1994).

Spheromaks are relaxed configurations verifying Taylor's minimum energy principle (Taylor 1976). According to such principle, the magnetic configuration tends to relax to a state which minimizes the magnetic energy

$$U \equiv \int \mathrm{d}V \cdot \frac{B^2}{2 \cdot \mu_0} \tag{B.76}$$

with the constraint of constant helicity

$$K \equiv \int \mathrm{d}V \cdot \vec{A} \cdot \vec{B} \tag{B.77}$$

with $\vec{A}$ being the vector potential and

$$\vec{B} = \nabla \times \vec{A} \tag{B.78}$$

the magnetic field (the integral is over the plasma volume). Minimizing U with the constraint K = const. leads to the equation

$$\nabla \times \vec{B} = \lambda \cdot \vec{B} \tag{B.79}$$

with λ being a global constant (it can be shown under simplified assumptions, that minimizing U corresponds to maximizing entropy). The solution of Eq. (B.79) is a force-free state

$$\vec{J} \times \vec{B} = 0 \tag{B.80}$$

The minimum energy principle has been successfully applied to the description of the reversed field pinch equilibrium, a plasma configuration which has several features in common with spheromaks. Note that, strictly speaking, relaxed states by definition have zero pressure gradient and are therefore irrelevant in plasma confinement. In practice, these configurations depart from a truly relaxed state and have finite pressure gradients.

B.3.4.1 Spheromak Formation

Six different schemes are currently employed for spheromak formation: (1) the flux core, (2) the θ-pinch, (3) the z-pinch, (4) the coaxial source, (5) the conical θ-pinch, and (6) the kinked z-pinch. All are described in Jarboe (1994). Only the coaxial source is reported here since it produces the best quality spheromaks (toroidal plasma current 1 MA, peak magnetic field 3 T, electron temperature 400 eV, plasma density close to 10^{20} m^{-3}, and energy confinement time 0.2 ms following a 10 ms pulse). For reference, the layout of the CTX experiment is shown in Fig. B.20. The formation sequence is shown in Fig. B.21.

Referring to the image on the left shown in Fig. B.21, the coaxial source is constituted by a pair of coaxial electrodes. Initially, a magnetic flux penetrates the inner electrode. A plasma gun injects gas between the electrodes that ionizes, forming a plasma frozen in the initial magnetic field. The electrode current is increased and, above a certain threshold, the plasma and magnetic field are ejected from the source into the flux conserver. After the coaxial current drops below a threshold value, the fields between the source and the spheromak reconnect and an isolated spheromak are formed.

The coaxial source can be also used to maintain steady-state conditions in the spheromak configuration that otherwise would decay due to dissipation in the plasma. Note that the whole magnetic configuration, including the toroidal current in the plasmoid, is sustained although the electric field produced by the gun is in the poloidal direction, namely orthogonal to the driven current. A similar situation arises in the reversed field pinch system (Bodin and Newton 1980) where a poloidal current associated with field reversal is maintained by a toroidal electric field. The generation of the magnetic field by the plasma is due to the so-called dynamo mechanism, which is typically a turbulent process. The drawback of this process is the generation of stochastic magnetic fields that can substantially reduce the confinement properties of these configurations.

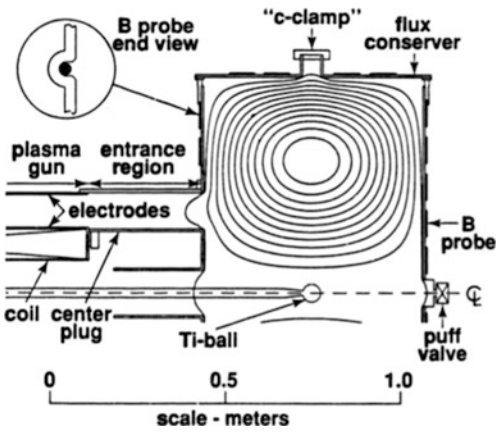

Fig. B.20 Layout of the CTX experiment showing a formed spheromak (Jarboe 1994)

B.3.4.2 Stability Limits of Spheromaks

The spheromak is generally considered a low- β configuration. However, experimental values of β in excess of 20% have been obtained, above the Mercier limit, i.e., the β limit for flute-like interchange modes (Jarboe 1994).

The most important unstable modes are briefly summarized below:

- Tilt modes: The dipole moment of a spheromak in a vertical field is antiparallel to the magnetic field. Hence, in a uniform magnetic field, the spheromak will tend to flip its axis to make the dipole moment parallel to the vertical field. The mode can be stabilized in a mirror field, but then the shift mode becomes unstable. If the equilibrium is provided by the flux conserver, instead of a vertical field, the axisymmetric solution is stable for oblate flux conservers (i.e., for a cylindrical flux conserver, if the length of the cylinder is lower than 1.67 times the radius).
- Current-Driven modes: Current-Driven modes may become unstable when the $J|/B$ radial profile ($J|$ is the current density component parallel to the equilibrium field) departs from a constant, which correspond to the minimum energy state predicted by theory ($J| = \lambda \cdot B$ from Eq. B.79). Internal current-driven modes have been observed in good agreement with the theoretical predictions.
- Pressure-driven modes: The spheromak has unfavorable flux-surface averaged curvature everywhere. Ideal interchange instability can arise if the Mercier criterion is violated.

It should be noted that many spheromaks have been modified by inserting a central conductor, making this configuration evolve toward an ultra-low aspect ratio tokamak. Such a modification is especially beneficial to stabilize the tilt mode (which is opposed by the presence of a central conductor). Whether such modified topology can still be of interest for space propulsion should be further investigated.

B.3.4.3 Confinement

Confinement in spheromaks is supposed to be heavily affected by the plasma turbulence that produces the dynamo effect, just as in reversed field pinches. The largest value of the energy confinement time (≈0.2 ms) has been obtained many years ago on the CTX reactor (Jarboe 1994). The local diffusivity is consistent with the expression, derived first by Rechester and Rosenbluth (1978), for the collisionless diffusion of a test particle in a stochastic magnetic field.

At this stage, it is unclear whether poor energy confinement is an inherent feature of spheromaks. As noted, relaxed configurations are sustained by the generation of magnetic

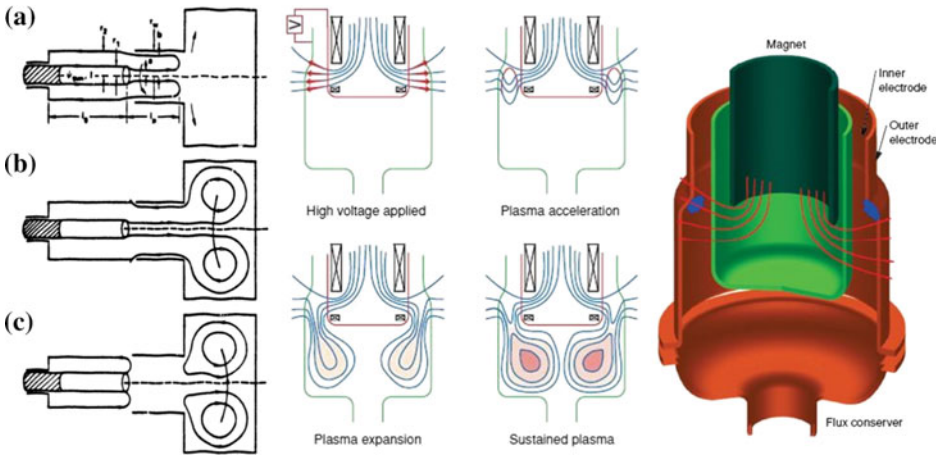

Fig. B.21 Spheromak formation sequence: *left* by coaxial plasma gun (Turner et al. 1983); (*middle and right*) LLNL's SSPX unit [Courtesy of LLNL]

fields through the dynamo process. Such mechanism can produce stochastic magnetic field lines and very poor confinement. The main issue to keep energy confinement at an acceptable level is therefore to keep the dynamo mechanism running with the minimum amount of turbulence. It should be noted that encouraging results have been obtained in recent years in several reversed field pinch experiments, where transport has been successfully reduced by controlling the level of plasma turbulence (Sarff et al. 2002). For example, when the so-called Quasi-Single-Helicity (QSH) states are produced (i.e., when turbulence with a given helicity component dominates), the volume of plasma filled with stochastic magnetic field lines is reduced and, as a consequence, confinement is improved.

B.3.4.4 Recent Experiments

The Sustained Spheromak Physics Experiment (SSPX) carried on at Livermore (Wood et al. 2004) had the primary goal of testing whether a favorable energy confinement scaling can be obtained in spheromak plasma sustained by coaxial helicity injection. Plasma temperature in the range of 200 eV and plasma density $\approx 10^{20}$ m^{-3} were reported, with confinement times around 0.2 ms. The plasma radius was about 0.23 m, and the discharge lasted up to a few ms.

Results from the Swarthmore College Spheromak Experiment (SSX), in operation since 1996, showed that spheromak formation is governed only by gun physics and is independent of the flux conserver dimension (Brown et al. 2009).

The SPHEX experiment (Rusbridge et al. 1996), conducted at the University of Manchester from 1989 to 1997, focused on the following: (a) partition of plasma into a high electric field central column and a low electric field toroidal annulus; (b) investigating the global (n = 1) mode responsible for carrying energy and helicity from the central column to the annulus; and (c) the MHD dynamo driving the current in the annulus. In the last years of activity, the reactor was equipped with a central rod to improve stability.

B.3.5 Levitated Dipole

The last concept to discuss is the magnetic dipole. So far receiving limited attention, theoretical analyses show it potentially capable of producing high- β plasmas (Hasegawa 1987).

Astrophysical observations indicate that the equilibrium configuration, consisting of a simple dipole field, exhibits remarkable MHD stability properties (for instance, β exceeds unity in the Jupiter magnetosphere). Interchange modes can indeed be shown to be stable if the pressure profile decreases sufficiently slowly toward the low field region. Furthermore, if the equilibrium density and temperature gradients are sufficiently weak, as required by MHD stability, these free energy sources are incapable of driving small-scale instability. The unwanted consequences of turbulent transport may be expected to be benign. In particular, the diamagnetic frequency tends to be smaller than the magnetic drift frequency, resulting in a strong stabilizing effect (Kesner et al. 1998).

A dipole configuration is produced by a large central coil levitated against gravity or local acceleration by a set of other coils that create a vertical field, see Fig. B.22. The combined field produces a magnetic separatrix. Outside the separatrix, a natural divertor configuration is formed. The presence of a magnetic separatrix can enhance MHD stability close to the separatrix and also by locally destabilizing drift waves, although the latter could also be stabilized by edge sheared flows similar to those observed in tokamak in conjunction with improved confinement regimes.

Very little is known experimentally about dipole configurations. The Levitated Dipole Experiment (LDX), a facility with a superconducting ring of 0.4 m radius built at MIT (Kesner et al. 1998), aimed at exploring plasmas at 300 eV temperature and up to 10^{18} m^{-3} density. LDX operation began at the end of 2004.

The use of an internal coil surrounded by plasma is the major drawback of the dipole configuration, since no external cooling (or power feed) is feasible. Following an early suggestion by John F. Dawson (Department of Physics, University of New Hampshire, Durham, New Hampshire), the assumption usually made is that radiative cooling from the ring surface balances the heat input to the ring (from radiation, heat conduction, and neutrons). The

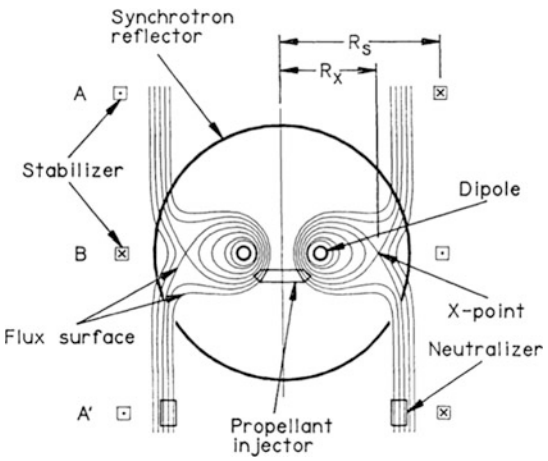

Fig. B.22 Levitated dipole reactor propulsion scheme from Teller et al. (1992)

power needed to cool the superconducting ring may be extracted from this heat flux by different energy conversion schemes. Note that since the surface heat temperature is limited by structural materials (e.g., 2700 K for tungsten), the above assumption sets a limit on the power that can reach the ring surface and therefore on the fusion power per unit volume.

A space propulsion application of levitated dipoles has been considered in Teller et al. (1992). This levitated dipole scheme has as major and minor radii 6 and 2 m, respectively. The magnetic field on the conductor is 15 T. The total fusion power (using D–^{3}He fuel) is 2 GW, with 60% available for thrust. With a total ring mass of 1180 t, the resulting specific power is close to 1 kW/kg, too low for space propulsion. Improvements may come from optimizing the coil mass and from new materials capable of higher surface temperature and radiated power, for instance ternary ultra-high-temperature ceramics (UHTC), a class of refractory ceramics that offer excellent stability at temperatures exceeding 2000 °C (2273 K).

The design of the superconducting coil includes a 1-mm-thick tungsten surface layer, capable of radiating 1 MW/m^2 at 2700 K, for a total radiated power of 400 MW, followed by a shield of C–C fiber composite (about 30% of the total ring mass) that reduces by 90% the neutron flux (the total neutron power is about 60 MW). This first shield is thermally insulated by a second shield consisting of a steel structure containing two layers of B–H_2O (with a radial width/working temperature of 0.24 and 0.66 m/300 K, respectively), reducing the neutron flux by a factor 5600. Only 467 W reach the superconducting magnet working at 4.2 K. Extracting heat from these sources of power at their working temperatures, and feeding it to the surface temperature (at 2700 K), requires, ideally, about 10 MW of electric power, available by converting the 400 MW of input power to the ring.

This visionary concept needs much in-depth work.

B.4 Further Issues in Investigating Fusion for Space Applications

B.4.1 Technology

A number of assumptions made in this study are based on zero-order physics awaiting further refinements, as discussed below.

Low-mass breeding blanket: The blanket (together with the magnet) is one heavy component of the reactor core. Research performed for the SOAR concept has pointed out that mass is minimized by using LiH blankets. On the basis of the experience gained in the last ten years in design and R&D of blankets for fusion reactors, neutronic and thermal analyses to assess the potential of this solution are in order.

Low-mass magnet: The magnet competes with the blanket for the heaviest reactor component. Detailed designs exist for magnets to be used in tokamak reactors, but these implementations have not considered the constraints arising from the low mass requirements of space applications. A superconducting and a cooled copper magnet for open magnetic field configurations should be designed to benchmark the (sometimes questionable) figures found in generic fusion rocket studies. High-temperature superconductors should be considered.

Auxiliary heating systems and cryoplant: All fusion concepts investigated rely on auxiliary systems for heating plasmas and on cryoplants to cool superconducting magnets. The assumptions made, for the sake of illustration in generic fusion rocket studies (1000 kg per kW of heat extracted for the cryoplant, and 2.5 kg per kW of auxiliary power), need definitely to be verified and consequences appraised. Significant R&D has been carried out in international fusion programs on heating methods (neutral beam injection, ion cyclotron resonance heating, and electron cyclotron resonant heating). The capability of low mass systems should be investigated together with high efficiency power generation.

Radiator: Typical figures for the radiator specific power (also called "radiator efficiency") used in propulsion studies are in the range of 5 kW of radiated power for each kg of radiator mass. Since also the radiator may become the heaviest propulsion component, its mass should be minimized. Values in the range of 100 kW/kg can be envisaged. Radiator efficiency depends on cycle temperature and material. Temperature should be the highest compatible with cycle efficiency and material structural limits. At this, industrial practice for space power generation assumes "low" cycle temperatures of order 800–900 K. If sufficiently large power is available, there is no reason why the "low" temperature could not be raised to 1200 °C without structural problems, substantially reducing radiator mass. This may be accomplished with nitride and carbide composites already available, but has never been tested: Experience with large space power generators (say, >20 kW) is essentially nonexistent. Nuclear space power generation will, in fact, have substantial impact on radiator technology. In any event, it seems advisable to investigate how to better exploit rejected heat prior to its disposal via a radiator, for instance, by utilizing thermionics or other more advanced physics. An assessment of the available technology is in order.

Thermal converter: Although the converter is typically not the heaviest component of the system, mass estimates cover a broad range.

Direct converter: A review of the present status of direct conversion could provide better estimates of efficiencies and mass budgets.

Vacuum vessel/first wall: In current fusion experiments, the mass of the vacuum vessel is not negligible. Space propulsion applications must be light and avoid massive radiators. A possible solution is an electrically conducting wall (made by Mo, graphite, or advanced carbon fiber) 50–70% transparent to bremsstrahlung and neutrons. Such solution should be investigated.

Magnetic nozzle: The conversion of high-energy charged particles into thrust depends on the design of the magnetic nozzle. Proposed schemes should be critically reviewed in order to identify reasonable values for the conversion efficiency and point out possible problems in the magnetic nozzle design.

B.4.2 Specific Design Studies

Colliding beam fusion reactor: FRC as a background neutralizer for nonthermal schemes, releasing fusion power by beam-beam reactions (CBFR), has been proposed also for propulsion (Cheung et al. 2004). Parameter optimization should be investigated for space propulsion applications, also by critically reviewing conventional plasma dynamics assumptions.

Spherical tokamak: The spherical tokamak is a closed configuration. Extracting high-energy particles from the reactor and toroidal magnet to produce thrust is not trivial, although probably less difficult than in conventional tokamak equipped with heavy magnets. Nevertheless, existing medium-scale experiments have already shown the significant potential of spherical tokamaks for energy production. Specific design studies, see Williams et al. (1998), exist for space propulsion systems based on spherical tokamaks, although the issue of particle extraction is not addressed in detail. The aim of future studies should be to design a divertor configuration capable of extracting particles from the reaction chamber, possibly looking at very low aspect ratio ($R/a \leq 1.5$) equilibria.

Levitated dipole coils: As discussed in the previous section, the levitated dipole coil must comply with the following requirements: high surface radiation (e.g., high surface temperature), good neutron shielding of the superconducting magnet, efficient energy conversion of the incoming heat into electricity to cool the system cooling, and low total mass. Present designs are only conceptual, and further assessments could set a limit on the coil mass (and therefore on the foreseeable specific power).

B.5 Fusion Propulsion Performance

The performance of fusion propulsion systems can be estimated by using the same approach and equations as introduced in Sects. 7.19 and 7.20. The basic trade-offs are the same, except conceptually power may be scaled up by a few orders of magnitude. It is assumed also that inert propellant is added to the propulsion system in some way to increase thrust. The spacecraft mass M (or M_{TOGW}) was chosen either 100 or 1000 t (the latter clearly an upper bound for many decades to come).

The analytical solutions in Sects. 7.19 and 7.20 are the result of having assumed, for simplicity, that the propellant mass can be neglected compared to M, and that the trajectories are composed of an accelerated segment to midcourse, followed by deceleration to final destination (ΔV for orbit capturing has been neglected in this approach).

In order to show the potential and limitations posed by these powered trajectories, consider propulsion solutions for a nominal Earth to Mars mission (average Earth to Mars distance, d, is assumed here $1.5 \cdot 10^8$ km). For the purpose of illustration, the round-trip distance d is then doubled to $3 \cdot 10^{11}$ m.

The matrix of input data is as follows: $M = 10^2$ and 10^3 t; $I_{\mathrm{sp}} = 10^5$, 10^6, and 10^7 m/s; and thrust power $P = 1$, 10, and 100 GW. The results are presented in Fig. B.23, plotting on log–log scales propellant mass consumed (m), acceleration time (t_{acc}), and ΔV (Δv in the figures) as a function of I_{sp} (in m/s) for spacecraft of mass $M = 100$ t (left) and $M = 1000$ t (right). Generally speaking, these results show the positive effect of I_{sp} on propellant mass consumption, and its negative effect on time to accelerate (trip time) and ΔV. In fact, at fixed power, increasing thrust comes at the expense of decreasing I_{sp}, so it takes longer and longer to reach smaller and smaller ΔV.

The curves show the sharp reduction of consumed propellant m by increasing I_{sp}. With a modest $I_{\mathrm{sp}} = 10^5$ m/s and for the larger spacecraft, the mission is doable *and* practical with thrust power $P = 1$ GW. The smaller spacecraft with $M = 100$ t case is not doable under the assumptions made, because m becomes of the same order of the spacecraft mass M.

At the intermediate $I_{\mathrm{sp}} = 10^6$ m/s, both spacecraft can perform the mission in reasonable times, the best being the case $M = 100$ t and $P = 10$ GW. Achieving the highest I_{sp} (10^7 m/s) would be very challenging, but if feasible such I_{sp} would enable missions with only 100 GW power. Scaling of open magnetic fusion reactors/thrusters is not established with the same level of confidence compared to tokamaks. Then, assuming this power would imply solving a host of

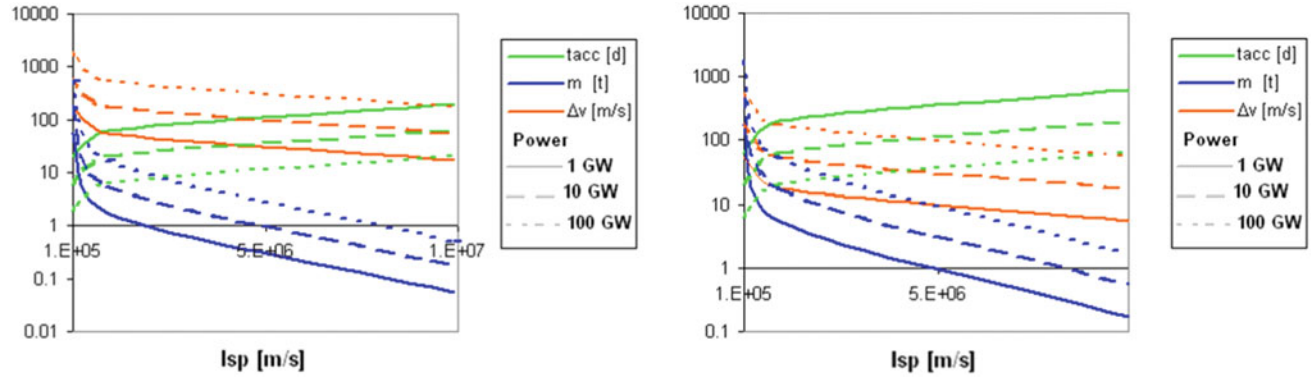

Fig. B.23 Spacecraft velocity increment, acceleration time and propellant consumed as a function of I_{sp} for **a** 100 t spacecraft (*left*) and **b** 1000 t spacecraft (*right*)

problems related to how to design, build, and operate such reactors.

From this first-order example, it seems that a preliminary design of a fusion rocket for a fast Mars mission would require thrust power of order 10 GW with an I_{sp} of order 10^6 m/s and a spacecraft mass of order 100 t. Since the trip would last no longer than 20 days, this mass may be adequate *if* the reactor can be made sufficiently compact and light. If that was not feasible, and mass must be of order 10^3 t, a practical "fast" Mars mission is possible only with a modest $I_{sp} = 10^5$ m/s rocket using 1 GW power.

B.6 Conclusions

Preliminary as they may be, some conclusions may be drawn from this analysis of magnetically confined fusion reactors as high-power propulsion systems candidates.

The mirror configuration may have some potential to become a future propulsion system. Indeed, its geometry allows converting 50% of fusion power to direct thrust power, and the rest to electricity by direct conversion *if* advanced fuels are employed. Significant values of β can be achieved with advanced fuels. Two main concepts were discussed in some detail. In this context:

- Feasibility of the tandem mirror (TM) concept has been experimentally proven in many devices. However, TM requires sophisticated techniques to tailor the plugging potential and has been limited so far to low-density operation.
- The gasdynamic mirror (GDM) concept is intrinsically simpler than the tandem mirror, but requires either very long, bulky, and *massive* systems, or very high-density plasma. This may raise the neutron flux at the wall beyond what is achievable within a medium-term material development program for fusion applications. A GDM design for a specific propulsion system (possibly based on ongoing efforts to design a volumetric neutron source) could be undertaken now. The goal would be to assess the potential of GDM using assumptions, data, and technologies far more realistic than so far found in the literature surveyed.

Field reversed configurations (FRC) can also produce either direct thrust or direct conversion to electrical power. Their main appeal is the possibility of achieving $\beta > 50\%$. However, stability of the configuration observed so far only at large ρ^* must still be demonstrated at (normalized) Larmor radii ρ^* of interest for energy production. Due to the very early stage of this line of research, it is difficult to predict global confinement. These configurations might be used in conjunction with nonthermal fusion schemes, for instance with a colliding beam fusion reactor. Such scheme might simultaneously solve the plasma formation/sustaining problem, and it might benefit from the presence of a population of fast ions to maintain the good stability properties of FRC.

Regarding magnetized target fusion (MTF), conclusions cannot be drawn at this stage, but the potential of this concept could be better assessed when results from FRX-L experiments become available.

The spheromaks geometry is conducive also to direct thrust and energy conversion. Overall, β is not as good as in field reversed configurations, but might be adequate for space propulsion provided $\beta > 10\%$ can be projected at typical reactor conditions. Plasma stability might require the insertion of a central conductor and ultra-low aspect ratio configurations akin to those of tokamak. Such configurations would require specific assessment. The main open question of spheromaks is whether they can effectively sustain a dynamo mechanism with minimal turbulence (laminar

dynamo), while keeping energy acceptably confined. Encouraging results in this direction have been obtained in reversed field pinch experiments.

The dipole configuration is very attractive from the point of view of direct thrust/direct energy generation and because of β. To assess its true potential requires testing of small-scale plasma stability and transport, for instance on the LDX facility. Theoretical predictions about good dipole stability at small scale must be experimentally confirmed. Technically, a noteworthy challenge is the construction of a superconducting coil capable of radiating all the incoming power, and how to produce the electrical power required for its cooling without excessive mass penalty.

Although not included here, the possible use of spherical tokamaks for space propulsion should be stressed. This configuration was not considered since it is a closed, not open, magnetic field configuration. Overall, it does not lend itself easily to propulsion application. However, it has the already proven advantage of conventional tokamak (in terms of confinement and stability) and can obtain very high β. Particles extraction to produce direct thrust has, in principle, the same difficulty of conventional tokamaks, where magnetic field lines do not escape from the reaction chamber, and non-trivial solutions should be investigated for the so-called divertor architecture. This possibility has been considered in the past for space propulsion, but further studies might be beneficial in clarifying its real potential.

Finally, as already noted in Chap. 8, *all* classes of fusion reactors considered here result in bulky and massive propulsion architectures. Some of the experiments in Sect. B.3 were indeed carried on with laboratory-size devices, and their power output (if any) was accordingly *orders of magnitude lower* than required for space propulsion. Mass estimates for GW-class propulsion systems are definitely alarming in view of the orbit lifting costs foreseeable near-term or midterm. This is due to fundamental physics, that is, to the impossibility of fusing at "high pressure," e.g., at pressure $\approx 10^{\circ}$ atm. Charged particles confinement would require $\vec{B}$ fields that are simply impossible to achieve. Therefore, in assessing the potential of fusion for propulsion, priority should be given to compact systems, perhaps even at the expense of efficiency and Q. This issue is critical in magnetically confined fusion.

Finally, Sect. B.1 made the case for fusion based on (1) fuel availability and on (2) the potential to produce large power (this is also the motivation for the ITER international fusion project). However, per unit mass converted into energy, this power is only a factor 3–4 of that obtainable from fission (see Chap. 7), the difference being the fuel itself. Whatever the class of fusion devices, the trade-off between I_{sp} and thrust is still an issue. Because fusion produces low molecular weight He, one may be tempted to use *only* the fusion products themselves as propellant. Leaving aside technology, this strategy implies very high exhaust speed (or I_{sp}), since the energy involved is of order MW/nucleon, and results thus in very low thrust. For instance, a 1 GW fusion propulsion system with I_{sp} in the 10^5 s range (see Fig. 8.5) means *ideally* a 1 kN thrust, in fact much less if the He jet cannot be perfectly collimated and if inevitable losses are accounted for.

For this reason, fast space travel may be achieved only by raising thrust, that is, *by adding inert* propellant to fusion products, with reduction in I_{sp}. This is also the conclusion in Petkow et al. (2008), bringing with it a number of questions connected with mixing a low momentum flux jet of very high-energy products with a much denser and much slower jet of inert propellant. Incidentally, this is the key issue in the air-breathing SCRJ engines discussed in Chaps. 2 to 4, but in fusion propulsion, this issue is exacerbated by the extreme velocity and temperature of fusion.

In summary, magnetic confinement fusion rockets are probably feasible. However, the bulk and mass assuming current technology and its projections are still excessive. Much testing will be necessary before self-sustained fusion for ground power is demonstrated. Only after that happens, space rockets will have a chance of being designed and tested.

Bibliography

Annenkov, V.V. et al (2016) "Book of Abstracts",*11th International Conference on Open Magnetic Systems for Plasma Confinement*, Budker Institute of Nuclear Physics, Novosibirsk,Russia, 08–12 August 2016.

Armentrout, C.J. (2013) "The MFTF-B Story – Fusion or ConFustion?", worldpress.com, March 2013.

Bodin, H.A.B. and Newton, A.A., (1980), "Reversed Field Pinch Research",*Nuclear Fusion*, Vol. 20, No. 10, October 1980, pp. 1255–1324.

Borowski, S.K., (1995), "Comparison of Fusion/Antiproton Propulsion Systems for Interplanetary Travel", in*Fusion Energy in Space Propulsion*, edited by T. Kammash, AIAA Progress in Astronautics and Aeronautics Series, Vol. 167, Washington, Ch. 4, 1995.

Brown, M.R., Cothran, C.D. et al. (2009) "3D Reconnection and Flow Dynamics in the SSX Experiment", CP 1154,*Current Trends in International Fusion Research*, Edited by E. Panarella and R. Raman,*Proceedings of the 7th Symposium*, American Institute of Physics, Vol. 1154, 2009, pp. 167–176.

Bussard, R.W. (1990) "Fusion as Electric Propulsion",*Journal of Propulsion*, Vol. 6, No. 5, September–October 1990, pp. 567-574.

Carpenter, S.A. and Deveny, M.E., (1992) "Mirror Fusion Propulsion System (MFPS): An Option for the Space Exploration Initiative (SEI)", Paper IAF-92-0613, presented at the*43rd Congress of the International Astronautical Federation*, Washington, DC, 28 August–05 September 1992.

Carpenter, S. and Deveny, M., (1993) "Overview of the Mirror Fusion Propulsion System (MFPS): An Optimised Open Magnetic Field Configuration Using D^3He", WCSAR-TR-AR3-9307-3,*Proceedings of the Second Wisconsin Symposium on Helium-3 and Fusion Power*, Madison, WI, 19–21 July 1993.

Casali, D. and Bruno, C., (2005), "Superconductive Materials Applied to Electric Propulsion",*AIAA Journal of Spacecraft and Rockets,* Vol. 41, No. 4, July–August 2004, pp. 671–676.

Casali, D. and Bruno, C., (2008), "Superconductivity", in*Advanced Propulsion Systems and Technologies, Today to 2020*, edited by C. Bruno and A. Accettura, Progress in Astronautics and Aeronautics Series, AIAA, Vol. 223, AIAA, Reston, VA, 2008, Chapter 11.

Chapman, M., Miley, G.H., Kernbichler, W. and Heindler, M. (1989) "Fusion Space Propulsion With a Field Reversed Configuration",*Fusion Technology*, Vol. 15, No., 2, 1989, pp. 1154–1162.

Cheung, A., Binderbauer, M. et al. (2004) "Colliding Beam Fusion Reactor Space Propulsion System",*Space Technology and Applications International Forum*, in*Proceedings STAIF-2004*, Vol. 699, February 2004, pp. 354–361.

Cho, T., Higaki, H., Hirata, M., Hojo, H., Ichimura, M., Ishii, K., et al. (2004) "Advances in Potential Formation and Findings in Sheared Radial Electric-Field Effects on Turbulence and Loss Suppression in GAMMA-10", Paper EX/9-6Rd,*Proceedings of the 20th IAEA Fusion Energy Conference,* Vilamoura, Portugal, 01–06 November 2004.

Cox, L.T. et al. (1990) "Thermonuclear Reaction Listing with Cross-Section Data for Four Advanced Reactions",*Fusion Science and Technology*, Vol. 18, No. 2, September 1990.

Emrich, W.J. (2002), "Current Status of the Gasdynamic Mirror Fusion Propulsion Experiment",*Space Technology and Applications International Forum Conference*, STAIF-2002, Albuquerque, NM, 3–7 February, 2002.

Gormezano, C. (1979) "Reduction of Losses in Open-Ended Magnetic Traps",*Nuclear Fusion*, Vol. 19, no. 8, August 1979, pp. 1085–1137.

Guss, W.C., Yao, X.Z. et al. (1988) "Atomic Hydrogen Density Measurements in the Tara Tandem Mirror Experiment", PFC/JA-88-46, Plasma Fusion Center, MIT, November 1988.

Hasegawa, A. (1987), "A Dipole Field Fusion Reactor",*Comments On Plasma Physics and Controlled Fusion*, Vol. 11, No. 3, 1987, pp. 147–151.

Hoffman, A.L., Guo, H.Y., Miller, K.E. and Milroy, R.D., (2005) "Long Pulse FRC Sustainment with Enhanced Edge Driven Rotating Magnetic Field Current Drive",*Nuclear* Fusion, Vol. 45, No. 3, 21 February 2005.

Huguet, M. et al. (2003) "The ITER Magnets: Preparation for Full Size Construction Based on the Results of the Model Coil Programme" Nuclear Fusion, Vol. 43, No. 5, 24 April 2003.

Jarboe, T.R., (1994) "Review of Spheromak Research",*Plasma Physics and Controlled Fusion*, Vol. 36, No. 6, January 1999, p. 945–990.

Kadomtsev B.B. (1992)*Tokamak Plasma: A Complex Physical System*, Plasma Physics Series, IOP Publishing Ltd, Bristol and Philadelphia, 1992.

Kadomtsev B.B. (1975) "Tokamaks and Dimensional Analysis"*Soviet Journal of Plasma Physics*, Vol. 1, 1975, p. 295.

Kammash, T., (1995) "Principles of Fusion Energy Utilization in Space Propulsion", in*Fusion Energy for Space Propulsion*, edited by T. Kammash, AIAA Progress in Astronautics and Aeronautics Series, Vol. 167, Reston, VA, 1995, Ch. 1.

Kammash, T. et al., (1995) "High-Performance Fusion Rocket for Manned Space Missions", in*Fusion Energy for Space Propulsion*, Edited by T. Kammash, AIAA Progress in Astronautics and Aeronautics Series, Vol. 167, Reston, VA, 1995, Ch. 1.

Kammash, T. and Emrich, W. (1998) "Physics Basis for the Gasdynamic Mirror (GDM) Fusion Rocket", Paper CP420,*Space Technology and Applications International Forum*, American Institute of Physics (AIP), Melville NY, 1998, pp. 1338–1343.

Kawamori, E., Murata, Y., Umeda, K., Hirota, D. et al., (2005) "Ion Kinetic Effect on Bifurcated Relaxation to a Field-Reversed Configuration in TS-4 CT Experiment",*Nuclear* Fusion, Vol. 45, No. 8, 27 July 2005.

Kesner, J., Bromberg, L., Garnier, D. and Mauel, M., (1998) "Plasma Confinement in a Magnetic Dipole", Paper ICP/09,*17th Fusion Energy Conference*, Yokohama, 22 October 1998, pp. 1165–1168.

Kruglyakov, E.P., Dimov, G.I., Ivanov, A.A. and Koidan V.S., (2002) "Axisymmetric Magnetic Mirrors for Plasma Confinement—Recent Development and Perspectives", Paper EX/C1-4Rb,*Proceedings 19th Fusion Energy Conference,* Lyon, France, 2002.

Kulcinski, G.L., Santarius, J.F. et al. (1987) "SOAR: Space Orbiting Advanced Fusion Power Reactor", Report UWFDM-722, Fusion Technology Institute, University of Wisconsin, Madison, Wisconsin, September 1987.

Kulcinski, G.L., Ashley, R.P., Santarius, J.F., Piefer, G. and Subramanian, K.M., (2000) "The Development of Lunar ^{3}He Resources: Near Term Applications and Long-Term Prospects", University of Wisconsin Report UWFDM-1128, Fusion Technology Institute, Department of Engineering Physics, University of Wisconsin, Madison, July 2000.

Lane, T. (2012) "It's Ten Times Hotter than the Sun, but also the Coldest Place on Earth, and It's being Built Deep in the French Countryside",*Building Magazine*, 23 March 2012, pp. 40–45.

Lawson, J.D. (1957) "Some Criteria for a Power Producing Thermonuclear Reactor",*Proceedings of the Physical Society*, Vol. 70, No. 1, Section B, 1957 [also in A.E.R.E. Report GP/R 1807, December 1955, declassified 09 April 1957].

Lee, B.J., Cho, K. et al. (2007) "Multi-Purpose Plasma (MP^2) Facility as a Steady State Divertor Simulator", presentation of Division of Plasma Application and Technology, NFRC, Japan-Korea Workshop, Gifu, Japan, 2007.

Miley, G.H., Gilligan, J.G. and Driemeyer, D. (1978) "Preliminary Design of a Self-Sustained, Advanced-Fueled Field Reversed Mirror Reactor: SAFFIRE",*Transactions of the American Nuclear Society*, Vol. 30, 1978, pp. 47–48.

Miley, G.H., (1987) "Advanced Propulsion Power: A Preliminary Assessment", Committee on Advanced Fusion Power, Air Force Studies Board, National Research Council, National Academy Press, Washington, D.C., 1987.

Miller, K., Slough, J. and Hoffman, A. (1998) "An Overview of the Star Thrust Experiment", Paper CP-420 in*AIP Conference Proceedings*, American Institute of Physics (AIP), Albuquerque, New Mexico, January 1998.

Mirnov, V.V. and Ryutov, D.D. (1979) "Linear Gasdynamic System for Plasma Confinement",*Soviet Technical Physics Letters*, Vol. 5, June 1979, pp. 279–280.

Nagornyj, V.P., Ryutov, D.D. and Stupakov, G.V. (1984) "Flute Instability of Plasma in a Gas Dynamic Trap",*Nuclear Fusion*, Vol. 24, No. 11, pp. 1421–1438.

Nakashima, H., Miley, G.H. and Nakao, Y. (1994) "Field Reversed Configuration (FRC) Fusion Rocket",*11th Symposium Space Nuclear Power and Space Propulsion Systems* (*STAIF*), Albuquerque, NM, 09–13 January 1994.

Okada, S., Fukuda, T., Kitano, K., Sumikura, H. et al. (2005) "Sustainment and Additional Heating of High-Beta Field-Reversed Configuration Plasmas", Paper IC/P6-6,*Nuclear Fusion*, Vol. 45, No. 9, 23 August 2005.

Ozima, M., Seki, K., Terada, N., Miura, Y.N., Podosek, F.A. and Shinagawa, H., (2005), "Terrestrial Nitrogen and Noble Gases in Lunar Soils",*Nature*, Vol. 436, No. 4, 04 August 2005, pp. 655–659.

Petkow, D., Herdrich, G., Laufer, R., Gabrielli, R. and Zeile, O., (2008), "Comparative Investigation of Fusion Reactions for Space Propulsion Applications", Paper ISTS 2008-b-09,*26th International Symposium on Space Technology and Science (ISTS)*, Hamamatsu, Japan, 01–08 June 2008.

Post, R.F., (1987) "The Magnetic Mirror Approach to Fusion",*Nuclear Fusion*, Vol. 27, No. 10, 1987, pp. 1579–1739.

Power, J.L. and Chapman, R.A. (1989) "Development of a High Power Microwave Thruster, With a Magnetic Nozzle, for Space Applications", NASA TM 102321, presented at the*24th Microwave Power Symposium*, Stamford, Connecticut, 21–23 August 1989.

Rechester, A.B. and Rosenbluth, M.N. (1978) "Electron Heat Transport in a Tokamak with Destroyed Magnetic Surfaces",*Physical Review Letters*, Vol. 40, No. 1, 02 January 1978, p. 38–41.

Rostoker, N. et al. (1993) "Magnetic Fusion with High Energy Self Colliding Ion Beams"*Science*, Vol. 278, 21 November 1997, pp. 1419–1422.

Rostoker, N., Binderbauer, M.W. and Monkhorst, H.J. (2003), "Colliding Beam Fusion Reactor",*Journal of Fusion Energy*, Vol. 83, 2003.

Roth, J.R., (1989) "Space Applications of Fusion Energy,"*Fusion Technology*, Vol. 15, 1989, pp. 1375–1394.

Rusbridge, M.G., Gee, S.J., Browning, P.K., Cunningham, G., et al. (1996) "The Design and Operation of the SPHEX Spheromak", *Plasma Physics and Controlled Fusion*, Vol. 39, No. 5, Issue 16, 1996, p. 683–714.

Santarius, J.F. et al. (1989), "Critical Issues for SOAR: The Space Orbiting Advanced Fusion Reactor", Presented at*Fifth Symposium on Space Nuclear Power Systems*, Albuquerque, NM, 11–14 January 1988, in*Space Nuclear Power Systems, 1988*, Edited by M.S. El-Genk and M.D. Also in: Hoover, Space Nuclear Power Systems, Vol. 5, Orbit Book Company, Malabar, FL, 1989, p. 161.

Santarius, J.F. and Logan, B.G., (1998) "Generic Magnetic Fusion Rocket Model",*Journal of Propulsion and Power*, Vol. 14, No. 4, July–August 1998, pp. 519–524.

Sarff, J.S., Almagri, A.F., Anderson, J.K., Biewer, T.M., et al., (2002) "Overview of Improved Confinement and Plasma Control in the MST Reversed Field Pinch", Paper IAEA-CN-94/OV/4-3,*Proceedings of the 19th Fusion Energy Conference,* Lyon, France, 2002.

Schulze, N.R., Miley, G.H. and Santarius, J.F. (1990) "Space Fusion Energy Conversion Using a Field Reversed Configuration Reactor", N91-28217,*Penn State Space Transportation Propulsion Technology Symposium*, Penn State University, State College, Pennsylvania, 25–29 June 1990.

Schulze, N.R. and J.R. Roth, (1990) "The NASA-Lewis Program on Fusion Energy for Space Power and Propulsion, 1958–1978", Conference Paper N91-22148, NASA CP 10059,*Vision-21: Space Travel for the Next Millennium*, Symposium held at NASA Lewis Research Center, Cleveland, Ohio, 03–04 April 1990.

Schulze, N.R. (1994) "Figures of Merit and Attributes for Space Fusion Propulsion,"*Fusion Science and Technology*, Volume 25, No. 2, March 1994, pp. 182–197.

Siemon, R., Peterson, P., Ryutov, D., Kirkpatrick, R. et al. (1999) "The Relevance of Magnetized Target Fusion (MTF) to Practical Energy Production", Los Alamos Laboratory Report LA-UR-99-2956, A White Paper for Consideration by the Fusion Community and the Fusion Energy Sciences Advisory Committee, Draft 2, 03 June 1999.

Simonen, T.C., et al. (1988) "TMX-U Thermal-Barrier Experiments", *IEEE Transactions on Plasma Science*, Vol. 16, Issue 1, February 1988.

Steinhauer, L.C. et al., (1996) "FRC 2001: A White Paper on FRC Development in the Next Five Years",*Fusion Science and Technology*, Vol. 30, No. 1, September 1996, pp. 116–127.

Stuhlinger, E. (1964)*Ion Propulsion for Space Flight*, McGraw-Hill, New York, 1964.

Taccetti, J. M., Intrator, T. P., Wurden, G. A., Zhang, S. Y. et al. (2003) "FRX-L: A Field-Reversed Configuration Plasma Injector for Magnetized Target Fusion",*Review of Scientific instruments*, Vol. 74, Issue 10, 2003, pp. 4314–4323.

Taylor, J.B., (1976) "Relaxation of Toroidal Discharges", in*Pulsed High Beta Plasmas,* Edited by D.E. Evans, Pergamon Press, Oxford, 1976, pp. 59–67.

Teller, E., Glass, A.J., Fowler, T.K., Hasegawa, A. and Santarius, J.F. (1992) "Space Propulsion by Fusion in a Magnetic Dipole",*Fusion Science and Technology*, Vol. 22, No. 1, August 1992, pp. 82–97.

Thio, Y., Freeze, R., Kirkpatrick, R., Landrum, B., Gerrish, H. and Schmidt, G.R. (1999) "High-Energy Space Propulsion Based on Magnetized Target Fusion", Paper AIAA 99-2703,*35th AIAA Joint Propulsion Conference and* Exhibit, Los Angeles, CA, 20–24 June 1999.

Tuszewski, M. (1988) "Field Reversed Configurations",*Nuclear Fusion*, Vol. 28, No. 11, 1988, pp. 2033–2092.

Williams, C.H., Borowski, S.K., Dudzinski, L.A., and Juhasz, A. J. (1998) "A Spherical Torus Nuclear Fusion Reactor Space Propulsion Vehicle Concept for Fast Interplanetary Travel", Paper AIAA-98-3591 presented at the*34th Joint AIAA/ASME/SAE/ASEE Propulsion Meeting*, Cleveland OH, 13–15 July 1998.

Wood, R.D., Cohen, B.I., Hill, D.N., Cohen, R.H. et al. (2004) "Improved Operation and Modeling of the SSPX Spheromak", Paper EX/9-5,*20th IAEA Fusion Energy Conference*, Vilamoura, Portugal, 01–06 November 2004.

Author Index

P.A. Czysz et al., *Future Spacecraft Propulsion Systems and Integration*,
Springer Praxis Books, DOI 10.1007/978-3-662-54,744-1

C

D

H

L

T

Subject Index

P.A. Czysz et al., *Future Spacecraft Propulsion Systems and Integration*,
Springer Praxis Books, DOI 10.1007/978-3-662-54,744-1

D

I

J

K

L

M

N

O

S

T